World Meteorological Organization
Global Ozone Research and Monitoring Project—Report No. 55

Scientific Assessment of Ozone Depletion: 2014

National Oceanic and Atmospheric Administration
National Aeronautics and Space Administration
United Nations Environment Programme
World Meteorological Organization
European Commission

World Meteorological Organization
7bis, avenue de la Paix
Case postale 2300
CH-1211, Geneva 2
Switzerland

United Nations Environment Programme
Ozone Secretariat
P.O. Box 30552
Nairobi, 00100
Kenya

U.S. Department of Commerce
National Oceanic and Atmospheric Administration
14th Street and Constitution Avenue NW
Herbert C. Hoover Building, Room 5128
Washington, D.C. 20230

National Aeronautics and Space Administration
Earth Science Division
NASA Headquarters
300 E Street SW
Washington, D.C. 20546-0001

European Commission
Directorate-General for Research and Innovation
B-1049 Bruxelles
Belgium

Published online December 2014

ISBN: 978-9966-076-01-4

This report and other components of the 2014 Ozone Assessment are available at the following locations:
http://www.wmo.int/pages/prog/arep/gaw/ozone_2014/ozone_asst_report.html
http://ozone.unep.org/en/assessment_panels_bodies.php?committee_id=7
http://ozone.unep.org/Assessment_Panels/SAP/SAP2014_Assessment_for_Decision-Makers.pdf
http://esrl.noaa.gov/csd/assessments/ozone/

This document should be cited as:
World Meteorological Organization (WMO), *Scientific Assessment of Ozone Depletion: 2014*, World Meteorological Organization, Global Ozone Research and Monitoring Project—Report No. 55, 416 pp., Geneva, Switzerland, 2014.

Example chapter citation:
L.J. Carpenter and S. Reimann (Lead Authors), J.B. Burkholder, C. Clerbaux, B.D. Hall, R. Hossaini, J.C. Laube, and S.A. Yvon-Lewis, Ozone-Depleting Substances (ODSs) and Other Gases of Interest to the Montreal Protocol, Chapter 1 in *Scientific Assessment of Ozone Depletion: 2014*, Global Ozone Research and Monitoring Project – Report No. 55, World Meteorological Organization, Geneva, Switzerland, 2014.

World Meteorological Organization
Global Ozone Research and Monitoring Project—Report No. 55

Scientific Assessment of Ozone Depletion: 2014

World Meteorological Organization
Global Ozone Research and Monitoring Project—Report No. 55

SCIENTIFIC ASSESSMENT OF OZONE DEPLETION: 2014

Pursuant to Article 6 of the Montreal Protocol
on Substances that Deplete the Ozone Layer

National Oceanic and Atmospheric Administration
National Aeronautics and Space Administration
United Nations Environment Programme
World Meteorological Organization
European Commission

LIST OF INTERNATIONAL AUTHORS, CONTRIBUTORS, AND REVIEWERS

Assessment Cochairs

Ayité-Lô Nohende Ajavon
Paul A. Newman
John A. Pyle
A.R. Ravishankara

Scientific Steering Committee

Ayité-Lô Nohende Ajavon
David J. Karoly
Malcolm K. Ko
Paul A. Newman
John A. Pyle
A.R. Ravishankara
Theodore G. Shepherd
Susan Solomon

Chapters, Lead Authors, and Chapter Editors

Chapter 1: Update on Ozone-Depleting Substances (ODSs) and Other Gases of Interest to the Montreal Protocol
Lucy J. Carpenter and Stefan Reimann [Lead Authors]
Andreas Engel and Stephen A. Montzka [Chapter Editors]

Chapter 2: Update on Global Ozone: Past, Present, and Future
Steven Pawson and Wolfgang Steinbrecht [Lead Authors]
Vitali E. Fioletov and Ulrike Langematz [Chaper Editors]

Chapter 3: Update on Polar Ozone: Past, Present, and Future
Martin Dameris and Sophie Godin-Beekmann [Lead Authors]
Slimane Bekki and Judith Perlwitz [Chapter Editors]

Chapter 4: Stratospheric Ozone Changes and Climate
Julie M. Arblaster and Nathan P.Gillett [Lead Authors]
Lesley J. Gray and David W.J. Thompson [Chapter Editors]

Chapter 5: Scenarios and Information for Policymakers
Neil R.P. Harris and Donald J. Wuebbles [Lead Authors]
Mack McFarland and Guus J.M. Velders [Chapter Editors]

Twenty Questions and Answers About the Ozone Layer: 2014 Update
Michaela I. Hegglin [Lead Authors]

Coordinating Editor

Christine A. Ennis

Authors, Contributors, and Reviewers

Jon Abbatt	Canada
Ayité-Lô Nohende Ajavon	Togo
Hideharu Akiyoshi	Japan
Joan M. Alexander	USA
Simon Alexander	Australia
Stephen O. Andersen	USA
Valentina Aquila	USA
Julie M. Arblaster	Australia/USA
Matthew Ashfold	Malaysia
Ghassem Asrar	USA
Pieter J. Aucamp	South Africa
Alkiviadis F. Bais	Greece
Mark P. Baldwin	UK
Elizabeth A. Barnes	USA
Steven L. Baughcum	USA
Gufran Beig	India
Slimane Bekki	France
Peter Bernath	USA
Tina Birmpili	UNEP
Thomas Birner	USA
Donald R. Blake	USA
Greg Bodeker	New Zealand
Rumen D. Bojkov	Germany
Geir O. Braathen	WMO
Peter Braesicke	Germany
Stefan Brönnimann	Switzerland
Dominik Brunner	Switzerland
James B. Burkholder	USA
John P. Burrows	Germany
Neal Butchart	UK
Amy H. Butler	USA
Wenju Cai	Australia
Francesco Cairo	Italy
Natalia Calvo	Spain
Pablo O. Canziani	Argentina
Lucy Carpenter	UK
Kenneth S. Carslaw	UK
Andrew J. Charlton-Perez	UK
Wissam Chehade	Germany
Martyn P. Chipperfield	UK
Bo Christiansen	Denmark
Irene Cionni	Italy
Cathy Clerbaux	France
Melanie Coldewey-Egbers	Germany
Martin Dameris	Germany
John S. Daniel	USA
Jos de Laat	The Netherlands
Andy Delcloo	Belgium
Sandip Dhomse	UK
Susana B. Diaz	Argentina
Marcel Dorf	Germany
Anne R. Douglass	USA
Geoffrey S. Dutton	USA
Richard S. Eckman	USA
Nawo Eguchi	Japan
James William Elkins	USA
Andreas Engel	Germany
Ines Engel	Germany
Christine A. Ennis	USA
Veronika Eyring	Germany
David W. Fahey	USA
Vitali Fioletov	Canada
Eric L. Fleming	USA
Piers M. Forster	UK
Paul Fraser	Australia
Stacey M. Frith	USA
Lucien Froidevaux	USA
Jan Fuglestvedt	Norway
Masatomo Fujiwara	Japan
John C. Fyfe	Canada
Annie Gabriel	Australia
Lenah Gaoetswe	Botswana
Chaim I. Garfinkel	Israel
Hella Garny	Germany
Marvin A. Geller	USA
Edwin P. Gerber	USA
Andrew Gettelman	USA
Tomasz Gierczak	Poland
Manuel Gil-Ojeda	Spain
Nathan P. Gillett	Canada
Sophie Godin-Beekmann	France
Marco González	Kenya
Lesley J. Gray	UK
Kevin M. Grise	USA
Jens-Uwe Grooß	Germany
Serge Guillas	UK
Joanna D. Haigh	UK
Bradley D. Hall	USA
Steven C. Hardiman	UK
Neil R.P. Harris	UK
Birgit Hassler	USA
Alain Hauchecorne	France
Peter Haynes	UK
Michaela I. Hegglin	UK
François Hendrick	Belgium
Peter Hitchcock	UK

Øivind Hodnebrog	Norway
Larry Horowitz	USA
Ryan Hossaini	UK
Jianxin Hu	China
Nathalie Huret	France
Dale F. Hurst	USA
Iolanda Ialongo	Finland
Mohammad Ilyas	Malaysia
Franz Immler	Belgium
Ivar S.A. Isaksen	Norway
Charles H. Jackman	USA
Michal Janouch	Czech Republic
Julie M. Jones	UK
Ashley Jones	Canada
Kenneth W. Jucks	USA
David J. Karoly	Australia
Alexey Yu. Karpechko	Finland
Yasuko Kasai	Japan
Philippe Keckhut	France
Sergey Khaykin	Russia
Doug Kinnison	USA
Andrew R. Klekociuk	Australia
Jeff R. Knight	UK
Malcolm K. Ko	USA
Yutaka Kondo	Japan
Karin Kreher	New Zealand
Kirstin Krüger	Norway
Paul B. Krummel	Australia
Lambert J.M. Kuijpers	The Netherlands
Markus Kunze	Germany
Michael J. Kurylo	USA
Paul J. Kushner	Canada
Erkki Kyrölä	Finland
Gabriela Lakkis	Argentina
Shyam Lal	India
Jean-François Lamarque	USA
Tom Land	USA
Ulrike Langematz	Germany
Johannes Laube	UK
Katharine Law	France
Franck Lefèvre	France
Bernard Legras	France
Jos Lelieveld	Germany
Qing Liang	USA
Eun-Pa Lim	Australia
Jintai Lin	China
Nathaniel Livesey	USA
Diego Loyola	Germany
Emmanuel Mahieu	Belgium
Desmond Manatsa	Zimbabwe
Gloria L. Manney	USA
Martin R. Manning	New Zealand
Elisa Manzini	Germany
Bella Maranion	USA
Daniel R. Marsh	USA
Amanda C. Maycock	UK
Mack McFarland	USA
Charles McLandress	Canada
Chris McLinden	Canada
Johan Mellqvist	Sweden
Michael P. Meredith	UK
Pauline M. Midgley	Switzerland
Daniel M. Mitchell	UK
Mario J. Molina	USA
Stephen Montzka	USA
Olaf Morgenstern	New Zealand
Jens Mühle	USA
Rolf Müller	Germany
Hiroaki Naoe	Japan
Thando Ndarana	South Africa
Paul A. Newman	USA
Ole John Nielsen	Denmark
Simon O'Doherty	UK
Keiichi Ohnishi	Japan
Luke D. Oman	USA
Vladimir L. Orkin	USA
Andrew Orr	UK
Yvan Orsolini	Norway
Steven Pawson	USA
Juan Carlos Peláez	Cuba
Stuart A. Penkett	UK
Judith Perlwitz	USA
Thomas Peter	Switzerland
Irina Petropavlovskikh	USA
Klaus Pfeilsticker	Germany
Daniel Phoenix	USA
Damaris K. Pinheiro	Brazil
Giovanni Pitari	Italy
Michael Pitts	USA
David Plummer	Canada
Lorenzo M. Polvani	USA
Jean-Pierre Pommereau	France
Lamont Poole	USA
Robert W. Portmann	USA
Michael J. Prather	USA
Michael Previdi	USA
Ronald G. Prinn	USA
John A. Pyle	UK
Birgit Quack	Germany
B. Rajakumar	India
S. Ramachandran	India
V. Ramaswamy	USA

Cora Randall	USA
William Randel	USA
Marilyn Raphael	USA
A.R. Ravishankara	USA
Stefan Reimann	Switzerland
James Renwick	New Zealand
Laura Revell	Switzerland
Markus Rex	Germany
Robert C. Rhew	USA
Harald E. Rieder	Austria
Martin Riese	Germany
Matt Rigby	UK
Vincenzo Rizi	Italy
Alan Robock	USA
Jose M. Rodriguez	USA
Eugene Rozanov	Switzerland
Vladimir Ryabinin	Switzerland
Alfonso Saiz-Lopez	Spain
Takatoshi Sakazaki	Japan
Ross J. Salawitch	USA
Michelle L. Santee	USA
Robert Sausen	Germany
Sue Schauffler	USA
Robyn Schofield	Australia
Dian J. Seidel	USA
Megumi Seki	UNEP
William Seviour	UK
Jonathan Shanklin	UK
Tiffany A. Shaw	USA
Rajendra Shende	India
Theodore G. Shepherd	UK
Kiyotaka Shibata	Japan
Keith Shine	UK
Masato Shiotani	Japan
Michael Sigmond	Canada
Peter Simmonds	UK
Isla R. Simpson	USA
Isobel J. Simpson	USA
Rajiv R. Singh	USA
Björn-Martin Sinnhuber	Germany
Karen L. Smith	USA
Susan Solomon	USA
Seok-Woo Son	Korea
Johannes Staehelin	Switzerland
Wolfgang Steinbrecht	Germany
Gabriele P. Stiller	Germany
Richard S. Stolarski	USA
William T. Sturges	UK
Tove M. Svendby	Norway
Neil C. Swart	Canada
David W. Tarasick	Canada
Susann Tegtmeier	Germany
Said Ali Thauobane	Comoros
Larry W. Thomason	USA
Owen Brian Toon	USA
Matthew B. Tully	Australia
David W.J. Thompson	USA
Simone Tilmes	USA
John Turner	UK
Joachim Urban	Sweden
Ronald van der A	The Netherlands
Guus J.M. Velders	The Netherlands
Daniel P. Verdonik	USA
Jean-Paul Vernier	USA
Martin K. Vollmer	Switzerland
Peter von der Gathen	Germany
Christian von Savigny	Germany
Timothy J. Wallington	USA
Darryn W. Waugh	USA
Ann R. Webb	UK
Mark Weber	Germany
Debra K. Weisenstein	USA
Ray F. Weiss	USA
Laura J. Wilcox	UK
Jeannette Wild	USA
Elian Augusto Wolfram	Argentina
Yutian Wu	USA
Donald J. Wuebbles	USA
Shi-Keng Yang	USA
Shigeo Yoden	Japan
Yoko Yokouchi	Japan
Paul J. Young	UK
Shari A. Yvon-Lewis	USA
Durwood Zaelke	USA
Christos S. Zerefos	Greece
Lingxi Zhou	China
Jerry Ziemke	USA

Chapter Editorial Contributors

Chapter 1:

Nada Derek	Australia
Jenny Hudson	UK

Remembrances

It is with sadness that we note the passing of the following scientists who have played leading roles in the science and international assessments of the ozone layer.

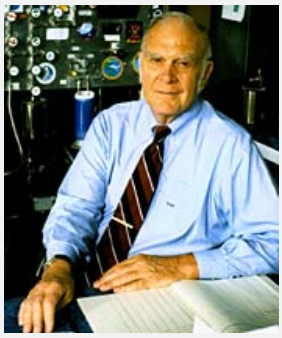

F. Sherwood "Sherry" Rowland (1927–2012) (Donald Bren research professor of chemistry in Earth system science at University of California, Irvine) passed away on 10 March 2012. Sherry was born on 28 June 1927 in Delaware, Ohio. He earned a B.A. in 1948 from Ohio Wesleyan University, his M.S. in 1951, and his Ph.D. in 1952 from the University of Chicago. In 1974, Mario Molina and Sherry warned that chlorofluorocarbons (CFCs) were increasing in the atmosphere, and were releasing chlorine in the stratosphere and thus depleting the ozone layer. Acting on this science spawned by Mario and Sherry, the nations of the world agreed in the 1985 Vienna Convention that ozone depletion was a real and serious problem. In 1987, the nations negotiated the Montreal Protocol on Substances that Deplete the Ozone Layer. The Montreal Protocol has now been strengthened to fully control the production and consumption of ozone depleting substances (ODSs), and has now been signed by every nation on Earth. In 1995, Sherry, Mario and Paul J. Crutzen shared the Nobel Prize for Chemistry "for their work in atmospheric chemistry, particularly concerning the formation and decomposition of ozone." Sherry's many other awards include the Tolman Award in 1976, the Tyler Prize for Environmental Achievement in 1983, the Japan Prize in 1989, the Peter Debye Award in 1993, the Albert Einstein World Award of Science in 1994, and the AGU Roger Revelle Medal in 1994. Sherry contributed in numerous ways to the WMO/UNEP assessments, in fact, it can be easily stated that he started the whole process with his seminal 1974 paper.

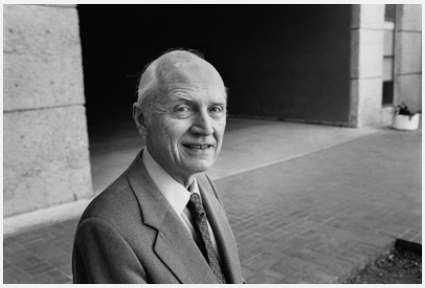

Harold "Hal" Johnston (1920–2012) died 20 October 2012 at the age of 92. He was born on 11 October 1920 in Woodstock, Georgia. He received his degree in chemistry from Emory University in 1941 and his Ph.D. from California Institute of Technology in 1948. After a few years at Stanford University, he was at UC Berkeley for his long and illustrious career. He was one of the pioneers of stratospheric research, having recognized the role of nitrogen oxides in destroying the ozone layer (simultaneously with Prof. Crutzen) and thus showing the potential impact of supersonic aircraft flying in the stratosphere. He was a major contributor to the Climatic Impact Assessment Program (CIAP) reports, an integrated assessment of the potential atmospheric impacts of the proposed American supersonic transport aircraft (SST) in the early 1970s. These reports predated the ozone layer assessments under the Montreal Protocol and laid the groundwork for stratospheric research. Hal received a number of awards and prizes, including the National Medal of Science, the Tyler World Prize for Environmental Achievement, the National Academy of Sciences Award for Chemistry in the Service to Society, and American Geophysical Union's Roger Revelle Medal.

Joseph C. Farman (1930–2013) died in Cambridge on 11 May 2013 at the age of 82. Joe led the British Antarctic Survey (BAS) team that made one of the major geophysical discoveries of the 20th century when it reported a very large decline in springtime stratospheric ozone, a phenomenon that became known as the Antarctic Ozone Hole. Joe was born on 7 August 1930 in Norwich, England. He received his M.A. in Natural Sciences from Corpus Christi College, Cambridge, where he was later a Fellow and Honorary Fellow. In 1956 he joined the Falkland Island Dependencies Survey (later British Antarctic Survey) with responsibility for establishing their geophysical measurements during the International Geophysical Year. He stayed at BAS until his retirement in 1990, then joining the European Ozone Research Coordinating Unit. He assisted directly and indirectly with a number of WMO/UNEP Ozone Assessments and played a key role in the development of the Montreal Protocol, well beyond his initial scientific input. His scientific life was characterized by a painstaking attention to detail, to the primacy of data, and for the need in geophysics for long data records.

CONTENTS

SCIENTIFIC ASSESSMENT OF OZONE DEPLETION: 2014

CHAPTER 4: STRATOSPHERIC OZONE CHANGES AND CLIMATE

Julie M. Arblaster and Nathan P. Gillett [Lead Authors]

Lesley J. Gray and David W.J. Thompson [Chapter Editors]

CHAPTER 5: SCENARIOS AND INFORMATION FOR POLICYMAKERS

Neil R.P. Harris and Donald J. Wuebbles [Lead Authors]

Mack McFarland and Guus J.M. Velders [Chapter Editors]

APPENDICES

PREFACE

This document is part of the information upon which the Parties to the United Nations Montreal Protocol will base their future decisions regarding ozone-depleting substances, their alternatives, and protection of the ozone layer. It is the latest in a long series of scientific assessments that have informed the Parties.

The Charge to the Assessment Panels

Specifically, the Montreal Protocol on Substances that Deplete the Ozone Layer[1] states (Article 6): "…the Parties shall assess the control measures…on the basis of available scientific, environmental, technical, and economic information." To provide the mechanisms whereby these assessments are conducted, the Protocol further states: "…the Parties shall convene appropriate panels of experts" and "the panels will report their conclusions…to the Parties."

To meet this request, the Scientific Assessment Panel (SAP), the Environmental Effects Assessment Panel (EEAP), and the Technology and Economic Assessment Panel (TEAP) have each prepared, about every 3–4 years, major assessment reports that updated the state of understanding in their purviews. These reports have been scheduled so as to be available to the Parties in advance of their meetings at which they consider the need to amend or adjust the Protocol.

The Sequence of Scientific Assessments

The present 2014 report is the latest in a series of 12 scientific Assessments prepared by the world's leading experts in the atmospheric sciences and under the international auspices of the World Meteorological Organization (WMO) and/or the United Nations Environment Programme (UNEP). This report is the eighth in the set of major Assessments that have been prepared by the Scientific Assessment Panel directly as input to the Montreal Protocol process. The chronology of all the scientific Assessments on the understanding of ozone depletion and their relation to the international policy process is summarized as follows:

Year	Policy Process	Scientific Assessment
1981		*The Stratosphere 1981 Theory and Measurements*. WMO No. 11
1985	Vienna Convention	*Atmospheric Ozone 1985*. WMO No. 16
1987	Montreal Protocol	
1988		*International Ozone Trends Panel Report 1988.* WMO No. 18
1989		*Scientific Assessment of Stratospheric Ozone: 1989*. WMO No. 20
1990	London Amendment and adjustments	
1991		*Scientific Assessment of Ozone Depletion: 1991*. WMO No. 25
1992		*Methyl Bromide: Its Atmospheric Science, Technology, and Economics* (Assessment Supplement). UNEP (1992).
1992	Copenhagen Amendment and adjustments	
1994		*Scientific Assessment of Ozone Depletion: 1994*. WMO No. 37
1995	Vienna adjustments	
1997	Montreal Amendment and adjustments	
1998		*Scientific Assessment of Ozone Depletion: 1998*. WMO No. 44
1999	Beijing Amendment and adjustments	
2002		*Scientific Assessment of Ozone Depletion: 2002*. WMO No. 47
2006		*Scientific Assessment of Ozone Depletion: 2006*. WMO No. 50
2007	Montreal adjustments	
2010		*Scientific Assessment of Ozone Depletion: 2010*. WMO No. 52
2014		*Scientific Assessment of Ozone Depletion: 2014*. WMO No. 55

[1] In this report, ozone-depleting substances (ODSs) refer to the gases listed in the Annexes to the Montreal Protocol. In addition to these gases, other chemicals also influence the ozone layer, and they are referred to as ozone-relevant gases.

The Current Information Needs of the Parties

The genesis of *Scientific Assessment of Ozone Depletion: 2014* was the 23rd Meeting of the Parties to the Montreal Protocol held during 21–25 November 2011 in Bali, Indonesia, at which the scope of the scientific needs of the Parties was defined in their Decision XXIII/13 (4), which stated that:

"*...for the 2014 report, the Scientific Assessment Panel should consider issues including:*

- *Assessment of the state of the ozone layer and its future evolution, including in respect of atmospheric changes from, for example, sudden stratospheric warming or accelerated Brewer-Dobson circulation;*
- *Evaluation of the Antarctic ozone hole and Arctic winter/spring ozone depletion and the predicted changes in these phenomena, with a particular focus on temperatures in the polar stratosphere;*
- *Evaluation of trends in the concentration in the atmosphere of ozone-depleting substances and their consistency with reported production and consumption of those substances and the likely implications for the state of the ozone layer and the atmosphere;*
- *Assessment of the interaction between the ozone layer and the atmosphere; including: (i) The effect of polar ozone depletion on tropospheric climate and (ii) The effects of atmosphere-ocean coupling;*
- *Description and interpretation of observed ozone changes and ultraviolet radiation, along with future projections and scenarios for those variables, taking into account among other things the expected impacts to the atmosphere;*
- *Assessment of the effects of ozone-depleting substances and other ozone-relevant substances, if any, with stratospheric influences, and their degradation products, the identification of such substances, their ozone-depletion potential and other properties;*
- *Identification of any other threats to the ozone layer*."

The 2014 SAP Assessment has addressed all the issues that were feasible to address to the best possible extent. Further, given the change in the structure of the report and the evolution of science, the UV changes are addressed by the Environmental Effects Assessment Panel (EEAP) of the Montreal Protocol. The SAP has provided the necessary information on ozone levels, now and in the future, to EEAP as input to their assessments.

The 2014 Assessment Process

The formal planning of the current Assessment was started early in 2013. The Cochairs considered suggestions from the Parties regarding experts from their countries who could participate in the process. Two key changes were incorporated for the 2014 Assessment: (1) creation of a Scientific Steering Committee consisting of the Cochairs and four other prominent scientists; and (2) instituting Chapter Editors for each chapter to ensure that the reviews were adequately and appropriately handled by the authors and key messages were clearly enunciated to take them to the next level. For this reason, the Chapter Editors are also Coauthors of the *Assessment for Decision Makers* (ADM) of the *Scientific Assessment of Ozone Depletion: 2014*. The plan for this Assessment was vetted by an ad hoc international scientific advisory group. This group also suggested participants from the world scientific community to serve as authors of the science chapters, reviewers, and other roles. In addition, this advisory group contributed to crafting the outline of this Assessment report. As in previous Assessments, the participants represented experts from the developed and developing world. The developing country experts bring a special perspective to the process, and their involvement in the process has also contributed to capacity building in those regions and countries.

The 2014 Scientific Assessment Panel (SAP) Report

The 2014 report of the Scientific Assessment Panel differs from the past seven reports in its structure and mode of publication. However, as in the past, it is a thorough examination and assessment of the science. The process by which this report was generated, as in the past, was also thorough; the documents underwent multiple reviews by international experts.

The Structure of the 2014 Report

The previous SAP reports have served well the Parties to the Montreal Protocol, the scientific community, and the managers who deal with the research activities. However, the Montreal Protocol process has

matured significantly and its needs have evolved. It was clear from the discussions between the Cochairs and both the Party representatives and the people involved in decision making that the previous very lengthy assessment reports would not meet the current needs of the Parties for a short, pithy, document that is written for them and not for the scientific community. Yet, it was also clear that the integrity of and the trust in the SAP reports come from the very thorough assessment of the science. Therefore, this 2014 Assessment was restructured to serve both purposes. The new structure is shown schematically below.

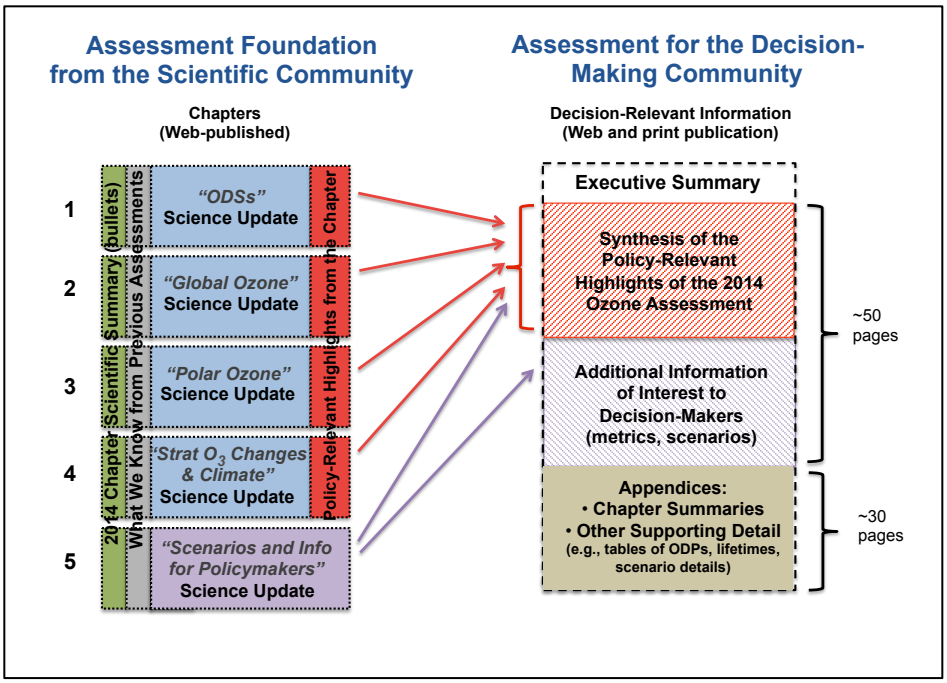

First, as in the past, a major scientific assessment process was carried out and the findings from these discussions and reviews constitute the five major chapters of the assessment foundation from the scientific community. This is shown on the left hand side of the diagram. The five scientific chapters are published only on the web but *are an integral part of the 2014 SAP report to the Parties*. Also, as discussed earlier, the assessment of the surface UV changes due to past ozone depletion or to projected future ozone levels are not included in this document. Readers are referred to the 2014 Environmental Effects Assessment Panel report for the UV discussion.

Second, the findings from the SAP's five scientific chapters were then synthesized and written in a language that is accessible to the Parties to the Protocol. The contents of the *Assessment for Decision-Makers* document—an Executive Summary and three sections—are shown on the right hand side. This short document, which contains all the major scientific summary points written in a clear and accessible language, is available in print and on the web. It is hoped that this new document will be useful to and usable by the Parties to the Protocol, countries, and high-level policymakers and managers. If more scientific details are needed, the complete document can be accessed via the web.

Third, for this Assessment, the *Twenty Questions and Answers About the Ozone Layer* has been only updated. This is because the overarching scientific understanding has not changed significantly from the previous Assessment. The update will ensure that the answers include the most current data and are consistent with the 2014 Assessment. These updated questions and answers are published separately (both in print and on the web) in a companion booklet to this report.

It is hoped that these steps will enhance the usefulness of the document to the Parties, meet the needs of the multiple user communities for the information, minimize the workload of the scientific community, and reduce costs.

The Process of Preparing the 2014 Assessment

The initial plans for the scientific chapters of the 2014 Scientific Assessment Panel's report were examined at a meeting that occurred on 10–11 June 2013 in Cambridge, UK. The Lead Authors, the Scientific Steering Committee, and Chapter Editors—along with a few representatives of other assessment panels and organizations—focused on the planned content of the chapters and on the need for coordination among the chapters.

The first drafts of the scientific chapters were mailed to 213 experts for written reviews. The chapters were revised to take into account the comments of the reviewers. The revised drafts were subsequently sent to 65 reviewers who either attended a review meeting in Boulder or communicated their comments back to the group. These second drafts were reviewed by 63 experts in person in Boulder, CO, USA during 8–10 April 2014. Final changes to the chapters were decided upon at this meeting, and the final chapter summary points were agreed. Subsequently, the chapters were revised for clarity and to address specific points that were agreed to at the Boulder meeting. Final drafts of the scientific chapters were completed in May 2014.

Subsequent to the finalization of the five chapters, an author team consisting of the Scientific Steering Committee, Chapter Lead Authors, and Chapter Editors wrote a draft of the *Assessment for Decision-Makers*. This document was based on the science findings of the five chapters. The draft ADM was made available on June 13 to the attendees of a Panel Review Meeting that took place in Les Diablerets, Switzerland, on 23–27 June 2014. The overall ADM was reviewed, discussed, and agreed to by the 59 participants. The Executive Summary of the ADM, contained herein (and posted on the UNEP and WMO websites on 10 September 2014), was prepared and completed by the attendees of the Les Diablerets meeting.

The final result of this two-year endeavor is the present assessment report. As the accompanying list indicates (Appendix A), the *Scientific Assessment of Ozone Depletion: 2014* is the product of 285 scientists from 36 countries[2] of the developed and developing world who contributed to its preparation and review (133 scientists prepared the report and 220 scientists participated in the peer review process).

[2] Argentina, Australia, Austria, Belgium, Botswana, Brazil, Canada, People's Republic of China, Comoros, Costa Rica, Cuba, Czech Republic, Denmark, Finland, France, Germany, Greece, India, Israel, Italy, Japan, Korea, Malaysia, New Zealand, Norway, Poland, Russia, South Africa, Spain, Sweden, Switzerland, The Netherlands, Togo, United Kingdom, United States of America, Zimbabwe.

EXECUTIVE SUMMARY
ASSESSMENT FOR DECISION-MAKERS

[This is the Executive Summary of the *Assessment for Decision-Makers* of the 2014 Ozone Assessment. It contains the policy-relevant major findings of the Assessment's five scientific chapters, which follow.]

Actions taken under the Montreal Protocol have led to decreases in the atmospheric abundance of controlled ozone-depleting substances (ODSs), and are enabling the return of the ozone layer toward 1980 levels.

- **The sum of the measured tropospheric abundances of substances controlled under the Montreal Protocol continues to decrease.** Most of the major controlled ODSs are decreasing largely as projected, and hydrochlorofluorocarbons (HCFCs) and halon-1301 are still increasing. Unknown or unreported sources of carbon tetrachloride are needed to explain its abundance.
- **Measured stratospheric abundances of chlorine- and bromine-containing substances originating from the degradation of ODSs are decreasing.** By 2012, combined chlorine and bromine levels (as estimated by Equivalent Effective Stratospheric Chlorine, EESC) had declined by about 10–15% from the peak values of ten to fifteen years ago. Decreases in atmospheric abundances of methyl chloroform (CH_3CCl_3), methyl bromide (CH_3Br), and chlorofluorocarbons (CFCs) contributed approximately equally to these reductions.
- **Total column ozone declined over most of the globe during the 1980s and early 1990s (by about 2.5% averaged over 60°S to 60°N). It has remained relatively unchanged since 2000,** with indications of a small increase in total column ozone in recent years, as expected. In the upper stratosphere there is a clear recent ozone increase, which climate models suggest can be explained by comparable contributions from declining ODS abundances and upper stratospheric cooling caused by carbon dioxide increases.
- **The Antarctic ozone hole continues to occur each spring**, as expected for the current ODS abundances. The Arctic stratosphere in winter/spring 2011 was particularly cold, which led to large ozone depletion as expected under these conditions.
- **Total column ozone will recover toward the 1980 benchmark levels over most of the globe** under full compliance with the Montreal Protocol. This recovery is expected to occur before midcentury in midlatitudes and the Arctic, and somewhat later for the Antarctic ozone hole.

The Antarctic ozone hole has caused significant changes in Southern Hemisphere surface climate in the summer.

- **Antarctic lower stratospheric cooling due to ozone depletion is very likely the dominant cause of observed changes in Southern Hemisphere tropospheric summertime circulation over recent decades**, with associated impacts on surface temperature, precipitation, and the oceans. In the Northern Hemisphere, no robust link has been found between stratospheric ozone depletion and tropospheric climate.

Changes in CO_2, N_2O, and CH_4 will have an increasing influence on the ozone layer as ODSs decline.

- **As controlled ozone-depleting substances decline, the evolution of the ozone layer in the second half of the 21st century will largely depend on the atmospheric abundances of CO_2, N_2O, and CH_4.** Overall, increasing carbon dioxide (CO_2) and methane (CH_4) elevate global ozone, while increasing nitrous oxide (N_2O) further depletes global ozone. The Antarctic ozone hole is less sensitive to CO_2, N_2O, and CH_4 abundances.
- **In the tropics, significant decreases in column ozone are projected during the 21st century.** Tropical ozone levels are only weakly affected by ODS decline; they are sensitive to circulation changes driven by CO_2, N_2O, and CH_4 increases.

The climate benefits of the Montreal Protocol could be significantly offset by projected emissions of HFCs used to replace ODSs.

The Montreal Protocol and its Amendments and adjustments have made large contributions toward reducing global greenhouse gas emissions. In 2010, the decrease of annual ODS emissions under the Montreal Protocol is estimated to be about 10 gigatonnes of avoided CO_2-equivalent emissions per year, which is about five times larger than the annual emissions reduction target for the first commitment period (2008–2012) of the Kyoto Protocol (from the Executive Summary of the *Scientific Assessment of Ozone Depletion: 2010*).[3]

- The sum of the hydrofluorocarbons (HFCs) currently used as ODS replacements makes a small contribution of about 0.5 gigatonnes CO_2-equivalent emissions per year. These emissions are currently growing at a rate of about 7% per year and are projected to continue to grow.
- If the current mix of these substances is unchanged, increasing demand could result in HFC emissions of up to 8.8 gigatonnes CO_2-equivalent per year by 2050, nearly as high as the peak emission of CFCs of about 9.5 gigatonnes CO_2-equivalent per year in the late 1980s.[4]
- Replacements of the current mix of high-Global Warming Potential (GWP) HFCs with low-GWP compounds or not-in-kind technologies would essentially avoid these CO_2-equivalent emissions.
- Some of these candidate low-GWP compounds are hydrofluoro-olefins (HFOs), one of which (HFO-1234yf) yields the persistent degradation product trifluoroacetic acid (TFA) upon atmospheric oxidation. While the environmental effects of TFA are considered to be negligible over the next few decades, potential longer-term impacts could require future evaluations due to the environmental persistence of TFA and uncertainty in future uses of HFOs.
- By 2050, HFC banks are estimated to grow to as much as 65 gigatonnes CO_2-equivalent. The climate change impact of the HFC banks could be reduced by limiting future use of high-GWP HFCs to avoid the accumulation of the bank, or by destruction of the banks.

Additional important issues relevant to the Parties to the Montreal Protocol and other decision-makers have been assessed.

- Derived emissions of carbon tetrachloride (CCl_4), based on its estimated lifetime and its accurately measured atmospheric abundances, have become much larger than those from reported production and usage over the last decade.

---

[3] GWP-weighted emissions, also known as CO_2-equivalent emissions, are defined as the amount of gas emitted multiplied by its 100-year Global Warming Potential (GWP). Part of the effect of ODSs as greenhouse gases is offset by the cooling due to changes in ozone.

[4] This is equivalent to about 45% of the fossil fuel and cement emissions of CO_2 in the late 1980s.

- As of 2009, the controlled consumption of methyl bromide declined below the reported consumption for quarantine and pre-shipment (QPS) uses, which are not controlled by the Montreal Protocol.
- Increased anthropogenic emissions of very short-lived substances (VSLS) containing chlorine and bromine, particularly from tropical sources, are an emerging issue for stratospheric ozone. The relative contribution of these emissions could become important as levels of ODSs controlled under the Montreal Protocol decline.
- As the atmospheric abundances of ODSs continue to decrease over the coming decades, N_2O, as the primary source of nitrogen oxides in the stratosphere, will become more important in future ozone depletion.
- Emissions of HFC-23, a by-product of HCFC-22 production, have continued despite mitigation efforts.
- While ODS levels remain high, a large stratospheric sulfuric aerosol enhancement due to a major volcanic eruption or geoengineering activities would result in a substantial chemical depletion of ozone over much of the globe.

While past actions taken under the Montreal Protocol have substantially reduced ODS production and consumption, additional, but limited, options are available to reduce future ozone depletion.

Emissions from the current banks are projected to contribute more to future ozone depletion than those caused by future ODS production, assuming compliance with the Protocol.

- Possible options to advance the return of the ozone layer to the 1980 level (analyses based on midlatitude EESC) are shown graphically. The cumulative effect of elimination of emissions from all banks and production advances this return by 11 years.

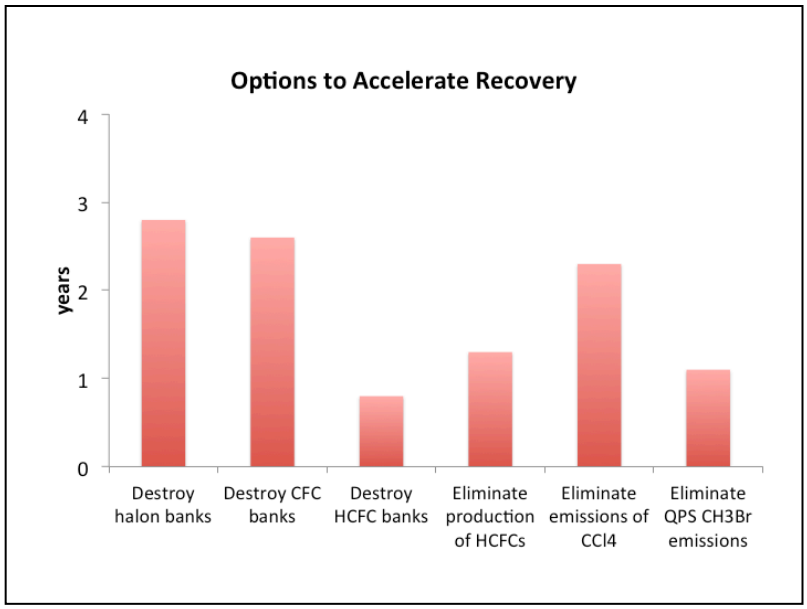

CHAPTER 1

Update on Ozone-Depleting Substances (ODSs) and Other Gases of Interest to the Montreal Protocol

Lead Authors:
L.J. Carpenter
S. Reimann

Coauthors:
J.B. Burkholder
C. Clerbaux
B.D. Hall
R. Hossaini
J.C. Laube
S.A. Yvon-Lewis

Contributors:
D.R. Blake
M. Dorf
G.S. Dutton
P.J. Fraser
L. Froidevaux
F. Hendrick
J. Hu
A. Jones
P.B. Krummel
L.J.M. Kuijpers
M.J. Kurylo
Q. Liang
E. Mahieu
J. Mühle
S. O'Doherty
K. Ohnishi
V.L. Orkin
K. Pfeilsticker
M. Rigby
I.J. Simpson
Y. Yokouchi

Chapter Editors:
A. Engel
S.A. Montzka

[Formatted for double-sided printing.]

From:
WMO (World Meteorological Organization), *Scientific Assessment of Ozone Depletion: 2014*, Global Ozone Research and Monitoring Project – Report No. 55, 416 pp., Geneva, Switzerland, 2014.

This chapter should be cited as:
L.J. Carpenter and S. Reimann (Lead Authors), J.B. Burkholder, C. Clerbaux, B.D. Hall, R. Hossaini, J.C. Laube, and S.A. Yvon-Lewis, Ozone-Depleting Substances (ODSs) and Other Gases of Interest to the Montreal Protocol, Chapter 1 in *Scientific Assessment of Ozone Depletion: 2014*, Global Ozone Research and Monitoring Project – Report No. 55, World Meteorological Organization, Geneva, Switzerland, 2014.

CHAPTER 1

UPDATE ON OZONE-DEPLETING SUBSTANCES (ODSs) AND OTHER GASES OF INTEREST TO THE MONTREAL PROTOCOL

Contents

SCIENTIFIC SUMMARY

Changes in the global atmospheric abundance of a substance are determined by the balance between its emissions and removal. Declines observed for ozone-depleting substances (ODSs) controlled under the Montreal Protocol are due to global emission reductions that have made emissions smaller than removals. Most ODSs are potent greenhouse gases. As the majority of ODSs have been phased out, demand for hydrochlorofluorocarbon (HCFC) and hydrofluorocarbon (HFC) substitutes for the substances controlled under the Montreal Protocol has increased; these are also greenhouse gases. HCFCs deplete much less ozone per kilogram emitted than chlorofluorocarbons (CFCs), while HFCs essentially deplete no ozone.

The amended and adjusted Montreal Protocol has continued to reduce emissions and atmospheric abundances of most controlled ozone-depleting substances. By 2012, the total combined abundance of anthropogenic ODSs in the troposphere (measured as Equivalent Chlorine) had decreased by nearly 10% from its peak value in 1994.

The contributions to the overall decline in tropospheric chlorine (Cl) and bromine (Br) from substances and groups of substances controlled and not controlled under the Montreal Protocol have changed since the previous Assessment. The observed declines in total tropospheric Cl and Br from controlled substances during the 5-year period 2008–2012 were 13.4 ± 0.9 parts per trillion (ppt) yr^{-1} and 0.14 ± 0.02 ppt yr^{-1}, respectively.[1]

Substances controlled under the Montreal Protocol

- −13.5 ± 0.5 ppt Cl yr^{-1} from chlorofluorocarbons (CFCs)
- −4.1 ± 0.2 ppt Cl yr^{-1} from methyl chloroform (CH_3CCl_3)
- −4.9 ± 0.7 ppt Cl yr^{-1} from carbon tetrachloride (CCl_4)
- −0.07 ± 0.01 ppt Cl yr^{-1} from halon-1211
- +9.2 ± 0.3 ppt Cl yr^{-1} from hydrochlorofluorocarbons (HCFCs)
- −0.06 ± 0.02 ppt Br yr^{-1} from halons
- −0.08 ± 0.02 ppt Br yr^{-1} from methyl bromide (CH_3Br)

Substances not controlled under the Montreal Protocol

- −1.7 ± 1.3 ppt Cl yr^{-1} from methyl chloride (CH_3Cl)
- +1.3 ± 0.2 ppt Cl yr^{-1} from very short-lived chlorine compounds (predominantly dichloromethane, CH_2Cl_2)

Tropospheric Chlorine

Total tropospheric chlorine from ODSs continued to decrease between 2009 and 2012 to 3300 parts per trillion (ppt) in 2012. The observed decline in controlled substances of 13.4 ± 0.9 ppt Cl yr^{-1} during 2008–2012 was in line with the A1 (baseline) scenario of the 2010 Assessment.

Of total tropospheric Cl in 2012:

- **CFCs, consisting primarily of CFC-11, -12, and -113, accounted for 2024 ± 5 ppt (about 61%) and are declining.** Their relative contribution is essentially unchanged from the 2010 Assessment (62% in 2008).
- **CCl_4 accounted for 339 ± 5 ppt (about 10%).** While our current understanding of the budget of CCl_4 is incomplete, mole fractions of CCl_4 declined largely as projected based on prior observations and the A1 scenario of the 2010 Assessment during 2009–2012.
- **HCFCs accounted for 286 ± 4 ppt (8.7%).** In total, the rate of increase for the sum of HCFCs has slowed by 25% since 2008 and has been lower than projected in the 2010 Assessment.

[1] All uncertainties are one standard deviation unless otherwise specified.

- **CH_3CCl_3, the largest contributor to the decrease in total tropospheric chlorine until around 2005, accounted for only 16 ± 1 ppt (0.5%).** This is 50% less than in 2008 (32 ppt) and a 95% reduction from its mean contribution to the total Cl decline during the 1980s. The fraction is declining in line with the A1 scenario of the 2010 Assessment.
- **CH_3Cl accounted for 540 ± 5 ppt (about 16%) and has remained essentially constant since 2008.** This gas is emitted predominantly from natural sources.
- **Very short-lived compounds (VSLS) contribute approximately 3%.**

Global emissions of HCFCs remain substantial, but relative emissions of individual constituents have changed notably since the last Assessment. Emissions of HCFC-22 have stabilized since 2008 at around 370 gigagrams per year (Gg yr^{-1}). HCFC-142b emissions decreased in the same period. In contrast emissions of HCFC-141b have increased since the last Assessment, in parallel with reported production and consumption in Article 5 Parties.

Estimated sources and sinks of CCl_4 remain inconsistent with observations of its abundance. The estimate of the total global lifetime (26 years) combined with the observed CCl_4 trend in the atmosphere (−1.1 to −1.4 ppt yr^{-1} in 2011–2012) implies emissions of 57 (40–74) Gg yr^{-1}, which cannot be reconciled with estimated emissions from net reported production. New evidence indicates that other poorly quantified sources, unrelated to reported production, could contribute to the currently unaccounted emissions.

Three CFCs (CFC-112, -112a, -113a) and one HCFC (HCFC-133a) have recently been detected in the atmosphere. These four chlorine-containing compounds are listed in the Montreal Protocol and contribute about 4 ppt or ~ 0.1% toward current levels of total chlorine, currently adding less than 0.5 ppt Cl yr^{-1}. Abundances of CFC-112 and CFC-112a are declining and those of CFC-113a and HCFC-133a are increasing. The sources of these chemicals are not known.

Stratospheric Inorganic Chlorine and Fluorine

Hydrogen chloride (HCl) is the major reservoir of inorganic chlorine (Cl_y) in the mid- to upper stratosphere. Satellite-derived measurements of HCl (50°N–50°S) in the mid- to upper stratosphere show a mean decline of 0.6% ± 0.1% yr^{-1} between 1997 and 2012. This is consistent with the measured changes in controlled chlorinated source gases. Variability in this decline is observed over shorter time periods based on column measurements above some ground-based sites, likely due to dynamic variability.

Measured abundances of stratospheric fluorine product gases (HF, COF_2, COClF) increased by about 1% yr^{-1} between 2008 and 2012. This is consistent with increases in measured abundances of fluorinated compounds and their degradation products. The increase was smaller than in the beginning of the 1990s, when the concentrations of fluorine-containing ODSs were increasing more rapidly.

Tropospheric Bromine

Total organic bromine from controlled ODSs continued to decrease in the troposphere and by 2012 was 15.2 ± 0.2 ppt, approximately 2 ppt below peak levels observed in 1998. This decrease was close to that expected in the A1 scenario of the 2010 Assessment and was primarily driven by declines in methyl bromide (CH_3Br), with some recent contribution from an overall decrease in halons. Total bromine from halons had stopped increasing at the time of the last Assessment, and a decrease is now observable.

CH_3Br mole fractions continued to decline during 2008–2012, and by 2012 had decreased to 7.0 ± 0.1 ppt, a reduction of 2.2 ppt from peak levels measured during 1996–1998. These atmospheric declines are driven primarily by continued decreases in total reported consumption of CH_3Br from fumigation. As of 2009, reported consumption for quarantine and pre-shipment (QPS) uses, which are exempted uses (not controlled) under the Montreal Protocol, surpassed consumption for controlled (non-

QPS) uses. As a result of the decrease in atmospheric CH_3Br, the natural oceanic source is now comparable to the oceanic sink.

Stratospheric Inorganic Bromine

Total inorganic stratospheric bromine (Br_y), derived from observations of bromine monoxide (BrO), was 20 (16–23) ppt in 2011, and had decreased at ~0.6 ± 0.1% yr^{-1} between peak levels observed in 2000–2001 and 2012. This decline is consistent with the decrease in total tropospheric organic Br based on measurements of CH_3Br and the halons.

Equivalent Effective Stratospheric Chlorine (EESC)

EESC is a sum of chlorine and bromine derived from ODS tropospheric abundances weighted to reflect their expected depletion of stratospheric ozone. The growth and decline in EESC depends on a given tropospheric abundance propagating to the stratosphere with varying time lags (on the order of years) associated with transport. Therefore the EESC abundance, its peak timing, and its rate of decline, are different in different regions of the stratosphere.

By 2012, EESC had declined by about 10% in polar regions and about 15% in midlatitudes from their peak values, with CH_3CCl_3, CH_3Br, and CFCs contributing approximately equally to these declines. This drop is about 40% of the decrease required for EESC in midlatitudes to return to the 1980 benchmark level, and about 20% of the decrease required for EESC in polar regions to return to the 1980 benchmark level.

Very Short-Lived Halogenated Substances (VSLS)

VSLS are defined as trace gases whose local lifetimes are comparable to, or shorter than, interhemispheric transport timescales and that have non-uniform tropospheric abundances. These local lifetimes typically vary substantially over time and space. As in prior Assessments, we consider species with annual mean lifetimes less than approximately 6 months to be VSLS. Of the VSLS identified in the current atmosphere, brominated and iodinated species are predominantly of oceanic origin, while the chlorinated species have significant industrial sources. These compounds will release their halogen atoms nearly immediately once they enter the stratosphere. The current contribution of chlorinated VSLS to Equivalent Chlorine (ECl) is about one-third as large as the contribution of VSLS brominated gases. Iodine from VSLS likely makes a minor contribution to ECl.

Total chlorinated VSLS source gases increased from 84 (70–117) ppt in 2008 to 91 (76–125) ppt in 2012 in the lower troposphere. Dichloromethane (CH_2Cl_2), a VSLS that has predominantly anthropogenic sources, accounted for the majority of this change, with an increase of ~60% over the last decade.

The estimated contribution of chlorinated VSLS to total stratospheric chlorine remains small. A lack of data on their concentrations in the tropical tropopause layer (TTL) limits our ability to quantify their contribution to the inorganic chlorine loading in the lower stratosphere. Current tropospheric concentrations of chlorinated VSLS imply a source gas injection of 72 (50–95) ppt, with 64 ppt from anthropogenic emissions (e.g., CH_2Cl_2, $CHCl_3$, 1,2 dichloroethane (CH_2ClCH_2Cl), tetrachloroethene (CCl_2CCl_2)). The product gases are estimated to contribute 0–50 ppt giving a total of ~ 95 ppt (50–145 ppt) against a total of 3300 ppt of chlorine from long-lived ODSs entering the stratosphere.

There is further evidence that VSLS contribute ~5 (2–8) ppt to a total of ~20 ppt of stratospheric bromine. Estimates of this contribution from two independent approaches are in agreement. New data suggest that previous estimates of stratospheric Br_y derived from BrO observations may in some cases have been overestimated, and imply a contribution of ~5 (2–8) ppt of bromine from VSLS. The second approach sums the quantities of observed, very short-lived source gases around the tropical tropopause with improved modeled estimates of VSLS product gas injection into the stratosphere, also giving a total contribution of VSLS to stratospheric bromine of ~5 (2–8) ppt.

Updated Lifetime Estimates

The uncertainties of estimated lifetimes for key long-lived ozone-depleting and related substances are better quantified following the SPARC Lifetimes Assessment (Stratosphere-troposphere Processes And their Role in Climate, 2013). Of note is the change in the estimated lifetime of CFC-11 (revised from 45 yr to 52 yr). The estimate of the total global lifetime of CCl_4 (26 yr) remains unchanged from the previous Assessment, although estimates of the relative importance of the multiple loss processes have been revised.

Other Trace Gases That Directly Affect Ozone and Climate

The emissions of CFCs, HCFCs, and HFCs in terms of their influence on climate (as measured by gigatonnes of carbon dioxide (CO_2)-equivalent emissions) were roughly equal in 2012. However, the emissions of HFCs are increasing rapidly, while the emissions of CFCs are going down and those of HCFCs are essentially unchanged. The 100-year GWP-weighted emissions for the sum of CFC, HCFC, and HFC emissions was 2.2 Gt CO_2-equivalent in 2012. The sum of GWP-weighted emissions of CFCs was 0.73 ± 0.25 Gt CO_2-equivalent yr^{-1} in 2012 and has decreased on average by 11.0 ± 1.2% yr^{-1} from 2008 to 2012. The sum of HCFC emissions was 0.76 ± 0.12 Gt CO_2-equivalent yr^{-1} in 2012 and has been essentially unchanged between 2008 and 2012. Finally, the sum of HFC emissions was 0.69 ± 0.12 Gt CO_2-equivalent yr^{-1} in 2012 and has increased on average by 6.8 ± 0.9% yr^{-1} from 2008 to 2012. The HFC increase partially offsets the decrease by CFCs. Current emissions of HFCs are, however, are less than 10% of peak CFC emissions in the early 1990s (>8 Gt CO_2-equivalent yr^{-1}).

From 2008 to 2012 the global mean mole fraction of nitrous oxide (N_2O), which leads to ozone depletion in the stratosphere, increased by 3.4 parts per billion (ppb), to 325 ppb. With the atmospheric burden of CFC-12 decreasing, N_2O is currently the third most important long-lived greenhouse gas contributing to radiative forcing (after CO_2 and methane (CH_4)).

Methane (CH_4) is an important greenhouse gas and influences stratospheric ozone. In 2012 the average background global mole fraction of CH_4 was 1808 ppb, with a growth rate of 5–6 ppb yr^{-1} from 2008 to 2012. This is comparable to the 2006–2008 period when the CH_4 growth rate began increasing again after several years of near-zero growth. The renewed increase is thought to result from a combination of increased CH_4 emissions from tropical and high-latitude wetlands together with increasing anthropogenic (fossil fuel) emissions, though the relative contribution of the wetlands and fossil fuel sources is uncertain.

Hydrofluorocarbons (HFCs) used as ODS substitutes are increasing in the global atmosphere. The most abundant HFC, HFC-134a, reached a mole fraction of nearly 68 ppt in 2012 with an increase of 5 ppt yr^{-1} (7.6%) in 2011–2012. HFC-125, -143a, and -32 have similar or even higher relative growth rates than HFC-134a, but their current abundances are considerably lower.

Worldwide emissions of HFC-23, a potent greenhouse gas and by-product of HCFC-22 production, reached a maximum of ~15 Gg in 2006, decreased to ~9 Gg in 2009, and then increased again to reach ~13 Gg yr^{-1} in 2012. While efforts in non-Article 5 Parties mitigated an increasing portion of HFC-23 emissions through 2004, the temporary decrease in emissions after 2006 is consistent with destruction of HFC-23 in Article 5 Parties owing to the Clean Development Mechanism (CDM) of the Kyoto Protocol. The average global mole fraction of HFC-23 reached 25 ppt in 2012, with an increase of nearly 1 ppt yr^{-1} in recent years.

Mole fractions of sulfur hexafluoride (SF_6), nitrogen trifluoride (NF_3), and sulfuryl fluoride (SO_2F_2) increased in recent years. Global averaged mole fractions of SF_6 reached 7.6 ppt in 2012, with an annual increase of 0.3 ppt yr^{-1} (4% yr^{-1}). Global averaged mole fractions of NF_3 reached 0.86 ppt in 2011, with an annual increase of 0.1 ppt yr^{-1} (12% yr^{-1}). Global averaged mole fractions of SO_2F_2 reached 1.8 ppt in 2012, with an annual increase of 0.1 ppt yr^{-1} (5% yr^{-1}). The considerable increases for these entirely anthropogenic, long-lived substances are caused by ongoing emissions.

1.1 SUMMARY OF THE PREVIOUS OZONE ASSESSMENT

Chapter 1 of the 2010 Assessment report (Montzka and Reimann et al., 2011) provided evidence of continued reductions of the atmospheric abundance of most ozone-depleting substances (ODSs), resulting from phase-out of controlled ODS production and consumption under the Montreal Protocol. Total tropospheric chlorine and bromine from long-lived chemicals continued to decrease between 2005 and 2008. The atmospheric reservoir for methyl chloroform (CH_3CCl_3) had reduced to the point that its contribution to the chlorine decline was surpassed by the chlorofluorocarbons (CFCs). Mole fractions of CFC-12, the single largest contributor to the atmospheric chlorine loading, declined for the first time in this period. The total tropospheric chlorine decline was however slower than expected because the sum of the CFC mole fractions did not drop as rapidly as projected and increases in hydrochlorofluorocarbons (HCFCs) were larger than anticipated. The stratospheric chlorine burden declined in accordance with the tropospheric decrease, within expected uncertainties. Chlorine-containing very short-lived substances (VSLS) and their degradation products contributed approximately 80 ppt (parts per trillion) of chlorine to the stratosphere, which was about 2% of the contribution from the longer-lived ODSs.

Chapter 1 of the 2010 Assessment documented the continued discrepancy between emissions of carbon tetrachloride (CCl_4) inferred from observed global trends with the much lower and more variable emissions derived from data reported to the United Nations Environment Programme (UNEP). These differences could not solely be explained by scaling the atmospheric lifetime. For other important ODSs (e.g., CFC-11), there was evidence that atmospheric lifetimes might be longer than reported in previous Assessments.

Tropospheric mole fractions of hydrofluorocarbons (HFCs), used as non-ozone-depleting ODS substitutes, continued to increase, which was reflected by an increase in column abundances of hydrogen fluoride (HF), one of their major degradation products. In total the sum of HFC emissions used as ODS replacements, weighted by direct, 100-year Global Warming Potentials (GWPs), increased by nearly 10% yr^{-1} from 2004 to 2008. In addition, emissions of the very potent greenhouse gas HFC-23 (CHF_3), which was mainly released from the production of HCFC-22 and therefore not labeled as an ODS replacement, had increased despite efforts to curb HFC-23 emissions.

The only regulated bromine compound still not decreasing in 2008 was halon-1301. The total tropospheric bromine levels from long-lived ODSs, however, continued to decrease because of the declining abundance of methyl bromide (CH_3Br) and because the sum of halons had stopped increasing. For the first time, measurements of stratospheric bromine showed a slight decrease over this period. Slightly more than 50% of the atmospheric bromine stemmed from sources not controlled by the Montreal Protocol (i.e., from natural sources and from quarantine and pre-shipment (QPS) uses of CH_3Br). The contribution from mostly natural short-lived compounds such as dibromomethane (CH_2Br_2) and tribromomethane ($CHBr_3$) and their degradation products to stratospheric bromine was estimated to be 1–8 ppt, which contributed substantially to the estimated total of 22.5 ppt of bromine in the stratosphere in 2008.

Equivalent Effective Stratospheric Chlorine (EESC) represents the overall influence on stratospheric ozone levels from the sum of the tropospheric abundances of chlorine and bromine ODSs. A discussion of the EESC concept can be found in Box 8-1 of the 2006 Assessment (Daniel and Velders, 2007). By the end of 2008, the EESC abundance in the midlatitude stratosphere had decreased by about 11% from its peak value in 1997. This represented 28% of the decrease required for EESC in the midlatitude stratosphere to return to the 1980 benchmark level. In the polar stratosphere, EESC had decreased by about 5% from its peak value in 2002, which is 10% of the decrease required for EESC in polar regions to return to the 1980 benchmark level.

1.2 LONGER-LIVED HALOGENATED SOURCE GASES

1.2.1 Updated Observations, Lifetimes, and Emissions

Global tropospheric observations of ODSs have been performed and updated by independent groups using both in situ and flask measurements as early as the late 1970s (Figure 1-1, Table 1-1). Data

from networks with global coverage (AGAGE: Advanced Global Atmospheric Gases Experiment; NOAA: National Oceanic and Atmospheric Administration; UCI: University of California, Irvine) are discussed primarily, except for substances where data from only one global network are available. For some ODSs, surface observations have been complemented with trends of total column measurements using satellite- and ground-based remote sensing techniques (Table 1-2).

Global steady-state lifetime estimates of the main ODSs and related substances appear in Table 1-3. Most are taken directly from SPARC (2013) and were derived from a weighted average of the lifetimes using different methods. Global steady-state lifetimes are derived from a combination of partial lifetimes for tropospheric hydroxyl radical (OH) reactive loss, stratospheric loss, and ocean and soil loss. Furthermore, updates to atmospheric budgets (emissions and sinks) of ODSs are discussed. Global mean mole fractions, trends, and emissions were calculated by combining the global network data with a two-dimensional model (Rigby et al., 2013, 2014).

1.2.1.1 CHLOROFLUOROCARBONS (CFCS)

Observations

The global surface mean dry air mole fractions of the three most abundant chlorofluorocarbons (CFC-12 (CCl_2F_2), CFC-11 (CCl_3F), and CFC-113 (CCl_2FCClF_2)) continued to decline since the last Assessment (Figure 1-1 and Table 1-1). Between 2008 and 2012 the trends observed for these three ODSs are consistent (within uncertainties) with those anticipated in the A1-2010 scenario (Daniel and Velders et al., 2011). For these three ODSs, differences in global abundances estimated by the three global networks in Table 1-1 were less than 1% in 2011–2012. This is comparable to differences of 1–2% for the measurement of these substances evaluated within the International Halocarbons in Air Comparison Experiment (IHALACE) (Hall et al., 2014). Differences between the global networks are used not only for estimating the uncertainty of the measurement data themselves, but also for assessing the accuracy and reliability of global emission estimates, which make use of these data.

Recent changes in the Northern Hemisphere abundances of CFC-11, CFC-12, and CFC-113 measured by ground-based infrared solar absorption spectroscopy (e.g., Zander et al., 2008) and space-based instruments (Brown et al., 2011; Kellmann et al., 2012) are largely consistent (within uncertainties) with those measured at the surface between 2004 and 2010 (Figure 1-2 and Table 1-2). Only CFC-113 from Atmospheric Chemistry Experiment-Fourier Transform Spectrometer (ACE-FTS) (Brown et al., 2011) shows a faster decrease than the ground-based measurements, which could be caused by measurement issues in the space-based instrument for this compound.

Global mole fractions of both CFC-114 ($CClF_2CClF_2$) and CFC-115 ($CClF_2CF_3$) have remained nearly constant since 2008 (Table 1-1). Measurements of CFC-114 include a fraction due to CFC-114a (CCl_2FCF_3), which is estimated to be around 10%, based on measurements in the 1990s (Oram, 1999). Furthermore, CFC-112 (CCl_2FCCl_2F), -112a ($CClF_2CCl_3$), -113a (CCl_3CF_3), and HCFC-133a (CH_2ClCF_3) (Section 1.2.1.5) were recently determined to be present in the atmosphere, with mole fractions of less than 1 ppt in 2010 (Laube et al., 2014). Abundances of CFC-112 and CFC-112a are declining but those of CFC-113a (and HCFC-133a) are increasing. These newly detected ODSs are listed in the Montreal Protocol and contribute about 4 ppt or ~ 0.1% toward current levels of total chlorine, currently adding less than 0.5 ppt Cl yr^{-1}.

Lifetimes and emissions

For CFC-11, a longer steady-state lifetime of 52 (43–67) years was recommended by SPARC (2013) compared with the 45-year lifetime used in the previous Assessments. Since the SPARC (2013) evaluation, a new CFC-11 UV absorption spectrum data set was reported by McGillen et al. (2013) that significantly reduced the overall estimated uncertainty in the CFC-11 spectrum from ~20%, as reported in SPARC (2013), to ~4%. This leads to a substantially reduced contribution to the CFC-11 lifetime uncertainty due to uncertainties in CFC-11 photolysis. The recommended CFC-11 steady-state lifetime of SPARC (2013) and its estimated uncertainty range, however, do not change significantly as a result. In

SPARC (2013) the lifetime and its range were primarily determined by the differences between observational data and various 3-D model calculations.

Another notable change discussed in SPARC (2013) was for CFC-115, for which the total lifetime was revised from 1020 to 540 years based on new $O(^1D)$ + CFC-115 reaction rate data from Baasandorj et al. (2013).

Results since SPARC (2013) include a suggested revision of the CFC-113a lifetime from ~45 to 59 (31–305) years by Laube et al. (2014), although uncertainties of the new estimate include the old number.

Global top-down emissions of CFC-11 derived from atmospheric observations, considering its new lifetime of 52 years, have been declining slowly over the past decade and are estimated to have been 57 (46–68) Gg in 2012 (Figure 1-3). Bottom-up estimated emissions are only available until 2003 and averaged 73 Gg yr^{-1} in the period 2000–2003 (UNEP, 2006). This was 19 Gg yr^{-1} smaller than estimated emissions using measurement-based top-down methods and a 52-year lifetime (Figure 1-3). The increase of the lifetime estimate from 45 years to 52 years considerably reduces the gap for CFC-11 emission estimates by the two methods from the previous Assessment (Montzka and Reimann et al., 2011).

Global CFC-12 emissions have been declining more rapidly than those of CFC-11. Top-down estimates (Figure 1-3) indicate emissions of CFC-12 were decreasing at a rate of ~7 Gg yr^{-1} in recent years to 40 (26–54) Gg in 2012. Global CFC-113 emissions have been consistently lower than 5 Gg yr^{-1} over recent years.

Emissions of the newly detected CFC-113a were estimated at 2 Gg in 2012 (Figure 1-3) and they could be caused by its usage as an intermediate in agrochemical production (Laube et al., 2014) or as a feedstock for HFC-125 (CHF_2CF_3) and HFC-134a (CH_2FCF_3) production (UNEP, 2013a). Although global production numbers for these HFCs are not available, the rapid increases in mole fractions and global emissions of HFC-125 and HFC-134a in the atmosphere (Figures 1-24, 1-25, and Table 1-14) indicate the potential for increasing releases of CFC-113a.

Measurements within specific regions and meteorological models are used to estimate emissions of ODSs and other halocarbons on regional scales. These regional source estimates are prone to considerable uncertainties due to inaccuracies in meteorological data, transport models, and in some instances, seasonal variations of emission. The summed effect of the errors in these parameters and their extrapolations can lead to large uncertainties for estimated regional emissions (see, e.g., Figure 1-4). When studied regions are substantially different from national scales, additional errors can be introduced by extrapolation of the regional estimates to national scales, which are often compared to national inventory-based estimates. Regional emissions of CFC-11, -12, and -113 were predominantly estimated to be from East Asia in recent years, due to the phase-out of these compounds in important Article 5 countries in 2010. In Figure 1-4 historical and projected bottom-up emissions in China (Wan et al., 2009) are compared with top-down regional emissions derived from atmospheric measurements (Palmer et al., 2003; Vollmer et al., 2009; Kim et al., 2010; An et al., 2012; Fang et al., 2012). The concurrent decline of emissions seen by both independent methods (top-down and bottom-up) shows the success of the Montreal Protocol in substantially decreasing CFC emissions in China. In 2000 CFC-12 top-down emission estimates were more than a factor of two higher than inventory-based estimates, but both estimates compare better in most recent years. Whereas CFC-11 emissions are still substantial but also declining, both top-down and bottom-up emissions of CFC-113, which was mostly used as a solvent, were found to be consistently small in recent years. However, measurements of these CFCs in urban environments in China, for example in the Pearl River Delta (Shao et al., 2011; Wu et al., 2014), still show mole fraction enhancements above background levels, indicating ongoing emissions from in-use equipment.

Recent estimates of emissions of CFC-11 and CFC-12 in the U.S. and Europe (Millet et al., 2009; Miller et al., 2012; Keller et al., 2012) were still comparable to those in China, although new production of CFCs for use was restricted in the U.S. and Europe in 1996/1995 (i.e., 14/15 years ahead of restrictions in China). For CFC-113, enhancements above background levels were not detected in the U.S. by Gentner et al. (2010) or Millet et al. (2009), suggesting very low emissions in this region of the world. In a source-specific study, Hodson et al. (2010) found that landfills were only small sources of CFC-11, CFC-12, and CFC-113 in the U.S. and in the United Kingdom.

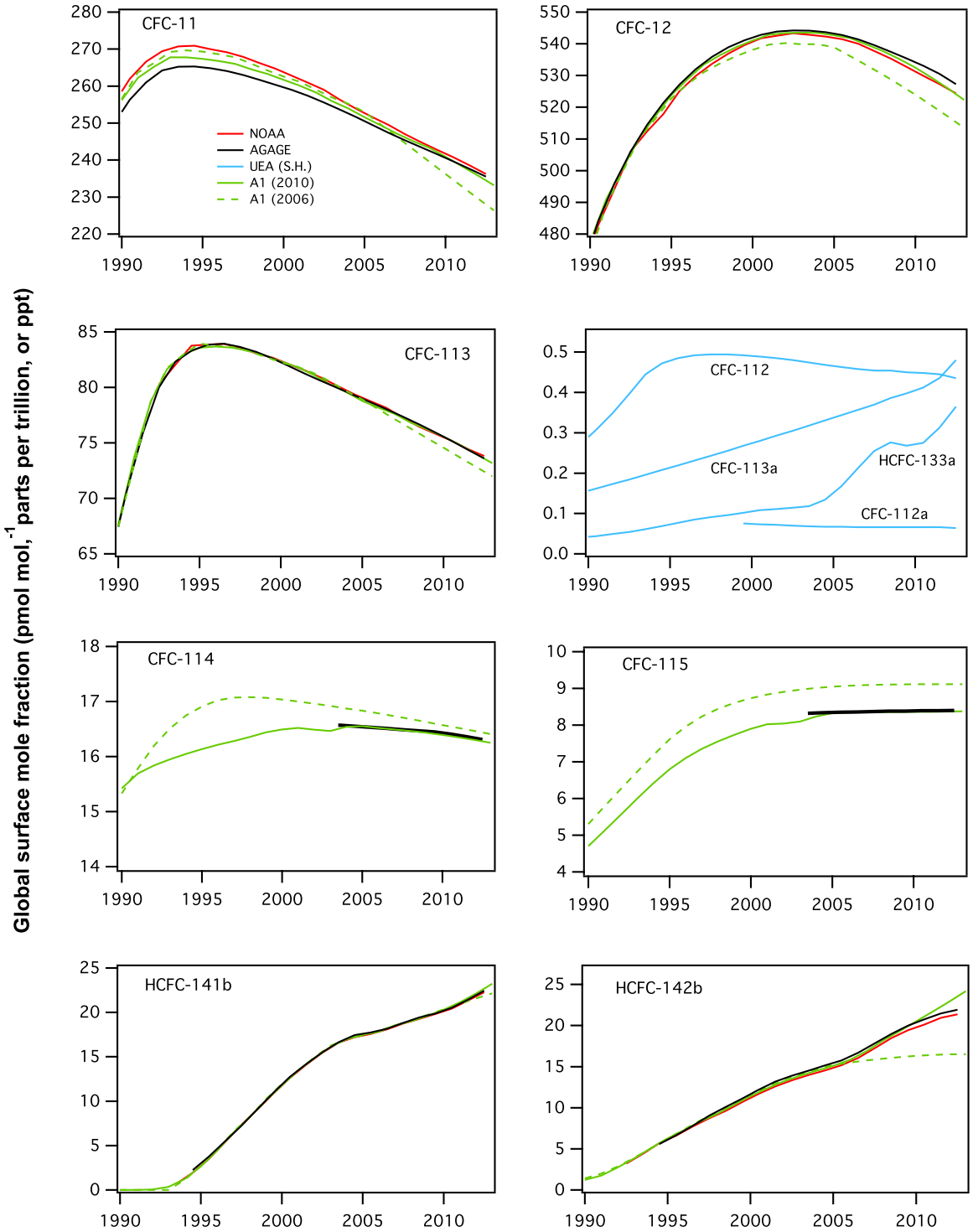

Figure 1-1. Mean global surface mole fractions (expressed as dry air mole fractions in parts per trillion or ppt) of ozone-depleting substances from independent sampling networks and from scenario A1 of the previous Ozone Assessments (Daniel and Velders et al., 2007, 2011) over the past 22 years (1990–2012). Measured global surface annual means are shown as red lines (NOAA data), black lines (AGAGE data), and blue lines (University of East Anglia (UEA) Southern Hemisphere (S.H.) data, ***(continued next page)***

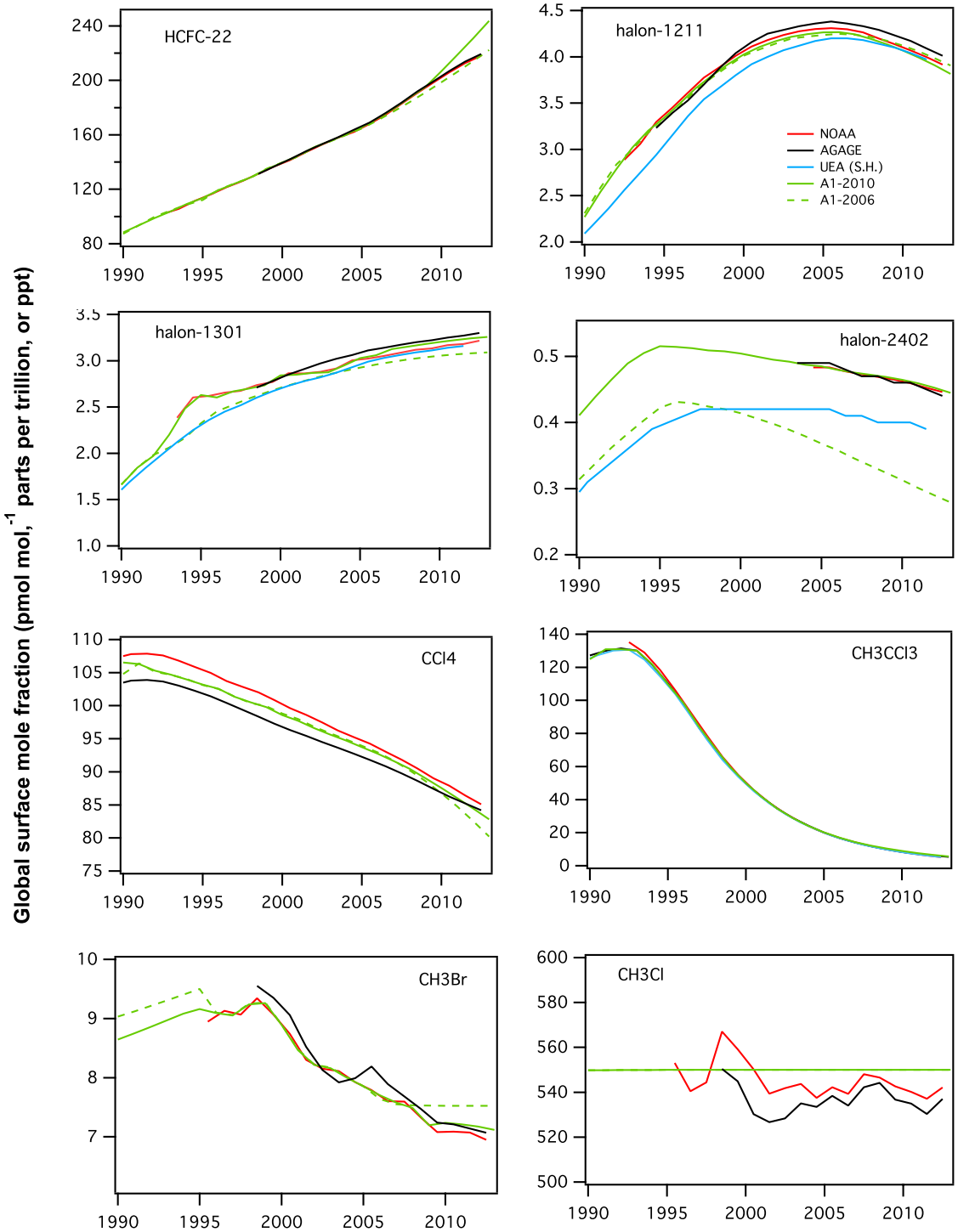

(Figure 1-1, continued) using Cape Grim archived air). Mole fractions from scenario A1 from the previous assessment (green lines) were derived to match observations in years before 2009 (Daniel and Velders et al., 2011). The scenario A1-2010 results shown in years after 2008 are projections made for 2009. Mole fractions from scenario A1 from the 2006 Assessment (green-dashed lines) were derived to match observations in years before 2005 (Daniel and Velders et al., 2007). The scenario A1-2006 results shown in years after 2004 are projections made in 2005.

Table 1-1. Measured mole fractions and changes of ozone-depleting gases from ground-based sampling networks.

Chemical Formula	Common or Industrial Name	Annual Mean Mole Fraction (ppt)			Change (2011–2012)		Network, Method
		2008	2011	2012	(ppt yr^{-1})	(% yr^{-1})	
CFCs							
CCl_3F	CFC-11	**243.4**	**237.6**	**235.5**	**−2.1**	**−0.9**	AGAGE, in situ [1]
		244.8	**238.6**	**236.3**	**−2.3**	**−1.0**	NOAA, flask & in situ
		244.2	**237.9**	**235.3**	**−2.6**	**−1.1**	UCI, flask
CCl_2F_2	CFC-12	**537.5**	**530.4**	**527.5**	**−2.9**	**−0.5**	AGAGE, in situ
		535.3	**527.2**	**524.4**	**−2.9**	**−0.5**	NOAA, flask & in situ
		532.6	**525.3**	**522.5**	**−2.8**	**−0.5**	UCI, flask
CCl_2FCCl_2F	CFC-112	*0.45*	*0.45*	*0.44*	*−0.01*	*−2*	UEA, flask (Cape Grim)
CCl_3CClF_2	CFC-112a	*0.065*	*0.066*	*0.064*	*−0.002*	*−3*	UEA, flask (Cape Grim)
CCl_2FCClF_2	CFC-113	**76.7**	**74.4**	**73.6**	**−0.8**	**−1.1**	AGAGE, in situ
		76.5	**74.5**	**73.8**	**−0.6**	**−0.8**	NOAA, flask & in situ
		77.1	**74.9**	**74.2**	**−0.7**	**−0.9**	UCI, flask
CCl_3CF_3	CFC-113a	*0.39*	*0.44*	*0.48*	*0.04*	*10*	UEA, flask (Cape Grim)
$CClF_2CClF_2$	CFC-114 [2]	**16.46**	**16.37**	**16.33**	**−0.04**	**−0.2**	AGAGE, in situ
		15.95	*15.77*	*15.75*	*−0.02*	*−0.1*	NIES, in situ (Japan)
$CClF_2CF_3$	CFC-115	**8.38**	**8.39**	**8.40**	**0.01**	**0.2**	AGAGE, in situ
		8.32	*8.44*	*8.48*	*0.04*	*0.5*	NIES, in situ (Japan)
HCFCs							
$CHClF_2$	HCFC-22	**191.8**	**214.2**	**219.8**	**5.6**	**2.6**	AGAGE, in situ
		190.9	**212.7**	**218.0**	**5.3**	**2.5**	NOAA, flask
		188.3	**209.0**	**214.5**	**5.5**	**2.6**	UCI, flask
$CHClFCF_3$	HCFC-124	**1.48**	**1.34**	**1.30**	**−0.04**	**−3**	AGAGE, in situ
CH_2ClCF_3	HCFC-133a	*0.275*	*0.313*	*0.365*	*0.052*	*17*	UEA, flask (Cape Grim)
CH_3CCl_2F	HCFC-141b	**19.5**	**21.4**	**22.5**	**1.1**	**5.1**	AGAGE, in situ
		19.3	**21.3**	**22.3**	**1.0**	**4.4**	NOAA, flask
		18.8	**20.8**	**21.8**	**1.0**	**4.8**	UCI, flask
CH_3CClF_2	HCFC-142b	**19.0**	**21.5**	**22.0**	**0.5**	**2.4**	AGAGE, in situ
		18.5	**20.9**	**21.3**	**0.4**	**2.0**	NOAA, flask
		18.0	**21.0**	**21.8**	**0.8**	**3.8**	UCI, flask
Halons							
CBr_2F_2	halon-1202	*0.026*	*0.020*	*0.019*	*−0.001*	*−5*	UEA, flask (Cape Grim)

(continued next page)

Chemical Formula	Common or Industrial Name	Annual Mean Mole Fraction (ppt)			Change (2011–2012)		Network, Method
		2008	2011	2012	(ppt yr^{-1})	(% yr^{-1})	
Table 1-1, continued.							
$CBrClF_2$	halon-1211	**4.29**	**4.09**	**4.01**	**−0.08**	**−2.0**	AGAGE, in situ
		4.20	**4.00**	**3.92**	**−0.08**	**−2.0**	NOAA, flask [3]
		4.25	**4.03**	**3.96**	**−0.07**	**−1.7**	NOAA, in situ
		4.24	**4.18**	**4.14**	**−0.04**	**−1.0**	UCI, flask
$CBrF_3$	halon-1301	**3.20**	**3.27**	**3.30**	**0.03**	**0.9**	AGAGE, in situ
		3.12	**3.18**	**3.22**	**0.04**	**1.1**	NOAA, flask
$CBrF_2CBrF_2$	halon-2402	***0.47***	***0.45***	***0.44***	***−0.01***	***−1.3***	AGAGE, in situ [4]
		0.47	**0.45**	**0.44**	**−0.01**	**−1.4**	NOAA, flask
		0.41	*0.394*	*0.387*	*−0.007*	*−2*	UEA, flask (Cape Grim)
Chlorocarbons							
CH_3Cl	methyl chloride	**544.2**	**530.3**	**537.1**	**6.8**	**1.3**	AGAGE, in situ
		546.6	**537.1**	**542.2**	**5.0**	**0.9**	NOAA, flask
		546	-	-	-	-	NOAA, in situ
CCl_4	carbon tetrachloride	**88.6**	**85.2**	**84.2**	**−1.1**	**−1.2**	AGAGE, in situ
		90.5	**86.4**	**85.1**	**−1.4**	**−1.6**	NOAA, flask & in situ
		91.5	**87.8**	**86.7**	**−1.1**	**−1.3**	UCI, flask
CH_3CCl_3	methyl chloroform	**10.6**	**6.26**	**5.20**	**−1.06**	**−17**	AGAGE, in situ
		10.8	**6.31**	**5.25**	**−1.06**	**−17**	NOAA, flask
		11.5	**6.8**	**5.7**	**−1.1**	**−16**	UCI, flask
Bromocarbons							
CH_3Br	methyl bromide	**7.47**	**7.14**	**7.07**	**−0.11**	**−1.0**	AGAGE, in situ
		7.33	**7.07**	**6.95**	**−0.12**	**−1.7**	NOAA, flask

Mole fractions in this table represent independent estimates measured by different groups for the years indicated. Results in bold text are estimates of global surface mean mole fractions. Regional data from relatively unpolluted sites are shown (in italics) where global estimates are not available, where global estimates are available from only one network, or where data from global networks do not represent independent calibration scales (e.g., halon-2402). Absolute changes (ppt yr^{-1}) are calculated as the difference in annual means; relative changes (% yr^{-1}) are the same difference relative to the 2011 value. Small differences between values from previous Assessments are due to changes in calibration scale and methods for estimating global mean mole fractions from a limited number of sampling sites.

These observations are updated from the following sources: Rowland et al. (1982); Butler et al. (1998); Fraser et al. (1999); Montzka et al. (1999); Oram (1999); Montzka et al. (2000); Prinn et al. (2000); Montzka et al. (2003); O'Doherty et al. (2004); Yokouchi et al. (2006); Simpson et al. (2007); Miller et al. (2008); Montzka et al. (2009); Newland et al. (2013); Laube et al. (2014). AGAGE, Advanced Global Atmospheric Gases Experiment (http://agage.eas.gatech.edu/); NOAA, National Oceanic and Atmospheric Administration, U.S. (http://www.esrl.noaa.gov/gmd/dv/site/); UEA, University of East Anglia, United Kingdom (http://www.uea.ac.uk/environmental-sciences/research/marine-and-atmospheric-sciences-group); UCI, University of California, Irvine, U.S. (http://ps.uci.edu/~rowlandblake/research_atmos.html); NIES, National Institute for Environmental Studies, Japan (http://db.cger.nies.go.jp/gem/moni-e/warm/Ground/st01.html). Cape Grim: Cape Grim Baseline Air Pollution Station, Australia.

Notes: [1]Global mean estimates from AGAGE are calculated using atmospheric data and a 12-box model (Cunnold et al., 1983; Rigby et al., 2013). AGAGE calibrations as specified in CDIAC (2014) and related primary publications. [2]Measurements of CFC-114 are a combination of CFC-114 and the CFC-114a isomer, with an assumed relative contribution of 10% CFC-114a (Oram, 1999). [3]The NOAA halon-1211 data have been updated following an instrument change in 2009. [4]AGAGE halon-2402 data are on the NOAA scale.

Table 1-2. Comparison of annual trends of ODSs, HFC-23, CF_4, and SF_6 from in-situ measurements vs. remote sensing measurements. Relative trends in ODSs and halogenated greenhouse gases for the common 2004–2010 time period (except when specified) derived from in-situ surface measurements and remote sensing observations from the ground and from space. Surface trends were derived from monthly mean mole fractions, weighted by surface area in the region 30°N–90°N. Shown are the average and standard deviation of trends derived independently from NOAA and AGAGE data (% yr^{-1} relative to 2007 annual mean). For CF_4 and HFC-23, only AGAGE data were used, and the uncertainty was derived from uncertainties (one standard deviation) in the slope and 2007 annual mean. For HFC-23, global mean data were used from 2007 through 2010, supplemented with data from Miller et al. (2010) for 2004–2007. Ground-based remote sensing trends were derived from daily mean total column measurements performed at Jungfraujoch (46.5ºN). The ACE-FTS trends were determined using tropical occultations (30ºN–30ºS), after averaging the mixing ratios in molecule-dependent altitude ranges (Brown et al., 2011). For HFC-23, the 40ºN–40ºS occultations were considered in the 10–25 km altitude range. For MIPAS CFC-11 and -12, mean rates of change for the 20ºN–20ºS and 10–15 km altitude range are provided, including observations between 2002 and 2011 (Kellmann et al., 2012). For SF_6, the trend characterizes the 2006–2009 time period between 17.5ºN–17.5ºS latitude and 9–15 km altitude (Stiller et al., 2012).

Substance	Annual Trend 2004–2010 (% yr^{-1} relative to 2007)			Data Sources
	In-situ 30°N–90°N	Remote sensing ground (total columns)	Remote sensing satellite	
CFC-11	−0.84 ± 0.09	−0.99 ± 0.10	MIPAS: −1.03±0.09 ACE-FTS: −0.9 ± 0.1	NOAA, AGAGE Zander et al., 2008 Kellmann et al., 2012 Brown et al., 2011
CFC-12	−0.39 ± 0.05	−0.38 ± 0.07	MIPAS: −0.51± 0.09 ACE-FTS: −0.4 ± 0.1	NOAA, AGAGE Zander et al., 2008 Kellmann et al., 2012 Brown et al., 2011
CFC-113	−0.93 ± 0.02		ACE-FTS: −1.2 ± 0.1	NOAA, AGAGE Brown et al., 2011
CCl_4	−1.35 ± 0.08	−1.31 ± 0.15	ACE-FTS −1.2 ± 0.1	NOAA, AGAGE Rinsland et al., 2012 Brown et al., 2011
HCFC-22	3.97 ± 0.06	3.52 ± 0.08	ACE-FTS 3.7 ± 0.1	NOAA, AGAGE Zander et al., 2008 Brown et al., 2011
HCFC-141b	2.57 ± 0.07		ACE-FTS 0.74 ± 0.5	NOAA, AGAGE Brown et al., 2011
HCFC-142b	5.44 ± 0.03		ACE-FTS 7.0 ± 0.4	NOAA, AGAGE Brown et al., 2011
HFC-23	4.2 ± 0.2		ACE-FTS 3.9 ± 1.2	AGAGE Harrison et al., 2012
CF_4	0.86 ± 0.01	1.02 ± 0.05	ACE-FTS 0.74 ± 0.04	AGAGE Mahieu et al., 2014 Brown et al., 2011
SF_6	4.27 ± 0.07	4.14 ± 0.32	MIPAS 4.3 ACE-FTS: 4.2 ± 0.1	NOAA, AGAGE Zander et al., 2008 Stiller et al., 2012 Brown et al., 2011

Table 1-3. Steady-state lifetimes for selected long-lived halocarbons (total lifetimes greater than 0.5 years). Total and partial lifetimes are defined in Box 1-1. Compounds included in the SPARC (2013) lifetime report are given in bold with the total lifetimes calculated using the SPARC (2013) atmospheric partial lifetime recommendation and the ocean and soil partial lifetimes reported here; stratospheric partial lifetimes for these compounds were taken from the SPARC (2013) model-mean unless noted otherwise. The footnotes contain specific details for each compound in the table. See Table 1-5 in Section 1.3 for local lifetime estimates for very short-lived substances (VSLS) and Table 1-11 in Section 1.3 for lifetimes of potential ODS replacement compounds.

Industrial Designation or Common Name	Chemical Formula	WMO (2011) Total Lifetime (years)	New Total Lifetime [a] (years)	SPARC (2013) Atmospheric Partial Lifetime & Estimated Uncertainty Range [b] (years)	Tropospheric OH Partial Lifetime [c] (years)	Stratospheric Partial Lifetime (years)	Ocean Partial Lifetime (years) [d]	Notes
Halogenated Methanes								
HFC-41	CH_3F	2.8	2.8		2.9	~65	1340	1, 2
HFC-32	**CH_2F_2**	5.2	5.4	5.4 [4.0–8.2]	5.5	124		1
HFC-23	**CHF_3**	222	228	228 [160–394]	243	4420		1
PFC-14 (Carbon tetrafluoride)	CF_4	>50,000	>50,000					3
Methyl chloride	**CH_3Cl**	1.0	0.9	1.3 [0.9–2.0]	1.57	30.4 [e]	12	4–7
Carbon tetrachloride	**CCl_4**	26	26	44 (36-58) [33-67]		44 [f]	94	7
HCFC-31	CH_2ClF	1.3	1.2		1.3	~35		1, 2, 8
HCFC-22	**$CHClF_2$**	11.9	11.9	12 [9.3–18]	13.0	161	1174	4
HCFC-21	$CHCl_2F$	1.7	1.7		1.8	~35	673	1, 2, 8
CFC-11	**CCl_3F**	45	52	52 (43–67) [35–89]		55		9
CFC-12	**CCl_2F_2**	100	102	102 (88–122) [78–151]		95.5		9
CFC-13	$CClF_3$	640	640					3
Methyl bromide	**CH_3Br**	0.8	0.8	1.5 [1.1–2.3]	1.8	26.3[e]	3.1	4, 7, 10
Halon-1201	$CHBrF_2$	5.2	5.1		6.0	~35		1, 2, 8
Halon-1301	**$CBrF_3$**	65	72	72 (61–89) [58–97]		73.5		9
Halon-1211	**$CBrClF_2$**	16	16	16 [10–39]		41		11
Halon-1202	**CBr_2F_2**	2.9	2.5	2.5 [1.5–7.3]		36		11
Halogenated Ethanes								
HFC-152a	**CH_3CHF_2**	1.5	1.6	1.6 [1.2–2.2]	1.55	39	1958	1
HFC-143	CH_2FCHF_2	3.5	3.5		3.70	~75		1, 2
HFC-143a	**CH_3CF_3**	47.1	51	51 [38–81]	57	612		1
HFC-134	CHF_2CHF_2	9.7	9.7		10.5	~135		1, 2
HFC-134a	**CH_2FCF_3**	13.4	14	14 [10–21]	14.1	267	5909	4
HFC-125	**CHF_2CF_3**	28.2	31	31 [22–48]	32	351	10650	1
PFC-116 (Perfluoroethane)	CF_3CF_3	>10,000	>10,000					3
Methyl chloroform	**CH_3CCl_3**	5.0	5.0 [g]	6.1 [4.7–5.4]	6.1 [f]	38	94	12
HCFC-141b	**CH_3CCl_2F**	9.2	9.4	9.4 [7.2–18]	10.7	72.3	9190	1
HCFC-142b	**CH_3CClF_2**	17.2	18	18 [14–25]	19.3	212	122200	1
HCFC-133a	CH_2ClCF_3	4.3	4.0		4.5	41		1, 2, 13
HCFC-123	$CHCl_2CF_3$	1.3	1.3		1.35	36		1, 14
HCFC-123a	$CHClFCF_2Cl$	4.0	4.0		4.3	~65		1, 2, 8
HCFC-123b	CHF_2CCl_2F	6.2	~6		~7	~50		2, 8, 15
HCFC-124	$CHClFCF_3$	5.9	5.9		6.3	111	1855	1, 14

(continued next page)

Industrial Designation or Common Name	Chemical Formula	WMO (2011) Total Lifetime (years)	New Total Life-time [a] (years)	SPARC (2013) Atmospheric Partial Lifetime & Estimated Uncertainty Range [b] (years)	Tropo-spheric OH Partial Lifetime [c] (years)	Strato-spheric Partial Lifetime (years)	Ocean Partial Lifetime (years) [d]	Notes
HCFC-124a	CHF_2CClF_2	9.1	~9.2		~10	~120		2, 16
CFC-112	CCl_2FCCl_2F		59			59		13
CFC-112a	$CClF_2CCl_3$		51			51		13
CFC-113	**CCl_2FCClF_2**	85	93	93 (82–109) [69–138]		88.4		9, 17
CFC-113a	CCl_3CF_3	~45	59			59		13
CFC-114	**$CClF_2CClF_2$**	190	189	189 [153–247]		191		9, 17
CFC-114a	CCl_2FCF_3	~100	~100			~100		18
CFC-115	**$CClF_2CF_3$**	1020	540	540 [404–813]		664		19
Halon-2311 (Halothane)	$CHBrClCF_3$	1.0	1.0		1.1	~16		1, 2, 8
Halon-2402	**$CBrF_2CBrF_2$**	20	28	28 [20–45]		41		11
Halogenated Propanes								
HFC-263fb	$CH_3CH_2CF_3$	1.2	1.1		1.16	~40		1, 2
HFC-245ca	$CH_2FCF_2CHF_2$	6.5	6.5		6.9	~105		1, 2
HFC-245ea	$CHF_2CHFCHF_2$	3.2	3.2		3.4	~70		1, 2
HFC-245eb	$CH_2FCHFCF_3$	3.1	3.2		3.3	~70		1, 2
HFC-245fa	**$CHF_2CH_2CF_3$**	7.7	7.9	7.9 [5.5–14]	8.2	149		1
HFC-236cb	$CH_2FCF_2CF_3$	13.1	~13		~14	~240		20
HFC-236ea	CHF_2CHFCF_3	11.0	11.0		11.9	~145		1, 2
HFC-236fa	$CF_3CH_2CF_3$	242	222		253	~1800		1, 21
HFC-227ea	**CF_3CHFCF_3**	38.9	36	36 [25–61]	37.5	673		4, 22
PFC-218 (Perfluoropropane)	$CF_3CF_2CF_3$	2,600	~7,000					23
PFC-c216 (Perfluorocyclo-propane)	c-C_3F_6	~3,000	~4,000					23
HCFC-243cc	$CH_3CF_2CCl_2F$	19.5	19.5		27.1	~70		1, 2, 8
HCFC-234fb	$CF_3CH_2CCl_2F$	49	~45		98	~85		1, 2, 8
HCFC-225ca	$CHCl_2CF_2CF_3$	1.9	1.9		2.0	44		1, 14
HCFC-225cb	$CHClFCF_2CClF_2$	5.9	5.9		6.3	101		1, 14
Halogenated Higher Alkanes								
HFC-365mfc	$CH_3CF_2CH_2CF_3$	8.7	8.7		9.3	~125		1, 2
HFC-356mcf	$CH_2FCH_2CF_2CF_3$	1.3	1.2		1.26	~40		1, 2
HFC-356mff	$CF_3CH_2CH_2CF_3$	8.3	8.3		8.9	~120		1, 2
HFC-338pcc	$CHF_2CF_2CF_2CHF_2$	12.9	12.9		14.0	~160		1, 2
HFC-329p	$CHF_2CF_2CF_2CF_3$	28.4	~30		~34	~260		2, 24
PFC-C318 (Perfluorocyclo-butane)	c-C_4F_8	3,200	3,200					3
PFC-31-10 (Perfluorobutane)	C_4F_{10}	2,600	~5,000					23
(*E*)-R316c ((*E*)-1,2-dichlorohexafluoro-cyclobutane)	(*E*)-1,2-c-$C_4F_6Cl_2$		75			76		9, 25
(*Z*)-R316c ((*Z*)-1,2-dichlorohexafluoro-cyclobutane)	(*Z*)-1,2-c-$C_4F_6Cl_2$		114			115		9, 25

(continued next page)

Industrial Designation or Common Name	Chemical Formula	WMO (2011) Total Lifetime (years)	New Total Life-time [a] (years)	SPARC (2013) Atmospheric Partial Lifetime & Estimated Uncertainty Range [b] (years)	Tropo-spheric OH Partial Lifetime [c] (years)	Strato-spheric Partial Lifetime (years)	Ocean Partial Lifetime (years) [d]	Notes
HFC-43-10mee	$CF_3CHFCHFCF_2CF_3$	16.1	16.1		17.9	157		1, 14
HFC-458mfcf	$CF_3CH_2CF_2CH_2CF_3$	22.9	22.9		25.5	~225		1, 2
PFC-41-12 (Perfluoropentane)	C_5F_{12}	4,100	4,100					3
HFC-55-10mcff	$CF_3CF_2CH_2CH_2CF_2CF_3$	7.5	7.5		8.0	~115		1, 2
HFC-52-13p	$CHF_2CF_2CF_2CF_2CF_2CF_3$	32.2	32.7		37.0	~280		2, 26
PFC-51-14 (Perfluorohexane)	C_6F_{14}	3,100	3,100					3
PFC-61-16 (Perfluoroheptane)	C_7F_{16}	~3,000	~3,000					23
PFC-71-18 (Perfluorooctane)	C_8F_{18}		~3,000					23
Perfluorodecalin	$C_{10}F_{18}$, (*E*)- and (*Z*)-isomers	~2,000	~2,000					23
Fluorinated Alcohols								
1,1,1,3,3,3-hexa-fluoroisopropanol	$(CF_3)_2CHOH$	1.9	1.9		2.0	~50		1, 2
Halogenated Ethers								
HFE-143a	CH_3OCF_3	4.8	4.8		5.1	~90		1, 2
HFE-134	CHF_2OCHF_2	24.4	25.4		28.4	~240		1, 2
HFE-125	CHF_2OCF_3	119	119		147	~620		1, 2
HFE-227ea	$CF_3OCHFCF_3$	51.6	46.7		54	~345		1, 2
HCFE-235da2 (Isoflurane)	$CHF_2OCHClCF_3$	3.5	3.5		3.7	~55		1, 2, 27
HFE-236ea2 (Desflurane)	$CHF_2OCHFCF_3$	10.8	10.8		11.7	~145		1, 2
HFE-236fa	$CF_3OCH_2CF_3$	7.5	~7.5		~8	~115		2, 28
HFE-245fa1	$CF_3OCH_2CHF_2$	6.6	~6.6		~7	~105		2, 29
HFE-245fa2	$CHF_2OCH_2CF_3$	5.5	5.5		5.8	~95		1, 2
HFE-245cb2	$CH_3OCF_2CF_3$	4.9	5.0		5.24	~90		1, 2
HFE-254cb2	$CH_3OCF_2CHF_2$	2.5	2.5		2.62	~60		1, 2
HFE-236ca	$CHF_2OCF_2CHF_2$	20.8	20.8		23.1	~210		1, 2
HFE-235ca2 (Enflurane)	CHF_2OCF_2CHFCl	4.3	4.3		4.62	~70		2, 8, 30
HFE–329mcc2	$CF_3CF_2OCF_2CHF_2$	22.5	~25		23–34	~220		2, 31
HFE–338mcf2	$CF_3CF_2OCH_2CF_3$	7.5	~7.5		~8	~130		2, 32
HFE–347mcc3	$CH_3OCF_2CF_2CF_3$	5.0	5.0		5.3	~90		1, 2
HFE–347mcf2	$CF_3CF_2OCH_2CHF_2$	6.6	~6.6		~7	~105		2, 33
HFC-347mcf	$CHF_2OCH_2CF_2CF_3$	5.7	5.6		6.0	~95		1, 2
HFE-347pcf2	$CF_3CH_2OCF_2CHF_2$	6.0	5.9		6.3	~100		1, 2
HFE–356mec3	$CH_3OCF_2CHFCF_3$	~3	~3		~3	~65		2, 34
HFE–356pcc3	$CH_3OCF_2CF_2CHF_2$	~3	~3		~3	~65		2, 34
HFE–356pcf2	$CHF_2CH_2OCF_2CHF_2$	5.7	~6		~6	~95		2, 35
HFE–356pcf3	$CHF_2OCH_2CF_2CHF_2$	3.5	3.5		3.7	~75		1, 2
HFE-347mmz1 (Sevoflurane)	$(CF_3)_2CHOCH_2F$	2.2	~2		~2	~50		2, 36
HFE-338mmz1	$(CF_3)_2CHOCHF_2$	21.2	21.2		23.5	~215		1, 2

(continued next page)

Industrial Designation or Common Name	Chemical Formula	WMO (2011) Total Lifetime (years)	New Total Life-time [a] (years)	SPARC (2013) Atmospheric Partial Lifetime & Estimated Uncertainty Range [b] (years)	Tropo-spheric OH Partial Lifetime [c] (years)	Strato-spheric Partial Lifetime (years)	Ocean Partial Lifetime (years) [d]	Notes
Perfluoroisopropyl methyl ether	$(CF_3)_2CFOCH_3$	3.7	3.6		3.8	~75		1, 2
HFE-7100	$CH_3O(CF_2)_3CF_3$	4.7	4.7		5.0	~85		1, 2
HFE-54-11mecf	$CF_3CHFCF_2OCH_2CF_2CF_3$	8.8	8.8		9.5	~125		2, 37
HFE-569sf2	$CH_3CH_2O(CF_2)_3CF_3$	0.8	~0.8		~0.8	~30		2, 38
HFE–236ca12	$CHF_2OCF_2OCHF_2$	25.0	25.0		28.0	235		1, 2
HFE–338pcc13	$CHF_2OCF_2CF_2OCHF_2$	12.9	12.9		14.0	~160		1, 2
HFE–43–10pccc	$CHF_2OCF_2OCF_2CF_2OCHF_2$	13.5	13.5		14.7	~165		1, 2
Trifluoromethyl formate	$CF_3OC(O)H$	<3.5	<3.5		3.7	~75		2, 39, 40
Perfluoroethyl formate	$C_2F_5OC(O)H$	<3.5	<3.5		3.7	~75		2, 40, 41
Perfluoro-n-propyl formate	$n\text{-}C_3F_7OC(O)H$	<2.6	<2.6		2.7	~60		2, 40, 41
Other Fluorinated Compounds								
Trifluoromethyl-sulfurpentafluoride	SF_5CF_3	650–950	650–950					42
Sulfur hexafluoride	SF_6	3,200	3,200					3
Nitrogen trifluoride	**NF_3**	500	569			740		43
Sulfuryl fluoride	SO_2F_2	36	36		>300	630	40	44

[a] Total lifetime includes tropospheric OH and Cl atom reaction and photolysis loss, stratospheric loss due to reaction (OH and $O(^1D)$) and photolysis, and ocean and soil uptake as noted in the table.
[b] The lifetimes given in parenthesis () represent the "most likely" lifetime range, while the lifetimes given in brackets [] represent the "possible" lifetime range, see SPARC (2013).
[c] Lifetime for tropospheric loss due to reaction with OH calculated relative to the lifetime for CH_3CCl_3, (6.1 years) and a temperature of 272 K (see Box 1-1).
[d] Ocean lifetimes were taken from Yvon-Lewis and Butler (2002) unless noted otherwise.
[e] Stratospheric lifetime from Chapter 5 of SPARC (2013).
[f] Stratospheric lifetime from SPARC (2013) was based on both tracer (40 years) and model-mean (49 years) derived lifetimes.
[g] The value of τ_{OH} of 6.1 years for methyl chloroform was derived from its measured overall lifetime of 5.0 years (Prinn et al., 2005; Clerbaux and Cunnold et al., 2007), taking into account an ocean partial lifetime of 94 years and stratospheric partial lifetime of 38 years.

Notes
1. OH rate coefficient data taken from Sander et al. (2011).
2. Stratospheric reactive loss ($O(^1D)$ and OH) partial lifetime estimate was based on an empirical correlation derived from data reported in Naik et al. (2000); log(Stratospheric reactive partial lifetime) = 1.537 + 0.5788*log(Tropospheric OH partial lifetime). This correlation was used in WMO (2011).
3. Total lifetime is a best estimate taken from Ravishankara et al. (1993) that includes mesospheric loss due to Lyman-α (121.567 nm) photolysis.
4. OH rate coefficient data taken from SPARC (2013) Chapter 3.
5. Lifetime due to reaction with Cl atom of 259 years taken from the SPARC (2013) Chapter 5 model-mean.
6. Ocean lifetime taken from Hu et al. (2013).
7. Total lifetime also includes soil uptake partial lifetimes: 4.2 years for CH_3Cl (Hu, 2012), 195 years for CCl_4 (Montzka and Reimann et al., 2011), and 3.35 years for CH_3Br (Montzka and Reimann et al., 2011).
8. Stratospheric photolysis lifetime was estimated using the empirical relationship given in Orkin et al. (2013a).
9. Tropospheric UV photolysis partial lifetime: 1870 years for CFC-11, 11600 years for CFC-12, 4490 years for halon-1301, 7620 years for CFC-113, 19600 years for CFC-114, 3600 years for (*E*)-R316c, and 10570 years for (*Z*)-R316c.
10. Ocean lifetime taken from Hu et al. (2012).
11. Lifetimes from 2-D model calculations using cross section data from Papanastasiou et al. (2013). The total lifetime includes a tropospheric photolysis partial lifetimes: 27.2 years for halon-1211, 2.74 years for halon-1202, and 85.5 years for halon-2402.
12. Tropospheric OH partial lifetime calculated from an overall lifetime of 5.0 years derived from the AGAGE and NOAA networks using a stratospheric partial lifetime of 38 years and an ocean partial lifetime of 94 years (Prinn et al., 2005).
13. Stratospheric partial lifetime of 51 (27–264) years taken from Laube et al. (2014) and scaled to a CFC-11 lifetime of 52 years.
14. Stratospheric partial lifetime taken from Naik et al. (2000).
15. Tropospheric OH partial lifetime estimated from that for CHF_2CF_3 taking into account the effects of chlorine substitution on the rate coefficients for CH_3CF_3 and CH_3CFCl_2.
16. Tropospheric OH partial lifetime estimated from that for CHF_2CF_3 taking into account the effects of chlorine substitution on the rate coefficients for CH_3CF_3 and CH_3CF_2Cl; stratospheric photolysis estimated to be the same as for CF_3CF_2Cl of 1590 years from SPARC (2013) Chapter 5 model mean.
17. The revised $O(^1D)$ rate coefficient recommended in SPARC (2013) Chapter 3 would decrease the model calculated stratospheric partial lifetime slightly.
18. UV photolysis is the expected predominant stratospheric loss process, however, no UV absorption spectrum data are available. Lifetimes assumed to be similar to CFC-12.

19. Stratospheric partial lifetime from 2-D model calculations using $O(^1D)$ rate coefficient data from Baasandorj et al. (2013). The total lifetime includes mesospheric loss due to Lyman-α (121.567 nm) photolysis.
20. Lifetimes estimated to be similar to that of HFC-134a (CH_2FCF_3).
21. Stratospheric partial lifetime estimated based on a reactivity comparison with CH_2F_2 and CF_3CHFCF_3.
22. Stratospheric partial lifetime calculated using 2-D model with OH and $O(^1D)$ rate coefficients recommended in SPARC (2013) Chapter 3.
23. Total lifetime estimated based on the increase in Lyman-α (121.567 nm) cross section with increasing number of $–CF_2–$ groups in the perfluorocarbon.
24. OH rate coefficient from Young et al. (2009) and an assumed temperature dependence the same as for CHF_2CF_3.
25. Lifetimes taken from the 2-D model calculations in Papadimitriou et al. (2013b).
26. OH rate coefficient data taken from Atkinson et al. (2008).
27. Stratospheric partial lifetime assumed to be the same as for HCFC-133a (CH_2ClCF_3).
28. Tropospheric OH partial lifetime estimated from that for $CF_3CH_2OCF_2CHF_2$ by adjusting for the reactivity contribution of $–CF_2CHF_2$ determined from the reactivity of $CF_3CF_2OCF_2CHF_2$.
29. Tropospheric OH partial lifetime estimated from those for CF_3OCH_3 and $CHF_2CH_2CF_3$.
30. OH rate coefficient taken from Tokuhashi et al. (1999).
31. Tropospheric OH partial lifetime estimated as being greater than that of $CHF_2CF_2OCHF_2$ and less than that of $CHF_2CF_2CF_2CF_3$.
32. Tropospheric OH partial lifetime assumed to be the same as that of $CF_3OCH_2CF_3$.
33. Tropospheric OH partial lifetime assumed to be the same as for $CHF_2CH_2OCF_3$.
34. Tropospheric OH partial lifetime assumed to be approximately that of $CH_3OCF_2CHF_2$.
35. Tropospheric OH partial lifetime estimated from the sum of the OH reaction loss of $CF_3CF_2OCF_2CHF_2$ and $CF_3CF_2OCH_2CHF_2$.
36. OH rate coefficient from the 298 K studies of Langbein et al. (1999) and Sulbaek Andersen et al. (2012) and an assumed *E*/R of 1500 K.
37. OH rate coefficient from Chen et al. (2005a).
38. OH rate coefficient from the 295 K study of Christensen et al. (1998) and an assumed *E*/R of 1000 K.
39. OH rate coefficient taken from Chen et al. (2004b).
40. Ocean loss for perfluoro esters has been estimated from hydrolysis and solubility data for non-fluorinated and partially fluorinated esters by Kutsuna et al. (2005). These authors suggest that the ocean sink can be comparable to the tropospheric reaction sink for perfluoro esters, thereby reducing the total lifetimes given in this table by as much as a factor of 2.
41. OH rate coefficient from Chen et al. (2004a).
42. Total lifetime taken from Table 1-4 in Clerbaux and Cunnold et al. (2007).
43. Lifetimes calculated based on 2-D model from Papadimitriou et al. (2013a); total lifetime includes tropospheric (84150 years) and mesospheric (2531 years) partial lifetimes.
44. From Papadimitriou et al. (2008) and Mühle et al. (2009).

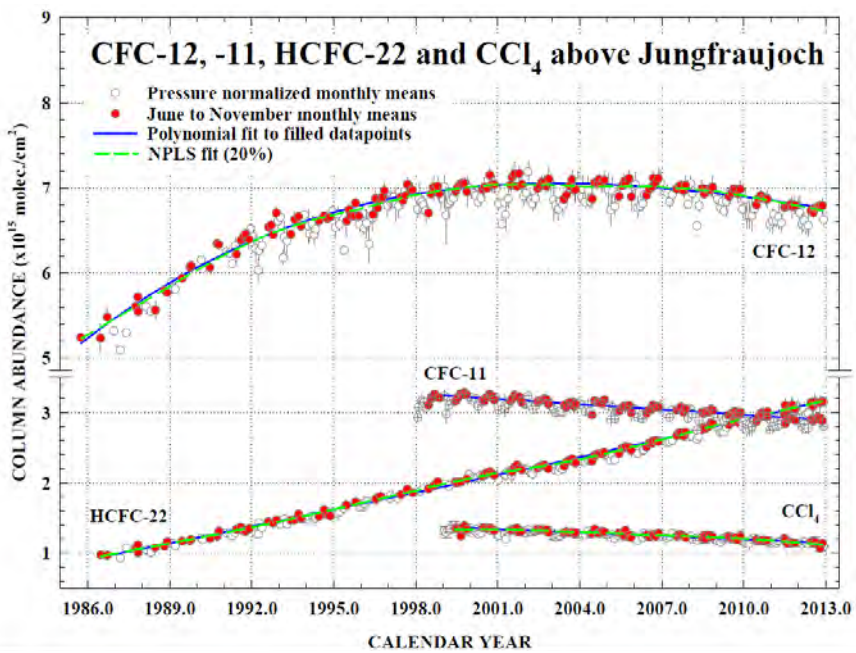

Figure 1-2. Time evolution of monthly-mean total vertical column abundances (in molecules per square centimeter) for CFC-12, CFC-11, CCl_4, and HCFC-22 above the Jungfraujoch station, Switzerland, through 2012 (updated from Zander et al. (2008), using the bootstrap resampling tool described by Gardiner et al. (2008) for the trend evaluations and Rinsland et al. (2012)). Note the discontinuity in the vertical scale. Solid blue lines show polynomial fits to the columns measured in June to November only so as to mitigate the influence of variability caused by atmospheric transport and tropopause subsidence during winter and spring (open circles) on derived trends. Dashed green lines show nonparametric least-squares fits (NPLS) to the June to November data.

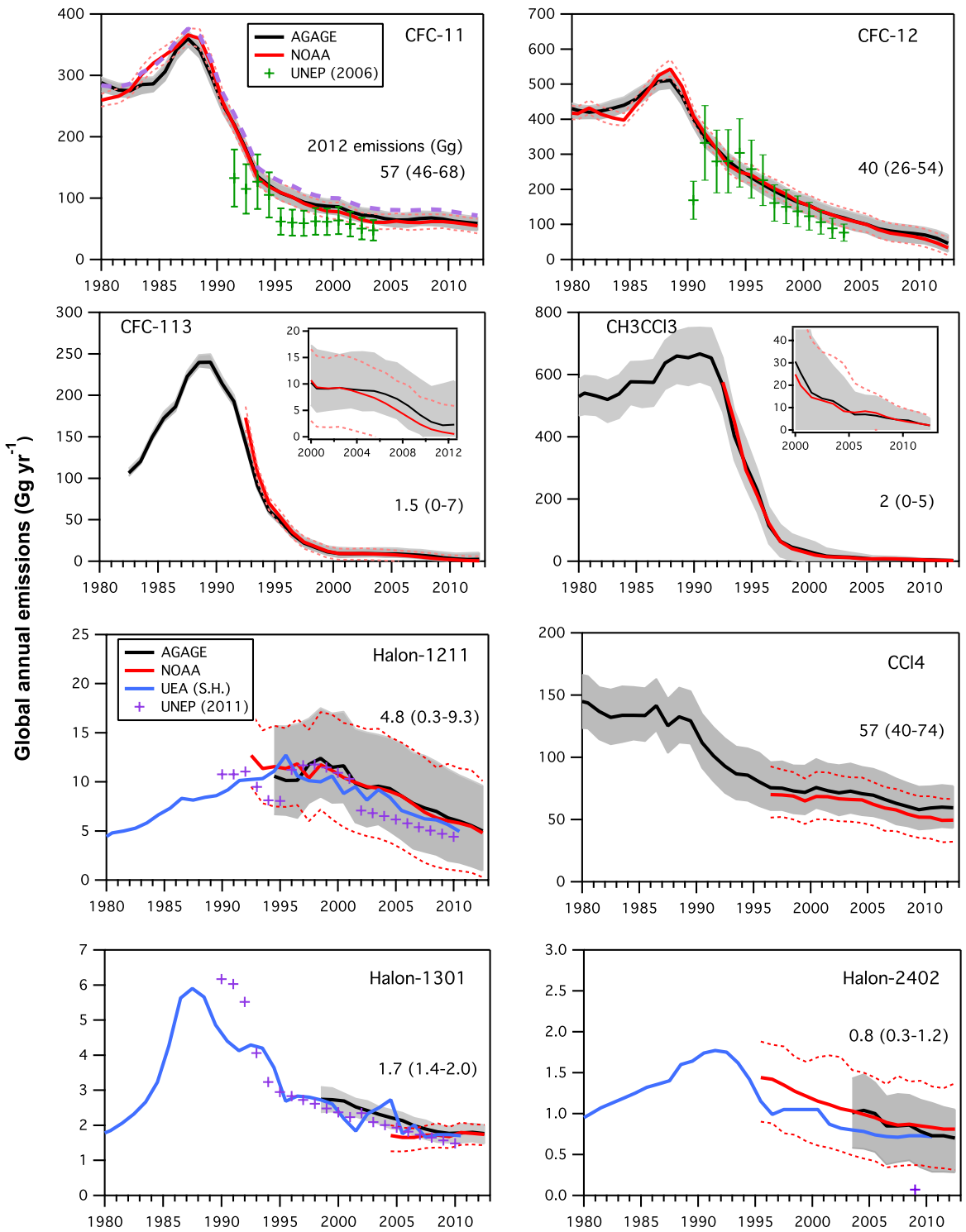

Figure 1-3. Top-down and bottom-up global emissions estimates (Gg yr^{-1}) for ozone-depleting substances. Top-down emissions from AGAGE (black) and NOAA (red) atmospheric data were calculated using a global 12-box model (Cunnold et al., 1983; Rigby et al., 2013). ***(continued next page)***

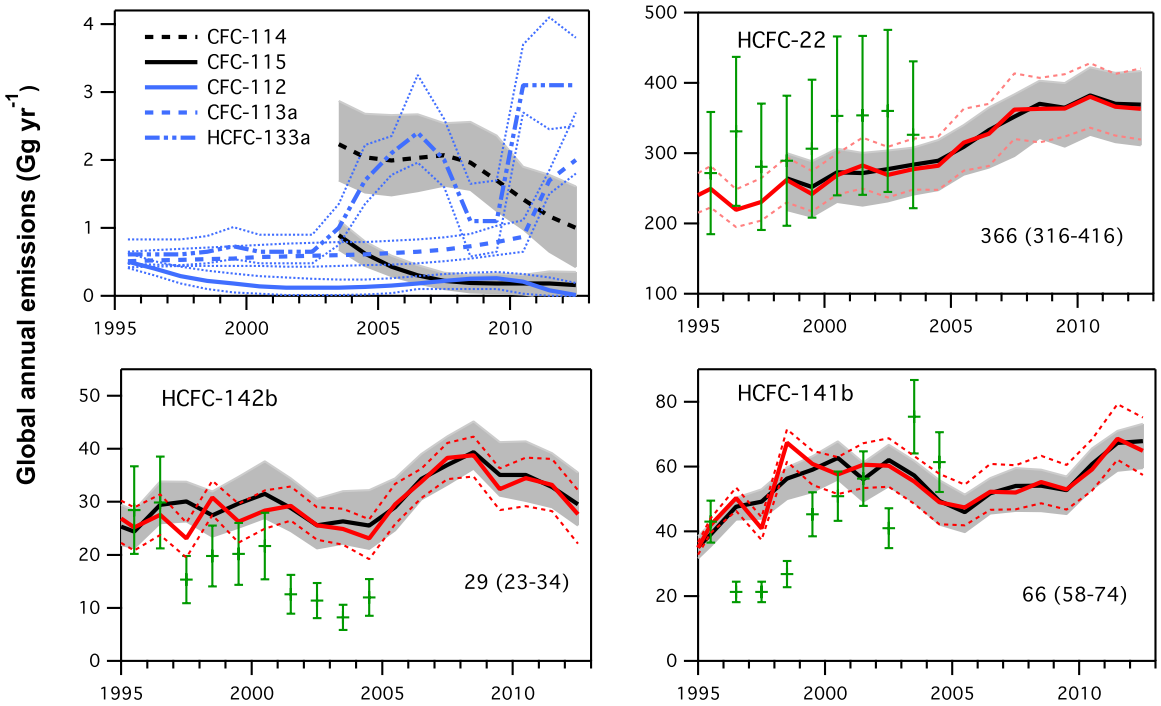

(Figure 1-3, continued) Additionally, for CFC-112, CFC-113a, HCFC-133a, and halons the emissions were calculated using UEA data from the Southern Hemisphere (S.H.) (Cape Grim archived air (blue); Laube et al., 2014). Lifetimes and ranges were taken from Newland et al. (2013), Laube et al. (2014), and SPARC (2013). Shaded bands indicate overall uncertainties derived from uncertainties in measurement, lifetimes, and prior emissions estimates. Mean values given in the text, and shown in figures for 2012, were calculated as the mean of AGAGE and NOAA estimates (when available). Ranges were taken from AGAGE data as shown in this figure unless AGAGE and NOAA ranges differed by more than 10%, in which case an average range was reported (e.g., CFC-113). CFC-11 emissions were also calculated using an older lifetime estimate of 45 years instead of 52 years (dashed violet line). Bottom-up estimates include UNEP (2006) (green) and UNEP (2011b) (violet). Note the x-axis ranges are not the same for all panels.

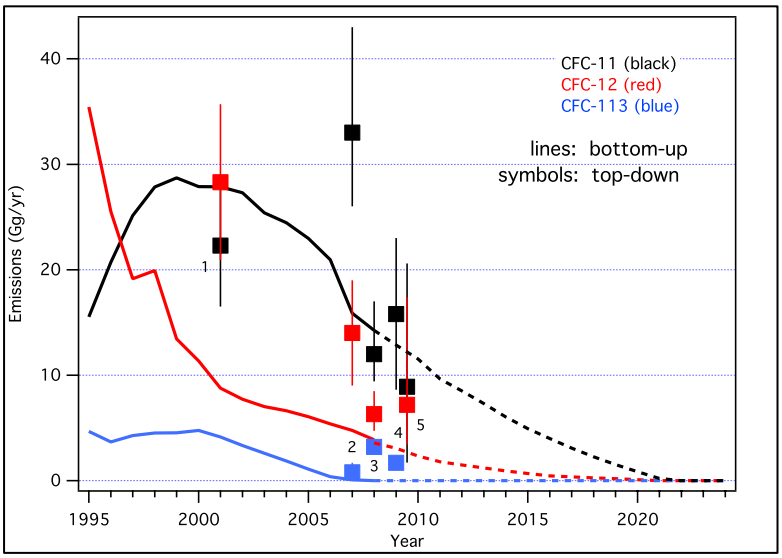

Figure 1-4. Regional emission estimates of CFC-11, CFC-12, and CFC-113 from China. Top-down estimates in years indicated were taken from [1]Palmer et al. (2003), [2]Vollmer et al. (2009), [3]Kim et al. (2010), [4]An et al. (2012), and [5]Fang et al. (2012). Bottom-up estimates (solid and dashed lines) are from Wan et al. (2009).

Box 1-1. Lifetimes and Removal Processes

The total lifetime (τ_{Total}) of a trace species is defined as the ratio of its global atmospheric burden (C_{Global}) to its total global loss rate (L_{Total})

$$\tau_{Total} = C_{Global}/L_{Total}$$

where L_{Total} is the sum of the loss rates for various removal processes

$$L_{Total} = L_{Atm} + L_{Soil} + L_{Ocean} + \cdots L_X$$

L_{Atm} represents the loss rate for processes occurring in the atmosphere (gas-phase reaction and photolysis), L_{Soil} is the loss rate due to soil uptake, and L_{Ocean} is the rate for loss to the oceans (additional loss rates are represented by L_X). Lifetimes are not constant values because they depend on the abundance of a chemical relative to the distribution of its sinks (and hence can vary with emission magnitude and location). Steady-state lifetimes refer to a lifetime when the emission and removal rates of a species are equal. A discussion of lifetimes and methods for defining their uncertainties is given in SPARC (2013).

Loss rates are associated with partial lifetimes such that

$$L_{Total} = C_{Global}/\tau_{Total} = C_{Global} \times (1/\tau_{Atm} + 1/\tau_{Soil} + 1/\tau_{Ocean} + \cdots 1/\tau_X)$$

$$\frac{1}{\tau_{Total}} = \frac{1}{\tau_{Atm}} + \frac{1}{\tau_{Soil}} + \frac{1}{\tau_{Ocean}} + \cdots \frac{1}{\tau_X}$$

where $(\tau_{Atm})^{-1} = (\tau_{OH})^{-1} + (\tau_{O_3})^{-1} + (\tau_{Cl})^{-1} + (\tau_{NO_3})^{-1} + (\tau_{O(^1D)})^{-1} + (\tau_J)^{-1}$

The atmospheric lifetime can also be separated into partial troposphere, stratosphere, and mesosphere lifetimes using the total global atmospheric burden and the loss rate integrated over the different atmospheric regions such that

$$\frac{1}{\tau_{Atm}} = \frac{1}{\tau_{Trop}} + \frac{1}{\tau_{Strat}} + \frac{1}{\tau_{Meso}}$$

Species with total lifetimes greater than ~0.5 years are well-mixed in the troposphere and, for the purposes of this Assessment, are considered long-lived. In this case, τ_{Total} is considered to be independent of the location of emission, and is considered to be a global lifetime that represents the compound's persistence in the Earth's atmosphere. The lifetime of a long-lived species due to reaction with tropospheric OH radicals is estimated relative to the corresponding tropospheric OH partial lifetime of methyl chloroform (CH_3CCl_3, MCF) such that

$$\tau_{OH}^{RH} = \frac{k_{MCF}(272\text{ K})}{k_{RH}(272\text{ K})} \times \tau_{OH}^{MCF}$$

where τ_{OH}^{RH} is the OH partial lifetime for compound RH, k_{RH}(272 K) and k_{MCF}(272 K) are the rate coefficients for the reactions of OH with RH and MCF at 272 K, respectively, and τ_{OH}^{MCF} = 6.1 years (see Table 1-3).

Very short-lived substances (VSLS) (i.e., compounds with atmospheric lifetimes less than ~0.5 years) typically have non-uniform tropospheric distributions, because this time period is comparable to or shorter than the characteristic time of mixing processes in the troposphere. Local atmospheric lifetimes of VSLS, therefore, depend on where and when the compound is emitted, as well as local atmospheric conditions (Table 1-5, page 1.35). The concept of a single global lifetime, an Ozone Depletion Potential (ODP), or a Global Warming Potential (GWP) is inappropriate for VSLS, as discussed in Chapter 5.

Since the last Assessment, SPARC (Stratosphere-Troposphere Processes And their Role in Climate)—a core project of the World Climate Research Programme (WCRP)—initiated a study of the "Lifetimes of Stratospheric Ozone-Depleting Substances, Their Replacements, and Related Species" (SPARC, 2013). The study included 27 long-lived key ozone-depleting substances (ODSs), replacement compounds, and greenhouse gases (see Table 1-3). Including CFC-11 was of particular importance since it is the reference species used in defining the ODPs of other ODSs. The lifetime evaluation was warranted because of advancements in

(Box 1-1, continued)
the ability of models to simulate atmospheric circulation (leading to better estimates of age of air) and new measurement data from ground-based networks, high-altitude sampling, and satellite observations. The recommended steady-state atmospheric lifetimes were derived using results from state-of-the art models and measurement-based estimates. The report also provides an in-depth analysis of the uncertainties in these lifetimes. The SPARC-recommended atmospheric steady-state lifetimes and estimated range of lifetimes given in Table 1-3 were obtained from a weighted average of the lifetimes derived from different methods, as described in SPARC (2013).

1.2.1.2 HALONS

Observations

Halon-1211 ($CBrClF_2$), halon-2402 ($CBrF_2CBrF_2$), and halon-1202 (CBr_2F_2) mole fractions continued to decline from peak values observed in the early and mid-2000s (Table 1-1; Figure 1-1; Newland et al., 2013). Recent trends in halon-1211, halon-1301, and halon-2402 agree with those anticipated in the A1-2010 scenario (Daniel and Velders et al., 2011). Although globally averaged mole fractions of halon-1301 (CF_3Br) continued to increase (reaching 3.26 ppt in 2012), the summed contribution of halons to total atmospheric bromine peaked around 2007. A decrease in global total bromine from halons was not evident at the time of the last Assessment, but is now significant, with an average rate of decline of −0.06 ppt yr^{-1} between 2008 and 2012.

Over the 2008–2012 period, estimates of the global abundances of halon-1301 and -1211 varied by 1–2% among global networks (Table 1-1). For halon-2402, Southern Hemispheric mole fractions from the University of East Anglia (UEA; Newland et al., 2013) were 7.5% lower than the NOAA scale.

Lifetimes and emissions

The new recommended steady-state lifetime of halon-1301 is 72 years (increased from 65 years) (SPARC, 2013). Revised lifetimes for halon-1202, halon-1211, and halon-2402, obtained using a 2-D model, are reported in this Assessment based on UV absorption cross section measurements made since the SPARC (2013) assessment (Papanastasiou et al., 2013). These halons are removed exclusively by photolysis in the troposphere and stratosphere. The lifetime uncertainty due solely to the uncertainty in the new cross section data for these substances (Table 1-3) is considerably smaller than reported in SPARC (2013), where the uncertainties were derived by averaging various 3-D approaches and observational data.

Global emission estimations derived from measured global mole fractions peaked around 1988 for halon-1301, 1993 for halon-2402, and 1995–1998 for halon-1211 (Figure 1-3). Emissions of halon-1211 and halon-2402 have been decreasing in recent years, while those of halon-1301 have remained approximately constant (Figure 1-3). This is broadly consistent with emission estimates from inventories (UNEP, 2011b). Continued emissions of halons are expected from banks (Box 5-1), since the primary use for these chemicals is in fire extinguishers. Therefore any impact of the 2010 global phase-out of halon production will likely not be observed in the atmosphere immediately. Top-down and bottom-up emissions estimates agree reasonably well for halon-1211 and halon-1301, but a large discrepancy continues to exist for halon-2402, which was predominantly produced and used in the former Soviet Union (McCulloch, 1992).

In 2010 halon banks were estimated by the Halons Technical Options Committee (HTOC); (UNEP, 2011b) as 43 Gg for halon-1301 and as 65 Gg for halon-1211. For the same year Newland et al. (2013) estimated an identical bank size for halon-1301, but only 37 Gg for halon-1211. The difference for halon-1211 may be partially explained by the relatively large uncertainty in the halon-1211 lifetime range (10–39 years), which translates into large uncertainties in emissions and bank sizes. With banks likely much larger than current emissions, it may take decades before halon-1211 and halon-1301 banks are depleted.

1.2.1.3 CARBON TETRACHLORIDE (CCl_4)

Observations

The global surface mean mole fraction of carbon tetrachloride (CCl_4) continued to decline from 2008 to 2012 (Table 1-1). The AGAGE and UCI networks report rates of decline of 1.2–1.3% from 2011–2012, whereas the rate of decline reported by the NOAA network was 1.6%. These relative declines in mole fractions at Earth's surface are comparable to declines in column abundances from remote sensing instruments of 1.2–1.3% yr^{-1} (Table 1-2).

Lifetimes and emissions

Historically, CCl_4 was used as a solvent and as a feedstock for production of CFCs and their replacements. Current production is limited to feedstock, process agent use (e.g., in chlor-alkali production plants), and minor other essential uses (UNEP, 2013b; Fraser et al., 2014). Sinks for CCl_4 include loss in the stratosphere (Sander, 2011; SPARC, 2013), degradation in the oceans (Krysell et al., 1994; Yvon-Lewis and Butler, 2002; Lee et al., 2012), and degradation in soils (Happell and Roche, 2003; Liu, 2006; Rhew et al., 2008; Mendoza et al., 2011). A revised best estimate of the partial lifetime with respect to stratospheric loss, including the results of Laube et al. (2013) and Volk et al. (1997), is 44 years (SPARC, 2013), updated from 35 years. The partial lifetime with respect to oceanic uptake is still 94 (82–191) years (Yvon-Lewis and Butler, 2002). The soil sink partial lifetime is estimated to be approximately 195 (108–907) years (Montzka and Reimann et al., 2011). The sum of these three updated partial loss rates results in a total lifetime estimate of 26 years, which is unchanged from the previous Assessment (Montzka and Reimann et al., 2011). If the soil sink was negligible this would result in total lifetime of ~30 years.

Since the last Assessment, the discrepancy between bottom-up and top-down CCl_4 emission estimates has not been resolved. Global emissions determined from AGAGE and NOAA atmospheric data, using a total lifetime of 26 years, averaged 57 (40–74) Gg in 2012. After 2005 these top-down emission estimates are considerably higher than bottom-up emissions (derived from reported production minus feedstock use and destruction) (Figure 1-6).

A further indication of ongoing CCl_4 emissions (mostly in the Northern Hemisphere) is provided by the difference in mean mole fraction between hemispheres (Northern Hemisphere minus Southern Hemisphere, or NH−SH), which has been virtually stable at about 1.3 ppt since 2006. This is between the NH-SH difference of CFC-11 (~2 ppt), with annual emissions of 57 (46–68) Gg (410 (330–490) Mmol) in 2012, and CFC-113, with virtually no interhemispheric gradient and only small annual emissions of 1.5 (0–7) Gg (9 (0–40) Mmol) in 2012 (Figure 1-5). This suggests that significant sources of CCl_4 remain in the NH, although the higher oceanic sink in the SH, caused by the larger ocean area, may also account for some of this difference (Montzka and Reimann et al., 2011).

Emissions of CCl_4 could potentially arise from old industrial sites and from feedstock usage. The magnitude of emissions from CCl_4 feedstock uses are highly uncertain (UNEP, 2012) but have been estimated to be approximately 0.5%–2% of the feedstock production (1–4 Gg yr^{-1} in 2012, Figure 1-6). Emissions from CCl_4 used as a process agent have also been suggested (UNEP, 2013b; Fraser et al., 2014). Fraser et al. (2014) detected enhanced abundances of CCl_4 downwind of industrial waste sites in Melbourne (Australia) and provided evidence that significant amounts of CCl_4 could be emitted from contaminated soils, toxic waste treatment facilities, and possibly chlor-alkali production plants. This finding is also supported by de Blas et al. (2013), who observed similar enhancements at an industrial site in Spain. On the other hand, UNEP (2013b) reported that CCl_4 emissions from process agent use are small and declining (<1 Gg yr^{-1}). Although it is possible that unreported fugitive emissions (e.g., in the manufacture of polymers) exist (UNEP, 2013b), it is unlikely that these sources can explain the 30–70 Gg yr^{-1} discrepancy between the top-down and bottom-up emission estimates.

The contributions of regional CCl_4 sources to global emissions are not well known. This is particularly true for developing countries, since the density of long-term surface measurements in these countries is still low. For North America, CCl_4 emissions between 0 and 0.4 Gg yr^{-1} were derived from regional

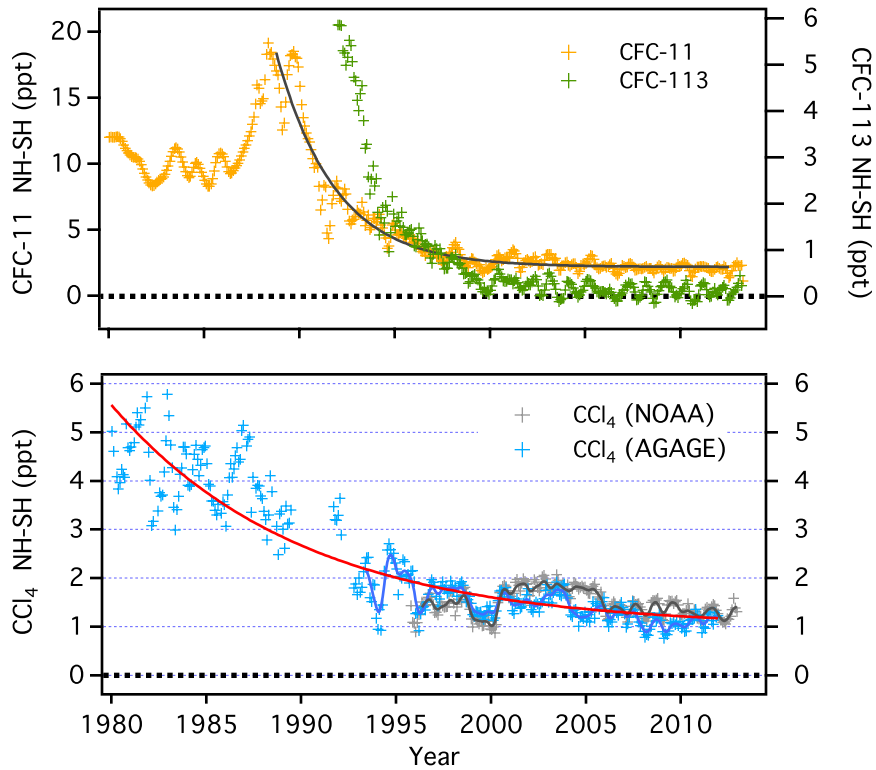

Figure 1-5. Trends in mean hemispheric mole fraction differences (NH minus SH ppt) for CFC-11 and CFC-113 (upper panel, NOAA data) and CCl_4 (lower panel; AGAGE data: blue symbols and blue line; NOAA data: gray symbols and black line). The red line is a fit to the AGAGE data.

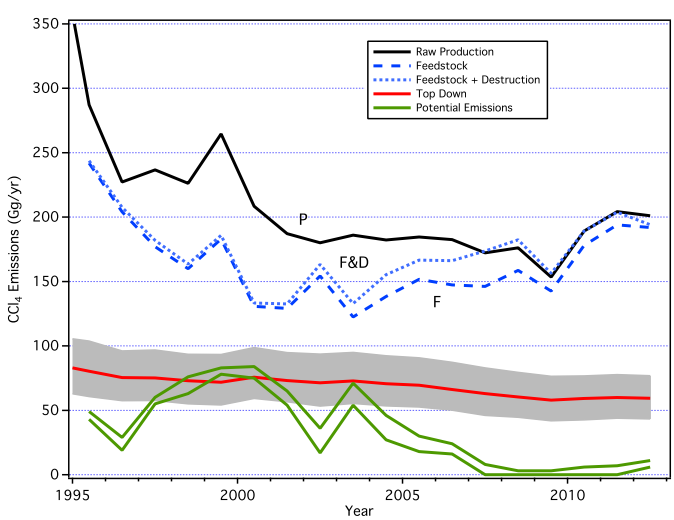

Figure 1-6. CCl_4 emissions derived from atmospheric measurements (red line and shading) and potential emissions estimated from production data (green lines). The lower potential emissions estimate (lower green line) was derived from the difference between total CCl_4 production reported to UNEP (solid black line labeled "P") and the sum of feedstock and amounts destroyed (dotted blue line labeled "F&D"), and also includes estimates of underreported feedstock production. The upper potential emissions estimate (upper green line) was derived similarly, but was augmented by fugitive emissions of 2% of reported CCl_4 feedstock use, and assuming an efficiency of only 75% for reported destruction. Production magnitudes related to feedstock alone are indicated with the dashed blue line labeled "F". Top-down estimates (red line) were derived using AGAGE data and a 12-box model as in Figure 1-2. The shaded region represents the uncertainty in the top-down emissions resulting from measurement uncertainty, prior emissions, and a range of lifetimes. A range of partial lifetimes with respect to stratospheric loss, loss to soils, and loss to the oceans, was considered. The mean total lifetime for CCl_4 was 26 years and the range was 22–32 years.

campaigns and extrapolated to the entire U.S. by Hurst et al. (2006), Millet et al. (2009), and Miller et al. (2012) between 2003 and 2009. Xiao et al. (2010a) used monthly means and their uncertainties from globally distributed sites and a global transport model to estimate emissions for several regions, constrained by the global total. They estimated CCl_4 emissions of 4.9 ± 1.4 Gg yr^{-1} for North America during 1995–2004. More significantly, their study indicated that S.E. Asia was responsible for ~53% (37–42 Gg yr^{-1}) of the average global CCl_4 emissions from 1996–2004. Palmer et al. (2003) (with a campaign downwind of China) and Vollmer et al. (2009) (with high-frequency observations at a site near Beijing) found that emissions from China in the early to mid-2000s were in the range of 15.0–17.6 Gg yr^{-1}, which is 20–25% of the global emissions estimated by top-down methods during that period. Furthermore, based on measurements at Cape Grim (Tasmania), Xiao et al. (2010a) and Fraser et al. (2014) estimated Australian CCl_4 emissions of 0.3–0.4 Gg in the late 1990s, declining to 0.1–0.2 Gg in the early 2010s.

In summary, the mismatch between bottom-up inventories and global top-down estimates of CCl_4 is still unresolved. There are, however, indications that some of the discrepancy could be explained by additional sources unrelated to reported production, such as contaminated soils and industrial waste (Fraser et al., 2014), although their global significance is highly uncertain. Additional explanations could include underreported emissions and incorrect partial lifetimes (stratosphere, ocean, or soil).

1.2.1.4 METHYL CHLOROFORM (CH_3CCl_3)

Observations

The global mole fraction of methyl chloroform (1,1,1-trichloroethane, CH_3CCl_3) has been declining steadily since reaching a maximum in the early 1990s (Figure 1-1). At ~5.4 ± 0.3 ppt in 2012, the global mean mole fraction is only 4% of its maximum. Thus, the contribution of CH_3CCl_3 to future changes in total Cl will likely be small. Atmospheric CH_3CCl_3 continues to be used to study the variability of the OH radical (Prinn et al., 2005; Montzka et al., 2011).

Lifetimes and emissions

Using atmospheric data and a global lifetime of 5.0 years (SPARC, 2013), global emissions of CH_3CCl_3 are estimated to have been < 10 Gg yr^{-1} since 2005 and decreased to ~2 Gg in 2012 (Figure 1-3). This behavior is consistent with the historical uses of this controlled chemical as a solvent, with generally rapid release to the atmosphere. However, small remaining banks and potential emissions from its feedstock usage could lead to ongoing emissions. Small but non-zero emissions have been reported for different years during the last decade for the U.S. (2.4–2.8 Gg yr^{-1}) by Millet et al. (2009) and Miller et al. (2012) as well as for China (1.7–3.3 Gg yr^{-1}) by Vollmer et al. (2009) and Li et al. (2011).

1.2.1.5 HYDROCHLOROFLUOROCARBONS (HCFCS)

Observations

The global surface mean mole fractions of the three most abundant hydrochlorofluorocarbons (HCFC-22, $CHClF_2$; HCFC-141b, CH_3CCl_2F; HCFC-142b, CH_3CClF_2) continue to increase (Table 1-1). However, the growth rates in 2012 differed significantly from those in 2008 (Figures 1-1, 1-7). Between 2008 and 2012 the growth rate declined by ~30% for HCFC-22 and by nearly 60% for HCFC-142b. In contrast, recent trends in HCFC-141b show a substantial increase (~70%) in the growth rate since 2008. Whereas the increase in HCFC-141b was anticipated under the A1-2010 scenario (Figure 1-1), the slower increases of HCFC-22 and HCFC-142b were not.

Trends in total column HCFC-22 are also available from remote sensing instruments (updated from Gardiner et al., 2008; Zander et al., 2008; Brown et al., 2011) and are similar to those derived from surface data (Table 1-2). On the other hand, trends for HCFC-142b and HCFC-141b derived from satellite observations (ACE-FTS) do not agree with those measured at the surface (Table 1-2). For HCFC-141b, the ACE-FTS column measurements are subject to interference from other trace gases, such as CFC-114

and HFC-23, particularly at lower altitudes (Brown et al., 2011), which may explain some of the discrepancy.

For HCFC-124 ($CHClFCF_3$) AGAGE measurements indicate a 9% decline in the global mole fraction between 2009 and 2012 (update of Prinn et al., 2000 and Miller et al., 2008). Laube et al. (2014) reported first measurements of HCFC-133a (CH_2ClCF_3), which is used in the production of pharmaceuticals and is an intermediate in HFC-134a production (Miller and Batchelor, 2012; UNEP, 2012). Mole fractions of HCFC-133a in the Southern Hemisphere increased slowly from the 1970s to 2003, then increased more rapidly from 2004 to 2008, and after a period of little change from 2008–2010, increased rapidly again to 0.365 ppt in 2012 (Laube et al., 2014; Figure 1-1 and Table 1-1).

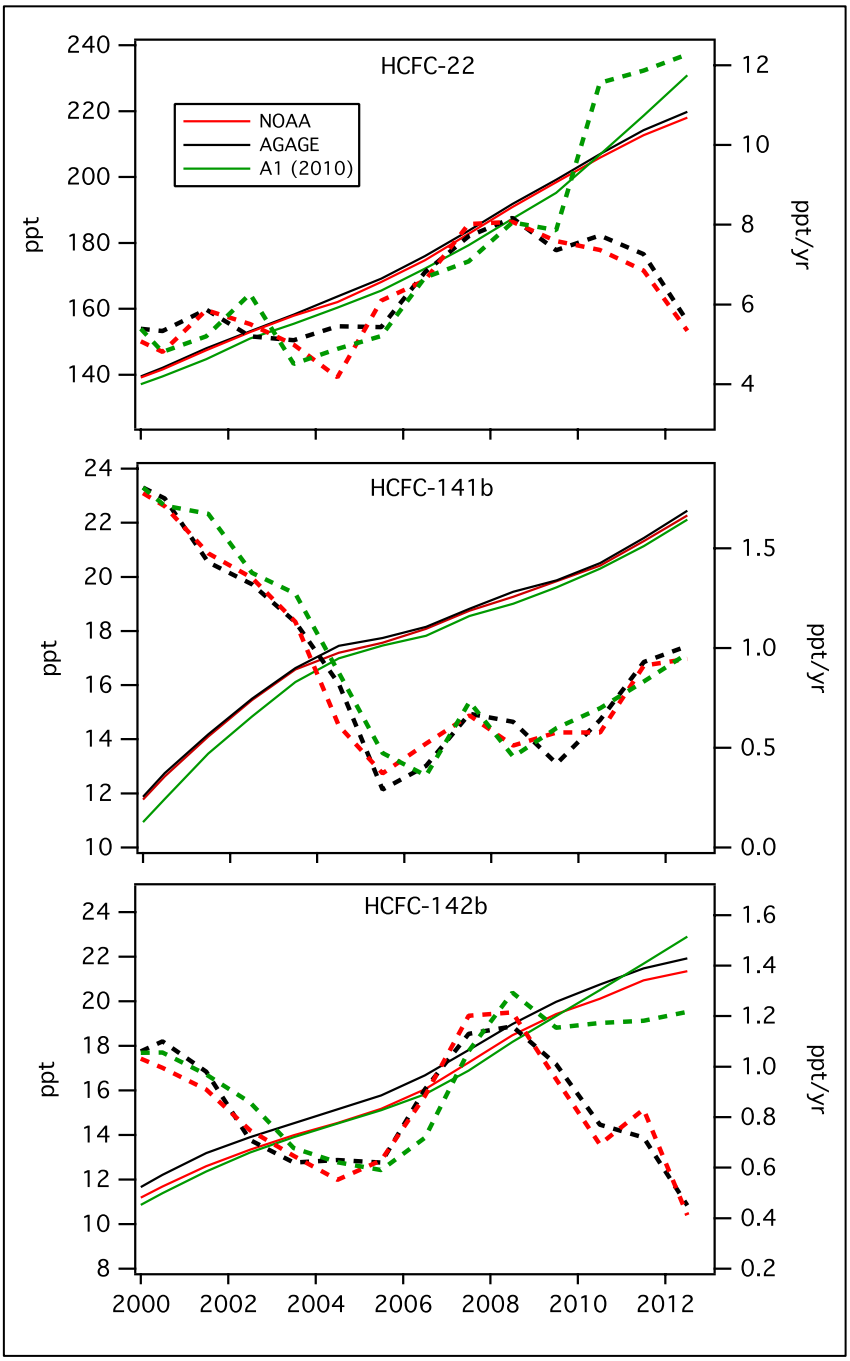

Figure 1-7. Recent trends for HCFC-22, HCFC-141b, and HCFC-142b estimated from AGAGE and NOAA global network data and the A1-2010 scenario: global mean mole fraction estimates (solid lines, left axis) and growth rates (dashed lines, right axis).

Lifetimes and emissions

With a large bank of HCFC-22 thought to exist in refrigeration systems, emissions are expected to continue, but should decline as new refrigerants are being adopted as a consequence of the freeze of HCFC production and consumption for dispersive uses in 2013 in developing (Article 5) countries. Global emissions of HCFC-22, calculated using surface measurements of HCFC-22, peaked in 2010 at 381 (331–431) Gg and were 366 (316–416) Gg in 2012 (Figure 1-3) (i.e., stable within the uncertainties).

The estimated lifetime of HCFC-142b was revised from 17.2 to 18.0 years (+5%) since the previous Assessment (SPARC, 2013). Global HCFC-142b emissions peaked at 39 (34–44) Gg yr^{-1} in 2008 and have since declined by 27% to 29 (23–34) Gg in 2012. This decline in emissions follows reduced production and consumption in non-Article 5 (non-A5) countries and a leveling off of production and consumption in Article 5 (A5) countries (Figure 1-8) (UNEP, 2014). Total global production in 2011 was only half that of 2009. On the other hand, feedstock use of HCFC-142b has increased markedly in recent years in both A5 and non-A5 countries. Emissions estimated from feedstock use vary, but are generally thought to be low (UNEP, 2013b).

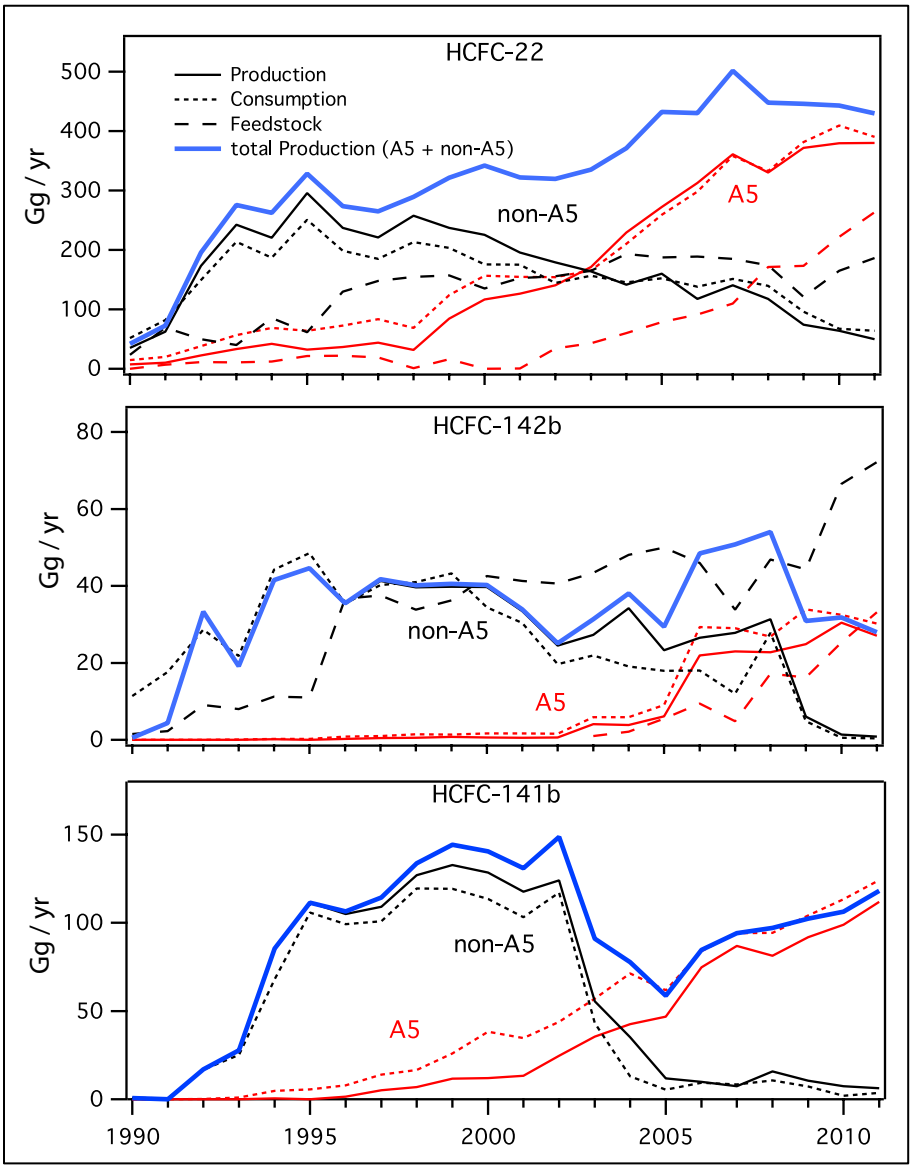

Figure 1-8. History of production, consumption, and feedstock use of HCFC-22, -142b, and -141b in Article 5 countries (red) and non-Article 5 countries (black) (UNEP, 2014). Total production (non-A5+A5) (blue) does not include feedstock production. Feedstock data for HCFC-141b are not shown because HCFC-141b feedstock use (15 Gg in 2010; UNEP, 2012) is thought to be small compared to that of HCFC-22 and HCFC-142b.

Current global HCFC-141b emissions are approaching the same level they were during peak production in the early 2000s (Figure 1-8). While production has decreased in non-A5 countries over the last decade, it has increased substantially in A5 countries since 2005 (UNEP, 2014). Regional studies indicate that China was responsible for about 15–30% of global HCFC-141b emissions in 2008–2009 (Wan et al., 2009; Stohl et al., 2010; Li et al., 2011; Fang et al., 2012).

Global and regional studies suggest a shift of HCFC emissions from midlatitudes to lower latitudes. Montzka et al. (2009) found a trend toward smaller intrahemispheric gradients as global emissions increased for HCFC-22, -141b, and -142b from 1996 to 2007. An updated gradient analysis using data through 2012 shows similar patterns to those described by Montzka et al. (2009), suggesting that recent shifts of production and consumption from non-A5 countries to A5 countries (Figure 1-8), which mostly are at lower latitudes, continue to be mirrored by higher emissions in these regions.

Recently, Saikawa et al. (2012) estimated regional HCFC-22 emissions between 1995 and 2009 using globally distributed surface data. They found a distinctive increase in emissions from Article 5 countries in Asia in recent years. A number of regional studies, along with bottom-up emission estimates and consideration of total HCFC production trends, suggest an increase in HCFC-22 emissions particularly from China in recent years (Figure 1-9) (Yokouchi et al., 2006; Stohl et al., 2010; Vollmer et al., 2009; Li et al., 2011; An et al., 2012; Fang et al., 2012). Apart from Vollmer et al. (2009) the temporal increase of the Chinese bottom-up emissions estimate from Wan et al. (2009) is consistent with several measurement-based studies (Figure 1-9). An et al. (2012) used an extension of the data set used by Vollmer et al. (2009) and found emissions that were comparable to those from Wan et al. (2009) (Figure 1-9). The reason for the difference between these two studies could be due to improvements in the regional transport simulation and in the inversion method used by An et al. (2012).

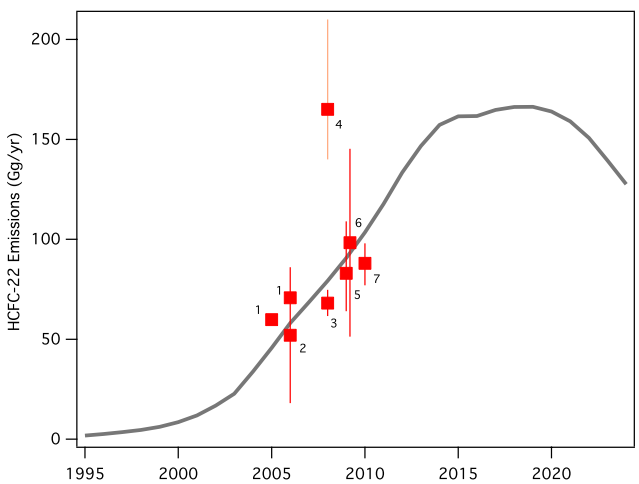

Figure 1-9. HCFC-22 emissions from China estimated by bottom-up (solid line; Wan et al., 2009) and top-down methods (filled squares): [1]Stohl et al. (2009); [2]Yokouchi et al. (2006); [3]Stohl et al. (2010); [4]Vollmer et al. (2009); [5]Li et al. (2011); [6]An et al. (2012); [7]Fang et al. (2012).

1.2.1.6 METHYL CHLORIDE (CH_3Cl)

Observations

The global surface mean mole fraction of methyl chloride (CH_3Cl) determined by the NOAA and AGAGE global networks was 540 ppt with a range from 537.1 to 542.2 ppt in 2012 (Table 1-1) and contributed ~16% to the total tropospheric chlorine. Only small changes were observed since the last Assessment, showing an enhanced interannual variability from 2011 to 2012 but an overall decline from 2008 to 2012 (Table 1-1, Figure 1-1).

Spatial and temporal variations in the distribution of CH_3Cl in the upper troposphere and stratosphere were assessed by Santee et al. (2013) using 8 years of Microwave Limb Sounder (MLS) satellite data. They found a correlation of enhanced CH_3Cl levels with regional biomass burning events, giving additional evidence for the importance of this highly fluctuating anthropogenically influenced source on the CH_3Cl budget.

Sources and sinks

While production and consumption of this primarily natural compound are not controlled by the Montreal Protocol, CH_3Cl shares many natural sources and sinks with CH_3Br, which is controlled. Sources of CH_3Cl include the ocean, biomass burning, fungi, salt marshes, wetlands, rice paddies, mangroves, and tropical forests (Table 1-4). As with CH_3Br, the budget for CH_3Cl remains unbalanced, with sinks outweighing sources (Table 1-4).

Since the last Assessment, the magnitude of the tropical source has been better defined. Individual studies have shown that tropical sources of CH_3Cl are significant. Saito et al. (2013) used an isotope tracer technique to separate the production of CH_3Cl from the degradation associated with tropical plants. They confirmed earlier studies (Yokouchi et al., 2002, 2007; Blei et al., 2010; Saito et al., 2008; Gebhardt et al., 2008) suggesting that tropical plants are a substantial net source of CH_3Cl. The modeling results of Xiao et al. (2010b) also suggest a substantial CH_3Cl source from the tropics. These studies together suggest an average tropical terrestrial flux of 2040 ± 610 Gg yr^{-1} (Table 1-4).

Sinks of CH_3Cl include reaction with hydroxyl radicals, uptake by soils, degradation in oceans, and photolysis in the stratosphere (Tables 1-3 and 1-4). Recently, Hu (2012) estimated a global soil uptake rate for CH_3Cl of 1058 (664–1482) Gg yr^{-1}. This rate was determined by scaling with the soil uptake rate for CH_3Br, as suggested by Rhew et al. (2011). The oceanic uptake and emission of CH_3Cl were recently revised by Hu et al. (2013) (Table 1-4), where the coastal ocean uptake and emissions were explicitly considered along with the open ocean fluxes and more degradation rate constant measurements.

1.2.1.7 METHYL BROMIDE (CH_3Br)

Observations

The global surface mean mole fraction of methyl bromide (CH_3Br) continued to decline since the last Assessment. The surface global mean mole fractions determined by NOAA and AGAGE networks was 7.0 ± 0.1 ppt in 2012 (Table 1-1). This represents a decline of around 25% from the 9.2 ppt observed in the mid-1990s (Yvon-Lewis et al., 2009). When data from ice core measurements from Butler et al. (1999), Saltzman et al. (2004), Trudinger et al. (2004), and Saltzman et al. (2008) are averaged, a natural background in the Southern Hemisphere of 5.5 ± 0.2 ppt results, which is consistent with the previous Assessment. Under the assumption that no natural interhemispheric gradient existed, this would signify that mole fractions of around 7 ppt in 2012 are still 27% above the natural background.

Sources and sinks

CH_3Br has both natural and anthropogenic sources. Our estimate of global sinks and sources for CH_3Br is not balanced, with known sinks outweighing known sources (Table 1-4). This imbalance persists from pre-phase-out (1995–1998) through the most recent years (Hu et al., 2012).

The primary anthropogenic source of CH_3Br has been from its use as a fumigant. Non-quarantine and pre-shipment (non-QPS) fumigation uses (mainly in agriculture) were the dominating anthropogenic source of atmospheric CH_3Br in the past, but are subject to phase-out and currently only limited amounts are still allowed for applications in critical-use exemptions. Quarantine and pre-shipment (QPS) uses, which are mainly related to pest control during transport and storage, are exempted from the phase-out and consumption from QPS uses was approximately stable in the last two decades (UNEP, 2014). Therefore, the declining atmospheric abundance of CH_3Br is the result of reductions in consumption for non-QPS uses (Figure 1-10). Accordingly, the non-QPS consumption became lower than the QPS consumption in 2009 and by 2012 it was only 43% of the QPS consumption, or 30% of the total fumigation use (Figure 1-10). Estimated emissions from non-QPS uses became lower than QPS uses after 2006, as emission factors are higher for QPS uses (84%) than for non-QPS uses (65%) (UNEP, 2007). These QPS/non-QPS uses do not include consumption as a chemical feedstock (Montzka and Reimann et al., 2011) or the application of CH_3Br as a transient in the conversion of methane to fuel (Ding et al., 2013), as CH_3Br is assumed to be released only in minor quantities from these processes.

Table 1-4. Sources and sinks for atmospheric CH_3Cl and CH_3Br in Gg yr^{-1} (adapted from Hu, 2012). The best values are shown with their possible ranges in parentheses. n.q. = not quantified. QPS = quarantine and pre-shipment. For CH_3Cl, figures represent the current knowledge. For CH_3Br changes in anthropogenic sources between 1995–1998 and 2012 are derived from reported information.

Source / Sink	CH_3Cl (Gg yr^{-1})	CH_3Br (Gg yr^{-1})	
		1995 – 1998	2012
SOURCES			
Anthropogenic Sources			
Leaded Gasoline	n.q.	3 (0.6–6)[18-21]	0–3
Coal Combustion; Waste Incineration; Industrial Activity	162 (29–295)[1]	n.q.	n.q.
Fumigation – QPS [a]	n.q.	8.1 (7.5–8.7)	7.4 (6.9–7.8)
Fumigation – non-QPS [b]	n.q.	39.9 (28.2–55.9)	2.5 (1.7–3.5)
Biomass Burning – Indoor Biofuel Use [c]	113 (56–169)	6 (3–9)	6 (3–9)
Biomass Burning – Open Field Burning [e]	355 (142–569)	17 (7–27) [d]	17 (7–27)
Ocean	700 (510–910)[2]	32 (22–44)[22]	32 (22–44)[22]
Terrestrial sources			
Tropical and Subtropical Plants; Tropical Leaf Litter [f]	2040 (1430–2650)[3-9]	n.q.	n.q.
Mangroves	12 (11–12)[10]	1.3 (1.2–1.3)[10]	1.3 (1.2–1.3)[10]
Rapeseed	n.q.	4.9 (3.8–5.8)[23]	5.1 (4.0–6.1)[23]
Fungus	145 (128–162)[7,11]	2.2 (1–5.7)[7,24]	2.2 (1–5.7)[7,24]
Salt Marshes	85 (1.1–170)[12,13]	7 (0.6–14)[26]	7 (0.6–14)[26]
Wetland	27 (5.5–48)[14,15]	0.6 (−0.1–1.3)[24]	0.6 (−0.1–1.3)[24]
Rice Paddies	3.7 (2.7–4.9)[16]	0.7 (0.1–1.7)[24]	0.7 (0.1–1.7)[24]
Shrublands	15 (9–21)[17]	0.7 (0.5–0.9)[17]	0.7 (0.5–0.9)[17]
Subtotal (Sources)	**3658**	**123**	**84**
SINKS [g]			
Reaction with OH [h]	2832 (2470–3420)	74 (63–83)	56 (48–63)
Loss in Soil	1058 (664–1482)	40 (25–54)	30 (19–41)
Loss in Ocean	370 (296–445)[2]	43 (27–58)[22]	33 (20–44) [22]
Loss in Stratosphere	146	5	4
Subtotal (Sinks)	**4406**	**162**	**123**
Net (Sources – Sinks)	**−748**	**−39**	**−39**

a. Data for fumigation — QPS consumptions of CH_3Br were downloaded from UNEP (http://ozone.unep.org/Data_Reporting/Data_Access) and the emission ratio is 84% (78%–90%) from UNEP (2007).

b. Data for fumigation — non-QPS consumptions of CH_3Br were downloaded from UNEP (http://ozone.unep.org/Data_Reporting/Data_Access) and the emission ratio is 65% (46%–91%) from UNEP (2007) and UNEP (2011c).

(continued next page)

Table 1-4, continued.

c. Emissions of indoor biofuel use were estimated based on the total dry matter burned for indoor biofuel use in 1995 (Yevich and Logan, 2003) and emission factors from Andreae and Merlet (2001).

d. Average biomass burning emissions were determined using the dry matter burned (van der Werf et al., 2010) and emission factors from Andreae and Merlet (2001).

e. Mean of observations with range of ±1σ.

f. Average value from Hu (2012).

g. For sinks, partial lifetimes from Table 1-3 were used. For the calculation of the atmospheric burden (B_a) the following equation was used: $B_a = \chi_a\ n_{tr}/r$, where χ_a is the sea-level mole fraction (CH_3Cl 540 ppt in 2012; CH_3Br 9.2 ppt in 1995-1998 and 7.0 ppt in 2012), n_{tr} is the number of moles in the troposphere (1.446×10^{20} moles), and r is the fraction of the total amount of the substance that resides in the troposphere (r = 0.95 for CH_3Br and 0.887 for CH_3Cl; Lal et al., 1994).

h. The sink due to the reaction with Cl-radicals is not included.

[1]McCulloch et al. (1999), [2]Hu et al. (2013), [3]Yokouchi et al. (2007), [4]Blei et al. (2010), [5]Saito et al. (2008), [6]Gebhardt et al. (2008), [7]Lee-Taylor et al. (2001), [8]Xiao et al. (2010b), [9]Yoshida et al. (2004), [10]Manley et al. (2007), [11]Watling and Harper (1998), [12]Rhew et al. (2000), [13]Cox et al. (2004), [14]Varner et al. (1999), [15]Dimmer et al. (2001), [16]Lee-Taylor and Redeker (2005), [17]Rhew et al. (2001), [18]Thomas et al. (1997), [19]Chen et al. (1999), [20]Baker et al. (1998), [21]Bertram and Kolowich (2000), [22] adapted from Hu et al. (2012) according to footnote g, [23]Mead et al. (2008), [24] Lee-Taylor and Holland (2000), [26]Montzka and Reimann et al. (2011).

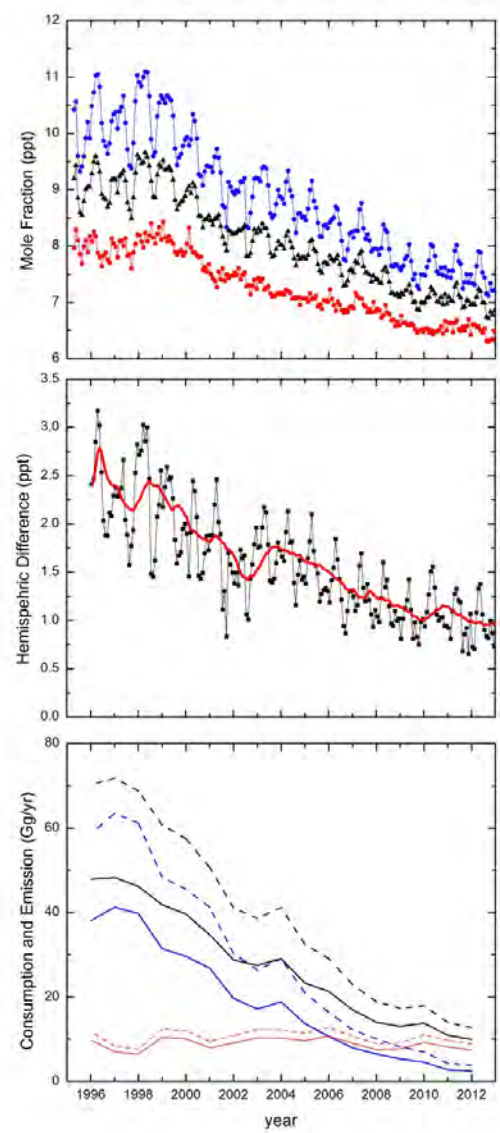

Figure 1-10. Upper panel: Trends since 1995 in methyl bromide (upper) mole fractions with NH (●) SH (■) and global (▲) NOAA data (Montzka et al., 2003, updated). Middle panel: Interhemispheric differences (NH−SH) as monthly means (•) and as a running average (—). Lower panel: consumption (dashed lines) as reported in the UNEP database (UNEP, 2014) for non-QPS uses (- - -), QPS uses (- - -) and total (- - -)., and emission (solid lines) from non-QPS uses (—), QPS uses (—) and total (—). Soil fumigation emission rates estimated as 65% (46–91%) of reported consumption rates (UNEP 2007). QPS emission rates estimated as 84% (78–90%) of reported consumption rates (UNEP 2007).

The total controlled and non-controlled fumigation emission is estimated to have accounted for 30 (22–40)% of the total global CH_3Br emissions during 1996–1998, before industrial production and consumption were reduced. By 2012, the total fumigation-related emissions, from controlled and non-controlled uses of CH_3Br, is estimated to have been reduced to 8 (7–10)% of the total global CH_3Br emissions.

Other anthropogenic sources of CH_3Br include the combustion of leaded gasoline, biomass burning, and emissions from certain crop species (e.g., canola/rapeseed, rice, mustard and cabbage) (references in Table 1-4). Biomass burning emissions are separated into open field burning, which can be anthropogenic or natural and indoor biofuel combustion (Yvon-Lewis et al., 2009; Hu, 2012). The combined burning emissions from these sources are comparable to the estimates in the previous Assessment (Table 1-4).

Natural sources of CH_3Br include the ocean, freshwater wetlands, fungus, tropical plants and leaf litter, and coastal saltmarshes (Table 1-4). Individual studies have shown that tropical sources are small or not significant (Gebhart et al., 2008; Blei et al., 2010). These studies were confirmed recently by Saito et al. (2013), who showed that the uptake of CH_3Br associated with tropical plants was nearly equal to its emission, resulting in only a small net source for CH_3Br from tropical plants. The variability in the magnitude of these tropical plant emissions has made them difficult to quantify over the global tropical region and they are therefore not included in the Table 1-4. An updated distribution of net fluxes from open and coastal oceans and of degradation rate constants has resulted in ocean emissions being revised downward from 42 Gg yr^{-1} (Montzka and Reimann et al., 2011) to 33 (20–44) Gg yr^{-1} (Table 1-4).

Since sink rates scale with the atmospheric burden, the rates of uptake by oceans, reaction with OH, photolysis, and soil microbial degradation continue to decline as the atmospheric concentrations have decreased (Table 1-4). In a recent study, Nilsson et al. (2013) proposed a significantly (~60%) faster reaction rate of CH_3Br with OH radicals than was recommended in SPARC (2013). However, due to the significant difference between the new reaction rate constant and the consistent values in the existing literature, no major change in the recommended rate constant could be justified. The rate constant recommended in SPARC (2013) is only slightly different from that used in previous Assessments. The partial CH_3Br lifetime with respect to reaction with OH and photolysis is 1.8 years, vs. 1.7 years in the previous Assessment. The partial lifetime for soil uptake, estimated at 3.35 years in the last Assessment, has been substantiated by results of Rhew et al. (2010) and Rhew (2011). The partial lifetime with respect to oceanic uptake has been revised upward to 3.1 (2.3–5.0) years (Hu et al., 2012) from the 2.2–2.4 years reported in the last Assessment based on Yvon-Lewis et al. (2009). However, when combined with the small reduction in the partial lifetime with respect to reaction with OH (discussed above) and the unchanged soil sink from the last Assessment, the overall lifetime remains unchanged at 0.8 years.

The reduction in the atmospheric abundance of CH_3Br since the time that the oceanic uptake rate was re-examined results in a lower uptake rate in Table 1-4 than that reported above by Hu et al. (2012). As a result of the decrease in atmospheric CH_3Br, the natural oceanic source is now comparable to the oceanic sink; this is consistent with the model prediction reported by Butler (1994) and Yvon-Lewis et al. (2009) and the near-equilibrium conditions observed in 2010 and reported by Hu et al. (2012).

1.3 VERY SHORT-LIVED HALOGENATED SUBSTANCES (VSLS)

As in previous Assessments, we consider VSLS to include very short-lived halogenated source gases (SGs), halogenated organic and inorganic product gases (PGs) arising from SG degradation, and other sources of tropospheric inorganic halogens.

Various lines of evidence suggest that VSLS may be transported from the boundary layer into the stratosphere, where they contribute to stratospheric halogen loading (Gettelman et al., 2009; Brioude et al., 2010; Montzka and Reimann et al., 2011; Marecal et al., 2012). Evaluating this contribution requires knowledge of VSLS tropospheric degradation and removal (Box 1-2), and the spatial and temporal variability of emissions, loss processes (Table 1-5), and transport processes (Box 1-3). These factors have consequences for the calculation of Ozone Depletion Potentials (ODPs) for VSLS, as the traditional concept of a single, geographically independent and time-independent value does not apply (Chapter 5: Section 5.3, Table 5-4).

Box 1-2. Atmospheric Chemistry of Very Short-Lived Ozone-Depleting Substances

For very short-lived (VSL) source gases (SGs), sinks include radical oxidation and photochemistry, resulting in typical mean local lifetimes of <6 months near Earth's surface (see Table 1-5). Photolysis of chlorinated SGs is slow and OH oxidation dominates tropospheric loss. Brominated SGs are removed by both OH oxidation and photolysis, with the latter more important for SGs containing multiple Br atoms (e.g., $CHBr_3$). Oxidation of SGs by Cl atoms is also possible but given the relatively low tropospheric abundance of Cl atoms (~10^3–10^4 molecules cm^{-3}) (Lawler et al., 2009), it is likely to be a relatively minor loss process for most SGs. Ultimately, the actual mean lifetime of a VSLS emission varies due to emission location/season, the distribution of tropospheric oxidants (e.g., Rex et al., 2014), and background conditions (e.g., temperature and solar flux). As SG lifetimes can be comparable to tropospheric transport timescales, the seasonal/spatial variability of transport processes (e.g., Aschmann et al., 2009) is also a key factor controlling stratospheric source gas injection (SGI).

Degradation of VSL SGs leads to a range of product gases (PGs), which may themselves be transported to the stratosphere via product gas injection (PGI). The breakdown of brominated and chlorinated SGs can lead to carbonyl compounds (e.g., CX_2O, CHXO) and minor products such as halogenated hydroperoxides (e.g., CHX_2OOH) or peroxynitrates (e.g., $CHX_2O_2NO_2$), where X=Br or Cl, the relative yield of which depends on background HO_x and NO_x loading (Krysztofiak et al., 2012). Once inorganic halogens are released, both gas-phase and heterogeneous reactions partition species among reactive (e.g., XO) and reservoir (e.g., HX) forms, controlling the fraction available for ozone destruction cycles or subject to tropospheric (dry/wet) deposition processes. Figure 1 highlights the principal reactions involved in the degradation of a typical tri-halogen SG, such as bromoform ($CHBr_3$). In global models, organic PG chemistry is generally bypassed as many of these species are short lived with respect to their parent SG. For example, CBr_2O and CHBrO have tropospheric lifetimes of ~7 and 2 days in the tropics, respectively (Hossaini et al., 2010). Therefore, instantaneous production of inorganic products is a reasonable approximation in the case of bromine (Sinnhuber and Folkins, 2006; Warwick et al., 2006a; Hossaini et al., 2010). PGI due to inorganic halogens may be enhanced by both multi-phase and heterogeneous reactions in/on liquid and frozen substrates (Crowley et al., 2010) that speciate halogens into radical form and thereby extend their lifetime against deposition processes (Aschmann and Sinnhuber, 2013).

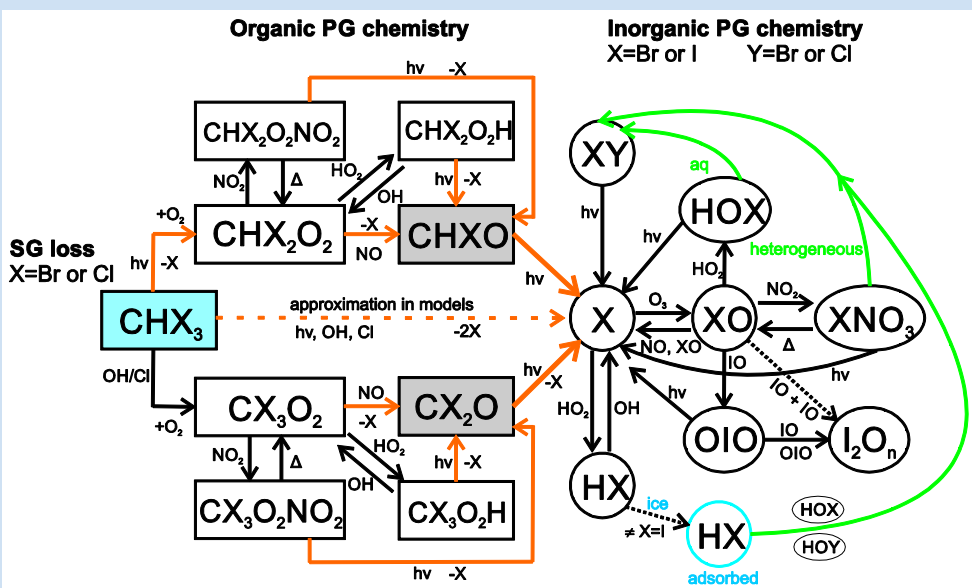

Box 1-2, Figure 1. The principal reactions involved in the degradation of a typical tri-halogen very short-lived source gas (blue shaded). The most stable organic intermediates are shaded gray. Orange arrows denote reactions that liberate halogen atoms. The approximation used in global models, that all three halogen atoms are released instantaneously on SG degradation, is denoted. Also shown are the primary gas-phase and heterogeneous reactions (green arrows) that cycle inorganic halogen species between active and reservoir forms. See also discussion in Ko and Poulet et al. (2003).

Box 1-3. Transport of Ozone-Depleting Substances to the Stratosphere in the Tropics

Ozone-depleting substances (ODSs) are transported to the stratosphere primarily in tropical regions where ascent through the troposphere is dominated by convection (Figure 1). Outflow from convective clouds, typically between 12–14 km (Folkins and Martin, 2005), can inject boundary layer air that may be rich in ODSs into the tropical tropopause layer (TTL) (e.g., Gettelman and Forster, 2002; Fueglistaler et al., 2009; Randel and Jensen, 2013). Here, over several kilometers, a transition occurs from the well-mixed, convectively dominated troposphere to a region of slow ascent controlled by the ascending branch of the stratospheric Brewer-Dobson circulation. The TTL is here defined as the layer between the level of maximum convective outflow (~12 km altitude, 345K potential temperature) and the cold-point tropopause (CPT, ~17 km, 380K). The level of zero radiative heating (LZRH) marks the transition from clear-sky radiative cooling to clear-sky radiative heating (Q_{clear}, ~15 km, 360K), and above which (in the "upper TTL") air masses may cross the CPT to enter the "tropical stratosphere" or "stratospheric overworld." For long lived and thus well-mixed halogenated source gases (see Section 1.2), the details of their troposphere-to-stratosphere transport are of minor importance. However, for very short-lived substances (VSLS), whose lifetimes may be comparable to tropospheric transport timescales, transport processes—along with physical and chemical processes that occur in the TTL—may strongly impact their stratospheric source gas and product gas injections.

The convective transport of air masses to the TTL is zonally asymmetric and exhibits significant seasonal and also interannual variability (e.g., Fueglistaler et al., 2004; Ashfold et al., 2012). Preferential transport into the TTL takes place in strong convective source regions. Examples include boreal winter over the Maritime Continent (e.g., Hosking et al., 2010; Bergman et al., 2012)—located within the tropical warm pool, between the Indian and Pacific Oceans—and also boreal summer within Indian monsoon regions (e.g., Devasthale and Grassl, 2009; Devasthale and Fueglistaler, 2010) and Southeast Asia (e.g., Wright et al., 2011; Chen et al., 2012). Air detrained into the lower TTL enters a region of large-scale subsidence and will mostly descend into the mid-troposphere. Air detrained above the LZRH can ascend through the upper TTL, where vertical velocities and residence times vary in both space and time. As zonal variation in these transport timescales can be large, the location at which air enters the TTL, along with its horizontal transport through regions of upwelling/downwelling in relation to the fluctuating LZRH, strongly impact transport into the stratosphere (e.g., Gettelman et al., 2004; Tzella and Legras, 2011; Bergman et al., 2012). In addition to these circulations, the TTL is also characterized by two-way exchange with the extratropics, which may strongly impact the abundance and seasonality of trace gases in the TTL, including ozone (e.g., Ploeger et al., 2012).

For particularly short-lived VSLS (i.e., those with a local lifetime of several days or less at the surface), significant transport to the upper TTL is unlikely unless emitted close to deep convection (Hossaini et al., 2012a). Residence times in this layer are estimated to be in the range of 24–45 days (Montzka and Reimann et al., 2011). For VSLS with comparable or shorter local lifetimes, significant source gas (SG) to product gas (PG) conversion could take place. If product gases are subsequently removed from this layer, for example due to adsorption onto cirrus ice followed by sedimentation, the net stratospheric input of halogen from VSLS will be reduced. Particularly deep overshooting convection can transport air masses directly up to or above the tropopause (e.g., Pommereau, 2010), providing rapid transport through the upper TTL. These events could allow even the shortest-lived VSLS to be transported to the stratospheric overworld, though they are relatively rare (Liu and Zipser, 2005; Takahashi and Luo, 2014) and at present their global-scale impact on stratospheric composition is uncertain. In addition to transport into the overworld, quasi-horizontal transport from the base of the TTL may provide a rapid transport route for VSLS to enter the extratropical lowermost stratosphere (i.e., above the tropopause but below the 380 K isentrope) (Levine et al., 2007). ***(continued next page)***

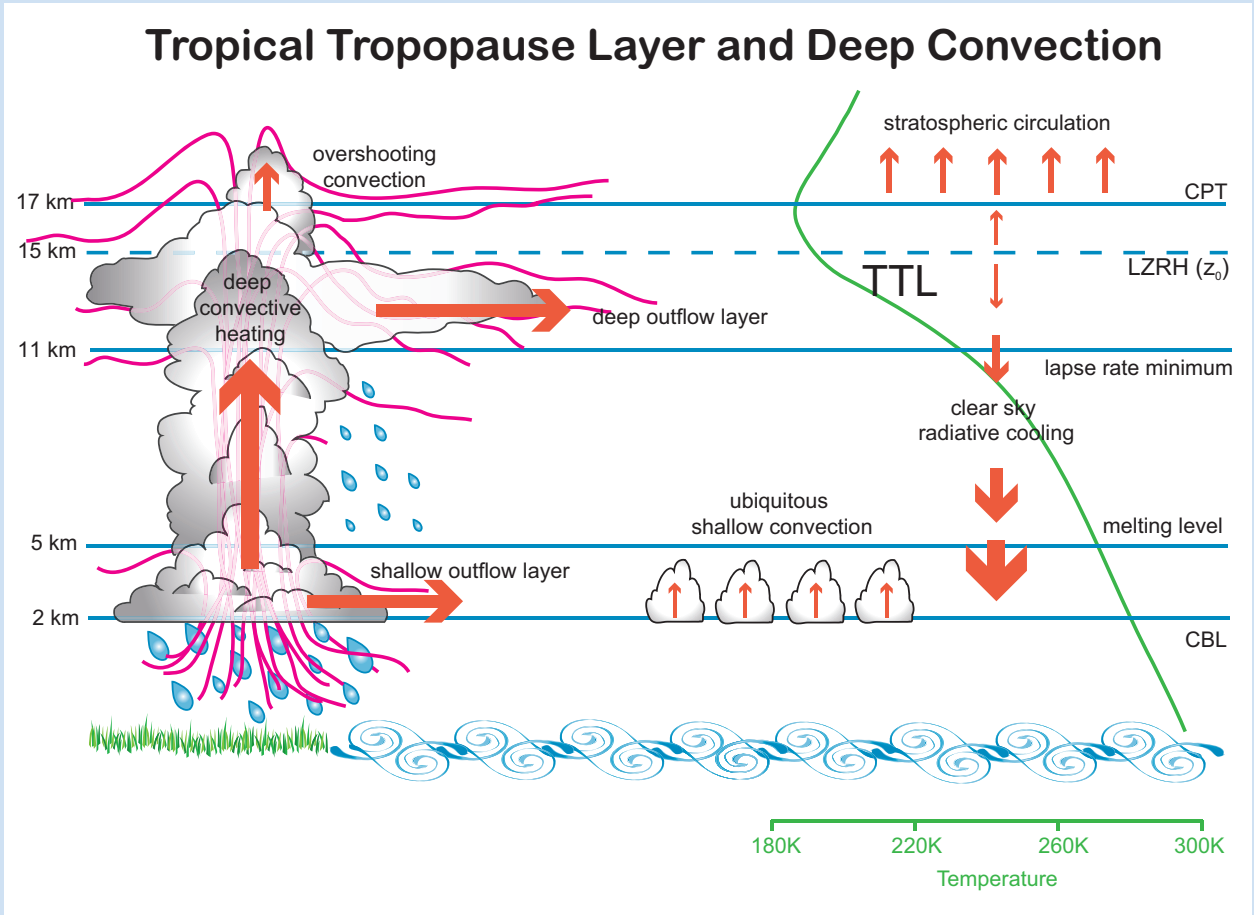

Box 1-3, Figure 1. Schematic of the convective boundary layer (CBL), tropical deep convection, and its interaction with the tropical tropopause layer (TTL). The temperature lapse rate minimum (typically between 10–12 km) is used to define the base of the TTL (taken here as 12 km) and the cold point tropopause (CPT) as the top (Gettelman and Forster, 2002). The level of zero radiative heating (LZRH, z_o) marks the transition from clear-sky radiative cooling to clear-sky radiative heating. The melting level indicates the altitude at which ice begins to melt. Red lines denote the redistribution of mass. Pink lines denote typical routes for tracer (e.g., VSLS) advection. A typical temperature profile is shown in green. Note, the arrow sizes are not representative of the relative importance of the various transport components. Figure courtesy of Diane Pendlebury (University of Toronto) and Thomas Birner (Colorado State University).

Table 1-5. Lifetime estimates for halogenated very short-lived (VSL) source gases. Local lifetimes for the tropospheric tropical and midlatitude regions were calculated using the OH and temperature climatology from Spivakovsky et al. (2000) and Prather and Remsberg (1993), respectively. Photolysis lifetimes were calculated using solar fluxes taken from the TOMCAT chemical transport model (e.g., Hossaini et al., 2012a). For the tropics, annually averaged values are reported along with the seasonal range of lifetimes given in parentheses. For midlatitudes, seasonally averaged local lifetimes (summer, fall, winter, spring) are reported. VSLS with new kinetic or photolysis laboratory studies available since the last Assessment are highlighted in bold, with local lifetimes calculated using the WMO (2011) method given in the footnotes.

Compound	WMO (2011) Local Lifetime (days) [1]	Loss Process	Local Lifetime [2] Tropics (25°S–25°N) (days)		Local Lifetime Midlatitude (25°N–65°N) (days)								Notes
			Boundary Layer	10 km	Boundary Layer				10 km				
					Su	F	W	Sp	Su	F	W	Sp	
Chlorocarbons													
CH_2Cl_2	144	OH	109 (98–133)	179 (171–185)	95	235	725	155	180	480	1070	430	3, 7
$CHCl_3$	149	OH	112 (100–136)	190 (182–197)	97	240	750	160	190	515	1145	460	4, 7
CH_3CH_2Cl	39	OH	30 (27–37)	47 (45–49)	26	65	200	43	47	125	280	111	5, 7
CH_2ClCH_2Cl	65	OH	47 (42–58)	90 (86–93)	41	103	320	69	90	250	555	225	4, 7
$CH_3CH_2CH_2Cl$	14	OH	11 (10–14)	14 (14–15)	10	24	70	15	14	37	80	32	5, 7
$CHClCCl_2$	4.9	OH	5 (4–6)	3 (3–4)	4	9	27	6	3	8	16	6	3, 7
CCl_2CCl_2	90	OH	67 (60–81)	119 (114–123)	58	145	450	96	120	325	725	290	3, 7
$CH_3CHClCH_3$	18	OH	15 (14–19)	17 (17–18)	13	32	95	21	17	44	95	38	5, 7
Bromocarbons													
CH_2Br_2	123	OH	94 (84–114)	150 (144–155)	80	200	620	135	150	405	890	360	3
	5000	*J*	–	–	–	–	–	–	–	–	–	–	
	123	*Total*	94 (84–114)	150 (144–155)	80	200	620	135	150	405	890	360	
$CHBr_3$	76	OH	40 (36–48)	46 (44–48)	34	84	250	54	45	117	250	101	6, 9
	36	*J*	23 (21–26)	27 (25–30)	25	59	130	33	28	70	135	40	
	24	*Total*	15 (13–17)	17 (16–18)	14	35	86	20	17	44	88	29	
CH_2BrCl	137	OH	103 (92–125)	174 (167–180)	89	220	685	147	175	470	1050	420	3, 7
$CHBrCl_2$	121	OH	65 (58–79)	82 (79–85)	56	137	410	89	81	210	460	185	6, 7
	222	*J*	108 (104–111)	114 (111–117)	120	305	610	160	130	300	550	165	
	78	*Total*	41 (37–46)	48 (46–49)	38	94	245	57	50	124	250	87	

(continued next page)

Compound	WMO (2011) Local Lifetime (days) [1]	Loss Process	Local Lifetime [2] Tropics (25°S–25°N) (days)		Local Lifetime Midlatitude (25°N–65°N) (days)								Notes
			Boundary Layer	10 km	Boundary Layer				10 km				
					Su	F	W	Sp	Su	F	W	Sp	
$CHBr_2Cl$	94	OH	50 (45–61)	59 (57–61)	43	105	310	67	58	150	325	130	6, 7
	161	*J*	91 (87–94)	55 (54–57)	120	360	820	170	72	195	415	97	
	59	*Total*	32 (30–37)	28 (28–29)	32	81	225	48	32	85	182	56	
CH_3CH_2Br	41	OH	32 (29–40)	45 (43–47)	28	69	210	45	45	118	260	103	3, 7
CH_2BrCH_2Br	70	OH	51 (46–62)	95 (91–99)	44	111	350	74	97	265	590	235	4, 7
n-C_3H_7Br	12.8	OH	11 (10–13)	12 (12–13)	9	23	67	15	12	30	65	26	3, 7
Iso-C_3H_7Br	16.7	OH	14 (13–17)	15 (15–16)	12	30	88	19	15	38	81	33	3, 7
Iodocarbons													
CH_3I	158	OH	114 (102–139)	223 (213–231)	99	250	780	165	230	620	1395	560	4
	7	*J*	4.2 (4.0–4.5)	3.6 (3.5–3.7)	4.3	9.6	19	5.6	3.5	7.5	13	4.6	
	7	*Total*	4.0 (3.8–4.3)	3.5 (3.4–3.6)	4.1	9.2	19	5.4	3.4	7.4	13	4.6	
CF_3I	4	*J*	0.97 (0.9–1.0)	0.85 (0.84–0.9)	0.9	2	4	1.1	0.7	1.6	2.9	1	3, 8
CH_3CH_2I	17.5	OH	16 (14–19)	14 (13–14)	14	33	94	21	13	34	71	28	4
	5	*J*	3.6 (3.3–3.8)	2.9 (2.8–2.9)	3.7	8.2	16.4	4.8	2.9	6.0	9.9	3.7	
	4	*Total*	2.9 (2.7–3.2)	2.4 (2.3–2.4)	2.9	6.6	13.9	3.9	2.4	5.1	8.7	3.3	

Notes:

1. Instantaneous local lifetimes for OH reactive loss were calculated with [OH] = 1×10^6 molecule cm^{-3} and T = 275 K; photolysis lifetimes taken from WMO (2011).
2. Annually averaged local lifetimes with the range in seasonal lifetimes given in parentheses.
3. OH reaction rate coefficient taken from JPL 10-6.
4. OH reaction rate coefficient taken from Atkinson et al. (2008).
5. OH reaction rate coefficient taken from Yujing and Mellouki (2001).
6. OH reaction rate coefficient taken from Orkin et al. (2013b); the instantaneous local lifetimes calculated as in WMO (2011) (see footnote 1) are 21 days (48 day OH reaction partial lifetime and 36 day partial lifetime for photolysis) for $CHBr_3$, 60 days for $CHBrCl_2$, and 80 days for $CHBr_2Cl$.
7. Photolysis is a negligible loss process; total local lifetime = local partial lifetime for OH reaction.
8. OH reaction is a negligible loss process; total local lifetime = local partial lifetime for photolysis.
9. Photolysis rates calculated using UV absorption cross sections from Papanastasiou et al. (2014); photolysis rates calculated using recommendations in Sander et al. (2011) are ~15% greater, see Papanastasiou et al. (2014).

1.3.1 Abundance, Trends, and Emissions of Very Short-Lived Source Gases

1.3.1.1 CHLORINE-CONTAINING VERY SHORT-LIVED SOURCE GASES

This section focuses on the chlorinated VSLS most widely reported in the background atmosphere, i.e., dichloromethane (CH_2Cl_2), trichloromethane ($CHCl_3$), tetrachloroethene (CCl_2CCl_2, shortened to C_2Cl_4), trichloroethene (C_2HCl_3), and 1,2-dichloroethane (CH_2ClCH_2Cl). Long-term global observations are available from the AGAGE (updated from O'Doherty et al., 2001, and Simmonds et al., 2006) and NOAA networks for CH_2Cl_2 and C_2Cl_4, and from AGAGE only for $CHCl_3$. Annual weighted sums of these globally distributed measurements are given in Table 1-6 and long-term trends are shown in Figure 1-11. It is notable that considerable differences exist between CH_2Cl_2 mole fractions reported by the two networks. These equate to an 11.2 ppt difference in tropospheric chlorine in 2012 (Table 1-6). Possible causes include differences in calibration scales and in measurement locations; the relatively short atmospheric lifetime of this compound (3–6 months in the tropics, Table 1-5) means that it shows large hemispheric and regional variability. However the observed relative growth in CH_2Cl_2 between 2001 and 2012 is comparable between the AGAGE (62%) and NOAA (67%) networks (i.e., during the period of onset of CH_2Cl_2 increases). In contrast, C_2Cl_4 abundances have decreased by 63% since the beginning of observations in 1994. AGAGE observations of C_2Cl_4 are only available from 2004 onward but both relative (−35%) and absolute (−0.6 ppt) changes compare well to NOAA trends in this period (−35%, −0.6 ppt).). For $CHCl_3$, no significant trends are apparent since the beginning of the record in 1994. Over the 5-year period between 2008 and 2012, we estimate that changes in the abundances of the three VSLS discussed above equate to an increase of 1.3 ± 0.2 ppt Cl yr^{-1}, and that total tropospheric chlorine from CH_2Cl_2, $CHCl_3$, CCl_2CCl_2, C_2HCl_3, and CH_2ClCH_2Cl increased from 84 (70–117) ppt to 91 (76–125) ppt, as shown in Table 1-7.

Other chlorinated VSLS such as vinyl chloride, 1,1-dichloroethane, 1,1-dichloroethene, 1,2-dichloropropane, 1,1,2-trichloroethane, 1,1,2,2-tetrachloroethane, hexachlorobutadiene, and chlorobenzene have been detected in urban air (e.g., Logue et al., 2010), but there is no observational evidence for these compounds in background air, the upper troposphere, or stratosphere.

Estimated global emissions for CH_2Cl_2, $CHCl_3$, and C_2Cl_4, calculated using a global 12-box model and using the observed mole fractions discussed above, are shown in Table 1-6. Emissions derived using either the NOAA or AGAGE observations (which have different station locations) are within the uncertainties of each other.

Table 1-6. Annual global mean mole fractions of chlorinated VSLS, and estimated emissions. Emissions from AGAGE and NOAA atmospheric data were calculated using a global 12-box model (Cunnold et al., 1983; Rigby et al., 2013, 2014), identical to the global emissions shown in Figure 1-3 for longer-lived ODSs.

Formula	Annual Mean Mole Fraction (ppt)			Growth (2011–2012)		Annual Global Emissions (Gg yr^{-1})			Laboratory
	2008	2011	2012	(ppt yr^{-1})	(% yr^{-1})	2008	2011	2012	
CH_2Cl_2	21.7	23.9	25.1	1.2	5.0	633 ± 142	681 ± 167	752 ± 177	AGAGE, in situ[1]
	24.8	28.4	30.7	2.3	8.1	709 ± 135	791 ± 182	841 ± 183	NOAA
$CHCl_3$	7.21	7.39	7.53	0.14	1.9	272 ± 51	277 ± 51	285 ± 53	AGAGE, in situ
C_2Cl_4	1.55	1.24	1.16	−0.08	−6.5	213 ± 40	167 ± 31	160 ± 30	AGAGE, in situ
	1.66	1.26	1.18	−0.08	−6.6	230 ± 50	164 ± 38	157 ± 33	NOAA

[1] AGAGE calibrations as specified in CDIAC (2014) and related primary publications.

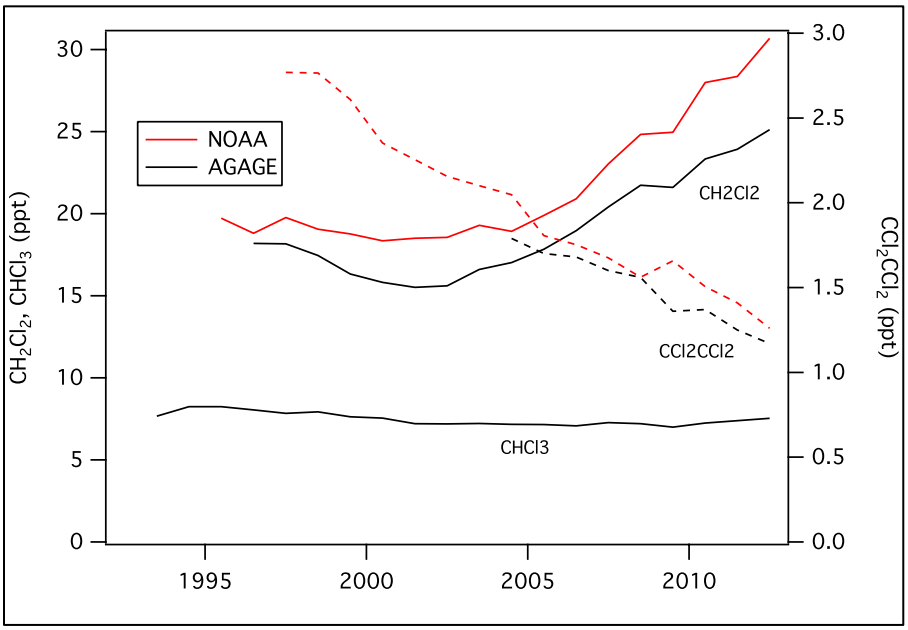

Figure 1-11. Global abundances of CH_2Cl_2, $CHCl_3$, and C_2Cl_4 as measured by the ground-based AGAGE (Simmonds et al., 2006, updated) and NOAA (Montzka et al., 2011, updated) networks. Global annual mean estimates were derived as weighted averages of monthly mean surface data from globally distributed observing sites (NOAA) and from the AGAGE 12-box model (AGAGE).

The atmospheric sources of chlorinated VSLS have been discussed in detail in Montzka and Reimann et al. (2011). In summary, anthropogenic emissions dominate strongly over natural sources with the exception of $CHCl_3$ and C_2H_5Cl. The anthropogenic emissions of $CHCl_3$ have been found to show a strong seasonality possibly affecting emission estimates (Gentner et al., 2010). Since the last Assessment various regional studies have confirmed anthropogenic and natural sources for chlorinated VSLS. For CH_2Cl_2, $CHCl_3$, C_2HCl_3, C_2Cl_4, and CH_2ClCH_2Cl, observation-based studies have reported emissions most likely related to industrial and commercial processes in North America (e.g., Millet et al., 2009; Russo et al., 2010; Miller et al., 2012) as well as East Asia (e.g., Shao et al., 2011; Xue et al., 2011; Bian et al., 2013). Natural sources including biomass burning ($CHCl_3$, C_2H_5Cl, and CH_2ClCH_2Cl), phytoplankton production (CH_2Cl_2), and soils ($CHCl_3$) such as drained peat land pasture soils or blanket peat bogs have also been reported (Simmonds et al., 2010; Ooki and Yokouchi, 2011; Simpson et al., 2011; Khan et al., 2012; Fraser et al., 2014). For $CHCl_3$ up to ~50% can be accounted for by anthropogenic sources (Trudinger et al., 2004; Worton et al., 2006). For C_2H_5Cl there are indications for both industrial and natural sources (e.g., Low et al., 2003; Simpson et al., 2011), but similar to C_2HCl_3 and CH_2ClCH_2Cl, no reliable global emission estimate is available to date.

1.3.1.2 Bromine-Containing Very Short-Lived Source Gases

Very short-lived brominated trihalomethanes (e.g., $CHBr_3$, $CHBrCl_2$, and $CHBr_2Cl$) and dibromomethane (CH_2Br_2) have primarily natural oceanic sources (Law and Sturges et al., 2007), with a small anthropogenic source from drinking water and cooling water chlorination for the trihalomethanes (Worton et al., 2006). There are also small anthropogenic sources of the VSLS 1-bromopropane (n-propyl bromide) and 1,2-dibromoethane (Montzka and Reimann et al., 2011); no new observations of these compounds have been reported since the last Assessment.

The atmospheric local lifetimes for $CHBr_3$, $CHBrCl_2$, and $CHBr_2Cl$ are revised from the previous Assessment (Table 1-5). This is due to new rate coefficient data for the OH reaction with $CHBr_3$, $CHBrCl_2$,

Table 1-7. Summary of observations of VSLS source gases from the marine boundary layer (MBL) to the tropical tropopause layer (TTL). All table entries are mole fractions, with units of parts per trillion (ppt). Note that many of the upper troposphere measurements were made at least one decade ago. For those gases that show trends (notably CH_2Cl_2 and CCl_2CCl_2), these data may no longer be appropriate for the present-day atmosphere. The mole fractions in the LZRH (used to derive the stratospheric input of VSLS chlorine source gases, see Table 1-9) have therefore been scaled to reflect their measured trends in the MBL; the new values are shown in bold. The scaling factor is the ratio of the current MBL mole fraction to that reported in the last Assessment (shown in italics in the MBL column), which are considered concurrent with the higher-altitude data.

	Marine Boundary Layer (MBL)		**Lower TTL**		**LZRH (z_0)[a]**		**Upper TTL**		**Tropical Tropopause**	
Height range			**12–14 km**		**14.5–15.5 km**		**15.5–16.5 km**		**16.5–17.5 km**	
Potential Temperature Range			**340–355 K**		**355–365 K**		**365–375 K**		**375–385 K**	
	Median[b]	**Range[c]**	**Mean[b]**	**Range[c]**	**Mean[b]**	**Range[c]**	**Mean[b]**	**Range[c]**	**Mean[b]**	**Range[c]**
CH_2Cl_2	28.4 (*17.5*)	21.8–34.4	17.1	7.8–38.1	14.3 (**23.2**)	10.8–27.8 (**17.5–27.8**)	13.2	9.8–28.6	12.6	7.2–30.4
$CHCl_3$	7.5	7.3–7.8	6.8	5.3–8.2	5.7	3.5–7.9	4.8	3.5–6.6	4.9	3.3–6.4
CH_2ClCH_2Cl	3.7	0.7–14.5	3.6	0.8–7.0	2.7	1.6–4.9	2.2	1.2–4.0	2.0	0.6–4.3
$CHClCCl_2$	0.5	0.05–2	0.08	0.0–0.7	0.03	0.00–0.17	0.02	0.00–0.05	0.03	0.00–0.17
CCl_2CCl_2	1.3 (*1.8*)	0.8–1.7	1.1	0.7–1.3	0.9 (**0.7**)	0.4–1.3 (**0.3–1.3**)	0.6	0.3–0.9	0.5	0.1–1.0
CH_2Br_2	0.9	0.6–1.7	0.89	0.6–1.2	0.74	0.59–0.99	0.66	0.43–0.83	0.52	0.3–0.86
$CHBr_3$	1.2	0.4–4.0	0.56	0.2–1.1	0.22	0.00–0.63	0.14	0.01–0.29	0.08	0.00–0.31
CH_2BrCl	0.10	0.07–0.12	0.12	0.13–0.16	0.10	0.06–0.13	0.11	0.1–0.12	0.07	0.05–0.11
$CHBr_2Cl$	0.3	0.1–0.8	0.11	0.04–0.26	0.06	0.03–0.11	0.05	0.01–0.11	0.02	0.00–0.14
$CHBrCl_2$	0.3	0.1–0.9	0.21	0.14–0.30	0.09	0.06–0.18	0.12	0.11–0.14	0.06	0.03–0.12
other brominated SG[d]					<0.2		<0.2		<0.2	
CH_3I	0.8	0.3–2.1	0.16	0.00–0.38	0.04	0.00–0.10	0.00	0.00–0.01	0.01	0.00–0.06
Total Cl	93.4[e] **91**[f]	70–134[e] **76–125**[f]	67	36–103	55 (**72**)	38–95 (**50–95**)	48	38–89	46	26–93
Anthrop. Cl[g]	76	55–115	48	22–96	39 (**64**)	27–72 (**34–85**)	34	24–68	32	17–73
Total Br	7.3	2.8–18.0	4.1	2.2–6.7	2.7	1.4–4.6	2.0	1.1–3.2	1.4	0.7–3.4
Total I	0.8	0.3–2.1	0.16	0.00–0.38	0.04	0.00–0.10	0.00	0.00–0.01	0.01	0.00–0.06

[a] LZRH(z_0) corresponds to the level of zero clear-sky radiative heating (see Box 1-3, Figure 1). As in the previous Assessment, this level is at about 15 km or 360 K, where there is a transition from clear-sky radiative cooling to clear-sky radiative heating. In general, air masses above this level are expected to enter the stratosphere.

[b] Note that calibration scales for VSLS differ among different research groups (see C.E. Jones et al., 2011; Hall et al., 2014). Abundances in the MBL are calculated from AGAGE and NOAA global 2012 data for CH_2Cl_2, $CHCl_3$, and CCl_2CCl_2, from the compilation of Ziska et al. (2013) for $CHBr_3$, CH_2Br_2, and CH_3I (20°N to 20°S), from Brinckmann et al. (2012) for CH_2BrCl, and from the last Assessment (Montzka and Reimann et al., 2011) for all other MBL data. Data in and above the upper troposphere have been compiled from observations during the PEM-Tropics A and B, TC4, Pre-AVE, and CR-AVE aircraft campaigns (Schauffler et al., 1999), from the SHIVA, HIPPO, and ATTREX aircraft campaigns (Tegtmeier et al., 2013), and from balloon observations (Laube et al., 2008, Brinckmann et al., 2012). See below for definition of field mission acronyms.

[c] The stated observed range represents the smallest mean minus 1 standard deviation and the largest mean plus 1 standard deviation.

[d] Estimated maximum contribution from species like C_2H_5Br, C_2H_4Br, and C_3H_7Br (Montzka and Reimann et al., 2011).

[e] Average median value and range.

[f] Mean value and range.

[g] The anthropogenic fraction of VSLS (Anthrop. Cl) has been calculated from the sum of 90% of CH_2Cl_2, 50% of $CHCl_3$, and 100% of CH_2ClCH_2Cl.

PEM-Tropics = Pacific Exploratory Missions-Tropics A (1996) and B (1999); TC4 = Tropical Composition, Cloud and Climate Coupling missions (2007); Pre-AVE = Pre-Aura Validation Experiment (2004); CR-AVE = Costa Rica-Aura Validation Experiment (2006); SHIVA = Stratospheric Ozone: Halogen Impacts in a Varying Atmosphere (SHIVA); HIPPO = HIAPER (High-Performance Instrumented Airborne Platform for Environmental Research) Pole-to-Pole Observations (2009–2011); ATTREX = Airborne Tropical Tropopause Experiment (2011).

and $CHBr_2Cl$ reported by Orkin et al. (2013b), measured over a more applicable temperature range than previous studies, and improved temperature-dependent UV absorption spectrum data for $CHBr_3$ reported by Papanastasiou et al. (2014). The new data result in a decrease of the calculated partial lifetime due to OH reaction for $CHBr_3$, $CHBrCl_2$, and $CHBr_2Cl$ by ~35% from those given in the previous Assessment, and an overall decrease in the atmospheric photolysis rate of $CHBr_3$ of the order of ~15% in the tropical troposphere, the region most critical for transport to the stratosphere. The combination of these new laboratory data implies that photolysis accounts for 50 to 70% of the $CHBr_3$ removal in the tropical troposphere (see Papanastasiou et al., 2014), which is less than obtained using the JPL10-6 recommendations used in the previous Assessment.

The relatively short local lifetimes of brominated VSLS, combined with spatially and temporally varying sources, means that determining global budgets for these gases requires extensive global-scale observations. For example, Ashfold et al. (2014) found that around two thirds of the measured $CHBr_3$ at a site in Borneo may be due to emissions in a region covering less than 1% of the tropics.

A number of emission estimates for brominated halocarbons have been reported since the last Assessment. Ziska et al. (2013) derived the first global climatology for $CHBr_3$ and CH_2Br_2 from a global database of measured halocarbon mole fractions, and determined a lower global flux of bromine from the oceans to the atmosphere than other estimates (Table 1-8). However the authors acknowledged that coastal (e.g., Carpenter et al., 2009; Liu et al., 2011) and other elevated emissions were likely underestimated in their climatology. Coastal VSLS emissions exhibit significant variability due to differing types and

Table 1-8. Fluxes of total bromine from bromoform ($CHBr_3$) and dibromomethane (CH_2Br_2) in Gg (Br) yr^{-1}, and iodine from methyl iodide (CH_3I) in Gg (I) yr^{-1}. Values in italics originate from regional studies while all other values are global studies.

Reference	$CHBr_3$ Flux (Gg Br yr^{-1})			CH_2Br_2 Flux (Gg Br yr^{-1})			CH_3I Flux (Gg I yr^{-1})		
	Global	Open Ocean	Coastal	Global	Open Ocean	Coastal	Global	Open Ocean	Coastal
Bell et al. (2002)							272		
Yokouchi et al. (2005)	*820* [a]								
Warwick et al. (2006a)[d,e]	560 [d]	280 [d]	280 [d]	100					
Butler et al. (2007)	800	150	650	280	50	230	550	270	280
Carpenter et al. (2009)			*200*						
O'Brien et al. (2009)	820 [a]								
Palmer and Reason (2009)		120 [c]							
Liang et al. (2010) [e]	430	260	170	57	34	23			
Jones et al. (2010) [f]							*300*	*240*	*60*
Youn et al. (2010)[g]							236		
Pyle et al. (2011)[h]	362								
Ordóñez et al. (2012) [e]	506			62			270		
Ziska et al. (2013) [i]	120–200			62–78			157–184		
Ashfold et al. (2014)	*213 (tropics only)*								
Liu et al. (2013) [j]		*19–304*			*9–62*				

[a] Scaled to CH_2Br_2 emissions from Ko and Poulet et al. (2003) based on global loss rates and an estimated global burden.
[b] Scaled to CH_2Br_2 emissions from Warwick et al. (2006b). [c] Tropical ocean only. [d] Modeling study: "Scenario 5": 70% of emissions in the tropics; August/September. [e] Top-down estimates based on modeling of airborne measurements primarily in the Pacific and North American troposphere and lower stratosphere. CH_3I estimate based upon Bell et al. (2002) inventory.
[f] Bottom-up estimate from north and tropical Atlantic data only. "Coastal" CH_3I emissions include shelf and upwelling fluxes.
[g] Based upon Bell et al. (2002) global inventory. [h] Update of "Scenario 5" from Warwick et al. (2006b). South East Asian emissions scaled to give better agreement with ground-based observations. [i] Net flux (source – sink) reported in Ziska et al. (2013) based on compiled sea-air flux data from the Halocat database (https://halocat.geomar.de/). Range represents global extrapolation of data using the robust fit (lower) or ordinary least squares (upper) technique. [j] Extrapolated global open ocean fluxes reported by (Liu et al., 2013) are based on 5 cruises in the Atlantic.

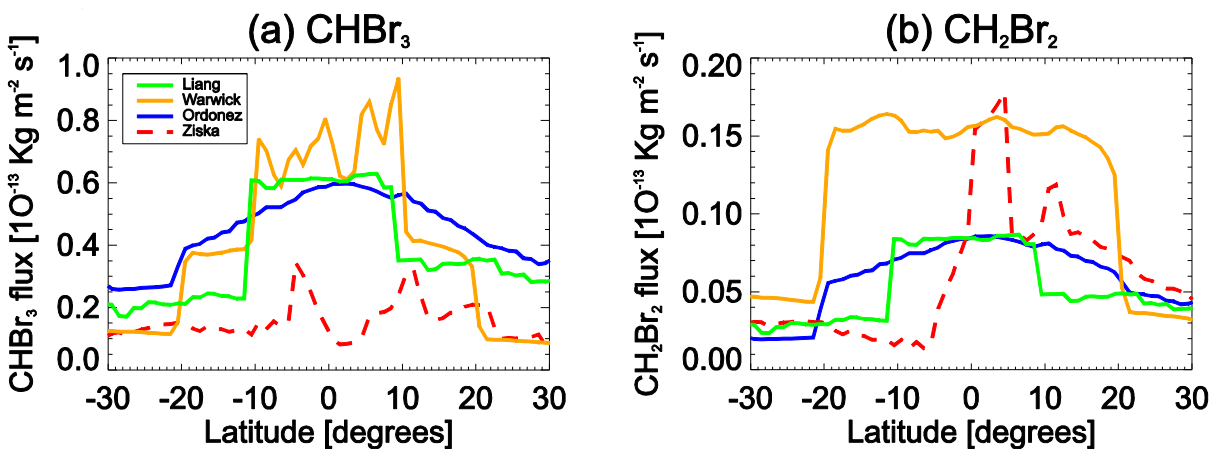

Figure 1-12. Latitudinal dependence of zonally averaged (a) $CHBr_3$ and (b) CH_2Br_2 emissions (10^{-13} kg m^{-2} s^{-1}) between 30°N and 30°S from recent top-down emission inventories (Warwick et al., 2006a [updated in Pyle et al., 2011]; Liang et al., 2010; Ordoñez et al., 2012) and bottom-up derived emission inventories (Ziska et al., 2013). The figure is modified from Hossaini et al. (2013).

amounts of macroalgae (Leedham et al., 2013), thus global extrapolation of coastal emissions is subject to high uncertainty. Liu et al. (2013) suggested that the Atlantic Ocean has comparable or possibly higher Br VSLS seawater concentrations than the Pacific Ocean, in contrast to an earlier study (Butler et al., 2007). These differing results may be due to differences in the locations of the observations and amount of data from each region. Several authors (e.g., Mattsson et al., 2013; Ziska et al., 2013) have also noted the existence of negative saturation anomalies (i.e., net flux from the atmosphere to the ocean) for $CHBr_3$ and CH_2Br_2, mostly in polar seas. Sparse data in these regions means that they may not be properly accounted for in global emission estimates. Although studies have attempted to map VSLS emissions by linking them to chlorophyll *a* (Ordoñez et al., 2012), brominated VSLS in seawater do not exhibit robust relationships with oceanic pigments (Roy, 2010; Roy et al., 2011; He et al., 2013), likely due to complex production mechanisms and interconversion processes (Lin and Manley, 2012; Hughes et al., 2013; Wever and van der Horst, 2013).

Ordoñez et al. (2012) assessed the ocean fluxes of $CHBr_3$ and CH_2Br_2 using a global chemistry-climate model combined with surface and aircraft observations. Global estimates were in the range of previous top-down emission estimates (e.g., Warwick et al., 2006a; Liang et al., 2010; Ordoñez et al., 2012) (Table 1-8). Hossaini et al. (2013) evaluated four global emission estimates, and found that no single inventory provided a satisfactory match between model and observations in all locations. For the tropics, the relatively low emissions of Ziska et al. (2013) provided the best fit with the limited available data. Discrepancies between top-down and bottom-up emission inventories (Figure 1-12 and Table 1-8) indicate that there are still insufficient data to constrain VSLS budgets to within a factor of 2–3.

1.3.1.3 Iodine-Containing Very Short-Lived Source Gases

Methyl iodide (CH_3I)

The ocean contributes over 80% of global CH_3I emissions with small contributions from rice production and other land sources (Redeker et al., 2000; Bell et al., 2002, Youn et al., 2010). Known oceanic production processes include photochemical degradation of organic matter in seawater (e.g., (Richter and Wallace, 2004) and phytoplankton production (e.g., Brownell et al., 2010). Observed surface seawater concentrations of CH_3I show best agreement with global model simulations that include a photochemical production pathway or both a photochemical and biological production pathway (Stemmler et al., 2013). CH_3I has potential anthropogenic sources since it is registered as a pesticide (as a replacement for CH_3Br) in a number of countries including the U.S., Japan, and Mexico. However the manufacturer has withdrawn it from the U.S. market.

Long-term time-series from the late 1990s of atmospheric CH_3I from several remote marine sites are now available (Yokouchi et al., 2012) and show a decreasing trend before 2003, but increases in CH_3I from 2003/2004 to 2009/2010 by several tens of percent. The interannual variation was linked with the Pacific Decadal Oscillation (PDO), suggesting that CH_3I emissions are affected by global-scale sea surface temperature oscillations (Yokouchi et al., 2012). Seasonally, CH_3I atmospheric mole fractions at remote marine locations outside of the polar regions tend to maximize in summer (Archer et al., 2007; Yokouchi et al., 2011, 2012), whereas winter maxima are observed in the Arctic due to long-range transport and slower atmospheric photooxidation (Yokouchi et al., 2012).

Globally, CH_3I emissions are not well constrained (Table 1-8). Recent top-down model estimates (Youn et al., 2010; Ordoñez et al., 2012), based on the CH_3I emission distribution of Bell et al. (2002), are about a factor of two lower than the global bottom-up estimate of Butler et al. (2007). While these model studies showed good agreement between simulated and observed marine boundary layer (MBL) mole fractions in some locations, there were regional discrepancies, indicating uncertain sources or sinks and/or model meteorology. A new global climatology (Ziska et al., 2013) has been calculated by interpolating available data onto a 1° × 1° grid, and results in even lower emissions of 158–184 Gg I yr^{-1}, depending on the fit used. The approach used may underrepresent locally elevated emissions. Quantifying emissions is challenging because oceanic and atmospheric abundances vary significantly in space and time, and there are also differences between measurement calibrations (up to about a factor of 2) (C.E. Jones et al., 2011) used by different research groups, although these are not as large as discrepancies in emission estimates.

Other iodine-containing VSLS

Recent observations indicate that the combined ocean-to-atmosphere flux of iodine-containing dihalomethanes (CH_2ICl, CH_2IBr, and CH_2I_2) provides a global iodine source of ~330 ± 190 Gg I yr^{-1}, comparable to that of CH_3I (Table 1-8), and a surface iodine atom source 3–4 times higher than CH_3I due to the rapid photolysis rates of these compounds (Jones et al., 2010). A number of studies have shown however that total organic iodine—including CH_3I, CH_2ICl, CH_2IBr, and CH_2I_2—cannot account for observations of IO in the MBL (Jones et al., 2010; Mahajan et al., 2010; Mahajan et al., 2012; Großmann et al., 2013), as they contribute only about 20% of the necessary reactive iodine flux. Laboratory measurements suggest that instead, inorganic emissions, namely I_2 and HOI (Carpenter et al., 2013), are the dominant contributors to MBL reactive iodine chemistry. These compounds are too reactive to be transported out of the MBL, though will be important contributors to particulate iodine, which has been observed in the upper troposphere and lower stratosphere (Murphy and Thomson, 2000).

1.3.2 Dynamics and Transport of VSLS

The last Assessment contained a comprehensive discussion of relevant dynamical processes controlling the transport of VSLS from the boundary layer (BL) to the tropical tropopause layer (TTL) and from the TTL into the stratosphere. Since then, theoretical and modeling studies have been performed that additionally constrain our understanding of the location and magnitude of the troposphere-stratosphere transport of VSLS, the relative importance of source gas injection (SGI) versus product gas injection (PGI), and the total contribution of VSLS to stratospheric bromine, chlorine, and iodine; also, new observations of both very short-lived source gases (SGs) and product gases (PGs) have been made.

Models continue to implicate the Maritime Continent as a strong convective source region where VSLS may be transported to the stratosphere rapidly (Levine et al., 2007; Aschmann et al., 2009; Pisso et al., 2010; Ashfold et al., 2012). However, uncertainties in parameterization of the boundary layer and convective transport (Hoyle et al., 2011; Schofield et al., 2011; Liang et al., 2014) limit the ability of models to calculate absolute amounts of VSLS reaching the stratosphere. The representation of very deep convection that penetrates the tropical tropopause (Liu and Zipser, 2005) is limited in global models (Hosking et al., 2010; Feng et al., 2011). A key constraint on the stratospheric SGI of VSLS is whether regions with particularly high surface mixing ratios are also preferred source regions for stratospheric air,

or whether a VSLS is sufficiently long-lived to be transported into these regions. Because transport processes also vary seasonally, the ODP (Ozone Depletion Potential; see Chapter 5) of a VSLS is dependent on both emission location and season (Pisso et al., 2010; Brioude et al., 2010).

Lagrangian transport calculations, combined with observed sea-to-air fluxes of VSLS in the Maritime Continent, have been used to infer the magnitudes of stratospheric SGI and PGI from $CHBr_3$, CH_2Br_2, and CH_3I (Tegtmeier et al., 2012, 2013). These results suggest sporadic injections of halogens from VSLS above the tropopause that are an order of magnitude larger than the global mean. These rare enhancements are highly localized in space and time and thus not representative of the global scale. However, they highlight a large variance that is not captured by coarse global-scale models. The "snap-shot" nature of observations during individual field campaigns makes an assessment of the relative importance of various geographical regions challenging. For VSLS, this is exacerbated by uncertainties in the magnitude of tropical emissions and how they are distributed with respect to convectively active regions. Based on global model simulations, Liang et al. (2014) found that the largest stratospheric input of bromine from VSLS occurred over the tropical Indian Ocean, where the modeled surface mixing ratio of $CHBr_3$ and CH_2Br_2 was large. Critically, these results depend on the validity of assumed surface emissions which, in sparsely sampled regions such as the Indian Ocean, are difficult to verify.

Interannual variability of VSLS troposphere-stratosphere transport is likely related to phases of the El Niño-Southern Oscillation (ENSO), through its impact on sea surface temperature (SST) (Aschmann et al., 2011; Ashfold et al., 2012). Using a model driven by offline meteorological analyses, Aschmann et al. (2011) reported 20% more $CHBr_3$ and 6% more CH_2Br_2 reaching the stratosphere during a strong El Niño event (relative to an ENSO-neutral year). While enhanced SGI is expected to be positively correlated with convective activity, PGI may be anticorrelated because inorganic PGs (e.g., HBr) are highly soluble and can be physically removed from the troposphere in convective rainfall. Liang et al. (2014) suggest that the net transport of bromine from VSLS into the stratosphere is largest under low convective conditions, because the associated increase in PGI (2–3 ppt) greatly exceeds the minor reduction in SGI.

1.3.2.1 SOURCE GAS INJECTION (SGI)

Source gases deliver halogens to the stratosphere in the same form as they were emitted at the surface. For a given SG, the efficiency of SGI is determined by its tropospheric loss rate versus timescales for troposphere-to-stratosphere transport. New aircraft observations of VSL SGs, especially the brominated gases, have been reported in tropical regions. These include observations from five aircraft missions spanning the global troposphere over different seasons and multiple years: HIAPER (High-performance Instrumented Airborne Platform for Environmental Research) Pole-to-Pole Observations (HIPPO 1–5) campaigns, 2009–2011; the Stratospheric Ozone: Halogen Impacts in a Varying Atmosphere (SHIVA) campaign in 2011, located in the previously poorly-sampled Maritime Continent region; and CARIBIC flights over the West Atlantic, Africa, and Southeast Asia. Aircraft observations during these campaigns were made at altitudes up to the lower TTL. Higher-altitude observations around the tropical tropopause have been made during the ongoing NASA Airborne Tropical Tropopause Experiment (ATTREX) campaign. These compiled data are reported in Table 1-7.

SGI from chlorinated VSLS

The majority of upper tropospheric data for the chlorinated VSLS shown in Table 1-7 were measured around a decade ago. Taken together with the surface data, the measurements apparently indicate a strong vertical gradient of CH_2Cl_2 within the troposphere, which is inconsistent with its relatively long lifetime compared to the analogous brominated SGs (see Table 1-5). The reason for this is most likely the temporal disparity between the (current) surface data and the higher-altitude data. Recent data from the HIPPO 1–5 campaign (Wofsy et al., 2011) show mean CH_2Cl_2 mixing ratios in the lower TTL of 23.5 (14.8–49.8) ppt, larger than the range of 14.9 (11.7–18.4) ppt reported in the last Assessment. The $CHCl_3$ mean mixing ratio in the lower TTL was 6.0 (4.7–8.2) ppt, within the range of

7.1 (5.9–9.2) ppt reported previously. No new observations of chlorinated VSLS have been reported above the level of zero radiative heating (LZRH), where previous measurements suggested a SGI of 55 (38–80) ppt of chlorine from VSLS (Montzka and Reimann et al., 2011). For CH_2Cl_2 and C_2Cl_4, gases that show observable trends in the boundary layer (Figure 1-11), we therefore scale mole fractions around the LZRH by the ratio of current MBL abundances to those reported in the last Assessment, which were concurrent with the compiled upper tropospheric data. We therefore suggest an increase in the VSLS chlorine SGI from 55 ppt to 72 (50–95) ppt, to take into account likely increases in CH_2Cl_2 abundances near the tropopause.

SGI from brominated VSLS

The estimated stratospheric SGI of bromine from VSLS, based on available observations around the tropical tropopause, is unchanged since the last Assessment (Table 1-7). Observations of the major brominated VSLS, $CHBr_3$ and CH_2Br_2, during HIPPO 1–5 show tropical mean mole fractions of 0.47 (0.14–1.13) ppt and 0.84 (0.58–1.09) ppt in the lower TTL, respectively. These values are generally in close agreement with the compiled mean and range reported in the last Assessment. Over Borneo, aircraft observations made during the SHIVA campaign show a total of 4.35 (±0.6) ppt of organic bromine from $CHBr_3$, CH_2Br_2, CH_2BrCl, $CHBr_2Cl$, and $CHBrCl_2$ at approximately 12 km (Sala et al., 2014). Similarly, a total of 4.2 ppt was obtained at 10–13 km from observations of the same suite of VSLS made during CARIBIC flights over Southeast Asia (Wisher et al., 2014). These estimates are in close agreement with the 4.3 (2.8–6.5) ppt of organic bromine reported in the last Assessment. At higher altitudes, in 2008 Brinckmann et al. (2012) reported balloon-borne observations of these five VSLS over Teresina, Brazil, up to the tropical tropopause. Around the LZRH, total organic bromine from VSLS was observed to be 2.25 ppt, in reasonable agreement with the 2.7 (1.4–4.6) ppt reported in the last Assessment. At 17.5 km, total organic bromine from VSLS was observed to be 1.35 ppt and thus within the previously reported range of 0.7–3.4 ppt.

Global model simulations suggest SGI contributes on average ~50% and ~90% of the total bromine reaching the stratosphere from $CHBr_3$ and CH_2Br_2, respectively (Aschmann et al., 2011; Hossaini et al., 2012a). Somewhat lower estimates of 21% ($CHBr_3$) and 74% (CH_2Br_2) were derived from a single set of balloon-borne observations (Brinckmann et al., 2012). For global models, explicit representation of SGI requires a sound treatment of VSLS emissions. The modeled contribution of VSLS to stratospheric bromine has been shown to vary by a factor of ~2 (Hossaini et al., 2013) when using the different available emission inventories (Liang et al., 2010; Pyle et al., 2011; Ordoñez et al., 2012; Ziska et al., 2013).

The proximity of emissions to convective source regions likely leads to geographical variation in SGI efficiency (Aschmann et al., 2009; Tegtmeier et al., 2012, 2013). The spatial distribution and seasonality of the primary tropospheric oxidant, the hydroxyl radical (OH), also leads to a significant variation in the lifetimes of less photolabile VSLS (Table 1-5). Over the West Pacific warm pool, an [OH] minimum has been inferred (Rex et al., 2014) based on reported low levels of tropospheric ozone from sonde, satellite, and aircraft data, in qualitative agreement with earlier observations (e.g., Kley et al., 1996). The lifetime of CH_2Br_2 was calculated to be up to a factor of 3 longer within this "OH hole" relative to typical Atlantic conditions (Figure 1-13), suggesting that regionally, a larger fraction of CH_2Br_2 may escape tropospheric oxidation to reach the TTL over the warm pool. Once in the TTL, the local lifetime of CH_2Br_2 can be long (~500 days) due to the strong temperature dependence of the CH_2Br_2 + OH reaction, meaning stratospheric SGI is likely (Hossaini et al., 2010). Future changes to tropospheric [OH], for example due to a projected methane increase/decrease, could alter the local lifetime and SGI of CH_2Br_2 substantially (Hossaini et al., 2012b) (Figure 1-14).

SGI from iodinated VSLS

Available high-altitude CH_3I observations in the last Assessment showed that mixing ratios in the TTL at 15 km were generally below 0.1 ppt, leading to the conclusion that no more than 0.05 ppt of iodine

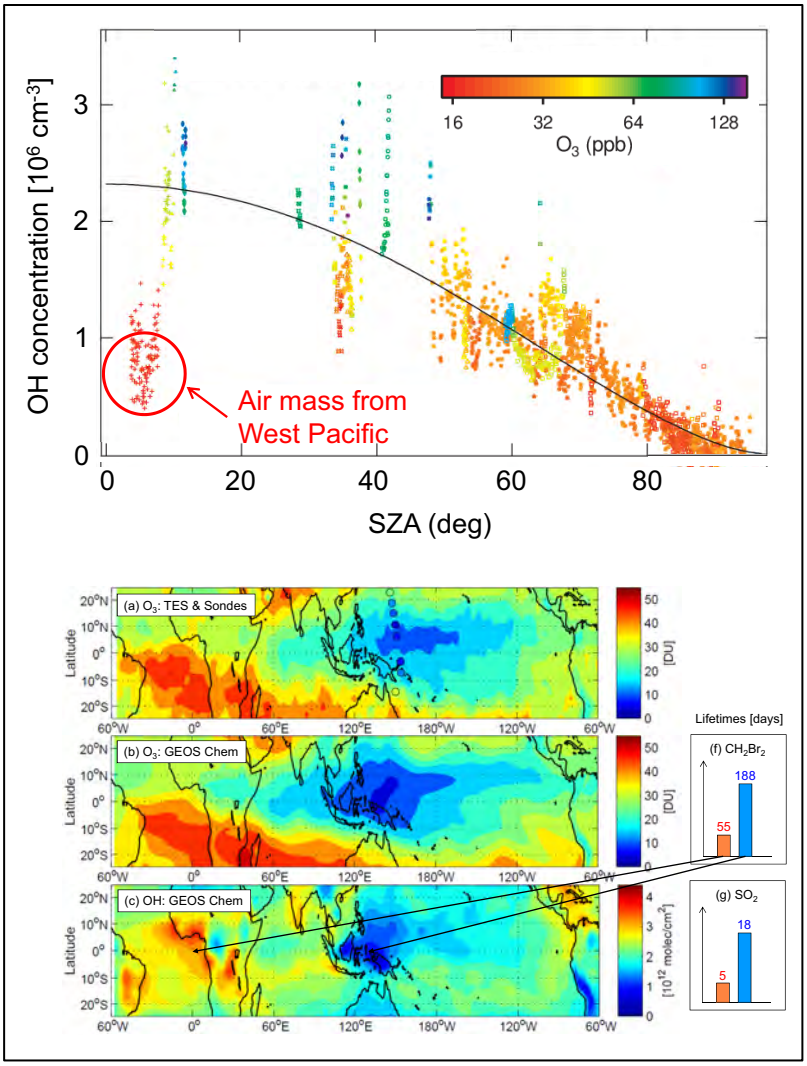

Figure 1-13. *Top*: Observed [OH] (10^6 molecules cm^{-3}) and O_3 mixing ratio (ppb) as a function of solar zenith angle (SZA) from the NASA Stratospheric Tracers of Atmospheric Transport (STRAT) aircraft mission (1995–1996) near Hawaii. Observations are taken above 11 km altitude. Analysis of back trajectories revealed an air mass originating from the West Pacific region containing relatively low O_3 and [OH]. The black line denotes the compact relation described in Hanisco et al. (2001). *Bottom*: Observed O_3 columns from satellite and sonde data, along with the modeled OH column from GEOS CHEM. This analysis indicates an "OH hole" region in the maritime continent, where the lifetime of CH_2Br_2 is significantly enhanced. Modified from Rex et al. (2014).

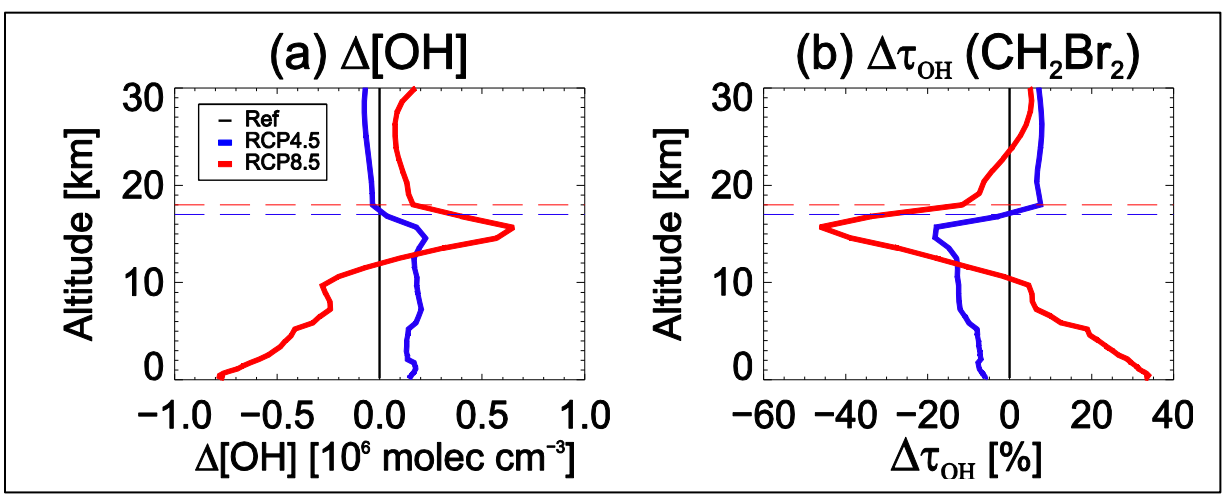

Figure 1-14. Modeled 2100 change in (a) OH abundance (molecules cm^{-3}) and (b) CH_2Br_2 lifetime due to OH oxidation, τ_{OH}, (%) under projected IPCC RCP 4.5 and 8.5 climate scenarios (relative to 2000). The dashed lines denote cold-point tropopause under each scenario. Modified from Hossaini et al. (2012a).

enters the stratosphere as CH_3I at the CPT. New high-altitude observations in the East Pacific region, along with associated modeling (Tegtmeier et al., 2013) are consistent with this conclusion, showing 0.01–0.02 ppt of CH_3I around the tropical CPT. The authors inferred considerably larger mixing ratios in the tropical West Pacific with 0.08 ppt CH_3I at the tropical CPT, calculated using a Lagrangian transport model and observed sea-air fluxes of CH_3I. The annual modeled mean over the inner tropical latitude bands between ~20°S and 20°N was ~0.05 ppt. Based on observed correlations between large oceanic CH_3I emissions and strong vertical uplift, however, a small amount of air was projected to carry larger amounts of CH_3I, with 5.5% of air at the tropical CPT calculated to have mixing ratios larger than 0.2 ppt.

Shorter-lived iodinated VSLS (e.g., CH_2ICl) with lifetimes of hours to a few days are unlikely to reach the stratosphere in significant amounts. Hossaini et al. (2012a) estimated with a global model that on average <1% of the surface mixing ratio of an idealized 6-hour lifetime tracer in the MBL was able to reach the CPT over the tropical West Pacific. However, such compounds contribute to longer-lived inorganic iodine product gases (Box 1-2; Saiz-Lopez et al., 2012), which could release reactive iodine at higher altitude.

1.3.2.2 PRODUCT GAS INJECTION (PGI)

The degradation of VSL SGs in the troposphere is expected to produce a range of organic and inorganic PGs. If these PGs evade tropospheric removal processes, such as dry/wet deposition, they may be transported to the stratosphere via PGI. Observational evidence for PGI is limited, and in general global models have limited representation of the multi-phase and microphysical processes that, coupled with sub-grid scale transport processes, determine the efficiency of PGI. Since the last Assessment, observations of inorganic PGs have been made in tropical regions, though observations in the TTL remain sparse. A number of recent modeling studies have also attempted to further constrain estimates of PGI from brominated VSLS.

PGI from chlorinated VSLS

The estimate of total stratospheric PGI from chlorinated VSLS is essentially unchanged since the last Assessment, at 25 (0–50) ppt Cl. This estimate is derived from observations of hydrogen chloride (HCl) and phosgene ($COCl_2$) observed around the LZRH (Marcy et al., 2007; Mebarki et al., 2010; Brown et al., 2011) of up to 20 and 32 ppt Cl, respectively. As noted in previous Assessments, chlorinated PGs are also produced following the breakdown of long-lived SGs in the stratosphere, and thus the possibility of "double counting" exists if they are recirculated into the troposphere (Montzka and Reimann et al., 2011). Thus, between 0 and 100% of the observed $COCl_2$ and HCl could originate from VSLS. Recent aircraft observations report evidence for episodic enhancements of ClO in the TTL (up to 40 ppt) in air of tropospheric origin (von Hobe et al., 2011). Heterogeneous chlorine activation, also observed around the tropopause at midlatitudes (Thornton et al., 2007), may occur on ice and/or liquid aerosol particles (von Hobe et al., 2011) at cold TTL temperatures.

PGI from brominated VSLS

Although there is now evidence for free tropospheric BrO originating from surface sources of VSLS, with tropospheric BrO columns of around $1–3 \times 10^{13}$ molecules cm^{-2} (Fitzenberger et al., 2000; Richter et al., 2002; Van Roozendael et al., 2002; Sinnhuber et al., 2005; Theys et al., 2007, 2011; Parrella et al., 2013), observational evidence for PG as BrO in the TTL is sparse (Dorf et al., 2008), and likely around the limit of detection (~1 ppt) for remote sensing instruments at the LZRH. Estimates of PGI from VSLS bromine are therefore derived from modeling studies. Such calculations of PGI are particularly sensitive to assumptions regarding partitioning of Br_y, wet scavenging, and heterogeneous recycling. Soluble inorganic bromine (Br_y) species, particularly HBr, are subject to wet deposition processes (Liang et al., 2010; Marecal et al., 2012) and have high uptake coefficients on ice (Crowley et al., 2010). HBr and HCl adsorbed to ice can be converted via heterogeneous reactions with hypohalous

acids (HOX) or halogen nitrates ($XONO_2$) to gas phase Br_2, BrCl, and/or Cl_2, which are readily photolyzed to halogen atoms (see Box 1-2).

Previous global modeling studies simplified tropospheric removal of Br_y by assuming a fixed and uniform loss rate (Sinnhuber and Folkins, 2006; Warwick et al., 2006a; Hossaini et al., 2010). In the last Assessment, PGI from $CHBr_3$ and CH_2Br_2 was estimated at 0.4–3.9 ppt Br based on a model sensitivity study (Hossaini et al., 2010) in which the prescribed "washout lifetime" of Br_y varied between 10 days and infinity (i.e., no tropospheric removal of Br_y). More recent models speciate Br_y in an explicit or semi-implicit manner and/or use a more complex representation of the dehydration processes (e.g., Aschmann et al., 2011; Hossaini et al., 2012a), and show that scavenging of Br_y from VSLS (Br_y^{VSLS}) is a minor loss process in the TTL, removing <10% (Aschmann et al., 2011; Aschmann and Sinnhuber, 2013; Liang et al., 2014). Models also indicate that organic PGs, such as CBr_2O and CHBrO, for which no observations exist, may also reach the TTL, although their contribution to the total bromine PGI is expected to be minor (Hossaini et al., 2010; Marecal et al., 2012). The tropospheric chemistry and speciation of organic PGs, which are likely sensitive to background NO_x and HO_x loading (Krysztofiak et al., 2012), was discussed in Ko and Poulet et al. (2003).

Based on the modeling work discussed above, PGI makes a non-negligible contribution to stratospheric bromine loading from VSLS but critically depends on how rapidly SGs can ascend through the troposphere, where the likelihood of Br_y washout decreases with altitude and may be minor once in the TTL (e.g., Aschmann et al., 2011). Independent model estimates of total PGI of bromine from $CHBr_3$ and CH_2Br_2 are 2.5 ppt Br (Liang et al., 2010), ~1.1 ppt Br (Hossaini et al., 2012b), 1.5 ppt Br (Aschmann and Sinnhuber, 2013), and ≥4 ppt Br (Liang et al., 2014). These models contain a more comprehensive treatment of Br_y than the calculations that formed the basis of the previous Assessment. However, care should be taken when making a direct comparison of these estimates due to variation in the modeling approaches. For example, only Aschmann and Sinnhuber (2013) considered the adsorption of HBr onto ice within the TTL, and the assumed VSLS emissions varied between these studies.

As in Montzka and Reimann et al. (2011), we estimate that PGI from minor brominated VSLS not considered in the studies mentioned above, such as $CHBr_2Cl$, $CHBrCl_2$, and CH_2BrCl, could contribute around 0 to 0.3 ppt Br. Therefore, overall we conclude that total PGI could range from 1.1 to 4.3 ppt Br, compared to the 0.4 to 4.2 ppt Br reported in the last Assessment.

PGI from iodinated VSLS or other iodine sources

There are no new observations of inorganic iodine (I_y) in the TTL since the last Assessment, when available Differential Optical Absorption Spectroscopy (DOAS) measurements (Bösch et al., 2003; Butz et al., 2009) suggested upper limits of 0.1 ppt IO and 0.1 ppt OIO and a total I_y level of <0.15 ppt. New observations of IO in the free troposphere suggest that similar levels are present (Puentedura et al., 2012; Dix et al., 2013). Such low levels of IO are challenging to retrieve accurately but indicate that most of the IO vertical column is above the MBL. This is surprising since the majority of sources are very short lived (Section 1.3.1.3), and could have implications for our understanding of iodine sources and/or the I_x (I + IO) lifetime with respect to irreversible uptake of reactive iodine to aerosol surfaces. Combined with uncertainties in transport and in iodine chemistry (Saiz-Lopez et al., 2012), the quantity of iodinated PGI is not known, up to the upper limits previously reported for IO and OIO in the TTL of 0.1 ppt (Butz et al., 2009).

1.3.2.3 TOTAL VSLS HALOGEN INPUT INTO THE STRATOSPHERE

As discussed above, VSLS contribute to stratospheric halogen loading by both SGI and PGI. Observations of SGs around the tropopause provide some constraint on the magnitude of SGI. Observational evidence for PGI is, however, still rather limited and as such its contribution remains a significant uncertainty. An updated estimate of SGI, PGI, and the total (SGI + PGI) contribution of VSLS to stratospheric halogen loading is given in Table 1-9 and is based on available SG/PG observations in the tropics and recent model studies.

TABLE 1-9. Summary of estimated VSLS source gas (SG) and product gas (PG) contributions to stratospheric halogens, based on observations and model results.

Halogen or Compound	Best Estimate (ppt Cl, Br, or I)
Chlorine	
VSL SGs	72 (50–95)
HCl PG	10 (0–20)
$COCl_2$ PG	15 (0–30)
Total chlorine	**95 (50–145)**
Bromine	
VSL SGs	0.7–3.4
PG sum	1.1–4.3
Total bromine	**5 (2–8)**
Iodine	
CH_3I SG	< 0.05
PG sum	< 0.1
Total iodine	**< 0.15**

Total input from chlorinated VSLS

As in the previous Assessment, "the best estimate" of total chlorine from VSLS reaching the stratosphere is obtained by summing the observed contribution from SGs (Table 1-7) at the tropopause and adding the estimated PG contribution from $COCl_2$ and HCl. This gives a best estimate and range of 95 (50–145) ppt. The anthropogenic fraction of VSLS chlorinated SG to the total SG at the tropopause is estimated to be around 70% (Table 1-7). Assuming this applies also to PGs, then we estimate ~70% of the total chlorine from VSLS entering the stratosphere is from anthropogenic sources.

Total input from brominated VSLS

The best estimate of bromine from VSLS that reaches the stratosphere, Br_y^{VSLS}, is based on SG observations around the tropical tropopause, two BrO profiles measurements in the TTL (Dorf et al., 2008), and an estimated PGI contribution from recent global modeling. A range is derived by summing the lower limits of SGI and PGI estimates as well as the upper limits (Table 1-9). This leads to a total estimated range of 2–8 ppt Br_y^{VSLS}, which is slightly narrower than the reported range of 1–8 ppt in the last Assessment, due to constraints on recent model estimates of PGI (Liang et al., 2010; Hossaini et al., 2012a; Aschmann and Sinnhuber, 2013; Liang et al., 2014).

An alternative approach to estimating Br_y^{VSLS} is to use observations of stratospheric BrO combined with model estimates of the BrO/Br_y ratio to calculate total stratospheric Br_y, and subtract the contribution of long-lived SGs. Uncertainties in the absolute mole fractions of long-lived source gases—CH_3Br and the halons—are small (< 5%) (see Section 1.2). The overall uncertainty in the BrO/Br_y ratio is dominated by uncertainties in chemical kinetics, which are estimated to be 10 to 30% (Hendrick et al., 2008; McLinden et al., 2010; Salawitch et al., 2010; Parrella et al., 2012). Based on balloon-borne observations over Kiruna (68°N) and photochemical modeling, Kreycy et al. (2013) inferred that the $j(BrONO_2)/k(BrO+NO_2)$ ratio (i.e., the ratio of bromine nitrate photolysis to production), could be larger by a factor of 1.7 (+0.4, −0.2) than that obtained using JPL recommendations. This result changes modeled BrO/Br_y ratios such that the total Br_y derived from BrO observations is reduced by about 1–2 ppt under conditions of high stratospheric NO_x levels (for which most Br_y assessments are made), although the impact could be near zero in regions where $BrONO_2$ is not important. While not affecting the trend in

Br_y (see Section 1.4.2.2), this study implies that Br_y^{VSLS} estimated from BrO observations could be smaller than considered previously.

Table 1-10 is an update from the previous Assessment and contains compiled Br_y^{VSLS} estimates from ground-, balloon-, aircraft- and satellite-based measurements of BrO, with associated uncertainties. Resolution of the measured total BrO columns from satellite UV-visible instruments into their stratospheric and tropospheric contributions depends upon assumptions regarding the presence of BrO in the troposphere and the spatial inhomogeneity of stratospheric BrO. Theys et al. (2011), Choi et al. (2012), and Sihler et al. (2012) have recently addressed many of the issues associated with retrieval of tropospheric BrO from the satellite sensors Ozone Monitoring Instrument (OMI), Global Ozone Monitoring Experiment (GOME-2), and Scanning Imaging Absorption Spectrometer for Atmospheric Chartography (SCIAMACHY), with results that support realistic separation of tropospheric fractions of the measured total BrO columns.

The three new estimates of Br_y^{VSLS} in Table 1-10 are based on measurements of BrO from the Aura Microwave Limb Sounder (MLS) instrument (Millán et al., 2012), SCIAMACHY (Parrella et al., 2013), and from a balloon-borne Submillimeterwave Heterodyne Limb Sounder (SLS) (Stachnik et al., 2013). These estimates of 5 (0.5–9.5) ppt, 7 (1–13) ppt, and 6 (3–9) ppt, respectively, fall within the previously reported range and support the "ensemble" value of 6 (3–8) ppt from the last Assessment (Montzka and Reimann, 2011). However, the discussion above regarding the $j(BrONO_2)/k(BrO+NO_2)$ ratio suggests that the lower bound of this estimate should be revised downward, giving a higher uncertainty

Table 1-10. Estimates of inorganic bromine from very short-lived substances (Br_y^{VSLS}) contribution to stratospheric bromine derived from BrO measurements. Update of Table 1-14 from the previous Assessment (Montzka and Reimann et al., 2011), extended with new results.

Data Source	Br_y^{VSLS} Central Value (ppt)	Br_y^{VSLS} Range (ppt)	References
Compilation of ground-based column BrO, aircraft & balloon BrO profiles, satellite BrO profiles from SCIAMACHY, MLS, and OSIRIS, and GOME and OMI satellite column BrO	6	3–8	Montzka and Reimann et al. (2011)
MLS satellite BrO profiles 55°S–55°N, 10–4.6 hPa	5	0.5–9.5	Millán et al. (2012)
SCIAMACHY satellite BrO profiles, 80°S–80°N, 15–30 km	7	1–13	Parrella et al. (2013)
SLS balloon BrO profiles Ft. Sumner, New Mexico (34°N)	6	3–9	Stachnik et al. (2013)
Ensemble	**6 (3–8)** [a]		
New, adjusted ensemble	**5 (2–8)** [b]		

SCIAMACHY, Scanning Imaging Absorption Spectrometer for Atmospheric Cartography; MLS, Microwave Limb Sounder; OSIRIS, Optical Spectrograph and InfraRed Imager System; GOME, Global Ozone Monitoring Experiment; OMI, Ozone Monitoring Instrument; SLS, Submillimeterwave Heterodyne Limb Sounder.

[a] Average and range of the central values of the 15 published estimates of Br_y^{VSLS}.

[b] Ensemble values, with mean and lower bound adjusted downwards by ~1 ppt to account for larger $j(BrONO_2)/k(BrO+NO_2)$ ratio (Kreycy et al., 2013).

range, since it is not yet clear how the new results of Kreycy et al. (2013) affect individual measurements. We therefore suggest a new ensemble value for Br_y^{VSLS} from BrO of 5 (2–8) ppt. This new ensemble range is the same as that based on SG observations and model PGI estimates (see above). Based on the similarity between these estimates from two different approaches, and the increased confidence in PGI estimates from models, we merge them to a best estimate of 5 (2–8) ppt Br_y^{VSLS}. This inferred quantity of Br_y^{VSLS} comprises a significant fraction of total stratospheric Br_y and is large enough to significantly affect the balance of ozone in the lower stratosphere, particularly at high latitudes (e.g., Feng et al., 2007) (see Section 1.3.3).

Total input from iodinated VSLS

The best estimate of iodine from VSLS that reaches the stratosphere, based on observed CH_3I around the tropopause and observed upper limits of stratospheric IO and OIO (Butz et al., 2009), is <0.15 ppt, which is unchanged from the last Assessment.

1.3.3 Potential Influence of VSLS on Ozone

A number of modeling studies have shown that inclusion of Br_y^{VSLS} in the stratosphere improves agreement between modeled and observed O_3 trends (Salawitch et al., 2005; Feng et al., 2007; Sinnhuber et al., 2009). These models show that the influence of Br_y^{VSLS} is largest during periods of elevated stratospheric aerosol, such as following large volcanic eruptions (e.g., Mt. Pinatubo in 1991), when heterogeneous halogen activation is enhanced. Therefore, proposed geoengineering strategies to combat climate change, such as stratospheric sulfate injections, may enhance the impact of VSLS on O_3 (Tilmes et al., 2012). In a volcanic quiescent year (2000) and relative to a model run with no VSLS, Feng et al. (2007) reported a column O_3 decrease of ~10 Dobson units (DU) at midlatitudes due to 6 ppt of Br_y^{VSLS} in the lower stratosphere during 2000.

Recent chemistry-climate model (CCM) studies have also included brominated VSLS (e.g., Ordoñez et al., 2012). Braesicke et al. (2013) reported up to a ~20% reduction in O_3 in the lower stratosphere in polar regions between a model run with and without Br_y^{VSLS} under 2000 stratospheric conditions.

The impact of chlorinated VSLS on O_3 trends has not been assessed, though relative to bromine it is likely to be small at present. Globally and annually averaged, the chemical effectiveness of bromine relative to chlorine for global O_3 destruction, the alpha factor, is estimated to be ~60 (Sinnhuber et al., 2009). The alpha factor for iodine is expected to be significantly larger, with an estimated range of 150–300 (Ko and Poulet et al., 2003). However, at the low levels of stratospheric iodine inferred from observed CH_3I around the tropopause and observed IO/OIO (Butz et al., 2009), models suggest that iodine is a very minor sink for O_3 (Bösch et al., 2003).

1.3.4 New Anthropogenic VSLS

A number of short-lived compounds have been proposed as replacements for long-lived ozone-depleting substances (ODSs) and radiatively active hydrofluorocarbons (HFCs). Several of these substances are halogenated VSLS (i.e., lifetimes <0.5 years) and were chosen due to their low Ozone Depletion Potentials (ODPs) and Global Warming Potentials (GWPs). An updated summary of the lifetimes of the proposed replacement substances is given in Table 1-11. These compounds are discussed further in Chapter 5.

Table 1-11. Local lifetimes of in-use and potential short-lived replacement compounds for long-lived ODSs. Local lifetimes were calculated for OH reactive loss with the OH and temperature climatology from Spivakovsky et al. (2000) and Prather and Remsberg (1993), respectively, unless noted otherwise. Note that local lifetimes are estimates because the actual lifetimes of short-lived gases are dependent on their emission location and season as well as local atmospheric conditions (e.g., OH concentration and temperature).

Compound	WMO (2011) [a] Local Lifetime (days)	Tropics (25°S–25°N) Annually Averaged Local Lifetime (days)		Midlatitude (25°N–65°N) Annually Averaged Local Lifetime (days)		Notes
		BL	10 km	BL	10 km	
Hydrocarbons						
$CH_2{=}CHCH_3$ (propene)	0.35	0.31	0.27	0.47	0.50	1
$(CH_3)_2C{=}CH_2$ (isobutene)	0.20	0.18	0.15	0.27	0.29	1
$CH_3CH_2CH_3$ (propane, R-600)	12.5	9.9	13.6	16	27	2
$(CH_3)_2CHCH_3$ (isobutane, R-600a)	6.0	5.2	5.6	8.1	10.7	1
$CH_3CH_2CH_2CH_2CH_3$ (n-pentane)	3.4	2.7	3.3	4.3	6.5	3
c-$CH_2CH_2CH_2CH_2CH_2$ (cyclopentane)	2.7	2.2	2.7	3.5	5.3	3
$(CH_3)_2CHCH_2CH_3$ (isopentane)	3.4	2.9	3.1	4.5	6.0	3
CH_3OCHO (methyl formate)	72	60	73	95	143	4
$(CH_3)_2CHOH$ (isopropanol)	2.0	1.9	1.5	2.9	2.7	2
$CH_3OCH_2OCH_3$ (methylal)	2.2	1.7	1.5	2.6	2.8	5
Hydrofluorocarbons						
CH_3CH_2F (HFC-161)	66	51	76	83	154	2
CH_2FCH_2F (HFC-152)	146	114	165	183	335	2
CH_3CHFCH_3 (HFC-281ea)	23	19	23	30	46	2
Unsaturated Fluorocarbons						
$CH_2{=}CHF$	2.1	2.0	1.4	3.1	2.6	2
$CH_2{=}CF_2$	4.0	3.7	3.0	5.7	5.4	2
$CF_2{=}CF_2$	1.1	1.0	0.7	1.6	1.3	2
$CH_2{=}CHCH_2F$	0.7	0.6	0.5	1.0	0.8	2
$CH_2{=}CHCF_3$	7.6	7.2	5.5	11	10	2
$CH_2{=}CFCF_3$ (HFC-1234yf)	10.5	9.6	8.4	15	16	2
$CF_2{=}CFCH_2F$		~2	~2	~2	~2	6
$CF_2{=}CHCHF_2$		<5	<5	<5	<5	6
$CHF{=}CFCHF_2$		<5	<5	<5	<5	6
$CF_2{=}CHCF_3$		~2	~2	~2	~2	6
(*E*)-$CHF{=}CHCF_3$ (HFC-1234ze(E))	16.4	15.0	12.8	23	24	2
(*E*)-$CHF{=}CFCF_3$	4.9	4.5	3.7	6.9	6.8	2
(*Z*)-$CHF{=}CFCF_3$	8.5	8.0	6.2	12	11	2
$CF_2{=}CFCF_3$	4.9	4.7	3.3	7.1	6.0	2
$CH_2{=}CHCF_2CF_3$	7.9	7.5	5.8	11.4	10.5	2
$CH_2{=}CHCF_2CF_2CF_3$		~8	~6	~10	~10	7
(*E*)-$CF_3CH{=}CHCF_3$		~22	~16	~30	~30	8
(*Z*)-$CF_3CH{=}CHCF_3$		21.2	16.3	32	30	9
$CF_2{=}CFCF{=}CF_2$	1.1	1.0	0.8	1.5	1.6	10
(*E*)-$CF_3CH{=}CHCF_2CF_3$		~22	~16	~30	~30	11
Unsaturated Chlorocarbons						
$CH_2{=}CHCl$	1.5	1.5	0.9	2.2	1.6	2

(continued next page)

Compound	WMO (2011) [a] Local Lifetime (days)	Tropics (25°S–25°N) Annually Averaged Local Lifetime (days)		Midlatitude (25°N–65°N) Annually Averaged Local Lifetime (days)		Notes
		BL	10 km	BL	10 km	
$CH_2{=}CCl_2$	0.9	0.9	0.5	1.3	0.9	2
CClH=CClH		4.4	3.2	6.7	5.9	12
$CHCl{=}CCl_2$	4.9	4.7	3.3	7.1	6.0	2, 13
$CCl_2{=}CCl_2$	90	66	119	109	245	2
$CF_2{=}CFCl$	1.4	1.4	0.8	2.1	1.4	14
(*E*)-$CF_3CH{=}CHCl$	26	24	21	37	39	15
(*Z*)-$CF_3CH{=}CHCl$		~25	~20	~40	~40	16
$CF_3CCl{=}CH_2$		~25	~20	~40	~40	16
$CF_2{=}CFCF_2Cl$	~5	~5	~3	~7	~6	17
$CF_2{=}CFCF_2CFCl_2$	~5	~5	~3	~7	~6	17
Unsaturated Bromocarbons						
$CFBr{=}CF_2$	1.4	1.3	0.9	2.0	1.6	18
$CHBr{=}CF_2$	2.3	2.3	1.5	3.4	2.7	18
$CH_2{=}CBrCF_3$	2.7	2.6	1.8	3.9	3.3	18
$CH_2{=}CBrCF_2CF_3$	3.1	3.0	2.0	4.6	3.6	18
$CH_2{=}CHCF_2CF_2Br$	6.5	6.2	4.7	9.5	8.6	18
Fluorinated Ethers, HFE						
$CH_3OCH_2CF_3$ (HFE-263fb2)	23	19	24	30	47	19, 20
$CH_3OCHFCF_3$ (HFE-254eb2)	88	69	99	111	200	2
$CH_3OCH_2CF_2CF_3$ (HFE–365mcf3)	21	17	21	27	42	20, 21
$CH_3CH_2OCF_2CHF_2$ (HFE–374pc2)	64	50	71	80	142	2
$CF_3CH_2OCH_2CF_3$ (HFE-356mff)	105	79	132	129	270	2
$CH_3OCH(CF_3)_2$ (HFE–356mm1)	61	49	64	79	128	22
Fluorinated Ketones						
$CF_3CF_2C(O)CF(CF_3)_2$ (FK 5-1-12)	7–14					23
$(CF_3)_2CFC(O)CF(CF_3)_2$						24
$CF_3CF_2CF_2C(O)CF(CF_3)_2$						24
Fluorinated Alcohols						
CH_2FCH_2OH	12.9	11	11	18	22	2
CHF_2CH_2OH	51	42	53	66	103	2
CF_3CH_2OH	142	111	161	180	325	2
$C_2F_5CH_2OH$	143	111	165	180	335	2
$C_4F_9CH_2OH$	142	111	164	178	330	2
$CF_3CHFCF_2CH_2OH$	112	85	137	138	280	1
Special Compounds						
$CF_3CF_2CF_2I$ (1-iodo-heptafluoropropane)	<2					25
CH_3I (methyl iodide)	7	4.0	3.5	9.6	7.1	26
COF_2 (carbonyl fluoride)	5–10					27
PBr_3	<0.01					28
NH_3	Few days					2, 29
CH_3CH_2Br (bromoethane)	41	32	45	52	90	30

(continued next page)

Notes:

a OH reactive loss partial lifetime was estimated with an OH abundance of 1×10^6 molecule cm^{-3} and a temperature of 275 K.
1. OH reaction rate coefficient taken from Atkinson et al. (2008).
2. OH reaction rate coefficient taken from JPL 10-6 (Sander et al., 2011).
3. OH reaction rate coefficient taken from Calvert et al. (2008).
4. OH reaction rate coefficient taken from Le Calvé et al. (1997).
5. OH reaction rate coefficient taken from Porter et al. (1997).
6. No experimental data available for the OH reaction; lifetime estimate was based on reactivity trends of fluorinated ethenes.
7. No experimental data available for the OH reaction; lifetime estimated to be similar to that of $CH_2{=}CHCF_2CF_3$.
8. No experimental data available for the OH reaction; lifetime estimated to be similar to that of (*Z*)-$CF_3CH{=}CHCF_3$.
9. OH reaction rate coefficient taken from Baasandorj et al. (2011).
10. OH reaction rate coefficient taken from Acerboni et al. (2001).
11. Lifetime estimated to be similar to that of (*E*)-$CF_3CH{=}CHCF_3$.
12. OH reaction rate coefficient from Zhang et al. (1991).
13. Photolysis lifetime taken from Table 2-4 in Ko and Poulet et al. (2003).
14. OH reaction rate coefficient taken from Abbatt and Anderson (1991).
15. Room temperature OH reaction rate coefficient taken from Sulbaek Andersen et al. (2008).
16. Local lifetime estimated as similar to that of (*E*)-$CF_3CH{=}CHCl$.
17. Local lifetime estimated as similar to that of $CF_3CF{=}CF_2$.
18. OH reaction rate coefficient taken from Orkin et al. (2002).
19. OH reaction rate coefficient taken from Oyaro et al. (2005).
20. Only room temperature rate coefficient data available; OH reaction lifetime calculated assuming E/R = 500 K.
21. OH reaction rate coefficient taken from Oyaro et al. (2004).
22. OH reaction rate coefficient from Chen et al. (2005b).
23. Estimated local lifetime range due to UV photolysis taken from Taniguchi et al. (2003).
24. Lifetime estimated to be similar to that of $CF_3CF_2C(O)CF(CF_3)_2$.
25. Estimated local lifetime taken from WMO (2011).
26. Losses due to OH reaction and UV photolysis, see Table 1-5.
27. Estimated local lifetime range due to heterogeneous uptake taken from Wallington et al. (1994).
28. Local lifetime taken from Table 2-1 in Law and Sturges et al. (2007); OH reaction rate coefficient taken from Jourdain et al. (1982); the local lifetime is probably determined by UV photolysis.
29. Local lifetime taken from IPCC/TEAP (2005); determined by washout rate.
30. See Table 1-5.

1.4 CHANGES IN ATMOSPHERIC HALOGENS

1.4.1 Tropospheric and Stratospheric Chlorine Changes

1.4.1.1 TROPOSPHERIC CHLORINE CHANGES

Total organic chlorine (CCl_y) in the troposphere peaked in 1993–1994 at 3660 ± 23 ppt and has then continuously declined for 20 years, initially at a rate of around 1% per year, reducing to a rate of around 0.5% yr^{-1} in recent years (Figure 1-15). By mid-2012, tropospheric organic Cl from anthropogenic (CFCs, HCFCs, and chlorinated solvents, including methyl chloroform) and natural (mainly CH_3Cl) sources had declined to 3300 ppt (Figure 1-15 and Table 1-12). This is a decrease of 1.5% since the 2010 Assessment report and of almost 10% when compared to the 1993 peak value, due to decreases in the anthropogenic Cl gases. In 2012, the CFCs and HCFCs accounted for 61% and 9%, respectively, of CCl_y in long-lived gases in the lower atmosphere. Table 1-12, updated from the 2010 Assessment, shows the contribution of halocarbons to the total chlorine budget for three milestones: 2004, 2008 and 2012.

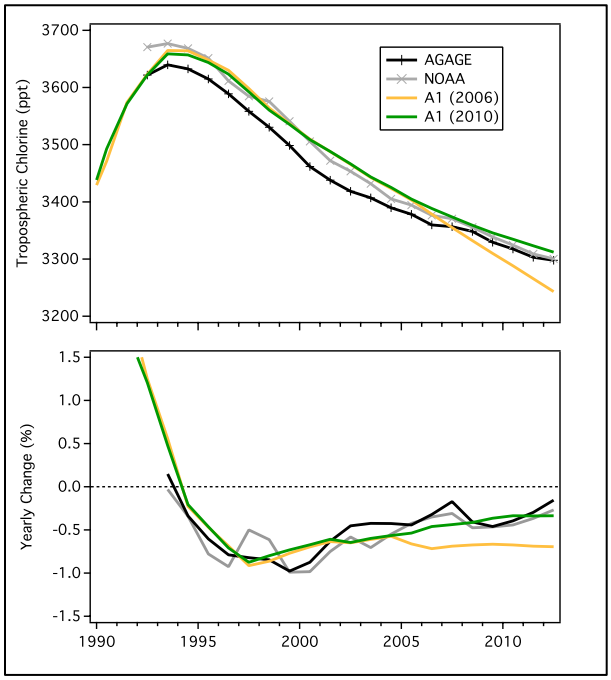

Figure 1-15. Total organic chlorine (CCl_y) from the NOAA (gray) and AGAGE (black) global measurement networks. Quantities are based on global mean mole fractions of CFC-11, CFC-12, CFC-113, CH_3CCl_3, CCl_4, CH_3Cl, HCFC-22, HCFC-141b, HCFC-142b, and halon-1211 determined by the respective networks. CFC-114, CFC-115, CFC-112, and CFC-113a were estimated from measurements of Cape Grim archive air samples (Prinn et al., 2000; Laube et al., 2014) and included in records from both networks. NOAA HCFC and halon-1211 data were included in the AGAGE record for years 1992–1993 to provide a more complete total chlorine record. An additional 75–91 ppt was added to NOAA and AGAGE records to account for the sum of $CHCl_3$, CH_2Cl_2, C_2Cl_4, and $COCl_2$ (see Table 1-12).

Table 1-12. Contributions of long-lived halocarbons to total chlorine in the troposphere.

	Total Cl (ppt) *			Contribution to Total (%)			Average Rate of Change of Total Cl ** (ppt yr^{-1})		
	2004	2008	2012	2004	2008	2012	2000–2004	2004–2008	2008–2012
All CFCs	2126	2078	2024	62.6	62.0	61.34	−7.7 (1.3)	–12.0 (1.0)	–13.5 (0.5)
CCl_4	376	358	339	11.1	10.7	10.3	–4.0 (0.6)	–4.4 (0.5)	–4.9 (0.7)
HCFCs	212	249	286	6.3	7.4	8.7	8.3 (0.4)	9.2 (0.2)	9.2 (0.3)
CH_3CCl_3	66	32	16	1.9	1.0	0.5	–17.6 (1.1)	–8.4 (0.5)	–4.1 (0.2)
CH_3Cl	535	545	540	15.8	16.3	16.4	–0.3 (2.8)	2.5 (0.9)	–1.7 (1.3)
halon-1211	4.33	4.24	3.96	0.13	0.13	0.12	0.05 (0.01)	–0.02 (0.01)	–0.07 (0.02)
Total Cl	3397	3352	3300				–21.0 (1.8)	–15.6 (1.3)	–13.4 (0.9)
							–0.60%	–0.46%	–0.40%

* Chlorine mid-year mole fractions were derived using AGAGE, NOAA, and archive data (see Figures 1-1, 1-15).

** Total and relative Cl changes over 5-year periods, as indicated. Uncertainties (in parentheses) are one standard deviation based on trends determined from different global networks. Relative changes in total chlorine (in percent) were calculated relative to values at the beginning of each period (3484 ppt in 2000).

Values for past years differ slightly from previous Assessments because of updated calibration information, different methods for determining global mean mole fractions, rounding errors, and the inclusion of CFC-112 and CFC-113a (Laube et al., 2014). Total Cl also includes 77, 84, and 91 ppt as VSLS in 2004, 2008, and 2012, respectively. Average trends in total Cl are based only on controlled species (not CH_3Cl and VSLS).

1.4.1.2 STRATOSPHERIC CHLORINE CHANGES

Most chlorine enters the stratosphere as organic chlorine (CCl_y) in long-lived source gases and undergoes photochemical oxidation to inorganic forms (Cl_y) as air is transported to higher altitudes within the stratosphere. In the upper stratosphere, total chlorine, i.e., the sum of CCl_y and Cl_y, lags the tropospheric CCl_y time series by up to 6 years owing to timescales for air to be transported to higher altitudes after crossing the tropopause, depicted in Figure 1-16. It is expected that total chlorine will continue to decrease in the stratosphere, with a time-delay as compared to tropospheric observations. The leveling off of inorganic chlorine occurred in 1996–1997 in the stratosphere (Rinsland et al., 2003).

The most abundant chlorine-containing gases in the stratosphere are the "reservoirs" HCl and $ClONO_2$, which can generate chlorine-containing radicals including ClO. Peak stratospheric abundances of $ClONO_2$, HCl, and ClO occur near 25–30 km, 50–60 km, and 25–45 km (daytime)/38–45km (night-time), respectively (Froidevaux et al., 2006; Sato et al., 2012; Kreyling et al., 2013).

Table 1-13 summarizes observed trends of HCl, $ClONO_2$, and ClO derived from ground-based and satellite measurements of partial and total columns. Over a broad latitudinal range, observed upper stratospheric HCl, which is the dominant Cl_y compound in this region, shows trends of −0.5 to −0.8% yr^{-1} for various time periods between 1997 and 2010. Between 1997 to 2013 and averaged over 50°N to 50°S, HCl trends of −0.5 to −0.6% yr^{-1} are derived from HALOE (Halogen Occultation Experiment) data from January 1997 to November 2005 and ACE-FTS (Atmospheric Chemistry Experiment Fourier Transform Spectrometer) data from February 2004 to February 2013 (A. Jones et al., 2011) (Figure 1-17). These measurements are made between 35 to 45 km, an altitude range particularly suitable for analysis due to the sensitivity of both instruments and because most source gases have been converted to inorganic species, primarily HCl. HALOE and ACE-FTS measurements are biased with respect to each other, due to non-uniform (time-dependent in the case of HALOE) sampling, and different time periods used. However the data shown in Figure 1-17 indicate a trend in HCl similar in magnitude to other observations over different time periods and locations (Table 1-13) and with the observed decrease in tropospheric CCl_y of 0.5 to 1% per year on average since 1993–1994 (Figure 1-15).

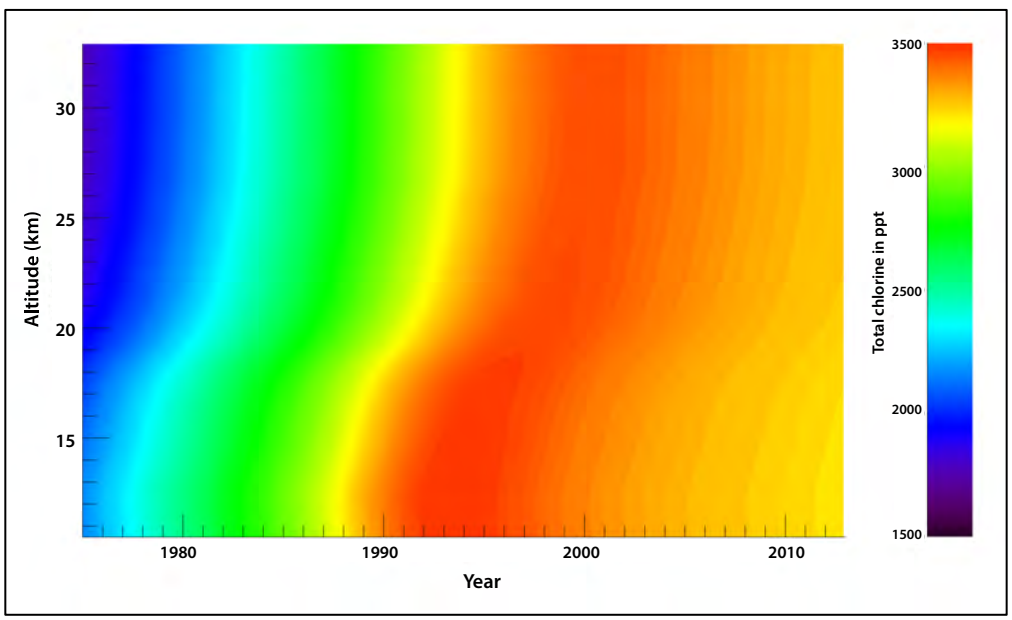

Figure 1-16. Midlatitude total chlorine evolution in the stratosphere, calculated using the vertical distribution of mean age (derived from observations of the age tracers SF_6 and CO_2) and assumptions on the width of the age spectrum. Tropospheric data from NOAA (using the data shown in Figure 1-15) are used exclusively as the basis of the calculation (updated from Engel et al., 2002).

Table 1-13. Observed inorganic chlorine changes in the upper atmosphere.

Data Source/ Location	Cl_y Species	Altitude Region	Rate of Change (yr^{-1})	Time Period	Reference
Ground-based microwave instrument (reanalysis) Mauna Kea, Hawaii (19.8°N, 204.5°E)	ClO	33 – 37 km	−0.64 ± 0.15%	1995–2012	Connor et al. (2013)
Aura MLS + Odin SMR 20°S–20°N	ClO	35 – 45 km	−0.71 ± 0.78%	Dec 2001–Nov 2008	A. Jones et al. (2011)
Aura MLS 60°S–60°N	HCl	50 – 65 km	−0.78 ± 0.08%	Aug 2004–Jan 2006	Froidevaux et al. (2006)
ACE-FTS (v3.0) 30°S–30°N	HCl	50 – 54 km	−0.7 ± 0.1%	2004–2010	Brown et al. (2011)
HALOE and ACE-FTS 30°N–50°N, 30°S–50°S, and 20°N–20°S	HCl	35 – 45 km	−0.51% (NH), −0.52% (SH), −0.58% (tropics)	1997–2008	A. Jones et al. (2011)
17 FTIR NDACC stations (80.1°N–77.8°S)	HCl	Total column	Between −0.36 ± 0.67% and −1.56 ± 0.64%	2000–2009, station dependent	Kohlhepp et al. (2012)
17 FTIR NDACC stations (80.1°N–77.8°S)	$ClONO_2$	Total column	Between −0.07 ± 0.52% and −4.56 ± 0.78%	2000–2009, station dependent, without Ny Alesund	Kohlhepp et al. (2012)

MLS = Microwave Limb Sounder; SMR = Sub-millimetre Radiometer; ACE-FTS = Atmospheric Chemistry Experiment Fourier Transform Spectrometer; HALOE = Halogen Occultation Experiment; FTIR = Fourier Transform Infrared; NDACC = Network for the Detection of Atmospheric Composition Change.

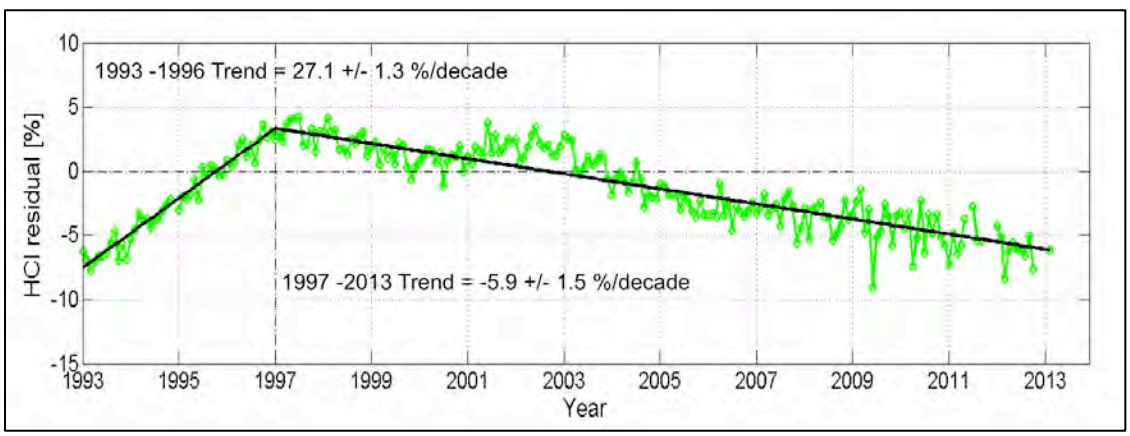

Figure 1-17. Time series of HCl anomalies at 35–45 km, averaged over 50°S–50°N. The anomalies represent de-seasonalized monthly averaged data for the all-instrument average (green) produced from HALOE v19 data from January 1997 to November 2005 and ACE-FTS v3.0/3.5 data from February 2004 to February 2013 (Ashley Jones, University of Toronto, extended from A. Jones et al., 2011). The anomalies are calculated by subtracting the climatological average value for each of the 12 months (calculated over the time span of each instrument) from each individual month (as in A. Jones et al., 2011). The vertical black dot-dash line at 1997 indicates the turnaround date. The solid black lines indicate the fitted trend to the all-instrument average before and after 1997. Trend values are given in percent per decade and uncertainties are 2 standard deviations.

Ground-based column data are more sensitive to HCl in the lower stratosphere, and are therefore potentially susceptible to short-term variability. At some ground-based stations, the total-column trends of HCl and $ClONO_2$ show significant differences, with much faster $ClONO_2$ decreases than HCl at low and high latitudes (Kohlhepp et al., 2012). However the mean annual cycles of HCl and $ClONO_2$ and the overall trend in the stratospheric chlorine content reported by Kohlhepp et al. (2012) were in agreement with five model calculations, also reported in the study, which were driven by baseline scenarios from WMO (2003) and WMO (2007).

Recently, Mahieu et al. (2013) updated the long-term Jungfraujoch HCl column measurement time series (Figure 1-18), and this update significantly impacts the derived trend (−0.7% yr^{-1} for 1997–2011 instead of –1.1% yr^{-1} for 1997–2007). Surprisingly, a flattening or even a positive trend (at the 2-σ uncertainty level) is found for the 2007–2011 time period, although these changes are relatively small in relation to the atmospheric variability. A change in atmospheric circulation over this period, with more frequent sampling of northerly air masses at the Jungfraujoch, is a possible explanation (Mahieu et al., 2013). Previous Assessments have also noted abrupt unexplained variations in HCl trends, i.e., which differ over short time periods from lagged tropospheric chlorine trends (Montzka and Fraser et al., 2003). The overall changes reported here for HCl, in Figure 1-17 and Table 1-13, and in previous Assessments are however generally consistent with expectations based on trends in tropospheric long-lived chlorine gases.

1.4.2 Tropospheric and Stratospheric Bromine Changes

1.4.2.1 Tropospheric Bromine Changes

Total organic bromine in the troposphere has declined by about 2 ppt since it peaked in 1998 (Figure 1-19), at an average rate of −0.86 ± 0.05% Br yr^{-1} from 1998–2012, and at −0.95 ± 0.13% Br yr^{-1} from 2008–2012. The majority of this decline results from reduced industrial production and emission of CH_3Br, although the rate of CH_3Br decline has slowed from ~0.14 ppt yr^{-1} during the last Assessment to 0.08 ± 0.02 ppt yr^{-1} since 2008. During 2008–2012 total bromine from CH_3Br and the halons decreased from 15.8 ± 0.2 ppt to 15.2 ± 0.2 ppt at an average rate of 0.14 ± 0.02 ppt yr^{-1}, based on two independent networks of surface observations (see Table 1-1). In the last Assessment, there were tentative signs of a decline in total Br from halons, from a peak around 2007; this decline is now larger and more robustly determined, decreasing at an average rate of 0.06 ± 0.02 ppt Br yr^{-1} since 2008 (see Table 1-1). Halon-1301 is the only anthropogenic bromocarbon that is still increasing, although the growth has slowed in recent years to 0.03 ± 0.01 ppt yr^{-1}.

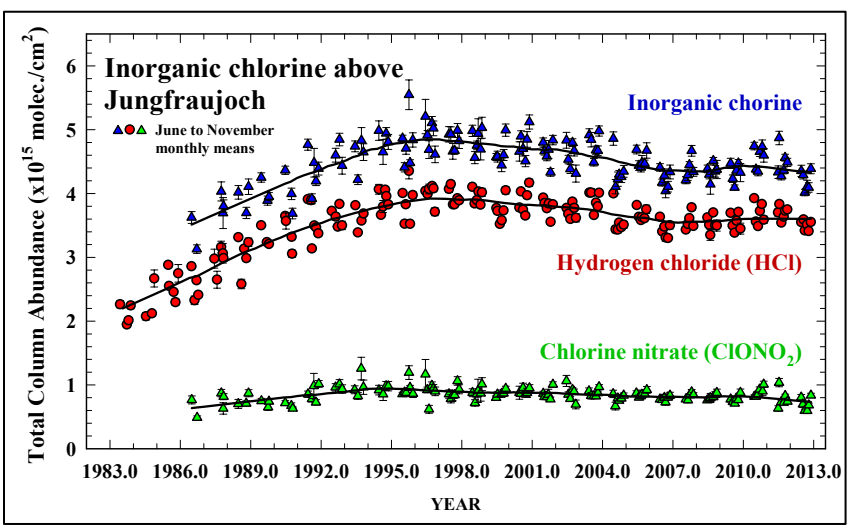

Figure 1-18. Time series (1983–2012) of monthly-mean total column HCl (red circles) and $ClONO_2$ (green triangles), as measured above the Jungfraujoch station (46.5°N). Cl_y total columns (blue triangles) were obtained by summing the corresponding HCl and $ClONO_2$ data points. To avoid the significant variability affecting measurements in winter and spring, the time series were derived from June to November data. Least-square fits were applied to these data sets (black curves) to provide trends estimates. Updated from Montzka and Reimann et al. (2011).

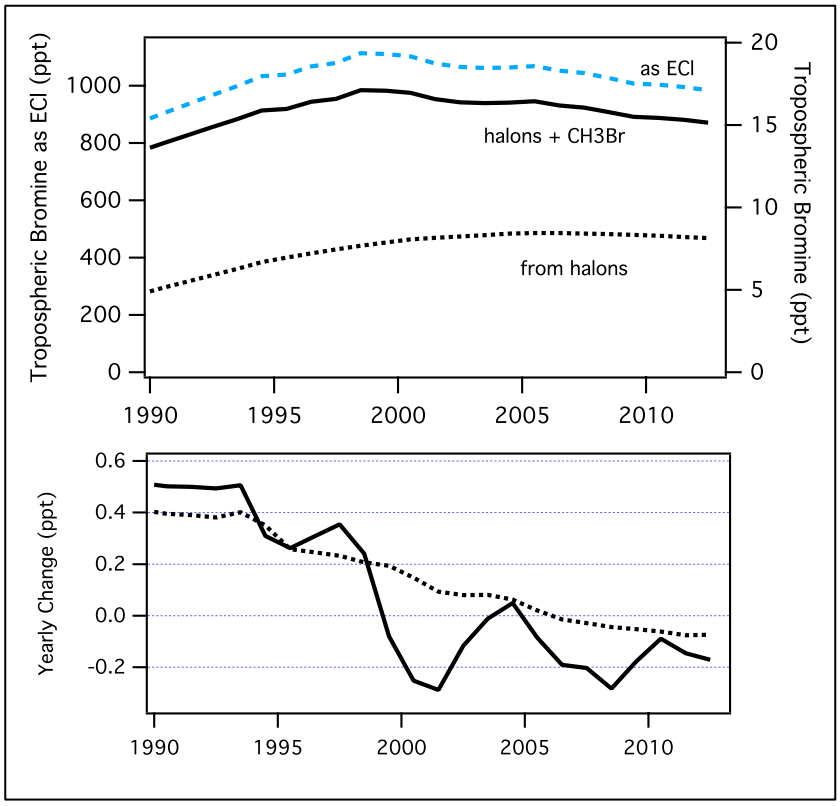

Figure 1-19. Tropospheric bromine expressed as bromine from halons, bromine from halons plus CH_3Br, and as Equivalent Chlorine (ECl, using α= 65) (upper panel) and annual changes in Br-halons and Br-halons+CH_3Br (lower panel). Sums are derived from the NOAA/AGAGE/UEA averaged data set.

1.4.2.2 Stratospheric Bromine Changes

Total stratospheric inorganic bromine (Br_y, which includes Br, BrO, $BrONO_2$, HOBr, BrCl, HBr, BrONO, and Br_2) can be determined through modeled estimates of the inorganic product gases arising from bromine source gases (see Section 1.3.2.2). Another method, as discussed in 1.3.2.3, is to use measurements of BrO in the stratosphere and estimate the concentrations of Br_y based on the calculated BrO/Br_y concentration ratios (e.g., Dorf et al., 2006; Millán et al., 2012). Figure 1-20 shows the updated stratospheric Br_y time series inferred from ground-based DOAS (Differential Optical Absorption Spectroscopy) BrO measurements at Lauder (45°S) and Harestua (60°N), and balloon-borne measurements (Dorf et al., 2006). The long-term time series of stratospheric BrO vertical column density measured at Harestua is shown in Figure 1-21 (update of Hendrick et al., 2008). The newly inferred trend values based on Harestua data alone, of +2.2 ± 0.3% yr^{-1} between 1995 and 2001 and of −0.6 ± 0.1% yr^{-1} between 2001 and 2012, are consistent with the previous estimates of Hendrick et al. (2008) of +2.5 ± 0.5% yr^{-1} and −0.9 ± 0.4% yr^{-1}, respectively, who identified a negative trend of stratospheric BrO of about 1% yr^{-1} from 2001 from observations in both hemispheres. The stratospheric Br_y decline is consistent with the observed temporal changes in total tropospheric bromine discussed above.

Recent BrO measurements imply a mean stratospheric Br_y burden of 20 (16–23) ppt in 2011 (Figure 1-20, Kreycy et al. (2013)). The estimated relative contribution to this burden from controlled uses of halons (~8.4 ppt in 2007, accounting for the mean age of stratospheric air) and CH_3Br (~0.3 ppt in 2007 from regulated agricultural use (non-QPS)) is within the range of the last Assessment's estimate of 40–45%, although it is declining slowly. Without accounting for the age of air, the estimated relative contributions to Br_y entering the stratosphere in 2012 from controlled uses are ~8.1 ppt for halons and ~0.15 ppt from regulated agricultural use (non-QPS) of CH_3Br. Thus, VSLS bromocarbons, natural sources of CH_3Br, and QPS uses of CH_3Br (which are not controlled by the Montreal Protocol) contribute more than half of the stratospheric Br_y burden.

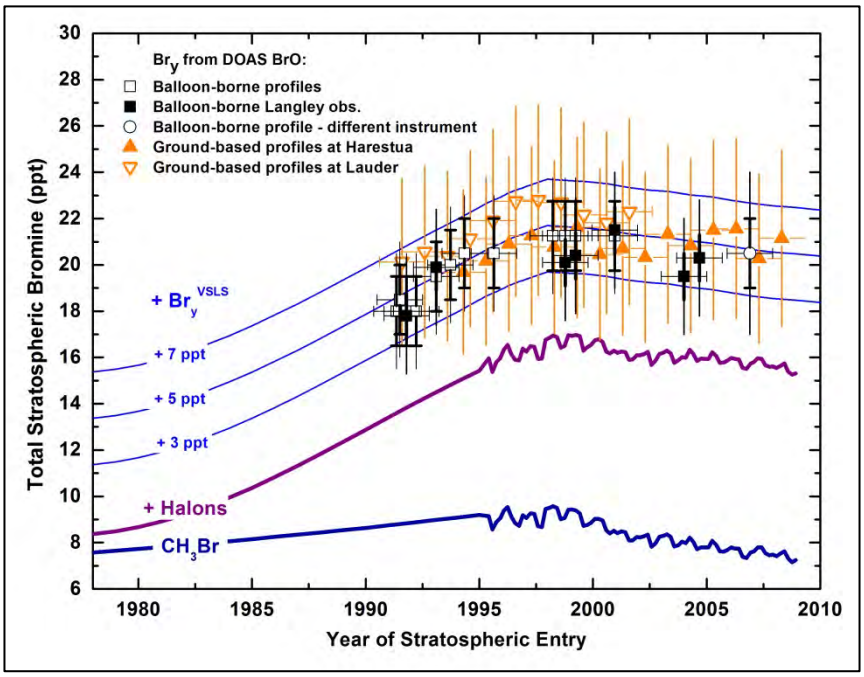

Figure 1-20. Changes in total stratospheric Br_y (ppt) derived from balloon-borne BrO observations (squares) (update of Dorf et al. (2006)) and annual mean mixing ratios calculated from ground-based UV-visible measurements of stratospheric BrO made at Harestua (60°N) and Lauder (45°S) (filled and open orange triangles, respectively) (adapted from Hendrick et al. (2007) and Hendrick et al. (2008)), using a common BrO absorption cross section. These stratospheric trends are compared to trends in measured bromine (ppt) at Earth's surface with additional constant amounts of Br_y added (thin lines). Dark blue line shows global tropospheric bromine from methyl bromide as measured in firn air (pre-1995, including consideration of a changing interhemispheric gradient; Butler et al., 1999) and ambient air (after 1995, Montzka et al., 2003) with no correction for tropospheric CH_3Br loss. Purple line shows global tropospheric bromine from the sum of methyl bromide plus halons (Butler et al. (1999) and Fraser et al. (1999) through 1995; Montzka et al. (2003) thereafter). Thin blue lines show bromine from CH_3Br, halons, plus additional constant amounts of 3, 5, and 7 ppt Br. Total inorganic bromine is derived from (i) stratospheric measurements of BrO and photochemical modeling that accounts for BrO/Br_y partitioning from slopes of Langley BrO observations above balloon float altitude (filled squares); and (ii) lowermost stratospheric BrO measurements (open squares and circles). For the balloon-borne observations, bold/faint error bars correspond to the precision/accuracy of the estimates, respectively. For the ground-based measurements (triangles), the error bars correspond to the total uncertainties in the Br_y estimates. For stratospheric data, the date corresponds to the time when the air was last in the troposphere, i.e., sampling date minus estimated mean age of the stratospheric air parcel. For tropospheric data, the date corresponds to the sampling time, i.e., no corrections are applied for the time required to transport air. This figure updates Figure 1-21 from the previous Assessment (Montzka and Reimann et al., 2011).

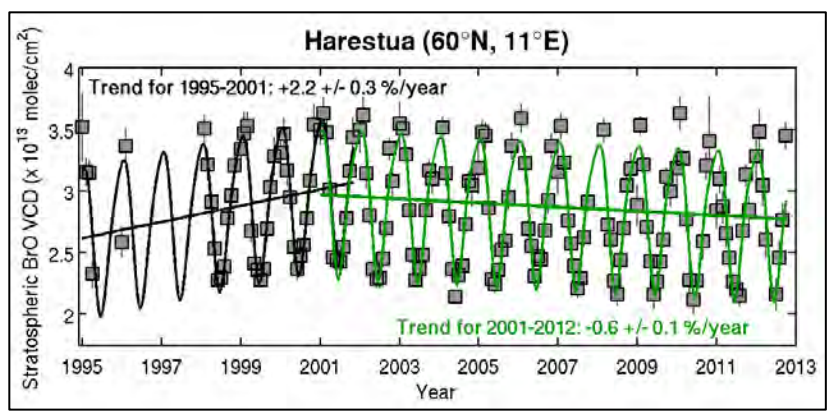

Figure 1-21. Times series of monthly averaged ground-based UV-visible BrO vertical column densities (VCDs) at Harestua (60°N) (update of Hendrick et al., 2008). The gray error bars correspond to the standard error of the monthly mean. The black and green thick solid lines represent the trend analyses for the 1995–2001 and 2001–2012 periods, respectively. The thick straight lines correspond to the linear trend for both periods. The full data set has been optimized using improved DOAS settings (mainly: new fitting window (342–357 nm), O_3 cross sections at 218K and 243K from Brion, Daumont, and Malicet (Brion et al., 1998; Daumont et al., 1992; Malicet et al., 1995), Taylor expansion of O_3 slant column densities in wavelength and vertical optical depth as in Pukite et al. (2010), and O_4 cross sections from Greenblatt et al. (1990)).

1.4.3 Tropospheric and Stratospheric Iodine Changes

1.4.3.1 Tropospheric Iodine Changes

More than a decade of atmospheric CH_3I observations at several remote sites, ranging in location from 82.5°N to 40.4°S, have revealed an increase from 2003–2004 to 2009–2010 by several tens of percent, with a decreasing trend before 2003 (Yokouchi et al., 2012). The interannual variability of the observations corresponded with the Pacific Decadal Oscillation (PDO), suggesting that CH_3I emissions are affected by SST-related processes on a global- and decadal scale.

1.4.3.2 Stratospheric Iodine Changes

There are no new observations of inorganic iodine in the upper troposphere/lower stratosphere (UTLS) since the last Assessment, when available measurements (Bösch et al., 2003; Butz et al., 2009) suggested upper limits of 0.1 ppt IO and 0.1 ppt OIO in the UTLS and a total inorganic stratospheric iodine (I_y) level of <0.15 ppt.

1.4.4 Changes in Ozone-Depleting Halogen Abundance in the Stratosphere Based Upon Long-Lived Source Gas Measurements: Equivalent Chlorine (ECl) and Equivalent Effective Stratospheric Chlorine (EESC)

Changes in the stratospheric burden of total inorganic halogens (Cl and Br) can be estimated from changes in the calculated abundance of Equivalent Effective Stratospheric Chlorine (EESC) (Daniel and Velders, 2007); changes in total tropospheric halogen (Cl and Br) abundance can be addressed with the Equivalent Chlorine (ECl) metric (WMO, 1992). At its peak in 1994–1995, the total abundance of ECl was ~4450 ppt. By 2012 ECl had decreased by nearly 10%, to ~4030 ppt.

EESC is a sum of chlorine and bromine derived from ODS tropospheric abundances weighted to reflect their potential influence on ozone. The EESC abundance and temporal behavior is derived for specific regions of the stratosphere (here, as in previous Assessments, for polar and midlatitude regions), because it is dependent on transport timescales and respective trace gas decomposition rates (see Montzka and Reimann et al. (2011) for further details). We continue to use the formulation of EESC introduced by Newman et al. (2007), which includes a variety of parameters such as transport times (expressed as mean ages of air), the efficiency of different halogens to deplete ozone (expressed as alpha factors), mixing processes, and age-of-air-dependent ODS decomposition rates (i.e., fractional release factors, FRFs), to predict inorganic halogen abundances and changes in the stratosphere based on tropospheric measurements of chlorinated and brominated source gases.

EESC has continued to decrease in both the midlatitude and polar stratosphere (Figure 1-22, upper panel), by 16.2 ± 0.4% and 8.9 ± 1.2%, respectively, between the times of its peak values through to 2012. Midlatitude EESC is calculated at a mean age of 3 years and polar EESC at 5.5 years, with the latter being generally larger due to enhanced ODS decomposition with increasing mean age. Using the average of model-derived fractional release factors from Newman et al. (2007), as used in the last Assessment, and from a new observation-based study by Laube et al. (2013), we find that between 2008 and 2012, EESC declined by 4.15% in midlatitudes and 3.2% in polar latitudes. As in the previous Assessment, we find that no single chemical class dominated these declines in EESC. In the polar stratosphere, CH_3CCl_3 was still the main contributor to this change (−1.3%), with similar contributions from CH_3Br (−1.1%) and long-lived CFCs (−0.9%). CCl_4 was a more minor contributor to the decline (change of −0.4%), whereas both HCFCs (+0.3%) and halons (+0.2%) were counteracting as they were still increasing. In the midlatitude stratosphere, the CH_3CCl_3 change (−1.25%) was less pronounced relative to the total, reflecting its decreasing contribution to total tropospheric Cl, with the EESC changes

mostly influenced by CH_3Br (−1.4%). CFCs contributed −1.0%, CCl_4 −0.55%, halons were contributors to an EESC decrease for the first time (change of −0.25%), and increases in HCFCs contributed +0.2%.

EESC calculations displayed in the lower panel of Figure 1-22 show changes in EESC relative to peak levels observed in the mid-1990s and amounts inferred for 1980 (Hofmann and Montzka, 2009), and are calculated separately using the FRFs from Newman et al. (2007) and Laube et al. (2013). The new FRFs do not appreciably change our understanding of the relative decline in EESC over time. We find 38–41% recovery to 1980 levels in midlatitudes (2008: 28%) and 16–21% recovery in polar latitudes (2008: 10%) by 2012. We note that ozone depletion is likely to have already been significant before the benchmark recovery date (1980).

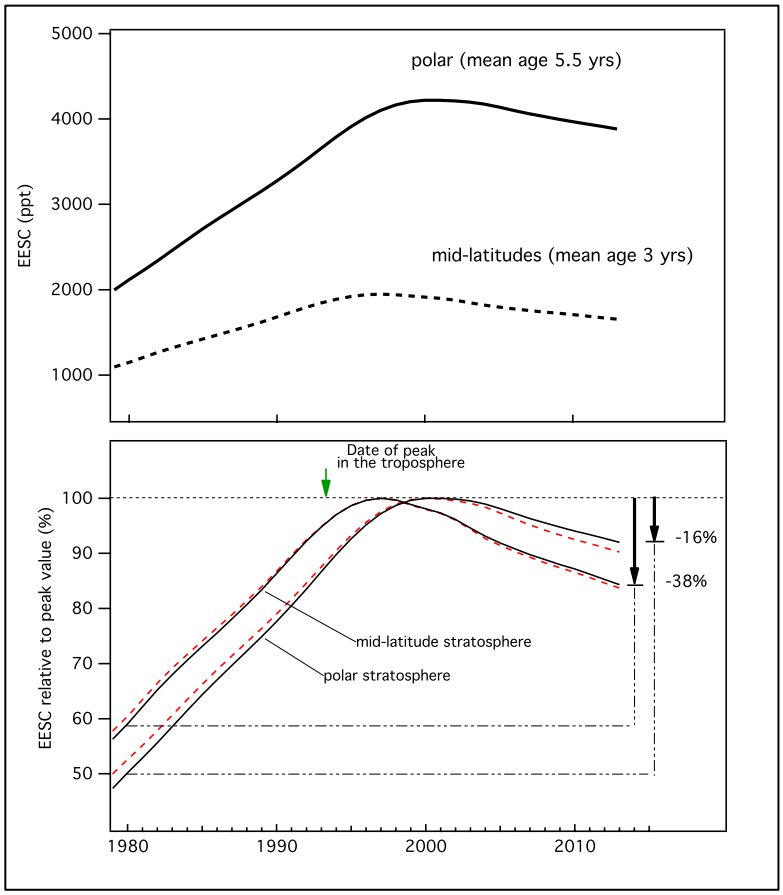

Figure 1-22. The Equivalent Effective Stratospheric Chlorine (EESC) was calculated for the midlatitude and polar stratosphere based on global mean mole fractions measured at the surface. Mean ages of 3 years (midlatitude) and 5.5 years (polar) were used along with spectral widths equal to one-half of the mean age. Surface data included CFC-11, CFC-12, CFC-113, CFC-114, CFC-115, CFC-112, CFC-113a, CH_3CCl_3, CCl_4, HCFC-22, HCFC-141b, HCFC-142b, halon-1211, halon-1301, halon-1202, halon-2402, CH_3Br, and CH_3Cl. Surface data were derived from NOAA and AGAGE global networks and from global means estimated from Cape Grim archive air samples (see Figure 1-1). Calibration scale adjustments were made as necessary. The lower panel shows EESC relative to peak levels. Percentages on the right indicate the observed changes in EESC relative to the changes needed for EESC to return to 1980 levels (note that in 1980, more than half the EESC abundance was already from anthropogenic origin). Here, two EESC cases are shown: (1) using age-of-air-dependent fractional release factors (FRF) from Newman et al. (2007) (black lines), and (2) using age-of-air-dependent FRF from Laube et al. (2013) (red lines). FRFs for CFC-112 and CFC-113a were derived as in Laube et al. (2014) for both cases. EESC returned 38–41% (midlatitude) and 16–21% (polar) of the way toward 1980 levels by the end of 2012.

Using the different FRFs (Newman et al., 2007; Laube et al., 2013), however, results in fairly significant differences in the absolute magnitude of reactive halogens as EESC, and different relative contributions of different gases to the EESC decline. The dominating limitations and uncertainties in EESC estimates are related to the methods used to derive inorganic halogen abundances in the stratosphere, which in turn relate to a limited understanding of ODS decomposition rates (expressed as FRFs), and mixing processes (Newman et al., 2007). Calculations of FRFs are dependent upon the methods used to calculate stratospheric mean ages of air (including assumptions on age spectra), interannual variability (especially in the Arctic winter), and long-term changes in stratospheric circulation (Engel et al., 2009; Stiller et al., 2012). Further, the relationship between a trace gas and the EESC derived from it could change with time if the tropospheric trends of the respective ODSs change (Laube et al., 2013); for trends changing by a few percent per year, the impact on the FRF is expected to be a few percent.

The study by Laube et al. (2013), who derived FRFs for 10 major ODSs (CFC-11, CFC-12, CFC-113, HCFC-22, HCFC-141b, HCFC-142b, CCl_4, CH_3CCl_3, halon-1211, and halon-1301), translates into a 22% reduction of the total abundance of EESC from these compounds in midlatitudes and 24% in polar latitudes in 2008, compared to WMO (2011). In terms of the relative importance of different ODS groups, using the Laube et al. (2013) fractional release leads to an increased relative contribution to total EESC from halons and solvents, and a decrease for CFCs and HCFCs, compared to WMO (2011). This would affect future projections depending on the temporal evolution of the individual ODSs; note that in Figure 1-22 the curves derived from the two fractional release data sets diverge most in recent years. In addition it should be noted that no VSLS are included in the EESC. This compound group quickly releases a large portion of its halogen in the lower stratosphere with fractional release factors close to one at relatively low mean ages (Pfeilsticker et al., 2000; Schauffler et al., 2003; Laube et al., 2008). The relative impact of VSLS on stratospheric Equivalent Chlorine is likely to be larger when using the Laube et al. (2013) fractional release.

1.4.5 Fluorine in the Troposphere and Stratosphere

Although the sum of fluorine from ODSs is declining, the tropospheric abundance of fluorine (F) (derived from CFCs -11, -12, -113, -114, -115; HCFCs -22, -141b, -142b, -124; halons -1211, -1301, -2402; HFCs -23, -32, -125, -134a, -143a, -152a, -227ea, -236fa, -245fa, -365mfc, -4310mee; C_1-C_8 perfluorocarbons (PFCs); SF_6; SF_5CF_3; SO_2F_2, and NF_3) was still increasing between 2009 and 2012 at a mean annual rate of 1.2% yr^{-1} or 33 ppt yr^{-1} and reached 2801 ppt in 2012. This recent growth in F, which is caused by the rising abundances of fluorine-containing replacement compounds (such as HFCs), is higher than that observed from 1995–2005 (29 ppt yr^{-1}), but lower than that of the 1980s (81 ppt yr^{-1}) during the period of unrestricted production and use of ODSs.

In the stratosphere, the reservoir species or product gases HF (hydrogen fluoride), COF_2 (carbonyl fluoride), and COClF (carbonyl chlorofluoride) are currently produced by major ODSs and other source gases. In order to estimate recent changes in stratospheric fluorine product gases, only source gases with stratospheric lifetimes of <100 years were considered (Table 1-3). This subset of fluorinated source gases decreased in the troposphere with a change of around −0.5% yr^{-1} during 2009–2012. Therefore, the recent stratospheric fluorine changes are likely to be between these two ranges (−0.5% to +1.2% yr^{-1}).

The stratospheric fluorine reservoir species HF, COF_2, and COClF are monitored by ACE-FTS (Brown et al., 2011; 2014), while the ground-based Network for the Detection of Atmospheric Composition Change (NDACC) Fourier Transform Infrared (FTIR) network (Kohlhepp et al., 2012) provides time series of the more abundant HF and COF_2 only. Using ACE-FTS occultation measurements, trends of total stratospheric fluorine were determined by Brown et al. (2014). Total stratospheric fluorine mole fractions increased from 2004 to 2009 by 24.3 ± 3.1 and 28.3 ± 2.7 ppt yr^{-1} (or 0.96 ± 0.12 and 1.12 ± 0.11% yr^{-1}), for the 30–70°S and 30–70°N latitude bands, respectively.

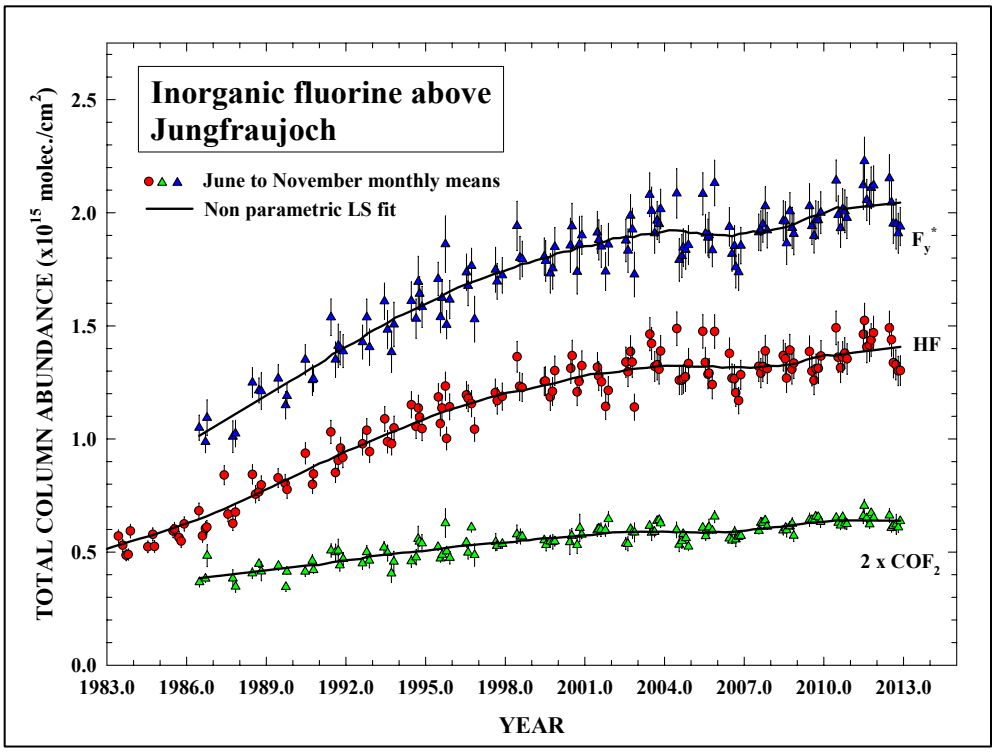

Figure 1-23. Time series of monthly-mean total column HF (red circles) and 2 x COF_2 (green triangles) (molecules per square centimeter), as derived from the Jungfraujoch station (46.5°N) for the June to November months, updated from Montzka and Reimann et al. (2011). The blue triangles correspond to the weighted sum of the HF and COF_2 total columns, i.e., a very good proxy of the total inorganic fluorine at northern midlatitudes (COClF is the only fluorine reservoir missing, with a contribution to the F_y budget estimated to be about 2%).

Kohlhepp et al. (2012) investigated the trend of HF at 16 NDACC stations covering the 80°N to 77.8°S latitude range through 2009. For the vast majority of sites, positive linear trends are reported, generally consistent with an increase of HF at rates close to 1% yr^{-1} when considering the 2000 loadings as reference. The Jungfraujoch time series for HF (Duchatelet et al., 2010) and COF_2 (Duchatelet et al., 2009) have been updated to include all observations up to the end of 2012 (Figure 1-23). The long-term trends for HF, COF_2, and their combination (F_y* = HF + 2×COF_2) above the Jungfraujoch are all positive and remain in line with values reported in Kohlhepp et al. (2012) as well as in Montzka and Reimann et al. (2011). Overall, the remote-sensing measurements of stratospheric F indicate global trends close to a 1% yr^{-1} increase between 2008 and 2012. This is smaller than trends observed during the late 1980s–early 1990s, but within the expected changes for fluorine based on tropospheric trends in ODSs, their substitutes, and other fluorinated gases in recent years.

1.5 CHANGES IN OTHER TRACE GASES THAT INFLUENCE STRATOSPHERIC OZONE AND CLIMATE

1.5.1 Updates to Mole Fractions, Budgets, Lifetimes, and Observations

In this section, anthropogenically emitted substances that are not covered by the Montreal Protocol but that indirectly affect stratospheric ozone are discussed. These include long-lived greenhouse gases such as CH_4, N_2O, hydrofluorocarbons (HFCs), other fluorinated chemicals (e.g., perfluorocarbons (PFCs), SF_6, NF_3), and some other sulfur-containing gases. HFCs are a focal point because they are potent

greenhouse gases and their increasing abundance in the atmosphere is a direct consequence of the restrictions on ODS production and consumption under the Montreal Protocol. Note that CO_2 is not discussed because it was thoroughly discussed in the recent Intergovernmental Panel on Climate Change (IPCC) 5th Assessment Report (IPCC, 2013).

1.5.1.1 F-GASES

F-gases define a class of source gases with fluorine as the only halogen attached either to carbon, sulfur, or nitrogen. F-gases are also called Kyoto Protocol synthetics are almost solely emitted from anthropogenic activities. Stratospheric reservoir species such as HF (hydrogen fluoride) or COF_2 (carbonyl fluoride) are not included here but in Section 1.4.5. F-gases do not deplete ozone but are potent greenhouse gases and therefore have an indirect effect on the ozone budget. They include the HFCs, the PFCs, sulfur hexafluoride (SF_6), sulfuryl fluoride (SO_2F_2), and nitrogen trifluoride (NF_3). Whereas HFCs have been introduced as replacements for ODSs under the Montreal Protocol for applications such as refrigeration and foam blowing, PFCs are by-products of the aluminum industry or are used in the semiconductor industry (IPCC/TEAP, 2005). Most HFCs and all PFCs are long-lived and have high Global Warming Potentials (GWPs). HFCs, in particular, were the subject of studies that forecasted that they could contribute considerably to climate change in the future (Velders et al., 2012, Rigby et al., 2014). In order to ease this environmental pressure, they are increasingly being replaced by shorter-lived alternatives such as unsaturated HFCs (also named hydrofluoro-olefins, HFOs), or by the non-halogenated gases such as hydrocarbons, CO_2, or not-in-kind alternatives (UNEP, 2011a, 2013a). In the group of sulfur-containing F-gases, SF_6 is used as insulator gas in electrical switchgear and to a minor extent in various industrial applications (Maiss and Brenninkmeijer, 1998), and SO_2F_2 is used as a replacement for CH_3Br in soil and grain fumigation (Mühle et al., 2009). Finally, NF_3 is increasingly used in the semiconductor industry as a replacement for PFCs (Prather and Hsu, 2008, 2010; Fthenakis et al., 2010).

Update on observations and on atmospheric budget

Updates of the global mean abundances of F-gases measured by global networks and from archived unpolluted air collected at Cape Grim, Tasmania (Langenfelds et al., 1996) are given in Table 1-14 and Figure 1-24. Global emissions were derived from these observations, their trends, and their loss rates (i.e., lifetimes) as in Section 1.2 for ODSs (Figure 1-25). Regional emissions can be assessed by either extracting information from globally distributed measurements (e.g., Stohl et al., 2009; Rigby et al., 2010) or by using measurements from the source regions (e.g., Miller et al., 2012; Kim et al., 2010; Keller et al., 2012).

HFC-134a (CH_2FCF_3)

Since the mid-1990s, HFC-134a has been used as replacement refrigerant for CFC-12 in mobile air conditioners, stationary refrigeration, as well as in foam-blowing applications, in aerosol inhalers, and for dry etching (Montzka et al., 1996; O'Doherty et al., 2004). In 2012 HFC-134a was the most abundant HFC and the two independent sampling networks (NOAA, AGAGE) show good agreement in its global mean mole fraction of 67.7 (67.5–67.8) ppt and also in the average annual trend of +5.0 ppt yr^{-1} (or 7.6% yr^{-1}) in 2011–2012 (Table 1-14). Furthermore, with a radiative forcing of 11 mW m^{-2}, HFC-134a was the F-gas with the largest radiative forcing in 2012. As HFC-134a has a high 100-year GWP of 1360 (Chapter 5), low-GWP refrigerants (e.g., HFC-1234yf) are being considered as alternatives for its use in mobile air conditioning and other applications.

Estimated global emissions of 176 ± 39 Gg in 2012 represent an increase of 4% yr^{-1} over emissions derived in 2008 (148 ± 24 Gg). Stohl et al. (2009) estimated that regional emissions were highest in Asia and the U.S., followed by Europe, with 29%, 28%, and 17% of the global emissions, respectively. Despite the extrapolations involved with most of these regional studies, results from more recent regional studies are largely in accordance with these findings for the U.S. (Barletta et al., 2011; Miller et al., 2012), Europe (Keller et al., 2012), and Asia (Kim et al., 2010; Stohl et al., 2010; Fang et al., 2012; Yao et al., 2012).

Table 1-14. Measured mole fractions of selected fluorinated compounds (HFCs, PFCs, SF_6, NF_3, SO_2F_2, SF_5CF_3) and CH_4, N_2O, and COS.

Chemical Formula	Common or Industrial Name	Annual Mean Mole Fraction (ppt)			Change (2011–2012)		Network, Method
		2008	2011	2012	ppt yr^{-1}	% yr^{-1}	
Hydrofluorocarbons (HFCs)							
CHF_3	HFC-23	21.9	24.1	25.0	0.9	3.6	AGAGE, in situ (Global)
CH_2F_2	HFC-32	2.7	5.2	6.3	1.1	19	AGAGE, in situ (Global)
CHF_2CF_3	HFC-125	6.1	9.7	11.2	1.5	7.1	AGAGE, in situ (Global)
CH_2FCF_3	HFC-134a	48.1	62.7	67.8	5.1	7.8	AGAGE, in situ (Global)
		47.6	62.7	67.5	4.9	7.5	NOAA, flask & in situ (Global)
		48.4	64.3	68.9	4.6	8.3	UCI, flask (Global)
CH_3CF_3	HFC-143a	8.6	12.1	13.4	1.3	11	AGAGE, in situ (Global)
CH_3CHF_2	HFC-152a	5.8	6.7	6.9	0.2	2.9	AGAGE, in situ (Global)
		5.6	6.5	6.7	0.2	3.0	NOAA, flask & in situ (Global)
$CHF_2CH_2CF_3$	HFC-245fa	0.86	1.28	1.44	0.16	12	AGAGE, in situ (Global)
$CH_3CF_2CH_2CF_3$	HFC-365mfc	0.44	0.59	0.65	0.06	9.7	AGAGE, in situ (Global)
CHF_3CHCF_3	HFC-227ea	0.44	0.66	0.74	0.08	11	AGAGE, in situ (Global)
$CF_3CF_2(CHF)_2CF_3$	HFC-43-10mee	0.15	0.20	0.21	0.01	7.9	AGAGE, in situ (Global)
Perfluorocarbons (PFCs)							
CF_4	PFC-14	77.1	79.0	79.7	0.8	1.0	AGAGE, *in situ* (Global)
C_2F_6	PFC-116	3.9	4.2	4.2	0.1	1.9	AGAGE, *in situ* (Global)
C_3F_8	PFC-218	0.50	0.56	0.57	0.01	2.1	AGAGE, *in situ* (Global)
c-C_4F_8	PFC-318c	*1.11*	*1.20*	*1.24*	*0.04*	*3.2*	*UEA, Cape Grim*
C_4F_{10}	PFC-31-10	0.17	0.17				AGAGE, flask (Global)
		0.174	0.178	0.177	0.00	n.s.	*UEA, Cape Grim*
C_5F_{12}	PFC-41-12	0.12	0.13				AGAGE, flask (Global)
		0.133	*0.136*	*0.134*	*0.00*	*n.s.*	*UEA, Cape Grim*
C_6F_{14}	PFC-51-14	0.26	0.27				AGAGE, flask (Global)
		0.245	0.252	0.252	0.00	*n.s.*	*UEA, Cape Grim*
C_7F_{16}	PFC-61-16	0.11	0.12				AGAGE, flask (Global)
		0.095	*0.108*	*0.107*	*0.00*	*n.s.*	*UEA, Cape Grim*
C_8F_{18}	PFC-71-18	0.09	0.09				AGAGE, flask (Global)
Other fluorinated compounds							
SF_6	Sulfur hexafluoride	6.42	7.28	7.58	0.30	4.1	AGAGE, in situ (Global)
		6.46	7.30	7.59	0.29	4.0	NOAA, flask & in situ (Global)

(continued next page)

Chemical Formula	Common or Industrial Name	Annual Mean Mole Fraction (ppt)			Change (2011–2012)		Network, Method
		2008	2011	2012	ppt yr^{-1}	% yr^{-1}	
NF_3	Nitrogen trifluoride	0.59	0.86				AGAGE, flask (Global)
SO_2F_2	Sulfuryl fluoride	1.5	1.7	1.8	0.1	5.4	AGAGE, in situ (Global)
SF_5CF_3		*0.149*	*0.152*	*0.153*	*0.001*	n.s.	*UEA, Cape Grim*
Other compounds							
CH_4 (ppb)	Methane[1]	1787.9	1803.8	1808.9	5.1	0.28	AGAGE, in situ (Global)
		1787.4	1803.1	1808.3	5.2	0.29	NOAA, flask & in situ (Global)
		1785.3	1798.1	1807.5	9.4	0.52	UCI, flask (Global)
		1785.2	1802.9	1806.5	3.6	0.20	CSIRO, flask (Global)
N_2O (ppb)	Nitrous oxide	321.6	324.1	325.0	0.85	0.26	AGAGE, in situ (Global)
		321.6	324.2	325.0	0.84	0.26	NOAA, flask & in situ (Global)
		321.4	324.0	324.9	0.93	0.29	CSIRO, flask (Global)
		321.7	324.2	325.1	0.9	0.28	WMO/GAW (Global)
COS (ppt)	Carbonyl sulfide	491	491	493	2	0.4	NOAA, flask & in situ (Global)

Mole fractions in this table represent independent estimates measured by different groups for the years indicated. Results indicated as "Global" are estimates of global surface mean mole fractions. Numbers in italics are from single sites that do not provide a global estimate.

Absolute changes (ppt yr^{-1}) are calculated as the difference in annual means; relative changes (% yr^{-1}) are the same difference relative to the average between 2011 and 2012 values. Small differences between values from previous Assessments are due to changes in calibration scale and methods for estimating global mean mole fractions from a limited number of sampling sites. n.s.: not significant.

These observations are updated from the following sources: Prinn et al. (2000); O'Doherty et al. (2004); Simpson et al. (2004); Montzka et al. (2007); Simpson et al. (2007); Miller et al. (2008); Montzka et al. (2009); Chevallier et al. (2010); Dlugokencky et al. (2011); Hall et al. (2011); Ivy et al. (2012a); Laube et al. (2012); Oram et al. (2012); Simpson et al. (2012); Sturges et al. (2012); Arnold et al. (2013); Thompson (2014).

AGAGE, Advanced Global Atmospheric Gases Experiment (http://agage.eas.gatech.edu/) with AGAGE calibrations as specified in CDIAC (2014) and related primary publications; NOAA, National Oceanic and Atmospheric Administration, U.S. (http://www.esrl.noaa.gov/gmd/dv/site/); UEA, University of East Anglia, United Kingdom (http://www.uea.ac.uk/environmental-sciences/research/marine-and-atmospheric-sciences-group); UCI, University of California, Irvine, U.S. (http://ps.uci.edu/~rowlandblake/research_atmos.html); Cape Grim: Cape Grim Baseline Air Pollution Station, Australia; WMO/GAW, World Meteorological Organization, Global Atmosphere Watch, World Data Center for Greenhouse Gases, http://ds.data.jma.go.jp/gmd/wdcgg.

[1]Global mean estimates for CH_4 from the WMO/GAW network are not included here because the criteria used for data selection in the WMO/GAW global mean mole fraction calculation are inconsistent with other global mean estimates shown. While NOAA, AGAGE, and CSIRO contribute data to the WMO/GAW network, the addition of inland and high-altitude sites in the WMO/GAW global mean leads to estimates for CH_4 that are ~11 ppb larger than those shown here.

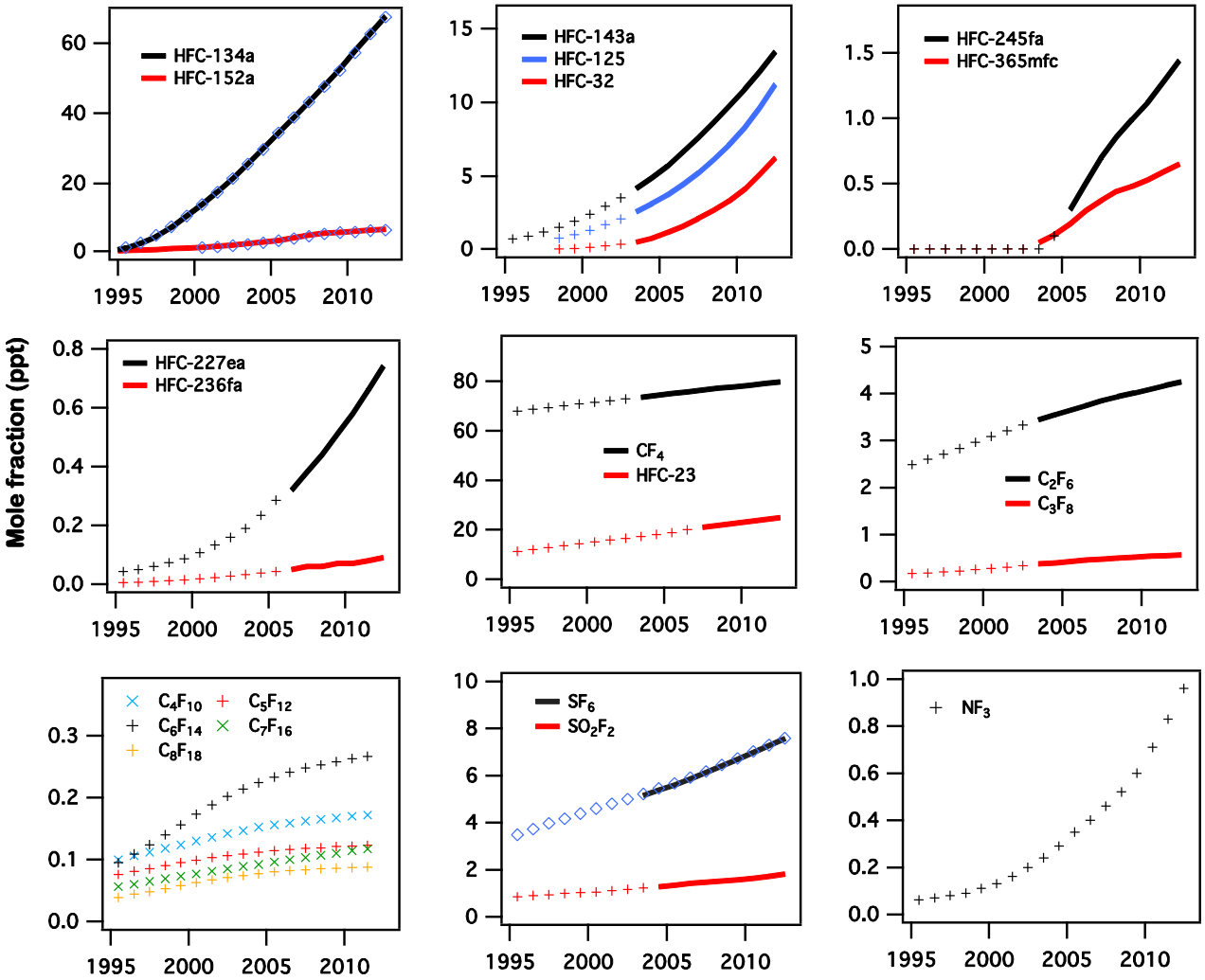

Figure 1-24. Global mole fractions of F-gases. Continuous measurements by the AGAGE network are shown as solid lines; NOAA data are shown by blue diamonds. Global mole fractions that have been compiled from grab samples or air archive measurements (e.g., from Cape Grim, Australia) are shown using additional symbols.

HFC-23 (CHF_3)

The mean global mole fraction of HFC-23 reached 25 ppt in 2012, and has increased at a rate of ~1 ppt yr^{-1} or 3.6% yr^{-1} in recent years (Table 1-14). At this global abundance, HFC-23 contributed 4.5 mW m^{-2} to the atmospheric radiative forcing in 2012. Trends of HFC-23 from ground-based measurements are similar to increases derived from remote sensing instruments (Harrison et al., 2012) (Table 1-2). However, calculated absolute mole fractions are around 30% higher from remote sensing data than from ground-based measurements.

HFC-23 is emitted into the atmosphere nearly exclusively as a by-product from over-fluorination during the production of HCFC-22, with only minor emissions from fire extinguishers, semiconductor industry, refrigeration, and as a feedstock for halon-1301 (Oram et al., 1998; Miller et al., 2010). Many HCFC-22 production facilities have destroyed the co-produced HFC-23 before it was emitted into the atmosphere or optimized the chemical process to minimize its formation (Miller et al., 2010; Han et al.,

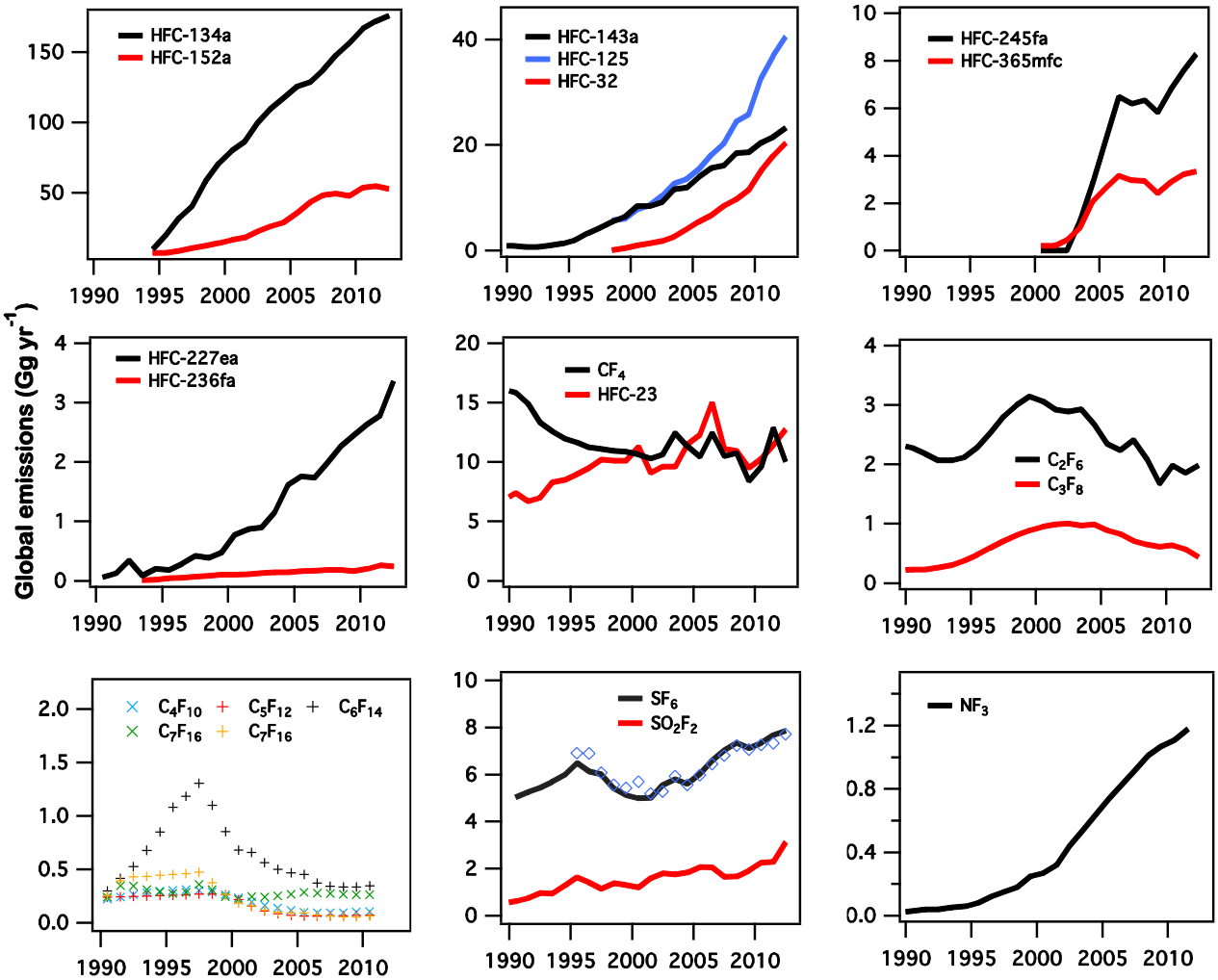

Figure 1-25. Global emissions of F-gases estimated by a global 12-box model (as described in Rigby et al. (2013)) using data shown in Figure 1-24 and lifetimes from SPARC (2013).

2012). For developing countries, this capability was facilitated by funding from the Clean Development Mechanism (CDM) under the Kyoto Protocol of the United Nations Framework Convention on Climate Change (UNFCCC).

Global emissions of HFC-23 estimated from measured and derived atmospheric trends reached a maximum of 15 Gg yr^{-1} in 2006, fell back to 8.6 Gg in 2009, and subsequently increased again to 12.8 Gg in 2012 (Figure 1-25, update of Miller et al., 2010 and Montzka et al., 2010). Whereas efforts in non-Article 5 countries mitigated an increasing portion of HFC-23 emissions through 2004, the temporal decrease from 2007 to 2009 was likely caused by destruction facilitated by the CDM, even though HCFC-22 production was highest around this time (Figure 1-8). The recent resurgence in emissions since 2009 could be the result of an increase in production of HCFC-22 (see Figure 1-8) with no subsequent incineration of HFC-23 (reference case in Miller and Kujipers, 2011), or less CDM-aided destruction of existing production in developing countries. Indeed, Miller and Kuijpers (2011) warned that HFC-23 emissions could surpass the historic peak values from 2006 if CDM projects ceased to be supported and feedstock production of HCFC-22 grows unabated.

Current emissions of HFC-23 occur foremost in East Asia. Studies from Yokouchi et al. (2006), Stohl et al. (2010), and Kim et al. (2010) estimate emissions in China to be in the range of 6 to 12 Gg yr^{-1} between 2004 and 2008. In contrast, Yao et al. (2012) estimated lower emissions of only 2.8 Gg yr^{-1} for China in 2010–2011, based on measurements at one site and a limited catchment area. In Europe, underreported emissions of HFC-23 from some HCFC-22 production facilities were found by Keller et al. (2011), but the difference of around 0.2 Gg yr^{-1} was small in comparison to global sources.

HFC-152a (CH_3CHF_2)

HFC-152a is used as a foam-blowing agent and as an aerosol propellant (Greally et al., 2007). Its growing average global mole fraction reached 6.8 ppt in 2012. The global mole fraction of HFC-152a grew at an average rate of 0.69 ± 0.04 ppt yr^{-1} from 2005–2008, but has slowed since 2008 to around 0.28 ppt yr^{-1} (Figure 1-24, Table 1-14). Global emissions derived from measured global mole fractions and trends appear to have stabilized at ~50 Gg yr^{-1} since 2010 (Figure 1-25). HFC-152a has a relatively small GWP_{100} (of 133; Chapter 5) and its direct radiative forcing is small compared to other HFCs.

Currently the U.S. is the world's most important source region for HFC-152a. Estimated U.S. emissions range from 25 (11–50) Gg yr^{-1} between 2004–2009 (Miller et al., 2012), to 12.3–15.1 Gg yr^{-1} in 2006 (Stohl et al., 2009), to 32 Gg yr^{-1} in 2008 (Barletta et al., 2011). European emissions were estimated to be 2.9 Gg in 2009 (Keller et al., 2012). Emissions from China were estimated to be 2.0–2.9 Gg yr^{-1} in 2010–2011 by Yao et al. (2012), which was lower than 3.4–5.7 Gg yr^{-1} estimated by Yokouchi et al. (2006), Kim et al. (2010), and Stohl et al. (2010) in former years.

HFC-32 (CH_2F_2), HFC-125 (CHF_2CF_3), HFC-143a (CH_3CF_3)

These three HFCs are mostly used as refrigerants. They are blended in various combinations, for stationary air conditioners as well as for various minor applications (e.g., for fire suppression) replacing HCFC-22 and CFC-115 (IPCC/TEAP, 2005; O'Doherty et al., 2009). Global background mole fractions of HFC-32, HFC-125, and HFC-143a are steadily growing (Table 1-14, Figure 1-24). Current annual growth rates of more than 1 ppt yr^{-1} are among the highest for all F-gases, showing the importance of these refrigeration blends in connection with the phase-out of ozone-depleting HCFCs and CFCs. Global estimates of their emissions in 2012 were 19 Gg yr^{-1}, 40 Gg yr^{-1}, and 24 Gg yr^{-1} for HFC-32, HFC-125, and HFC-143a, respectively. During 2009–2012 the emissions approximately doubled for HFC-32 and HFC-125, and increased by ~50% for HFC-143a. The combined radiative forcing of these three substances was 5.4 mW m^{-2} in 2012, with highest impact from HFC-125 (2.6 mW m^{-2}).

Regional emissions of these three gases have been estimated by several studies in recent years (2004–2011). However, differing time periods and the rapid increase of emissions hinder the direct comparison with total global emission estimates. Estimated emissions from the last decade from East Asia as estimated by Li et al. (2011) and Yao et al. (2012) were of the same order of magnitude as estimated emissions from Europe (O'Doherty et al., 2009; Keller et al., 2012) and from the U.S. (Miller et al., 2012) for different years during this same period.

HFC-245fa ($CF_3CH_2CHF_2$) and HFC-365mfc ($CF_3CH_2CF_2CH_3$)

HFC-245fa and HFC-365mfc are replacements for HCFC-141b in foam-blowing applications (Vollmer et al., 2006; Stemmler et al., 2007; Vollmer et al., 2011). In 2012 global average mole fractions reached 1.44 and 0.65 ppt for HFC-245fa and HFC-365mfc (Table 1-14), respectively, and were increasing between 2011–2012 at similar rates of 12% and 10% (Table 1-14). The approximately factor-of-two difference in the global mean mole fractions for these two compounds is also reflected in the 2011–2012 growth rates of 0.17 ppt and 0.07 ppt for HFC-245a and HFC-365mfc, respectively. Global atmospheric-derived emissions of HFC-245fa and HFC-365mfc leveled off after 2006 but showed a renewed increase since 2010 and reached 8.2 Gg yr^{-1} for HFC-245fa and 3.1 Gg yr^{-1} for HFC-365mfc by 2012 (Figure 1-25).

HFC-227ea (CF_3CHFCF_3)

HFC-227ea is used in fire suppression, metered dose inhalers, refrigeration, and foam blowing. Vollmer et al. (2011) recently used archived air from both hemispheres to reconstruct the atmospheric history of HFC-227ea. They inferred that the global background mole fraction of HFC-227ea has grown from less than 0.1 ppt in the 1990s to 0.58 ppt in 2010 and that the annual growth rate of HFC-227ea increased from 0.026 ppt yr^{-1} in 2000 to 0.069 ppt yr^{-1} in 2010 (Vollmer et al., 2011). Global emissions were estimated to be 2.5 Gg yr^{-1} in 2010. These results were confirmed by firn air samples from Greenland (Laube et al., 2010), which showed similarly low mole fractions in the 1990s and increasing global emissions of nearly 2 Gg yr^{-1} in 2007. In 2012 the global background mole fraction was 0.74 ppt (Table 1-14) and global emissions were estimated at 3.3 Gg yr^{-1} (Figure 1-25).

HFC-43-10mee ($CF_3CF_2CHFCHFCF_3$)

HFC-43-10mee is used as a cleaning solvent in the electronics industry. First published measurements by Arnold et al. (2014) show a rising global mean mole fraction between 2000 and 2012 (0.04 ± 0.03 ppt to 0.21 ±0.05 ppt). Based on these measurements, global emissions were estimated as 1.13 ± 0.31 Gg yr^{-1} in 2012.

HFC-1234yf (CH_2=$CFCF_3$) and HFC-1234ze(E) (E-CHF=$CHCF_3$)

HFC-1234yf and HFC-1234ze(E) are unsaturated hydrofluorocarbons (also referred to as hydrofluoro-olefins, HFOs) with estimated tropospheric OH-lifetimes of 8–16 days and 13–24 days, respectively (Table 1-11). These substances have small Global Warming Potentials (GWPs) and are therefore considered as replacement compounds for long-lived HFCs with high GWPs. Whereas HFC-1234ze(E) is already used for foam blowing, HFC-1234yf has only recently been accepted as a replacement for HFC-134a in mobile air conditioners and other refrigeration uses (UNEP, 2011a) (Chapter 5).

Although these unsaturated HFCs degrade within days to weeks in the troposphere, there are concerns regarding the impact of their degradation products on the environment. Whereas HFC-1234ze(E) degrades to short-lived intermediates, the atmospheric degradation of HFC-1234yf almost exclusively yields trifluoroacetic acid ($CF_3C(O)OH$, TFA) (Hurley et al., 2008). TFA is resistant to further degradation in the environment and exhibits some herbicidal properties (Boutonnet et al., 1999). Under an upper-limit scenario of full replacement of HFC-134a by HFC-1234yf, Henne et al. (2012) and Papasavva et al. (2009) estimate that European and U.S. emissions of HFC-1234yf could reach ~20 Gg yr^{-1} and 11–25 Gg yr^{-1}, respectively. There is currently no imminent danger connected to this potential input of TFA into the environment (Chapter 5). Accumulation of TFA in specific biomes from the long-term usage of HFC-1234yf is discussed in Cahill et al. (2001) and Russell et al. (2012).

Perfluorocarbons (PFCs)

Perfluorocarbons (PFCs) exclusively consist of carbon and fluorine. They are not substitutes for ODSs, and they have very long atmospheric lifetimes of up to several thousand years (Table 1-3). In combination with their very large radiative efficiencies, they will have a long-lasting influence on the radiative balance of the atmosphere (Ravishankara et al., 1993; Myrhe et al., 2013). The combined radiative forcing of the PFCs was 6.0 mW m^{-2} in 2012, with CF_4 as the main contributor.

Four PFCs were reported in the last Assessment (PFC-14 or CF_4, PFC-116 or C_2F_6, PFC-218 or C_3F_8, and PFC-c-318 or c-C_4F_8). Ground-based mole fractions and growth rates for CF_4, C_2F_6, and C_3F_8 were updated from Mühle et al. (2010) and are shown in Table 1-14 and Figure 1-24. CF_4 observations based on remote-sensing techniques (Mahieu et al., 2014) find a comparable trend in the atmospheric abundance as for the ground-based measurements (Table 1-2). Furthermore, mole fractions and trends of c-C_4F_8 have been updated by Saito et al. (2010) and Oram et al. (2012), with a global mole fraction in 2012 estimated at 1.24 ppt (Table 1-14) and estimated global emissions of 1.1 Gg yr^{-1} in 2007 (Oram et al., 2012). PFC-218 was shown to be a minor PFC emission from aluminium smelting, the major PFCs being PFC-14 and PFC-116 (Fraser et al., 2013).

Since the previous Assessment, atmospheric mole fractions and emissions have been newly reported for n-C_4F_{10}, n-C_5F_{12}, n-C_6F_{14}, n-C_7F_{16}, and n-C_8F_{18} in three recent publications (Ivy et al., 2012a, 2012b; Laube et al., 2012). As shown in Table 1-14, the mole fractions of all five long-chain PFCs are currently below 0.3 ppt. Their current growth rates are small and have continued to decrease in recent years, which could be due to the introduction of emission reduction techniques in industrial applications (Tsai et al., 2002). With nearly 1.5 Gg yr^{-1} in the 1990s highest emissions from these group of compounds was reached by n-C_6F_{14} (Figure 1-25). In recent years emissions of all these PFCs were stable and smaller than 0.5 Gg yr^{-1}.

Lifetime estimates for the perfluorocarbons (PFCs) C_3F_8, c-C_3F_6, and C_4F_{10} were revised in this Assessment (Table 1-3). PFCs are persistent greenhouse gases removed primarily in the upper-stratosphere and mesosphere (>65 km) mainly by Lyman-α (121.6 nm) photolysis. Lifetime estimates for PFCs (>2000 yr) are typically obtained from model calculations and are highly dependent on transport from the lower atmosphere. The revised lifetime estimates of these three PFCs shown in Table 1-3 are based on a correlation of an increase in Lyman-α absorption cross section with an increase in the $-CF_2$-sub-units within the molecule. Baasandorj et al. (2012) reported improved upper-limits for $O(^1D)$ reactive rate coefficients for C_2F_6, c-C_4F_8, n-C_5F_{12}, and n-C_6F_{14}, which reduces the calculated contribution of $O(^1D)$ reaction to their atmospheric loss further from the rate coefficient studies of Zhao et al. (2010) and Ravishankara et al. (1993). Furthermore, the lifetime for C_8F_{18} was estimated to be ~3000 years by (Ivy et al., 2012a), which was adopted in this Assessment.

Sulfur hexafluoride (SF_6)

The global average mole fraction of sulfur hexafluoride (SF_6) continues to increase, and reached 7.6 ppt in 2012 (Table 1-14). The global average mole fraction at the surface was increasing at ~0.22 ppt yr^{-1} in the early 2000s, but has averaged ~0.28 ppt yr^{-1} since 2007 (Rigby et al., 2010; Hall et al., 2011). Due to its long lifetime (3200 years; Table 1-3) combined with a high radiative efficiency, the contribution of SF_6 to radiative forcing is increasing accordingly. The resulting radiative forcing in 2012 was 4.3 mW m^{-2}.

Remote sensing techniques have also contributed to the monitoring of SF_6 over the recent years. Brown et al. (2011) using ACE-FTS data, Stiller et al. (2012) using MIPAS global data, and Zander et al. (2008) using ground-based solar spectroscopy at Jungfraujoch all found growth rates which were comparable with the in-situ measurements (Table 1-2).

Global atmospheric-based emissions of SF_6 were estimated by Levin et al. (2010) and Rigby et al. (2010) at 7.2–7.5 Gg yr^{-1} in 2008. Emissions since then have increased and were at their highest historic levels in 2012 at almost 8 Gg yr^{-1} in 2012 (Figure 1-25). Rigby et al. (2010) found that the rise in global emissions from 2004–2008 was likely mostly due to emissions from Asian developing countries. Consistent with this, Fang et al. (2013) estimated the contribution from East Asia to SF_6 emissions to be 3.8 ± 0.5 Gg yr^{-1} in 2009, or a contribution of about 50% to global SF_6 emissions. In addition, based on an extrapolation of results from the northeastern U.S. only, Miller et al. (2012) reported U.S. emissions of 1.4 (0.7–3.0) Gg yr^{-1} from 2004–2009, which is equivalent to about 20% of global emissions in 2008.

Trifluoromethylsulfurpentafluoride (SF_5CF_3)

This substance was discovered in the atmosphere by Sturges et al. (2000), with a global background mole fraction of 0.12 ppt in 1999 and 0.15 ppt in 2010 (Sturges et al., 2012). SF_5CF_3 is very long lived, with an estimated lifetime of 650–950 years (Table 1-3). SF_5CF_3 levels have been stable in recent years and therefore Sturges et al. (2012) concluded that emission sources have ceased. They provide strong indications that SF_5CF_3 was released as a by-product of the production of perfluorooctanyl sulfonate (PFOS) and similar compounds. Furthermore, they used firn air measurements to place the onset of SF_5CF_3 emissions in the early 1960s. Baasandorj et al. (2012) reported improved upper limits for the $O(^1D)$ reactive rate coefficient of SF_5CF_3, thereby enhancing knowledge of its atmospheric loss processes from previous studies but not changing its lifetime estimate (Ravishankara et al., 1993; Zhao et al., 2010).

Nitrogen trifluoride (NF_3)

NF_3 is used in the production of flat panel displays, in plasma etching, and in the semiconductor industry as a replacement for PFCs (Weiss et al., 2008; Fthenakis et al., 2010). It was first measured in the atmosphere by Weiss et al. (2008). The measured record was recently extended and revised with a new calibration (Arnold et al., 2012, 2013). Its global tropospheric mole fraction was 0.86 ± 0.04 ppt in 2011 (Table 1-14) with a yearly rate of increase of 0.10 ± 0.01 ppt (11%) between 2010 and 2011.

Global emissions of NF_3 increased continuously from 0.21 Gg yr^{-1} in 1998 to 1.18 Gg yr^{-1} in 2011 (Arnold et al., 2013; Figure 1-25). With a radiative forcing of just 0.2 mW m^{-2}, the effect of NF_3 on climate was still very small in 2011. However, its large atmospheric growth rate and its application in the growing semiconductor industry have a high potential to increase its importance in the future. Therefore, NF_3 was added to the basket of greenhouse gases in the Doha Amendment to the Kyoto Protocol, which covers emissions in a second commitment period of 2013–2020 (UNFCCC, 2014).

The NF_3 lifetime estimate was revised in SPARC (2013) to 569 (454–764) years based on 2-D model calculations that included the NF_3 UV absorption spectrum temperature dependence reported by Papadimitriou et al. (2013a). SPARC (2013) also recommended a revision of the $O(^1D) + NF_3$ reaction rate coefficient, although the impact of the revision on the NF_3 lifetime is minor.

Sulfuryl fluoride (SO_2F_2)

Sulfuryl fluoride (SO_2F_2) replaced the ozone-depleting CH_3Br as a fumigant against animal pests in buildings and other places susceptible to infestation (e.g., flour mills, grain silos, transport containers). The average global mole fraction of SO_2F_2 has increased to 1.8 ppt in 2012, with a yearly increase (2011–2012) of 0.1 ppt (5%) (update of Mühle et al., 2009; Table 1-14). The total atmospheric lifetime of SO_2F_2 is 36 ± 11 yr (Mühle et al., 2009), with a partial lifetime for the oceanic uptake of 40 ± 13 yr as its most important contributor. Global emissions calculated from atmospheric observations and the estimated lifetime were 3.1 Gg in 2012. This is an increase of nearly a factor of two in comparison with 2008.

1.5.1.2 NITROUS OXIDE (N_2O)

Nitrous oxide (N_2O) has both natural and anthropogenic sources and unlike most other chemicals discussed in this section, it has a direct chemical influence on ozone (Ravishankara et al., 2009). The influence of N_2O on stratospheric ozone and on climate has been the focus of a recent review (UNEP, 2013c). Photochemical degradation of N_2O in the stratosphere leads predominately to N_2 and O_2, but about 10% is converted to nitrogen oxides (NO, NO_2) (UNEP, 2013c), which contribute to stratospheric ozone depletion. Current ODP-weighted emissions of N_2O from anthropogenic activities are larger than those of any other ozone-depleting species (Ravishankara et al., 2009). Nitrous oxide is also a greenhouse gas, and with the atmospheric burden of CFC-12 decreasing, both of these gases contribute about equally to radiative forcing (Myhre et al., 2013) and are after CO_2 and CH_4 the most important anthropogenic greenhouse gases.

Atmospheric N_2O has increased from a pre-industrial mole fraction of 271 ppb (Ciais et al., 2013) to 325 ppb in 2012 (Table 1-14) with a fairly constant growth rate of 0.8 ppb yr^{-1} over the last decade (3.4 ppb between 2008 and 2012). According to UNEP (2013c), current natural emissions (e.g., from terrestrial, marine, and atmospheric sources) are roughly 11 Tg N_2O-N yr^{-1}. Total gross anthropogenic emissions are estimated to contribute another 6.2 Tg N_2O-N yr^{-1}. Anthropogenic sources include agriculture, biomass burning, and industry (including combustion, production of nitric acid and adipic acid), as well as indirect emissions from reactive nitrogen leaching, runoff, and atmospheric deposition. The observed increase in atmospheric N_2O over preindustrial levels is largely the result of nitrogen-based fertilizer use (Park et al., 2012). Ciais et al. (2013) have estimated that food production was likely responsible for 80% of the increase in atmospheric N_2O in recent decades.

The IPCC AR5 report lists total global N_2O emissions of 17.8 Tg-N yr^{-1} in 2006 (Ciais et al., 2013). This value is consistent with global emissions of 17.5 to 20.1 Tg-N yr^{-1} estimated between 1999 and 2009 (calculated from atmospheric observations and the estimated lifetime (Thompson et al., 2014)), and also with bottom-up estimates of 17.6 Tg-N yr^{-1} from UNEP (2013c). There are, however, substantial

uncertainties associated with both bottom-up and top-down emissions estimates due to uncertain emission factors (bottom-up) and uncertainties in the stratospheric sink (top-down). Revision of emissions factors between AR4 and AR5 resulted in reapportionment of global emissions among anthropogenic sources, but did not significantly affect the global total (Ciais et al., 2013). The global lifetime of N_2O has also recently been updated from 114 yr to 123 yr with a range of 104–152 yr (SPARC, 2013).

1.5.1.3 METHANE (CH_4)

In addition to its influence on radiative forcing, methane affects the efficiency for ODSs to deplete stratospheric ozone by acting as a sink for reactive chlorine (producing HCl as a reservoir species) and as a source of stratospheric water vapor. In the upper stratosphere, enhanced CH_4 concentrations lead to ozone loss through the HO_x catalytic cycle, but also reduce ozone loss by sequestering reactive chlorine. In the lower stratosphere and troposphere, additional CH_4 leads to more ozone through photochemical smog chemistry and CH_4 also reacts with OH radicals, which leads to an influence on the lifetimes of ODSs that also react with OH (such as HCFCs and VSLS). In general, an increase in global CH_4 results in an increase in column ozone (Portmann et al., 2012; Revell et al., 2012; Shindell et al., 2013).

Wetlands are the primary natural source of CH_4, with smaller contributions from sources such as geological seeps and freshwater (Ciais et al., 2013). Anthropogenic sources include agriculture (e.g., rice production, ruminants), landfills, biomass burning, and the extraction and processing of fossil fuels (Kirschke et al., 2013). The global mean mole fraction of CH_4 was 1803 ppb in 2011 (Hartmann et al., 2013) and 1808 ppb in 2012 (Table 1-14). Mole fractions today are more than 2 times greater than those in preindustrial times (1750) (Hartmann et al., 2013). After increasing from ~1750 to the 1980s, global CH_4 mole fractions increased more slowly in the late 1990s and started to stabilize in the early 2000s, but increased again from 1781 ppb in 2007 to 1808 ppb in 2012. Reasons for the growth rate slow-down in the 1990s and renewed increase beginning in 2007 are debated (Rigby et al., 2008; Dlugokencky et al., 2009; Aydin et al., 2011; Bousquet et al., 2011; Kai et al., 2011; Levin et al., 2012; Simpson et al., 2012; Kirschke et al., 2013). The subsequent increase of global CH_4 levels since 2006 is likely due to increased emissions from natural wetlands and fossil fuels, although their relative contributions remain uncertain (Kirschke et al., 2013).

1.5.1.4 COS, SO_2

Carbonyl sulfide (COS) and other sulfur-containing gases such as sulfur dioxide (SO_2) contribute to stratospheric sulfate aerosols (SSA) (SPARC, 2006).

Sources of SO_2 include fossil fuel combustion, volcanoes, and oxidation of precursors. Fossil fuel combustion accounts for the largest part of the total flux of sulfur gases to the atmosphere, mainly from sources in the Northern Hemisphere (SPARC, 2006). While SO_2 emissions were reduced in the U.S. and Europe in the 1980s and 1990s as part of efforts to reduce acid rain, emissions from East Asia have increased in recent years (Lu et al., 2010).

Sources of COS include the oxidation of dimethyl sulfide (DMS) and carbon disulfide (CS_2), and ocean-atmosphere gas exchange (SPARC, 2006). Sinks of COS include uptake by terrestrial plants and soils, and oxidation by OH radicals. Current tropospheric mole fractions of COS (~490 ppt, Table 1-14) are substantially higher than preindustrial values of 300–400 ppt (Montzka et al., 2004). Total column COS measurements above Jungfraujoch indicate a decrease in the total column from 1990–2002 followed by an increase from 2002–2008 (update from Zander et al., 2005). A relatively small trend in global COS derived from surface observations (1.8 ppt yr^{-1}) was reported in the last Assessment for the period 2000–2008 (Montzka and Reimann et al., 2011). Recent observations from the NOAA surface network updated through 2012 suggest that any systematic changes in global COS since 2000 have been small (<3%), with an increase of 0.4% from 2011–2012 (Table 1-14).

The fraction of COS contributing to SSA is uncertain, but could be about 30% (SPARC, 2006). This is supported by recent work by Hattori et al. (2011), Brühl et al. (2012), and Schmidt et al. (2013). However, it is not yet possible to reconcile these studies with an earlier study from Leung et al. (2002), who concluded that COS is only a minor contributor to SSA.

1.6 POLICY-RELEVANT INFORMATION HIGHLIGHTS

1.6.1 HCFCs Becoming a Larger Fraction of Tropospheric Chlorine; Bromine from Halons Now Decreasing

As a result of the Montreal Protocol, the overall abundance of controlled ozone-depleting substances (ODSs) in the atmosphere has been decreasing for over 15 years. The reduction in the atmospheric abundance of an ODS in response to controls on production depends principally on two factors: (1) how rapidly an ODS is used and released to the atmosphere after being produced and (2) the lifetime for the removal of the ODS from the atmosphere. Much of the decline in tropospheric chlorine since the peak in the 1990s was due to decreases in methyl chloroform (CH_3CCl_3), which has a relatively short atmospheric lifetime of about 5 years. This substance still continues to make a significant contribution to declines in total chlorine, although decreases in chlorofluorocarbons (CFCs) are now the largest contributor. Hydrochlorofluorocarbon (HCFC) mixing ratios continue to increase, although at a declining rate.

CFCs still represent the largest fraction of tropospheric chlorine, but their contribution has been decreasing since 2005. The rapid decrease of CH_3CCl_3 in the atmosphere means that its relative contribution to the tropospheric ODS abundance is now approaching zero. Since the peak in total tropospheric chlorine, the relative contribution of carbon tetrachloride (CCl_4) has not changed significantly, due to its relatively slow decline. The abundance of methyl chloride (CH_3Cl), the largest natural contributor to chlorine, has remained fairly constant over the last decades, currently contributing around 17% of tropospheric chlorine. A large proportional change to the total chlorine-containing ODS abundance however comes from HCFCs; their contribution has more than doubled since the mid 1990s.

The largest contributor to the decline in tropospheric bromine is methyl bromide (CH_3Br), which has both natural and anthropogenic sources. The rate of CH_3Br decline has slowed as phase out of controlled emissions is now almost complete, and the balance of emissions is now overwhelmingly of natural origin, with the remainder mostly from non-controlled emissions. While the contribution of halons to total tropospheric bromine has increased since the mid-1990s, bromine from halons is now showing robust signs of decline. Natural sources contribute over half of the abundance of total tropospheric bromine.

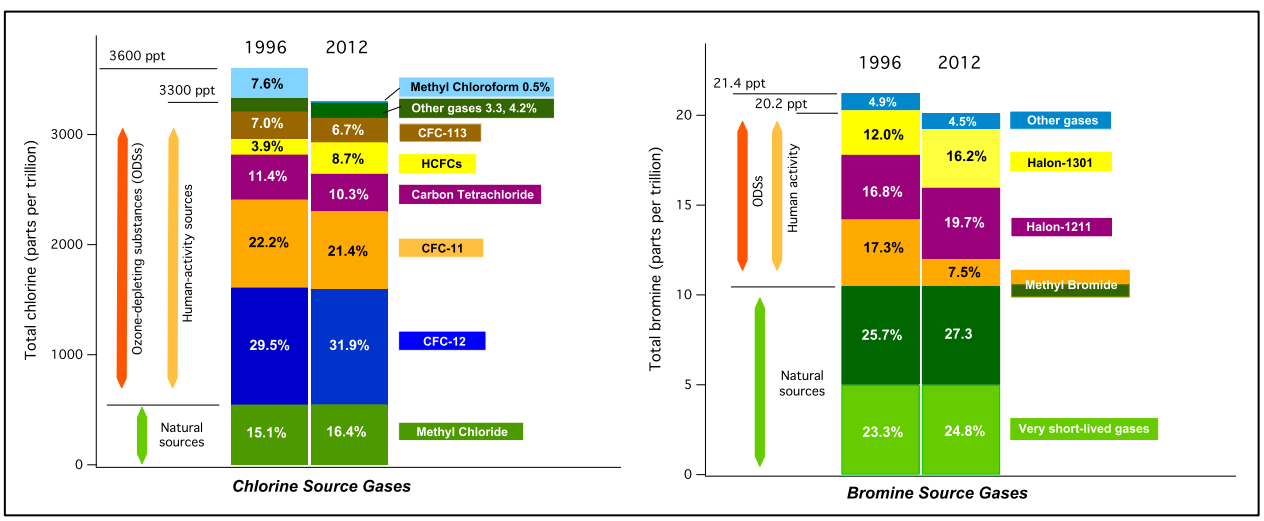

Figure 1-6-1. Relative contribution to total tropospheric chlorine and total tropospheric bromine from individual and groups of compounds in 1996 and 2012. The sum of very short-lived species (CH_2Cl_2, $CHCl_3$, C_2Cl_4, $COCl_2$) is shown as "other gases" for chlorine, while halon-1202 and halon-2402 are included as "other gases" for bromine.

1.6.2 VSLS Chlorinated Compounds Become More Relevant for Stratospheric Ozone

The current (2008–2012) increase in tropospheric very short-lived substance (VSLS) chlorine source gases is ~1.3 ± 0.3 ppt Cl yr^{-1}, compared to the decline in long-lived controlled chlorinated substances of 13.4 ± 0.9 ppt Cl yr^{-1}. Averaged over the longer time period of 2004–2013, the combined trend of the three major VSLS chlorine source gases CH_2Cl_2, C_2Cl_4, and $CHCl_3$ is 1.8 ± 0.2 ppt Cl yr^{-1} (Figure 1-6-2). Increased levels of dichloromethane (CH_2Cl_2), which has predominantly anthropogenic sources, account for the majority of this change. The globally averaged surface abundance of CH_2Cl_2 has increased by ~60% over the last decade. The majority (>80%) of VSLS chlorinated gases and associated product gases are expected to reach the stratosphere, based upon observed vertical profiles of CH_2Cl_2 and and model calculations of CH_2Br_2, a gas with a similar atmospheric lifetime.

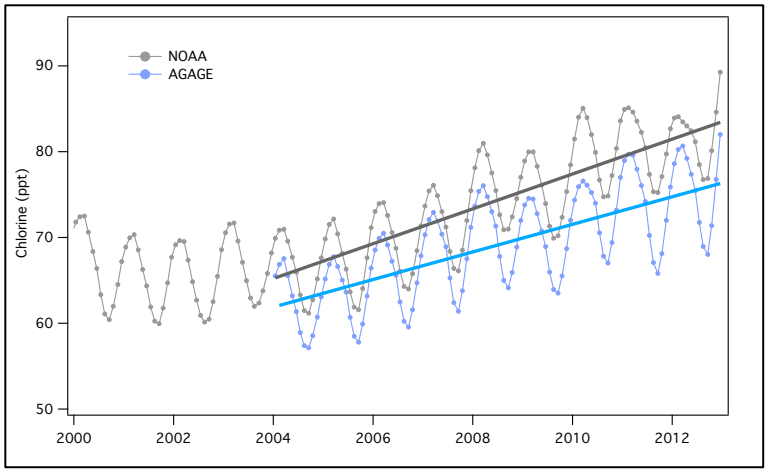

Figure 1-6-2. Average global, monthly mean values of total tropospheric chlorine from three VSLS gases (CH_2Cl_2, C_2Cl_4, and $CHCl_3$) derived from 12-box model output using NOAA and AGAGE data (Simmonds et al., 2006; Montzka et al., 2011). Linear fits are shown as the thicker lines, starting 2004. The trend from AGAGE: 1.6 ± 0.2 ppt Cl yr^{-1}; from NOAA: 2.0 ± 0.2 ppt Cl yr^{-1}; average trend: 1.8 ppt Cl yr^{-1}. A constant 21 ppt, derived from AGAGE data, was used to represent the contribution of $CHCl_3$.

1.6.3 Radiative Forcing of ODSs and ODS Replacement Compounds

Update on the effect on the radiative budget of F-gases

In Figure 1-6-3 the radiative forcing values for ODSs and F-gases (source gases with fluorine as the only halogen attached either to carbon, sulfur, or nitrogen; also called Kyoto Protocol synthetics) are compared against those of carbon dioxide (CO_2), methane (CH_4), and nitrous oxide (N_2O). In 2012 the total contribution from the F-gases was 33 mW m^{-2}, with 22 mW m^{-2} from hydrofluorocarbons (HFCs), 6 mW m^{-2} from perfluorocarbons (PFCs), and 5mW m^{-2} from SF_6, SO_2F_2, and NF_3. The most important single HFC in terms of climate forcing in 2012 was the cooling agent HFC-134a. However, other HFCs used in cooling applications, such as HFC-125, HFC-32, and HFC-143a, are increasing and the sum of their radiative forcing surpassed that of HFC-23 (a by-product of HCFC-22 production) and is now equal to the sum of the PFCs. Radiative forcing from SF_6 has continued its growth at a stable rate of 0.16–0.17 mW yr^{-1} in recent years. SO_2F_2 and NF_3 currently contribute very little to climate forcing.

In 2012 the total contribution of the F-gases was still small in comparison to the total anthropogenic-induced climate forcing due to the major greenhouse gases (1850 mW m^{-2} for CO_2, 490 mW m^{-2} for CH_4, and 170 mW m^{-2} for N_2O) and also compared to the total ODS contribution (330 mW m^{-2}), which has remained virtually stable since the last Assessment.

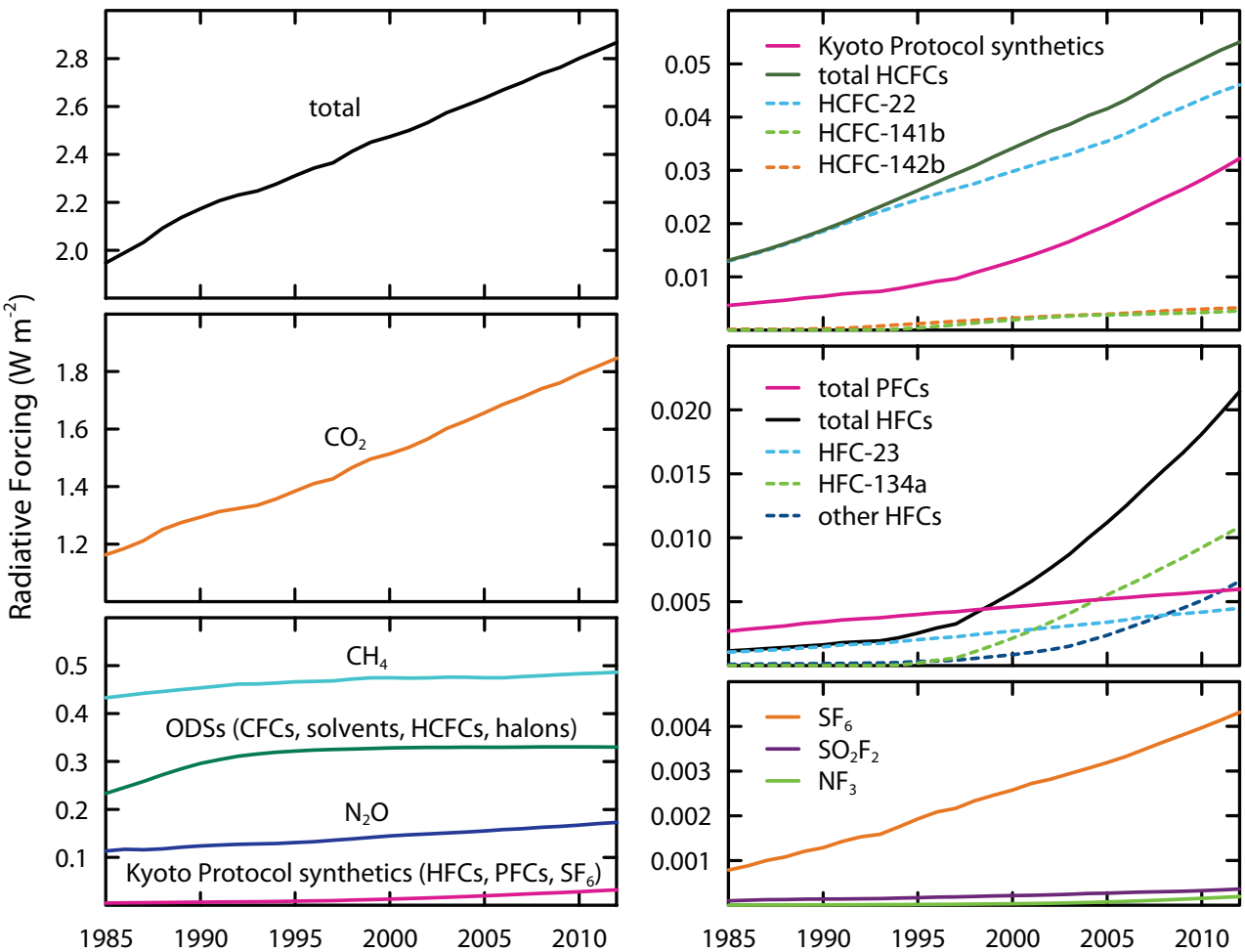

Figure 1-6-3. *Left panels*: The evolution of radiative forcing in W m^{-2} from the sum of the major greenhouse gases (CO_2, CH_4, N_2O), the ODSs (CFCs, HCFCs, halons, solvents (CH_3CCl_3, CCl_4)), and the Kyoto Protocol synthetic gases (F-gases (HFCs, PFCs, SF_6). *Right panels*: The evolution of radiative forcing from Kyoto Protocol synthetic gases (and their sums) as well as specified F-gases. Other HFCs combine all measured HFCs from Table 1-14, except HFC-134a and HFC-23. Data are from Table 1-1 and Table 1-14; radiative efficiencies are from Chapter 5. Radiative forcings are calculated according to Myhre et al. (2013). This figure represents an update of Figure 1-25 from the last Assessment (Montzka and Reimann et al., 2011).

1.6.4 GWP-Weighted Emissions of ODS and ODS Replacement Compounds

The emissions of CFCs, HCFCs, and HFCs in terms of their influence on climate (as measured by $GtCO_2$-equivalent yr^{-1} emissions) were roughly equal in 2012. However, the emissions of HFCs are increasing rapidly, while the emissions of CFCs are going down and those of HCFCs are essentially unchanged. The 100-year GWP weighted emissions for the sum of CFC, HCFC, HFC, halons, and chlorinated solvents emissions was 2.3 $GtCO_2$-eq in 2012. The sum of GWP-weighted emissions of CFCs was 0.73 ± 0.25 $GtCO_2$-eq yr^{-1} in 2012 and has decreased on average by 11.0 ± 1.2% yr^{-1} from 2008 to 2012. The sum of HCFC emissions was 0.76 ± 0.12 $GtCO_2$-eq yr^{-1} in 2012 and has been essentially unchanged between 2008 and 2012. Finally, the sum of HFC emissions was 0.69 ± 0.12

$GtCO_2$-eq yr^{-1} in 2012 and has increased on average by 6.8 ± 0.9% yr^{-1} from 2008 to 2012. The HFC increase partially offsets the decrease by CFCs. Current emissions of HFCs are, however, less than 10% of peak CFC emissions in the early 1990s (>8 Gt CO_2-eq yr^{-1}).

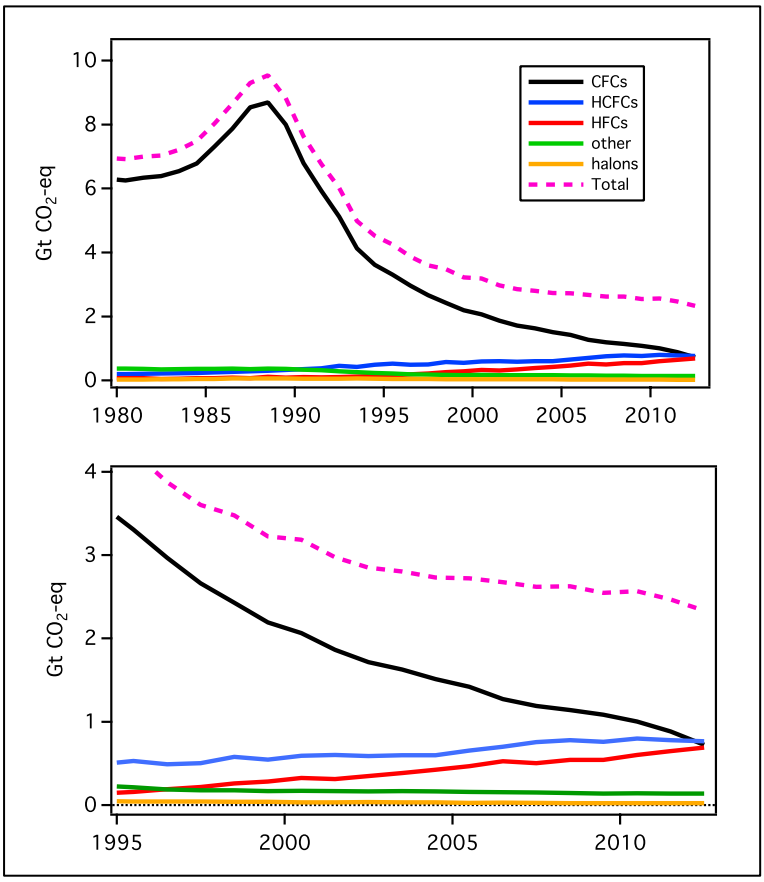

Figure 1-6-4. Emissions of ODSs and ODS replacements weighted by 100-yr Global Warming Potential. The lower figure is an expanded version of the upper figure. In 2012, CO_2-equivalent emissions of CFCs, HCFCs, and HFCs were nearly equal. In this figure, "other" includes CCl_4, CH_3CCl_3, and CH_3Cl.

1.6.5 Ongoing Mismatch between Estimated Sources of CCl_4 from Measurements and from Inventories

Carbon tetrachloride (CCl_4) accounted for about 10% of total tropospheric Cl in 2012, and during 2009–2012 declined largely as projected in the A1 scenario of the 2010 Assessment. However, estimated sources and sinks remain inconsistent with observations of CCl_4, so the budget of this key gas remains unclear. When combined with the current estimate of the total atmospheric lifetime of CCl_4 (26 years), the observed CCl_4 trend in the atmosphere (−1.1 to −1.4 ppt yr^{-1} in 2012, right panel of Figure 1-6-5) implies sources of 57 (40–74) Gg yr^{-1} (red line in left panel of Figure 1-6-5), which cannot be reconciled by estimated emissions from feedstock and other uses (green lines). These industry-based estimates together with a global atmospheric CCl_4 lifetime of 26 years result in calculated CCl_4 mole fractions (dotted black line, right panel) much lower than measured abundances in the past decade, with an increasing divergence. The stable and significant interhemispheric CCl_4 difference of 1.3 ppt in recent years could be an indicator for ongoing anthropogenic emissions in the Northern Hemisphere, although the distribution of CCl_4 sources is not well understood.

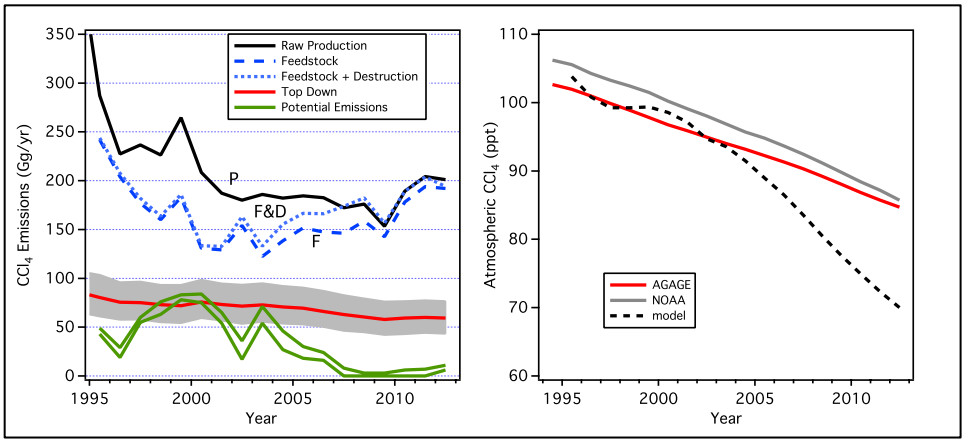

Figure 1-6-5. *Left panel*: Global top-down emissions of CCl_4 and global potential emissions of CCl_4, derived from raw production, feedstock, and destruction. For further explanation see caption of Figure 1-6. *Right panel*: Global mole fractions from NOAA and AGAGE measurements along with the theoretical mole fraction (black dotted line) derived from potential emissions and a global lifetime of 26 years using a 1-box model and observed concentrations in 1994, from 1994 through 2012.

1.6.6 Quarantine and Pre-Shipment (QPS) Consumption of CH_3Br Has Exceeded Non-QPS Consumption

Quarantine and pre-shipment (QPS) consumption of methyl bromide (CH_3Br) exceeded non-QPS consumption in 2009 (Figure 1-6-6). Article 5 and non-Article 5 countries consume similar amounts of CH_3Br for QPS uses. There was a slight increase in QPS consumption by Article 5 countries in the mid-2000s, with fairly steady consumption since then. QPS consumption by non-Article 5 countries was 34% of the total QPS consumption in 2012. With non-QPS emissions totaling just 30% of the 2012 total fumigation emissions, increases in QPS consumption/emissions will begin to reverse the reductions in tropospheric bromine gained from the reductions in non-QPS production, consumption, and emission.

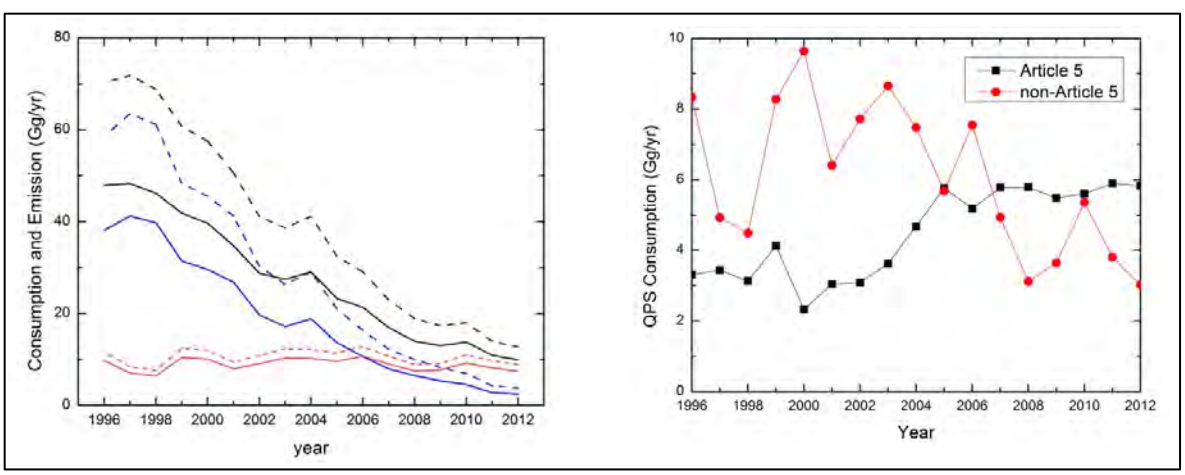

Figure 1-6-6. *Left panel:* Trends in methyl bromide consumption (dashed lines) as reported in the UNEP database for non-QPS uses (- - -), QPS uses (- - -), and total (- - -); and trends in methyl bromide emission (solid lines) from non-QPS uses (—), QPS uses (—), and total (—). *Right panel:* Quarantine and pre-shipment (QPS) consumption for Article 5 and non-Article 5 Parties to the Montreal Protocol (UNEP, 2014).

REFERENCES

Abbatt, J.P.D., and J.G. Anderson, High-pressure discharge flow kinetics and frontier orbital mechanistic analysis for OH + CH_2CCl_2, *cis*-CHClCHCl, *trans*-CHClCHCl, $CFClCF_2$, and CF_2CCl_2 → products, *J. Phys. Chem.*, *95* (6), 2382-2390, doi: 10.1021/j100159a049, 1991.

Acerboni, G., J.A. Beukes, N.R. Jensen, J. Hjorth, G. Myhre, C.J. Nielsen, and J.K. Sundet, Atmospheric degradation and global warming potentials of three perfluoroalkenes, *Atmos. Environ.*, *35*, 4113-4123, doi: 10.1016/S1352-2310(01)00209-6, 2001.

An, X.Q., S. Henne, B. Yao, M.K. Vollmer, L.X. Zhou, and Y. Li, Estimating emissions of HCFC-22 and CFC-11 in China by atmospheric observations and inverse modeling, *Sci. China Chem.*, *55* (10), 2233-2241, doi: 10.1007/s11426-012-4624-8, 2012.

Andreae, M.O., and P. Merlet, Emission of trace gases and aerosols from biomass burning, *Global Biogeochem. Cycles*, *15* (4), 955-966, doi: 10.1029/2000GB001382, 2001.

Archer, S.D., L.E. Goldson, M.I. Liddicoat, D.G. Cummings, and P.D. Nightingale, Marked seasonality in the concentrations and sea-to-air flux of volatile iodocarbon compounds in the western English Channel, *J. Geophys. Res.*, *112* (C8), C08009, doi: 10.1029/2006JC003963, 2007.

Arnold, T., J. Mühle, P.K. Salameh, C.M. Harth, D.J. Ivy, and R.F. Weiss, Automated measurement of nitrogen trifluoride in ambient air, *Anal. Chem.*, *84* (11), 4798-4804, doi: 10.1021/ac300373e, 2012.

Arnold, T., C.M. Harth, J. Mühle, A.J. Manning, P.K. Salameh, J. Kim, D.J. Ivy, L.P. Steele, V.V. Petrenko, J.P. Severinghaus, D. Baggenstos, and R.F. Weiss, Nitrogen trifluoride global emissions estimated from updated atmospheric measurements, *Proc. Natl. Acad. Sci.*, *110* (6), 2029-2034, doi: 10.1073/pnas.1212346110, 2013.

Arnold, T., D.J. Ivy, C.M. Harth, M.K. Vollmer, J. Mühle, P.K. Salameh, L.P. Steele, P.B. Krummel, R.H..J. Wang, D. Young, C.R. Lunder, O. Hermansen, T.S. Rhee, J. Kim, S. Reimann, S. O'Doherty, P.J. Fraser, P.G. Simmonds, R.G. Prinn, and R.F. Weiss, HFC-43-10mee atmospheric abundances and global emission estimates, *Geophys. Res. Lett.*, *41* (6), 2228-2235, doi: 10.1002/2013GL059143, 2014.

Aschmann, J., and B.-M. Sinnhuber, Contribution of very short-lived substances to stratospheric bromine loading: Uncertainties and constraints, *Atmos. Chem. Phys.*, *13* (3), 1203-1219, doi: 10.5194/acp-13-1203-2013, 2013.

Aschmann, J., B.-M. Sinnhuber, E.L. Atlas, and S.M. Schauffler, Modeling the transport of very short-lived substances into the tropical upper troposphere and lower stratosphere, *Atmos. Chem. Phys.*, 9 (23), 9237-9247, doi: 10.5194/acp-9-9237-2009, 2009.

Aschmann, J., B.-M. Sinnhuber, M.P. Chipperfield, and R. Hossaini, Impact of deep convection and dehydration on bromine loading in the upper troposphere and lower stratosphere, *Atmos. Chem. Phys.*, *11* (6), 2671-2687, doi: 10.5194/acp-11-2671-2011, 2011.

Ashfold, M.J., N.R.P. Harris, E.L. Atlas, A.J. Manning, and J.A. Pyle, Transport of short-lived species into the Tropical Tropopause Layer, *Atmos. Chem. Phys.*, *12* (14), 6309-6322, doi: 10.5194/acp-12-6309-2012, 2012.

Ashfold, M.J., N.R.P. Harris, A.J. Manning, A.D. Robinson, N.J. Warwick, and J.A. Pyle, Estimates of tropical bromoform emissions using an inversion method, *Atmos. Chem. Phys.*, *14* (2), 979-994, doi: 10.5194/acp-14-979-2014, 2014.

Atkinson, R., D.L. Baulch, R.A. Cox, J.N. Crowley, R.F. Hampson, R.G. Hynes, M.E. Jenkin, M.J. Rossi, J. Troe, and T.J. Wallington, Evaluated kinetic and photochemical data for atmospheric chemistry: Volume IV – gas phase reactions of organic halogen species, *Atmos. Chem. Phys.*, *8* (15), 4141-4496, doi: 10.5194/acp-8-4141-2008, 2008.

Aydin, M., K.R. Verhulst, E.S. Saltzman, M.O. Battle, S.A. Montzka, D.R. Blake, Q. Tang, and M.J. Prather, Recent decreases in fossil-fuel emissions of ethane and methane derived from firn air, *Nature*, *476* (7359), 198-201, doi: 10.1038/nature10352, 2011.

Baasandorj, M., A.R. Ravishankara, and J.B. Burkholder, Atmospheric chemistry of (*Z*)-$CF_3CH{=}CHCF_3$: OH radical reaction rate coefficient and global warming potential, *J. Phys. Chem. A*, *115* (38), 10539-10549, doi: 10.1021/jp206195g, 2011.

Baasandorj, M., B.D. Hall, and J.B. Burkholder, Rate coefficients for the reaction of $O(^1D)$ with the atmospherically long-lived greenhouse gases NF_3, SF_3CF_3, CHF_3, C_2F_6, c-C_4F_8, n-C_5F_{12}, and n-C_6F_{14}, *Atmos. Chem. Phys.*, *12* (23), 11753-11764, doi: 10.5194/acp-12-11753-2012, 2012.

Baasandorj, M., E.L. Fleming, C.H. Jackman, and J.B. Burkholder, $O(^1D)$ kinetic study of key ozone depleting substances and greenhouse gases, *J. Phys. Chem. A*, *117* (12), 2434-2445, doi: 10.1021/jp312781c, 2013.

Baker, J.M., C.E. Reeves, S.A. Penkett, L.M. Cardenas, and P.D. Nightingale, An estimate of the global emissions of methyl bromide from automobile exhausts, *Geophys. Res. Lett.*, *25* (13), 2405-2408, doi: 10.1029/98GL01795, 1998.

Barletta, B., P. Nissenson, S. Meinardi, D. Dabdub, F. Sherwood Rowland, R.A. VanCuren, J. Pederson, G.S. Diskin, and D.R. Blake, HFC-152a and HFC-134a emission estimates and characterization of CFCs, CFC replacements, and other halogenated solvents measured during the 2008 ARCTAS campaign (CARB phase) over the South Coast Air Basin of California, *Atmos. Chem. Phys.*, *11* (6), 2655-2669, doi: 10.5194/acp-11-2655-2011, 2011.

Bell, N., L. Hsu, D.J. Jacob, M.G. Schultz, D.R. Blake, J.H. Butler, D.B. King, J.M. Lobert, and E. Maier-Reimer, Methyl iodide: Atmospheric budget and use as a tracer of marine convection in global models, *J. Geophys. Res.*, *107* (D17), 4340, doi: 10.1029/2001JD001151, 2002.

Bergman, J.W., E.J. Jensen, L. Pfister, and Q. Yang, Seasonal differences of vertical-transport efficiency in the tropical tropopause layer: On the interplay between tropical deep convection, large-scale vertical ascent, and horizontal circulations, *J. Geophys. Res.*, *117* (D5), D05302, doi: 10.1029/2011JD016992, 2012.

Bertram, F.J., and J.B. Kolowich, A study of methyl bromide emissions from automobiles burning leaded gasoline using standardized vehicle testing procedures, *Geophys. Res. Lett.*, *27* (9), 1423-1426, doi: 10.1029/1999GL011008, 2000.

Bian, H., P.R. Colarco, M. Chin, G. Chen, J.M. Rodriguez, Q. Liang, D. Blake, D.A. Chu, A. da Silva, A.S. Darmenov, G. Diskin, H.E. Fuelberg, G. Huey, Y. Kondo, J.E. Nielsen, X. Pan, and A. Wisthaler, Source attributions of pollution to the Western Arctic during the NASA ARCTAS field campaign, *Atmos. Chem. Phys.*, *13* (9), 4707-4721, doi: 10.5194/acp-13-4707-2013, 2013.

Blei, E., C.J. Hardacre, G.P. Mills, K.V. Heal, and M.R. Heal, Identification and quantification of methyl halide sources in a lowland tropical rainforest, *Atmos. Environ.*, *44* (8), 1005-1010, doi: 10.1016/j.atmosenv.2009.12.023, 2010.

Bösch, H., C. Camy-Peyret, M.P. Chipperfield, R. Fitzenberger, H. Harder, U. Platt, and K. Pfeilsticker, Upper limits of stratospheric IO and OIO inferred from center-to-limb-darkening-corrected balloon-borne solar occultation visible spectra: Implications for total gaseous iodine and stratospheric ozone, *J. Geophys. Res.*, *108* (D15), 4455, doi: 10.1029/2002JD003078, 2003.

Bousquet, P., B. Ringeval, I. Pison, E.J. Dlugokencky, E.-G. Brunke, C. Carouge, F. Chevallier, A. Fortems-Cheiney, C. Frankenberg, D.A. Hauglustaine, P.B. Krummel, R.L. Langenfelds, M. Ramonet, M. Schmidt, L.P. Steele, S. Szopa, C. Yver, N. Viovy, and P. Ciais, Source attribution of the changes in atmospheric methane for 2006–2008, *Atmos. Chem. Phys.*, *11* (8), 3689–3700, doi: 10.5194/acp-11-3689-2011, 2011.

Boutonnet, J.C., P. Bingham, D. Calamari, C. de Rooij, J. Franklin, T. Kawano, J.-M. Libre, A. McCulloch, G. Malinverno, J.M. Odom, G.M. Rusch, K. Smythe, I. Sobolev, R. Thompson, and J.M. Tiedje, Environmental risk assessment of trifluoroacetic acid, *Hum. Ecol. Risk Assess.*, *5* (1), 59-124, doi: 10.1080/10807039991289644, 1999.

Braesicke, P., J. Keeble, X. Yang, G. Stiller, S. Kellmann, N.L. Abraham, A.T. Archibald, P. Telford, and J.A. Pyle, Circulation anomalies in the Southern Hemisphere and ozone changes, *Atmos. Chem. Phys.*, *13* (21), 10677-10688, doi: 10.5194/acp-13-10677-2013, 2013.

Brinckmann, S., A. Engel, H. Bönisch, B. Quack, and E. Atlas, Short-lived brominated hydrocarbons – observations in the source regions and the tropical tropopause layer, *Atmos. Chem. Phys.*, *12* (3), 1213-1228, doi: 10.5194/acp-12-1213-2012, 2012.

Brion, J., A. Chakir, J. Charbonnier, D. Daumont, C. Parisse, and J. Malicet, Absorption spectra measurements for the ozone molecule in the 350-830 nm region, *J. Atmos. Chem., 30* (2), 291-299, doi: 10.1023/A:1006036924364, 1998.

Brioude, J., R.W. Portmann, J.S. Daniel, O.R. Cooper, G.J. Frost, K.H. Rosenlof, C. Granier, A.R. Ravishankara, S.A. Montzka, and A. Stohl, Variations in ozone depletion potentials of very short-lived substances with season and emission region, *Geophys. Res. Lett.*, *37* (19), L19804, doi: 10.1029/2010GL044856, 2010.

Brown, A.T., M.P. Chipperfield, C. Boone, C. Wilson, K.A. Walker, and P.F. Bernath, Trends in atmospheric halogen containing gases since 2004, *J. Quant. Spectrosc. Raiat. Transfer*, *112* (16), 2552-2566, doi: 10.1016/j.jqsrt.2011.07.005, 2011.

Brown, A.T., M.P. Chipperfield, N.A.D. Richards, C. Boone, and P.F. Bernath, Global stratospheric fluorine inventory for 2004-2009 from Atmospheric Chemistry Experiment Fourier Transform Spectrometer (ACE-FTS) measurements and SLIMCAT model simulations, *Atmos. Chem. Phys.*, *14* (1), 267-282, doi: 10.5194/acp-14-267-2014, 2014.

Brownell, D.K., R.M. Moore, and J.J. Cullen, Production of methyl halides by *Prochlorococcus* and *Synechococcus*, *Global Biogeochem. Cycles*, *24* (2), GB2002, doi: 10.1029/2009GB003671, 2010.

Brühl, C., J. Lelieveld, P.J. Crutzen, and H. Tost, The role of carbonyl sulphide as a source of stratospheric sulphate aerosol and its impact on climate, *Atmos. Chem. Phys.*, *12* (3), 1239-1253, doi: 10.5194/acp-12-1239-2012, 2012.

Butler, J.H., The potential role of the ocean in regulating atmospheric CH_3Br, *Geophys. Res. Lett.*, *21* (3), 185-188, doi: 10.1029/94GL00071, 1994.

Butler, J.H., S.A. Montzka, A.D. Clarke, J.M. Lobert, and J.W. Elkins, Growth and distribution of halons in the atmosphere, *J. Geophys. Res.*, *103* (D1), 1503-1511, doi: 10.1029/97JD02853, 1998.

Butler, J.H., M. Battle, M.L. Bender, S.A. Montzka, A.D. Clarke, E.S. Saltzman, C.M. Sucher, J.P. Severinghaus, and J.W. Elkins, A record of atmospheric halocarbons during the twentieth century from polar firn air, *Nature*, *399* (6738), 749-755, doi: 10.1038/21586, 1999.

Butler, J.H., D.B. King, J.M. Lobert, S.A. Montzka, S.A. Yvon-Lewis, B.D. Hall, N.J. Warwick, D.J. Mondeel, M. Aydin, and J.W. Elkins, Oceanic distributions and emissions of short-lived halocarbons, *Global Biogeochem. Cycles*, *21*, GB1023, doi: 10.1029/2006GB002732, 2007.

Butz, A., H. Bösch, C. Camy-Peyret, M.P. Chipperfield, M. Dorf, S. Kreycy, L. Kritten, C. Prados-Roman, J. Schwärzle, and K. Pfeilsticker, Constraints on inorganic gaseous iodine in the tropical upper troposphere and stratosphere inferred from balloon-borne solar occultation observations, *Atmos. Chem. Phys.*, *9* (18), 7229-7242, doi: 10.5194/acp-9-7229-2009, 2009.

Cahill, T.M., C.M. Thomas, S.E. Schwarzbach, and J.N. Seiber, Accumulation of trifluoroacetate in seasonal wetlands in California, *Environ. Sci. Technol.*, *35* (5), 820-825, doi: 10.1021/es0013982, 2001.

Calvert, J.G., R.G. Derwent, J.J. Orlando, G.S. Tyndall, and T.J. Wallington, *Mechanisms of Atmospheric Oxidation of the Alkanes*, 1008 pp., Oxford University Press, New York, NY, 2008.

Carpenter, L.J., C.E. Jones, R.M. Dunk, K.E. Hornsby, and J. Woeltjen, Air-sea fluxes of biogenic bromine from the tropical and North Atlantic Ocean, *Atmos. Chem. Phys.*, *9* (5), 1805-1816, doi: 10.5194/acp-9-1805-2009, 2009.

Carpenter, L.J., S.M. MacDonald, M.D. Shaw, R. Kumar, R.W. Saunders, R. Parthipan, J. Wilson, and J.M.C. Plane, Atmospheric iodine levels influenced by sea surface emissions of inorganic iodine, *Nature Geosci.*, *6* (2), 108-111, doi: 10.1038/ngeo1687, 2013.

CDIAC (Carbon Dioxide Information Analysis Center), *The ALE/GAGE/AGAGE Network (DB1001),* available: http://cdiac.esd.ornl.gov/ndps/alegage.html, 2014.

Chen, B., X.D. Xu, S. Yang, S., and T.L. Zhao, Climatological perspectives of air transport from atmospheric boundary layer to tropopause layer over Asian monsoon regions during boreal summer inferred from Lagrangian approach, *Atmos. Chem. Phys.*, *12* (13), 5827-5839, doi: 10.5194/acp-12-5827-2012, 2012.

Chen, L., S. Kutsuna, K. Tokuhashi, and A. Sekiya, Kinetics study of the gas-phase reactions of $C_2F_5OC(O)H$ and n-$C_3F_7OC(O)H$ with OH radicals at 253-328 K, *Chem. Phys. Lett.*, *400* (4-6), 563-568, doi: 10.1016/j.cplett.2004.11.019, 2004a.

Chen, L., S. Kutsuna, K. Tokuhashi, and A. Sekiya, Kinetics of the gas-phase reaction of $CF_3OC(O)H$ with OH radicals at 242-328 K, *Int. J. Chem. Kinet.*, *36* (6), 337-344, doi: 10.1002/kin.20004, 2004b.

Chen, L., S. Kutsuna, K. Tokuhashi, and A. Sekiya, Kinetics study of the gas-phase reactions of $-CHF_2CF_2OCHF_2$ and $CF_3CHFCF_2OCH_2CF_2CF_3$ with OH radicals at 253-328 K, *Chem. Phys. Lett.*, *403* (1-3), 180-184, doi: 10.1016/j.cplett.2005.01.002, 2005a.

Chen, L., S. Kutsuna, K. Tokuhashi, A. Sekiya, R. Tamai, and Y. Hibino, Kinetics and mechanism of $(CF_3)_2CHOCH_3$ reaction with OH radicals in an environmental reaction chamber, *J. Phys. Chem. A*, *109* (21), 4766-4771, doi: 10.1021/jp050491f, 2005b.

Chen, T.-Y., D.R. Blake, J.P. Lopez, and F.S. Rowland, Estimation of global vehicular methyl bromide emissions: Extrapolation from a case study in Santiago, Chile, *Geophys. Res. Lett.*, *26* (3), 283-286, doi: 10.1029/1998 GL900214, 1999.

Chevallier, F., P. Ciais , T. J. Conway, T. Aalto, B.E. Anderson, P. Bousquet, E.G., Brunke, L. Ciattaglia, Y. Esaki, M. Fröhlich, A. Gomez, A.J. Gomez-Pelaez, L. Haszpra, P.B. Krummel, R.L. Langenfelds, M. Leuenberger, T. Machida, F. Maignan, H. Matsueda, J.A. Morguí, H. Mukai, T. Nakazawa, P. Peylin, M. Ramonet, L. Rivier, Y. Sawa, M. Schmidt, L.P. Steele, S.A. Vay, A.T. Vermeulen, S. Wofsy, and D. Worthy, CO_2 surface fluxes at grid point scale estimated from a global 21 year reanalysis of atmospheric measurements, *J. Geophys. Res.*, *115* (D21), D21307, doi: 10.1029/2010JD013887, 2010.

Choi, S., Y. Wang, R.J. Salawitch, T. Canty, J. Joiner, T. Zeng, T.P. Kurosu, K. Chance, A. Richter, L.G. Huey, J. Liao, J.A. Neuman, J.B. Nowak, J.E. Dibb, A.J. Weinheimer, G. Diskin, T.B. Ryerson, A. da Silva, J. Curry, D. Kinnison, S. Tilmes, and P.F. Levelt, Analysis of satellite-derived Arctic tropospheric BrO columns in conjunction with aircraft measurements during ARCTAS and ARCPAC, *Atmos. Chem. Phys.*, *12* (3), 1255-1285, doi: 10.5194/acp-12-1255-2012, 2012.

Christensen, L.K., J. Sehested, O.J. Nielsen, M. Bilde, T.J. Wallington, A. Guschin, L.T. Molina, and M.J. Molina, Atmospheric chemistry of HFE-7200 ($C_4F_9OC_2H_5$): Reaction with OH radicals and fate of $C_4F_9OCH_2CH_2O(\bullet)$ and $C_4F_9OCHO(\bullet)CH_3$ radicals, *J. Phys. Chem. A*, *102* (25), 4839-4845, doi: 10.1021/jp981128u, 1998.

Ciais, P., and C. Sabine (Co-ordinating Lead Authors), G. Bala, L. Bopp, V. Brovkin, J. Canadell, A. Chhabra, R. DeFries, J. Galloway, M. Heimann, C. Jones, C. Le Quéré, R.B. Myneni, S. Piao, and P. Thornton (Lead Authors), Carbon and other biogeochemical cycles, Chapter 6 in *Climate Change 2013: The Physical Science Basis. Contribution of Working Group I to the Fifth Assessment Report of the Intergovernmental Panel on Climate Change*, edited by T.F. Stocker, D. Qin, G.-K. Plattner, M. Tignor, S.K. Allen, J. Boschung, A. Nauels, Y. Xia, V. Bex, and P.M. Midgley, 1535 pp., Cambridge University Press, Cambridge, U.K. and New York, NY, 2013.

Clerbaux, C. and D.M. Cunnold (Lead Authors), J. Anderson, A. Engel, P.J. Fraser, E. Mahieu, A. Manning, J. Miller, S.A. Montzka, R. Nassar, R. Prinn, S. Reimann, C.P. Rinsland, P. Simmonds, D. Verdonik, R. Weiss, D. Wuebbles, and Y. Yokouchi, Long-lived compounds, Chapter 1 in *Scientific Assessment of Ozone Depletion, 2006*, Global Ozone Research and Monitoring Project–Report No. 50, Geneva, Switzerland, 2007.

Connor, B.J., T. Mooney, G. E. Nedoluha, J.W. Barrett, A. Parrish, J. Koda, M.L. Santee, and R.M. Gomez, Re-analysis of ground-based microwave ClO measurements from Mauna Kea, 1992 to early 2012, *Atmos. Chem. Phys*., *13* (17), 8643-8650, doi: 10.5194/acp-13-8643-2013, 2013.

Cox, M.L., P.J. Fraser, G.A. Sturrock, S.T. Siems, and L.W. Porter, Terrestrial sources and sinks of halomethanes near Cape Grim, Tasmania, *Atmos. Environ.*, *38* (23), 3839-3852, doi: 10.1016/j.atmosenv.2004.03.050, 2004.

Crowley, J.N., M. Ammann, R.A. Cox, R.G. Hynes, M.E. Jenkin, A. Mellouki, M.J. Rossi, J. Troe, and T.J. Wallington, Evaluated kinetic and photochemical data for atmospheric chemistry: Volume V – heterogeneous reactions on solid substrates, *Atmos. Chem. Phys.*, *10* (18), 9059-9223, doi: 10.5194/acp-10-9059-2010, 2010.

Crutzen, P.J., The influence of nitrogen oxides on the atmospheric ozone content, *Quart. J. Roy. Meteorol. Soc.*, *96* (408), 320-325, doi: 10.1002/qj.49709640815, 1970.

Cunnold, D.M., R.G. Prinn, R.A. Rasmussen, P.G. Simmonds, F.N. Alyea, C.A. Cardelino, A.J. Crawford, P.J. Fraser, and R.D. Rosen, The Atmospheric Lifetime Experiment 3. Lifetime methodology and application to three years of $CFCl_3$ data, *J. Geophys. Res., 88* (C13), 8379-8400, doi: 10.1029/JC088iC13p08379, 1983.

Daniel, J.S., and G.J.M Velders (Coordinating Lead Authors), A.R. Douglass, P.M.D. Forster, D.A. Hauglustaine, I.S.A. Isaksen, L.J.M. Kuijpers, A. McCulloch, and T.J. Wallington, Halocarbon scenarios, ozone depletion potentials, and global warming potentials, Chapter 8 in *Scientific Assessment of Ozone Depletion: 2006*, Global Ozone Research and Monitoring Project–Report No. 50, 572 pp., World Meteorological Organization, Geneva, Switzerland, 2007.

Daniel, J.S., and G.J.M. Velders (Coordinating Lead Authors), H. Akiyoshi, A.F. Bais, E.L. Fleming, C.H. Jackman, L.J.M. Kuijpers, M. McFarland, S.A. Montzka, O. Morgenstern, M.N. Ross, S. Tilmes, D.W. Toohey, M.B. Tully, T.J. Wallington, and D.J. Wuebbles, A Focus on Information and Options for Policymakers, Chapter 5 in *Scientific Assessment of Ozone Depletion: 2010*, Global Ozone Research and Monitoring Project–Report No. 52, World Meteorological Organization, Geneva, Switzerland, 2011.

Daumont, D., J. Brion, J. Charbonnier, and J. Malicet, Ozone UV spectroscopy.I. Absorption cross-sections at room temperature, *J. Atmos. Chem., 15* (2), 145-155, doi: 10.1007/BF00053756, 1992.

de Blas, M., M. Navazo , L. Alonso, N. Durana, and J. Iza, Trichloroethylene, tetrachloroethylene and carbon tetrachloride in an urban atmosphere: Mixing ratios and temporal patterns, *Intern. J. Environ. Anal. Chem.*, *93* (2), 228-244, doi: 10.1080/03067319.2011.629346, 2013.

Devasthale, A., and H. Grassl, A daytime climatological distribution of high opaque ice cloud classes over the Indian summer monsoon region observed from 25-year AVHRR data, *Atmos. Chem. Phys.*, *9* (12), 4185-4196, doi: 10.5194/acp-9-4185-2009, 2009.

Devasthale, A., and S. Fueglistaler, A climatological perspective of deep convection penetrating the TTL during the Indian summer monsoon from the AVHRR and MODIS instruments, *Atmos. Chem. Phys.*, *10* (10), 4573-4582, doi: 10.5194/acp-10-4573-2010, 2010.

Dimmer, C.H., P.G. Simmonds, G. Nickless, and M.R. Bassford, Biogenic fluxes of halomethanes from Irish peatland ecosystems, *Atmos. Environ.*, *35* (2), 321-330, doi: 10.1016/S1352-2310(00)00151-5, 2001.

Ding, K., H. Metiu, and G.D. Stucky, The selective high-yield conversion of methane using iodine-catalyzed methane bromination, *ACS Catal.*, *3* (3), 474-477, doi: 10.1021/cs300775m, 2013.

Dix, B., S. Baidar, J.F. Bresch, S.R. Hall, K.S. Schmidt, S. Wang, and R. Volkamer, Detection of iodine monoxide in the tropical free troposphere, *Proc. Natl. Acad. Sci.*, *110* (6), 2035-2040, doi: 10.1073/pnas.1212386110, 2013.

Dlugokencky, E.J., L. Bruhwiler, J.W.C. White, L.K. Emmons, P.C. Novelli, S.A. Montzka, K.A. Masarie, P.M. Lang, A.M. Crotwell, J.B. Miller, and L.V. Gatti, Observational constraints on recent increases in the atmospheric CH_4 burden, *Geophys. Res. Lett.*, *36*, L18803, doi: 10.1029/2009GL039780, 2009.

Dlugokencky, E.J., E.G., Nisbet, R. Fisher, and D. Lowry, Global atmospheric methane: Budget, changes and dangers, *Phil. Trans. R. Soc. A*, *369* (1943), 2058–2072, doi: 10.1098/rsta.2010.0341, 2011.

Dorf, M., J.H. Butler, A. Butz, C. Camy-Peyret, M.P. Chipperfield, L. Kritten, S.A. Montzka, B. Simmes, F. Weidner, and K. Pfeilsticker, Long-term observations of stratospheric bromine reveal slow down in growth, *Geophys. Res. Lett.*, *33*, L24803, doi: 10.1029/2006GL027714, 2006.

Dorf, M., A. Butz, C. Camy-Peyret, M.P. Chipperfield, L. Kritten, and K. Pfeilsticker, Bromine in the tropical troposphere and stratosphere as derived from balloon-borne BrO observations, *Atmos. Chem. Phys.*, *8* (23), 7265-7271, doi: 10.5194/acp-8-7265-2008, 2008.

Duchatelet, P., E. Mahieu, R. Ruhnke, W. Feng, M. Chipperfield, P. Demoulin, P. Bernath, C.D. Boone, K.A. Walker, C. Servais, and O. Flock, An approach to retrieve information on the carbonyl fluoride (COF_2) vertical distributions above Jungfraujoch by FTIR multi-spectrum multi-window fitting, *Atmos. Chem. Phys.*, *9* (22), 9027-9042, doi: 10.5194/acp-9-9027-2009, 2009.

Duchatelet, P., P. Demoulin, F. Hase, R. Ruhnke, W. Feng, M.P. Chipperfield, P.F. Bernath, C.D. Boone, K.A. Walker, and E. Mahieu, Hydrogen fluoride total and partial column time series above the Jungfraujoch from long-term FTIR measurements: Impact of the line-shape model, characterization of the error budget and seasonal cycle, and comparison with satellite and model data, *J. Geophys. Res.*, *115* (D22), D22306, doi: 10.1029/2010jd014677, 2010.

Engel, A., M. Strunk, M. Müller, H.-P. Haase, C. Poss, I. Levin, and U. Schmidt, Temporal development of total chlorine in the high-latitude stratosphere based on reference distributions of mean age derived from CO_2 and SF_6, *J. Geophys. Res.*, *107* (D12), 4136, doi: 10.1029/2001JD000584, 2002.

Engel, A., T. Möbius, H. Bönisch, U. Schmidt, R. Heinz, I. Levin, E. Atlas, S. Aoki, T. Nakazawa, S. Sugawara, F. Moore, D. Hurst, J. Elkins, S. Schauffler, A. Andrews, and K. Boering, Age of stratospheric air unchanged within uncertainties over the past 30 years, *Nature Geosci.*, *2* (1), 28-31, doi: 10.1038/ngeo388, 2009.

Fang, X., J. Wu, S. Su, J. Han, Y. Wu, Y. Shi, D. Wan, X. Sun, J. Zhang, and J. Hu, Estimates of major anthropogenic halocarbon emissions from China based on interspecies correlations, *Atmos. Environ.*, *62*, 26-33, doi: 10.1016/j.atmosenv.2012.08.010, 2012.

Fang, X., X. Hu, G. Janssens-Maenhout, J. Wu, J. Han, S. Su, J. Zhang, and J. Hu, Sulfur hexafluoride (SF_6) emission estimates for China: An inventory for 1990–2010 and a projection to 2020, *Environ. Sci. Technol.*, *47* (8), 3848-3855, doi: 10.1021/es304348x, 2013.

Feng, W., M.P. Chipperfield, M. Dorf, K. Pfeilsticker, and P. Ricaud, Mid-latitude ozone changes: Studies with a 3-D CTM forced by ERA-40 analyses, *Atmos. Chem. Phys*., *7* (9), 2357-2369, doi: 10.5194/acp-7-2357-2007, 2007.

Feng, W., M.P. Chipperfield, S. Dhomse, B.M. Monge-Sanz, X. Yang, K. Zhang, and M. Ramonet, Evaluation of cloud convection and tracer transport in a three-dimensional chemical transport model, *Atmos. Chem. Phys.*, *11* (12), 5783-5803, doi: 10.5194/acp-11-5783-2011, 2011.

Fitzenberger, R., H. Bösch, C. Camy-Peyret, M.P. Chipperfield, H. Harder, U. Platt, B.-M. Sinnhuber, T. Wagner, and K. Pfeilsticker, First profile measurements of tropospheric BrO, *Geophys. Res. Lett.*, *27* (18), 2921-2924, doi: 10.1029/2000GL011531, 2000.

Folkins, I., and R.V. Martin, The vertical structure of tropical convection and its impact on the budgets of water vapor and ozone, *J. Atmos. Sci.*, *62* (5), 1560-1573. doi: 10.1175/JAS3407.1, 2005.

Fraser, P.J., D.E. Oram, C.E. Reeves, S.A. Penkett, and A. McCulloch, Southern Hemispheric halon trends (1978–1998) and global halon emissions, *J. Geophys. Res.*, *104* (D13), 15985-15999, doi: 10.1029/1999JD900113, 1999.

Fraser. P., P. Steele, and M.A. Cooksey, PFC and carbon dioxide emissions from an Australian aluminium smelter using time-integrated stacksampling and GC-MS, GC-FID analysis, in *Light Metals 2013*, edited by B. Sadler, 871-876, John Wiley & Sons, Inc., Hoboken, New Jersey, doi: 10.1002/9781118663189.ch148, 2013.

Fraser, P.J., B.L. Dunse, A.J. Manning, S.Walsh, R.H.J. Wang, P.B. Krummel, L.P. Steele, L.W. Porter, C.Allison, S. O'Doherty, P.G. Simmonds, J. Mühle, R.F. Weiss, and R.G. Prinn, Australian carbon tetrachloride emissions in a global context, *Environ. Chem.*, *11*, 77-88**,** doi: 10.1071/EN13171, 2014.

Froidevaux, L., N.J. Livesey, W.G. Read, R.J. Salawitch, J.W. Waters, B. Drouin, I.A. MacKenzie, H.C. Pumphrey, P. Bernath, C. Boone, R. Nassar, S. Montzka, J. Elkins, D. Cunnold, and D. Waugh, Temporal decrease in upper atmospheric chlorine, *Geophys. Res. Lett*., *33*, L23812, doi: 10.1029/2006GL027600, 2006.

Fthenakis, V., D.O. Clark, M. Moalem, P. Chandler, R.G. Ridgeway, F.E. Hulbert, D.B. Cooper, and P.J. Maroulis, Life-cycle nitrogen trifluoride from photovoltaics, *Environ. Sci. Technol.*, *44* (22), 8750–8757, doi: 10.1021/es100401y, 2010.

Fueglistaler, S., H. Wernli, and T. Peter, Tropical troposphere-to-stratosphere transport inferred from trajectory calculations, *J. Geophys. Res.*, *109* (D3), D03108, doi: 10.1029/2003JD004069, 2004.

Fueglistaler, S., A.E. Dessler, T.J. Dunkerton, I. Folkins, Q. Fu, and P.W. Mote, Tropical tropopause layer, *Rev. Geophys.*, *47*, RG1004, doi: 10.1029/2008RG000267, 2009.

Gardiner, T., A. Forbes, M. de Mazière, C. Vigouroux, E. Mahieu, P. Demoulin, V. Velazco, J. Notholt, T. Blumenstock, F. Hase, I. Kramer, R. Sussmann, W. Stremme, J. Mellqvist, A. Strandberg, K. Ellingsen, and M. Gauss, Trend analysis of greenhouse gases over Europe measured by a network of ground-based remote FTIR instruments, *Atmos. Chem. Phys.*, *8* (22), 6719-6727, doi: 10.5194/acp-8-6719-2008, 2008.

Gebhardt, S., A. Colomb, R. Hofmann, J. Williams, and J. Lelieveld, Halogenated organic species over the tropical South American rainforest, *Atmos. Chem. Phys.*, *8* (12), 3185-3197, doi: 10.5194/acp-8-3185-2008, 2008.

Gentner, D.R., A.M. Miller, and A.H. Goldstein, Seasonal variability in anthropogenic halocarbon emissions, *Environ. Sci. Technol.*, *44* (14), 5377-5382, doi: 10.1021/es1005362, 2010.

Gettelman, A., and P.M. de F. Forster, A climatology of the tropical tropopause layer, *J. Meteorol. Soc. Japan.*, *80* (4B), 911-924, doi: 10.2151/jmsj.80.911, 2002.

Gettelman, A., P.M. de F. Forster, M. Fujiwara, Q. Fu, H. Vömel, L.K. Gohar, C. Johanson, and M. Ammerman, Radiation balance of the tropical tropopause layer, *J. Geophys. Res.*, *109* (D7), D07103, doi: 10.1029/2003 JD004190, 2004.

Gettelman, A., P.H. Lauritzen, M. Park, and J.E. Kay, Processes regulating short-lived species in the tropical tropopause layer, *J. Geophys. Res*., *114*, D13303, doi: 10.1029/2009JD011785, 2009.

Greally, B.R., A.J. Manning, S. Reimann, A. McCulloch, J. Huang, B.L. Dunse, P.G. Simmonds, R.G. Prinn, P.J. Fraser, D.M. Cunnold, S. O'Doherty, L.W. Porter, K. Stemmler, M.K. Vollmer, C.R. Lunder, N. Schmidbauer, O. Hermansen, J. Arduini, P.K. Salameh, P.B. Krummel, R.H.J. Wang, D. Folini, R.F. Weiss, M. Maione, G. Nickless, F. Stordal, and R.G. Derwent, Observations of 1,1-difluoroethane (HFC-152a) at AGAGE and SOGE monitoring stations in 1994–2004 and derived global and regional emission estimates, *J. Geophys. Res.*, *112* (D6), D06308, doi: 10.1029/2006JD007527, 2007.

Greenblatt, G.D., J.J. Orlando, J.B. Burkholder, and A.R. Ravishankara, Absorption measurements of oxygen between 330 and 1140 nm, *J. Geophys. Res.,* 95 (D11), 18557-18582, doi: 10.1029/JD095iD11p18577, 1990.

Großmann, K., U. Frieß, E. Peters, F. Wittrock, J. Lampel, S. Yilmaz, J. Tschritter, R. Sommariva, R. von Glasow, B. Quack, K. Krüger, K. Pfeilsticker, and U. Platt, Iodine monoxide in the Western Pacific marine boundary layer, *Atmos. Chem. Phys.*, *13* (6), 3363-3378, doi: 10.5194/acp-13-3363-2013, 2013.

Hall, B.D., G.S. Dutton, D.J. Mondeel, J.D. Nance, M. Rigby, J.H. Butler, F.L. Moore, D.F. Hurst, and J.W. Elkins, Improving measurements of SF_6 for the study of atmospheric transport and emissions, *Atmos. Meas. Tech.*, *4* (11), 2441-2451, doi: 10.5194/amt-4-2441-2011, 2011.

Hall, B.D., A. Engel, J. Mühle, J.W. Elkins, F. Artuso, E. Atlas, M. Aydin, D.R. Blake, E.-G. Brunke, S. Chiavarini, P.J. Fraser, J. Happell, P.B. Krummel, I. Levin, M. Loewenstein, M. Maione, S.A. Montzka, S. O'Doherty, S. Reimann, G. Rhoderick, E.S. Saltzman, H.E. Scheel, L.P. Steele, M.K. Vollmer, R.F. Weiss, D. Worthy, and Y. Yokouchi, Results from the International Halocarbons in Air Comparison Experiment (IHALACE), *Atmos. Meas. Tech.*, *7* (2), 469-490, doi: 10.5194/amt-7-469-2014, 2014.

Han, W., Y. Li, H. Tang, and H. Liu, Treatment of the potent greenhouse gas, CHF_3 – An overview, *J. Fluorine Chem.*, *140*, 7-16, doi: 10.1016/j.jfluchem.2012.04.012, 2012.

Hanisco, T.F., E.J. Lanzendorf, P.O. Wennberg, K.K. Perkins, R.M. Stimpfle, P.B. Voss, J.G. Anderson, R.C. Cohen, D.W. Fahey, R.S. Gao, E.J. Hintsa, R.J. Salawitch, J.J. Margitan, C.T. McElroy, and C. Midwinter, Sources, sinks, and the distribution of OH in the lower stratosphere, *J. Phys. Chem. A*, *105* (9), 1543-1553, doi: 10.1021/jp002334g, 2001.

Happell, J.D., and M.P. Roche, Soils: A global sink of atmospheric carbon tetrachloride, *Geophys. Res. Lett.*, *30* (2), 1088, doi: 10.1029/2002GL015957, 2003.

Harrison, J.J., C.D. Boone, A.T. Brown, N.D.C. Allen, G.C. Toon, and P.F. Bernath, First remote sensing observations of trifluoromethane (HFC-23) in the upper troposphere and lower stratosphere, *J. Geophys. Res.*, *117* (D5), D05308, doi: 10.1029/2011JD016423, 2012.

Hartmann, D.L., A.M.G. Klein Tank, M. Rusticucci, L.V. Alexander, S. Brönnimann, Y. Charabi, F.J. Dentener, E.J. Dlugokencky, D.R. Easterling, A. Kaplan, B.J. Soden, P.W. Thorne, M. Wild, and P.M. Zhai, Observations: Atmosphere and surface, Chapter 2 in *Climate Change 2013: The Physical Science Basis. Contribution of Working Group I to the Fifth Assessment Report of the Intergovernmental Panel on Climate*

Change, edited by T.F. Stocker, D. Qin, G.-K. Plattner, M. Tignor, S.K. Allen, J. Boschung, A. Nauels, Y. Xia, V. Bex, and P.M. Midgley, Cambridge University Press, Cambridge, U.K. and New York, NY, 2013.

Hattori, S., S.O. Danielache, M.S. Johnson, J.A. Schmidt, H.G. Kjaergaard, S. Toyoda, Y. Ueno, and N. Yoshida, Ultraviolet absorption cross sections of carbonyl sulfide isotopologues $OC^{32}S$, $OC^{33}S$, $OC^{34}S$ and $O^{13}CS$: Isotopic fractionation in photolysis and atmospheric implications, *Atmos. Chem. Phys.*, *11* (19), 10293-10303, doi: 10.5194/acp-11-10293-2011, 2011.

He, Z., G.P. Yang, and X.L. Lu, Distributions and sea-to-air fluxes of volatile halocarbons in the East China Sea in early winter, *Chemosphere*, *90* (2), 747-757, doi: 10.1016/j.chemosphere.2012.09.067, 2013.

Hendrick, F., M. Van Roozendael, M.P. Chipperfield, M. Dorf, F. Goutail, X. Yang, C. Fayt, C. Hermans, K. Pfeilsticker, J.P. Pommereau, J.A. Pyle, N. Theys, and M. De Maziere, Retrieval of stratospheric and tropospheric BrO profiles and columns using ground-based zenith-sky DOAS observations at Harestua, 60 degrees N, *Atmos. Chem. Phys., 7* (18), 4869-4885, 2007.

Hendrick, F., P.V. Johnston, M. De Mazière, C. Fayt, C. Hermans, K. Kreher, N. Theys, A. Thomas, and M. Van Roozendael, One-decade trend analysis of stratospheric BrO over Harestua (60°N) and Lauder (45°S) reveals a decline, *Geophys. Res. Lett.*, *35* (14), L14801, doi: 10.1029/2008GL034154, 2008.

Henne, S., D.E. Shallcross, S. Reimann, P. Xiao, D. Brunner, S. O'Doherty, and B. Buchmann, Future emissions and atmospheric fate of HFC-1234yf from mobile air conditioners in Europe, *Environ. Sci. Technol.*, *46* (3), 1650-1658, doi: 10.1021/es2034608, 2012.

Hodson, E.L., D. Martin, and R.G. Prinn, The municipal solid waste landfill as a source of ozone-depleting substances in the United States and United Kingdom, *Atmos. Chem. Phys.*, *10* (4), 1899-1910, doi: 10.5194/acp-10-1899-2010, 2010.

Hofmann, D.J., and S.A. Montzka, Recovery of the ozone layer: The Ozone Depleting Gas Index, *EOS Transactions*, *90* (1), 1-2, doi: 10.1029/2009EO010001, 2009.

Hosking, J.S., M.R. Russo, P. Braesicke, and J.A. Pyle, Modelling deep convection and its impacts on the tropical tropopause layer, *Atmos. Chem. Phys.*, *10* (22), 11175-11188, doi: 10.5194/acp-10-11175-2010, 2010.

Hossaini, R., M.P. Chipperfield, B.M. Monge-Sanz, N.A.D. Richards, E. Atlas, and D.R. Blake, Bromoform and dibromomethane in the tropics: A 3-D model study of chemistry and transport, *Atmos. Chem. Phys*., *10* (2), 719-735, doi: 10.5194/acp-10-719-2010, 2010.

Hossaini, R., M.P. Chipperfield, S. Dhomse, C. Ordoñez, A. Saiz-Lopez, N.L. Abraham, A. Archibald, P. Braesicke, P. Telford, N. Warwick, X. Yang, and J. Pyle, Modelling future changes to the stratospheric source gas injection of biogenic bromocarbons, *Geophys. Res. Lett.*, *39* (20), L20813, doi: 10.1029/2012GL053401, 2012a.

Hossaini, R., M.P. Chipperfield, W. Feng, T.J. Breider, E. Atlas, S.A. Montzka, B.R. Miller, F. Moore, and J. Elkins, The contribution of natural and anthropogenic very short-lived species to stratospheric bromine, *Atmos. Chem. Phys.*, *12* (1), 371-380, doi: 10.5194/acp-12-371-2012, 2012b.

Hossaini, R., Mantle, H., Chipperfield, M.P., Montzka, S.A., Hamer, P., Ziska, F., Quack, B., Krüger, K., Tegtmeier, S., Atlas, E., Sala, S., Engel, A., Bönisch, H., Keber, T., Oram, D., Mills, G., Ordóñez, C., Saiz-Lopez, A., Warwick, N., Liang, Q., Feng, W., Moore, F., Miller, B.R., Marécal, V., Richards, N.A.D., Dorf, M., and Pfeilsticker, K., Evaluating global emission inventories of biogenic bromocarbons, *Atmos. Chem. Phys*., *13* (23), 11819-11838, doi: 10.5194/acp-13-11819-2013, 2013.

Hoyle, C.R., V. Marecal, M.R. Russo, G. Allen, J. Arteta, C. Chemel, M.P. Chipperfield, F. D'Amato, O. Dessens, W. Feng, J.F. Hamilton, N.R.P. Harris, J.S. Hosking, A.C. Lewis, O. Morgenstern, T. Peter, J.A. Pyle, T. Reddmann, N.A.D. Richards, P.J. Telford, W. Tian, S. Viciani, A. Volz-Thomas, O. Wild, X. Yang, and G. Zeng, Representation of tropical deep convection in atmospheric models - Part 2: Tracer transport, *Atmos. Chem. Phys.*, *11* (15), 8103-8131, doi: 10.5194/acp-11-8103-2011, 2011.

Hu, L., The Role of the Ocean in the Atmospheric Budgets of Methyl Bromide, Methyl Chloride and Methane, Doctoral dissertation, Texas A&M University, College Station, TX, U.S.A., 2012.

Hu, L., S.A. Yvon-Lewis, Y. Liu, and T.S. Bianchi, The ocean in near equilibrium with atmospheric methyl bromide, *Global Biogeochem. Cycles*, *26* (3), GB3016, doi: 10.1029/2011GB004272, 2012.

Hu, L., S.A. Yvon-Lewis, J.H. Butler, J.M. Lobert, and D.B. King, An improved oceanic budget for methyl chloride, *J. Geophys. Res.*, *118* (2), 715-725, doi: 10.1029/2012JC008196, 2013.

Hughes, C., M. Johnson, R. Utting, S. Turner, G. Malin, A. Clarke, and P.S. Liss, Microbial control of bromocarbon concentrations in coastal waters of the western Antarctic Peninsula, *Mar. Chem.*, *151*, 35-46, doi: 10.1016/j.marchem.2013.01.007, 2013.

Hurley, M.D., T.J. Wallington, M.S. Javadi, and O.J. Nielsen, Atmospheric chemistry of $CF_3CF{=}CH_2$: Products and mechanisms of Cl atom and OH radical initiated oxidation, *Chem. Phys. Lett*., *450* (4-6), 263-267, doi: 10.1016/j.cplett.2007.11.051, 2008.

Hurst, D.F., J.C. Lin, P.A. Romashkin, B.C. Daube, C. Gerbig, D.M. Matross, S.C. Wofsy, B.D. Hall, and J.W. Elkins, Continuing global significance of emissions of Montreal Protocol-restricted halocarbons in the United States and Canada, *J. Geophys. Res.*, *111*, D15302, doi: 10.1029/2005JD006785, 2006.

IPCC (Intergovernmental Panel on Climate Change), *Climate Change 2013: The Physical Science Basis: Contribution of Working Group I to the Fifth Assessment Report of the Intergovernmental Panel on Climate Change*, edited by T.F. Stocker, D. Qin, G.-K. Plattner, M. Tignor, S.K. Allen, J. Boschung, A. Nauels, Y. Xia, V. Bex, and P.M. Midgley, 1535 pp., Cambridge University Press, Cambridge, UK and New York, NY, USA, 2013.

IPCC/TEAP (Intergovernmental Panel on Climate Change/Technology and Economic Assessment Panel), *IPCC/TEAP Special Report on Safeguarding the Ozone Layer and the Global Climate System: Issues Related to Hydrofluorocarbons and Perfluorocarbons*, prepared by Working Groups I and III of the Intergovernmental Panel on Climate Change, and the Technical and Economic Assessment Panel, Cambridge University Press, Cambridge, U.K. and New York, NY, U.S.A., 2005.

Ivy, D.J., T. Arnold, C.M. Harth, L.P. Steele, J. Mühle, M. Rigby, P.K. Salameh, M. Leist, P.B. Krummel, P.J. Fraser, R.F. Weiss, and R.G. Prinn, Atmospheric histories and growth trends of C_4F_{10}, C_5F_{12}, C_6F_{14}, C_7F_{16} and C_8F_{18}, *Atmos. Chem. Phys.*, *12* (9), 4313-4325, doi: 10.5194/acp-12-4313-2012, 2012a.

Ivy, D.J., M. Rigby, M. Baasandorj, J.B. Burkholder, and R.G. Prinn, Global emission estimates and radiative impact of C_4F_{10}, C_5F_{12}, C_6F_{14}, C_7F_{16} and C_8F_{18}, *Atmos. Chem. Phys.*, *12* (16), 7635-7645, doi: 10.5194/acp-12-7635-2012, 2012b.

Jones, A., J. Urban, D.P. Murtagh, C. Sanchez, K.A. Walker, N.J. Livesey, L. Froidevaux, and M.L. Santee, Analysis of HCl and ClO time series in the upper stratosphere using satellite data sets, *Atmos. Chem. Phys.*, *11* (11), 5321-5333, doi: 10.5194/acp-11-5321-2011, 2011.

Jones, C.E., K.E. Hornsby, R. Sommariva, R.M. Dunk, R. von Glasow, G.B. McFiggans, and L.J. Carpenter, Quantifying the contribution of marine organic gases to atmospheric iodine, *Geophys. Res. Lett.*, *37* (18), L18804, doi: 10.1029/2010GL043990, 2010.

Jones, C.E., S.J. Andrews, L.J. Carpenter, C. Hogan, F.E. Hopkins, J.C. Laube, A.D. Robinson, T.G. Spain, S.D. Archer, N.R.P. Harris, P.D. Nightingale, S.J. O'Doherty, D.E. Oram, J.A. Pyle, J.H. Butler, and B.D. Hall, Results from the first national UK inter-laboratory calibration for very short-lived halocarbons, *Atmos. Meas. Tech.*, *4* (5), 865-874, doi: 10.5194/amt-4-865-2011, 2011.

Jourdain, J.L., G. Le Bras, and J. Combourieu, Kinetic study by electron paramagnetic resonance and mass spectrometry of the elementary reactions of phosphorus tribromide with H, O, and OH radicals, *J. Phys. Chem.*, *86* (21), 4170-4175, doi: 10.1021/j100218a016, 1982.

Kai, F.M., S.C. Tyler, J.T. Randerson, and D.R. Blake, Reduced methane growth rate explained by decreased Northern Hemisphere microbial sources, *Nature*, *476* (7359), 194-197, 2011.

Keller, C.A., D. Brunner, S. Henne, M.K. Vollmer, S. O'Doherty, and S. Reimann, Evidence for under-reported western European emissions of the potent greenhouse gas HFC-23, *Geophys. Res. Lett.*, *38* (15), L15808, doi: 10.1029/2011GL047976, 2011.

Keller, C.A., M. Hill, M.K. Vollmer, S. Henne, D. Brunner, S. Reimann, S. O'Doherty, J. Arduini, M. Maione, Z. Ferenczi, L. Haszpra, A.J. Manning, and T. Peter, European emissions of halogenated greenhouse gases inferred from atmospheric measurements, *Environ. Sci. Technol.*, *46* (1), 217-225, doi: 10.1021/es202453j, 2012.

Kellmann, S., T. von Clarmann, G.P. Stiller, E. Eckert, N. Glatthor, M. Höpfner, M. Kiefer, J. Orphal, B. Funke, U. Grabowski, A. Linden, G.S. Dutton, and J.W. Elkins, Global CFC-11 (CCl_3F) and CFC-12 (CCl_2F_2) measurements with the Michelson Interferometer for Passive Atmospheric Sounding (MIPAS): Retrieval, climatologies and trends, *Atmos. Chem. Phys.*, *12* (24), 11857-11875, doi: 10.5194/acp-12-11857-2012, 2012.

Khan, M.A.H., M.E. Whelan, and R.C. Rhew, Effects of temperature and soil moisture on methyl halide and chloroform fluxes from drained peatland pasture soils, *J. Environ. Monit.*, *14* (1), 241-249, doi: 10.1039/c1em10639b, 2012.

Kim, J., S. Li, K.-R. Kim, A. Stohl, J. Mühle, S.-K. Kim, M.-K. Park, D.-J. Kang, G. Lee, C.M. Harth, P.K. Salameh, and R.F. Weiss, Regional atmospheric emissions determined from measurements at Jeju Island, Korea: Halogenated compounds from China, *Geophys. Res. Lett.*, *37*, L12801, doi: 10.1029/2010GL043263, 2010.

Kirschke, S., P. Bousquet, P. Ciais, M. Saunois, J.G. Canadell, E.J. Dlugokencky, P. Bergamaschi, D. Bergmann, D.R. Blake, L. Bruhwiler, P. Cameron-Smith, S. Castaldi, F. Chevallier, L. Feng, A. Fraser, M. Heimann, E.L. Hodson, S. Houweling, B. Josse, P.J. Fraser, P.B. Krummel, J.-F. Lamarque, R.L. Langenfelds, C. Le Quere, V. Naik,. S. O'Doherty, I. Palmer, I. Pison, D. Plummer, B. Poulter, R.G. Prinn, M. Rigby, B. Ringeval, M. Santini, M. Schmidt, D.T. Shindell, I.J. Simpson, R. Spahni, L.P. Steele, S.A. Strode, K. Sudo,. S. Szopa, G.R. van der

Werf, A. Voulgarakis, M. van Weele, R.F. Weiss, J.E. Williams, and G. Zeng, Three decades of global methane sources and sinks, *Nature Geosci.*, *6* (10), 813-823, doi: 10.1038/ngeo1955, 2013.

Kley, D., P.J. Crutzen, H.G.J. Smit, H. Vömel, S.J. Oltmans, H. Grassl, and V. Ramanathan, Observations of near-zero ozone concentrations over the convective Pacific: Effects on air chemistry, *Science*, *274* (5285), 230-233, doi: 10.1126/science.274.5285.230, 1996.

Ko, M.K.W., and G. Poulet (Lead Authors), D.R. Blake, O. Boucher, J.H. Burkholder, M. Chin, R.A. Cox, C. George, H.-F. Graf, J.R. Holton, D.J. Jacob, K.S. Law, M.G. Lawrence, P.M. Midgley, P.W. Seakins, D.E. Shallcross, S.E. Strahan, D.J. Wuebbles, and Y. Yokouchi, Very short-lived halogen and sulfur substances, Chapter 2 in *Scientific Assessment of Ozone Depletion: 2002*, Global Ozone Research and Monitoring Project–Report No. 47, World Meteorological Organization, Geneva, Switzerland, 2003.

Kohlhepp, R., R. Ruhnke, M.P. Chipperfield, M. De Maziere, J. Notholt, S. Barthlott, R.L. Batchelor, R.D. Blatherwick, T. Blumenstock, M.T. Coffey, P. Demoulin, H. Fast, W. Feng, A. Goldman, D.W.T. Griffith, K. Hamann, J.W. Hannigan, F. Hase, N.B. Jones, A. Kagawa, I. Kaiser, Y. Kasai, O. Kirner, W. Kouker, R. Lindenmaier, E. Mahieu, R.L. Mittermeier, B. Monge-Sanz, I. Morino, I. Murata, H. Nakajima, M. Palm, C. Paton-Walsh, U. Raffalski, T. Reddmann, M. Rettinger, C.P. Rinsland, E. Rozanov, M. Schneider, C. Senten, C. Servais, B.-M. Sinnhuber, D. Smale, K. Strong, R. Sussmann, J.R. Taylor, G. Vanhaelewyn, T. Warneke, C. Whaley, M. Wiehle, and S.W. Wood, Observed and simulated time evolution of HCl, $ClONO_2$, and HF total column abundances, *Atmos. Chem. Phys.*, *12* (7), 3527-3556, doi: 10.5194/acp-12-3527-2012, 2012.

Kreycy, S., C. Camy-Peyret, M.P. Chipperfield, M. Dorf, W. Feng, R. Hossaini, L. Kritten, B. Werner, and K. Pfeilsticker, Atmospheric test of the $J(BrONO_2)/k_{BrO+NO2}$ ratio: Implications for total stratospheric Br_y and bromine-mediated ozone loss, *Atmos. Chem. Phys.*, *13* (13), 6263-6274, doi: 10.5194/acp-13-6263-2013, 2013.

Kreyling, D., H. Sagawa, I. Wohltmann, R. Lehmann, and Y. Kasai, SMILES zonal and diurnal variation climatology of stratospheric and mesospheric trace gasses: O_3, HCl, HNO_3, ClO, BrO, HOCl, HO_2, and temperature, *J. Geophys. Res.*, *118* (20), doi: 10.1002/2012JD019420, 2013.

Krysell, M., E. Fogelqvist, and T. Tanhua, Apparent removal of the transient tracer carbon tetrachloride from anoxic seawater, *Geophys. Res. Lett.*, *21* (23), 2511-2514, doi: 10.1029/94GL02336, 1994.

Krysztofiak, G., V. Catoire, G. Poulet, V. Marécal, M. Pirre, F. Louis, S. Canneaux, and B. Josse, Detailed modeling of the atmospheric degradation mechanism of very-short lived brominated species, *Atmos. Environ.*, *59*, 514-532, doi: 10.1016/j.atmosenv.2012.05.026, 2012.

Kutsuna, S., L. Chen, T. Abe, J. Mizukado, T. Uchimaru, K. Tokuhashi, and A. Sekiya, Henry's law constants of 2,2,2-trifluoroethyl formate, ethyl trifluoroacetate, and non-fluorinated analogous esters, *Atmos. Environ.*, *39* (32), 5884-5892, doi: 10.1016/j.atmosenv.2005.06.021, 2005.

Lal, S., R. Borchers, P. Fabian, P.K. Patra, and B. H. Subbaraya, Vertical distribution of methyl bromide over Hyderbad, India, *Tellus B, 46,* 373-377, doi: 10.1034/j.1600-0889.1994.t01-3-00003.x, 1994.

Langbein, T., H. Sonntag, D. Trapp, A. Hoffmann, W. Malms, E.P. Roth, V. Mors, and R. Zellner, Volatile anaesthetics and the atmosphere: Atmospheric lifetimes and atmospheric effects of halothane, enflurane, isoflurane, desflurane and sevoflurane, *British J. Anaesthesia*, *82* (1), 66-73, doi: 10.1093/bja/82.1.66, 1999.

Langenfelds, R.L., P.J. Fraser, R.J. Francey, L.P. Steele, L.W. Porter, and C.E. Allison, The Cape Grim Air Archive: The first seventeen years, 1978-1995, in *Baseline Atmospheric Program (Australia) 1994-95*, edited by R.J. Francey, A.L. Dick, and N. Derek, 53-70, Bureau of Meteorology and CSIRO Division of Atmospheric Research, Melbourne, Australia, 1996.

Laube, J.C., A. Engel, H. Bönisch, T. Möbius, D.R. Worton, W.T. Sturges, K. Grunow, and U. Schmidt, Contribution of very short-lived organic substances to stratospheric chlorine and bromine in the tropics—a case study, *Atmos. Chem. Phys.*, *8* (23), 7325-7334, doi: 10.5194/acp-8-7325-2008, 2008.

Laube, J.C., P. Martinerie, E. Witrant, T. Blunier, J. Schwander, C.A.M Brenninkmeijer, T.J. Schuck, M. Bolder, T. Röckmann, C. van der Veen, H. Bönisch, A. Engel, G.P. Mills, M.J. Newland, D.E. Oram, C.E. Reeves, and W.T. Sturges, Accelerating growth of HFC-227ea (1,1,1,2,3,3,3-heptafluoropropane) in the atmosphere, *Atmos. Chem. Phys.*, *10* (13), 5903-5910, doi: 10.5194/acp-10-5903-2010, 2010.

Laube, J.C., C. Hogan, M.J. Newland, F.S. Mani, P.J. Fraser, C.A.M. Brenninkmeijer, P. Martinerie, D.E. Oram, T. Röckmann, J. Schwander, E. Witrant, G.P. Mills, C.E. Reeves, and W.T. Sturges, Distributions, long term trends and emissions of four perfluorocarbons in remote parts of the atmosphere and firn air, *Atmos. Chem. Phys.*, *12* (9), 4081-4090, doi: 10.5194/acp-12-4081-2012, 2012.

Laube, J.C., A. Keil, H. Bönisch, A. Engel, T. Röckmann, C.M. Volk, and W.T. Sturges, Observation-based assessment of stratospheric fractional release, lifetimes, and ozone depletion potentials of ten important source gases, *Atmos. Chem. Phys.*, *13* (5), 2779-2791, doi: 10.5194/acp-13-2779-2013, 2013.

Laube, J.C., M.J. Newland, C. Hogan, C.A.M. Brenninkmeijer, P.J. Fraser, P. Martinerie, D.E. Oram, C.E. Reeves, T. Röckmann, J. Schwander, E. Witrant, and W.T. Sturges, Newly detected ozone-depleting substances in the atmosphere, *Nature Geosci.*, *7* (4), 266–269, doi: 10.1038/ngeo2109, 2014.

Law, K.S., and W.T. Sturges (Lead Authors), D.R. Blake, N.J. Blake, J.B. Burkholder, J.H. Butler, R.A. Cox, P.H. Haynes, M.K.W. Ko, K. Kreher, C. Mari, K. Pfeilsticker, J.M.C. Plane, R.J. Salawitch, C. Schiller, B.-M. Sinnhuber, R. von Glasow, N.J. Warwick, D.J. Wuebbles, and S.A. Yvon-Lewis, Halogenated very short-lived substances, Chapter 2 in *Scientific Assessment of Ozone Depletion: 2006*, Global Ozone Research and Monitoring Project—Report No.50, World Meteorological Organization, Geneva, Switzerland, 2007.

Lawler, M.J., B. D. Finley, W.C. Keene, A.A.P. Pszenny, K.A. Read, R. von Glasow, and E.S. Saltzman, Pollution-enhanced reactive chlorine chemistry in the eastern tropical Atlantic boundary layer, *Geophys. Res. Lett.*, *36* (8), L08810, doi: 10.1029/2008GL036666, 2009.

Le Calvé, S., G. Le Bras, and A. Mellouki, Temperature dependence for the rate coefficients of the reactions of the OH radical with a series of formates, *J. Phys. Chem. A*, *101* (30), 5489-5493, doi: 10.1021/jp970554x, 1997.

Lee, Y., S. Bae, and W. Lee, Degradation of carbon tetrachloride in modified Fenton reaction, *Korean J. Chem. Eng.*, *29* (6), 769-774, doi: 10.1007/s11814-011-0261-8, 2012.

Lee-Taylor, J.M., and E.A. Holland, Litter decomposition as a potential natural source of methyl bromide, *J. Geophys. Res.*, *105* (D7), 8857-8864, doi: 10.1029/1999JD901112, 2000.

Lee-Taylor, J., and K.R. Redeker, Reevaluation of global emissions from rice paddies of methyl iodide and other species, *Geophys. Res. Lett.*, *32*, L15801, doi: 10.1029/2005GL022918, 2005.

Lee-Taylor, J.M., G.P. Brasseur, and Y. Yokouchi, A preliminary three-dimensional global model study of atmospheric methyl chloride distributions, *J. Geophys. Res.*, *106* (D24), 34221-34233, doi: 10.1029/2001 JD900209, 2001.

Leedham, E.C., C. Hughes, F.S.L. Keng, S.-M. Phang, G. Malin, and W.T. Sturges, Emission of atmospherically significant halocarbons by naturally occurring and farmed tropical macroalgae, *Biogeosciences*, *10* (6), 3615-3633, doi: 10.5194/bg-10-3615-2013, 2013.

Leung, F.-Y.T., A.J. Colussi, M.R. Hoffmann, and G.C. Toon, Isotopic fractionation of carbonyl sulfide in the atmosphere: Implications for the source of background stratospheric sulfate aerosol, *Geophys. Res. Lett.*, *29* (10), 112-111-112-114, doi: 10.1029/2001GL013955, 2002.

Levin, I., T. Naegler, R. Heinz, D. Osusko, E. Cuevas, A. Engel, J. Ilmberger, R.L. Langenfelds, B. Neininger, C. von Rohden, L.P. Steele, R. Weller, D.E. Worthy, and S.A. Zimov, The global SF_6 source inferred from long-term high precision atmospheric measurements and its comparison with emission inventories, *Atmos. Chem. Phys.*, *10* (6), 2655-2662, doi: 10.5194/acp-10-2655-2010, 2010.

Levin, I., C. Veidt, B.H. Vaughn, G. Brailsford, T. Bromley, R. Heinz, D. Lowe, J.B. Miller, C. Poß, and J.W.C. White, No inter-hemispheric $\delta^{13}CH_4$ trend observed, *Nature*, 486 (7404), E3–E4, doi: 10.1038/nature11175, 2012.

Levine, J.G., P. Braesicke, N.R.P. Harris, N.H. Savage, and J.A. Pyle, Pathways and timescales for troposphere-to-stratosphere transport via the tropical tropopause layer and their relevance for very short lived substances, *J. Geophys. Res.*, *112* (D4), D04308, doi: 10.1029/2005JD006940, 2007.

Li, S., J. Kim, K.R. Kim, J. Mühle, S.K. Kim, M.K. Park, A. Stohl, D.J. Kang, T. Arnold, C.M. Harth, P.K. Salameh, and R.F. Weiss, Emissions of halogenated compounds in East Asia determined from measurements at Jeju Island, Korea, *Environ. Sci. Technol.*, *45* (13), 5668-5675, doi: 10.1021/es104124k, 2011.

Liang, Q., R.S. Stolarski, S.R. Kawa, J.E. Nielsen, J.M. Rodriguez, A.R. Douglass, J.M. Rodriguez, D.R. Blake, E.L. Atlas, and L.E. Ott, Finding the missing stratospheric Br_y: A global modeling study of $CHBr_3$ and CH_2Br_2, *Atmos. Chem. Phys.*, *10* (5), 2269-2286, doi: 10.5194/acp-10-2269-2010, 2010.

Liang, Q., E. Atlas, D. Blake, M. Dorf, K. Pfeilsticker, and S. Schauffler, Convective transport of very-short-lived bromocarbons to the stratosphere, *Atmos. Chem. Phys.*, *14,* 5781-5792, doi: 10.5194/acp-14-5781-2014, 2014.

Lin, C.Y., and S.L. Manley, Bromoform production from seawater treated with bromoperoxidase, *Limnol. Oceanogr.*, *57* (6), 1857-1866, doi: 10.4319/lo.2012.57.06.1857, 2012.

Liu, C., and E.J. Zipser, Global distribution of convection penetrating the tropical tropopause, *J. Geophys. Res.*, *110* (D23), D23104, doi: 10.1029/2005JD006063, 2005.

Liu, X.-F., Evidence of Biodegradation of Atmospheric Carbon Tetrachloride in Soils: Field and Microcosm Studies, Ph.D. thesis, 139 pp., Columbia University, New York, NY, U.S.A., 2006.

Liu, Y., S.A. Yvon-Lewis, L. Hu, J.E. Salisbury, and J.E. O'Hern, $CHBr_3$, CH_2Br_2, and $CHClBr_2$ in U.S. coastal waters during the Gulf of Mexico and East Coast Carbon cruise, *J. Geophys. Res.*, *116* (C10), C10004, doi: 10.1029/2010JC006729, 2011.

Liu, Y., S.A. Yvon-Lewis, D.C.O. Thornton, J.H. Butler, T.S. Bianchi, L. Campbell, L. Hu, and R.W. Smith, Spatial and temporal distributions of bromoform and dibromomethane in the Atlantic Ocean and their relationship with photosynthetic biomass, *J. Geophys. Res.*, *118* (8), 3950–3965, doi: 10.1002/jgrc.20299, 2013.

Logue, J.M., M.J. Small, D. Stern, J. Maranche, and A.L. Robinson, Spatial variation in ambient air toxics concentrations and health risks between industrial-influenced, urban, and rural sites, *J. Air Waste Manag. Assoc.*, *60* (3), 271-286, doi: 10.3155/1047-3289.60.3.271, 2010.

Low, J.C., N.Y. Wang, J. Williams, and R.J. Cicerone, Measurements of ambient atmospheric C_2H_5Cl and other ethyl and methyl halides at coastal California sites and over the Pacific Ocean, *J. Geophys. Res.*, *108* (D19), 4608, doi: 10.1029/2003JD003620, 2003.

Lu, Z., D.G. Streets, Q. Zhang, S. Wang, G.R. Carmichael, Y.F. Cheng, C. Wei, M. Chin, T. Diehl, and Q. Tan, Sulfur dioxide emissions in China and sulfur trends in East Asia since 2000, *Atmos. Chem. Phys.*, *10* (13), 6311-6331, doi: 10.5194/acp-10-6311-2010, 2010.

Mahajan, A.S., J.M.C. Plane, H. Oetjen, L. Mendes, R.W. Saunders, A. Saiz-Lopez, C.E. Jones, L.J. Carpenter, and G.B. McFiggans, Measurement and modelling of tropospheric reactive halogen species over the tropical Atlantic Ocean, *Atmos. Chem. Phys.*, *10* (10), 4611-4624, doi: 10.5194/acp-10-4611-2010, 2010.

Mahajan, A.S., J.C. Gómez Martín, T.D. Hay, S.-J. Royer, S. Yvon-Lewis, Y. Liu, L. Hu, C. Prados-Roman, C. Ordóñez, J.M.C. Plane, and A. Saiz-Lopez, Latitudinal distribution of reactive iodine in the Eastern Pacific and its link to open ocean sources, *Atmos. Chem. Phys.*, *12* (23), 11609-11617, doi: 10.5194/acp-12-11609-2012, 2012.

Mahieu, E., R. Zander, P.F. Bernath, C.D. Boone, and K.A. Walker, Recent trend anomaly of hydrogen chloride (HCl) at northern mid-latitudes derived from Jungfraujoch, HALOE and ACE-FTS Infrared solar observations, in *The Atmospheric Chemistry Experiment ACE at 10: A Solar Occultation Anthology*, edited by P.F. Bernath, 239-249, A. Deepak Publishing, Hampton, Virginia, 2013.

Mahieu, E., R. Zander, G.C. Toon, M.K. Vollmer, S. Reimann, J. Mühle, W. Bader, B. Bovy, B. Lejeune, C. Servais, P. Demoulin, G. Roland, P.F. Bernath, C.D. Boone, K.A. Walker, and P. Duchatelet, Spectrometric monitoring of atmospheric carbon tetrafluoride (CF_4) above the Jungfraujoch station since 1989: Evidence of continued increase but at a slowing rate, *Atmos. Meas. Tech.*, *7* (1), 333-344, doi: 10.5194/amt-7-333-2014, 2014.

Maiss, M., and C.A.M. Brenninkmeijer, Atmospheric SF_6: Trends, sources and prospects, *Environ. Sci. Technol.*, *32* (20), 3077-3086, doi: 10.1021/es9802807, 1998.

Malicet, J., D. Daumont, J. Charbonnier, C. Parisse, A. Chakir, and J. Brion, Ozone U.V. spectroscopy. II. Absorption cross-sections and temperature dependence, *J. Atmos. Chem., 21* (3), 263-273, doi: 10.1007/BF 00696758, 1995.

Manley, S.L., N.-Y. Wang, M.L. Walser, and R.J. Cicerone, Methyl halide emissions from greenhouse-grown mangroves, *Geophys. Res. Lett.*, *34* (1), L01806, doi: 10.1029/2006GL027777, 2007.

Marcy, T.P., P.J. Popp, R.S. Gao, D.W. Fahey, E.A. Ray, E.C. Richard, T.L. Thompson, E.L. Atlas, M. Loewenstein, S.C. Wofsy, S. Park, E.M. Weinstock, W.H. Swartz, and M.J. Mahoney, Measurements of trace gases in the tropical tropopause layer, *Atmos. Environ.*, *41* (34), 7253-7261, doi: 10.1016/j.atmosenv. 2007.05.032, 2007.

Marécal, V., M. Pirre, G. Krysztofiak, P.D. Hamer, and B. Josse, What do we learn about bromoform transport and chemistry in deep convection from fine scale modelling?, *Atmos. Chem. Phys.*, *12* (14), 6073-6093, doi: 10.5194/acp-12-6073-2012, 2012.

Mattsson, E., A. Karlsson, and K. Abrahamsson, Regional sinks of bromoform in the Southern Ocean, *Geophys. Res. Lett.*, *40* (15), 3991-3996, doi: 10.1002/grl.50783, 2013.

McCulloch, A., Global production and emissions of bromochlorodifluoromethane and bromotrifluoromethane (halons 1211 and 1301), *Atmos. Environ., Part A*, *26* (7), 1325–1329, doi: 10.1016/0960-1686(92)90392-X, 1992.

McCulloch, A., M.L. Aucott, C.M. Benkovitz, T.E. Graedel, G. Kleiman, P.M. Midgley, and Y.-F. Li, Global emissions of hydrogen chloride and chloromethane from coal combustion, incineration and industrial activities: Reactive Chlorine Emissions Inventory, *J. Geophys. Res.*, *104* (D7), 8391–8403, doi: 10.1029/1999JD900025, 1999.

McGillen, M.R., E.L. Fleming, C.H. Jackman, and J.B. Burkholder, $CFCl_3$ (CFC-11): UV absorption spectrum temperature dependence measurements and the impact on its atmospheric lifetime and uncertainty, *Geophys. Res. Lett.*, *40* (17), 4772–4776, doi: 10.1002/grl.50915, 2013.

McLinden, C.A., C.S. Haley, N.D. Lloyd, F. Hendrick, A. Rozanov, B.-M. Sinnhuber, F. Goutail, D.A. Degenstein, E.J. Llewellyn, C.E. Sioris, M. Van Roozendael, J.P. Pommereau, W. Lotz, and J.P. Burrows, Odin/OSIRIS

observations of stratospheric BrO: Retrieval methodology, climatology, and inferred Br_y, *J. Geophys. Res.*, *115*, D15308, doi: 10.1029/2009JD012488, 2010.

Mead, M.I., I.R. White, G. Nickless, K.-Y. Wang, and D.E. Shallcross, An estimation of the global emission of methyl bromide from rapeseed (*Brassica napus*) from 1961 to 2003, *Atmos. Environ.*, *42* (2), 337-345, doi: 10.1016/j.atmosenv.2007.09.020, 2008.

Mébarki, Y., V. Catoire, N. Huret, G. Berthet, C. Robert, and G. Poulet, More evidence for very short-lived substance contribution to stratospheric chlorine inferred from HCl balloon-borne in situ measurements in the tropics, *Atmos. Chem. Phys.*, *10* (2), 397-409, doi: 10.5194/acp-10-397-2010, 2010.

Mendoza, Y., K.D. Goodwin, and J.D. Happell, Microbial removal of atmospheric carbon tetrachloride in bulk aerobic soils, *Appl. Environ. Microbiol.*, *77* (17), 5835-5841, doi: 10.1128/AEM.05341-11, 2011.

Millán, L., N. Livesey, W. Read, L. Froidevaux, D. Kinnison, R. Harwood, I.A. MacKenzie, and M.P. Chipperfield, New Aura Microwave Limb Sounder observations of BrO and implications for Br_y, *Atmos. Meas. Tech.*, *5* (7), 1741-1751, doi: 10.5194/amt-5-1741-2012, 2012.

Miller, B.R., and L.J.M. Kuijpers, Projecting future HFC-23 emissions, *Atmos. Chem. Phys.*, *11* (24), 13259-13267, doi: 10.5194/acp-11-13259-2011, 2011.

Miller, B.R., R.F. Weiss, P.K. Salameh, T. Tanhua, B.R. Greally, J. Mühle, and P.G. Simmonds, Medusa: A sample preconcentration and GC/MS detector system for in situ measurements of atmospheric trace halocarbons, hydrocarbons, and sulfur compounds, *Anal. Chem.*, *80* (5), 1536-1545, doi: 10.1021/ac702084k, 2008.

Miller, B.R, M. Rigby, L.J.M. Kuijpers, P.B. Krummel, L.P. Steele, M. Leist, P.J. Fraser, A. McCulloch, C. Harth, P. Salameh, J. Mühle, R.F. Weiss, R.G. Prinn, R.H.J. Wang, S. O'Doherty, B.R. Greally, and P.G. Simmonds, HFC-23 (CHF_3) emission trend response to HCFC-22 ($CHClF_2$) production and recent HFC-23 emission abatement measures, *Atmos. Chem. Phys.*, *10* (16), 7875-7890, doi: 10.5194/acp-10-7875-2010, 2010.

Miller, J.B., S.J. Lehman, S.A. Montzka, C. Sweeney, B.R. Miller, A. Karion, C. Wolak, E.J. Dlugokencky, J. Southon, J.C. Turnbull, and P.P. Tans, Linking emissions of fossil fuel CO_2 and other anthropogenic trace gases using atmospheric $^{14}CO_2$, *J. Geophys. Res.*, *117*, D08302, doi: 10.1029/2011JD017048, 2012.

Miller, M., and T. Batchelor, Information paper on feedstock uses of ozone-depleting substances, 72 pp., available at http://ec.europa.eu/clima/policies/ozone/research/docs/feedstock_en.pdf, 2012.

Millet, D.B., E.L. Atlas, D.R. Blake, N.J. Blake, G.S. Diskin, J.S. Holloway, R.C. Hudman, S. Meinardi, T.B. Ryerson, and G.W. Sachse, Halocarbon emissions from the United States and Mexico and their global warming potential, *Environ. Sci. Technol.*, *43* (4), 1055-1060, doi: 10.1021/es802146j, 2009.

Montzka, S.A., R.C. Myers, J.H. Butler, J.W. Elkins, L.T. Lock, A.D. Clarke, and A.H. Goldstein, Observations of HFC-134a in the remote troposphere, *Geophys. Res. Lett.*, *23* (2), 169-172, doi: 10.1029/95GL03590, 1996.

Montzka, S.A., J.H. Butler, J.W. Elkins, T.M. Thompson, A.D. Clarke, and L.T. Lock, Present and future trends in the atmospheric burden of ozone-depleting halogens, *Nature*, *398*, 690-694, doi: 10.1038/19499, 1999.

Montzka, S.A., C.M. Spivakovsky, J.H. Butler, J.W. Elkins, L.T. Lock, and D.J. Mondeel, New observational constraints for atmospheric hydroxyl on global and hemispheric scales, *Science*, *288* (5465), 500-503, doi: 10.1126/science.288.5465.500, 2000.

Montzka, S.A., and P.J. Fraser (Lead Authors), J.H. Butler, P.S. Connell, D.M. Cunnold, J.S. Daniel, R.G. Derwent, S. Lal, A. McCulloch, D.E. Oram, C.E. Reeves, E. Sanhueza, L.P. Steele, G.J.M. Velders, R.F. Weiss, and R.J. Zander, Controlled substances and other source gases, Chapter 1 in *Scientific Assessment of Ozone Depletion: 2002*, Global Ozone Research and Monitoring Project—Report No. 47, Geneva, Switzerland, 2003.

Montzka, S.A., J.H. Butler, B.D. Hall, D.J. Mondeel, and J.W. Elkins, A decline in tropospheric organic bromine, *Geophys. Res. Lett.*, *30* (15), 1826, doi: 10.1029/2003GL017745, 2003.

Montzka, S.A., M. Aydin, M. Battle, J.H. Butler, E.S. Saltzman, B.D. Hall, A.D. Clarke, D. Mondeel, and J.W. Elkins, A 350-year atmospheric history for carbonyl sulfide inferred from Antarctic firn air and air trapped in ice, *J. Geophys. Res.*, *109*, D22302, doi: 10.1029/2004JD004686, 2004.

Montzka, S.A., P. Calvert, B.D. Hall, J.W. Elkins, T.J. Conway, P.P. Tans, and C. Sweeney, On the global distribution, seasonality, and budget of atmospheric carbonyl sulfide (COS) and some similarities to CO_2, *J. Geophys. Res.*, *112*, D09302, doi: 10.1029/2006JD007665, 2007.

Montzka, S.A., B.D. Hall, and J.W. Elkins, Accelerated increases observed for hydrochlorofluorocarbons since 2004 in the global atmosphere, *Geophys. Res. Lett.*, *36*, L03804, doi: 10.1029/2008GL036475, 2009.

Montzka, S.A., L. Kuijpers, M.O. Battle, M. Aydin, K.R. Verhulst, E.S. Saltzman, and D.W. Fahey, Recent increases in global HFC-23 emissions, *Geophys. Res. Lett.*, *37*, L02808, doi: 10.1029/ 2009GL041195, 2010.

Montzka, S.A., and S. Reimann (Coordinating Lead Authors), A. Engel, K. Krüger, S. O'Doherty, W.T. Sturges, D.R. Blake, M. Dorf, P.J. Fraser, L. Froidevaux, K. Jucks, K. Kreher, M.J. Kurylo, A. Mellouki, J. Miller, O.-J. Nielsen, V.L. Orkin, R.G. Prinn, R. Rhew, M.L. Santee, and D.P. Verdonik, Ozone-Depleting Substances

(ODSs) and related chemicals, Chapter 1 in *Scientific Assessment of Ozone Depletion: 2010*, Global Ozone Research and Monitoring Project—Report No. 52, World Meteorological Organization, Geneva, Switzerland, 2011.

Montzka, S.A., M. Krol, E. Dlugokencky, B. Hall, P. Jöckel, and J. Lelieveld, Small interannual variability of global atmospheric hydroxyl, *Science*, *331* (6013), 67-69, doi: 10.1126/science.1197640, 2011.

Mühle, J., J. Huang, R.F. Weiss, R.G. Prinn, B.R. Miller, P.K. Salameh, C.M. Harth, P.J. Fraser, L.W. Porter, B.R. Greally, S. O'Doherty, and P.G. Simmonds, Sulfuryl fluoride in the global atmosphere, *J. Geophys. Res.*, *114*, D05306, doi: 10.1029/2008JD011162, 2009.

Mühle, J., A.L. Ganesan, B.R. Miller, P.K. Salameh, C.M. Harth, B.R. Greally, M. Rigby, L.W. Porter, L.P. Steele, C.M. Trudinger, P.B. Krummel, S. O'Doherty, P.J. Fraser, P.G. Simmonds, R.G. Prinn, and R.F. Weiss, Perfluorocarbons in the global atmosphere: Tetrafluoromethane, hexafluoroethane, and octafluoropropane, *Atmos. Chem. Phys.*, *10* (11), 5145-5164, doi: 10.5194/acp-10-5145-2010, 2010.

Murphy, D.M., and D.S. Thomson, Halogen ions and NO^+ in the mass spectra of aerosols in the upper troposphere and lower stratosphere, *Geophys. Res. Lett.*, *27* (19), 3217-3220, doi: 10.1029/1999GL011267, 2000.

Myhre, G., and D. Shindell (Coordinating Lead Authors), F.-M. Bréon, W. Collins, J. Fuglestvedt, J. Huang, D. Koch, J.-F. Lamarque, D. Lee, B. Mendoza, T. Nakajima, A. Robock, G. Stephens, T. Takemura, and H. Zhang (Lead Authors), Anthropogenic and natural radiative forcing, Chapter 8 in *Climate Change 2013: The Physical Science Basis. Contribution of Working Group I to the Fifth Assessment Report of the Intergovernmental Panel on Climate Change*, edited by Stocker, T.F., D. Qin, G.-K. Plattner, M. Tignor, S.K. Allen, J. Boschung, A. Nauels, Y. Xia, V. Bex, and P.M. Midgley, 1535 pp., Cambridge University Press, Cambridge, U.K. and New York, NY, 2013.

Naik, V., A.K. Jain, K.O. Patten, and D.J. Wuebbles, Consistent sets of atmospheric lifetimes and radiative forcings on climate for CFC replacements: HCFCs and HFCs, *J. Geophys. Res.*, *105* (D5), 6903-6914, doi: 10.1029/1999JD901128, 2000.

Newland, M.J., C.E. Reeves, D.E. Oram, J.C. Laube, W.T. Sturges, C. Hogan, P. Begley, and P.J. Fraser, Southern hemispheric halon trends and global halon emissions, 1978-2011, *Atmos. Chem. Phys.*, *13* (11), 5551-5565, doi: 10.5194/acp-13-5551-2013, 2013.

Newman, P.A., J.S. Daniel, D.W. Waugh, and E.R. Nash, A new formulation of equivalent effective stratospheric chlorine (EESC), *Atmos. Chem. Phys.*, *7* (17), 4537-4552, doi: 10.5194/acp-7-4537-2007, 2007.

Nilsson, E.J.K., L.M.T. Joelsson, J. Heimdal, M.S. Johnson, and O.J. Nielsen, Re-evaluation of the reaction rate coefficient of CH_3Br + OH with implications for the atmospheric budget of methyl bromide, *Atmos. Environ.*, *80*, 70-74, doi: 10.1016/j.atmosenv.2013.07.046, 2013.

O'Brien, L.M., N.R.P. Harris, A.D. Robinson, B. Gostlow, N. Warwick, X. Yang, and J.A. Pyle, Bromocarbons in the tropical marine boundary layer at the Cape Verde Observatory – measurements and modelling, *Atmos. Chem. Phys*., *9* (22), 9083-9099, doi: 10.5194/acp-9-9083-2009, 2009.

O'Doherty, S., D.M. Cunnold, A. Manning, B.R. Miller, R.H.J. Wang, P.B. Krummel, P.J. Fraser, P.G. Simmonds, A. McCulloch, R.F. Weiss, P. Salameh, L.W. Porter, R.G. Prinn, J. Huang, G. Sturrock, D. Ryall, R.G. Derwent, and S.A. Montzka, Rapid growth of hydrofluorocarbon 134a and hydrochlorofluorocarbons 141b, 142b, and 22 from Advanced Global Atmospheric Gases Experiment (AGAGE) observations at Cape Grim, Tasmania, and Mace Head, Ireland, *J. Geophys. Res.*, *109*, D06310, doi: 10.1029/2003JD004277, 2004.

O'Doherty, S., D.M. Cunnold, B.R. Miller, J. Mühle, A. McCulloch, P.G. Simmonds, A.J. Manning, S. Reimann, M.K. Vollmer, B.R. Greally, R.G. Prinn, P.J. Fraser, L.P. Steele, P.B. Krummel, B.L. Dunse, L.W. Porter, C.R. Lunder, N. Schmidbauer, O. Hermansen, P.K. Salameh, C.M. Harth, R.H.J. Wang, and R.F. Weiss, Global and regional emissions of HFC-125 (CHF_2CF_3) from in situ and air archive atmospheric observations at AGAGE and SOGE observatories, *J. Geophys. Res.*, *114*, D23304, doi: 10.1029/2009JD012184, 2009.

O'Doherty, S., P.G. Simmonds, D.M. Cunnold, H.J. Wang, G.A. Sturrock, P.J. Fraser, D. Ryall, R.G. Derwent, R.F., Weiss, P. Salameh, B.R. Miller, and R.G. Prinn, In situ chloroform measurements at Advanced Global Atmospheric Gases Experiment atmospheric research stations from 1994 to 1998, *J. Geophys. Res.*, *106* (D17), 20429-20444, doi: 10.1029/2000JD900792, 2001.

Ooki, A., and Y. Yokouchi, Dichloromethane in the Indian Ocean: Evidence for in-situ production in seawater, *Mar. Chem.*, *124* (1-4), 119-124, doi: 10.1016/j.marchem.2011.01.001, 2011.

Oram, D.E., Trends of Long-Lived Anthropogenic Halocarbons in the Southern Hemisphere and Model Calculations of Global Emissions, Ph.D. thesis, University of East Anglia, Norwich, U.K., 249 pp., 1999.

Oram, D.E., W.T. Sturges, S.A. Penkett, A. McCulloch, and P.J. Fraser, Growth of fluoroform (CHF_3, HFC-23) in the background atmosphere, *Geophys. Res. Lett.*, *25* (1), 35-38, doi: 10.1029/97GL03483, 1998.

Oram, D.E., F.S. Mani, J.C. Laube, M.J. Newland, C.E. Reeves, W.T. Sturges, S.A. Penkett, C.A.M. Brenninkmeijer, T. Röckmann, and P.J. Fraser, Long-term tropospheric trend of octafluorocyclobutane (c-C_4F_8 or PFC-318), *Atmos. Chem. Phys.*, *12* (1), 261-269, doi: 10.5194/acp-12-261-2012, 2012.

Ordoñez, C., J.-F. Lamarque, S. Tilmes, D.E. Kinnison, E.L. Atlas, D.R. Blake, G. Sousa Santos, G. Brasseur, and A. Saiz-Lopez, Bromine and iodine chemistry in a global chemistry-climate model: Description and evaluation of very short-lived oceanic sources, *Atmos. Chem. Phys.*, *12* (3), 1423-1447, doi: 10.5194/acp-12-1423-2012, 2012.

Orkin, V.L., F. Louis, R.E. Huie, and M.J. Kurylo, Photochemistry of bromine-containing fluorinated alkenes: Reactivity toward OH and UV spectra, *J. Phys. Chem. A*, *106* (43), 10195-10199, doi: 10.1021/jp014436s, 2002.

Orkin, V.L., V.G. Khamaganov, E.E. Kasimovskaya, and A.G. Guschin, Photochemical properties of some Cl-containing halogenated alkanes, *J. Phys. Chem. A*, *117* (26), 5483-5490, doi: 10.1021/jp400408y, 2013a.

Orkin, V.L., V.G. Khamaganov, S.N. Kozlov, and M.J. Kurylo, Measurements of rate constants for the OH reactions with bromoform ($CHBr_3$), $CHBr_2Cl$, $CHBrCl_2$, and epichlorohydrin (C_3H_5ClO), *J. Phys. Chem. A*, *117* (18), 3809-3818, doi: 10.1021/jp3128753, 2013b.

Oyaro, N., S.R. Sellevåg, and C.J. Nielsen, Study of the OH and Cl-initiated oxidation, IR absorption cross-section, radiative forcing, and global warming potential of four C_4-hydrofluoroethers, *Environ. Sci. Technol.*, *38* (21), 5567-5576, doi: 10.1021/es0497330, 2004.

Oyaro, N., S.R. Sellevåg, and C.J. Nielsen, Atmospheric chemistry of hydrofluoroethers: Reaction of a series of hydrofluoroethers with OH radicals and Cl atoms, atmospheric lifetimes, and global warming potentials, *J. Phys. Chem. A*, *109* (2), 337-346, doi: 10.1021/jp047860c, 2005.

Palmer, C.J., and C.J. Reason, Relationships of surface bromoform concentrations with mixed layer depth and salinity in the tropical oceans, *Global Biogeochem. Cycles*, *23*, GB2014, doi: 10.1029/ 2008GB003338, 2009.

Palmer, P.I., D.J. Jacob, L.J. Mickley, D.R. Blake, G.W. Sachse, H.E. Fuelberg, and C.M. Kiley, Eastern Asian emissions of anthropogenic halocarbons deduced from aircraft concentration data, *J. Geophys. Res.*, *108* (D24), 4753, doi: 10.1029/2003JD003591, 2003.

Papadimitriou, V.C., R.W. Portmann, D.W. Fahey, J. Mühle, R.F. Weiss, and J.B. Burkholder, Experimental and theoretical study of the atmospheric chemistry and global warming potential of SO_2F_2, *J. Phys. Chem. A*, *112* (49), 12657-12666, doi: 10.1021/jp806368u, 2008.

Papadimitriou, V.C., M.R. McGillen, E.L. Fleming, C.H. Jackman, and J.B. Burkholder, NF_3: UV absorption spectrum temperature dependence and the atmospheric and climate forcing implications, *Geophys. Res. Lett.*, *40* (2), 440-445, doi: 10.1002/grl.50120, 2013a.

Papadimitriou, V.C., M.R. McGillen, S.C. Smith, A.M. Jubb, R.W. Portmann, B.D. Hall, E.L. Fleming, C.H. Jackman, and J.B. Burkholder, 1,2-Dichlorohexafluoro-cyclobutane (1,2-c-$C_4F_6Cl_2$, R-316c) a potent ozone depleting substance and greenhouse gas: Atmospheric loss processes, lifetimes, and ozone depletion and global warming potentials for the (*E*) and (*Z*) stereoisomers, *J. Phys. Chem. A*, *117* (43), 11049-11065, doi: 10.1021/jp407823k, 2013b.

Papanastasiou, D.K., N. Rontu Carlon, J.A. Neuman, E.L. Fleming, C.H. Jackman, and J.B. Burkholder, Revised UV absorption spectra, ozone depletion potentials, and global warming potentials for the ozone-depleting substances CF_2Br_2, CF_2ClBr, and CF_2BrCF_2Br, *Geophys. Res. Lett.*, *40* (2), 464-469, doi: 10.1002/grl.50121, 2013.

Papanastasiou, D.K., S.A. McKeen, and J.B. Burkholder, The very short-lived ozone depleting substance $CHBr_3$ (bromoform): Revised UV absorption spectrum, atmospheric lifetime and ozone depletion potential, *Atmos. Chem. Phys.*, *14* (6), 3017-3025, doi: 10.5194/acp-14-3017-2014, 2014.

Papasavva, S., D.J. Luecken, R.L. Waterland, K.N. Taddonio, and S.O. Andersen, Estimated 2017 refrigerant emissions of 2,3,3,3-tetrafluoropropene (HFC-1234yf) in the United States resulting from automobile air conditioning, *Environ. Sci. Technol.*, *43* (24), 9252-9259, doi: 10.1021/es902124u, 2009.

Park, S., P. Croteau, K.A. Boering, D.M. Etheridge, D. Ferretti, P.J. Fraser, K.-R. Kim, P.B. Krummel, R.L. Langenfelds, T.D. van Ommen, L.P. Steele, and C.M. Trudinger, Trends and seasonal cycles in the isotopic composition of nitrous oxide since 1940, *Nature Geosci.*, *5* (4), 261-265, doi: 10.1038/ngeo1421, 2012.

Parrella, J.P., D.J. Jacob, Q. Liang, Y. Zhang, L.J. Mickley, B. Miller, M.J. Evans, X. Yang, J.A. Pyle, N. Theys, and M. Van Roozendael, Tropospheric bromine chemistry: Implications for present and pre-industrial ozone and mercury, *Atmos. Chem. Phys.*, *12* (15), 6723-6740, doi: 10.5194/acp-12-6723-2012, 2012.

Parrella, J.P., K. Chance, R.J. Salawitch, T. Canty, M. Dorf, and K. Pfeilsticker, New retrieval of BrO from SCIAMACHY limb: An estimate of the stratospheric bromine loading during April 2008, *Atmos. Meas. Tech.*, *6* (10), 2549-2561, doi: 10.5194/amt-6-2549-2013, 2013.

Pfeilsticker, K., W.T. Sturges, H. Bösch, C. Camy-Peyret, M.P. Chipperfield, A. Engel, R. Fitzenberger, M. Müller, S. Payan, and B.-M. Sinnhuber, Lower stratospheric organic and inorganic bromine budget for the Arctic winter 1998/99, *Geophys. Res. Lett.*, *27* (20), 3305-3308, 2000.

Pisso, I., P.H. Haynes, and K.S. Law, Emission location dependent ozone depletion potentials for very short-lived halogenated species, *Atmos. Chem. Phys.*, *10* (24), 12025-12036, doi: 10.5194/acp-10-12025-2010, 2010.

Ploeger, F., P. Konopka, R. Müller, S. Fueglistaler, T. Schmidt, J.C. Manners, J.-U. Grooβ, G. Günther, P.M. Forster, and M. Riese, Horizontal transport affecting trace gas seasonality in the Tropical Tropopause Layer (TTL), *J. Geophys. Res.*, *117* (D9), D09303, doi: 10.1029/2011JD017267, 2012.

Pommereau, J.-P., Troposphere-to-stratosphere transport in the tropics, *Comptes Rendus Géoscience*, *342* (4-5), 331-338, doi: 10.1016/j.crte.2009.10.015, 2010.

Porter, E., J. Wenger, J. Treacy, H. Sidebottom, A. Mellouki, S. Téton, and G. LeBras, Kinetic studies on the reactions of hydroxyl radicals with diethers and hydroxyethers, *J. Phys. Chem. A*, *101* (32), 5770-5775, doi: 10.1021/jp971254i, 1997.

Portmann, R.W., J.S. Daniel, and A.R. Ravishankara, Stratospheric ozone depletion due to nitrous oxide: Influences of other gases, *Phil. Trans. R. Soc. Lond. B. Biol. Sci.*, *367* (1593), 1256-1264, doi: 10.1098/rstb.2011.0377, 2012.

Prather, M.J., and J. Hsu, NF_3, the greenhouse gas missing from Kyoto, *Geophys. Res. Lett.*, *35* (12), L12810, doi: 10.1029/2008GL034542, 2008.

Prather, M.J., and J. Hsu, Correction to "NF_3, the greenhouse gas missing from Kyoto," *Geophys. Res. Lett.*, *37*, L11807, doi: 10.1029/2010GL043831, 2010.

Prather, M. J., and E.E. Remsberg (editors), *The Atmospheric Effects of Stratospheric Aircraft: Report of the 1992 Models and Measurements Workshop*, National Aeronautics and Space Administration, NASA Ref. Publ. 1292, available http://ntrs.nasa.gov, 1993.

Prinn, R.G., R.F. Weiss, P.J. Fraser, P.G. Simmonds, D.M. Cunnold, F.N. Alyea, S. O'Doherty, P. Salameh, B.R. Miller, J. Huang, R.H.J. Wang, D.E. Hartley, C. Harth, L.P. Steele, G. Sturrock, P.M. Midgley, and A. McCulloch, A history of chemically and radiatively important gases in air deduced from ALE/GAGE/AGAGE, *J. Geophys. Res.*, *105* (D14), 17751-17792, doi: 10.1029/2000JD900141, 2000.

Prinn, R.G., J. Huang, R.F. Weiss, D.M. Cunnold, P.J. Fraser, P.G. Simmonds, A. McCulloch, C. Harth, S. Reimann, P. Salameh, S. O'Doherty, R.H.J. Wang, L.W. Porter, B.R. Miller, and P.B. Krummel, Evidence for variability of atmospheric hydroxyl radicals over the past quarter century, *Geophys. Res. Lett.*, *32*, L07809, doi: 10.1029/2004GL022228, 2005.

Puentedura, O., M. Gil, A. Saiz-Lopez, T. Hay, M. Navarro-Comas, A. Gómez-Pelaez, E. Cuevas, J. Iglesias, and L. Gomez, Iodine monoxide in the north subtropical free troposphere, *Atmos. Chem. Phys.*, *12* (11), 4909-4921, doi: 10.5194/acp-12-4909-2012, 2012.

Puķīte, J., S. Kühl, T. Deutschmann, S. Dörner, P. Jöckel, U. Platt, and T. Wagner, The effect of horizontal gradients and spatial measurement resolution on the retrieval of global vertical NO_2 distributions from SCIAMACHY measurements in limb only mode, *Atmos. Meas. Tech., 3* (4), 1155-1174, 2010.

Pyle, J.A., M.J. Ashfold, N.R.P. Harris, A.D. Robinson, N.J. Warwick, G.D. Carver, B. Gostlow, L.M. O'Brien, A.J. Manning, S.M. Phang, S.E. Yong, K.P. Leong, E.H. Ung, and S. Ong, Bromoform in the tropical boundary layer of the Maritime Continent during OP3, *Atmos. Chem. Phys.*, *11* (2), 529-542, doi: 10.5194/acp-11-529-2011, 2011.

Randel, W.J., and E.J. Jensen, Physical processes in the tropical tropopause layer and their role in a changing climate, *Nature Geosci.*, *6* (3), 169-176, doi: 10.1038/ngeo1733, 2013.

Ravishankara, A.R., S. Solomon, A.A. Turnipseed, and R.F. Warren, Atmospheric lifetimes of long-lived halogenated species, *Science*, *259* (5092), 194-199, doi: 10.1126/science.259.5092.194, 1993.

Ravishankara, A.R., J.S. Daniel, and R.W. Portmann, Nitrous oxide (N_2O): The dominant ozone-depleting substance emitted in the 21st century, *Science*, *326* (5949), 123-125, doi: 10.1126/science.1176985, 2009.

Redeker, K.R., and R.J. Cicerone, Environmental controls over methyl halide emissions from rice paddies, *Global Biogeochem. Cycles*, *18*, GB1027, doi: 10.1029/2003GB002092, 2004.

Reeves, C.E., W.T. Sturges, G.A. Sturrock, K. Preston, D.E. Oram, J. Schwander, R. Mulvaney, J.-M. Barnola, and J. Chappellaz, Trends of halon gases in polar firn air: Implications for their emission distributions, *Atmos. Chem. Phys.*, *5* (8), 2055-2064, doi: 10.5194/acp-5-2055-2005, 2005.

Revell, L.E., G.E. Bodeker, P.E. Huck, B.E. Williamson, and E. Rozanov, The sensitivity of stratospheric ozone changes through the 21st century to N_2O and CH_4, *Atmos. Chem. Phys.*, *12* (23), 11309-11317, doi: 10.5194/acp-12-11309-2012, 2012.

Rex, M., I. Wohltmann, T. Ridder, R. Lehmann, K. Rosenlof, P. Wennberg, D. Weisenstein, J. Notholt, K. Krüger, V. Mohr, and S. Tegtmeier, A Tropical West Pacific OH minimum and implications for stratospheric composition, *Atmos. Chem. Phys.*, *14* (9), 4827-4841, doi: 10.5194/acp-14-4827-2014, 2014.

Rhew, R.C., Sources and sinks of methyl bromide and methyl chloride in the tallgrass prairie: Applying a stable isotope tracer technique over highly variable gross fluxes, *J. Geophys. Res.*, *116* (G3), G03026, doi: 10.1029/2011JG001704, 2011.

Rhew, R.C., B.R. Miller, and R.F. Weiss, Natural methyl bromide and methyl chloride emissions from coastal salt marshes, *Nature*, *403*, 292-295, doi: 10.1038/35002043, 2000.

Rhew, R.C., B.R. Miller, M.K. Vollmer, and R.F. Weiss, Shrubland fluxes of methyl bromide and methyl chloride, *J. Geophys. Res.*, *106* (D18), 20875-20882, doi: 10.1029/2001JD000413, 2001.

Rhew, R.C., B.R. Miller, and R.F. Weiss, Chloroform, carbon tetrachloride and methyl chloroform fluxes in southern California ecosystems, *Atmos. Environ.*, *42* (30), 7135-7140, doi: 10.1016/j.atmosenv.2008.05.038, 2008.

Rhew, R.C., C. Chen, Y.A. Teh, and D. Baldocchi, Gross fluxes of methyl chloride and methyl bromide in a California oak-savanna woodland, *Atmos. Environ.*, *44* (16), 2054-2061, doi: 10.1016/j.atmosenv.2009.12.014, 2010.

Richter, U., and D.W.R. Wallace, Production of methyl iodide in the tropical Atlantic Ocean, *Geophys. Res. Lett.*, *31* (23), L23S03, doi: 10.1029/2004GL020779, 2004.

Richter, A., F. Wittrock, A. Ladstätter-Weißenmayer, and J.P. Burrows, GOME measurements of stratospheric and tropospheric BrO, *Adv. Space Res.*, *29* (11), 1667-1672, doi: 10.1016/S0273-1177(02)00123-0, 2002.

Rigby, M., R.G. Prinn, P.J. Fraser, P.G. Simmonds, R.L. Langenfelds, J. Huang, D.M. Cunnold, L.P. Steele, P.B. Krummel, R.F. Weiss, S. O'Doherty, P.K. Salameh, H.J. Wang, C.M. Harth, J. Mühle, and L.W. Porter, Renewed growth of atmospheric methane, *Geophys. Res. Lett.*, *35*, L22805, doi: 10.1029/2008GL036037, 2008.

Rigby, M., J. Mühle, B.R. Miller, R.G. Prinn, P.B. Krummel, L.P. Steele, P.J. Fraser, P.K. Salameh, C.M. Harth, R.F. Weiss, B.R. Greally, S. O'Doherty, P.G. Simmonds, M.K. Vollmer, S. Reimann, J. Kim, K.-R. Kim, H.J. Wang, J.G.J. Olivier, E.J. Dlugokencky, G.S. Dutton, B.D. Hall, and J.W. Elkins, History of atmospheric SF_6 from 1973 to 2008, *Atmos. Chem. Phys.*, *10* (21), 10305-10320, doi: 10.5194/acp-10-10305-2010, 2010.

Rigby, M., R.G. Prinn, S. O'Doherty, S.A. Montzka, A. McCulloch, C.M. Harth, J. Mühle, P.K. Salameh, R.F. Weiss, D. Young, P.G. Simmonds, B.D. Hall, G.S. Dutton, D. Nance, D.J. Mondeel, J.W. Elkins, P.B. Krummel, L.P. Steele, and P.J. Fraser, Re-evaluation of the lifetimes of the major CFCs and CH_3CCl_3 using atmospheric trends, *Atmos. Chem. Phys.*, *13* (5), 2691-2702, doi: 10.5194/acp-13-2691-2013, 2013.

Rigby, M., R.G. Prinn, S. O'Doherty, B.R. Miller, D. Ivy, J. Mu□hle, C.M. Harth, P.K. Salameh, T. Arnold, R.F. Weiss, P.B. Krummel, L.P. Steele, P.J. Fraser, D. Young, and P.G. Simmonds, Recent and future trends in synthetic greenhouse gas radiative forcing, *Geophys. Res. Lett.*, *41* (7), doi: 10.1002/2013GL059099, 2014.

Rinsland, C.P., E. Mahieu, R. Zander, N.B. Jones, M.P. Chipperfield, A. Goldman, J. Anderson, J.M. Russell III, P. Demoulin, J. Notholt, G.C. Toon, J.-F.Blavier, B. Sen, R. Sussmann, S.W. Wood, A. Meier, D.W.T. Griffith, L.S. Chiou, F.J. Murcray, T.M. Stephen, F. Hase, S. Mikuteit, A. Schulz, and T. Blumenstock, Long-term trends of inorganic chlorine from ground-based infrared solar spectra: Past increases and evidence for stabilization, *J. Geophys. Res.*, *108* (D8), 4252, doi: 10.1029/ 2002JD003001, 2003.

Rinsland, C.P., E. Mahieu, P. Demoulin, R. Zander, C. Servais, and J.-M. Hartmann, Decrease of the carbon tetrachloride (CCl_4) loading above Jungfraujoch, based on high resolution infrared solar spectra recorded between 1999 and 2011, *J. Quant. Spectrosc. Radiat. Transfer*, *113* (11), 1322-1329, doi: 10.1016/j.jqsrt.2012.02.016, 2012.

Rowland, F.S., S.C. Tyler, D.C. Montague, and Y. Makide, Dichlorodifluoromethane, CCl_2F_2, in the Earth's atmosphere, *Geophys. Res. Lett.*, *9* (4), 481-484, doi: 10.1029/GL009i004p00481, 1982.

Roy, R., Short-term variability in halocarbons in relation to phytoplankton pigments in coastal waters of the central eastern Arabian Sea, *Estuar. Coast. Shelf Sci.*, *88* (3), 311-321, doi: 10.1016/j.ecss.2010.04.011, 2010.

Roy, R., A. Pratihary, G. Narvenkar, S. Mochemadkar, M. Gauns, and S.W.A. Naqvi, The relationship between volatile halocarbons and phytoplankton pigments during a *Trichodesmium* bloom in the coastal eastern Arabian Sea, *Estuar. Coast. Shelf Sci.*, *95* (1), 110-118, doi: 10.1016/j.ecss.2011.08.025, 2011.

Russell, M.H., G. Hoogeweg, E.M. Webster, D.A. Ellis, R.L. Waterland, and R.A. Hoke, TFA from HFO-1234yf: Accumulation and aquatic risk in terminal water bodies, *Environ. Toxicol. Chem.*, *31* (9), 1957-1965, doi: 10.1002/etc.1925, 2012.

Russo, R.S., Y. Zhou, M.L. White, H. Mao, R. Talbot, and B.C. Sive, Multi-year (2004-2008) record of nonmethane hydrocarbons and halocarbons in New England: Seasonal variations and regional sources, *Atmos. Chem. Phys.*, *10* (10), 4909-4929, doi: 10.5194/acp-10-4909-2010, 2010.

Saikawa, E., M. Rigby, R.G. Prinn, S.A. Montzka, B.R. Miller, L.J.M. Kuijpers, P.J.B. Fraser, M.K. Vollmer, T. Saito, Y. Yokouchi, C.M. Harth, J. Mühle, R.F. Weiss, P.K. Salameh, J. Kim, S. Li, S. Park, K.-R. Kim, D. Young, S. O'Doherty, P.G. Simmonds, A. McCulloch, P.B. Krummel, L.P. Steele, C. Lunder, O. Hermansen, M. Maione, J. Arduini, B. Yao, L.X. Zhou, H.J. Wang, J.W. Elkins, and B. Hall, Global and regional emission estimates for HCFC-22, *Atmos. Chem. Phys.*, *12* (21), 10033-10050, doi: 10.5194/acp-12-10033-2012, 2012.

Saito, T., Y. Yokouchi, Y. Kosugi, M. Tani, E. Philip, and T. Okuda, Methyl chloride and isoprene emissions from tropical rain forest in Southeast Asia, *Geophys. Res. Lett.*, *35* (19), L19812, doi: 10.1029/2008GL035241, 2008.

Saito, T., Y. Yokouchi, A. Stohl, S. Taguchi, and H. Mukai, Large emissions of perfluorocarbons in East Asia deduced from continuous atmospheric measurements, *Environ. Sci. Technol.*, *44* (11), 4089-4095, doi: 10.1021/es1001488, 2010.

Saito, T., Y. Yokouchi, E. Phillip, and T. Okuda, Bidirectional exchange of methyl halides between tropical plants and the atmosphere, *Geophys. Res. Lett.*, *40* (19), 5300–5304, doi: 10.1002/grl.50997, 2013.

Saiz-Lopez, A., J.M.C. Plane, A.R. Baker, L.J. Carpenter, R. von Glasow, J.C.G. Martín, G. McFiggans, and R.W. Saunders, Atmospheric chemistry of iodine, *Chem. Rev.*, *112* (3), 1773-1804, doi: 10.1021/cr200029u, 2012.

Sala, S., H. Bönisch, T. Keber, D.E. Oram, G. Mills, and A. Engel, Deriving an atmospheric budget of total organic bromine using airborne in-situ measurements from the Western Pacific during SHIVA, *Atmos. Chem. Phys.*, *14* (13), 6903-6923, doi: 10.5194/acp-14-6903-2014, 2014.

Salawitch, R.J., D.K. Weisenstein, L.J. Kovalenko, C.E. Sioris, P.O. Wennberg, K. Chance, M.K.W. Ko, and C.A. McLinden, Sensitivity of ozone to bromine in the lower stratosphere, *Geophys. Res. Lett.*, *32*, L05811, doi: 10.1029/2004GL021504, 2005.

Salawitch, R.J., T. Canty, T. Kurosu, K. Chance, Q. Liang, A. da Silva, S. Pawson, J.E. Nielsen, J.M. Rodriguez, P.K. Bhartia, X. Liu, L.G. Huey, J. Liao, R.E. Stickel, D.J. Tanner, J.E. Dibb, W.R. Simpson, D. Donohoue, A. Weinheimer, F. Flocke, D. Knapp, D. Montzka, J.A. Neuman, J.B. Nowak, T.B. Ryerson, S. Oltmans, D.R. Blake, E.L. Atlas, D.E. Kinnison, S. Tilmes, L.L. Pan, F. Hendrick, M. Van Roozendael, K. Kreher, P.V. Johnston, R.S. Gao, B. Johnson, T.P. Bui, G. Chen, R.B. Pierce, J.H. Crawford, and D.J. Jacob, A new interpretation of total column BrO during Arctic spring, *Geophys. Res. Lett.*, *37* (21), L21805, doi: 10.1029/2010GL043798, 2010.

Saltzman, E.S., M. Aydin, W.J. De Bruyn, D.B. King, and S.A. Yvon-Lewis, Methyl bromide in preindustrial air: Measurements from an Antarctic ice core, *J. Geophys. Res.*, *109* (D5), D05301, doi: 10.1029/2003JD004157, 2004.

Saltzman, E.S., M. Aydin, C. Tatum, and M.B. Williams, 2,000-year record of atmospheric methyl bromide from a South Pole ice core, *J. Geophys. Res.*, *113*, D05304, doi: 10.1029/2007JD008919, 2008.

Sander, S.P., J. Abbatt, J.R. Barker, J.B. Burkholder, R.R. Friedl, D.M. Golden, R.E. Huie, C.E. Kolb, M.J. Kurylo, G.K. Moortgat, V.L. Orkin, and P.H. Wine, *Chemical Kinetics and Photochemical Data for Use in Atmospheric Studies*, *Evaluation Number 17*, JPL Publication 10-6, Jet Propulsion Laboratory, Pasadena, Calif., http://jpldataeval.jpl.nasa.gov/pdf/JPL%2010-6%20Final%2015June2011.pdf, 2011.

Santee, M.L., N.J. Livesey, G.L. Manney, A. Lambert, and W.G. Read, Methyl chloride from the Aura Microwave Limb Sounder: First global climatology and assessment of variability in the upper troposphere and stratosphere, *J. Geophys. Res.*, *118* (24), 13532–13560, doi: 10.1002/2013JD020235, 2013.

Sato, T.O., H. Sagawa, D. Kreyling, T. Manabe, S. Ochiai, K. Kikuchi, P. Baron, J. Mendrok, J. Urban, D. Murtagh, M. Yasui, and Y. Kasai, Strato-mesospheric ClO observations by SMILES: Error analysis and diurnal variation, *Atmos. Meas. Tech.*, *5* (11), 2809-2825, doi: 10.5194/amt-5-2809-2012, 2012.

Schauffler, S.M., E.L. Atlas, D.R. Blake, F. Flocke, R.A. Lueb, J.M. Lee-Taylor, V. Stroud, and W. Travnicek, Distributions of brominated organic compounds in the troposphere and lower stratosphere, *J. Geophys. Res.*, *104* (D17), 21513-21536, doi: 10.1029/1999jd900197, 1999.

Schauffler, S.M., E.L. Atlas, S.G. Donnelly, A. Andrews, S.A. Montzka, J.W. Elkins, D.F. Hurst, P.A. Romashkin, G.S. Dutton, and V. Stroud, Chlorine budget and partitioning during the Stratospheric Aerosol and Gas Experiment (SAGE) III Ozone Loss and Validation Experiment (SOLVE), *J. Geophys. Res.*, *108* (D5), 4173, doi: 10.1029/2001JD002040, 2003.

Schmidt, J.A., M.S. Johnson, S. Hattori, N. Yoshida, S. Nanbu, and R. Schinke, OCS photolytic isotope effects from first principles: Sulfur and carbon isotopes, temperature dependence and implications for the stratosphere, *Atmos. Chem. Phys.*, *13* (3), 1511-1520, doi: 10.5194/acp-13-1511-2013, 2013.

Schofield, R., K. Kreher, B.J. Connor, P.V. Johnston, A. Thomas, D. Shooter, M.P. Chipperfield, C.D. Rodgers, and G.H. Mount, Retrieved tropospheric and stratospheric BrO columns over Lauder, New Zealand, *J. Geophys. Res.*, *109*, D14304, doi: 10.1029/2003JD004463, 2004.

Schofield, R., P.V. Johnston, A. Thomas, K. Kreher, B.J. Connor, S. Wood, D. Shooter, M.P. Chipperfield, A. Richter, R. von Glasow, and C.D. Rodgers, Tropospheric and stratospheric BrO columns over Arrival Heights, Antarctica, 2002, *J. Geophys. Res.*, *111*, D22310, doi: 10.1029/2005JD007022, 2006.

Schofield, R., S. Fueglistaler, I. Wohltmann, and M. Rex, Sensitivity of stratospheric Br_y to uncertainties in very short lived substance emissions and atmospheric transport, *Atmos. Chem. Phys.*, *11* (4), 1379-1392, doi: 10.5194/acp-11-1379-2011, 2011.

Shao, M., D. Huang, D. Gu, S. Lu, C. Chang, and J. Wang, Estimate of anthropogenic halocarbon emission based on measured ratio relative to CO in the Pearl River Delta region, China, *Atmos. Chem. Phys.*, *11* (10), 5011-5025, doi: 10.5194/acp-11-5011-2011, 2011.

Shindell, D.T., O. Pechony, A. Voulgarakis, G. Faluvegi, L. Nazarenko, J.-F. Lamarque, K. Bowman, G. Milly, B. Kovari, R. Ruedy, and G.A. Schmidt, Interactive ozone and methane chemistry in GISS-E2 historical and future climate simulations, *Atmos. Chem. Phys.*, *13* (5), 2653-2689, doi: 10.5194/acp-13-2653-2013, 2013.

Sihler, H., U. Platt, S. Beirle, T. Marbach, S. Kühl, S. Dörner, J. Verschaeve, U. Frieβ, D. Pöhler, L. Vogel, R. Sander, and T. Wagner, Tropospheric BrO column densities in the Arctic derived from satellite: Retrieval and comparison to ground-based measurements, *Atmos. Meas. Tech.*, *5* (11), 2779-2807, doi: 10.5194/amt-5-2779-2012, 2012.

Simmonds, P.G., A.J. Manning, D.M. Cunnold, A. McCulloch, S. O'Doherty, R.G. Derwent, P.B. Krummel, P.J. Fraser, B. Dunse, L.W. Porter, R.H.J. Wang, B.R. Greally, B.R. Miller, P. Salameh, R.F. Weiss, and R.G. Prinn, Global trends, seasonal cycles, and European emissions of dichloromethane, trichloroethene, and tetrachloroethene from the AGAGE observations at Mace Head, Ireland, and Cape Grim, Tasmania, *J. Geophys. Res*., *111*, D18304, doi: 10.1029/2006JD007082, 2006.

Simmonds, P.G., R.G. Derwent, A.J. Manning, S. O'Doherty, and G. Spain, Natural chloroform emissions from the blanket peat bogs in the vicinity of Mace Head, Ireland over a 14-year period, *Atmos. Environ.*, *44* (10), 1284-1291, doi: 10.1016/j.atmosenv.2009.12.027, 2010.

Simpson, I.J., S. Meinardi, N.J. Blake, F.S. Rowland, and D.R. Blake, Long-term decrease in the global atmospheric burden of tetrachloroethene (C_2Cl_4), *Geophys. Res. Lett.*, *31* (8), L08108, doi: 10.1029/2003GL019351, 2004.

Simpson, I.J., N.J. Blake, D.R. Blake, S. Meinardi, M.P.S. Andersen, and F.S. Rowland, Strong evidence for negligible methyl chloroform (CH_3CCl_3) emissions from biomass burning, *Geophys. Res. Lett.*, *34* (10), L10805, doi: 10.1029/2007GL029383, 2007.

Simpson, I.J., S.K. Akagi, B. Barletta, N.J. Blake, Y. Choi, G.S. Diskin, A. Fried, H.E. Fuelberg, S. Meinardi, F.S. Rowland, S.A. Vay, A.J. Weinheimer, P.O. Wennberg, P. Wiebring, A. Wisthaler, M. Yang, R.J. Yokelson, and D.R. Blake, Boreal forest fire emissions in fresh Canadian smoke plumes: C_1-C_{10} volatile organic compounds (VOCs), CO_2, CO, NO_2, NO, HCN and CH_3CN, *Atmos. Chem. Phys.*, *11* (13), 6445-6463, doi: 10.5194/acp-11-6445-2011, 2011.

Simpson, I.J., M.P. Sulbaek Andersen, S. Meinardi, L. Bruhwiler, N.J. Blake, D. Helmig, F.S. Rowland, and D.R. Blake, Long-term decline of global atmospheric ethane concentrations and implications for methane, *Nature*, *488* (7412), 490-494, doi: 10.1038/nature11342, 2012.

Sinnhuber, B.-M., and I. Folkins, Estimating the contribution of bromoform to stratospheric bromine and its relation to dehydration in the tropical tropopause layer, *Atmos. Chem. Phys.*, *6* (12), 4755-4761, doi: 10.5194/acp-6-4755-2006, 2006.

Sinnhuber, B.-M., A. Rozanov, N. Sheode, O.T. Afe, A. Richter, M. Sinnhuber, F. Wittrock, J.P. Burrows, G.P. Stiller, T. von Clarmann, and A. Linden, Global observations of stratospheric bromine monoxide from SCIAMACHY, *Geophys. Res. Lett.*, *32* (20), L20810, doi: 10.1029/2005GL023839, 2005.

Sinnhuber, B.-M., N. Sheode, M. Sinnhuber, M.P. Chipperfield, and W. Feng, The contribution of anthropogenic bromine emissions to past stratospheric ozone trends: A modelling study, *Atmos. Chem. Phys.*, *9* (8), 2863-2871, doi: 10.5194/acp-9-2863-2009, 2009.

Sioris, C.E., L.J. Kovalenko, C.A. McLinden, R.J. Salawitch, M. Van Roozendael, F. Goutail, M. Dorf, K. Pfeilsticker, K. Chance, C. von Savigny, X. Liu, T.P. Kurosu, J.-P. Pommereau, H. Bösch, and J. Frerick, Latitudinal and vertical distribution of bromine monoxide in the lower stratosphere from Scanning Imaging Absorption Spectrometer for Atmospheric Chartography limb scattering measurements, *J. Geophys. Res.*, *111*, D14301, doi: 10.1029/2005JD006479, 2006.

Solomon, S., R.W. Portmann, R.R. Garcia, W. Randel, F. Wu, R. Nagatani, J. Gleason, L. Thomason, L.R. Poole, and M.P. McCormick, Ozone depletion at mid-latitudes: Coupling of volcanic aerosols and temperature variability to anthropogenic chlorine, *Geophys. Res. Lett.*, *25* (11), 1871-1874, doi: 10.1029/98GL01293, 1998.

SPARC (Stratosphere-troposphere Processes And their Role in Climate), *SPARC Assessment of Stratospheric Aerosol Properties*, edited by L. Thomason and Th. Peter, World Climate Research Program Report 124, SPARC Report 4, WMO/TD- No. 1295, 346 pp., Verrières le Buisson, France, 2006.

SPARC (Stratosphere-troposphere Processes And their Role in Climate), *SPARC Report on the Lifetimes of Stratospheric Ozone-Depleting Substances, Their Replacements, and Related Species*, edited by M. Ko, P. Newman, S. Reimann, and S. Strahan, SPARC Report No. 6, WCRP-15/2013, 2013.

Spivakovsky, C.M., J.A. Logan, S.A. Montzka, Y.J. Balkanski, M. Foreman-Fowler, D.B.A. Jones, L.W. Horowitz, A.C. Fusco, C.A.M. Brenninkmeijer, M.J. Prather, S.C. Wofsy, and M.B. McElroy, Three-dimensional climatological distribution of tropospheric OH: Update and evaluation, *J. Geophys. Res.*, *105* (D7), 8931-8980, doi: 10.1029/1999JD901006, 2000.

Stachnik, R.A., L. Millán, R. Jarnot, R. Monroe, C. McLinden, S. Kühl, J. Puķīte, M. Shiotani, M. Suzuki, Y. Kasai, F. Goutail, J.P. Pommereau, M. Dorf, and K. Pfeilsticker, Stratospheric BrO abundance measured by a balloon-borne submillimeterwave radiometer, *Atmos. Chem. Phys.*, *13* (6), 3307-3319, doi: 10.5194/acp-13-3307-2013, 2013.

Stemmler, K., D. Folini, S. Ubl, M.K. Vollmer, S. Reimann, S. O'Doherty, B.R. Greally, P.G. Simmonds, and A.J. Manning, European emissions of HFC-365mfc, a chlorine-free substitute for the foam blowing agents HCFC-141b and CFC-11, *Environ. Sci. Technol.*, *41* (4), 1145-1151, doi: 10.1021/es061298h, 2007.

Stemmler, I., M. Rothe, I. Hense, and H. Hepach, Numerical modelling of methyl iodide in the eastern tropical Atlantic, *Biogeosciences, 10* (6), 4211-4225, doi: 10.5194/bg-10-4211-2013, 2013.

Stiller, G.P., T. von Clarmann, F. Haenel, B. Funke, N. Glatthor, U. Grabowski, S. Kellmann, M. Kiefer, A. Linden, S. Lossow, and M. López-Puertas, Observed temporal evolution of global mean age of stratospheric air for the 2002 to 2010 period, *Atmos. Chem. Phys.*, *12* (7), 3311-3331, doi: 10.5194/acp-12-3311-2012, 2012.

Stohl, A., P. Seibert, J. Arduini, S. Eckhardt, P. Fraser, B.R. Greally, C. Lunder, M. Maione, J. Mühle, S. O'Doherty, R.G. Prinn, S. Reimann, T. Saito, N. Schmidbauer, P.G. Simmonds, M.K. Vollmer, R.F. Weiss, and Y. Yokouchi, An analytical inversion method for determining regional and global emissions of greenhouse gases: Sensitivity studies and application to halocarbons, *Atmos. Chem. Phys.*, *9* (5), 1597-1620, doi: 10.5194/acp-9-1597-2009, 2009.

Stohl, A., J. Kim, S. Li, S. O'Doherty, J. Mühle, P.K. Salameh T. Saito, M.K. Vollmer, D. Wan, R.F. Weiss, B. Yao, Y. Yokouchi, and L.X. Zhou, Hydrochlorofluorocarbon and hydrofluorocarbon emissions in East Asia determined by inverse modeling, *Atmos. Chem. Phys.*, *10* (8), 3545-3560, doi: 10.5194/acp-10-3545-2010, 2010.

Sturges, W.T., T.J. Wallington, M.D. Hurley, K.P. Shine, K. Sihra, A. Engel, D.E. Oram, S.A. Penkett, R. Mulvaney, and C.A.M. Brenninkmeijer, A potent greenhouse gas identified in the atmosphere: SF_5CF_3, *Science*, *289* (5479), 611-613, doi: 10.1126/science.289.5479.611, 2000.

Sturges, W.T., D.E. Oram, J.C. Laube, C.E. Reeves, M.J. Newland, C. Hogan, P. Martinerie, E. Witrant, C.A.M. Brenninkmeijer, T.J. Schuck, and P.J. Fraser, Emissions halted of the potent greenhouse gas SF_5CF_3, *Atmos. Chem. Phys.*, *12* (8), 3653-3658, doi: 10.5194/acp-12-3653-2012, 2012.

Sulbaek Andersen, M.P., E.J.K. Nilsson, O.J. Nielsen, M.S. Johnson, M.D. Hurley, and T.J. Wallington, Atmospheric chemistry of *trans*-$CF_3CH{=}CHCl$: Kinetics of the gas-phase reactions with Cl atoms, OH radicals, and O_3, *J. Photochem. Photobio. A: Chemistry*, *199* (1), 92-97, doi: 10.1016/j.jphotochem.2008.05.013, 2008.

Sulbaek Andersen, M.P., O.J. Nielsen, B. Karpichev, T.J. Wallington, and S.P. Sander, Atmospheric chemistry of isoflurane, desflurane, and sevoflurane: Kinetics and mechanisms of reactions with chlorine atoms and OH radicals and global warming potentials, *J. Phys. Chem. A*, *116* (24), 5806-5820, doi: 10.1021/jp2077598, 2012.

Takahashi, H., and Luo, Z.J., Characterizing tropical overshooting deep convection from joint analysis of CloudSat and geostationary satellite observations, *J. Geophys. Res.*, *119* (1), 112–121, doi: 10.1002/2013JD020972, 2014.

Taniguchi, N., T.J. Wallington, M.D. Hurley, A.G. Guschin, L.T. Molina, and M.J. Molina, Atmospheric chemistry of $C_2F_5C(O)CF(CF_3)_2$: Photolysis and reaction with Cl atoms, OH radicals, and ozone, *J. Phys. Chem. A*, *107* (15), 2674-2679, doi: 10.1021/jp0220332, 2003.

Tegtmeier, S., K. Krüger, B. Quack, E.L. Atlas, I. Pisso, A. Stohl, and X. Yang, Emission and transport of bromocarbons: From the West Pacific ocean into the stratosphere, *Atmos. Chem. Phys.*, *12* (22), 10633-10648, doi: 10.5194/acp-12-10633-2012, 2012.

Tegtmeier, S., K. Krüger, B. Quack, E. Atlas, D.R. Blake, H. Boenisch, A. Engel, H. Hepach, R. Hossaini, M.A. Navarro, S. Raimund, S. Sala, Q. Shi, and F. Ziska, The contribution of oceanic methyl iodide to stratospheric iodine, *Atmos. Chem. Phys., 13* (23), 11869-11886, doi: 10.5194/acp-13-11869-2013, 2013.

Theys, N., M. Van Roozendael, F. Hendrick, C. Fayt, C. Hermans, J.-L. Barray, F. Goutail, J.-P. Pommereau, and M. De Mazière, Retrieval of stratospheric and tropospheric BrO columns from multi-axis DOAS measurements at Reunion Island (21°S, 56°E), *Atmos. Chem. Phys.*, *7* (18), 4733-4749, doi: 10.5194/acp-7-4733-2007, 2007.

Theys, N., M. Van Roozendael, F. Hendrick, X. Yang, I. De Smedt, A. Richter, M. Begoin, Q. Errera, P.V. Johnston, K. Kreher, and M. De Mazière, Global observations of tropospheric BrO columns using GOME-2 satellite data, *Atmos. Chem. Phys.*, *11* (4), 1791-1811, doi: 10.5194/acp-11-1791-2011, 2011.

Thomas, V.M., J.A. Bedford, and R.J. Cicerone, Bromine emissions from leaded gasoline, *Geophys. Res. Lett., 24* (11), 1371-1374, doi: 10.1029/97GL01243, 1997.

Thompson, R.L., F. Chevallier, A.M. Crotwell, G. Dutton, R.L. Langenfelds, R.G. Prinn, R.F. Weiss, Y. Tohjima, T. Nakazawa, P.B. Krummel, L.P. Steele, P. Fraser, S. O'Doherty, K. Ishijima, and S. Aoki, Nitrous oxide emissions 1999–2009 from a global atmospheric inversion, *Atmos. Chem. Phys.*, *14* (4), 1801-1817, doi: 10.5194/acp-14-1801-2014, 2014.

Thornton, B.F., D.W. Toohey, A.F. Tuck, J.W. Elkins, K.K. Kelly, S.J. Hovde, E.C. Richard, K.H. Rosenlof, T.L. Thompson, M.J. Mahoney, and J.C. Wilson, Chlorine activation near the midlatitude tropopause, *J. Geophys. Res.*, *112* (D18), D18306, doi: 10.1029/2006JD007640, 2007.

Tilmes, S., D.E. Kinnison, R.R. Garcia, R. Salawitch, T. Canty, J. Lee-Taylor, S. Madronich, and K. Chance, Impact of very short-lived halogens on stratospheric ozone abundance and UV radiation in a geo-engineered atmosphere, *Atmos. Chem. Phys.*, *12* (22), 10945-10955, doi: 10.5194/acp-12-10945-2012, 2012.

Tokuhashi, K., A. Takahashi, M. Kaise, and S. Kondo, Rate constants for the reactions of OH radicals with CH_3OCF_2CHFCl, CHF_2OCF_2CHFCl, $CHF_2OCHClCF_3$, and $CH_3CH_2OCF_2CHF_2$, *J. Geophys. Res*., *104* (D15), 18681-18688, doi: 10.1029/1999JD900278, 1999.

Trudinger, C.M., D.M. Etheridge, G.A. Sturrock, P.J. Fraser, P.B. Krummel, and A. McCulloch, Atmospheric histories of halocarbons from analysis of Antarctic firn air: Methyl bromide, methyl chloride, chloroform, and dichloromethane, *J. Geophys. Res.*, *109* (D22), D22310, doi: 10.1029/2004JD004932, 2004.

Tsai, W.-T., H.-P. Chen, and W.-Y. Hsien, A review of uses, environmental hazards and recovery/recycle technologies of perfluorocarbons (PFCs) emissions from the semiconductor manufacturing processes, *J. of Loss Prevent. Proc.*, *15* (2), 65-75, doi: 10.1016/S0950-4230(01)00067-5, 2002.

Tzella, A., and B. Legras, A Lagrangian view of convective sources for transport of air across the Tropical Tropopause Layer: Distribution, times and the radiative influence of clouds, *Atmos. Chem. Phys.*, *11* (23), 12517-12534, doi: 10.5194/acp-11-12517-2011, 2011.

UNEP (United Nations Environment Programme), *Technology and Economic Assessment Panel: Task Force On Emissions Discrepancies Report*, 80 pp., Nairobi, Kenya, http://montreal-protocol.org/Assessment_Panels/TEAP/Reports/TEAP_Reports/TEAP-Discrepancy-report.pdf, 2006.

UNEP (United Nations Environment Programme), *2006 Report of the Methyl Bromide Technical Options Committee: 2006 Assessment*, coordinated by M. Pizano, I. Porter, M. Marcotte, M. Besri, and J. Banks, 453 pp., Nariobi, Kenya, http://montreal-protocol.org/Assessment_Panels/TEAP/Reports/MBTOC/MBTOC-2006-Assessment%20Report.pdf, 2007.

UNEP (United Nations Environment Programme), *HFCs: A Critical Link in Protecting Climate and the Ozone Layer*, 36 pp., Nairobi, Kenya, http://www.unep.org/dewa/Portals/67/pdf/HFC_report.pdf, 2011a.

UNEP (United Nations Environment Programme), *2010 Report Of The Halons Technical Options Committee*, coordinated by D. Catchpole, S. Kopylov, and D Verdonik, 168 pp., Nairobi, Kenya, http://montreal-protocol.org/Assessment_Panels/TEAP/Reports/HTOC/HTOC-Assessment-Report-2010.pdf, 2011b.

UNEP (United Nations Environment Programme), *Report of the Methyl Bromide Technical Options Committee: 2010 Assessment*, coordinated by M. Besri, M. Marcotte, M. Pizano, and I. Porter, 397 pp., Nairobi, Kenya, http://montreal-protocol.org/Assessment_Panels/TEAP/Reports/MBTOC/MBTOC-Assesment-Report-2010.pdf, 2011c.

UNEP (United Nations Environment Programme), *May 2012 Report of the Technology and Economic Assessment Panel*: *Volume 1 Progress Report*, 222 pp, Nairobi, Kenya, http://montreal-protocol.org/Assessment_Panels/TEAP/Reports/TEAP_Reports/teap-progress-report-may2012.pdf, 2012.

UNEP (United Nations Environment Programme), *May 2013 Report of the Technology and Economic Assessment Panel*: *Decision XXIV/7 Task Force Report, Additional Information on Alternatives to ODS, Volume 2*, 124 pp, Nairobi, Kenya, http://montreal-protocol.org/Assessment_Panels/TEAP/Reports/TEAP_Reports/TEAP_Task Force%20XXIV-7-May2013.pdf, 2013a.

UNEP (United Nations Environment Programme), *May 2013 Report of the Technology and Economic Assessment Panel*: *Volume 1 Progress Report*, 156 pp, Nairobi, Kenya, http://montreal-protocol.org/Assessment_Panels/TEAP/Reports/TEAP_Reports/TEAP_Progress_Report_May_2013.pdf, 2013b.

UNEP (United Nations Environment Programme), *Drawing Down N_2O to Protect Climate and the Ozone Layer. A UNEP Synthesis Report,* 57 pp., Nairobi, Kenya, http://www.unep.org/pdf/UNEPN2Oreport.pdf, 2013c.

UNEP (United Nations Environment Programme), http://ozone.unep.org/new_site/en/ozone_data_tools_access.php, retrieved in May 2014, 2014.

UNFCCC (United Nations Framework Convention on Climate Change), http://unfccc.int/kyoto_protocol/doha_amendment/items/7362.php, retrieved in May 2014, 2014.

van der Werf, G.R., J.T. Randerson, L. Giglio, G.J. Collatz, M. Mu, P.S. Kasibhatla, D.C. Morton, R.S. DeFries, Y. Jin, and T.T. van Leeuwen, Global fire emissions and the contribution of deforestation, savanna, forest, agricultural, and peat fires (1997-2009), *Atmos. Chem. Phys.*, *10* (23), 11707-11735, doi: 10.5194/acp-10-11707-2010, 2010.

Van Roozendael, M., T. Wagner, A. Richter, I. Pundt, D.W. Arlander, J.P. Burrows, M. Chipperfield, C. Fayt, P.V. Johnston, J.-C. Lambert, K. Kreher, K. Pfeilsticker, U. Platt, J.-P. Pommereau, B.-M. Sinnhuber, K.K. Tørnkvist, and F. Wittrock, Intercomparison of BrO measurements from ERS-2 GOME, ground-based and balloon platforms, *Adv. Space Res*., *29* (11), 1661-1666, 2002.

Varner, R.K., P.M. Crill, and R.W. Talbot, Wetlands: A potentially significant source of atmospheric methyl bromide and methyl chloride, *Geophys. Res. Lett.*, *26* (16), 2433-2436, doi: 10.1029/1999GL900587, 1999.

Velders, G.J.M., A.R. Ravishankara, M.K. Miller, M.J. Molina, J. Alcamo, J.S. Daniel, D.W. Fahey, S.A. Montzka, and S. Reimann, Preserving Montreal Protocol climate benefits by limiting HFCs, *Science*, *335* (6071), 922-923, doi: 10.1126/science.1216414, 2012.

Volk, C.M., J.W. Elkins, D.W. Fahey, G.S. Dutton, J.M. Gilligan, M. Loewenstein, J.R. Podolske, K.R. Chan, and M.R. Gunson, Evaluation of source gas lifetimes from stratospheric observations, *J. Geophys. Res.*, *102* (D21), 25543-25564, doi: 10.1029/97JD02215, 1997.

Vollmer, M.K., S. Reimann, D. Folini, L.W. Porter, and L.P. Steele, First appearance and rapid growth of anthropogenic HFC-245fa ($CHF_2CH_2CF_3$) in the atmosphere, *Geophys. Res. Lett.*, *33*, L20806, doi: 10.1029/2006GL026763, 2006.

Vollmer, M.K., L.X. Zhou, B.R. Greally, S. Henne, B. Yao, S. Reimann, F. Stordal, D.M. Cunnold, X.C. Zhang, M. Maione, F. Zhang, J. Huang, and P.G. Simmonds, Emissions of ozone-depleting halocarbons from China, *Geophys. Res. Lett*., *36*, L15823, doi: 10.1029/2009GL038659, 2009.

Vollmer, M.K., B.R. Miller, M. Rigby, S. Reimann, J. Mühle, P.B. Krummel, S. O'Doherty, J. Kim, T.S. Rhee, R.F. Weiss, P.J. Fraser, P.G. Simmonds, P.K. Salameh, C.M. Harth, R.H.J. Wang, L.P. Steele, D. Young, C.R. Lunder, O. Hermansen, D. Ivy, T. Arnold, N. Schmidbauer, K.-R. Kim, B.R. Greally, M. Hill, M. Leist, A. Wenger, and R.G. Prinn, Atmospheric histories and global emissions of the anthropogenic hydrofluorocarbons HFC-365mfc, HFC-245fa, HFC-227ea, and HFC-236fa, *J. Geophys. Res.*, *116* (D8), D08304, doi: 10.1029/2010JD015309, 2011.

von Hobe, M., J.-U. Grooß, G. Günther, P. Konopka, I. Gensch, M. Krämer, N. Spelten, A. Afchine, C. Schiller, A. Ulanovsky, N. Sitnikov, G. Shur, V. Yushkov, F. Ravegnani, F. Cairo, A. Roiger, C. Voigt, H. Schlager, R. Weigel, W. Frey, S. Borrmann, R. Müller, and F. Stroh, Evidence for heterogeneous chlorine activation in the tropical UTLS, *Atmos. Chem. Phys.*, *11* (1), 241-256, doi: 10.5194/acp-11-241-2011, 2011.

Wallington, T.J., W.F. Schneider, D.R. Worsnop, O.J. Nielsen, J. Sehested, W.J. DeBruyn, and J.A. Shorter, The environmental impact of CFC replacements – HFCs and HCFCs, *Environ. Sci. Technol*., *28* (7), 320A-326A, doi: 10.1021/es00056a002, 1994.

Wan, D., J. Xu, J. Zhang, X. Tong, and J. Hu, Historical and projected emissions of major halocarbons in China, *Atmos. Environ*., *43* (36), 5822-5829, doi: 10.1016/j.atmosenv.2009.07.052, 2009.

Warwick, N.J., J.A. Pyle, G.D. Carver, X. Yang, N.H. Savage, F.M. O'Connor, and R.A. Cox, Global modeling of biogenic bromocarbons, *J. Geophys. Res.*, *111* (D24), D24305, doi: 10.1029/2006JD007264, 2006a.

Warwick, N.J., J.A. Pyle, and D.E. Shallcross, Global modelling of the atmospheric methyl bromide budget, *J. Atmos. Chem.*, *54* (2), 133-159, doi: 10.1007/s10874-006-9020-3, 2006b.

Watling, R., and D.B. Harper, Chloromethane production by wood-rotting fungi and an estimate of the global flux to the atmosphere, *Mycol. Res.*, *102* (7), 769-787, doi: 10.1017/S0953756298006157, 1998.

Weiss, R.F., J. Mühle, P.K. Salameh, and C.M. Harth, Nitrogen trifluoride in the global atmosphere, *Geophys. Res. Lett.*, *35* (20), L20821, doi: 10.1029/2008GL035913, 2008.

Wever, R., and M.A. van der Horst, The role of vanadium haloperoxidases in the formation of volatile brominated compounds and their impact on the environment, *Dalton Trans.*, *42* (33), 11778-11786, doi: 10.1039/c3dt50525a, 2013.

Wisher, A., D.E. Oram, J.C. Laube, G.P. Mills, P. van Velthoven, A. Zahn, and C.A.M. Brenninkmeijer, Very short-lived bromomethanes measured by the CARIBIC observatory over the North Atlantic, Africa and Southeast Asia during 2009–2013, *Atmos. Chem. Phys., 14* (7), 3557-3570, doi: 10.5194/acp-14-3557-2014, 2014.

WMO, (World Meteorological Organization), *Scientific Assessment of Ozone Depletion: 1991 Global Ozone Research and Monitoring Project–Report No. 25*, Geneva, Switzerland, 1992.

WMO (World Meteorological Organization), *Scientific Assessment of Ozone Depletion: 2002*, Global Ozone Research and Monitoring Project–Report No. 47, Geneva, Switzerland, 2003.

WMO (World Meteorological Organization), *Scientific Assessment of Ozone Depletion: 2006*, Global Ozone Research and Monitoring Project–Report No. 50, 572 pp., Geneva, Switzerland, 2007.

WMO, (World Meteorological Organization), *Scientific Assessment of Ozone Depletion: 2010,* Global Ozone Research and Monitoring Project–Report No. 52, Geneva, Switzerland, 2011.

Wofsy, S.C., HIPPO Science Team, and Cooperating Modellers and Satellite Team, HIAPER Pole-to-Pole Observations (HIPPO): Fine-grained, global-scale measurements of climatically important atmospheric gases and aerosols, *Phil. Trans. R. Soc. A*, *369* (1943), 2073-2086, doi: 10.1098/rsta.2010.0313, 2011.

Worton, D.R., W.T. Sturges, J. Schwander, R. Mulvaney, J.-M. Barnola, and J. Chappellaz, 20th century trends and budget implications of chloroform and related tri- and dihalomethanes inferred from firn air, *Atmos. Chem. Phys.*, *6* (10), 2847-2863, doi: 10.5194/acp-6-2847-2006, 2006.

Wright, J.S., R. Fu, S. Fueglistaler, Y.S. Liu, and Y. Zhang, The influence of summertime convection over Southeast Asia on water vapor in the tropical stratosphere, *J. Geophys. Res.*, *116* (D12), D12302, doi: 10.1029/2010JD015416, 2011.

Wu, J., X. Fang, J.W. Martin, Z. Zhai, S. Su, X. Hu, J. Han, S., Lu, C., Wang, J., Zhang, and J., Hu, Estimated emissions of chlorofluorocarbons, hydrochlorofluorocarbons, and hydrofluorocarbons based on an interspecies correlation method in the Pearl River Delta region, China, *Sci. Total. Environ.*, *470–471*, 829-834, doi: 10.1016/j.scitotenv.2013.09.071, 2014.

Xiao, X., R.G. Prinn, P.J. Fraser, R.F. Weiss, P.G. Simmonds, S. O'Doherty, B.R. Miller, P.K. Salameh, C.M. Harth, P.B. Krummel, A. Golombek, L.W. Porter, J.W. Elkins, G.S. Dutton, B.D. Hall, L.P. Steele, R.H.J. Wang, and D.M. Cunnold, Atmospheric three-dimensional inverse modeling of regional industrial emissions and global oceanic uptake of carbon tetrachloride, *Atmos. Chem. Phys.*, *10* (21), 10421-10434, doi: 10.5194/acp-10-10421-2010, 2010a.

Xiao, X., R.G. Prinn, P.J. Fraser, P.G. Simmonds, R.F. Weiss, S. O'Doherty, B.R. Miller, P.K. Salameh, C.M. Harth, P.B. Krummel, L.W. Porter, J. Mühle, B.R. Greally, D. Cunnold, R. Wang, S.A. Montzka, J.W. Elkins, G.S. Dutton, T.M. Thompson, J.H. Butler, B.D. Hall, S. Reimann, M.K. Vollmer, F. Stordal, C. Lunder, M. Maione, J. Arduini, and Y. Yokouchi, Optimal estimation of the surface fluxes of methyl chloride using a 3-D global chemical transport model, *Atmos. Chem. Phys.*, *10* (12), 5515-5533, doi: 10.5194/acp-10-5515-2010, 2010b.

Xue, L.K., T. Wang, I.J. Simpson, A.J. Ding, J. Gao, D.R. Blake, X. Z. Wang, W.X. Wang, H.C. Lei, and D.Z. Jing, Vertical distributions of non-methane hydrocarbons and halocarbons in the lower troposphere over northeast China, *Atmos. Environ.*, *45* (36), 6501-6509, doi: 10.1016/j.atmosenv.2011.08.072, 2011.

Yao, B., M.K. Vollmer, L.X. Zhou, S. Henne, S. Reimann, P.C. Li, A. Wenger, and M. Hill, In-situ measurements of atmospheric hydrofluorocarbons (HFCs) and perfluorocarbons (PFCs) at the Shangdianzi regional background station, China, *Atmos. Chem. Phys.*, *12* (21), 10181-10193, doi: 10.5194/acp-12-10181-2012, 2012.

Yevich, R., and J.A. Logan, An assessment of biofuel use and burning of agricultural waste in the developing world, *Global Biogeochem. Cycles*, *17* (4), 1095, doi: 10.1029/2002GB001952, 2003.

Yokouchi, Y., M. Ikeda, Y. Inuzuka, and T. Yukawa, Strong emission of methyl chloride from tropical plants, *Nature*, *416*, 163-165, doi: 10.1038/416163a, 2002.

Yokouchi, Y., F. Hasebe, M. Fujiwara, H. Takashima, M. Shiotani, N. Nishi, Y. Kanaya, S. Hashimoto, P. Fraser, D. Toom-Sauntry, H. Mukai, and Y. Nojiri, Correlations and emission ratios among bromoform, dibromochloromethane, and dibromomethane in the atmosphere, *J. Geophys. Res.*, *110*, D23309, doi: 10.1029/2005JD006303, 2005.

Yokouchi, Y., S. Taguchi, T. Saito, Y. Tohjima, H. Tanimoto, and H. Mukai, High frequency measurements of HFCs at a remote site in east Asia and their implications for Chinese emissions, *Geophys. Res. Lett.*, *33* (21), L21814, doi: 10.1029/2006GL026403, 2006.

Yokouchi, Y., T. Saito, C. Ishigaki, and M. Aramoto, Identification of methyl chloride-emitting plants and atmospheric measurements on a subtropical island, *Chemosphere*, *69* (4), 549-553, doi: 10.1016/j.chemosphere.2007.03.028, 2007.

Yokouchi, Y., T. Saito, A. Ooki, and H. Mukai, Diurnal and seasonal variations of iodocarbons (CH_2ClI, CH_2I_2, CH_3I, and C_2H_5I) in the marine atmosphere, *J. Geophys. Res.*, *116* (D6), D06301, doi: 10.1029/2010JD015252, 2011.

Yokouchi, Y., Y. Nojiri, D. Toom-Sauntry, P. Fraser, Y. Inuzuka, H. Tanimoto, H. Nara, R. Murakami, and H. Mukai, Long-term variation of atmospheric methyl iodide and its link to global environmental change, *Geophys. Res. Lett.*, *39* (23), L23805, doi: 10.1029/2012GL053695, 2012.

Yoshida, Y., Y.H. Wang, T. Zeng, and R. Yantosca, A three-dimensional global model study of atmospheric methyl chloride budget and distributions, *J. Geophys. Res.*, *109* (D24), D24309, doi: 10.1029/2004JD004951, 2004.

Youn, D., K.O. Patten, D.J. Wuebbles, H. Lee, and C.-W. So, Potential impact of iodinated replacement compounds CF_3I and CH_3I on atmospheric ozone: A three-dimensional modeling study, *Atmos. Chem. Phys.*, *10* (20), 10129-10144, doi: 10.5194/acp-10-10129-2010, 2010.

Young, C.J., M.D. Hurley, T.J. Wallington, and S.A. Mabury, Atmospheric chemistry of CF_3CF_2H and $CF_3CF_2CF_2CF_2H$: Kinetics and products of gas-phase reactions with Cl atoms and OH radicals, infrared spectra, and formation of perfluorocarboxylic acids, *Chem. Phys. Lett.*, *473* (4-6), 251-256, doi: 10.1016/j.cplett. 2009.04.001, 2009.

Yujing, M., and A. Mellouki, Rate constants for the reactions of OH with chlorinated propanes, *Phys. Chem. Chem. Phys.*, *3*, 2614-2617, doi: 10.1039/b102971c, 2001.

Yvon-Lewis, S.A., and J.H. Butler, Effect of oceanic uptake on atmospheric lifetimes of selected trace gases, *J. Geophys. Res.*, *107* (D20), 4414, doi: 10.1029/2001JD001267, 2002.

Yvon-Lewis, S.A., E.S. Saltzman, and S.A. Montzka, Recent trends in atmospheric methyl bromide: Analysis of post-Montreal Protocol variability, *Atmos. Chem. Phys.*, *9* (16), 5963-5974, doi: 10.5194/acp-9-5963-2009, 2009.

Zander, R., E. Mahieu, P. Demoulin, P. Duchatelet, G. Roland, C. Servais, M. De Mazière, and C.P. Rinsland, Evolution of a dozen non-CO_2 greenhouse gases above central Europe since the mid-1980s, *Environ. Sci.*, *2* (2-3), 295-303, 2005.

Zander, R., E. Mahieu, P. Demoulin, P. Duchatelet, G. Roland, C. Servais, M. De Mazière, S. Reimann, and C.P. Rinsland, Our changing atmosphere: Evidence based on long-term infrared solar observations at the Jungfraujoch since 1950, *Sci. Tot. Environ.*, *391* (2-3), 184-195, doi: 10.1016/j.scitotenv.2007.10.018, 2008.

Zhang, Z., R. Liu, R.E. Huie, and M.J. Kurylo, A gas-phase reactivity study of OH radicals with 1,1-dichloroethene and *cis*- and *trans*-1,2-dichloroethene over the temperature range 240-400 K, *J. Phys. Chem.*, *95* (1), 194-196, doi: 10.1021/j100154a039, 1991.

Zhao, Z., P.L. Laine, J.M. Nicovich, and P.H. Wine, Reactive and nonreactive quenching of $O(^1D)$ by the potent greenhouse gases SO_2F_2, NF_3, and SF_5CF_3, *Proc. Natl. Acad. Sci.*, *107* (15), 6610-6615, doi: 10.1073/ pnas.0911228107, 2010.

Ziska, F., B. Quack, K. Abrahamsson, S.D. Archer, E. Atlas, T. Bell, J.H. Butler, L.J. Carpenter, C.E. Jones, N.R.P. Harris, H. Hepach, K.G. Heumann, C. Hughes, J. Kuss, K. Krüger, P. Liss, R.M. Moore, A. Orlikowska, S. Raimund, C.E. Reeves, W. Reifenhäuser, A.D. Robinson, C. Schall, T. Tanhua, S. Tegtmeier, S. Turner, L. Wang, D. Wallace, J. Williams, H. Yamamoto, S. Yvon-Lewis, and Y. Yokouchi, Global sea-to-air flux climatology for bromoform, dibromomethane and methyl iodide, *Atmos. Chem. Phys.*, *13* (17), 8915-8934, doi: 10.5194/acp-13-8915-2013, 2013.

CHAPTER 2

Update on Global Ozone: Past, Present, and Future

Lead Authors:
S. Pawson
W. Steinbrecht

Coauthors:
A.J. Charlton-Perez
M. Fujiwara
A.Yu. Karpechko
I. Petropavlovskikh
J. Urban
M. Weber

Contributors:
V. Aquila
W. Chehade
I. Cionni
M. Coldewey-Egbers
A. Delcloo
S.S. Dhomse
V. Eyring
E. Fleming
S.M. Frith
L. Froidevaux
N.P. Gillett
B. Hassler
M.I. Hegglin
D.E. Kinnison
D. Loyola
C.A. McLinden
L.D. Oman
D.A. Plummer
L.E. Revell
T. Sakazaki
W. Seviour
S. Tegtmeier
R.J. van der A
J. Wild

Chapter Editors:
V.E. Fioletov
U. Langematz

[Formatted for double-sided printing.]

From:
WMO (World Meteorological Organization), *Scientific Assessment of Ozone Depletion: 2014*, Global Ozone Research and Monitoring Project – Report No. 55, 416 pp., Geneva, Switzerland, 2014.

This chapter should be cited as:
Pawson, S., and W. Steinbrecht (Lead Authors), A.J. Charlton-Perez, M. Fujiwara, A.Yu. Karpechko, I. Petropavlovskikh, J. Urban, and M. Weber, Update on global ozone: Past, present, and future, Chapter 2 in *Scientific Assessment of Ozone Depletion: 2014*, Global Ozone Research and Monitoring Project – Report No. 55, World Meteorological Organization, Geneva, Switzerland, 2014.

CHAPTER 2

UPDATE ON GLOBAL OZONE: PAST, PRESENT, AND FUTURE

Contents

SCIENTIFIC SUMMARY

Past Changes in Total Column Ozone

This chapter deals with the evolution of global ozone outside of the polar regions. The increase of ozone-depleting substance (ODS) concentrations caused the large ozone decline observed from 1980 to the mid-1990s. Since the late 1990s, concentrations of ODSs have been declining due to the successful implementation of the Montreal Protocol. As reported in the last Assessment, global ozone levels have remained stable since 2000. Ozone columns observed in the last four years have largely remained in the range observed since 2000.

Over the next decades we expect increasing global-mean stratospheric ozone columns, as ODSs decline further. Climate change and emissions of greenhouse gases, especially carbon dioxide (CO_2), methane (CH_4), and nitrous oxide (N_2O), also affect the evolution of global stratospheric ozone, particularly in the second half of the 21st century, when ODS concentrations are expected to be low.

- Compared to 1964–1980 total column ozone, ground-based and space-based observations show that present-day (circa 2008–2013) ozone columns are:
    - lower by about 2% for the near-global average (60°S–60°N), compared to 2.5% reported in the last Assessment;
    - lower by about 3.5% in the Northern Hemisphere (35°N–60°N), as reported in the last Assessment;
    - lower by about 6% in the Southern Hemisphere (35°S–60°S), as reported in the last Assessment. The larger depletion in the Southern Hemisphere is linked to the Antarctic ozone hole; and
    - almost unchanged in the tropics (20°S–20°N), as in the last Assessment.

- **Ground- and space-based observations indicate that near-global (60°S–60°N) column ozone has increased by around 1% ± 1.7% (2 sigma) between 2000 and 2013.** However, there is substantial disagreement among the data sets about the magnitude and statistical significance of this increase. Two out of three independent data sets show increases at the upper end; one recently updated data set shows an increase at the lower end. The CCMVal-2 multi-model mean predicts a 1% increase between 2000 and 2013 for the near-global (60°S–60°N) column ozone.

- **Total column ozone (dominated by lower stratospheric ozone) displays large, dynamically forced year-to-year variability in the middle and high latitudes, exemplified by unusually high ozone in 2010 and low ozone in 2011 in the Northern Hemisphere, and low ozone in 2006 in the Southern Hemisphere.** The recent decline (15% since 1997) in concentrations of ODSs, as described by Equivalent Effective Stratospheric Chlorine (EESC), is expected to have had only a small impact on total ozone recovery (approximately 3 Dobson units (DU), or 1%, since 2000). Separation of the small recent ODS-related ozone increase from the large natural variability (up to 15 DU or 5% change from one year to the next) can currently not be made with a high level of confidence.

Past Changes in Ozone Profiles

Additional and improved data sets have strengthened our ability to assess ozone profile changes over the last 10 to 15 years. Data from the upper stratosphere now confirm the significance of ozone increases that were already suggested in the last Assessment. Large ozone variability in the lower stratosphere complicates the identification of long-term ozone changes in this region. Chemistry-climate model (CCM) simulations that include realistic time variations of greenhouse gas (GHG) and ODS concentrations

capture changes in the ozone profile that agree quite well with those observed. These CCM simulations provide a means of attributing changes in ozone to different processes.

- **Measurements show a statistically significant increase in upper stratospheric ozone (35–45 km altitude) in middle latitudes and the tropics since around 2000.** Following a large observed decline of 5–8% per decade through the 1980s and middle 1990s, ozone has increased by 2.5–5% per decade over the 2000 to 2013 period.
- **About half of the upper stratospheric ozone increase after 2000 can be attributed to the decline of ODS since the late 1990s.** Increasing CO_2 concentrations have led to a cooling of the upper stratosphere. CCM simulations reveal that, between the 1980s and the present this has contributed to an increase in ozone concentrations. Before the middle 1990s, this ozone increase was substantially smaller than the ozone decrease caused by ODS increases. From 2000 to 2013, the ozone increase arising from the decline in ODS concentrations is of comparable magnitude to that caused by upper stratospheric cooling.
- **As reported in the last Assessment (WMO, 2011), CCMs consistently show a long-term decline of ozone in the lowermost tropical stratosphere by up to 20% between 1960 and 2060.** This modeled ozone decline is caused by an increase in the strength of upwelling in the tropical lower stratosphere. This increased upwelling is associated with a strengthening Brewer-Dobson circulation caused by GHG-induced climate change.
- **In-situ and space-based observations reveal that ozone concentrations in the lowermost tropical stratosphere have declined by as much as 10% between 1984 and 2005.** There are several additional data sets available since 2002. Continued ozone decreases are not detected in the presence of large natural variability during 2002–2013. This observed behavior is consistent with that computed in CCMs, which also show periods of strong interannual and decadal variability.

Future Ozone Changes

The chemistry-climate model simulations used in the last Assessment are still the main source for projection of future ozone levels and the dates of return of ozone to 1980 levels. Declining ODS concentrations, upper stratospheric cooling because of increased CO_2, and the possible strengthening of the Brewer-Dobson circulation from climate change are all likely to affect recovery of global column ozone, with different relative contributions in various latitude regions.

- Estimates of the likely return dates of total column ozone concentrations to their 1980 values have not changed since the last Assessment. The best estimates are:
    - by midcentury for global mean annually averaged ozone;
    - between 2015 and 2030 for annually averaged Northern Hemisphere midlatitude ozone;
    - between 2030 and 2040 for annually averaged Southern Hemisphere midlatitude ozone; and
    - for annual average tropical column ozone, slowly increasing until the middle of the 21st century, before leveling off at values about 0–3% below 1980s columns.
- **The updated lifetimes estimated for ODSs in the SPARC lifetimes report have no significant impact on model projections of future ozone evolution.**
- **Projections of future ozone levels depend substantially on the assumed scenario of greenhouse gas (GHG) emissions, especially in the later half of the 21st century.** Six chemistry-climate model simulations show that projected total ozone columns in 2100 differ by up to 20 DU or 7% in the global average, by up to 40 DU or 12% in midlatitudes, and by up to 10 DU or 4% in the tropics between minimum and maximum radiative forcing Representative Concentration Pathway scenarios for future CO_2, N_2O, and CH_4 emissions. These new estimates of scenario uncertainty are broadly consistent with previous estimates from different models and scenarios reported in the last

Assessment. Our confidence in the magnitude of this scenario uncertainty remains low because of the small number of models and scenarios assessed.

- **Part of the scenario uncertainty in future column ozone is due to differences in emissions of N_2O and CH_4 between different scenarios.** Increases of stratospheric N_2O and CH_4 impact the chemical cycles relevant for ozone. Higher N_2O emissions tend to reduce column ozone, whereas higher CH_4 tends to increase column ozone, each by a few percent from 2020 to 2100. The magnitude of these effects on ozone is comparable to what is expected from stratospheric cooling by CO_2 increases. The influence of each individual trace gas on ozone also depends on emissions of the others, meaning that their impacts on ozone are strongly scenario dependent.

- **Given that ODS levels remain high, a large enhancement of stratospheric sulfate aerosol in the next decade, e.g., due to a volcanic eruption of the same size as Mt. Pinatubo, could result in chemical losses of at least 2% in total ozone columns over much of the globe.** Confidence in this conclusion is strengthened because the long-standing puzzle about the midlatitude hemispheric asymmetry in the midlatitude ozone response to Mt. Pinatubo aerosols is now much better understood. Studies have shown that enhanced ozone transport in the Brewer-Dobson circulation more than compensated the enhanced chemical loss in the Southern Hemisphere.

2.1 INTRODUCTION

2.1.1 Main Findings of WMO-UNEP 2010

The 2010 Assessment (WMO, 2011) provided strong evidence that the limitations imposed by the Montreal Protocol on ozone-depleting substance (ODS) emissions were leading to a slowdown in chemical ozone destruction after 1997. Observations showed a leveling off of ozone values at almost all latitudes and altitudes, with a distinct change in the trend: A strong negative ozone trend between the 1970s and the late 1990s was superseded by a period of almost no significant change in ozone until the end of the record in 2009. A broad range of numerical modeling studies, using chemical transport models (CTMs) and chemistry-climate models (CCMs), demonstrated that we have a robust scientific understanding of the mechanisms of ozone depletion. Further, the CCMs demonstrated at least three important connections between climate change and ozone depletion. First, observations and models demonstrated that the ozone hole impacts atmospheric heating rates, leading to a dynamical response of the springtime polar vortex that couples to the summertime dynamics of the Antarctic troposphere. Second, model simulations indicated that increasing greenhouse gases (GHGs) would further cool the stratosphere, thus slowing gas-phase reactions that destroy ozone in the upper stratosphere, and generally increase ozone and accelerate ozone increases. Third, the model simulations consistently predicted an increase in the strength of the Brewer-Dobson circulation (BDC), leading to lower ozone concentrations in the tropical lower stratosphere and higher values in the extratropics than might be otherwise expected. In WMO (2011) the observational evidence for this latter change was weak.

These changes in stratospheric temperatures and tropical upwelling contribute substantially to projections of ozone change through the 21st century. CCM projections showed that, in the extratropics, ozone would recover to 1980 levels as ODSs were flushed from the atmosphere, with "return dates" occurring in the 2030s to 2060s. As GHG-induced climate change continued to increase the tropical upwelling, many CCMs indicated that ozone concentrations in the tropical lower stratosphere would continue to decrease through the 21st century. In the tropics, this dynamically induced decline in ozone would offset the impacts of chemical recovery. Likewise, CCMs predicted that, in the upper stratosphere, the lower temperature resulting from increasing GHGs and declining ODSs would lead to ozone increases through the 21st century.

2.1.2 Major New Developments Since 2010

With the decline in emissions of ODSs and the consequent decrease in stratospheric chlorine- and bromine-containing compounds, a major component of the present Assessment concerns the detectability of any positive ozone trends over the past decade. The four additional years of observations available for analysis facilitate a new look at the potential recovery of ozone concentrations, with evidence that the positive trend associated with ODS reductions is becoming significant in some regions. Global ozone has been observed by spaceborne sensors for about 35 years. A continuous ozone profile data set based on one type of observations with global coverage is, however, not available. Since WMO (2011) the records of several instruments have been extended. These contribute substantially to the database of ozone profiles that supplements the sparse ground-based data sets. Long-term ozone profile data sets have been constructed by merging data from different instruments. New observations available since WMO (2011) have facilitated the investigation of the diurnal cycle of stratospheric ozone. This positions the research community to improve estimates of data set biases induced by diurnal effects (e.g., due to orbits that drift in local time), which can be particularly important in the upper stratosphere. The 2006 and 2010 Ozone Assessments drew heavily on model comparisons conducted by the SPARC (Stratosphere-troposphere Processes and their Role in Climate) Chemistry-Climate Model Validation (CCMVal) activity (Eyring et

al., 2010), with a consequent focus on differences among model predictions of ozone and some emphasis on the robustness of model simulations. Because the models used in CCMVal have not been substantially updated, no new multi-model comparison has been performed. New CCM simulations focus on different aspects of ozone change resulting from ODSs and GHGs, with a particular focus on the possible ozone distributions in the late 21st century, when chemical ozone destruction by halogens will have almost disappeared, and the main changes in ozone are driven by the assumed scenarios in greenhouse gas growth rates.

A main focus of this Assessment thus relies on better detection of ozone change, its attribution, and the robustness of recent changes detected in observations. The second main focus is on how ozone is expected to evolve in the presence of ODS reductions and how assumptions about greenhouse gas pathways impact future ozone change.

2.2 PAST OZONE IN OBSERVATIONS AND MODEL SIMULATIONS

2.2.1 Data Sources

As in the previous Assessments, carefully assessed, long-term ozone data sets have been used for trend analysis. Several new data sets have now become sufficiently long to examine ozone changes since 2000, particularly from instruments on the Odin, Envisat, and Aura satellite platforms, available since 2001, 2002, and 2004, respectively. Information about the ozone data sets used for this Assessment is summarized in Tables 2-1 (total ozone column) and 2-2 (ozone profiles). Detailed information about spatial and temporal coverage, vertical resolution, and systematic uncertainties is available from previous Assessments (WMO, 2007, 2011), and from recent SPARC initiatives on the evaluation of trace gas and aerosol climatologies (SPARC Data Initiative; Tegtmeier et al., 2013), and on past changes in the vertical distribution of ozone (SPARC/IO3C/IGACO-O3/NDACC = SI2N; Hassler et al., 2014).

Because trend detection requires time series of observations that are longer than the lifetime of most satellite instruments, several new merged ozone time series are used in this Assessment. Challenges for such long-term records come from inter-instrument biases, drifts, differing local measurement times, different coordinate systems (e.g., ozone mixing ratio in a pressure-based coordinate system, or number density in an altitude-based system), different vertical and temporal resolution, and different sampling patterns. Box 2-1, for example, discusses differences in ozone profile trends that can arise from the coordinate system used. Section 2.3.1 discusses possible effects of diurnal variations, which are, however, presently not corrected for in any merged data set. This Assessment draws heavily on recent activities to combine and homogenize ozone data sets for trend studies. The following data sets are used here:

- The most recent update of the monthly-mean zonal mean data set combining Brewer spectrometer, Dobson spectrometer, filter, and SAOZ (Système d'Analyse par Observation Zénithale) total ozone data from the ground covering the period from 1964 to present (Fioletov et al., 2002; WMO, 2011).
- Merged total ozone data sets from the Global Ozone Monitoring Experiments (GOME, GOME-2) and the Scanning Imaging Absorption Spectrometer for Atmospheric Chartography (SCIAMACHY): The Global Total Ozone data set (GTO: Chiou et al., 2014; Lerot et al., 2014) is based on the GODFIT (GOME Direct-FITting) retrieval (Loyola et al., 2009). An alternative data set is the weighting function differential optical absorption (WFDOAS) GOME/SCIAMACHY/ GOME-2 data set (GSG: Kiesewetter et al., 2010; Weber et al., 2011, 2013).
- The Multi Sensor Reanalysis (MSR), an assimilated total ozone data set using various satellite data (SBUVs, GOME, SCIAMACHY, GOME-2) and variants of retrieval algorithms as input (van der A et al., 2010). All satellite data sets have been bias corrected with respect to colocated ground Brewer and Dobson data.

Table 2-1. Merged total ozone column data sets used in this report (zonal monthly-mean data).

Data Set	Instruments	Record Length	Reference	URL
Ground-Based	Dobson, Brewer, SAOZ	01/1964 to 12/2013	Fioletov et al., 2002, 2008; Hendrick et al., 2011	http://www.woudc.org ftp://ftp.tor.ec.gc.ca/pub/woudc/Projects-Campaigns/Zonal Means
SBUV MOD V8	BUV Nimbus-4, SBUV/TOMS Nimbus-7, SBUV/2 NOAA 9 to 19, OMI, TOMS EP	11/1978 to 12/2012	Stolarski and Frith, 2006	http://acd-ext.gsfc.nasa.gov/Data_ services/merged/
SBUV V8.6 NASA (MOD V8.6)	BUV Nimbus-4, SBUV Nimbus-7, SBUV/2 NOAA 9 to 19	BUV: 01/1970 to 05/1976 SBUV: 11/1978 to 12/2013	Chiou et al., 2014; Labow et al., 2013; McPeters et al., 2013	http://acd-ext.gsfc.nasa.gov/Data_ services/merged/
SBUV V8.6 NOAA	SBUV Nimbus-7, SBUV/2 NOAA 9 to 19	11/1978 to 12/2013		ftp://ftp.cpc.ncep.noaa.gov/SBUV_CDR/
GSG - Bremen	GOME, SCIAMACHY, GOME2	07/1995 to 12/2013	Weber et al., 2013	http://www.iup.uni-bremen.de/gome/wfdoas/
GTO - ESA/DLR	GOME, SCIAMACHY, GOME2	07/1995 to 12/2013	Chiou et al., 2014; Lerot et al., 2014	http://www.esa-ozone-cci.org
Multiple Satellite Reanalysis	assimilated TOMS, SBUV, GOME, SCIAMACHY, OMI	11/1978 to 12/2013	van der A et al., 2010	http://www.temis.nl/protocols/O3global.html

- Merged total ozone and ozone profile data sets from the V8.6 retrievals of the Solar Backscatter Ultraviolet (SBUV) instruments from NASA (MOD V8.6: DeLand et al., 2012; McPeters et al., 2013; Chiou et al., 2014), which supersede the SBUV/Total Ozone Mapping Spectrometer (TOMS)/Ozone Monitoring Instrument (OMI) MOD V8 data set (Stolarski and Frith, 2006; WMO, 2011). Another merged SBUV V8.6 data set from NOAA (MA-NOAA) uses inter-satellite adjustments similar to the previous SBUV/TOMS/OMI MOD V8 data set. It provides ozone time series very similar to MOD V8. Within the uncertainty margins discussed by Stolarski and Frith (2006), the new NASA and MA-NOAA SBUV V8.6 merged data sets agree over most of their 40-year time series (i.e., total ozone columns are usually within 1% or better; profile ozone data are within 5% or better). Trend results from both data sets are similar. The NOAA SBUV V8.6 merged data set is not used in this Assessment, because currently no validation has been published for this recently merged data set.
- Stratospheric Aerosol and Gas Experiment II (SAGE II) data, updated from Version 6.2 to 7.0 (Damadeo et al., 2013). For ozone, the new data version has not resulted in significant changes of SAGE II derived trends or long-term variability (Remsberg, 2014).
- The NASA "Making Earth System Data Records for Use in Research Environments" (MEaSUREs) Global OZone Chemistry And Related trace gas Data records for the Stratosphere (GOZCARDS) project (R. Wang et al., 2013), combining satellite ozone records primarily from Stratospheric Aerosol and Gas Experiments I and II (SAGE I, II, V6.20), Halogen Occultation Experiment (HALOE), Microwave Limb Sounders (Upper Atmosphere Research Satellite MLS, Aura MLS), and Atmospheric Chemistry Experiment (ACE-Fourier Transform Spectrometer). The quality of these data sets contributing to GOZCARDS was recently assessed in the SPARC Data Initiative

(Tegtmeier et al., 2013), which also considered results from the limb sounding instruments presented in the next bullet.

- The HARMonized data set of OZone profiles (HARMOZ: Sofieva et al., 2013) produced by the European Space Agency Ozone Climate Change Initiative (ESA O3-CCI). HARMOZ consists of quality-screened European individual limb sounder data sets that are provided in common ozone units and altitude grid. HARMOZ consists of ozone data from the Optical Spectrograph and Infrared Imaging System (OSIRIS), the Sub-Millimetre Radiometer (SMR), both on the Odin satellite since 2001, and from the Global Ozone Monitoring by Occultation of Stars (GOMOS), the Michelson Interferometer for Passive Atmospheric Sounding (MIPAS), and the Scanning Imaging Absorption Spectrometer for Atmospheric Chartography (SCIAMACHY), all on the Envisat platform from 2002 to 2012. Tegtmeier et al. (2013) and Sofieva et al. (2013) discuss these individual data sets and their differences. In the Assessment, only ozone anomalies averaged over all available HARMOZ instruments are used. This removes the average bias of individual instruments, and reduces effects from spurious anomalies and drifts of individual instruments (see also Steinbrecht et al., 2006; Jones et al., 2009; Nair et al., 2012). Results for individual instruments from the HARMOZ data set have been reported by Kyrölä et al. (2013), Eckert et al. (2014), and Gebhardt et al. (2014).

Table 2-2. Main ozone profile data sets used in this report.

Data Set	Instruments Most Relevant for Trend	Record Length	References	URL
SBUV V8.6 NASA (MOD V8.6)	BUV Nimbus-4, SBUV Nimbus-7, SBUV/2 NOAA 9 to 19	BUV: 01/1970 to 05/1976 SBUV: 11/1978 to 07/2013	Kramarova et al., 2013a; McPeters et al., 2013	http://acd-ext.gsfc.nasa.gov/ Data_ services/merged/
SBUV V8.6 NOAA	SBUV Nimbus-7, SBUV/2 NOAA 9 to 19	11/1978 to 12/2012		ftp://ftp.cpc.ncep.noaa.gov/ SBUV_CDR/
GOZCARDS	SAGE I, SAGE II, HALOE, MLS-Aura	02/1979 to 12/2013 Gap: 11/1981 to 10/1984	R. Wang et al., 2013	https://gozcards.jpl.nasa.gov/
SAGE II, V7.0	SAGE II	10/1984 to 08/2005	Damadeo et al., 2013	https://eosweb.larc.nasa.gov/project/ sage2/sage2_table
HARMOZ	ODIN: OSIRIS, SMR ACE-FTS; Envisat: GOMOS, MIPAS, SCIAMACHY	10/2001 to 12/2012 08/2002 to 12/2011	Sofieva et al., 2013	http://www.esa-ozone-cci.org
NDACC ground-based	lidars, microwave radiometers, FTIRs about 5 stations	late 1980s/early 1990s to 2012/2013, depending on station	Steinbrecht et al., 2009; Vigoroux et al., 2008	http://www.ndacc.org see also Table 2-3
Umkehr	about 5 stations	1956 (Arosa) 1984 (Lauder) to 2012	Petropavlovskikh et al., 2005 ; Tourpali et al., 2007	http://www.esrl.noaa.gov/gmd/ozwv/ umkehr/
Ozonesondes	about 50 stations	Late 1960s / mid-1990s to 2012/2013 depending on station	Smit et al., 2007; Deshler et al., 2008; Thompson et al., 2012	http://www.woudc.org http://www.ndacc.org http://nadir.nilu.no http://croc.gsfc.nasa.gov/shadoz/

Box 2-1. Ozone Trends in Different Coordinates

Different instruments retrieve ozone in different fundamental units. SAGE and lidars, for example, provide ozone number density as a function of altitude. MLS provides ozone mixing ratio as a function of pressure. SBUV retrieves partial column ozone between two pressure levels, equivalent to mixing ratio versus pressure. All these quantities are linked through the background stratosphere (pressure and temperature), which is changing due to ozone and climate changes. Changing temperature and pressure profiles affect the different ozone coordinate systems. Since most ozone data sets come without corresponding temperature measurements, background atmospheres from operational meteorological analyses, or reanalyses (all with uncertainties; see Chapter 4), have to be used for unit conversion. This adds uncertainty to the comparison of ozone trends in different units.

McLinden and Fioletov (2011) assessed these differences using observed decadal temperature trends (see Chapter 4) to determine changes in the standard atmosphere. Stratospheric cooling leads to a contraction of the stratosphere, so pressure and ozone mixing ratio are shifted to lower geometric altitudes. As a result, above the mixing ratio peak (5 hPa, 35 km), lower ozone from higher altitudes replaces higher values at constant height surfaces. This makes ozone trends in mixing ratio versus altitude more negative than in mixing ratio versus pressure. The effect is enhanced for number density versus altitude trends by smaller pressures at the same altitude. Below the ozone maximum, atmospheric "shrinking" due to cooling is less pronounced and the contraction brings down higher ozone mixing ratios from above. Lower temperatures enhance number densities. As a consequence, below ~10 hPa or 30 km, number density versus altitude trends are slightly more positive than mixing ratio versus pressure trends.

The figure panel shows the result of McLinden and Fioletov (2011) applied to trends in mixing ratio versus pressure, *VMR(p)*, and in number density vs. altitude, *nd(z)*. Trends are shown for the two periods: 1979–1997, when both stratospheric ozone and temperature declined; and 2000–2013, when ozone increased and the temperature decreased. The biggest effects of cooling and the largest differences in ozone trends occur above 35 km. The clear 1–2% per decade effect near 2 hPa before 1997 is consistent with differences between upper stratospheric trends from SAGE (*nd(z)*) and SBUV (*VMR(p)*). After 2000, the trend differences are smaller (1% per decade or less), because the temperature decline was 60% less than that before 1997 (see Chapter 4). The substantial uncertainty of ozone trends derived from any given instrument means that the smaller coordinate-related differences after 2000 are hard to resolve.

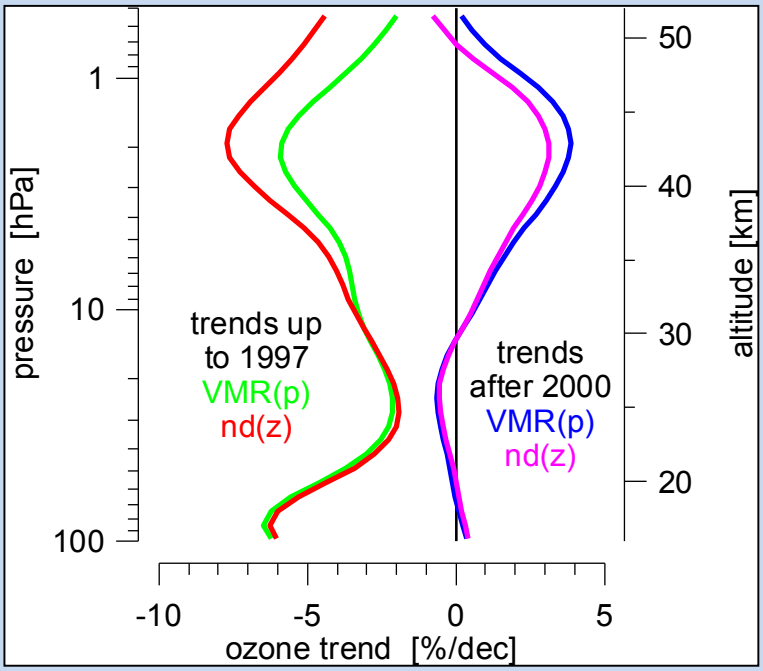

2.2.2 Data Quality

Since the WMO (2011) Assessment there have been small improvements, but no major changes in data quality and uncertainty estimates for ground- and space-based ozone observing systems. Uncertainties for total ozone columns, monthly or annual means, are typically below 1%. Biases of individual systems are typically also 1% or less. Recent studies confirm this: UV total ozone data sets created from GOME, SCIAMACHY, and GOME-2 ozone records (Table 2-1), for example, show very good agreement with ground data and other satellites, within 1% in monthly zonal means, and with drifts generally well below 1%/decade (Weber et al., 2005; Koukouli et al., 2012; Chiou et al., 2014; Lerot et al., 2014). Comparisons of column ozone from SBUV V8.6 with Dobson- and Brewer-spectrometer data also show agreement, 1% or better, over a thirty-year time span (Labow et al., 2013; McPeters et al., 2013).

For ozone profiles, uncertainties are generally larger, of the order of 2 to 5% for the best instruments. Since the last Assessment (WMO, 2011), the SPARC Data Initiative (Tegtmeier et al., 2013), and the SI2N initiative on Past changes in the Vertical Distribution of Ozone (Hassler et al., 2014) have provided platforms to assess accuracy, precision, and stability of existing ozone profile records. Final results from SI2N are not yet available, but nearly all recent studies confirm the general picture that ozone profile uncertainties are smallest between 20 and 40 km altitude (pressures between 50 and 2 hPa), and are usually better than 10% for most instruments, and better than 2 to 5% for some instruments, including SAGE II, MLS, OSIRIS, and GOMOS (Tegtmeier et al., 2013; Adams et al., 2013, 2014; Eckert et al., 2014; Damadeo et al., 2013; Kramarova et al., 2013a; Remsberg, 2014). Above this region, ozone decreases rapidly and uncertainties increase, for many instruments to 20% and more. Diurnal variations also play an increasing role above 30 to 40 km (10 to 2 hPa pressure), see Section 2.3.1. Below 20 km (pressure higher than 50 hPa), transport-driven ozone variability increases considerably. Sharp vertical ozone gradients occur and, especially near the tropopause, ozone concentrations are very low. In this region uncertainties increase substantially, to values larger than 20 to 30%, also due to limitations in sampling and altitude resolution. Limb sounding instruments, for example, have typical altitude resolutions of only 2–3 km in this region (Tegtmeier et al., 2013; Sofieva et al., 2013; Hassler et al., 2014). SBUV ozone retrievals cannot separate contributions from lower stratospheric and tropospheric ozone (McPeters et al., 2013; Kramarova et al., 2013b).

Time series of monthly-mean inter-instrument differences evaluated, e.g., in the SPARC Data Initiative (Tegtmeier et al., 2013; see Figure 2-1) confirm that monthly, zonal-mean ozone values from several limb-sounding satellites usually differ by less than 10–15% near 16 km (100 hPa), and less than 2 –5% near 33 km (7 hPa). Some instruments, however, show substantial drifts and larger biases. A striking example is given in the left panel of Figure 2-1. At this particular pressure and latitude band, one data set (GOMOS) exhibits a clear drift and should probably not be used. Near 7 hPa (see Figure 2-1) SCIAMACHY shows a large time-varying bias against the other instruments, about ±5% in phase with the QBO. For SBUV, a QBO related bias is attributed to SBUV's very coarse altitude resolution (Kramarova et al., 2013b). Good long-term stability and drifts of less than 2% per decade over the altitude range from 20 to 40 km are reported for SAGE, HALOE, UARS MLS, and Aura MLS ozone records against ground-based lidars (Nair et al., 2011, 2012; Kirgis et al., 2013). More details on the various systems can be found in Appendix 2A. Overall, drift uncertainties in the best individual ozone profile records are usually smaller than 2 to 5% per decade, but larger in the lowermost stratosphere. Only multiple independent records allow identification of bad records (like GOMOS in Figure 2-1). Averaging over several records removes noise and improves the precision. In this Assessment, averaging is done (on the basis of anomalies where the average annual cycle and bias of each instrument has been removed) for the HARMOZ record, which combines six European satellite limb sounders. The ozone profile time series in Section 2.2.4 indicate that for the best data sets drifts, and trend uncertainties, better than 1 to 2% can be achieved over the last 10 to 15 years, where many ozone profile records exist. Before 1990, however, only few records exist and profile trend uncertainties are larger.

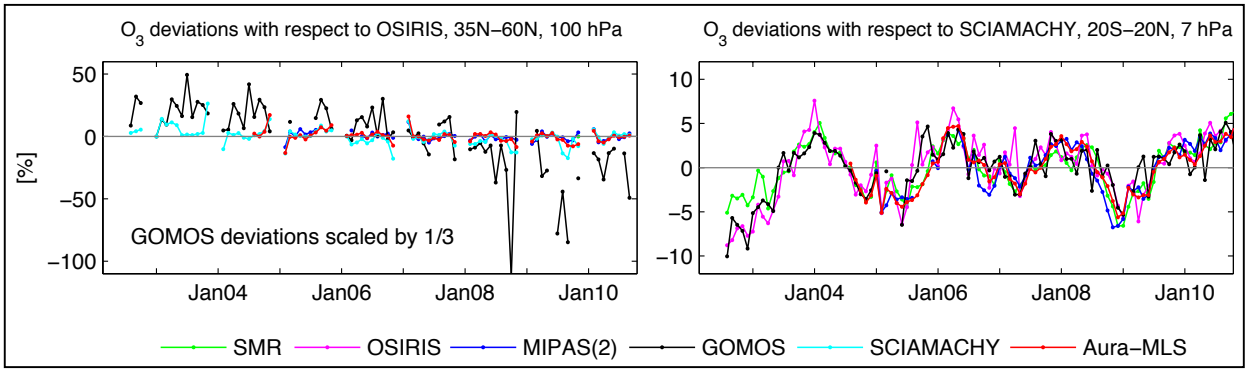

Figure 2-1. Time series showing zonal-, monthly-mean ozone differences between different instruments for 2002–2010. Differences are expressed as a percentage from the reference. The left-hand panel shows differences at northern middle latitudes near 100 hPa, using OSIRIS V5.0 data as the reference data set. Differences are shown for SMR (green), MIPAS (blue), SCIAMACHY (cyan), and Aura-MLS (red). Differences for GOMOS (V5.0) data are also shown (black) but these are scaled by 0.33 as they are much larger than those for the other data sets. Similarly, the right-hand panel shows differences relative to SCIAMACHY (V2.5) near 7 hPa in the tropics. Colors are the same as in the previous panel and the OSIRIS curve is shown in pink. Adapted from Tegtmeier et al. (2013).

2.2.3 Changes in Total Column Ozone

2.2.3.1 Time Series

For the total ozone data sets in Table 2-1, Figure 2-2 shows time-series of annual-mean total ozone anomalies since 1964 for four regions: global (60°S–60°N), midlatitudes in both hemispheres (35°–60°), and tropics (20°S–20°N). Anomalies were computed from monthly zonal mean total ozone data by subtracting the annual cycle over the period 1998–2008, individually for all data sets. This reference period was chosen because: (1) levels of ozone and ODSs were fairly constant from 1998 to 2008; (2) nearly all total column and profile ozone data sets provide data for a large part of this period; (3) it is long enough to cover one solar cycle and provide a stable baseline; and (4) it is not influenced by major volcanic eruptions.

In addition to the observations, the gray range in Figure 2-2 shows the range of simulated total ozone anomalies from the Chemistry-Climate Model Validation 2 activity (CCMVal-2, see Box 2-2: Eyring et al., 2010; SPARC, 2010). This ensemble of simulations from 17 CCMs was used in the WMO (2011) Assessment. Four of the same models have recently simulated ozone time series on the basis of recently updated ODS lifetimes, as described in Chapter 1 and SPARC (2013), but the long-term changes in ozone are virtually the same as those in CCMVal-2 (see Section 2.4.1). Thus the CCMVal-2 ozone results used in WMO (2011) remain viable for use in this Assessment.

The gray range of CCMVal-2 simulations in Figure 2-2 gives the multi-model mean anomaly (from the 1998 to 2008 baseline) and 2 standard deviations of individual annual mean anomalies. The multi-model mean (and standard deviation) comes from 15 CCMs. Two models (MRI and CNRM-CMM) with known deficiencies were omitted (see Oman et al., 2010b; Michou, 2011). This approach to presenting the CCMVal-2 results differs from the last Assessment, where the complex Time Series Adaptive Method (Scinocca et al., 2010; WMO, 2011) was used to define the range of simulated ozone values. Because the TSAM method cannot readily be applied to observed time series, the simpler approach of computing means and standard deviation over sliding five-year windows and multiple models defines the range of simulated interannual, and, to a lesser degree, intermodel variability. The use of a

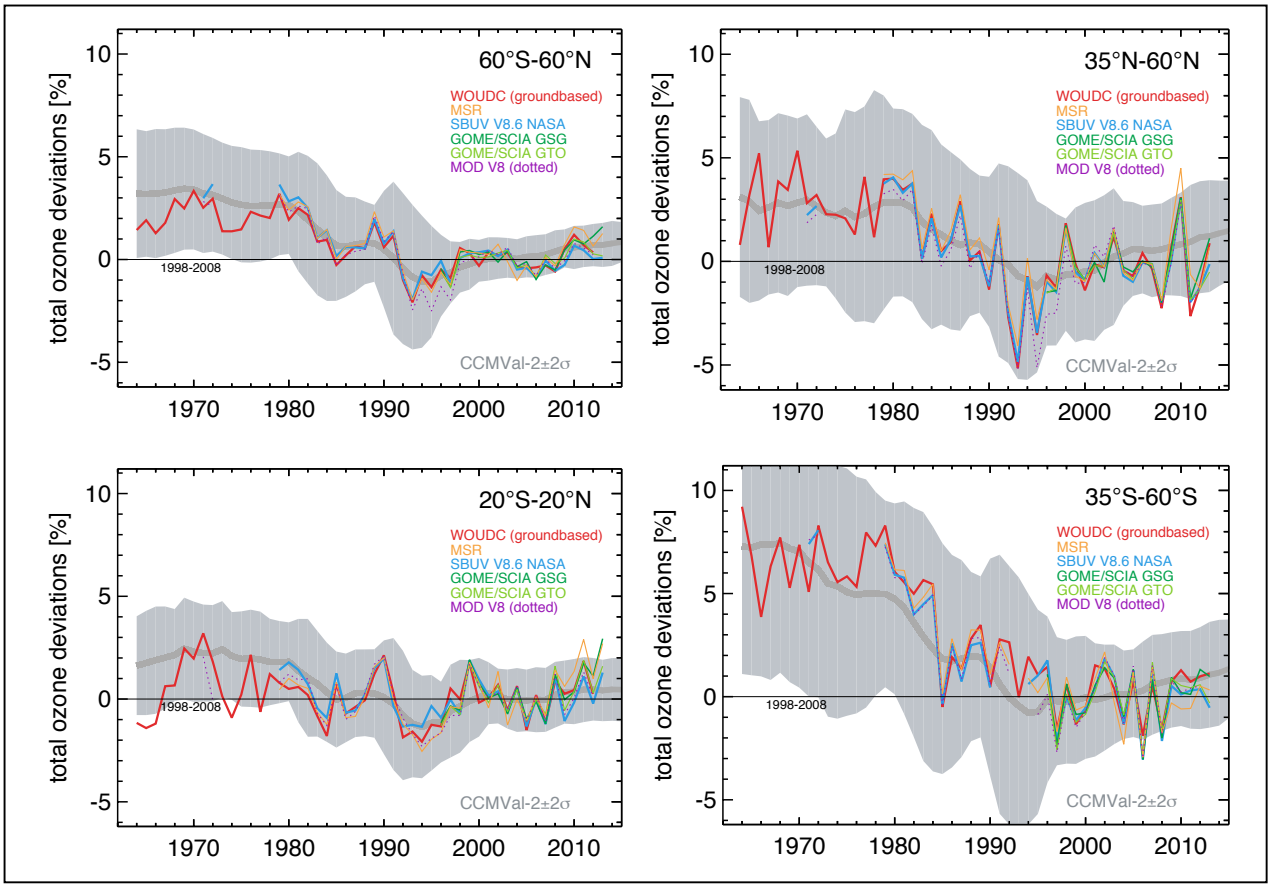

Figure 2-2. Total column ozone annual mean anomalies for different data sets. Anomalies are with respect to the 1998 to 2008 mean of each individual data set. Top left: 60°S–60°N (global), top right: 35°N–60°N (Northern Hemisphere), bottom left: 20°S–20°N (tropics), bottom right: 35°S–60°S (Southern Hemisphere). Colored lines give observed results for the data sets from Table 2-1. Gray line and gray range give multi-model mean and ±2 standard deviation range of annual mean anomalies simulated by CCMVal-2 models (Eyring et al., 2010; WMO, 2011). The model simulations account for changing ODSs, GHGs, and a QBO. Up to about 2000, all simulations also account for the 11-year solar cycle, volcanic aerosol, observed sea surface temperatures, and sea ice coverage. After about 2000, sea surface temperature and sea ice are prescribed from other model simulations, and no solar cycle is included for most models. See text for details.

1998–2008 baseline spreads systematic differences to the beginning and end of the time series. The nearly identical treatment of simulations and observations in Figure 2-2 (and later Figures 2-5 to 2-8) allows direct comparison of observed ozone variations with the range of simulated interannual variations. Note that reducing the number of models used (e.g., from 15 to 9 or 7) barely changes the width of the gray range in Figure 2-2 and later figures (see also Eyring et al., 2010; WMO, 2011). While recent studies discuss reducing the uncertainty range of multi-model simulations (Charlton-Perez et al., 2010; Strahan et al., 2011; Douglass et al., 2012; Karpechko et al., 2013), by selecting only a few (say, better-performing) models, this has not been done for the present Assessment. One motivation is that scenario uncertainty is not covered by the current CCMVal-2 simulations (all use the same scenario, see next paragraph), but will increase the range of simulated ozone, especially in the second half of the 21st century (Eyring et al., 2013; see also Section 2.4.3).

Box 2-2. Model Simulations

This Assessment uses simulations from a range of atmospheric models that have been used in previous Ozone Assessments and in recent international multi-model intercomparisons. These models can be divided into several general types:

- Chemical Transport Models (CTMs): CTMs are used for detailed calculations of chemical processes, using wind and temperature fields specified from meteorological analyses or from another model. There is no coupling between chemical species and radiation and transport in CTMs. They are often used for investigations of chemical processes.
- Chemistry-Climate Models (CCMs): These models explicitly couple chemical processes to radiation and transport in the model, but generally do not couple to ocean models. The chemistry mechanism can be appropriate for the stratosphere only, the troposphere only, or coupled troposphere-stratosphere investigations.
- Atmosphere-ocean general circulation models (AOGCMs): These models include a dynamic ocean and coupled atmosphere-land-ocean-sea ice interactions and are primarily developed to understand surface and tropospheric climate variability and change. They generally do not include interactive chemistry processes, and rely on prescribed data sets for ozone and other radiatively important species. Until recently, these models typically had coarse resolution in the stratosphere and lower model upper boundaries than CCMs.

While CCMs and AOGCMs have traditionally been used for different purposes, some AOGCMs now include some interactive chemistry and higher upper boundaries. Similarly, some CCMs now include a dynamical ocean and sea ice. CCMs and AOGCMs have been used in three recent multi-model intercomparisons that are drawn on in this Assessment:

- The second *Chemistry-Climate Model Validation (CCMVal-2)* activity (SPARC CCMVal, 2010) is a comparison of CCMs with stratospheric chemistry and a resolved stratosphere. This activity focused on understanding and projecting the evolution of stratospheric ozone and ozone-climate interactions. In these experiments, ozone-depleting substances (ODSs) followed the adjusted halogen scenario of WMO (2007). Greenhouse gases followed the Special Report on Emissions Scenarios (SRES) A1B scenario from the Intergovernmental Panel on Climate Change (IPCC) (2007). See Table 1 (below) for scenarios used. Many results from CCMVal-2 were discussed in the last Ozone Assessment (WMO, 2011).
- The *Coupled Model Intercomparison Project, Phase 5 (CMIP5)* (Taylor et al., 2012) is a comparison of AOGCMs that contributed significantly to the IPCC Assessment Report 5 (IPCC, 2013). Most (80%) of these models do not include interactive chemistry, and only one-third of them resolve the full stratosphere (model tops above 1 hPa). Both historical (1850–2005) and future scenario experiments (2006–2100) are included. See Table 1 for scenarios used.
- The *Atmospheric Chemistry and Climate Model Intercomparison Project (ACCMIP)* (Lamarque et al., 2013) is a comparison of CCMs with troposphere or troposphere-stratosphere chemistry. ACCMIP supplemented the CMIP5 simulations, focusing on tropospheric chemistry-climate interactions.

Box 2-2, Table 1: Summary of chemistry-climate model experiments used for this report.

Activity	Scenario	Model Type	Years	Stratospheric Ozone Forcing (ODS and precursor changes)	Other Forcings	Strato-spheric Chemistry	Interactive Ocean
CCMVal-2 [1]	REF-B1	CCM	1960–~2004	Observed	Observed GHGs, solar variability, volcanic aerosols, SST [x]	Yes	1 of 17 models
CCMVal-2 [1]	REF-B2	CCM	1960–2100	A1 scenario WMO (2007)	SRES A1B GHGs (IPCC, 2007), model SST, fixed solar [x, y]	Yes	1 of 17 models
CMIP5 [2]	Historical	AOGCM	1850–2005	Observed	Observed GHGs, volcanic and anthropogenic aerosols, solar variability [x]	18 out of 45 models	Yes
CMIP5 [2]	RCP 2.6, 4.5, 6.0, 8.5	AOGCM	2006–2100	A1 scenario WMO (2003)	Four RCP scenarios, aerosols, land-use, tropospheric ozone, repeating solar cycle [x]	18 out of 45 models	Yes
CMIP3 [3]	SRES A1B	AOGCM	2000–2099	A1 scenario WMO (2003)	Mid-range GHG emissions, aerosols, tropospheric ozone, fixed solar	No	Yes

[1] WMO (2011); Eyring et al. (2010). [2] Taylor et al. (2012); Eyring et al. (2013). [3] Meehl et al. (2007).
[x] Most CCMVal-2 simulations include a nudged or model-generated quasi-biennial oscillation (QBO), whereas most CMIP5 model simulations do not include a QBO. [y] Several CCMVal-2 models include variable solar cycle forcing in their REF-B2 simulations.

For Figure 2-2, (and Figures 2-5 to 2-8) up to 2004 (1999 for some models), the simulations account for changing ODSs (adjusted A1 scenario, WMO, 2007), changing GHGs (SRES A1B scenario, IPCC, 2007), solar cycle and volcanic forcings, observed sea surface temperatures and sea ice coverage, and the quasi-biennial oscillation (QBO) (REF-B1 scenario, see Table 1 in Box 2-2). After 2004 (or 1999 for some models), the simulations include changing ODSs and GHGs (same scenarios as above), modeled sea surface temperatures and sea ice, and an internally generated QBO (for models that have one), but no volcanic forcing and usually no solar cycle forcing (REF-B2 scenario). Three of the CCMs apply solar cycle forcing. The common 1998 to 2008 baseline and the sliding five-year window allow these REF-B1 and REF-B2 simulations to be combined, but the absence of volcanic and solar forcing substantially reduced the variability range after 2000 in Figure 2-2.

Figure 2-2 extends results from previous Assessments. At midlatitudes, and in the 60°S to 60°N near-global mean, total ozone columns show a clear decline from the late 1970s to the mid-1990s. This decline has stopped. Since about 2000, observed ozone columns have been fluctuating around a more or less constant level (compare with the 1998 to 2008 baseline in Figure 2-2). This long-term behavior is in good agreement with previous Assessments. Agreement between different data sets is also good, typically better than 1% (see also Section 2.2.2).

CCMVal-2 model simulations attribute most of the long-term ozone decrease before the mid-1990s to increasing ODSs and the subsequent leveling off to the small decline of ODSs, by about 15% since 2000 (WMO, 2003, 2007, 2011). The pronounced minimum in the Northern Hemispheric ozone in the 1990s arose from additional loss associated with the Mt. Pinatubo eruption in 1991 and several cold Arctic stratospheric winters (WMO, 2003, 2007, 2011). A clear minimum related to the Mt. Pinatubo eruption was not observed in the Southern Hemisphere (see also Section 2.3.4).

In the tropics, observed total ozone has remained nearly unchanged, with substantial interannual variability due to the QBO, tropical El Niño and La Niña events (El Niño-Southern Oscillation (ENSO)), and the 11-year solar cycle (see previous Assessments and Sections 2.3.2 and 2.3.3). Tropical ozone columns in recent years show a slight increase, as expected, at least in part, from the maximum of solar cycle 24 in 2012 to 2014. In contrast to the observations, which show little long-term column-ozone change from the 1960s/1970s to the 1990s, the CCMVal-2 simulations show a decline (Figure 2-2, lower left). However, this difference is less obvious in Figure 2-2 than reported in WMO (2011). Note that the difference relies on ground-based observations in the early years only, and is roughly twice the 1% systematic uncertainty of total ozone columns from Dobson spectrometers (Fioletov et al., 2008; Labow et al., 2013; Appendix 2A).

Between 60°S and 60°N current ozone levels are on average 2% below the 1964–1980 mean. At northern midlatitudes, ozone levels are on average 3.5% below the pre-1980 values. In the Southern Hemisphere, current levels are on average 6% below pre-1980 values. These numbers are essentially the same as reported in WMO (2011). Figure 2-2 shows superimposed substantial year-to-year variations by several percent, also in the last decade, which clearly complicate the identification of small trends, like the small increase expected since about 2000 from the turnaround of ODS and from model simulations.

2.2.3.2 INTERANNUAL VARIATIONS

Figure 2-3 focuses on ozone variations since the year 2000, a period with little overall change in total ozone levels (see Figure 2-2 and previous Assessments for variations before 2000). Most obvious are the QBO-related variations in the tropics and (usually of opposite sign) in the extratropics (Baldwin et al., 2001). Sometimes the tropical anomalies seem to be exported to the extratropics, delayed by about a year (Tegtmeier et al., 2010). The largest interannual variations occur in winter and at high latitudes, for example the high total ozone at northern midlatitudes in 2002/2003, 2009/2010, and 2013, or in the Southern Hemisphere in late 2002 (polar vortex split) and 2012/2013. Examples for large ozone deficits in the Northern Hemisphere (NH) are 2008 and 2011 (large polar ozone loss: see Chapter 3; Manney et al., 2011), or 2006 in the Southern Hemisphere (SH, largest ozone hole on record: see Chapter 3).

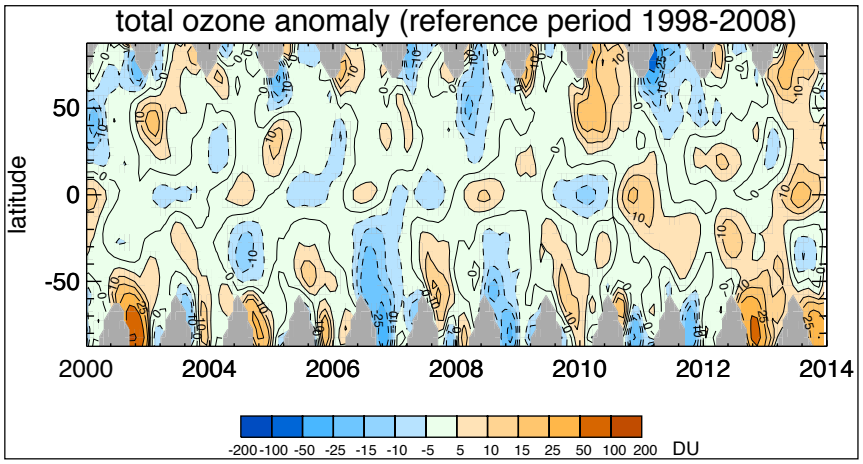

Figure 2-3. Observed monthly zonal mean total ozone anomalies as a function of time and latitude. Results are from the GOME/SCIAMACHY/GOME-2 (GSG) merged data set (see Table 2-1). Anomalies are with respect to the mean annual cycle obtained for the period 1998 to 2008. For clarity, data are smoothed over three months and three 5° latitude bands.

It is well known that these interannual variations are due to year-to-year variations in the strength of the polar winter vortices, (random) stratospheric warmings, and variation of the Brewer-Dobson circulation (BDC), which transports ozone from low latitudes to the winter pole (WMO, 1999, 2003, 2007, 2011). Recent studies have confirmed this and have quantified some of the very large variations observed since the last Assessment. The unusually high total ozone columns in the NH in 2010, for example, are related to the negative phase of the AO (Arctic Oscillation) or NAO (North Atlantic Oscillation) (Rieder et al., 2010a, 2010b; Ossó et al., 2011; Steinbrecht et al., 2011; Weber et al., 2011). Both oscillations are related to the BDC, and both describe nearly the same atmospheric anomalies. In the SH, the Antarctic Oscillation (AAO) plays a role for the high ozone columns in 2012 (Kramarova et al., 2014). Progress has been made on influences from ENSO (Brönnimann et al., 2013; Oman et al., 2013; Rieder et al., 2013; see also Section 2.3.3). Long-term variations in these large meteorological influences, which easily exceed 5% or 15 DU (see Figure 2-3; or Frossard et al., 2013), and uncertainty on the 11-year solar cycle variation (around 2% or 5 DU peak-to-peak, Brönniman et al., 2013; see also Section 2.3.2), complicate detection of the expected small total ozone increase due to declining ODSs, which is only about 1% or 3 DU since 2000; see the CCMVal-2 mean in Figure 2-2.

2.2.3.3 TOTAL OZONE TRENDS

As in previous Assessments (WMO, 1995, 2003, 2007, 2011), multiple linear regression (MLR) is used to estimate ozone trends and to account for the just-mentioned ozone variations due to natural factors (QBO, ENSO, volcanic aerosol, solar cycle). Here we use MLR on the basis of annual means for total ozone and monthly means for profile data (Section 2.2.4). ODS values reached their maximum around 1997 (Chapter 1) and there are different approaches to express ODS changes in the regression:

(a) Two simple linear trends that are not necessarily joined at the ODS inflection time.
(b) Piecewise linear trends (PWLT), with two linear trends connected at the ODS inflection time, or, alternatively, a continuous linear trend plus a trend-change term. Mathematically, both yield the same regressed time series (Newchurch et al., 2003; Reinsel et al., 2005; Jones et al., 2009; Nair et al., 2013; Chehade et al., 2014).
(c) Fitting Equivalent Effective Stratospheric Chlorine (EESC; Newman et al., 2007), as in Yang et al. (2006), Mäder et al. (2010), Steinbrecht et al. (2011), Nair et al. (2013), Frossard et al. (2013), and Chehade et al. (2014).

A disadvantage of fitting EESC is that the ratio of ozone "trend before" to "trend after" (the ODS inflection time) is prescribed by the shape of the EESC curve. While the goodness of EESC fits does indicate overall agreement of ozone and ODS changes, the prescribed shape of the EESC curve precludes the independent estimation of an ozone increase after the ODS maximum. This is possible with PWLT,

and most studies use 1997 as the inflection time (Harris et al., 2008; WMO, 2011), although the exact year is not very critical (Mäder et al., 2010). Low ozone values around the inflection time (e.g., due to Mt. Pinatubo aerosol after 1991) can result in a larger decline before 1997, and a larger increase after 1997 (see Figure 2-2). Therefore, in this Assessment a three-step process corresponding to regression approach (a) is used, similar to Newchurch et al. (2003). (1) A full MLR including PWLT (or EESC) contribution is applied to the time series, mainly to estimate QBO, ENSO, solar-cycle, and aerosol related ozone variations. (2) Ozone "residuals" are obtained by subtracting the QBO, ENSO, solar-cycle, and aerosol variations from step (1). These ozone "residuals" will then be rid of all contributions but still contain the long-term trends. (3) Two simple linear trends, from the beginning of each record up to 1997 and from 2000 to the end of each record, are fitted separately to the ozone "residuals." The year 2000 was selected as starting point for the second trend because: (1) it is after the peak of stratospheric chlorine loading; (2) the period between 2000 and the end of most data records (2011 to 2013) covers one full solar cycle, so this should minimize uncertainties in accounting for the solar cycle; and (3) 2000 is close to the beginning of the Odin- and Envisat-based HARMOZ ozone profile data sets starting in 2001/2002, allowing better comparison with results from this ozone profile data set.

Uncertainties for the derived trends are estimated from the standard deviation of the fit residual, as in Newchurch et al. (2003), Kyrolä et al. (2013), or Gebhardt et al. (2014), and are corrected for first-order autocorrelation in the fit residuals (Weatherhead et al., 2000). Note that this is not enough to account for longer-range correlations, so uncertainty bars may still be underestimated by a factor up to 1.5 (Vyushin et al., 2007, 2010). For the CCMVal-2 simulations, trends are estimated by linear regression, similar to the trend estimation for the observations. Trends are estimated individually for each model from the REF-B2 runs, which do not include forcing by solar cycle and volcanic aerosol. Individual model trends are then averaged over all models. Mean and standard deviation are used as CCMVal-2 multi-model trend and uncertainty (see also Figure 2-25 of WMO, 2011).

Figure 2-4 shows the resulting total ozone trends from 1979 to 1997, and from 2000 to 2013, as a function of latitude. Observed trends, derived by the three-step method, are given by the colored bars, which also give their uncertainty range. Dashed lines show the range of ozone trends obtained from fitting EESC to the observations (Approach c). The gray background gives the range of trends obtained from the CCMVal-2 simulations (see also Figure 2-2). Before 1997, the observed linear trends are negative everywhere, except for the inner tropics, and in good agreement with EESC trends, within uncertainty. Except for the tropics, observed trends before 1997 are also in good agreement with the simulations. These have a larger uncertainty range (Figure 2-2) due to differing sensitivity of models to ODS and other influences (Charlton-Perez et al., 2010; Strahan et al., 2011; Douglass et al., 2012). The negative ozone trends before 1997 are consistent with previous Assessments. Outside of the tropics they are largely due to increasing ODS (WMO, 1999, 2003, 2007, 2011).

After 2000, the computed linear trends are positive, around 1 to 2% per decade, at most latitudes. As expected due to the shorter period, uncertainty bars, ±1 to 2% per decade (2σ), are larger than for 1979 to 1997. Poleward of 40°N, the post-2000 trends are not significant for most of the data sets. SBUV V8.6 trends are not significantly different from zero in the entire NH. Poleward of 30° latitude in both hemispheres, the observed linear trends agree between data sets. There, they also agree with the range of trends obtained by fitting EESC (over the entire 40-year period) and with the range of CCMVal-2 simulated trends. Especially in the NH, transport variations play a significant role (e.g., Kiesewetter et al., 2010; Steinbrecht et al., 2011; Weber et al., 2011; Frossard et al., 2013; Rieder et al., 2013), but are not accounted for in the present regression (as in WMO, 2007, 2011). This contributes to the uncertainties.

Between 30°S and 30°N, however, the large observed 2000 to 2013 trends from ground-based, GOME-SCIAMACHY-GOME-2, and Multi-Satellite-Reanalysis (MSR) data are often outside of the ranges expected from EESC (dashed lines) and simulations (gray range). Trends from SBUV V8.6 (and V8.0) are smaller, and are compatible with EESC and with simulations. The reason for the fairly large positive trends of some data sets in the tropics is currently not clear. Changing the initial year for the trend computation (e.g., from 2000 to 1997) does not change the trends significantly. Figure 2-2 (lower left

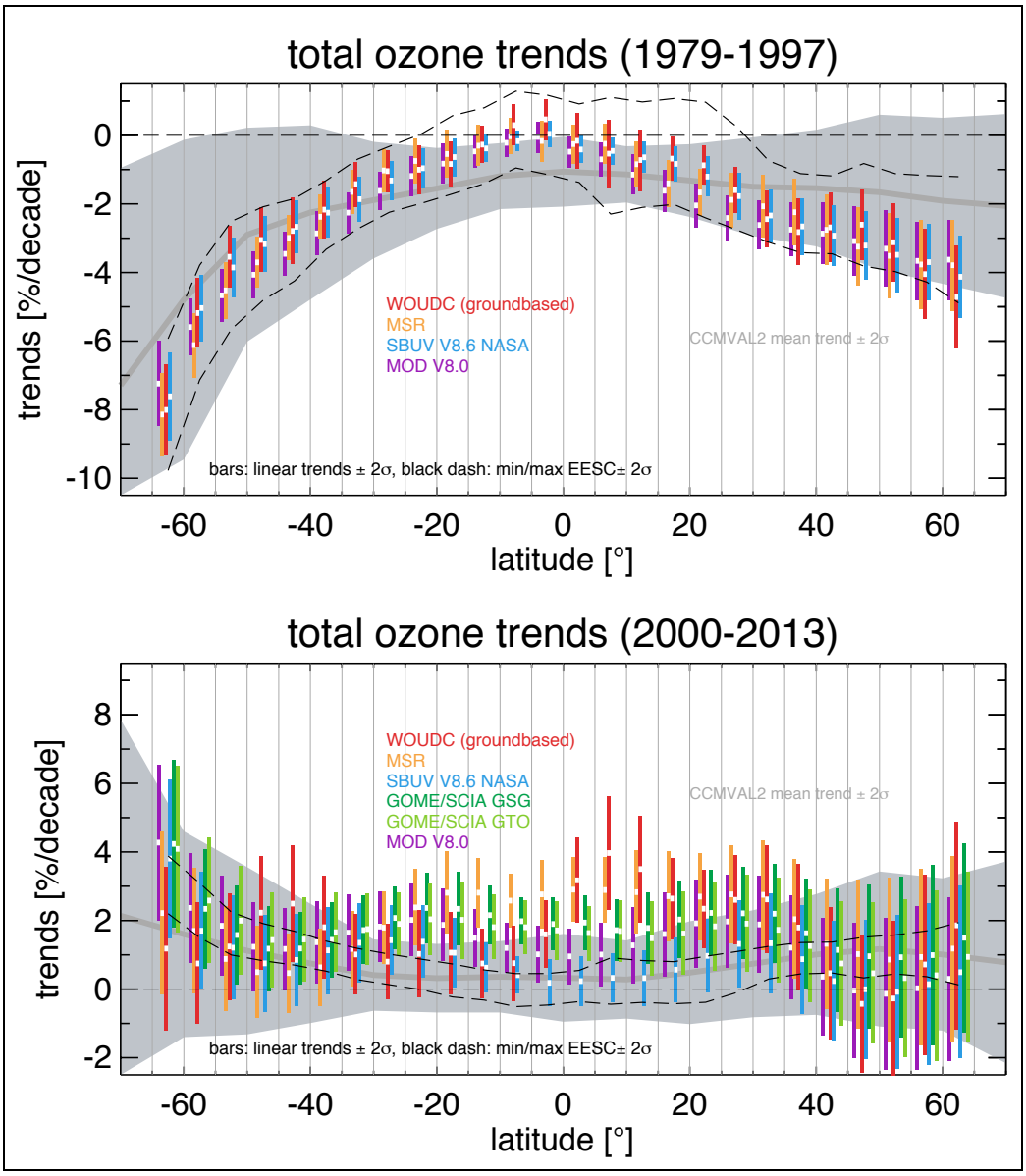

Figure 2-4. Ozone trends for different merged total ozone data sets, as a function of latitude. Top: Trends from 1979 to 1997. Bottom: Trends from 2000 to 2013. Observed trends are derived using multiple linear regression (MLR) to account for solar cycle, QBO, volcanic aerosols, and ENSO. See text for details. The white dots give the linear trend in % per decade, the colored vertical bars indicate the ±2σ uncertainty range from the regression. Gray areas give average trend and ±2 standard deviation range of individual model trends from CCMVal-2 simulations (Eyring et al., 2010; WMO, 2011). Model trends were derived from REF-B2 simulations accounting for ODS and GHG changes, and including an internal QBO, but using only modeled sea surface temperatures and sea ice. Different from Figure 2-2, forcings from volcanic aerosol and 11-year solar cycle were not included in these simulations (except for three models that did include the solar cycle). The black dashed lines give the range of linear trends arising from MLR fits to the observations that include Equivalent Effective Stratospheric Chlorine (EESC) as a proxy for ODS changes. The fitted EESC coefficients usually give a negative ozone trend while EESC increases from 1979 to 1997, and a positive ozone trend while EESC declines from 2000 to 2013. For the EESC, a mean age-of-air of three years and width of 1.5 years were assumed (Newman et al., 2007).

panel) indicates that instrumental uncertainties may play a role, since the different data sets diverge by about 1% in the last years. Also, due to the different lengths of the data sets (50 years ground-based, >30 years SBUV, <20 years GSG), accounting for the solar cycle in the regression may make some difference (see also Section 2.3.2). Uncertainties may also be underestimated (Vyushin et al., 2007, 2010). Discrepancies between simulated and observed total ozone column trends in the tropics, therefore, remain. Before 1997, the decline detected from observations was smaller than in the CCMs (WMO, 1999, 2003, 2007, 2011). Since 2000, the total-ozone increases in some data sets are larger than those simulated.

Figure 2-4 shows that the total ozone column at most latitudes has a positive trend since 2000, but in many regions this trend is not statistically different from zero. This is consistent with WMO (2011) and with more recent studies using station data (e.g., Steinbrecht et al., 2011; Nair et al., 2013; Tully et al., 2013) and global data (e.g., Ziemke and Chandra, 2012; Krzyścin, 2012). As indicated by the black dashed lines for EESC trends in the lower panel of Figure 2-4, ODS-related total ozone increases since 1997 to 2000 should be small, <1% per decade at most latitudes, and not yet be detectable with the large current uncertainty margins of observed trends (mostly > ±1%/decade). Figure 2-4, thus, shows that total ozone has not been decreasing further after the mid-1990s, confirming the effectiveness of the Montreal Protocol. However, a clear attribution of total ozone increases to declining ODSs is not yet possible. This is essentially the same conclusion as reached in the last Assessment (WMO, 2011).

2.2.4 Trends in Ozone Profiles

2.2.4.1 Time Series

Like Figure 2-2 for total ozone, Figures 2-5 to 2-8 show time series of ozone profile annual mean anomalies at selected altitude or pressure levels. Section 2.2.1 and Table 2-2 summarize the profile data sets that were used. Data sets using altitude coordinates are for the altitudes given in the figures; data sets using pressure coordinates are at the given pressures. Ground-based station data are also included, although the number of stations in the tropical and southern midlatitude bands is very limited (see Figure 2A-1 of Appendix 2A). All data sets are normalized to their 1998 to 2008 average annual cycles (same as for total ozone in Section 2.2.3).

These updates and additions give a comprehensive picture of ozone profile variations, but they have not resulted in major changes of our understanding from the last Assessment (WMO, 2011). For the upper stratosphere near 42 km/2 hPa, Figure 2-5 shows the well known ozone decline due to increasing ODS from the 1970s to the mid-1990s (WMO, 1999, 2003). Since 1995 to 2000, the decline is followed by a leveling off, as expected from the turnaround of ODSs after 1997 (WMO, 2007, 2011). In the last years, in most panels, the ozone values are usually above the zero line (=1998 to 2008 climatology), and indicate an ozone increase from around 2000 to 2012 or 2013. This increase is most visible in the 35°N to 60°N and 60°S to 35°S latitude bands. In the tropical band, data in recent years indicate little or no increase, only elevated ozone around the solar-cycle maxima, near 2001 and 2012. For the 60°S to 60°N mean, data points since 2009 also lie above the zero line.

Ozone time series at lower levels (Figures 2-6 to 2-8) also show the ODS-related long-term decline until the mid-1990s, and are generally leveling off since around 2000. However, long-term changes at these lower levels are less pronounced than at 2 hPa. Several aspects of Figures 2-6 to 2-8 are worth mentioning:

- At 31 km/10 hPa and at 26 km/20 hPa (Figures 2-6 and 2-7), QBO-related variations are pronounced, especially in the tropics (Baldwin, 2001; Kirgis et al., 2013; Kramarova et al., 2013b; Gebhardt et al., 2014).
- Near 31 km/10 hPa in the tropics (Figure 2-6), fairly high ozone values are recorded by several instruments between 2000 and 2003, whereas ozone has often been low after 2005. Thus, trend analyses over this period, e.g., of ozone records from instruments on the Odin and Envisat satellites, tend to indicate a decadal decline in the tropics around 31 to 35 km/10 to 5 hPa (Kyrölä et al., 2013; Eckert et al., 2014; Gebhardt et al., 2014).

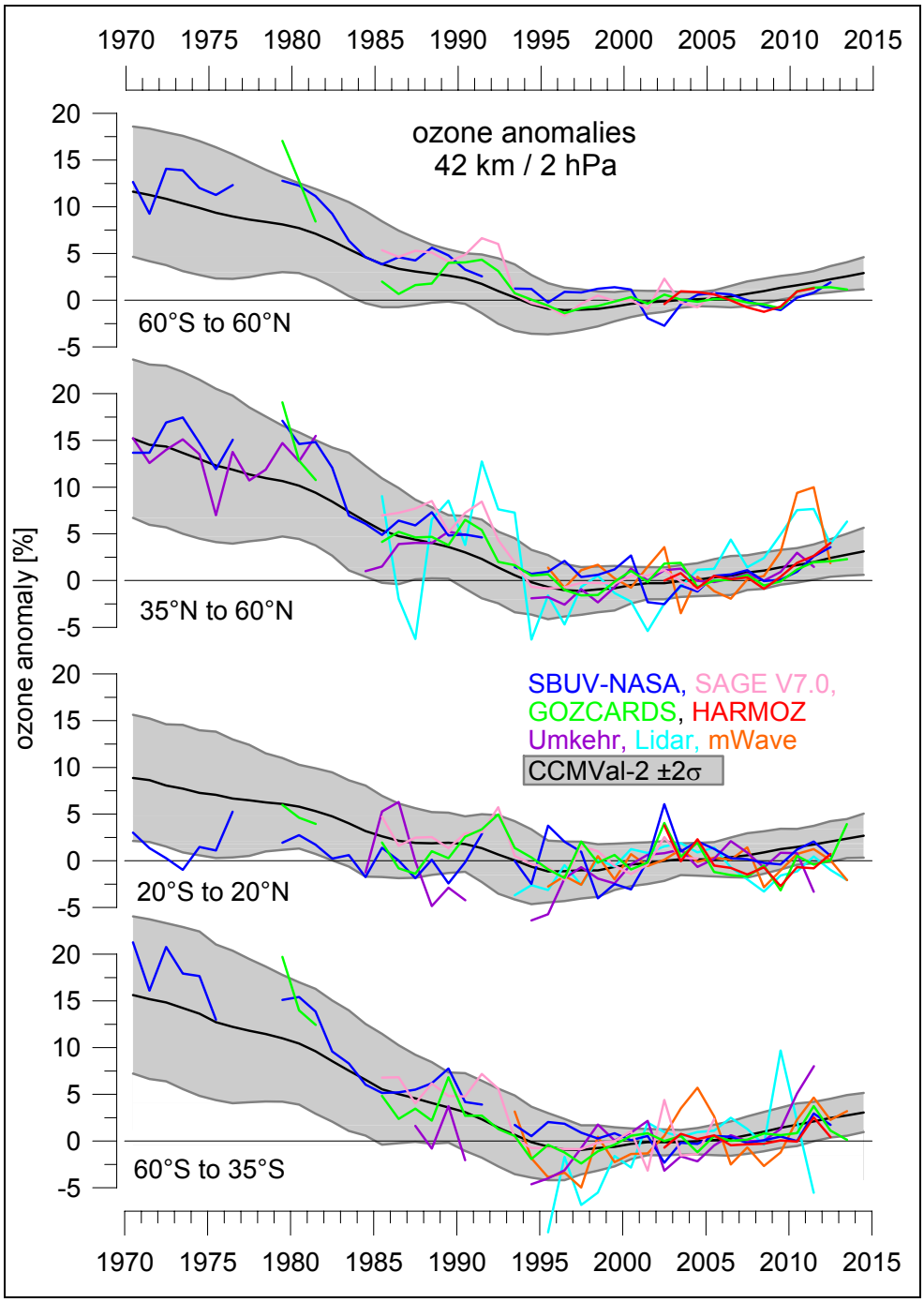

Figure 2-5. Annual mean ozone anomaly time series for different latitude bands, at 42 km altitude (for data sets using altitude coordinates) or at 2 hPa pressure (for data sets using pressure coordinates). Satellite data (see Table 2-2) are based on zonal means. NASA SBUV V8.6 (MOD V8.6) is given in blue, SAGE II V7.0 in pink, GOZCARDS in green, HARMOZ in red. Ground-based station data (Umkehr, lidar, microwave; see Table 2-3, and also Figure 2A-1 of Appendix 2A) are averaged over the zonal bands. Umkehr data in purple, lidar in cyan, microwave data in orange. The gray background gives the CCMVal-2 multi-model mean, and ±2 standard-deviation range of individual annual means, same as in Figure 2-2 for total ozone. All anomalies are with respect to the average annual cycle during 1998 to 2008, determined individually for each data set/instrument/model.

Table 2-3. Remote sensing stations used for ozone profile data sets in this report.

Station	Latitude / Longitude	FTIR	Lidar	Microwave	Umkehr
Lauder	45.0°S / 169.7°E	01/2001 to 12/2012	12/1994 to 06/2012	10/1992 to 10/2013	02/1987 to12/2011
Wollongong	34.4°S / 150.9°E	05/1996 to 12/2012			
Mauna Loa	19.5°N / 155.6°W		07/1993 to 08/2013	07/1995 to 10/2013	01/1984 to 12/2011
Izana	28.3°N / 16.5°W	03/1999 to 10/2012			
Table Mountain	34.4°N / 117.7°W		02/1988 to 08/2013		
Tateno Rikubetsu	36.0°N / 140.1°W 43.5°N / 143.8°E	05/1995 to 12/2009			08/1957 to 12/2011
Boulder	40.0°N / 105.3°W				05/1979 to 12/2011
Haute Provence	43.9°N / 5.7°E		07/1985 to 05/2013		01/1984 to 12/2011
Arosa Jungfraujoch	46.8°N / 9.7°E 46.6°N / 8.0°E	03/1995 to 12/2012			01/1956 to 12/2011
Bern Payerne	47.0°N / 7.5°E 46.8°N / 7.0°E			01/1994 to 12/2012 01/2004 to 12/2013	
Hohenpeissenberg	47.8°N / 11.0°E		09/1987 to 12/2013		

- Near 31 km/10 hPa and 26 km/20 hPa in the Southern Hemisphere (Figures 2-6 and 2-7), recent years indicate an ozone decrease from 2002 to 2005, and an increase from about 2005 to 2011, whereas in the Northern Hemisphere, ozone values were more or less constant over the last decade.
- Consistent with the high total column ozone observed in 2010 in the Northern Hemisphere (see Figures 2-2 and 2-3, and Section 2.2.3; Steinbrecht et al., 2011), the Northern Hemisphere profile data also report high ozone in 2010 from 19 to 31 km/70 to 10 hPa.
- In the tropical lower stratosphere (19 km/70 hPa, Figure 2-8), SAGE II data (V7.0), and the GOZCARDS record, which is based on SAGE II (V6.20), indicate a long-term decline from 1985 to about 2005 (Randel and Thompson, 2011; Sioris et al., 2014). However, also from Figure 2-8 it appears that this decline has not continued over the last decade (Gebhardt et al., 2014). Note further the importance of El Niño in the tropical lower stratosphere, i.e., low ozone values associated with El Niño events (e.g., 1998, 2010), and high values associated with La Niña events (e.g., 1985, 1989, 1999/2000, 2011). See Section 2.3.3 for further discussion.

Unlike the largely ODS-related ozone changes at most altitudes and latitudes, the ozone decline in the tropical lowermost stratosphere (19 km/70 hPa, Figure 2-8) has been attributed to a long-term increase of the mean meridional upwelling of the Brewer-Dobson circulation (BDC) (Randel and Thompson, 2011; Randel and Jensen, 2013), which enhances vertical transport of ozone-poor air in the tropics. CCMs predict such an increase and simulate a continuing ozone decline in the tropical lowermost stratosphere (Eyring et al., 2010; WMO, 2011). However, model simulations (black line and gray range in Figure 2-8) and observations also indicate substantial interannual and decadal variability, and no clear decline since 1997. Observational evidence for the long-term decline before 1997 relies substantially on the high ozone values reported by SAGE II from 1985 to 1990. SAGE II has only sparse sampling in the tropics, but is

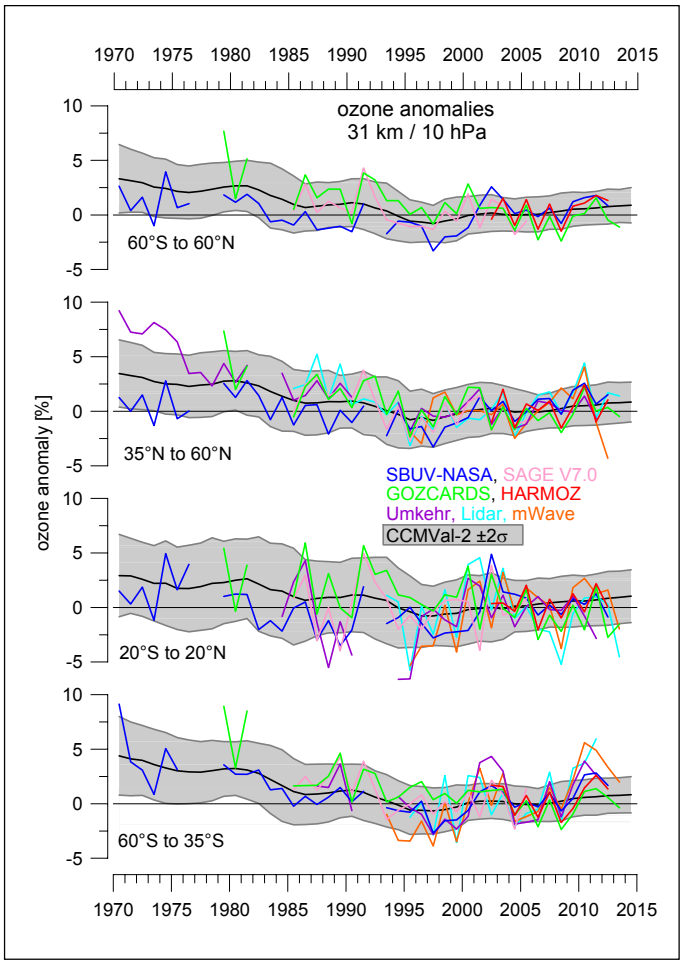

Figure 2-6. Same as Figure 2-5, but for the 31 km/10 hPa level.

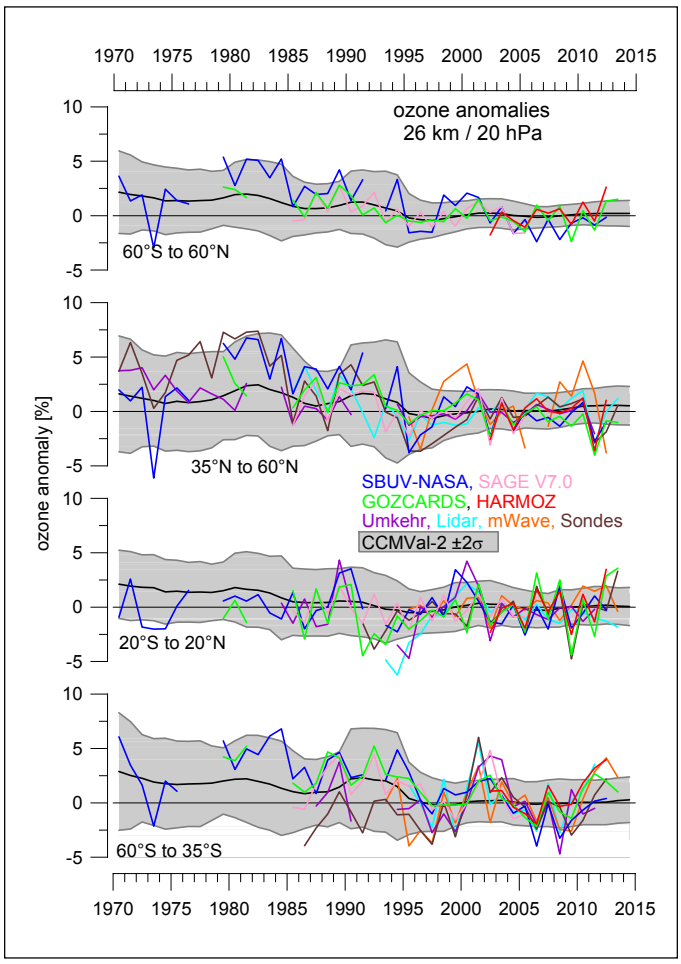

Figure 2-7. Same as Figures 2-5 and 2-6, but for the 26 km/20 hPa level. In addition, data from about 50 ozonesondes stations, averaged over the respective latitude bands are shown (see Figure 2-25). Note that SBUV NASA has only very coarse altitude resolution (10 to 15 km), and reports only one layer from the ground to ≈20 hPa/26 km for the 20°S to 20°N latitude belt.

the only credible observational data set for the tropical lowermost stratosphere before 1991. This, together with the leveling off of ozone in the tropical lowermost stratosphere since about 2000, suggested by multiple data sets in Figure 2-8, means that observational evidence for the modeled long-term ozone decline due to a strengthening BDC remains weak (see also Solomon et al., 2012). For further discussion see Section 2.4.2 and the more comprehensive discussion of the BDC in Chapter 4.

Figures 2-5 to 2-8 also contain information about uncertainty of the available ozone records and about possible drifts. Nearly all data sets show very similar ozone evolution, especially over the last 10–15 years (also due to normalization to the 1998 to 2008 period). The relative differences are larger in the early years (e.g., up to 15% between SBUV, Umkehr, and ozonesondes in the 1970s: Figures 2-6 and 2-7). Before 1985, and before 2000 at 19 km/70 hPa, there are not enough observations to determine ozone levels with a high level of confidence in the tropics and the SH. After 2000, the availability of multiple

and redundant data sets generally provides a higher level of confidence. Sampling issues also play a role, particularly when single station data are compared to zonal means (Gabriel et al., 2011a). This can be seen in the sometimes larger deviations of ground-based station data, such as lidars and microwave radiometers near 2 hPa in the 35°N to 60°N latitude band in 1986 and in 2010–2012 (Figure 2-5), or near 20 hPa from 1994 to 1996 for Umkehr and lidar data at Mauna Loa, which is located at 20°N near the edge of the tropics (Figure 2-8). Generally, however, Figures 2-5 to 2-8 confirm statements about data quality and drifts from Section 2.2.2.

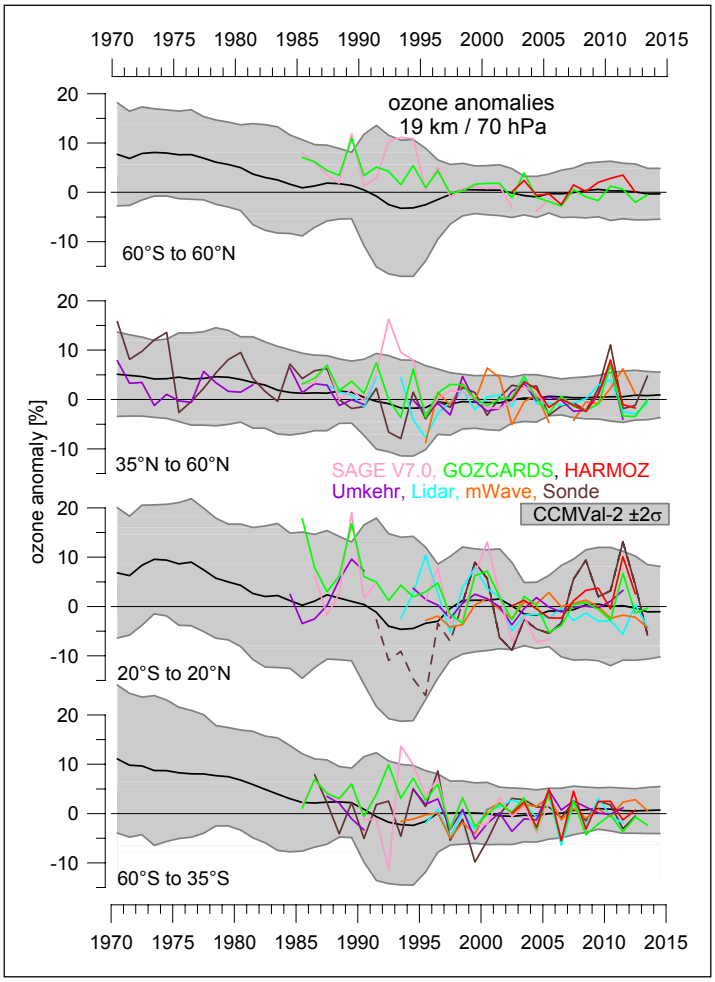

Figure 2-8. Same as Figure 2-7, but for the 19 km/70 hPa level. SBUV NASA data are not included because they have only very coarse altitude resolution, 10 to 15 km, in the lowermost stratosphere. The dashed line for the sonde data in the tropical belt indicates that before 1998 only data from the sonde station at Hilo, Hawaii (20°N), were used here. Umkehr, microwave and lidar data are also only from a few stations, e.g., Hawaii only in the tropical belt.

2.2.4.2 OZONE TRENDS UP TO 1997

Previous Assessments have established the latitude-altitude pattern of ozone decline due to increasing ODSs (WMO, 1999, 2003, 2007, 2011). The largest negative trends, −6 to −8% per decade, were found around 42 km/2 hPa (e.g., Figure 2-4 of WMO, 2011). This section briefly revisits the latitude-pressure pattern of ozone trends before the turnaround of stratospheric chlorine loading, i.e., before 1997, based on the new data sets, and based on the regression described in Section 2.2.3.3.

Figure 2-9 shows resulting linear ozone trends for the declining period up to 1997, for the GOZCARDS data set (in pressure coordinates), which is largely based on SAGE I and SAGE II (V6.20) over this trend period from 1978 to 1997, for the SBUV-NASA data set (trend period 1970 to 1997, in pressure coordinates), and for the SAGE II V7.0 data set (trend period 1984 to 1997, in altitude coordinates). The corresponding pattern from the CCMVal-2 model simulations (trend period 1970 to

1997) is shown as well. Note that small differences between trends can arise from the use of pressure or altitude in different observing systems (Box 2-1).

The observations all show the largest ozone decline near 42 km/2 hPa, between 30° and 70°, in both hemispheres. This highly significant (>3σ) decline is also simulated by the CCMVal-2 models, which show the largest loss near the poles, where SBUV and SAGE cannot observe during polar night. The trends from Figure 2-9 are consistent with previous Assessments (e.g., WMO, 2011), and with recent trend studies based on SAGE II V7.0 data (Remsberg, 2014), as well as the combined SAGE II – GOMOS (Kyrolä et al., 2013) data set. Below 22 km/50 hPa, all observational data sets also report significant ozone decline in both hemispheres. This decline is also largely due to ozone depletion through ODSs, especially near the poles (WMO, 2003, 2007, 2011).

In the tropical lowermost stratosphere below 22 km/50 hPa, the CCMVal-2 simulations indicate a long-term decline that is very pronounced in SAGE-II observations and captured in GOZCARDS, but is absent in the SBUV record. However, SBUV data have only very coarse altitude resolution below 25 km, where the retrieval mixes contributions from stratospheric and tropospheric ozone (Kramarova et al., 2013b).

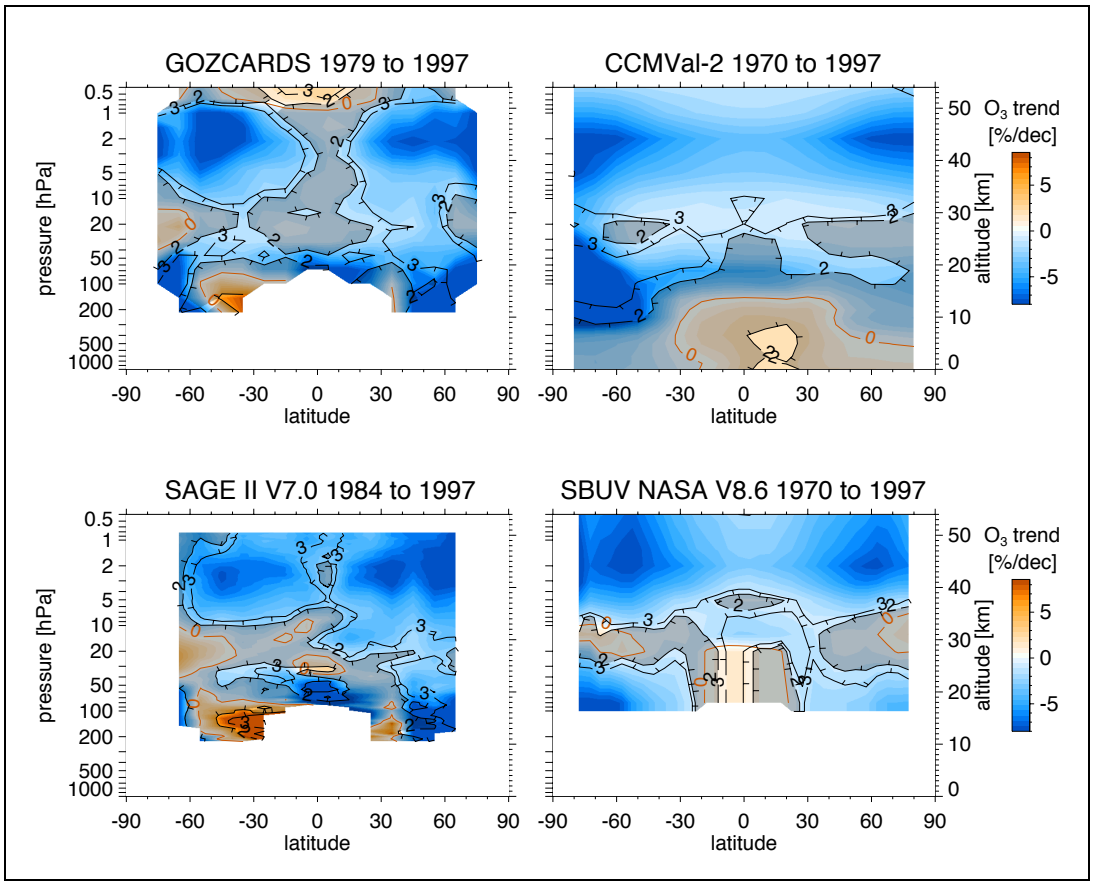

Figure 2-9. Ozone trends (in % per decade) before 1997 as a function of latitude and pressure. SAGE II altitude coordinates are converted to approximate pressure. Results are from multi-linear regression accounting for QBO, solar cycle, volcanic aerosol and ENSO related variations. See text for details. Top left: GOZCARDS record from 1979 to 1997. Top right: CCMVal-2 multi-model mean from 1970 to 1997 (REF-B1 runs, including volcanos and solar cycle, see text). Bottom left: SAGE II V7.0 from 1984 to 1997. Bottom right: BUV/SBUV/2 V8.6 NASA MOD data set from 1970 to 1997. See Table 2-2 for data sources. Trend magnitude is given by the color scale. The black contour lines give the ratio of trend to uncertainty, i.e., the statistical significance of the trends. The line labeled 3 corresponds to 3σ, 2 corresponds to 2σ. Gray shading indicates regions where the trends are not significant at the 2σ level. See text for details on the uncertainties.

2.2.4.3 OZONE TRENDS SINCE 2000

Upper stratospheric chlorine has been decreasing at a rate of 5–6%/decade since about 1997, following a strong increase in the early 1990s (Jones et al., 2011; see also Chapter 1). Despite the clear decline of upper stratospheric chlorine after 1997, a corresponding significant increase of upper stratospheric ozone had not been identified at the time of the last Assessment (WMO, 2011). There was, however, broad consensus that a significant change in the trend of midlatitude, upper stratospheric ozone had occurred in the second half of the 1990s (Reinsel et al., 2002; Newchurch et al., 2003; Miller et al., 2006; Steinbrecht et al., 2009; Jones et al., 2009), and that the negative trend of ozone had slowed down and eventually ended (WMO, 2007, 2011). Ozone time series are now longer and more data sets are available. Several studies have reported statistically significant increases of ozone in the upper stratosphere since 2001 (Kyrölä et al., 2013; Gebhardt et al., 2014; Eckert et al., 2014).

Confirming these studies, Figure 2-10 gives ozone trends since 2000 for three independent observational data sets and for the CCMVal-2 simulations. In the upper stratosphere, between 36 and 48

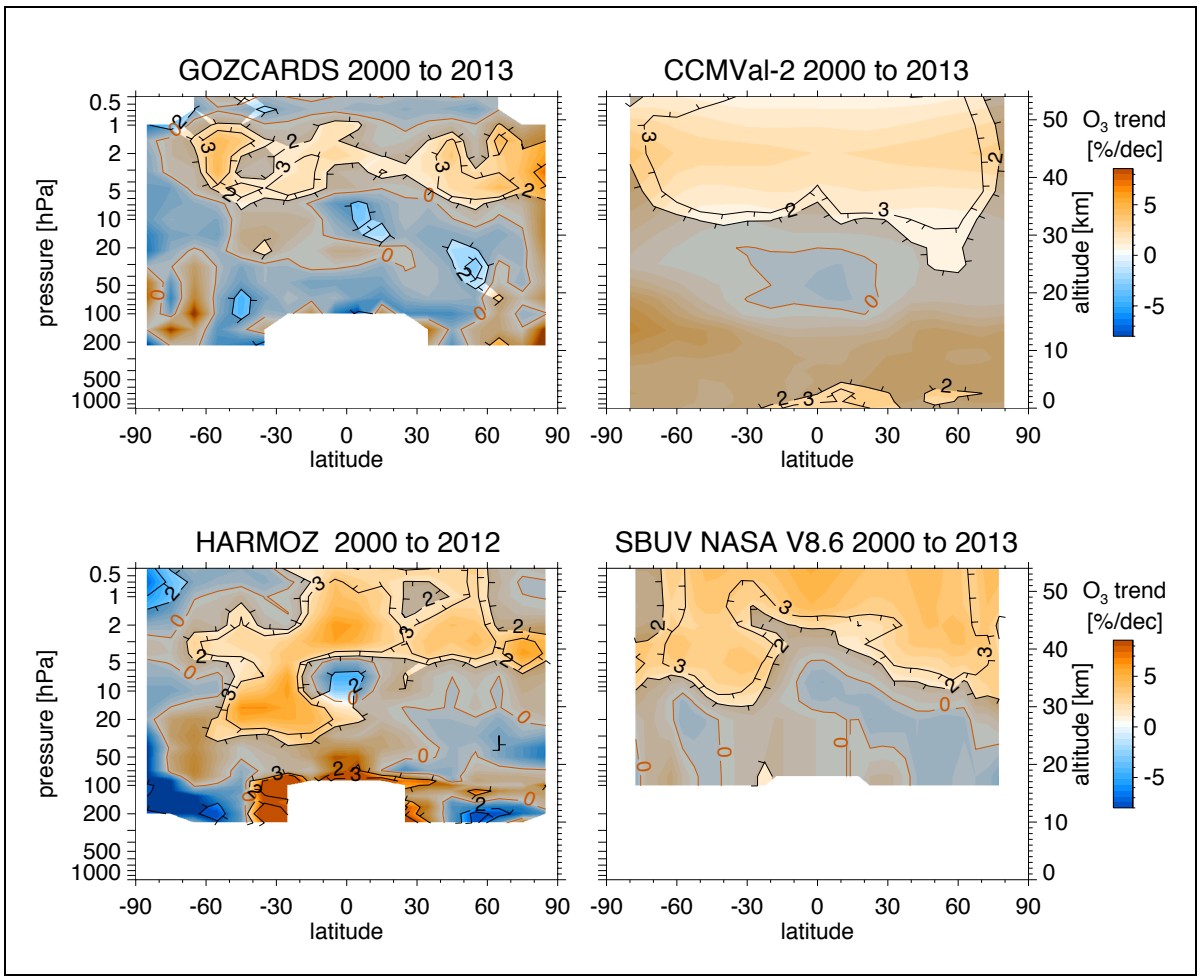

Figure 2-10. Same as Figure 2-9, but for ozone trends (in % per decade) since 2000. In the lower left panel, the trend derived from average ozone anomalies of the HARMOZ data set is given instead of SAGE II V7.0 trends. See Table 2-2 for details on the data sources. CCMVal-2 trend is for the REF-B2 simulations (not including volcanos and solar cycle, see text).

km/5 hPa and 1 hPa, all observations show significant ozone increases, up to 5% per decade, at most latitudes north of 60°S. Very similar increases are reported for individual instruments (Kyrölä et al., 2013; Gebhardt et al., 2014; Eckert et al., 2014). Here, ozone anomalies from these instruments have been averaged to obtain the HARMOZ trend in Figure 2-10. Upper stratospheric ozone increases since 2000, which have a peak near 2 hPa, are generally reproduced by the CCMVal-2 simulations (top right panel of Figure 2-10), although the simulated pattern is much smoother than the noisy observed pattern. Ozone increases in the upper stratosphere were mentioned in Figures 2-7 and 2-25 of WMO (2011). Four additional years of data, the new SBUV V8.6 data, and the additional GOZCARDS and HARMOZ data sets, now confirm these increases. In particular, the statistical significance of the increases is now higher (>2σ) than in WMO (2011).

In the mid- and lower stratosphere, ozone trends since 2000 are generally not significant. In the SH middle stratosphere (around 30 km/15 hPa), HARMOZ and SBUV show significant ozone increases, which are also evident, but not significant, in GOZCARDS. This increase was also reported for GOMOS, SCIAMACHY, and MIPAS by the studies mentioned above. In the NH, the observations show small ozone decreases between 30°N and 80°N at most levels below 32 km/10 hPa. These decreases are not statistically significant. At this point, the interhemispheric difference in Figure 2-10 is interesting, but not statistically significant.

In the tropical stratosphere, 20°S to 20°N, observations agree on decreases between 32 and 36 km/10 hPa and 5 hPa, largely due to high ozone values in the years 2000 to 2003 (see discussion of Figure 2-6; also Gebhardt et al., 2014; Eckert et al., 2014). In the lowermost tropical stratosphere, between 100 hPa and 50 hPa, 16 and 21 km, HARMOZ data indicate an increase, while GOZCARDS (and simulations) indicate a decrease: none of these are significant. There are substantial differences in trends since 2000 computed from individual instruments. Sioris et al. (2014) report a decline for OSIRIS data and Gebhardt et al. (2014) report an increase for SCIAMACHY and Aura MLS data. At this point, differences among trends computed from different data sets in the tropical lowermost stratosphere remain an open question.

2.2.4.4 TREND PROFILES

Trend profiles for the three latitude bands 60°S–35°S, 20°S–20°N, and 35°N–60°N are given in Figure 2-11. Results from the ground-based stations are averaged over available stations in each latitude belt, and are shown along with the satellite zonal mean data. CCMVal-2 model trends are given as gray background. In all three zonal bands, and at most pressure/altitude levels, the observed trends computed for the different observational data sets agree to within uncertainty bars, and for both periods (before 1997 and after 2000). The simulated trends also agree, within the uncertainty limits, with the observed trends. Some uncertainty bars are quite large, especially for the sparse ground-based data. There is only one station providing lidar, microwave, and Umkehr data in each of the tropical (Mauna Loa) and SH (Lauder) belts.

In addition to the individual trend estimates, the average trend of satellite and ground-based data sets is also plotted in Figure 2-11 (thick black line). This average trend is calculated as the weighted mean of the trends from all individual data sets, weighted by their inverse squared uncertainty. In order to account for possible instrumental drifts, a 2% per decade uncorrelated systematic uncertainty has been added to the individual trend uncertainties before building the weighted average. This results in more similar weights, and a larger and more conservative uncertainty estimate for the average trend. Table 2-4 summarizes these observed profile trends and compares them with the observed total column ozone trends from Figure 2-4.

Consistent with Figure 2-9 and previous Assessments (WMO, 1999, 2003, 2007, 2011), the left panel of Figure 2-11 shows significant ozone decline before 1997 at most levels. This decline peaks around 42 km/2 hPa at about −7% per decade in the Northern Hemisphere, at −4% per decade in the tropics, and at −8% per decade in the Southern Hemisphere. Near 26 km/20 hPa, the ozone decline

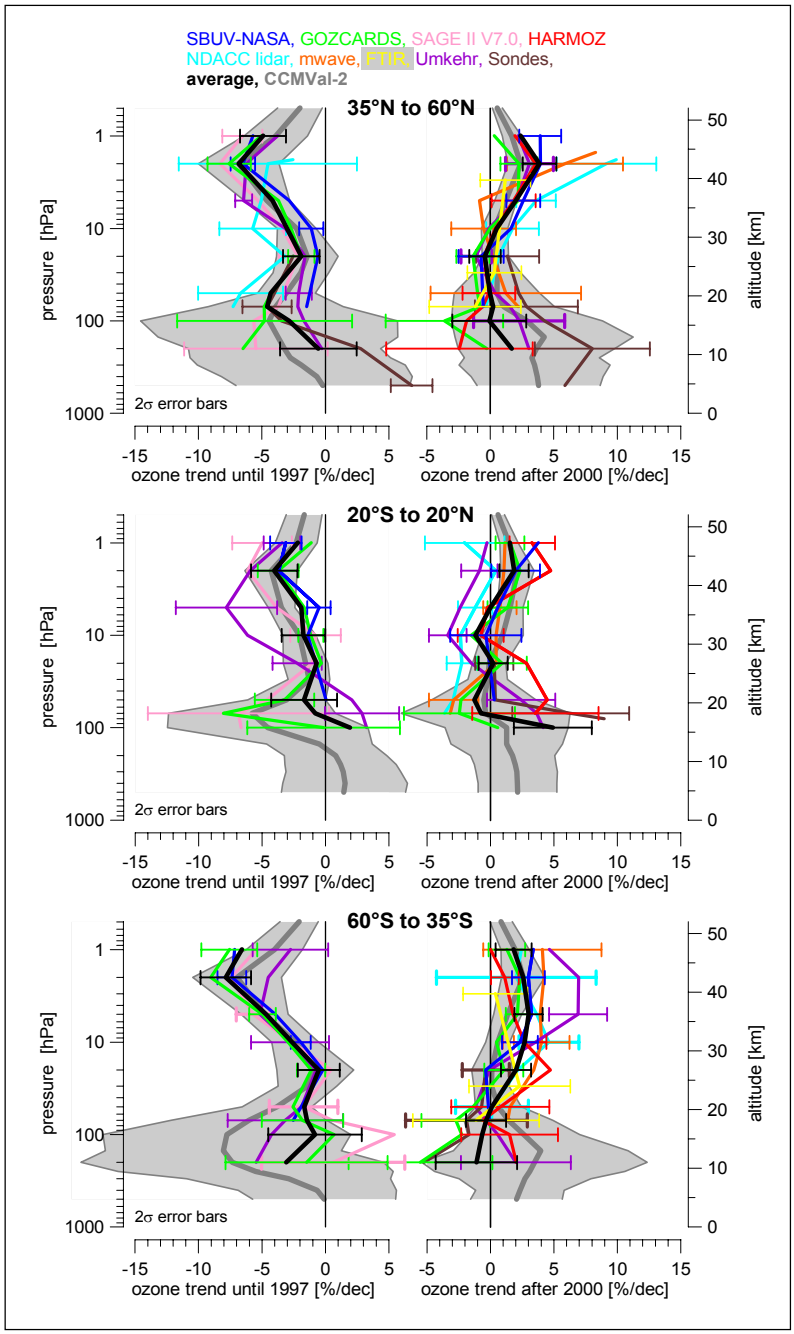

Figure 2-11. Ozone trends for the periods up to 1997 and after 2000 from various observed data sets and CCMVal-2 model simulations and for selected latitude bands. Length of period depends on length of data record for each system. See Tables 2-1 and 2-2. For CCMVal-2 simulations, the trend periods are 1979 to 1997 and 2000 to 2013. Data sets using pressure co-ordinates are plotted on the pressure axis, data sets using altitude coordinates are plotted on the altitude axis. Observed trends are from multi-linear regression accounting for QBO, solar cycle, volcanic aerosol and ENSO, same as in Figures 2-4, 2-9, and 2-10. Gray areas give multi-model average trend and ±2 standard deviation range of individual model trends from CCMVal-2 REF-B2 simulations (not including volcanos and solar cycle, see text).

before 1997 is small and barely significant. A second region with large declines before 1997, but also with large interannual variability and large uncertainty, occurs in the lower stratosphere, where trends peak around 100 hPa, and around −5% per decade. As in previous Assessments, trend uncertainties in the lowermost stratosphere are large, especially around the tropopause (10 km/200 hPa in the extratropics, 17 km/100 hPa in the tropics). This is due both to large natural variability and large gradients in this region (see also the large width of the gray range of model results), and due to less reliable observations at these altitudes.

The right-hand panels of Figure 2-11 indicate significant ozone increases since 2000 near 42 km/2 hPa, by about +3% per decade in Southern and Northern midlatitudes, and by about +2% per decade in the tropics. The CCMVal-2 simulations reproduce these observed increases (gray range in Figure 2-11). Between 16 and 31 km (100 to 10 hPa), ozone trends since 2000 are not significantly different from zero in the Northern Hemisphere, and in the tropics. In the Southern Hemisphere, they are significantly positive above 27 km/20 hPa. This hemispheric asymmetry has already been mentioned (see previous section, and Figure 2-10).

Table 2-4. Summary of ozone trends. Given uncertainty margins are ±2σ. Statistically significant trends are printed in bold. Trends are derived for 1979 to 1997 and 2000 to 2013, as described in Section 2.2.3 for total column ozone and in Section 2.2.4 for ozone profile trends.

Ozone Trends (% per decade)	60°S to 60°N		60°S to 35°S		20°S to 20°N		35°N to 60°N	
	up to 1997	since 2000	up to 1997	since 2000	up to 1997	since 2000	up to 1997	since 2000
Total column	**-2.0±0.7**	+1.1±1.7	**-3.8±1.2**	+1.6±1.7	-0.6±0.7	+1.1±2.1	**-3.3±1.4**	+0.8±2.3
70 hPa / 20 km	**-3.8±2.0**	-0.2±1.4	-1.5±2.9	-0.1±1.6	-0.8±4.0	-0.7±1.8	**-4.6±2.2**	+0.2±1.8
10 hPa / 30 km	**-2.9±1.4**	+0.1±1.1	**-2.6±1.9**	**+2.7±1.2**	-1.7±1.9	-1.2±1.3	**-3.0±1.5**	+0.5±1.2
2 hPa / 40 km	**-6.1±1.7**	**+3.6±1.2**	**-7.8±2.0**	**+2.6±1.3**	**-4.0±1.8**	**+1.9±1.2**	**-6.8±1.8**	**+3.9±1.3**

Positive ozone trends of about +3% per decade near 2 hPa since 1997 (or 2000) were already noted in Figures 2-7 and 2-25 of WMO (2011). Since then, these positive trends have now become clearer and statistically more significant. As discussed later (Section 2.4.2), the CCMVal-2 model simulations attribute this upper stratospheric ozone increase to declining ODSs and to stratospheric cooling by increasing GHGs.

2.2.4.5 Consistency Between Total Column Trends and Integrated Profile Trends

Although the long-term evolution of tropospheric ozone columns is only measured at a few sonde stations, and the vertical resolution and sampling of many instruments are limited in the lowermost stratosphere, it is useful and good practice from past Assessments to compare observed total ozone column trends with integrated profile trends. Generally, the profile ozone trends reported here (Figures 2-9 to 2-11) are consistent within uncertainty bars with the total column ozone trends reported in Figure 2-4. There are, however, two points worth noting:

Previous Assessments (WMO, 2003, 2007, 2011) have discussed that the large ozone decline reported in the tropical lowermost stratosphere from 1984 to 1997 by SAGE II (see Figure 2-8) is not consistent with the observed near constant total column ozone in the tropics. The observed, near-constant total ozone columns in the tropics were also not consistent with the long-term decline simulated by the CCMVal-2 models at these latitudes. New model results presented in Figure 2-12 now indicate that a long-term increase in tropospheric column ozone may resolve this long-standing discrepancy (Shepherd et al., 2014). The model simulation in Figure 2-12 shows good agreement between observed and simulated total ozone columns in the tropics, with little or no long-term decline (top panel). The middle panel shows good agreement also between observed stratospheric ozone columns from limb-sounding satellites and simulated stratospheric columns, both giving significant long-term decline. The new model simulations include a better simulation of tropospheric ozone changes. Figure 2-12 (bottom panel) indicates that a long-term increase of tropospheric ozone columns may have occurred. This could resolve the long-standing discrepancy mentioned above. Unfortunately, reliable long-term observations of tropospheric column ozone in the tropics are not available before 1998, precluding direct observational confirmation of this new model result.

Total ozone column increases of 2% per decade reported from 2000 to 2013 by several data sets (Figure 2-4) are larger than the vertically integrated ozone profile changes between 20°S and 30°N (from Figures 2-10 and 2-11). There, the vertically integrated trends give only small and insignificant column increases of 0–1% per decade, with error bars of about 1% per decade. These vertically integrated changes are, however, consistent with the small total column changes reported by SBUV V8.6 (and TOMS/SBUV V8.0) between 30°S and 30°N (see Figure 2-4). Reasons for the larger total column trends

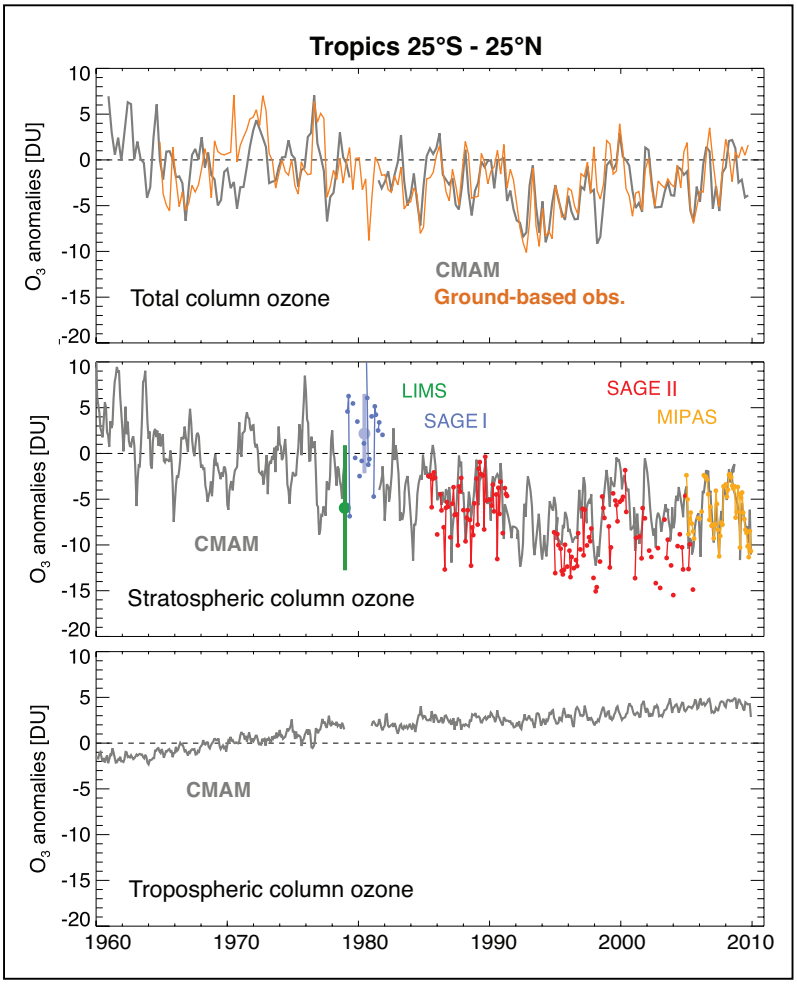

Figure 2-12. Total ozone columns in the tropical belt (top panel), and partial ozone columns for the stratosphere (middle panel) and troposphere (bottom panel). For total column and stratospheric column ozone, results from observations (colored lines) are compared to simulations by one chemistry-climate model (CCM), driven by observed meteorology (gray lines). For the troposphere, a consistent long-term observational record is not available. CCM simulations are from the Canadian Middle Atmosphere Model (CMAM) and are driven by meteorological conditions from the ERA-40 and ERA-Interim reanalyses. Figure adapted from Shepherd et al. (2014).

from some data sets are currently not known. However, as mentioned in the discussion of Figure 2-4, systematic uncertainties in the total column data of the order of 1% have to be considered as well.

2.3 UPDATES ON NATURAL OZONE VARIATIONS

This section discusses recent advances in understanding of ozone variability in the upper troposphere and stratosphere. An assessment of recent advances in diurnal ozone variations (Section 2.3.1) is included to demonstrate the importance of time-of-day sampling in sun-synchronous (and other) satellite observations. This is followed by discussions of recent advances in understanding of low-frequency ozone variability caused by the solar cycle and ENSO. It is well known that these two factors impact stratospheric composition, through their effects on chemistry and transport. As reported again by Kirgis et al. (2013) and Nair et al. (2013), the QBO is also an important contributor to interannual variability, both in the tropics and at higher latitudes (see also Figure 2-3). Dynamical feedbacks in the Earth System lead to effects of originally tropical phenomena, such as the QBO and ENSO, on midlatitude wave structures and wave propagation. This affects the Brewer-Dobson circulation and ozone transport in the stratosphere. Many variations thus impact detection and attribution of long-term changes. Finally, effects of volcanic and other aerosols are discussed in Section 2.3.4, since variations of such aerosols and their impacts on ozone chemistry must also be quantified.

2.3.1 Diurnal Ozone Variations and Their Impacts on Evaluating Long-Term Trends

The diurnal variation of ozone is large and well established in the mesosphere and lower thermosphere, i.e., above 50 km (e.g., Huang et al., 1997; Schneider et al., 2005; Dikty et al., 2010a; Huang et al., 2008, 2010). Since WMO (2011), several studies have improved our understanding of diurnal ozone variations, demonstrating in particular that substantial diurnal variations occur also between 20 km and 50 km and even in the total column (e.g., Sakazaki et al., 2013; Studer et al., 2014).

Diurnal variations of ozone in the tropics and midlatitudes can be obtained from measurements by satellites with non-sun-synchronous orbit. Figure 2-13 shows tropical (10°S–10°N) diurnal ozone variations derived from data from the Superconducting Submillimeter-Wave Limb-Emission Sounder (SMILES) during Northern Hemisphere winter from October 2009 to April 2010 (Sakazaki et al., 2013). At 20–30 km, ozone levels have a maximum in the morning and a minimum in the late afternoon with typical variations of 1% above and below the daily mean. At 30–40 km, ozone levels are smallest after dawn and highest in the afternoon with variations of 2–3% above and below the daily mean. At 40–50 km, ozone concentrations are minimum during daytime and maximum in the late afternoon with variations of 4% above and below the daily mean. UARS MLS and Sounding of the Atmosphere using Broadband Emission Radiometry (SABER) data show a similar altitude and local time dependence in the tropics (Huang et al., 1997, 2010) but there is disagreement about the size of the diurnal variation between the three instruments, particularly in the lower stratosphere.

Measurements of the diurnal cycle in ozone from ground-based microwave radiometers located in the extratropics are consistent with the results from satellites in the middle and upper stratosphere (Haefele et al., 2008; Studer et al., 2014). The vertical resolution of these radiometers is reported to be 6–20 km. The diurnal cycle of ozone levels above two stations in Switzerland (Payerne (47°N, 7°E) and Bern (48°N, 7°E)) and a station at Mauna Loa (20°N, 116°E) shows an afternoon maximum at 30–40 km (approximately 2–4% larger than the nighttime value) and daytime depletion above 40 km. Haefele et al. (2008) and Studer et al. (2013) also noted a seasonal dependence of the diurnal cycle, with the largest amplitude in summer. Figure 2-14 shows their seasonal variations of the diurnal ozone cycle at 5.8 hPa (~35 km in altitude) at 48°N. The peak-to-peak difference is 6% in summer and 3% in winter.

Generally, there is good agreement between the diurnal cycle of ozone in measurements and in CCMs and CTMs (Haefele et al., 2008; Sakazaki et al., 2013; Studer et al., 2014). Figure 2-13, for example, indicates good agreement between SMILES observations and model results for the whole tropical stratosphere. CTMs and CCMs show seasonal variations in the amplitude of the diurnal cycle that are, at least qualitatively, in agreement with space- and ground-based measurements.

The CTM simulations by Sakazaki et al. (2013) show that diurnal ozone variations in the stratosphere can be explained by a combination of photochemical processes (in the altitude region above 30 km) and dynamical processes in association with vertical ozone transport by atmospheric tides.

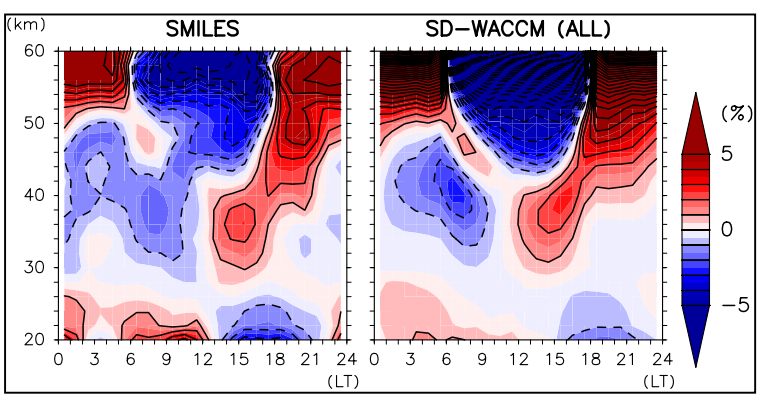

Figure 2-13. Diurnal ozone variations, relative to the daily mean, and averaged over 10°S–10°N, as a function of local time and altitude. Left panel: SMILES observations. Right panel: Specified Dynamics-Whole-Atmosphere Community Climate Model (SD-WACCM) simulation. A low-pass filter (three-point running mean in both time and vertical domains) was applied to the SMILES observations. The WACCM simulation is given for the full grid, not subsampled to the SMILES observation points. Adapted from Sakazaki et al. (2013).

Dynamical processes are important at 20–30 km and at 40–50 km where the vertical ozone gradient is large. Photochemical contributions are important at all latitudes, while the dynamical contributions are important only in the tropics. The latter means that the diurnal variations are enhanced in the tropics, at 20–30 km and at 40–50 km. The combined effect of these dynamical/photochemical changes results in a peak-to-peak difference of up to 1% in the total ozone column in the tropics (Sakazaki et al., 2013). Semidiurnal variations are seen with maxima at 01:00 local time (LT) and 15:00 LT. The former maximum is caused by the variations at 20–30 km due to dynamics, while the latter is caused by the variations at 30–40 km due to photochemistry. In CTM simulations, the diurnal cycle in total ozone is large at high latitudes in the summer hemisphere (e.g., the peak-to-peak difference is up to 6 DU (1.5%) at 70°S and <1 DU (<0.2%) at 70°N in January).

Diurnal variations are important for ozone trend analyses because data from satellite measurements have biases due to the difference in local time of measurements. It is well known that data from solar occultation satellite sensors show a sunset-sunrise bias. The SAGE II sunset profiles exhibit, for example, up to 10% more ozone than the sunrise profiles between 35 km and 55 km in the tropics (McLinden et al., 2009; Kyrölä et al., 2013). The results presented here suggest that at least half of the sunset-sunrise bias in SAGE II can be attributed to diurnal variations. Second, the diurnal variation of ozone should be considered when creating merged ozone time series that combine data from different satellites measuring at different local solar times. Furthermore, the local solar time of satellite measurements may change as their orbits drift. For example, the local time of measurements by Solar Backscatter Ultraviolet (SBUV) instruments on several NOAA satellites changed from early afternoon to late afternoon over a few years (e.g., McPeters et al., 2013). None of the (merged) data sets at this time tries to correct for such diurnal effects. The results presented here indicate that, in severe cases, systematic differences due to changing local times could reach 5% even below 45 km altitude, and more at higher altitudes. Depending on the timescale of satellite changes or local time drifts, trend uncertainties of several percent per decade could result. For instruments with nearly fixed local time sampling, the effects should be substantially smaller, but the need to combine data from several instruments with different sampling complicates the issues.

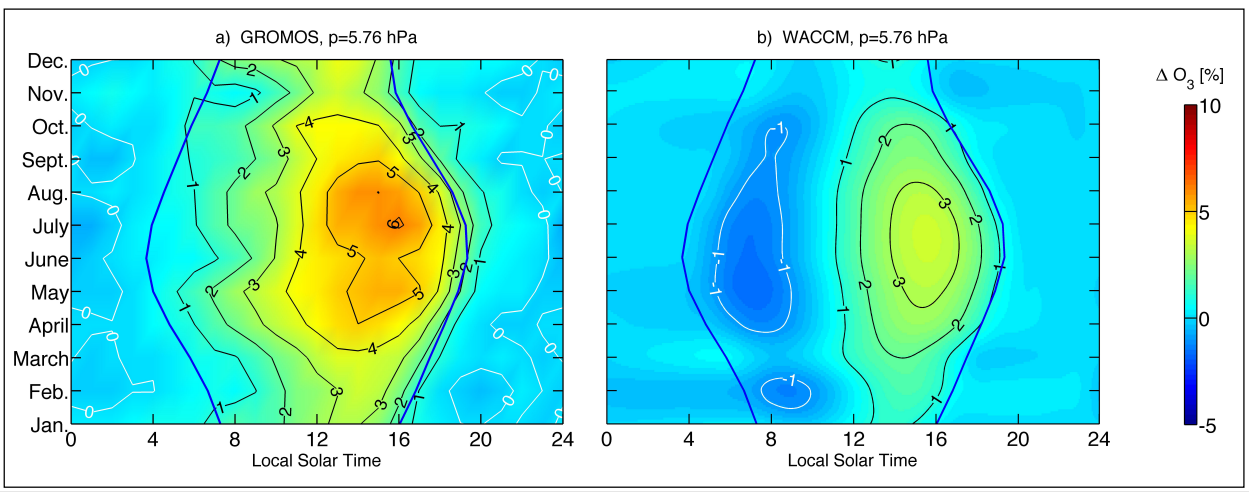

Figure 2-14. (a) Seasonal variation of diurnal ozone cycle with respect to the mean nighttime value (22:30–01:30) at 5.76 hPa/35 km as derived from the Ground-Based Millimeter-Wave Ozone Spectrometer (GROMOS) radiometer measurements at Berne (48°N, 7°E) during 1994–2011. (b) As for (a) but from WACCM free-running simulation. Color bar is shown at the right. Contour interval is 1%. The thick lines near 4 to 8 local time and near 16 to 19 local time give the sunrise and sunset times for Berne, Switzerland. Adapted from Studer et al. (2014).

2.3.2 Solar Variability

WMO (2011) reported a solar cycle effect on upper and lower stratospheric ozone of 2% to 4% between solar minimum and solar maximum. In the tropical middle stratosphere the observed solar cycle response is weaker and statistically insignificant (Soukharev and Hood, 2006; Randel and Wu, 2007). The solar cycle effect on upper stratospheric ozone is a direct radiative effect of heating and photochemistry. The lower stratospheric response in ozone (and also in total column ozone), however, occurs predominantly through a dynamical response to solar ultraviolet variations (e.g., Sitnov, 2009; Hood and Soukharev, 2012). The exact mechanism of the dynamical response to solar cycle variations is not fully understood and cannot be reproduced fully by CCMs (Gray et al., 2010). Ozone changes in the middle and upper stratosphere are also in phase with 27-day sun-rotation UV variation (Fioletov, 2009; Gruzdev et al., 2009; Dikty et al., 2010b; Kubin et al., 2012).

Remsberg and Lingenfelser (2010) and Remsberg (2014) found a stratospheric 11-year solar ozone response of around 2% for HALOE data and a response of up to 4% for SAGE II data. The differences between HALOE and SAGE II in the upper stratosphere solar response can be in part explained by the conversion between pressure and height coordinates that are used by the two data sets (see also Box 2-1). A minimum ozone response to the solar cycle in the middle stratosphere reported by Randel and Wu (2007) was not confirmed by Remsberg and Lingenfelser (2010). From a combined SAGE II/GOMOS data set, a solar cycle-induced stratospheric ozone response of 1–3% was derived (Kyrölä et al., 2013). These values are all in accord with WMO (2011).

Regarding total column ozone, in line with earlier studies (e.g., WMO, 2007, 2011), Hood and Soukharev (2012) confirmed a solar-induced 3% change in total column ozone from the SBUV/TOMS data set. This solar total ozone response is visible in the time-series of Figure 2-2, particularly in the tropics. The solar modulation of total ozone is likely driven by decadal variations of the Brewer-Dobson circulation (BDC) (Hood and Soukharev, 2012). Model simulations show that zonal asymmetries in the ozone, water vapor, and temperature fields are modulated by the 11-year solar cycle (Gabriel et al., 2011b). This provides a direct link between the solar cycle, zonal asymmetries, planetary waves, and the BDC, all of which affect stratospheric ozone.

Based on a CTM driven by analyzed meteorological fields, a double-peak profile with a minimum in the middle stratosphere was found in the tropical solar cycle (Dhomse et al., 2011), in agreement with Randel and Wu (2007). This modeled solar response was in better agreement with HALOE than with SAGE-corrected SBUV (McLinden et al., 2009) or SAGE II. However, uncertainties in analyzed upper stratospheric temperatures and in the various ozone data sets still complicate the assessment of solar responses in models and observations (Dhomse et al., 2011).

Since solar irradiance variations over the 11-year solar cycle are the main driver of the corresponding ozone variation, data from the Solar Radiation and Climate Experiment (SORCE) satellite, suggesting a significantly stronger variability by a factor of 4–6 in the ultraviolet (UV) spectral range compared to other solar data (Harder et al., 2009; Haigh et al., 2010; Figure 2-15), have received a lot of attention. Most spectral solar irradiance (SSI) observations and solar models, with the exception of SORCE, had so far provided a qualitatively consistent picture of SSI variability over the 11-year solar cycle.

In order to preserve total solar irradiance (TSI or solar constant), which is SSI integrated over the entire wavelength range, the large UV variability reported for SORCE data by Harder et al. (2009) requires that the visible SSI from SORCE has to decrease from solar minimum to solar maximum. Most solar models and other observations, however, indicate a positive (but weak) change in the visible (Ermolli et al., 2013; Figure 2-15). A careful analysis of the green spectral channel of VIRGO (Variability of solar IRradiance and Gravity Oscillations) confirmed a positive SSI change in the visible toward solar maximum (Wehrli et al., 2013). DeLand and Cebula (2012) and Lean and DeLand (2012) provide arguments that the SORCE data may be affected by optical degradation during the first years of the mission, near solar maximum. An additional investigation on the SORCE SSI variability closer to

solar minimum came to the conclusion that the SORCE UV SSI variability is about halved from the original studies but still higher than other observations and solar models (Ermolli et al., 2013; see Figure 2-15).

The large UV variation from SORCE has triggered several reinvestigations, comparing CCM runs using both the SORCE SSI and Naval Research Laboratory Solar Spectral Irradiance Model (NRLSSI) reconstructions. NRLSSI is representative for typical SSI variations assumed before SORCE data become available, and is commonly used in CCM simulations (e.g., Morgenstern et al., 2010). The CCMs generally showed a larger in-phase solar ozone response in the lower and middle stratosphere and out-of-phase (opposite) response above 37 to 45 km for simulations using SORCE SSI compared to simulations using NRLSSI (Haigh et al., 2010; Merkel et al., 2011; Swartz et al., 2012; Ermolli et al., 2013; see Figure 2-16a). SABER (2002–2010) and Aura MLS (2004–2007) daytime ozone observations seem to confirm the anti-cyclic ozone behavior in the mesosphere (Haigh et al., 2010; Merkel et al., 2011). Other results remain inconclusive as to which CCM simulations fit the observations better (Swartz et al., 2012; Shapiro et al., 2013; see Figure 2-15a). CTM simulations with different SSI implementations, including SORCE SSI, also provide very similar ozone responses in the middle atmosphere (Dhomse et al., 2013).

In the upper stratosphere and mesosphere, ozone is influenced substantially by odd-hydrogen (HO_x) chemistry. The observed decadal variability of hydroxyl (OH) total columns above 21 hPa, on the order of 7%, matches CCM results using SORCE SSI better than using NRLSSI (S. Wang et al., 2013). Many CCMs and general circulation models (GCMs) also show larger stratospheric temperature and shortwave heating rate responses for the SORCE SSI (Cahalan et al., 2010; Oberländer et al., 2012; Swartz et al., 2012; Ermolli et al., 2013). The modeled solar response of total ozone using SORCE SSI agrees better with SBUV/TOMS satellite data, but the run with NRLSSI agrees better with ground-based data (Swartz et al., 2012; Figure 2-16b).

In summary, recent studies have confirmed a 2–4% variation of stratospheric ozone (3% in total ozone) in phase with the 11-year solar cycle. However, the exact shape of the solar response profile depends on the type of data and/or analysis, the length of data records, and the time periods under investigation. There is evidence that SORCE SSI strongly overestimates UV solar cycle variability. However, a clear conclusion on which SSI fits ozone observations best can currently not be drawn, because (1) available ozone records are too short (only a few solar cycles), and have limited accuracy, (2) spectral resolution of the radiation schemes in global models is not sufficient (Oberländer et al., 2012; Swartz et al., 2012), and (3) solar cycle induced changes in atmospheric transport compete with the direct radiative effects (Shapiro et al., 2013; Dhomse et al., 2013).

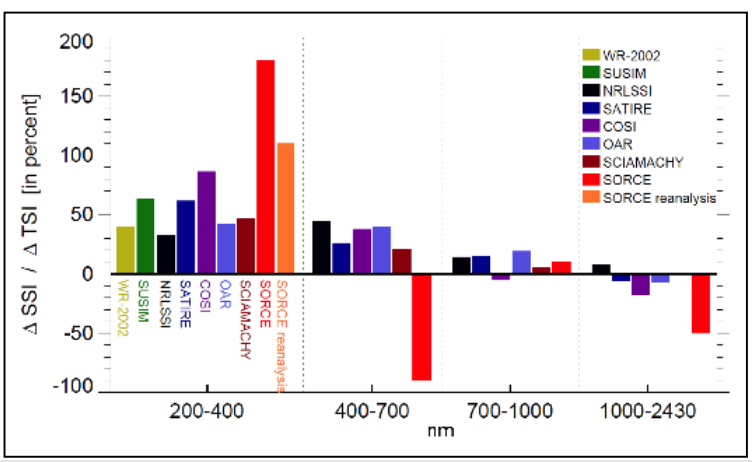

Figure 2-15. Spectral solar irradiance (SSI) changes over a solar cycle and in various spectral regions. SSI changes are normalized to total solar irradiance changes (TSI, solar constant), and are given for several data sets. WR-2002 (Woods and Rottman, 2002), SORCE, Solar Ultraviolet Spectral Irradiance Monitor (SUSIM), and SCIAMACHY are derived from observations. SATIRE, COSI, and OAR are solar models. NRLSSI is a solar reconstruction from Lean (2000). Except for SORCE (2004–2008) all values were derived from solar maximum to minimum conditions. As reported in Ermolli et al. (2013) a reanalysis of SORCE data close to solar minimum in 2009 revealed a weaker sensitivity in the UV, shown as SORCE reanalysis here. Adapted from Ermolli et al. (2013).

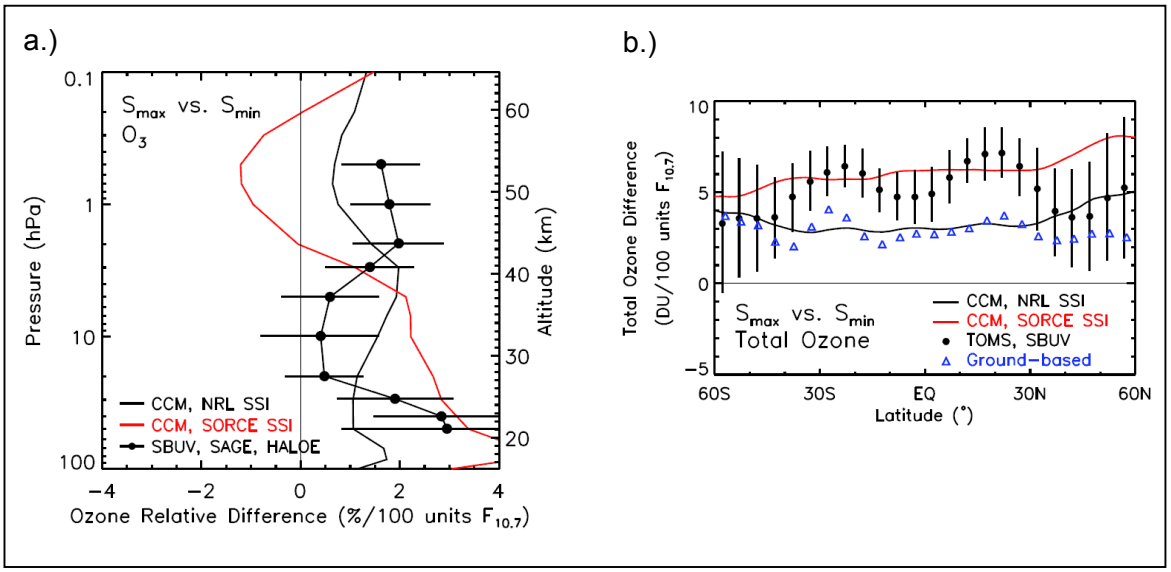

Figure 2-16. Solar cycle response of ozone from Goddard Earth Observing System Chemistry-Climate Model (GEOSCCM) simulations using SORCE SSI (red line) and NRLSSI (black, Lean and DeLand, 2012). a.) Comparison to profile response in SAGE II data from Randel and Wu (2007). b.) Comparison to response in zonal mean total ozone from SBUV/TOMS data and from ground-based Dobson and Brewer data. Both panels from Swartz et al. (2012).

2.3.3 Variations Associated with El Niño-Southern Oscillation

The El Niño-Southern Oscillation (ENSO) is an important mode of interannual variability in the tropical ocean and atmosphere. ENSO-forced variations in tropical upwelling lead to temperature and water vapor variations in the tropical lower stratosphere and have impacts on the chemistry and transport of ozone (e.g., Randel et al., 2009). Atmospheric teleconnections lead to ENSO-related impacts on the strength of planetary waves and the Brewer-Dobson circulation. Both affect stratospheric ozone distributions in middle and high latitudes.

Since WMO (2011), several studies have refined our understanding of ozone variations associated with ENSO. Randel and Thompson (2011) describe ENSO-related variations of tropical ozone found in the SAGE II and Southern Hemisphere Additional Ozonesondes (SHADOZ) data sets. In the tropical lower stratosphere (17–21 km), ENSO warm events lead to enhanced tropical upwelling that results in a reduction of zonal-mean ozone concentrations. A similar analysis using combined SAGE II and OSIRIS ozone data (Sioris et al., 2014) demonstrates that ENSO cold events (La Niña) in 1988–1989 and 1999–2000 led to positive anomalies in lower stratospheric ozone, see also Figure 2-8. Oman et al. (2013) used the spatially dense MLS and Tropospheric Emission Spectrometer (TES) observations to demonstrate the zonal symmetry of the ENSO signal in stratospheric ozone. ENSO-related signals (Figure 2-17) are strongest just above the tropical tropopause; at higher levels they appear with a one- to two-month delay and are weaker than QBO-related signals in ozone.

In contrast to the zonal-mean response in the lower stratosphere, these studies (Randel and Thompson, 2011; Oman et al., 2013) isolate a strong longitudinal dependence of the ENSO influence on tropical tropospheric ozone, which peaks in the upper troposphere (11–16km). It is also detected in total column ozone (Ziemke et al., 2010). This spatial structure is defined by an out-of-phase relationship between the Indonesian/western Pacific (high upper tropospheric ozone during ENSO warm events) and eastern Pacific regions (low ozone during ENSO warm events). Simulations using GEOSCCM (Oman et al., 2011, 2013), which include no year-to-year variations in biomass-burning emissions of ozone

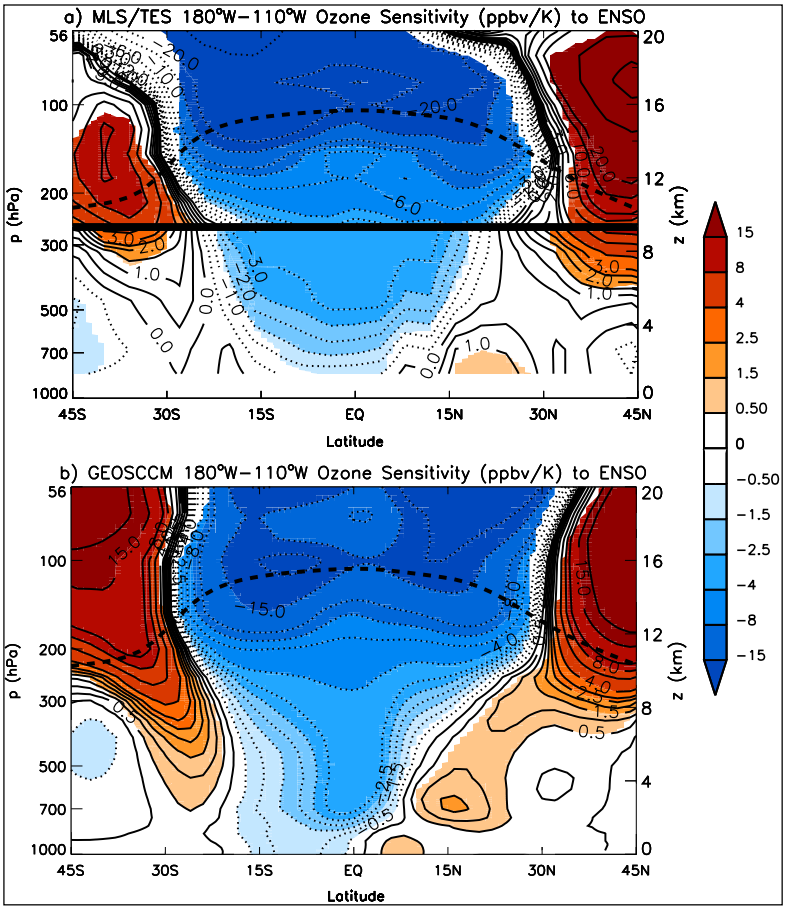

Figure 2-17. Sensitivity coefficient of ozone over the eastern Pacific (longitudinal average from 180°W to 110°W) to sea surface temperature anomalies in the Niño 3.4 region of the tropical Pacific (parts per billion by volume (ppbv) per Kelvin). Results of multiple linear regression analysis by Oman et al. (2013). Top panel: Observation results from Microwave Limb Sounder (MLS) and Tropospheric Emission Spectrometer (TES). The thick black line at 260 hPa separates MLS data used above from TES data used below. Bottom panel: Same for model simulations by the GEOSCCM model. Only regions that are significant at the 2σ level are colored. The dashed black line gives the mean model tropopause. From Oman et al. (2013).

precursors, demonstrate that the ENSO-related longitudinal structure is mainly caused by changes in atmospheric circulation that impact transport and photochemistry. Impacts of ENSO-related variations of biomass-burning emissions might have additional effects (e.g., Ott et al., 2010).

Several studies have examined the sensitivity of midlatitude ozone columns to the occurrence of ENSO through changes in planetary waves and their propagation and damping in the middle atmosphere (e.g., Hood et al., 2010; Gabriel et al., 2011b). Extratropical ozone variations due to ENSO are opposite to the tropical effects (Figure 2-17). There is also some evidence for hemispheric asymmetry, especially in the West Pacific (70°E–140°E). Smaller or negative sensitivity of ozone to ENSO is found in the SH midlatitude lower stratosphere, at least in these short records since 2004. Rieder et al. (2013) show a spatially complex relationship between midlatitude ozone column and ENSO index in both hemispheres during December-January-February and March-April-May between 30° and 50°N. Brönnimann et al. (2013) showed a similar zonal mean response to ENSO using an assimilated ozone data set covering much of the 20th century.

2.3.4 Effects of Increased Stratospheric Aerosol Loading

Previous Assessments have described how stratospheric sulfate aerosols impact ozone concentrations through both direct impacts on heterogeneous chemical processes and indirect impacts on temperature and transport. Figure 2-18 (Trickl et al., 2013) shows the well-documented, rapid increases in sulfate aerosol loading associated with the El Chichón (1982) and Mt. Pinatubo (1991) volcanic eruptions

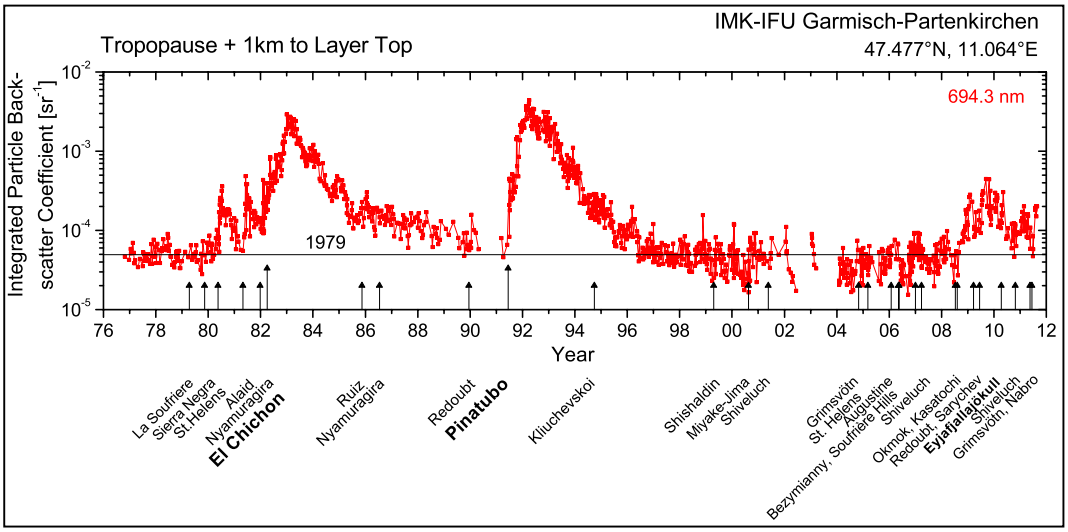

Figure 2-18. Aerosol backscatter coefficient measured since 1976 by lidar at Garmisch-Partenkirchen (47.5°N, 11.0°E) as a measure of stratospheric aerosol loading. Backscatter coefficient is integrated over the stratospheric aerosol layer, from 1 km above the tropopause to above 30 km altitude. Arrows mark the eruption of volcanoes that have, most likely, resulted in the observed aerosol enhancements. Note the recent aerosol enhancement after 2008. From Trickl et al. (2013).

followed by several years of gradual reductions. The figure also reveals an increase in the stratospheric aerosol burden after 2006 to 2008.

The recent aerosol increases are likely to impact stratospheric ozone. The 4–10% increase in the stratospheric aerosol burden is about twice as large in the tropics as in the middle latitudes (Vernier et al., 2011; Trickl et al., 2013). While Hofmann et al. (2009) hypothesized that this aerosol increase could come from increasing Asian fossil-fuel emissions, other studies (Nagai et al., 2010; Vernier et al., 2011; Neely et al., 2013; Trickl et al., 2013) show that volcanic sulfate aerosols are the likely cause. Most volcanic sulfates are injected directly into the lowermost stratosphere, but some may also be transported there via monsoonal circulations from the upper troposphere (Bourassa et al., 2012; 2013). The exact path of aerosols and precursors is not always clear (Vernier et al., 2013; Fromm et al., 2013; Bourassa et al., 2013). Quantitative assessments of the impact on ozone of this observed stratospheric aerosol increase are needed, especially in the context of other changes in the tropical lower stratosphere. Most likely, given the current (high) stratospheric chlorine and bromine burden, heterogeneous reactions on the increased aerosol surface area will result in some lower-stratospheric ozone destruction. Using a total column depletion of typically 2%, maximum 5%, after Mt. Pinatubo as a reference (Telford et al., 2009; see also Figure 2-2, WMO, 1999), the current effect on the total column should be below 0.2 to 0.5%, since aerosol loading is about a factor of 10 smaller, and chlorine levels are comparable. Major stratospheric aerosol perturbations, however, are likely to lead to substantial ozone loss until stratospheric halogen loading falls to values expected in about 2030–2050 (Pitari et al., 2014). Note that bromine released from very short-lived halocarbons that are transported into the lowermost stratosphere contributes substantially, up to 50%, to the aerosol-related ozone destruction (Salawitch et al., 2005; Sinnhuber et al., 2009). These very short-lived halocarbon sources are not expected to decrease in the future, providing potential for ozone loss due to enhanced stratospheric aerosol even when controlled ODSs have largely disappeared from the stratosphere.

Mt. Pinatubo was the most recent major volcanic eruption to increase global stratospheric aerosol levels by an order of magnitude or more, injecting about 17 teragrams (Tg) of sulfur dioxide into the stratosphere, which oxidized into about 30 Tg of sulfate aerosol (WMO, 1995, 1999). This aerosol

remained in the stratosphere for several years (see Figure 2-18) and was transported in approximately equal amounts to both hemispheres. The observed sudden depletion of stratospheric nitrogen dioxide (NO_2) in both hemispheres (WMO, 1995, 1999) provided evidence that the volcanic aerosol had enhanced heterogeneous chemistry at all latitudes. However, while observations showed enhanced ozone depletion in the NH, a small increase of the ozone column was detected, surprisingly, in the SH during the year following the eruption (see Figure 2-2). This remained unexplained in WMO (2011). Recent studies have now provided explanations. Poberaj et al. (2011) suggested that in the SH, enhanced ozone transport in late 1991 and early 1992 more than compensated the aerosol-induced chemical ozone loss. The enhanced transport was related to enhanced wave forcing of the SH stratosphere. A set of CCM simulations by Aquila et al. (2013) demonstrated that aerosol-induced longwave heating in the lower stratosphere would increase tropical upwelling, leading in turn to an enhanced BDC. This also increases ozone in the southern midlatitudes. Both mechanisms have likely acted together, and can explain the lack of a clear ozone decline in the SH after the Mt. Pinatubo eruption.

2.3.5 Impacts of Ozone-Depleting Substances and Greenhouse Gas Changes on Ozone Trends

Although the concentrations of ozone-depleting substances (ODSs) in the stratosphere continue to decrease, the detection of ozone recovery from ODSs remains a challenging scientific task. Essentially it is a statistical problem, complicated by the fact that influences other than ODSs, such as greenhouse gas (GHG) concentration increases, atmospheric dynamical variability, solar irradiance variations, and volcanic aerosol all affect stratospheric ozone (see previous sections). In the lower stratosphere and for total ozone, dynamical variability influences ozone directly, via changes in transport. Ozone is also affected indirectly by dynamical temperature changes, which affect rates of chemical production and destruction of ozone.

In the following we report how our capability to connect observed changes in total column ozone, and ozone in the upper stratosphere, to changes in ODSs and GHGs has improved. We also report on recent studies that examine observational evidence, from ozone in the lowermost tropical stratosphere, for an acceleration of the mean meridional Brewer-Dobson circulation (BDC). This acceleration has been simulated by most chemistry-climate model (CCM) simulations. These remain the major tool for estimating contributions from different processes, which usually cannot be separated on the basis of observations alone.

2.3.5.1 Changes in Total and Lower Stratospheric Ozone and ODS and GHG Changes

To detect the influence of ODSs on ozone changes, WMO (2011) relied on multiple-linear regression analysis. Equivalent Effective Stratospheric Chlorine (EESC) or piecewise linear trends (PWLT), both closely resembling the increase and the beginning of the decline of ODSs, were used as proxies describing the effect of ODSs (see also Section 2.2.3.3). In addition chemical transport models (CTMs) forced with winds and temperatures from meteorological analyses have been used to separate the influences of ODSs and dynamical variability. WMO (2007) attributed about 30% of the observed negative total ozone column trend from 1979 to the mid-1990s to changes in the lower stratospheric circulation. WMO (2011) also found that total ozone column increases observed since mid-1990 were significantly larger than expected from ODS decreases, and that dynamical variability contributed to these increases. Several new studies, reviewed below, follow the same approach.

Kiesewetter et al. (2010), for example, used a CTM and attributed at least 50% of the linear negative trend in total ozone from 1979 to 1999 to gas-phase chemistry. They found that insignificant ozone increases over the period 2000–2009 were dominated by changes in transport (see also Section 2.2.3.3). This is expected since stratospheric halogen loading has not yet decreased substantially over the last decade (compare EESC lines in Figure 2-4, or see Chapter 1). Kobayashi and Shibata (2011) also

used a CTM driven with observed meteorological conditions and pointed out that, in the northern midlatitudes, meteorological changes drive ozone changes on interannual to decadal timescales in the lower stratosphere, whereas upper stratospheric ozone decreases until the mid-1990s were dominated by changes in halogen loading, in agreement with previous studies.

Several studies assessed by WMO (2011) (e.g., Li et al., 2009; Waugh et al., 2009) used CCM model simulations driven by individual forcings to separately detect the influence of ODSs and GHGs on the past ozone trends. These results, corroborated by Plummer et al. (2010) and Fleming et al. (2011), have shown that ODS-induced changes dominated ozone during recent decades everywhere except for the lower tropical stratosphere (where little change has been observed; see Figure 2-8). However, none of these studies tested specifically whether observed ozone changes are consistent with responses to each of the forcings taking into account both the temporal evolution and spatial distribution of the changes. Such a test was performed by Gillett et al. (2011), who applied detection and attribution techniques common in other branches of climate science (e.g., Hegerl et al., 1996) to simulations from the CCMVal-2 ensemble, including simulations driven by all forcing, anthropogenic-only forcing, and GHG and ODS changes only over the period 1979–2005. Figure 2-19 (adapted from Gillett et al., 2011) shows a good agreement between observed total ozone trends and those simulated in response to the combined natural and anthropogenic forcing as well as to ODS changes alone. This suggests that the ODS changes are the dominant cause of the global ozone trends from 1979 to 2005, as concluded in WMO (2011). By applying optimal regression, Gillett et al. (2011) showed that the response of total column ozone to ODSs as well as to natural forcing (i.e., volcanoes and solar cycle) is detectable in observations. Furthermore, the observed and simulated responses to these forcings are of comparable magnitude. They also showed that the response of total ozone to GHG forcing is not yet detectable using this method. Note, however, that Gillett et al. (2011) attributed overall ozone changes over the entire 1979 to 2005 period to ODS and GHG changes, without considering a possible change in the trend since around 2000.

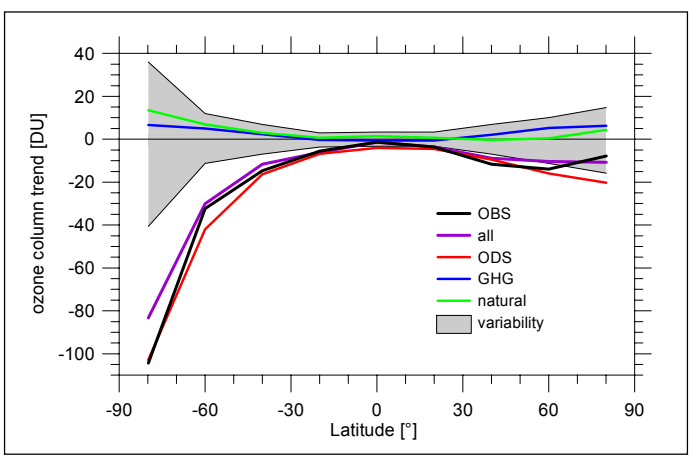

Figure 2-19. Comparison of observed (black line, OBS) and simulated linear trends in zonal mean total column ozone in Dobson units (DU) over the 27-year period 1979–2005. Observed total column ozone is taken from the merged TOMS/SBUV V8.0 data set. Simulated trends are from CCMVal-2 simulations and are shown for separate responses to ODS, GHG, and natural forcing, and all forcings combined (all, purple line). Gray band shows the estimated 5 to 95 percentile ranges of internal variability. Adapted from Gillett et al. (2011).

2.3.5.2 Changes in Upper Stratospheric Ozone and ODS and GHG Changes

As shown in previous Assessments (WMO, 1999, 2003, 2007, 2011), and reaffirmed by recent studies (e.g., Gillett et al., 2011), the large increase of ODSs from the 1970s to the late 1990s has been the main driver of the negative trend in upper stratospheric ozone until the late 1990s (see also Section 2.2, Figures 2-5, 2-9, 2-11). Model simulations have indicated that stratospheric cooling due to increasing GHGs is another important driver of the ozone evolution in the upper stratosphere (WMO, 1999; Jonsson et al., 2009; Eyring et al., 2010; Oman et al., 2010b; Gillett et al., 2011; Fleming et al., 2011; WMO, 2011; Stolarski et al., 2012).

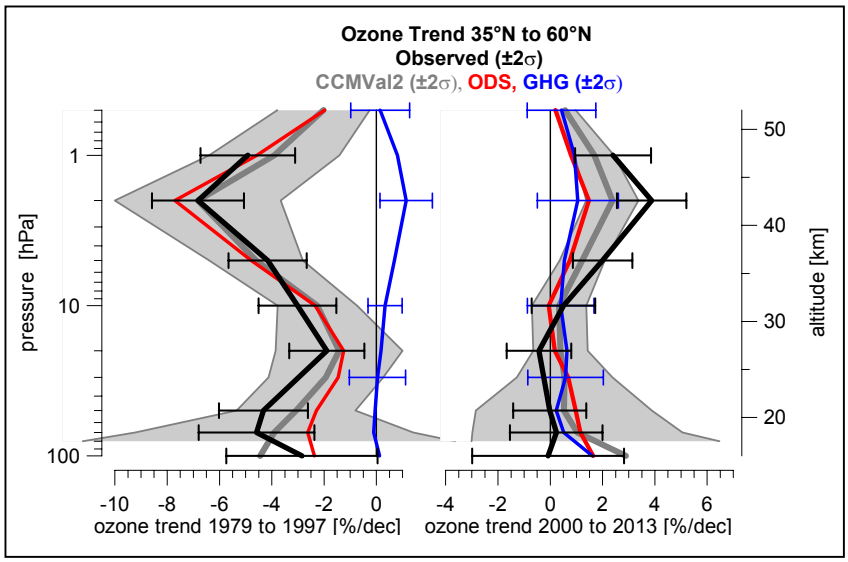

Figure 2-20. Observed and modeled ozone trend profiles. Left panel: For the period 1979 to 1997. Right panel: For the period 2000 to 2013. Black line: Average of all available observations in the 35°N to 60°N latitude band (same as in Figure 2-11). Gray line with shading: Corresponding mean trends from CCMVal-2 model simulations (same as Figure 2-11, but only for the subset of 7 models that did simulations with fixed GHGs), with uncertainty range given by ±2 standard deviations of individual model trends. Red line: Trend attributed to ODS changes alone, from CCMVal-2 simulations with fixed GHG concentrations (7 models). Blue line: Trend attributed to increasing GHGs alone, from CCMVal-2 simulations with fixed ODS concentrations (9 models). See Tables 1 and 2 of Eyring et al. (2010) or Tables 3-1 and 3-2 of WMO (2011) for details on CCMVal-2 fixed GHG and fixed ODS simulations.

The left panel of Figure 2-20 illustrates the influences of ODS and GHG changes on midlatitude ozone amounts during the period of ozone decline. The figure compares the observed ozone trend profiles (already shown in Figure 2-11; see also Figure 2-25 of WMO, 2011) to simulations from models in the CCMVal-2 ensemble forced by ODSs (red) and GHGs (blue) concentrations alone, in addition to simulations with all forcings (gray line and shading). Consistent with Oman et al. (2010a), simulations forced with ODS changes alone and with all forcings produce a large decline (−7% per decade) in ozone at 2 hPa until the mid-1990s. Within observational and model uncertainty these changes are consistent with the observed decline. Ozone increases due to GHG-driven cooling are smaller at around 1% per decade and also peak around 2 hPa.

The more recent impacts of declining ODSs and increasing GHGs in the early 21st century are illustrated in the right panel of Figure 2-20. Since 2000, declining chlorine and the continued slowing of gas-phase ozone destruction cycles due to declining temperatures both act to increase upper stratospheric ozone. Each factor contributes about one-half to the simulated upper stratospheric ozone increases (Eyring et al., 2010; Oman et al., 2010b; Fleming et al., 2011; Shepherd and Jonsson, 2011; WMO, 2011). The simulations also indicate that the contributions from ODSs and GHGs add linearly to produce the overall ozone change over this period (WMO, 2011).

Figure 2-20 indicates that this combined effect of GHG and ODS on upper stratospheric ozone can already be observed in the NH midlatitude upper stratosphere. Around 42 km (2 hPa), both ODS and GHG forced simulations each indicate a trend of 1–2% per decade in ozone concentration, compared to a mean observed trend of 2.5–5% per decade. Only when models are forced with both ODS and GHG changes are they able to capture trends as large as observed at these levels.

Since WMO (2011), four years of additional observations and the availability of more data sets have decreased the uncertainty margins for the observed trends. There are now stronger indications that a significant ozone increase is detectable in the upper stratosphere since 2000, and that about half of this increase is due to declining ODSs, with another half coming from the photochemical response to the cooling of the upper stratosphere by increasing GHGs.

2.3.5.3 TROPICAL OZONE CHANGES

WMO (2011) reported negative ozone trends in the tropical lower stratosphere (about 18–19 km) for 1985–2005, based on SAGE II data. While the uncertainty in this trend was large, the ozone decrease was consistent with that simulated by CCMs. These simulations indicate a long-term increase in tropical upwelling and an increased Brewer-Dobson circulation (BDC), resulting in declining ozone in the tropical lowermost stratosphere. New studies that merge SAGE II data for 1984 to 2005 with either SHADOZ ozonesonde data for 1998–2009 (Randel and Thompson, 2011) or OSIRIS satellite data for 2001–2012 (Sioris et al., 2014) seem to confirm a negative long-term ozone trend in the lowermost tropical stratosphere, −2% to −4% per decade for the 17 to 21 km altitude range, see also Figure 2-8. The magnitude and vertical profile of this ozone decline from 1984 to around 2000 are similar to the results from twelve different CCMVal-2 simulations (Eyring et al., 2010; WMO, 2011; Randel and Thompson, 2011).

However, as discussed in Section 2.2, recent analyses of shorter satellite data sets, between 2002 and 2012, do not show significant lower stratospheric ozone trends. This is the case for both SCIAMACHY (Gebhardt et al., 2014) and MIPAS data (Eckert et al., 2014). Analysis of a combined SAGE II-GOMOS data set for 1984–2011 (Kyrölä et al., 2013) shows a significant negative trend between 20-22 km for the period 1984–1997 but an insignificant trend for 1997–2011. Examination of the tropical ozone time series near 70 hPa in Figure 2-8 reveals the large year-to-year variations of ozone in this region, and variations around a relatively constant level since 1997. The CCMVal-2 simulations in Figure 2-8 also do not indicate a clear decline over the last 10–15 years in the tropical belt. The absence of a significant trend in the most recent observations is therefore not unexpected.

Overall these new results indicate substantial decadal variability of ozone in the tropical lowermost stratosphere. Based on existing tropical ozone records, there is little evidence for a continuing ozone decline in the tropical lowermost stratosphere since around 2000 that would be driven by a strengthening BDC. In agreement with WMO (2011), ozone values appear to have declined between 1984 and about 2000. Chapter 4 of this Assessment examines the BDC and its possible long-term change in more detail. The general expectation from model simulations is that, in the long term, ozone in the tropical lowermost stratosphere will continue to decrease due to enhanced upwelling and increases of the BDC driven by increasing GHGs (WMO, 2011).

2.4 UPDATE ON FUTURE OZONE CHANGES

2.4.1 Expected Return to 1960 or 1980 Levels and Ozone Recovery

The past two Ozone Assessments (WMO, 2007; 2011) have used chemistry-climate models (CCMs) as the primary tool for future ozone projections. WMO (2011) based their future projections on the simulations of 17 models, all of which participated in CCMVal-2 (Eyring et al., 2010). This ensemble remains the most comprehensive set of coordinated simulations of past and future stratospheric ozone changes. It is therefore the basis of future projections in the current Assessment. These CCMs have been extensively evaluated by CCMVal and the results are documented in the SPARC CCMVal Report (2010). Recent new simulations by four CCMVal-2 models using the revised estimates of ODS lifetimes (SPARC, 2013; also Chapter 1) are shown in Figure 2-21. These simulations indicate that the expected future evolution of near-global total ozone columns changes very little when using the revised ODS lifetimes. Changes in expected recovery dates to 1980 levels, for example, are typically less than a few years and are usually not significant given the large interannual variability and the intermodel differences. The estimates of return dates in different regions (Table 2-5) are not updated from WMO (2011). At this point there is not enough new evidence to motivate a revision of the estimates of ozone recovery presented in the previous Assessment.

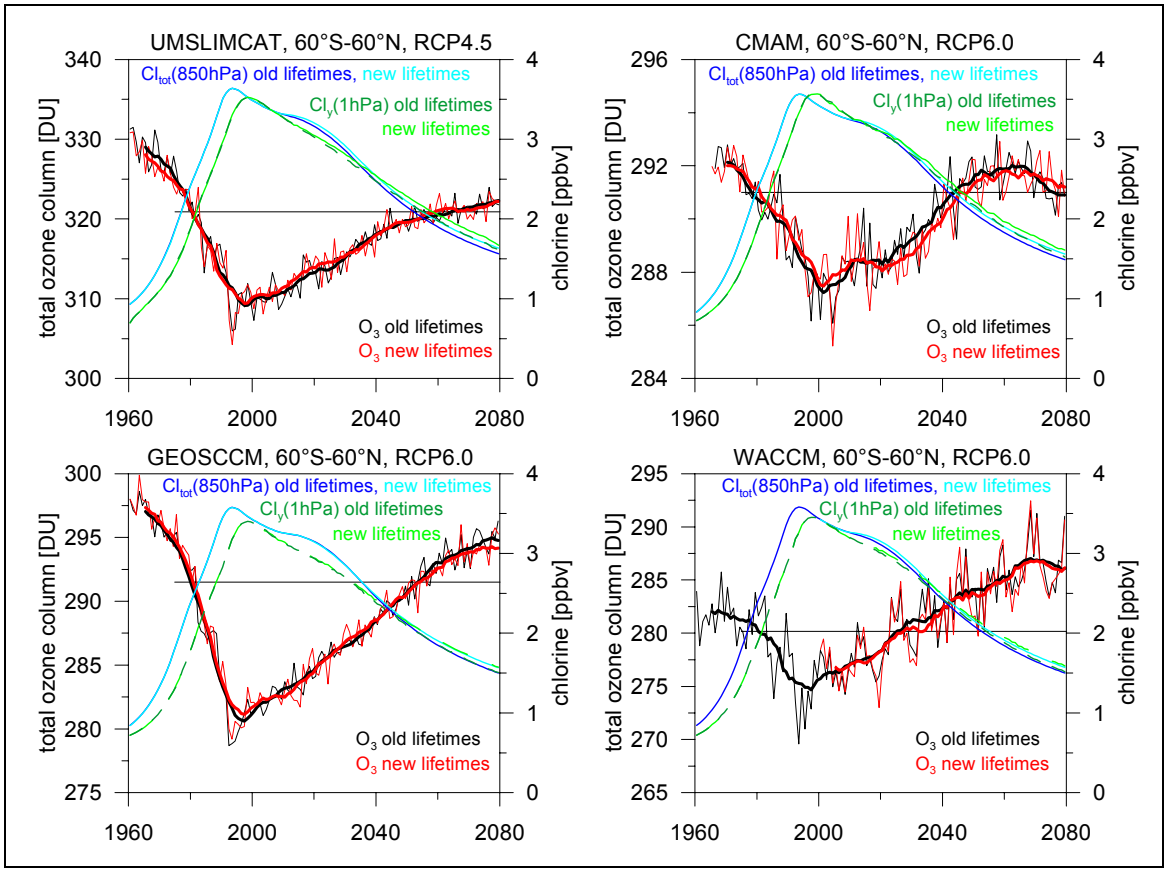

Figure 2-21. Comparison of total ozone column evolutions simulated using "old" ODS lifetimes from WMO (2010), black lines, and simulations using updated "new" ODS lifetimes from SPARC (2013), red lines. Also shown, on the axes on the right, are total organic chlorine at 850 hPa in the troposphere (Cl_{tot}, blue and cyan lines) and chlorine in the upper stratosphere at 1 hPa (Cl_y, dark green and light green lines). Annual means, averaged from 60°S to 60°N, are used. Results are from simulations with the chemistry-climate models UMSLIMCAT (Unified Model Single-Layer Isentropic Model of Chemistry and Transport; top left), CMAM (top right), GEOSCCM (bottom left, Oman and Douglass, 2014), and WACCM (bottom right). All models are described in Eyring et al. (2010) and WMO (2011). For greenhouse gases (GHGs) the simulations use the Representative Concentration Pathway (RCP) 6.0 scenario, except for UMSLIMCAT, which uses the RCP4.5 scenario. WACCM is coupled to an interactive ocean; the other simulations use prescribed sea surface temperatures. For total ozone, sliding 11-year averages are also plotted (thick lines).

WMO (2011) constructed its ozone projections by combining all available simulations from chemistry-climate model ensembles. WMO (2011) also gave equal weights to all simulations, and used multi-model means as the best estimate of future ozone and intermodel spread as a measure of uncertainty. This mean estimate of the CCMVal-2 ensemble can be seen in the black line in Figure 2-23, which will be discussed later in Section 2.4.3.1.

Table 2-5 shows that the simulations predict a later return date for SH midlatitudes than for the NH. This is the opposite of the currently observed total column trends in Figure 2-4, or profile trends in Figures 2-10 and 2-11, which tend to indicate slightly more increase since 2000 in the SH. The differences are not very significant though. As mentioned (e.g., in Sections 2.2.3 and 2.2.4) decadal changes in transport play an important role. WMO (2011) assumes that long-term changes in transport, i.e., in the Brewer-Dobson circulation (BDC), cause the earlier NH return dates. Garny et al. (2013)

suggest other possible reasons for the asymmetry in return dates between NH and SH midlatitudes. They hypothesize that transport effects play only a small role in this asymmetry and that differences in column return dates are related to less efficient destruction of ozone by nitrogen-oxides (NO_x) cycles in the NH and more efficient destruction of ozone by total inorganic chlorine (Cl_y) in the SH due to the larger polar vortex. These results should be interpreted cautiously because they rely on attribution of ozone changes in a single CCM and use a relatively novel and complex attribution method.

Since WMO (2011) there has been discussion about the possibility of using prior physical constraints to weight ozone projections from different models in order to reduce the significant uncertainty in current multi-model ozone projections. Challenges associated with combining projections from multi-model ensembles are common in all areas of climate science. Several weighting methods have been proposed. An overview of strategies for analyzing model ensembles and recommendations for good practice in applying multi-model ensembles is given in Knutti et al. (2010). Moreover, for CCMs the SPARC CCMVal Report (2010) presented a comprehensive set of diagnostics of model performance that are useful for model discrimination.

Several recent studies demonstrate that, at least for some regions, the performance-based weighting may give a more realistic ozone projection than the multi-model mean approach used by WMO (2011). Strahan et al. (2011) argued that in the tropical lower stratosphere the spread of ozone projections from the full set of models is unrealistically large. They evaluated CCM performance based on several transport diagnostics and found that tropical ozone agreed best with observations in the models whose transport was the most realistic. They further demonstrated that models with the most realistic transport in the tropical stratosphere produced a smaller spread of ozone projections compared to the full set of models. Douglass et al. (2014) demonstrate that selecting models based on their realistic performance can reduce the intermodel spread in the ensemble of projected ozone changes, although this comes at the expense of severely reducing the sample size.

Douglass et al. (2012) showed that, in agreement with expectation based on photochemical theory of upper stratospheric ozone, models with cold biases in upper stratospheric temperatures have higher ozone levels and stronger ozone sensitivity to chlorine changes. Thus, intermodel spread is not always an appropriate measure of uncertainty in future upper stratospheric ozone projections, but is also indicative of systematic errors that depend on model biases in simulated temperature, ozone, and reactive nitrogen climatologies.

Table 2-5. Expected return years when ozone columns will return to 1960 or 1980 values. Results from multi-model projections from the entire CCMVal-2 model simulation ensemble are repeated here from WMO (2011). Four new simulations using the recently updated longer ODS lifetimes from SPARC (2013; see also Chapter 1) indicate insignificant delays, about 2 years, in these return years (see Figure 2-21). Interannual variability of ozone columns, systematic differences between models, and uncertainty about future emissions (see Figure 2-23) cause larger uncertainty in the estimated return years.

Region	Date of Return	Mean Estimate	Lower Bound	Upper Bound
Global annual mean	1960	2053	2046	2064
	1980	2032	2027	2038
Tropics annual mean	1960	---	---	---
	1980	2042	2028	---
Northern midlatitude annual mean	1960	2029	2024	2036
	1980	2021	2017	2026
Southern midlatitude annual mean	1960	2055	2049	2064
	1980	2035	2030	2040

Karpechko et al. (2013) used the dependence of Antarctic ozone projections on simulated biases in present-day transport to constrain future projections. They showed that constraining projections resulted in a slightly delayed ozone recovery compared to the multi-model mean; however the difference between the two estimates was within the uncertainty limits. Waugh and Eyring (2008) and WMO (2011) also reported little difference between weighted and unweighted ozone projections, providing some support for using multi-model mean projections, as done in Section 2.2. The agreement between weighted and unweighted projections can be expected if models have opposite biases that nearly compensate each other within the ensemble. However when the models tend to have common biases, weighted projections can differ considerably from the multi-model mean.

These studies suggest that physically based model weighting approaches may help to reduce uncertainty in future ozone projections for regions where ozone is dominated by a small number of well understood processes, which are poorly simulated by some models. For consistency with the last Assessment, however, this chapter uses unweighted multi-model mean and intermodel spread from all relevant CCMVal-2 models, as in Eyring et al. (2010) and WMO (2011), as discussed in Section 2.2.3.1. Further, as shown in Douglass et al. (2014), performance metrics based on observations of meteorology and transport do not currently reduce the ensemble spread of the impacts of climate change on ozone in the late 21st century because the response of any model to climate change is not closely related to its transport skill.

2.4.2 Effects of Future Stratospheric Temperature and Circulation Changes

Future increases in greenhouse gases (GHGs), especially carbon dioxide (CO_2) are important for global ozone because they result in stratospheric cooling, slowing some chemical ozone destruction rates in the middle and upper stratosphere (e.g., Stolarski et al., 2012). According to model simulations, GHG-forced climate change leads to increased upwelling in the tropics and to changes in planetary waves that drive an increase in the strength of the BDC, which in turn affects the distribution of ozone in the stratosphere and the transport of ODSs, nitrous oxide (N_2O), methane (CH_4), and water vapor (H_2O) between the stratosphere and troposphere. For a mid-range GHG emission scenario, such as SRES A1B used in CCMVal-2, the dominant impact on stratospheric temperatures is from CO_2 changes. Future changes in transport due to the BDC, however, depend more on the amount of tropospheric warming, which will reflect the radiative forcing of the total mixture of future GHGs. Projecting future changes in the BDC is more difficult since the processes involved span the troposphere and stratosphere and are not well constrained in climate models. Observational evidence for changes in stratospheric temperatures and circulation is discussed in Chapter 4 of this Assessment.

Figure 2-22 shows a simple, illustrative experiment using the Solar-Climate-Ozone Links (SOCOL) CCM (Zubov et al., 2013) that separates the direct effects of GHG-induced temperature change on ozone from those resulting from stratospheric circulation change. This is achieved by performing timeslice experiments in which GHG and sea surface temperature and sea ice are varied independently. In the lower tropical stratosphere, large negative percentage changes of ozone below 20 hPa (Figure 2-22d) are driven almost completely by increased sea surface temperatures driven by tropospheric warming due to GHG increases (Figure 2-22c). As described in detail in WMO (2011), or Oberländer et al. (2013), the increased surface temperatures result in enhanced upward transport, especially in the tropics, and planetary wave driven increases in the mean meridional BDC. In midlatitudes, the same process is responsible for the enhancement of ozone in the lower stratosphere as ozone-rich air is transported from above. WMO (2011) concluded that CCMs consistently predict a strengthening of the BDC of around 2% per decade between 1960 and 2100, but that this strengthening had not been confirmed in observations (see also Section 2.3.5.3 and Figure 2-8). Recent work (see Chapter 4) separately considers changes in the shallow and deep branches of the BDC. Lin and Fu (2013) show that for the CCMVal-2 models, less than one-quarter of the predicted increase in tropical mass flux can be attributed to changes in the deep branch. CCM projections of changes to the shallow branch of the

BDC are sensitive to changes in the strength of the tropospheric subtropical jets and warming in the tropical upper troposphere (Lin and Fu, 2013), following the mechanism described by Shepherd and McLandress (2011). As well as the transport-induced impacts on lower stratospheric ozone concentrations, Meul et al. (2014) demonstrate using a CCM that the increased upwelling also leads to changes in chemical production and loss of tropical stratospheric ozone. The projected changes in lower stratospheric ozone concentrations in the late 21st century are thus caused by a combination of direct transport-induced changes and various chemical impacts that vary considerably with altitude in the low stratosphere.

In the upper stratosphere, above 10 hPa, the local cooling effect of CO_2 on ozone amounts (Figure 2-22b) is dominant, with little contribution from changes in transport. It is of comparable size to the increases in ozone driven by ODS reduction (Figure 2-22a; see also Figure 2-20 and Section 2.3.5.2). In midlatitudes, the upper stratospheric ozone increase from CO_2 cooling is roughly similar to that in the tropics, whereas the ODS-driven ozone increases are larger at midlatitudes. These upper stratospheric increases, combined with enhanced transport, drive an increase in ozone also in the lower stratosphere, resulting in increases in total column amounts (with a stronger signal expected in the NH; see also Shepherd, 2008; Li et al., 2009).

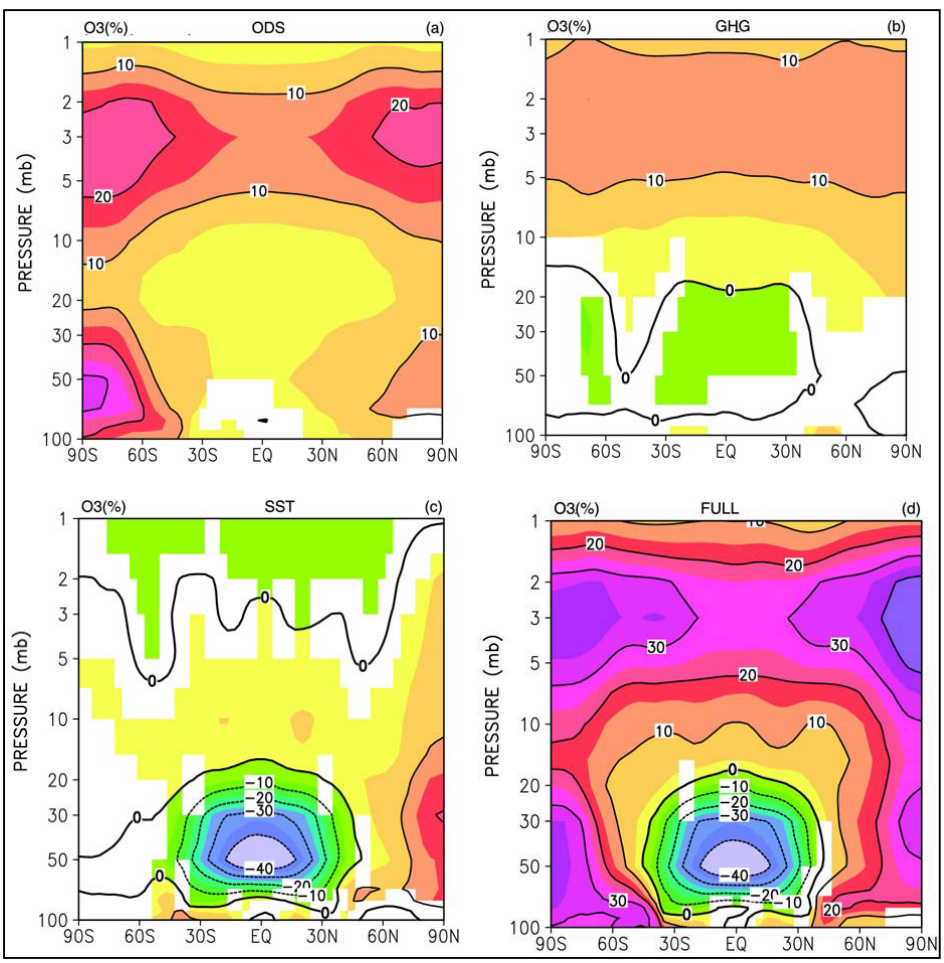

Figure 2-22. Zonal, annual and ensemble mean percentage changes of the ozone mixing ratio between different timeslice integrations of the SOCOL CCM for 2100 and for 2000 conditions.
(a) Ozone changes from 2000 to 2100 when only ODSs are changed.
(b) Ozone changes from 2000 to 2100 due to GHG changes only.
(c) Ozone changes due to changes in sea surface temperature and sea ice, driven by tropospheric warming.
(d) Ozone changes when ODS, GHG, sea surface temperature, and sea ice are all changed together. White regions indicate nonsignificant changes at the 5% confidence level. Adapted from Zubov et al. (2013).

2.4.3 Sensitivity to the Specification of Different Future Scenarios

As recognized in WMO (2011), numerous factors other than ODSs, including concentrations of CO_2, N_2O, and CH_4, will affect the future evolution of ozone in the stratosphere. In addition, changes in stratospheric water vapor are important for HO_x and NO_x chemistry, as reviewed by WMO (2011). Apart from methane oxidation, stratospheric water vapor concentrations are strongly influenced by stratospheric and tropospheric temperature and circulation changes. All are reviewed in detail in Chapter 4, Section 4.2.2 of this Assessment. Both natural and anthropogenic influences on the stratospheric aerosol layer also have the potential to influence ozone in the next decades, while ODS levels remain high. Since WMO (2011) our understanding of the influence of the 1991 Mt. Pinatubo eruption on ozone has increased, enhancing confidence in predictions of the future effects of these changes (Section 2.3.4).

Assessing the impact on ozone of future changes in CO_2, N_2O, and CH_4 is complicated by the significant, nonlinear interactions between them (Portmann et al., 2012). The following subsections address impacts on ozone of various future scenarios, and the complex effects of changes in N_2O and CH_4.

2.4.3.1 EFFECTS OF DIFFERENT REPRESENTATIVE CONCENTRATION PATHWAYS (RCP) SCENARIOS

Quantifying the combined influence of CO_2, CH_4, and N_2O increases on ozone over the 21st century requires an estimate of the potential range of future anthropogenic emissions of these gases and subsequent calculations of the effect of these changes on ozone abundance using CCMs. Given the computational complexity and cost of CCMs, the number of simulations available for these calculations is limited.

As introduced in WMO (2011) the scenarios used for the latest Climate Model Intercomparison Project experiment (CMIP5) are the so-called Representative Concentration Pathways (RCPs, van Vuuren et al., 2011). These scenarios will also be the basis for most future runs of the next generation of CCMs, so they are reviewed here. It is important to note that the RCPs are chosen to represent some of the many different potential future emissions pathways and are produced using a complex chain of different Integrated Assessment Models (IAMs). RCPs are named to reflect their total radiative forcing in 2100. The evolution of emissions of CO_2, CH_4, N_2O, and other GHGs in each scenario is complex and the ordering of emissions of each gas as a function of scenario changes with respect to time over the 21st century. Key points to note are that CH_4 emissions are much larger (by a factor of more than 2) in the RCP8.5 scenario than the other three scenarios and that N_2O emissions in the RCP6.0 and 8.5 scenarios are much larger than those of the RCP2.6 and 4.5 scenarios by midcentury. Since the emissions trajectories for GHGs in the RCP scenarios are complex and have differing rates of change over time, this will lead to differing rates of change for key processes in CCMs, both in the stratosphere and in the troposphere.

WMO (2011) reported early calculations of the sensitivity of future ozone to the GHG scenario and concluded that the GHG scenarios had a measurable impact on future ozone concentrations in the stratosphere and troposphere, particularly during the latter half of the 21st century, but that model uncertainty was at least as large as scenario uncertainty for all regions.

More recently, Eyring et al. (2013) considered the sensitivity of ozone projections to GHG scenario for those models submitted to CMIP5 that had a representation of stratospheric ozone chemistry. The results of Eyring et al. (2013) are qualitatively consistent with WMO (2011), increasing confidence in our understanding of the scenario uncertainty associated with future ozone projections. However, the CMIP5 results from Eyring et al. (2013) deviate quantitatively from the projections made by the CCMVal-2 models (WMO, 2011). As shown in Figure 2-23, the multi-model mean of the CCMVal-2 models assessed by WMO (2011), and used in this Assessment, differs in timing of minimum total ozone columns and in other aspects from the CMIP5 model projections. Most noteworthy are the differences between CCMVal-2 simulations using the SRES A1B intermediate radiative forcing (6 W

m^{-2}) scenario from IPCC (2007), and CMIP5 simulations using the similar RCP6.0 scenario. These deviations may be due to differences in the models used in each ensemble, in the ensemble sizes, and differences in the scenarios themselves. It should also be noted that the RCP scenarios do not sample all possible future emission changes relevant to ozone, for example different ODS scenarios. As noted in WMO (2011), it will only be possible to refine estimates of scenario uncertainty by comparing a large number of CCM integrations forced with different emissions scenarios.

Given these caveats, all simulations in Figure 2-23 project substantial changes in total ozone columns in the future. Outside of the tropics, simulations for the scenarios with higher radiative forcing project a recovery of total ozone columns to 1980 values or even larger columns, with contributions from declining ODS, continued stratospheric cooling, and strengthening of the BDC (see previous sections). Future increases in tropospheric column ozone also contribute to the expected larger columns. In the tropics, projected future increases of tropospheric ozone column are particularly large in the RCP8.5 scenario, where they more than compensate the projected decline of tropical stratospheric column ozone. Depending on the assumed scenario, total ozone columns in 2100 could vary by up to 10 DU or 4% in the tropics, by up to 20 DU or 7% in the global mean, and by up to 40 DU or 12% at midlatitudes. This large variation shows that, apart from the expected decline of ODS, future emissions of GHGs will have a substantial influence on ozone levels.

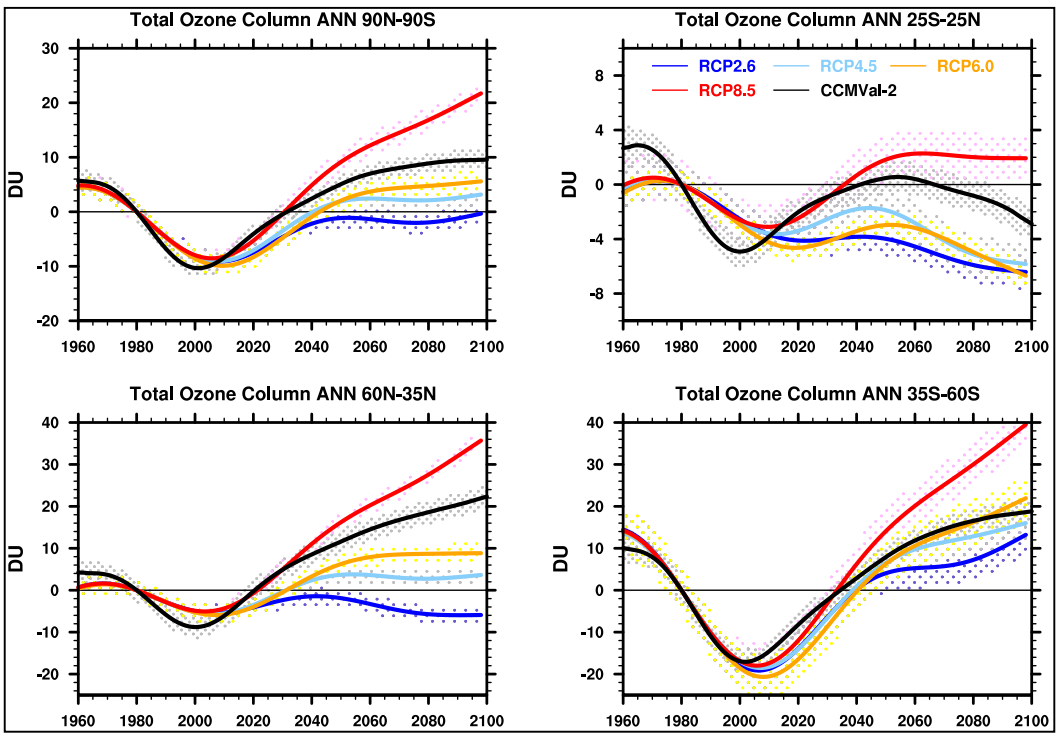

Figure 2-23. 1980-baseline adjusted total column (tropospheric plus stratospheric) ozone time series for CMIP5 runs of models that follow four RCP scenarios for GHGs, and the A1 scenario from WMO (2003) for ODS. The RCP2.6 scenario is shown in the solid blue line with the 95% confidence interval for the mean of 5 models shown in blue stippling. The RCP4.5 scenario is shown in the light blue line and averages 6 models. The RCP6.0 scenario is shown in the orange line and averages 5 models. The RCP8.5 scenario is shown in the red line and averages 6 models. Five models are common to all scenarios. Also included is the CCMVal-2 multi-model mean (black line), which is based on different models, the SRES A1B scenario for GHGs, and the adjusted A1 scenario from WMO (2007) for ODS (see Section 2.2.3). Adapted from Eyring et al. (2013).

2.4.3.2 INFLUENCES OF NITROUS OXIDE AND METHANE

As well as being important GHGs, N_2O and CH_4 are key source gases for the NO_x and HO_x chemical cycles, which directly impact ozone amounts. About 90% of stratospheric NO_x arises from N_2O oxidation (Vitt and Jackman, 1996). At low halogen levels, chemical ozone destruction is dominated by the NO_x loss cycle in the middle stratosphere and by the HO_x loss cycle below 20 km and above ~50 km (in the mesosphere). As the ODS burden declines over the 21st century, ozone changes will depend strongly on the N_2O and CH_4 burdens, which are assumed to change in very different ways in the RCP scenarios. These impacts are considered in this section.

In the global mean, for a mid-range N_2O emissions scenario, simulations compute a total ozone reduction by around ~5 DU by 2050, compared to preindustrial values. Similar changes are computed by both 2-D (Fleming et al., 2011; Portmann et al., 2012) and 3-D (Revell et al., 2012a, b) models. This reduction, shown by the green line in Figure 2-24, is about one-quarter of the isolated maximum effect of the ODS changes in 2000 (blue line in Figure 2-24), and comparable to the increases in total column ozone due to the isolated effects of CO_2 and of CH_4 through the 21st century (red and yellow lines in Figure 2-24). These studies found that the depletion of the total column due to the isolated effect of N_2O does not exceed that due to ODSs until ~2080. The efficiency of N_2O in destroying ozone can be compared to ODSs by computing the Ozone Depletion Potential for these gases (Ravishankara et al., 2009; Daniel et al., 2010). This is discussed further in Chapter 5 (Sections 5.3–5.4), along with policy-relevant information about future N_2O increases.

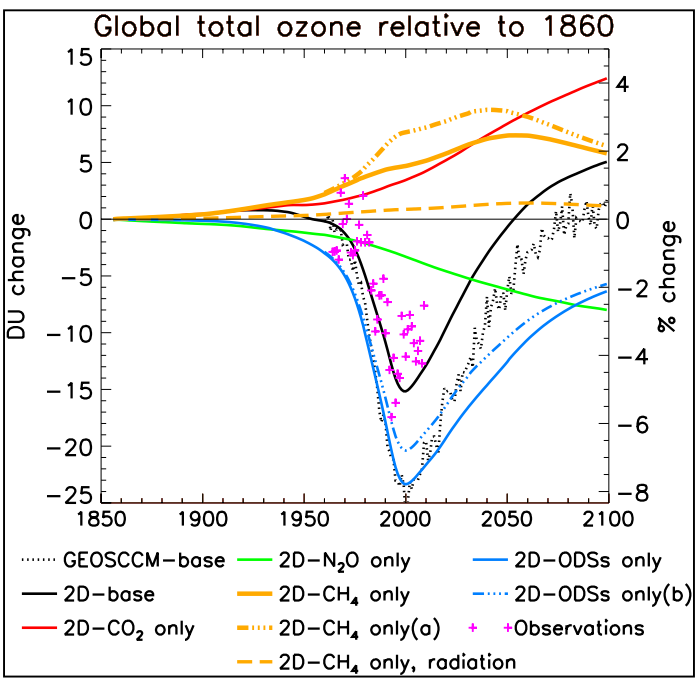

Figure 2-24. Global and annual average total ozone time series relative to 1860 values from model simulations (lines) and ground-based data (pink crosses, updated from from Fioletov et al., 2002). The black dotted line shows a base simulation of the 3-D chemistry-climate model GEOSCCM with the A1 scenario of WMO (2007) for ODS concentrations and the SRES A1B scenario for GHG concentrations (same as for the CCMVal-2 simulations). The black solid line shows the simulation of a 2-D chemical transport model that uses the same forcings. The other colored lines show additional scenarios of the 2-D model in which only selected forcings are varied in time (while keeping the others at 1850 levels). The experiments are as follows: Red-line: Only CO_2 varies. Green line: Only N_2O varies. Yellow solid line: Only CH_4 varies. Blue solid line: Only ODSs vary. Also shown are experiments in which both ODSs and CH_4 are varied. The orange dot dashed line shows the effects of CH_4 in the presence of time-dependent ODS changes (difference between simulation with CH_4 and ODSs changing and simulation with only ODSs changing). The blue dot dashed line shows the effects of ODSs in the presence of time-dependent CH_4 changes (difference between simulation with CH_4 and ODSs changing and simulation with only CH_4 changing). Finally, the orange dashed line shows the impact of CH_4 on ozone when its effects are confined to impacts on the radiation budget only. Adapted from Fleming et al. (2011).

Revell et al. (2012a) provided a study of the sensitivity to N_2O/NO_x by comparing three RCP scenarios, bounded by RCP2.6 (lower N_2O growth) and RCP8.5 (higher N_2O growth). They performed a suite of CCM simulations in which each of the gases is varied in isolation along four different future N_2O and CH_4 pathways. Their results demonstrate clear links between the assumed GHG scenario and stratospheric ozone. Increased N_2O emissions lead to higher NO_x concentrations and faster chemical ozone destruction in the middle stratosphere. Middle stratospheric ozone concentrations in the late 21st century are thus substantially lower for the RCP8.5 N_2O scenario than for the RCP2.6 scenario (Figure 2-25a, b). In the lower tropical stratosphere the differences are of opposite sign because of enhanced ozone production following CH_4 oxidation caused in the troposphere by the higher NO_x concentrations in the RCP8.5 scenario (this mechanism is discussed below). Some of this lower stratospheric ozone increase could also be due to "self-healing" wherein the ozone decreases in the middle and upper stratosphere allow more solar UV radiation to penetrate to lower altitudes, leading to ozone enhancements in the lower stratosphere (Mills et al., 2008).

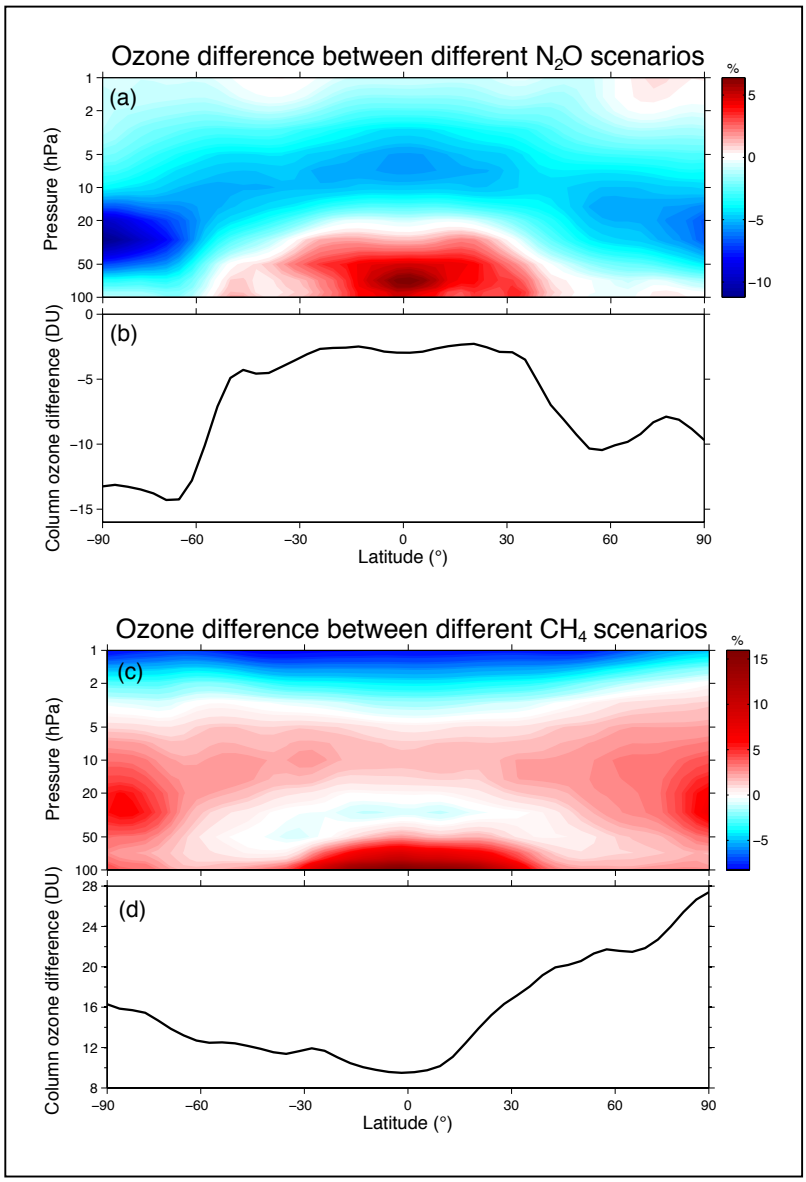

Figure 2-25. Ozone changes in the 2090s due to different N_2O and CH_4 scenarios, computed with the National Institute of Water and Atmospheric Research (NIWA)-SOCOL chemistry-climate model. (a) Difference between ozone in the 2090s under the N_2O-RCP8.5 scenario and ozone under the N_2O-RCP2.6 scenario, calculated as a per-centage of N_2O-RCP2.6 ozone, as a function of latitude and pressure. In 2100, N_2O mixing ratio is 340 parts per billion by volume (ppbv) for the RCP2.6 scenario, and 430 ppbV for the RCP8.5 scenario, com-pared to 320 ppbv in 2010. (b) Same but for the change in total column ozone (in Dobson units). Both simulations use the same scenario for CH_4 and CO_2 (IPCC SRES A1B), and the adjusted A1 scenario from WMO (2007) for the halocarbons. (c, d) same but for CH_4-RCP8.5 ozone minus CH_4-RCP2.6 ozone in the 2090s decade, otherwise using the same scenario for N_2O and CO_2 (IPCC SRES A1B), and the adjusted A1 scenario from WMO (2007) for the halocarbons. In 2100, the CH_4 mixing ratio is 1.25 parts per million by volume (ppmv) for the RCP2.6 scenario, and 3.75 ppmv for the RCP8.5 scenario; com-pared to 1.8 ppmv in 2010. Adapted from Revell et al. (2012a).

Various feedbacks are also important. The recovering ozone layer will reduce the penetration of UV radiation to the middle stratosphere and reduce the photolytic production of $O(^1D)$ (Rosenfield and Douglass, 1998; Fleming et al., 2011; Chipperfield et al., 2014), thereby reducing the production of NO_y via N_2O oxidation. Upper stratospheric cooling caused by GHG increases leads to enhanced conversion of NO_y to N_2 and less ozone destruction (Rosenfield and Douglass, 1998; Plummer et al., 2010). Portmann et al. (2012) computed that in 2100, the ozone destruction caused by increased N_2O was reduced by roughly 20% when the CO_2-induced stratospheric cooling effects on NO_y were included in the model simulations. Oman et al. (2010a) showed that the upper stratospheric cooling was greater when CCM simulations used the SRES A2 scenario than when they used the SRES A1b scenario. This enhanced cooling moderated the NO_y increase relative to the N_2O growth in the A2 scenario. Climate change-induced changes to the circulation, including an enhancement of the BDC, also modify the photochemical breakdown of N_2O (Rosenfield and Douglass, 1998; Plummer et al., 2010). A stronger Brewer-Dobson circulation will increase the loss of NO_y by increasing the rate of NO_y transport to the extratropical troposphere, where it is removed via nitric acid (HNO_3) washout. By comparing CCM simulations of N_2O increases, with and without the radiative and dynamical impacts of GHGs, Plummer et al. (2010) showed that GHG-induced cooling and circulation changes reduced the N_2O-induced increase of stratospheric NO_y by more than 50% by the end of the century.

The sensitivity of ozone to CH_4 is also complex, arising from a combination of direct and indirect effects (e.g., Brasseur and Solomon, 2005). Ozone is decreased through the direct impact of enhanced HO_x–ozone loss cycles as CH_4 is oxidized to H_2O. This mechanism dominates above ~45 km, so that the net impact of CH_4 is to reduce ozone in the very upper stratosphere and mesosphere. Figure 2-25c, d show the sensitivity of ozone in the late 21st century to the choice of high (RCP8.5) or low (RCP2.6) CH_4 scenarios. Below 45 km, and in the total column, increased CH_4 loading leads to increases in ozone via several mechanisms:

1) CH_4 converts active chlorine to the reservoir HCl via the reaction:
   $CH_4 + Cl \rightarrow HCl + CH_3$. This reduces the chlorine-catalyzed ozone loss, as long as chlorine levels are high (red areas around 20 hPa near the poles in Figure 2-25c).
2) CH_4 oxidation (mainly CH_4 + OH) leads to enhanced NO_x-induced ozone production in the troposphere and lowermost stratosphere ("photochemical smog chemistry," red area below 50 hPa in Figure 2-25c).
3) Increased H_2O, from methane oxidation, enhances stratospheric cooling and reduces chemical ozone loss rates (shown by the red area in Figure 2-25c around 10 to 20 hPa in the tropics and midlatitudes, and around 20 hPa near the poles).

For present-day chlorine loading, roughly two-thirds of the total column increase due to methane loading can be attributed to mechanism (1), but this will be much less important by the late 21st century. The process also reduces the effectiveness of present-day chlorine in depleting ozone by 15–20% (Fleming et al., 2011; Portmann et al., 2012). Mechanism (3) is most important in the middle stratosphere to lower mesosphere (30–60 km); it contributes about 20% to the total projected CH_4-induced increase in total column ozone during the 21st century (Figure 2-25d). By 2100, mechanism (2) will likely have the greatest impact. Methane oxidation (mechanism 2) is also affected by lower stratospheric NO_x produced by N_2O oxidation (e.g., Portmann and Solomon, 2007), as seen in Figure 2-25a. Also, CH_4 loading will increase stratospheric HO_x, which can (a) sequester NO_x in the reservoir HNO_3 (Nevison et al., 1999; Randeniya et al., 2002), and (b) enhance the HO_x-ozone loss, thereby reducing atomic oxygen abundance which in turn will reduce the NO_x-ozone loss cycles (Revell et al., 2012b).

Based on the SRES A1B GHG scenario, 2-D model calculations show that the total column response of ozone to CH_4 is around half to two-thirds that of N_2O at the end of the 21st century, with a CH_4-induced increase in the global ozone column of between 3 DU (Portmann et al., 2012) and 5 DU (Fleming et al., 2011) by 2100 (see Figure 2-24). However, quantifying the impact of CH_4 on ozone amounts toward the end of the century will have a large uncertainty due to the wide variation among the

RCP CH_4 scenarios, especially RCP8.5 (Section 2.4.3.1). Finally, uncertainties in the kinetic and photolytic loss rate parameters of both CH_4 and N_2O will have significant impacts on future ozone amounts (SPARC, 2013).

2.5 HIGHLIGHTS FOR POLICYMAKERS

This Assessment confirms the success of the international Montreal Protocol for the protection of the ozone layer.

As reported in previous Assessments, the decline of stratospheric ozone has been stopped in the late 1990s. Since about 2000, ozone levels in most parts of the stratosphere have remained approximately constant, or have been increasing slightly. Assessment of the most recent ozone observations since 2010 confirms these overall trends.

In the upper stratosphere, around 40 km altitude, ozone levels have been increasing in the last 10 years, and at a statistically significant rate. This increase is expected and is consistent with scientific understanding. About half of the ozone increase is due to declining ozone-depleting substances (ODSs, declining due to the Montreal Protocol). The other half is due to cooling of the stratosphere due to carbon dioxide (CO_2) increases, which slows chemical ozone destruction cycles in the upper stratosphere.

Not only ozone-depleting substances, but also increasing greenhouse gases affect the ozone layer.

Radiatively active greenhouse gases (GHGs) absorb thermal infrared radiation in the troposphere (global warming). Less thermal radiation reaches the stratosphere. In addition, GHGs, especially CO_2, emit radiation from the stratosphere to space. Both effects result in cooling of the stratosphere with increasing GHG levels. It is expected that GHG levels will increase throughout this century, and that the cooling of the stratosphere will continue.

A small acceleration of the global stratospheric Brewer-Dobson circulation (BDC) over the next century is expected from model simulations. This change is caused by GHG-induced warming of the troposphere and cooling of the stratosphere. Acceleration of the BDC will reduce ozone in the tropics and enhance ozone at higher latitudes.

As shown in previous Assessments, the continuing slow decline of ODSs, and the expected further increase of CO_2, will contribute to a recovery of stratospheric ozone. Model simulations indicate that total column ozone outside of the tropics will recover to 1980s values by 2020 to 2050 and to 1960s values by 2025 to 2060, later in the Antarctic. The recovery dates will depend on future GHG emissions but are expected to remain in this range for different plausible emission scenarios. In the second half of the century, ozone columns may even exceed historical levels. Figure 2-26 shows the expected range of near global (60°S to 60°N) annual mean total column ozone anomalies. In the tropics, ozone columns will probably not recover to 1960 values, but past ozone decline in the tropics has also been small.

Importance of future nitrous oxide and methane emissions

Since the last Assessment, model simulations have confirmed that not only ODSs and CO_2, but also future levels of nitrous oxide (N_2O) and methane (CH_4) will play a significant role in the recovery of stratospheric ozone over this century. By itself, increasing N_2O will increase ozone loss. This would delay and negate part of the expected ozone recovery (due to declining ODSs and stratospheric cooling).

Increasing methane, on the other hand, will generally increase ozone levels by tying up chlorine and by enhancing ozone production in the lower stratosphere. In the second half of the century, lower chlorine levels, stratospheric cooling, and other factors will reduce the efficiency by which CH_4 and N_2O emissions affect ozone.

Continued monitoring

Apart from future ODS levels, future levels of GHGs, especially carbon dioxide (CO_2), nitrous oxide (N_2O), methane (CH_4), and water vapor (H_2O) are expected to have important effects on the evolution of stratospheric ozone. Although most scenarios predict a recovery of stratospheric ozone, only continued measurements of ozone and these trace gases, and the combination of observations and model simulations, can verify that the ozone layer is recovering.

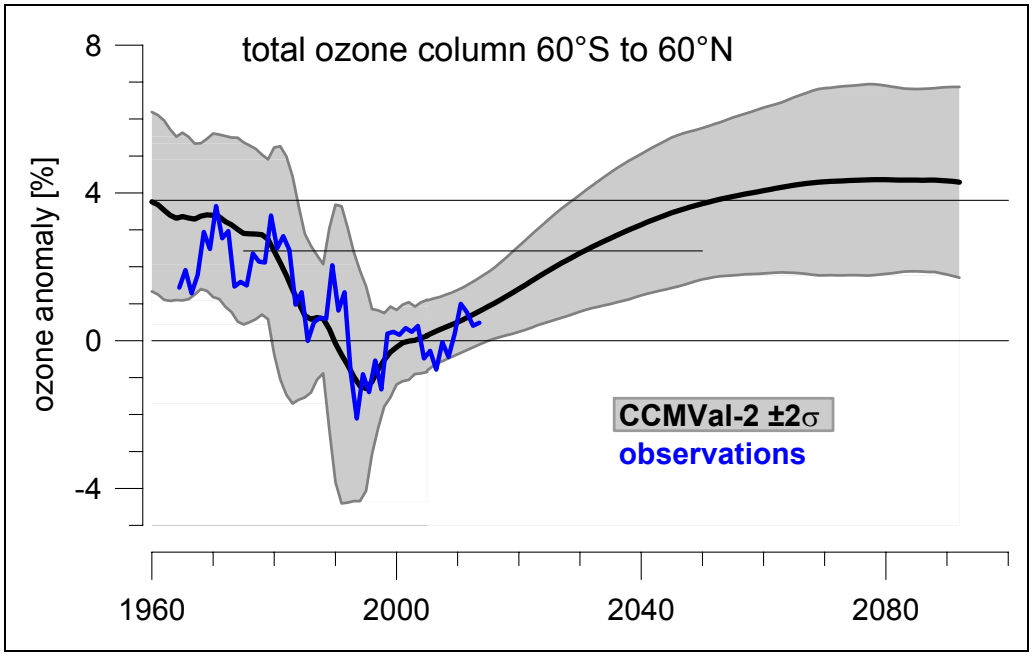

Figure 2-26. Simulated and observed evolution of the near global total ozone column. Observations are annual mean anomalies averaged over all available ground- and satellite-based measurements (blue line). Black line and gray range give multi-model mean and ±2 standard deviations of simulated individual model annual mean anomalies for the CCMVal-2 simulations already used in WMO (2011). Only the subset of 9 models performing runs for fixed ODS and for all forcings is used. All data are referenced to the 1998 to 2008 period. Up to 2000, the simulations account for changing ODSs, GHGs, observed sea surface temperatures and sea ice, volcanic aerosol, the 11-year solar-cycle, and the QBO (REF-B1 scenario, Eyring et al., 2010; WMO, 2011). After 2000 the adjusted A1 scenario of WMO (2007) is used for ODSs, the SRES A1B scenario is used for GHGs, sea surface temperatures and sea ice are from other models, the QBO is generated internally, there is no volcanic aerosol, and most models, except for 3, do not include the solar cycle (REF-B2 scenario, Eyring et al., 2010; WMO, 2011).

REFERENCES

Adams, C., A.E. Bourassa, A.F. Bathgate, C.A. McLinden, N.D. Lloyd, C.Z. Roth, E.J. Llewellyn, J.M. Zawodny, D.E. Flittner, G.L. Manney, W.H. Daffer, and D.A. Degenstein, Characterization of Odin-OSIRIS ozone profiles with the SAGE II dataset, *Atmos. Meas. Tech.*, *6* (5), 1447-1459, doi: 10.5194/amt-6-1447-2013, 2013.

Adams, C., A.E. Bourassa, V. Sofieva, L. Froidevaux, C.A. McLinden, D. Hubert, J.-C. Lambert, C.E. Sioris, and D.A. Degenstein, Assessment of Odin-OSIRIS ozone measurements from 2001 to the present using MLS, GOMOS, and ozonesondes, *Atmos. Meas. Tech.*, *7* (1), 49-64, doi: 10.5194/amt-7-49-2014, 2014.

Antón, M., M. Kroon, M. López, J.M. Vilaplana, M. Bañón, R. van der A, J.P. Veefkind, P. Stammes, and L. Alados-Arboledas, Total ozone column derived from GOME and SCIAMACHY using KNMI retrieval algorithms: Validation against Brewer measurements at the Iberian Peninsula, *J. Geophys. Res.*, *116* (D22), D22303, doi: 10.1029/2011JD016436, 2011.

Aquila, V., L.D. Oman, R. Stolarski, A.R. Douglass, and P.A. Newman, The response of ozone and nitrogen dioxide to the eruption of Mt. Pinatubo at southern and northern midlatitudes, *J. Atmos. Sci.*, *70* (3), 894-900, doi: 10.1175/JAS-D-12-0143.1, 2013.

Baldwin, M.P., L.J. Gray, T.J. Dunkerton, K. Hamilton, P.H. Haynes, W.J. Randel, J.R. Holton, M.J. Alexander, I. Hirota, T. Horinouchi, D.B.A. Jones, J.S. Kinnersley, C. Marquardt, K. Sato, and M. Takahashi, The quasi-biennial oscillation, *Rev. Geophys.*, *39* (2), 179-229, doi: 10.1029/1999RG000073, 2001.

Barath, F.T., M.C. Chavez, R.E. Cofield, D.A. Flower, M.A. Frerking, M.B. Gram, W.M. Harris, J.R. Holden, R.F. Jarnot, W.G. Kloezeman, G.J. Klose, G.K. Lau, M.S. Loo, B.J. Maddison, R.J. Mattauch, R.P. McKinney, G.E. Peckham, H.M. Pickett, G. Siebes, F.S. Soltis, R.A. Suttie, J.A. Tarsala, J.W. Waters, and W.J. Wilson, The Upper Atmosphere Research Satellite microwave limb sounder instrument, *J. Geophys. Res.*, *98* (D6), 10751-10762, doi: 10.1029/93JD00798, 1993.

Bertaux, J.L., E. Kyrölä, D. Fussen, A, Hauchecorne, F. Dalaudier, V. Sofieva, J. Tamminen, F. Vanhellemont, O. Fanton d'Andon, G. Barrot, A. Mangin, L. Blanot, J.C. Lebrun, K. Pérot, T. Fehr, L. Saavedra, G.W. Leppelmeier, and R. Fraisse, Global ozone monitoring by occultation of stars: An overview of GOMOS measurements on ENVISAT, *Atmos. Chem. Phys.*, *10* (24), 12091-12148, doi: 10.5194/acp-10-12091-2010, 2010.

Bhartia, P.K., R.D. McPeters, L.E. Flynn, S. Taylor, N.A. Kramarova, S. Frith, B. Fisher, and M. DeLand, Solar Backscatter UV (SBUV) total ozone and profile algorithm, *Atmos. Meas. Tech.*, *6* (10), 2533-2548, doi: 10.5194/amt-6-2533-2013, 2013.

Bodeker, G.E., B. Hassler, P.J. Young, and R.W. Portmann, A vertically resolved, global, gap-free ozone database for assessing or constraining global climate model simulations, *Earth Syst. Sci. Data*, *5* (1), 31-43, doi: 10.5194/essd-5-31-2013, 2013.

Bojkov, R.D., V.E. Fioletov, and A.M. Shalamjansky, Total ozone changes over Eurasia since 1973 based on reevaluated filter ozonometer data, *J. Geophys. Res.*, *99* (D11), 22985-22999, doi: 10.1029/94JD02006, 1994.

Bourassa, A.E., A. Robock, W.J. Randel, T. Deshler, L.A. Rieger, N.D Lloyd, E.J. Llewellyn, and D.A. Degenstein, Large volcanic aerosol load in the stratosphere linked to Asian Monsoon transport, *Science*, *337* (6090), 78-81, doi: 10.1126/science.1219371, 2012.

Bourassa, A.E., A. Robock, W.J. Randel, T. Deshler, L.A. Rieger, N.D Lloyd, E.J. Llewellyn, and D.A. Degenstein, Response to comments on "Large volcanic aerosol load in the stratosphere linked to Asian Monsoon transport," *Science*, *339* (6120), 647, doi: 10.1126/science.1227961, 2013.

Boyd, I.S., A.D. Parrish, L. Froidevaux, T. von Clarmann, E. Kyrölä, J.M. Russell III, and J.M. Zawodny, Ground-based microwave ozone radiometer measurements compared with Aura-MLS v2.2 and other instruments at two Network for Detection of Atmospheric Composition Change sites, *J. Geophys. Res.*, *112* (D24), D24S33, doi: 10.1029/2007JD008720, 2007.

Brasseur, G., and S. Solomon, *Aeronomy of the Middle Atmosphere*, 3rd ed., Dordrecht, The Netherlands, 2005.

Brönnimann, S., J. Bhend, J. Franke, S. Flückiger, A.M. Fischer, R. Bleisch, G. Bodeker, B. Hassler, E. Rozanov, and M. Schraner, A global historical ozone data set and prominent features of stratospheric variability prior to 1979, *Atmos. Chem. Phys.*, *13* (18), 9623-9639, doi: 10.5194/acp-13-9623-2013, 2013.

Cahalan, R.F., G. Wen, J.W. Harder, and P. Pilewskie, Temperature responses to spectral solar variability on decadal time scales, *Geophys. Res. Lett.*, *37* (7), L07705, doi: 10.1029/2009GL041898, 2010.

Charlton-Perez, A.J., E. Hawkins, V. Eyring, I. Cionni, G.E. Bodeker, D.E. Kinnison, H. Akiyoshi, S.M. Frith, R. Garcia, A. Gettelman, J.F. Lamarque, T. Nakamura, S. Pawson, Y. Yamashita, S. Bekki, P. Braesicke, M.P.

Chipperfield, S. Dhomse, M. Marchand, E. Mancini, O. Morgenstern, G. Pitari, D. Plummer, J.A. Pyle, E. Rozanov, J. Scinocca, K. Shibata, T.G. Shepherd, W. Tian, and D.W. Waugh, The potential to narrow uncertainty in projections of stratospheric ozone over the 21st century, *Atmos. Chem. Phys.*, *10*, 9473-9486, doi: 10.5194/acp-10-9473-2010, 2010.

Chehade, W., M. Weber, and J.P. Burrows, Total ozone trends and variability during 1979-2012 from merged data sets of various satellites, *Atmos. Chem. Phys.*, *14* (13), 7059-7074, doi: 10.5194/acp-14-7059-2014, 2014.

Chiou, E.W., P.K. Bhartia, R.D. McPeters, D.G. Loyola, M. Coldewey-Egbers, V.E. Fioletov, M. Van Roozendael, R. Spurr, C. Lerot, and S.M. Frith, Comparison of profile total ozone from SBUV (v8.6) with GOME-type and ground-based total ozone for the 16-year period (1996 to 2011), *Atmos. Meas. Tech.*, *7* (6), 1681-1692, doi: 10.5194/amt-7-1681-2014, 2014.

Chipperfield, M.P., Q. Liang, S.E. Strahan, O. Morgenstern, S.S. Dhomse, N.L. Abraham, A.T. Archibald, S. Bekki, P. Braesicke, G. Di Genova, E.L. Fleming, S.C. Hardiman, D. Iachetti, C.H. Jackman, D.E. Kinnison, M. Marchand, G. Pitari, J.A. Pyle, E. Rozanov, A. Stenke, and F. Tummon, Multimodel estimates of atmospheric lifetimes of long-lived ozone-depleting substances: Present and future, *J. Geophys. Res.*, *119* (5), 2555-2573, doi: 10.1002/2013JD021097, 2014.

Coldewey-Egbers, M., M. Weber, L.N. Lamsal, R. deBeck, M. Buchwitz, and J.P. Burrows, Total ozone retrieval from GOME UV spectral data using the weighting function DOAS approach, *Atmos. Chem. Phys.*, *5* (4), 1015-1025, doi: 10.5194/acp-5-1015-2005, 2005.

Damadeo, R.P., J.M. Zawodny, L.W. Thomason, and N. Iyer, SAGE version 7.0 algorithm: Application to SAGE II, *Atmos. Meas. Tech.*, *6* (12), 3539-3561, doi: 10.5194/amt-6-3539-2013, 2013.

Daniel, J.S., E.L. Fleming, R.W. Portmann, G.J.M. Velders, C.H. Jackman, and A.R. Ravishankara, Options to accelerate ozone recovery: Ozone and climate benefits, *Atmos. Chem. Phys.*, *10* (16), 7697-7707, doi: 10.5194/acp-10-7697-2010, 2010.

DeLand, M.T., and R.P. Cebula, Solar UV variations during the decline of Cycle 23, *J. Atmos. Sol. Terr. Phys.*, *77*, 225-234, doi: 10.1016/j.jastp.2012.01.007, 2012.

DeLand, M.T., S.L. Taylor, L.K. Huang, and B.L. Fisher, Calibration of the SBUV version 8.6 ozone data product, *Atmos. Meas. Tech.*, *5* (11), 2951-2967, doi: 10.5194/amt-5-2951-2012, 2012.

Deshler, T., J.L. Mercer, H.G.J. Smit, R. Stubi, G. Levrat, B.J. Johnson, S.J. Oltmans, R. Kivi, A.M. Thompson, J. Witte, J. Davies, F.J. Schmidlin, G. Brothers, and T. Sasaki, Atmospheric comparison of electrochemical cell ozonesondes from different manufacturers, and with different cathode solution strengths: The Balloon Experiment on Standards for Ozonesondes, *J. Geophys. Res.*, *113*, D04307, doi: 10.1029/2007JD008975, 2008.

Dhomse, S., M.P. Chipperfield, W. Feng, and J.D. Haigh, Solar response in tropical stratospheric ozone: A 3-D chemical transport model study using ERA reanalyses, *Atmos. Chem. Phys.*, *11* (24), 12773-12786, doi: 10.5194/acp-11-12773-2011, 2011.

Dhomse, S.S., M.P. Chipperfield, W. Feng, W.T. Ball, Y.C. Unruh, J.D. Haigh, N.A. Krivova, S.K. Solanki, and A.K. Smith, Stratospheric O_3 changes during 2001-2010: The small role of solar flux variations in a chemical transport model, *Atmos. Chem. Phys.*, *13* (19), 10113-10123, doi: 10.5194/acp-13-10113-2013, 2013.

Dikty, S., H. Schmidt, M. Weber, C. von Savigny, and M.G. Mlynczak, Daytime ozone and temperature variations in the mesosphere: A comparison between SABER observations and HAMMONIA model, *Atmos. Chem. Phys.*, *10* (17), 8331-8339, doi: 10.5194/acp-10-8331-2010, 2010a.

Dikty, S., M. Weber, C. von Savigny, T. Sonkaew, A. Rozanov, and J.P. Burrows, Modulations of the 27 day solar rotation signal in stratospheric ozone from Scanning Imaging Absorption Spectrometer for Atmospheric Cartography (SCIAMACHY) (2003-2008), *J. Geophys. Res.*, *115*, D00I15, doi: 10.1029/2009JD012379, 2010b.

Douglass, A.R., R.S. Stolarski, S.E. Strahan, and L.D. Oman, Understanding differences in upper stratospheric ozone response to changes in chlorine and temperature as computed using CCMVal-2 models, *J. Geophys. Res.*, *117*, D16306, doi: 10.1029/2012JD017483, 2012.

Douglass, A.R., S.E. Strahan, L.D. Oman, and R.S. Stolarski, Understanding differences in chemistry climate model projections of stratospheric ozone, *J. Geophys. Res.*, *119* (8), 4922-4939, doi: 10.1002/2013JD021159, 2014.

Eckert, E., T. von Clarmann, M. Kiefer, G.P. Stiller, S. Lossow, N. Glatthor, D.A. Degenstein, L. Froidevaux, S. Godin-Beekmann, T. Leblanc, S. McDermid, M. Pastel, W. Steinbrecht, D.P.J. Swart, K.A. Walker, and P.F. Bernath, Drift-corrected trends and periodic variations in MIPAS IMK/IAA ozone measurements, *Atmos. Chem. Phys.*, *14* (5), 2571-2589, doi: 10.5194/acp-14-2571-2014, 2014.

Ermolli, I., K. Matthes, T. Dudok de Wit, N.A. Krivova, K. Tourpali, M. Weber, Y.C. Unruh, L. Gray, U. Langematz, P. Pilewskie, E. Rozanov, W. Schmutz, A. Shapiro, S.K. Solanki, and T.N. Woods, Recent variability of the solar spectral irradiance and its impact on climate modelling, *Atmos. Chem. Phys.*, *13* (8), 3945-3977, doi: 10.5194/acp-13-3945-2013, 2013.

Eyring, V., I. Cionni, G.E. Bodeker, A.J. Charlton-Perez, D.E. Kinnison, J.F. Scinocca, D.W. Waugh, H. Akiyoshi, S. Bekki, M.P. Chipperfield, M. Dameris, S. Dhomse, S.M. Frith, H. Garny, A. Gettelman, A. Kubin, U. Langematz, E. Mancini, M. Marchand, T. Nakamura, L.D. Oman, S. Pawson, G. Pitari, D.A. Plummer, E. Rozanov, T.G. Shepherd, K. Shibata, W. Tian, P. Braesicke, S.C. Hardiman, J.F. Lamarque, O. Morgenstern, J.A. Pyle, D. Smale, and Y. Yamashita, Multi-model assessment of stratospheric ozone return dates and ozone recovery in CCMVal-2 models, *Atmos. Chem. Phys.*, *10*, 9451-9472, doi: 10.5194/acp-10-9451-2010, 2010.

Eyring, V., J.M. Arblaster, I. Cionni, J. Sedláček, J. Perlwitz, P.J. Young, S. Bekki, D. Bergmann, P. Cameron-Smith, W.J. Collins, G. Faluvegi, K.-D. Gottschaldt, L.W. Horowitz, D.E. Kinnison, J.-F. Lamarque, D.R. Marsh, D. Saint-Martin, D.T. Shindell, K. Sudo, S. Szopa, and S. Watanabe, Long-term ozone changes and associated climate impacts in CMIP5 simulations, *J. Geophys. Res.*, *118* (10), 5029-5060, doi: 10.1002/jgrd.50316, 2013.

Fioletov, V.E., Estimating the 27-day and 11-year solar cycle variations in tropical upper stratospheric ozone, *J. Geophys. Res.*, *114*, D02302, doi: 10.1029/2008JD010499, 2009.

Fioletov, V.E., G.E. Bodeker, A.J. Miller, R.D. McPeters, and R. Stolarski, Global and zonal total ozone variations estimated from ground-based and satellite measurements: 1964–2000, *J. Geophys. Res.*, *107* (D22), 4647, doi: 10.1029/2001JD001350, 2002.

Fioletov, V.E., G. Labow, R. Evans, E.W. Hare, U. Köhler, C.T. McElroy, K. Miyagawa, A. Redondas, V. Savastiouk, A.M. Shalamyansky, J. Staehelin, K. Vanicek, and M. Weber, Performance of ground-based total ozone network assessed using satellite data, *J. Geophys. Res.*, *113*, D14313, doi: 10.1029/2008JD009809, 2008.

Fleming, E.L., C.H. Jackman, R.S. Stolarski, and A.R. Douglass, A model study of the impact of source gas changes on the stratosphere for 1850-2100, *Atmos. Chem. Phys.*, *11* (16), 8515-8541, doi: 10.5194/acp-11-8515-2011, 2011.

Froidevaux, L., Y.B. Jiang, A. Lambert, N.J. Livesey, W.G. Read, J.W. Waters, E.V. Browell, J.W. Hair, M.A. Avery, T.J. McGee, L.W. Twigg, G.K. Sumnicht, K.W. Jucks, J.J. Margitan, B. Sen, R.A. Stachnik, G.C. Toon, P.F. Bernath, C.D. Boone, K.A. Walker, M.J. Filipiak, R.S. Harwood, R.A. Fuller, G.L. Manney, M.J. Schwartz, W.H. Daffer, B.J. Drouin, R.E. Cofield, D.T. Cuddy, R.F. Jarnot, B.W. Knosp, V.S. Perun, W.V. Snyder, P.C. Stek, R.P. Thurstans, and P.A. Wagner, Validation of Aura Microwave Limb Sounder stratospheric ozone measurements, *J. Geophys. Res.*, *113* (D15), D15S20, doi: 10.1029/2007JD008771, 2008.

Fromm, M., G. Nedoluha, and Z. Charvát, Comment on "Large volcanic aerosol load in the stratosphere linked to Asian monsoon transport," *Science*, *339* (6120), 647, doi: 10.1126/science.1228605, 2013.

Frossard, L., H.E. Rieder, M. Ribatet, J. Staehelin, J.A. Maeder, S. Di Rocco, A.C. Davison, and T. Peter, On the relationship between total ozone and atmospheric dynamics and chemistry at mid-latitudes – Part 1: Statistical models and spatial fingerprints of atmospheric dynamics and chemistry, *Atmos. Chem. Phys.*, *13* (1), 147-164, doi: 10.5194/acp-13-147-2013, 2013.

Gabriel, A., H. Körnich, S. Lossow, D.H.W. Peters, J. Urban, and D. Murtagh, Zonal asymmetries in middle atmospheric ozone and water vapour derived from Odin satellite data 2001-2010, *Atmos. Chem. Phys.*, *11* (18), 9865-9885, doi: 10.5194/acp-11-9865-2011, 2011a.

Gabriel, A., H. Schmidt, and D.H.W. Peters, Effects of the 11 year solar cycle on middle atmospheric stationary wave patterns in temperature, ozone, and water vapor, *J. Geophys. Res.*, *116*, D23301, doi: 10.1029/2011JD015825, 2011b.

Garny, H., G.E. Bodeker, D. Smale, M. Dameris, and V. Grewe, Drivers of hemispheric differences in return dates of mid-latitude stratospheric ozone to historical levels, *Atmos. Chem. Phys.*, *13* (15), 7279-7300, doi: 10.5194/acp-13-7279-2013, 2013.

Gebhardt, C., A. Rozanov, R. Hommel, M. Weber, H. Bovensmann, J.P. Burrows, D. Degenstein, L. Froidevaux, and A.M. Thompson, Stratospheric ozone trends and variability as seen by SCIAMACHY from 2002 to 2012, *Atmos. Chem. Phys.*, *14* (2), 831-846, doi: 10.5194/acp-14-831-2014, 2014.

Gillett, N.P., H. Akiyoshi, S. Bekki, P. Braesicke, V. Eyring, R. Garcia, A.Yu. Karpechko, C.A. McLinden, O. Morgenstern, D.A. Plummer, J.A. Pyle, E. Rozanov, J. Scinocca, and K. Shibata, Attribution of observed changes in stratospheric ozone and temperature, *Atmos. Chem. Phys.*, *11* (2), 599-609, doi: 10.5194/acp-11-599-2011, 2011.

Gottwald, M., and H. Bovensmann, *SCIAMACHY - Exploring the Changing Earth's Atmosphere*, Dordrecht Heidelberg London New York, doi: 10.1007/978-90-481-9896-2, 2011.

Gray, L.J., J. Beer, M. Geller, J.D. Haigh, M. Lockwood, K. Matthes, U. Cubasch, D. Fleitmann, G. Harrison, L. Hood, J. Luterbacher, G.A. Meehl, D. Shindell, B. van Geel, and W. White, Solar influence on climate, *Rev. Geophys.*, *48*, RG4001, doi: 10.1029/2009RG000282, 2010.

Gruzdev, A.N., H. Schmidt, and G.P. Brasseur, The effect of the solar rotational irradiance variation on the middle and upper atmosphere calculated by a three-dimensional chemistry-climate model, *Atmos. Chem. Phys.*, *9* (2), 595-614, doi: 10.5194/acp-9-595-2009, 2009.

Haefele, A., K. Hocke, N. Kämpfer, P. Keckhut, M. Marchand, S. Bekki, B. Morel, T. Egorova, and E. Rozanov, Diurnal changes in middle atmospheric H_2O and O_3: Observations in the Alpine region and climate models, *J. Geophys. Res.*, *113* (D17), D17303, doi: 10.1029/2008JD009892, 2008.

Haigh, J.D., A.R. Winning, R. Toumi, and J.W. Harder, An influence of solar spectral variations on radiative forcing of climate, *Nature*, *467*, 696-699, doi: 10.1038/nature09426, 2010.

Harder, J.W., J.M. Fontenla, P. Pilewskie, E.C. Richard, and T.N. Woods, Trends in solar spectral irradiance variability in the visible and infrared, *Geophys. Res. Lett.*, *36*, L07801, doi: 10.1029/2008GL036797, 2009.

Harris, N.R.P., E. Kyrö, J. Staehelin, D. Brunner, S.-B. Andersen, S. Godin-Beekmann, S. Dhomse, P. Hadjinicolaou, G. Hansen, I. Isaksen, A. Jrrar, A. Karpetchko, R. Kivi, B. Knudsen, P. Krizan, J. Lastovicka, J. Maeder, Y. Orsolini, J.A. Pyle, M. Rex, K. Vanicek, M. Weber, I. Wohltmann, P. Zanis, and C. Zerefos, Ozone trends at northern mid- and high latitudes – a European perspective, *Ann. Geophys.*, *26*, 1207-1220, 2008.

Hassler, B., G.E. Bodeker, I. Cionni, and M. Dameris, A vertically resolved, monthly mean, ozone database from 1979 to 2100 for constraining global climate model simulations, *Int. J. Remote Sens.*, *30* (15-16), 4009-4018, doi: 10.1080/01431160902821874, 2009.

Hassler, B., I. Petropavlovskikh, J. Staehelin, T. August, P.K. Bhartia, C. Clerbaux, D. Degenstein, M. De Mazière, B.M. Dinelli, A. Dudhia, G. Dufour, S.M. Frith, L. Froidevaux, S. Godin-Beekmann, J. Granville, N.R.P. Harris, K. Hoppel, D. Hubert, Y. Kasai, M.J. Kurylo, E. Kyrölä, J.-C. Lambert, P.F. Levelt, C.T. McElroy, R.D. McPeters, R. Munro, H. Nakajima, A. Parrish, P. Raspollini, E.E. Remsberg, K.H. Rosenlof, A. Rozanov, T. Sano, Y. Sasano, M. Shiotani, H.G.J. Smit, G. Stiller, J. Tamminen, D.W. Tarasick, J. Urban, R.J. van der A, J.P. Veefkind, C. Vigouroux, T. von Clarmann, C. von Savigny, K.A. Walker, M. Weber, J. Wild, and J. Zawodny, SI2N overview paper: Ozone profile measurements: Techniques, uncertainties and availability, *Atmos. Meas. Tech.*, 7, 1395-1427, doi: 10.5194/amt-7-1395-2014, 2014.

Hegerl G.C., H. von Storch, K. Hasselmann, B.D. Santer, U. Cubasch, and P.D. Jones, Detecting greenhouse-gas-induced climate change with an optimal fingerprint method, *J. Clim.*, *9* (10), 2281-2306, doi: 10.1175/1520-0442(1996)009<2281:DGGICC>2.0.CO;2, 1996.

Hendrick, F., J.-P. Pommereau, F. Goutail, R.D. Evans, D. Ionov, A. Pazmino, E. Kyrö, G. Held, P. Eriksen, V. Dorokhov, M. Gil, and M. Van Roozendael, NDACC/SAOZ UV-visible total ozone measurements: Improved retrieval and comparison with correlative ground-based and satellite observations, *Atmos. Chem. Phys.*, *11* (12), 5975-5995, doi: 10.5194/acp-11-5975-2011, 2011.

Hofmann, D., J. Barnes, M. O'Neill, M. Trudeau, and R. Neely, Increase in background stratospheric aerosol observed with lidar at Mauna Loa Observatory and Boulder, Colorado, *Geophys. Res. Lett.*, *36*, L15808, doi: 10.1029/2009GL039008, 2009.

Hood, L.L., and B.E. Soukharev, The lower-stratospheric response to 11-yr solar forcing: Coupling to the troposphere-ocean response, *J. Atmos. Sci.*, *69* (6), 1841-1864, doi: 10.1175/JAS-D-11-086.1, 2012.

Hood, L.L., B.E. Soukharev, and J.P. McCormack, Decadal variability of the tropical stratosphere: Secondary influence of the El Niño-Southern Oscillation, *J. Geophys. Res.*, *115* (D11), D11113, doi: 10.1029/2009 JD012291, 2010.

Huang, F.T., C.A. Reber, and J. Austin, Ozone diurnal variations observed by UARS and their model simulation, *J. Geophys. Res.*, *102* (D11), 12971-12985, doi: 10.1029/97JD00461, 1997.

Huang, F.T., H.G. Mayr, J.M. Russell III, M.G. Mlynczak, and C.A. Reber, Ozone diurnal variations and mean profiles in the mesosphere, lower thermosphere, and stratosphere, based on measurements from SABER on TIMED, *J. Geophys. Res.*, *113* (A4), A04307, doi: 10.1029/2007JA012739, 2008.

Huang, F.T., H.G. Mayr, J.M. Russell III, and M.G. Mlynczak, Ozone diurnal variations in the stratosphere and lower mesosphere, based on measurements from SABER on TIMED, *J. Geophys. Res.*, *115* (D24), D24308, doi: 10.1029/2010JD014484, 2010.

IPCC (Intergovernmental Panel on Climate Change), *Climate Change 2007: The Physical Science Basis: Contribution of Working Group I to the Fourth Assessment Report of the Intergovernmental Panel on Climate Change*, edited by Solomon, S., D. Qin, M. Manning, Z. Chen, M. Marquis, K.B. Averyt, M. Tignor, and H.L. Miller, 996 pp., Cambridge University Press, Cambridge, U.K., and New York, NY, U.S.A., 2007.

IPCC (Intergovernmental Panel on Climate Change), *Climate Change 2013: The Physical Science Basis: Contribution of Working Group I to the Fifth Assessment Report of the Intergovernmental Panel on Climate Change*, edited by T.F. Stocker, D. Qin, G.-K. Plattner, M. Tignor, S.K. Allen, J. Boschung, A. Nauels, Y. Xia, V. Bex, and P.M. Midgley, 1535 pp., Cambridge University Press, Cambridge, UK, and New York, NY, USA, 2013.

Jones, A., J. Urban, D.P. Murtagh, P. Eriksson, S. Brohede, C. Haley, D. Degenstein, A. Bourassa, C. von Savigny, T. Sonkaew, A. Rozanov, H. Bovensmann, and J. Burrows, Evolution of stratospheric ozone and water vapour time series studied with satellite measurements, *Atmos. Chem. Phys.*, *9* (16), 6055-6075, doi: 10.5194/acp-9-6055-2009, 2009.

Jones, A., J. Urban, D.P. Murtagh, C. Sanchez, K.A. Walker, N.J. Livesey, L. Froidevaux, and M.L. Santee, Analysis of HCl and ClO time series in the upper stratosphere using satellite data sets, *Atmos. Chem. Phys.*, *11* (11), 5321-5333, doi: 10.5194/acp-11-5321-2011, 2011.

Jonsson, A.I., V.I. Fomichev, and T.G. Shepherd, The effect of nonlinearity in CO_2 heating rates on the attribution of stratospheric ozone and temperature changes. *Atmos. Chem. Phys.*, *9*, 8447-8452, doi: 10.5194/acp-9-8447-2009, 2009.

Karpechko, A.Y., D. Maraun, and V. Eyring, Improving Antarctic total ozone projections by a process-oriented multiple diagnostic ensemble regression, *J. Atmos. Sci.*, *70* (12), 3959-3976, doi: 10.1175/JAS-D-13-071.1, 2013.

Kiesewetter, G., B.-M., Sinnhuber, M. Weber, and J.P. Burrows, Attribution of stratospheric ozone trends to chemistry and transport: A modelling study, *Atmos. Chem. Phys.*, *10* (24), 12073-12089, doi: 10.5194/acp-10-12073-2010, 2010.

Kirgis, G., T. Leblanc, I.S. McDermid, and T.D. Walsh, Stratospheric ozone interannual variability (1995-2011) as observed by lidar and satellite at Mauna Loa Observatory, HI and Table Mountain Facility, CA, *Atmos. Chem. Phys.*, *13* (9), 5033-5047, doi: 10.5194/acp-13-5033-2013, 2013.

Knutti, R., G. Abramowitz, M. Collins, V. Eyring, P.J. Gleckler, B. Hewitson, and L. Mearns, Good practice guidance paper on assessing and combining multi model climate projections, *IPCC Expert Meeting on Assessing and Combining Multi Model Climate Projections*, edited by T. Stocker, D. Qin, G.-K. Plattner, M. Tignor, and P.M. Midgley, 13 pp., University of Bern, Bern, Switzerland, 2010.

Kobayashi C., and K. Shibata, Evaluation of dynamical contribution to lower stratospheric ozone trends in northern mid-latitudes over the last three decades (1980–2006) using a Chemical Transport Model, *J. Meteorol. Soc. Japan.*, *89* (4), 363-376, doi: 10.2151/jmsj.2011-405, 2011.

Koukouli, M.E., D.S. Balis, D. Loyola, P. Valks, W. Zimmer, N. Hao, J.-C. Lambert, M. Van Roozendael, C. Lerot, and R.J.D. Spurr, Geophysical validation and long-term consistency between GOME-2/MetOp-A total ozone column and measurements from the sensors GOME/ERS-2, SCIAMACHY/ENVISAT and OMI/Aura, *Atmos. Meas. Tech.*, *5* (9), 2169-2181, doi: 10.5194/amt-5-2169-2012, 2012.

Kramarova, N.A., S.M. Frith, P.K. Bhartia, R.D. McPeters, S.L. Taylor, B.L. Fisher, G.J. Labow, and M.T. DeLand, Validation of ozone monthly zonal mean profiles obtained from the version 8.6 Solar Backscatter Ultraviolet algorithm, *Atmos. Chem. Phys.*, *13* (14), 6887-6905, doi: 10.5194/acp-13-6887-2013, 2013a.

Kramarova, N.A., P.K. Bhartia, S.M. Frith, R.D. McPeters, and R.S. Stolarski, Interpreting SBUV smoothing errors: An example using the quasi-biennial oscillation, *Atmos. Meas. Tech.*, *6* (8), 2089-2099, doi: 10.5194/amt-6-2089-2013, 2013b.

Kramarova, N.A., E.R. Nash, P.A. Newman, P.K. Bhartia, R.D. McPeters, D.F. Rault, C.J. Seftor, P.Q. Xu, and G.J. Labow, Measuring the Antarctic ozone hole with the new Ozone Mapping and Profiler Suite (OMPS), *Atmos. Chem. Phys.*, *14* (5), 2353-2361, doi: 10.5194/acp-14-2353-2014, 2014.

Kroon, M., J.P. Veefkind, M. Sneep, R.D. McPeters, P.K. Bhartia, and P.F. Levelt, Comparing OMI-TOMS and OMI-DOAS total ozone column data, *J. Geophys. Res.*, *113* (D16), D16S28, doi: 10.1029/2007JD008798, 2008.

Kroon, M., J.F. de Haan, J.P. Veefkind, L. Froidevaux, R. Wang, R. Kivi, and J.J. Hakkarainen, Validation of operational ozone profiles from the Ozone Monitoring Instrument, *J. Geophys. Res.*, *116* (D18), D18305, doi: 10.1029/2010JD015100, 2011.

Krzyścin, J.W., Onset of the total ozone increase based on statistical analyses of global ground-based data for the period 1964–2008, *Int. J. Clim.*, *32* (2), 240-246, doi: 10.1002/joc.2264, 2012.

Kubin, A., U. Langematz, and C. Brühl, Chemistry climate model simulations of the effect of the 27 day solar rotational cycle on ozone, *J. Geophys. Res.*, *116* (D15), D15301, doi: 10.1029/2011JD015665, 2011.

Kyrölä, E., J. Tamminen, V. Sofieva, J.L. Bertaux, A. Hauchecorne, F. Dalaudier, D. Fussen, F. Vanhellemont, O. Fanton d'Andon, G. Barrot, M. Guirlet, T. Fehr, and L. Saavedra de Miguel, GOMOS O_3, NO_2, and NO_3 observations in 2002–2008, *Atmos. Chem. Phys.*, *10* (16), 7723-7738, doi: 10.5194/acp-10-7723-2010, 2010.

Kyrölä, E., M. Laine, V. Sofieva, J. Tamminen, S.-M. Päivärinta, S. Tukiainen, J. Zawodny, and L. Thomason, Combined SAGE II-GOMOS ozone profile data set for 1984-2011 and trend analysis of the vertical distribution of ozone, *Atmos. Chem. Phys.*, *13* (21), 10645-10658, doi: 10.5194/acp-13-10645-2013, 2013.

Labow, G.J., R.D. McPeters, P.K. Bhartia, and N. Kramarova, A comparison of 40 years of SBUV measurements of column ozone with data from the Dobson/Brewer network, *J. Geophys. Res.*, *118* (13), 7370-7378, doi: 10.1002/jgrd.50503, 2013.

Lamarque, J.-F., D.T. Shindell, B. Josse, P.J. Young, I. Cionni, V. Eyring, D. Bergmann, P. Cameron-Smith, W.J. Collins, R. Doherty, S. Dalsoren, G. Faluvegi, G. Folberth, S.J. Ghan, L.W. Horowitz, Y.H. Lee, I.A. MacKenzie, T. Nagashima, V. Naik, D. Plummer, M. Righi, S.T. Rumbold, M. Schulz, R.B. Skeie, D.S. Stevenson, S. Strode, K. Sudo, S. Szopa, A. Voulgarakis, and G. Zeng, The Atmospheric Chemistry and Climate Model Intercomparison Project (ACCMIP): Overview and description of models, simulations and climate diagnostics, *Geosci. Model Dev.*, *6* (1), 179-206, doi: 10.5194/gmd-6-179-2013, 2013.

Lean, J., Evolution of the sun's spectral irradiance since the Maunder Minimum, *Geophys. Res. Lett.*, *27* (16), 2425-2428, doi: 10.1029/2000GL000043, 2000.

Lean, J.L., and M.T. DeLand, How does the sun's spectrum vary?, *J. Clim.*, *25* (7), 2555-2560, doi: 10.1175/JCLI-D-11-00571.1, 2012.

Lerot, C., M. Van Roozendael, R. Spurr, D. Loyola, M. Coldewey-Egbers, S. Kochenova, J. van Gent, M. Koukouli, D. Balis, J.-C. Lambert, J. Granville, and C. Zehner, Homogenized total ozone data records from the European sensors GOME/ERS-2, SCIAMACHY/Envisat, and GOME-2/MetOp-A, *J. Geophys. Res.*, *119* (3), 1639-1662, doi: 10.1002/2013JD020831, 2014.

Li, F., R.S. Stolarski, and P.A. Newman, Stratospheric ozone in the post-CFC era, *Atmos. Chem. Phys.*, *9* (6), 2207-2213, doi: 10.5194/acp-9-2207-2009, 2009.

Lin, P., and Q. Fu, Changes in various branches of the Brewer-Dobson circulation from an ensemble of chemistry climate models, *J. Geophys. Res.*, *118*, 73-84, doi: 10.1029/2012JD018813, 2013.

Liu, J., D.W. Tarasick, V.E. Fioletov, C. McLinden, T. Zhao, S. Gong, C. Sioris, J.J. Jin, G. Liu, and O. Moeini, A global ozone climatology from ozone soundings via trajectory mapping: A stratospheric perspective, *Atmos. Chem. Phys.*, *13* (22), 11441-11464, doi: 10.5194/acp-13-11441-2013, 2013.

Livesey, N.J., W. Van Snyder, W.G. Read, and P.A. Wagner, Retrieval algorithms for the EOS Microwave Limb Sounder (MLS), *IEEE Trans. Geosci. Rem. Sens.*, *44* (5), 1144-1155, doi: 10.1109/TGRS.2006.872327, 2006.

Loyola, D.G., R.M. Coldewey-Egbers, M. Dameris, H. Garny, A. Stenke, M. Van Roozendael, C. Lerot, D. Balis, and M. Koukouli, Global long-term monitoring of the ozone layer — a prerequisite for predictions, *Int. J. Remote Sens.*, *30*, 4295-4318, doi: 10.1080/01431160902825016, 2009.

Manney, G.L., M.L. Santee, M. Rex, N.J. Livesey, M.C. Pitts, P. Veefkind, E.R. Nash, I. Wohltmann, R. Lehmann, L. Froidevaux, L.R. Poole, M.R. Schoeberl, D.P. Haffner, J. Davies, V. Dorokhov, H. Gernandt, B. Johnson, R. Kivi, E. Kyrö, N. Larsen, P.F. Levelt, A. Makshtas, C.T. McElroy, H. Nakajima, M.C. Parrondo, D.W. Tarasick, P. von der Gathen, K.A. Walker, and N.S. Zinoviev, Unprecedented Arctic ozone loss in 2011, *Nature*, *478*, 469-475, doi: 10.1038/nature10556, 2011.

Mäder, J.A., J. Staehelin, T. Peter, D. Brunner, H.E. Rieder, and W.A. Stahel, Evidence for the effectiveness of the Montreal Protocol to protect the ozone layer, *Atmos. Chem. Phys.*, *10* (24), 12161-12171, doi: 10.5194/acp-10-12161-2010, 2010.

McLinden, C.A., and V. Fioletov, Quantifying stratospheric ozone trends: Complications due to stratospheric cooling, *Geophys. Res. Lett.*, *38* (3), L03808, doi: 10.1029/2010GL046012, 2011.

McLinden, C.A., S. Tegtmeier, and V. Fioletov, Technical note: A SAGE-corrected SBUV zonal-mean ozone data set, *Atmos. Chem. Phys.*, *9* (20), 7963-7972, doi: 10.5194/acp-9-7963-2009, 2009.

McLinden, C.A., A.E. Bourassa, S. Brohede, M. Cooper, D.A. Degenstein, W.J.F. Evans, R.L. Gattinger, C.S. Haley, E.J. Llewellyn, N.D. Lloyd, P. Loewen, R.V. Martin, J.C. McConnell, I.C. McDade, D. Murtagh, L. Rieger, C. von Savigny, P.E. Sheese, C.E. Sioris, B. Solheim, and K. Strong, OSIRIS: A decade of scattered light, *Bull. Am. Meteorol. Soc.*, *93* (12), 1845-1863, doi: 10.1175/BAMS-D-11-00135.1, 2012.

McPeters, R.D., P.K. Bhartia, D. Haffner, G.J. Labow, and L. Flynn, The version 8.6 SBUV ozone data record: An overview, *J. Geophys. Res.*, *118* (14), 8032-8039, doi: 10.1002/jgrd.50597, 2013.

Meehl, G.A., C. Covey, T. Delworth, M. Latif, B. McAvaney, J.F.B. Mitchell, R.J. Stouffer, and K.E. Taylor, The WCRP CMIP3 multi-model dataset: A new era in climate change research, *Bull. Amer. Meteorol. Soc.*, *88* (9), 1383-1394, doi: 10.1175/BAMS-88-9-1383, 2007.

Merkel, A.W., J.W. Harder, D.R. Marsh, A.K. Smith, J.M. Fontenla, and T.N. Woods, The impact of solar spectral irradiance variability on middle atmospheric ozone, *Geophys. Res. Lett.*, *38* (13), L13802, doi: 10.1029/2011 GL047561, 2011.

Meul, S., U. Langematz, S. Oberländer, H. Garny, and P. Jöckel, Chemical contribution to future tropical ozone change in the lower stratosphere, *Atmos. Chem. Phys*., *14*, 2959-2971, doi: 10.5194/acp-14-2959-2014, 2014.

Michou, M., D. Saint-Martin, H. Teyssèdre, A. Alias, F. Karcher, D. Olivié, A. Voldoire, B. Josse, V.-H. Peuch, H. Clark, J.N. Lee, and F. Chéroux, A new version of the CNRM Chemistry-Climate Model, CNRM-CCM: Description and improvements from the CCMVal-2 simulations, *Geosci. Model Dev.*, *4* (4), 873-900, doi: 10.5194/gmd-4-873-2011, 2011.

Miller, A.J., A. Cai, G. Taio, D.J. Wuebbles, L.E. Flynn, S.-K. Yang, E.C. Weatherhead, V. Fioletov, I. Petropavlovskikh, X.-L. Meng, S. Guillas, R.M. Nagatani, and G.C. Reinsel, Examination of ozonesonde data for trends and trend changes incorporating solar and Arctic oscillation signals, *J. Geophys. Res.*, *111*, D13305, doi: 10.1029/2005JD006684, 2006.

Mills, M.J., O.B. Toon, R.P. Turco, D.E. Kinnison, and R.R. Garcia, Massive global ozone loss predicted following regional nuclear conflict, *Proc. Nat. Acad. Sci.*, *105* (14), 5307-5312, doi: 10.1073/pnas.0710058105, 2008.

Morgenstern, O., M.A. Giorgetta, K. Shibata, V. Eyring, D.W. Waugh, T.G. Shepherd, H. Akiyoshi, J. Austin, A.J.G. Baumgaertner, S. Bekki, P. Braesicke, C. Brühl, M.P. Chipperfield, D. Cugnet, M. Dameris, S. Dhomse, S.M. Frith, H. Garny, A. Gettelman, S.C. Hardiman, M.I. Hegglin, P. Jöckel, D.E. Kinnison, J.-F. Lamarque, E. Mancini, E. Manzini, M. Marchand, M. Michou, T. Nakamura, J.E. Nielsen, D. Olivié, G. Pitari, D.A. Plummer, E. Rozanov, J.F. Scinocca, D. Smale, H. Teyssèdre, M. Toohey, W. Tian, and Y. Yamashita, Review of the formulation of present-generation stratospheric chemistry-climate models and associated external forcings, *J. Geophys. Res.*, *115*, D00M02, doi: 10.1029/2009JD013728, 2010.

Nagai, T., B. Liley, T. Sakai, T. Shibata, and O. Uchino, Post-pinatubo evolution and subsequent trend of the stratospheric aerosol layer observed by mid-latitude lidars in both hemispheres, *Sola*, *6*, 69-72, doi: 10.2151/sola.2010-018, 2010.

Nair, P.J., S. Godin-Beekmann, A. Pazmiño, A. Hauchecorne, G. Ancellet, I. Petropavlovskikh, L.E. Flynn, and L. Froidevaux, Coherence of long-term stratospheric ozone vertical distribution time series used for the study of ozone recovery at a northern mid-latitude station, *Atmos. Chem. Phys.*, *11* (10), 4957-4975, doi: 10.5194/acp-11-4957-2011, 2011.

Nair, P.J., S. Godin-Beekmann, L. Froidevaux, L.E. Flynn, J.M. Zawodny, J.M. Russell III, A. Pazmiño, G. Ancellet, W. Steinbrecht, H. Claude, T. Leblanc, S. McDermid, J.A.E van Gijsel, B. Johnson, A. Thomas, D. Hubert, J.-C. Lambert, H. Nakane, and D.P.J. Swart, Relative drifts and stability of satellite and ground-based stratospheric ozone profiles at NDACC lidar stations, *Atmos. Meas. Tech.*, *5* (6), 1301-1318, doi: 10.5194/ amt-5-1301-2012, 2012.

Nair, P.J., S. Godin-Beekmann, J. Kuttippurath, G. Ancellet, F. Goutail, A. Pazmiño, L. Froidevaux, J.M. Zawodny, R.D. Evans, H.J. Wang, J. Anderson, and M. Pastel, Ozone trends derived from the total column and vertical profiles at a northern mid-latitude station, *Atmos. Chem. Phys.*, *13* (20), 10373-10384, doi: 10.5194/acp-13-10373-2013, 2013.

Neely, R.R. III, O.B. Toon, S. Solomon, J.-P. Vernier, C. Alvarez, J.M. English, K.H. Rosenlof, M.J. Mills, C.G. Bardeen, J.S. Daniel, and J.P. Thayer, Recent anthropogenic increases in SO_2 from Asia have minimal impact on stratospheric aerosol, *Geophys. Res. Lett.*, *40* (5), 999-1004, doi: 10.1002/grl.50263, 2013.

Nevison, C.D, S. Solomon, and R.S. Gao, Buffering interactions in the modelled response of stratospheric O_3 to increased NO_x and HO_x, *J. Geophys. Res.*, *104*, 3741-3754, doi: 10.1029/1998JD100018, 1999.

Newchurch, M.J., E.-S. Yang, D.M. Cunnold, G.C. Reinsel, J.M. Zawodny, and J.M. Russell III, Evidence for slowdown in stratospheric ozone loss: First stage of ozone recovery, *J. Geophys. Res.*, *108* (D16), 4507, doi: 10.1029/2003JD003471, 2003.

Newman, P.A., J.S. Daniel, D.W. Waugh, and E.R. Nash, A new formulation of equivalent effective stratospheric chlorine (EESC), *Atmos. Chem. Phys.*, *7* (17), 4537-4522, doi: 10.5194/acp-7-4537-2007, 2007.

Oberländer, S., U. Langematz, K. Matthes, M. Kunze, A. Kubin, J. Harder, N.A. Krivova, S.K. Solanki, J. Pagaran, and M. Weber, The Influence of spectral solar irradiance data on stratospheric heating rates during the 11 year solar cycle, *Geophys. Res. Lett.*, *39* (1), L01801, doi: 10.1029/2011GL049539, 2012.

Oberländer S., U. Langematz, and S. Meul, Unravelling impact factors for future changes of the Brewer-Dobson circulation, *J. Geophys. Res.*, *118* (18), 10296-10312, doi: 10.1002/jgrd. 50775, 2013.

Oman, L.D., and A.R. Douglass, Improvements in total column ozone in GEOSCCM and comparisons with a new ozone-depleting substances scenario, *J. Geophys. Res.*, *119* (9), doi: 10.1002/2014JD021590, 2014.

Oman, L.D., D.W. Waugh, S.R. Kawa, R.S. Stolarski, A.R. Douglass, and P.A. Newman, Mechanisms and feedbacks causing changes in upper stratospheric ozone in the 21st century, *J. Geophys. Res.*, *115*, D05303, doi: 10.1029/2009JD012397, 2010a.

Oman, L.D., D.A. Plummer, D.W. Waugh, J. Austin, J.F. Scinocca, A.R. Douglass, R.J. Salawitch, T. Canty, H. Akiyoshi, S. Bekki, P. Braesicke, N. Butchart, M.P. Chipperfield, D. Cugnet, S. Dhomse, V. Eyring, S. Frith, S.C. Hardiman, D.E. Kinnison, J.-F. Lamarque, E. Mancini, M. Marchand, M. Michou, O. Morgenstern, T. Nakamura, J.E. Nielsen, D. Olivié, G. Pitari, J. Pyle, E. Rozanov, T.G. Shepherd, K. Shibata, R.S. Stolarski, H. Teyssèdre, W. Tian, Y. Yamashita, and J.R. Ziemke, Multimodel assessment of the factors driving stratospheric ozone evolution over the 21st century, *J. Geophys. Res.*, *115* (D24), D24306, doi: 10.1029/2010 JD014362, 2010b.

Oman, L.D., J.R. Ziemke, A.R. Douglass, D.W. Waugh, C. Lang, J.M. Rodriguez, and J.E. Nielsen, The response of tropical tropospheric ozone to ENSO, *Geophysical Res. Lett.*, *38* (13), L13706, doi: 10.1029/2011 GL047865, 2011.

Oman, L., A. Douglass, J. Ziemke, J. Rodriguez, D. Waugh, and J. Nielsen, The ozone response to ENSO in Aura satellite measurements and a chemistry-climate simulation, *J. Geophys. Res.*, *118* (2), 965-976, doi: 10.1029/2012JD018546, 2013.

Ossó, A., Y. Sola, J. Bech, and J. Lorente, Evidence for the influence of the North Atlantic Oscillation on the total ozone column at northern low latitudes and midlatitudes during winter and summer seasons, *J. Geophys. Res.*, *116* (D24), D24122, doi: 10.1029/2011JD016539, 2011.

Ott, L., B. Duncan, S. Pawson, P. Colarco, M. Chin, C. Randles, T. Diehl, and E. Nielsen, Influence of the 2006 Indonesian biomass burning aerosols on tropical dynamics studied with the GEOS-5 AGCM, *J. Geophys. Res.*, *115* (D14), D14121, doi: 10.1029/2009JD013181, 2010.

Petropavlovskikh, I., P.K. Bhartia, and J.J. DeLuisi, New Umkehr ozone profile retrieval algorithm optimized for climatological studies, *Geophys. Res. Lett.*, *32*, L16808, doi: 10.1029/2005GL023323, 2005.

Pitari, G., V. Aquila, B. Kravitz, A. Robock, S. Watanabe, I. Cionni, N. De Luca, G. Di Genova, E. Mancini, and S. Tilmes, Stratospheric ozone response to sulfate geoengineering: Results from the Geoengineering Model Intercomparison Project (GeoMIP), *J. Geophys. Res.*, *119* (5), 2629-2653, doi: 10.1002/2013JD020566, 2014.

Plummer, D.A., J.F. Scinocca, T.G. Shepherd, M.C. Reader, and A.I. Jonsson, Quantifying the contributions of stratospheric ozone changes from ozone depleting substances and greenhouse gases, *Atmos. Chem. Phys.*, *10* (18), 8803-8820, doi: 10.5194/acp-10-8803-2010, 2010.

Poberaj, C.S., J. Staehelin, and D. Brunner, Missing stratospheric ozone decrease at southern hemisphere middle latitudes after Mt. Pinatubo: A dynamical perspective, *J. Atmos. Sci.*, *68* (9), 1922-1945, doi: 10.1175/JAS-D-10-05004.1, 2011.

Portmann, R.W., and S. Solomon, Indirect radiative forcing of the ozone layer during the 21st century, *Geophys. Res. Lett*., *34*, L02813, doi: 10.1029/2006GL028252, 2007.

Portmann, R.W., J.S. Daniel, and A.R. Ravishankara, Stratospheric ozone depletion due to nitrous oxide: Influences of other gases, *Phil. Trans. R. Soc. Lond. B Biol. Sci.*, *367* (1593), 1256-1264, doi: 10.1098/rstb.2011.0377, 2012.

Randel, W.J., and E.J. Jensen, Physical processes in the tropical tropopause layer and their roles in a changing climate, *Nature Geosci*., *6* (3), 169-176, doi: 10.1038/ngeo1733, 2013.

Randel, W.J., and A.M. Thompson, Interannual variability and trends in tropical ozone derived from SAGE II satellite data and SHADOZ ozonesondes, *J. Geophys. Res.*, *116* (D7), D07303, doi: 10.1029/2010JD015195, 2011.

Randel, W.J., and F. Wu, A stratospheric ozone profile data set for 1979–2005: Variability, trends, and comparisons with column ozone data, *J. Geophys. Res.*, *112*, D06313, doi: 10.1029/2006JD007339, 2007.

Randel, W.J., R.R. Garcia, N. Calvo, and D. Marsh, ENSO influence on zonal mean temperature and ozone in the tropical lower stratosphere, *Geophys. Res. Lett.*, *36* (15), L15822, doi: 10.1029/2009GL039343, 2009.

Randeniya, L.K., P.F. Vohralik, and I.C. Plumb, Stratospheric ozone depletion at northern mid latitudes in the 21st century: The importance of future concentrations of greenhouse gases nitrous oxide and methane, *Geophys. Res. Lett.*, *29* (4), 1051, doi: 10.1029/2001GL014295, 2002.

Ravishankara, A.R., J.S. Daniel, and R.W. Portmann, Nitrous oxide (N_2O): The dominant ozone-depleting substance emitted in the 21st century, *Science*, *326* (5949), 123-125, doi: 10.1126/science.1176985, 2009.

Reinsel, G.C., E.C. Weatherhead, G.C. Tiao, A.J. Miller, R.M. Nagatani, D.J. Wuebbles, and L.E. Flynn, On detection of turnaround and recovery in trend for ozone, *J. Geophys. Res.*, *107* (D10), 4078, doi: 10.1029/2001JD000500, 2002.

Reinsel, G.C., A.J. Miller, E.C. Weatherhead, L.E. Flynn, R. Nagatani, G.C. Tiao, and D.J. Wuebbles, Trend analysis of total ozone data for turnaround and dynamical contributions, *J. Geophys. Res.*, *110*, D16306, doi: 10.1029/2004JD004662, 2005.

Remsberg, E.E., Decadal-scale responses in middle and upper stratospheric ozone from SAGE II version 7 data, *Atmos. Chem. Phys.*, *14*, 1039-1053, doi: 10.5194/acp-14-1039-2014, 2014.

Remsberg, E., and G. Lingenfelser, Analysis of SAGE II ozone of the middle and upper stratosphere for its response to a decadal-scale forcing, *Atmos. Chem. Phys.*, *10* (23), 11779-11790, doi: 10.5194/acp-10-11779-2010, 2010.

Revell L.E., G.E. Bodeker, P.E. Huck, B.E. Williamson, and E. Rozanov, The sensitivity of stratospheric ozone changes through the 21st century to N_2O and CH_4, *Atmos. Chem. Phys.*, 12, 11309-11317, doi: 10.5194/acp-12-11309-2012, 2012a.

Revell L.E., G.E. Bodeker, D. Smale, R. Lehmann, P.E. Huck, B.E. Williamson, E. Rozanov, and H. Struthers, The effectiveness of N_2O in depleting stratospheric ozone, *Geophys. Res. Lett.*, *39* (15), L15806, doi: 10.1029/2012GL052143, 2012b.

Rieder, H.E., J. Staehelin, J.A. Maeder, T. Peter, M. Ribatet, A.C. Davison, R. Stübi, P. Weihs, and F. Holawe, Extreme events in total ozone over Arosa – Part 1: Application of extreme value theory, *Atmos. Chem. Phys.*, *10*, 10021-10031, doi: 10.5194/acp-10-10021-2010, 2010a.

Rieder, H.E., J. Staehelin, J.A. Maeder, T. Peter, M. Ribatet, A.C. Davison, R. Stübi, P. Weihs, and F. Holawe, Extreme events in total ozone over Arosa – Part 2: Fingerprints of atmospheric dynamics and chemistry and effects on mean values and long-term changes, *Atmos. Chem. Phys.*, *10* (20), 10033-10045, doi: 10.5194/acp-10-10033-2010, 2010b.

Rieder, H.E., L. Frossard, M. Ribatet, J. Staehelin, J.A. Maeder, S. Di Rocco, A.C. Davison, T. Peter, P. Weihs, and F. Holawe, On the relationship between total ozone and atmospheric dynamics and chemistry at mid-latitudes – Part 2: The effects of the El Niño/Southern Oscillation, volcanic eruptions and contributions of atmospheric dynamics and chemistry to long-term total ozone changes, *Atmos. Chem. Phys.*, *13* (1), 165-179, doi: 10.5194/acp-13-165-2013, 2013.

Rosenfield, J.E., and A.R. Douglass, Doubled CO_2 effects on NO_y in a coupled 2D model, *Geophys. Res. Lett.*, *25* (23), 4381-4384, 1998.

Sakazaki, T., M. Fujiwara, C. Mitsuda, K. Imai, N. Manago, Y. Naito, T. Nakamura, H. Akiyoshi, D. Kinnison, T. Sano, M. Suzuki, and M. Shiotani, Diurnal ozone variations in the stratosphere revealed in observations from the Superconducting Submillimeter-Wave Limb-Emission Sounder (SMILES) on board the International Space Station (ISS), *J. Geophys. Res.*, *118* (7), 2991-3006, doi: 10.1002/jgrd.50220, 2013.

Salawitch, R.J., D.K. Weisenstein, L.J. Kovalenko, C.E. Sioris, P.O. Wennberg, K. Chance, M.K.W. Ko, and C.A. McLinden, Sensitivity of ozone to bromine in the lower stratosphere, *Geophys. Res. Lett.*, *32*, L05811, doi: 10.1029/2004GL021504, 2005.

Scarnato, B., J. Staehelin, R. Stübi, and H. Schill, Long term total ozone observations at Arosa (Switzerland) with Dobson and Brewer instruments (1988–2007), *J. Geophys. Res.*, *115*, D13306, doi: 10.1029/2009JD011908, 2010.

Schneider, N., F. Selsis, J. Urban, O. Lezeaux, J. De La Noë, and P. Ricaud, Seasonal and diurnal ozone variations: Observations and modeling, *J. Atmos. Chem.*, *50* (1), 25-47, doi: 10.1007/s10874-005-1172-z, 2005.

Scinocca, J.F., D.B. Stephenson, T.C. Bailey, and J. Austin, Estimates of past and future ozone trends from multimodel simulations using a flexible smoothing spline methodology, *J. Geophys. Res.*, *115* (D3), D00M12, doi: 10.1029/2009JD013622, 2010.

Shapiro, A.V., E.V. Rozanov, A.I. Shapiro, T.A. Egorova, J. Harder, M. Weber, A.K. Smith, W. Schmutz, and T. Peter, The role of the solar irradiance variability in the evolution of the middle atmosphere during 2004-2009, *J. Geophys. Res.*, *118* (9), 3781-3793, doi: 10.1002/jgrd.50208, 2013.

Shepherd, T.G., Dynamics, stratospheric ozone, and climate change, *Atmos.-Ocean*, *46* (1), 117-138, doi: 10.3137/ao.460106, 2008.

Shepherd, T.G., and A.I. Jonsson, On the attribution of stratospheric ozone and temperature changes to changes in ozone-depleting substances and well-mixed greenhouse gases, *Atmos. Chem. Phys*., *8* (5), 1435-1444, doi: 10.5194/acp-8-1435-2008, 2008.

Shepherd, T.G., and C. McLandress, A robust mechanism for strengthening of the Brewer-Dobson circulation in response to climate change: Critical-layer control of subtropical wave breaking, *J. Atmos. Sci.*, *68* (4), 784-797, doi: 10.1175/2010JAS3608.1, 2011.

Shepherd, T.G., D.A. Plummer, J.F. Scinocca, M.I. Hegglin, V.E. Fioletov, M.C. Reader, E. Remsberg, T. von Clarmann, and H.J. Wang, Reconciliation of halogen-induced ozone loss with the total-column ozone record, *Nature Geosci*., *7*, 443-449, doi: 10.1038/ngeo2155, 2014.

Sinnhuber, B.-M., N. Sheode, M. Sinnhuber, M.P. Chipperfield, and W. Feng, The contribution of anthropogenic bromine emissions to past stratospheric ozone trends: A modelling study, *Atmos. Chem. Phys.*, *9* (8), 2863-2871, doi: 10.5194/acp-9-2863-2009, 2009.

Sioris, C.E., C.A. McLinden, V.E. Fioletov, C. Adams, J.M. Zawodny, A.E. Bourassa, C.Z. Roth, and D.A. Degenstein, Trend and variability in ozone in the tropical lower stratosphere over 2.5 solar cycles observed by SAGE II and OSIRIS, *Atmos. Chem. Phys.*, *14* (7), 3479-3496, doi: 10.5194/acp-14-3479-2014, 2014.

Sitnov, S., Influence of the 11-year solar cycle on the effects of the equatorial quasi-biennial oscillation, manifesting in the extratropical northern atmosphere, *Clim. Dyn.*, *32*, 1-17, doi: 10.1007/s00382-007-0362-6, 2009.

Smit, H.G.J., W. Straeter, B.J. Johnson, S.J. Oltmans, J. Davies, D.W. Tarasick, B. Goegger, R. Stubi, F.J. Schmidlin, T. Northam, A.M. Thompson, J.C. Witte, I. Boyd, and F. Posny, Assessment of the performance of ECC ozonesondes under quasi-flight conditions in the environmental simulation chamber: Insights from the Juelich Ozone Sonde Intercomparison Experiment (JOSIE), *J. Geophys. Res.*, *112*, D19306, doi: 10.1029/2006 JD007308, 2007.

Sofieva, V.F., N. Rahpoe, J. Tamminen, E. Kyrölä, N. Kalakoski, M. Weber, A. Rozanov, C. von Savigny, A. Laeng, T. von Clarmann, G. Stiller, S. Lossow, D. Degenstein, A. Bourassa, C. Adams, C. Roth, N. Lloyd, P. Bernath, R.J. Hargreaves, J. Urban, D. Murtagh, A. Hauchecorne, F. Dalaudier, M. van Roozendael, N. Kalb, and C. Zehner, Harmonized dataset of ozone profiles from satellite limb and occultation measurements, *Earth Syst. Sci. Data*, *5* (2), 349-363, doi: 10.5194/essd-5-349-2013, 2013.

Solomon, S., P.J. Young, and B. Hassler, Uncertainties in the evolution of stratospheric ozone and implications for recent temperature changes in the tropical lower stratosphere, *Geophys. Res. Lett.*, *39* (17), L17706, doi: 10.1029/2012GL052723, 2012.

Soukharev, B.E., and L.L. Hood, Solar cycle variation of stratospheric ozone: Multiple regression analysis of long-term satellite data sets and comparisons with models, *J. Geophys. Res*., *111*, D20314, doi: 10.1029/2006 JD007107, 2006.

SPARC (Stratosphere-troposphere Processes And their Role in Climate), SPARC Report on the Lifetimes of Stratospheric Ozone-Depleting Substances, Their Replacements, and Related Species, edited by M. Ko, P. Newman, S. Reimann, and S. Strahan, SPARC Report No. 6, WCRP-15/2013, 2013.

SPARC CCMVal (Stratosphere-troposphere Processes And their Role in Climate), *SPARC Report on the Evaluation of Chemistry-Climate Models*, edited by V. Eyring, T.G. Shepherd, and D.W. Waugh, SPARC Report No. 5, WCRP-132, WMO/TD-No. 1526, 478 pp., available: http://www.atmosp.physics.utoronto.ca/ SPARC/ccmval_final/ index.php, 2010.

Steinbrecht, W., H. Claude, F. Schönenborn, I.S. McDermid, T. Leblanc, S. Godin, T. Song, D.P.J. Swart, Y.J. Meijer, G.E. Bodeker, B.J. Connor, N. Kämpfer, K. Hocke, Y. Calisesi, N. Schneider, J. de la Noë, A.D. Parrish, I.S. Boyd, C. Brühl, B. Steil, M.A. Giorgetta, E. Manzini, L.W. Thomason, J.M. Zawodny, M.P. McCormick, J.M. Russell III, P.K. Bhartia, R.S. Stolarski, and S.M. Hollandsworth-Frith, Long-term evolution of upper stratospheric ozone at selected stations of the Network for the Detection of Stratospheric Change (NDSC), *J. Geophys. Res.*, *111* (D10), D10308, doi: 10.1029/2005JD006454, 2006.

Steinbrecht, W., H. Claude, F. Schönenborn, I.S. McDermid, T. Leblanc, S. Godin-Beekmann, P. Keckhut, A. Hauchecorne, J.A.E. Van Gijsel, D.P.J. Swart, G.E. Bodeker, A. Parrish, I.S. Boyd, N. Kämpfer, K. Hocke, R.S. Stolarski, S.M. Frith, L.W. Thomason, E.E. Remsberg, C. Von Savigny, A. Rozanov, and J.P. Burrows, Ozone and temperature trends in the upper stratosphere at five stations of the Network for the Detection of Atmospheric Composition Change, *Int. J. Remote Sens.*, *30*, 3875-3886, doi: 10.1080/01431160902821841, 2009.

Steinbrecht, W., U. Köhler, H. Claude, M. Weber, J.P. Burrows, and R.J. van der A, Very high ozone columns at northern mid-latitudes in 2010, *Geophys. Res. Lett.*, *38* (6), L06803, doi: 10.1029/2010GL046634, 2011.

Stolarski, R.S., and S.M. Frith, Search for evidence of trend slow-down in the long-term TOMS/SBUV total ozone data record: The importance of instrument drift uncertainty, *Atmos. Chem. Phys.*, *6*, 4057-4065, 2006.

Stolarski, R.S., A.R. Douglass, E.E. Remsberg, N.J. Livesey, and J.C. Gille, Ozone temperature correlations in the upper stratosphere as a measure of chlorine content, *J. Geophys. Res.*, *117* (D10), D10305, doi: 10.1029/2012 JD017456, 2012.

Strahan, S.E., A.R. Douglass, R.S. Stolarski, H. Akiyoshi, S. Bekki, P. Braesicke, N. Butchart, M.P. Chipperfield, D. Cugnet, S. Dhomse, S.M. Frith, A. Gettelman, S.C. Hardiman, D.E. Kinnison, J.-F. Lamarque, E. Mancini, M. Marchand, M. Michou, O. Morgenstern, T. Nakamura, D. Olivié, S. Pawson, G. Pitari, D.A. Plummer, J.A. Pyle, J.F. Scinocca, T.G. Shepherd, K. Shibata, D. Smale, H. Teyssèdre, W. Tian, and Y. Yamashita, Using transport diagnostics to understand chemistry climate model ozone simulations, *J. Geophys. Res.*, *116* (D17), D17302, doi: 10.1029/2010JD015360, 2011.

Studer, S., K. Hocke, A. Shanz, H. Schmidt, and N. Kämpfer, A climatology of the diurnal variations of stratospheric and mesospheric ozone over Bern, Switzerland, *Atmos. Chem. Phys.*, *14* (12), 5905-5919, doi: 10.5194/acp-14-5905-2014, 2014.

Swartz, W.H., R.S. Stolarski, L.D. Oman, E.L. Fleming, and C.H. Jackman, Middle atmosphere response to different descriptions of the 11-yr solar cycle in spectral irradiance in a chemistry-climate model, *Atmos. Chem. Phys.*, *12* (13), 5937-5948, doi: 10.5194/acp-12-5937-2012, 2012.

Taylor, K.E., R.J. Stouffer, and G.A. Meehl, An overview of CMIP5 and the experiment design, *Bull. Amer. Meteorol. Soc.*, *93* (4), 485-498, doi: 10.1175/BAMS-D-11-00094.1, 2012.

Tegtmeier, S., V.E. Fioletov, and T.G. Shepherd, A global picture of the seasonal persistence of stratospheric ozone anomalies, *J. Geophys. Res.*, *115* (D18), D18119, doi: 10.1029/2009JD013011, 2010.

Tegtmeier, S., M.I. Hegglin, J. Anderson, A. Bourassa, S. Brohede, D. Degenstein, L. Froidevaux, R. Fuller, B. Funke, J. Gille, A. Jones, Y. Kasai, K. Krüger, E. Kyrölä, G. Lingenfelser, J. Lumpe, B. Nardi, J. Neu, D. Pendlebury, E. Remsberg, A. Rozanov, L. Smith, M. Toohey, J. Urban, T. von Clarmann, K.A. Walker, and R.H.J. Wang, SPARC Data Initiative: A comparison of ozone climatologies from international satellite limb sounders, *J. Geophys. Res.*, *118* (21), 12229-12247, doi: 10.1002/2013JD019877, 2013.

Telford, P., P. Braesicke, O. Morgenstern, and J. Pyle, Reassessment of causes of ozone column variability following the eruption of Mount Pinatubo using a nudged CCM, *Atmos. Chem. Phys.*, *9* (13), 4251-4260, doi: 10.5194/acp-9-4251-2009, 2009.

Thompson, A.M., S.K. Miller, S. Tilmes, D.W. Kollonige, J.C. Witte, S.J. Oltmans, B.J. Johnson, M. Fujiwara, F.J. Schmidlin, G.J.R. Coetzee, N. Komala, M. Maata, M. Mohamad, J. Nguyo, C. Mutai, S.-Y. Ogino, F. Raimundo Da Silva, N.M. Paes Leme, F. Posny, R. Scheele, H.B. Selkirk, M. Shiotani, R. Stübi, G. Levrat, B. Calpini, V. Thouret, H. Tsuruta, J. Valverde Canossa, H. Vömel, S. Yonemura, J. Andrés Diaz, N.T. Tan Thanh, and H.T. Thuy Ha, Southern Hemisphere Additional Ozonesondes (SHADOZ) ozone climatology (2005-2009): Tropospheric and tropical tropopause layer (TTL) profiles with comparisons to OMI-based ozone products, *J. Geophys. Res.*, *117* (D23), D23301, doi: 10.1029/2011JD016911, 2012.

Tourpali, K., C.S. Zerefos, D.S. Balis, and A.F. Bais, The 11-year solar cycle in stratospheric ozone: Comparison between Umkehr and SBUVv8 and effects on surface erythemal irradiance, *J. Geophys. Res.*, *112* (D12), D12306, doi: 10.1029/2006JD007760, 2007.

Trickl, T., H. Giehl, H. Jäger, and H. Vogelmann, 35 yr of stratospheric aerosol measurements at Garmisch-Partenkirchen: From Fuego to Eyjafjallajökull, and beyond, *Atmos. Chem. Phys.*, *13* (10), 5205-5225, doi: 10.5194/acp-13-5205-2013, 2013.

Tully, M.B., A.R. Klekociuk, and S.K. Rhodes, Trends and variability in total ozone from a mid-latitude Southern Hemisphere site: The Melbourne Dobson record 1978-2012, *Atmos. Ocean*, *0*, 1-8, doi: 10.1080/07055900. 2013.869192, 2013.

Urban, J., N. Lautié, C. Jimenez, E. Le Flochmoën, C. Jiménez, P. Eriksson, J. de la Nöe, E. Dupuy, M. Ekström, L. El Amraoui, U. Frisk, D. Murtagh, M. Olberg, and P. Ricaud, Odin/SMR limb observations of stratospheric trace gases: Level 2 processing of ClO, N_2O, HNO_3, and O_3, *J. Geophys. Res.*, *110*, D14307, doi: 10.1029/ 2004JD005741, 2005.

van der A, R.J., M.A.F. Allaart, and H.J. Eskes, Multi sensor reanalysis of total ozone, *Atmos. Chem. Phys.*, *10* (22), 11277-11294, doi: 10.5194/acp-10-11277-2010, 2010.

Van Roozendael, M., R. Spurr, D. Loyola, C. Lerot, D. Balis, J.-C. Lambert, W. Zimmer, J. van Gent, J. van Geffen, M. Koukouli, J. Granville, A. Doicu, C. Fayt, and C. Zehner, Sixteen years of GOME/ERS-2 total

ozone data: The new direct-fitting GOME Data Processor (GDP) version 5 – Algorithm description, *J. Geophys. Res.*, *117* (D3), D03305, doi: 10.1029/2011JD016471, 2012.

van Vuuren D.P., J. Edmonds, M. Kainuma, K. Riahi, A. Thomson, K. Hibbard, G.C. Hurtt, T. Kram, V. Krey, J.-F. Lamarque, T. Masui, M. Meinshausen, N. Nakicenovic, S.J. Smith, and S.K. Rose, The representative concentration pathways: An overview, *Clim. Change*, *109*, 5-31. doi: 10.1007/s10584-011-0148-z, 2011.

Vernier, J.-P., L.W. Thomason, J.-P. Pommereau, A. Bourassa, J. Pelon, A. Garnier, A. Hauchecorne, L. Blanot, C. Trepte, D. Degenstein, and F. Vargas, Major influence of tropical volcanic eruptions on the stratospheric aerosol layer during the last decade, *Geophys. Res. Lett.*, *38* (12), L12807. doi: 10.1029/2011GL047563, 2011.

Vernier, J-P., L.W. Thomason, T.D. Fairlie, P. Minnis, R. Palikonka, and K.M. Bedka, Comment on "Large volcanic aerosol load in the stratosphere linked to asian monsoon transport," *Science*, *339* (6120), 647, doi: 10.1126/science.1227817, 2013.

Vigouroux C., M. De Mazière, P. Demoulin, C. Servais, F. Hase, T. Blumenstock, I. Kramer, M. Schneider, J. Mellqvist, A. Strandberg, V. Velazco, J. Notholt, R. Sussmann, W. Stremme, A. Rockmann, T. Gardiner, M. Coleman, and P. Woods, Evaluation of tropospheric and stratospheric ozone trends over Western Europe from ground-based FTIR network observations, *Atmos. Chem. Phys.*, *8* (23), 6865-6886, doi: 10.5194/acp-8-6865-2008, 2008.

Vitt, F.M., and C.H. Jackman, A comparison of sources of odd nitrogen production from 1974 through 1993 in the Earth's middle atmosphere as calculated using a two-dimensional model, *J. Geophys. Res.*, *101* (D3), 6729-6739, doi: 10.1029/95JD03386, 1996.

von Clarmann, T., M. Höpfner, S. Kellmann, A. Linden, S. Chauhan, B. Funke, U. Grabowski, N. Glatthor, M. Kiefer, T. Schieferdecker, G.P. Stiller, and S. Versick, Retrieval of temperature, H_2O, O_3, HNO_3, CH_4, N_2O, $ClONO_2$ and ClO from MIPAS reduced resolution nominal mode limb emission measurements, *Atmos. Meas. Tech.*, *2* (1), 159-175, doi: 10.5194/amt-2-159-2009, 2009.

Vyushin, D., V.E. Fioletov, and T.G. Shepherd, Impact of long-range correlations on trend detection in total ozone, *J. Geophys. Res.*, *112*, D14307, doi: 10.1029/2006JD008168, 2007.

Vyushin, D., T.G. Shepherd, and V.E. Fioletov, On the statistical modeling of persistence in total ozone anomalies, *J. Geophys. Res.*, *115*, D16306, doi: 10.1029/2009JD013105, 2010.

Wang, R., L. Froidevaux, J. Anderson, R.A. Fuller, P.F. Bernath, M.P. McCormick, N.J. Livesey, J.M. Russell III, K.A. Walker, and J.M. Zawodny, GOZCARDS merged data for ozone monthly zonal means on a geodetic latitude and pressure grid, version 1.01, Greenbelt, MD, USA, NASA Goddard Earth Science Data and Information Services Center, doi: 10.5067/MEASURES/GOZCARDS/DATA3006, 2013.

Wang, S., K.-F. Li, T.J. Pongetti, S.P. Sander, Y.L. Yung, M.-C. Liang, N.J. Livesey, M.L. Santee, J.W. Harder, M. Snow, and F.P. Mills, Midlatitude atmospheric OH response to the most recent 11-y solar cycle., *Proc. Natl. Acad. Sci.*, *110* (6), 2023-2028, doi: 10.1073/pnas.1117790110, 2013.

Waters, J.W., L. Froidevaux, R.S. Harwood, R.F. Jarnot, H.M. Pickett, W.G. Read, P.H. Siegel, R.E. Cofield, M.J. Filipiak, D.A. Flower, J.R. Holden, G.K. Lau, N.J. Livesey, G.L. Manney, H.C. Pumphrey, M.L. Santee, D.L. Wu, D.T. Cuddy, R.R. Lay, M.S. Loo, V.S. Perun, M.J. Schwartz, P.C. Stek, R.P. Thurstans, M.A. Boyles, K.M. Chandra, M.C. Chavez, G.-S. Chen, B.V. Chudasama, R. Dodge, R.A. Fuller, M.A. Girard, J.H. Jiang, Y. Jiang, B.W. Knosp, R.C. LaBelle, J.C. Lam, K.A. Lee, D. Miller, J.E. Oswald, N.C. Patel, D.M. Pukala, O. Quintero, D.M. Scaff, W. Van Snyder, M.C. Tope, P.A. Wagner, and M.J. Walch, The Earth Observing System Microwave Limb Sounder (EOS MLS) on the Aura satellite, *IEEE Trans. Geosci. Rem. Sens.*, *44* (5), 1075-1092, doi: 10.1109/TGRS.2006.873771, 2006.

Waugh, D.W., and V. Eyring, Quantitative performance metrics for stratospheric-resolving chemistry-climate models, *Atmos. Chem. Phys.*, *8* (18), 5699-5713, doi: 10.5194/acp-8-5699-2008, 2008.

Waugh, D.W., L. Oman, S.R. Kawa, R.S. Stolarski, S. Pawson, A.R. Douglass, P.A. Newman, and J.E. Nielsen, Impacts of climate change on stratospheric ozone recovery, *Geophys. Res. Lett.*, *36*, L03805, doi: 10.1029/2008GL036223, 2009.

Weatherhead, E.C., G.C. Reinsel, G.C. Tiao, C.H. Jackman, L. Bishop, S.M.H. Frith, J. DeLuisi, T. Keller, S.J. Oltmans, E.L. Fleming, D.J. Wuebbles, J.B. Kerr, A.J. Miller, J. Herman, R. McPeters, R.M. Nagatani, and J.E. Frederick, Detecting the recovery of total column ozone, *J. Geophys. Res.*, *105* (D17), 22201-22210, 2000.

Weber, M., L.N. Lamsal, M. Coldewey-Egbers, K. Bramstedt, and J.P. Burrows, Pole-to-pole validation of GOME WFDOAS total ozone with groundbased data, *Atmos. Chem. Phys.*, *5* (5), 1341-1355, doi: 10.5194/acp-5-1341-2005, 2005.

Weber, M., S. Dikty, J.P. Burrows, H. Garny, M. Dameris, A. Kubin, J. Abalichin, and U. Langematz, The Brewer-Dobson circulation and total ozone from seasonal to decadal time scales, *Atmos. Chem. Phys.*, *11* (21), 11221-11235, doi: 10.5194/acp-11-11221-2011, 2011.

Weber, M., W. Chehade, V.E. Fioletov, S.M. Frith, C.S. Long, W. Steinbrecht, and J.D. Wild, Stratospheric ozone [in "State of the Climate in 2012"], *Bull. Amer. Meteorol. Soc.*, *94* (8), S36-S37, doi: 10.1175/2013BAMS StateoftheClimate.1, 2013.

Wehrli, C., W. Schmutz, and A.I. Shapiro, Correlation of spectral solar irradiance with solar activity as measured by VIRGO, *Astron. Astrophys.*, *556* (L3), doi: 10.1051/0004-6361/201220864, 2013.

WMO (World Meteorological Organization), *Scientific Assessment of Ozone Depletion: 1994*, Global Ozone Research and Monitoring Project–Report No. 37, Geneva, Switzerland, 1995.

WMO (World Meteorological Organization), *Scientific Assessment of Ozone Depletion: 1998*, Global Ozone Research and Monitoring Project–Report No. 44, Geneva, Switzerland, 1999.

WMO (World Meteorological Organization), *Scientific Assessment of Ozone Depletion: 2002*, Global Ozone Research and Monitoring Project–Report No. 47, Geneva, Switzerland, 2003.

WMO (World Meteorological Organization), *Scientific Assessment of Ozone Depletion: 2006*, Global Ozone Research and Monitoring Project–Report No. 50, 572 pp., Geneva, Switzerland, 2007

WMO (World Meteorological Organization), *Scientific Assessment of Ozone Depletion: 2010*, *Global Ozone Research and Monitoring Project–Report No. 52*, Geneva, Switzerland, 2011.

Woods, T.N., and G.J. Rottman, Solar ultraviolet variability over time periods of aeronomic interest, in *Atmospheres in the Solar System: Comparative Aeronomy*, edited by M. Mendillo, A. Nagy, and J.H. Waite, vol. 130 of AGU Monographs, p. 221, American Geophysical Union, Washington DC, doi: 10.1029/130GM14, 2002.

Yang, E.-S., D.M. Cunnold, R.J. Salawitch, M.P. McCormick, J. Russell III, J.M. Zawodny, S. Oltmans, and M.J. Newchurch, Attribution of recovery in lower-stratospheric ozone, *J. Geophys. Res.*, *111*, D17309, doi: 10.1029/2005JD006371, 2006.

Ziemke, J.R., S. Chandra, L.D. Oman, and P.K. Bhartia, A new ENSO index derived from satellite measurements of column ozone, *Atmos. Chem. Phys.*, *10* (8), 3711-3721, doi: 10.5194/acp-10-3711-2010, 2010.

Ziemke, J.R., and S. Chandra, Development of a climate record of tropospheric and stratospheric column ozone from satellite remote sensing: Evidence of an early recovery of global stratospheric ozone, *Atmos. Chem. Phys.*, *12*, 5737-5753, doi: 10.5194/acp-12-5737-2012, 2012.

Zubov, V., E. Rozanov, T. Egorova, I. Karol and W. Schmutz, The role of external factors in the evolution of the ozone layer and stratospheric circulation in 21st century, *Atmos. Chem. Phys.*, *13* (9), 4697-4706, doi: 10.5194/acp-13-4697-2013, 2013.

APPENDIX 2A
Ozone Data Sets

1) Ground-Based Measurement Systems

The World Ozone and Ultraviolet Data Centre (WOUDC) archives a record of ground-based total column ozone observations (http://www.woudc.org). This includes Dobson spectrophotometers (since the 1920s), automated Brewer spectrometers (since the 1980s), and filter instruments (Bojkov et al., 1994; Fioletov et al., 2008). At many ground stations, the Brewer instruments have supplemented or replaced the Dobsons (Scarnato et al., 2010). Dobson Umkehr ozone profiles provide a long historical record, with regular measurements beginning in 1957 at several stations around the world (Figure 2A-1). In addition to Dobson spectrometers, Brewer instruments in principle also provide Umkehr measurements since the 1990s (Petropavlovskikh et al., 2005).

Zenith-sky visible spectral measurements from SAOZ (Système d'Analyse par Observation Zénithale) instruments (Hendrick et al., 2011) are another source of total column ozone data, as are Fourier-Transform Infrared spectrometers (FTIRs). Both SAOZ and FTIR instruments are part of the NDACC network (Network for Detection of Atmospheric Composition Change, http://www.ndsc.ncep.noaa.gov/) and the GAW (Global Atmosphere Watch) network (Table 2-3). Selected time series extend back to the early 1990s (SAOZ) and 1995 (FTIR). In addition to the total ozone column, the FTIR instruments also provide low vertical resolution ozone profiles.

Ozonesondes have been used since the middle 1960s for routine monitoring of ozone profiles at a number of stations around the world. Figure 2A-1 shows the network of ozonesonde stations, and other ground-based ozone profiling stations used in this Assessment. Most networks are biased toward populated Northern Hemisphere areas (Figure 2A-1), with additional capabilities over Antarctica (Liu et al., 2013). The Southern Hemisphere Additional Ozonesondes project (SHADOZ: Thompson et al., 2012) has added substantially to the global coverage since 1998. Ozonesonde observations are also the backbone of the MATCH network of measurements (see Chapter 3), which are made in unpopulated regions of the NH and are crucial for monitoring ozone depletion in Arctic winter and spring.

Ozone measurements by lidar systems have been in operation since the late 1980s (Steinbrecht et al., 2009; Nair et al., 2012; Kirgis et al., 2013). Currently they are available at 12 stations, mostly in the NH, but fewer stations have long records that are used in this Assessment (Table 2-3; Figure 2A-1).

Ground-based microwave radiometers have been used for stratospheric ozone monitoring since the 1990s (Boyd et al., 2007; Studer et al., 2014). Stations are mostly in the Northern Hemisphere, with one station operating in the Southern Hemisphere (Lauder, New Zealand, see Figure 2A-1).

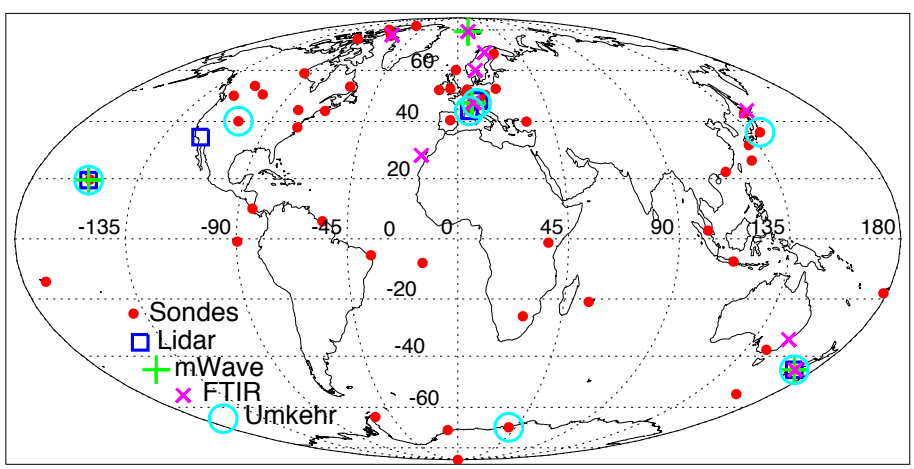

Figure 2A-1. Ground-based ozone profiling stations used in this Assessment. See Table 2-3 for details on the few stations running lidars, microwave radiometers, Fourier-Transform Infrared spectrometers (FTIRs), or Umkehr measurements.

2) Nadir-Viewing Satellite Instruments

The longest available satellite ozone record comes from Solar Backscatter Ultraviolet (SBUV) measurements. The Nimbus-4 BUV instrument collected ozone profiles between 1970 and 1976 from a sun-synchronous polar orbit. Routine measurements of profiles and total ozone from polar-orbiting satellites began in the late 1970s with the Nimbus-7 SBUV, followed by SBUV/2 instruments on several NOAA satellites. At least one SBUV instrument has been operational at all times since 1978. SBUV retrievals provide coarse-resolution vertical profiles. Partial column data are integrated to produce a total column ozone record. A series of similar instruments (i.e., Ozone Monitoring Instrument (OMI) and Ozone Mapping and Profiler Suite (OMPS)) have also flown on more recent research satellites (e.g., Kroon et al., 2011; Kramarova et al., 2014), with sensors designed to detect total ozone with smaller spatial footprints than the SBUV instruments. WMO (2011) used total ozone obtained using the V8 retrieval algorithm, which included a homogenization of the time series (Stolarski and Frith, 2006). SBUV data based on the more recent retrieval algorithm (V8.6: Bhartia et al., 2013; McPeters et al., 2013) are used in this Assessment.

Several European instruments have collected global data from the satellite polar orbiting platforms since 1995. These are: the Global Ozone Monitoring Experiment (GOME: 1995–2011); the Scanning Imaging Spectrometer for Atmospheric Chartography (SCIAMACHY: 2002–2012), Ozone Monitoring Instrument (OMI: since 2004) and GOME-2 aboard Metop-A (since 2007) and Metop-B (since 2012). Various UV total ozone algorithms are applied to these sensors: WFDOAS (Coldewey-Egbers et al., 2005), TOSOMI/TOGOMI (Antón et al., 2011), and GDP5/GODFIT (van Roozendael et al., 2012; Lerot et al., 2014). Generally, all algorithms show very good agreement (within 1%) with ground-based data and with other satellite data (e.g., Weber et al., 2005, 2013; Koukouli et al., 2012; Lerot et al., 2014). A variant of the TOSOMI/TOGOMI algorithm called OMI-DOAS (Kroon et al., 2008) has routinely been used to retrieve total column ozone from OMI (since 2004).

3) Solar and Stellar Occultation Instruments

Solar and stellar occulation instruments provide the highest vertical resolution in ozone profile measurements from space, typically 2 km, and generally provide very accurate ozone profiles. However, their global sampling is rather sparse compared to limb-scattering and limb-emission instruments. These instruments are:

- The Stratospheric Aerosol and Gas Experiment II (SAGE II) provides one of the longest single instrument data sets (1984 to 2005) of ozone profile information. The ozone values in the new version (v7.0, see Table 2-2) are 1–2% lower than in the previous version (6.2) due to the change of the ozone absorption cross section used in the retrieval (Damadeo et al., 2013; Remsberg, 2014).
- The Halogen Occultation Experiment (HALOE) aboard the Upper Atmosphere Research Satellite (UARS) has collected ozone profiles (cloud to mesosphere) from 1991 to 2005 with ~2 km resolution. Further information about profiles can be found at NASA Goddard Earth Sciences Data & Information Services Center (GES DISC): http://daac.gsfc.nasa.gov/. Although the HALOE record is not used directly in this Assessment, it is part of the Global OZone Chemistry And Related trace gas Data records for the Stratosphere (GOZCARDS) data set (R. Wang et al., 2013).
- The Global Ozone Monitoring by Occultation of Stars (GOMOS) on Envisat is a star-occultation instrument measuring in the UV, visible and near infrared spectrum. It provided global, nighttime ozone profiles in the altitude range 15–100 km with 2–3 km vertical resolution (e.g., Bertaux et al., 2010; Kyrölä et al., 2010, 2013).
- The Atmospheric Chemistry Experiment-Fourier Transform Spectrometer (ACE-FTS) was launched in 2004 aboard the SCISAT satellite. Although its record is short for trend analysis, it is used in the The HARMonized data set of OZone profiles (HARMOZ) database (Sofieva et al., 2013).

4) Limb-Scattering Instruments

Limb-scattering instruments have a typical vertical resolution of 3–4 km and provide very dense sampling of the daytime portion of the globe using backscattered solar radiation. These instruments are:

- The Optical Spectrograph and Infrared Imager System (OSIRIS) instrument was launched in 2001 on the Odin satellite (McLinden et al., 2012).
- The Scanning Imaging Absorption spectroMeter for Atmospheric CHartographY (SCIAMACHY) was launched on Envisat in 2002 and operated until 2012 (Gottwald and Bovensmann, 2011).
- The OMPS (Ozone Mapping and Profiler Suite) is a mission providing limb scatter ozone profiles since 2012 (Kramarova et al., 2014). While its record is too short for ozone assessment, it is the only recently launched new limb sounder. OMPS may play an important role in extending the observational record beyond the lifetime of other existing satellite ozone profilers.

5) Limb-Emission Instruments

Limb emission instruments operate in the thermal infrared and microwave part of the spectrum, meaning they can provide measurements in both day and night, and they provide a much denser sampling than the occultation instruments. They have similar vertical resolution and sampling characteristics as the limb-scattering instruments.

- Since 2001, the Sub-Millimetre Radiometer (SMR) aboard the Odin platform has provided twice-weekly measurements of global stratospheric ozone between 12 and 60 km altitude with random uncertainty estimated at 20%. Retrieved ozone profiles have a vertical resolution of about 3 km in the stratosphere (Urban et al., 2005).
- Sounding of the Atmosphere using Broadband Emission Radiometry (SABER) is another emission instrument providing ozone profiles. SABER data are not used for trend analysis in this Ozone Assessment, but the orbital characteristics make the data useful for estimating the diurnal cycle (Studer et al., 2014; Section 2.3.2). Further information can be found at http://saber.gats-inc.com/overview.php.
- The Michelson Interferometer for Passive Atmospheric Sounding (MIPAS) on board Envisat provided daily infrared sensing of global ozone profiles, and many other trace gases, from late 2002, and in a different mode, from late 2004 until April 2012, covering the ~10–70 km altitude range with resolution decreasing from 2 km at the bottom to 5 km at the top of the profile (von Clarmann et al., 2009). Several processers for MIPAS exist. MIPAS data are included in the HARMOZ data set (Sofieva et al., 2013).
- Since 2004, the EOS-Aura Microwave Limb Sounder (Aura MLS) has provided near-global information on ozone profiles (and many other trace gases) between the upper troposphere and the mesosphere. Ozone profiles are retrieved from microwave emissions (Waters et al., 2006; Livesey et al., 2006). The Upper Atmosphere Research Satellite (UARS) Microwave Limb Sounder (UARS MLS) is a predecessor to Aura MLS (Barath et al., 1993). Both MLS records are used in the GOZCARDS combined data set (Froidevaux et al., 2008; R. Wang et al., 2013).

6) Additional Combined Ozone Data Sets Not Used in the Assessment

- SBUV V8.6 NOAA merged data set, where bias corrections in overlapping periods have been applied (see http://larss.science.yorku.ca/QOS2012pdf/6071.pdf; data available at ftp://ftp.cpc.ncep.noaa.gov/SBUV_CDR/).
- SWOOSH (Stratospheric Water and Ozone Satellite Homogenized, http://www.esrl.noaa.gov/csd/groups/csd8/swoosh/)
- BDBP (Binary Data Base of Profiles; Hassler et al., 2009, 2014; Bodeker et al., 2013).
- The trajectory-mapped ozonesonde data set (Liu et al., 2013).

CHAPTER 3

Update on Polar Ozone: Past, Present, and Future

Lead Authors:
M. Dameris
S. Godin-Beekmann

Coauthors:
S. Alexander
P. Braesicke
M. Chipperfield
A.T.J. de Laat
Y. Orsolini
M. Rex
M.L. Santee

Contributors:
R. van der A
I. Cionni
S. Dhomse
S. Diaz
I. Engel
P. von der Gathen
J.-U. Grooß
B. Hassler
L. Horowitz
K. Kreher
M. Kunze
U. Langematz
G.L. Manney
R. Müller
G. Pitari
M. Pitts
L. Poole
R. Schofield
S. Tilmes
M. Weber

Chapter Editors:
S. Bekki
J. Perlwitz

[Formatted for double-sided printing.]

From:
WMO (World Meteorological Organization), *Scientific Assessment of Ozone Depletion: 2014*, Global Ozone Research and Monitoring Project – Report No. 55, 416 pp., Geneva, Switzerland, 2014.

This chapter should be cited as:
Dameris, M., and S. Godin-Beekmann (Lead Authors), S. Alexander, P. Braesicke, M. Chipperfield, A.T.J. de Laat, Y. Orsolini, M. Rex, and M.L. Santee, Update on Polar ozone: Past, present, and future, Chapter 3 in *Scientific Assessment of Ozone Depletion: 2014*, Global Ozone Research and Monitoring Project – Report No. 55, World Meteorological Organization, Geneva, Switzerland, 2014.

CHAPTER 3

UPDATE ON POLAR OZONE: PAST, PRESENT, AND FUTURE

Contents

SCIENTIFIC SUMMARY

Polar Ozone Changes

As stated in the previous Assessments, ozone-depleting substance (ODS) levels reached a maximum in the polar regions around the beginning of this century and have been slowly decreasing since then, consistent with the expectations based on compliance with the Montreal Protocol and its Amendments and adjustments. Considering the current elevated levels of ODSs, and their slow rate of decrease, changes in the size and depth of the Antarctic ozone hole and in the magnitude of the Arctic ozone depletion since 2000 have been mainly controlled by variations in temperature and dynamical processes.

- **Over the 2010–2013 period, the Antarctic ozone hole continued to appear each spring.** The continued occurrence of an Antarctic ozone hole is expected because ODS levels have declined by only about 10% from the peak values reached at the beginning of this century.

- **Larger year-to-year variability of Antarctic springtime total ozone was observed over the last decade compared to the 1990s.** The main driver of this pronounced variability has been variations in meteorological processes, notably the occurrence of dynamically induced disturbances of the Antarctic polar vortex.

- **A small increase of about 10–25 Dobson units (DU) in springtime Antarctic total ozone since 2000 can be derived by subtracting an estimate of the natural variability from the total ozone time series.** However, uncertainties in this estimate and in the total ozone measurements preclude definitive attribution of this increase to the reduction of ODSs over this period.

- **Exceptionally low ozone abundances in the Arctic were observed in spring of 2011.** These low ozone levels were due to anomalously persistent low temperatures and a strong, isolated polar vortex in the lower stratosphere that led to a large extent of halogen-induced chemical ozone depletion, and also to atypically weak transport of ozone-rich air into the vortex from lower latitudes. State-of-the-art chemical transport models (CTMs), which use observed winds and temperatures in the stratosphere together with known chemical processes, successfully reproduce the observed ozone concentrations.

Understanding of Polar Ozone Processes

Since the last Assessment, new laboratory measurements have strengthened our knowledge of polar ozone loss processes. Simulations using updated and improved models have been tested using the wealth of currently available measurements from satellites, ground-based networks, and dedicated campaigns.

- **CTMs are generally able to reproduce the observed polar chlorine activation by stratospheric particles and the rate of the resulting photochemical ozone loss.** Since the last Assessment, better constraint of a key photochemical parameter based on recent laboratory measurements, i.e., the ClOOCl (ClO dimer) photolysis cross section, has increased confidence in our ability to quantitatively model polar ozone loss processes in CTMs.

- **Chemistry-climate models (CCMs), which calculate their own temperature and wind fields, do not fully reproduce the range of polar ozone variability.** Most CCMs have limitations in simulating the temperature variability in polar regions in winter and spring, as well as the temporal and spatial variation of the polar vortex.

Future Changes in Polar Ozone

Projections of future ozone levels in this Assessment are mainly based on the CCM simulations used in the last Assessment. Individual studies using results from climate models provide new insights into the effects of carbon dioxide (CO_2), nitrous oxide (N_2O), and methane (CH_4) on future polar ozone levels by the end of this century.

- **Arctic and Antarctic ozone abundances are predicted to increase as a result of the expected reduction of ODSs.** A return to values of ozone in high latitudes similar to those of the 1980s is likely during this century, with polar ozone predicted by CCMs to recover about 20 years earlier in the Arctic (2025–2035) than in the Antarctic (2045–2060). Updated ODS lifetimes have no significant effect on these estimated return dates to 1980 values.

- **During the next few decades, while stratospheric halogens remain elevated, large Arctic ozone loss events similar to that observed in spring 2011 would occur again under similar long-lasting cold stratospheric conditions.** CCM simulations indicate that dynamic variability will lead to occasional cold Arctic winters in the stratosphere but show no indication for enhanced frequency of their occurrence.

- **Climate change will be an especially important driver for polar ozone change in the second half of the 21st century.** Increases in CO_2 concentrations will lead to a cooling of the stratosphere and increases in all greenhouse gases are projected to strengthen the transport of ozone-rich air to higher latitudes. Under conditions of low halogen loading both of these changes are anticipated to increase polar ozone amounts. The changes are expected to have a larger impact on ozone in the Arctic than in the Antarctic due to a larger sensitivity of dynamical processes in the Northern Hemisphere to climate change. Polar ozone levels at the end of the century might be affected by changing concentrations of N_2O and CH_4 through their direct impact on atmospheric chemistry. The atmospheric concentrations of both of these gases are projected to increase in most future scenarios, but these projections are very uncertain.

- **Substantial polar ozone depletion could result from enhancements of sulfuric aerosols in the stratosphere during the next few decades when stratospheric halogen levels remain high. Such enhancements could result from major volcanic eruptions in the tropics or deliberate "geoengineering" efforts.** The surface area and number density of aerosol in polar regions are important parameters for heterogeneous chemistry and chlorine activation. The impact of sulfur dioxide (SO_2) injection of either natural or anthropogenic origin on polar ozone depends on the halogen loading. In the next several decades, enhanced amounts of sulfuric acid aerosols would increase polar ozone depletion.

3.1 INTRODUCTION

This chapter presents and assesses the latest results from the peer-reviewed literature about our knowledge and understanding of the past, present, and future of polar ozone, i.e., in the stratospheric region defined from 60° to 90° in both hemispheres. In the last *WMO Scientific Assessment of Ozone Depletion: 2010* (WMO, 2011), information about polar ozone was distributed in both Chapter 2 (Stratospheric Ozone and Surface Ultraviolet Radiation) and Chapter 3 (Future Ozone and its Impact on Surface UV). The chapter begins with a brief compilation of the main conclusions from the previous Assessment and a description of the aims and content of the chapter.

3.1.1 State of Science in 2010

As reported in WMO (2011), the Antarctic ozone hole had continued to appear each spring, in spite of a moderate decrease of ozone-depleting substances (ODSs) between 2005 and 2010 (WMO, 2011). Since 1997 both the depth and magnitude of the Antarctic ozone hole were controlled primarily by variations in stratospheric temperature and dynamical processes. In comparison, ozone loss in the Arctic winter and spring remained highly variable but in a range comparable to values that have been determined since the early 1990s.

WMO (2011) reaffirmed the important role of halogen chemistry in polar ozone depletion. Some recent laboratory measurements of the chlorine monoxide dimer (ClOOCl) dissociation cross sections, together with analyses of chlorine partitioning from aircraft and satellite observations, had in part questioned the fundamental understanding of polar springtime ozone depletion. After further study, the earlier measurements of ClOOCl absorption cross section were confirmed and the then more recent study (Pope et al., 2007) was shown to be incorrect. The dominant role of the catalytic ozone destruction cycle in polar springtime ozone depletion, initiated by the ClO + ClO reaction, coupled with a significant contribution from the catalytic destruction cycle initiated by the reaction BrO + ClO, was confirmed. The climatology of polar stratospheric clouds (PSCs) in both polar regions was revisited, based on measurements from a new class of satellite instruments that provide daily vortex-wide information on PSC formation. The new climatology showed that PSCs over Antarctica occur more frequently in early June and less frequently in September than expected based on the previous PSC satellite climatology, which was developed from solar occultation instruments.

It was pointed out that numerical calculations constrained to match observed temperatures and halogen levels (e.g., with chemical transport models, CTMs) produced Antarctic ozone losses that were close to those derived from measured data. Free-running chemistry-climate models (CCMs) simulated many aspects of the Antarctic ozone hole quite well. However, they did not uniformly reproduce the necessary very low temperatures at high southern latitudes, the isolation of polar air masses from middle latitudes, the dynamically isolated vortex characterized by strong vertical descent, and high amounts of halogens inside the polar vortex. Furthermore, most CCMs underestimated the mean Arctic ozone loss that had been derived from observations primarily because the simulated mean northern winter vortices were too dynamically disturbed, implying warmer conditions and larger mixing with lower-latitude air masses.

CCM simulations predicted that Antarctic total column ozone values during spring would return to pre-1980 levels after the mid-21st century. This was later than estimated in any other region of the stratosphere, yet it was earlier than the expected return of stratospheric halogen loading to 1980 values. The latter finding was explained by the global middle and upper stratospheric cooling due to enhanced greenhouse gas (GHG) concentrations (mainly due to carbon dioxide (CO_2) increases). This cooling induces a slowing down of ozone-destroying gas-phase reactions and an increase in the rate of the production of ozone from the pressure-dependent reaction of oxygen atoms with oxygen molecules at

these stratospheric altitudes. Moreover, in most CCMs, GHG-induced changes (including corresponding changes of sea surface temperatures) accelerate the stratospheric meridional circulation (the so-called Brewer-Dobson circulation, BDC), resulting in a faster decrease in stratospheric halogen loading. Nevertheless, it was stated that Antarctic ozone holes could persist up to the end of the 21st century. Overall the confidence in the accuracy of our understanding of changes in Antarctic ozone was higher than that for other stratospheric regions.

Arctic total column ozone values during spring (March) were projected to return to pre-1980 levels two to three decades before polar halogen loading returns to 1980 levels. Most CCMs did not capture the extreme low stratospheric temperatures observed in some winters and, on average, underestimated Arctic ozone loss. In summary it was considered possible that this return date was biased early. In addition, a strengthening of the BDC through the 21st century leads to increases in springtime Arctic column ozone. As a consequence, by 2100, Arctic ozone was projected by models to lie well above 1980 levels.

3.1.2 Scope of Chapter

This chapter updates the state of our knowledge about ozone in both polar regions from measurements and model studies. It focuses on the recent evolution of stratospheric ozone in the winter and springtime, compared to changes that occurred in the preceding decades. As about 10–15 years have passed since the peak of stratospheric content of ODSs in the polar regions, one important issue is whether a decrease of polar ozone depletion has been detected that can unambiguously be attributed to the decrease of ODSs in the stratosphere. Recent evolution in polar temperatures and PSC formation are discussed, together with improvements in our understanding of chemical and dynamical processes influencing polar ozone, especially in the winter and springtime. The most recent projections of stratospheric ozone in the polar regions are compiled from global model simulations, based on the Chemistry-Climate Model Validation-2 (CCMVal2) exercise (SPARC CCMVal, 2010) and some Coupled Model Intercomparison Project Phase 5 (CMIP5) investigations for the Fifth Assessment Report (AR5) of the Intergovernmental Panel on Climate Change (IPCC, 2013). The chapter closes with a discussion of uncertainties in future polar ozone due to climate change and potential effects of eruptions of large volcanoes as well as possible geoengineering activities.

3.2 RECENT POLAR OZONE CHANGES

3.2.1 Measurements of Ozone and Related Constituents

Over the last three decades, an array of instruments on a number of satellite platforms has provided an expansive suite of measurements crucial for understanding the chemical and dynamical processes controlling ozone in the polar stratosphere. The last decade in particular was unique in its wealth of measurements of many atmospheric constituents of importance in studies of polar processes. Table 3A-1 in Appendix 3A summarizes the main satellite data sets of ozone, related trace gases, aerosols, and clouds of particular relevance for the polar regions.

It is worth noting that many of the instruments listed here are no longer operational, and others have exceeded their planned mission lifetimes. Table 3A-1 focuses exclusively on satellite measurements that have been or can be useful in polar studies; information about other available space-based ozone data sets can be found in Chapter 2 of this Assessment. Chapter 2 also includes discussion of long-term merged and/or homogenized ozone data records and climatologies, which are not covered here. General overviews of satellite ozone profile measurements are also given by Tegtmeier et al. (2013) and Hassler et al. (2013).

In addition to the satellite observing systems listed in Table 3A-1, several ground-based networks and other stations provide measurements of ozone and related constituents in the polar regions.

Information on NDACC (Network for Detection of Atmospheric Composition Change, http://www.ndsc.ncep.noaa.gov/) measurements and other data sets archived at the World Ozone and Ultraviolet Data Centre (WOUDC) is provided in Chapter 2.

3.2.2 Recent Evolution of Polar Temperatures and Vortex Characteristics

3.2.2.1 Polar Temperatures

The annual climatological cycle (1979–2012) of 50 hPa polar minimum temperature is illustrated for the Arctic and Antarctic in Figure 3-1. The 50 hPa polar minimum temperatures during recent winters are highlighted by the colored lines in Figure 3-1, along with the Arctic 1996–97 polar minimum temperature.

Arctic minimum temperatures show considerable year-to-year variations. Recent Arctic winter variability has included new minimum temperatures during spring 2011, a time during which significant ozone depletion occurred (Manney et al., 2011; Pommereau et al., 2013). These low temperatures were associated with a small and strong polar vortex, low planetary wave activity, and weak meridional transport to high latitudes, as well as a relatively late final warming date (Hurwitz et al., 2011; Isaksen et al., 2012; Strahan et al., 2013). High stratospheric temperatures during some Arctic winters are due to the occurrence of sudden stratospheric warmings (SSWs), which are characterized by the reversal of the meridional temperature gradient.

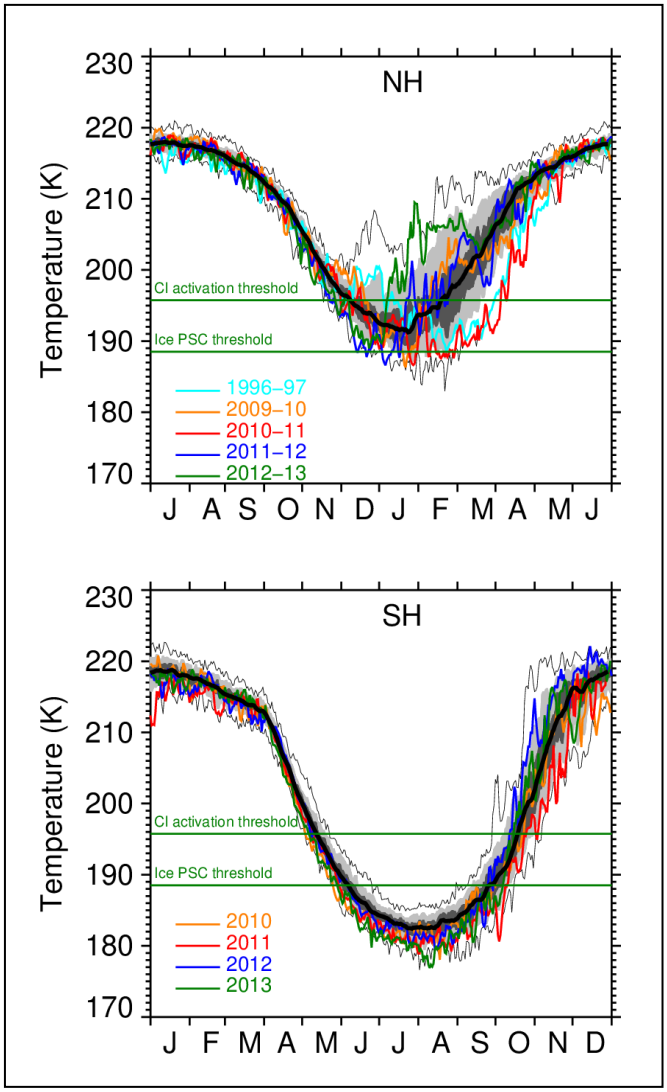

Figure 3-1. The annual cycle and variability at 50 hPa of minimum temperature for the Northern Hemisphere (50°N–90°N, top) and the Southern Hemisphere (50°S–90°S, bottom) from MERRA reanalysis data (Rienecker et al., 2011). The thick black line shows the climatological mean annual cycle; the light and dark gray shading indicate the 30–70% and 10–90% probabilities, respectively; and the thin black lines indicate the record maximum and minimum values, all for the period 1978/79–2012/13 (Northern Hemisphere) and 1979–2012 (Southern Hemisphere). The thresholds for chlorine activation (see Section 3.3, Box 3-1) and ice PSC formation are indicated by the green lines. Recent winters are highlighted by the colored lines, along with Northern Hemisphere winter 1996–97. Updated from Figure 4-1 in WMO (2007) with MERRA data sourced from ozonewatch.gsfc.nasa.gov.

For major SSWs, the 10 hPa zonal mean zonal wind at 60°N changes from westerly to easterly (Labitzke and Naujokat, 2000). Section 3.2.3.2 describes in detail the meteorological and chemical conditions leading to the severe ozone loss in the Arctic in 2011.

Recent 50 hPa Antarctic polar minimum temperatures have been lower than the climatological mean (1979–2012) during winter and September (Figure 3-1). In October and November 2012, the minimum temperatures at 50 hPa were higher than during other recent years. As emphasized in Section 3.2.4, the 2012 ozone hole was significantly weaker than the 1990–2011 average due to the strong springtime planetary-wave forcing that year, which raised the polar mean temperature (Newman et al., 2013). In contrast, 50 hPa minimum temperatures in 2011 were lower as a result of relatively weak winter and spring planetary wave forcing (Newman et al., 2012). Planetary wave activity also adiabatically warmed the stratosphere in July and September 2010 (Newman et al., 2011; de Laat and van Weele, 2011; Klekociuk et al., 2011).

3.2.2.2 POLAR VORTEX BREAKUP DATES

The polar vortex decays and then finally breaks up during spring due to the warming of the polar stratosphere by the returning sun and forcing by planetary waves, which decelerate the winds in the jet and further warm the polar stratosphere. The date on which the vortex breaks up is calculated from a wind average along the vortex edge (Nash et al., 1996). The first decade of the 21st century was characterized by major stratospheric sudden warmings during several Arctic winters (Manney et al., 2005; WMO, 2007; Manney et al., 2009; Ayarzagüena et al., 2011) and the date of final Arctic warming exhibited larger interannual variability in the 2000s than in the 1990s (Figure 3-2). Since the last Ozone Assessment in 2010, the Antarctic vortex has continued to break up in November and December. The presence of the Antarctic ozone hole has resulted in a delay in the breakup date in recent decades, consistent with a vortex intensification following additional springtime radiative cooling (e.g., Waugh et al., 1999; Langematz and Kunze, 2006). However, interannual variability in the date of the Antarctic breakup is visible in Figure 3-2; for example, the 2012 vortex broke up several weeks earlier than in other recent years. The variability in the Antarctic breakup date is most likely due to meteorological variability rather than being a sign of a trend.

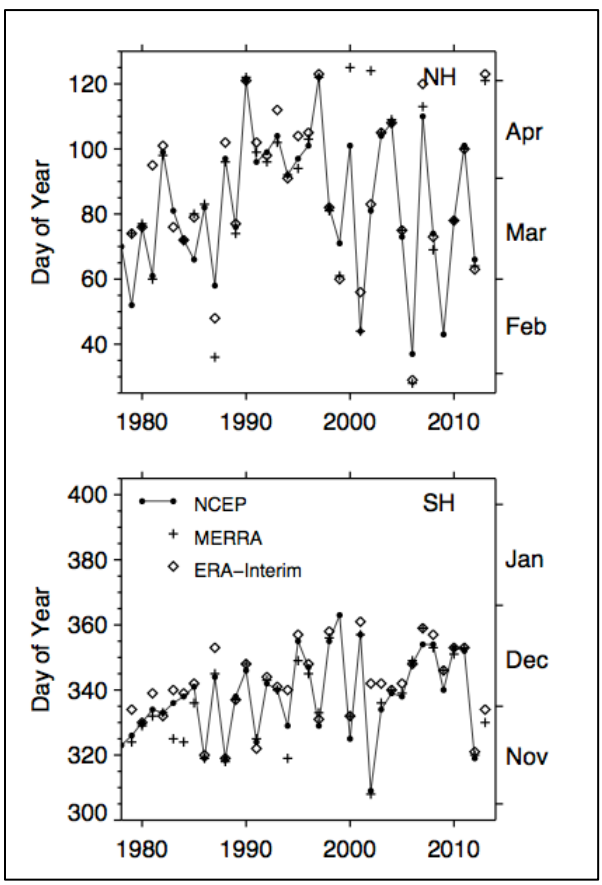

Figure 3-2. The Arctic (top) and Antarctic (bottom) vortex breakup dates on the 500 K isentropic surface following Nash et al. (1996). NCEP (Kalnay et al., 1996); MERRA (Rienecker et al., 2011) and ERA-Interim (Dee et al., 2011) reanalyses are used to calculate these dates. Updated from Figure 4-4 in WMO (2007).

3.2.2.3 LONG-TERM EVOLUTION OF PSC VOLUME

The volume of air inside the vortex at temperatures below the nitric acid trihydrate (NAT) polar stratospheric cloud (PSC) formation threshold, referred to as V_{PSC}, is a commonly used diagnostic for multidecadal polar ozone depletion studies. This NAT PSC formation threshold is defined using a standard, non-denitrified profile of nitric acid (HNO_3) (Rex et al., 2003). Thus V_{PSC} is a temperature threshold (dependent on altitude) rather than a PSC threshold. The volume of air with temperature below this threshold, V_{PSC}, is a proxy for ozone loss (Rex et al., 2003). V_{PSC} is calculated using radiosonde data as well as reanalyses, thus investigation of the long-term evolution of Arctic PSC volumes must account for changes in the data sources with time. Radiosondes provide the longest data record, however, the use of their data for analyzing long-term evolution requires a careful account of the non-homogenized nature of the radiosondes. Non-homogenized radiosonde data overestimate stratospheric cooling trends when compared with homogenized data and furthermore there are large uncertainties between different homogenization approaches (Randel et al., 2009). Besides, the observational coverage of radiosondes has changed with time. The Freie University (FU-Berlin) analyses are based solely on radiosonde measurements over the period 1967–2001, although they are not objectively homogenized with respect to the station network. Radiosondes are more likely to capture temperature extremes than satellite radiometers due to the coarse vertical integration of the latter (e.g., Pawson et al., 1999). In the satellite era (post 1979), reanalyses incorporate observations in the lower stratosphere from the Microwave Sounding Unit (MSU), which make them more reliable in the stratosphere. There is some long-term drift of stratospheric temperatures in reanalyses but it is less severe in more recent reanalyses. Due to differences in data assimilation, individual reanalysis should not be combined with each other or with other observational data sets, in order to avoid inconsistencies in the records used for variability analysis.

Using both FU-Berlin soundings and European Centre for Medium-Range Forecasts (ECMWF) analyses, Rex et al. (2004, 2006) found that during the time period since 1965, recent decades showed larger extreme values of V_{PSC} than earlier decades, i.e., cold Arctic stratospheric winters have become colder. Cold winters were defined by Rex et al. (2004) as the coldest winter in each 5-year interval. This trend result was statistically significant at the 99% level. For the shorter period since 1979, Rieder and Polvani (2013) used three reanalyses (MERRA, NCEP, ERA-Interim) to calculate V_{PSC} and demonstrated the high correlation among the three reanalysis. Using a different definition of extreme V_{PSC}, they found that in these reanalyses, increases in maximum values of V_{PSC} are not statistically significant at the 95% confidence level; however, they are significant at the 80–93% level (varying for each reanalysis). Using ERA-Interim data, Pommereau et al. (2013) reported high variability but no trend in total sunlit V_{PSC} (i.e., PSC volume in sunlight) between 1994 and 2012. Thus, recent research has made conclusions of larger extreme V_{PSC} values in the coldest Arctic winters in recent decades less certain than it was stated in the previous Assessment (WMO, 2011). Individual winters clearly exhibit extremely cold conditions, leading to large values of V_{PSC}. This interannual variability is illustrated clearly in Figure 3-3, which combines results from several published time series of both Arctic V_{PSC} and V_{PSC} divided by the volume of the polar vortex, calculated using MERRA, NCEP, ERA-Interim reanalyses and FU-Berlin radiosondes (update from Rex et al., 2006, based on new reanalysis products). V_{PSC} is an absolute measure of the area affected by polar ozone loss and thus related to the absolute amount of ozone destruction. The fraction of the vortex area below the V_{PSC} temperature threshold, V_{PSC}/V_{vortex}, is a proxy for chemical processing in the polar vortex, and thus particularly important for the Arctic, where a large interannual variability of the vortex is observed (Tilmes et al., 2006). Cold extreme conditions in the Arctic are likely related to the absence of sudden stratospheric warmings in some winters and are likely to continue to occur in the future. Whether there is a long-term trend in extreme values of the derived V_{PSC} time series depends upon the specific definition of an extreme and, given the short observational record, further extreme-value analysis is warranted.

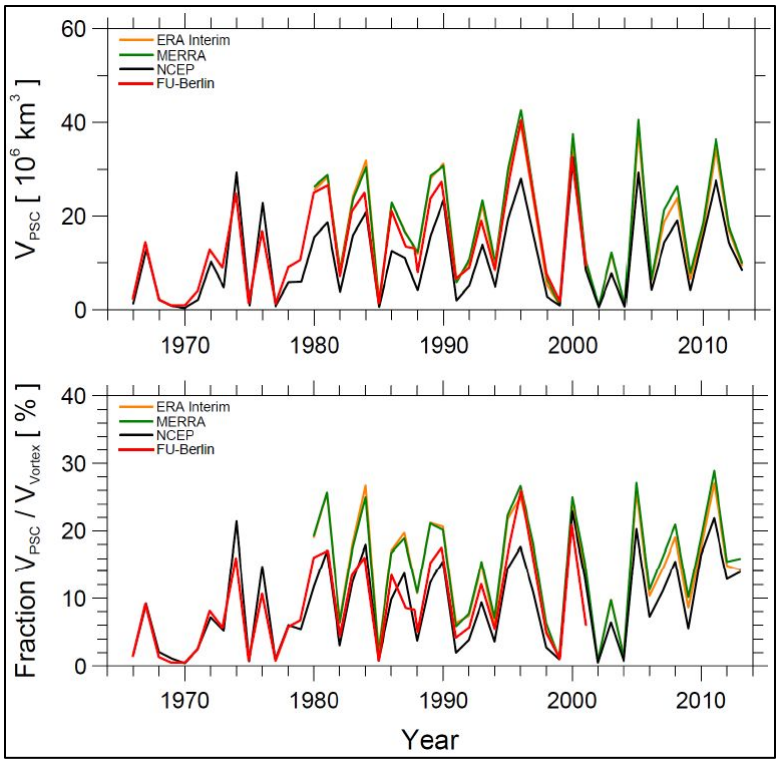

Figure 3-3. Arctic V_{PSC} (top) and V_{PSC} divided by the volume of the polar vortex (bottom), based on different meteorological reanalyses: ECMWF ERA-Interim (orange line), MERRA (green line), NCEP (black line), and FU-Berlin (red line). Update from Rex et al. (2006) based on new reanalysis products.

3.2.3 Ozone Depletion in Recent Arctic Winters

The recent evolution of polar ozone is shown in Figure 3-4, which represents the springtime average of total ozone poleward of 63° geographic latitude in the Arctic and Antarctic, derived from satellite measurements. The gray shading in the figure highlights the difference between the average total ozone values computed over the period 1970–1982 (represented by the horizontal black lines) and the ozone abundances observed in individual years. Such a figure has been featured in the last several WMO/UNEP Ozone Assessments. However, because the size, shape, position, and breakup date of the Arctic vortex are highly variable, the March polar-cap averages depicted in Figure 3-4 reflect differing amounts of extravortex air (which may have higher or lower total ozone abundances than those inside the vortex in any given year, depending primarily on the relationship between the vortex and the cold region, which are often not concentric). Alternatively, Figure 3-5 shows the minimum of the daily average total ozone within the 63° contour of equivalent latitude, which more closely follows the position of the polar vortex. Arctic winters with early final warmings, for which March mean total ozone values convey little information about ozone loss, are excluded from the time series (as indicated by the dotted segments of the line in the top panel of the figure). As for Figure 3-4, interpretation of Figure 3-5 is complicated by the fact that dynamically induced low total ozone abundances are strongly spatially correlated with the cold region in the lower stratosphere and not necessarily with the vortex (e.g., Petzoldt, 1999); thus in the Arctic, because dynamical effects almost always dominate over chemical destruction, both high and low column values are included in the means in Figures 3-4 and 3-5. Moreover, Figure 3-5 only partially alleviates the issue of mixing vortex and extravortex air, because the area encompassed within the 63° contour of equivalent latitude is a constant, whereas the size of the vortex varies over the course of the month and from year to year. The very low total ozone in the Arctic spring of 2011 stands out in both figures. However, as column ozone is strongly influenced by both chemical destruction and transport effects (e.g., Tegtmeier et al., 2008), it is not possible to diagnose the degree of chemical loss from inspection of the total ozone values in Figure 3-4 or Figure 3-5 alone. That the Arctic vortex was smaller than usual in March 2011 (Manney et al., 2011) further complicates interpretation of that average polar

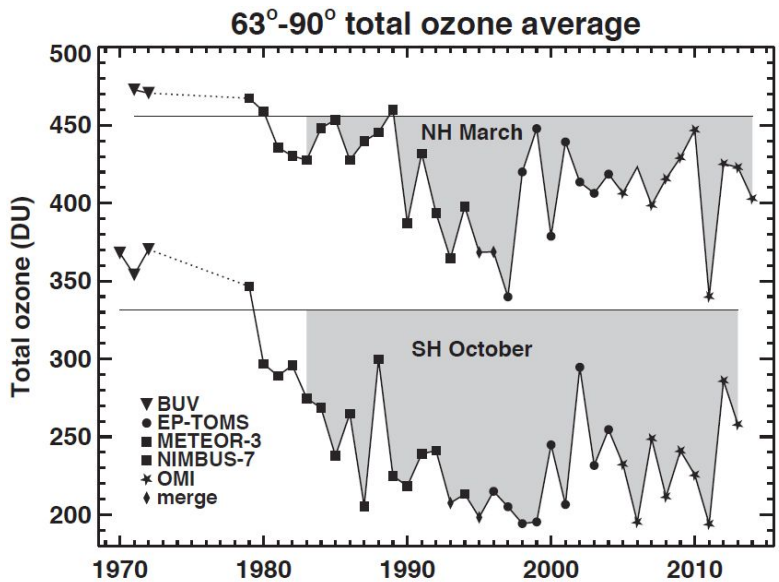

Figure 3-4. Total ozone average (Dobson units) over 63°-90° latitude in March (Northern Hemisphere, NH) and October (Southern Hemisphere, SH). Symbols indicate the satellite data that have been used in different years. The horizontal gray lines represent the average total ozone for the years prior to 1983 in March for the NH and in October for the SH. Updated from Figure 2-8, WMO (2011).

Figure 3-5. Time series of the minimum of the daily average column ozone (Dobson units) within the 63° contour of equivalent latitude (Φ_e) in March in the Arctic and October in the Antarctic. Arctic winters in which the polar vortex broke up before March (1987, 1999, 2001, 2006, 2009, and 2013) are shown by open symbols; dotted lines connect surrounding years. Figure adapted from Müller et al. (2008) and WMO (2011), updated using the Bodeker Scientific combined total column ozone database (version 2.8; circles) through the Arctic winter of 2012, and Aura OMI measurements thereafter (diamonds).

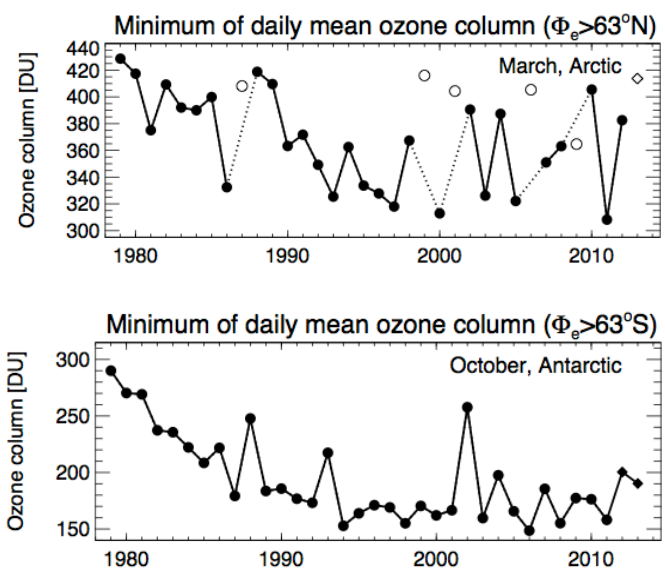

cap total ozone value relative to those in other cold years. Ozone loss in the 2010/2011 Arctic winter/spring is discussed in detail in Section 3.2.3.2.

With the present availability of satellite stratospheric measurements, the extent of polar ozone destruction processes during the winter can be evaluated from the evolution of key species involved in those processes, such as hydrogen chloride (HCl), chlorine monoxide (ClO), and nitric acid (HNO_3), in addition to ozone. Decreases in gas-phase HNO_3 are indicative of the formation of PSCs, while decreases in HCl and increases in ClO signify the occurrence of chlorine activation through heterogeneous reactions on PSC particles and/or cold binary aerosols (see Section 3.3.1). Figure 3-6 (discussed in more detail below) shows the vortex-averaged evolution of these key constituents at a representative level in the lower stratosphere during the last four Arctic winters, as measured by the Microwave Limb Sounder (MLS) instrument onboard NASA's Aura satellite. The envelope of behavior over the 2005–2009 period is also shown for comparison.

3.2.3.1 Ozone Depletion in the Arctic Winters of 2009/2010, 2011/2012, and 2012/2013

The meteorology of the wintertime Arctic lower stratosphere is characterized by substantial interannual variability. Although all recent winters had at least brief intervals cold enough for chlorine activation, they were also, with the exception of 2010/2011, marked by considerable intraseasonal variations in temperature (Figure 3-1) and in the size, strength, and persistence of the polar vortex (Figure 3-2), conditions that govern the cumulative amount of chemical ozone loss. The 2009/2010 early winter was extremely cold with unusually extensive PSC formation, including a rare outbreak of synoptic-scale ice PSCs in mid-January 2010 (Pitts et al., 2011; Dörnbrack et al., 2012). The vortex was shifted off the pole during the midwinter cold spell, allowing greater exposure to sunlight than usual and hence prompting intense chlorine activation (Figure 3-6), which induced a moderate degree of ozone loss (Kuttippurath et al., 2010b; Wohltmann et al., 2013) prior to the onset of a major SSW in February 2010

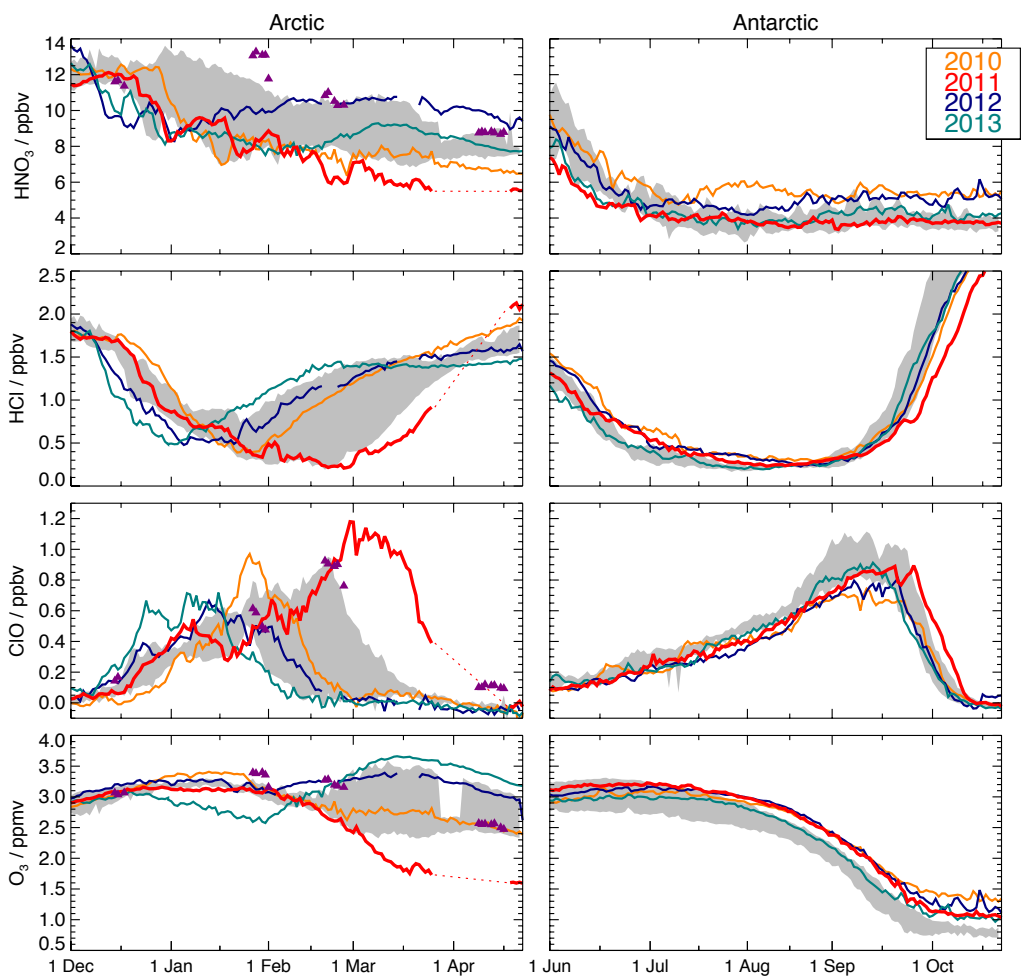

Figure 3-6. Time series of vortex-averaged HNO_3, HCl, ClO, and O_3 from Aura Microwave Limb Sounder (MLS) on the 485 K potential temperature surface (~18 km, ~50 hPa) for winters in the Arctic (left panels) and Antarctic (right panels). Gray shading shows the envelope of behavior observed by Aura MLS over the 2005–2009 period. The last four winters are highlighted by colored lines as indicated in the legend (for the Arctic, the year given refers to the spring). An instrument anomaly caused Aura MLS operations to be suspended from 27 March to 20 April 2011; dotted red lines have been used to fill the resulting data gap to guide the eye. Purple triangles on Arctic panels show 1996/1997 values from UARS MLS. Updated from Manney et al. (2011).

(Kuttippurath and Nikulin, 2012). Similarly, the 2011/2012 and 2012/2013 winters were characterized by low minimum temperatures in December that triggered PSC formation and chlorine activation. In late January 2012, a strong SSW (Chandran et al., 2013) halted further chemical processing. In December 2012 and January 2013, the vortex was again substantially shifted off the pole, ClO was strongly enhanced, and ozone abundances dropped (Figure 3-6). However, temperatures rose abruptly to near-record values in early January as a very strong and prolonged SSW began (Goncharenko et al., 2013). As a result, chlorine deactivation by early February 2013 precluded the exceptional loss that can occur when low temperatures persist into spring.

3.2.3.2 OZONE DEPLETION IN THE ARCTIC WINTER 2010/2011

The Arctic winter/spring of 2010/2011 has been widely studied. It was characterized by an unprecedented degree of chemical ozone loss, coupled with atypically weak transport of ozone to the lower stratospheric polar vortex, which led to exceptionally low values of springtime total ozone (Figures 3-4, 3-5, and 3-8). It must be emphasized, however, that the occurrence of this extreme event has not challenged our fundamental understanding of the processes controlling polar ozone. Unusual (for the Arctic) meteorological conditions in 2010/2011 resulted in record-low ozone through known chemical and dynamical mechanisms. If similar conditions were to arise again in the Arctic while stratospheric chlorine loading remains high, similarly severe chemical ozone loss would take place. Uncertainties in current climate models preclude confident quantification of the likelihood of repeated episodes of extensive Arctic ozone depletion in the present or future climate (e.g., Charlton-Perez et al., 2010; Garcia, 2011), as discussed in Section 3.5.

In spring 2011, the transport barrier at the edge of the lower stratospheric polar vortex was the strongest (in either hemisphere) in the previous 32 years (Manney et al., 2011). Unusually weak tropospheric planetary wave driving allowed the vortex to remain strong, stable, and cold for an extended period, with its mid-April breakup date one of the latest in the satellite era. The mechanisms responsible for the weak wave activity in 2011 have not been definitively determined but may be related to high sea surface temperatures in the North Pacific (Hurwitz et al., 2011; Section 3.3.3.2). Recent analyses suggest that the atypically high frequency of extreme total negative eddy heat flux events and the absence of extreme positive events at 50 hPa during spring 2011 may have contributed to weakened downward transport, cooling, and strengthening of the Arctic lower stratospheric vortex, and a delayed final warming (Shaw and Perlwitz, 2014). Daily minimum temperatures were only moderately low (i.e., rarely below ice PSC formation thresholds), but the cold region was uncommonly long lasting and vertically extensive, leading to a winter-mean vortex fractional volume of air with the potential for PSC formation that was the largest ever observed in the Arctic (Manney et al., 2011), and a March Arctic polar cap temperature at 50 hPa more than two standard deviations below the climatological mean (Hurwitz et al., 2011). The persistence of a strong, cold vortex for more than three months (from December through the end of March) is typical in the Antarctic but unique in the observational record in the Arctic (Manney et al., 2011).

Consistent with the temperature distribution, ice PSCs were rare, but other PSCs types (see Box 3-1, p. 3.17) were abundant until mid-March (Arnone et al., 2012; Lindenmaier et al., 2012). CALIPSO data show that not only were PSCs present far later in 2011 than is typical in the Arctic, but they also spanned a vertical range comparable to that in the Antarctic (Manney et al., 2011). Widespread and persistent PSCs led to severely depleted gas-phase HNO_3 (Figure 3-6). That HNO_3 mixing ratios remained much lower than observed in any previous Arctic winter well after the last PSCs had dissipated is evidence for the occurrence of considerable denitrification (Sinnhuber et al., 2011; Kuttippurath et al., 2012).

The persistent low temperatures supported extensive chlorine activation on the surfaces of PSC particles and/or cold binary aerosols. Although some chlorine activation has occurred in all recent Arctic winters, it has never been as prolonged or as intense as that in 2011, when vortex-averaged ClO values exceeded the range previously observed in the Arctic from late February through March (Manney et al.,

2011). In addition, very low values of chlorine nitrate ($ClONO_2$) (Sinnhuber et al., 2011; Arnone et al., 2012; Lindenmaier et al., 2012) and HCl (Figure 3-6) were observed in the vortex in March. In contrast to previous cold Arctic winters, when chlorine deactivation had already been completed by mid-March, in 2011 ClO began decreasing rapidly only about a week earlier than is typical in the corresponding season in the Antarctic (Figure 3-6). For the ozone and odd nitrogen abundances normally found in the Arctic, the primary chlorine deactivation mechanism is the reformation of $ClONO_2$, whereas under the severely denitrified and ozone-depleted conditions characteristic of the Antarctic ozone hole, production of $ClONO_2$ is suppressed and that of HCl favored. Figure 3-6 shows that chlorine was initially repartitioned into HCl to a greater (more Antarctic-like) extent than typical in the Arctic, suggesting that denitrification and low ozone abundances may have inhibited $ClONO_2$ reformation to some extent (Manney et al., 2011; Arnone et al., 2012; Lindenmaier et al., 2012). Nevertheless, the steep rise in $ClONO_2$ associated with the decline in ClO after mid-March indicates that deactivation did occur predominantly into that reservoir even in 2011 (Sinnhuber et al., 2011; Arnone et al., 2012).

The meteorological conditions (persistent low temperatures inside a strong, isolated polar vortex), consequent chlorine activation, and denitrification in the 2011 Arctic vortex led to severe chemical ozone destruction between 16 and 22 km altitude (Figure 3-7), with 60–80% of the vortex ozone at ~18–20 km removed by early April (Manney et al., 2011; Sinnhuber et al., 2011). Because of the delayed chlorine deactivation, lower stratospheric ozone loss rates in March 2011 reached over 4 parts per billion by volume (ppbv) per sunlit hour (Kuttippurath et al., 2012) or 0.7%/d (Pommereau et al., 2013), larger than previously observed in mid-March in the Arctic and similar to those routinely seen in September in the Antarctic. Peak chemical ozone loss had been as large in some previous cold Arctic winters (e.g., the winters of 2000 and 2005; Manney et al., 2011), but significant loss extended over a much broader altitude region in 2011 (Manney et al., 2011). In addition to chemical ozone destruction, unusually weak diabatic descent and wave-driven horizontal transport also played major roles in 2011, with the late final warming delaying influx of ozone-rich air into the polar lower stratosphere (Hurwitz et al., 2011; Isaksen et al., 2012; Strahan et al., 2013). Although CTM studies consistently show that the exceptionally low

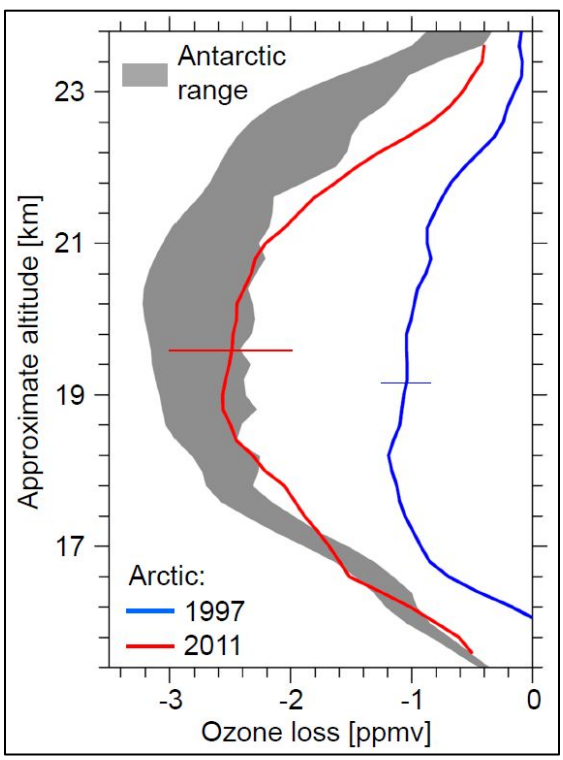

Figure 3-7. Profiles of observed vortex-average chemical ozone loss from the cold Arctic winter/spring periods of 1997 and 2011 derived from ozonesondes. Note that significant differences (up to ~0.4 parts per million by volume (ppmv) at the end of March 2011) in ozone loss estimates for a given year derived from various methods and data sets imply some uncertainty in the chemical loss determination. However, year-to-year differences in the amount of ozone loss obtained from any given method/data set combination are very similar, indicating a high degree of precision in the relative amount of calculated loss between different years and hemispheres. Also shown is an indicative range of ozone loss for typical Antarctic winter/spring periods, illustrated by the loss that has been derived from ozone observations for a relatively weak early Antarctic ozone hole (1985, upper limit of the gray shading) and the loss in a strong Antarctic ozone hole (2003, lower limit of the gray shading). Error bars show uncertainty estimates of the derived ozone losses based on a methodology described in Harris et al. (2002). Figure adapted from Manney et al. (2011).

ozone abundances in spring 2011 were brought about by both extreme chemical loss and weak dynamical resupply, they disagree on the relative contributions of the two factors, with Isaksen et al. (2012) attributing roughly 25% of the observed ozone column anomaly to chemistry and the rest to transport effects, whereas Strahan et al. (2013) found chemical and transport effects to contribute equally.

Together, the anomalous chemical and meteorological conditions induced record-low ozone in March 2011, as characterized by a variety of metrics. Sinnhuber et al. (2011) reported Michelson Interferometer for Passive Atmospheric Sounding (MIPAS) measurements showing that vortex-averaged ozone at 475 K decreased from ~3 parts per million by volume (ppmv) in early December to ~1.5 ppmv in early April, in good agreement with the MLS measurements shown at 485 K in Figure 3-6. Using Ozone Monitoring Instrument (OMI) data, Manney et al. (2011) calculated that the fraction of the Arctic vortex in March with total ozone less than 275 Dobson units (DU), typically near zero, reached nearly 45% in 2011 (see also Figure 3-8); minimum vortex total ozone values were continuously below 250 DU for 27 days. Integrated over the column, the 2011 Arctic ozone "deficit" (the difference between the daily total ozone amount from OMI and a reference value minimally affected by chemical ozone loss) was comparable to that in the Antarctic vortex core in recent years (Figure 3-8; Manney et al., 2011). Similarly, column ozone measurements from UV-visible spectrometers located in eight Systèmes d'Analyse par Observation Zénithale (SAOZ)/NDACC stations distributed around the Arctic indicate a reduction in total ozone of ~38% (170 DU) by late March 2011, the largest in the SAOZ record dating back to 1994 and comparable to that in the 2002 Antarctic winter (Pommereau et al., 2013). Ground-based measurements at the Polar Environment Atmospheric Research Laboratory (PEARL) at Eureka, Canada, also registered the lowest ozone columns in their 11-year record, 237–247 DU, when the vortex was overhead in mid-March (Adams et al., 2012). On the basis of the long-term total ozone data set updated from Stolarski and Frith (2006), in 2011 March total ozone averaged over the 60–80°N region was the lowest of the satellite era (Hurwitz et al., 2011; see also Figure 3-4). Similarly, record-low zonal mean (60–90°N) column ozone values, reaching as low as ~310 DU in mid-March, were seen in Global Ozone Monitoring Experiment 2 (GOME-2) data (Balis et al., 2011; Isaksen et al., 2012).

It is important to emphasize that because downward transport in the winter polar vortex is stronger in the Arctic, background ozone levels are ~100 DU higher there than in the Antarctic (e.g., Tegtmeier et al., 2008). As a result, although the evolution of Arctic ozone and related constituents in spring 2011 more closely followed that characteristic of the Antarctic than ever before, the springtime total ozone values remained considerably higher than those reached in a typical year in the Antarctic (Figures 3-4, 3-5, and 3-8). Moreover, ozone loss in cold and prolonged Antarctic winters is substantially greater throughout the profile (Figure 3-7). Finally, because the areal extent of the 2011 Arctic vortex was only ~60% the size of a typical Antarctic vortex, the low-ozone region was more spatially confined (Figure 3-8).

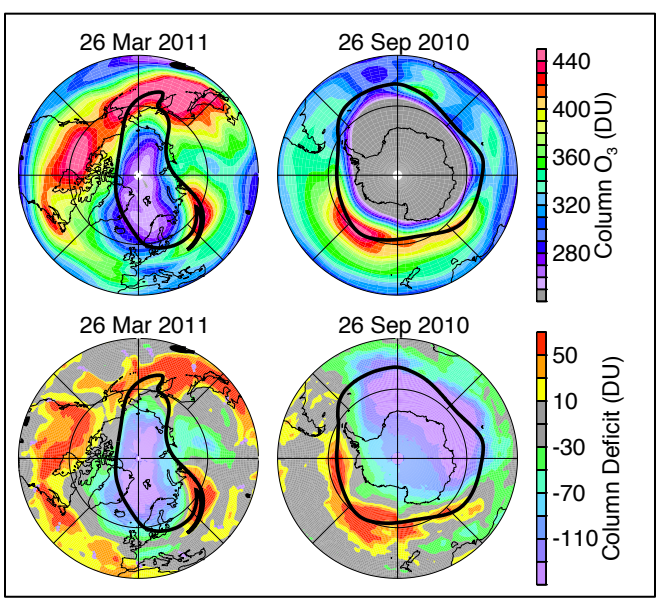

Figure 3-8. Maps of total column ozone from Aura Ozone Monitoring Instrument (OMI) (top row) and ozone "deficit" (bottom row) for the Arctic (left) and Antarctic (right). Total ozone deficit is defined as the difference between daily values and a reference total ozone field minimally affected by chemical loss. Overlaid black contours mark the size and shape of the polar vortex on the 460 K potential temperature surface. Adapted from Manney et al. (2011).

3.2.3.3 TWO ARCTIC SPRINGS WITH VERY LOW TOTAL OZONE: 1997 AND 2011

Figure 3-4 shows that March polar-cap average total ozone abundances were comparably low in 1997 and 2011, and much lower than those in any other year in the satellite record. Similarly, Figure 3-5 shows that the minimum daily mean ozone column amount reached in March was very low in both 1997 and 2011, although in this view 2000 was also an exceptional year, and the 1997 value is not as striking. As discussed in Section 3.2.3.2, an unprecedented degree of chemical ozone loss took place in 2011, whereas only moderate chemical ozone loss occurred in 1997 (Manney et al., 1997; Tegtmeier et al., 2008). In fact, chemical loss also was more severe in the Arctic springs of 1996 and 2005 than in 1997 (WMO, 2007; Manney et al., 2011; Pommereau et al., 2013), yet those years show larger March average total ozone in both Figures 3-4 and 3-5. That the March total ozone values in these two years are so similar reflects how strongly Arctic column ozone is influenced by dynamical effects (e.g., Petzoldt, 1999; Tegtmeier et al., 2008). Here, the chemical and dynamical conditions in the two years are compared and contrasted to underline the fact that total ozone abundances cannot by themselves be used as a proxy for quantifying chemical loss in the lower stratosphere.

Similarities between 1997 and 2011:

- The polar stratospheric chlorine burden peaked in the period 2000–2002 and has been declining slowly since then (WMO, 2011; see also Chapter 1); thus the amount of total inorganic chlorine available was approximately the same in the two years.
- Lower stratospheric temperatures below the threshold associated with chlorine activation on PSC particles and/or cold binary aerosols (see Section 3.3.1) persisted through March in both years (Coy et al., 1997; Manney et al., 2011; Figure 3-1), prolonging the potential for heterogeneous processing into a period of greater exposure to sunlight than in more typical years.
- The lower stratospheric vortices were unusually persistent into the spring, consistent with abnormal patterns of total eddy heat fluxes at 50 hPa (Shaw and Perlwitz, 2014); as a result, vortex breakup dates in both years were among the latest on record, delaying dynamical resupply of ozone to northern high latitudes and keeping March total ozone abundances anomalously low (Hurwitz et al., 2011; Isaksen et al., 2012; Strahan et al., 2013).

Differences between 1997 and 2011:

- The transport barrier at the edge of the 2011 Arctic vortex was unusually strong throughout the winter (the strongest on record during February and March), whereas the 1997 vortex was among the weakest until February, and near average strength thereafter (Manney et al., 2011).
- Lower stratospheric minimum temperatures were continuously below the threshold for chlorine activation (through heterogeneous reactions on PSC particles and/or cold binary aerosol; see Section 3.3.1) from mid-December through March in 2011 (Manney et al., 2011), whereas they did not drop significantly below that threshold until mid-January in 1997 (Coy et al., 1997; Figure 3-1)
- Temperatures persistently (for more than 100 days) below the chlorine activation threshold covered a larger vertical domain in 2011 than in 1997 (15–23 km vs. 20–23 km), with a consequently broader range of ClO enhancement as well as larger maximum ClO abundances, especially at lower altitudes (Manney et al., 2011).
- Early-winter cold conditions and chlorine activation prompted ozone destruction, resulting in ~0.7–0.8 ppmv less O_3 at lower stratospheric levels by March in 2011 than in 1997 (Figure 3-6).
- The persistent cold in 2011 led to extensive PSC formation and severe denitrification (Sinnhuber et al., 2011; Arnone et al., 2012; Lindenmaier et al., 2012), with ~4 ppbv less HNO_3 at lower stratospheric levels by March in 2011 than in 1997 (Figure 3-6).
- Denitrification delayed chlorine deactivation in 2011, when ClO started to decline rapidly only in mid-March (Figure 3-6), compared to late February in 1997 (Santee et al., 1997); the late onset of chlorine deactivation allowed ozone loss rates in March 2011 to reach values typical in the Antarctic

at an equivalent time but not observed previously in the Arctic at this period of time (Kuttippurath et al., 2012; Pommereau et al., 2013).

- Photochemical box model results suggest that by prolonging the period of rapid springtime ozone destruction, denitrification caused an additional 0.6 ppmv of loss in March and April 2011 (Manney et al., 2011).
- Together, the early-winter loss and greater springtime loss induced by denitrification roughly account for the ~1.5 ppmv lower ozone observed in the lower stratosphere in 2011 than in 1997 (Manney et al., 2011).

In summary, anomalous meteorological conditions played a large role in bringing about low total ozone in the Arctic springs of both 1997 and 2011. Chlorine-catalyzed ozone destruction was much greater in 2011 than in 1997. Although a cold polar vortex persisted into April in both years, chemical loss as severe as that in 2011 requires additional conditions that did not occur in 1997, namely: temperatures low enough to trigger chlorine activation early in winter, and cold regions extensive enough to allow widespread denitrification before March. Even in 2011, however, denitrification was not so severe and vertically extensive as to allow ozone destruction on the scale typically seen in Antarctica over a large altitude range (e.g., Manney et al., 2011; Arnone et al., 2012; Solomon et al., 2014).

3.2.4 Recent Antarctic Winters

The Antarctic winters of 2010, 2012, and 2013 were on average characterized by larger ozone columns than has been typical for the Antarctic stratosphere since the early 1990s (Figure 3-4). The ozone mass deficits (OMD) during those years were approximately one-third smaller than during most years of the 2000s, and losses were close to half of the maximum recorded OMD in 2006 (based on the Multi Sensor Reanalysis (MSR) total ozone data set, following de Laat and van Weele, 2011). In contrast, in 2011 the reduction of springtime Antarctic ozone columns was more typical of that observed in the 2000s.

The 2010 Antarctic vortex was characterized by a midwinter (mid-July) minor SSW, which increased the descending motion within the polar vortex (a minor SSW is a warming not accompanied by a 10 hPa zonal wind reversal around 65ºS). Correspondingly, V_{PSC}, the potential NAT volume (see Section 3.2.2.3) based on MERRA reanalysis data remained well below the 1979–2012 average and less denitrification than typical occurred during the Antarctic winter of 2010. The SSW penetrated down to 50 hPa. The average temperature between 60º-90ºS around 30 hPa rose by approximately 5–10 K from 190 K to 195–200 K and thus above the threshold temperature for efficient heterogeneous chlorine activation. As a result, in 2010 photochemical springtime ozone destruction around 30 hPa became less effective. Combined with a late onset of ozone depletion around 30 hPa within the vortex which occurred two to four weeks later than typical during the last decade (de Laat and van Weele, 2011; Klekociuk et al., 2011) ozone columns throughout the 2010 Antarctic spring remained larger than what has been typical for the 2000s. Note that, as midlatitude wave activity remained weak during the rest of the winter and spring, the vortex remained stable into December.

The occurrence of an Antarctic ozone hole with much less ozone loss is not without precedent. Other years that have shown less than typical (for the period) Antarctic ozone loss are 1986, 1988, 2002, and 2004. It has long been established that the much lower ozone loss during these years compared to previous years is related to above-average wave activity (e.g., Schoeberl et al., 1989; Kanzawa and Kawaguchi, 1990; WMO, 2007). Furthermore, it is well documented that this reduction occurred at altitudes between approximately 20 and 25 km (Hofmann et al., 1997; Hoppel et al., 2005), above the 15–20 km layer typically associated with complete ozone destruction.

Using trace gas measurements from Aura MLS, de Laat and van Weele (2011) showed that the primary cause of the smaller ozone loss in 2004 and 2010 was a change in chemistry triggered by vortex dynamics. Enhanced midlatitude wave activity induced SSWs during the Antarctic winter (July–August). Although the amplitude of these minor warmings is small in an absolute sense—only a few degrees

Kelvin at maximum and not comparable to the magnitude of sudden warmings seen in the Arctic—they nevertheless strongly inhibit the formation of PSCs at altitudes between 20 and 25 km where temperatures are close to PSC formation thresholds. The reduced PSC formation limits denitrification and dehydration as seen in water vapor and nitric acid measurements from MLS. Due to this pre-conditioning, once sunlight returns to the Antarctic stratosphere from mid-August onward, reduced availability of active halogen lessens the efficiency of catalytic ozone destruction.

In 2011, stratospheric temperatures during Austral winter and spring remained persistently lower than the long-term mean and on average close to the lowest stratospheric temperatures seen since 1979 throughout, with only a single small warming period during midwinter. Estimates of the potential NAT volume in 2011 were well above its climatological mean, and ozone destruction was not reduced.

In 2012, meteorological conditions to some extent mimicked those in 2010, i.e., in early winter (late June) a minor SSW occurred, which reduced the potential NAT volume and preconditioned the Antarctic lower stratosphere for less ozone depletion. However, the 2012 winter SSW was not as pronounced as that in 2010. On the other hand, in contrast to 2010, springtime 2012 was characterized by several minor SSWs. As a result, stratospheric temperatures between 10 to 50 hPa remained above the long-term climatological mean. These minor warmings were indicative of a less stable vortex, which led to an early dissipation of the Antarctic vortex halfway through October (Kramarova et al., 2014). This explains the relatively large total ozone column values in October 2012 in Figures 3-4 and 3-5.

In 2013, no midwinter warming events occurred. Yet, from mid-August onward, the Antarctic vortex was disrupted by several minor SSWs, mimicking the year 2012 with stratospheric temperatures between 10 to 50 hPa remaining above the long-term climatological mean, and similar to 2013, an early dissipation of the vortex.

Note that detailed analyses of the 2012 and 2013 Antarctic ozone hole seasons have not been performed at the time of this Assessment. Hence, it is not known to what degree modified chemistry and changes in vortex dynamics and transport processes have contributed to the smaller than typical OMDs in 2012 and 2013.

In summary, the Antarctic ozone hole has seen very different amounts of ozone loss over the period 2010–2013 due to variations in polar vortex dynamics. In particular, minor SSWs, as well as reduced vortex stability, have led to significantly reduced Antarctic springtime ozone depletion during several years.

3.3 UNDERSTANDING OF POLAR OZONE PROCESSES

Overall, there have been no major changes in our understanding of polar ozone loss processes since WMO (2011). Our knowledge of polar chemical and dynamical processes was already based on a large body of research, and models could reproduce observed chemical polar ozone depletion and its variability well (e.g., Chipperfield et al., 2005; Frieler et al., 2006). Recent work has improved our detailed understanding of polar ozone processes, such as the formation mechanism of nitric acid trihydrate (NAT) particles; validated previous assumptions; and reduced uncertainty. For example, uncertainty in the photolysis rate of the ClO dimer (Cl_2O_2 or ClOOCl), a key parameter in polar chemical ozone loss, has been reduced by a factor of three (see Section 3.3.2.2). The very cold winter of 2010/11 increased the range of meteorological variability seen in the Arctic over the past few decades and provided a new extreme test case for models.

3.3.1 Polar Stratospheric Clouds

Polar stratospheric clouds (PSCs) play two major roles in stratospheric ozone depletion (Solomon, 1999). First, heterogeneous chemical reactions that convert chlorine from HCl and $ClONO_2$ reservoirs to active, ozone-destroying species are catalyzed by PSC particles (primarily supercooled ternary solution (STS) droplets; see Box 3-1), as well as by cold binary aerosols (Portmann et al., 1996;

Drdla and Müller, 2012). Second, the gravitational sedimentation of large nitric acid trihydrate (NAT) PSC particles irreversibly removes gaseous odd nitrogen (denitrification) (Salawitch et al., 1989), thereby slowing the reformation of the benign chlorine reservoirs and extending the ozone depletion process.

Box 3-1. Stratospheric Particles and Their Roles in Ozone Depletion

- Stratospheric aerosols – liquid sulfuric acid/water (H_2SO_4/H_2O) droplets: They are present at all latitudes in the lower stratosphere; typical mean radius ≈ 0.05–0.1 μm. Their background abundance can be greatly enhanced by volcanic eruptions that reach the stratosphere. These aerosols cause the conversion of gaseous nitrogen oxides (NO_x: NO + NO_2) species to nitric acid (HNO_3) and can initiate chlorine activation at low temperatures (≈195 K).
- Supercooled ternary solution (STS) polar stratospheric clouds (PSCs) – liquid nitric acid/sulfuric acid/water ($HNO_3/H_2SO_4/H_2O$) droplets: They grow from stratospheric aerosols at low temperatures (≈195 K) without a phase change; maximum radius ≈0.3–0.5 μm. They are responsible for reversible removal of HNO_3 by condensation and play a major role in chlorine activation.
- Solid nitric acid trihydrate (NAT) PSCs – HNO_3•3 H_2O particles: They can form at temperatures below the NAT existence temperature, typically around 195 K, but require significant super-cooling to form readily from the gas or liquid phase. They are responsible for irreversible removal of HNO_3 (denitrification) when they sediment and can play a role in chlorine activation, though their effect is likely masked by activation on STS particles. NAT particles have a typical radius of 1 μm, but can grow to 10 μm radius or larger. These larger particles have been referred to as "NAT-rocks."
- Solid water ice PSCs – H_2O particles: They can exist only at temperatures below the frost point, typically around 188 K; typical radii range from ~1 μm for mountain wave-induced ice PSCs to 5–10 μm for synoptic-scale ice PSCs. They are responsible for irreversible removal of H_2O (dehydration) but play a minor role in chlorine activation.

3.3.1.1 RECENT OBSERVATIONS

An extensive set of PSC observations was produced by the RECONCILE field campaign conducted in the Arctic during January–March 2010 (von Hobe et al., 2013). These include observations from in-situ particle probes, a HNO_3 content probe, in situ backscatter probe, infrared limb-sounding instrumentation, and upward- and downward-looking lidar onboard the high-altitude M55-Geophysica aircraft; from ground-based lidars; and from the balloon-borne Compact Optical Backscatter and AerosoL Detector (COBALD) aerosol backscatter sondes. In addition, the spaceborne lidar (Cloud-Aerosol Lidar with Orthogonal Polarization, CALIOP) on the Cloud-Aerosol Lidar and Infrared Pathfinder Satellite Observation (CALIPSO) satellite provided a view of PSC properties on nearly vortex-wide spatial scales and spanning the entire winter, complementing the more localized campaign measurements. Significant findings related to PSC processes include:

1) Extensive regions of NAT PSCs were observed by CALIOP during 15–30 December 2009 prior to the occurrence of ice PSCs (Pitts et al., 2011). This is the first time NAT PSCs have been observed on vortex-wide scales prior to the occurrence of ice PSCs and corroborates the conclusions of Pagan et al. (2004) and Voigt et al. (2005) that ice nuclei are not a prerequisite for NAT formation. A non-ice NAT nucleation mechanism operating on vortex-wide scales has important implications for denitrification and potential enhancement of ozone depletion.

2) Unusually large PSC particles ("NAT-rocks") were detected during the 2010 winter and again in the winter of 2011 when synoptic scale PSCs formed in the Arctic (von Hobe et al., 2013). Visual evidence for particles with diameters as large as 35 μm was provided by shadow-cast images. However, if the particles are assumed to be NAT spheres, the total mass of all optically detected particles with diameters greater than 2 μm exceeds the available total reactive nitrogen (NO_y) (as measured and also reconstructed from model calculations) beyond the measurement uncertainties. Thus, new theoretical concepts, e.g., that the particles are highly aspherical or consist mostly of ice with a NAT coating, must be explored.
3) In situ measurements of submicron background aerosols showed that up to 75% of the particles larger than 10 nm in diameter were non-volatile or contained non-volatile cores and thus could not consist solely of sulfuric acid (H_2SO_4) and H_2O (von Hobe et al., 2013). This high refractory particle fraction was consistently found within the Arctic polar vortex during three measurement campaigns in 2003, 2010, and 2011, with the largest amount of refractory material occurring at the lowest nitrous oxide (N_2O) mixing ratios. Thus, subsiding air masses in the vortices transported non-volatile particulate matter—possibly of meteoric origin—from the upper stratosphere and lower mesosphere into the upper troposphere/lower stratosphere (UT/LS) region. Especially in times of relative volcanic quiescence or low stratospheric background (H_2SO_4/H_2O) aerosol, such particles may be involved in heterogeneous PSC nucleation (e.g., Hoyle et al., 2013; Engel et al., 2013).
4) A rare outbreak of synoptic-scale Arctic ice PSCs was observed by CALIOP from 15–21 January 2010. During this same period, unprecedented evidence of water redistribution and irreversible dehydration in the Arctic stratosphere was obtained (Engel et al., 2014). Simultaneous balloon-borne measurements of water vapor and aerosol backscatter on 17 January provided a unique high-resolution snapshot of repartitioning of water vapor into ice particles. For the first time, signatures of rehydration could be measured in the Arctic and attributed to the observed dehydration. The movement of the dehydrated air masses around the polar vortex was seen in the Aura MLS water vapor data. A modeling study by Engel et al. (2014) showed that the observed redistribution of water cannot be explained by homogeneous ice nucleation alone. A selective, heterogeneous nucleation mechanism is required that allows the ice particles to grow to larger sizes compared to homogeneously nucleated ice particles, which remain too small to cause the significant dehydration in the observed case.

3.3.1.2 REVISED HETEROGENEOUS NAT AND ICE NUCLEATION SCHEME

The formation of NAT PSCs is a prerequisite for denitrification by sedimenting particles, which prolongs seasonal ozone loss. The extensive and deep denitrification in the Antarctic vortex helps to drive the almost complete O_3 loss inside the Southern Hemisphere polar vortex (Solomon et al., 2014). In contrast, denitrification in the Arctic is smaller and more variable from year to year. A more accurate representation of NAT PSC nucleation and particle characteristics leads to better model simulations of denitrification and hence ozone loss. For example, a Single-Layer Isentropic Model of Chemisty and Transport (SLIMCAT) chemical transport model (CTM) simulation of the 2004/2005 Arctic winter using the microphysics-based Denitrification by Lagrangian Particle Sedimentation (DLAPSE) denitrification scheme showed much better agreement with observed HNO_3 and column O_3 loss than a simulation using the standard thermodynamic equilibrium PSC approach (Feng et al., 2011).

CALIOP observations of widespread NAT PSCs and synoptic-scale ice PSCs in the Arctic during the 2009/2010 winter (Pitts et al., 2011) have stimulated new microphysical modeling studies (Hoyle et al., 2013; Engel et al., 2013). PSC optical parameters computed using Mie and T-Matrix scattering codes were compared to selected CALIPSO PSC observations made in December 2009 and January 2010. The best agreement between model and observations was achieved by (1) allowing for NAT and ice to

nucleate heterogeneously on pre-existing solid particles and (2) superimposing small-scale temperature fluctuations onto synoptic-scale parcel trajectories as suggested by Murphy and Gary (1995). The nucleation properties of NAT and ice can be approximated the same way as heterogeneous ice nucleation on Arizona test dust in the immersion mode as demonstrated in previous laboratory experiments (Marcolli et al., 2007). Whereas artificially produced Arizona test dust is composed of various mineral species with a composition similar to that of dust originating from desert, non-volatile solid inclusions were observed in 67% of the stratospheric background aerosols by Curtius et al. (2005) and up to 75% of the submicron aerosol measurements during the 2010 RECONCILE campaign (von Hobe et al., 2013). Coagulated meteoritic smoke particles or micrometeorites may be suitable nuclei for heterogeneous NAT and ice formation as speculated by the above mentioned authors and have also been used in early laboratory experiments by Biermann et al. (1996). It now appears that the upper limits of measured NAT nucleation rate coefficients on foreign material by Biermann et al. (1996) might be sufficient to explain the CALIPSO PSC observations of low number density NAT PSCs from December 2009.

The newly introduced heterogeneous nucleation pathways of NAT and ice are allowed to compete with the conventional accepted pathways of PSC formation, namely, the growth of liquid particles into supercooled ternary solution (STS) droplets due to uptake of HNO_3 and H_2O (Carslaw et al., 1995), the homogeneous ice nucleation at around 3 K below the ice frost point (Koop et al., 2000), and the subsequent nucleation of NAT on ice upon warming, which typically occurs in mountain-wave-driven localized cold pools (Carslaw et al., 1998).

Grooß et al. (2014) implemented a new saturation-dependent NAT nucleation parameterization into the Chemical Lagrangian Model of the Stratosphere (CLaMS) model based on the theory described in Hoyle et al. (2013) and found that the model reproduces the locations and extent of NAT PSCs observed by CALIOP somewhat better than when a constant nucleation rate is assumed (Grooß et al., 2005).

3.3.1.3 IMPROVED UNDERSTANDING OF PSC COMPOSITION

Recent studies by Lambert et al. (2012) and Pitts et al. (2013) demonstrated the usefulness of combining nearly coincident data from the CALIOP lidar on CALIPSO and MLS on Aura to study the temperature-dependent uptake of HNO_3 in PSCs; this procedure is very similar to the method of Spang and Remedios (2003), who combined Cryogenic Infrared Spectrometers and Telescopes for the Atmosphere (CRISTA) measurements of HNO_3 and particle properties for a PSC type classification in the Southern Hemisphere. Comparing observations with theoretical HNO_3 uptake for STS (Carslaw et al., 1995) and NAT (Hanson and Mauersberger, 1988) allows one to judge how well PSCs can be assigned to the various composition classes by CALIOP and also offers insight into PSC growth kinetics. Pitts et al. (2013) showed that CALIOP PSCs in the STS, liquid-NAT mixture (external mixtures of NAT and stratospheric aerosols or STS), and ice classes conform well to their expected temperature existence regimes, providing more confidence in our understanding of PSC particle composition. Pitts et al. (2013) also found that liquid-NAT mixture PSCs exhibit two preferred modes of HNO_3 uptake, one that is closely aligned with the theoretical HNO_3 uptake curve for STS, and a second that is more closely aligned with the theoretical HNO_3 uptake curve for NAT as shown in Figure 3-9a.

Analysis of temperature histories along parcel trajectories (Figure 3-9b) show that liquid-NAT mixture PSCs with HNO_3 uptake more like that of STS had been below the NAT existence temperature T_{NAT} for only short periods of time. Since the growth of large, low-number-density NAT particles is kinetically limited, HNO_3 uptake in these mixtures of PSCs is dominated by STS droplets. On the other hand, liquid-NAT mixture PSCs with HNO_3 uptake more like that of NAT had been below T_{NAT} for much longer periods of time, allowing the thermodynamically favored NAT particles to approach equilibrium (Figure 3-9b). Wegner et al. (2013) showed that allowing the formation of non-equilibrium NAT mixtures in the Whole Atmosphere Community Climate Model (WACCM) global 3-D model significantly improves the agreement of the model with gas-phase HNO_3 observations.

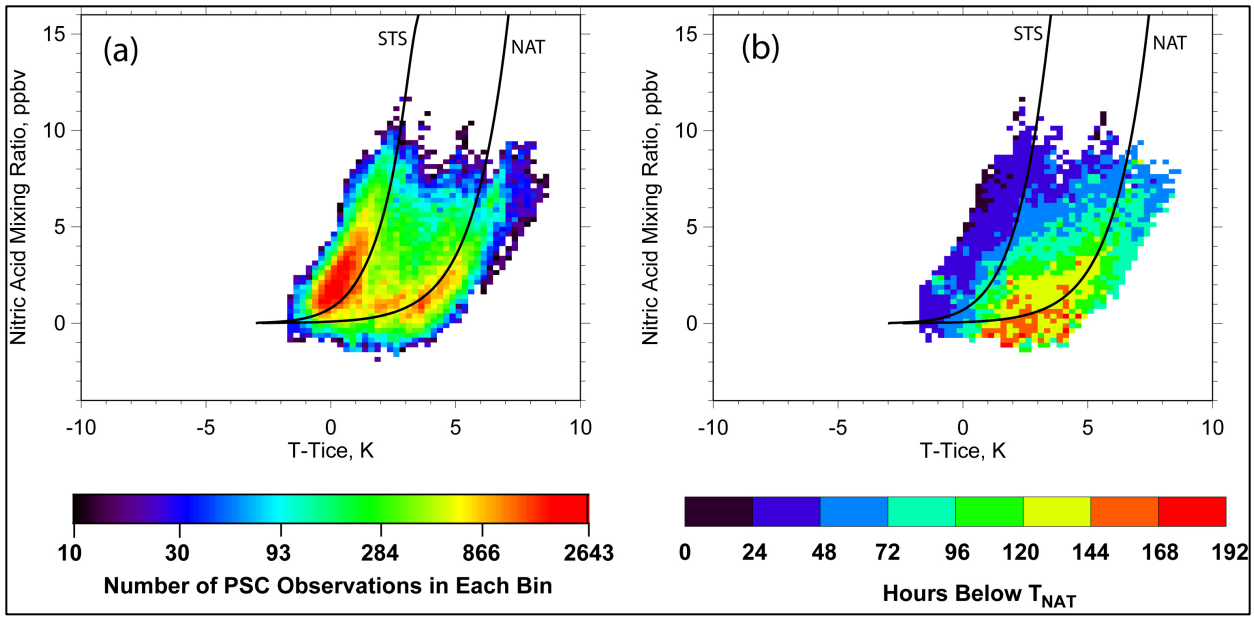

Figure 3-9. (a) Uptake of nitric acid as a function of $T - T_{ice}$ for CALIOP Arctic NAT mixture PSC observations during 1 December 2009–31 January 2010. (b) Temperature histories along air parcel trajectories for CALIOP Arctic NAT mixture PSC observations during 1 December 2009–31 January 2010. The color scale for panel (b) indicates the average number of hours each air parcel associated with the NAT mixture observations falling within each bin was exposed to temperatures below T_{NAT}. Black lines are reference equilibrium uptake curves for STS and NAT assuming 16 ppbv HNO_3 and 5 ppbv H_2O. The histogram bin size is 0.25 ppbv × 0.25 K. Adapted from Pitts et al. (2013).

3.3.1.4 PSC Forcing Mechanisms

PSCs can form in the winter polar stratosphere once the synoptic-scale temperature drops below the NAT and ice PSC existence temperatures, but the formation of NAT particles requires significant supercooling below the NAT equilibrium temperature. Small-scale orographic gravity waves provide an additional forcing mechanism for PSC formation when synoptic-scale temperatures are close to the PSC formation thresholds (Godin et al., 1994; Carslaw et al., 1999). The PSCs formed by orographic gravity waves can cause the conversion of a large fraction of inactive chlorine species to reactive chlorine species (Carslaw et al., 1998), despite the limited spatial and temporal scales of the waves. Early-season PSC formation in the Antarctic winter has been linked to orographic wave forcing (Höpfner et al., 2006; Eckermann et al., 2009), with quantifiable changes in the abundance of trace gas species (Lambert et al., 2012). PSC formation due to orographic wave forcing occurs throughout winter near the polar vortex edge, where synoptic-scale temperatures remain close to the frost-point temperature (Alexander et al., 2011; Kohma and Sato, 2011). Recent satellite data sets indicate the occurrence of midwinter PSCs linked to orographic wave forcing in both the Arctic and the Antarctic (Khosrawi et al., 2011; Noel and Pitts, 2012; Alexander et al., 2013). Analyses of satellite observations indicate that the location and occurrence of resolved orographic gravity waves are well reproduced by meteorological analyses such as ECMWF, but the amplitudes can be significantly underestimated (e.g., Schroeder et al., 2009). Kohma and Sato (2013) demonstrated that the simultaneous occurrence of upper tropospheric clouds and PSCs is preferentially promoted by tropospheric blocking linked to high-pressure systems.

3.3.2 Polar Chemistry

3.3.2.1 HETEROGENEOUS CHEMISTRY

During polar winter, heterogeneous reactions can convert reservoir chlorine species (HCl and $ClONO_2$) into more reactive species, together termed ClO_x, that destroy ozone (Solomon et al., 1986). The seasonal evolution of the balance between the heterogeneous chlorine activation rates and mostly gas-phase chlorine deactivation rates (i.e., the reformation of HCl and/or $ClONO_2$) largely controls the amount of ozone loss in a given polar winter.

Chlorine activation reactions occur on a variety of surface types such as liquid binary aerosol, STS, and NAT (Box 3-1), although with rates that, at a given temperature, vary with the surface type and increase substantially with decreasing temperature. All of these particles are included in typical models used to simulate stratospheric ozone. Drdla and Müller (2012) proposed that the temperature threshold for the onset of polar chlorine activation is controlled by the reactivity of liquid aerosols. They further report that different assumptions about the types of PSC and rates of heterogeneous reactions have only a minor impact on simulated polar chlorine activation rates, at least for the range of conditions studied (the Arctic winter 1999/2000 and the Antarctic winter 2000). Fast chlorine activation on liquid particles means that these particles control the onset of polar chlorine activation at temperatures just higher than T_{NAT}, and Drdla and Müller (2012) argue they are sufficient to reproduce the morphology of chlorine activation and the evolution of ClO_x levels throughout winter. They suggest that this is the case even for cold binary (H_2SO_4/H_2O) stratospheric aerosols. In reality, these particles will take up HNO_3 as temperatures decrease, turning them into STS and further increasing their reactivity. Wohltmann et al. (2013) found that the difference in simulated column ozone loss over the winter 2009/2010 caused by a variety of assumptions about heterogeneous activation rates is less than 10%. For other winters it remains to be studied how sensitive ozone loss calculations are to these assumptions. When temperatures remain low until later during the season compared to 2009/2010, these sensitivities can potentially be larger.

Vortex-averaged satellite observations by the MLS instrument for the Arctic winters 2004/2005 to 2010/2011 (Figure 3-10) show that the initial removal of HCl and HNO_3 from the gas-phase in December/January are not correlated (Wegner et al., 2012) and therefore there is no definite connection between the PSC particles that lead to chlorine activation and those that deplete gas-phase HNO_3. HNO_3 loss exhibits large interannual variability depending on prevailing temperatures while HCl loss is continuous through December with small inter- or intra-annual variability. Hence, the occurrence of HNO_3-containing PSC particles does not seem to have a significant effect on the rate of initial chlorine activation on a vortex-wide scale.

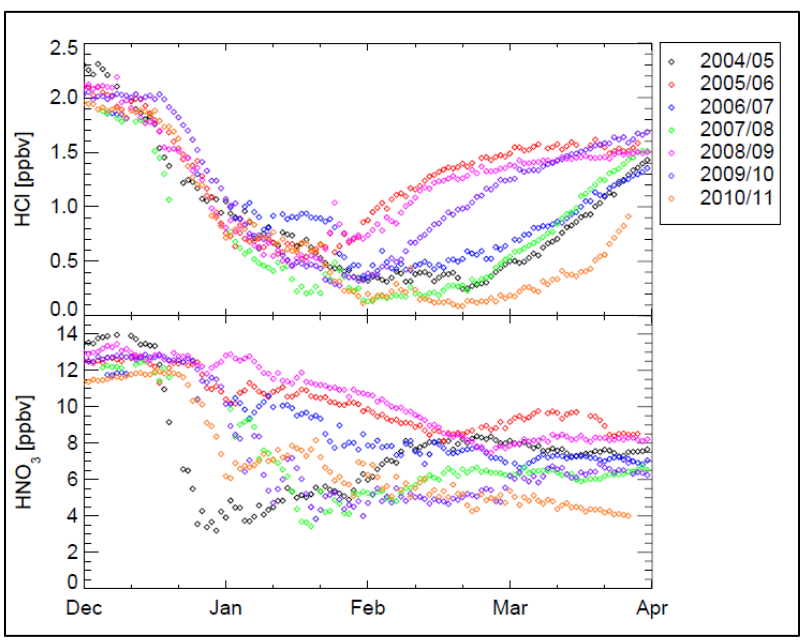

Figure 3-10. HCl and HNO_3 observations by MLS for the Arctic winters 2004/2005 to 2010/2011 on 500 K potential temperature in the vortex core (equivalent latitude >75°N). Adapted from Wegner et al. (2012).

Overall the body of work presented above corrobates the view that chlorine activation rates are mainly controlled by temperature (e.g., Kawa et al., 1997), with a limited dependence on the different particle types. Nonetheless, the formation of STS and NAT particles is important as these particles significantly alter gas-phase chemistry through the uptake of HNO_3. Further, the formation of NAT particles is important as sedimentation and thus denitrification can only occur if large NAT particles form in the stratosphere (see Section 3.3.1).

Antarctic observations have shown that extremely low ozone mixing ratios below about 0.5 ppmv are reached (e.g., Solomon, 2005). The lower limit of these low ozone values has been investigated by Grooß et al. (2011), extending earlier work by Douglass et al. (1995). Grooß et al. showed that continuous rapid heterogeneous reactions on polar stratospheric clouds were required to produce the extreme low ozone values observed in the Antarctic. They show that under such low ozone conditions with continued PSC existence a balance is maintained by gas-phase production of both HCl and hypochlorous acid (HOCl) followed by heterogeneous reaction between these two compounds, which inhibits deactivation of chlorine via the formation of HCl and therefore allows the ozone loss to continue. Thereafter, a very rapid, irreversible chlorine deactivation into HCl occurs, either when ozone drops to values low enough for gas-phase HCl production to exceed chlorine activation processes or when temperatures increase above the polar stratospheric cloud formation threshold.

3.3.2.2 GAS-PHASE CHEMISTRY

Recent observational studies and laboratory investigations have largely confirmed our understanding of how chlorine and bromine compounds drive polar ozone losses. The major cause of gas-phase chemical springtime polar ozone loss is due to the ClO + ClO and ClO + BrO cycles, for example:

$$\mathrm{ClO + ClO + M \leftrightarrow ClOOCl + M} \quad \text{(R1)}$$
$$\mathrm{ClOOCl + h\nu \rightarrow Cl + ClOO} \quad \text{(R2a)}$$
$$\mathrm{ClOO + M \rightarrow Cl + O_2 + M} \quad \text{(R3)}$$
$$\mathrm{2\{Cl + O_3 \rightarrow ClO + O_2\}}$$
$$\text{Net: } \mathrm{2\,O_3 \rightarrow 3\,O_2}$$

The efficiency of ozone loss via this cycle largely depends on the rate of ClOOCl photolysis (R2a). Pope et al. (2007) reported very low values for the ClOOCl photolysis cross section, but these are now attributed to an overcorrection of the molecular chlorine (Cl_2) interference (von Hobe et al., 2009). Following Pope et al. (2007) a large number of new laboratory studies of the ClOOCl photolysis cross sections and quantum yields were carried out. This additional body of work led to a comprehensive re-evaluation of the absorption spectra (WMO, 2011) and to a new recommendation for the cross sections given in the Jet Propulsion Laboratory (JPL) 2011 report (Sander et al., 2011), which is now based on the study of Papanastasiou et al. (2009). These are larger than previously recommended values. At the same time the uncertainty range in the recommendation has been reduced compared to earlier JPL recommendations, based on the considerable amount of new laboratory data that was published after Pope et al. (2007). Recent experiments by Young et al. (2014) are consistent with the current JPL recommendation but their measurements extend to longer wavelengths and also directly quantify the Cl_2 interference, further confirming our understanding of this photolysis process. The higher ClOOCl photolysis cross section in JPL 2011 (Sander et al., 2011), which is based only on laboratory measurements, is now also consistent with previous studies of the ClO dimer reaction that are based on atmospheric observations (e.g., Stimpfle et al., 2004; Frieler et al., 2006) and with more recent evaluations based on ClO observations from ground-based microwave measurements in the Antarctic (Kremser et al., 2011), and in situ (Sumińska-Ebersoldt et al., 2012) and remote-sensing (Kleinböhl et al., 2014) aircraft observations in the Arctic.

The products of ClOOCl photolysis in (R2a) have been questioned by Huang et al. (2011). They argue that ClOOCl photolyzes directly into $2\,Cl + O_2$. Under stratospheric conditions this mechanism would be slightly more rapid than the thermal decomposition of ClOO in (R3) but otherwise it has a

limited impact on modeling the ozone loss process. More important, Huang et al. (2011) also support the findings of Moore et al. (1999) on the existence of a minor channel for (R2) that produces ClO via photolysis with a yield of 19%, compared to a value of 10 ± 10% in Moore et al. (1999), while previous JPL recommendations do not mention this channel. This minor channel has now been adopted in the JPL 2011 recommendation (Sander et al., 2011). Plenge et al. (2005) estimated that the impact of a 10% yield decreases the ozone loss due to the dimer cycle by 5%.

Progress has also been made in understanding the forward (i.e., formation of ClOOCl) and backward (i.e., thermal decomposition of ClOOCl) reactions that determine the equilibrium described by process (R1). Recent atmospheric observations of nighttime ClO (Sumińska-Ebersoldt et al., 2012) are consistent with the Plenge et al. (2005) laboratory measurements of the thermal equilibrium constant given by (R1), which is considerably smaller than JPL 2006 recommendations (Sander et al., 2006). This agrees with previous atmospheric observations, which also support a thermal equilibrium constant smaller than laboratory-based recommendations (see WMO, 2011). The JPL 2011 recommendation, while smaller than the JPL 2006 recommendation, is still 2.5–3 times larger than the value derived by Plenge et al. (2005) for stratospherically relevant temperatures of 190–210K. While a quantitative understanding of the equilibrium constant is important for understanding the budget between ClO and ClOOCl in particular during night and twilight conditions, it does not significantly affect our understanding of ozone loss rates, which, in a chemical model, are not very sensitive to assumptions about this particular kinetic parameter.

The ClO + BrO catalytic cycles are responsible for about 50% of the ozone loss in the polar lower stratosphere, with the contribution being slightly larger in the Arctic where the overall ozone depletion is smaller (e.g., Frieler et al., 2006). Chapter 1 discusses recent work that has better quantified the contribution from very short-lived substances (VSLS) to the stratospheric bromine budget. Overall the result of Chapter 1 is that VSLS increase the stratospheric bromine burden to some extent, compared to what it would be in the absence of VSLS transport into the stratosphere. Considering the VSLS contribution to stratospheric bromine leads to larger ozone loss in chemical models and this VSLS contribution is necessary for models to reproduce observed ozone loss rate.

Atmospheric balloon observations of bromine monoxide (BrO) and ClO (Kreycy et al., 2013) support a larger photolysis rate for bromine nitrate ($BrONO_2$) and a smaller reaction rate of BrO + NO_2 affecting the BrO and NO_2 cycles. This reduces the amount of total inorganic bromine (Br_y) required to reconcile stratospheric BrO measurements with models, and reduces the inferred contribution of VSLS (see Chapter 1). The overall effect on stratospheric ozone of such changes in the photolysis and reaction rates is small to negligible (<1% ozone change everywhere), due to canceling effects of overestimating Br_y (ozone loss suppressing) and underestimating BrO/Br_y (ozone loss enhancing).

3.3.2.3 OZONE LOSS PROCESSES

We now discuss the effect of the progress presented in Section 3.3.2.2 on our ability to calculate ozone loss rates with chemical models. Figure 3-11 illustrates the progress in our quantitative understanding of chemical ozone loss rates since the last Assessment (WMO, 2011). It compares observed ClO_x in the cold Arctic winter of 1999/2000 with chemical box model calculations, which are based on ozone loss rates that were diagnosed with the Match approach (Rex et al., 2002) from ozonesonde observations. With the updates in ClOOCl cross sections described in Section 3.3.2.2, and including a contribution from stratospheric Br_y from VSLS (see Chapter 1 of this Assessment), the model reproduces observed ClO_x much better than based on WMO (2011) assumptions, and uncertainties of the model calculations are largely reduced compared to the status in WMO (2011).

Since WMO (2011) a number of studies have quantified chemical ozone loss rates as vortex averages or at a single location and confirmed our understanding. Moreover, the cold Arctic winter of 2010/11 provided a new, more extreme test case for ozone loss models. Kuttippurath et al. (2010a and 2010b) examined the UV-visible SAOZ spectrometer network, Hassler et al. (2011b) examined ozonesondes

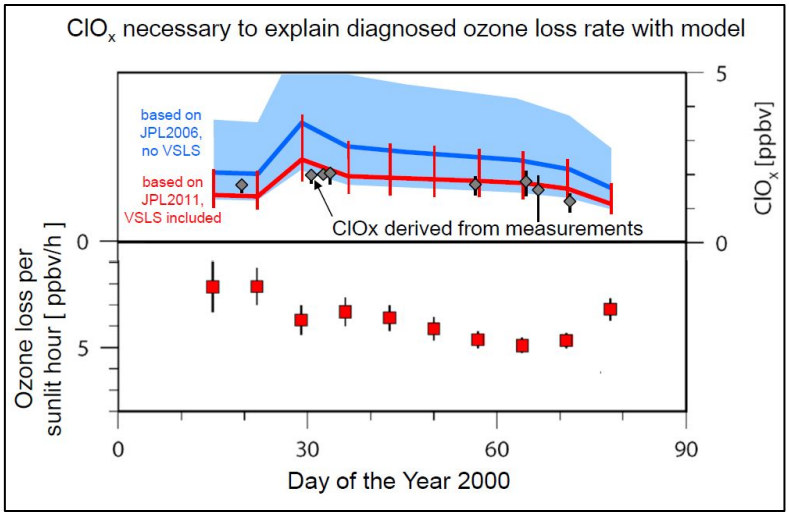

Figure 3-11. Ozone loss per sunlit hour (lower panel) based on results of Match analysis for Arctic winter 1999/2000. The upper panel shows the abundance of ClO_x (ppbv) needed to reproduce the observed loss rates in a photochemical box model based on JPL 2006 (blue) and JPL 2011 (red) recommendations for $J_{Cl_2O_2}$ and their respective uncertainties. Observations of ClO_x are also shown (gray diamonds). The diagram illustrates the progress in quantitative understanding of polar chemical ozone loss and the reduced uncertainty in modeling this process. Both calculations include a contribution to stratospheric Br_y from VSLS based on Chapter 1. Update of Frieler et al. (2006) and WMO (2011).

at South Pole, and Sonkaew et al. (2013) examined the SCanning Imaging Absorption spectroMeter for Atmospheric CHartographY (SCIAMACHY) ozone profiles. Differences between the SCIAMACHY Antarctic loss rates of 45 ± 6 ppbv per day and South Pole sonde-derived rates of 70 ± 10 ppbv per day for the peak chemical ozone loss rates at 475 K over the 2002–2010 period are likely explained by the very different sampling of the polar vortex.

A number of studies have compared inferred chemical ozone loss rates with models for the cold Arctic winter 2010/2011. Figure 3-12 shows the results from a range of 3-D CTMs compared with ozone observations from MIPAS and from MLS. Overall all models shown in the figure were able to reproduce the observed ozone loss, clearly showing that the unprecedented loss during Arctic spring 2011 has been caused by well-known chemistry. Adams et al. (2012) also found that their 3-D CTM could reproduce the loss inferred from ground-based observations. Pommereau et al. (2013) found good agreement between observations and models for the diagnosed ozone column loss, when taking into account changes in partial ozone column at high altitudes (above ~550K, ~20km). Together, these studies indicate that the large loss seen in Arctic winter 2010/2011 is consistent with our current understanding of chemical processes and was driven by the very specific meteorological conditions, as described in Section 3.2.3.2. Overall the ability of 3D-CTMs to reproduce the observed loss for such an event that has extended the previous range of variability increases confidence that the models are now mature and capture the processes that are relevant for Arctic ozone loss.

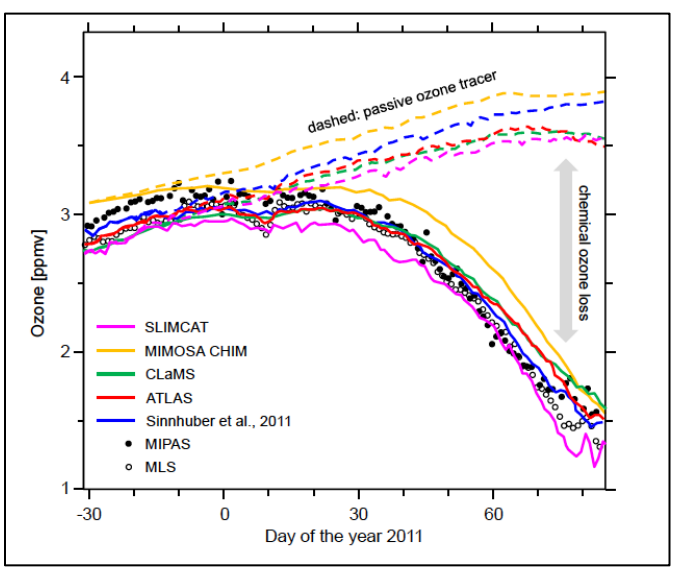

Figure 3-12. Evolution of ozone mixing ratio at 475 K (~18km) observed by the MLS and MIPAS satellite instruments (open and solid black dots) and simulated by several chemical transport models (CTMs, solid color lines). Figure based on updated calculations with CTMs described in Feng et al. (2011; SLIMCAT), Kuttippurath et al., (2012; MIMOSA CHIM), Grooß et al. (2005, 2014; CLaMS), Wohltmann and Rex (2009; ATLAS), and Sinnhuber et al. (2011).

3.3.3 Polar Dynamical Processes

3.3.3.1 Relation Between Wave Driving and Polar Ozone

Ozone inside the polar vortex and in the collar region surrounding the polar vortex experiences large year-to-year variations (WMO, 2011). The main driver for this variability is variations in atmospheric dynamics (Fusco and Salby, 1999; Randel et al., 2002; Weber et al., 2003, 2011; Hood and Soukharev, 2005; Salby, 2008). Variability in the planetary wave activity driving the winter Brewer-Dobson circulation modulates both dynamical and chemical processes affecting polar ozone (e.g., Tegtmeier et al., 2008). The links between planetary waves and polar ozone losses results from the temperature modulation (e.g., Newman et al., 2001). Mass circulations associated with momentum deposition by the planetary waves leads to adiabatic compression of polar air masses (and immediate warming, e.g., SSWs (Ayarzaguëna et al., 2011)) and expansion in the tropical lower stratosphere (cooling). The return toward radiative equilibrium (slow diabatic cooling) in the polar region then results in enhanced transport into the polar vortex and subsidence inside the vortex area. The combination of enhanced transport and warmer polar temperatures in a given winter is then responsible for higher polar ozone levels, reduced polar ozone losses, and leads to higher spring total ozone (e.g., Chipperfield and Jones, 1999; de Laat and van Weele, 2011; Kuttipurath et al., 2010b; Kuttipurrath and Nikulin, 2012; Kramarova et al., 2014). Our understanding of the mechanisms that determine the degree of wave driving of the polar stratosphere is still incomplete, but some progress has been made.

Weber et al. (2011) showed a compact relationship between the mean winter eddy heat flux at 100 hPa, a measure for the planetary wave activity and BDC strength, and spring-to-fall polar ozone ratio combining data from both hemispheres (Figure 3-13). The planetary wave activity is much lower in the Southern Hemisphere and, therefore, results in spring-to-fall ozone ratios smaller than 1 (polar ozone loss outweighs ozone transport). In the Northern Hemisphere this ratio is always above 1 (ozone transport outweighs polar ozone loss). The various extreme events like the split of the Antarctic vortex in 2002 (with an ozone ratio above 1), the record Antarctic ozone hole in 2006, the cold Arctic winters in 1996, 1997, and 2011 (e.g., Manney et al., 2011), and high Arctic ozone in 2010 (Steinbrecht et al., 2011) follow this compact linear relationship.

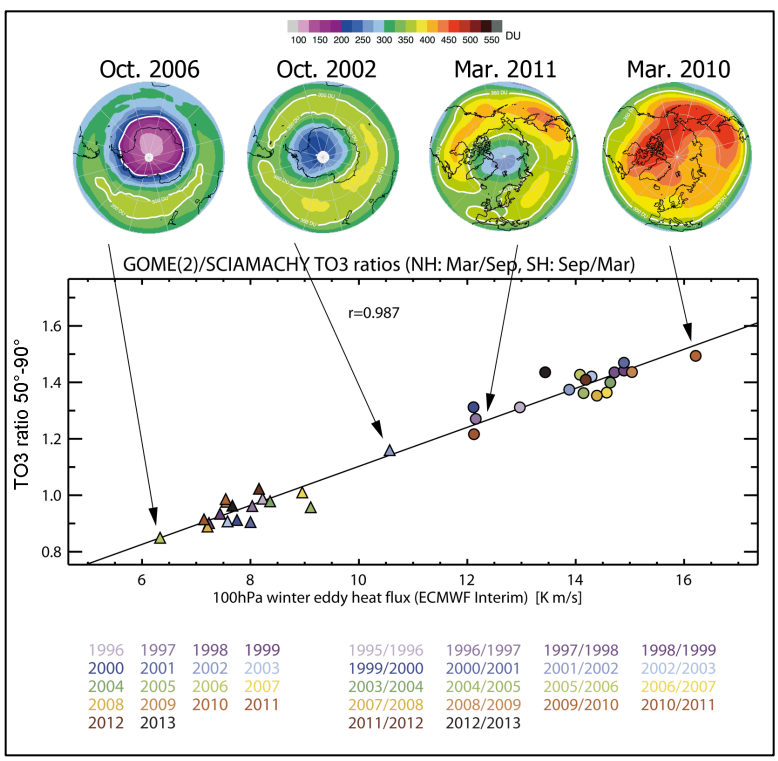

Figure 3-13. Spring-to-fall ratio of observed polar cap total ozone (>50°) as a function of the absolute extra-tropical winter mean eddy heat flux (September to March in the Northern Hemi-sphere and March to September in the Southern Hemisphere) derived from ECMWF ERA-Interim data. Data from the Southern Hemisphere are shown as triangles (September over March ozone ratios) and from the Northern Hemisphere as solid circles (March over September ratios). Selected polar total ozone distributions for selected years are shown at the top. Updated from Weber et al. (2011).

This linear relationship between eddy heat flux and polar cap ozone was also found in two CCMs, indicating that current models realistically describe the variability in stratospheric circulation and its effect on total ozone (Weber et al., 2011). Both models show a positive trend in the winter mean eddy heat flux (and winter BDC strength) in both hemispheres until year 2050, however, the interannual variability (peak-to-peak) is two to three times larger than the change in the decadal means between 1960 and 2050 (Weber et al., 2011). Substantial polar ozone losses could occur in the case of particularly cold winters in the coming decades despite the ongoing decrease of ODS levels in the stratosphere.

3.3.3.2 THE ROLE OF LEADING MODES OF DYNAMICAL VARIABILITY

The respective influences of natural variability and anthropogenic climate change on polar stratospheric temperatures are difficult to disentangle given the short observational record in the satellite era. Using reanalyses and radiosonde data, Bohlinger et al. (2014) showed a wintertime positive trend in Arctic temperatures at 50 hPa over the past three decades, and a corresponding increase in planetary wave activity diagnosed as the meridional eddy heat fluxes at 100 hPa. In addition, they have identified a residual radiative cooling trend of about −0.5 K/decade. Nevertheless, the processes in the troposphere that govern the large interannual variability and the trend in these temperatures remain to be fully understood. It is particularly important to understand the origin of very strong vortex events that drive the ozone loss, either short-duration intense cooling episodes as observed in January 2010 (Dörnbrack et al., 2012), or else prolonged coolings like that observed during the late winter and spring 2011 (Manney et al., 2011). Several recent observational studies have shown that tropospheric highs (e.g., blockings) can lead to either warming or cooling of the Northern Hemisphere polar stratosphere, depending upon their geographical location (Nishii et al., 2011; Woollings et al., 2010; Castanheira and Barriopedro, 2010). This dual effect arises from the potential interaction of transient waves with climatological planetary waves, thereby increasing or lowering the wave activity flux into the stratosphere. North Pacific blockings distinctly lead to polar stratospheric coolings (Nishii et al., 2010), and brief vortex cooling episodes observed during the 2009/10 (Dörnbrack et al., 2012). Also the 2010/2011 winter, described in Section 3.2.3.2, was clearly associated with North Pacific highs and a precursory enhanced Western Pacific teleconnection pattern (Orsolini et al., 2009). The exact cause of the prolonged cold stratosphere in March and April 2011, which led to the record ozone loss, remains unclear, but may involve complex dynamical positive feedbacks between a small intense polar vortex and equatorward-deflected planetary waves. Recent observational and modeling studies emphasize the role of a warm anomaly in North Pacific sea surface temperatures in leading to the cold vortex in 2011 (Hurwitz et al., 2011, 2012). Hence, a better understanding of the variability of the coupled ocean-atmosphere circulation not only in the North Atlantic but also in the key Eastern Eurasia/North Pacific region where wave activity fluxes into the stratosphere are climatologically the strongest, may lead to a better understanding of polar stratospheric temperature variability.

Kiesewetter et al. (2010) showed that the stratospheric Northern Annular Mode (NAM) index is strongly correlated with Arctic ozone anomalies. The different phases of the NAM are driven by the variability in planetary wave driving. Extreme phases of the NAM index (strong and weak vortex events) are associated with negative and positive ozone anomalies that descend from the uppermost stratosphere and then rapidly cover the upper and middle stratosphere, from where they then slowly descend into the lowermost stratosphere within 5 months.

Another important factor in modulating the strength of the polar vortices is the equatorial quasi-biennal oscillation (QBO). The QBO influences the propagation of waves, e.g., during QBO easterlies the waves are more directed toward the polar region, decelerating the polar night jet and perturbing the polar vortex (Holton and Tan, 1980; Baldwin et al., 2001; Naoe and Shibata, 2010; Anstey and Shepherd, 2014; Watson et al., 2014). There is a close link between the QBO and the occurrence of SSWs and the date of the final warming (Thiéblemont et al., 2011). Similarly, planetary wave activity tends to be stronger during warm phases of the El Niño-Southern Oscillation (ENSO) (e.g., Garfinkel and Hartmann, 2008).

Trends and changes in the amplitude of Southern Hemisphere stationary waves in reanalyses are associated with polar ozone depletion and changes in the strength of the subtropical jets driven by sea surface temperature (SST) forcing (Wang et al., 2013; Agosta and Canziani, 2011). Sonkaew et al. (2013) showed that the variable Arctic ozone loss as determined from SCIAMACHY limb ozone profiles during 2002–2009 correlate with the QBO phase, meaning larger ozone losses were generally observed during QBO west phases, although the studied period is relatively short. Hurwitz et al. (2011) showed that the dynamical conditions prevailing during Arctic winter 2011 were characterized as expected by a QBO westerly phase and a concurrent La Niña phase. However, these features alone cannot explain the persistence of the low temperature anomaly into March 2011. As mentioned above, they identified the positive North Pacific SST anomaly as a potential driver for the cold Arctic vortex in late winter 2011.

3.3.3.3 MERIDIONAL MIXING

Blessmann et al. (2012a) showed that a larger fraction of ozone from lower latitudes is mixed into the Arctic vortex in early winter when the wave activity in late fall has been high. In the contrasting case of low wave activity, a larger fraction of early winter polar vortex ozone has subsided from the upper stratosphere during fall. The amount and variability (10%) of early winter Arctic ozone below 750 K (~30 km) are largely determined by dynamical processes in the early vortex formation period (Blessmann et al., 2012b).

Using ozone observations above Antarctica in combination with a CTM model, Roscoe et al. (2012) confirmed earlier studies that the polar ozone depletion starts earlier for stations that are closer to the vortex edge than those in the core region. They also showed from dynamical considerations that air parcels from the core region and the vortex edge region mix only weakly. As the vortex edge region is more strongly exposed to sunlight and is generally warmer, a cooling trend in the stratosphere could extend the region where PSC formation is possible, potentially delaying ozone recovery. This contrasts to the core region where the formation of PSCs is saturated and is less impacted by additional cooling.

3.4 RECOVERY OF POLAR OZONE

Detection of polar ozone recovery is an important milestone in assessing the effectiveness of the Montreal Protocol. As indicated in Chapter 1 of this assessment, the stratospheric chlorine and bromine burden as expressed by the Equivalent Effective Stratospheric Chlorine (EESC) has decreased by about 10% in the polar regions from its peak level reached in the beginning of this century. This section assesses whether an increase in ozone is observed in the polar regions that can be attributed to the decrease in ODSs. Recent changes in understanding of polar ozone trends are discussed in the context of what has been discussed in previous assessments. The focus is on observed polar ozone changes. Future polar ozone evolution is discussed in detail in Section 3.5.

3.4.1 Polar Ozone Recovery in Previous Assessments

The WMO/UNEP 2006 Ozone Assessment Report (WMO, 2007; see Section 6.2.2) outlined in detail the different stages of current and future ozone: slowdown of ozone decline, turn around and onset of ozone increases, and full recovery from ODSs. The latter will be discussed in the context of future polar ozone in Section 3.5. WMO (2007) established that slowing and cessation of ozone decline had already occurred and that 1997 was the most likely turnaround year. That report also included predictions of a slow recovery of Antarctic column ozone, with an increase in springtime ozone of 5–10% between 2000 and 2020, or 0.25–0.5%/year over that period.

The WMO/UNEP 2010 Ozone Assessment Report (WMO, 2011) firmly established that for detection of the second stage of ozone recovery—the occurrence of statistically significant increases in ozone above previous minimum values due to declining EESC—it is required to separate dynamical from

chemical influences on ozone (Newman et al., 2006; Yang et al., 2008). A standard approach for detection that was discussed in WMO (2011, see Section 2.1.2; Box 3-2) is to use a multivariate regression model that quantifies the relation between ozone and different dependent variables that simultaneously describe natural and anthropogenic forcings. The long-term trend can either be described by fitting a piece-wise linear trend function (PWLT) or the EESC. For the PWLT, the turning point is typically defined at the EESC maximum. Alternatively, the turning point can also be derived from a break-point analysis of the ozone record (Yang et al., 2005, 2008; Chehade et al., 2014).

WMO (2011) also discussed the available regression studies, which at that time had focused on tropical and midlatitude ozone. However, analyzing polar ozone for long-term trends and signs of onset of ozone increases had not been performed before WMO (2011), as it is more complicated due to the need to include polar vortex dynamics, which results in larger year-to-year variability in polar regions than at midlatitudes and in the tropics. In WMO (2011), Antarctic trends were only briefly discussed, as essentially only one regression study was available at the time (Yang et al., 2008). Furthermore, that study only considered temperature as a dependent variable and focused on the first stage of ozone recovery, the leveling off of Antarctic ozone loss and reversal of the EESC trend from increasing during the 1980s and 1990s to a decrease after 2000. It was concluded that the leveling off of Antarctic ozone since the late 1990s could be attributed to changes in Antarctic stratospheric halogen loading.

In addition, WMO (2011) noted based on model studies that increases in greenhouse gas (GHG) concentrations do not have a significant direct effect (due to radiative processes) on springtime Antarctic polar temperatures and ozone for the period up to 2100. Indirect effects of GHG on ozone via changes in vortex dynamics were not reported in WMO (2011). Furthermore, there are large uncertainties associated with the ozone recovery path, and model uncertainties rather than those of GHG scenarios dominate uncertainties in ozone recovery. Hence, it is unlikely that recent Antarctic stratospheric ozone changes were affected by increases in GHGs. See further Section 3.5 on the impact of GHGs on future Antarctic ozone recovery.

For the Arctic, WMO (2007) already noted that compared to the Antarctic, the Arctic shows larger interannual variability in springtime ozone and smaller ozone depletion. As a result, detection of changes in ozone due to decreases in EESC will likely take longer than in the Antarctic. For the Arctic, no slowing of a decline in ozone had been found. WMO (2011) reported little progress in assessing Arctic ozone recovery since WMO (2007).

3.4.2 Long-Term Antarctic Ozone Trends

3.4.2.1 Vertically Resolved Ozone

Hassler et al. (2011a) assessed 25 years of ozonesonde measurements made at the South Pole station and presented an update and expansion of earlier South Pole ozonesonde studies (Hofmann et al., 1997; Solomon et al., 2005; Hofmann et al., 2009). The study analyzed the height dependence of ozone loss rates throughout Antarctic spring (late August to late September) for five-year periods, which reduces the effect of year-to-year variability in ozone (Figure 3-14). The study concluded that ozone loss rates changed little over the period 1996–2010, although a small but statistically insignificant reduction in ozone loss rates after 2000 was identified. The lack of clear reduction in ozone loss rates (Figure 3-14) could be partly related to saturation of loss at certain pressure levels which results in the near-complete ozone destruction at pressure levels around 70 hPa (typically 50–100 hPa; see also Yang et al. (2008)). It thus may take some time for air masses at certain pressure levels to become “desaturated” with regard to ozone loss. Furthermore, the decrease in EESC during the period 2000–2010 is approximately 5–10%, depending on the choice of age of air (Newman et al., 2007), suggesting that no large decrease in ozone destruction can be expected to have occurred yet. Assuming a future linear relation between the reduction in EESC and ozone loss rates and assuming that future dynamical variability of the Antarctic stratosphere will remain similar to the variability observed during the last two decades as well as assuming that no

major volcanic eruption will occur, Hassler et al. (2011a) find that a statistically significant reduction in South Pole ozone loss rates for August–September as measured by ozonesondes is only expected to occur at the end of the 2010–2020 period if the current decline in EESC continues unabated. They also noted that there are uncertainties with this methodology, in particular how to account for changes in greenhouse gas concentrations, which likely will affect future Antarctic stratospheric dynamics. Another complicating factor for the detection of height-dependent ozone increases is changes in stratospheric temperatures (cooling), which lead to trends in air density and layer thickness (McLinden and Fioletov, 2011).

Miyagawa et al. (2014) assessed ground-based ozone profile Dobson Umkehr measurements at the Antarctic coastal station Syowa (69.0°S, 39.6°E). Based on a multivariate regression method to account for Antarctic polar vortex dynamics, and consistent with Hassler et al. (2011a), they report a small but statistically insignificant increase in springtime Antarctic stratospheric ozone after 2001 over Syowa that can be attributed to decreasing EESC. They find that Antarctic vortex dynamics have a large impact on stratospheric ozone at Syowa, and conclude that differences in lower, middle, and upper stratospheric transport processes have different effects on lower, middle, and upper stratospheric Antarctic stratospheric ozone. Furthermore, they point at possible delays in upper stratospheric ozone recovery by both effects of the solar cycle, as well as by longer transport time of air masses to reach the upper stratosphere.

In summary, in situ measurements of the vertical distribution of Antarctic ozone do not yet show a significant reduction in ozone loss rates, and this is not expected to become apparent until approximately 2020.

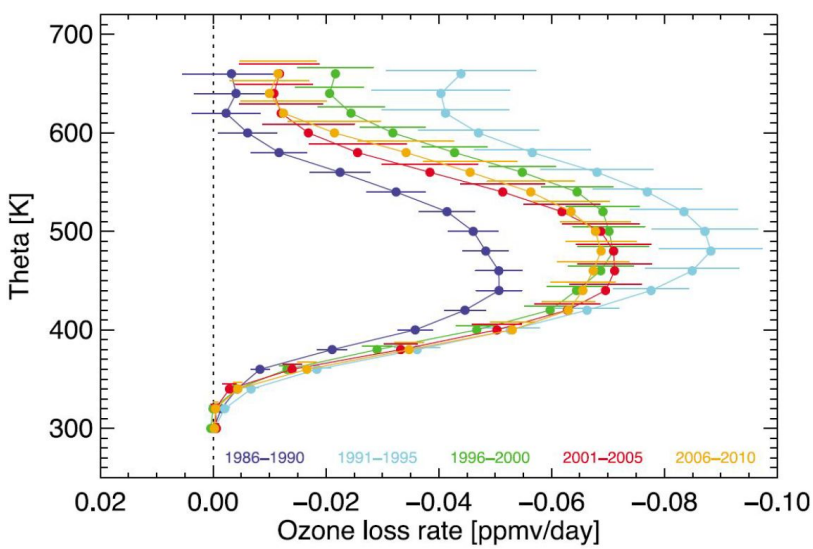

Figure 3-14. Vertical profile of ozone loss rates for five time periods (1986–1990, 1991–1995, 1996–2000, 2001–2005 without 2002, 2006–2010) based on 25 years of ozonesonde measurements taken at the South Pole, as determined by a linear fit to all available data for each pressure level between day 235 and 270 (late August to end of September). Ozone loss rates are given in [ppmv/day], error bars represent 1-σ uncertainties. After Hassler et al. (2011b).

3.4.2.2 SPRINGTIME TOTAL OZONE

Hassler et al. (2011b) analyzed October mean total ozone columns from four surface stations around Antarctica for the period 1966 to 2008. While these stations show a similar emergence of the ozone hole from 1960 to 1980, their records diverge after 1980, with annual mean differences between stations as large as 50 DU. By screening measurements based on whether they are obtained within or outside the vortex, ozone behavior over the last two decades for the four stations was found to be very similar. Similar conclusions have been reached for the Arctic stratosphere based on satellite data and methodologies (e.g., Kiesewetter et al., 2010).

Salby et al. (2011, 2012) presented the first claim of detection of the second phase of recovery of Antarctic ozone, i.e., a statistically significant increase in ozone due to declining EESC. They applied a two-parameter regression model to analyze annual springtime (September–November) Total Ozone Mapping Spectrometer (TOMS)/OMI total ozone over Antarctica poleward of 70°S (vortex core). Total ozone measurements were regressed against the upward Eliassen-Palm (EP) flux at 70 hPa, averaged poleward of 40°S during the period August–September, and the QBO, represented by tropical 30 hPa winds. Salby et al. (2011) reported a correlation (R^2) of springtime vortex core total ozone variations by their two-parameter regression model of 0.96. By applying these regressions, dynamical processes that determine year-to-year variability in Antarctic vortex strength and ozone destruction can be removed from the total ozone record, leaving an ozone residual that can be probed for the presence of trends. A positive linear trend for the period 1996–2008 was reported with a statistical significance of 99.5% using a two-tailed t-test. Note that the results from Salby et al. (2011, 2012) cannot directly be compared to those of Hassler et al. (2011a), in part because they look at different springtime periods, and also because Salby et al. (2011, 2012) investigate a vortex-average total ozone amount, whereas Hassler et al. (2011a) investigate ozone profiles taken at one specific location.

Kuttippurath et al. (2013) presented more extensive multivariate regression analyses of Antarctic polar vortex total ozone for the period 1979–2010. They analyzed two different satellite total ozone data sets (TOMS/OMI and MSR), as well as averaged ground-based Antarctic measurements of total ozone. They further applied the multivariate regression to three total ozone time series based on three different Antarctic ozone records: average total ozone inside the vortex and the vortex core, both based on passive tracer transport model simulations, as well as average total ozone for equivalent latitudes between 65° and 90°S. Finally, they applied two different trend estimates to the total ozone time series: either the EESC or PWLT were used as fit parameters in the multivariate regression. Trends were calculated for the periods both before and after 2000. The multivariate regression model includes effects of the solar flux, QBO, stratospheric aerosols, the heat flux (or Eliassen-Palm flux), and the Antarctic oscillation (or Southern Annular Mode). Taking these effects into account, the three types of measurements, the three vortex definitions, and the two linear trend methods all show a statistically significant positive trend in Antarctic total ozone for the period 2000–2010. The recovery rates based on the PWLT trend estimates are approximately 25 DU/decade or 8%/decade, while the EESC fit provides an estimate of approximately 10 DU/decade or 3%/decade. Both trend estimates are significant at the 95% confidence level. Differences between PWLT and EESC trend estimates indicate that vortex dynamics are important and should be considered, consistent with findings from Kiesewetter et al. (2010) and Hassler et al. (2011a).

The correlation of the multivariate regression in Kuttipurrath et al. (2013) does not exceed 0.90 (R^2), which appears inconsistent with the 0.96 (R^2) correlation found by Salby et al. (2011), despite the latter study being based on only two dependent variables. The cause of this discrepancy is currently unclear, but it should be kept in mind that although both studies include the same dependent variables (QBO and heat flux), they use different underlying base data (40 hPa tropical wind speed QBO and ECMWF ERA Interim heat flux in Kuttippurath et al. (2013); 30 hPa wind speed QBO and NCEP heat flux in Salby et al. (2011, 2012)). The time period over which total ozone data are averaged is also different (between September and November in the former case, over October in the latter case), as well as the length of the period under consideration (1996–2008 for Salby et al. (2011, 2012), and 2000–2010 for Kuttippurath et al. (2013)). In addition, these studies do not address several other sources of uncertainty, like regression parameter choices, regressor errors, and sensitivity to the time period over which the regressors are taken.

In summary, although findings of multivariate regression studies of springtime Antarctic total ozone are consistent with a beginning of ozone recovery, i.e., they report increases in ozone after 2000, uncertainties in measurements and regressors as well as uncertainties in statistical analyses preclude the definitive conclusion that Antarctic stratospheric ozone is increasing due to declining ODSs.

3.4.3 Long-Term Ozone Trend in the Arctic

Previous WMO/UNEP Ozone Assessments have noted that the large degree of interannual variability in meteorological conditions, and the strong dependence on the start and end dates used for the analysis render robust determination of ozone trends in the Arctic extremely problematic. The picture remains largely unchanged for this Assessment. Although several studies have placed the exceptional 2011 Arctic spring ozone values in context through comparisons with multiyear (in some cases multidecade) ozone data sets (Manney et al., 2011; Balis et al., 2011; Hurwitz et al., 2011; Arnone et al., 2012; Adams et al., 2012; Kuttippurath et al., 2012; Lindemaier et al., 2012; Isaksen et al., 2012; Pommereau et al., 2013; Strahan et al., 2013), few have specifically quantified long-term changes in Arctic lower stratospheric ozone. It is thus not possible to make a definitive statement about Arctic ozone trends at this time.

3.5 FUTURE CHANGES IN POLAR OZONE

Future changes in ozone can be assessed with models of varying complexity (parametric, two- and three-dimensional models). In recent years the state-of-the-art for assessing stratospheric ozone changes in a climate context has moved to comprehensive three-dimensional chemistry-climate models (CCMs). A major milestone for the CCM community was the CCMVal-2 model intercomparison report (SPARC CCMVal, 2010) that preceded the WMO/UNEP 2010 Ozone Assessment (WMO, 2011) and informed the conclusions therein. Progress with CCMs since has been continuous and new studies have either consolidated or added details to results from CCMVal-2. No recent study has challenged our fundamental understanding of how ozone will develop in the future, based on decreasing ODSs and continued evaluation of climate change sensitivities.

No intercomparison on the scale of CCMVal-2 has been carried out in time for this Ozone Assessment. The SPARC lifetime assessment (SPARC, 2013) has reassessed lifetimes of a number of ODSs using observations and models. The CCMs that contributed to the modeling part of the lifetime assessment have been updated since CCMVal-2 and will be used for future integrations and collaborative efforts, including the Chemistry-Climate Model Initiative (CCMI). Even though the modeling part of the lifetime assessment is extremely valuable for attributing past ozone changes by providing additional model integrations covering the recent past, it is investigating time-slice experiments for the future (Chipperfield et al., 2014), which are not directly comparable to the transient integrations projecting 2100 ozone levels in CCMVal-2. However, changed lifetimes of ODSs can be used in an indicative way and in updated model integrations. If key lifetimes are significantly increased, projected ozone recovery will be delayed. Table 6.1 in SPARC (2013) summarizes the new lifetimes for CFC-11 and CFC-12, among others. The recommended lifetimes increased from 45 to 52 years for CFC-11 and from 100 to 102 years for CFC-12. This lifetime adjustment does not suggest a major change of return and recovery dates reported in WMO (2011). Commonly the lifetime information of a species is used in conjunction with the assumed surface fluxes to calculate surface mixing ratios. The time-dependent surface mixing ratios are subsequently used as boundary conditions for CCM integrations. Four CCMs used in CCMVal-2 (SPARC CCMVal, 2010) and subsequently presented in WMO (2011), i.e., CMAM, GEOSCCM, UMSLIMCAT, and WACCM, compared the impact of changing from the WMO (2011) mixing ratio time series of ODSs to the SPARC (2013) recommendations (Figure 3-15). In Figure 3-15 the thick black line is the multi-model mean (MMM) polar total ozone from the four CCMs as contributed to WMO (2011) using Special Report on Emissions Scenarios (SRES) A1B scenario for well-mixed GHG and the WMO (2011) recommended ODS concentrations. The thin colored lines are pairwise differences added to the MMM for each of the four models. The models used Representative Concentration Pathway (RCP) 6.0 (GEOSCCM, WACCM, and CMAM) or RCP 4.5 (UMSLIMCAT) scenarios for well-mixed GHG in the updated runs. The turquoise shading is the one standard deviation interannual variability for March or October respectively added/subtracted to the MMM. Note that the differences are small and that they lie

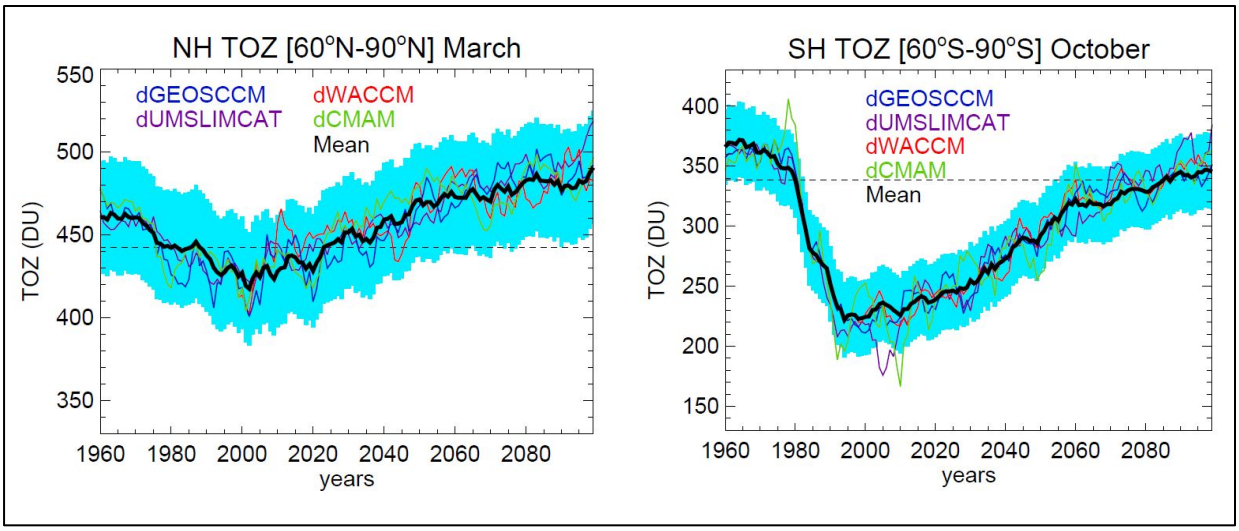

Figure 3-15. The thick black line is showing multi-model mean (MMM) polar total ozone (60°-90°; left: Northern Hemisphere March, right: Southern Hemisphere October) from four CCMs (see legend) that contributed to WMO (2011) using SRES A1B for well-mixed GHG and the WMO (2011) recommended ODS concentrations. The thin colored lines are pairwise differences ("old-new" ODS scenarios; "old": WMO, 2011; "new": SPARC, 2013) added to the MMM for each of the four models. The "new" integrations used RCP 6.0 (CMAM, GEOSCCM, and WACCM) or RCP 4.5 (UMSLIMCAT) for well-mixed GHG. The turquoise shading is the one standard deviation interannual variability for March (left) and October (right) from GEOSCCM added/subtracted to the MMM. Horizontal dashed lines are 1980 values.

largely within the one standard deviation range, thus suggesting that the ODS lifetime change had no significant impact on the polar ozone recovery in either the Northern or Southern Hemisphere. However it should be noted that this "by chance ensemble" provides a MMM that is returning late to 1980s ozone values in the Southern Hemisphere, compared to the full WMO (2011) MMM.

3.5.1 Factors Controlling Polar Ozone Amounts

Section 3.3 describes our level of understanding of processes influencing polar ozone changes. CCMs are an attempt to utilize this process understanding to simulate (in a comprehensive way) chemistry-climate interactions, allowing us to make projections into the future. Such models are of increasing complexity (e.g., consider more and more Earth system components with higher complexity). Like all models, CCMs have to compromise in terms of complexity and resolution, to provide the length of integrations required to evaluate interactions between composition and climate on longer timescales. Continuous validation of the model performance for the recent past is a key to our judgment of model projections, even though good model performance for the past does not necessarily guarantee reliable predictions.

Two main factors determine future ozone amounts: How fast are the stratospheric chlorine and bromine amounts changing, and what is the impact of increasing GHGs on ozone? Box 3-2 summarizes many important aspects relating to this issue. To illustrate the success of the Montreal Protocol, it is useful to consider so-called "world avoided" simulations. Since the last Assessment, Garcia et al. (2012) used an updated version of the Whole Atmosphere Community Climate Model (WACCM) model, illustrating the expected strong impact of heterogeneous chemistry on the ozone budget and quantifying the ozone loss avoided by the Montreal Protocol. Their results are in good agreement with earlier studies that have been reported in WMO (2011).

For tracing the success of the Montreal Protocol, previous WMO/UNEP ozone assessments have introduced the concepts of ozone recovery and return. As emphasized in Section 3.4, ozone recovery relates to the physical effects ODSs have on stratospheric ozone. When ODSs no longer significantly

affect ozone chemistry, full ozone recovery has been achieved. For this consideration, transport effects, e.g., the removal of chlorine-containing species from the stratosphere, are most important (indicated with a downward pointing arrow in Box 3-2).

Return relates to the achievement of a threshold ozone amount that was observed in the past. When ODS abundances decline in the stratosphere, ozone will increase. In addition ozone will increase due to a cooling of the upper stratosphere that is caused by increasing GHGs (Box 3-2). Simultaneously, changes in meridional transport would modify the high-latitude ozone budget, with current CCMs indicating a strengthening of the BDC for GHG increases. This has been extensively discussed in WMO (2011) and it was concluded that, "A stronger BDC would decrease the abundance of tropical lower stratospheric ozone, increase poleward transport of ozone, and could reduce the atmospheric lifetimes of long-lived ODSs and other trace gases." A detailed discussion of the recent findings regarding the evolution of the BDC is presented in Chapter 4 of the present Assessment.

Baumgaertner et al. (2010) add a nuance to the general picture by pointing out that upper stratospheric NO_x enhancement due to a stronger BDC would cause additional ozone loss, but that the ozone loss would be more or less canceled by more poleward ozone transport. The added effects of decreasing ODSs, increasing GHGs, and changing meridional transport will lead to polar ozone return dates that are earlier than the recovery dates. Arguably the evolution of return dates, in particular in total ozone, is more straightforward and easier to measure than the exact timing of recovery.

Even though two important factors determining future ozone are well understood, namely, the ozone change due to decreasing ODSs and the stratospheric cooling due to GHGs, many mechanisms exist that are uncertain in their future development. One of the uncertainties lies with the PSCs (Box 3-2). How will they develop under climate change? Will there be more PSCs due to radiatively controlled cooling, or less due to dynamically induced warming? Hurwitz and Newman (2010) looked at the development of the PSC area in projections using the Goddard Chemistry-Climate Model (GEOSCCM). In their model, future trends in the PSC area in October over Antarctica were negative, thus "helping" ozone return. In addition, Deushi and Shibata (2011) investigated the impact of GHGs on ozone recovery. In their model, resolved wave forcing is decreased in spring over Antarctica, due to an earlier breakdown of the polar vortex in the future. If this is a verifiable result, it would indicate a potential mechanism for earlier ozone return dates. More examples are discussed in Sections 3.3.3 and in 3.5.3.1.

3.5.2 Long-Term Projection of Polar Ozone Amounts

A multi-model mean (MMM) total ozone time series relative to a particular year is a relatively robust representation of an "average" behavior for the future. An uncertainty range can be described by the inter-model standard deviation that is usually large. The large standard deviations arise because the models are potentially biased and their meteorology will differ in the same nominal year. However each individual model ozone time series is referenced to its own climatological base period. Therefore a large spread does not mean that models disagree on the general temporal development of ozone. The spread is merely highlighting that the models differ.

Following considerations in Austin et al. (2010a) and WMO (2011), Figure 3-16 presents a MMM anomaly total ozone time series. In Figure 3-16, 1980 ozone values are indicated with a dashed line. The thick red line indicates the MMM total ozone anomaly for the Arctic in March (Figure 3-16, top) and for Antarctica in October (Figure 3-16, bottom). The spread is indicated by a two standard deviation interval (gray shading). The MMM time series indicate an earlier return date with respect to 1980 values for the Arctic (near 2030) than for the Antarctic (near 2050). Note that the CCMVal-2 integrations have been performed with a particular Special Report on Emission Scenario (SRES) climate changes scenario (A1B). For the recent IPCC report (AR5; IPCC, 2013), SRES scenarios have been superseded by Representative Concentration Pathways (RCP) scenarios (van Vuuren et al., 2011). Both SRES and RCP are descriptions of the possible evolution of climate forcings that depend on assumptions, e.g., how energy consumption will develop in the future, and a range of possibilities is considered. This scenario

Box 3-2. Factors Determining Future Polar Ozone

Ozone-depleting substances (ODSs) are the drivers of polar ozone loss. Due to the Montreal Protocol and its Amendments, ODS amounts are decreasing and ozone will recover. Here, we discuss factors that influence details of the recovery process. Factors influencing future ozone amounts in high latitudes at different heights are: **changes in meridional transport** (indicated by bold open arrows), **temperature changes** from increased long-lived GHGs (indicated by blue or red shaded areas), and **chemical effects** (the future potential to form PSCs that can activate available halogens, e.g., chlorine and to a lesser extent bromine, and changes in temperature-dependent reaction rates). Each effect is changing ozone at certain heights. A combination of all effects is manifested in the total ozone, the vertically integrated amount of ozone.

The sketch below shows polar latitudes (with the North or South Pole to the left) versus altitude. The altitude scale is roughly indicated by the position of the polar tropopause (black dashed line). Stratospheric cooling and tropospheric warming are indicated with color-shaded areas. Poleward transport and generally descending motion, as well as air exchange between the stratosphere and the troposphere, are indicated with bold open arrows. The blue half ellipse shows the region where PSCs occur when temperatures are low enough. The green half ellipse denotes the ozone maximum in partial pressure or number density.

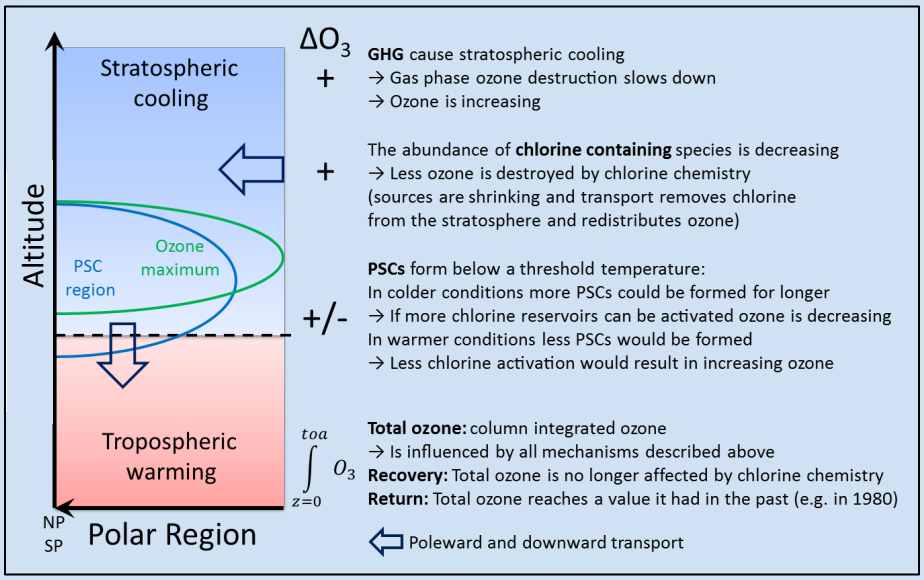

Changes in transport under climate change: Models predict a strengthening of the Brewer-Dobson circulation (BDC) for increased long-lived GHG concentrations. Increased poleward transport would provide a gain in polar ozone. Increased downward transport and more efficient air exchange between the stratosphere and the troposphere would provide a more efficient removal mechanism for halogen-containing species, the main driver of ozone destruction.

Changes in temperature under climate change: The increase of long-lived GHGs has led to a warming in the troposphere and cooling in the stratosphere. Many processes and reactions that change ozone are temperature dependent. In colder conditions more PSCs could be formed, thus providing a greater potential for halogen activation and ozone destruction. Furthermore, PSC formation depends on the availability of water vapor; future trends in water vapor are uncertain.

Chemical effects: They are closely coupled to the transport and temperature changes. In the lower stratosphere they depend on the availability of halogen-containing species and the occurrence, amount, and timing of PSCs. In the upper stratosphere, chlorine chemistry also plays a role. However, lower temperatures there slow down the gas-phase destruction of ozone, thus resulting in more ozone. In addition, changes in N_2O and CH_4 concentrations could affect ozone chemistry as well.

Because all effects above contribute to changes in polar total ozone, it is more difficult to monitor **total ozone recovery** than **return**. **Total ozone recovery** relies on the concept that ozone amounts are no longer significantly affected by halogen chemistry and **full recovery** would imply that halogens of anthropogenic origin no longer play a role in determining ozone amounts. **Total ozone return** is a simpler milestone to monitor, answering the question "When do we reach a level of ozone that we had in the past?"

uncertainty will be discussed further in Section 3.5.3. The blue line in Figure 3-16 is derived from observations (see also Figure 3-4) indicating the overall qualitative agreement with model results (see also Chapter 2 of this Assessment).

Austin et al. (2010a) compared 1960 and 1980 baseline projections for CCMVal-2, highlighting the issue of a later return to 1960 values. One factor limiting our confidence in the timing of return date projections is the large inter-model spread, even though Austin et al. (2010a) presented some evidence that the situation had improved since CCMVal-1. Note however that this Assessment uses a recent climatological base period and indicates the 1980-return date separately (black dashed lines in Figure 3-16).

Certain aspects of the inter-model spread in return dates can be understood by investigating physical properties of the models. Note however that the spread in return dates is smaller than the envelope in Figure 3-16 (see WMO, 2011 for details). Strahan et al. (2011) evaluated CCMVal-2 model results by characterizing transport performance and the resulting vortex Cl_y (80°S, 50hPa) concentrations. Results showed that models with no diagnosable chlorine chemistry deficiencies showed a quasi-linear relationship between polar vortex Cl_y in 2005 and the projected return dates. As expected from our chemical understanding of ozone loss, models with high Cl_y in 2005 showed late return dates, with return dates to 1980 values ranging from around 2040 to 2070.

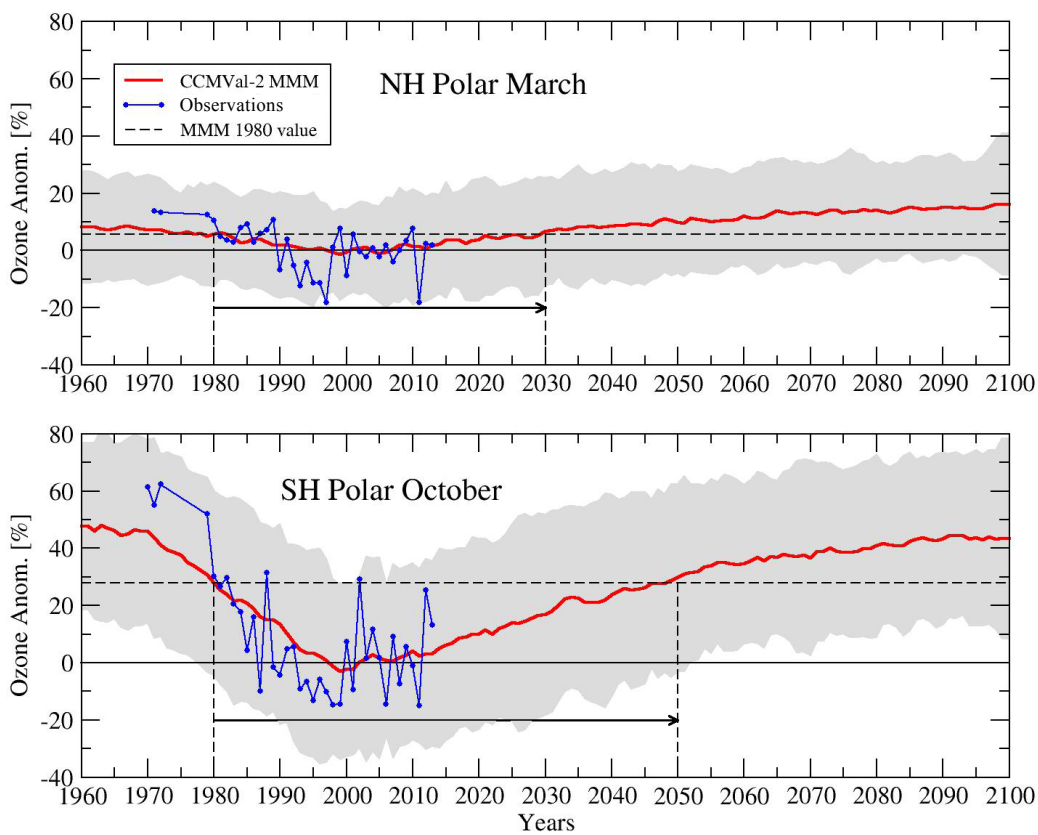

Figure 3-16. The solid red line is showing multi-model mean (MMM) polar total ozone anomalies in percent (60°-90°; top: Northern Hemisphere March, bottom: Southern Hemisphere October) relative to a 1998 to 2008 base period. The MMM values predict a return date relative to the year 1980 in the Northern Hemisphere before the middle of the 21st century (near 2030, indicated with black dashed lines) and in the SH for around the middle of the 21st century (near 2050). The spread between the CCMs used for estimating the MMM values is indicated by the gray ranges (two standard deviations). Observations are indicated by the blue lines showing ozone anomalies derived from ozone values presented in Figure 3-4 of this Assessment.

3.5.3 Uncertainties of Future Polar Ozone Changes

We can distinguish three different contributors to uncertainty: internal variability of the atmosphere, model uncertainty, and scenario uncertainty. Depending on the quantity, internal variability can be a small or large source of uncertainty. In contrast model uncertainty is commonly significant. Scenario uncertainty is less problematic in the near future (e.g., for the next twenty years), because different RCPs diverge more for the far future than for the near future. Consequently scenario uncertainty increases rapidly for the later decades, because we do not know which path will be chosen in the far future.

Charlton-Perez et al. (2010) estimated uncertainty contributions in multi-model mean projections of annual and global mean total ozone. They use global and annual mean data to keep the contribution of internal variability small. The spatial and temporal averaging mitigates the magnitude of internal variability that would be far more dominant for, e.g., seasonal or monthly mean data. Indications are that scenario uncertainties are increased in the late 21st century with RCP (used in Coupled Model Intercomparison Project Phase 5, CMIP5) compared to SRES A1B (used in Coupled Model Intercomparison Project Phase 3 (CMIP3) and WMO, 2011) scenarios. In the following subsections, we will discuss aspects of internal variability/model uncertainty and scenario uncertainty in more detail.

3.5.3.1 INTERNAL VARIABILITY AND MODEL UNCERTAINTY

Stratospheric cooling from increasing carbon dioxide levels will likely alter the forcing from upward-propagating tropospheric waves, which affect cold and warm winters, and thus internal variability itself, in different ways. Overall increasing wave activity in the stratosphere, as predicted by some climate models, would make dynamically quiet periods less frequent. However, as already mentioned in Section 3.3.3.2, amplified tropospheric wave activity does not necessarily imply enhanced wave fluxes into the stratosphere. Consequently the evolution of polar stratospheric temperatures over the next hundred years has a number of uncertainties.

Chemistry-climate models (CCMs) do not reproduce the derived long-term changes in Arctic V_{PSC} (Hitchcock et al., 2009). V_{PSC} is an integrated measure of polar temperatures (see Section 3.2.2). Although there is a suggestion that multidecadal variability in V_{PSC} extremes can happen through internal variability (Rieder and Polvani, 2013), the question remains open as to whether more extremely cold Arctic winters are projected in the future (e.g., Hitchcock et al., 2009). Langematz et al. (2014) analyzed future V_{PSC} in transient and timeslice simulations, finding an increase in V_{PSC} until the middle of the 21st century and a drop afterwards.

One of the uncertainties in modeling polar ozone amounts arises from ongoing changes in the Northern Hemisphere land or ocean cryospheres, which might impact the high-latitude stratosphere. Both the Eurasian snow cover and the Arctic sea ice loss have the potential to modulate the upward propagation of planetary waves. Increased Eurasian snow cover during autumn amplifies wave trains propagating upward into the polar stratosphere (e.g., Fletcher et al., 2009; Orsolini and Kvamstø, 2009; Smith et al., 2010). Arctic sea ice loss first leads to a strong warming of the lower troposphere in autumn, when ocean heat loss is strong, but ultimately changes synoptic and global circulation patterns. An observational study contrasting recent decades with low or high sea ice extent (Jaiser et al., 2012) and a case study with a high-resolution coupled ocean-atmosphere model for the year 2007 characterized by a very large summer sea ice loss (Orsolini et al., 2012), have shown enhanced stratospheric planetary waves in early winter. The springtime response to observed or projected sea ice decrease was also investigated using models of various complexity, i.e., a coupled atmosphere-ocean model in Screen et al. (2013), a CCM in Cai et al. (2012), and a CCM coupled to an ocean in Scinocca et al. (2009), the three studies qualitatively agreeing on a springtime stratospheric cooling.

Given the small number of studies with models of various complexity, the high internal atmospheric variability in winter, the different sea ice decrease scenarios, and the potential seasonality of

the response, further studies are needed to determine whether there exists a real multi-model consensus on the impact on stratospheric variability.

Model biases pose an ongoing challenge for modelers and influence the estimate of model uncertainty. Biases can have far reaching consequences for model performance. For example a temperature bias will impact the formation of PSCs and thus influence chemical ozone destruction significantly. WMO (2011) and in more detail Austin et al. (2010b) showed that many models participating in CCMVal-2 underestimated the present-day ozone hole area in the projection runs and that the future development of the ozone hole area differed significantly between models. In a case study, Brakebusch et al. (2013) showed an improvement in modeled ozone in their nudged CCM for the winter 2004–2005 when temperatures for heterogeneous chemistry reactions were reduced by 1.5 K, indicating, for instance, less chlorine activation in the model under observed conditions. This indicates that underlying climate model biases affect the performance of a CCM regarding the simulation of future polar ozone.

3.5.3.2 SCENARIO UNCERTAINTY

As discussed in WMO (2011) and detailed in Eyring et al. (2010), the relative contributions of ODSs and GHGs on projected ozone changes can be estimated with CCM experiments in which different forcings are fixed, for example an integration from 1960 to 2100 with fixed ODSs. For instance, the role of increasing GHGs in speeding up ozone return was investigated by Oman et al. (2010). Using CCMVal-2 model results, they showed that decreasing halogens and declining upper atmospheric temperatures (due to GHGs), contribute almost equally to increases in modeled upper stratospheric ozone (Box 3-2 and accompanying description). A similar conclusion is reached by Plummer et al. (2010) studying sensitivities in one particular model that is included in Oman et al. (2010).

The recent CMIP5 exercise focused on broader climate change issues in support of the IPCC AR5 (IPCC, 2013). Models with and without interactive chemistry participated. Models without interactive chemistry had the option of using an ozone climatology derived from observations, CCMVal-2 data, and complementary data (Cionni et al., 2011). Eyring et al. (2013) compared the ozone evolution in CMIP5 models with interactive ozone to the climatology constructed for non-interactive models (Cionni et al., 2011), thus achieving some insight in the scenario uncertainty due to different climate change scenarios (Figure 3-17). For the Northern Hemisphere (NH) polar region in March, the total ozone column for all RCP scenarios agrees well until ~2025. After the year 2025 ozone modeled with RCP6.0 agrees well with the CCMVal-2 data. This is expected, because RCP6.0 is close to the SRES A1B forcing used in CCMVal-2.

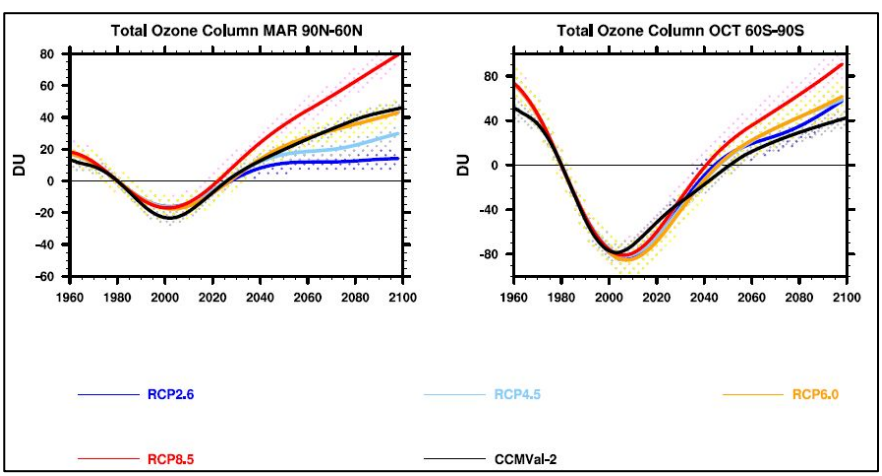

Figure 3-17. The 1980 baseline-adjusted total ozone column time series from 1960 to 2100 for the CMIP5 CHEM multi-model mean (colored lines) and CCMVal-2 multi-model mean ozone database (black line) for Northern Hemisphere (left) and Southern Hemisphere (right) spring polar regions. All time series by construction go through 0 in 1980. The RCP 2.6, RCP 4.5, RCP6.0, and RCP 8.5 are shown in blue, light blue, orange, and red, respectively. The corresponding color-coded stippled areas show the 95% confidence interval of the CHEM multi-model mean simulations. Derived from Figure 6 in Eyring et al. (2013).

For RCP8.5, ozone increases fastest and rises significantly above the 1980 amounts. For RCP2.6, ozone increases slower after ~2040 compared to RCP6.0 and the ozone enhancement relative to 1980 amounts is smaller. The situation is less clear in the Southern Hemisphere (SH). The RCP-driven models show higher ozone values compared to the CCMVal-2 multi-model mean during October in the SH polar region. All ozone trajectories stay close together until ~2030. After ~2040, distinct scenario differences are apparent, with RCP8.5 showing the largest ozone amounts in later years. Note that there are some clear differences between the different scenarios with respect to SRES A1B. Obviously many aspects influence scenario uncertainty. Revell et al. (2012) evaluated the ozone response to different nitrous oxide (N_2O) and methane (CH_4) scenarios in a number of model sensitivity studies. Large N_2O concentrations were associated with smaller ozone increases, whereas larger CH_4 concentrations were associated with larger ozone increases. All this highlights the importance of the chosen concentration pathway for the discussion of recovery dates.

In addition, scenario uncertainty includes events we cannot foresee and that can potentially affect stratospheric ozone: for example a major volcanic eruption or the decision to use stratospheric aerosol for solar radiation management (i.e., "geoengineering"). Details about possible geoengineering activities and the issue of potential impact to global stratospheric ozone and climate are also discussed in Chapters 2, 4, and 5 of this Assessment.

Austin et al. (2013) discuss how past volcanic eruptions have changed ozone in the stratosphere using a version of the GFDL CCM. The more recent eruptions (El Chichón and Mt. Pinatubo) resulted in a globally averaged total ozone decrease (Figure 3-18, top) caused by severe ozone depletion in the lower stratosphere (confirmed by many earlier studies as well, including the CCMVal-2 Report). The earlier eruptions (Krakatau, Santa Maria, and Agung) resulted in globally averaged total ozone increases (Figure 3-18, top). The difference in ozone response is caused by the changed chemistry due to the increased availability of chlorine. However, changes in polar latitudes are more complex and depend on the meteorology as well (Figure 3-18, middle and bottom). Past volcanic aerosol episodes (only two events are well described based on a wealth of measurements) can be used as templates for assessing possible future impacts, highlighting that the impact on ozone at global scale will depend on stratospheric halogen loading and on many other factors in polar latitudes.

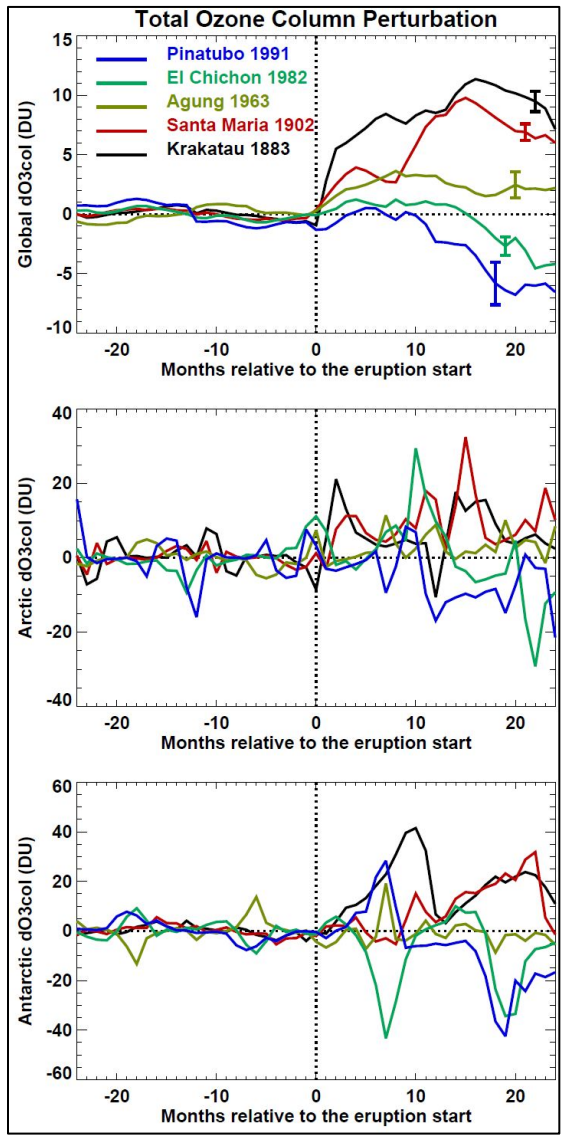

Figure 3-18. Simulated total ozone anomalies for the global mean (top), the Arctic mean (middle), and the Antarctic mean (bottom) within two years of each of the five major volcanic eruptions since 1860. The results are plotted relative to the mean for the two-year period prior to the date that the aerosol surface area density significantly exceeded the background value at the 63-hPa level. The mean annual cycle has been subtracted from the results. The error bars denote twice the standard deviation of the monthly values for the two-year pre-volcanic period. Extension of Figure 11 in Austin et al. (2013).

Tilmes et al. (2008, 2009) investigated the relationship between ozone depletion and chlorine activation to estimate how sulfuric acid aerosol might affect polar ozone. In their model, an injection of sulphur large enough to compensate surface warming caused by the doubling of atmospheric CO_2 would strongly enhance Arctic ozone depletion during the present century for cold winters and would cause a considerable delay in Antarctic ozone recovery. Pitari et al. (2014) presented results from two general circulation models (GCMs) and two CCMs. On average, the models simulate a decrease in globally averaged ozone up to about 2 DU during the middle of the century (2040–2049) due to an increase in sulfate aerosol surface area density similar to conditions a year after the Mt. Pinatubo eruption. Enhanced heterogeneous chemistry on sulfate aerosols leads to an ozone increase in low and middle latitudes, whereas enhanced heterogeneous reactions in polar regions and increased tropical upwelling lead to a reduction of stratospheric ozone.

A further uncertainty for polar ozone amounts is the change in natural halogen-containing source gases levels, and in particular in very short-lived substances (VSLS). Considerations include the characterization of VSLS sources in models (Hossaini et al., 2013) and how the sources will change under climate change, how VSLS and their breakdown products will be transported (Hossaini et al., 2012), and how efficient the brominated species originating from VSLS will be in depleting ozone (Tilmes et al., 2012; Braesicke et al., 2013; Oman and Douglass, 2014). For example, Braesicke et al. (2013) diagnose in their model a possible sensitivity of total ozone to an increase in VSLS, with up to 20 DU ozone loss in the Southern Hemisphere polar region. Of course this sensitivity depends on the chlorine loading and will change in the future as well.

In summary, while we have a sound understanding of processes determining future polar ozone (Box 3-2), there are significant uncertainties in determining recovery and return dates. Part of the uncertainty can be understood through physical considerations (for example transport and chemical lifetimes), and are expected to be reduced in the future. Other uncertainties, in particular in the scenarios, are beyond our direct control and we can only gauge possibilities.

3.6 KEY MESSAGES OF CHAPTER 3 FOR THE DECISION-MAKING COMMUNITY

3.6.1 Recent Polar Ozone Changes

An Antarctic ozone hole has continued to form each year during the period 2010–2013. The continued occurrence of an Antarctic ozone hole was expected because the amount of ozone-depleting substances in polar regions has decreased only moderately (by about 10%) over the last decade. The period was also characterized by enhanced variability in Antarctic polar vortex dynamics that had an impact on the year-to-year variations of vortex-averaged total ozone during the springtime.

In the Arctic, exceptionally low ozone abundances were observed within the vortex during the spring of 2011. These low ozone values were due to an unprecedented degree of chemical ozone loss, coupled with very weak transport of ozone to the lower stratospheric polar vortex. This exceptional event was caused by unusual meteorological conditions in the Arctic during the winter 2010/2011, characterized by persistent low temperatures and a strong isolated polar vortex. With the present availability of stratospheric satellite measurements, the extent of polar ozone destruction processes throughout the winter could be evaluated from the evolution of key species involved in chemical ozone depletion, such as hydrogen chloride (HCl), chlorine monoxide (ClO), and nitric acid (HNO_3). The persistence of low temperatures led to the formation of widespread and vertically extensive polar stratospheric clouds, which induced strong chlorine activation and denitrification in the 2011 Arctic vortex. These mechanisms led to severe chemical ozone destruction between 16 and 22 km altitude, with 60–80% of the vortex ozone at ~18–20 km removed by early April (Figure 3-19).

State-of-the-art chemical transport models (CTMs) reproduce the observed ozone values during spring 2011 well, confirming that the extremely low ozone values resulted from known processes, not

unusual or unexpected chemistry. The occurrence of this extreme event has thus not challenged our fundamental understanding of the processes controlling polar ozone.

The derived ozone loss in the Arctic spring 2011 was comparable to ozone losses observed in Antarctica in the 1980s (Figure 3-19). Because transport from low to high latitudes is more prominent in the Northern Hemisphere (NH) than in the Southern Hemisphere (SH), background ozone levels in the Arctic are ~100 DU higher than in the Antarctic. As a result, although the evolution of Arctic ozone and related constituents in spring 2011 more closely followed that characteristic of the Antarctic than ever before, the springtime total ozone values remained considerably higher than those reached in a typical year in the Antarctic. In addition, the areal extent of the 2011 Arctic vortex was only ~60% the size of a typical Antarctic vortex, thus the low-ozone region was more spatially confined (Figure 3-19).

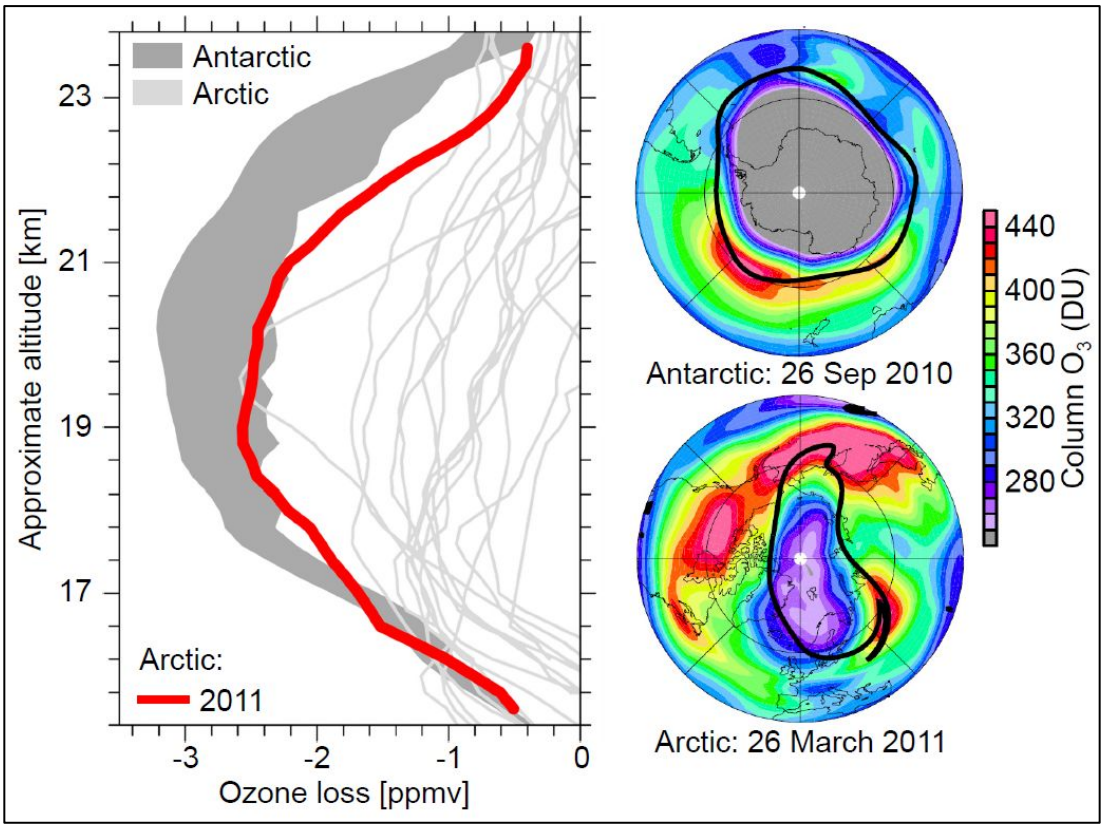

Figure 3-19. *Left:* Representative spring profiles of observed vortex-average chemical ozone loss (in parts per million by volume, ppmv). The light gray curves indicate the results for individual Arctic spring periods (1992–2010). The red curve indicates the result in Arctic spring 2011. Also shown is an indicative range of ozone loss for typical Antarctic spring periods, illustrated by the loss that has been derived from ozone observations for a relatively weak early Antarctic ozone hole (1985, upper limit of the gray shading) and the loss in a strong Antarctic ozone hole (2003, lower limit of the gray shading). *Right:* Maps of total column ozone from the Aura satellite's Ozone Monitoring Instrument (OMI) for the Antarctic (top; ozone hole situation 2010) and Arctic (bottom; strong ozone column reduction in March 2011). Overlaid black contours mark the size and shape of the polar vortex on the 460 K potential temperature surface. Different charts are adapted from Manney et al. (2011). The figure shows that the degree of chemical ozone loss in the Arctic in spring 2011 was in the range of observations from weak Antarctic ozone holes (within uncertainties; left panel), but that the abundance of ozone above the Arctic was still substantially larger than in Antarctic ozone holes, mainly because the undisturbed ozone layer is thicker in the Arctic compared to the Antarctic, due to natural differences in transport between the two hemispheres.

If similar conditions were to arise again in the Arctic while stratospheric chlorine loading remains high, similarly severe chemical ozone loss would take place. Uncertainties in current climate models preclude confident quantification of the likelihood of repeated episodes of extensive Arctic ozone depletion in the present or future climate (a point also made in Section 3.5).

3.6.2 Understanding of Polar Ozone Processes

Generally, there have been no major changes in our understanding of polar ozone loss processes since WMO (2011). The scientific knowledge of polar chemical and dynamical processes was already based on a large body of research. As mentioned, numerical model studies of the atmosphere using CTMs reproduce observed chemical polar ozone depletion and its variability well.

Recent work has improved the detailed understanding of polar ozone processes (such as the formation mechanism of polar stratospheric clouds (PSCs), in particular nitric acid trihydrate (NAT) particles), validated previous assumptions, and reduced uncertainty. The formation of NAT PSCs is a prerequisite for denitrification by sedimenting particles, which prolongs seasonal ozone loss. A more accurate representation of NAT PSC nucleation and particle characteristics leads to better model simulations of denitrification and hence ozone loss.

The uncertainty range in the photolysis rate of dichlorine peroxide (ClOOCl, the ClO dimer), a key parameter in polar chemical ozone loss, has been reduced significantly, providing a better constraint for the simulation of polar ozone in late winter and spring. The overall understanding of chemical processes involved in polar ozone loss is well developed and remains unchanged.

It is now clear that the ClO + BrO catalytic cycles are responsible for about 50% of the ozone loss in the polar lower stratosphere, with the contribution being slightly larger in the Arctic, where the overall depletion is less. Recent work has better quantified the contribution from very short-lived substances (VSLS) to the overall stratospheric bromine budget. In the photochemically aged air masses of the polar lower stratosphere, both long-lived and short-lived brominated species will have decomposed to inorganic bromine. Therefore, the source of bromine is not important, but any contribution of VSLS to bromine will translate into a contribution to polar ozone loss, which is proportional to the fraction of overall bromine that comes from the breakdown of VSLS.

Regarding polar stratospheric dynamics, the very cold Northern Hemisphere winter of 2010/2011 expanded the range of stratospheric dynamical variability seen in the Arctic over the past decades and provided a new extreme test case for models (i.e., CTMs as well as chemistry-climate models, CCMs).

The current understanding of the mechanisms that determine planetary wave driving (or the lack of it) of the polar stratosphere is still incomplete, but some progress has been made. It is particularly important to understand the origin of very strong polar vortex events that drive the ozone loss, either short-duration intense cooling episodes as observed in January 2010, or prolonged cooling like that observed during the late winter and spring 2011. Several recent observational studies have shown that tropospheric highs (e.g., blockings) can lead to either warming or cooling of the Northern Hemisphere polar stratosphere, depending upon their geographical location.

3.6.3 Recovery of Polar Ozone

Recent WMO/UNEP ozone assessments (WMO, 2007, 2011) have firmly established that intensification of Antarctic springtime ozone depletion is no longer occurring. The stabilization of Antarctic polar ozone loss occurred most likely after 1997. The previous ozone assessment (WMO, 2011) concluded that it was not yet possible to confidently state that there had been increases in Antarctic springtime stratospheric ozone, nor that these could be attributed to decreasing ozone-depleting substances (ODSs).

Current investigations indicate a small increase of 10–25 DU (3–8%) after 2000 in springtime Antarctic ozone observations, after taking year-to-year variability into account. This slight rise in Antarctic springtime ozone content is consistent with expectations considering the decrease in ODSs.

However, uncertainties in separating chemical from dynamical effects on Antarctic springtime ozone, combined with only a slow decline in ODSs and the strong dependence of results on the start and end dates used for the analyses, prevent—for now—unambiguously attributing the decrease in ozone depletion to decreasing ODSs.

The expected continued slow decline in ODSs will make attribution of decreasing Antarctic springtime ozone depletion to decreasing ODSs possible as time progresses.

3.6.4 Future Changes in Polar Ozone

A major milestone for the CCM community was the CCMVal-2 model intercomparison report (SPARC CCMVal, 2010) that preceded the WMO/UNEP 2010 assessment (WMO, 2011) and informed the conclusions therein. Progress with CCMs since has been continuous and new studies have either consolidated or added details to results from CCMVal-2. No recent study has challenged our fundamental understanding of how ozone will develop in the future, based on decreasing ODSs and continued evaluation of climate change sensitivities.

Arctic and Antarctic ozone is predicted to increase as a result of the expected reduction of ODSs due to regulations of the Montreal Protocol. A return to values of ozone in high latitudes similar to those of the 1980s is likely during this century, with Northern Hemisphere (NH) polar ozone predicted to recover earlier as compared to the Southern Hemisphere (SH) polar ozone (Figure 3-16). Uncertainties in the assessed return dates result in particular from incomplete knowledge of future greenhouse gas (GHG) levels and corresponding climate change consequences (Figure 3-17), and incomplete description of processes and their feedbacks in numerical prediction tools, including CCMs.

Updated ODS lifetimes (SPARC, 2013) have only a minor effect on previously estimated dates of ozone return to 1980 values. Lifetimes of ODSs have been reassessed and some lifetimes have changed since the last Assessment. Our physical understanding and first CCM studies do not indicate any significant changes for ozone return dates due to the changed ODS lifetimes.

Climate change is an important driver for polar ozone amounts late this century. Due to a larger sensitivity of NH dynamical processes, climate change is expected to have a larger impact on ozone in the Arctic than in the Antarctic. However, we do not know how climate change forcings will develop in detail. The possibilities have been gauged by using four different "Representative Concentration Pathways (RCPs)" adopted by IPCC (5th Assessment Report, 2013) in climate model studies (Coupled Model Intercomparison Project Phase 5, CMIP5) (Figure 3-17). Conversely, it is now evident that considering ozone in a comprehensive way is important for climate projections.

Another driver for the development of ozone are VSLS emissions, especially brominated species. There are large uncertainties about current-day VSLS emissions and the sensitivity of polar ozone loss to changes in Br_y requires further characterization. Nevertheless, some model studies indicate a sensitivity of total ozone sensitivity to increased VSLS emissions, with up to 20 DU ozone loss in the Southern Hemisphere polar region. How VSLS sources will change in a changing climate is yet unknown.

Major volcanic eruptions can perturb stratospheric ozone. Volcanic effects on stratospheric ozone have been simulated by several CCMs. Observations and model simulations show that recent major eruptions (e.g., El Chichón in 1982 and Mt. Pinatubo in 1991) resulted in globally averaged total ozone decreases caused by severe ozone destruction in the lower stratosphere. In contrast, model results suggest that earlier eruptions (e.g., Krakatau in 1883, Santa Maria in 1902, and Agung in 1963) resulted in globally averaged total ozone increases. The difference in the response of ozone to the earlier and later volcanos is attributable to catalytic ozone destruction enabled by the increased availability of stratospheric chlorine. Hence, in the next few decades while stratospheric chlorine content remains high, ozone depletion could worsen in the event of large volcanic eruptions.

REFERENCES

Adams, C., K. Strong, X. Zhao, M.R. Bassford, M.P. Chipperfield, W. Daffer, J.R. Drummond, E.E. Farahani, W. Feng, A. Fraser, F. Goutail, G. Manney, C.A. McLinden, A. Pazmino, M. Rex, and K.A. Walker, Severe 2011 ozone depletion assessed with 11 years of ozone, NO_2, and OClO measurements at 80°N, *Geophys. Res. Lett.*, *39* (5), L05806, doi: 10.1029/2011GL050478, 2012.

Agosta, E.A., and P.O. Canziani, Austral spring stratospheric and tropospheric circulation interannual variability, *J. Clim.*, *24* (11), 2629-2647, doi: 10.1175/2010JCLI3418.1, 2011.

Alexander, S.P., A.R. Klekociuk, M.C. Pitts, A.J. McDonald, and A. Arevalo-Torres, The effect of orographic gravity waves on Antarctic polar stratospheric cloud occurrence and composition, *J. Geophys. Res.*, *116* (D6), D06109, doi: 10.1029/2010JD015184, 2011.

Alexander, S.P., A.R. Klekociuk, A.J. McDonald, and M.C. Pitts, Quantifying the role of orographic gravity waves on polar stratospheric cloud occurrence in the Antarctic and the Arctic, *J. Geophys. Res*., *118* (20), 11493-11507, doi: 10.1002/2013JD020122, 2013.

Anstey, J.A., and T.G. Shepherd, High-latitude influence of the quasi-biennial oscillation, *Quart. J. Roy. Meteorol. Soc.*, *140* (678), 1-21, doi: 10.1002/qj.2132, 2014.

Arnone, E., E. Castelli, E. Papandrea, M. Carlotti, and B.M. Dinelli, Extreme ozone depletion in the 2010–2011 Arctic winter stratosphere as observed by MIPAS/ENVISAT using a 2-D tomographic approach, *Atmos. Chem. Phys., 12* (19), 9149-9165, doi: 10.5194/acp-12-9149-2012, 2012.

August, T., D. Klaes, P. Schlüssel, T. Hultberg, M. Crapeau, A. Arriaga, A. O'Carroll, D. Coppens, R. Munro, and X. Calbet, IASI on Metop-A: Operational Level 2 retrievals after five years in orbit, *J. Quant. Spectrosc. Radiat. Transfer*, *113* (11), 1340-1371, doi: 10.1016/j.jqsrt.2012.02.028, 2012.

Austin, J., J. Scinocca, D. Plummer, L. Oman, D. Waugh, H. Akiyoshi, S. Bekki, P. Braesicke, N. Butchart, M. Chipperfield, D. Cugnet, M. Dameris, S. Dhomse, V. Eyring, S. Frith, R.R. Garcia, H. Garny, A. Gettelman, S.C. Hardiman, D. Kinnison, J.F. Lamarque, E. Mancini, M. Marchand, M. Michou, O. Morgenstern, T. Nakamura, S. Pawson, G. Pitari, J. Pyle, E. Rozanov, T.G. Shepherd, K. Shibata, H. Teyssèdre, R.J. Wilson, and Y. Yamashita, Decline and recovery of total column ozone using a multimodel time series analysis, *J. Geophys. Res.*, *115* (D3), D00M10, doi: 10.1029/2010JD013857, 2010a.

Austin, J., H. Struthers, J. Scinocca, D.A. Plummer, H. Akiyoshi, A.J.G. Baumgaertner, S. Bekki, G.E. Bodeker, P. Braesicke, C. Brühl, N. Butchart, M.P. Chipperfield, D. Cugnet, M. Dameris, S. Dhomse, S. Frith, H. Garny, A. Gettelman, S.C. Hardiman, P. Jöckel, D. Kinnison, A. Kubin, J.F. Lamarque, U. Langematz, E. Mancini, M. Marchand, M. Michou, O. Morgenstern, T. Nakamura, J.E. Nielsen, G. Pitari, J. Pyle, E. Rozanov, T.G. Shepherd, K. Shibata, D. Smale, H. Teyssèdre, and Y.Yamashita, Chemistry-climate model simulations of spring Antarctic ozone, *J. Geophys. Res.*, *115*, D00M11, doi: 10.1029/2009JD013577, 2010b.

Austin, J., L.W. Horowitz, M.D. Schwarzkopf, R.J. Wilson, and H. Levy II, Stratospheric ozone and temperature simulated from the preindustrial era to the present day, *J. Clim.*, *26* (11), 3528-3543, doi: 10.1175/JCLI-D-12-00162.1, 2013.

Ayarzagüena, B., U. Langematz, and E. Serrano, Tropospheric forcing of the stratosphere: A comparative study of the two different major stratospheric warmings in 2009 and 2010, *J. Geophys. Res.*, *116* (D18), D18114, doi: 10.1029/2010JD015023, 2011.

Bai, K., C. Liu, R. Shi, Y. Zhang, and W. Gao, Global validation of FY-3A total ozone unit (TOU) total ozone columns using ground-based Brewer and Dobson measurements, *Int. J. Remote Sens., 34* (14), 5228-5242, doi: 10.1080/01431161.2013.788264, 2013.

Baldwin, M.P., L.J. Gray, T.J. Dunkerton, K. Hamilton, P.H. Haynes, W.J. Randel, J.R. Holton, M.J. Alexander, I. Hirota, T. Horinouchi, D.B.A. Jones, J.S. Kinnersley, C. Marquardt, K. Sato, and M. Takahashi, The quasi-biennial oscillation, *Rev. Geophys.*, *39* (2), 179-229, doi: 10.1029/1999RG000073, 2001.

Balis, D., I.S.A. Isaksen, C. Zerefos, I. Zyrichidou, K. Eleftheratos, K. Tourpali, R. Bojkov, B. Rognerud, F. Stordal, O.A. Søvde, and Y. Orsolini, Observed and modelled record ozone decline over the Arctic during winter/spring 2011*, Geophys. Res. Lett.*, *38* (23)*,* L23801, doi: 10.1029/2011GL049259*,* 2011.

Barath, F.T., M.C. Chavez, R.E. Cofield, D.A. Flower, M.A. Frerking, M.B. Gram, W.M. Harris, J.R. Holden, R.F. Jarnot, W.G. Kloezeman, G.J. Klose, G.K. Lau, M.S. Loo, B.J. Maddison, R.J. Mattauch, R.P. McKinney, G.E. Peckham, H.M. Pickett, G. Siebes, F.S. Soltis, R.A. Suttie, J.A. Tarsala, J.W. Waters, and W.J. Wilson, The Upper Atmosphere Research Satellite microwave limb sounder instrument, *J. Geophys. Res.*, *98* (D6), 10751-10762, doi: 10.1029/93JD00798, 1993.

Barret, B., P. Ricaud, M. Santee, J.-L. Attié, J. Urban, E. Le Flochmoën, G. Berthet, D.P. Murtagh, P. Eriksson, A. Jones, J. de la Noë, E. Dupuy, L. Froidevaux, N.J. Livesey, J.W. Waters, and M.J. Filipiak, Intercomparisons of

trace gases profiles from the Odin/SMR and Aura/MLS limb sounders, *J. Geophys. Res.*, *111* (D21), D21302, doi: 10.1029/2006JD007305, 2006.

Baumgaertner, A.J.G., P. Jöckel, M. Dameris, and P.J. Crutzen, Will climate change increase ozone depletion from low-energy-electron precipitation?, *Atmos. Chem. Phys.*, *10* (19), 9647-9656, doi: 10.5194/acp-10-9647-2010, 2010.

Beer, R., TES on the Aura mission: Scientific objectives, measurements, and analysis overview, *IEEE Trans. Geosci. Rem. Sens.*, *44* (5), 1102-1105, doi: 10.1109/TGRS.2005.863716, 2006.

Bernath, P.F., C.T. McElroy, M.C. Abrams, C.D. Boone, M. Butler, C. Camy-Peyret, M. Carleer, C. Clerbaux, P.-F. Coheur, R. Colin, P. DeCola, M. DeMaziere, J.R. Drummond, D. Dufour, W.F.J. Evans, H. Fast, D. Fussen, K. Gilbert, D.E. Jennings, E.J. Llewellyn, R.P. Lowe, E. Mahieu, J.C. McConnell, M. McHugh, S.D. McLeod, R. Michaud, C. Midwinter, R. Nassar, F. Nichitiu, C. Nowlan, C.P. Rinsland, Y.J. Rochon, N. Rowlands, K. Semeniuk, P.Simon, R. Skelton, J.J Sloan, M.-A. Soucy, K. Strong, P. Tremblay, D. Turnbull, K.A. Walker, I. Walkty, D.A. Wardle, V. Wehrle, R. Zander, and J. Zou, Atmospheric Chemistry Experiment (ACE): Mission overview, *Geophys. Res. Lett.*, *32* (15), L15S01, doi: 10.1029/2005GL022386, 2005.

Bertaux, J. L., E. Kyrölä, D. Fussen, A. Hauchecorne, F. Dalaudier, V. Sofieva, J. Tamminen, F. Vanhellemont, O. Fantond'Andon, G. Barrot, A. Mangin, L. Blanot, J.C. Lebrun, K. Pérot, T. Fehr, L. Saavedra, G.W. Leppelmeier, and R. Fraisse, Global ozone monitoring by occultation of stars: An overview of GOMOS measurements on ENVISAT, *Atmos. Chem. Phys.*, *10* (24), 12091-12148, doi: 10.5194/acp-10-12091-2010, 2010.

Bevilacqua, R.M., C.P. Aellig, D.J. Debrestian, M.D. Fromm, K. Hoppel, J.D. Lumpe, E.P. Shettle, J.S. Hornstein, C.E. Randall, D.W. Rusch, and J.E. Rosenfield, POAM II ozone observations in the Antarctic ozone hole in 1994, 1995, and 1996, *J. Geophys. Res.*, *102* (D19), 23643-23657, doi: 10.1029/97JD01623, 1997.

Bhartia, P.K., and C. Wellemeyer, TOMS-V8 total O_3 algorithm, in *OMI Algorithm Theoretical Basis Document, Vol. II*, OMI Ozone Products, ATBD-OMI-02, edited by P. K. Bhartia, pp. 15-31, NASA Goddard Space Flight Center, Greenbelt, MD, (Available: at http://eospso.gsfc.nasa.gov/eos_homepage/for_scientists/atbd/index.php), 2002.

Bhartia, P.K., R.D. McPeters, L.E. Flynn, S. Taylor, N.A. Kramarova, S. Frith, B. Fisher, and M. DeLand, Solar Backscatter UV (SBUV) total ozone and profile algorithm, *Atmos. Meas. Tech.*, *6* (10), 2533-2548, doi: 10.5194/amt-6-2533-2013, 2013.

Biermann, U.M., T. Presper, T. Koop, J. Mößinger, P.J. Crutzen, and Th. Peter, The unsuitability of meteoritic and other nuclei for polar stratospheric cloud freezing, *Geophys. Res. Lett.*, *23* (13), 1693-1696, doi: 10.1029/96GL 01577, 1996.

Blessmann, D., I. Wohltmann, and M. Rex, Influence of transport and mixing in autumn on stratospheric ozone variability over the Arctic in early winter, *Atmos. Chem. Phys*., *12* (17), 7921-7930, doi: 10.5194/acp-12-7921-2012, 2012a.

Blessmann, D., I. Wohltmann, R. Lehmann, and M. Rex, Persistence of ozone anomalies in the Arctic stratospheric vortex in autumn, *Atmos. Chem. Phys.*, *12* (11), 4817-4823, doi: 10.5194/acp-12-4817-2012, 2012b.

Bodeker, G.E., J.C. Scott, K. Kreher, and R.L. McKenzie, Global ozone trends in potential vorticity coordinates using TOMS and GOME intercompared against the Dobson network: 1978–1998, *J. Geophys. Res.*, *106* (D19), 23029-23042, doi: 10.1029/2001JD900220, 2001.

Bohlinger, P., B.-M. Sinnhuber, R. Ruhnke, and O. Kirner, Radiative and dynamical contributions to past and future Arctic stratospheric temperature trends, *Atmos. Chem. Phys.*, *14* (3), 1679-1688, doi: 10.5194/acp-14-1679-2014, 2014.

Boone, C.D., R. Nassar, K.A. Walker, Y. Rochon, S.D. McLeod, C.P. Rinsland, and P.F. Bernath, Retrievals for the atmospheric chemistry experiment Fourier-transform spectrometer, *Appl. Opt.*, *44* (33), 7218-7231, doi: 10.1364/AO.44.007218, 2005.

Bovensmann, H., J.P. Burrows, M. Buchwitz, J. Frerick, S. Noël, V.V. Rozanov, K.V. Chance, and A.H.P. Goede, SCIAMACHY: Mission objectives and measurement modes, *J. Atmos. Sci.*, *56* (2), 127-150, 1999.

Bowman, K.W., S.S. Kulawik, J. Worden, E. Sarkissian, G. Osterman, M. Lou, A. Eldering, H. Worden, M. Gunson, R. Beer, C.D. Rodgers, T. Steck, M. Shephard, S. Clough, M. Lampel, P. Brown, and C. Rinsland, Tropospheric Emission Spectrometer: Retrieval method and error analysis, *IEEE Trans. Geosci. Remote Sens.*, *44* (5), 1297-1306, 2006.

Braesicke, P., J. Keeble, X. Yang, G. Stiller, S. Kellmann, N.L. Abraham, A. Archibald, P. Telford, and J.A. Pyle, Circulation anomalies in the Southern Hemisphere and ozone changes, *Atmos. Chem. Phys.*, *13* (21), 10677-10688, doi: 10.5194/acp-13-10677-2013, 2013.

Brakebusch, M., C.E. Randall, D.E. Kinnison, S. Tilmes, M.L. Santee, and G.L. Manney, Evaluation of Whole Atmosphere Community Climate Model simulations of ozone during Arctic winter 2004-2005, *J. Geophys. Res.*, *118* (6), 2673-2688, doi: 10.1002/jgrd.50226, 2013.

Brohede, S.M., C.S. Haley, C.A. McLinden, C.E. Sioris, D.P. Murtagh, S.V. Petelina, E.J. Llewellyn, A. Bazureau, F. Goutail, C.E. Randall, J.D. Lumpe, G. Taha, L.W. Thomasson, and L.L. Gordley, Validation of Odin/OSIRIS stratospheric NO_2 profiles, *J. Geophys. Res.*, *112* (D7), D07310, doi: 10.1029/2006JD007586, 2007.

Cai, D., M. Dameris, H. Garny, and T. Runde, Implications of all season Arctic sea-ice anomalies on the stratosphere, *Atmos. Chem. Phys.*, *12* (24), 11819-11831, doi: 10.5194/acp-12-11819-2012, 2012.

Carslaw, K.S., B.P. Luo, and T. Peter, An analytic expression for the composition of aqueous HNO_3-H_2SO_4 stratospheric aerosols including gas phase removal of HNO_3, *Geophys. Res. Lett.*, *22* (14), 1877-1880, doi: 10.1029/95GL01668, 1995.

Carslaw, K.S., M. Wirth, A. Tsias, B.P. Luo, A. Dörnbrack, M. Leutbecher, H. Volkert, W. Renger, J.T. Bacmeister, E. Reimer, and Th. Peter, Increased stratospheric ozone depletion due to mountain-induced atmospheric waves, *Nature, 391*, 675-678, doi: 10.1038/35589, 1998.

Carslaw, K.S., T. Peter, J.T. Bacmeister, and S.D. Eckermann, Widespread solid particle formation by mountain waves in the Arctic stratosphere, *J. Geophys. Res.*, *104* (D1), 1827-1836, doi: 10.1029/1998JD100033, 1999.

Castanheira, J.M., and D. Barriopedro, Dynamical connection between tropospheric blockings and stratospheric polar vortex, *Geophys. Res. Lett.*, *37* (13), L13809, doi: 10.1029/2010GL043819, 2010.

Chandran, A., R.R. Garcia, R.L. Collins, and L.C. Chang, Secondary planetary waves in the middle and upper atmosphere following the stratospheric sudden warming event of January 2012, *Geophys. Res. Lett.*, *40* (9), 1861-1867, doi: 10.1002/grl.50373, 2013.

Charlton-Perez, A.J., E. Hawkins, V. Eyring, I. Cionni, G.E. Bodeker, D.E. Kinnison, H. Akiyoshi, S.M. Frith, R. Garcia, A. Gettelman, J.F. Lamarque, T. Nakamura, S. Pawson, Y. Yamashita, S. Bekki, P. Braesicke, M.P. Chipperfield, S. Dhomse, M. Marchand, E. Mancini, O. Morgenstern, G. Pitari, D. Plummer, J.A. Pyle, E. Rozanov, J. Scinocca, K. Shibata, T.G. Shepherd, W. Tian, and D.W. Waugh, The potential to narrow uncertainty in projections of stratospheric ozone over the 21st century, *Atmos. Chem. Phys.*, *10*, 9473-9486, doi: 10.5194/acp-10-9473-2010, 2010.

Chehade, W., M. Weber, and J.P. Burrows, Total ozone trends and variability during 1979–2012 from merged data sets of various satellites, *Atmos. Chem. Phys*., *14*, 7059-7074, doi: 10.5194/acp-14-7059-2014, 2014.

Chipperfield, M.P., and R.L. Jones, Relative influences of atmospheric chemistry and transport on Arctic ozone trends, *Nature*, *400*, 551-554, doi: 10.1038/22999, 1999.

Chipperfield, M., W. Feng, and M. Rex, Arctic ozone loss and climate sensitivity: Updated three-dimensional model study, *Geophys. Res. Lett.*, *32*, L11813, doi: 10.1029/2005GL022674, 2005.

Chipperfield, M.P., Q. Liang, S.E. Strahan, O. Morgenstern, S.S. Dhomse, N.L. Abraham, A.T. Archibald, S. Bekki, P. Braesicke, G. Di Genova, E.L. Fleming, S.C. Hardiman, D. Iachetti, C.H. Jackman, D.E. Kinnison, M. Marchand, G. Pitari, J.A. Pyle, E. Rozanov, A. Stenke, and F. Tummon, Multimodel estimates of atmospheric lifetimes of long-lived ozone-depleting substances: Present and future, *J. Geophys. Res.*, *119* (5), 2555-2573, doi: 10.1002/2013JD021097, 2014.

Cionni, I., V. Eyring, J.F. Lamarque, W.J. Randel, D.S. Stevenson, F. Wu, G.E. Bodeker, T.G. Shepherd, D.T. Shindell, and D.W. Waugh, Ozone database in support of CMIP5 simulations: Results and corresponding radiative forcing, *Atmos. Chem. Phys.*, *11* (21), 11267-11292, doi: 10.5194/acp-11-11267-2011, 2011.

Coheur, P.-F., B. Barret, S. Turquety, D. Hurtmans, J. Hadji-Lazaro, and C. Clerbaux, Retrieval and characterization of ozone vertical profiles from a thermal infrared nadir sounder, *J. Geophys. Res.*, *110* (D24), D24303, doi: 10.1029/2005JD005845, 2005.

Coy, L., E.R. Nash, and P.A. Newman, Meteorology of the polar vortex: Spring 1997, *Geophys. Res. Lett.*, *24* (22), 2693-2696, doi: 10.1029/97GL52832, 1997.

Cunnold, D.M., W.P. Chu, R.A. Barnes, M.P. McCormick, and R.E. Veiga, Validation of SAGE II ozone measurements, *J. Geophys. Res.*, *94* (D6), 8447-8460, doi: 10.1029/JD094iD06p08447, 1989.

Curtius, J., R. Weigel, H.-J. Vössing, H. Wernli, A. Werner, C.-M. Volk, P. Konopka, M. Krebsbach, C. Schiller, A. Roiger, H. Schlager, V. Dreiling, and S. Borrmann, Observations of meteoric material and implications for aerosol nucleation in the winter Arctic lower stratosphere derived from in situ particle measurements, *Atmos. Chem. Phys.*, *5* (11), 3053-3069, doi: 10.5194/acp-5-3053-2005, 2005.

Damadeo, R.P., J.M. Zawodny, L.W. Thomason, and N. Iyer, SAGE version 7.0 algorithm: Application to SAGE II, *Atmos. Meas. Tech.*, *6* (12), 3539-3561, doi: 10.5194/amt-6-3539-2013, 2013.

de Laat, A.T.J., and M. van Weele, The 2010 Antarctic ozone hole: Observed reduction in ozone destruction by minor sudden stratospheric warmings, *Sci. Rep.*, *1*, doi: 10.1038/srep00038, 2011.

Dee, D.P., S.M. Uppala, A.J. Simmons, P. Berrisford, P. Poli, S. Kobayashi, U. Andrae, M.A. Balmaseda, G. Balsamo, P. Bauer, P. Bechtold, A.C.M. Beljaars, L. van de Berg, J. Bidlot, N. Bormann, C. Delsol, R. Dragani, M. Fuentes, A.J. Geer, L. Haimberger, S.B. Healy, H. Hersbach, E.V. Hólm, L. Isaksen, P. Kållberg, M. Köhler, M. Matricardi, A.P. McNally, B.M. Monge-Sanz, J.-J. Morcrette, B.-K. Park, C. Peubey, P. de Rosnay, C. Tavolato, J.-N. Thépaut, and F. Vitart, The ERA-Interim reanalysis: Configuration and performance of the data assimilation system, *Quart. J. Roy. Meteorol. Soc.*, *137* (656), 553-597, doi: 10.1002/qj.828, 2011.

Deushi, M., and K. Shibata, Impacts of increases in greenhouse gases and ozone recovery on lower stratospheric circulation and the age of air: Chemistry-climate model simulations up to 2100, *J. Geophys. Res.*, *116* (D7), D07107, doi: 10.1029/2010JD015024, 2011.

Divakarla, M., C. Barnet, M. Goldberg, E. Maddy, F. Irion, M. Newchurch, X. Liu, W. Wolf, L. Flynn, G. Labow, X. Xiong, J. Wei, and L. Zhou, Evaluation of Atmospheric Infrared Sounder ozone profiles and total ozone retrievals with matched ozonesonde measurements, ECMWF ozone data, and Ozone Monitoring Instrument retrievals, *J. Geophys. Res.*, *113* (D15), D15308, doi: 10.1029/2007JD009317, 2008.

Dong, C., J. Yang, Z. Yang, N. Lu, J. Shi, P. Zhang, Y. Liu, B. Cai, and W. Zhang, An overview of a new Chinese weather satellite FY-3A, *Bull. Amer. Meteorol. Soc.*, *90* (10), 1531-1544, doi: 10.1175/2009BAMS2798.1, 2009.

Douglass A.R., M.R. Schoeberl, R.S. Stolarski, J.W. Waters, J.M. Russell III, A.E. Roche, and S.T. Massie, Interhemispheric differences in springtime production of HCl and $ClONO_2$ in the polar vortices, *J. Geophys. Res.*, *100* (D7), 13967-13978, doi: 10.1029/95JD00698, 1995.

Dörnbrack, A., M.C. Pitts, L.R. Poole, Y.J. Orsolini, K. Nishii, and H. Nakamura, The 2009–2010 Arctic stratospheric winter – general evolution, mountain waves and predictability of an operational weather forecast model, *Atmos. Chem. Phys.*, *12* (8), 3659-3675, doi: 10.5194/acp-12-3659-2012, 2012.

Drdla, K., and R. Müller, Temperature thresholds for chlorine activation and ozone loss in the polar stratosphere, *Ann. Geophys.*, *30* (7), 1055-1073, doi: 10.5194/angeo-30-1055-2012, 2012.

Eckermann, S.D., L. Hoffmann, M. Höpfner, D.L. Wu, and M.J. Alexander, Antarctic NAT PSC belt of June 2003: Observational validation of the mountain wave seeding hypothesis, *Geophys. Res. Lett.*, *36*, L02807, doi: 10.1029/2008GL036629, 2009.

Engel, I., B.P. Luo, M.C. Pitts, L.R. Poole, C.R. Hoyle, J.-U. Grooß, A. Dörnbrack, and T. Peter, Heterogeneous formation of polar stratospheric clouds – Part 2: Nucleation of ice on synoptic scales, *Atmos. Chem. Phys.*, *13* (21), 10769-10785, doi: 10.5194/acp-13-10769-2013, 2013.

Engel, I., B.P. Luo, S.M. Khaykin, F.G. Wienhold, H. Vömel, R. Kivi, C.R. Hoyle, J.-U. Grooβ, M.C. Pitts, and T. Peter, Arctic stratospheric dehydration - Part 2: Microphysical modeling, *Atmos. Chem.Phys.*, *14* (7), 3231-3246, doi: 10.5194/acp-14-3231-2014, 2014.

Eyring, V., I. Cionni, G.E. Bodeker, A.J. Charlton-Perez, D.E. Kinnison, J.F. Scinocca, D.W. Waugh, H. Akiyoshi, S. Bekki, M.P. Chipperfield, M. Dameris, S. Dhomse, S.M. Frith, H. Garny, A. Gettelman, A. Kubin, U. Langematz, E. Mancini, M. Marchand, T. Nakamura, L.D. Oman, S. Pawson, G. Pitari, D.A. Plummer, E. Rozanov, T.G. Shepherd, K. Shibata, W. Tian, P. Braesicke, S.C. Hardiman, J.F. Lamarque, O. Morgenstern, J.A. Pyle, D. Smale, and Y. Yamashita, Multi-model assessment of stratospheric ozone return dates and ozone recovery in CCMVal-2 models, *Atmos. Chem. Phys.*, *10*, 9451-9472, doi: 10.5194/acp-10-9451-2010, 2010.

Eyring, V., J.M. Arblaster, I. Cionni, J. Sedláček, J. Perlwitz, P.J. Young, S. Bekki, D. Bergmann, P. Cameron-Smith, W.J. Collins, G. Faluvegi, K.-D. Gottschaldt, L.W. Horowitz, D.E. Kinnison, J.-F. Lamarque, D.R. Marsh, D. Saint-Martin, D.T. Shindell, K. Sudo, S. Szopa, and S. Watanabe, Long-term ozone changes and associated climate impacts in CMIP5 simulations, *J. Geophys. Res.*, *118* (10), 5029-5060, doi: 10.1002/jgrd.50316, 2013.

Feng W., M.P. Chipperfield, S. Davies, G.W. Mann, K.S. Carslaw, S. Dhomse, L. Harvey, C. Randall, and M.L. Santee, Modelling the effect of denitrification on polar ozone depletion for Arctic winter 2004/2005, *Atmos. Chem. Phys.*, *11* (13), 6559-6573, doi: 10.5194/acp-11-6559-2011, 2011.

Fischer, H., M. Birk, C. Blom, B. Carli, M. Carlotti, T. von Clarmann, L. Delbouille, A. Dudhia, D. Ehhalt, M. Endemann, J.M. Flaud, R. Gessner, A. Kleinert, R. Koopman, J. Langen, M. López-Puertas, P. Mosner, H. Nett, H. Oelhaf, G. Perron, J. Remedios, M. Ridolfi, G. Stiller, and R. Zander, MIPAS: An instrument for atmospheric and climate research, *Atmos. Chem. Phys.*, *8* (8), 2151-2188, doi: 10.5194/acp-8-2151-2008, 2008.

Fletcher, C.G., S.C. Hardiman, P.J. Kushner, and J. Cohen, The dynamical response to snow cover perturbations in a large ensemble of atmospheric GCM integrations, *J. Clim.*, *22* (5), 1208-1222, doi: 10.1175/2008JCLI2505.1, 2009.

Frieler, K., M. Rex, R.J. Salawitch, T. Canty, M. Streibel, R.M. Stimpfle, K. Pfeilsticker, M. Dorf, D.K. Weisenstein, and S. Godin-Beekmann, Toward a better quantitative understanding of polar stratospheric ozone loss, *Geophys. Res. Lett.*, *33*, L10812, doi: 10.1029/2005GL025466, 2006.

Froidevaux, L., Y.B. Jiang, A. Lambert, N.J. Livesey, W.G. Read, J.W. Waters, R.A. Fuller, T.P. Marcy, P.J. Popp, R.S. Gao, D.W. Fahey, K.W. Jucks, R.A. Stachnik, G.C. Toon, L.E. Christensen, C.R. Webster, P.F. Bernath, C.D. Boone, K.A. Walker, H.C. Pumphrey, R.S. Harwood, G.L. Manney, M.J. Schwartz, W.H. Daffer, B.J. Drouin, R.E. Cofield, D.T. Cuddy, R.F. Jarnot, B.W. Knosp, V.S. Perun, W.V. Snyder, P.C. Stek, R.P. Thurstans, and P.A. Wagner, Validation of Aura Microwave Limb Sounder HCl measurements, *J. Geophys. Res*., *113*, D15S25, doi: 10.1029/2007JD009025, 2008.

Fromm, M., J. Alfred, and M. Pitts, A unified, long-term, high-latitude stratospheric aerosol and cloud database using SAM II, SAGE II, and POAM II/III data: Algorithm description, database definition, and climatology, *J. Geophys. Res.*, 108 (D12), 4366, doi: 10.1029/2002JD002772, 2003.

Fusco, A.C., and M.L. Salby, Interannual variations of total ozone and their relationship to variations of planetary wave activity, *J. Clim.*, *12* (6), 1619-1629, 1999.

Garcia, R.R., Atmospheric science: An Arctic ozone hole?, *Nature*, *478* (7370), 462-463, doi: 10.1038/478462a, 2011.

Garcia, R.R., D.E. Kinnison, and D.R. Marsh, "World avoided" simulations with the Whole Atmosphere Community Climate Model, *J. Geophys. Res.*, *117* (D23), D23303, doi: 10.1029/2012JD018430, 2012.

Garfinkel, C.I., and D.L. Hartmann, Different ENSO teleconnections and their effects on the stratospheric polar vortex, *J. Geophys. Res.*, *113* (D18), D18114, doi: 10.1029/2008JD009920, 2008.

Gille, J.C., and J.M. Russell III, The Limb Infrared Monitor of the Stratosphere: Experiment description, performance, and results, *J. Geophys. Res.*, *89* (D4), 5125-5140, doi: 10.1029/JD089iD04p05125, 1984.

Gille, J., J. Barnett, P. Arter, M. Barker, P. Bernath, C. Boone, C. Cavanaugh, J. Chow, M. Coffey, J. Craft, C. Craig, M. Dials, V. Dean, T. Eden, D.P. Edwards, G. Francis, C. Halvorson, L. Harvey, C. Hepplewhite, R. Khosravi, D. Kinnison, C. Krinsky, A. Lambert, H. Lee, L. Lyjak, J. Loh, W. Mankin, S. Massie, J. McInerney, J. Moorhouse, B. Nardi, D. Packman, C. Randall, J. Reburn, W. Rudolf, M. Schwartz, J. Serafin, K. Stone, B. Torpy, K. Walker, A. Waterfall, R. Watkins, J. Whitney, D. Woodard, and G. Young, High Resolution Dynamics Limb Sounder: Experiment overview, recovery and validation of initial temperature data, *J. Geophys. Res.*, *113* (D16), D16S43, doi: 10.1029/2007JD008824, 2008.

Girard, A., and N. Louisnard, Stratospheric water vapor, nitrogen dioxide, nitric acid and ozone measurements deduced from spectroscopic observations, *J. Geophys. Res.*, *89* (D4), 5109-5114, doi: 10.1029/JD089i D04p05109, 1984.

Glaccum, W., R.L. Lucke, R.M. Bevilacqua, E.P. Shettle, J.S. Hornstein, D.T. Chen, J.D. Lumpe, S.S. Krigman, D.J. Debrestian, M.D. Fromm, F. Dalaudier, E. Chassefière, C. Deniel, C.E. Randall, D.W. Rusch, J.J. Olivero, C. Brogniez, J. Lenoble, and R. Kremer, The Polar Ozone and Aerosol Measurement instrument, *J. Geophys. Res.*, *101* (D9), 14479-14487, doi: 10.1029/96JD00576, 1996.

Godin, S., G. Mégie, C. David, D. Haner, C. Flesia, and Y. Emery, Airborne lidar observation of mountain-wave-induced polar stratospheric clouds during EASOE, *Geophy. Res. Lett.*, *21* (13), 1335-1338, doi: 10.1029/93GL 02894, 1994.

Goncharenko, L., J.L. Chau, P. Condor, A. Coster, and L. Benkevitch, Ionospheric effects of sudden stratospheric warming during moderate-to-high solar activity: Case study of January 2013, *Geophys. Res. Lett.*, *40* (19), 4982-4986, doi: 10.1002/grl.50980, 2013.

Grooß, J.-U., G. Günther, R. Müller, P. Konopka, S. Bausch, H. Schlager, C. Voigt, C.M. Volk, and G.C. Toon, Simulation of denitrification and ozone loss for the Arctic winter 2002/2003, *Atmos. Chem. Phys.*, *5* (6), 1437-1448, doi: 10.5194/acp-5-1437-2005, 2005.

Grooß, J.-U., K. Brautzsch, R. Pommrich, S. Solomon, and R. Müller, Stratospheric ozone chemistry in the Antarctic: What determines the lowest ozone values reached and their recovery?, *Atmos. Chem. Phys.*, *11* (23), 12217-12226, doi: 10.5194/acp-11-12217-2011, 2011.

Grooß, J.-U., I. Engel, S. Borrmann, W. Frey, G. Günther, C.R. Hoyle, R. Kivi, B.P. Luo, S. Molleker, T. Peter, M.C. Pitts, H. Schlager, G. Stiller, H. Vömel, K.A. Walker, and R. Müller, Nitric acid trihydrate nucleation and denitrification in the Arctic stratosphere, *Atmos. Chem. Phys.,14,* doi: 10.5194/acp-14-1055-2014, 1055-1073, 2014.

Hanson, D., and K. Mauersberger, Laboratory studies of the nitric acid trihydrate: Implications for the south polar stratosphere, *Geophys. Res. Lett.*, *15* (8), 855-858, doi: 10.1029/GL015i008p00855, 1988.

Harris, N.R.P., M. Rex, F. Goutail, B.M. Knudsen, G.L. Manney, R. Müller, and P. von der Gathen, Comparison of empirically derived ozone loss rates in the Arctic vortex, *J. Geophys. Res.*, *107* (D20), SOL 7-1-SOL 7-11, doi: 10.1029/2001JD000482, 2002.

Hassler, B., G.E. Bodeker, S. Solomon, and P.J. Young, Changes in the polar vortex: Effects on Antarctic total ozone observations at various stations, *Geophys. Res. Lett.*, *38* (1), L01805, doi: 10.1029/2010GL045542, 2011a.

Hassler, B., J.S. Daniel, B.J. Johnson, S. Solomon, and S.J. Oltmans, An assessment of changing ozone loss rates at South Pole: Twenty-five years of ozonesonde measurements, *J. Geophys. Res.*, *116* (D22), D22301, doi: 10.1029/2011JD016353, 2011b.

Hassler, B., I. Petropavlovskikh, J. Staehelin, T. August, P.K. Bhartia, C. Clerbaux, D. Degenstein, M. De Mazière, B.M. Dinelli, A. Dudhia, G. Dufour, S.M. Frith, L. Froidevaux, S. Godin-Beekmann, J. Granville, N.R.P. Harris, K. Hoppel, D. Hubert, Y. Kasai, M.J. Kurylo, E. Kyrölä, J.-C. Lambert, P.F. Levelt, C.T. McElroy, R.D. McPeters, R. Munro, H. Nakajima, A. Parrish, P. Raspollini, E.E. Remsberg, K.H. Rosenlof, A. Rozanov, T. Sano, Y. Sasano, M. Shiotani, H.G.J. Smit, G. Stiller, J. Tamminen, D.W. Tarasick, J. Urban, R.J. van der A, J.P. Veefkind, C. Vigouroux, T. von Clarmann, C. von Savigny, K.A. Walker, M. Weber, J. Wild, and J. Zawodny, SI^2N overview paper: Ozone profile measurements: Techniques, uncertainties and availability, *Atmos. Meas. Tech. Discuss.*, *6* (6), 9857-9938, doi: 10.5194/amtd-6-9857-2013, 2013.

Herman, J.R., R. McPeters, R. Stolarski, D. Larko, and R. Hudson, Global average ozone change from November 1978 to May 1990, *J. Geophys. Res.*, *96* (D9), 17279-17305, doi: 10.1029/91JD01553, 1991.

Hervig, M.E., K.S. Carslaw, T. Peter, T. Deshler, L.L. Gordley, G. Redaelli, U. Biermann, and J.M. Russell III, Polar stratospheric clouds due to vapor enhancement: HALOE observations of the Antarctic vortex in 1993, *J. Geophys. Res.*, *102* (D23), 28185-28193, doi: 10.1029/97JD02464, 1997.

Hitchcock, P., T.G. Shepherd, and C. McLandress, Past and future conditions for polar stratospheric cloud formation simulated by the Canadian middle atmosphere model, *Atmos. Chem. Phys.*, *9* (2), 483-495, doi: 10.5194/acp-9-483-2009, 2009.

Hofmann, D.J., S.J. Oltmans, J.M. Harris, B.J. Johnson, and J.A. Lathrop, Ten years of ozonesonde measurements at the south pole: Implications for recovery of springtime Antarctic ozone. *J. Geophys. Res.*, *102* (D7), 8931-8943, doi: 10.1029/96JD03749, 1997.

Hofmann, D.J., B.J. Johnson, and S.J. Oltmans, Twenty-two years of ozonesonde measurements at the South Pole, *Int. J. Remote Sens.*, *30* (15-16), 3995-4008, doi: 10.1080/01431160902821932, 2009.

Holton, J.R., and H.-C. Tan, The influence of the equatorial quasi-biennial oscillation on the global circulation at 50 mb, *J. Atmos. Sci.*, *37* (10), 2200-2208, doi: 10.1175/1520-0469(1980)037<2200:TIOTEQ>2.0.CO;2, 1980.

Höpfner, M., N. Larsen, R. Spang, B.P. Luo, J. Ma, S.H. Svendsen, S.D. Eckermann, B. Knudsen, P. Massoli, F. Cairo, G. Stiller, T. v. Clarmann, and H. Fischer, MIPAS detects Antarctic stratospheric belt of NAT PSCs caused by mountain waves, *Atmos. Chem. Phys.*, *6* (5), 1221-1230, doi: 10.5194/acp-6-1221-2006, 2006.

Hood, L.L., and B.E. Soukharev, Interannual variations of total ozone at northern midlatitudes correlated with stratospheric EP flux and potential vorticity, *J. Atmos. Sci.*, *62* (10), 3724-3740, doi: 10.1175/JAS3559.1, 2005.

Hoppel, K., G. Nedoluha, M. Fromm, D. Allen, R. Bevilacqua, J. Alfred, B. Johnson, and G. König-Langlo, Reduced ozone loss at the upper edge of the Antarctic Ozone Hole during 2001–2004, *Geophys. Res. Lett.*, *32* (20), L20816, doi: 10.1029/2005GL023968, 2005.

Hossaini, R**.,** M.P. Chipperfield, S. Dhomse, C. Ordóñez, A. Saiz-Lopez, N.L. Abraham, A. Archibalid, P. Braesicke, P. Telford, N. Warwick, X. Yang, and J. Pyle, Modelling future changes to the stratospheric source gas injection of biogenic bromocarbons, *Geophys. Res. Lett*., *39* (20), L20813, doi: 10.1029/2012GL053401, 2012.

Hossaini, R., H. Mantle, M.P. Chipperfield, S.A. Montzka, P. Hamer, F. Ziska, B. Quack, K. Krüger, S. Tegtmeier, E. Atlas, S. Sala, A. Engel, H. Bönisch, T. Keber, D. Oram, G. Mills, C. Ordóñez, A. Saiz-Lopez, N. Warwick, Q. Liang, W. Feng, F. Moore, B.R. Miller, V. Marécal, N.A.D. Richards, M. Dorf, and K. Pfeilsticker, Evaluating global emission inventories of biogenic bromocarbons, *Atmos. Chem. Phys.*, *13* (23), 11819-11838, doi: 10.5194/acp-13-11819-2013, 2013.

Hoyle, C.R., I. Engel, B.P. Luo, M.C. Pitts, L.R. Poole, J.-U. Grooß, and T. Peter, Heterogeneous formation of polar stratospheric clouds – Part 1: Nucleation of nitric acid trihydrate (NAT), *Atmos. Chem. Phys.*, *13* (18), 9577-9595, doi: 10.5194/acp-13-9577-2013, 2013.

Huang, W.-T., A.F. Chen, I.-C. Chen, C.-H. Tsai, and J.J.-M. Lin, Photodissociation dynamics of ClOOCl at 248.4 and 308.4 nm, *Phys. Chem. Chem. Phys.*, *13* (18), 8195-8203, doi: 10.1039/c0cp02453h, 2011.

Hurwitz, M.M., and P.A. Newman, 21st century trends in Antarctic temperature and polar stratospheric cloud (PSC) area in the GEOS chemistry-climate model, *J. Geophys. Res.*, *115* (D19), D19109, doi: 10.1029/2009JD013397, 2010.

Hurwitz, M.M., P.A. Newman, and C.I. Garfinkel, The Arctic vortex in March 2011: A dynamical perspective, *Atmos. Chem. Phys.*, *11* (22), 11447-11453, doi: 10.5194/acp-11-11447-2011, 2011.

Hurwitz, M.M., P.A. Newman, and C.I. Garfinkel, On the influence of North Pacific sea surface temperature on the Arctic winter climate, *J. Geophys. Res.*, *117* (D19), D19110, doi: 10.1029/2012JD017819, 2012.

IPCC (Intergovernmental Panel on Climate Change), *Climate Change 2013: The Physical Science Basis: Contribution of Working Group I to the Fifth Assessment Report of the Intergovernmental Panel on Climate Change*, edited by T.F. Stocker, D. Qin, G.-K. Plattner, M. Tignor, S.K. Allen, J. Boschung, A. Nauels, Y. Xia, V. Bex, and P.M. Midgley, 1535 pp., Cambridge University Press, Cambridge, UK, and New York, NY, USA, 2013.

Irie, H., T. Sugita, H. Nakajima, T. Yokota, H. Oelhaf, G. Wetzel, G.C. Toon, B. Sen, M.L. Santee, Y. Terao, N. Saitoh, M.K. Ejiri, T. Tanaka, Y. Kondo, H. Kanzawa, H. Kobayashi, and Y. Sasano, Validation of stratospheric nitric acid profiles observed by Improved Limb Atmospheric Sectrometer (ILAS)-II, *J. Geophys. Res.*, *111* (D11), D11S03, doi: 10.1029/2005JD006115, 2006.

Isaksen, I.S.A., C. Zerefos, W.-C. Wang, D. Balis, K. Eleftheratos, B. Rognerud, F. Stordal, T.K. Berntsen, J.H. LaCasce, O.A. Søvde, D. Olivié, Y.J. Orsolini, I. Zyrichidou, M. Prather, and O.N.E. Tuinder, Attribution of the Arctic ozone column deficit in March 2011, *Geophys.Res. Lett.*, *39* (24), L24810, doi: 10.1029/2012GL053876, 2012.

Jaiser, R., K. Dethloff, D. Handorf, A. Rinke, and J. Cohen, Impact of sea ice cover changes on the Northern Hemisphere atmospheric winter circulation, *Tellus A.*, *64*, 11595, doi: 10.3402/tellusa.v64i0.11595, 2012.

Jones, A., K.A. Walker, J.J. Jin, J.R. Taylor, C.D. Boone, P.F. Bernath, S. Brohede, G.L. Manney, S. McLeod, R. Hughes, and W. H. Daffer, Technical Note: A trace gas climatology derived from the Atmospheric Chemistry Experiment Fourier Transform Spectrometer (ACE-FTS) data set, *Atmos. Chem. Phys.*, *12* (11), 5207-5220, doi: 10.5194/acp-12-5207-2012, 2012.

Jucks, K.W., D.G. Johnson, K.V. Chance, W.A. Traub, J.M. Margitan, R. Stachnik, Y. Sasano, T. Yokota, H. Kanzawa, K. Shibasaki, M. Suzuki, and T. Ogawa, Validation of ILAS v5.2 data with FIRS-2 balloon observations, *J. Geophys. Res.*, *107* (D24) doi: 10.1029/2001JD000578, 2002.

Kalnay, E., M. Kanamitsu, R. Kistler, W. Collins, D. Deaven, L. Gandin, M. Iredell, S. Saha, G. White, J. Woollen, Y. Zhu, M. Chelliah, W. Ebisuzaki, W. Higgins, J. Janowiak, K.C. Mo, C. Ropelewski, J. Wang, A. Leetmaa, R. Reynolds, R. Jenne, and D. Joseph, The NCEP/NCAR 40-year reanalysis project, *Bull. Amer. Meteorol. Soc.*, *77* (3), 437-471, doi: 10.1175/1520-0477(1996)077<0437:TNYRP>2.0.CO;2, 1996.

Kanzawa, H., and S. Kawaguchi, Large stratospheric sudden warming in the Antarctic late winter and shallow ozone hole in 1988, *Geophys. Res. Lett.*, *17* (1), 77-80, doi: 10.1029/GL017i001p00077, 1990.

Kawa, S.R., P.A. Newman, L.R. Lait, M.R. Schoeberl, R.M. Stimpfle, D.W. Kohn, C.R. Webster, R.D. May, D. Baumgardner, J.E. Dye, J.C. Wilson, K.R. Chan, and M. Loewenstein, Activation of chlorine in sulfate aerosol as inferred from aircraft observations, *J. Geophys. Res.*, *102*, 3921-3933, 1997.

Kent, G.S., and M.P. McCormick, SAGE and SAM II measurements of global stratospheric aerosol optical depth and mass loading, *J. Geophys. Res.*, *89* (D4), 5303-5314, doi: 10.1029/JD089iD04p05303, 1984.

Khosrawi, F., J. Urban, M.C. Pitts, P. Voelger, P. Achtert, M. Kaphlanov, M.L. Santee, G.L. Manney, D. Murtagh, and K.-H. Fricke, Denitrification and polar stratospheric cloud formation during the Arctic winter 2009/2010, *Atmos. Chem. Phys.*, *11* (16), 8471-8487, doi: 10.5194/acp-11-8471-2011, 2011.

Kiesewetter, G., B.-M. Sinnhuber, M. Weber, and J.P. Burrows, Attribution of stratospheric ozone trends to chemistry and transport: A modelling study, *Atmos. Chem. Phys.*, *10* (24), 12073-12089, doi: 10.5194/acp-10-12073-2010, 2010.

Kinnison, D.E., J. Gille, J. Barnett, C. Randall, V.L. Harvey, A. Lambert, R. Khosravi, M.J. Alexander, P.F. Bernath, C.D. Boone, C. Cavanaugh, M. Coffey, C. Craig, V.C. Dean, T. Eden, D. Ellis, D.W. Fahey, G. Francis, C. Halvorson, J. Hannigan, C. Hartsough, C. Hepplewhite, C. Krinsky, H. Lee, B. Mankin, T.P. Marcy, S. Massie, B. Nardi, D. Packman, P.J. Popp, M.L. Santee, V. Yudin, and K.A. Walker, Global observations of HNO3 from the High Resolution Dynamics Limb Sounder (HIRDLS): First results, *J. Geophys. Res.*, *113* (D16), D16S44, doi: 10.1029/2007JD008814, 2008.

Kleinböhl, A., M. Khosravi, J. Urban, T. Canty, R.J. Salawitch, G.C. Toon, H. Küllmann, and J. Notholt, Constraints for the photolysis rate and the equilibrium constant of ClO-dimer from airborne and balloon-borne measurements of chlorine compounds, *J. Geophys. Res.*, *119* (11), 6916-6937, doi: 10.1002/2013JD021433, 2014.

Klekociuk, A.R., M.B. Tully, S.P. Alexander, R.J. Dargaville, L.L. Deschamps, P.J. Fraser, H.P. Gies, S.I. Henderson, J. Javorniczky, P.B. Krummel, S.V. Petelina, J.D. Shanklin, J.M. Siddaway, and K.A. Stone, The Antarctic ozone during 2010, *Aust. Meteorol. Oceanographic J.*, *61*, 253-267, 2011.

Kohma, M., and K. Satao, The effects of atmospheric waves on the amounts of polar stratospheric clouds, *Atmos. Chem. Phys.*, *11* (22), 11535-11552, doi: 10.5194/acp-11-11535-2011, 2011.

Kohma, M., and K. Sato, Simultaneous occurrence of polar stratospheric clouds and upper-tropospheric clouds caused by blocking anticyclones in the Southern Hemisphere, *Atmos. Chem. Phys.*, *13* (7), 3849-3864, doi: 10.5194/acp-13-3849-2013, 2013.

Koop, T., B. Luo, A. Tsias, and T. Peter, Water activity as the determinant for homogeneous ice nucleation in aqueous solutions, *Nature*, *406*, 611-614, doi: 10.1038/35020537, 2000.

Kramarova, N.A., E.R. Nash, P.A. Newman, P.K. Bhartia, R.D. McPeters, D.F. Rault, C.J. Seftor, P.Q. Xu, and G.J. Labow, Measuring the Antarctic ozone hole with the new Ozone Mapping and Profiler Suite (OMPS), *Atmos. Chem. Phys.*, *14* (5), 2353-2361, doi: 10.5194/acp-14-2353-2014, 2014.

Kremser, S., R. Schofield, G.E. Bodeker, B.J. Connor, M. Rex, J. Barret, T. Mooney, R.J. Salawitch, T. Canty, K. Frieler, M.P. Chipperfield, U. Langematz, and W. Feng, Retrievals of chlorine chemistry kinetic parameters from Antarctic ClO microwave radiometer measurements, *Atmos. Chem. Phys.*, *11* (11), 5183-5193, doi: 10.5194/acp-11-5183-2011, 2011.

Kreycy, S., C. Camy-Peyret, M.P. Chipperfield, M. Dorf, W. Feng, R. Hossaini, L. Kritten, B. Werner, and K. Pfeilsticker, Atmospheric test of the $J(BrONO_2)/k_{BrO+NO_2}$ ratio: Implications for total stratospheric Br_y and bromine-mediated ozone loss, *Atmos. Chem. Phys.*, *13* (13), 6263-6274, doi: 10.5194/acp-13-6263-2013, 2013.

Kroon, M., J.F. de Haan, J.P. Veefkind, L. Froidevaux, R. Wang, R. Kivi, and J.J. Hakkarainen, Validation of operational ozone profiles from the Ozone Monitoring Instrument, *J. Geophys. Res.*, *116* (D18), D18305, doi: 10.1029/2010JD015100, 2011.

Kumer, J.B., J.L. Mergenthaler, A.E. Roche, R.W. Nightingale, G.A. Ely, W.G. Uplinger, J.C. Gille, S.T. Massie, P.L. Bailey, M.R. Gunson, M.C. Abrams, G.C. Toon, B. Sen, J.-F. Blavier, R.A. Stachnik, C.R. Webster, R.D. May, D.G. Murcray, F.J. Murcray, A. Goldman, W.A. Traub, K.W. Jucks, and D.G. Johnson, Comparison of correlative data with HNO_3 version 7 from the CLAES instrument deployed on the NASA Upper Atmosphere Research Satellite, *J. Geophys. Res.*, *101* (D6), 9621-9656, doi: 10.1029/95JD03759, 1996.

Kuttippurath, J., and G. Nikulin, A comparative study of the major sudden stratospheric warmings in the Arctic winters 2003/2004–2009/2010, *Atmos. Chem. Phys.*, *12* (17), 8115-8129, doi: 10.5194/acp-12-8115-2012, 2012.

Kuttippurath, J., F. Goutail, J.-P. Pommereau, F. Lefèvre, H.K. Roscoe, A. Pazmiño, W. Feng, M.P. Chipperfield, and S. Godin-Beekmann, Estimation of Antarctic ozone loss from ground-based total column measurements, *Atmos. Chem. Phys.*, *10* (14), 6569-6581, doi: 10.5194/acp-10-6569-2010, 2010a.

Kuttippurath, J., S. Godin-Beekmann, F. Lefèvre, and F. Goutail, Spatial, temporal, and vertical variability of polar stratospheric ozone loss in the Arctic winters 2004/2005–2009/2010, *Atmos. Chem. Phys.*, *10* (20), 9915-9930, doi: 10.5194/acp-10-9915-2010, 2010b.

Kuttippurath, J., S. Godin-Beekmann, F. Lefèvre, G. Nikulin, M.L. Santee, and L. Froidevaux, Record-breaking ozone loss in the Arctic winter 2010/2011: Comparison with 1996/1997, *Atmos. Chem. Phys.*, *12* (15), 7073-7085, doi: 10.5194/acp-12-7073-2012, 2012.

Kuttippurath, J., F. Lefèvre, J.-P. Pommereau, H.K. Roscoe, F. Goutail, A. Pazmiño, and J.D. Shanklin, Antarctic ozone loss in 1979–2010: First sign of ozone recovery, *Atmos. Chem. Phys.*, *13* (3), 1625-1635, doi: 10.5194/acp-13-1625-2013, 2013.

Kyrölä, E., J. Tamminen, G.W. Leppelmeier, V. Sofieva, S. Hassinen, J.L. Bertaux, A. Hauchecorne, F. Dalaudier, C. Cot, O. Korablev, O. Fanton d'Andon, G. Barrot, A. Mangin, B. Théodore, M. Guirlet, F. Etanchaud, P. Snoeij, R. Koopman, L. Saavedra, R. Fraisse, D. Fussen, and F. Vanhellemont, GOMOS on Envisat: An overview, *Adv. Space Res.*, *33* (7), 1020-1028, doi: 10.1016/S0273-1177(03)00590-8, 2004.

Labitzke, K., and B. Naujokat, The lower arctic stratosphere in winter since 1952, SPARC Newsletter No.15, 11-14, 2000.

Lambert, A., M.L. Santee, D.L. Wu, and J.H. Chae, A-train CALIOP and MLS observations of early winter Antarctic polar stratospheric clouds and nitric acid in 2008, *Atmos. Chem. Phys.*, *12* (6), 2899-2931, doi: 10.5194/acp-12-2899-2012, 2012.

Langematz, U., and M. Kunze, An update on dynamical changes in the Arctic and Antarctic stratospheric polar vortices, *Clim. Dyn.*, *27*, 647-660, doi: 10.1007/s00382-006-0156-2, 2006.

Langematz, U., S. Meul, K. Grunow, E. Romanowsky, S. Oberländer, J. Abalichin, and A. Kubin, Future Arctic temperature and ozone: The role of stratospheric composition changes, *J. Geophys. Res.*, *119* (5), 2092-2112, doi: 10.1002/2013JD021100, 2014.

Lindenmaier, R., K. Strong, R.L. Batchelor, M.P. Chipperfield, W.H. Daffer, J.R. Drummond, T.J. Duck, H. Fast, W. Feng, P.F. Fogal, F. Kolonjari, G.L. Manney, A. Manson, C. Meek, R.L. Mittermeier, G.J. Nott, C. Perro, and K.A. Walker, Unusually low ozone, HCl, and HNO_3 column measurements at Eureka, Canada during winter/spring 2011, *Atmos. Chem. Phys.*, *12* (8), 3821-3835, doi: 10.5194/acp-12-3821-2012, 2012.

Liu, X., P.K. Bhartia, K. Chance, R.J.D. Spurr, and T.P. Kurosu, Ozone profile retrievals from the Ozone Monitoring Instrument, *Atmos. Chem. Phys.*, *10* (5), 2521-2537, doi: 10.5194/acp-10-2521-2010, 2010.

Livesey, N.J., W.G. Read, L. Froidevaux, J.W. Waters, H.C. Pumphrey, D.L. Wu, Z. Shippony, and R.F. Jarnot, The UARS Microwave Limb Sounder version 5 dataset: Theory, characterization, and validation, *J. Geophys. Res.*, *108* (D13), 4378, doi: 10.1029/2002JD002273, 2003.

Livesey, N.J., W. Van Snyder, W.G. Read, and P.A. Wagner, Retrieval algorithms for the EOS Microwave Limb Sounder (MLS) instrument, *IEEE Trans. Geosci. Remote Sens.*, *44* (5), 1144-1155, doi: 10.1109/TGRS.2006.872327, 2006.

Llewellyn, E.J., N.D. Lloyd, D.A. Degenstein, R.L. Gattinger, S.V. Petelina, A.E. Bourassa, J.T. Wiensz, E.V. Ivanov, I.C. McDade, B.H. Solheim, J.C. McConnell, C.S. Haley, C. von Savigny, C.E. Sioris, C.A. McLinden, E. Griffioen, J. Kaminski, W.F.J. Evans, E. Puckrin, K. Strong, V. Wehrle, R.H. Hum, D.J.W. Kendall, J. Matsushita, D.P. Murtagh, S. Brohede, J. Stegman, G. Witt, G. Barnes, W.F. Payne, L. Piché, K. Smith, G. Warshaw, D.-L. Deslauniers, P. Marchand, E.H. Richardson, R.A. King, I. Wevers, W. McCreath, E. Kyrölä, L. Oikarinen, G.W. Leppelmeier, H. Auvinen, G. Mégie, A. Hauchecorne, F. Lefèvre, J. de La Nöe, P. Ricaud, U. Frisk, F. Sjoberg, F. von Schéele, and L. Nordh, The OSIRIS instrument on the Odin Spacecraft, *Can. J. Phys.*, *82*, 411-422, doi: 10.1139/P04-005, 2004.

Lucke, R.L., D.R. Korwan, R.M. Bevilacqua, J.S. Hornstein, E.P. Shettle, D.T. Chen, M. Daehler, J.D. Lumpe, M.D. Fromm, D. Debrestian, B. Neff, M. Squire, G. König-Langlo, and J. Davies, The Polar Ozone and Aerosol Measurement (POAM) III instrument and early validation results, *J. Geophys. Res.*, *104* (D15), 18785-18799, doi: 10.1029/1999JD900235, 1999.

Lumpe, J.D., R.M. Bevilacqua, K.W. Hoppel, S.S. Krigman, D.L. Kriebel, C.E. Randall, D.W. Rusch, C. Brogniez, R. Ramananahérosa, E.P. Shettle, J.J. Olivero, J. Lenoble, and P. Pruvost, POAM II retrieval algorithm and error analysis, *J. Geophys. Res.*, *102* (D19), 23593-23614, doi: 10.1029/97JD00906, 1997.

Lumpe, J.D., R.M. Bevilacqua, K.W. Hoppel, and C.E. Randall, POAM III retrieval algorithm and error analysis, *J. Geophys. Res.*, *107* (D21), 4575, doi: 10.1029/2002JD002137, 2002.

Manney, G.L., L. Froidevaux, M.L. Santee, R.W. Zurek, and J.W. Waters, MLS observations of Arctic ozone loss in 1996-97, *Geophys. Res. Lett.*, *24* (22), 2967-2700, doi: 10.1029/97GL52827, 1997.

Manney, G.L., K. Krüger, J.L. Sabutis, S.A. Sena, and S. Pawson, The remarkable 2003–2004 winter and other recent warm winters in the Arctic stratosphere since the late 1990s, *J. Geophys. Res.*, *110* (D4), D04107, doi: 10.1029/2004JD005367, 2005.

Manney, G.L., M.J. Schwartz, K. Krüger, M.L. Santee, S. Pawson, J.N. Lee, W.H. Daffer, R.A. Fuller, and N.J. Livesey, Aura Microwave Limb Sounder observations of dynamics and transport during the record-breaking 2009 Arctic stratospheric major warming, *Geophys. Res. Lett.*, *36* (12), L12815, doi: 10.1029/2009GL038586, 2009.

Manney, G.L., M.L. Santee, M. Rex, N.J. Livesey, M.C. Pitts, P. Veefkind, E.R. Nash, I. Wohltmann, R. Lehmann, L. Froidevaux, L.R. Poole, M.R. Schoeberl, D.P. Haffner, J. Davies, V. Dorokhov, H. Gernandt, B. Johnson, R. Kivi, E. Kyrö, N. Larsen, P.F. Levelt, A. Makshtas, C.T. McElroy, H. Nakajima, M.C. Parrondo, D.W. Tarasick, P. von der Gathen, K.A.Walker, and N.S. Zinoviev, Unprecedented Arctic ozone loss in 2011, *Nature*, *478* (7370), 469-475, doi: 10.1038/nature10556, 2011.

Marcolli, C., S. Gedamke, T. Peter, and B. Zobrist, Efficiency of immersion mode ice nucleation on surrogates of mineral dust, *Atmos. Chem. Phys.*, *7* (19), 5081-5091, doi: 10.5194/acp-7-5081-2007, 2007.

Massie, S.T., J.C. Gille, D.P. Edwards, P.L. Bailey, L.V. Lyjak, C.A. Craig, C.P. Cavanaugh, J.L. Mergenthaler, A.E. Roche, J.B. Kumer, A. Lambert, R.G. Grainger, C.D. Rodgers, F.W. Taylor, J.M. Russell III, J.H. Park, T. Deshler, M.E. Hervig, E.F. Fishbein, J.W. Waters, and W.A. Lahoz, Validation studies using multiwavelength Cryogenic Limb Array Etalon Spectrometer (CLAES) observations of stratospheric aerosol, *J. Geophys. Res.*, *101*, 9757-9773, doi: 10.1029/95JD03225, 1996.

McCormick, M.P., and C.R. Trepte, SAM II Measurements of Antarctic PSC's and Aerosols, *Geophys. Res. Lett.*, *13* (12), 1276-1279, doi: 10.1029/GL013i012p01276, 1986.

McCormick, M.P., W.P Chu, G.W. Grams, P. Hamill, B.M. Herman, L.R. McMaster, T.J. Pepin, P.B. Russell, H.M. Steele, and T.J. Swissler, High-latitude stratospheric aerosols measured by the SAM-II satellite system in 1978 and 1979, *Science*, *214* (4518), 328-331, doi: 10.1126/science.214.4518.328, 1981.

McCormick, M.P., T.J. Swissler, E. Hilsenrath, A.J. Krueger, and M.T. Osborn, Satellite and correlative measurements of stratospheric ozone: Comparison of measurements made by SAGE, ECC balloons, chemiluminescent, and optical rocketsondes, *J. Geophys. Res.*, *89* (D4), 5315-5320, doi: 10.1029/JD089iD04p05315, 1984.

McCormick, M.P., J.M. Zawodny, R.E. Veiga, J.C. Larsen, and P.H. Wang, An overview of SAGE I and SAGE II ozone measurements, *Planet. Space Sci.*, *37* (12), 1567-1586, doi: 10.1016/0032-0633(89)90146-3, 1989.

McElroy, C.T., C.R. Nowlan, J.R. Drummond, P.F. Bernath, D.V. Barton, D.G. Dufour, C. Midwinter, R.B. Hall, A. Ogyu, A. Ullberg, D.I. Wardle, J. Kar, J. Zou, F. Nichitiu, C.D. Boone, K.A. Walker, and N. Rowlands, The ACE-MAESTRO instrument on SCISAT: Description, performance, and preliminary results, *Appl. Opt.*, *46* (20), 4341-4356, doi: 10.1364/AO.46.004341, 2007.

McLinden, C.A., and V. Fioletov, Quantifying stratospheric ozone trends: Complications due to stratospheric cooling, *Geophys. Res. Lett.*, *38* (3), L03808, doi: 10.1029/2010GL046012, 2011.

McLinden, C.A., V.E. Fioletov, C.S. Haley, N. Lloyd, C. Roth, D. Degenstein, A. Bourassa, C.T. McElroy, and E.J. Lewellyn, An evaluation of Odin/OSIRIS limb pointing and stratospheric ozone through comparisons with ozonesondes, *Can. J. Phys.*, *85* (11), 1125-1141, doi: 10.1139/p07-112, 2007.

McPeters, R.D., P.K. Bhartia, D. Haffner, G.J. Labow, and L. Flynn, The version 8.6 SBUV ozone data record: An overview, *J. Geophys. Res.*, *118* (14), 8032-8039, doi: 10.1002/jgrd.50597, 2013.

Miyagawa, K., I. Petropavlovskikh, R.D. Evans, C. Long, J. Wild, G.L. Manney, and W.H. Daffer, Long-term changes in the upper stratospheric ozone at Syowa, Antarctica, *Atmos. Chem. Phys.*, *14* (8), 3945-3968, doi: 10.5194/acp-14-3945-2014, 2014.

Moore, T.A., M. Okumura, J.W. Seale, and T.K. Minton, UV photolysis of ClOOCl, *J. Phys. Chem. A*, *103* (12), 1691-1695, 1999.

Müller, R., J.-U. Grooß, C. Lemmen, D. Heinze, M. Dameris, and G. Bodeker, Simple measures of ozone depletion in the polar stratosphere, *Atmos. Chem. Phys.*, *8* (2), 251-264, doi: 10.5194/acp-8-251-2008, 2008.

Murphy, D.M., and B.L. Gary, Mesoscale temperature fluctuations and polar stratospheric clouds, *J. Atmos. Sci.*, *52*, 1753-1760, doi: 10.1175/1520-0469(1995)0522.0.CO;2, 1995.

Nakajima, H., M. Suzuki, A. Matsuzaki, T. Ishigaki, K. Waragai, Y. Mogi, N. Kimura, N. Araki, T. Yokota, H. Kanzawa, T. Sugita, and Y. Sasano, Characteristics and performance of the Improved Limb Atmospheric Spectrometer (ILAS) in orbit, *J. Geophys. Res.*, *107* (D24), 8213, doi: 10.1029/2001JD001439, 2002.

Naoe, H., and K. Shibata, Equatorial quasi-biennial oscillation influence on the northern winter extratropical circulation, *J. Geophys. Res.*, *115* (D19), D19102, doi: 10.1029/2009JD012952, 2010.

Nardi, B., J.C. Gille, J.J. Barnett, C.E. Randall, V.L. Harvey, A. Waterfall, W.J. Reburn, T. Leblanc, T.J. McGee, L.W. Twigg, A.M. Thompson, S. Godin-Beekmann, P.F. Bernath, B.R. Bojkov, C.D. Boone, C. Cavanaugh, M.T. Coffey, J. Craft, C. Craig, V. Dean, T.D. Eden, G. Francis, L. Froidevaux, C. Halvorson, J.W. Hannigan, C.L. Hepplewhite, D.E. Kinnison, R. Khosravi, C. Krinsky, A. Lambert, H. Lee, J. Loh, S.T. Massie, I.S. McDermid, D. Packman, B. Torpy, J. Valverde-Canossa, K.A. Walker, D. Whiteman, J.C. Witte, and G. Young, Initial validation of ozone measurements from the High Resolution Dynamics Limb Sounder, *J. Geophys. Res.*, *113* (D16), D16S36, doi: 10.1029/2007JD008837, 2008.

Nash, E.R., P.A. Newman, J.E. Rosenfield, and M.R. Schoeberl, An objective determination of the polar vortex using Ertel's potential vorticity, *J. Geophys. Res.*, *101* (D5), 9471-9478, doi: 10.1029/96JD00066, 1996.

Nassar, R., J.A. Logan, H.M. Worden, I.A. Megretskaia, K.W. Bowman, G.B. Osterman, A.M. Thompson, D.W. Tarasick, S. Austin, H. Claude, M.K. Dubey, W.K. Hocking, B.J. Johnson, E. Joseph, J. Merrill, G.A. Morris, M. Newchurch, S.J. Oltmans, F. Posny, F.J. Schmidlin, H. Vömel, D.N. Whiteman, and J.C. Witte, Validation of Tropospheric Emission Spectrometer (TES) nadir ozone profiles using ozonesonde measurements. *J. Geophys. Res.*, *113* (D15), D15S17, doi: 10.1029/2007JD008819, 2008.

Newman, P.A., R. Stolarski, M. Schoeberl, R. McPeters, and A. Krueger, The 1990 Antarctic Ozone Hole as observed by TOMS, *Geophys. Res. Lett.*, *18* (4), 661-664, doi: 10.1029/91GL00546, 1991.

Newman, P.A., J.F. Gleason, R.D. McPeters, and R.S. Stolarski, Anomalously low ozone over the Arctic, *Geophys. Res. Lett.*, *24* (22), 2689-2692, doi: 10.1029/97GL52831, 1997.

Newman, P.A., E.R. Nash, and J.E. Rosenfield, What controls the temperature of the Arctic stratosphere during the spring?, *J. Geophys. Res.*, *106* (D17), 19999-20010, doi: 10.1029/2000JD000061, 2001.

Newman, P.A., E.R. Nash, S.R. Kawa, S.A. Montzka, and S.M. Schauffler, When will the Antarctic ozone hole recover?, *Geophys. Res. Lett.*, *33*, L12814, doi: 10.1029/2005GL025232, 2006.

Newman, P.A., J.S. Daniel, D.W. Waugh, and E.R. Nash, A new formulation of equivalent effective stratospheric chlorine (EESC), *Atmos. Chem. Phys.*, *7* (17), 4537-4522, doi: 10.5194/acp-7-4537-2007, 2007.

Newman, P.A., E.R. Nash, C.S. Long, M.C. Pitts, B. Johnson, M.L. Santee, and J. Burrows, [Antarctic] Ozone depletion, in *State of the Climate in 2010*, edited by J. Blunden, D.S. Arndt, and M.O. Baringer, Special Supplement to the *Bull. Amer. Meteorol. Soc*., *92* (6), S170-S171, 2011.

Newman, P.A., E.R. Nash, C.S. Long, M.C. Pitts, B. Johnson, M.L. Santee, J. Burrows, and G.O. Braathen, [Antarctic] Ozone depletion, in *State of the Climate in 2011*, Special Supplement to the *Bull. Amer. Meteorol. Soc*., *93* (7), S159-S161, 2012.

Newman, P.A., N. Kramarova, E.R. Nash, C.S. Long, M.C. Pitts, B. Johnson, M.L. Santee, J. Burrows, and G.O. Braathen, [Antarctic] Ozone depletion, in *State of the Climate in 2012*, Special Supplement to the *Bull. Amer. Meteorol. Soc*., *94* (8), S142-146, 2013.

Nishii, K., H. Nakamura, and Y.J. Orsolini, Cooling of the wintertime Arctic stratosphere induced by the Western Pacific teleconnection pattern, *Geophys. Res. Lett.*, *37* (13), L13805, doi: 10.1029/2010GL043551, 2010.

Nishii, K., H. Nakamura, and Y.J. Orsolini, Geographical dependence observed in blocking high influence on the stratospheric variability through enhancement and suppression of upward planetary-wave propagation, *J. Clim.*, *24* (24), 6408-6423, doi: 10.1175/JCLI-D-10-05021.1, 2011.

Noel, V., and M. Pitts, Gravity wave events from mesoscale simulations, compared to polar stratospheric clouds observed from spaceborne lidar over the Antarctic Peninsula, *J. Geophys. Res.*, *117* (D11), D11207, doi: 10.1029/2011JD017318, 2012.

Nowlan, C.R., C.T. McElroy, and J.R. Drummond, Measurements of the O_2A- and B-bands for determining temperature and pressure profiles from ACE-MAESTRO: Forward model and retrieval algorithm, *J. Quant. Spectrosc. Radiat. Transfer*, *108* (3), 371-388, doi: 10.1016/j.jqsrt.2007.06.006, 2007.

Ohyama, H., S. Kawakami, K. Shiomi, and K. Miyagawa, Retrievals of total and tropospheric ozone from GOSAT thermal infrared spectral radiances, *IEEE Trans. Geosci. Remote Sens.*, *50* (5), 1770-1784, doi: 10.1109/TGRS.2011.2170178, 2012.

Oman, L.D., and A.R. Douglass, Improvements in total column ozone in GEOSCCM and comparisons with a new ozone-depleting substances scenario, *J. Geophys. Res.*, *119* (9), 5613-5624, doi: 10.1002/2014JD021590, 2014.

Oman, L.D., D.A. Plummer, D.W. Waugh, J. Austin, J.F. Scinocca, A.R. Douglass, R.J. Salawitch, T. Canty, H. Akiyoshi, S. Bekki, P. Braesicke, N. Butchart, M.P. Chipperfield, D. Cugnet, S. Dhomse, V. Eyring, S. Frith, S.C. Hardiman, D.E. Kinnison, J.-F. Lamarque, E. Mancini, M. Marchand, M. Michou, O. Morgenstern, T. Nakamura, J.E. Nielsen, D. Olivié, G. Pitari, J. Pyle, E. Rozanov, T.G. Shepherd, K. Shibata, R.S. Stolarski, H. Teyssèdre, W. Tian, Y. Yamashita, and J.R. Ziemke, Multimodel assessment of the factors driving stratospheric ozone evolution over the 21st century, *J. Geophys. Res.*, *115* (D24), D24306, doi: 10.1029/2010JD014362, 2010.

Orsolini, Y.J., and N.G. Kvamstø, Role of Eurasian snow cover in wintertime circulation: Decadal simulations forced with satellite observations, *J. Geophys. Res.*, *114* (D19), D19108, doi: 10.1029/2009JD012253, 2009.

Orsolini, Y.J., A.Y. Karpechko, and G. Nikulin, Variability of the Northern Hemisphere polar stratospheric cloud potential: The role of North Pacific disturbances, *Quart. J. Roy. Meteorol. Soc.*, *135* (641), 1020-1029, doi: 10.1002/qj.409, 2009.

Orsolini, Y.J., R. Senan, R.E. Benestad, A. Melsom, Autumn atmospheric response to the 2007 low Arctic sea ice extent in coupled ocean-atmosphere hindcasts, *Clim. Dyn.*, *38* (11-12), 2437-2448, doi: 10.1007/s00382-011-1169-z, 2012.

Pagan, K.L., A. Tabazadeh, K. Drdla, M.E. Hervig, S.D. Eckermann, E.V. Browell, M.J. Legg, and P.G. Foschi, Observational evidence against mountain-wave generation of ice nuclei as a prerequisite for the formation of three solid nitric acid polar stratospheric clouds observed in the Arctic in early December 1999, *J. Geophys. Res.*, *109* (D4), D04312, doi: 10.1029/2003JD003846, 2004.

Papanastasiou, D.K., V.C. Papadimitriou, D.W. Fahey, and J.B. Burkholder, UV absorption spectrum of the ClO dimer (Cl_2O_2) between 200 and 420 nm, *J. Phys. Chem. A*, *113* (49), 13711-13726, doi: 10.1021/jp9065345, 2009.

Pawson, S., K. Krüger, R. Swinbank, M. Bailey, and A. O'Neill, Intercomparison of two stratospheric analyses: Temperatures relevant to polar stratospheric cloud formation, *J. Geophys. Res.*, *104* (D2), 2041-2050, doi: 10.1029/98JD02279, 1999.

Petzoldt, K., The role of dynamics in total ozone deviations from their long-term mean over the Northern Hemisphere, *Ann. Geophys.*, *17*, 231-241, doi: 10.1007/s00585-999-0231-1, 1999.

Pitari, G., V. Aquila, B. Kravitz, A. Robock, S. Watanabe, I. Cionni, N. De Luca, G. Di Genova, E. Mancini, and S. Tilmes, Stratospheric ozone response to sulfate geoengineering: Results from the Geoengineering Model Intercomparison Project (GeoMIP), *J. Geophys. Res.*, *119* (5), 2629-2653, doi: 10.1002/2013JD020566, 2014.

Piters, A.J.M., K. Bramstedt, J.-C. Lambert, and B. Kirchhoff, Overview of SCIAMACHY validation: 2002–2004, *Atmos. Chem. Phys*., *6* (1), 127-148, doi: 10.5194/acp-6-127-2006, 2006.

Pitts, M.C., L.R. Poole, and L.W. Thomason, CALIPSO polar stratospheric cloud observations: Second-generation detection algorithm and composition discrimination, *Atmos. Chem. Phys.*, *9* (19), 7577-7589, doi: 10.5194/acp-9-7577-2009, 2009.

Pitts, M.C., L.R. Poole, A. Dörnbrack, and L.W. Thomason, The 2009–2010 Arctic polar stratospheric cloud season: A CALIPSO perspective, *Atmos. Chem. Phys.*, *11* (5), 2161-2177, doi: 10.5194/acp-11-2161-2011, 2011.

Pitts, M.C., L.R. Poole, A. Lambert, and L.W. Thomason, An assessment of CALIOP polar stratospheric cloud composition classification, *Atmos. Chem. Phys.*, *13* (6), 2975-2988, doi: 10.5194/acp-13-2975-2013, 2013.

Plenge, J., S. Kühl, B. Vogel, R. Müller, F. Stroh, M. von Hobe, R. Flesch, and E. Rühl, Bond strength of chlorine peroxide, *J. Phys. Chem. A*, *109* (30), 6730-6734, doi: 10.1021/jp044142h, 2005.

Plummer, D.A., J. F. Scinocca, T.G. Shepherd, M.C. Reader, and A.I. Jonsson, Quantifying the contributions to stratospheric ozone changes from ozone depleting substances and greenhouse gases, *Atmos. Chem. Phys.*, *10* (18), 8803-8820, doi: 10.5194/acp-10-8803-2010, 2010.

Pommereau, J.-P., F. Goutail, F. Lefèvre, A. Pazmino, C. Adams, V. Dorokhov, P. Eriksen, R. Kivi, K. Stebel, X. Zhao, and M. van Roozendael, Why unprecedented ozone loss in the Arctic in 2011? Is it related to climate change?, *Atmos. Chem. Phys.*, *13* (10), 5299-5308, doi: 10.5194/acp-13-5299-2013, 2013.

Pope, F.D., J.C. Hansen, K.D. Bayes, R.R. Friedl, and S.P. Sander, Ultraviolet absorption spectrum of chlorine peroxide, ClOOCl, *J. Phys. Chem., 111*, 4322-4332, 2007.

Portmann, R.W., S. Solomon, R.R. Garcia, L.W. Thomason, L.R. Poole, and M.P. McCormick, Role of aerosol variations in anthropogenic ozone depletion in the polar regions, *J. Geophys. Res.*, *101* (D17), 22991-23006, 1996.

Randel, W., F. Wu, and R. Stolarski, Changes in column ozone correlated with the stratospheric EP flux, *J. Meteorol. Soc. Japan*, *80*, 849-862, doi: 10.2151/jmsj.80.849, 2002.

Randel, W.J., K.P. Shine, J. Austin, J. Barnett, C. Claud, N.P. Gillett, P. Keckhut, U. Langematz, R. Lin, C. Long, C. Mears, A. Miller, J. Nash, D.J. Seidel, D.W.J. Thompson, F. Wu, and S. Yoden, An update of observed stratospheric temperature trends, *J. Geophys. Res*., *114*, D02107, doi: 10.1029/2008JD01042, 2009.

Rault, D.F., and R.P. Loughman, The OMPS Limb Profiler environmental data record algorithm theoretical basis document and expected performance, *IEEE Trans. Geosci. Remote Sens*., *51* (5), 2505-2527, doi: 10.1109/TGRS.2012.2213093, 2013.

Remsberg, E., G. Lingenfelser, M. Natarajan, L. Gordley, B.T. Marshall, and E. Thompson, On the quality of the Nimbus 7 LIMS version 6 ozone for studies of the middle atmosphere, *J. Quant. Spectrosc. Radiat. Transfer*, *105* (3), 492-518, doi: 10.1016/j.jqsrt.2006.12.005, 2007.

Remsberg, E., M. Natarajan, B.T., Marshall, L.L. Gordley, R.E. Thompson, and G. Lingenfelser, Improvements in the profiles and distributions of nitric acid and nitrogen dioxide with the LIMS version 6 dataset, *Atmos. Chem. Phys.*, *10* (10), 4741-4756, doi: 10.5194/acp-10-4741-2010, 2010.

Revell, L.E., G.E. Bodeker, P.E. Huck, B.E. Williamson, and E. Rozanov, The sensitivity of stratospheric ozone changes through the 21st century to N_2O and CH_4, *Atmos. Chem. Phys.*, *12* (23), 11309-11317, doi: 10.5194/acp-12-11309-2012, 2012.

Rex, M., R.J. Salawitch, N,R.P. Harris, P. von der Gathen, G.O. Braathen, A. Schulz, H. Deckelmann, M. Chipperfield, B.-M. Sinnhuber, E. Reimer, R. Alfier, R. Bevilacqua, K. Hoppel, M. Fromm, J. Lumpe, H. Küllmann, A. Kleinböhl, H. Bremer, M. von König, K. Künzi, D. Toohey, H. Vömel, E. Richard, K. Aikin, H. Jost, J.B. Greenblatt, M. Loewenstein, J.R. Podolske, C.R. Webster, G.J. Flesch, D.C. Scott, R.L. Herman, J.W. Elkins, E.A. Ray, F.L. Moore, D.F. Hurst, P. Romashkin, G.C. Toon, B. Sen, J.J. Margitan, P. Wennberg, R. Neuber, M. Allart, B.R. Bojkov, H. Claude, J. Davies, W. Davies, H. De Backer, H. Dier, V. Dorokhov, H. Fast, Y. Kondo, E. Kyrö, Z. Litynska, I.S. Mikkelsen, M.J. Molyneux, E. Moran, T. Nagai, H. Nakane, C. Parrondo, F. Ravegnani, P. Skrivankova, P. Viatte, and V. Yushkov, Chemical depletion of Arctic ozone in winter 1999/2000, *J. Geophys. Res.*, *107* (D20), 8276, doi: 10.1029/2001JD000533, 2002.

Rex, M., R.J. Salawitch, M.L. Santee, J.W. Waters, K. Hoppel, and R. Bevilacqua, On the unexplained stratospheric ozone losses during cold Arctic Januaries, *Geophys. Res. Lett.*, *30* (1), 1008, doi: 10.1029/2002GL016008, 2003.

Rex, M., R.J. Salawitch, P. von der Gathen, N.R.P. Harris, M.P. Chipperfield, and B. Naujokat, Arctic ozone loss and climate change, *Geophys. Res. Lett.*, *31*, L04116, doi: 10.1029/2003GL018844, 2004.

Rex, M., R.J. Salawitch, H. Deckelmann, P. von der Gathen, N.R.P. Harris, M.P. Chipperfield, B. Naujokat, E. Reimer, M. Allaart, S.B. Andersen, R. Bevilacqua, G.O. Braathen, H. Claude, J. Davies, H. De Backer, H. Dier, V. Dorokhov, H. Fast, M. Gerding, S. Godin-Beekmann, K. Hoppel, B. Johnson, E. Kyrö, Z. Litynska, D.

Moore, H. Nakane, M.C. Parrondo, A.D. Risley Jr., P. Skrivankova, R. Stübi, P. Viatte, V. Yushkov, and C. Zerefos, Arctic winter 2005: Implications for stratospheric ozone loss and climate change, *Geophys. Res. Lett.*, *33*, L23808, doi: 10.1029/2006GL026731, 2006.

Rieder, H.E., and L.M. Polvani, Are recent Arctic ozone losses caused by increasing greenhouse gases?, *Geophys. Res. Lett.*, *40* (16), 4437-4441, doi: 10.1002/grl.50835, 2013.

Rienecker, M.M., M.J. Suarez, R. Gelaro, R. Todling, J. Bacmeister, E. Liu, M.G. Bosilovich, S.D. Schubert, L. Takacs, G.-K. Kim, S. Bloom, J. Chen, D. Collins, A. Conaty, A. da Silva, W. Gu, J. Joiner, R.D. Koster, R. Lucchesi, A. Molod, T. Owens, S. Pawson, P. Pegion, C.R. Redder, R. Reichle, F.R. Robertson, A.G. Ruddick, M. Sienkiewicz, and J. Woollen, MERRA: NASA's Modern-Era Retrospective Analysis for Research and Applications, *J. Clim.*, *24* (14), 3624-3648, doi: 10.1175/JCLI-D-11-00015.1, 2011.

Roche, A.E., J.B. Kumer, J.L. Mergenthaler, G.A. Ely, W.G. Uplinger, J.F. Potter, T.C. James, and L.W. Sterrit, The cryogenic limb array etalon spectrometer (CLAES) on UARS: Experiment description and performance, *J. Geophys. Res.*, *98* (D6), 10763-10775, doi: 10.1029/93JD00800, 1993.

Roscoe, H.K., W. Feng, M.P. Chipperfield, M. Trainic, and E.F. Shuckburgh, The existence of the edge region of the Antarctic stratospheric vortex, *J. Geophys. Res.*, *117*, D04301, doi: 10.1029/2011JD015940, 2012.

Russell III, J.M., L.L. Gordley, J.H. Park, S.R. Drayson, W.D. Hesketh, R.J. Cicerone, A.F. Tuck, J.E. Frederick, J.E. Harries, and P.J. Crutzen, The halogen occultation experiment, *J. Geophys. Res.*, *98* (D6), 10777-10797, doi: 10.1029/93JD00799, 1993.

Salawitch, R.J., G.P. Gobbi, S.C. Wofsy, and M.B. McElroy, Denitrification in the Antarctic stratosphere, *Nature*, *339*, 525-527, doi: 10.1038/33952a0, 1989.

Salby, M.L., Involvement of the Brewer–Dobson circulation in changes of stratospheric temperature and ozone, *Dynam. Atmos. Oceans*, *44* (3-4), 143-164, doi: 10.1016/j.dynatmoce.2006.11.002, 2008.

Salby, M., E. Titova, and L. Deschamps, Rebound of Antarctic ozone, *Geophys. Res. Lett.*, *38* (9), L09702, doi: 10.1029/2011GL047266, 2011.

Salby, M.L., E.A. Titova, and L. Deschamps, Changes of the Antarctic ozone hole: Controlling mechanisms, seasonal predictability, and evolution, *J. Geophys. Res.*, *117* (D10), D10111, doi: 10.1029/2011JD016285, 2012.

Sander, S.P., R.R. Friedl, D.M. Golden, M.J. Kurylo, G.K. Moortgat, H. Keller-Rudek, P.H. Wine, A.R. Ravishankara, C.E. Kolb, M.J. Molina, B.J. Finlayson-Pitts, R.E. Huie, and V.L. Orkin, *Chemical Kinetics and Photochemical Data for Use in Atmospheric Studies*, Evaluation Number 15, JPL Publication 06-02, Jet Propulsion Laboratory, Pasadena, Calif., 2006.

Sander, S.P., J. Abbatt, J.R. Barker, J.B. Burkholder, R.R. Friedl, D.M. Golden, R.E. Huie, C.E. Kolb, M.J. Kurylo, G.K. Moortgat, V.L. Orkin, and P.H. Wine, *Chemical Kinetics and Photochemical Data for Use in Atmospheric Studies*, Evaluation Number 17, JPL Publication 10-6, Jet Propulsion Laboratory, Pasadena, Calif., available: http://jpldataeval.jpl.nasa.gov/, 2011.

Santee, M.L., G.L. Manney, L. Froidevaux, R.W. Zurek, and J.W. Waters, MLS observations of ClO and HNO_3 in the 1996–97 Arctic Polar Vortex, *Geophys. Res. Lett.*, *24* (22), 2713-2716, doi: 10.1029/97GL52830, 1997.

Santee, M.L., A. Lambert, W.G. Read, N.J. Livesey, G.L. Manney, R.E. Cofield, D.T. Cuddy, W.H. Daffer, B.J. Drouin, L. Froidevaux, R.A. Fuller, R.F. Jarnot, B.W. Knosp, V.S. Perun, W.V. Snyder, P.C. Stek, R.P. Thurstans, P.A. Wagner, J.W. Waters, B. Connor, J. Urban, D. Murtagh, P. Ricaud, B. Barrett, A. Kleinböehl, J. Kuttippurath, H. Küllmann, M. von Hobe, G.C. Toon, and R.A. Stachnik, Validation of the Aura Microwave Limb Sounder ClO measurements, *J. Geophys. Res.*, *113* (D15), D15S22, doi: 10.1029/2007JD008762, 2008.

Schoeberl, M.R., R.S. Stolarksi, and A.J. Krueger, The 1988 Antarctic ozone depletion: Comparison with previous year depletions, *Geophys. Res. Lett.*, *16* (5), 377-380, doi: 10.1029/GL016i005p00377, 1989.

Schoeberl, M.R., M. Luo, and J.E. Rosenfield, An analysis of the Antarctic Halogen Occultation Experiment trace gas observations, *J. Geophys. Res.*, *100* (D3), 5159-5172, doi: 10.1029/94JD02749, 1995.

Schroeder, S., P. Preusse, M. Ern, and M. Riese, Gravity waves resolved in ECMWF and measured by SABER, *Geophys. Res. Lett.*, *36* (10), L10805, doi: 10.1029/2008GL037054, 2009.

Scinocca, J.F., M.C. Reader, D.A. Plummer, M. Sigmond, P.J. Kushner, T.G. Shepherd, and A.R. Ravishankara, Impact of sudden Arctic sea-ice loss on stratospheric polar ozone recovery, *Geophys. Res. Lett.*, *36*, L24701, doi: 10.1029/2009GL041239, 2009.

Screen, J.A., I. Simmonds, C. Deser, and R. Thomas, The atmospheric response to three decades of observed Arctic sea ice loss, *J. Clim.*, *26* (4), 1230-1248, doi: 10.1175/JCLI-D-12-00063.1, 2013.

Seftor, C.J., G. Jaross, M. Kowitt, M. Haken, J. Li, and L.E. Flynn, Postlaunch performance of the Suomi National Polar-orbiting Partnership Ozone Mapping and Profiler Suite (OMPS) nadir sensors, *J. Geophys. Res.*, *119* (7), 4413-4428, doi: 10.1002/2013JD020472, 2014.

Shaw, T.A., and J. Perlwitz, On the control of the residual circulation and stratospheric temperatures in the Arctic by planetary wave coupling, *J. Atmos. Sci.*, *71* (1), 195-206, doi: 10.1175/JAS-D-13-0138.1, 2014.

Sinnhuber, B.-M., G. Stiller, R. Ruhnke, T. von Clarmann, S. Kellmann, and J. Aschmann, Arctic winter 2010/2011 at the brink of an ozone hole, *Geophys. Res. Lett.*, *38* (24), L24814, doi: 10.1029/2011GL049784, 2011.

Smith, K.L., C.G. Fletcher, and P.J. Kushner, The role of linear interference in the annular mode response to extratropical surface forcing, *J. Clim.*, *23*, 6036-6050, doi: 10.1175/2010JCLI3606.1, 2010.

Solomon, S., Stratospheric ozone depletion: A review of concepts and history, *Rev. Geophys.*, *37* (3), 275-316, doi: 10.1029/1999RG900008, 1999.

Solomon, S., R.R. Garcia, F.S. Rowland, and D.J. Wuebbles, On the depletion of Antarctic ozone, *Nature*, *321*, 755-758, doi: 10.1038/321755a0, 1986.

Solomon, S., R.W. Portmann, T. Sasaki, D.J. Hofmann, and D.W.J. Thompson, Four decades of ozonesonde measurements over Antarctica, *J. Geophys. Res.*, *110* (D21), D21311, doi: 10.1029/2005JD005917, 2005.

Solomon, S., J. Haskins, D.J. Ivy, and F. Min, Fundamental differences between Arctic and Antarctic ozone depletion, *Proc. Natl. Acad. Sci.*, *111* (17), 6220-6225, doi: 10.1073/pnas.1319307111, 2014.

Sonkaew, T., C. von Savigny, K.-U. Eichmann, M. Weber, A. Rozanov, H. Bovensmann, J.P. Burrows, and J.-U. Grooß, Chemical ozone losses in Arctic and Antarctic polar winter/spring season derived from SCIAMACHY limb measurements 2002–2009, *Atmos. Chem. Phys.*, *13* (4), 1809-1835, doi: 10.5194/acp-13-1809-2013, 2013.

Spang, R., and J.J. Remedios, Observations of a distinctive infra-red spectral feature in the atmospheric spectra of polar stratospheric clouds measured by the CRISTA instrument, *Geophys. Res. Lett.*, *30* (16), 1875, doi: 10.1029/2003GL017231, 2003.

SPARC CCMVal (Stratosphere-troposphere Processes And their Role in Climate), *SPARC Report on the Evaluation of Chemistry-Climate Models*, edited by V. Eyring, T.G. Shepherd, and D.W. Waugh, SPARC Report No. 5, WCRP-132, WMO/TD-No. 1526, 478 pp., available: http://www.atmosp.physics.utoronto.ca/SPARC/ccmval_final/index.php, 2010.

SPARC (Stratosphere-troposphere Processes And their Role in Climate), *SPARC Report on the Lifetimes of Stratospheric Ozone-Depleting Substances, Their Replacements, and Related Species*, edited by M. Ko, P. Newman, S. Reimann, and S. Strahan, SPARC Report No. 6, WCRP-15/2013, 2013.

Steinbrecht, W., U. Köhler, H. Claude, M. Weber, J.P. Burrows, and R.J. van der A, Very high ozone columns at northern mid-latitudes in 2010, *Geophys. Res. Lett.*, *38* (6), L06803, doi: 10.1029/2010GL046634, 2011.

Stimpfle, R., D.M. Wilmouth, R.J. Salawitch, and J.G. Anderson, First measurements of ClOOCl in the stratosphere: The coupling of ClOOCl and ClO in the Arctic polar vortex, *J. Geophys. Res.*, *109*, D03301, doi: 10.1029/2003JD003811, 2004.

Stolarski, R.S., and S.M. Frith, Search for evidence of trend slow-down in the long-term TOMS/SBUV total ozone data record: The importance of instrument drift uncertainty, *Atmos. Chem. Phys.*, *6*, 4057-4065, 2006.

Stolarski, R.S., P. Bloomfield, R.D. McPeters, and J.R. Herman, Total Ozone trends deduced from Nimbus-7 TOMS data, *Geophys. Res. Lett.*, *18* (6), 1015-1018, doi: 10.1029/91GL01302, 1991.

Strahan, S.E., A.R. Douglass, R.S. Stolarski, H. Akiyoshi, S. Bekki, P. Braesicke, N. Butchart, M.P. Chipperfield, D. Cugnet, S. Dhomse, S.M. Frith, A. Gettelman, S.C. Hardiman, D.E. Kinnison, J.-F. Lamarque, E. Mancini, M. Marchand, M. Michou, O. Morgenstern, T. Nakamura, D. Olivié, S. Pawson, G. Pitari, D.A. Plummer, J.A. Pyle, J.F. Scinocca, T.G. Shepherd, K. Shibata, D. Smale, H. Teyssèdre, W. Tian, and Y. Yamashita, Using transport diagnostics to understand chemistry climate model ozone simulations, *J. Geophys. Res.*, *116* (D17), D17302, doi: 10.1029/2010JD015360, 2011.

Strahan, S.E., A.R. Douglass, and P.A. Newman, The contributions of chemistry and transport to low arctic ozone in March 2011 derived from Aura MLS observations, *J. Geophys. Res.*, *118* (3), 1563-1576, doi: 10.1002/jgrd.50181, 2013.

Sugita, T., T. Yokota, H. Nakajima, H. Kanzawa, H. Nakane, H. Gernandt, V. Yushkov, K. Shibasaki, T. Deshler, Y. Kondo, S. Godin, F. Goutail, J.-P. Pommereau, C. Camy-Peyret, S. Payan, P. Jeseck, J.-B. Renard, H. Bösch, R. Fitzenberger, K. Pfeilsticker,M. von König, H. Bremer, H. Küllmann, H. Schlager, J.J. Margitan, B. Stachnik, G.C. Toon, K. Jucks, W.A. Traub, D.G. Johnson, I. Murata, H. Fukunishi, and Y. Sasano, Validation of ozone measurements from the Improved Limb Atmospheric Spectrometer, *J. Geophys. Res.*, *107* (D24), 8212, doi: 10.1029/2001JD000602, 2002.

Sugita, T., H. Nakajima, T. Yokota, H. Kanzawa, H. Gernandt, A. Herber, P. von der Gathen, G. König-Langlo, K. Sato, V. Dorokhov, V.A. Yushkov, Y. Murayama, M. Yamamori, S. Godin-Beekmann, F. Goutail, H.K. Roscoe, T. Deshler, M. Yela, P. Taalas, E. Kyrö, S.J. Oltmans, B.J. Johnson, M. Allaart, Z. Litynska, A. Klekociuk, S.B. Andersen, G.O. Braathen, H. De Backer, C.E. Randall, R.M. Bevilacqua, G. Taha, L.W. Thomason, H. Irie, M.K. Ejiri, N. Saitoh, T. Tanaka, Y. Terao, H. Kobayashi, and Y. Sasano, Ozone profiles in

the high-latitude stratosphere and lower mesosphere measured by the Improved Limb Atmospheric Spectrometer (ILAS)-II: Comparison with other satellite sensors and ozonesondes, *J. Geophys. Res.*, *111* (D11), D11S02, doi: 10.1029/2005JD006439, 2006.

Sumińska-Ebersoldt, O., R. Lehmann, T. Wegner, J.-U. Grooβ, E. Hösen, R. Weigel, W. Frey, S. Griessbach, V. Mitev, C. Emde, C.M. Volk, S. Borrmann, M. Rex, F. Stroh, and M. von Hobe, ClOOCl photolysis at high solar zenith angles: Analysis of the RECONCILE self-match flight, *Atmos. Chem. Phys.*, *12* (3), 1353-1365, doi: 10.5194/acp-12-1353-2012, 2012.

Tegtmeier, S., M. Rex, I. Wohltmann, and K. Krüger, Relative importance of dynamical and chemical contributions to Arctic wintertime ozone, *Geophys. Res. Lett.*, *35*, L17801, doi: 10.1029/ 2008GL034250, 2008.

Tegtmeier, S., M.I. Hegglin, J. Anderson, A. Bourassa, S. Brohede, D. Degenstein, L. Froidevaux, R. Fuller, B. Funke, J. Gille, A. Jones, Y. Kasai, K. Kru□ger, E. Kyrölä, G. Lingenfelser, J. Lumpe, B. Nardi, J. Neu, D. Pendlebury, E. Remsberg, A. Rozanov, L. Smith, M. Toohey, J. Urban, T. von Clarmann, K.A. Walker, and R.H.J. Wang, SPARC Data Initiative: A comparison of ozone climatologies from international satellite limb sounders, *J. Geophys. Res.*, *118* (21), 12229-12247, doi: 10.1002/2013JD019877, 2013.

Thiéblemont, R., N. Huret, Y.J. Orsolini, A. Hauchecorne, and M.-A. Drouin, Frozen-in anticyclones occurring in polar Northern Hemisphere during springtime: Characterization, occurrence and link with quasi-biennial oscillation, *J. Geophys. Res.*, *116* (D20), D20110, doi: 10.1029/2011JD016042, 2011.

Tilmes, S., R. Müller, A. Engel, M. Rex, and J. M. Russell, Chemical ozone loss in the Arctic and Antarctic stratosphere between 1992 and 2005, *Geophys. Res. Lett.*, *33*, L20812, doi: 10.1029/ 2006GL026925, 2006.

Tilmes, S., R. Müller, and R. Salawitch, The sensitivity of polar ozone depletion to proposed geoengineering schemes, *Science*, *320*, 1201-1204, 2008.

Tilmes, S., R.R. Garcia, D.E. Kinnison, A. Gettelman, and P.J. Rasch, Impact of geoengineered aerosols on the troposphere and stratosphere, *J. Geophys. Res.*, *114*, D12305, doi: 10.1029/2008JD011420, 2009.

Tilmes, S., D.E. Kinnison, R.R. Garcia, R. Salawitch, T. Canty, J. Lee-Taylor, S. Madronich, and K. Chance, Impact of very short-lived halogens on stratospheric ozone abundance and UV radiation in a geo-engineered atmosphere, *Atmos. Chem. Phys.*, *12* (22), 10945-10955, doi: 10.5194/acp-12-10945-2012, 2012.

Urban, J., N. Lautié, E. Le Flochmoën, C. Jimènez, P. Eriksson, J. de La Noë, E. Dupuy, M. Ekström, L. El Amraoui, U. Frisk, D. Murtagh, M. Olberg, and P. Ricaud, Odin/SMR limb observations of stratospheric trace gases: Level-2 processing of ClO, N_2O, HNO_3, and O_3, *J. Geophys. Res.*, *110* (D14), D14307, doi: 10.1029/ 2004JD005741, 2005.

van Peet, J.C.A., R.J. van der A, O.N.E. Tuinder, E. Wolfram, J. Salvador, P.F. Levelt, and H.M. Kelder, Ozone ProfilE Retrieval Algorithm (OPERA) for nadir-looking satellite instruments in the UV-VIS, *Atmos. Meas. Tech.*, *7* (3), 859-876, doi: 10.5194/amt-7-859-2014, 2014.

van Roozendael, M., R. Spurr, D. Loyola, C. Lerot, D. Balis, J.-C. Lambert, W. Zimmer, J. van Gent, J. van Geffen, M. Koukouli, J. Granville, A. Doicu, C. Fayt, and C. Zehner, Sixteen years of GOME/ERS-2 total ozone data: The new direct-fitting GOME Data Processor (GDP) version 5 - Algorithm description, *J. Geophys. Res.*, *117* (D3), D03305, doi: 10.1029/2011JD016471, 2012.

van Vuuren, D.P., J. Edmonds, M. Kainuma, K. Riahi, A. Thomson, K. Hibbard, G.C. Hurtt, T. Kram, V. Krey, J.-F. Lamarque, T. Masui, M. Meinshausen, N. Nakicenovic, S.J. Smith, and S.K. Rose, The representative concentration pathways: An overview, *Climatic Change*, *109* (1-2), 5-31, doi: 10.1007/s10584-011-0148-z, 2011.

Veefkind, J.P., J.F. de Haan, E.J. Brinksma, M. Kroon, and P.F. Levelt, Total ozone from the Ozone Monitoring Instrument (OMI) using the DOAS technique, *IEEE Trans. Geosci. Rem. Sens.*, *44* (5), 1239-1244, doi: 10.1109/TGRS.2006.871204, 2006.

Voigt, C., H. Schlager, B.P. Luo, A. Dörnbrack, A. Roiger, P. Stock, J. Curtius, H. Vössing, S. Borrmann, S. Davies, P. Konopka, C. Schiller, G. Shur, and T. Peter, Nitric Acid Trihydrate (NAT) formation at low NAT supersaturation in Polar Stratospheric Clouds (PSCs), *Atmos. Chem. Phys.*, *5*, 1371-1380, doi: 10.5194/acp-5-1371-2005, 2005.

von Clarmann, T., M. Höpfner, S. Kellmann, A. Linden, S. Chauhan, B. Funke, U. Grabowski, N. Glatthor, M. Kiefer, T. Schieferdecker, G.P. Stiller, and S. Versick, Retrieval of temperature, H_2O, O_3, HNO_3, CH_4, N_2O, $ClONO_2$ and ClO from MIPAS reduced resolution nominal mode limb emission measurements, *Atmos. Meas. Tech.*, *2* (1), 159-175, doi: 10.5194/amt-2-159-2009, 2009.

von Hobe, M., F. Stroh, H. Beckers, T. Benter, and H. Willner, The UV/Vis absorption spectrum of matrix-isolated dichlorine peroxide, ClOOCl, *Phys. Chem. Chem. Phys.*, *11*, 1571-1580, doi: 10.1039/b814373k, 2009.

von Hobe, M., S. Bekki, S. Borrmann, F. Cairo, F. D'Amato, G. Di Donfrancesco, A. Dörnbrack, A. Ebersoldt, M. Ebert, C. Emde, I. Engel, M. Ern, W. Frey, S. Genco, S. Griessbach, J.-U. Grooß, T. Gulde, G. Günther, E.

Hösen, L. Hoffmann, V. Homonnai, C.R. Hoyle, I.S.A. Isaksen, D.R. Jackson, I.M. Jánosi, K. Kandler, C. Kalicinsky, A. Keil, S.M. Khaykin, F. Khosrawi, R. Kivi, J. Kuttippurath, J.C. Laube, F. Lefèvre, R. Lehmann, S. Ludmann, B.P. Luo, M. Marchand, J. Meyer, V. Mitev, S. Molleker, R. Müller, H. Oelhaf, F. Olschewski, Y. Orsolini, T. Peter, K. Pfeilsticker, C. Piesch, M.C. Pitts, L.R. Poole, F.D. Pope, F. Ravegnani, M. Rex, M. Riese, T. Röckmann, B. Rognerud, A. Roiger, C. Rolf, M.L. Santee, M. Scheibe, C. Schiller, H. Schlager, M. Siciliani de Cumis, N. Sitnikov, O.A. Søvde, R. Spang, N. Spelten, F. Stordal, O. Sumińska-Ebersoldt, A. Ulanovski, J. Ungermann, S. Viciani, C.M. Volk, M. vom Scheidt, P. von der Gathen, K. Walker, T. Wegner, R. Weigel, S. Weinbuch, G. Wetzel, F.G. Wienhold, J. Wintel, I. Wohltmann, W. Woiwode, I.A.K. Young, V. Yushkov, B. Zobrist, and F. Stroh, Reconciliation of essential process parameters for an enhanced predictability of Arctic stratospheric ozone loss and its climate interactions (RECONCILE): Activities and results, *Atmos. Chem. Phys.*, *13* (18), 9233-9268, doi: 10.5194/acp-13-9233-2013, 2013.

Wang, H.-J., D.M. Cunnold, C. Trepte, L.W. Thomason, and J.M. Zawodny, SAGE III solar ozone measurements: Initial results, *Geophys. Res. Lett.*, *33*, L03805, doi: 10.1029/2005GL025099, 2006.

Wang, L., P.J. Kushner, and D.W. Waugh, Southern hemisphere stationary wave response to changes of ozone and greenhouse gases, *J. Clim.*, *26* (24), 10205-10217, doi: 10.1175/JCLI-D-13-00160.1, 2013.

Waters, J.W., L. Froidevaux, W.G. Read, G.L. Manney, L.S. Elson, D.A. Flower, R.F. Jarnot, and R.S. Harwood, Stratospheric ClO and ozone from the Microwave Limb Sounder on the Upper Atmosphere Research Satellite, *Nature*, *362* (6421), 597-602, doi: 10.1038/362597a0, 1993.

Waters, J.W., L. Froidevaux, R.S. Harwood, R.F. Jarnot, H.M. Pickett, W.G. Read, P.H. Siegel, R.E. Cofield, M.J. Filipiak, D.A. Flower, J.R. Holden, G.K. Lau, N.J. Livesey, G.L. Manney, H.C. Pumphrey, M.L. Santee, D.L. Wu, D.T. Cuddy, R.R. Lay, M.S. Loo, V.S. Perun, M.J. Schwartz, P.C. Stek, R.P. Thurstans, M.A. Boyles, K.M. Chandra, M.C. Chavez, G.-S. Chen, B.V. Chudasama, R. Dodge, R.A. Fuller, M.A. Girard, J.H. Jiang, Y. Jiang, B.W. Knosp, R.C. LaBelle, J.C. Lam, K.A. Lee, D. Miller, J.E. Oswald, N.C. Patel, D.M. Pukala, O. Quintero, D.M. Scaff, W. Van Snyder, M.C. Tope, P.A. Wagner, and M.J. Walch, The Earth Observing System Microwave Limb Sounder (EOS MLS) on the Aura satellite, *IEEE Trans. Geosci. Rem. Sens.*, *44* (5), 1075-1092, doi: 10.1109/TGRS.2006.873771, 2006.

Watson, P.A.G., and L.J. Gray, How does the quasi-biennial oscillation affect the stratospheric polar vortex?, *J. Atmos. Sci.*, *71* (1), 391-409, doi: 10.1175/JAS-D-13-096.1, 2014.

Waugh, D., W. Randel, S. Pawson, P. Newman, and E. Nash, Persistence of the lower stratospheric polar vortices, *J. Geophys. Res.*, *104* (D22), 27191-27201, 1999.

Weber, M., S. Dhomse, F. Wittrock, A. Richter, B.-M. Sinnhuber, and J.P. Burrows, Dynamical control of NH and SH winter/spring total ozone from GOME observations in 1995-2002, *Geophys. Res. Lett.*, *30* (11), 1583, doi: 10.1029/2002GL016799, 2003.

Weber, M., S. Dikty, J.P. Burrows, H. Garny, M. Dameris, A. Kubin, J. Abalichin, and U. Langematz, The Brewer-Dobson circulation and total ozone from seasonal to decadal time scales, *Atmos. Chem. Phys.*, *11* (21), 11221-11235, doi: 10.5194/acp-11-11221-2011, 2011.

Wegner, T., J.-U. Grooß, M. von Hobe, F. Stroh, O. Sumińska-Ebersoldt, C.M. Volk, E. Hösen, V. Mitev, G. Shur, and R. Müller, Heterogeneous chlorine activation on stratospheric aerosols and clouds in the Arctic polar vortex, *Atmos. Chem. Phys.*, *12* (22), 11095-11106, doi: 10.5194/acp-12-11095-2012, 2012.

Wegner, T., D.E. Kinnison, R.R. Garcia, and S. Solomon, Simulation of polar stratospheric clouds in the specified dynamics version of the whole atmosphere community climate model, *J. Geophys. Res.*, *118* (10), 4991-5002, doi: 10.1002/jgrd.50415, 2013.

Wespes, C., D. Hurtmans, C. Clerbaux, M.L. Santee, R.V. Martin, and P.F. Coheur, Global distributions of nitric acid from IASI/MetOP measurements, *Atmos. Chem. Phys.*, *9* (20), 7949-7962, doi: 10.5194/acp-9-7949-2009, 2009.

Winker, D.M., M.A. Vaughan, A. Omar, Y. Hu, and K.A. Powell, Overview of the CALIPSO mission and CALIOP data processing algorithms, *J. Atmos. Oceanic Technol.*, *26* (11), 2310-2323, doi: 10.1175/2009JTECHA 1281.1, 2009.

WMO (World Meteorological Organization), *Scientific Assessment of Ozone Depletion: 2006*, Global Ozone Research and Monitoring Project–Report No. 50, 572 pp., Geneva, Switzerland, 2007.

WMO (World Meteorological Organization), *Scientific Assessment of Ozone Depletion: 2010*, *Global Ozone Research and Monitoring Project–Report No. 52*, Geneva, Switzerland, 2011.

Wohltmann, I., and M. Rex, The Lagrangian chemistry and transport model ATLAS: Validation of advective transport and mixing, *Geosci. Model Dev.*, *2* (2), 153-173, doi: 10.5194/gmd-2-153-2009, 2009.

Wohltmann, I., T. Wegner, R. Müller, R. Lehmann, M. Rex, G.L. Manney, M. Santee, P. Bernath, O. Sumińska-Ebersoldt, F. Stroh, M. von Hobe, C.M. Volk, E. Hösen, F. Ravegnani, A. Ulanovsky, and V. Yushkov,

Uncertainties in modeling heterogeneous chemistry and Arctic ozone depletion in the winter 2009/2010, *Atmos. Chem. Phys.*, *13* (8), 3909-3929, doi: 10.5194/acp-13-3909-2013, 2013.

Woollings, T., A. Charlton-Perez, S. Ineson, A.G. Marshall, and G. Masato, Associations between stratospheric variability and tropospheric blocking, *J. Geophys. Res.*, *115* (D6), D06108, doi: 10.1029/2009JD012742, 2010.

Yang, E.-S., D.M. Cunnold, M.J. Newchurch, and R.J. Salawitch, Change in ozone trends at southern high latitudes, *Geophys. Res. Lett.*, *32*, L12812, doi: 10.1029/2004GL022296, 2005.

Yang, E.-S., D.M. Cunnold, M.J. Newchurch, R.J. Salawitch, M.P. McCormick, J.M. Russell, J.M. Zawodny, and S.J. Oltmans, First stage of Antarctic ozone recovery, *J. Geophys. Res.*, *113*, D20308, doi: 10.1029/2007 JD009675, 2008.

Yokota, T., H. Nakajima, T. Sugita, H. Tsubaki, Y. Itou, M. Kaji, M. Suzuki, H. Kanzawa, J.H. Park, and Y. Sasano, Improved Limb Atmospheric Spectrometer (ILAS) data retrieval algorithm for Version 5.20 gas profile products, *J. Geophys. Res.*, *107* (D24), 8216, doi: 10.1029/2001JD000628, 2002.

Young, I.A.K., R.L. Jones, and F.D. Pope, The UV and visible spectra of chlorine peroxide: Constraining the atmospheric photolysis rate, *Geophys. Res. Lett.*, *41* (5), 1781-1788, doi: 10.1002/2013GL058626, 2014.

Appendix 3A

Satellite Measurements Useful for Polar Studies

Table 3A-1. Main satellite measurements of ozone and related constituents in polar regions.

Instrument	Record Length	Latitudinal Range	Constituents	Vertical Resolution*	References
Total Column					
TOMS on Nimbus-7, Meteor-3 TOMS on ADEOS, Earth Probe	Nov 1978 – Dec 1994 Jul 1996 – Dec 2006	Near-global coverage [1]	Ozone SO_2, aerosol	Total column	Herman et al., 1991; Stolarski et al., 1991; Newman et al., 1991; Newman et al., 1997; Bodeker et al., 2001
AIRS on Aqua	May 2002 – present	Global coverage	Ozone CH_4	Total column	Divakarla et al., 2008
TOU on Feng-Yun 3A	May 2008 – present	Near-global coverage [1]	Ozone	Total column	Dong et al., 2009; Bai et al., 2013
TANSO-FTS on GOSAT	Apr 2009 – present	Near-global coverage [1]	Ozone CH_4, NO_2, HNO_3, NO_2, SO_2	Total column	Ohyama et al., 2012
OMPS-NM on Suomi-NPP	Nov 2011 – present	Near-global coverage [1]	Ozone SO_2, aerosol	Total column	Kramarova et al., 2014; Seftor et al., 2014
Total Column and Profiles					
SBUV on Nimbus 7 SBUV on NOAA-9, NOAA-11, NOAA-14, NOAA-16, NOAA-17, NOAA-18, NOAA-19	Nov 1978 – Jun 1990 Feb 1985 – present	Near-global coverage [1]	Ozone	Total column & profiles (nadir) Between 16 hPa and 40 hPa – top of the atmosphere Vertical resolution between 6 km and 15 km	Bhartia et al., 2013; McPeters et al., 2013
SCIAMACHY on Envisat	Aug 2002 – Apr 2012	Global coverage	Ozone NO_2, BrO, SO_2, OClO, aerosol	Total column & profiles (nadir/limb) ~10 km – ~60 km Vertical resolution 3–5 km	Bovensmann et al., 1999; Piters et al., 2006
OMI on EOS-Aura	Aug 2004 – present	Near-global coverage [1]	Ozone NO_2, BrO, SO_2, OClO, aerosol	Total column & profiles (nadir) Troposphere – top of atmosphere (18 layers) Vertical resolution 6–15 km	Bhartia and Wellemeyer, 2002; Veefkind et al., 2006; Liu et al., 2010; Kroon et al., 2011

TES on EOS-Aura	Aug 2004 – present	Global coverage	Ozone CH_4, HNO_3	Total column & profiles (nadir/limb) 0 km – 33 km Vertical resolution ~6–7 km	Beer, 2006; Bowman et al., 2006; Nassar et al., 2008
IASI on Metop-A IASI on Metop-B	Nov 2006 – present Nov 2012 – present	Global coverage	Ozone CH_4, HNO_3	Total column & profiles (nadir) Tropospheric layer – top of atmosphere Vertical resolution ~7 km	Coheur et al., 2005; Wespes et al., 2009; August et al., 2012
GOME-2 on Metop-A GOME-2 on Metop-B	Jan 2007 – present Dec 2012 – present	Near-global coverage [1]	Ozone NO_2, BrO, SO_2, OClO, aerosol	Total column & profiles (nadir) Surface – top of atmosphere Vertical resolution ~7–15 km	van Roozendael et al., 2012; van Peet et al., 2014
OMPS-NP on Suomi-NPP	Nov 2011 – present	Near-global coverage [1]	Ozone SO_2, aerosol	Total column & profiles (nadir) Between 16 hPa and 40 hPa – top of the atmosphere Vertical resolution 6–15 km	Seftor et al., 2014
Profiles					
LIMS on Nimbus 7	Nov 1978 – May 1979	64°S – 84°N	Ozone H_2O, HNO_3, NO_2	Profiles (limb) Cloud top – ~0.01 hPa Vertical resolution ~3.7 km	Gille and Russell, 1984; Girard and Louisnard, 1984; Remsberg et al., 2007; Remsberg et al., 2010
SAM II on Nimbus 7	Nov 1978 – Dec 1993	64°S – 80°S and 64°N – 80°N [2] (coverage changed over the lifetime of the instrument)	PSCs, aerosol	Profiles (solar occultation) Surface – ~160 km Vertical resolution ~0.5 km	Kent and McCormick, 1984; McCormick et al., 1981; McCormick and Trepte, 1986
SAGE I on AEM-B	Feb 1979 – Nov 1981	79°S – 79°N [2]	Ozone NO_2, aerosol	Profiles (solar occultation) Tropopause – ~55 km Vertical resolution 1 km	McCormick et al., 1984; Kent and McCormick, 1984; McCormick et al., 1989
SAGE II on ERBS	Oct 1984 – Jul 2005	80°S – 80°N [2]	Ozone NO_2, H_2O, aerosol	Profiles (solar occultation) Tropopause – ~55 km Vertical resolution 1 km	Cunnold et al., 1989; McCormick et al., 1989; Damadeo et al., 2013
MLS on UARS	Sep 1991 – Mar 2000	From 34° on one side of the equator to 80° on the other side – alternating every ~36 days	Ozone ClO, HNO_3, H_2O	Profiles (limb) 100 hPa – 0.22 hPa; Vertical resolution 3.5–5 km in the stratosphere, 5–8 km in the mesosphere	Barath et al., 1993; Waters et al., 1993; Livesey et al., 2003

CLAES on UARS	Oct 1991 – Apr 1993	From 34° on one side of the equator to 80° on the other – alternating every ~36 days	Ozone N_2O, CFC-11, CFC-12, CH_4, H_2O, NO, NO_2, HNO_3, $ClONO_2$, HCl, N_2O_5, PSCs, aerosol	Profiles (limb) 10 km – 60 km Vertical resolution ~2.5 km	Roche et al., 1993; Kumer et al., 1996; Massie et al., 1996
HALOE on UARS	Oct 1991 – Nov 2005	80°S – 80°N [2]	Ozone NO_2, H_2O, NO, CH_4, HCl, HF, PSCs, aerosol	Profiles (solar occultation) Cloud top – ~0.005 hPa Vertical resolution ~2.3 km	Russell et al., 1993; Schoeberl et al., 1995; Hervig et al., 1997
POAM II on SPOT-3	Sep 1993 – Nov 1996	55°N – 73°N, 63°S – 88°S [2]	Ozone NO_2, H_2O, PSCs, aerosol	Profiles (solar occultation) ~5 km – ~60 km Vertical resolution ~1.5 km	Glaccum et al., 1996; Lumpe et al., 1997 ; Bevilacqua et al., 1997 ; Fromm et al., 2003
ILAS on ADEOS	Oct 1996 – Jun 1997	57°N – 71°N, 64°S – 88°S [2]	Ozone HNO_3, NO_2, N_2O, CH_4, H_2O, PSCs, aerosol	Profiles (solar occultation) ~10 km – top of atmosphere Vertical resolution ~2 km	Sugita et al., 2002; Jucks et al., 2002; Nakajima et al., 2002; Yokota et al., 2002
POAM III on SPOT-4	Mar 1998 – Dec 2005	55°N – 73°N, 63°S – 88°S [2]	Ozone NO_2, H_2O, PSCs, aerosol	Profiles (solar occultation) ~5km – ~60km Vertical resolution ~1.5 km	Lucke et al., 1999; Lumpe et al., 2002; Fromm et al., 2003
OSIRIS on Odin	Nov 2001 – present	Near-global coverage [1]	Ozone NO_2, BrO, aerosol	Profiles (limb) Cloud tops – 55 km Vertical resolution 1.5 km in UTLS, 2 km higher up	Llewellyn et al., 2004; Brohede et al., 2007; McLinden et al., 2007
SMR on Odin	Nov 2001 – present	~83°S – ~83°N	Ozone N_2O, HNO_3, H_2O, ClO, NO, NO_y	Profiles (limb) Vertical resolution 2.5–3.5 km	Urban et al., 2005; Barret et al., 2006
SAGE III on Meteor-3M [3]	Feb 2002 – Dec 2005	50°S – 30°S, 50°N – 80°N [2]	Ozone, NO_2, H_2O, OClO, aerosol	Profiles (solar occultation) Tropopause – ~55 km Vertical resolution 1 km	Wang et al., 2006
MIPAS on Envisat	Jun 2002 – Apr 2012	Global coverage	Ozone N_2O, NO, NO_2, HNO_3, N_2O_5, $ClONO_2$, CFCs, HOCl, ClO, H_2O, H_2O_2, CH_4, CO	Profiles (limb) ~8 km (20/40 km; middle/upper atmosphere mode) – 72 km (100 km; middle/upper atmosphere mode) Vertical resolution from ~2 km to ~8 km (depending on altitude)	Fischer et al., 2008; von Clarmann et al., 2009
GOMOS on Envisat	Aug 2002 – Apr 2012	Global coverage	Ozone NO_2, H_2O, PSCs, aerosol	Profiles (stellar occultation) ~15 km – ~100 km Vertical resolution 2–3 km	Kyrölä et al., 2004; Bertaux et al., 2010

ILAS II on ADEOS II	Apr 2003 – Oct 2003	57°N – 71°N and 64°S – 88°S [2]	Ozone HNO_3, NO_2, N_2O, CH_4, H_2O, $ClONO_2$, N_2O_5, CFC-11, CFC-12, PSCs, aerosol	Profiles (solar occultation) ~10 km – top of atmosphere Vertical resolution ~1.5 km	Sugita et al., 2006; Irie et al., 2006
ACE-MAESTRO on SCISAT	Feb 2004 – present	Near-global coverage [2]	Ozone NO_2, PSCs, aerosol	Profiles (solar occultation) 5 km – 35 km Vertical resolution ~1.2 km	McElroy et al., 2007; Nowlan et al., 2007
ACE-FTS on SCISAT	Feb 2004 – present	Near-global coverage [2]	Ozone H_2O, CH_4, N_2O, NO_2, NO, NO_3, HCl, HF, CO, CFC-11, CFC-12, N_2O_5, $ClONO_2$, CH_3Cl, SF_6, H_2O_2, CCl_4, HCFCs, ClO, HOCl	Profiles (solar occultation) ~5 km – 95 km Vertical resolution 3–4 km	Bernath et al., 2005; Boone et al., 2005; Jones et al., 2012
MLS on EOS-Aura	Aug 2004 – present	82°S – 82°N	Ozone BrO, CH_3Cl, ClO, CO, H_2O, HCl, HNO_3, HO_2, OH, OCl, N_2O, SO_2	Profiles (limb) 215 hPa – 0.02 hPa Vertical resolution ~3 km in stratosphere, degrading to 4–6 km for pressures of 0.1 hPa or less	Waters et al., 2006; Livesey et al., 2006; Froidevaux et al., 2008; Santee et al., 2008
HIRDLS on EOS-Aura	Jan 2005 – Mar 2008	63°S – 80°N	Ozone HNO_3, CFC-11, CFC-12, NO_2, N_2O_5, H_2O, N_2O, NO_2, $ClONO_2$, aerosol	Profiles (limb) 10 km – 55 km Vertical resolution ~1 km	Gille et al., 2008; Kinnison et al., 2008; Nardi et al., 2008
CALIOP on CALIPSO	Apr 2005 – present	82°S – 82°N	PSCs, aerosol	Profiles (nadir) Surface – 40km Vertical resolution 30–60 m	Winker et al., 2009; Pitts et al., 2009
OMPS-LP on Suomi-NPP	Nov 2011 – present	Near-global coverage [1]	Ozone	Profiles (limb) 10 km – 60 km Vertical resolution 2 km	Rault and Loughman, 2013

* Vertical resolution only applies to ozone.

[1] Apart from polar night latitudes.

[2] Because of their particular viewing geometry and measurement technique, solar occultation instruments do not provide global coverage on a daily basis.

[3] A replica of the SAGE III Meteor-3M instrument is scheduled to be deployed on the International Space Station (ISS) in 2015. Although SAGE-III/ISS will measure ozone, water vapor, and a few other atmospheric constituents (NO_2, NO_3, and OClO, as well as aerosols and clouds), its coverage will be focused on middle and low latitudes.

CHAPTER 4

Stratospheric Ozone Changes and Climate

Lead Authors:
J.M. Arblaster
N.P. Gillett

Coauthors:
N. Calvo
P.M. Forster
L.M. Polvani
S.-W. Son
D.W. Waugh
P.J. Young

Contributors:
E.A. Barnes
I. Cionni
C.I. Garfinkel
E.P. Gerber
S.C. Hardiman
D.F. Hurst
J.-F. Lamarque
E.-P. Lim
M.P. Meredith
J. Perlwitz
R.W. Portmann
M. Previdi
M. Sigmond
N.C. Swart
J.-P. Vernier
Y. Wu

Chapter Editors:
L.J. Gray
D.W.J. Thompson

[Formatted for double-sided printing.]

From:
WMO (World Meteorological Organization), *Scientific Assessment of Ozone Depletion: 2014*, Global Ozone Research and Monitoring Project – Report No. 55, 416 pp., Geneva, Switzerland, 2014.

This chapter should be cited as:
Arblaster, J.M., and N.P Gillett (Lead Authors), N. Calvo, P.M. Forster, L.M. Polvani, S.-W. Son, D.W. Waugh, and P.J. Young, Stratospheric ozone changes and climate, Chapter 4 in *Scientific Assessment of Ozone Depletion: 2014*, Global Ozone Research and Monitoring Project – Report No. 55, World Meteorological Organization, Geneva, Switzerland, 2014.

CHAPTER 4

STRATOSPHERIC OZONE CHANGES AND CLIMATE

Contents

SCIENTIFIC SUMMARY

Since the last Assessment, new research has better quantified the impact of stratospheric ozone changes on climate. Additional model and observational analyses are assessed which examine the influence of stratospheric ozone changes on stratospheric temperatures and circulation, Southern Hemisphere tropospheric circulation and composition, surface climate, oceans, and sea ice.

- **Stratospheric ozone changes are the dominant driver of observed globally averaged long-term temperature changes in the lower stratosphere.** Between 1979 and 1995 global mean lower stratospheric temperature decreased by about 1 K but has since remained approximately constant.
  - Models broadly reproduce the evolution of global mean lower stratospheric temperature change. Stratospheric ozone changes are the dominant driver of these changes, with volcanic aerosol driving episodic warming, and greenhouse gas increases having only a minor contribution.
  - Observed mid- and upper-stratospheric temperatures decreased from 1979 to 2005, but the magnitude of the cooling is uncertain. A newly reprocessed data set of satellite measurements exhibits substantially different cooling trends compared to the existing data set. Models indicate that increasing greenhouse gases, as well as ozone changes, both made comparable contributions to observed cooling in the mid and upper stratosphere.
  - There was little overall change in global lower stratospheric water vapor concentration between 2000 and 2012, based on satellite measurements, which show a decrease between 2000 and 2004 followed by an increase to 2012.
  - The observed cooling of the Antarctic lower stratosphere since 1979 during austral spring is consistent with the average simulated cooling in models forced with observed ozone depletion. There is a large range in the magnitude of the simulated cooling, with models that underestimate the ozone depletion also underestimating the temperature trends.

- **Climate models consistently predict a long-term increase in the strength of the Brewer-Dobson circulation due to greenhouse gas increases, with important impacts on stratospheric and tropospheric composition.**
  - The predicted increase in the strength of the Brewer-Dobson circulation extends throughout the depth of the stratosphere.
  - Observations of changes in temperature, ozone, and trace gases over the past three to five decades are suggestive of increased upwelling in the tropical lower stratosphere, consistent with a strengthening of the shallow branch of the Brewer-Dobson circulation predicted by models. There is large uncertainty in changes in the deep branch of the Brewer-Dobson circulation inferred from observations in the mid and upper stratosphere.
  - Stratospheric ozone recovery and an acceleration of the Brewer-Dobson circulation in the future would both tend to increase the global tropospheric ozone burden. The projected net changes in tropospheric ozone and other compounds vary regionally and are scenario and model dependent.

- **Stratospheric temperature changes due to Antarctic ozone depletion are very likely the dominant driver of the observed changes in Southern Hemisphere tropospheric circulation in summer over recent decades, with associated surface climate and ocean impacts.**
  - The contribution of Antarctic ozone depletion to the observed increase in the Southern Annular Mode index in austral summer is substantially larger in most models than the contribution from greenhouse gas increases over the past three to five decades. An increase in this index corresponds to a decrease in atmospheric pressure at high latitudes, an increase at midlatitudes, and a poleward shift of the midlatitude jet. The role of ozone depletion is largest in summer. Observations and models suggest smaller Southern Annular Mode trends in other seasons.
  - Stratospheric ozone depletion has likely contributed to the observed expansion of the Southern Hemisphere Hadley Cell in austral summer.

- Climate models simulate a poleward shift of the Southern Hemisphere midlatitude maximum in precipitation and a moistening of the subtropics in response to stratospheric ozone depletion in austral summer. There is some evidence of a consistent pattern of trends in observations.
- Observational and modeling studies present a broadly consistent picture of the ocean's response to surface wind stress changes, which have likely been substantially caused by stratospheric ozone changes, with intensification of the subtropical ocean gyres and the meridional overturning circulations, and a subsurface warming. The impact of these wind stress changes on oceanic carbon uptake remains uncertain. The role of ocean eddies, which modify the ocean circulation and temperature response to wind stress changes, is better understood than at the time of the last Ozone Assessment, but remains a source of uncertainty.
- The influence of stratospheric ozone depletion on Antarctic sea ice increases reported in the last Ozone Assessment is not supported by a number of new coupled modeling studies. These suggest that ozone depletion drives a decrease in Southern Hemisphere sea ice extent and thus did not lead to the small observed increase. However, there is low confidence in this model result because of large uncertainties in the simulation of Antarctic sea ice.
- No robust link between stratospheric ozone changes and Northern Hemisphere tropospheric climate has been found, consistent with the conclusions of the previous Ozone Assessment.

- **There is further evidence that in austral summer over the next 50 years, Antarctic stratospheric ozone recovery and increases in greenhouse gases will have opposite effects on the Southern Hemisphere tropospheric circulation, with associated surface climate and ocean impacts.**
  - Ozone recovery is expected to drive a weakening and equatorward shift of the midlatitude jet, while increases in greenhouse gases are expected to drive a strengthening and poleward shift of the jet. Under a low greenhouse gas emissions scenario, ozone recovery is expected to dominate the effect of greenhouse gas increases on Southern Hemisphere tropospheric circulation in austral summer to give a weakening and equatorward shift of the midlatitude jet over the next 50 years, whereas in a high emissions scenario the jet is projected to continue to strengthen and shift poleward.
  - An equatorward shift in the Southern Hemisphere Hadley Cell boundary and extratropical rainfall in summer is simulated in response to ozone recovery. These changes offset a scenario-dependent fraction of projected greenhouse-gas induced changes in these variables.
  - Simulations from multiple models indicate that if the concentrations of ozone-depleting substances (ODSs) had continued to increase in the absence of the Montreal Protocol, the enhanced ozone depletion from uncontrolled ODSs would be expected to have led to substantial additional cooling in the Antarctic polar stratosphere, with associated changes in Southern Hemisphere circulation and rainfall patterns.

- **New estimates of global mean ozone radiative forcing due to emissions of ozone-depleting substances, which account for stratospheric ozone change and its indirect effect on tropospheric ozone, indicate a stronger surface cooling effect than that due to stratospheric ozone changes alone.**
  - The overall global mean ozone radiative forcing from the effects of ODS emissions on both tropospheric and stratospheric ozone is assessed to be −0.15 (−0.3 to 0) watts per square meter (W m^{-2}) in 2011. Approximately three quarters of this results from ozone changes in the stratosphere.
  - Models indicate that ODS-induced stratospheric ozone depletion has acted to decrease tropospheric ozone. This ODS-driven decrease in tropospheric ozone contributes to the overall negative ozone radiative forcing, although the magnitude is uncertain.
  - The radiative forcing due to observed decreases in stratospheric ozone concentration alone is estimated to be −0.05 W m^{-2} (−0.15 to 0.05) W m^{-2} in 2011. A rapid adjustment to radiative forcing may also arise from cloud changes, resulting from the circulation changes driven by ODS-induced ozone depletion. The radiative effect of this cloud adjustment may be of a larger magnitude than the non-adjusted forcing.
  - Uncertainty in future lower stratospheric ozone trends in the tropics precludes a confident assessment of the sign of future stratospheric ozone radiative forcing. Current models give a range of stratospheric ozone radiative forcing of −0.05 to +0.25 W m^{-2} in 2100 under a high greenhouse gas emissions scenario, which is generally suggestive of a slight warming contribution relative to present.

4.1 INTRODUCTION AND SCOPE

4.1.1 Summary of the Previous Ozone Assessment

Chapter 4 of the 2010 Ozone Assessment (Forster and Thompson et al., 2011) assessed stratospheric changes and their influence on climate. The chapter considered the tropospheric response to stratospheric change induced by greenhouse gases (GHGs), solar variability, and volcanic eruptions, as well as ozone. New data sets and improved simulations allowed an improved characterization of lower stratospheric temperature trends, and the influence of both natural and human factors was identified. The evolution of lower stratospheric temperature was described, with progressive cooling from 1960 to the late 1990s followed by a period with approximately constant temperature. Based on updated data sets the observed cooling was found to have occurred in the tropics as well as the extratropics and to have been similar at all latitudes in the annual mean. Ozone decreases were assessed to be the dominant driver of the observed long-term lower stratospheric cooling, with volcanic eruptions causing episodic warming. Temperature trends in the mid and upper stratosphere were assessed to be relatively uncertain, due to the existence of only a single reconstruction of satellite observed mid- and upper-stratospheric temperature available at the time.

The 2010 Ozone Assessment described an upward trend in stratospheric water vapor from 1980 to around 2000, followed by an abrupt decrease that was assessed to be sustained through to 2009 based on measurements available at the time. An increase of stratospheric aerosol concentrations of 4–7% yr^{-1} between the late 1990s and 2009 was reported, though the causes of the trend were not clear, with both volcanic sources and increased coal burning cited as possible contributors.

The radiative impact of stratospheric ozone on climate was concluded to be smaller than had previously been thought. The chapter concluded that much of the observed southward shift of the Southern Hemisphere tropospheric midlatitude jet in summer was due to Antarctic ozone depletion, which in turn had driven trends in surface winds and temperature over Antarctica. It was concluded with somewhat less confidence that Antarctic ozone depletion had contributed to the observed increase in Antarctic sea ice extent, a southward shift of the Southern Hemisphere storm track and associated precipitation, a warming of the subsurface Southern Ocean, and decreases of carbon uptake over the Southern Ocean. No link between Arctic ozone depletion and tropospheric circulation had been established.

Projected changes in stratospheric temperature were discussed, with GHGs driving a cooling, moderated by ozone increases driven by this cooling itself and by decreasing concentrations of ozone-depleting substances (ODSs). The opposing effects of ozone recovery and GHG increases on the latitude of the Southern Hemisphere midlatitude jet in summer were discussed, and the net effect of these forcings was assessed to be uncertain. The chapter reported that climate models simulate an increase in the Brewer-Dobson circulation (BDC) in response to GHG increases, consistent with earlier assessments. It was concluded that stratospheric ozone recovery would increase the transport of ozone into the troposphere.

4.1.2 Scope of the Chapter

The previous chapters of this report have described and assessed past and projected future changes in stratospheric ozone. This chapter assesses new research since the 2010 Ozone Assessment on the impact of those changes on climate. To facilitate easy comparison with the 2010 Ozone Assessment, this chapter will follow a similar structure to Chapter 4 of that Assessment (Forster and Thompson et al., 2011). Stratospheric ozone changes, together with changes in other stratospheric constituents, directly affect the radiative budget of the stratosphere, causing changes in stratospheric temperature and

circulation, which in turn influence tropospheric climate. Therefore after assessing observed variations in stratospheric constituents that relate to climate (Section 4.2), the chapter will continue to assess simulated and observed variations in stratospheric temperature and circulation, with a focus on attribution of observed changes to variations in ozone and other drivers (Section 4.3). The chapter will then assess the influence of stratospheric ozone changes on the troposphere, surface, and ocean, as requested by the Parties to the Montreal Protocol. In 1987 when the Montreal Protocol was signed, the impacts of stratospheric ozone depletion on tropospheric climate were not generally known, but over the past fifteen years an increasingly mature body of research on these impacts has developed. While the 2010 Ozone Assessment also considered the tropospheric response to other stratospheric changes, including changes in stratospheric water vapor, stratospheric aerosol, and solar irradiance variations, these topics were comprehensively assessed in the recently published Fifth Assessment Report of the Intergovernmental Panel on Climate Change (IPCC, 2013). For this reason this chapter will focus on the influence of stratospheric ozone change, with the influence of other stratospheric changes on climate discussed only briefly for context. Sections on the influence of stratospheric ozone on the troposphere in the past (Section 4.4) and future (Section 4.5) will start by considering ozone-induced effects on tropospheric circulation and resulting climate impacts, followed by sections considering radiative effects and chemical effects in turn.

4.2 OBSERVED CHANGES IN STRATOSPHERIC CONSTITUENTS THAT RELATE TO CLIMATE

The stratospheric constituents considered in this section impact climate directly through radiative effects and indirectly through their influence on stratospheric ozone. We review and assess observed variations in these constituents to inform our understanding and attribution of changes in stratospheric temperature and circulation.

4.2.1 Long-Lived Greenhouse Gases and Ozone-Depleting Substances

Carbon dioxide (CO_2), methane (CH_4), nitrous oxide (N_2O), and ODSs are all gases of tropospheric origin that impact climate both directly by absorbing and emitting long-wave radiation and indirectly by impacting stratospheric ozone. ODSs, N_2O, and CH_4 are source gases for compounds that deplete stratospheric ozone, whereas changes in CO_2 impact ozone through changes in stratospheric temperature and circulation.

Recent measurements and growth rates for ODSs and N_2O are covered in Chapter 1 of this report, with a summary of recent growth rates shown in Tables 1-1 and 1-12. The measurements and growth rates for CO_2 and CH_4 are covered in detail in the IPCC Fifth Assessment Report (Hartmann et al., 2013) and are briefly summarized here. The tropospheric abundance of CO_2 was around 390.5 parts per million (ppm) in 2011, which is around 40% greater than in 1750, and the average annual increase in globally averaged CO_2 concentration from 1980 to 2011 was 1.7 ppm yr^{-1} (2.0 ppm yr^{-1} since 2001) (Hartmann et al., 2013). There are large year-to-year variations (from an annual increase of around 0.7 ppm in 1992 to 2.9 ppm in 1998) that are primarily due to small changes in the balance between carbon fluxes from photosynthesis and respiration on land. Tropospheric CH_4 abundance was around 1803 ppb in 2011, which is 150% greater than before 1750. There have been substantial changes in the growth rate of CH_4 since 1980: there was an increase in the global-average annual abundance from 1980 to 1998, little change from 1999 to 2006, and an increase in atmospheric burden since 2007 (Ciais et al., 2013).

4.2.2 Stratospheric Water Vapor

Stratospheric water vapor is important for Earth's radiative balance (influencing stratospheric and tropospheric temperatures) and for stratospheric chemistry. Changes in stratospheric water vapor can alter

stratospheric ozone chemistry in several different ways: Water vapor is the main source of reactive hydrogen oxide molecules (HO_x) that destroy ozone, and changes in water vapor alter stratospheric temperatures (and hence rates of chemical reactions) and the formation of polar stratospheric clouds. Changes in stratospheric water vapor can also impact the stratospheric circulation, as well as the tropospheric midlatitude jets (Maycock et al., 2013).

As discussed in the previous Ozone Assessment (Forster and Thompson et al., 2011), satellite measurements of lower stratospheric H_2O from the early 1990s to the present show substantial variability, with a large (~ 0.6 ppmv) step-like decrease after 2001 followed by roughly constant values. In more recent years these measurements show an increase in both tropical and midlatitude lower stratospheric water vapor, and there is only a small net change between 2000 and 2012 both in the midlatitudes and in the tropics (Randel and Jensen 2013; Fueglistaler et al., 2013). These changes are observed in both balloon-borne and satellite measurements. Figure 4-1 compares balloon-borne measurements at Boulder, Colorado, with corresponding zonal mean satellite observations (Hurst et al., 2011). There are unresolved discrepancies between the balloon and satellite measurements over the period 1992–1996. An updated trend analysis of the full (1980–2010) Boulder record shows sensitivity to the time period considered for the trends (due to the large decadal variability, Figure 4-1) and to the altitude (Hurst et al., 2011). For the full 30-year period there is a net increase of 1.0 ± 0.2 ppm between 16–26 kilometers (which corresponds to around 0.75% yr^{-1}).

The principal sources of water vapor in the bulk of the stratosphere are entry through the tropical tropopause and CH_4 oxidation. There is a small additional source from oxidation of molecular hydrogen (H_2). In the extratropical lowermost stratosphere, an additional source of water vapor is quasi-horizontal (isentropic) transport across the subtropical tropopause and deep convection, while dehydration in the polar lower stratosphere is a sink. Long-term H_2O trends are due to trends in the flux of water vapor entering the stratosphere and increased production of H_2O from CH_4 oxidation (for example, around 30% of the 1980–2010 increase in water vapor over Boulder can be attributed to increases in CH_4; Fujiwara et al., 2010; Hurst et al., 2011). Many of the year-to-year and longer variations in the observational H_2O record can be linked to observed changes in tropical tropopause temperatures but some discrepancies still exist (e.g., Schoeberl et al., 2012; Fueglistaler et al., 2013; Randel and Jensen, 2013). For example, the long-term trends cannot be reproduced with trajectory-based models based on observed changes in tropical

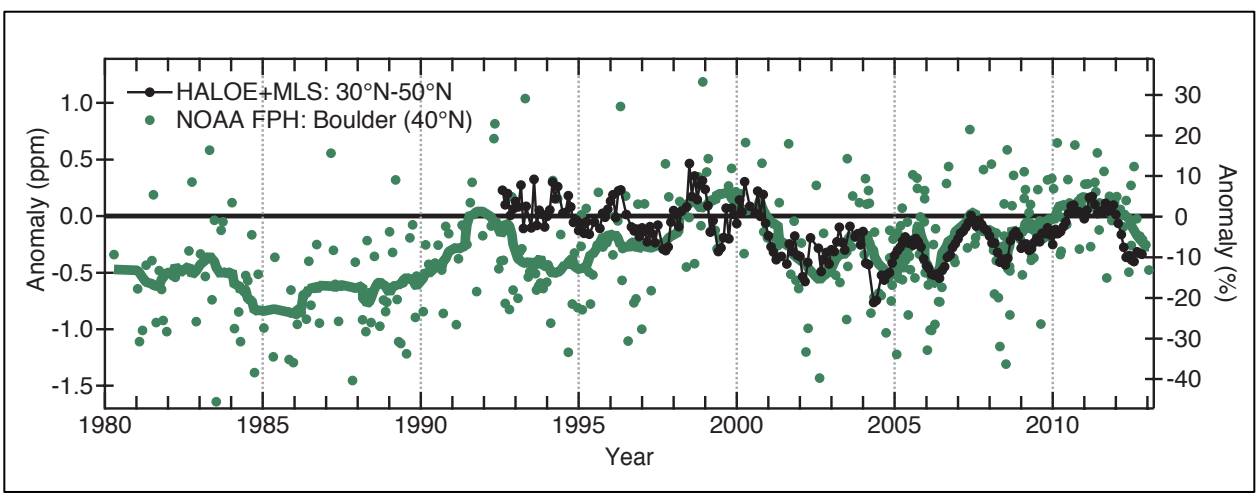

Figure 4-1. Water vapor anomalies in the Northern Hemisphere lower stratosphere (~16–19 km) from satellite sensors and in situ measurements normalized to 2000–2011. Approximately monthly balloon-borne measurements (FPH = frost point hygrometer) of stratospheric water vapor from Boulder, Colorado, at 40°N (green dots; green curve is 15-point running mean) averaged over 16–18 km and monthly means at 83 hPa for 30°N–50°N (black) determined from Halogen Occultation Experiment (HALOE) and Microwave Limb Sounder (MLS) satellite sensors. Updated from Figure 2.5 of Hartmann et al. (2013), which is updated from Solomon et al. (2011).

tropopause temperatures. It is still unclear whether the inability to model the observed trends is due to the large uncertainties in the observed stratospheric water vapor and tropical tropopause temperatures (e.g., Wang et al., 2012), uncertainties in the models, or whether the models have missing mechanisms.

4.2.3 Stratospheric Aerosols

Stratospheric aerosols influence climate in many ways, including shortwave radiative forcing (with surface cooling following an increase in stratospheric aerosols), changes in circulation caused by differential (vertical or horizontal) heating, and by changing stratospheric ozone with its associated radiative and circulation impacts. Observed changes in stratospheric aerosols are discussed in Section 2.3.4 of Chapter 2 of this Assessment. Briefly, the eruption of Mt. Pinatubo in 1991 was the last major volcanic eruption and the current stratospheric aerosol concentrations are much lower than in the years immediately following this eruption**.** However, as reported in the previous Ozone Assessment (Forster and Thompson et al., 2011), there has been an increase in stratospheric aerosol optical depth since the late 1990s, with an average increase of 4–10% per year from 2000–2010 (see Figure 2-18 of Chapter 2).

4.2.4 Ozone

As discussed in detail in this chapter, changes in stratospheric ozone influence climate both by direct radiative effects and by affecting stratospheric and tropospheric circulation. Past changes in global and polar stratospheric ozone are reviewed in Chapters 2 and 3, respectively, and only the key points are briefly summarized here.

There is substantial year-to-year variability in extratropical column ozone, but there have been only weak trends since 2000, especially compared to the large decreases observed from 1980 to the mid-1990s. The differences between total column ozone in the recent past (circa 2008–2012) and pre-1980 values are similar to those quoted for 2006–2008 in the previous Ozone Assessment (Forster and Thompson et al., 2011), i.e., near-global (60°N–60°S) column ozone is approximately 2% lower than pre-1980 values. The Antarctic ozone hole has continued to form each year, with springtime Antarctic (October, 60–90°S) column ozone values substantially lower than pre-1980 values. There has, however, been large year-to-year variability in the ozone amount in the last few years, due to variability in stratospheric temperatures and dynamical processes. Large year-to-year variability is also evident in tropical lower stratospheric ozone concentrations, complicating the detection of long-term trends there.

4.3 OBSERVED AND SIMULATED CHANGES IN STRATOSPHERIC CLIMATE

The previous section summarized the observed changes in long-lived GHGs and ODSs, as well as stratospheric water vapor, aerosols, and ozone (see also Chapters 1–3 of this Assessment). Changes in these constituents have a direct impact on stratospheric temperatures through their radiative effects, which in turn can affect the stratospheric circulation. In this section, we assess observed changes in stratospheric temperature and circulation and simulated changes in the past and future, as well as current understanding of the causes of these changes. In addition to influencing tropospheric climate, stratospheric temperature and circulation are also important drivers of stratospheric ozone change (Box 3-2 of Chapter 3).

4.3.1 Stratospheric Temperature

4.3.1.1 OBSERVATIONS

Identifying robust long-term trends in stratospheric temperature requires records of at least a few decades and global coverage. Observations of stratospheric temperatures are mainly derived from

balloon-borne radiosondes and satellite retrievals. Radiosondes provide measurements since 1957 over an irregular network with quasi-global coverage, although certain regions such as the oceans and the Antarctic are poorly sampled. Radiosondes have very good vertical resolution in the lower stratosphere, but coverage does not extend to the middle and upper stratosphere. Microwave Sounding Unit (MSU) and Stratospheric Sounding Unit (SSU) satellite instruments provided global coverage measurements from late 1978 to 2005. However, their vertical resolution is coarse as they measure over broad altitude ranges corresponding to the instrument weighting functions. The highest MSU channel (MSU channel 4) peaks in the lower stratosphere near 20 km, while SSU channels peak in the middle and upper stratosphere, at 25–35 km (SSU channel 1), 35–45 km (SSU channel 2), and 40–50 km (SSU channel 3). SSU channels 1, 2, and 3 are also referred in the literature as channels 25, 26, and 27, respectively. MSU and SSU instruments have now been replaced by the Advanced Microwave Sounding Unit (AMSU; in service since 1998), which has channels covering the domains of both the MSU and SSU instruments.

New trend estimates in the lower stratosphere, published since the last Ozone Assessment and based on longer records of several radiosonde and satellite temperature data sets, agree with previous estimates of temperature trends in this region. The global mean temperature in the lower stratosphere decreased by around 1 K from 1979 to 2012, as shown in Figure 4-2 in MSU channel 4 data processed by three different institutions (RSS, UAH, and NOAA; see also Hartmann et al., 2013). Short-term warming periods appear after the volcanic eruptions of El Chichón (1982) and Mt. Pinatubo (1991), and a lack of any statistically significant trend in globally averaged lower stratospheric temperatures since the mid-1990s continues to 2012 (Thompson et al., 2012; Seidel et al., 2011). Estimates of lower stratospheric temperature trends from radiosondes and the MSU instrument up to 2012 are listed in Table 2.8 from the IPCC AR5 (Hartmann et al., 2013).

Interest in temperature trends in the middle and upper stratosphere has grown recently. While the tropospheric climate response may be most sensitive to changes in stratospheric composition and temperature in the lower stratosphere (e.g., Forster and Shine, 1997), trends in the middle and upper stratosphere are potentially useful for understanding stratospheric circulation changes. The number of temperature data sets available in the middle and upper stratosphere is much smaller than in the lower stratosphere and as discussed below, the trend uncertainties are larger. SSU data from a series of instruments are available from 1979, SSU and AMSU data are available from 1998 to 2005, and only AMSU data are available after 2005. Like most satellite data, SSU data require several corrections before they can be used for climatic studies. These corrections are related to 1) the cell of CO_2 that is used to calibrate the long-wave emissions, which leaks over time, changing the altitudes measured, and whose CO_2 content also varies among SSU instruments (Kobayashi et al., 2009); 2) interactions between the large amplitudes of the diurnal and semidiurnal thermal tides in the middle and upper stratosphere and satellite orbital drift (Nash and Forrester, 1986), and 3) the long-term increase in CO_2 in the atmosphere, which can change the weighting function of the instruments and thus the altitudes measured (Shine et al., 2008). In addition, there is no overlap period between several pairs of consecutive satellites and thus, merging data from different satellites may produce inaccurate results. Comparison with radiosonde observations is also not possible since radiosonde data are not generally available at these altitudes.

Only two independent analyses of SSU data are available. Originally, SSU data were processed by scientists at the U.K. Met Office in the 1980s (Nash and Forrester, 1986; Nash, 1988) and this data set was subsequently updated by Shine et al. (2008) and Randel et al. (2009). Recently, an additional alternative analysis of SSU data has been generated by Wang et al. (2012), taking advantage of improvements in radiative transfer modeling. Figure 4-2 (left panels) shows the global mean stratospheric temperature anomalies since 1979 in the three SSU channels as produced by Wang et al. (NOAA STAR, red line) and Shine et al. (Met Office, blue line). Comparison of these data sets (Thompson et al., 2012) shows that global mean trends are similar in the upper stratosphere (SSU channel 3). However, in the middle stratosphere, the two data sets exhibit differences in SSU channels 1 and 2 of as large as 0.5 K decade^{-1}, with the NOAA STAR data set showing a global mean cooling almost twice as large as the Met Office data set (Wang et al., 2012; Thompson et al., 2012). The full reasons for these discrepancies remain unknown (e.g., Nash and Saunders, 2013), but planned updates to the data sets may resolve the discrepancies in part.

Thus, the agreement between satellite measurements and radiosonde observations over the longer record since the 2010 Ozone Assessment increases confidence in the robustness of the temperature trends in the lower stratosphere. Observed changes in global-mean temperature in the middle and upper stratosphere are considerably more uncertain. All data sets exhibit a cooling trend from 1979 to 2005 (to 2012 for the lower stratosphere), which is stronger in the upper stratosphere than at lower levels, consistent with physical understanding.

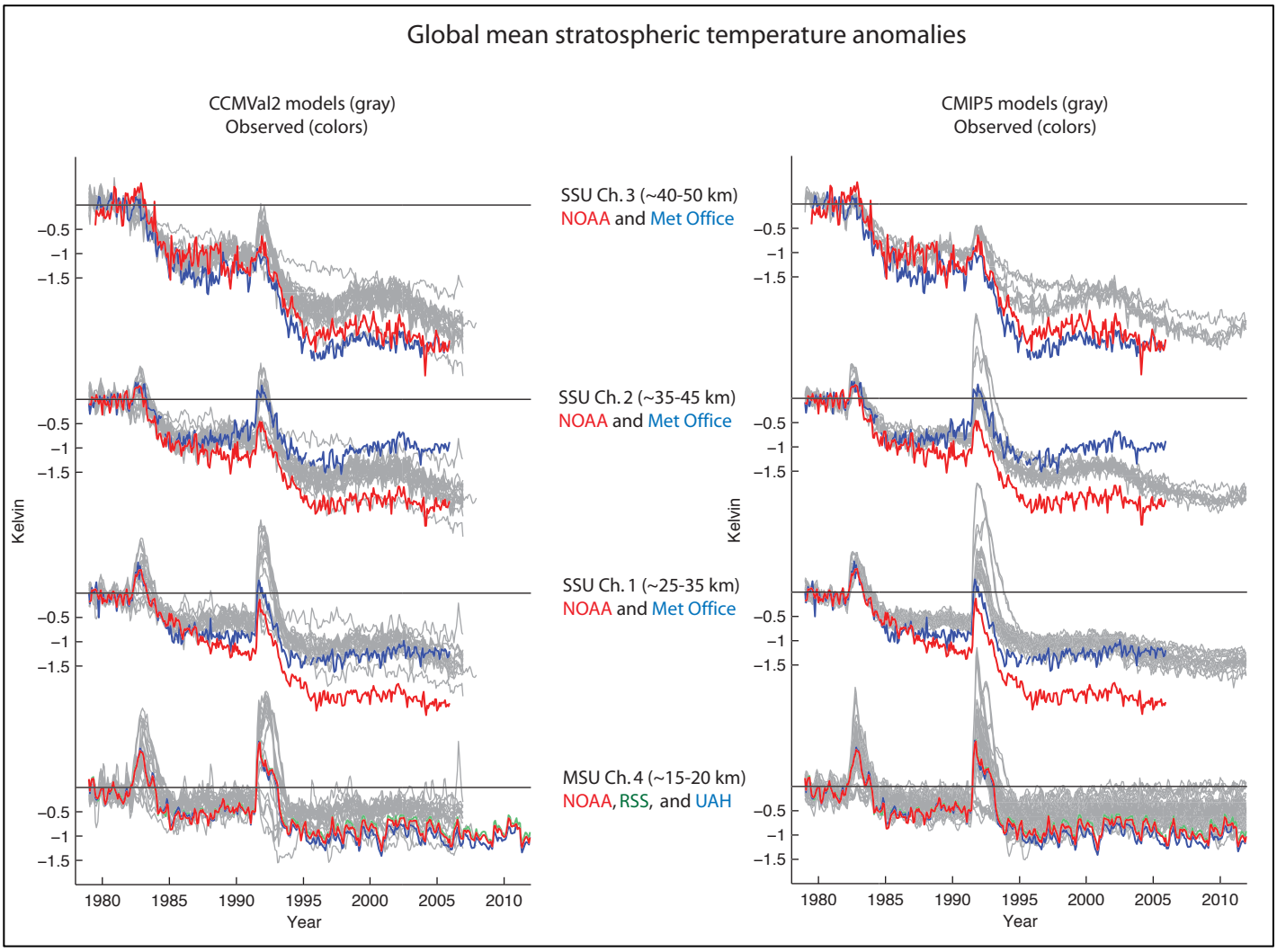

Figure 4-2. Time series of global mean stratospheric temperature anomalies from 1979 to 2012 for SSU channels 1-3 (*top three rows*) and MSU channel 4 (*bottom row*) for the altitude ranges, data sets, and model output indicated. Colored lines indicate results based on observations processed by different research groups: the Met Office (blue in top three panels), Remote Sensing Systems (green), the University of Alabama-Huntsville (blue in bottom panel) and the National Oceanic Atmospheric Administration Center for Satellite Applications and Research (red). Gray lines indicate results from the Chemistry-Climate Model Validation-2 (CCMVal2) and Coupled Model Intercomparison Project Phase 5 (CMIP5) models weighted by the appropriate satellite weighting function for easy comparison with observations. Time series are plotted so that their 1979–1982 mean anomalies are zero. Adapted from Thompson et al. (2012).

Seasonal and spatial structure of trends

Changes in the seasonal and spatial patterns of stratospheric temperature trends can arise from the radiative response to homogeneous changes in long-lived GHGs (Fels et al., 1980; Forster and Shine, 1999), constituents with a strong spatial and seasonal structure (such as ozone), as well as changes in the stratospheric mean meridional circulation (as will be discussed in Section 4.3.2). The pattern of zonal mean lower stratospheric temperature trends as a function of month over the period 1979–2012 (Figure 4-3a, b) is similar to that shown over the period 1979–2007 in the previous Ozone Assessment (Forster and Thompson et al., 2011). The largest trends in lower stratospheric temperatures occur over the Antarctic in November and December in satellite data (Figure 4-3a) and October–November in HadAT (Hadley Centre Atmospheric Temperature) radiosonde data (Figure 4-3b) following the maximum in ozone depletion in October. However, this feature is somewhat sensitive to the period over which the trend is calculated due partly to the

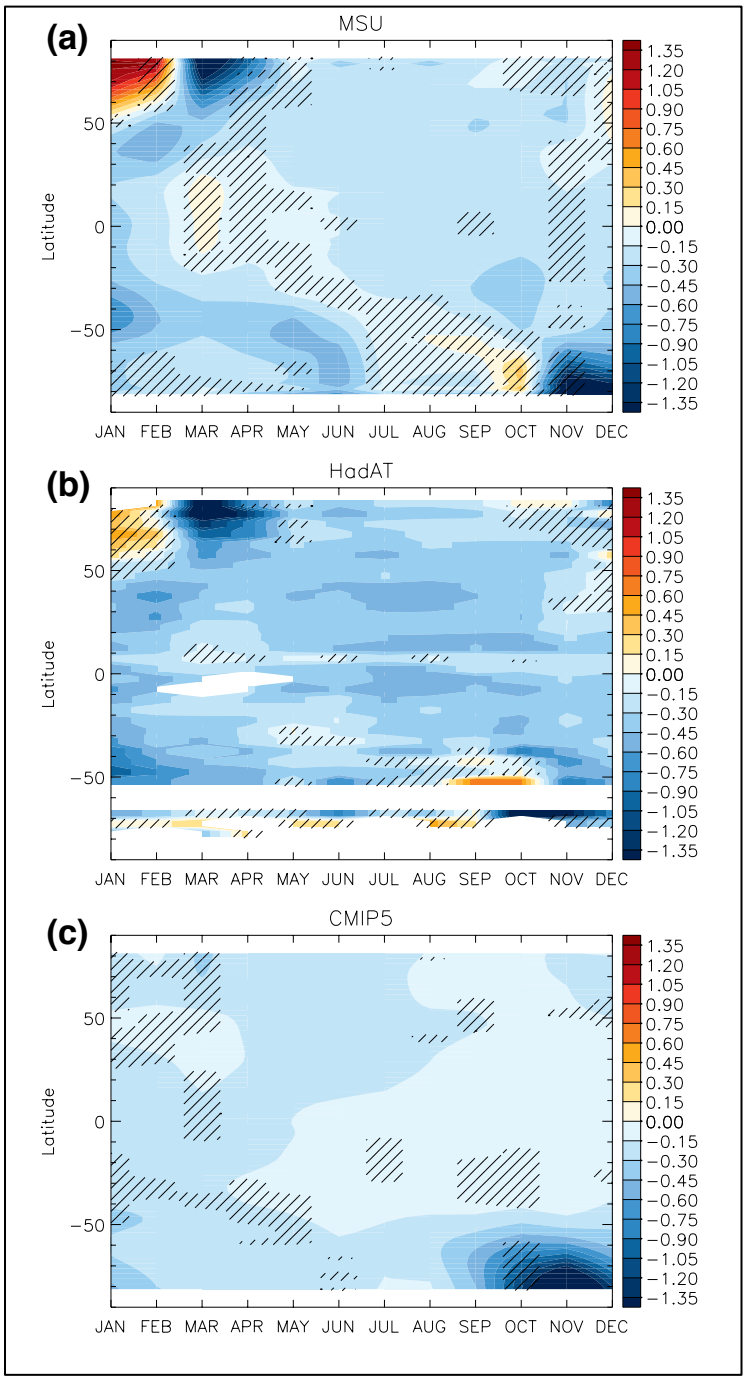

Figure 4-3. Lower stratospheric temperature trends over the period 1979–2012 in K per decade as a function of latitude and month from (a) satellite MSU RSS v3.3 (channel 4); (b) HadAT radiosonde (averaged with the MSU channel 4 weighting function), and (c) synthetic MSU channel 4 temperatures from merged CMIP5 historical and RCP8.5 (Representative Concentration Pathway) simulations covering 1979–2012 taken from Santer et al. (2013). The following volcano years are treated as missing data (1982, 1983, 1991, 1992, 1993) and trends are calculated where at least 50% of monthly anomalies are present over the 1979–2012 period. The hatching in a) and b) shows where the observed trend is within the 5–95% range of simulated internal variability and thus not significant, where internal variability is assessed from the spread of trends in the CMIP5 historical simulations. Hatching in c) shows where the observed MSU trend in (a) lies outside the 5–95% range of trends simulated in the 33 individual CMIP5 simulations, thus showing thus showing areas where the simulated and observed trends are inconsistent.

large internal variability in this region (Figure 4-4). Anomalously warm conditions over Antarctica in 2002–2006 were followed by anomalously low temperatures in the period 2007–2010. In the Arctic, both satellite and radiosonde observations agree on a large warming trend in January and February and large cooling trend in March and April (Figure 4-3a and b) although some of these trends are not statistically robust, likely because of the large interannual variability at high latitudes, particularly in the Northern Hemisphere, and decadal variability possibly associated with changes in the seasonal distribution of Sudden Stratospheric Warmings (Gómez-Escolar et al., 2012). In the tropics, the seasonal cycle is amplified through the significant cooling from June to October and December to February observed in satellite data (Figure 4-3a) as pointed out in the last Ozone Assessment (Forster and Thompson et al., 2011) and confirmed in radiosonde observations (Figure 4-3b and Free et al., 2011). However, it is not clear whether the changes in the seasonal patterns in the tropical lowermost stratosphere represent a long-term trend or are related to decadal-scale variability (Free, 2011).

In the middle and upper stratosphere, there are large differences between the latitudinal structure of the trends in the NOAA STAR (Wang et al., 2012) and Met Office (Shine et al., 2008) SSU data sets (not shown; see Thompson et al., 2012). Large meridional variations are present in the NOAA STAR data set, with the largest cooling trend in the tropics, and decreasing trends toward the high latitudes, with smaller trends in the Antarctic than in the Arctic. In contrast, the Met Office data set shows a relatively uniform cooling at all latitudes in the middle stratosphere (channels 1 and 2). Near the stratopause (channel 3), the high-latitude differences between the data sets reverse and the Met Office data set exhibits a larger cooling than the NOAA STAR data set (Thompson et al., 2012).

In summary, in the lower stratosphere, there is high confidence in the observations of the global mean trends and good agreement across different data sets. This is not the case in the mid and upper stratosphere, where only satellite data are available and different satellite reconstructions exhibit different trends. Changes in mid- and upper-stratospheric temperature are relevant to the climate change signal detection problem and as explained in Section 4.3.2, they are used to characterize changes in the BDC, which in turn can affect the amount of ozone entering the troposphere. Uncertainties in the seasonal and spatial patterns of stratospheric temperature trends are larger than those in the global mean especially in the dynamically active season in each hemisphere, boreal winter and austral spring.

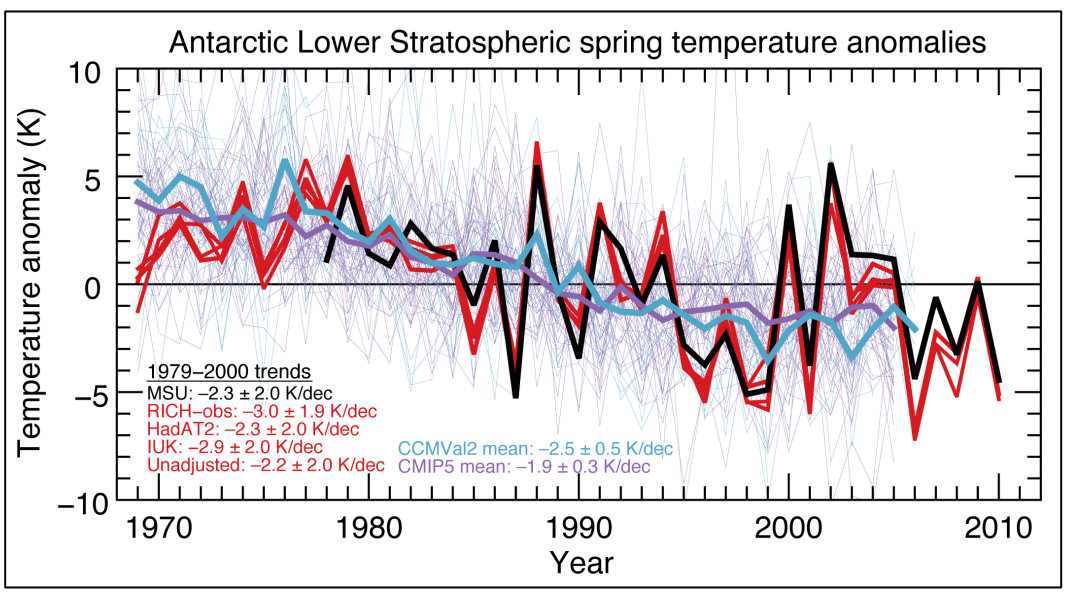

Figure 4-4. Time series of MSU channel 4-weighted temperature anomalies for the October to January average for four different radiosonde data sets and the unadjusted radiosondes at the Antarctic locations examined by Thompson and Solomon (2002) (red), MSU channel 4 data (black), the CMIP5 ensemble mean (purple), and the CCMVal-2 models and ensemble mean (blue). Individual model results are shown with the thin blue and purple lines. Adapted from Young et al. (2013b).

4.3.1.2 SIMULATED PAST AND FUTURE CHANGES

Temperature changes in the stratosphere can have a natural or anthropogenic origin, and attribution of the past or projected changes to a given driver relies on using climate model simulations. Since the last Ozone Assessment, two types of models have been widely analyzed for climate purposes in the stratosphere: Chemistry-Climate Models (CCMs) and atmosphere-ocean general circulation models (AOGCMs). They are described in Box 2-2, along with details of the model intercomparison projects in which such models are compared. While the last Ozone Assessment (Forster and Thompson et al., 2011) relied principally on CCM simulations, this Assessment makes use of results from a more comprehensive set of CCM and AOGCM simulations.

Figure 4-2 shows time series of global mean stratospheric temperatures simulated by CCMs (from the Chemistry-Climate Model Validation-2 (CCMVal-2) experiment) and AOGCMs (from the Coupled Model Intercomparison Project Phase 5 (CMIP5) experiment) together with the time evolution of satellite observations from different channels, corresponding to the different altitude ranges already discussed above. Model data have been weighted by the satellite weighting functions. The model simulations were forced with changes in well-mixed GHGs, anthropogenic aerosols, and stratospheric ozone or ODSs, as well as with changes in solar irradiance, volcanic aerosols, and in the case of most CMIP5 simulations, land use change. It is clear that both sets of models exhibit a global mean cooling trend at all levels, which is larger in the upper stratosphere in general agreement with the observations. Nevertheless, there are discrepancies in the magnitude of the long-term cooling.

For the lower stratosphere, both sets of models underestimate the global mean cooling seen in the MSU channel 4 measurements (Thompson et al., 2012; Santer et al., 2013; Charlton-Perez et al., 2013). The cause (or causes) of the model-observation discrepancy remains unexplained at this time, but could relate to forcing errors related to ozone trends or prescribed stratospheric aerosol loadings (Free and Lanzante, 2009; Solomon et al., 2011; Santer et al., 2013), as well as errors in the evolution of the modeled stratospheric water vapor (Gettelman et al., 2010; Maycock et al., 2014), or even errors in the model radiation code (Forster et al., 2011). For example, the prescribed ozone data set used by most of the CMIP5 models without interactive chemistry (Cionni et al., 2011) has been shown to underestimate Antarctic ozone depletion relative to the 1979–2007 observations (Cionni et al., 2011; Hassler et al., 2013), although only a subset of models in Figure 4-2 used this data set and the discrepancy shown here is for the global mean temperature. Stratospheric water vapor changes (Section 4.2.2) are estimated to have cooled the lower stratosphere by up to ~0.2 K decade^{-1} in the global and annual mean from 1980–2010, a substantial portion of the total trend (Maycock et al., 2014). However, stratospheric water vapor changes in this region are likely dominated by indirect climate feedbacks due to global warming (Dessler et al., 2013), rather than forced by increases in methane.

In the middle stratosphere at around 30 km (SSU channel 1), both the CCMVal2 and CMIP5 models exhibit cooling trends more in agreement with the Nash and Forrester (1986) Met Office SSU data set than the Wang et al. (2012) NOAA SSU data set. At altitudes centered around 40 km (SSU channel 2) the models lie in between both observational data sets. In the upper stratosphere, where the agreement between the two SSU data sets is better, the models show a smaller cooling than observed. Some of the model-observation differences were already highlighted in the previous Ozone Assessment based on the CCMVal2 models (Forster and Thompson et al., 2011). The fact that the differences remain in the CMIP5 AOGCMs (Thompson et al., 2012; Santer et al., 2013) suggests that they are not related to coupling to the ocean. The reasons for these model-observation differences or the discrepancy between SSU data sets remain unknown.

When comparing the latitudinal and seasonal distribution of lower stratospheric zonal mean temperature trends (Figure 4-3) there is a tendency for models to overestimate the seasonal extent of the Southern Hemisphere polar cooling and underestimate the tropical cooling over the past three decades, compared to the observations (see also Thompson et al., 2012; Santer et al., 2013). Over the Antarctic, the simulated cooling trend over the 1979–2012 period is more consistent with observations than over the shorter 1979–2005 period (Charlton-Perez et al., 2013; Santer et al., 2013). At high latitudes, there are

large differences between the pattern of zonal mean trends in the models and satellite observations (Thompson et al., 2012), which may reflect trends in the circulation (see Section 4.3.2.1).

For the high latitude Southern Hemisphere in particular, modeling studies have shown that stratospheric ozone depletion is the main driver of polar temperature trends in the lower stratosphere region during austral spring and summer (e.g., McLandress et al., 2011; Polvani et al., 2011b). The comparison of CCMs carried out as part of CCMVal-2 (SPARC CCMVal, 2010) concluded that the ensemble mean temperature showed too strong a cooling between 1969–1998, as compared with observations reported by Thompson and Solomon (2002), which has been used as a benchmark in this type of study. Recently, Young et al. (2013b) compared several different sets of radiosondes and found a cooling trend in November at 100 hPa in the range of −3.8 to −4.7 K decade^{-1} for the same period, around 50% larger than that reported by Thompson and Solomon (2002). Comparing over different periods with several observational data sets, Calvo et al. (2012) and Young et al. (2013b) concluded that the ensemble mean of both CCMVal-2 and CMIP5 exhibits cooling trends for the Southern Hemisphere lower stratosphere polar cap that are not significantly different from observations, although there is a large spread for individual models (Figure 4-4), and those underestimating ozone depletion also underestimate the temperature trends (Young et al., 2013b). Lower stratosphere temperature trends for the Southern Hemisphere polar cap are also characterized by zonal asymmetries in September and October (e.g., Lin et al., 2009). However, while Wang and Waugh (2012) found that CCMs forced with observed sea surface temperatures (SSTs) can qualitatively reproduce the observed seasonal pattern of lower stratospheric temperature variations, there is a large contribution from internal variability, and the pattern of the trends can differ substantially between different realizations from the same model. This is consistent with a large role for internal variability in generating the observed seasonal and spatial pattern of trends.

Over the recent past, global mean lower stratospheric temperatures calculated from simulations with individual forcings (Figure 4-5) suggest that ozone changes (or equivalently ODSs) are the dominant driver of lower stratospheric cooling, with greenhouse gas increases making a smaller cooling contribution, and volcanic aerosol driving episodic warming following large volcanic eruptions (Eyring et al., 2006; Ramaswamy et al., 2006; Dall'Amico et al., 2010; Gillett et al., 2011; Lott et al., 2013). An analysis of five CMIP5 model simulations of the combined response to all major anthropogenic and natural influences shows they are able to reproduce the observed evolution of global mean lower stratospheric temperature reasonably well, although with the caveats mentioned above (Figure 4-5). The

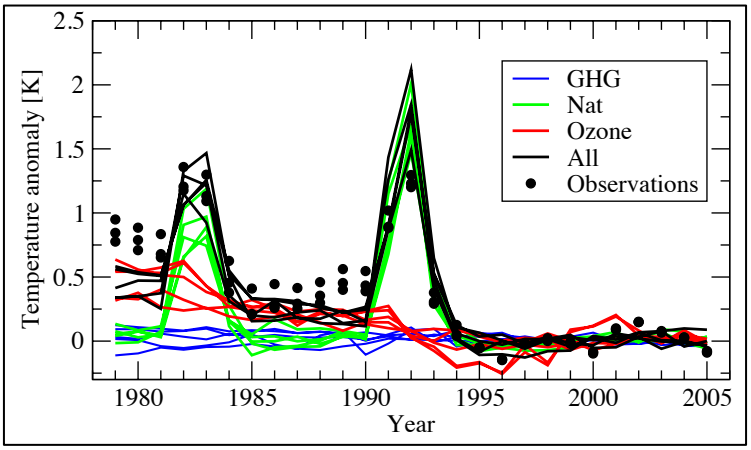

Figure 4-5. Time series of observed (black dots) and simulated global mean (82.5°S–82.5°N) synthetic MSU lower stratosphere temperature anomalies in a subset of CMIP5 simulations forced with anthropogenic and natural forcings (black), well mixed greenhouse gases (blue), natural forcings (green) and stratospheric and tropospheric ozone (red). Anomalies are calculated relative to 1996–2005. Ensemble means of the following models are shown: CCSM4, CESM1-CAM5, CanESM2, GISS-E2-H, GISS-E2-R. Adapted from Ramaswamy et al. (2006) and Bindoff et al. (2013).

models generally capture the step-like temperature reduction after episodic warming from major volcanic eruptions but the overall cooling trend (−0.29 ± 0.03 K decade^{-1}) from 1979–2005 is slightly less than observed (–0.34 ± 0.05 K decade^{-1}). Simulated changes in stratospheric and tropospheric ozone alone lead to much larger lower stratospheric temperature trends (–0.20 ± 0.04 K decade^{-1}) than increases in GHGs (–0.01 ± 0.03 K decade^{-1}). Simulations with individual forcings have also been used to examine the drivers of temperature trends in the tropical lower stratosphere. Polvani and Solomon (2012) suggested that the observed seasonal cycle of tropical lower stratospheric temperature trends correlates well with the seasonal cycle of tropical ozone trends, although these appear to be largely driven by trends in the BDC (Lamarque and Solomon, 2010; Mclandress et al., 2010) (see Section 4.3.2).

Such individual forcing simulations may also be used to attribute observed changes in stratospheric temperature by regressing observed changes onto the patterns of response simulated by the models in an attribution analysis. Gillett et al. (2011) used output from the CCMVal-2 simulations to partition observed MSU lower stratospheric temperature trends into components attributable to changes in GHGs, ODSs, and natural forcings. They found that both natural forcings and ODSs contributed significantly to the observed lower stratospheric cooling over the 1979–2005 period, with the influence of ODSs dominating, whereas the influence of greenhouse gas changes was not detectable in the observations. In the mid and upper stratosphere, Gillett et al. (2011) could detect the response to combined anthropogenic forcing (ODSs + GHGs) and natural forcings in SSU measurements, but the GHG and ODS influences were not separately detectable. However, conclusions related to the SSU data should be treated as tentative due to the large uncertainties in these observations, as discussed above. The attribution of temperature trends using one model was found to be sensitive to the height of the model top (Mitchell et al., 2013), though Charlton-Perez et al. (2013) did not find significant differences between lower stratospheric temperature trends in high-top and low-top CMIP5 models.

An important driver of the future evolution of stratospheric temperatures is the relative rate of increase of GHGs and stratospheric ozone. Relative to present day, the recovery of the ozone layer will act to warm the stratosphere over future decades. Increasing GHGs both cool the stratosphere radiatively and induce changes in the stratospheric mean meridional circulation, as discussed in Section 4.3.2. Hence, the projected GHG and ozone changes oppose each other and their relative importance in future projections varies across scenarios and models (Figure 4-6). Projected temperature changes also vary both regionally and with altitude. In the tropics, models simulate a stratospheric cooling trend that is larger at higher altitudes (e.g., Oman et al., 2010) as a result of increasing GHGs. They also exhibit tropical cooling (Figure 4-6) which increases with the magnitude of the GHG forcing. At high latitudes, the future response in the lower stratosphere exhibits seasonal structure. For the Southern Hemisphere high latitudes, warming is projected in late spring and early summer, and cooling in winter. The Northern Hemisphere high latitudes are projected to warm in winter and early spring although the trends are not statistically significant.

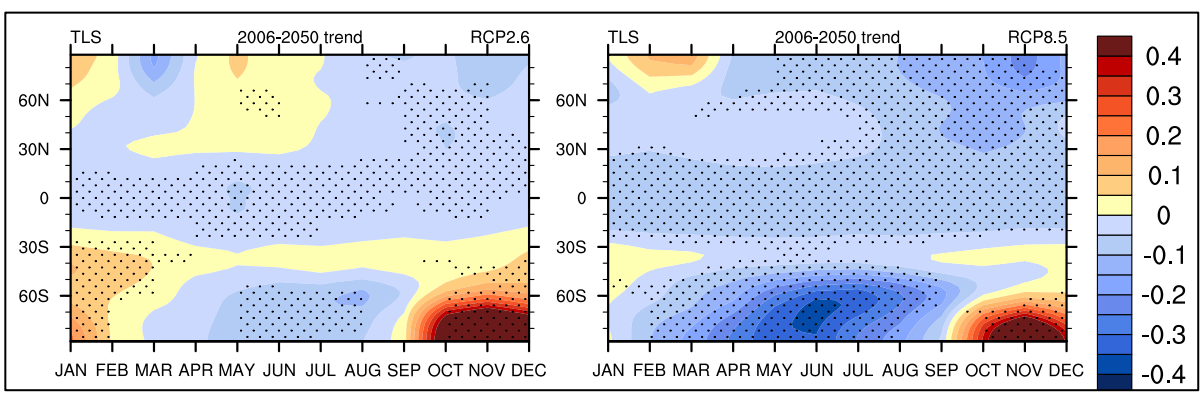

Figure 4-6. CMIP5 multi-model mean zonal mean lower stratospheric temperature trends (K per decade) over the period 2006–2050 under the low emissions scenario, RCP2.6 (*left*) and the high emissions scenario, RCP8.5 (*right*). Multi-model mean trends significant at the 5% level are stippled.

4.3.2 Stratospheric Meridional Circulation

4.3.2.1 OBSERVATIONS

Since the 2010 Ozone Assessment, many studies have advanced our understanding of the stratospheric meridional circulation (the so-called Brewer-Dobson circulation, BDC) and its changes. While before 2010 most of the focus of the investigations was on the changes in the tropical upwelling in the lower stratosphere, recent studies have highlighted the importance of differentiating two branches of the stratospheric circulation, the shallow and deep branches (Plumb 2002; Birner and Bönisch 2011; Bönisch et al., 2011). The shallow branch appears in the lowermost stratosphere with rising air in the tropics and descending air in the subtropics and middle latitudes, while the deep branch reaches the upper stratosphere and the descending branches extend to the mid and high latitudes, shown schematically in Figure 4-7. Birner and Bönisch (2011) compared these two branches of the Brewer-Dobson circulation and found that the deep branch was characterized by a much longer transit time (defined as the time an air parcel needs to be transported from the entry point at the tropical tropopause to a given arrival location), smaller integrated mass flux, and stratospheric entry latitudes closer to the equator. As the circulation is driven by wave dissipation, and different waves dissipate in different regions, the type of waves driving the shallow and deep branches differs.

It is now well established across many different model simulations that a strengthening of the BDC is simulated in response to increasing GHG concentrations through changes in wave dissipation driven by climate change (e.g., Butchart, 2014). Ozone changes on regional and seasonal scales also modulate changes in the meridional circulation at these scales through changes in local radiative heating, temperature, and zonal wind patterns, impacting wave-mean flow interactions (e.g., Lin and Fu, 2013). As pointed out in the last Ozone Assessment (Forster and Thompson et al., 2011), trends in the BDC are not easy to detect in observations because trends are small and thus difficult to separate from natural variability, and the BDC cannot be measured directly with available observations, so needs to be inferred from changes in other variables such as the latitudinal distribution of temperature, the amplitude of the quasi-biennial oscillation (QBO), chemical constituents, and the estimated age of air.

Based on the out-of-phase relationship between temperature changes in the tropics and high latitudes, the 2010 Ozone Assessment noted that observed changes in temperature are consistent with an acceleration of the BDC in the lower stratosphere (e.g., Thompson and Solomon, 2009; Fu et al., 2010). This has been corroborated recently by studies of radiosonde data sets (Free, 2011; Young et al., 2012) and satellite data (Young et al., 2012), although the role of decadal variability in the apparent trend and the possible role of changes in the seasonal cycle of the circulation are not clear yet. Kawatani and

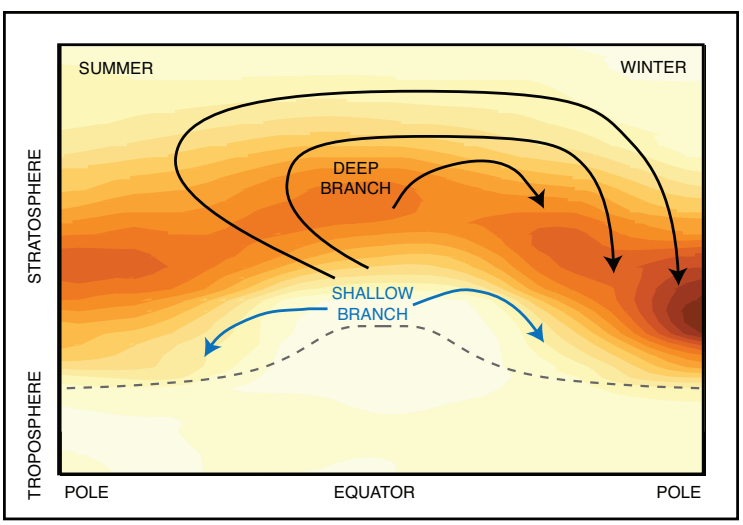

Figure 4-7. Schematic illustration of the shallow and deep branches of the Brewer-Dobson circulation in the stratosphere at solstices. Also shown is the meridional cross section of Northern Hemisphere winter ozone density (color shading, with darker shades indicating larger ozone concentrations, based on the Bodeker et al. (2013) climatology), and the approximate location of the tropopause (dashed curve). Adapted from Plumb (2002) and IPCC/TEAP (2005).

Hamilton (2013) found a significant decrease in the amplitude of the QBO at 70hPa between 1953 and 2013 based on radiosonde zonal wind measurements at near-equatorial stations and attributed it to an increased upwelling in the lowermost stratosphere that hampered the downward penetration of the QBO into this region. At higher levels in the stratosphere, Young et al. (2012) used the Met Office SSU data to diagnose a strengthening of the Northern Hemisphere branch of the BDC in December and the Southern Hemisphere branch of the BDC in August over 1979–2005, but only after removing year-to-year variability. However, as noted in Section 4.3.1.1, the Met Office SSU temperature trends have a different latitudinal structure to the NOAA STAR data (Thompson et al., 2012), meaning that the BDC trend inferred from each data set would be different. Thus, there are large uncertainties in the changes in the upper branch of the BDC inferred from temperature observations.

In addition to inferences made from observed temperature variations, changes in the BDC can also be inferred from measurements of chemical species. Decreasing ozone in the lowermost tropical stratosphere has been measured by satellite instruments and ozonesondes from 1985 to 2010 (Randel and Thompson, 2011; Sioris et al., 2014), consistent with an acceleration of the BDC in the lower stratosphere. However, the early years of the record are subject to substantial observational uncertainties (Solomon et al., 2012). Several recent studies using shorter records, subject to large interannual variability, are not long enough to corroborate such trends. More details on tropical ozone changes can be found in Chapter 2 (Section 2.3.5.3).

Recently, Stiller et al. (2012) presented new age-of-air estimates derived from more than 10^6 SF_6 profiles retrieved from the Michelson Interferometer for Passive Atmospheric Sounding (MIPAS) limb emission mid-infrared spectrometer for 2002–2010, with almost global coverage and about 3 km vertical resolution. Stiller et al. (2012) show that trends of differing sign occur at different levels in the stratosphere. In the lower stratosphere, their results show a decrease in age of air consistent with an acceleration of the BDC. As discussed in the last Ozone Assessment, Engel et al. (2009) found no significant decrease in the mean age of air above 24 km based on measurements of CO_2 and SF_6. In the middle and upper stratosphere, the results of Stiller et al. (2012) corroborate those of Engel et al. (2009) for northern midlatitudes, showing a statistically robust increase in age of air in that region, consistent with a weakening of the deep branch of the BDC there, in contrast to the strengthening inferred from stratospheric temperatures (Young et al., 2012).

As also discussed in the 2010 Ozone Assessment, inhomogeneities in observations and reanalysis products complicate the diagnosis of long-term trends in reanalysis data (e.g., Iwasaki et al., 2009). The new generation of reanalysis products, however, do show some improvements (e.g., for ERA-Interim reanalysis data as discussed by Dee et al. (2011) and Monge-Sanz et al. (2012)). Using ERA-Interim reanalysis data, changes in the BDC circulation were investigated based on the Transformed Eulerian Mean residual circulation (Sevior et al., 2011) and age of air with transport models of different complexity (Monge-Sanz et al., 2013; Diallo et al., 2012). Seviour et al. (2012) found that trends in the BDC inferred from tropical upwelling in the lower stratosphere were dependent on the altitude and tropical latitudes considered. Statistically significant trends in the lower stratosphere were found by Seviour et al. (2011) and Diallo et al. (2012) consistent with an enhancement of the BDC in this region, while Monge-Sanz et al. found significant changes above 25 km in the Northern Hemisphere that were consistent with a weakening of the deep branch of the BDC in the Northern Hemisphere and in broad agreement with findings by Engel et al. (2009) and Stiller et al. (2012). However, Diallo et al. (2012) found little or no statistical significance in the changes in age of air above 20 km (in agreement with Bönisch et al., 2011).

In summary, changes in temperature, ozone, and age of air all agree in showing an acceleration of the tropical upwelling in the lowermost stratosphere (shallow branch) and, as discussed in Section 4.3.2.2, this change is consistent with that simulated by climate models. However, the behavior of the trends in the BDC in the middle and upper stratosphere is not as clear, as temperature changes (albeit from only one data set) indicate a strengthening of the deep branch while BDC changes inferred from age of air point to no change or even weakening of the deep branch.

4.3.2.2 SIMULATED PAST AND FUTURE CHANGES

In the 2010 Ozone Assessment, it was assessed that chemistry-climate models consistently simulate an acceleration of the BDC in response to increasing GHG concentrations, although most studies had focused on the lower stratosphere. More recent modeling studies all consistently simulate an acceleration of the BDC in response to increasing GHG concentrations in past and future simulations (e.g., Butchart, 2014). The 2010 Ozone Assessment highlighted a primary caveat associated with the non-statistically significant trend found in stratospheric age-of-air estimates from SF_6 and CO_2 measurements (Engel et al., 2009) and also noted difficulties in comparing the tropical upwelling and its forcings across different studies because of the different definitions used (e.g., fixed latitudes versus turnaround latitudes, where the residual vertical velocity changes sign), and in quantifying the role of parameterized gravity waves (versus resolved waves) in models, especially in the lower stratosphere. Since the last Ozone Assessment, new research has clarified some of these issues.

New studies demonstrated that observational results of Engel et al. (2009) may not be inconsistent with simulated stratospheric circulation changes and that BDC changes in climate models agree with new observational age-of-air measurements in the lower stratosphere (Stiller et al., 2012). Ray et al. (2010) were able to reproduce the observed age of air and ozone trends over the last 30 years in their simple model assuming a small strengthening of the mean circulation in the lower stratosphere and a moderate weakening of the mean circulation in the middle and upper stratosphere. Garcia et al. (2011) identified issues associated with using natural species, with non-uniform growth rates, as proxies for trends in the stratospheric circulation. Their CCM was able to simulate non-statistically significant trends in age of air, as observed by Engel et al. (2009), when it was sampled sparsely as in the observations, demonstrating the large uncertainty in trends determined from sparsely sampled data.

Recent studies have confirmed that the role of parameterized gravity waves in driving modeled changes in tropical upwelling is larger in the middle and upper stratosphere (Bunzel and Schmidt et al., 2013; Oberländer et al., 2013; Palmeiro et al., 2014). This is in agreement with previous results from Garcia and Randel (2008) and McLandress and Shepherd (2009). In the lowermost stratosphere, orographic wave forcing dominates over non-orographic contributions and the trend in orographic gravity wave forcing is larger in the subtropics than in the deep tropics (McLandress and Shepherd, 2009). Thus the contribution of orographic gravity waves to the total trend in tropical upwelling is larger when the turnaround latitudes are used to compute the upwelling (e.g., McLandress and Shepherd, 2009) instead of using fixed latitudes encompassing the deep tropics (e.g., Calvo and Garcia, 2009).

Understanding of the role of resolved waves in driving the tropical upwelling has advanced. New individual modeling studies indicate that resolved waves are the main driver of the trend in tropical upwelling in the lower stratosphere (Bunzel and Schmidt, 2013; Oberländer et al., 2013; Palmeiro et al., 2014; Okamoto et al., 2011) while the role of orographic gravity waves seems to be largely dependent on the model. Previous multi-model studies already highlighted the large spread in the contribution of both types of waves to the trend (e.g., Butchart et al., 2010), which could be in part explained by the compensation between resolved and parameterized orographic wave driving found in this region (Cohen et al., 2013; Sigmond and Shepherd, 2014 and references therein). The fact that representation of parameterized waves varies between models hampers a systematic multi-model comparison to assess the degree of consensus in the role of resolved versus parameterized waves.

The contribution of stationary and transient waves to the trend in the shallow branch tropical upwelling varies with latitude in models. The contribution of stationary waves dominates in the deep tropics, whereas transient waves are more important at higher latitudes in the subtropics (Garny et al., 2011; Shepherd and McLandress, 2011). This explains discrepancies found in previous studies, because the contribution of these waves is expected to be different depending on how the tropical upwelling is defined (in the deep tropics or between the turnaround latitudes).

It is still difficult to attribute changes in wave forcing to changes in wave propagation or wave generation, because changes in both processes are hard to disentangle in a free-running climate model. Garny et al. (2011) found that warmer tropical SSTs under increasing GHGs cause a strengthening of the

subtropical jets and changes in deep convection affecting latent heat release, which modulate the wave propagation and wave generation, respectively, although the former dominates in their model. Shepherd and McLandress (2011) propose that critical-layer control of Rossby wave breaking (Randel and Held, 1991) is the mechanism that explains the simulated changes in wave drag that ultimately force the strengthened tropical upwelling in the lower stratosphere. The tropospheric warming in response to climate change leads to a strengthening and upward displacement of the upper flanks of the subtropical jets in the lower stratosphere (e.g., Garcia and Randel, 2008), which causes the critical layers on the equatorward side of the jets to move upward and the Rossby wave drag to occur at higher altitudes and further equatorward, allowing more Rossby wave activity to penetrate into the subtropical lower stratosphere. This mechanism can also explain the simulated increase in parameterized lower-stratospheric orographic gravity wave drag (e.g., Li et al., 2008; McLandress and Shepherd, 2009) as an upward shift of the wave-breaking levels due to the strengthened upper flank of the subtropical jets.

As discussed above, a few recent studies have been devoted to exploring the behavior of the deep branch of the circulation and understanding its driving mechanisms in future climates (Hardiman et al., 2013; Palmeiro et al., 2014; Lin and Fu, 2013; Oberländer et al., 2013). A strengthening of the deep branch of the circulation has been found in response to increasing GHG concentrations in CCMs (Lin and Fu, 2013) and in "high top" CMIP5 models (i.e., those with their lid above 1 hPa; Hardiman et al., 2013; Palmeiro et al., 2014; Figure 4-8). In addition, changes in the width of the tropical upwelling region have been found to vary with height, so that the upwelling region narrows below 20 hPa and widens above 20 hPa (Hardiman et al., 2013; also compare black and red lines in Figure 4-8). This indicates that different mechanisms might operate in forcing the changes in each branch of the circulation. Changes in the

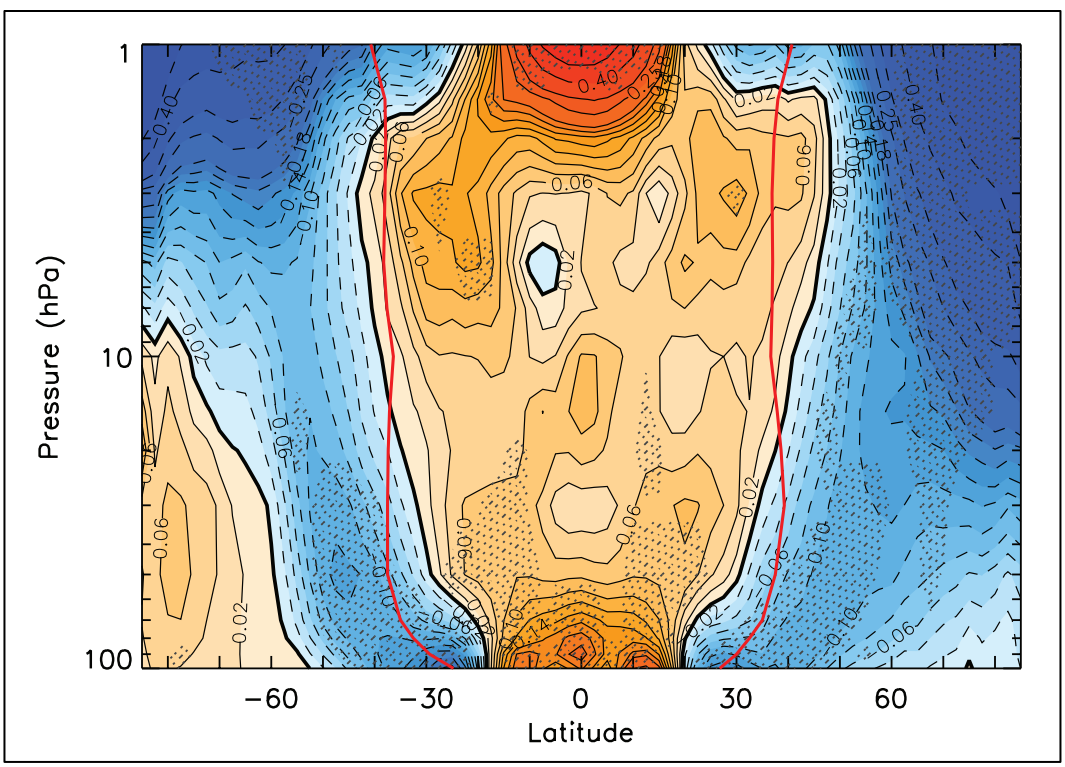

Figure 4-8. Multi-model mean CMIP5 simulated differences in annual mean residual vertical velocity (mm/s) in RCP8.5, 2080–2099 climatology minus 2006–2025 climatology. Solid/Dashed contours show positive/negative values (increases/decreases in residual vertical velocity). Stippling denotes regions where 90% of models show a statistically significant change in residual vertical velocity at the 5% level. Red lines denote the position of the turnaround latitudes (where residual vertical velocity is zero) for the 2006–2025 climatology. Adapted from Hardiman et al. (2013).

dissipation of parameterized gravity waves appear to be the key to explaining the acceleration of the deep branch of the BDC under climate change (Oberländer et al., 2013; Palmeiro et al., 2014), although there is no consensus in the type of gravity waves involved. Thus, modeling evidence is currently too limited to assess the contribution of gravity waves to the deep branch of the circulation in the upper stratosphere.

Overall, studies have found that the projected increase in the tropical upwelling in the upper stratosphere is robust across models and balanced by an increase in extratropical downwelling. In the Northern Hemisphere, a robust increase in downwelling is simulated at high latitudes throughout the entire stratosphere (Figure 4-8) while in the Southern Hemisphere, the increased downwelling mainly occurs at midlatitudes although the agreement across models is not as robust. Reduced downwelling is simulated over the Antarctic in austral spring and summer, driving the annual mean behavior in this region. Recent studies have shown that the reduced downwelling is in response to future ozone recovery (Hardiman et al., 2013; Palmeiro et al., 2014; Lin and Fu, 2013), in agreement with the enhanced downwelling in austral summer found in response to ozone depletion (e.g., Manzini et al., 2003; Li et al., 2008) but in contrast with McLandress and Shepherd (2009), who found reduced downwelling in the future in Antarctic spring in response to increasing GHGs.

In summary, modeling studies show an acceleration of the shallow and deep branches of the BDC with climate change. In the lower stratosphere, these results are in agreement with observations from changes in temperature, trace gases, and age of air, which all agree in showing an intensification of the BDC in this region. In the middle and upper stratosphere, changes in the deep branch of the BDC inferred from changes in temperatures, trace gases, and age-of-air observations are uncertain. Further research is needed to assess the changes in the BDC in the middle and upper stratosphere and the underlying mechanisms.

4.3.3 Stratospheric Zonal Flow

The characteristics of the stratospheric zonal flow, and in particular the stratospheric polar vortices, play an important role in determining polar ozone concentrations and in the dynamical coupling between the stratosphere and troposphere. Changes in the zonal flow and vortices can have an impact on tropospheric climate. The observed changes in vortex characteristics, the cause of these changes, and projected future changes are discussed in Chapter 3 of this Assessment, and are only briefly reviewed here.

In general, there is larger interannual variability in the characteristics of the Arctic vortex than the Antarctic vortex. However, as discussed in Chapter 3, there has been an increase in the year-to-year variability in both hemispheres in recent years, with increased variability in lower stratospheric polar temperatures (Figure 3-1) and the breakup date of the vortices (Figure 3-2). Also, whereas there were few Arctic major sudden warmings during the 1990s, there were many during the first decade of the 21st century (Chapter 3). In the Antarctic there has been a trend toward a stronger vortex (e.g., stronger zonal flow; see Figure 4-10) and later breakup dates since 1980 (Figure 3-2). In most recent years the vortex broke up in early to mid-December, although the 2012 vortex broke up in mid-November.

The variability in the strength and lifetime of the polar vortices is connected to similar variability in planetary wave activity, since there is generally a stronger, longer-lasting vortex in winters with lower mean winter eddy heat flux (see Section 3.3.3). However, whether changes in wave activity and the resulting vortex strength are due to natural variability or the response to anthropogenic forcing is generally not known. An exception is the strengthening and delay in breakup date of the Antarctic vortex, which is due primarily to diabatic cooling associated with the Antarctic ozone hole (see Section 4.3.1).

Climate model simulations also show a strengthening of the Antarctic vortex during the latter part of the 20th century in response to stratospheric ozone depletion, and a weakening in spring as ozone recovers (Figures 4-6, 4-10). The simulations show a shift to later breakup dates in the latter part of the 20th century and then a return to earlier breakup dates (e.g., McLandress et al., 2010; Deushi and Shibata 2011; Shaw et al., 2011; Wilcox et al., 2013; Orr et al., 2013). There is some indication of a shift toward later final warming dates in the latter half of the 21st century for a high GHG emission scenario (Wilcox et

al., 2013). However, Sheshadri et al. (2014) found that a delayed stratospheric final warming could not explain the trend in Southern Hemisphere tropospheric zonal mean zonal wind in recent decades (see Section 4.4).

In contrast to the clear trends in the Antarctic, models generally show small, insignificant trends in Arctic polar temperatures and vortex breakup dates over the 21st century (CCMVal 2010; Hitchcock et al., 2009; Langematz et al., 2014).

4.4 EFFECTS OF PAST CHANGES IN STRATOSPHERIC OZONE ON THE TROPOSPHERE AND SURFACE

The influence of stratospheric ozone change on Southern Hemisphere tropospheric and surface climate has been analyzed and investigated in an increasingly mature body of research, with its signature now well documented (e.g., recent reviews of Thompson et al., 2011; Previdi and Polvani, 2014; Canziani et al., 2014). We focus here on what has been learned since the 2010 Ozone Assessment (Forster and Thompson et al., 2011), notably, improved quantification of the relative roles of ozone and GHGs in driving observed Southern Hemisphere circulation changes. Consistent with the last Assessment, ozone depletion is assessed to be the dominant driver of austral summer (December-January-February, DJF) atmospheric circulation changes over the last several decades. We begin by assessing the effects of stratospheric ozone changes on the tropospheric circulation, followed by an assessment of the resultant impacts on surface climate, the ocean, and sea ice.

4.4.1 Tropospheric Circulation Effects

The Southern Hemisphere

As described in the previous section, the primary effect of stratospheric ozone depletion is to produce a strong cooling in the lower stratosphere over the Antarctic in austral spring. Simulations indicate that this cooling acts to strengthen and shift the Southern Hemisphere tropospheric midlatitude jet poleward in austral summer, and to drive an increase in the Southern Annular Mode (SAM) index corresponding to decreases in sea level pressure over high latitudes and increases over midlatitudes. We first evaluate the observed evidence for the impact of ozone depletion on the tropospheric circulation followed by an assessment of the current understanding of the mechanisms through which this shift occurs. We note that here and elsewhere in this chapter, we use the term “midlatitude jet” to refer to the band of strong westerly winds, climatologically centered around 50°S, which are associated with synoptic-scale eddies (i.e., typical storms in the midlatitudes). The latitude of the midlatitude jet is generally defined as the location of the maximum zonal mean westerly winds at 850 hPa. This definition is used because it distinguishes the Southern Hemisphere midlatitude jet from the upper-level subtropical jet that is present in some seasons.

The SAM is the leading mode of variability in the extratropical circulation and the SAM index gives an indication of changes in the characteristics of the midlatitude jet, though there is not necessarily a one-to-one relationship between SAM index anomalies and variations in the strength or location of the midlatitude jet. Whereas changes in the jet strength and location can only be determined from reanalysis data sets, the SAM index can be calculated from sea level pressure observations, which are available over a longer period. After 1979, there is generally good agreement between the SAM index calculated from station observations and that calculated from reanalyses, whereas prior to 1979 some reanalyses are known to have deficiencies (Marshall, 2003). Since a longer period is often used in model attribution studies, two periods are discussed here. Figure 4-9 shows trends in the SAM index from station observations of sea level pressure (based on an update of Marshall, 2003) for 1979–2012 (which encompasses the satellite era) and 1958–2012 (which begins at the International Geophysical Year). The largest seasonal trends are found in DJF over both periods and significant trends (shown in red) are observed

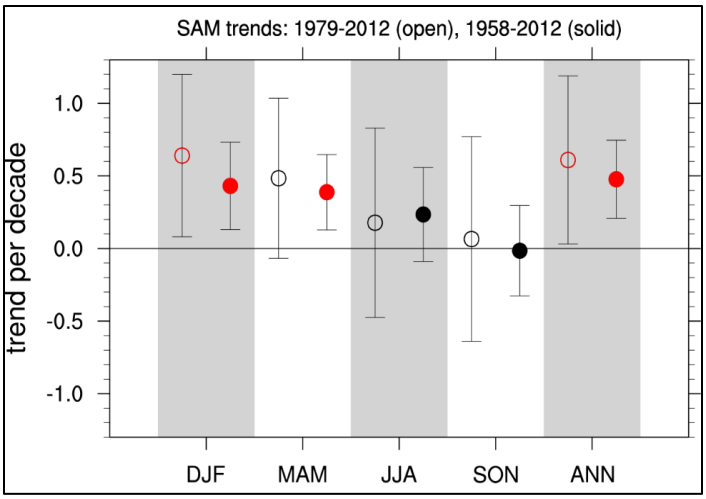

Figure 4-9. SAM trends per decade calculated over 1979–2012 (open circles) and 1958–2012 (closed circles) from the seasonal and annual data of Marshall (2003; http://www.nerc-bas.ac.uk/icd/gjma/sam.html). Error bars indicate the 95% confidence interval of the trends with the auto-correlation accounted for. Trends significant at the 5% level based on a two-sided t-test are colored red. The SAM index is dimensionless (Marshall, 2003).

in the annual mean and DJF for 1979–2012 and in the annual mean, DJF, and March-April-May (MAM) for 1958–2012.

The connection of these surface changes to the stratosphere is evident in Figure 4-10a, which shows the austral summer climatology and trends in the zonal mean zonal winds over the period 1979–2005 in one reanalysis data set (Eyring et al., 2013). There is a clear asymmetry between the Northern and Southern Hemisphere trends over this period, with the largest wind changes in the Southern Hemisphere stratosphere. These features lend support to ozone depletion being the dominant cause of the Southern Hemisphere trends, and these trends are well captured by the CMIP5 historical experiments (see Box 2-2 in Chapter 2 of this Assessment), driven by natural and anthropogenic forcings including ozone depletion (Figure 4-10b).

Swart and Fyfe (2012) analyzed recent trends in surface wind stress over the Southern Ocean in various reanalyses (Figure 4-11). They report no statistically significant trends in the annual mean midlatitude jet location (defined based on surface wind stress) over the 1979–2010 period, but note the existence of a significant poleward shift in austral summer (DJF), which is found consistently across six reanalysis data sets. They find that the Southern Hemisphere DJF midlatitude jet has shifted poleward by -0.7 ± 0.5 degrees latitude per decade, averaged across the different reanalyses (their Figure 3). Swart and Fyfe (2012) also report a *strengthening* of the midlatitude jet in the annual mean and in DJF, but the large spread across the reanalyses in Figure 4-11 precludes a confident assessment of this metric.

A recent study by Lee and Feldstein (2013) also found a dominant role for ozone depletion in summertime extratropical circulation trends in the ERA-Interim reanalyses in the last few decades. These authors applied a cluster analysis technique to zonal mean zonal wind data, identified trends in the occurrence frequency of two of the clusters, and by simply comparing the patterns of zonal mean wind anomalies associated with each cluster with the simulated response to GHGs and ozone from other studies, inferred that changes in occupation frequency of one cluster were due to GHG changes and changes in the occurrence frequency of the other were due to ozone depletion. Based on this, they inferred that ozone depletion has contributed about 50% more than increasing GHGs toward the jet shift in austral summer. Son et al. (2013) and Bandoro et al. (2014) further showed that stratospheric ozone variability can change the tropospheric circulation on interannual timescales.

Since the previous Ozone Assessment, several modeling studies have compared the influence of ozone depletion and GHGs on the tropospheric circulation. McLandress et al. (2011), performed transient simulations with a coupled-chemistry stratosphere-resolving model with a fully coupled (non-eddy resolving) ocean; Polvani et al. (2011b), performed time-slice integrations with a much simpler atmosphere-only (low-top) climate model, with prescribed ozone concentrations, sea surface temperatures, and sea ice; while Gillett et al. (2013) and Fyfe et al. (2012) compared sea level pressure trends in CMIP5 simulations that included GHG changes only and ozone (stratospheric and tropospheric) changes only. Considering spatio-temporal patterns of sea level pressure change over the whole globe and for all four

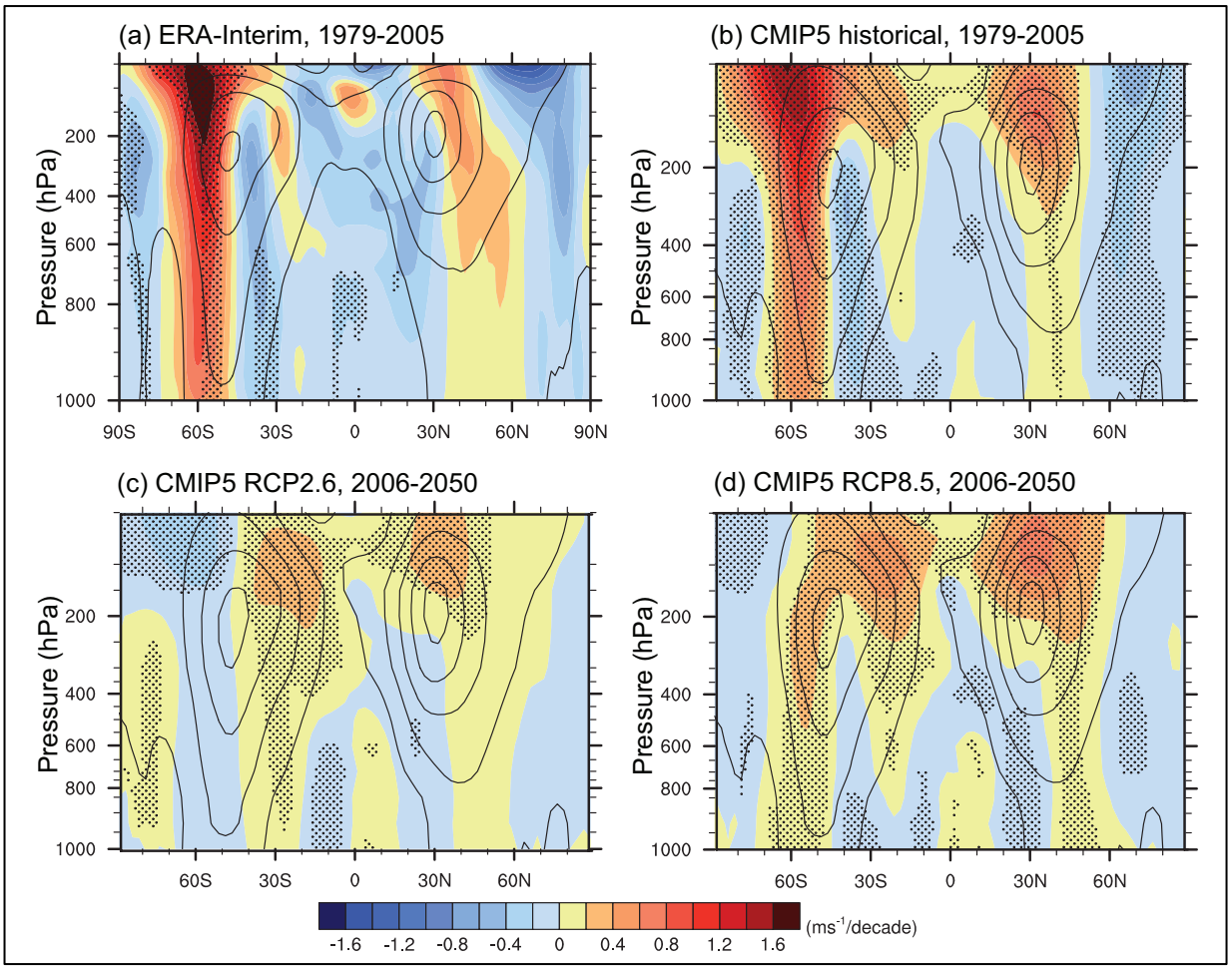

Figure 4-10. Long-term mean (thin black contour) and linear trend (color) of zonal mean DJF zonal winds for (a) ERA-interim over 1979–2005; (b) the mean of the CMIP5 historical experiments over 1979–2005; (c) CMIP5 RCP2.6 multi-model mean over 2006–2050 and (d) CMIP5 RCP8.5 multi-model mean over 2006–2050. Contour intervals of climatological wind are 10 m s^{-1} starting from −20 m s^{-1}. Trends that are statistically significant at the 5% level are stippled. Adapted from Eyring et al. (2013).

seasons, Gillett et al. (2013) separately detected the influence of ozone changes and GHG changes in observations, using attribution techniques that employ the distinctive patterns of response to each forcing simulated by CMIP5 models. Gillett et al. (2013) also examined seasonal SAM trends across the CMIP5 individual forcing simulations (see Figure 4-12). In all studies apart from Fyfe et al. (2012), simulations showed that the shift in the latitude of the midlatitude jet and the SAM index trend in DJF were considerably larger in response to stratospheric ozone depletion than in response to GHG changes over the last fifty years or so (McLandress et al., 2011; Polvani et al., 2011b; Gillett et al., 2013). Fyfe et al. (2012) find a comparable contribution of GHGs and ozone to trends in their DJF sea level pressure index over 1957–2010, although they note that the prescribed ozone forcing used in their simulations may be weaker than observed.

In seasons other than DJF, the relative amplitude of the circulation response to anthropogenic and natural forcings depends on the metric used and on the period over which trends are calculated. Observations and most models show smaller SAM trends in these seasons, and simulations show a relatively uniform response to GHGs in all months (e.g., Staten et al., 2012; Gillett et al., 2013). In MAM, when the observed SAM index trends are significant over longer timescales (Figure 4-9), Polvani et al. (2011b) and McLandress et al. (2011) find larger contributions from GHGs compared to ozone depletion,

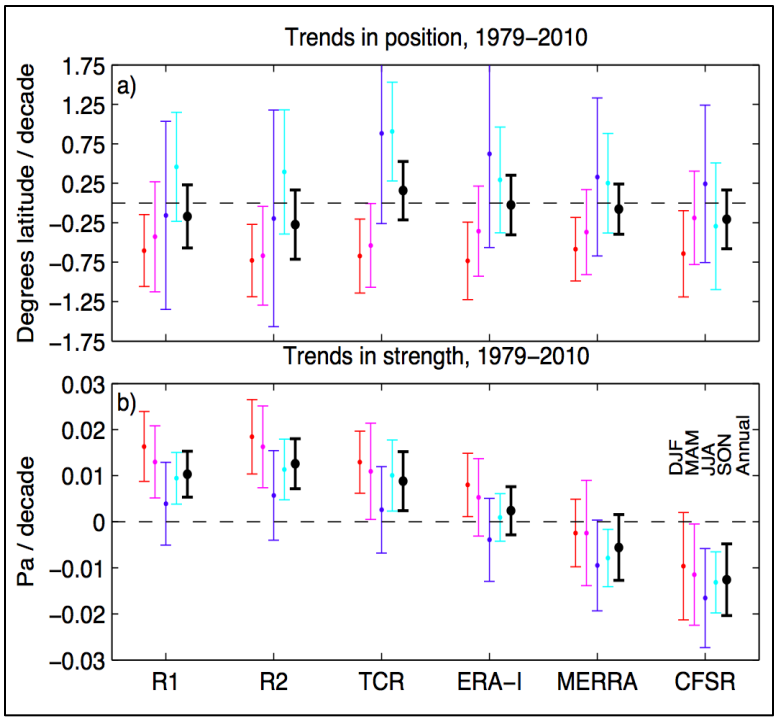

Figure 4-11. Historical trends in the Southern Hemisphere surface westerly wind-stress jet position (a) and strength (b). Trends are computed over the period 1979–2010 from six reanalysis products: NCEP-NCAR Reanalysis 1 (R1), NCEP-DOE Reanalysis 2 (R2), ECMWF ERA-Interim Reanalysis (ERA-I), NOAA-CIRES Twentieth Century Reanalysis Version 2 (TCR), NASA Modern Era-Retrospective Analysis for Research and Applications (MERRA), and NCEP Climate Forecast System Reanalysis (CFSR); the analysis has been adapted from Swart and Fyfe (2012) to include the NASA MERRA and NCEP CFSR data sets that were not included in the main text. The error bars show the 95% confidence interval of the trends, where auto-correlation has been accounted for. Trends are computed for seasonal means and annual means of the zonal-mean zonal wind-stress. Adapted from Swart and Fyfe (2012).

Figure 4-12. Simulated and observed trends in the Northern Annular Mode and Southern Annular Mode indices. Observed trends in the (a) NAM and (b) SAM over the period 1951–2011 are shown for each season based on HadSLP2 / HadSLP2r_lowvar (solid line), the 20th Century Reanalysis (dotted), and in the case of the SAM, the Marshall SAM index over the period 1958–2011 (dashed). No normalization was used when computing the annular mode indices. Gray bars show the 5–95% centered range of trends in the control simulations. Colored boxes show the ensemble mean and its 5–95% confidence range for the simulated response to GHGs, aerosols (AER), tropospheric and stratospheric ozone changes (OZ), and natural forcings (NAT), based on available individual forcing simulations. Black boxes show the 5–95% range of trends simulated in response to ALL forcings. Note the different scales on (a) and (b). Adapted from Gillett et al. (2013).

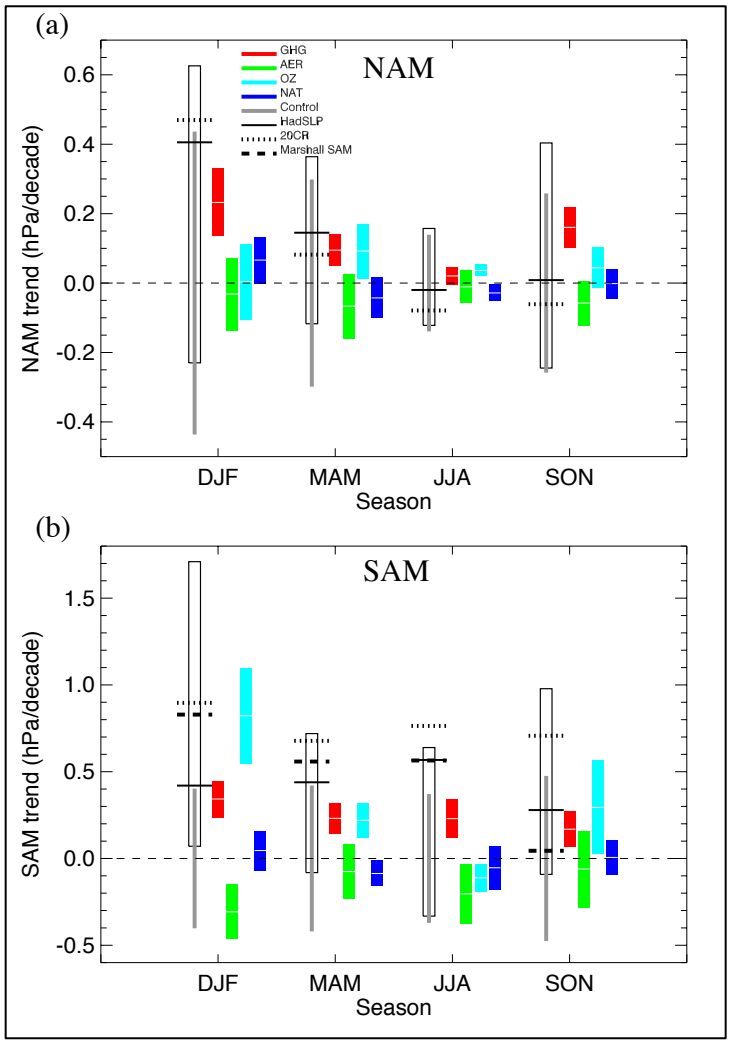

while Staten et al. (2012) and Gillett et al. (2013) suggest comparable contributions from both (see Figure 4-12). A comparable contribution of GHGs and ozone is also found in annual mean trends in the SAM in studies where it was diagnosed (Sigmond et al., 2011; Staten et al., 2012), consistent with earlier studies (e.g., Arblaster and Meehl, 2006; Shindell and Schmidt, 2004). Recent modeling studies suggest that the response to other forcings is weaker, though aerosol changes may have driven opposing, negative trends in the SAM (Gillett et al., 2013; Xie et al., 2013).

In summary, the contribution of Antarctic ozone depletion to the observed increase in the Southern Annular Mode index in austral summer is substantially larger in most models than the contribution from greenhouse gas increases over the past three to five decades. The role of ozone depletion is largest in summer. Observations and models suggest smaller Southern Annular Mode trends in other seasons. In most models, GHGs drive consistently positive trends in the SAM across the seasonal cycle and likely contribute partially to the observed changes seen.

In the Southern Hemisphere midlatitudes, in association with the shift of the jet, several additional impacts of stratospheric ozone depletion, beyond those already mentioned in the previous Ozone Assessment have now been documented. Ndarana et al. (2012) reported a large increase in summertime Rossby wave breaking events on the equatorward side of the tropospheric midlatitude jet in the Southern Hemisphere (and weak decreases on the poleward side), over the last 30 years in meteorological analyses. Such events are of interest because they are often linked to weather extremes and stratosphere-troposphere exchange of trace gases. Using model integrations with single forcings, Ndarana et al. (2012) showed that trends consistent with the reanalyses are simulated in response to stratospheric ozone depletion. Using the same model integrations, Grise et al. (2014) showed how ozone depletion can also cause a significant poleward shift in the position of midlatitude storms over the Southern Ocean, indicating that the storm tracks are tightly linked with the position of the midlatitude jet.

Recent studies have shown that the impact of stratospheric ozone depletion is not confined to the mid to high latitudes but extends well into the low latitudes. Notably, new studies have shown that ozone depletion has likely contributed to a broadening of the Hadley Cell in austral summer (McLandress et al., 2011; Polvani et al., 2011b; Min and Son, 2013), confirming the tentative conclusion of the last Ozone Assessment (Forster and Thompson et al., 2011; Son et al., 2010). This is illustrated in Figure 4-13, which shows a broad variety of simulated circulation metrics exhibit substantial trends in austral summer, in a model forced with stratospheric ozone changes alone (via changes in ODSs). Note, in particular, the Hadley cell width in panel (d), and how the ozone forcing yields a much stronger broadening than greenhouse gas forcing, over the period 1960–2005. The response of the Hadley Cell width to ozone depletion has also been detected in observations in austral summer by Min and Son (2013), using several reanalyses and CMIP3 and CMIP5 models. Nonetheless, large observational uncertainties remain and the observed trend in the Hadley Cell width is considerably larger than that simulated in response to ozone and GHG changes by climate models (Quan et al., 2013; Min and Son, 2013; Lucas et al., 2013, 2014). Understanding of the influence of stratospheric ozone depletion on the low-latitude atmospheric circulation has also improved since the last Ozone Assessment. Although the direct response to polar ozone depletion is primarily a shift of the jet in the midlatitudes, the width of the tropical circulation is very tightly coupled to the position of the jet in austral summer (Kang and Polvani, 2011).

In spite of the modeling and observational evidence that stratospheric ozone depletion affects the tropospheric circulation, a precise mechanism linking stratospheric ozone loss to the jet shift is still the subject of active research. Experiments with simplified atmospheric models (e.g., Polvani and Kushner, 2002, and Butler et al., 2010) have established that the impact of ozone depletion on the troposphere is effected through a cooling of the lower polar stratosphere, which is associated with anomalously strong westerly winds that alter the wave driving of the stratosphere, producing a positive anomaly in potential vorticity. It is well accepted that the balanced response of the troposphere to this positive potential vorticity anomaly is an acceleration of the zonal flow on the poleward flank of the storm track, consistent with the sign of the observed shift in the circulation (e.g., Hartley et al., 1998; Thompson et al., 2006). It is unlikely, however, that this balanced response is sufficiently large to explain the magnitude of the observed circulation shift.

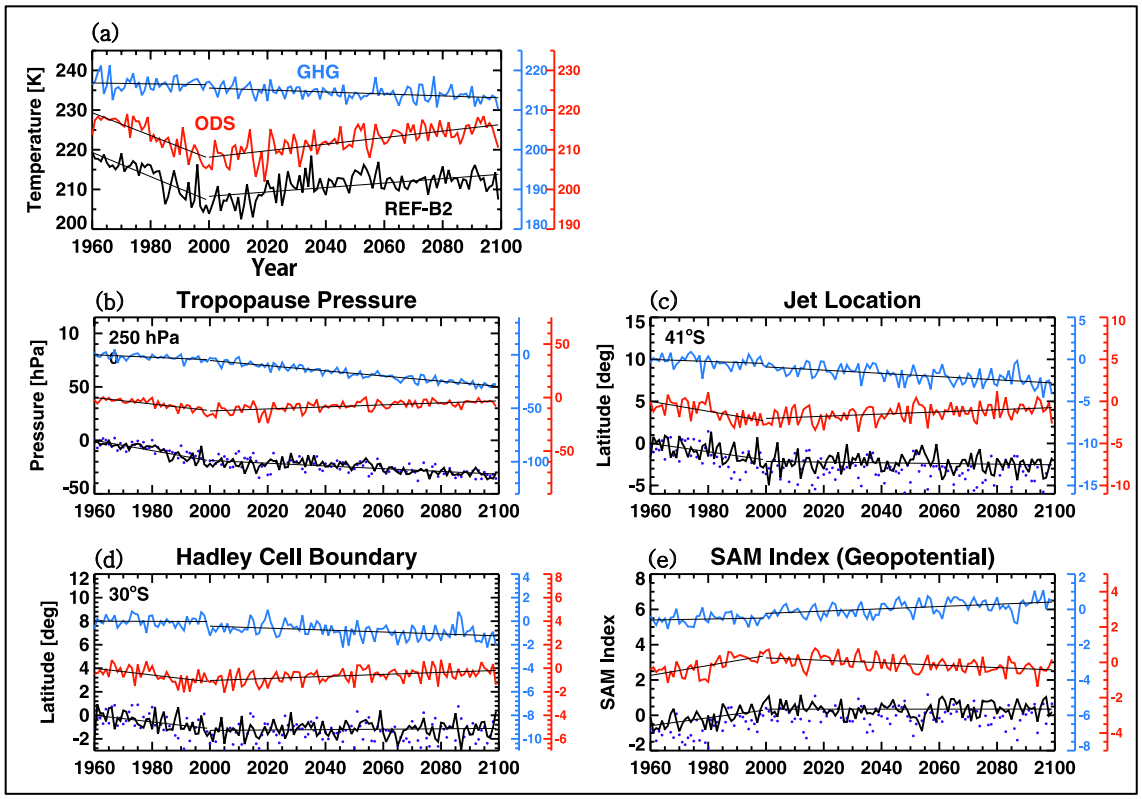

Figure 4-13. Time series of (a) 100-hPa temperature for October–January area-averaged over 70° to 90°S, (b) DJF tropopause pressure anomaly averaged over 45° to 90°S, (c) DJF jet-location anomaly defined by the latitude of 850-hPa zonal-mean zonal wind maximum, (d) DJF Hadley cell boundary anomaly defined as the zero-crossing latitude of 500-hPa mass streamfunction, and (e) DJF SAM-index anomaly derived from 850-hPa geopotential. The REF-B2 (black), ODS (red), and GHG (blue) simulations denote an experiment with time-varying ODS and GHG concentrations, an experiment with time-varying ODS concentration but GHG concentrations fixed at 2000 values, and an experiment with time-varying GHG concentration and ODS concentrations fixed at 2000 values, respectively. The sum of the GHG and ODS responses is denoted by purple dots. The straight lines are linear fits computed from 1960 to 1999 and 2000 to 2099. The red and blue curves are shifted with respect to the black; their color-coded axes are given on the right. In (b-d), anomalies are computed with respect to 1960 baselines; the average baseline (i.e., average of the REF-B2, ODS, and GHG baselines) is shown in the top-left corner of each panel. The 1960 baseline has not been removed from the SAM index time series. Adapted from McLandress et al. (2011).

Studies with idealized atmospheric models in particular suggest that tropospheric eddy feedbacks amplify the impact of stratospheric cooling, and so play a critical role in the mechanism (Kushner and Polvani, 2004; Song and Robinson, 2004); a number of pathways for the lower stratosphere to directly influence tropospheric eddies have been proposed. Several mechanisms focus on the direct influence of the lower stratosphere on tropospheric eddy momentum fluxes: linear theories consider the propagation and refraction of synoptic waves (Limpasuvan and Hartmann, 2000; Chen and Held, 2007; Simpson et al., 2009), while nonlinear mechanisms focus on the wave breaking itself (Wittman et al., 2004; Kunz et al., 2009). Other studies have focussed on the impact of stratospheric anomalies on the generation of wave activity through baroclinic instability, which in turn drives changes in the eddy momentum fluxes (Rivière, 2011; Thompson and Birner, 2012).

Crook et al. (2008) and Waugh et al. (2009) find that the zonal structure of ozone loss amplifies its impact on the troposphere, suggesting a role for planetary-scale wave interactions. The potential for constructive and destructive interferences between forced and climatological planetary waves has been shown to impact coupling between the stratosphere and troposphere in the Northern Hemisphere (Smith et al., 2010), and there is evidence that the ozone hole has modified planetary wave coupling in the Southern Hemisphere (Shaw et al., 2011).

Tropospheric eddy feedbacks have been observed in the jet response in comprehensive model studies (McLandress et al., 2011; Orr et al., 2012), but Garfinkel et al. (2013) illustrate the difficulty in separating and confirming many of the proposed mechanisms, even in an idealized atmospheric model. Tropospheric eddy feedbacks overwhelm the initial perturbation generated by the stratosphere, controlling the ultimate amplitude of the response. Both comprehensive and idealized models tend to overestimate the strength of the tropospheric eddy feedbacks (e.g., Gerber et al., 2010), complicating the effort to connect model-based analysis to the real atmosphere. A number of studies have also noted the equatorward bias in the position of the Southern Hemisphere DJF midlatitude jet in the CMIP3 and CMIP5 models compared to the reanalyses (Wilcox et al., 2012, Swart and Fyfe, 2012), which may impact their response to stratospheric ozone changes (Sigmond and Fyfe, 2014). Swart and Fyfe (2012) find this bias has somewhat improved from CMIP3 to CMIP5. Despite these uncertainties and the lack of clarity on the mechanism, the influence of stratospheric ozone on the troposphere is robust across a range of comprehensive and idealized atmospheric models.

The Northern Hemisphere

The last Ozone Assessment assessed that no robust linkages between stratospheric ozone depletion and tropospheric circulation had been established in the Northern Hemisphere, consistent with the relatively weak ozone depletion observed in the Arctic (see, e.g., Figure 3-4). However, Morgenstern et al. (2010) find a weak but significant anticorrelation between Northern Hemisphere column ozone and the NAM index in spring (March-May, MAM) in the CCMVal-2 models, suggesting that in these models Arctic ozone depletion drives an increase in the NAM index in MAM. The CMIP5 models also exhibit an increase in the NAM index in MAM in response to combined changes in stratospheric and tropospheric ozone (Figure 4-12), though simulations with one model suggest that this response may be driven by tropospheric ozone changes (Gillett et al., 2013). No statistically significant trend in the NAM index has been observed in MAM (e.g., Gillett et al., 2013). Thus our assessment remains that no robust link between stratospheric ozone depletion and Northern Hemisphere circulation has been established.

4.4.1.1 SURFACE IMPACTS

An important development since the previous Ozone Assessment has been the improved understanding of the influence of ozone depletion on Southern Hemisphere precipitation. The effect of ozone depletion on midlatitude precipitation is directly related to the position of the midlatitude jet, and has been documented in a number of studies (e.g., Fyfe et al., 2012; Previdi and Polvani, 2014). What has become apparent more recently is that ozone depletion may also be impacting precipitation in the subtropics, notably the latitudinal band 15–35°S (Kang et al., 2011). Over this region a positive trend in precipitation has been observed over the last decades of the 20th century during austral summer (Kang et al., 2011; Previdi and Polvani, 2014).

The connection between observed Southern Hemisphere precipitation changes and the SAM trends in austral summer is illustrated in Figure 4-14, which shows the DJF zonal mean observed GPCP (Global Precipitation Climatology Project) precipitation trend over both land and ocean points over the period 1979–2000. Note how most of the observed precipitation changes (red) are linearly congruent with the SAM (blue; see caption for details). This is particularly the case for the midlatitude zone. The subtropical trends are less significant, with more year-to-year variability in that latitude band compared to higher

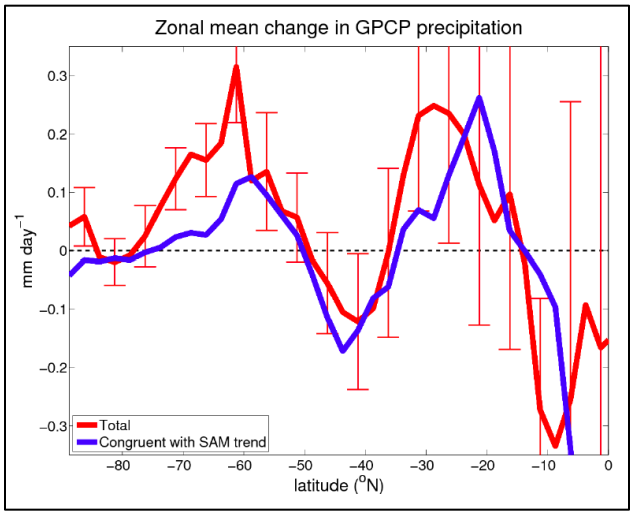

Figure 4-14. Zonal-mean change in GPCP (Global Precipitation Climatology Project) DJF precipitation during 1979–2000. The total precipitation change is plotted in red, and is based on the linear trend in the seasonal-mean precipitation at each latitude. The component of the precipitation change that is linearly congruent with the SAM trend is plotted in blue. This is calculated by regressing the seasonal detrended precipitation onto the SAM index and multiplying by the trend in the SAM. Error bars show the plus and minus one standard deviation range of the detrended seasonal-mean data, providing an indication of the year-to-year precipitation variability. From Previdi and Polvani (2014).

latitudes, yet are also largely congruent with the observed positive trend in the SAM index. Attribution of precipitation trends to SAM trends on more regional scales is more difficult. For example, the observed summer rainfall increases in subtropical northern Australia are larger than can be explained by the SAM changes alone (Hendon et al., 2007; Thompson et al., 2011).

Kang et al. (2011), using models forced with ozone depletion alone, showed that the precipitation response in austral summer was consistent with that observed and resulted from an expansion of the tropical circulation in their simulations. This moves the downwelling branch of the tropical circulation poleward, which results in enhanced upwelling in the subtropics and hence enhanced precipitation, in austral summer. A recent regional study by Gonzalez et al. (2013), contrasting models forced with ozone depletion and increasing GHGs, suggested that ozone depletion is a driver of observed precipitation increases in South East South America in austral summer, with its effect comparable to that due to increasing GHGs. Fyfe et al. (2012) identified a poleward shift in Southern Hemisphere extratropical austral summer precipitation from merged reanalysis and satellite-based observations that was inconsistent with simulated internal variability, but consistent with the simulated response to anthropogenic and natural forcings. In individual forcing simulations from one model, they found that both GHGs and ozone depletion contributed to a shift in precipitation consistent with that observed, with their influence partially opposed by the response to aerosols.

Previous Ozone Assessments have noted that the observed warming of the Antarctic Peninsula and cooling observed over the rest of continental Antarctica observed in austral summer are largely congruent with the positive trend in the SAM, suggesting that ozone depletion has contributed to these trends (e.g., Forster and Thompson et al., 2011). Since the last Ozone Assessment, several studies have directly examined the surface temperature trends simulated in response to ozone changes in coupled ocean-atmosphere models. Consistent with the last Ozone Assessment, McLandress et al. (2011) simulate cooling over eastern Antarctica and warming over western Antarctica in austral summer in response to ozone depletion. Sigmond and Fyfe (2010) also simulate a weak cooling over the Antarctic interior in austral summer in response to ozone depletion, but no significant response over the Antarctic Peninsula. They simulate a maximum surface temperature response to ozone depletion over the Southern Ocean at around 60°S in late winter where a pronounced warming is associated with the simulated decrease in sea ice extent (Section 4.4.1.3). In the annual mean, Bitz and Polvani (2012) also simulate the largest surface temperature response to ozone depletion over the high latitude Southern Ocean at around 60°S, in standard and high-resolution models. Over Antarctica itself, the simulated surface temperature response is small in the annual mean in their simulations. Thus recent studies find that in models at least, the largest annual mean surface temperature response to ozone depletion is not over Antarctica itself, but warming over the high latitude Southern Ocean. Other studies have noted the summertime contribution of the positive SAM trend to surface warming over southern Africa (Manatsa et al., 2013) and Patagonia

(Thompson et al., 2011) and the mitigation of warming in central-east Australia (Hendon et al., 2007), with a recent study suggesting springtime ozone losses can be directly implicated in these impacts (Bandoro et al., 2014).

4.4.1.2 OCEAN IMPACTS

As discussed above, observations show a strengthening and poleward shift of the band of maximum surface wind stress over the southern oceans since 1979 (Figure 4-11), largest in austral summer. Modeling evidence indicates that in summer, stratospheric ozone depletion has been the dominant driver of these changes, with greenhouse gas increases and stratospheric ozone making comparable contributions in the annual mean (see discussion above). The westerly wind stress plays a fundamental role in driving the oceanic circulation, including creating (via so-called Ekman transport) a region of divergence and upwelling on the poleward side of the surface wind maximum, and convergence and downwelling equatorward of the maximum. As discussed in the 2010 Ozone Assessment (Forster and Thompson et al., 2011), given the observed trends in the surface wind stress, one expects an enhancement of this Ekman response, causing increased upwelling of deep waters south of the Antarctic Circumpolar Current (ACC), increased northward surface flow at the latitude of the ACC, and increased downwelling north of the ACC. Recent observational and modeling studies have considerably improved our understanding of the response of the southern oceans to changing winds.

We first consider changes in the southern subtropical oceans (~15–45°S), where observations show increases in the horizontal circulation, and transport consistent with the increase in maximum wind stress (and wind stress curl). Analysis of satellite altimetry and ship and float hydrographic data shows an increase in the strength of the southern subtropical horizontal circulation ("gyres") from the early 1990s to early 2000s that agrees with the expected response to the increase in the wind stress curl (Roemmich et al., 2007; Cai, 2006). Model simulations indicate that at least half of the changes in DJF are induced by Antarctic ozone depletion (Cai and Cowan, 2007). This intensification of the subtropical gyres and associated changes in Ekman-driven downwelling north of the ACC would be expected to contribute to more rapid transport of surface waters into the interior ("ventilation") of the upper southern subtropical oceans. Recent analysis of repeat measurements of chlorofluorocarbons (CFCs) in the southern oceans shows such an increase in ventilation, with a decrease in the mean age of water at the subtropical thermocline between the early 1990s and mid-late 2000s (Waugh et al., 2013; Figure 4-15). The mean age of ocean water is analogous to the mean age of stratospheric air, and is defined as the mean time for transport from the surface to the interior ocean. Further, there is quantitative agreement in observed changes in wind stress curl, gyre strength, and subtropical age, with all changing by around 20–30% (Waugh, 2014).

The new analysis of ocean CFC measurements also indicates decadal changes in the ventilation of the subpolar southern oceans, but with an increase in the mean age between the early 1990s and mid-late 2000s (Huhn et al., 2013; Waugh et al., 2013; Figure 4-15). This increase is consistent with theoretical considerations and modeling studies, which (as discussed in the last Assessment) indicate that an intensification of the surface winds will lead to an intensification in the meridional overturning circulation, with an increase of upwelling in subpolar waters and an increase in downwelling in subtropical waters. The increase in subpolar upwelling will bring up more deep, old waters that mix with surrounding waters and increase the ages in subpolar waters. The contrast between the decrease in age in subtropical waters and increase in subpolar waters inferred from CFC observations is also found in modeling studies (Bryan et al., 2006; Gnanadesikan et al., 2007; Waugh, 2013).

An intensification of surface winds is also expected to lead to changes in subsurface ocean temperatures. A subsurface warming is observed below and north of the ACC (around 40–60°S), and this is consistent with a poleward shift of the temperature structure (Böning et al., 2008; Gille, 2008; Cai et al., 2010). However, the extent to which the Southern Ocean warming is caused by shifting of the ACC versus other processes, such as an acceleration of poleward heat flux caused by the increasing eddy intensity (Hogg et al., 2008), is currently unclear. A subsurface warming, extending deepest in the midlatitudes, is

also found in modeling studies examining the impact of ozone depletion on Antarctic sea ice (Sigmond and Fyfe, 2010; Bitz and Polvani, 2012; Smith et al., 2012), as described in Section 4.4.1.3 below.

The above observational and modeling studies present a consistent picture for the ocean's response to increasing surface wind stress, with intensification of the subtropical horizontal (gyre) and the meridional overturning circulations, more rapid ventilation of the subtropical waters but older subpolar waters, and a subsurface warming. However, large uncertainties remain. This is in part due to limited historical oceanic data that prevents observational quantification of the (potentially large) natural decadal variability. An additional complication is the role of oceanic mesoscale (10–50 km scale) eddies. As discussed in the 2010 Ozone Assessment, these play an important role in the ocean response to changing forcing, but the climate models used to examine ozone impacts generally do not explicitly resolve these eddies and it is uncertain how much the effect of eddies oppose the direct wind-forced acceleration of the zonal flow (e.g., ACC transport) and overturning circulation. However, there has been recent progress in testing these ideas, and we now have a better understanding of the Southern Ocean eddy field and circulation response to changing winds. Theoretical arguments have been made that indicate that an invariant ACC transport (eddy saturation) is dynamically distinct from an invariant overturning circulation (eddy compensation), and one does not imply the other (Meredith et al., 2012). These arguments have been tested with various eddy permitting and eddy resolving models with different configurations, and it has been found that in the eddy saturated limit, only partial compensation of the overturning circulation is expected in response to decadally-changing winds (Meredith et al., 2012; Morrison and Hogg, 2013; Farneti et al., 2010). Widely used parameterizations for the role of mesoscale eddies have typically failed to capture this response adequately, though recent improvements in their implementation have shown progress (Hofmann and Morales Maqueda, 2011; Gent and Danabasoglu, 2011). Investigations are continuing, including into what sets the level of (incomplete) eddy compensation, and hence the magnitude of the overturning response to changing winds (Abernathey et al., 2011). These advances in understanding imply that an increase in Southern Ocean overturning (and corresponding changes in the ventilation) in response to changing winds is a reasonable expectation.

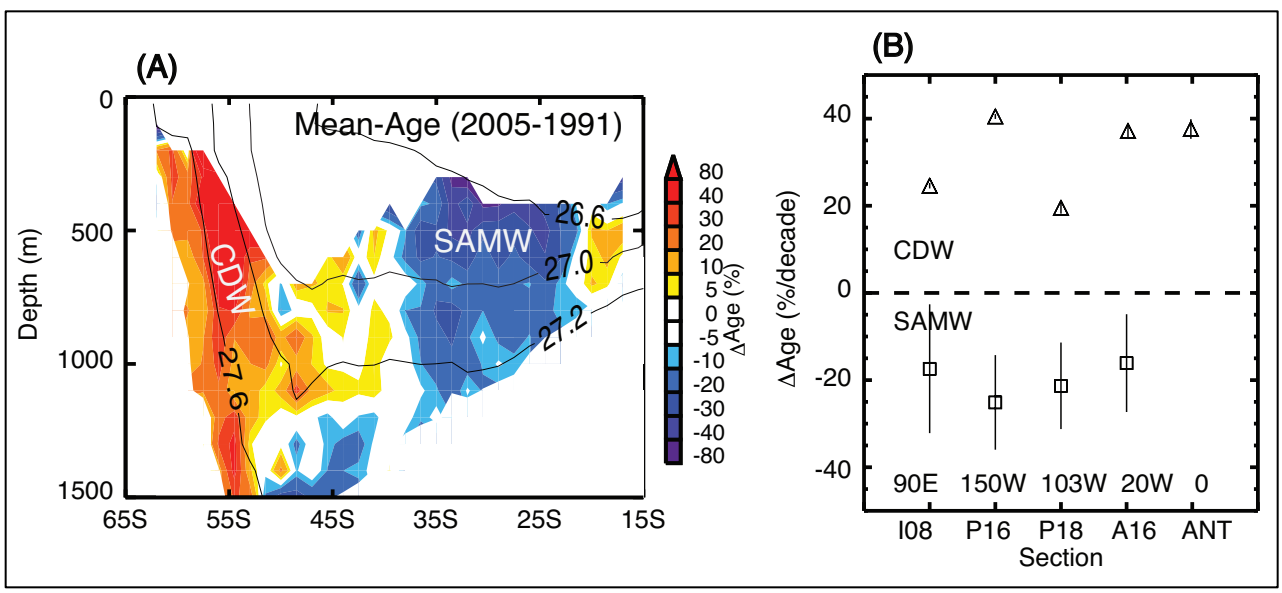

Figure 4-15. (a) Depth-latitude cross-sections of the change in mean age of ocean water between 1991 and 2005 based on CFC-12 measurements along 150°W. (b) Difference in mean age, expressed as percentage change per decade relative to age from original cruise, for circumpolar deep water (CDW) and Subantarctic Mode Water (SAMW) water masses for the repeat sampling of meridional sections at 90°E, 150°W, 103°W, 20°W, and 0°E. Adapted from Waugh et al. (2013) and Huhn et al. (2013).

Ocean carbon

The southern oceans play a critical role in the oceanic uptake of atmospheric carbon dioxide, and, as discussed in the last Assessment, there is evidence that the intensification and poleward shift of the surface winds has led to a reduction in the CO_2 uptake in Antarctic waters. This reduction is linked to more transport of carbon-rich deep waters to the surface, which decreases the surface air-sea gradients and oceanic uptake. An increase in the upwelling of carbon-rich deep waters is consistent with the increase in the age of subpolar water discussed above. However, the southern oceans are very poorly sampled (especially for carbon), and there are large uncertainties in the estimates of the carbon uptake.

In a recent study, Lenton et al. (2013) compared estimates of 1990–2009 Southern Ocean air-sea CO_2 fluxes from several different methods, including a synthesis of surface ocean observations, five ocean biogeochemical models coupled to ocean general circulation models, eleven atmosphere inversions, and ten ocean inversions (the atmospheric inversions estimate carbon fluxes from atmospheric CO_2 measurements, while the ocean inversions estimate fluxes from ocean measurements). They show large interannual variability in the air-sea fluxes (up to 25% of annual mean) and some substantial differences between fluxes inferred using different methods. In particular, there is a large spread in the 1990–2009 trends, with atmospheric inversions generally showing a slowdown in the uptake (broadly consistent with Le Quéré et al., 2007), while the ocean biogeochemical models indicate an uptake consistent with the growth of atmospheric CO_2 (i.e., no slow-down). Further complicating the picture, recent observational studies indicate large zonal variations in the ocean uptake of carbon (Sallée et al., 2012), and the changes in the efficiency of the Southern Ocean sink may not be zonally uniform (Lenton et al., 2013). Given the poor sampling in southern oceans, the zonal and interannual variability, and large uncertainties in all methods, longer data records will be needed to determine if there are any trends in the oceanic uptake of CO_2 (and even then it may not be possible to determine if these trends are linked to stratospheric ozone depletion).

4.4.1.3 SEA ICE IMPACTS

Significant increases in Antarctic sea ice extent of 2.5 ± 2.0% have been observed in austral summer from 1979–2012 (Vaughan et al., 2013). The sea ice trends vary regionally, with large increases in the Ross Sea and decreases in the Bellingshausen and Amundsen seas (Vaughan et al., 2013). At the time of the 2010 Assessment, the influence of stratospheric ozone trends on Antarctic sea ice was unclear, with some studies arguing that ozone depletion might be responsible for the observed positive trends in Antarctic sea ice extent (e.g., Turner et al., 2009), leading the last Assessment to conclude that there was some evidence that the ozone-induced summer SAM trend had caused the summer increase in Antarctic sea ice extent (Forster and Thompson et al., 2011). However, the studies assessed in the last Assessment focused on the relationship between sea ice and the SAM on monthly timescales, instead of on how stratospheric ozone changes affect sea ice on decadal timescales. Since the last Ozone Assessment, Simpkins et al. (2012) argued, based on observations, that the increase in sea ice extent is not linked to the trend in the SAM and several studies have now explicitly addressed the question of how stratospheric ozone depletion affects Antarctic sea ice.

The first of these studies is by Sigmond and Fyfe (2010); they contrasted time-slice model integrations before and after the formation of the ozone hole and concluded that ozone depletion would result in a reduction of Antarctic sea ice extent. The second is a study by Bitz and Polvani (2012), which also contrasted model runs with and without an ozone hole; they confirmed the results of Sigmond and Fyfe (2010) and corroborated them by using an eddy-resolving ocean model. This same result was further strengthened by the study of Smith et al. (2012), who used a fully coupled chemistry-climate model to study the effect of ozone recovery on sea ice. Finally, Sigmond and Fyfe (2014) found that a decrease in annual mean sea ice extent was simulated in response to ozone changes over the 1951–2005 period in all five CMIP5 models with ozone-only simulations available. The ozone-induced strengthening of the

Southern Ocean overturning circulation (Section 4.4.1.2) is found to enhance the upwelling of warm water beneath the mixed-layer and enhance convection, driving upper ocean warming (Section 4.4.1.2) and decreases in sea ice extent in all seasons (Bitz and Polvani, 2012).

Thus, in all models that have isolated the impact of stratospheric ozone depletion, Antarctic sea ice extent declines in all seasons. However, confidence in the simulated response to ozone depletion is limited by the fact that even with all major forcings, climate models on average simulate a decrease in sea ice extent (Turner et al., 2013; Zunz et al., 2013), whereas observations show Antarctic sea ice extent to have increased (albeit at a rather small rate) over the observational period (Parkinson and Cavalieri, 2012; Vaughan et al., 2013). Some studies have found that the observed positive trend is within the range of simulated trends, perhaps just reflecting a multi-decadal natural variation (Polvani and Smith, 2013; Zunz et al., 2013; Mahlstein et al., 2013), though Turner et al. (2013) and Zunz et al. (2013) also note the difficulties the models have in reproducing both the climatological and interannual variability of the observed sea ice extent. Another hypothesis is that the observed sea ice growth is due to enhanced freshwater input from dynamic mass loss (Bintanja et al., 2013), which is not included in the models, though this effect may not be large enough to explain the discrepancy (Swart and Fyfe, 2013). Overall, as concluded in the IPCC Fifth Assessment Report, the fundamental cause for the observed sea ice increase remains unknown and there is low confidence in the scientific understanding of this trend (Bindoff et al., 2013).

4.4.2 Radiative Effects

Stratospheric ozone exerts an influence on the troposphere directly by affecting the longwave and shortwave irradiances in the troposphere. Since 2000, a limited number of studies have investigated the radiative effects of stratospheric ozone concentration change, as assessed in previous IPCC and Ozone Assessments. These assessments have all reached similar conclusions, that stratospheric ozone depletion since 1979 likely contributes a net negative radiative forcing of around −0.05 W m^{-2} ± 0.1 W m^{-2} (e.g., Myhre et al., 2013). For context the forcing from CO_2 changes over 1979–2010 was 0.8 W m^{-2} (Myhre et al., 2013). The sign of the ozone forcing remains uncertain due to uncertainties from: i) quantifying ozone changes near the tropopause where the relative forcing is strongest; ii) cancellation between positive shortwave and negative longwave forcing, and iii) the dominant role of stratospheric adjustment in contributing a negative longwave forcing. Because of these factors considerable uncertainties remain when deriving forcing from observations and these uncertainties impact the testing of model-derived forcings. The radiative forcing from stratospheric ozone change is comparable in magnitude to that from changes in stratospheric water vapor due to methane oxidation (discussed in Section 4.2.2), which is assessed to be 0.07 (0.02–0.12) W m^{-2} in the IPCC Fifth Assessment Report (Myhre et al., 2013). Changes in stratospheric water vapor due to changes in transport or circulation are considered to be a feedback rather than a forcing by Myhre et al. (2013).

Hassler et al. (2013) compared stratospheric ozone forcings derived from different observation-based data sets over 1979–1997 and found a factor of four difference in net globally averaged radiative forcing (−0.03 W m^{-2} to −0.12 W m^{-2}; Figure 4-16). Uncertainties in derived ozone trends, corresponding to differences between data sets, at both high latitudes and over the equator lead to uncertainties in forcing, and to uncertainties in the simulated response to ozone changes. This uncertainty is illustrated in Figure 4-16 where the mean forcing derived from models (−0.04 ± 0.06 W m^{-2}) is similar to the forcings derived using the SPARC (Stratosphere-troposphere Processes and their Role in Climate; Cionni et al., 2011) data set but smaller than those derived from the BDBP (Binary Database of Profiles; Bodeker et al., 2013) data set. There is also additional uncertainty introduced by the radiative transfer and stratospheric adjustment method (compare the two dashed lines in Figure 4-16). The weaker ozone and radiative forcing trends in the SPARC data set, used in many CMIP5 simulations (Eyring et al., 2013), could lead to an underestimate of the magnitude of the simulated response to ozone changes in many CMIP5 models, although it is not clear whether simulations forced with the BDBP data set could lead to overestimates in the response (e.g., Solomon et al., 2012).

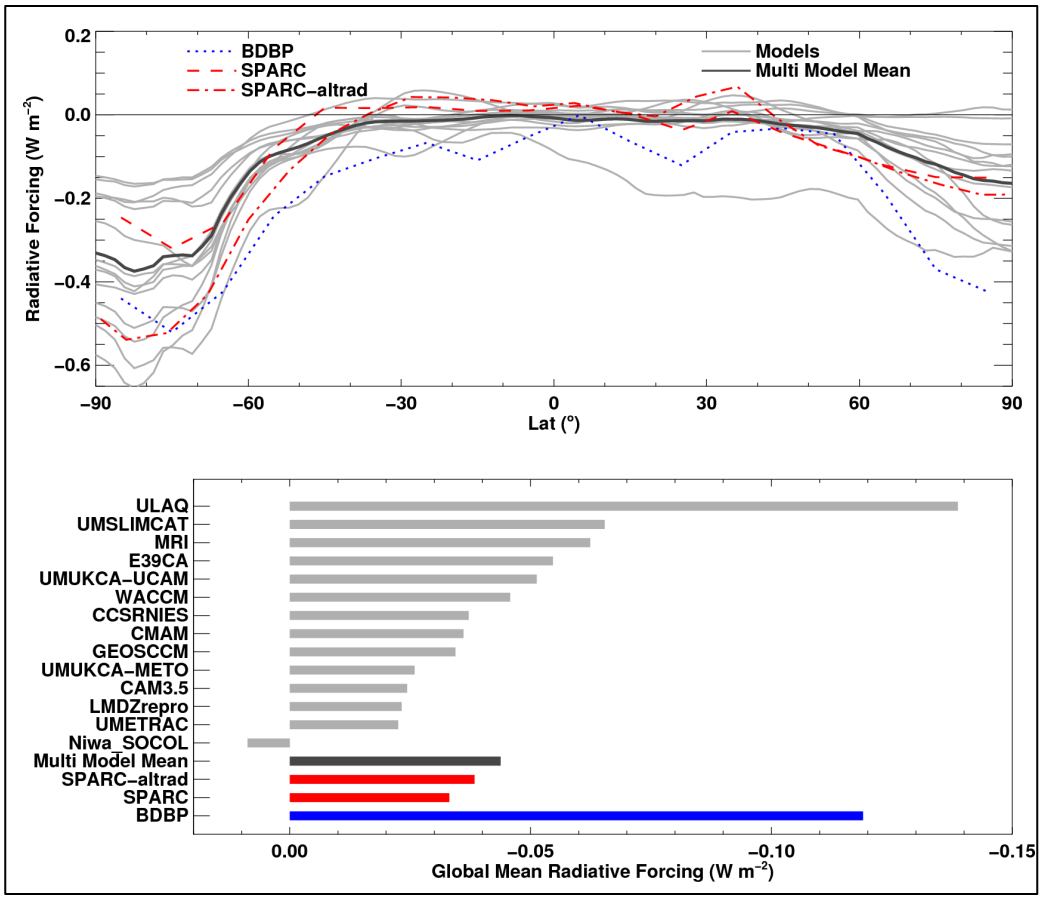

Figure 4-16. *Top:* Annual mean radiative forcing due to stratospheric ozone changes between 1979–1981 and 1995–1997 averages for the BDBP (solid blue line), and the SPARC (dashed red lines) ozone data sets (reproduced from Hassler et al., 2013). Two different radiation and stratospheric adjustment schemes are used with the SPARC data to give a measure of methodological uncertainty. Model forcings are calculated using their ozone fields with a single radiation scheme (CAMRT- J.F. Lamarque). Calculations for CAM3.5, CCSRNIES, CMAM, E39CA, GEOSCCM, LMDZrepro, MRI, Niwa_SOCOL, ULAQ, UMETRAC, UMSLIMCAT, UMUKCA-METO, UMUKCA-UCAM, WACCM CCMVAL-2 models are shown, as well as the multi-model mean. *Bottom:* Same as above but for the global average.

Previous Ozone Assessments have considered the radiative forcing due to stratospheric ozone concentration changes, but this is not necessarily the same as the ozone forcing from ODS emissions, as both ODSs and stratospheric precursors such as methane can affect stratospheric ozone concentrations (see Section 4.4.3). Further, ODS emissions can induce changes in ozone in both the stratosphere and troposphere (see Section 4.4.3). Therefore, as discussed in the IPCC Fifth Assessment Report (Myhre et al., 2013), progress has been made toward merging observation and model results (e.g., Søvde et al., 2011; Shindell et al., 2013a) to derive the radiative forcing from ozone changes due to ODS emissions, considering effects on both tropospheric and stratospheric ozone. There have also been ongoing multi-model intercomparison efforts (e.g., Shindell et al., 2013b; Conley et al., 2013; Stevenson et al., 2013) that help to assess the uncertainties in the ozone radiative forcing. The net radiative forcing due to stratospheric and tropospheric ozone changes induced by ODSs relative to preindustrial levels was calculated to be −0.26 W m^{-2} based on simulations of the Oslo CTM2 (Søvde et al., 2011) and −0.28 W m^{-2} based on simulations of the GISS-E2-R model (Shindell et al., 2013a). Based on these two studies, Myhre et al. (2013) assess the radiative forcing from the effect of ODSs on ozone to be –0.15 (–0.3 to 0.0) W m^{-2} from 1750 to 2010. The best estimate was assessed to be smaller than the estimates of Søvde et al. (2011) and Shindell et al. (2013a) because the models used in those studies had stronger

stratospheric ozone radiative forcing than the Atmospheric Chemistry and Climate Model Intercomparison Project (ACCMIP) multi-model mean (Myhre et al., 2013). About three-quarters of the ozone forcing from ODS emissions results from ozone changes in the stratosphere. The indirect changes in tropospheric ozone account for the other quarter (Shindell et al., 2013a).

The IPCC Fifth Assessment Report (Myhre et al., 2013) also uses effective radiative forcings to quantify the drivers of climate change. This effective radiative forcing goes beyond the traditional definition of radiative forcing and is defined to additionally account for the forcing from rapid cloud and circulation adjustments in the troposphere, not associated with global mean climate change. Myhre et al. (2013) assumed that any rapid adjustment associated with ozone was small and the effective radiative forcing matched the radiative forcing quoted above, i.e., any indirect forcings from cloud changes were small. However, some studies suggest otherwise. Grise et al. (2013) find a cloud radiative forcing due to the fact that the modeled poleward jet shift caused by the ozone hole moves the Southern Hemisphere clouds poleward, exposing the surface to higher insolation on average. In their model this effect contributed a positive indirect radiative forcing of +0.25 W m^{-2} averaged over the Southern Hemisphere in the annual mean (and around +0.2 W m^{-2} in the global mean). Their result is subject to considerable uncertainty and would likely be model dependent. A further possible effect relates to the modification of surface wind driven sea salt fluxes and thereby cloud condensation nuclei and clouds (Korhonen et al., 2010; Struthers et al., 2013). Korhonen et al. (2010) show that this could be of a similar magnitude, but is a cooling effect (–0.7 W m^{-2} over the 50°S to 65°S latitude band in the summer, and around −0.1 W m^{-2} in the global mean). Therefore, it is expected that Southern Hemisphere effective forcings exist due to shifts in the midlatitude jet. These are of indeterminate sign, could exert a large local forcing, and could be of a comparable magnitude to the direct ODS-induced ozone radiative forcing in the global mean.

In summary ODS emissions likely contributed a small negative radiative forcing of −0.15 ± 0.15 W m^{-2} in 2010 due to ozone. However, the possibility of a similarly sized adjusted forcing from circulation-driven cloud changes leads to an effective radiative forcing from ODSs of undetermined sign. The regional nature of this adjusted forcing could be important for Southern Hemisphere climate change.

4.4.3 Chemistry Effects

Ozone levels in the troposphere are affected by natural and anthropogenic emissions of reactive compounds, the prevailing climate, and the influence of the stratosphere. At the global scale, the impact of these drivers on tropospheric ozone is assessed by examining its budget terms, with production from in situ photochemistry and a net influx from the stratosphere (via stratosphere-troposphere exchange, STE), and loss from in situ chemistry and deposition to surfaces (e.g., Wild, 2007). The role of stratospheric change for tropospheric ozone is both direct and indirect. The direct influence is via changes in the net influx of stratospheric ozone, mediated by increases or decreases in stratospheric ozone concentrations and changes in the patterns and strength of the stratospheric transport and circulation (e.g., the BDC) that bring ozone to the troposphere (e.g., Hegglin and Shepherd, 2009). The indirect influence is mainly through stratospheric ozone-modulated changes in UV radiation and the subsequent impacts on tropospheric photochemistry (e.g., Tang et al., 2011), although stratospherically driven tropospheric climate changes could have an additional small impact. Changes in tropospheric ozone and the UV flux are important because these have impacts on all chemically active tropospheric constituents, including impacting air quality (Tang et al., 2011; Lin et al., 2012) and the lifetimes of chemically active GHGs such as methane (Voulgarakis et al., 2013).

Global chemistry models remain the main tools for understanding the tropospheric ozone budget (see Box 2-2 in Chapter 2 of this Assessment). A major improvement to many chemistry-climate models since the last Assessment is the merging of tropospheric and stratospheric chemistry schemes (e.g., Naik et al., 2013; Shindell et al., 2013c), enabling studies that examine impacts and feedbacks between the two domains. Ten of the fifteen models used to assess preindustrial to projected future ozone changes in the Atmospheric Chemistry and Climate Model Intercomparison Project (ACCMIP) (Young et al., 2013a)

included a chemistry scheme appropriate for both stratospheric and tropospheric chemical processes, although there was a broad range in the complexity of the schemes (the number of species simulated ranged from 16 to 130). However, despite the overall increase in complexity of the models, simulations of present day tropospheric ozone do not differ markedly from those considered in the 2010 Ozone Assessment (see also Stevenson et al., 2006), including in their ability to reproduce the seasonal and geographical features in ozone observations (Myhre et al., 2013; Young et al., 2013a).

Since the 2010 Ozone Assessment, there have been several model studies examining the drivers of past tropospheric composition that explicitly consider the influence of stratospheric ozone change caused by ODSs (John et al., 2012; Lang et al., 2012; Shindell et al., 2013c; Young et al., 2013a; Reader et al., 2013). Lang et al. (2012) examined the changes between 1960 and 2005, using sensitivity simulations to isolate the role of ODS changes between those periods. They found that, in the absence of other changes, the increase of ODSs between 1960 and 2005 reduced ozone concentrations globally, with the chemically induced reduction of stratospheric ozone resulting in a decreased net ozone influx to the troposphere of 5.4% in the Northern Hemisphere and 21.6% in the Southern Hemisphere. The decrease in STE ozone flux was slightly offset by an ODS-driven increase in the strength of the meridional circulation, which increases the STE mass flux (Oman et al., 2009) (see also Section 4.3.2.2). John et al. (2012) note the importance of decreased stratospheric ozone in decreasing methane lifetime in the last decades of the 20th century (through enhanced UV increasing the concentration of the hydroxyl radical, OH), but do not quantify the effect.

The main focus of the other studies is on the drivers of preindustrial (PI; ~1850) to present-day changes. All three studies (Shindell et al., 2013c; Young et al., 2013a; Reader et al., 2013) report a much lower tropospheric ozone column/burden in the PI (reduced 25–30% compared to present day), driven by the lower ozone precursor emissions in the past. Shindell et al. (2013c) found that the net stratospheric influx of ozone into the troposphere was ~25% greater in their PI simulation. Such an increase might indeed be expected, given the higher stratospheric ozone concentrations and the lower tropospheric ozone concentrations (meaning a higher *net* import of ozone into the troposphere), although the range of changes in the net stratospheric influx reported by Young et al. (2013a) (~0–50%) shows that there is little agreement on the magnitude of this impact. Reader et al. (2013) suggest that the combined increase in tropospheric ozone (through precursor emission increases) and decrease in stratospheric ozone since the PI means that the global total ozone column has changed little.

Overall, the move by many groups toward combined troposphere-stratosphere chemistry-climate models allows better characterization of the links between the two domains, albeit with the caveat that it is hard to unambiguously assign magnitudes to individual drivers in such an interrelated system. While most models agree that ODS-driven ozone depletion has reduced the magnitude of the net stratospheric influx of ozone into the troposphere, our assessment of the magnitude of the effect is hampered by the range of stratospheric treatments in different models (i.e., fully interactive to passive/prescribed), which is likely one driver of inter-model variability in the results. Furthermore, improvements in measurement techniques will be needed to better constrain STE processes in models (Tang and Prather, 2012), although new observational analyses are providing insights into the main locations of STE events (Jin et al., 2013), which will be valuable for future validations.

4.5 EFFECTS OF FUTURE CHANGES IN STRATOSPHERIC OZONE ON THE TROPOSPHERE AND SURFACE

This section assesses the climate impacts of future variations in stratospheric ozone over the next century. It follows an identical structure to Section 4.4, discussing the climate impacts from a radiative, dynamical, and chemistry perspective. Earlier chapters have outlined future projections of stratospheric ozone for the globe (Chapter 2) and polar regions (Chapter 3). These projections involve a complex interaction between projected changes in GHGs, ODSs, and the climate system. While a declining stratospheric halogen loading is expected to lead to an increase in stratospheric ozone, GHG changes will

also influence ozone concentrations through direct chemical effects, climate-induced changes in chemistry, and changes in the stratospheric circulation.

The studies assessed incorporate climate model results from a number of intercomparison projects. These include experiments run under new scenarios of future emissions named Representative Concentration Pathways (RCPs) that were developed in preparation for the IPCC Fifth Assessment Report. Box 4-1 gives a description of the RCPs and how they differ from the Special Report on Emissions Scenarios (SRES) scenarios considered in the 2010 Ozone Assessment.

4.5.1 Tropospheric Circulation Effects

It is now well established that the Southern Hemisphere circulation response to the anticipated ozone recovery is largely opposite to that resulting from ozone depletion in the past (Section 4.4.1), offsetting GHG-induced circulation change in the austral summer. This offsetting effect may then result in a much weaker rate of Southern Hemisphere circulation change, and associated impacts, in the next few decades than in the recent past. In this section the possible effects of stratospheric ozone recovery on Southern Hemisphere climate are assessed, updating the 2010 Ozone Assessment by integrating recent findings. Since projected circulation changes are all assessed from climate models and many models exhibit biases, for example in the climatological jet location, projected circulation changes are subject to considerable uncertainty. In line with Section 4.4.1, overall assessments are focused on the Southern Hemisphere especially over austral summer, DJF, when ozone-related tropospheric climate changes are strongest. The potential impact of ozone recovery on the Northern Hemisphere climate is only briefly assessed. The benefit of the Montreal Protocol is also documented by considering recent simulations of the effects of unregulated ODS emissions.

The Southern Hemisphere

Since the 2010 Ozone Assessment significant progress has been made in our understanding of stratospheric ozone-related Southern Hemisphere climate change in the future. A number of studies have been conducted either by performing climate model sensitivity tests with and without stratospheric ozone recovery (Shindell and Schmidt, 2004; Perlwitz et al., 2008; Karpechko et al., 2010; McLandress et al., 2011; Polvani et al., 2011a; Arblaster et al., 2011; Staten et al., 2012; Watson et al., 2012) or by examining multi-model projections of the CMIP3 (Miller et al., 2006; Son et al., 2009), CCMVal-2 (Son et al., 2010), and CMIP5 models where stratospheric ozone concentration is prescribed or predicted internally (Swart and Fyfe, 2012; Eyring et al., 2013; Barnes et al., 2014; Gerber and Son, 2013).

Figure 4-13 summarizes the overall climate effects of stratospheric ozone recovery as simulated by the Canadian CCM (CMAM) under the SRES A1B GHG emission scenario (McLandress et al., 2011). Although this is based on single model's experiments, these experiments are qualitatively consistent with results that were reported by Polvani et al. (2011a) based on simulations from the CAM3 model. In the absence of other climate forcing, the increase in stratospheric ozone concentration since 2000 (red lines) warms the stratosphere, with a maximum warming in the Antarctic lower stratosphere during austral spring and summer (Figure 4-13a, Figure 4-6). This warming reduces the temperature lapse rate near the tropopause, lowering polar tropopause height and increasing tropopause pressure (Figure 4-13b). The polar warming also reduces the meridional temperature gradient in the upper troposphere and lower stratosphere that will likely lead to a weakening of the Antarctic polar vortex. As discussed in Section 4.4.1 and shown in Figure 4-13c, the wind change is not limited to the upper troposphere and lower stratosphere. A significant response is also simulated near the surface. Specifically, the midlatitude jet is simulated to shift equatorward in response to ozone recovery. This change strongly projects onto the negative polarity of the SAM. Recent studies have shown that the latitudinal shift of the austral-summer jet is mostly eddy-driven (Lorenz and DeWeaver, 2007; Butler et al., 2010; McLandress et al., 2011) and highly correlated with the long-term trend of the southern edge of the Southern Hemisphere Hadley Cell

Box 4-1. Representative Concentration Pathways

Future anthropogenic emission projections typically follow a scenario approach based on a set of assumed socio-economic choices that may be expected over the next century. In the lead-up to the Intergovernmental Panel on Climate Change (IPCC) Fifth Assessment Report, the scientific community, for the first time in 12 years, developed new scenarios for climate change research. These Representative Concentration Pathways (RCPs) differ from the previous Special Report on Emissions Scenarios (SRES) scenarios in that they are concentration scenarios based around general characteristics of radiative forcing at 2100, rather than emissions scenarios (van Vuuren et al., 2011). This allowed both emission and socio-economic scenarios to be developed in parallel.

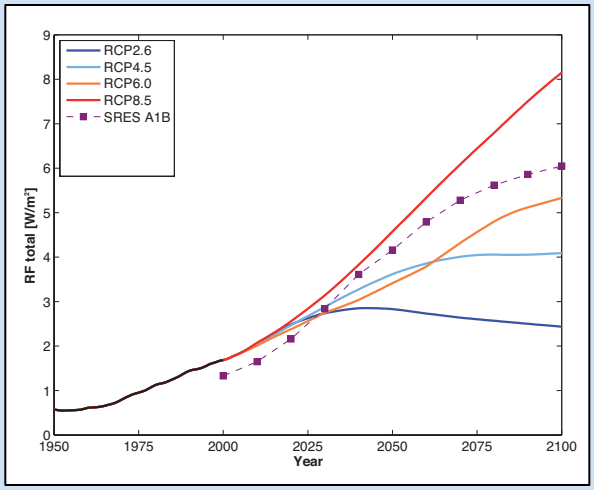

Box 4-1: Figure 1. Historical and projected total anthropogenic radiative forcing (RF; W m^{-2}) relative to preindustrial (~1765) between 1950 and 2100 for the SRES A1B and RCP scenarios. Adapted from Cubasch et al. (2013).

For the Coupled Model Intercomparison Project-Phase 5 (CMIP5), four pathways were chosen from the existing literature to span a range of radiative forcing in 2100 which are outlined in Figure 1: RCP2.6 (peak and decline; 2.6 W m^{-2}), RCP4.5 (stabilization without over-shoot; 4.5 W m^{-2}), RCP6.0 (stabilization without over-shoot; 6.0 W m^{-2}), and RCP8.5 (rising; 8.5 W m^{-2}). By 2100, the radiative forcing of the SRES A1B scenario, used in most of the chemistry-climate model simulations assessed in SPARC CCMVal (2010), is closest to RCP6.0. The RCPs explicitly define emissions and concentrations of GHGs (Figure 2), aerosols, tropospheric ozone precursors, and land-use change. They do not give specific guidance on variations in natural forcings, such as volcanic eruptions and solar input for the future, however most CMIP5 models included some form of the 11-year solar cycle in their RCP simulations while returning volcanic aerosols to zero or preindustrial background volcanic aerosol values (Collins et al., 2013). Emissions of most ozone-depleting substances follow the A1 scenario (WMO, 2003), which has a similar trajectory to the adjusted A1 halon scenario used in the 2010 Ozone Assessment, and is identical for all RCPs. See Meinshausen et al. (2011) for more details.

The main set of climate model simulations underlying the IPCC Fifth Assessment Report were those included in CMIP5. For models without interactive chemistry, the International Global Atmospheric Chemistry (IGAC) and Stratosphere-troposphere Processes and Their Role in Climate (SPARC) communities developed an ozone concentrations database covering the period 1850–2100 (Cionni et al., 2011). For the future period, zonal mean stratospheric ozone concentrations in this database were computed from the average of 13 CCMVal-2 models run under the SRES A1B scenario. Thus, the stratospheric ozone concentrations are identical for each RCP. Tropospheric ozone was based on the CAM3.5 chemistry-climate model (Lamarque et al., 2011). Eyring et al. (2013) document the implementation of ozone forcing in each model that participated in CMIP5. Of the 46 models assessed, a little over half prescribed ozone concentrations from the IGAC/SPARC database and the others used either semi-offline or interactive chemistry. For the latter, the ozone concentrations were simulated interactively under the four RCPs, providing some variation in stratospheric ozone across scenarios and models. The CMIP5 ozone projections are within the spread of those from the CCMVal-2 models used in the 2010 Ozone Assessment.

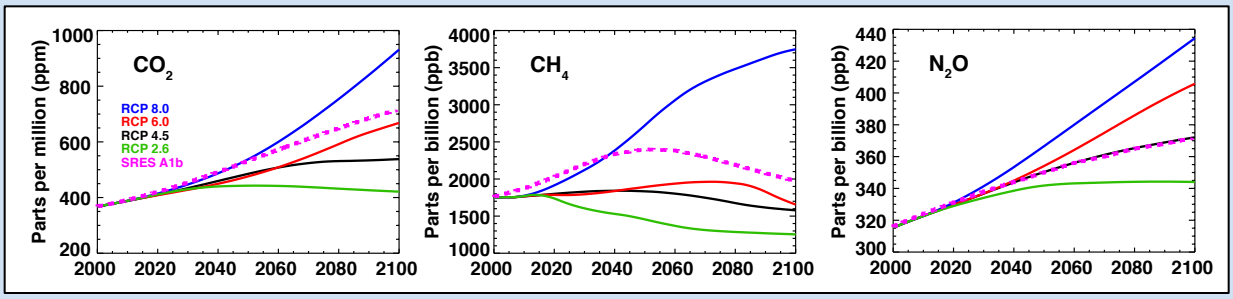

Box 4-1: Figure 2. Concentrations of CO_2, CH_4, and N_2O under the four RCPs and the SRES A1B scenario.

(Son et al., 2009; Kang and Polvani, 2011; Gerber and Son, 2013). Although weak, this equatorward shift of the Hadley Cell edge is evident in Figure 4-13d.

All of these projected changes are essentially opposite to those resulting from stratospheric ozone depletion in the past (compare 1960–2000 and 2001–2099 trends in Figure 4-13). More importantly, they oppose atmospheric circulation changes associated with ongoing GHG increases (blue lines in Figure 4-13). As a result, Southern Hemisphere summer circulation changes in the next few decades are likely to be much weaker than those in the late 20th century (black lines in Figure 4-13).

The relative importance of GHG increases and ozone recovery for the simulated future midlatitude jet shift depends on the GHG emissions scenario and season. Multi-model analyses using the CMIP5 models (e.g., Swart and Fyfe, 2012; Eyring et al., 2013; Barnes et al., 2014) have shown that in austral summer the Southern Hemisphere circulation effects of stratospheric ozone recovery in the first half of 21st century likely overwhelm those of GHG increases under a low GHG emissions scenarios, e.g., RCP2.6 (Box 4-1), as shown in Figures 4-10c and 4-17a. In the RCP8.5 scenario, which has high GHG emissions, the influence of GHGs likely dominates (Figures 4-10d, 4-17a), whereas near cancellation is simulated under moderate emission scenarios such as RCP4.5 and RCP6.0 (Box 4-1). In austral winter (JJA), the jet shift is weaker and scales with the strength of the GHG emissions (Figure 4-17b). Differences in radiative forcing between RCP scenarios are small in the near term (Box 4-1), and hence the difference in projected jet trends between RCP scenarios may not be significant until the middle of 21st century (Figure 4-17; Simpkins and Karpechko, 2012).

Projected changes in the Southern Hemisphere midlatitude jet are also dependent on the Antarctic lower stratosphere ozone trend itself. The CCMVal-2 and CMIP5 models with interactive chemistry exhibit a range in future projections of stratospheric ozone. For example, the dates when global-mean total column ozone returns to its 1980 values vary by about 20 years between CCMVal-2 models (Eyring et al., 2010; see also Section 2.4 of Chapter 2 of this Assessment). Consideration of the effects of differing ODS emissions scenarios, and the effects of solar and volcanic forcing changes, would further increase this spread (see Sections 2.4 and 5.4 of Chapters 2 and 5 of this Assessment).

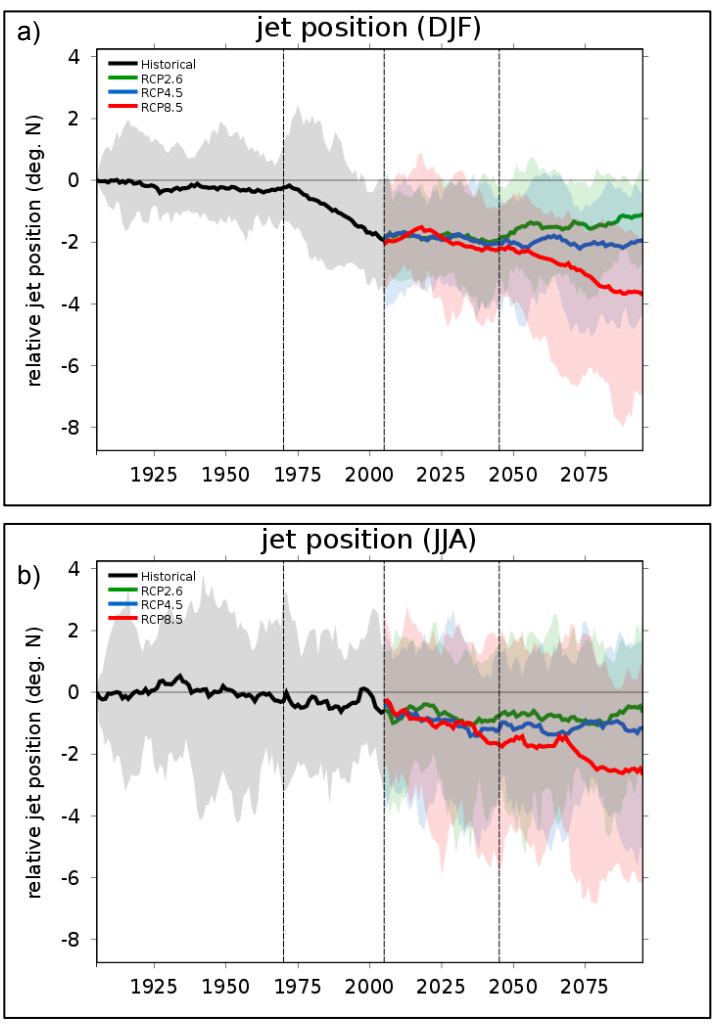

Figure 4-17. Time series of the CMIP5 Southern Hemisphere DJF (panel a) and JJA (panel b) jet position anomalies relative to the 1900–1910 value in the historical simulations and three climate scenario simulations (RCP8.5, RCP4.5, and RCP2.6). Thick lines show the multi-model means and shading indicates the model spread. Time series have been smoothed using a 10-year moving average filter. Adapted from Barnes et al. (2014).

The degree of simulated cancellation between ozone-related and GHG-related climate changes further depends on climate sensitivity (Arblaster et al., 2011; Watson et al., 2012). For the same GHG emissions scenario, upper tropospheric tropical temperature changes differ widely between models (bottom panel of Figure 4-18) partly because of uncertainties in physical parameterizations of atmospheric processes (e.g., Watson et al., 2012). Likewise the same ODS emissions scenario results in different Antarctic ozone and lower stratospheric temperature trends in different models (top panel of Figure 4-18). These uncertainties in tropical upper troposphere and polar lower stratosphere temperature changes, or uncertainties in equator-to-pole temperature gradient changes in the upper troposphere and lower stratosphere, contribute to the uncertainty in projections of future Southern Hemisphere climate change in austral summer (Lorenz and DeWeaver, 2007; Wilcox et al., 2012; Gerber and Son, 2013; Harvey et al., 2013). In general a larger poleward shift of the midlatitude jet is associated with a larger temperature gradient change in the upper troposphere and lower stratosphere (e.g., Wilcox et al., 2012). Even for models with similar climate sensitivity, the atmospheric and surface climate response to external forcings can differ substantially, in part due to differing biases in the mean state (Kidston and Gerber, 2010; Son et al., 2010), since the mean state bias is correlated with the projected Southern Hemisphere midlatitude jet change (Kidson and Gerber, 2010; Son et al., 2010; Simpson et al., 2012; Sigmond and Fyfe, 2014). The projected circulation change is typically larger if the climatological jet is biased equatorward. However, the causal relationship is not clear as there are other deficiencies in climate models. For example, Simpson

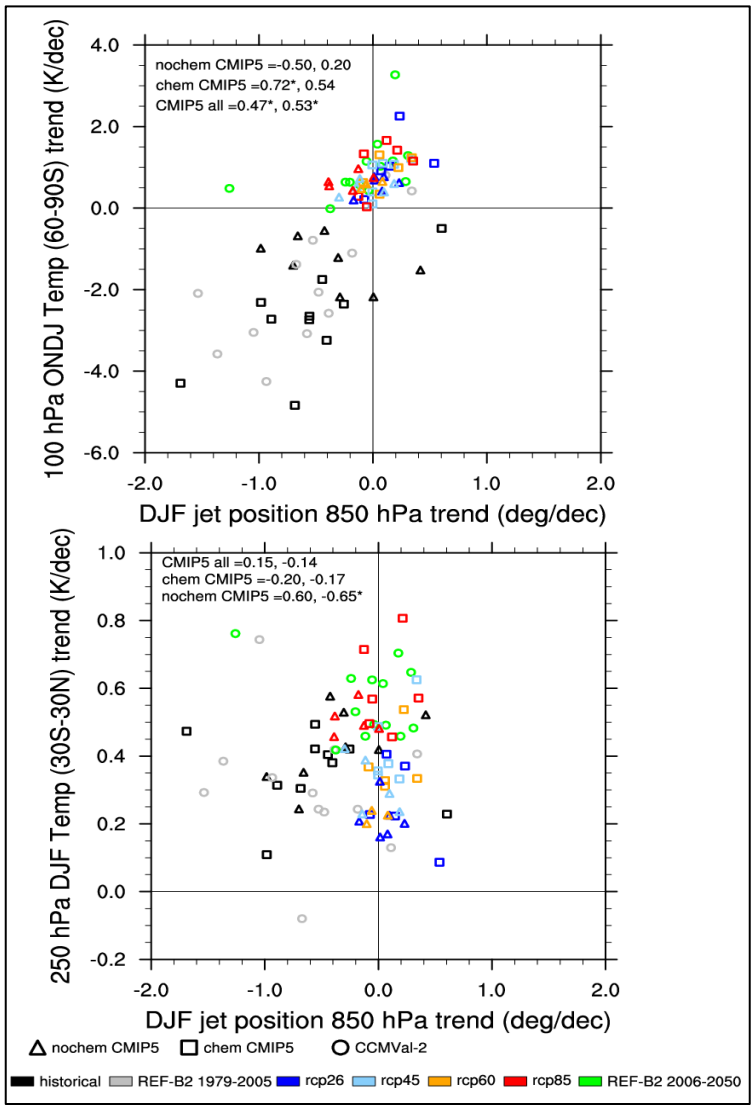

Figure 4-18. The relationship between the trends of the latitudinal location of the DJF near-surface westerly maximum and (*top*) ONDJ polar lower-stratospheric temperature trends and (*bottom*) DJF tropical upper-tropospheric temperature trends. The trends are calculated over 1979–2005 for the past (black or gray) and 2006–2050 for the future (different colors for various GHG emissions scenarios). Both CCMVal-2 (circles) and CMIP5 models (squares for the models with interactive chemistry and triangles for models without it) are used. The correlation between the two variables is computed for all CMIP5 models and for the subset of CMIP5 models with and without interactive chemistry for the past (first number) and for the future (second number). The correlation coefficients that are statistically significant at the 95% confidence level are indicated with an asterisk. Adapted from Eyring et al. (2013).

et al. (2013) showed that the CMIP5 models do not have realistic planetary wave-zonal mean flow feedback, overestimating the time scale of SAM anomalies. This bias in eddy feedback can introduce more uncertainty in future Southern Hemisphere climate changes.

The Northern Hemisphere

Hu et al. (2011) recently argued that the anticipated recovery of stratospheric ozone will substantially enhance tropospheric and surface warming in the first half of the 21st century. They examined CMIP3 models with and without ozone recovery and suggested that ozone-induced tropospheric warming will be strongest during winter in the extratropical Northern Hemisphere, despite the fact that ozone recovery will be strongest in the Southern Hemisphere during springtime. This surprising result was shown by Previdi and Polvani (2012) and McLandress et al. (2012) to be caused not by stratospheric ozone forcing but by different responses of the climate models to GHG forcing. By examining the same two groups of models in GHG-only simulations, Previdi and Polvani (2012) found essentially the same result as Hu et al. (2011), clearly attributing the differences to climate sensitivity. McLandress et al. (2012) further confirmed that Northern Hemisphere surface temperature response to stratospheric ozone recovery is negligible in their coupled chemistry-climate model integrations.

4.5.1.1 Surface Impacts

Projected future tropospheric circulation changes are accompanied by surface climate changes, as were past changes (Section 4.4.1.1). These include changes in sea level pressure, surface air temperature, and precipitation (McLandress et al., 2011; Polvani et al., 2011a). In response to ozone recovery, sea level pressure is projected to increase in high latitudes and decrease in midlatitudes in austral summer, consistent with the negative SAM trend. This will likely change Antarctic surface temperature (Son et al., 2009), but projected changes are relatively small (e.g., McLandress et al., 2011). Hydro-climate systems are also projected to change in response to ozone recovery in austral summer. Specifically the ozone-induced equatorward shift of the surface wind and the associated storm track in summer is expected to drive high-latitude drying and midlatitude moistening (Purich and Son, 2012; Polvani et al., 2011a) and potentially modify the frequency of extreme precipitation events (Purich and Son, 2012; Kang et al., 2013). Projected ozone-induced precipitation and circulation changes approximately cancel GHG-induced changes in the mid and high latitudes of the Southern Hemisphere in summer under the SRES A1B scenario over the 2000–2060 period (Polvani et al., 2011a).

4.5.1.2 Ocean Impacts

The possible influences of stratospheric ozone recovery on the southern oceans have been discussed in the literature, based mainly on past climate simulations (Forster and Thompson et al., 2011). However, a few recent studies have directly addressed this issue using CCMs coupled with coarse-resolution ocean and sea-ice models (Sigmond et al., 2011; Smith et al., 2012).

The equatorward shift and weakening of surface westerlies, or negative SAM trend, simulated in response to ozone recovery will tend to reverse the changes in the southern oceans due to ozone depletion (discussed in Section 4.4.1.2). For example, ozone recovery is expected to reduce northward Ekman transport in the austral summer, weaken the meridional overturning circulation, and weaken the baroclinic component of the ACC (e.g., Figure 4-19). While this effect may be overestimated in some simulations because of unresolved mesoscale eddies, these circulation changes are expected to offset GHG-induced changes to some degree (Sigmond et al., 2011).

There is uncertainty in the timescales of response of different aspects of the ocean circulation to changes in the wind stress. The Ekman response to a change in winds will be almost instantaneous, but the contributions due to eddies will increase over time on a timescale of decades (Meredith and Hogg,

2006; Screen et al., 2009). Changes due to advection of surface perturbations (due to the wind stress change) into the interior ocean will also take longer than the instantaneous Ekman response. Thus there will likely be a delay between changes in the wind stress and changes in the ocean circulation, with the delay depending on the relative role of Ekman and eddy responses in causing changes in a particular aspect of the circulation. For example, the simulations in Sigmond et al. (2011) showed a delay of around 20 years in the response of the ACC to changes in the surface wind stress (see Figure 4-19).

There have been no studies of the impact of ozone recovery on the oceanic uptake of CO_2, but it is likely there will be a reversal of the impact of ozone depletion.

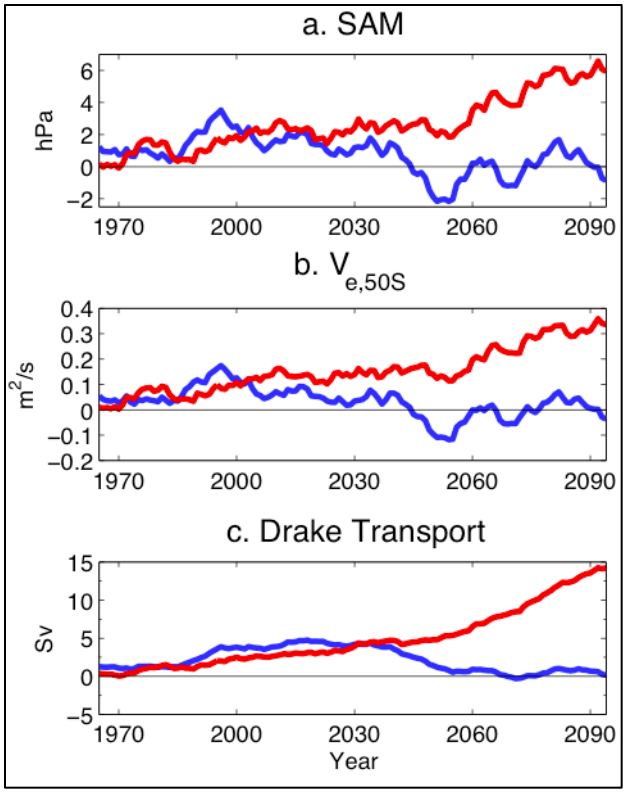

Figure 4-19. Annual mean response to GHG (red) and ODS forcings (blue) of (a) the SAM index, (b) the zonal-mean meridional Ekman transport at 50°S, and (c) the zonal transport through the Drake passage. The time series are smoothed with an 11-year moving average. Three sets of CMAM experiments (GHG, ODS, and control simulations) are used in this figure, each with three ensemble members simulating the 1960–2100 period. The GHG simulation is forced with time-varying GHGs and fixed ODSs at 1960 levels. Conversely, the ODS simulation is forced with time-varying ODSs and other GHGs at 1960 levels. The control simulation is forced with time-varying ODSs and GHGs. To account for model drift, the response to the ODS forcing is defined as the difference between the control and GHG simulations. Likewise GHG-related response is defined as the difference between the control and ODS simulations. Updated from Sigmond et al. (2011).

4.5.1.3 Sea Ice Impacts

Smith et al. (2012) showed that ozone recovery is projected to slow down the Antarctic sea ice decline that is projected in response to GHG increases. This compensation, which results from modulation of the Ekman transport and upper-ocean temperature near the Antarctic continent (Sigmond and Fyfe, 2010; Smith et al., 2012), is found to occur in all seasons because of the long-term memory of ocean temperature. However, this result, which is largely opposite to the simulated Antarctic sea ice response to ozone depletion (Section 4.4.1.3), is based on a single model experiment coupled with a coarse-resolution ocean model. Verification of this result will require further evaluations using high-resolution ocean models.

4.5.1.4 The World Avoided by the Montreal Protocol

The ozone-related climate changes described above are all based on the successful regulation of ODS emissions in accordance with the Montreal Protocol (considered here together with its Amendments and adjustments). However, it is pertinent to ask, what would have happened if the Montreal Protocol had

not been implemented? In other words, what is the benefit of the Montreal Protocol and actions taken so far? Climate models suggest that continued accumulation of ODSs in the absence of the Montreal Protocol would have led to a collapse of the global ozone layer by the mid-21st century. For example, recent studies suggest a decrease of global total ozone from about 315 DU in 1974 to about 110 DU in 2065 in the absence of the Montreal Protocol (Newman et al., 2009; Garcia et al., 2012). Because ODSs are effective GHGs (e.g., Velders et al., 2007; WMO, 2011), increasing ODS concentrations would also enhance surface warming. The combined effects of lower-stratospheric cooling by continued ozone depletion and tropospheric warming by increased ODS emissions would then drive much stronger climate changes in both the Southern Hemisphere and Northern Hemisphere in the 21st century than those simulated in the latter half of the 20th century (Morgenstern et al., 2008; Newman et al., 2009; Wu et al., 2013).

A series of modeling studies, the so-called "world avoided" simulations, have recently been performed either by increasing the concentration of ODSs in CCMs (Morgenstern et al., 2008; Newman et al., 2009; Garcia et al., 2012) or by prescribing unregulated ODSs and corresponding ozone concentrations in an atmospheric general circulation model (AGCM) (Wu et al., 2013). Such simulations show significant stratospheric cooling in the next 20–50 years, with a maximum cooling in the Antarctic lower stratosphere in response to the increased ODS concentrations (e.g., Wu et al., 2013). This cooling would maintain the polar vortex year-round by the mid-21st century (Newman et al., 2009), resulting in no final warming in the Southern Hemisphere stratosphere. Simulated tropospheric warming due to the direct radiative effects of the ODSs would also be substantial. For example, Garcia et al. (2012) found surface warming of over 2 K in response to enhanced ODSs in the tropics, 6 K in the Arctic, and about 4 K in Antarctic from 2000 to 2070 (Figure 4-20). This is of comparable magnitude to GHG warming under the RCP4.5 scenario (Garcia et al., 2012), indicating that global warming over next few decades could have been doubled in the absence of the Montreal Protocol.

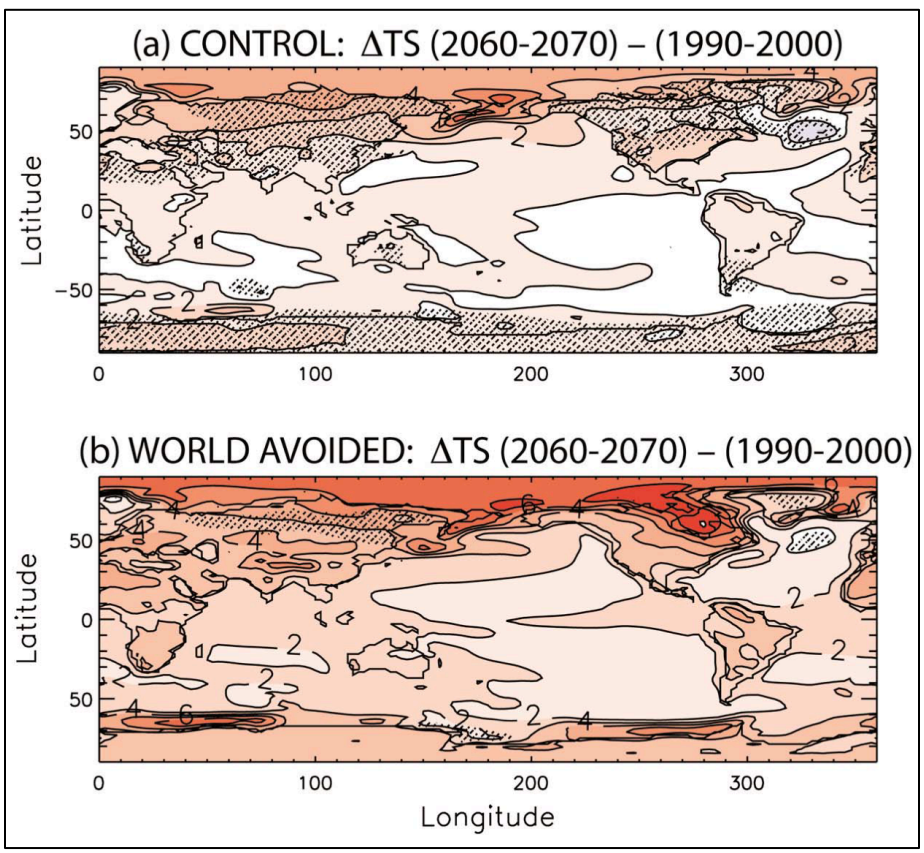

Figure 4-20. Surface temperature change (K) between the decades of 1990–2000 and 2060–2070 in the (a) control and (b) world-avoided simulations. The former is driven by RCP 4.5 and an ODS emissions scenario that is based on the Montreal Protocol. However, in the latter, ODS emissions are not regulated until 2070. Changes in the stippled regions are not significant at the 95% confidence level. From Garcia et al. (2012).

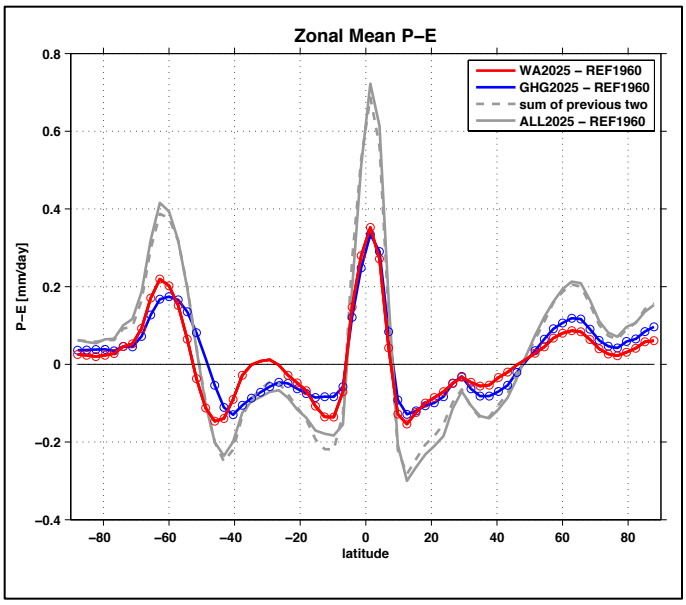

Figure 4-21. The precipitation minus evaporation (P-E) change between a reference simulation (REF1960) and a simulation with increased ODSs but fixed GHGs (WA2025; red), a simulation with GHG increases only (GHG2025; blue), the sum of the two (gray dashed), and a simulation with both ODS and GHG increases (ALL202; gray solid line). In REF1960, CO_2, CH_4, N_2O, CFC-11, CFC-12, and O_3 concentrations are prescribed at levels corresponding to the year 1960. In WA2025, the concentrations of CFC-11, CFC-12, and stratospheric O_3 are increased from the reference level to the world-avoided levels, averaged over the decade 2020–29. In GHG2025 the concentrations of CO_2, CH_4, and N_2O are increased by approximately 37%, 66%, and 15%, respectively, relative to the reference level. Updated from Wu et al. (2013).

Focusing on near-future climate impacts, Wu et al. (2013) examined atmospheric and surface responses to unregulated ODS emissions in the 2020s. They showed that not only the Southern Hemisphere, but also the tropics and Northern Hemisphere would experience substantial hydro-climate changes in the absence of the Montreal Protocol (Figure 4-21; Wu et al., 2013). As the ODS concentration increases, tropical and extratropical wet regions become wetter, whereas subtropical dry regions become drier in both hemispheres (red line in Figure 4-21). These changes in global precipitation minus evaporation (P-E) are of comparable magnitude to those associated with the increase in other GHGs alone (blue line in Figure 4-21). This result suggests that hydro-climate change by 2025 would be almost doubled in the absence of the Montreal Protocol, highlighting the importance of the Montreal Protocol in mitigating future climate change.

4.5.2 Radiative Effects

Stratospheric ozone forcing is very sensitive to the altitude of ozone change, and GHG increases as well as future circulation changes are expected to influence the distribution of ozone. Therefore, as stratospheric chlorine levels decline, stratospheric ozone is not expected to return to its 1970 or preindustrial spatial distribution or total column. As a result, the stratospheric ozone radiative forcing does not simply scale with stratospheric chlorine loading and would not be expected to return to zero in the future (Portmann et al., 2012). Bekki et al. (2013) found a large spread between CCMVal-2 models, with radiative forcing due to stratospheric ozone staying negative in some models but increasing by up to +0.25 W m^{-2} by 2100 in others. On average the multi-model mean showed an increase in forcing to +0.06 W m^{-2} by 2100 from a value of −0.05 W m^{-2} today. The spread is driven by differences in modeled ozone change near the tropopause. The expected high-altitude increase in ozone would have little effect on forcing.

4.5.3 Chemistry Effects

Kawase et al. (2011), a single model study, and the ACCMIP multi-model study of Young et al. (2013a) present the most detailed account of the 21st century tropospheric ozone projections under the RCP scenarios (see Box 4-1), supported by complementary findings of Lamarque et al. (2011), Shindell

et al. (2013b), and – for the CMIP5 models – Eyring et al. (2013). These model studies find that tropospheric ozone changes over the 21st century are dominated by changes in precursor emissions (oxides of nitrogen, carbon monoxide, and volatile organic compounds) (see Lamarque et al., 2011, 2013). A decrease in the tropospheric ozone burden is found for the RCP2.6, 4.5, and 6.0 simulations, driven by falling emissions of ozone precursors. RCP8.5 simulations project ozone increases throughout the troposphere, partially driven by the near doubling of methane concentrations by 2100 (compared to the present day), and occurring in spite of the decreasing emissions prescribed for the other ozone precursors. In these studies, the expected recovery of stratospheric ozone concentrations, due to reduced ODSs, combines with an enhanced STE, due to the projected strengthening of the BDC (Section 4.3.2.2), to somewhat negate the tropospheric ozone decrease in RCP2.6, 4.5, and 6.0, and enhance the increase in RCP8.5.

Both Kawase et al. (2011) and Young et al. (2013a) quantify the increases in the net influx of stratospheric ozone to the troposphere for the RCPs. For 2100, Kawase et al. (2011) report net influx increases of 45%, 80%, 111%, and 109% compared to the present day for RCP2.6, 4.5, 6.0, and 8.5 respectively (RCP8.5 has a lower net influx due to the large tropospheric ozone increases). The ACCMIP models (Young et al., 2013a) exhibit a wide range of net influx increases: 14–90% and 24–139% for RCP2.6 and 8.5, respectively. Using different climate and emissions scenarios (and neglecting changes in ozone precursor emissions), Zeng et al. (2010) separated the impacts on the net stratospheric ozone influx from increasing GHG concentrations (strengthening the BDC) and from ozone recovery, finding that approximately half their overall 43% increase in the influx by 2100 was attributable to each factor. Moreover, the combined impact of ozone recovery and a strengthened BDC was enough to cancel the reduction in tropospheric ozone due to climate change (from enhanced water vapor, leading to more ozone destruction; e.g., Johnson et al. (2001). Morgenstern et al. (2014) found a 33% increase in the net stratospheric influx by 2050, caused predominantly by ozone recovery.

The range of stratospheric influx changes between models is related to: different treatments of the stratosphere, such as whether the model explicitly calculates stratospheric ozone concentrations or uses an offline stratospheric ozone data set; what the vertical extent and resolution of the stratosphere is in the model, which may influence how the modeled circulation responds to GHG forcing; and the magnitude of the troposphere-stratosphere gradient in ozone concentrations, which is important since we are concerned with the *net* ozone influx from STE. Furthermore, different tropopause definitions can affect comparisons between studies. Despite the inter-model differences, there is general agreement in the spatial patterns of tropospheric ozone change that are qualitatively attributable to an increased stratospheric influx between models, such as enhanced ozone in the upper troposphere (at the flanks of the jets), and a quasi-zonal increase in the midlatitude tropospheric ozone column (Kawase et al., 2011; Eyring et al., 2013; Stevenson et al., 2013; Young et al., 2013a).

As with past changes (Section 4.4.3), the potential impacts of projected stratospheric ozone change through UV attenuation have received less attention. Model studies by Voulgarakis et al. (2013) and Morgenstern et al. (2014) (correcting Morgenstern et al., 2013) investigated OH and methane lifetime changes, finding a significant impact of the modeled stratospheric ozone column changes on the mean tropospheric OH concentration (mediated through ozone photolysis), suggesting that differences in stratospheric ozone could contribute to the model spread in methane lifetimes.

Overall, simulations are in agreement that stratospheric ozone recovery and climate change (through circulation impacts) mean that the net influx of stratospheric ozone could become a more important term in the tropospheric ozone budget. Simulations also agree on the broad spatial patterns of an enhanced stratospheric input, but there remains a large degree of uncertainty in the magnitude of the impact. Models are beginning to include more interactive processes relevant for understanding the role of stratospheric change on tropospheric composition (e.g., stratospheric chemistry, interactive photolysis calculations), but it remains to be seen whether an ensemble of models with more consistent processes will reduce or increase the inter-model spread.

POLICY-RELEVANT INFORMATION

There is further evidence that Antarctic ozone depletion has influenced the Southern Hemisphere surface climate and ocean.

The Antarctic ozone hole was first linked to changes in the tropospheric circulation in the early 2000s. In the decade or so since, a strong case has been built for the dominance of ozone depletion in driving the Southern Hemisphere summertime circulation changes in recent decades. A poleward shift in the circulation, including the position of the midlatitude jet and storm tracks, has been observed in austral summer. Since the last Ozone Assessment, the contribution of ozone depletion to Southern Hemisphere summertime circulation changes over the past three to five decades has been better quantified and shown to be considerably larger than that from greenhouse gases, in most studies. No robust link between stratospheric ozone changes and Northern Hemisphere tropospheric climate has been found, consistent with the conclusions of the previous Ozone Assessment.

The ozone hole impacts the Southern Hemisphere tropospheric circulation by cooling the polar lower stratosphere in spring, which increases the gradient in temperature between the equator and pole. While the precise mechanism by which this then shifts the tropospheric midlatitude jet poleward is still unclear, such a response is robustly simulated in models. New research has found that ozone depletion has likely contributed to the observed expansion of the Southern Hemisphere Hadley Cell, with models simulating an associated pattern of increased summertime precipitation in the subtropics. An improved understanding of the role of ocean eddies in the response of the Southern Ocean to observed wind stress changes (partly due to ozone depletion) has also been gained, and models and observations provide evidence that these wind stress changes have strengthened the overturning circulation in the Southern Ocean. This may have led to a reduction in the amount of carbon uptake by the Southern Ocean, but large uncertainties remain in both observing and simulating this process. Additional research since the previous Ozone Assessment has shown that coupled models simulate a decrease in hemispheric-mean Antarctic sea-ice extent in response to ozone depletion. However, there is low confidence in this model result because these models also simulate a decrease in Antarctic sea-ice extent when driven by all major anthropogenic and natural forcings, in contrast to the small observed increase since 1979. Figure 4-22 schematically summarizes the impact of ozone depletion on the climate system.

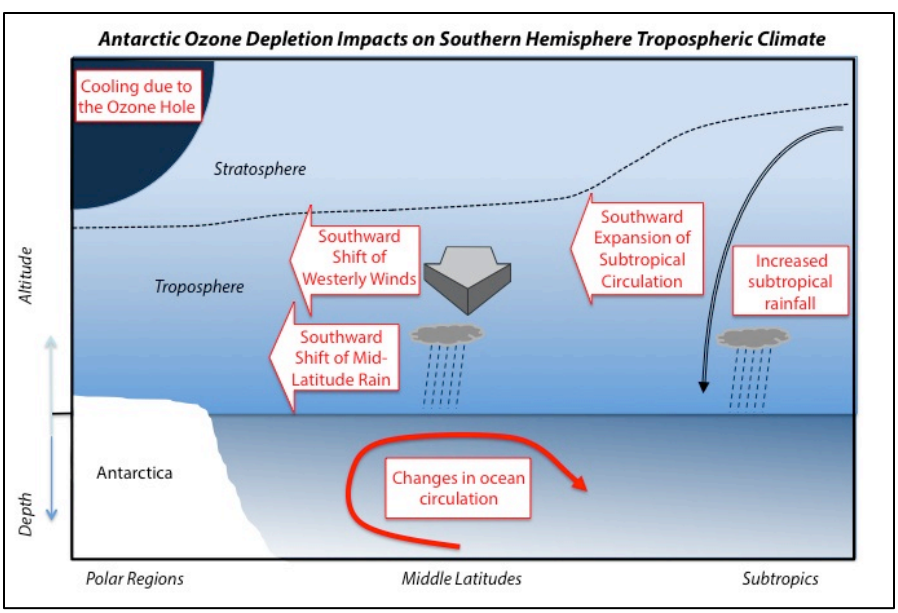

Figure 4-22. Schematic illustration of Southern Hemisphere climate impacts in austral summer associated with Antarctic ozone depletion. Ozone depletion has cooled the Antarctic stratosphere, very likely shifting the region of strong westerly winds and associated rainfall southward in the summer. These changes in midlatitude winds have likely led to changes in the ocean circulation. Ozone depletion has also likely contributed to a southward expansion of the tropical circulation in summer, and may have increased subtropical rainfall.

With the ozone hole expected to recover over coming decades, the climate impacts of stratospheric ozone change in the future will be opposite to those of the past. Meanwhile, GHGs are projected to keep increasing, driving circulation effects that oppose those of ozone recovery. Hence, climate model simulations show that summer trends in the Southern Hemisphere tropospheric circulation over the next fifty years will likely be weaker than those over the past few decades. New simulations since the last Ozone Assessment have allowed an assessment of the impacts of ozone recovery under various scenarios of future emissions, compared to the single emissions scenario previously assessed. In all scenarios, ozone recovery acts to weaken the circulation changes induced by greenhouse gases alone. In a scenario with low greenhouse gas emissions, ozone recovery is found to dominate the Southern Hemisphere summer circulation changes, shifting the midlatitude jet equatorward.

Stratospheric ozone changes are the dominant driver of globally averaged cooling in the lower stratosphere.

Stratospheric temperature changes are important indicators of the impact of anthropogenic emissions on climate. There is robust evidence that changes in composition in the stratosphere have resulted in radiative cooling of the stratosphere over the past three decades. Weather balloons have been providing vertically resolved temperatures since 1958 but are sparse geographically and only cover the lower stratosphere. Hence, most of the information about stratospheric temperature change comes from satellite measurements. Satellite observations provide good global coverage of the stratosphere since the late 1970s but have coarser vertical resolution than the balloon data.

New research since the previous Ozone Assessment has led to a better understanding of the uncertainties in stratospheric temperature changes. Lower stratospheric temperature trends have been analyzed by numerous groups and, while some differences exist between data sets, a global cooling of approximately 1°C over the 1979–2012 period is found across these data sets. For the middle and upper stratosphere, however, only one data set was available at the time of the 2010 Ozone Assessment, making estimates of uncertainty difficult. An additional analysis of the Stratospheric Sounding Unit (SSU) satellite measurements published in 2012 tells quite a different story from the previous data set. While both data sets show global cooling, the new data set shows a cooling almost twice as large as the original analysis in the middle stratosphere. Comparison with modeled trends provided little insight into the cause of these differences, though planned updates to the data sets may help to resolve some of the discrepancies.

Since the previous Ozone Assessment, a number of carefully designed model experiments have been undertaken to quantify the contribution of ozone depletion to recent climate change. Based on these and earlier experiments, cooling in the lower stratosphere over Antarctica in spring and summer has been clearly attributed to Antarctic ozone depletion by multiple studies. In the tropics, one study suggests that ozone depletion is the main driver of lower stratospheric cooling there, though uncertainties in ozone concentrations used to force the models are tightly linked to uncertainties in the temperatures. Globally, several studies have shown that ozone changes are the dominant driver of lower stratospheric cooling.

New estimates of global mean ozone radiative forcing due to emissions of ozone-depleting substances, which account for stratospheric ozone change and its indirect effect on tropospheric ozone, indicate a stronger surface cooling effect than that due to stratospheric ozone changes alone.

Radiative forcing — the net change in the energy balance at the tropopause due to an imposed perturbation — has been further developed within the IPCC Fifth Assessment Report. A new term "Effective Radiative Forcing" was defined to encompass rapid adjustments in the troposphere as well as the traditional stratospheric adjustment. This quantity is more closely associated with the resulting temperature changes. Radiative forcings are assessed at 2010.

This Assessment, for the first time, considers the radiative forcing from the effects of ODS emissions on ozone, including impacts on both tropospheric and stratospheric ozone, which is assessed to

be −0.15 [−0.3 to 0] W m^{-2}. Approximately three-quarters of this radiative forcing results from ozone changes in the stratosphere. There is also the possibility of an induced forcing from rapid adjustment effects on clouds, associated with ozone-driven changes in the Southern Hemisphere tropospheric circulation, and a second possible effect due to ozone-induced wind changes increasing sea salt aerosol over the Southern Ocean. These rapid adjustments could be of a comparable size to the direct ozone radiative forcing and could be of either sign. Overall, this makes the sign of the Effective Radiative Forcing, which includes such adjustments, unknown at present.

Estimates of radiative forcing are very sensitive to the latitudinal and vertical distribution of ozone. Observations and models suggest that increasing greenhouse gases have accelerated the shallow branch of the Brewer-Dobson circulation, leading to a decrease of lower stratospheric ozone in the tropics and an increase in midlatitudes, with additional impacts on tropospheric ozone. A further acceleration of the Brewer-Dobson circulation is projected due to future greenhouse gas increases. This implies that the distribution of ozone will not recover to its pre-depletion spatial state, which has implications for projections of radiative forcing. Model estimates for stratospheric ozone radiative forcing by 2100 are highly uncertain, ranging from slightly negative to exceeding +0.25 W m^{-2} under a high greenhouse gas emissions scenario.

REFERENCES

Abernathey, R., J. Marshall, and D. Ferreira, The dependence of Southern Ocean meridional overturning on wind stress, *J. Phys. Oceanogr.*, *41*, 2261-2278, doi: 10.1175/JPO-D-11-023.1, 2011.

Arblaster, J.M., G.A. Meehl, and D.J. Karoly, Future climate change in the Southern Hemisphere: Competing effects of ozone and greenhouse gases, *Geophys. Res. Lett.*, *38*, L02701, doi: 10.1029/2010GL045384, 2011.

Bandoro, J., S. Solomon, A. Donohoe, D. Thompson, and B. Santer, Influences of the Antarctic ozone hole on Southern Hemisphere summer climate change, *J. Clim.*, *27* (16), 6245-6264, doi: 10.1175/JCLI-D-13-00698.1, 2014.

Barnes, E.A., N.W. Barnes, and L.M. Polvani, Delayed Southern Hemisphere climate change induced by stratospheric ozone recovery, as projected by the CMIP5 models, *J. Clim.*, *27*, 852-867, doi: 10.1175/JCLI-D-13-00246.1, 2014.

Bekki, S., A. Rap, V. Poulain, S. Dhomse, M. Marchand, F. Lefevre, P.M. Forster, S. Szopa, and M.P. Chipperfield, Climate impact of stratospheric ozone recovery, *Geophys. Res. Lett.*, *40*, 2796–2800, doi: 10.1002/grl.50358, 2013.

Bindoff, N.L., and P.A. Stott (Coordinating Lead Authors), K. Mirle AchutaRao, M. Allen, N. Gillett, D. Gutzler, K. Hansingo, G. Hegerl, Y. Hu, S. Jain, I. Mokhov, J. Overland, J. Perlwitz, R. Sebbari, and X. Zhang (Lead Authors), Detection and attribution of climate change: From global to regional, Chapter 10 in *Climate Change 2013: The Physical Science Basis. Contribution of Working Group I to the Fifth Assessment Report of the Intergovernmental Panel on Climate Change*, edited by T.F. Stocker, D. Qin, G.-K. Plattner, M. Tignor, S.K. Allen, J. Boschung, A. Nauels, Y. Xia, V. Bex and P.M. Midgley, Cambridge University Press, Cambridge, UK, and New York, NY, USA, 2013.

Bintanja, R., G.J. van Oldenborgh, S.S. Drijfhout, B. Wouters, and C.A. Katsman, Important role for ocean warming and increased ice-shelf melt in Antarctic sea-ice expansion, *Nature Geosci.*, *6*, 376-379, doi: 10.1038/ngeo1767, 2013.

Birner, T., and H. Bönisch, Residual circulation trajectories and transit times into the extratropical lowermost stratosphere, *Atmos. Chem. Phys.*, *11*, 817-827, doi: 10.5194/acp-11-817-2011, 2011.

Bitz, C.M., and L.M. Polvani, Antarctic climate response to stratospheric ozone depletion in a fine resolution ocean climate model, *Geophys. Res. Lett.*, *39*, L20705, doi: 10.1029/2012GL053393, 2012.

Bodeker, G.E., B. Hassler, P.J. Young, and R.W. Portmann, A vertically resolved, global, gap-free ozone database for assessing or constraining global climate model simulations, *Earth Syst. Sci. Data*, *5*, 31-43, doi: 10.5194/essd-5-31-2013, 2013.

Böning C.W., A. Dispert, M. Visbeck, S.R. Rintoul, and F.U. Schwarzkopf, The response of the Antarctic Circumpolar Current to recent climate change, *Nature Geosci*., *1*, 864-869, doi: 10.1038/ngeo362, 2008.

Bönisch, H., A. Engel, Th. Birner, P. Hoor, D.W. Tarasick, and E.A. Ray, On the structural changes in the Brewer-Dobson Circulation after 2000, *Atmos. Chem. Phys.*, *11*, 3937-3948, doi: 10.5194/acp-11-3937-2011, 2011.

Bryan, F.O., G. Danabasoglu, P.R. Gent and K. Lindsay, Changes in ocean ventilation during the 21st century in the CCSM3, *Ocean Model.*, *15*, 141-156, doi: 10.1016/j.ocemod.2006.01.002, 2006.

Bunzel, F., and H. Schmidt, The Brewer-Dobson circulation in a changing climate: Impact of the model configuration, *J. Atmos. Sci.*, *70*, 1437-1455, doi: 10.1175/JAS-D-12-0215.1, 2013.

Butchart, N., The Brewer-Dobson circulation, *Rev. Geophys*, *52* (2), 157-184, doi: 10.1002/2013RG000448, 2014.

Butchart, N., I. Cionni, V. Eyring, T.G. Shepherd, D.W. Waugh, H. Akiyoshi, J. Austin, C. Brühl, M.P. Chipperfield, E. Cordero, M. Dameris, R. Deckert, S. Dhomse, S.M. Frith, R.R. Garcia, A. Gettelman, M.A. Giorgetta, D.E. Kinnison, F. Li, E. Mancini, C. McLandress, S. Pawson, G. Pitari, D.A. Plummer, E. Rozanov, F. Sassi, J.F. Scinocca, K. Shibata, B. Steil, and W. Tian, Chemistry-climate model simulations of 21st century stratospheric climate and circulation changes, *J. Clim*., *23* (20), 5349-5374, doi: 10.1175/2010JCLI3404.1, 2010.

Butler, A.H., D.W.J. Thompson, and R. Heikes, The steady-state atmospheric circulation response to climate change-like thermal forcings in a simple general circulation model, *J. Clim.*, *23*, 3474-3496, doi: 10.1175/ 2010JCLI3228.1, 2010.

Cai, W., Antarctic ozone depletion causes an intensification of the Southern Ocean super-gyre circulation, *Geophys. Res. Lett*., *33*, L03712, doi: 10.1029/ 2005GL024911, 2006.

Cai, W., and T. Cowan, Trends in Southern Hemisphere circulation in IPCC AR4 models over 1950–99: Ozone depletion versus greenhouse forcing, *J. Clim*., *20* (4), 681-693, doi: 10.1175/JCLI4028.1, 2007.

Cai, W., T. Cowan, S. Godfrey, and S. Wijffels, Simulations of processes associated with the fast warming rate of the southern mid-latitude ocean, *J. Clim.*, *23*, 197-206, doi: 10.1175/2009JCLI3081.1, 2010.

Calvo, N., and R.R. Garcia, Wave forcing of the tropical upwelling in the lower stratosphere under increasing concentrations of greenhouse gases, *J. Atmos. Sci*., *66* (10), 3184-3196, doi: 10.1175/2009JAS3085.1, 2009.

Calvo, N., R.R. Garcia, D.R. Marsh, M.J. Mills, D.E. Kinnison, and P.J. Young, Reconciling modeled and observed temperature trends over Antarctica, *Geophys. Res. Lett*., *39*, L16803, doi: 10.1029/2012GL052526, 2012.

Canziani, P.O., A. O'Neill, R. Schofield, M. Raphael, G.J. Marshall, and G. Redaelli, World climate research programme special workshop on climatic effects of ozone depletion in the southern hemisphere, *Bull. Amer. Meteorol. Soc.*, *95*, ES101-ES105, doi: 10.1175/BAMS-D-13-00143.1, 2014.

Charlton-Perez, A.J., M.P. Baldwin, T. Birner, R.X. Black, A.H. Butler, N. Calvo, N.A. Davis, E.P. Gerber, N. Gillett, S. Hardiman, J. Kim, K. Krüger, Y.-Y. Lee, E. Manzini, B.A. McDaniel, L. Polvani, T. Reichler, T.A. Shaw, M. Sigmond, S.-W. Son, M. Toohey, L. Wilcox, S. Yoden, B. Christiansen, F. Lott, D. Shindell, S. Yukimoto, and S. Watanabe, On the lack of stratospheric dynamical variability in low-top versions of the CMIP5 models, *J. Geophys. Res*., *118*, 2494-2505, doi: 10.1002/jgrd.50125, 2013.

Chen, G., and I.M. Held, Phase speed spectra and the recent poleward shift of Southern Hemisphere surface westerlies, *Geophys. Res. Lett.*, *34*, L21805, doi: 10.1029/2007GL031200, 2007.

Ciais, P., and C. Sabine (Coordinating Lead Authors), G. Bala, L. Bopp, V. Brovkin, J. Canadell, A. Chhabra, R. DeFries, J. Galloway, M. Heimann, C. Jones, C. Le Quéré, R.B. Myneni, S. Piao, and P. Thornton (Lead Authors), Carbon and other biogeochemical cycles, Chapter 6 in *Climate Change 2013: The Physical Science Basis. Contribution of Working Group I to the Fifth Assessment Report of the Intergovernmental Panel on Climate Change*, edited by T.F. Stocker, D. Qin, G.-K. Plattner, M. Tignor, S.K. Allen, J. Boschung, A. Nauels, Y. Xia, V. Bex, and P.M. Midgley, Cambridge University Press, Cambridge, UK, and New York, NY, USA, 2013.

Cionni, I., V. Eyring, J.F. Lamarque, W.J. Randel, D.S. Stevenson, F. Wu, G.E. Bodeker, T.G. Shepherd, D.T. Shindell, and D.W. Waugh, Ozone database in support of CMIP5 simulations: Results and corresponding radiative forcing, *Atmos. Chem. Phys.*, *11*, 11267-11292, doi: 10.5194/acp-11-11267-2011, 2011.

Collins, M., and R. Knutti (Coordinating Lead Authors), J. Arblaster, J.-L. Dufresne, T. Fichefet, P. Friedlingstein, X. Gao, W.J. Gutowski, T. Johns, G. Krinner, M. Shongwe, C. Tebaldi, A.J. Weaver, and M. Wehner (Lead Authors), Long-term climate change: Projections, commitments and irreversibility, Chapter 12 in *Climate Change 2013: The Physical Science Basis. Contribution of Working Group I to the Fifth Assessment Report of the Intergovernmental Panel on Climate Change*, edited by T.F. Stocker, D. Qin, G.-K. Plattner, M. Tignor, S.K. Allen, J. Boschung, A. Nauels, Y. Xia, V. Bex and P.M. Midgley, Cambridge University Press, Cambridge, UK, and New York, NY, USA, 2013.

Conley, A.J., J.-F. Lamarque, F. Vitt, W.D. Collins, and J. Kiehl, PORT, a CESM tool for the diagnosis of radiative forcing, *Geosci. Model Dev.*, *6*, 469-476, doi: 10.5194/gmd-6-469-2013, 2013.

Crook, J.A., N.P. Gillett, and S.P.E. Keeley, Sensitivity of Southern Hemisphere climate to zonal asymmetry in ozone, *Geophys. Res. Lett.*, *35*, L07806, doi: 10.1029/2007GL032698, 2008.

Cubasch, U., and D. Wuebbles (Coordinating Lead Authors), D. Chen, M.C. Facchini, D. Frame, N. Mahowald, and J.-G. Winther (Lead Authors), Introduction, Chapter 1 in *Climate Change 2013: The Physical Science Basis. Contribution of Working Group I to the Fifth Assessment Report of the Intergovernmental Panel on Climate Change*, edited by T.F. Stocker, D. Qin, G.-K. Plattner, M. Tignor, S.K. Allen, J. Boschung, A. Nauels, Y. Xia, V. Bex, and P.M. Midgley, Cambridge University Press, Cambridge, UK, and New York, NY, USA, 2013.

Dall'Amico, M., P.A. Stott, A.A. Scaife, L.J. Gray, K.H. Rosenlof, and A.Y. Karpechko, Impact of stratospheric variability on tropospheric climate change, *Clim. Dyn.*, *34*, 399-417, doi: 10.1007/s00382-009-0580-1, 2010.

Dee, D.P., S.M. Uppala, A.J. Simmons, P. Berrisford, P. Poli, S. Kobayashi, U. Andrae, M.A. Balmaseda, G. Balsamo, P. Bauer, P. Bechtold, A.C.M. Beljaars, L. van de Berg, J. Bidlot, N. Bormann, C. Delsol, R. Dragani, M. Fuentes, A.J. Geer, L. Haimberger, S.B. Healy, H. Hersbach, E.V. Hólm, L. Isaksen, P. Kållberg, M. Köhler, M. Matricardi, A.P. McNally, B.M. Monge-Sanz, J.-J. Morcrette, B.-K. Park, C. Peubey, P. de Rosnay, C. Tavolato, J.-N. Thépaut, and F. Vitart, The ERA-Interim reanalysis: Configuration and performance of the data assimilation system, *Quart. J. Roy. Meteorol. Soc.*, *137*, 553-597, doi: 10.1002/qj.828, 2011.

Dessler, A.E., M.R. Schoeberl, T. Wang, S.M. Davis, and K.H. Rosenlof, Stratospheric water vapor feedback, *Proc. Natl. Acad. Sci.*, *110*, 18087-18091, doi: 10.1073/pnas.1310344110, 2013.

Deushi, M., and K. Shibata, Impacts of increases in greenhouse gases and ozone recovery on lower stratospheric circulation and the age of air: Chemistry-climate model simulations up to 2100, *J. Geophys. Res.*, *116*, D07107, doi: 10.1029/2010JD015024, 2011.

Diallo, M., B. Legras, and A. Chédin, Age of stratospheric air in the ERA-Interim, *Atmos. Chem. Phys*., *12*, 12133-12154, doi: 10.5194/acp-12-12133-2012, 2012.

Engel, A., T. Möbius, H. Bönisch, U. Schmidt, R. Heinz, I. Levin, E. Atlas, S. Aoki, T. Nakazawa, S. Sugawara, F. Moore, D. Hurst, J. Elkins, S. Schauffler, A. Andrews, and K. Berine, Age of stratospheric air unchanged within uncertainties over the past 30 years, *Nature Geosci.*, *2*, 28-31, doi: 10.1038/GEO388, 2009.

Eyring, V., N. Butchart, D.W. Waugh, H. Akiyoshi, J. Austin, S. Bekki, G.E. Bodeker, B.A. Boville, C. Brühl, M.P. Chipperfield, E. Cordero, M. Dameris, M. Deushi, V.E. Fioletov, S.M. Frith, R.R. Garcia, A. Gettelman, M.A. Giorgetta, V. Grewe, L. Jourdain, D.E. Kinnison, E. Mancini, E. Manzini, M. Marchand, D.R. Marsh, T. Nagashima, P.A. Newman, J.E. Nielsen, S. Pawson, G. Pitari, D.A. Plummer, E. Rozanov, M. Schraner, T.G. Shepherd, K. Shibata, R.S. Stolarski, H. Struthers, W. Tian, and M. Yoshiki, Assessment of temperature, trace species, and ozone in chemistry-climate model simulations of the recent past, *J. Geophys. Res.*, *111*, D22308, doi: 10.1029/2006JD007327, 2006.

Eyring, V., I. Cionni, J.-F. Lamarque, H. Akiyoshi, G.E. Bodeker, A.J. Charlton-Perez, S.M. Frith, A. Gettelman, D.E. Kinnison, T. Nakamura, L.D. Oman, S. Pawson, and Y. Yamashita, Sensitivity of 21st century stratospheric ozone to greenhouse gas scenarios, *Geophys. Res. Lett.*, *37*, L16807, doi: 10.1029/2010GL044443, 2010.

Eyring, V., J.M. Arblaster, I. Cionni, J. Sedlacek, J. Perlwitz, P.J. Young, S. Bekki, D. Bergmann, P. Cameron-Smith, W. Collins, G. Faluvegi, K.-D. Gottschaldt, L. Horowitz, D. Kinnison, J.-F. Lamarque, D.R. Marsh, D. Saint-Martin, D. Shindell, K. Sudo, S. Szopa, and S. Watanabe, Long-term changes in tropospheric and stratospheric ozone and associated climate impacts in CMIP5 simulations, *J. Geophys. Res.*, *118*, 5029-5060, doi: 10.1002/jgrd.50316, 2013.

Farneti R., T.L. Delworth, A.J. Rosati, S.M. Griffies, and F. Zeng, The role of mesoscale eddies in the rectification of the Southern Ocean response to climate change, *J. Phys. Oceanogr.*, *40*, 1539-1557, doi: 10.1175/2010JPO 4353.1, 2010.

Fels, S.B., J.D. Mahlman, M.D. Schwarzkopf, and R.W. Sinclair, Stratospheric sensitivity to perturbations in ozone and carbon dioxide: Radiative and dynamical response, *J. Atmos. Sci.*, *37*, 2265-2297, doi: 10.1175/1520-0469(1980)037<2265:SSTPIO>2.0.CO;2, 1980.

Forster, P.M., and K.P. Shine, Radiative forcing and temperature trends from stratospheric ozone changes, *J. Geophys. Res.*, *102*, 10841-10855, doi: 10.1029/96JD03510, 1997.

Forster, P.M., and K.P. Shine, Stratospheric water vapour changes as a possible contributor to observed stratospheric cooling, *Geophys. Res. Lett.*, *26*, 3309-3312, doi: 10.1029/1999GL010487, 1999.

Forster, P.M., V.I. Fomichev, E. Rozanov, C. Cagnazzo, A.I. Jonsson, U. Langematz, B. Fomin, M.J. Iacono, B. Mayer, E. Mlawer, G. Myhre, R.W. Portmann, H. Akiyoshi, V. Falaleeva, N. Gillett, A. Karpechko, J. Li, P. Lemennais, O. Morgenstern, S. Oberländer, M. Sigmond, and K. Shibata, Evaluation of radiation scheme performance within chemistry climate models, *J. Geophys. Res.*, *116*, D10302, doi: 10.1029/2010JD015361, 2011.

Forster, P.M., and D.W.J. Thompson (Coordinating Lead Authors), M.P. Baldwin, M.P. Chipperfield, M. Dameris, J.D. Haigh, D.J. Karoly, P.J. Kushner, W.J. Randel, K.H. Rosenlof, D.J. Seidel, S. Solomon, G. Beig, P. Braesicke, N. Butchart, N.P. Gillett, K.M. Grise, D.R. Marsh, C. McLandress, T.N. Rao, S.-W. Son, G.L. Stenchikov, and S. Yoden, Stratospheric changes and climate, Chapter 4 in *Scientific Assessment of Ozone Depletion: 2010*, Global Ozone Research and Monitoring Project-Report No. 52, 516 pp., World Meteorological Organization, Geneva, Switzerland, 2011.

Free, M., The seasonal structure of temperature trends in the tropical lower stratosphere, *J. Clim.*, *24*, 859-866, doi: 10.1175/2010JCLI3841.1, 2011.

Free, M., and J. Lanzante, Effect of volcanic eruptions on the vertical temperature profile in radiosonde data and climate models, *J. Clim*., *22*, 2925-2939, doi: 10.1175/2008JCLI2562.1, 2009.

Fu, Q., S. Solomon, and P. Lin, On the seasonal dependence of tropical lower-stratospheric temperature trends, *Atmos. Chem. Phys*., *10*, 2643-2653, doi: 10.5194/acp-10-2643-2010, 2010.

Fueglistaler, S., Y.S. Liu, T.J. Flannaghan, P.H. Haynes, D.P. Dee, W.J. Read, E.E. Remsberg, L.W. Thomason, D.F. Hurst, J.R. Lanzante, and P.F. Bernath, The relation between atmospheric humidity and temperature trends for stratospheric water, *J. Geophys. Res.*, *118*, 1052-1074, doi: 10.1002/jgrd.50157, 2013.

Fujiwara, M., H. Vömel, F. Hasebe, M. Shiotani, S.-Y. Ogino, S. Iwasaki, N. Nishi, T. Shibata, K. Shimizu, E. Nishimoto, J.M. Valverde Canossa, H.B. Selkirk, and S.J. Oltmans, Seasonal to decadal variations of water vapor in the tropical lower stratosphere observed with balloon-borne cryogenic frost point hygrometers, *J. Geophys. Res.*, *115*, D18304, doi: 10.1029/2010JD014179, 2010.

Fyfe, J.C., N.P. Gillett, and G.J. Marshall, Human influence on extratropical Southern Hemisphere summer precipitation, *Geophys. Res. Lett.*, *39*, L23711, doi: 10.1029/2012GL054199, 2012.

Fyfe, J.C., N.P. Gillett, and F.W. Zwiers, Overestimated global warming over the past 20 years, *Nature Climate Change*, *3*, 767-769, doi: 10.1038/nclimate1972, 2013.

Garcia, R.R., and W.J. Randel, Acceleration of the Brewer-Dobson circulation due to increases in greenhouse gases, *J. Atmos. Sci.*, *65* (8), 2731-2739, doi: 10.1175/2008JAS2712.1, 2008.

Garcia, R.R., W.J. Randel, and D.E. Kinnison, On the determination of age of air trends from atmospheric trace species, *J. Atmos. Sci*., *68*, 139-154, doi: 10.1175/2010JAS3527.1, 2011.

Garcia, R.R., D.E. Kinnison, and D.R. Marsh, "World avoided" simulations with the Whole Atmosphere Community Climate Model, *J. Geophys. Res.*, *117*, D23303, doi: 10.1029/2012JD018430, 2012.

Garfinkel, C.I., D.W. Waugh, and E.P. Gerber, The effect of tropospheric jet latitude on coupling between the stratospheric polar vortex and the troposphere, *J. Clim.*, *26*, 2077-2097, doi: 10.1175/JCLI-D-12-00301.1, 2013.

Garny H., M. Dameris, W. Randel, G.E. Bodeker, and R. Deckert, Dynamically forced increase of tropical upwelling in the lower stratosphere, *J. Atmos. Sci.*, *68*, 1214-1233, doi: 10.1175/2011JAS3701.1, 2011.

Gent P.R., and G. Danabasoglu, Response to increasing Southern Hemisphere winds in CCSM4, *J. Clim.*, *24*, 4992-4998, doi: 10.1175/JCLI-D-10-05011.1, 2011.

Gerber, E.P., and S.-W. Son, Quantifying the summertime Austral jet stream and Hadley Cell response to stratospheric ozone and greenhouse gases, *J. Clim.*, *27*, 5538-5559, 2014.

Gerber, E.P., M.P. Baldwin, H. Akiyoshi, J. Austin, S. Bekki, P. Braesicke, N. Buchart, M. Chipperfield, M. Dameris, S. Dhomse, S.M. Firth, R.R. Garcia, H. Garney, A. Gettelman, S.C. Hardiman, O. Morgenstern, J.E. Nielsen, S. Pawson, T. Peter, D.A. Plummer, J.A. Pyle, E. Rozanov, J.F. Scinocca, T.G. Shepherd, and D. Smale, Stratosphere-troposphere coupling and annular mode variability in chemistry-climate models, *J. Geophys. Res.*, *115*, D00M06, doi: 10.1029/2009JD013770, 2010.

Gettelman, A., M.I. Hegglin, S.-W. Son, J. Kim, M. Fujiwara, T. Birner, S. Kremser, M. Rex, J.A. Añel, H. Akiyoshi, J. Austin, S. Bekki, P. Braesike, C. Brühl, N. Butchart, M. Chipperfield, M. Dameris, S. Dhomse, H. Garny, S.C. Hardiman, P. Jöckel, D.E. Kinnison, J.F. Lamarque, E. Mancini, M. Marchand, M. Michou, O. Morgenstern, S. Pawson, G. Pitari, D. Plummer, J.A. Pyle, E. Rozanov, J. Scinocca, T.G. Shepherd, K. Shibata, D. Smale, H. Teyssèdre, and W. Tian, Multimodel assessment of the upper troposphere and lower stratosphere: Tropics and trends, *J. Geophys. Res.*, *115*, D00M08, doi: 10.1029/2009JD013638, 2010.

Gille, S.T., Decadal-scale temperature trends in the Southern Hemisphere ocean, *J. Clim.*, *21* (18), 4749-4765, doi: 10.1175/2008JCLI2131.1, 2008.

Gillett, N.P., H. Akiyoshi, S. Bekki, P. Braesicke, V. Eyring, R. Garcia, A. Yu. Karpechko, C.A. McLinden, O. Morgenstern, D.A. Plummer, J.A. Pyle, E. Rozanov, J. Scinocca, and K. Shibata, Attribution of observed changes in stratospheric ozone and temperature, *Atmos. Chem. Phys*., *11* (2), 599-609, doi: 10.5194/acp-11-599-2011, 2011.

Gillett, N.P., J.C. Fyfe, and D.E. Parker, Attribution of observed sea level pressure trends to greenhouse gas, aerosol, and ozone changes, *Geophys. Res. Lett.*, *40*, 2302-2306, doi: 10.1002/grl.50500, 2013.

Gnanadesikan, A., J.L. Russell, and F. Zeng, How does ocean ventilation change under global warming?, *Ocean Sci.*, *3* (1), 43-53, doi: 10.5194/os-3-43-2007, 2007.

Gómez-Escolar, M., S. Fueglistaler, N. Calvo, and D. Barriopedro, Changes in polar stratospheric temperature climatology in relation to stratospheric sudden warming occurrence, *Geophys. Res. Lett*., *39*, L22802, doi: 10.1029/2012GL053632, 2012.

Gonzalez, P.L.M., L.M. Polvani, R. Seager, and G.J.P. Correa, Stratospheric ozone depletion: A key driver of recent precipitation trends in south eastern South America, *Clim. Dyn*., *42*, 1775-1792, doi: 10.1007/s00382-013-1777-x, 2013.

Grise, K.M., L.M. Polvani, G. Tselioudis, Y. Wu, and M.D. Zelinka, The ozone hole indirect effect: Cloud-radiative anomalies accompanying the poleward shift of the eddy-driven jet in the Southern Hemisphere, *Geophys. Res. Lett*., *40*, 1-5, doi: 10.1002/grl.50675, 2013.

Grise, K.M., S.-W. Son, G.P.J. Correa, and L.M. Polvani, The response of extratropical cyclones in the Southern Hemisphere to stratospheric ozone depletion in the 20th century, *Atmos. Sci. Lett.*, *15*, 29-36, doi: 10.1002/asl2.458, 2014.

Hardiman, S., N. Butchart, and N. Calvo, The morphology of the Brewer-Dobson circulation and its response to climate change in CMIP5 simulations, *Q. J. Roy. Meteorol. Soc.*, *140* (683), 1958-1965, doi: 10.1002/qj.2258, 2013.

Hartley, D.E., J.T. Villarin, R.X. Black, and C.A. Davis, A new perspective on the dynamical link between the stratosphere and troposphere, *Nature*, *391*, 471-474, 1998.

Hartmann, D.L., A.M.G. Klein Tank, and M. Rusticucci (Coordinating Lead Authors), L.V. Alexander, S. Brönnimann, Y. Charabi, F.J. Dentener, E.J. Dlugokencky, D.R. Easterling, A. Kaplan, B.J. Soden, P.W. Thorne, M. Wild, and P.M. Zhai, Observations: Atmosphere and surface, Chapter 2 in *Climate Change 2013: The Physical Science Basis. Contribution of Working Group I to the Fifth Assessment Report of the Intergovernmental Panel on Climate Change*, edited by T.F Stocker, D. Qin, G.-K. Plattner, M. Tignor, S.K. Allen, J. Boschung, A. Nauels, Y. Xia, V. Bex, and P.M. Midgley, Cambridge University Press, Cambridge, UK, and New York, NY, USA, 2013.

Harvey, B.J., L.C. Shaffrey, and T.J. Woollings, Equator-to-pole temperature differences and the extra-tropical storm track response of the CMIP5 climate models, *Clim. Dyn.*, *43*, 1171-1182, doi: 10.1007/s00382-013-1883-9, 2013.

Hassler, B., P.J. Young, R.W. Portmann, G.E. Bodeker, J.S. Daniel, K.H. Rosenlof, and S. Solomon, Comparison of three vertically resolved ozone data bases: Climatology, trends and radiative forcings, *Atmos. Chem. Phys.*, *13*, 5533-5550, doi: 10.5194/acp-13-5533-2013, 2013.

Hegglin, M.I., and T.G. Shepherd, Large climate-induced changes in stratosphere-to-troposphere ozone flux and ultraviolet index, *Nature Geosci.*, *2*, 687-691, doi: 10.1038/NGEO604, 2009.

Hendon, H.H., D.W.J. Thompson, and M.C.Wheeler, Australian rainfall and surface temperature variations associated with the Southern Hemisphere Annular Mode, *J. Clim.*, *20* (11), 2452-2467, doi: 10.1175/JCLI 4134.1, 2007.

Hitchcock, P., T.G. Shepherd, and C. McLandress, Past and future conditions for polar stratospheric cloud formation simulated by the Canadian middle atmosphere model, *Atmos. Chem. Phys.*, *9* (2), 483-495, doi: 10.5194/acp-9-483-2009, 2009.

Hofmann, M., and M.A. Morales Maqueda, The response of Southern Ocean eddies to increased mid-latitude westerlies: A non-eddy resolving model study, *Geophys. Res. Lett.*, *38*, L03605, doi: 10.1029/2010GL045972, 2011.

Hogg A.M., M.P. Meredith, J.R. Blundell, and C. Wilson, Eddy heat flux in the southern ocean: Response to variable wind forcing, *J. Clim*., *21*, 608-620, 2008.

Hu, Y., Y. Xia, and Q. Fu, Tropospheric temperature response to stratospheric ozone recovery in the 21st century, *Atmos. Chem. Phys*., *11*, 7687-7699, doi: 10.5194/acp-11-7687-2011, 2011.

Huhn O., M. Rhein, M. Hoppema, and S. van Heuven, Decline of deep and bottom water ventilation and slowing down of anthropogenic carbon storage in the Weddell Sea, 1984-2011, *Deep-Sea Research I*, *76*, 66-84, doi: 10.1016/j.dsr.2013.01.005, 2013.

Hurst, D.F., S.J. Oltmans, H. Vömel, K.H. Rosenlof, S.M. Davis, E.A. Ray, E.G. Hall, and A.F. Jordan, Stratospheric water vapor trends over Boulder, Colorado: Analysis of the 30 year Boulder record, *J. Geophys. Res*., *116*, D02306, doi: 10.1029/2010JD015065, 2011.

IPCC (Intergovernmental Panel on Climate Change), *Climate Change 2013: The Physical Science Basis: Contribution of Working Group I to the Fifth Assessment Report of the Intergovernmental Panel on Climate Change*, edited by T.F. Stocker, D. Qin, G.-K. Plattner, M. Tignor, S.K. Allen, J. Boschung, A. Nauels, Y. Xia,

V. Bex, and P.M. Midgley, 1535 pp., Cambridge University Press, Cambridge, UK, and New York, NY, USA, 2013.

Iwasaki, T., H. Hamada, and K. Miyazaki, Comparisons of Brewer-Dobson circulations diagnosed from reanalyses, *J. Meteor. Soc. Jap.*, *87* (6), 997-1006, 2009.

Jin, J.J., N.J. Livesey, G.L. Manney, J.H. Jiang, M.J. Schwartz, and W.H. Daffer, Chemical discontinuity at the extratropical tropopause and isentropic stratosphere-troposphere exchange pathways diagnosed using Aura MLS data, *J. Geophys. Res.*, *118*, 3832-3847, doi: 10.1002/jgrd.50291, 2013.

John, J.G., A.M. Fiore, V. Naik, L.W. Horowitz, and J.P. Dunne, Climate versus emission drivers of methane lifetime against loss by tropospheric OH from 1860-2100, *Atmos. Chem. Phys.*, *12*, 12021-12036, doi: 10.5194/acp-12-12021-2012, 2012.

Johnson, C.E., D.S. Stevenson, W.J. Collins, and R.G. Derwent, Role of climate feedback on methane and ozone studied with a coupled Ocean-Atmosphere-Chemistry model, *Geophys. Res. Lett.*, *28*, 1723-1726, doi: 10.1029/2000GL011996, 2001.

Kang, S.M., and L.M. Polvani, The interannual relationship between the eddy-driven jet and the edge of the Hadley Cell, *J. Clim.*, *24*, 563-568, doi: 10.1175/2010JCLI4077.1, 2011.

Kang, S.M., L.M. Polvani, J.C. Fyfe, and M. Sigmond, Impact of polar ozone depletion on subtropical precipitation, *Science*, *332*, 951-954, doi: 10.1126/science.1202131, 2011.

Kang, S.M., L.M. Polvani, J.C. Fyfe, S.-W. Son, M. Sigmond, and G.J.P. Correa, Modeling evidence that ozone depletion has impacted extreme precipitation in the austral summer, *Geophys. Res. Lett.*, *40*, 4054-4059, doi: 10.1002/grl.50769, 2013.

Karpechko, A.Y., N.P. Gillett, L.J. Gray, and M. Dall'Amico, Influence of ozone recovery and greenhouse gas increases on Southern Hemisphere circulation, *J. Geophys. Res.*, *115*, D22117, doi: 10.1029/2010JD014423, 2010.

Kawase, H., T. Nagashima, K. Sudo, and T. Nozawa, Future changes in tropospheric ozone under Representative Concentration Pathways (RCPs), *Geophys. Res. Lett.*, *38*, L05801, doi: 10.1029/2010GL046402, 2011.

Kawatani, Y., and K. Hamilton, Weakened stratospheric quasibiennial oscillation driven by increased tropical mean upwelling, *Nature*, *497*, 478-481, doi: 10.1038/nature12140, 2013.

Kidston, J., and E.P. Gerber, Intermodel variability of the poleward shift of the austral jet stream in the CMIP3 integrations linked to biases in 20th century climatology, *Geophys. Res. Lett.*, *37*, L09708, doi: 10.1029/2010GL042873, 2010.

Kobayashi, S., M. Matricardi, D. Dee, and S. Uppala, Toward a consistent reanalysis of the upper stratosphere based on radiance measurements from SSU and AMSU-A, *Quart. J. Roy. Meteor. Soc.*, *135*, 2086-2099, doi: 10.1002/qj.514, 2009.

Korhonen, H., K.S. Carslaw, P.M. Forster, S. Mikkonen, N.D. Gordon, and H. Kokkola, Aerosol climate feedback due to decadal increases in Southern Hemisphere wind speeds, *Geophys. Res. Lett.*, *37*, L02805, doi: 10.1029/2009GL041320, 2010.

Kunz, T., K. Fraedrich, and F. Lunkeit, Synoptic scale wave breaking and its potential to drive NAO-like circulation dipoles: A simplified GCM approach, *Quart. J. Roy. Meteorol. Soc.*, *135*, 1-19, doi: 10.1002/qj.351, 2009.

Kushner, P.J., and L.M. Polvani, Stratosphere-troposphere coupling in a relatively simple AGCM: The role of eddies, *J. Clim.*, *17* (3), 629-639, 2004.

Lamarque, J.-F., and S. Solomon, Impact of changes in climate and halocarbons on recent lower stratosphere ozone and temperature trends, *J. Clim.*, *23* (10), 2599-2611, doi: 10.1175/2010JCLI3179.1, 2010.

Lamarque, J.-F., G.P. Kyle, M. Meinshausen, K. Riahi, S.J. Smith, D.P. Vuuren, A.J. Conley, and F. Vitt, Global and regional evolution of short-lived radiatively-active gases and aerosols in the Representative Concentration Pathways, *Clim. Change*, *109*, 191-212, doi: 10.1007/s10584-011-0155-0, 2011.

Lamarque, J.-F., D.T. Shindell, B. Josse, P.J. Young, I. Cionni, V. Eyring, D. Bergmann, P. Cameron-Smith, W.J. Collins, R. Doherty, S. Dalsoren, G. Faluvegi, G. Folberth, S.J. Ghan, L.W. Horowitz, Y.H. Lee, I.A. MacKenzie, T. Nagashima, V. Naik, D. Plummer, M. Righi, S.T. Rumbold, M. Schulz, R.B. Skeie, D.S. Stevenson, S. Strode, K. Sudo, S. Szopa, A. Voulgarakis, and G. Zeng, The Atmospheric Chemistry and Climate Model Intercomparison Project (ACCMIP): Overview and description of models, simulations and climate diagnostics, *Geosci. Model Dev.*, *6* (1), 179-206, doi: 10.5194/gmd-6-179-2013, 2013.

Lang, C., D.W. Waugh, M.A. Olsen, A.R. Douglass, Q. Liang, J.E. Nielsen, L.D. Oman, S. Pawson, and R.S. Stolarski, The impact of greenhouse gases on past changes in tropospheric ozone, *J. Geophys. Res.*, *117*, D23304, doi: 10.1029/2012JD018293, 2012.

Langematz, U., S. Meul, K. Grunow, E. Romanowsky, S. Oberländer, J. Abalichin, and A. Kubin, Future Arctic temperature and ozone: The role of stratospheric composition changes, *J. Geophys. Res.*, *119*, 2092-2112, doi:

10.1002/2013JD021100, 2014.

Le Quéré, C., C. Rodenbeck, E.T. Buitenhuis, T.J. Conway, R. Langenfelds, A. Gomez, C. Labuschagne, M. Ramonet, T. Nakazawa, N. Metzl, N. Gillett, and M. Heimann, Saturation of the Southern Ocean CO_2 sink due to recent climate change, *Science*, *316*, 1735-1738, doi: 10.1126/science.1136188, 2007.

Lee, S., and S.B. Feldstein, Detecting ozone- and greenhouse-gas-driven wind trends with observational data, *Science*, *339*, 563-567, doi: 10.1126/science.1225154, 2013.

Lenton, A., B. Tilbrook, R. Law, D. Bakker, S.C. Doney, N. Gruber, M. Hoppema, M. Ishii, N.S. Lovenduski, R.J. Matear, B.I. McNeil, N. Metzl, S.E. Mikaloff Fletcher, P. Monteiro, C. Rödenbeck, C. Sweeney, and T. Takahashi, Sea-air CO_2 fluxes in the Southern Ocean for the period 1990-2009, *Biogeosciences*, *10*, 4037-4054, doi: 10.5194/bg-10-4037-2013, 2013.

Li, F., J. Austin, and J. Wilson, The strength of the Brewer-Dobson circulation in a changing climate: Coupled chemistry-climate model stimulation, *J. Clim.*, *21* (1), 40-57, doi: 10.1175/2007.JCLI1663.1, 2008.

Limpasuvan, V., and D.L. Hartmann, Wave-maintained annular modes of climate variability, *J. Clim.*, *13*, 4414-4429, 2000.

Lin, P., and Q. Fu, Changes in various branches of the Brewer Dobson circulation from an ensemble of chemistry climate models, *J. Geophys. Res.*, *118*, 73-84, doi: 10.1029/2012JD018813, 2013.

Lin, P., Q. Fu, S. Solomon, and J.M. Wallace, Temperature trend patterns in Southern Hemisphere high latitudes: Novel indicators of stratospheric change, *J. Clim.*, *22* (23), 2009.

Lin, M., A.M. Fiore, O.R. Cooper, L.W. Horowitz, A.O. Langford, H. Levy II, B.J. Johnson, V. Naik, S.J. Oltmans, and C.J. Senff, Springtime high surface ozone events over the western United States: Quantifying the role of stratospheric intrusions, *J. Geophys. Res.*, *117*, D00V22, doi: 10.1029/2012JD018151, 2012.

Lorenz, D.J., and E.T. DeWeaver, Tropopause height and zonal wind response to global warming in the IPCC scenario integrations, *J. Geophys. Res.*, *112*, D10119, doi: 10.1029/2006JD008087, 2007.

Lott, F.C., P.A. Stott, D.M. Mitchell, N. Christidis, N.P. Gillet, L. Haimberger, J. Perlwitz, and P.W. Thorne, Models versus radiosondes in the free atmosphere: A new detection and attribution analysis of temperature, *J. Geophys. Res.*, *118*, 2609-2619, doi: 10.1002/jgrd.50255, 2013.

Lucas, C., H. Nguyen, and B. Timbal, An observational analysis of Southern Hemisphere tropical expansion, *J. Geophys. Res.*, *117*, D17112, doi: 10.1029/2011JD017033, 2013.

Lucas, C., B. Timbal, and H. Nguyen, The expanding tropics: A critical assessment of the observational and modeling studies, *WIREs Clim Change*, *5* (1), 89-112. doi: 10.1002/wcc.251, 2014.

Mahlstein I., P.R. Gent, and S. Solomon, Historical Antarctic mean sea ice area, sea ice trends, and winds in CMIP5 simulations, *J. Geophys. Res. 118* (11), 5105-5110, doi: 10.1002/jgrd.50443, 2013.

Manatsa, D., Y. Morioka, S.K. Behera, T. Yamagata, and C.H. Matarira, Link between Antarctic ozone depletion and summer warming over southern Africa, *Nature Geoscience.*, 6, 934-939, doi: 10.1038/ngeo1968, 2013.

Marshall, G., Trends in the Southern Annular Mode from observations and reanalyses, *J. Clim.*, *16* (24), 4134-4143, doi: 10.1175/1520-0442(2003)016<4134:TITSAM>2.0.CO;2, 2003.

Maycock, A.C., M.M. Joshi, K.P. Shine, A.A. Scaife, The circulation response to idealized changes in stratospheric water vapor, *J. Clim.*, *26*, 545-561, doi: 10.1175/JCLI-D-12-00155.1, 2013.

Maycock, A.C., M.M. Joshi, K.P. Shine, S.M. Davis, and K.H. Rosenlof, The potential impact of changes in lower stratospheric water vapour on stratospheric temperatures over the past 30 years, *Quart. J. Roy. Meteor. Soc.*, *140* (684), 2176-2185, doi: 10.1002/qj.2287, 2014.

McLandress, C., and T.G. Shepherd, Simulated anthropogenic changes in the Brewer-Dobson circulation, including its extension to high latitudes, *J. Clim.*, *22*, 1516-1540, doi: 10.1175/2008JCLI2679.1, 2009.

Mclandress, C., A.I. Jonsson, D.A. Plummer, M.C. Reader, J.F. Scinocca, and T.G. Shepherd, Separating the dynamical effects of climate change and ozone depletion Part I: Southern Hemisphere stratosphere, *J. Clim.*, *23*, 5002-5020, doi: 10.1175/2010JCLI3586.1, 2010.

McLandress, C., T.G. Shepherd, J.F. Scinocca, D.A. Plummer, M. Sigmond, A.I. Jonsson, and M.C. Reader, Separating the dynamical effects of climate change and ozone depletion. Part II: Southern Hemisphere troposphere, *J. Clim.*, *24*, 1850-1868, doi: 10.1175/2010JCLI3958.1, 2011.

McLandress, C., J. Perlwitz, and T.G. Shepherd, Comment on "Tropospheric temperature response to stratospheric ozone recovery in the 21st century" by Hu et al. (2011), *Atmos. Chem. Phys.*, *12*, 2533-2540, doi: 10.5194/acp-12-2533-2012, 2012.

Meinshausen, M., S.J. Smith, K.V. Calvin, J.S. Daniel, M.L.T. Kainuma, J.-F. Lamarque, K. Matsumoto, S.A. Montzka, S.C.B. Raper, K. Riahi, A. Thomson, G.J.M. Velders, and D.P.P. van Vuuren, The RCP greenhouse gas concentrations and their extensions from 1765 to 2300, *Clim. Change*, *109*, 213-241, doi: 10.1007/s10584-011-0156-z, 2011.

Meredith, M.P., and A.M. Hogg, Circumpolar response of the Southern Ocean eddy activity to a change in the Southern Annular Mode, *Geophys. Res. Lett.*, *33*, L16608, doi: 10.1029/2006GL026499, 2006.

Meredith, M.P., A.C. Naveira Garabato, A.M. Hogg, and R. Farneti, Sensitivity of the overturning circulation in the Southern Ocean to decadal changes in wind forcing, *J. Clim.*, *25*, 99-110, doi: 10.1175/2011JCLI4204.1, 2012.

Miller, R.L., G.A. Schmidt, and D.T. Shindell, Forced annular variations in the 20th century Intergovernmental Panel on Climate Change Fourth Assessment Report models, *J. Geophys. Res.*, *111*, D18101, doi: 10.1029/2005JD006323, 2006.

Min, S.-K., and S.-W. Son, Multi-model attribution of the Southern Hemisphere Hadley Cell widening: Major role of ozone depletion, *J. Geophys. Res*., *118*, 3007-3015, doi: 10.1002/jgrd.50232, 2013.

Mitchell, D.M., P.A. Stott, L.J. Gray, M.R. Allen, F.C. Lott, N. Butchart, S.C. Hardiman, and S.M. Osprey, The impact of stratospheric resolution on the detectability of climate change signals in the free atmosphere, *Geophys. Res. Lett.*, *40*, 937-942, doi: 10.1002/grl.50177, 2013.

Monge-Sanz, B.M., M.P. Chipperfield, D.P. Dee, A.J. Simmons, and S.M. Uppala, Improvements in the stratospheric transport achieved by a CTM with ECMWF (re)analyses: Identifying effects and remaining challenges, *Qurt. J. Roy. Meteorol. Soc.*, *139*, 654-673, doi:_10.1002/qj.1996, 2012.

Monge-Sanz, B.M., M.P. Chipperfield, A. Untch, J.-J. Morcrette, A. Rap, and A.J. Simmons, On the uses of a new linear scheme for stratospheric methane in global models: Water source, transport tracer and radiative forcing, *Atmos. Chem. Phys.*, *13*, 9641-9660, doi:_10.5194/acp-13-9641-2013, 2013.

Morgenstern, O., P. Braesicke, M.M. Hurwitz, F.M. O'Connor, A.C. Bushell, C.E. Johnson, and J.A. Pyle, The world avoided by the Montreal Protocol, *Geophys. Res. Lett.*, *35*, L16811, doi: 10.1029/2008GL034590, 2008.

Morgenstern, O., H. Akiyoshi, S. Bekki, P. Braesicke, N. Butchart, M.P. Chipperfield, D. Cugnet, M. Deushi, S.S. Dhomse, R.R. Garcia, A. Gettelman, N.P. Gillett, S.C. Hardiman, J. Jumelet, D.E. Kinnison, J.-F. Lamarque, F. Lott, M. Marchand, M. Michou, T. Nakamura, D. Olivié, T. Peter, D. Plummer, J.A. Pyle, E. Rozanov, D. Saint-Martin, J.F. Scinocca, K. Shibata, M. Sigmond, D. Smale, H. Teyssèdre, W. Tian, A. Voldoire, and Y. Yamashita, Anthropogenic forcing of the Northern Annular Mode in CCMVal-2 models, *J. Geophys. Res.*, *115* (D00M03), doi: 10.1029/2009JD013347, 2010.

Morgenstern, O., G. Zeng, N.L. Abraham, P.J. Telford, P. Braesicke, J.A. Pyle, S.C. Hardiman, F.M. O'Connor, and C.E. Johnson, Impacts of climate change, ozone recovery, and increasing methane on the tropospheric oxidizing capacity, *J. Geophys. Res.*, *118*, 1028-1041, doi: 10.1029/2012JD018382, 2013.

Morgenstern, O., G. Zeng, N.L. Abraham, P.J. Telford, P. Braesicke, J.A. Pyle, S.C. Hardiman, F.M. O'Connor, and C.E. Johnson, Correction to "Impacts of climate change, ozone recovery, and increasing methane on surface ozone and the tropospheric oxidizing capacity," *J. Geophys. Res.*, *119* (8), 5028-5036, doi: 10.1002/2014 JD021515, 2014.

Morrison, A.K., and A.M. Hogg, On the relationship between Southern Ocean overturning and ACC transport, *J. Phys. Oceanogr*., *43* (1), 140-148, doi: 10.1175/JPO-D-12-057.1, 2013.

Myhre, G., and D. Shindell (Coordinating Lead Authors), F.-M. Bréon, W. Collins, J. Fuglestvedt, J. Huang, D. Koch, J.-F. Lamarque, D. Lee, B. Mendoza, T. Nakajima, A. Robock, G. Stephens, T. Takemura, and H. Zhang, Anthropogenic and natural radiative forcing, Chapter 8 in *Climate Change 2013: The Physical Science Basis. Contribution of Working Group I to the Fifth Assessment Report of the Intergovernmental Panel on Climate Change*, edited by T.F. Stocker, D. Qin, G.-K. Plattner, M. Tignor, S.K. Allen, J. Boschung, A. Nauels, Y. Xia, V. Bex, and P.M. Midgley, Cambridge University Press, Cambridge, UK, and New York, NY, USA, 2013.

Naik, V., L.W. Horowitz, A.M. Fiore, P. Ginoux, J. Mao, A.M. Aghedo, and H. Levy II, Impact of preindustrial to present day changes in short-lived pollutant emissions on atmospheric composition and climate forcing, *J. Geophys. Res.*, *118*, 8086-8110, doi: 10.1002/jgrd.50608, 2013.

Nash, J., Extension of explicit radiance observations by the Stratospheric Sounding Unit into the lower stratosphere and lower mesosphere, *Quart. J. Roy. Meteorol. Soc*., *114*, 1153-1171, 1988.

Nash, J., and G.F. Forrester, Long-term monitoring of stratospheric temperature trends using radiance measurements obtained by the TIROS-N series of NOAA spacecraft, *Adv. Space Res.*, *6* (10), 37-44, doi: 10.1016/0273-1177(86)90455-2, 1986.

Nash, J., and R. Saunders, A review of Stratospheric Sounding Unit radiance observations in support of climate trends investigations and reanalysis, *Forecasting Research Technical Report No. 586*, Met Office, 2013.

Ndarana, T., D.W. Waugh, L.M. Polvani, G.J.P. Correa, and E.P. Gerber, Antarctic ozone depletion and trends in tropopause Rossby wave breaking, *Atmos. Sci. Lett*., *13*, 164-168, doi: 10.1002/asl.384, 2012.

Newman, P.A., L.D. Oman, A.R. Douglass, E.L. Fleming, S.M. Frith, M.M. Hurwitz, S.R. Kawa, C.H. Jackman, N.A. Krotkov, E.R. Nash, J.E. Nielsen, S. Pawson, R.S. Stolarski, and G.J.M. Velders, What would have happened to the ozone layer if chlorofluorocarbons (CFCs) had not been regulated?, *Atmos. Chem. Phys*., *9* (6),

2113-2128, doi: 10.5194/acp-9-2113-2009, 2009.
Oberländer, S., U. Langematz, and S. Meul, Unravelling impact factors for future changes in the Brewer-Dobson circulation, *J. Geophys. Res.*, *118*, 10296-10312, doi: 10.1002/jgrd50775, 2013.
Okamoto, K., K. Sato, and H. Akiyoshi, A study on the formation and trends of the Brewer-Dobson circulation, *J. Geophys. Res*., *116*, D10117, doi: 10.1029/2010JD014953, 2011.
Oman, L., D.W. Waugh, S. Pawson, R.S. Stolarski, and P.A. Newman, On the influence of anthropogenic forcings on changes in the stratospheric mean age, *J. Geophys. Res*., *114*, doi: 10.1029/2008JD010378, 2009.
Oman, L.D., D.W. Waugh, S.R. Kawa, R.S. Stolarski, A.R. Douglass, and P.A. Newman, Mechanisms and feedbacks causing changes in upper stratospheric ozone in the 21st century, *J. Geophys. Res.*, *115*, D05303, doi: 10.1029/2009JD012397, 2010.
Orr, A., T.J. Bracegirdle, J.S. Hosking, T. Jung, J.D. Haigh, T. Phillips, and W. Feng, Possible Dynamical Mechanisms for Southern Hemisphere Climate Change due to the Ozone Hole, *J. Atmos. Sci.*, *69*, 2917-2932, doi: 10.1175/JAS-D-11-0210.1, 2012.
Orr, A., T.J. Bracegirdle, J.S. Hosking, W. Feng, H.K. Roscoe, and J.D. Haigh, Strong dynamical modulation of the cooling of the polar stratosphere associated with the Antarctic ozone hole, *J. Clim.*, *26*, 662-668, doi: 10.1175/JCLI-D-12-00480.1, 2013.
Palmeiro, F., N. Calvo, and R.R. Garcia, Future changes in the Brewer-Dobson circulation under different GHG concentrations, *J. Atmos. Sci.*, *71*, 2962-2975, doi: 10.1175/JAS-D-13-0289.1, 2014.
Parkinson, C.L., and D.J. Cavalieri, Antarctic sea ice variability and trends, 1979-2010, *Cryosphere*, *6* (4), 871-880, doi: 10.5194/tc-6-871-2012, 2012.
Perlwitz, J., S. Pawson, R.L. Fogt, J.E. Nielsen, and W.D. Neff, Impact of stratospheric ozone hole recovery on Antarctic climate, *Geophys. Res. Lett.*, *35*, L08714, doi: 10.1029/2008GL033317, 2008.
Plumb, R.A., Stratospheric transport, *J. Meteor. Soc. Japan*, *80*,793-809, 2002.
Polvani, L.M., and P.J. Kushner, Tropospheric response to stratospheric perturbations in a relatively simple general circulation model, *Geophys. Res. Lett.*, *29*, doi: 10.1029/2001GL014284, 2002.
Polvani, L.M., and K.L. Smith, Can natural variability explain observed Antarctic sea ice trends? New modeling evidence from CMIP5, *Geophys. Res. Lett*., *40*, 3195-3199, doi: 10.1002/grl.50578, 2013.
Polvani, L.M., and S. Solomon, The signature of ozone depletion on tropical temperature trends, as revealed by their seasonal cycle in model integrations with single forcings, *J. Geophys. Res*., *117*, D17102, doi: 10.1029/2012 JD017719, 2012.
Polvani, L.M., M. Previdi, and C. Deser, Large cancellation, due to ozone recovery, of future Southern Hemisphere atmospheric circulation trends, *Geophys. Res. Lett.*, *38*, L04707, doi: 10.1029/2011GL046712, 2011a.
Polvani, L.M., D.W. Waugh, G.J.P. Correa, and S.-W. Son, Stratospheric ozone depletion: The main driver of 20th Century atmospheric circulation changes in the Southern Hemisphere, *J. Clim.*, *24*, 795-812, doi: 10.1175/2010 JCLI3772.1, 2011b.
Portmann, R.W., J.S. Daniel, and A.R. Ravishankara, Stratospheric ozone depletion due to nitrous oxide: Influences of other gases, *Phil. Trans. R. Soc. B. Bio. Sci.*, *367*, 1256-1264, doi: 10.1098/rstb.2011.0377, 2012.
Previdi, M., and L.M. Polvani, Comment on "Tropospheric temperature response to stratospheric ozone recovery in the 21st century" by Hu et al. (2011), *Atmos. Chem. Phys.*, *12*, 4893-4896, doi: 10.5194/acp-12-4893-2012, 2012.
Previdi, M., and L.M. Polvani, Climate system response to stratospheric ozone depletion and recovery, *Quart. J. Roy. Meteorol. Soc.*, in press, doi: 10.1002/qj.2330, 2014.
Purich, A., and S.-W. Son, Impact of Antarctic ozone depletion and recovery on Southern Hemisphere precipitation, evaporation, and extreme changes, *J. Clim.*, *25* (9), 3145-3154, doi:_10.1175/JCLI-D-11-00383.1, 2012.
Quan, X.-W., M.P. Hoerling, J. Perlwitz, H.F. Diaz, and T. Xu, How fast are the tropics expanding?, *J. Clim.*, *27* (5), 1999-2013, doi: 10.1175/JCLI-D-13-00287.1, 2013.
Ramaswamy, V., M.D. Schwarzkopf, W.J. Randel, B.D. Santer, B.J. Soden, and G.L. Stenchikov, Anthropogenic and natural influences in the evolution of lower stratospheric cooling, *Science*, *311* (5764), 1138-1141, 2006.
Randel, W.J., and I.M. Held, Phase speed spectra of transient eddy fluxes and critical layer absorption, *J. Atmos. Sci.*, *48* (5), 688-697, doi: 10.1175/1520-0469(1991)048<0688:PSSOTE>2.0.CO;2, 1991.
Randel, W.J., and E.J. Jensen, Physical processes in the tropical tropopause layer and their roles in a changing climate, *Nature Geoscience*, *6*, 169-176, doi: 10.1038/ngeo1733, 2013.
Randel, W.J., and A.M. Thompson, Interannual variability and trends in tropical ozone derived from SAGE II satellite data and SHADOZ ozonesondes, *J. Geophys. Res.*, *116* (D7), D07303, doi: 10.1029/2010JD015195, 2011.
Randel, W.J., K.P. Shine, J. Austin, J. Barnett, C. Claud, N.P. Gillett, P. Keckhut, U. Langematz, R. Lin, C. Long,

C. Mears, A. Miller, J. Nash, D.J. Seidel, D.W.J. Thompson, F. Wu, and S. Yoden, An update of observed stratospheric temperature trends, *J. Geophys. Res.*, *114,* D02107, doi: 10.1029/2008JD010421, 2009.

Ray, E.A., F.L. Moore, K.H. Rosenlof, S.M. Davis, H. Boenisch, O. Morgenstern, D. Smale, E. Rozanov, M. Hegglin, G. Pitari, E. Mancini, P. Braesicke, N. Butchart, S. Hardiman, F. Li, K. Shibata, and D.A. Plummer, Evidence for changes in stratospheric transport and mixing over the past three decades based on multiple data sets and tropical leaky pipe analysis. *J. Geophys. Res.*, *115* (D21), D21304, doi: 10.1029/2010JD014206, 2010.

Reader, M.C., D.A. Plummer, J.F. Scinocca, and T.G. Shepherd, Contributions to twentieth century total column ozone change from halocarbons, tropospheric ozone precursors, and climate change, *Geophys. Res. Lett.*, *40* (23), 6276-6281, doi: 10.1002/2013GL057776, 2013.

Rivière, G., A dynamical interpretation of the poleward shift of the jet streams in global warming scenarios, *J. Atmos. Sci.*, *68* (6), 1253-1272, doi: 10.1175/2011JAS3641.1, 2011.

Roemmich D., J. Gilson, R. Davis, P. Sutton, S. Wijffels, and S. Riser, Decadal spinup of the South Pacific subtropical gyre., *J. Phys. Oceanogr.*, *37*, 162-173, doi: 10.1175/JPO3004.1, 2007.

Sallée, J.-B., R.J. Matear, S.R. Rintoul, and A. Lenton, Localized subduction of anthropogenic carbon dioxide in the Southern Hemisphere oceans, *Nature Geoscience*, *5*, 579-584, doi: 10.1038/ngeo1523, 2012.

Santer, B.D., J.F. Painter, C.A. Mears, C. Doutriaux, P. Caldwell, J.M. Arblaster, P.J. Cameron-Smith, N.P. Gillett, P.J. Gleckler, J. Lanzante, J. Perlwitz, S. Solomon, P.A. Stott, K.E. Taylor, L. Terray, P.W. Thorne, M.F. Wehner, F.J. Wentz, T.M.L. Wigley, L.J. Wilcox, and C.-Z. Zou, Identifying human influences on atmospheric temperature, *Proc. Natl. Acad. Sci. USA*, *110* (1), 26-33, doi: 10.1073/pnas.1210514109, 2013.

Schoeberl, M.R., A.E. Dessler, and T. Wang, Simulation of stratospheric water vapor and trends using three reanalyses, *Atmos. Chem. Phys*., *12* (14), 6475-6487, doi: 10.5194/acp-12-6475-2012, 2012.

Screen, J.A., N.P. Gillett, D.P. Stevens, G.J. Marshall, and H.K. Roscoe, The role of eddies in the Southern Ocean temperature response to the Southern Annular Mode, *J. Clim.*, *22* (3), 806-818, doi: 10.1175/2008JCLI2416.1, 2009.

Seidel, D.J., N.P. Gillet, J.R. Lanzante, K.P. Shine, and P.W. Thorne, Stratospheric temperature trends: Our evolving understanding, *WIREs Clim. Change*, *2* (4), 592-616, doi: 10.1002/wcc.125, 2011.

Seviour, W.J.M., N. Butchart, and S. Hardiman, The Brewer-Dobson circulation inferred from ERA-Interim, *Q.J.R. Meteorol. Soc.*, *138* (665), 878-888. doi: 10.1002/qj.966, 2012.

Shaw, T.A., J. Perlwitz, N. Harnik, P.A. Newman, and S. Pawson, The impact of stratospheric ozone changes on downward wave coupling in the southern hemisphere, *J. Clim., 24* (16), 4210-4229, doi: 10.1175/2011JCLI 4170.1, 2011.

Shepherd, T.G., and C. McLandress, A robust mechanism for strengthening of the Brewer-Dobson circulation in response to climate change: Critical-layer control of subtropical wave breaking, *J. Atmos. Sci*., *68* (4), 784-797, doi: 10.1175/2010JAS3608.1, 2011.

Sheshadri, A., R.A. Plumb, and D.I.V. Domeisen, Can the delay in Antarctic polar vortex breakup explain recent trends in surface westerlies?, *J. Atmos. Sci.*, *71* (2), 566-573, doi: 10.1175/JAS-D-12-0343.1, 2014.

Shindell, D., and G.A. Schmidt, Southern Hemisphere climate response to ozone changes and greenhouse gas increases, *Geophys. Res. Lett.*, *31*, L18209, doi: 10.1029/2004GL020724, 2004.

Shindell, D., G. Faluvegi, L. Nazarenko, K. Bowman, J.-F. Lamarque, A. Voulgarakis, G.A. Schmidt, O. Pechony, and R. Rudy, Attribution of historical ozone forcing to anthropogenic emissions, *Nature Clim. Change*, *3*, 567-570, doi: 10.1038/nclimate1835, 2013a.

Shindell, D.T., J.-F. Lamarque, M. Schulz, M. Flanner, C. Jiao, M. Chin, P.J. Young, Y.H. Lee, L. Rotstayn, N. Mahowald, G. Milly, G. Faluvegi, Y. Balkanski, W.J. Collins, A.J. Conley, S. Dalsoren, R. Easter, S. Ghan, L. Horowitz, X. Liu, G. Myhre, T. Nagashima, V. Naik, S.T. Rumbold, R. Skeie, K. Sudo, S. Szopa, T. Takemura, A. Voulgarakis, J.-H. Yoon, and F. Lo, Radiative forcing in the ACCMIP historical and future climate simulations, *Atmos. Chem. Phys*., *13* (6), 2939-2974, doi: 10.5194/acp-13-2939-2013, 2013b.

Shindell, D.T., O. Pechony, A. Voulgarakis, G. Faluvegi, L. Nazarenko, J.-F. Lamarque, K. Bowman, G. Milly, B. Kovari, R. Ruedy, and G.A. Schmidt, Interactive ozone and methane chemistry in GISS-E2 historical and future climate simulations, *Atmos. Chem. Phys*., *13* (5), 2653-2689, doi: 10.5194/acp-13-2653-2013, 2013c.

Shine, K.P., J.J. Barnett, and W.J. Randel, Temperature trends derived from Stratospheric Sounding Unit radiances: The effect of increasing CO_2 on the weighting function, *Geophys. Res. Lett.*, *35*, L02710, doi: 10.1029/ 2007GL032218, 2008.

Sigmond, M., and J.C. Fyfe, Has the ozone hole contributed to increased Antarctic sea ice extent?, *Geophys. Res. Lett*., *37* (18), L18502, doi: 10.1029/2010GL044301, 2010.

Sigmond, M., and J.C. Fyfe, The Antarctic sea ice response to the ozone hole in climate models, *J. Clim.*, *27* (3), 1336-1342, doi: 10.1175/JCLI-D-13-00590.1, 2014.

Sigmond, M., and T.G. Shepherd, Compensation between resolved wave driving and parameterized orographic gravity wave driving of the Brewer-Dobson circulation and its response to climate change, *J. Clim.*, *27* (14), 5601-5610, doi: 10.1775/JCLI-D-13-00644.1, 2014.

Sigmond, M., M.C. Reader, J.C. Fyfe, and N.P. Gillett, Drivers of past and future Southern Ocean change: Stratospheric ozone versus greenhouse gas impacts, *Geophys. Res. Lett.*, *38* (12), L12601, doi: 10.1029/2011GL047120, 2011.

Simpkins, G.R., and A.Y. Karpechko, Sensitivity of the southern annular mode to greenhouse gas emission scenarios, *Clim. Dyn.*, *38* (3-4), 563-572, doi: 10.1007/s00382-011-1121-2, 2012.

Simpkins, G.R., L.M. Ciasto, D.W.J. Thompson, and M.H. England, Seasonal relationships between large-scale climate variability and Antarctic sea ice concentration, *J. Clim.*, *25* (16), 5451-5469, doi: 10.1175/JCLI-D-11-00367.1, 2012.

Simpson, I.R., M. Blackburn, and J.D. Haigh, The role of eddies in driving the tropospheric response to stratospheric heating perturbations, *J. Atmos. Sci.*, *66* (5), 1347-1365, doi: 10.1175/2008JAS2758.1, 2009.

Simpson, I.R., M. Blackburn, and J.D. Haigh, A mechanism for the effect of tropospheric jet structure on the annular mode-like response to stratospheric forcing, *J. Atmos. Sci.*, *69* (7), 2152-2170, doi: 10.1175/JAS-D-11-0188.1, 2012.

Simpson, I.R., T.G. Shepherd, P. Hitchcock, and J.F. Scinocca, Southern annular mode dynamics in observations and models. Part II: Eddy feedbacks, *J. Clim.*, *26* (14), 5220-5241, doi: 10.1175/JCLI-D-12-00495.1, 2013.

Sioris, C.E., C.A. McLinden, V.E. Fioletov, C. Adams, J.M. Zawodny, A.E. Bourassa, C.Z. Roth, and D.A. Degenstein, Trend and variability in ozone in the tropical lower stratosphere over 2.5 solar cycles observed by SAGE II and OSIRIS, *Atmos. Chem. Phys.*, *14* (7), 3479-3496, doi: 10.5194/acp-14-3479-2014, 2014.

Smith, K.L., C.G. Fletcher, and P.J. Kushner, The role of linear interference in the annular mode response to extratropical surface forcing, *J. Clim.*, *23*, 6036-6050, doi: 10.1175/2010JCLI3606.1, 2010.

Smith, K.L., L.M. Polvani, and D.R. Marsh, Mitigation of 21st century Antarctic sea ice loss by stratospheric ozone recovery, *Geophys. Res. Lett.*, *39* (20), L20701, doi: 10.1029/2012GL053325, 2012.

Solomon, S, J.S. Daniel, R.R. Neely III, J.-P. Vernier, E.G. Dutton, and L.W. Thomason, The persistently variable "background" stratospheric aerosol layer and global climate change, *Science*, *333* (6044), 866-870, doi: 10.1126/science.1206027, 2011.

Solomon, S., P.J. Young, and B. Hassler, Uncertainties in the evolution of stratospheric ozone and implications for recent temperature changes in the tropical lower stratosphere, *Geophys. Res. Lett.*, *39* (17), L17706, doi: 10.1029/2012GL052723, 2012.

Son, S.-W., L.M. Polvani, D.W. Waugh, T. Birner, H. Akiyoshi, R.R. Garcia, A. Gettelman, D.A. Plummer, and E. Rozanov, The impact of stratospheric ozone recovery on tropopause height trends, *J. Clim.*, *22* (2), 429-445, doi: 10.1175/2008JCLI2215.1, 2009.

Son, S.-W., E.P. Gerber, J. Perlwitz, L.M. Polvani, N.P. Gillett, K.-H. Seo, V. Eyring, T.G. Shepherd, D. Waugh, H. Akiyoshi, J. Austin, A. Baumgaertner, S. Bekki, P. Braesicke, C. Brühl, N. Butchart, M.P. Chipperfield, D. Cugnet, M. Dameris, S. Dhomse, S. Frith, H, Garny, R. Garcia, S.C. Hardiman, P. Jöckel, J.F. Lamarque, E. Mancini, M. Marchand, M. Michou, T. Nakamura, O. Morgenstern, G. Pitari, D.A. Plummer, J. Pyle, E. Rozanov, J.F. Scinocca, K. Shibata, D. Smale, H. Teyssèdre, W. Tian, and Y. Yamashita, Impact of stratospheric ozone on Southern Hemisphere circulation change: A multimodel assessment, *J. Geophys. Res.*, *115*, D00M07, doi: 10.1029/2010JD014271, 2010.

Son, S.-W., A. Purich, H.H. Hendon, B.-M. Kim, and L.M. Polvani, Improved seasonal forecast using ozone hole variability?, *Geophy. Res. Lett.*, *40* (23), 6231-6235, doi: 10.1002/2013GL057731, 2013.

Song, Y., and W.A. Robinson, Dynamical mechanisms for stratospheric influences on the troposphere, *J. Atmos. Sci.*, *61* (14), 1711-1725, 2004.

Søvde, O.A., C.R. Hoyle, G. Myhre, and I.S.A. Isaksen, The HNO_3 forming branch of the HO_2 + NO reaction: Pre-industrial-to-present trends in atmospheric species and radiative forcings, *Atmos. Chem. Phys.*, *11*, 8929-8943, doi: 10.5194/acp-11-8929-2011, 2011.

SPARC CCMVal (Stratosphere-troposphere Processes And their Role in Climate), *SPARC Report on the Evaluation of Chemistry-Climate Models*, edited by V. Eyring, T.G. Shepherd, and D.W. Waugh, SPARC Report No. 5, WCRP-132, WMO/TD-No. 1526, 478 pp., available: http://www.atmosp.physics.utoronto.ca/SPARC/ccmval_final/index.php, 2010.

Staten, P.W., J.J. Rutz, T. Reichler, and J. Lu, Breaking down the tropospheric circulation response by forcing, *Clim, Dyn.*, *39* (9-10), 2361-2375, doi: 10.1007/s00382-011-1267-y, 2012.

Stevenson, D.S., F.J. Dentener, M.G. Schultz, K. Ellingsen, T.P.C. vanNoije, O. Wild, G. Zeng, M. Anann, C.S. Atherton, N. Bell, D.J. Bergmann, I. Bey, T. Butler, J. Cofala, W.J. Collins, R.G. Derwent, R.M. Doherty, J.

Drevet, H.J. Eskes, A.F. Fiore, M. Gauss, D.A. Hauglustaine, L.W. Horowitz, I.S.A. Isaksen, M.C. Krol, J.-F. Lamarque, M.G. Lawrence, V. Montanaro, J.-F. Müller, G. Pitari, M.J. Prather, S.A. Pyle, S. Rast, J.M. Rodriguez, M.G. Sanderson, H.H. Savage, D.T. Shindell, S.E. Strahan, K. Sudo, and S. Szopa, Multi-model ensemble of present-day and near-future tropospheric ozone, *J. Geophys. Res.*, *111*, D8301, doi: 10.1029/2005JD006338, 2006.

Stevenson, D.S., P.J. Young, V. Naik, J.-F. Lamarque, D.T. Shindell, A. Voulgarakis, R.B. Skeie, S.B. Dalsoren, G. Myhre, T.K. Berntsen, G.A. Folberth, S.T. Rumbold, W.J. Collins, I.A. MacKenzie, R.M. Doherty, G. Zeng, T.P.C. van Noije, A. Strunk, D. Bergmann, P. Cameron-Smith, D.A. Plummer, S.A. Strode, L. Horowitz, Y.H. Lee, S. Szopa, K. Sudo, T. Nagashima, B. Josse, I. Cionni, M. Righi, V. Eyring, A. Conley, K.W. Bowman, O. Wild, and A. Archibald, Tropospheric ozone changes, radiative forcing and attribution to emissions in the Atmospheric Chemistry and Climate Model Intercomparison Project (ACCMIP), *Atmos. Chem. Phys*., *13* (6), 3063-3085, doi: 10.5194/acp-13-3063-2013, 2013.

Stiller, G.P., T. von Clarmann, F. Haenel, B. Funke, N. Glatthor, U. Grabowski, S. Kellmann, M. Kiefer, A. Linden, S. Lossow, and M. López-Puertas, Observed temporal evolution of global mean age of stratospheric air for the 2002 to 2010 period, *Atmos. Chem. Phys*., *12* (7), 3311-3331, doi: 10.5194/acp-12-3311-2012, 2012.

Struthers H., A.M.L. Ekman, P. Glantz, T. Iversen, A. Kirkevåg, Ø. Seland, E.M. Mårtensson, K. Noone, and E.D. Nilsson, Climate-induced changes in sea salt aerosol number emissions: 1870 to 2100, *J. Geophys. Res.*, *118* (2), 670-682, doi: 10.1002/jgrd.50129, 2013.

Swart, N.C., and J.C. Fyfe, Observed and simulated changes in the Southern Hemisphere surface westerly wind-stress, *Geophys. Res. Lett*., *39* (16), L16711, doi: 10.1029/2012GL052810, 2012.

Swart, N.C., and J.C. Fyfe, The influence of recent Antarctic ice sheet retreat on simulated sea ice area trends, *Geophys. Res. Lett.*, *40* (16), 4328-4332, doi: 10.1002/grl.50820, 2013.

Tang, Q., and M.J. Prather, Five blind men and the elephant: What can the NASA Aura ozone measurements tell us about stratosphere-troposphere exchange?, *Atmos. Chem. Phys.*, *12* (5), 2357-2380, doi: 10.5194/acp-12-2357-2012, 2012.

Tang, X., S.R. Wilson, K.R. Solomon, M. Shao, and S. Madronich, Changes in air quality and tropospheric composition due to depletion of stratospheric ozone and interactions with climate, *Photochem. Photobiol. Sci.*, *10* (2), 280-291, doi: 10.1039/c0pp90039g, 2011.

Thompson, D.W.J., and T. Birner, On the linkages between the tropospheric isentropic slope and eddy fluxes of heat during Northern Hemisphere winter, *J. Atmos. Sci*., *69* (6), 1811-1823, doi: 10.1175/JAS-D-11-0187.1, 2012.

Thompson, D.W.J., and S. Solomon, Interpretation of recent Southern Hemisphere climate change, *Science*, *296* (5569), 895-899, 2002.

Thompson, D.W.J., and S. Solomon, Understanding recent stratospheric climate change, *J. Clim.*, *22* (8), 1934-1943, doi: 10.1175/2008JCLI2482.1, 2009.

Thompson, D.W.J., J.C. Furtado, and T.G. Shepherd, On the tropospheric response to anomalous stratospheric wave drag and radiative heating, *J. Atmos. Sci.*, *63* (10), 2616-2629, 2006.

Thompson, D.W.J., S. Solomon, P.J. Kushner, M.H. England, K.M. Grise, and D.J. Karoly, Signatures of the Antarctic ozone hole in Southern Hemisphere surface climate change, *Nature Geoscience*, *4*, 741-749. doi: 10.1038/ngeo1296, 2011.

Thompson, D.W.J., D.J. Seidel, W.J. Randel, C.-Z. Zou, A.H. Butler, C. Mears, A. Osso, C. Long, and R. Lin, The mystery of recent stratospheric temperature trends, *Nature*, *491*, 692-697, doi: 10.1038/Nature11579, 2012.

Turner, J., J.C. Comiso, G.J. Marshall, T.A. Lachlan-Cope, T. Bracegirdle, T. Maksym, M.P. Meredith, Z. Wang, and A. Orr, Non-annular atmospheric circulation change induced by stratospheric ozone depletion and its role in the recent increase of Antarctic sea ice extent, *Geophys. Res. Lett.*, *36*, L08502, doi: 10.1029/2009GL037524, 2009.

Turner, J., T.J. Bracegirdle, T. Phillips, G.J. Marshall, and J.S. Hosking, An initial assessment of Antarctic sea ice extent in the CMIP5 models, *J. Clim*., *26* (5), 1473-1484, doi: 10.1175/JCLI-D-12-00068.1, 2013.

van Vuuren, D.P., J. Edmonds, M. Kainuma, K. Riahi, A. Thomson, K. Hibbard, G.C. Hurtt, T. Kram, V. Krey, J.-F. Lamarque, T. Masui, M. Meinshausen, N. Nakicenovic, S.J. Smith, and S.K. Rose, The representative concentration pathways: An overview, *Clim. Change*, *109*, 5-31, doi: 10.1007/s10584-011-0148-z, 2011.

Vaughan, D.G., and J.C. Comiso (Coordinating Lead Authors), I. Allison, J. Carrasco, G. Kaser, R. Kwok, P. Mote, T. Murray, F. Paul, J. Ren, E. Rignot, O. Solomina, K. Steffen, and T. Zhang (Lead Authors), Observations: Cryosphere, Chapter 4 in *Climate Change 2013: The Physical Science Basis. Contribution of Working Group I to the Fifth Assessment Report of the Intergovernmental Panel on Climate Change*, T.F. Stocker, D. Qin, G.-K. Plattner, M. Tignor, S.K. Allen, J. Boschung, A. Nauels, Y. Xia, V. Bex and P.M. Midgley, Cambridge University Press, Cambridge, UK, and New York, NY, USA, 2013.

Velders, G.J.M., S.O. Andersen, J.S. Daniel, D.W. Fahey, and M. McFarland, The importance of the Montreal Protocol in protecting climate, *Proc. Natl. Acad. Sci.*, *104* (12), 4814-4819, doi: 10.1073/pnas.0610328104, 2007.

Voulgarakis, A., V. Naik, J.-F. Lamarque, D.T. Shindell, P.J. Young, M.J. Prather, O. Wild, R.D. Field, D. Bergman, P. Cameron-Smith, I. Cionni, W.J. Collins, S.B. Dalsøren, R.M. Doherty, V. Eyring, G. Faluvegi, G.A. Folberth, L.W. Horowitz, B. Josse, I.A. McKenzie, T. Nagashima, D.A. Plummer, M. Righi, S.T. Rumbold, D.S. Stevenson, S.A. Strode, K. Sudo, S. Szopa, and G. Zeng., Analysis of present day and future OH and methane lifetime in the ACCMIP simulations, *Atmos. Chem. Phys*., *13* (5), 2563-2587, doi: 10.5194/acp-13-2563-2013, 2013.

Wang, L., and D.W. Waugh, Chemistry-climate model simulations of recent trends in lower stratospheric temperature and stratospheric residual circulation, *J. Geophys. Res*., *117* (D9), D09109, doi: 10.1029/2011 JD017130, 2012.

Wang, L., C-Z. Zou, and H. Qian, Constructions of stratospheric temperature data records from stratospheric sounding units, *J. Clim.*, *25* (8), 2931-2946, doi: 10.1175/JCLI-D-11-00350.1, 2012.

Watson, P.A.G., D.J. Karoly, M.R. Allen, N. Faull, and D.S. Lee, Quantifying uncertainty in future Southern Hemisphere circulation trends, *Geophys. Res. Lett*., *39* (23), L23708, doi: 10.1029/2012GL054158, 2012.

Waugh, D.W., Changes in the ventilation of the southern oceans, *Phil. Trans. R. Soc. A*, *372* (2019), doi: 10.1098/ rsta.2013.0269, 2014.

Waugh, D.W., L. Oman, S.R. Kawa, R.S. Stolarski, S. Pawson, A.R. Douglass, P.A. Newman, and J.E. Nielsen, Impacts of climate change on stratospheric ozone recovery, *Geophys. Res. Lett.*, *36*, L03805, doi: 10.1029/ 2008GL036223, 2009.

Waugh, D.W., F. Primeau, T. DeVries, and M. Holzer, Recent changes in the ventilation of the southern oceans, *Science*, *339* (6119), 568-570, doi: 10.1126/science.1225411, 2013.

Wilcox, L.J., A.J. Charlton-Perez, and L.J. Gray, Trends in Austral jet position in ensembles of high- and low-top CMIP5 models, *J. Geophys. Res*., *117*, D13115, doi: 10.1029/2012JD017597, 2012.

Wilcox, L.J., and A.J. Charlton-Perez, Final warming of the Southern Hemisphere polar vortex in high- and low-top CMIP5 models, *J. Geophys. Res.*, *118* (6), 2535-2546, doi: 10.1002/jgrd.50254, 2013.

Wild, O., Modelling the global tropospheric ozone budget: Exploring the variability in current models, *Atmos. Chem. Phys.*, *7* (10), 2643-2660, doi: 10.5194/acp-7-2643-2007, 2007.

Wittman, M.A.H., L.M. Polvani, R.K. Scott, and A.J. Charlton, Stratospheric influence on baroclinic lifecycles and its connection to the Arctic Oscillation, *Geophys. Res. Lett.*, *31*, L16113, doi: 10.1029/2004GL020503, 2004.

WMO (World Meteorological Organization), *Scientific Assessment of Ozone Depletion: 2002*, Global Ozone Research and Monitoring Project–Report No. 47, Geneva, Switzerland, 2003.

WMO (World Meteorological Organization), *Scientific Assessment of Ozone Depletion: 2010,* Global Ozone Research and Monitoring Project - Report No. 52, Geneva, Switzerland, 2011.

Wu, Y., L.M. Polvani, and R. Seager, The importance of the Montreal Protocol in protecting Earth's hydroclimate, *J. Clim.*, *26* (12), 4049-4068, doi: 10.1175/JCLI-D-12-00675.1, 2013.

Xie S.-P., B. Lu, and B. Xiang, Similar spatial patterns of climate responses to aerosol and greenhouse gas changes, *Nature Geoscience*, *6*, 828-832, doi: 10.1038/ngeo1931, 2013.

Young, P.J., K.H. Rosenlof, S. Solomon, S.C. Sherwood, Q. Fu, and J.-F. Lamarque, Changes in stratospheric temperatures and their implications for changes in the Brewer-Dobson circulation, 1979-2005, *J. Clim.*, *25* (5), 1759-1772, doi: 10.1175/2011JCLI4048.1, 2012.

Young, P.J., A.T. Archibald, K.W. Bowman, J.-F. Lamarque, V. Naik, D.S. Stevenson, S. Tilmes, A. Vougarakis, O. Wild, D. Bergmann, P. Cameron-Smith, I. Cionni, W.J. Collins, S.B. Dalsøren, R.M. Doherty, V. Eyring, G. Faluvegi, L.W. Horowitz, B. Josse, Y.H. Lee, I.A. MacKenzie, T. Nagashima, D.A. Plummer, M. Righi, S.T. Rumbold, R.B. Skeie, D.T. Shindell, S.A. Strode, K. Sudo, S. Szopa, and G. Zeng, Pre-industrial to end 21st century projections of tropospheric ozone from the Atmospheric Chemistry and Climate Model Intercomparison Project (ACCMIP), *Atmos. Chem. Phys*., *13* (4), 2063-2090, doi: 10.5194/acp-13-2063-2013, 2013a.

Young, P.J., A.H. Butler, N. Calvo, L. Haimberger, P.J. Kushner, D.R. Marsh, W.J. Randel, and K.R. Rosenlof, Agreement in late twentieth century Southern Hemisphere stratospheric temperature trends in observations and CCMVal-2, CMIP3, and CMIP5 models, *J. Geophys. Res*., *118* (2), 605-613, doi: 10.1002/jgrd.50126, 2013b.

Zeng, G., O. Morgenstern, P. Braesicke, and J.A. Pyle, Impact of stratospheric ozone recovery on tropospheric ozone and its budget, *Geophys. Res. Lett*., *37* (9), L09805, doi: 10.1029/2010GL042812, 2010.

Zunz, V., H. Goosse, and F. Massonnet, How does internal variability influence the ability of CMIP5 models to reproduce the recent trend in Southern Ocean sea ice extent?, *The Cryosphere*, *7* (2), 451-468, doi: 10.5194/tc-7-451-2013, 2013.

CHAPTER 5

Scenarios and Information for Policymakers

Lead Authors:
N.R.P. Harris
D.J. Wuebbles

Coauthors:
J.S. Daniel
J. Hu
L.J.M. Kuijpers
K.S. Law
M.J. Prather
R. Schofield

Contributors:
J.B. Burkholder
E.L. Fleming
Ø. Hodnebrog
R. Hossaini
C.H. Jackman
D. Phoenix

Chapter Editors:
M. McFarland
G.J.M. Velders

[Formatted for double-sided printing.]

From:
WMO (World Meteorological Organization), *Scientific Assessment of Ozone Depletion: 2014*, Global Ozone Research and Monitoring Project – Report No. 55, 416 pp., Geneva, Switzerland, 2014.

This chapter should be cited as:
N.R.P. Harris and D.J.Wuebbles (Lead Authors), J.S. Daniel, J. Hu, L.J.M. Kuijpers, K.S. Law, M.J. Prather, and R. Schofield, Scenarios and information for policymakers, Chapter 5 in *Scientific Assessment of Ozone Depletion: 2014*, Global Ozone Research and Monitoring Project – Report No. 55, World Meteorological Organization, Geneva, Switzerland, 2014.

CHAPTER 5

SCENARIOS AND INFORMATION FOR POLICYMAKERS

Contents

SCIENTIFIC SUMMARY

A new baseline scenario for ozone-depleting substances (ODSs) is presented in Chapter 5 that reflects our current understanding of atmospheric mixing ratios, production levels, and bank sizes. Elimination of future emissions, from either production or existing banks of various ODSs, is applied to this scenario to evaluate the maximum impacts of various hypothetical policy options including phase-outs and destruction (see Table S5-1). Some specific findings corresponding to this table include:

- **Emissions from the current banks (taking 2015 as being current) over the next 35 years are projected to lead to greater future ozone depletion and climate forcing than those caused by future ODS production.** Capture and destruction of these banks could avoid 1.8 million Ozone Depletion Potential-tonnes (ODP-tonnes) of future emission through 2050; this compares with an estimated 1.6 million ODP-tonnes of emissions that have occurred over the last decade (from 2005–2014).
- **Of all of the ODS banks, the banks of halons in 2015 are projected to contribute most to ozone depletion over the next 35 years (as Equivalent Effective Stratospheric Chlorine, EESC), while chlorofluorocarbon (CFC) and hydrochlorofluorocarbons (HCFC) banks are expected to contribute most in terms of Global Warming Potential-weighted (GWP-weighted) emissions.**
- **If future production and all ODS 2015 banks are considered, HCFCs represent the halocarbon group that contributes most to future GWP-weighted emissions. HCFCs can be reduced in the future by both bank recapture and destruction and by production elimination.**

Table S5-1. Summary of mitigation options for accelerating the recovery of the ozone layer and reducing CO_2-equivalent emissions. The table gives the reductions in integrated EESC (Equivalent Effective Stratospheric Chlorine) and integrated CO_2-equivalent emissions relative to the baseline scenario that can be achieved for mitigation options beginning in 2015 or 2020. The integrated EESC is defined as the total EESC amount integrated from 2015 until the time EESC returns to the 1980 level (before 2050 for all scenarios). Bank recapture and destruction is assumed to be 100% effective and either applies to the bank existing in 2015 or the bank existing in 2020. Any potential contribution from very short-lived substances is neglected. These calculations use the lifetimes derived from SPARC, 2013 (Stratosphere-troposphere Processes And their Role in Climate).

Substance or Group of Substances	Reductions (%) in Integrated Midlatitude EESC Integrated from 2015 until EESC Returns to 1980 Levels		Reduction in Cumulative GWP-Weighted Emissions from 2015 to 2050 (Gigatonnes of CO_2-equivalent)	
Bank recapture and destruction in 2015 or 2020:	**2015 bank**	**2020 bank**	**2015 bank**	**2020 bank**
CFCs	8.9	5.3	4.7	3.3
halons	12	6.8	0.2	0.2
HCFCs	6.4	5.5	4.6	4.6
Production elimination from 2015 onward:				
HCFCs	6.4		7.8	
CH_3Br (only quarantine and pre-shipment)	5.3		0.0	
Total emissions elimination from 2015 onward:				
CCl_4	9.8		1.2	
CH_3CCl_3	0.0		0.0	
HFCs	0.0		Up to 165*	

* Reduction relative to hypothetical future upper range scenario and would depend on actual growth rate of HFC use.

- **The impact on ozone-layer recovery of further policy actions on already controlled ozone-depleting substances is becoming smaller.** Nonetheless, if all ODS emissions – including those emanating from many widely dispersed banks – were to be stopped in 2015, then the return to 1980 midlatitude EESC values would be brought forward to 2036 compared with 2047 in the baseline scenario.
- **Updated Ozone Depletion Potentials (ODPs) are almost all numerically smaller, ranging from no change (for carbon tetrachloride, CCl_4) to more than a factor of two smaller (for CFC-115), with most of these smaller by 10–30% than the values reported in WMO (2011).** These changes largely reflect the revised estimate for the atmospheric lifetime of CFC-11 (from 45 to 52 years) reported in SPARC (2013); CFC-11 is the reference gas in determining ODPs so this change affects all ODPs. Uncertainties in the atmospheric lifetimes, the fractional release values, and atmospheric chemistry generally result in overall uncertainties in ODPs on the order of 30% for the CFCs and CCl_4, but are higher for HCFCs and halons (about 60% for the HCFCs and halon-1301, to over 80% for halon-1202 and halon-1211).
- **New atmospheric model studies continue to emphasize that ODPs for very short-lived substances (VSLS) that contain bromine or chlorine are strongly dependent on the geographic location and season of emission.** Impacts from VSLS are much larger (with ODPs approaching values of 1) if emissions occur in regions close to convective regions in the tropics. There is still insufficient research available to confidently compare the mitigation options of anthropogenic VSLS emissions with those of the longer-lived halogenated hydrocarbons; overall the VSLS have smaller ODPs than longer-lived ODS. However, if long-lived controlled halocarbons (and their banks) follow their projected decline, then chlorine- and bromine-containing anthropogenic VSLS emissions will play a relatively larger role in future ozone depletion, but the absolute effects are smaller than that of ODSs today while remaining uncertain.
- **The projection of CCl_4 remains more uncertain than projections for other ODSs due to our incomplete understanding of the current CCl_4 budget (likely a missing source; see Chapter 1).** In the scenarios examined (see table above), CCl_4 human-related emissions from 2015 through 2050 are comparable to those of the HCFCs in terms of ODP-weighted emissions and are about 10% in terms of GWP-weighted emissions. It is expected that future emissions of CCl_4 will remain an important factor in the evolution of EESC.
- **The total anthropogenic emissions of methyl bromide (CH_3Br) have declined in response to controls of the Montreal Protocol.** Overall, reported consumption has gone down from ~70,000 tonnes/yr in the late 1990s to ~13,000 tonnes/yr in 2012.
- **Quarantine and pre-shipment (QPS) uses of CH_3Br are exempted uses (not controlled) by the Montreal Protocol and in 2012 constitute an annual consumption of CH_3Br (~9,000 tonnes) that is larger than the annual consumption for 2012 from uses controlled by the Protocol (~4,000 tonnes).** The elimination of future emissions from QPS uses could bring forward the date of EESC return to 1980 levels by 1.1 years, smaller than the 1.6 years estimated in the previous Assessment. Critical-use exemptions continue to be granted, but at levels significantly reduced compared with four years ago. A continuation of critical-use exemptions at the current level would delay the return of EESC to 1980 levels by 0.2 years.
- **Carbon dioxide (CO_2), nitrous oxide (N_2O), and methane (CH_4) are each important to climate forcing and to the levels of stratospheric ozone (see Chapter 2).** In terms of the globally averaged ozone column, additional N_2O leads to lower ozone levels, whereas additional CO_2 and CH_4 lead to higher ozone levels. Ozone depletion to date would have been greater if not for the historical increases in CO_2 and CH_4. The net impact on ozone recovery and future levels of stratospheric ozone thus depends on the future abundances of these gases. For many of the scenarios used in the most recent Intergovernmental Panel on Climate Change (IPCC) Assessment (IPCC, 2013), global ozone

will increase to above pre-1980 levels due to future trends in the gases. Latitudinal and altitudinal responses are expected to vary. Note that scenarios used in IPCC consider a future with all three major greenhouse gases increasing and thus it is important to assess the net balance of these perturbations on stratospheric ozone.

- **Global Warming Potentials (GWPs) for a range of halocarbons have been updated based on IPCC (2013) and SPARC (2013).** The CO_2 Absolute Global Warming Potential (AGWP; the denominator for the GWP of other greenhouse gases) has increased by 6% compared to the previous Assessment (WMO, 2011). As a result, GWP values for many non-CO_2 greenhouse gases decreased slightly. GWPs also changed because of revised values for the lifetime and the radiative efficiency of the individual greenhouse gases. The revised SPARC-based lifetimes for a range of ODSs have been updated due to new analyses of observations and models and are included here; the largest differences in GWPs are found for CFC-11, CFC-115, halon-1301, halon-2402, and halon-1202. For hydrofluorocarbons (HFCs), some examples of the IPCC 100-year GWPs and the SPARC lifetime adjusted values are given below. The numbers in parentheses represent the effects of uncertainties in the SPARC lifetimes, radiative efficiency, and the AGWP for CO_2 based on 90% confidence. In addition, the IPCC (2013) stated uncertainties in the 100-year GWP for HFC-134a is ±35% (90% confidence) as representative for similar gases. The IPCC and updated GWPs that use the SPARC lifetimes are consistent within their uncertainties.

Substance	IPCC AR5 100-yr GWP	Updated 100-yr GWP (90% uncertainty range)
HFC-23	12,400	12,500 (8880–16,300)
HFC-32	677	704 (453–1070)
HFC-125	3170	3450 (2230–5140)
HFC-134a	1300	1360 (857–2050)
HFC-143a	4800	5080 (3460–7310)
HFC-152a	138	148 (96–211)

- **Global Temperature Potentials (GTPs) are discussed and values reported for the first time in a WMO-UNEP Ozone Assessment.** The GTP metric gives the relative temperature increase at a specified time horizon due to emissions of a greenhouse gas, relative to that caused by the same weight of CO_2 emissions. This metric may be useful as an alternative to GWPs. These metrics are different in construction and have both advantages and disadvantages. The revised SPARC-based lifetimes affect GTPs (relative to IPCC, 2013) in the same way as GWPs. The table below shows updated GTPs for the same HFCs listed above.

Substance	Updated 20-yr GTP	Updated 50-year GTP	Updated 100-year GTP
HFC-23	11,500	13,000	12,800
HFC-32	1440	154	98
HFC-125	6040	3350	1180
HFC-134a	3170	771	214
HFC-143a	7110	5390	2830
HFC-152a	191	26	21

- **The current direct radiative forcing (RF) from ODS halocarbons (CFCs, halons, and HCFCs) is about 0.33 W m^{-2} and is near its expected peak.** The RF is projected to decrease to about 0.20 W m^{-2} by about 2050, depending on the particular emission scenario adopted. By 2100, the radiative forcing from these halocarbons is projected to be near 0.10 W m^{-2} independent of the specific emission scenarios considered here.

- **While HFCs currently constitute less than 1% of the radiative forcing on climate (0.02 W m^{-2}), if the current mix of HFCs is unchanged, increasing demand could imply a radiative forcing for HFCs as high as 0.4 W m^{-2} by 2050.** For all scenarios (Special Report on Emissions Scenarios (SRES) and Representative Concentration Pathway (RCP)) used in the recent IPCC Assessments, the HFC radiative forcing increases by 0.1 W m^{-2} or less by 2050; however, these scenarios did not consider recent market trends. Scenarios based on projections of HFC markets yield radiative forcings that range from 0.16 W m^{-2} to 0.4 W m^{-2} by 2050.
- **Replacements of the current mix of high-GWP HFCs with low- or zero-ODP, low-GWP compounds, could lead to a decrease in the radiative forcing on climate over the coming decades, possibly by as much as 0.07 W m^{-2} by 2030 relative to baseline scenarios assuming continued growth in high-GWP HFC production.** Such reductions are comparable to possible reductions in radiative forcing for some other non-CO_2 emissions (e.g., for black carbon emissions). Even by 2050, the RF from the low-GWP replacement compounds would be negligibly small. For the uses projected, such replacements are likely to have a negligible effect on stratospheric ozone, despite some replacements containing chlorine or bromine and having non-zero ODPs.
- **The impact of HFC mitigation on future climate change that only considers radiative forcing of HFCs through a particular year is underestimated if the future commitment to climate forcing in the HFC banks is neglected.** This bank size represents a substantially larger fraction of the cumulative HFC production and emission than was the case for CFCs in the 1980s; this is because current and projected applications for HFCs emit those HFCs much more slowly than applications historically did for CFCs.
- **Unsaturated HFCs (also known as hydrofluoro-olefins, HFOs) are replacement compounds for long-lived HCFCs and HFCs.** Unsaturated HFCs have short atmospheric lifetimes (days) and small GWPs (<10). Atmospheric degradation of one of these substances (HFC-1234yf) produces the persistent degradation product trifluoroacetic acid (TFA). While the environmental effects of TFA are considered negligible over the next decades, potential longer-term impacts could require future evaluations due to the environmental persistence of TFA and uncertainty in future uses of HFC-1234yf.
- **CFC-316c ((*E*)- and (*Z*)- isomers of cyclic 1,2-$C_4F_6Cl_2$) are possible ODS replacement compounds, and have long lifetimes (75 and 114 years), with correspondingly high ODPs (0.46 and 0.54) and GWPs (4160 and 5400).**
- **Emissions of biogenically produced bromocarbons will likely increase as a result of changes in the management of their human-related production (e.g., marine aquaculture).** However, uncertainties in all natural emissions and in transport to the stratosphere are large, making it difficult to quantify their effects on ozone.
- **Current emissions from aviation and rockets have only a small effect on total ozone (<1%). However, new technologies and potential market growth in aviation and rockets will require further assessment as they could potentially lead to effects on ozone.**
- **Geoengineering the climate system via anthropogenic increases of stratospheric sulfate aerosols within the next few decades would be expected to deplete stratospheric ozone, with the largest effects in the polar regions.** The current level of understanding of how other possible geoengineering approaches would affect the stratosphere is limited.
- **The proposed cosmic-ray-driven breakdown of CFCs in ice particles is of negligible importance in polar ozone loss.**

5.1 INTRODUCTION

The series of WMO Ozone Assessments have reported the success of the control measures introduced under the Montreal Protocol. These have included striking reductions first in the rate of increase in atmospheric ozone-depleting substances (ODSs) and subsequently in the total amount of ODSs in the atmosphere (see Chapter 1). Signs of an increase in stratospheric ozone amounts are emerging (Chapter 2), pointing to the success of these measures in reducing ozone depletion and hence limiting the resulting increases in surface UV radiation. As successive Amendments and adjustments to the Montreal Protocol have been introduced, opportunities for further significant measures affecting stratospheric ozone have become scarcer. Accordingly, policy-relevant issues are now largely concentrated on (i) issues connected with new compounds with the potential to deplete ozone and (ii) the other atmospheric effects of ODSs and their replacements. In addition, the Montreal Protocol and its Amendments have at this point contributed more to climate change mitigation than any other existing international agreement.

In this section, the main points from the WMO Ozone Assessment (2011) are first summarized. Then, the objectives and the contents of this chapter are described.

5.1.1 Main Issues from WMO-UNEP 2010 and Other Reports

In several respects, this chapter is an update of Chapter 5 in WMO (2011). In that chapter, Ozone Depletion Potentials (ODPs) and Global Warming Potentials (GWPs) for ODSs and their replacements were updated. New scenarios were generated to explore the potential impacts of hypothetical ODS and nitrous oxide (N_2O) emissions reductions on future ozone depletion and climate forcing. The WMO (2011) chapter additionally included assessments of some processes and activities (e.g., from rockets or from the possible uses of geoengineering as a response to climate change) that may affect future ozone levels through mechanisms that do not necessarily involve the emission of chlorine- and bromine-containing source gases. It was found that some of these processes could affect future ozone levels more than future emissions of controlled ODSs. The impact of the Montreal Protocol on climate forcing was discussed. Finally, the chapter showed how the Montreal Protocol and its Amendments and adjustments had averted many profound changes to Earth and its atmosphere. In particular, because many ODSs are potent greenhouse gases, the Montreal Protocol has successfully avoided larger potential changes to the Earth's climate. Two specific issues raised there are worth mentioning as they are looked into again here.

First, the effects of the accelerated phase-out of HCFCs (hydrochlorofluorocarbons) agreed to by the Parties to the Montreal Protocol in 2007 were projected as a reduction in cumulative HCFC emissions between 2011 and 2050 of 0.6–0.8 million ODP-tonnes, equivalent to bringing forward the year in which Equivalent Effective Stratospheric Chlorine (EESC) returns to 1980 levels by 4–5 years. In addition, the accelerated HCFC phase-out was projected to reduce emissions by 0.4–0.6 gigatonnes of carbon dioxide-equivalents ($GtCO_2$-eq) per year averaged over 2011–2050. The *net* climate benefit is determined, in part, by the climate impact of the compounds used to replace the HCFCs. If high GWP HFCs (hydro-fluorocarbons) were to be used without mitigation, it was estimated that the HFC growth could result in GWP-weighted emissions up to 8.8 $GtCO_2$-eq per year by 2050. This amount is comparable to the GWP-weighted emissions of chlorofluorocarbons (CFCs) at their peak in 1988. The projected radiative forcing in 2050 from these compounds (up to 0.4 watts per square meter ($W\ m^{-2}$)) could be reduced by using replacement compounds with lower GWP values that also have low ODPs.

Second, the options available for further reductions in future halocarbon emissions were recognized as becoming more limited. However, for reducing the risk of future increases in atmospheric concentrations, the Assessment showed it would be important to minimize any leakage of CFCs and halons from banked storage (or "banks," the largest source of current ODP-weighted emissions of ODSs). A delay of four years, from 2011 to 2015, in the capture and destruction of the estimated CFC and halon banks was estimated to reduce the potential ozone and climate benefits from these actions by about 30%.

Since the last WMO Assessment, several reports have addressed topics of direct interest for this chapter:

1) *The UNEP synthesis report, "HFCs: A Critical Link in Protecting Climate and the Ozone Layer" (UNEP, 2011).* It concluded that limiting the future growth of HFCs could result in unrealized emissions (emissions that would have otherwise occurred) corresponding to as much as 7–19% of the CO_2 emissions that year. Alternative technological options exist that minimize the climate impact of HFCs. Issues related to future scenarios in HFC and other ODS alternatives are addressed in this chapter.
2) *The SPARC report, "Lifetimes of Stratospheric Ozone-Depleting Substances, Their Replacements, and Related Species" (SPARC, 2013).* This report provides a thorough and consistent re-assessment of the lifetimes for a number of halocarbons as well as in-depth analysis of the associated uncertainties (Chapter 1, Box 1-1). These values are discussed in Chapter 1 and are used in the metric and scenario evaluations presented in this chapter.
3) *Reports produced by the UNEP Technology and Economic Assessment Panel (TEAP).* These reports continue to assess the technological and economic possibilities for phasing in commercially available replacements for ODSs (e.g., UNEP, 2013).
4) *The Fifth Assessment Report of the Intergovernmental Panel on Climate Change, "Climate Change 2013 – The Physical Science Basis" (IPCC, 2013).* This report includes updated values of metrics such as Global Warming Potentials. These are updated in this chapter using the SPARC (2013) lifetimes.

5.1.2 Objectives of This Assessment

The overall aim of this chapter is to present policy-relevant information. It includes an assessment of the possible options available to policymakers related to protection of stratospheric ozone (and effects on climate from halocarbons). In Section 5.2, recent developments in the understanding of the main ozone-depleting compounds, anthropogenic and natural, are summarized with emphasis on their importance for future stratospheric ozone depletion, other impacts such as the role of their breakdown products, and their influence on climate. The impacts of real and potential replacement products are similarly discussed. Special attention is given to the additional complexities associated with evaluating the effects from short-lived substances with spatially and temporally varying sources and sinks. Finally in Section 5.2, other potential influences on stratospheric ozone (e.g., other atmospheric changes, rockets, geoengineering) are considered.

Simple quantitative measures have been used to provide information about the effect of emissions from human activity on the atmosphere. These include Ozone Depletion Potentials (ODPs), Global Warming Potentials (GWPs), and radiative forcing (RF), which can be used to compare the relative effect of individual gases, as well as Equivalent Effective Stratospheric Chlorine (EESC) which is a measure of the combined impact of all chlorine- and bromine-containing gases. Estimates of these are discussed in Section 5.3, and updated values are presented based on the recently updated estimates of atmospheric lifetimes (SPARC, 2013). In addition, newer measures, such as Global Temperature change Potentials (GTPs), are discussed here for the first time in a WMO Assessment.

Section 5.4 concludes the chapter with an examination of a range of scenarios. These are compared to a new baseline that is consistent with the existing observational record for atmospheric concentrations of halocarbons and the current limits on emissions contained in the Montreal Protocol. The scenarios investigate effects of hypothetical changes in emissions and are illustrative of potential mitigation actions such as controls on banks (see Box 5-1). The halocarbon lifetimes used are those reported in SPARC (2013). The baseline emission scenario for CO_2, methane (CH_4), and N_2O is taken as the RCP6.0 scenario (van Vuuren et al., 2011; IPCC, 2013). The sensitivity of the calculated impact on the stratosphere is investigated by additionally using the RCP4.5 and RCP8.5 scenarios. (Representative Concentration Pathways are well established in the climate community and used as a basis for climate modeling experiments (van Vuuren et al., 2011; Chapter 4).) EESC is used where possible and additional calculations are performed using a two-dimensional (2-D) coupled chemistry-radiation-dynamics model (Fleming et al., 2011).

Box 5-1. Halocarbon Banks

The bank of a manufactured compound is defined as the quantity of that compound stored in equipment and products and held as chemical inventory. The size of the bank will increase as long as the production of a compound is larger than the release into the atmosphere. Any compound produced and kept in equipment will either increase the size of the bank or be used to compensate for leakage. Leakage is the amount released to the environment by physical leakage or by accidental leakage occurring in regular use, accidents, and maintenance.

For ODS and their replacements, bottom-up estimates of the banks are calculated on the basis of the total amount of equipment and products manufactured per year per country (or per region), and their assumed charges (or contents in the case of products). These bottom-up estimates are generally less accurate than either the amount of a given compound produced or the amount in the atmosphere, which is accurately known from atmospheric measurements. An alternative way to estimate the bank is by taking the difference between the amount produced and the amount released to the atmosphere.

Banks tend to decrease when products and equipment are taken from the market or their use stops. In the absence of specific measures, there will be leakage of the contents of the products to the environment. This release can be avoided by recovery and capture. The captured material can either be used or destroyed. Reporting the amounts of ODSs recovered, recycled, or destroyed is not required under the Montreal Protocol, leading to uncertainty in the size of the bank. However, the success of this option can be limited as a result of either cost or logistical problems. TEAP report XX/8 2009 describes the options for destroying ODS chemicals for different regions and a range of scenarios (UNEP, 2009).

Scenarios of future banks and their composition are based on assumptions of economic development, patterns in society (e.g., number of coolers in supermarkets, air conditioners, etc.), and the expected market penetration of alternative compounds and technologies. Containment, recovery and recycling, and destruction at the end of product life can reduce emissions to the atmosphere. This can be achieved by reducing leakage during operation and use and/or by ensuring high rates of recovery and capture at the end of the useful lifetime of equipment. The potential impact of such controls on atmospheric concentrations of CFCs, halons, HCFCs, and HFCs are investigated in Section 5.4.

5.2 ISSUES OF POTENTIAL IMPORTANCE TO STRATOSPHERIC OZONE AND CLIMATE

5.2.1 Halocarbons Controlled Under the Montreal Protocol

The success of the Montreal Protocol in limiting the atmospheric abundance of ODSs is now well documented. Implementation of its measures has resulted in significantly lower EESC than would otherwise have occurred (WMO, 2011 and preceding reports) as well as reductions in radiative forcing of climate change. Chapter 1 in this report finds that this success in limiting CFC and halon abundances has continued, though it notes large discrepancies between top-down and bottom-up emission estimates for halon-2402 and carbon tetrachloride (CCl_4). In WMO (2011), leakage of CFCs and halons from their banks (see Box 5-1) was found to be the largest source to the atmosphere, and so the main policy option presented was to reduce the leakage. This issue is investigated further in Section 5.4. Revised ODPs and GWPs for the CFCs and halons are presented in Section 5.3 based on the recommendations for the lifetimes made in SPARC (2013).

Part of the decrease in CFC usage in the 1990s was achieved by finding chemical substitutes for CFCs, including HCFCs and HFCs. Due to their lower, but non-zero ODPs, the HCFCs were defined by the Parties as transitional compounds and a first phase-out schedule for them was established in 1992. In order to accelerate the reduction in EESC, accelerated phase-out schedules for HCFCs were agreed under the Montreal Protocol in 2007. The implementation of these measures has been occurring gradually since that time, and it is expected that the overall effects will be observed as a decrease in first the growth rate

and then the atmospheric abundance of HCFCs. Chapter 1 reports that the increases over 2009–2012 for the main three HCFCs are smaller than those for 2006–2009. Presumably this has occurred in anticipation of the introduction of new measures following the accelerated phase-out agreement in 2007. Updated atmospheric measurements and lifetimes for HCFCs are used in the revised ODPs and GWPs presented and discussed in Section 5.3 and the scenarios presented in Section 5.4.

An inconsistency in the carbon tetrachloride (CCl_4) budget was reported in WMO (2011), as the decline in atmospheric CCl_4 concentrations was less than expected. Chapter 1 in this Assessment concludes that this discrepancy remains as there is a continued imbalance between the emissions of CCl_4 inferred from the observed changes in global concentration and the bottom-up estimates of the anthropogenic emissions. This difference cannot solely be explained by adjusting the atmospheric lifetime. Chapter 1 suggests that there may be ongoing anthropogenic emissions in the Northern Hemisphere. The implications of this uncertainty on future EESC are discussed further in Section 5.4.

Atmospheric methyl bromide (CH_3Br) results from anthropogenic and natural emissions. The partitioning between them has been the subject of much debate in the past (WMO, 2003, 2007. 2011). The continued decline in tropospheric CH_3Br amounts is caused by reductions in the controlled industrial production, consumption, and emission (see Chapter 1 for further analysis of the CH_3Br emissions and budget). The anthropogenic uses fall into three categories: (1) the controlled applications (soil and postharvest fumigation and commodity disinfestation); (2) quarantine and pre-shipment (QPS) exempted applications, which are reported under the Montreal Protocol; and (3) feedstock uses exempted but reported under the Montreal Protocol. The annual global total consumption for non-QPS uses of CH_3Br has decreased steadily as a result of the implementation of the Montreal Protocol, from over 50,000 tonnes/yr in the late 1990s to about 4,000 tonnes/yr in 2012 (Figure 1-6-6 of UNEP, 2013). This compares to a change in total consumption from about 70,000 tonnes/yr to about 20,000 tonnes/yr over the same period. Critical-use exemptions for the controlled uses are applied for by developed country (non-Article 5) Parties and have been granted annually since 2005. Fewer critical-use exemptions are being granted, as alternative approaches are more often available. The phase-out of controlled uses in Article 5 Parties by 1/1/2015 may result in additional applications for critical-use exemptions in the coming years (four Article 5 Parties have already applied for critical-use exemptions for 2015). The annual use for QPS is currently about 9,000 tonnes and is approximately steady (UNEP, 2013; Figure 1-6-6). In general, use for QPS has decreased in non-Article 5 and increased in Article 5 Parties. Feedstock production is estimated at about 3,900 tonnes in 2012; however, this should not result in any significant emissions. Total global production in 2012 was 16,700 tonnes, down from 35,000 tonnes in 2006. Scenarios for possible future emissions of CH_3Br are discussed in Section 5.4.

5.2.2 Replacement Compounds

The majority of the reduction in ODS emissions has occurred as a result of not-in-kind technology, such as containment, recovery and recycling, and non-fluorocarbon solutions. However, some of the decrease in the use of CFCs, and now HCFCs, has resulted in increased HFC use, particularly in the refrigeration and air conditioning sectors and, to a lesser degree, in the foam and fire protection sectors. While most HFCs have GWPs similar to those of the HCFCs they are replacing, some have higher GWPs (UNEP, 2011). The potential growth in the use of these high-GWP HFCs has given rise to concerns about the possible climate impact of the growth in HFC use (and emission) by the year 2050 (Velders et al., 2009, 2012; WMO, 2011; UNEP, 2011; Wuebbles at al., 2013). To minimize the impact on the ozone layer and climate, HCFC replacements would ideally have low ODPs and GWPs, even if the replacements contain chlorine or bromine. Meeting such conditions implies that the replacement compounds have short lifetimes and/or weak IR absorptions. A number of possible compounds, many of which have low GWPs, are now being considered. Technical aspects of new compounds are assessed by TEAP once their commercial potential has been shown (UNEP, 2013). Scenarios of future replacement compounds are considered in Section 5.4 and the possible impacts on ozone depletion and climate are assessed.

1,2-dichlorohexafluorocyclobutane ($C_4Cl_2F_6$, CFC-316c) is a proposed replacement substance, especially as a refrigerant. Papadimitriou (2013) evaluated the most likely atmospheric removal processes for the (*E*)- and (*Z*)- isomers of CFC-316c in a series of laboratory studies. 2-D model calculations included in their work show that stratospheric photolysis is the predominant loss process for both isomers, with lifetimes of 75 and 114 years for the (*E*)- and (*Z*)- isomers, respectively (see Table 1-3). Ozone Depletion Potentials and Global Warming Potentials were also reported, demonstrating that both isomers are potent ozone-depleting substances and greenhouse gases (ODPs are 0.46 for (*E*)-R-316c and 0.54 for (*Z*)-R-316c; GWP_{100} are 4160 for (*E*)-R-316c and 5400 for (*Z*)-R-316c).

A number of short-lived compounds have been proposed as replacements for long-lived ODSs and hydrofluorocarbons (HFCs) (see Table 1-11). Some of these substances are halogenated VSLS (i.e., lifetimes <0.5 years) and were chosen due to their low ODPs and GWPs. An updated summary of the partial and total lifetimes of the proposed replacement substances is given in Table 1-11. Further discussion of the ODPs and GWPs for a number of these compounds is given in Section 5.3.

5.2.3 HFC-23

HFC-23 is an unwanted by-product in the manufacture of HCFC-22. A major and increasing use of HCFC-22 is as a feedstock in the production of other chemicals, the most important of which is polytetrafluoroethylene (PTFE). The amount of HFC-23 produced in HCFC-22 manufacturing is far larger than the small amounts currently required for its direct use in some low temperature refrigeration and fire protection equipment. HFC-23 emissions are sometimes not considered in the emissions total from the mix of HFCs used or predicted to be used. Global emissions of HFC-23 have risen since 2009 after a period of decrease (Chapter 1). HFC-23 is a strong infrared absorber, and has a long lifetime of 220 years and a high GWP (12,400 for a 100-year time horizon GWP) (IPCC, 2013). Its radiative forcing in 2012 was 0.005 W m^{-2}, about 25% of the RF from all HFCs (Chapter 1). The annual emission of 12.8 ktonne per year (Chapter 1) corresponds to 150 Gt CO_2-eq per year.

The fraction produced in HCFC-22 manufacture depends on the details of the manufacturing process. It is assumed to be at most 3% of the amount of HCFC-22 produced, and in optimal manufacturing conditions (which are difficult to maintain) it can be brought down to 1.5%. Atmospheric emissions can be avoided if the HFC-23 is incinerated, which makes it possible to recover hydrofluoric acid (HF), the raw feedstock. Globally, a significant fraction of the HFC-23 produced in HCFC-22 facilities has been incinerated since 2006, due to the fact that incineration projects in developing countries could be supported through the Kyoto Protocol Clean Development Mechanism (CDM). Future HFC-23 emissions will depend on the amount of HCFC-22 produced, the efficiency of avoiding unwanted HFC-23 byproducts, and whether the amount of residual HFC-23 incinerated increases or decreases. This is directly related to future policy choices including those related to the granting of new HFC-23 incineration credits in the CDM (Miller and Kuijpers, 2011) and on other initiatives to avoid and destroy HFC-23. The impact of different emission scenarios is discussed in Section 5.4. More information can be found in Chapter 1 and references therein.

5.2.4 Biogenically Produced Short-Lived Halocarbons

Biogenically produced very short-lived substances (VSLS) are thought to contribute significantly to the stratospheric halogen budget, particularly for bromine (Chapter 1). The main processes affecting the effectiveness of these compounds (emissions, convective transport, and chemical processing) could all change in the coming decades as a result of changes in climate or in human activities. Bromoform ($CHBr_3$) and methylene bromide (CH_2Br_2) are expected to remain the two most important species. Their emissions could increase as a result of changes in managed production (e.g., algae farming for food, pharmaceuticals, or carbon capture). Currently 99% of cultivation comes from 7 countries in Asia and the volume produced has grown by ~8%/yr since 1990 (FAO, 2012). A study in Malaysia found that while current bromocarbon

emissions from aquaculture are negligible, they could become significant in the next decade (>10% of regional seaweed emissions) (Leedham et al., 2013). With multiple ecosystem, dynamical, and chemical components contributing to oceanic VSLS emissions, predicting future emissions will be a major challenge.

Transport of these species into and across the tropical tropopause is the major way for them to enter the stratosphere. Tropical convection is thus a critical process in determining their flux into the stratosphere, and any changes in its strength or frequency as a result of a changing climate will affect their future stratospheric concentrations. These changes will happen in concert with any changes in the strength of the stratospheric circulation. The Coupled Model Intercomparison Project Phase 5 (CMIP5) climate models suggest that the flux of air into the stratosphere will increase at the same time as ozone depletion reduces and as greenhouse gas concentrations increase (see Figure 4-8 and related discussion). For shorter-lived species, some features of the convection are particularly important in determining how much of any emitted substance (or their reaction products) reaches the stratosphere: these include the overall mass transport in convection, the altitudes where the air flows into and out of the convection, the frequency of strong events (particularly the high altitude outflow), and the location of the convection relative to the emissions. These all have significant uncertainties associated with them (e.g., Schofield et al., 2011). In addition, the boundary layer mixing and stratospheric advection processes have been shown to cause significant differences in simulated VSLS reaching the stratosphere (Hoyle et al., 2011). Differences are amplified for shorter-lived compounds. The implications for the contribution of short-lived species to stratospheric chlorine and bromine amounts and to the calculation of ODPs are discussed in Section 5.3.

Modeling studies have shown that climate-driven changes to tropospheric transport may affect stratospheric VSLS loading (Dessens et al., 2009; Pyle et al., 2011). Hossaini et al. (2012a) calculate increased injection of $CHBr_3$ into the stratosphere for a 2100 simulation based on the Representative Concentration Pathways (RCPs) 4.5 and 8.5 scenarios (IPCC, 2013; also see Chapters 2 and 4). This increase was largest under RCP8.5, a scenario with stronger warming, and mostly attributed to an enhanced convective mass flux in the tropical troposphere, which agrees qualitatively with earlier model studies (Stevenson et al., 2005; Dessens et al., 2009). Overall, Hossaini et al. (2012a) project an increase in the direct injection of bromine into the stratosphere contained in the five major VSLS of 0.3 ppt and 1.0 ppt Br under RCP4.5 and RCP8.5, respectively. These increases are attributed to both the dynamical and chemical perturbations, both of which carry large uncertainty, while climate-driven changes to emissions and changes in anthropogenic use were not considered. As discussed in Chapter 1, there remains significant uncertainty in the role of convection in determining the amount of bromine and chlorine reaching the lower stratosphere.

Changes in the tropospheric oxidizing capacity will impact the lifetimes of VSLS (SPARC, 2013), particularly those whose primary sink is through hydroxyl radical (OH) oxidation (e.g., CH_2Br_2, CH_2Cl_2). Hossaini et al. (2012a) find significant variation in projected tropical tropospheric [OH] between the RCP scenarios. The local lifetime of CH_2Br_2 (against oxidation) varies significantly (±40%) (e.g., see Figure 1-14). Despite OH production being favored under warm and humid conditions, tropical [OH] in 2100 is projected to decrease by 25% near the surface, due to a projected doubling of methane (CH_4) under RCP8.5. Voulgarakis et al. (2013) find similar [OH] decreases of −22 ± 4.6% from a multi-model intercomparison. Under more moderate climate scenarios, such as RCP2.6 and RCP4.5, models project an increase in tropospheric [OH] of up to ~10% below 500 hectoPascals (hPa) (Hossaini et al., 2012a; John et al., 2012; Voulgarakis et al., 2013). These studies underline the sensitivity of future OH concentrations and distribution to future CH_4 emissions. Results also depend on responses to relative decreases in nitrogen oxides ($NO_x = NO + NO_2$) and carbon monoxide (CO) in the different scenarios over polluted regions. In addition sub-annual and regional variations, such as the low ozone concentrations found (and low OH concentration inferred) in the West Pacific (Rex et al., 2014), could affect VSLS.

The future impact of VSLS on ozone has yet to be fully assessed. While some studies suggest a potential increase in bromine from VSLS toward the end of the century, stratospheric chlorine will have decreased substantially by 2100 due to the phase-out of the long-lived chlorinated source gases under the Montreal Protocol. Therefore, bromine-mediated O_3 destruction via the BrO + ClO catalytic cycle would be reduced.

5.2.5 Breakdown Products

Certain HCFCs, HFCs, HFEs (hydrofluoroethers), and HFOs (hydrofluoroolefins) can contribute to tropospheric ozone formation and degrade to produce toxic compounds. The atmospheric degradation of HCFCs, HFCs, HFEs, and HFOs is initiated by reaction with OH radicals leading to the formation of halogenated carbonyl compounds, which undergo further oxidation to yield HF, HCl, CO_2, and, in some cases, trifluoroacetic acid (TFA, $CF_3C(O)OH$) (e.g., see prior Assessments such as IPCC/TEAP 2005; WMO, 2011). There is a special concern regarding the production of TFA because of its possible effects on life in aquatic environments (see the discussion in WMO, 2011). The chlorine production is considered in the discussion of EESC in Section 5.4; the effects on HF and CO_2 are likely to be extremely small. Examples of halocarbons that lead to the formation of TFA (and related compounds) include: HCFC-123, HCFC-124, HFC-125, HFC-134a, HFC-227ea, and HFO-1234yf (Young and Mabury, 2010). While it is well established that TFA is a ubiquitous natural component in rivers, lakes, and other surface water bodies, uncertainties remain, as discussed in WMO (2011), regarding its natural and anthropogenic sources, long-term fate, and abundances. TFA formation depends on whether CF_3CFO or CF_3CClO are formed as intermediates in the parent compound degradation. The sole atmospheric fate of CF_3CFO is hydrolysis to give TFA (Wallington, et al., 1994). The atmospheric fate of CF_3CClO is hydrolysis, to give TFA, or photolysis. For halogenated propenes, HFOs, if there is a fluorine atom on the central carbon, the TFA yield is expected to be high; such as found with $CF_3CF{=}CH_2$ (HFO-1234yf) (Papadimitriou et al. 2011; Wallington et al., 2010). On the other hand, if there is a hydrogen on the central carbon atom there is no TFA formation, such as in $CF_3CH{=}CHF$ (HFO-1234ze) or $CF_3CH{=}CHCl$ (trans-1-chloro-3,3,3-trifluoropropylene or tCFP; also referred to as HFO-1233zd) or HFC-152a. While some studies suggest that the extensive use of some TFA source compounds could dramatically increase the amount of TFA in wetlands (e.g., Luecken et al., 2010; Henne et al., 2012), the potential effects on associated ecosystems remains unclear and may not be as large a problem as initially envisioned (Boutonnet et al., 1999; Benesch et al., 2002; WMO, 2007, 2011). UNEP (2010) concluded that even when added to existing amounts from natural sources, risks from TFA (and the more toxic monofluoroacetic acid (MFA)) from halocarbons to humans and organisms in the aquatic environment are judged to be negligible. Nonetheless, there remains significant uncertainty about the potential effects of TFA in the future environment.

5.2.6 Nitrous Oxide, Methane, and Carbon Dioxide

Any future changes in halogen concentrations will be taking place against the backdrop of other atmospheric changes. From a stratospheric chemistry and circulation standpoint, the most important direct changes are likely to be those of CH_4, N_2O, and CO_2 (also see Chapters 2 and 4). The concentrations of these gases have changed and are continuing to change as a result of human activities (IPCC, 2013). Continued changes in the stratospheric concentrations of these gases will lead to changing odd hydrogen (HO_x) and NO_x concentrations during the period that halogen levels are falling. At the same time, continued increases in the CO_2 concentrations will lead to stratospheric cooling, which will slow the ozone chemical loss rates. Increases in CO_2 also are projected to cause a strengthening of the stratospheric Brewer-Dobson circulation, which will redistribute ozone.

In general the chemical effects of these three gases occur in different locations in the stratosphere, but overall the increases in CH_4 and CO_2 will have the opposite effect on stratospheric ozone as that of N_2O. Future ozone levels will be strongly dependent on the actual future emissions and concentrations of these gases. How ozone will change as the future concentrations of these gases change is explored in Section 5.4 (see also Section 2.4).

5.2.7 Stratospheric Water Vapor

Stratospheric water vapor is critically important for the gas-phase chemistry, the particle distribution, and the radiative balance of the stratosphere. The large majority of stratospheric water vapor

enters the stratosphere in the tropics in the form of either CH_4 or H_2O. However, it can also enter the lowermost stratosphere through mixing processes around the extratropical tropopause. One such process is direct injection through midlatitude convection. Increased midlatitude convection could thus result in increased injection of water vapor and a greater occurrence of ice crystals. While EESC remains high, there is thus a chance of enhanced chemical destruction of ozone by catalytic halogen chemistry on these additional surfaces (Anderson et al., 2012). The comprehensive measurements by the Aura Microwave Limb Sounder (MLS) satellite instrument (Schwartz et al., 2013) confirmed that the lower stratosphere over North America is episodically moist (as seen in the aircraft campaigns reported in Anderson et al., 2012). However, Schwartz et al. (2013) caution that chemical ozone depletion as a result of convectively enhanced H_2O of the scale suggested by Anderson et al. (2012) does not seem readily apparent or likely in the current stratosphere; moreover, dilution effects from low O_3 values lofted by tropospheric air would complicate the detection and attribution issues. Comparison of the Aura MLS observations with the CLaMS model (Chemical Lagrangian Model of the Stratosphere) further suggest that the annual cycle in water above 360 K at northern midlatitudes is dominated by horizontal transport of water vapor from low latitudes (Ploeger et al., 2013). The importance of northern midlatitude convection in the lower stratosphere is therefore unclear. Two points can be made with confidence: any chemical ozone depletion (i) is already included in the changes seen in the existing observational record; and (ii) will continue to reduce as EESC decreases.

Future stratospheric water vapor levels will be affected by any changes in the amount of water entering the stratosphere in the tropics. This could occur through changes in the large-scale structure of the tropical tropopause layer (Davis and Rosenlof, 2012; Randel and Jensen, 2013); and in the strength of the vertical transport of tropospheric air associated with features such as the Asian monsoon anticyclone (Ploeger et al., 2013). Such changes are included implicitly in the discussions in Sections 2.4 and 3.5. Given the uncertainties in possible future changes of stratospheric water vapor, the effect on ozone depletion is not investigated further with the simple models in this chapter.

Finally, it has been proposed that the observed correlation between stratospheric water levels and higher tropospheric temperatures implies a positive feedback of stratospheric water vapor on climate, with one-third of the feedback resulting from increases in water vapor entering the stratosphere in the tropics and the rest occurring from increases entering through the extratropical tropopause (Dessler et al., 2013).

5.2.8 Stratospheric Aerosols

Stratospheric aerosols can have a significant influence on stratospheric ozone (e.g., Solomon et al., 1996; Chapter 2). The stratospheric aerosol layer has been increasing during the volcanically quiescent period of 2000–2009 by ~3.8% (Nagai et al., 2010). This has been shown to have a direct climate impact (Solomon et al., 2011). The increase is probably caused by the cumulative effect of minor volcanic eruptions with subsequent transport of sulfur dioxide (SO_2) into the stratosphere (Vernier et al., 2009; Neely et al., 2013). The impact of tropospheric pollution is now thought to be small (Siddaway and Petelina, 2011; Vernier et al., 2011; Section 8.4.2.2 in IPCC, 2013; Chapter 4). Changes in anthropogenic carbonyl sulfide (COS) emissions could also affect future background aerosol levels (Brühl et al., 2012). Other than in the discussion on geoengineering below, the effect on stratospheric ozone of possible changes in the stratospheric aerosol layer is not considered further in this chapter and so represents a source of uncertainty in the results presented.

5.2.9 Other Proposed Influences on Stratospheric Ozone

AVIATION

Since WMO (2011), studies have continued toward understanding the effects of emissions from commercial aviation on ozone in the upper troposphere and lower stratosphere (UTLS) and on climate (e.g., see Brasseur et al., 2013, Holmes et al., 2011; Lee et al., 2009). Aircraft emit gases and particles into the atmosphere, especially in the region of the UTLS. These emissions include carbon dioxide,

nitrogen oxides, water vapor, sulfates, and soot. The gases and soot tend to have a positive radiative forcing (RF), a surface warming effect, while other particles like sulfates produce a negative RF, a surface cooling effect. NO_x produces ozone in the UTLS that then leads to additional OH production in the troposphere and a resulting decrease in methane. Current commercial aviation emissions are estimated to increase UTLS ozone at northern midlatitudes by 5–7% (2.3–9.1% in the range of models from recent studies: Olsen et al., 2013; Brasseur et al., 2013; Skowron et al., 2013). The net effect on the total ozone column, however, is small, an increase of less than 0.3% globally- and annually-averaged. By 2050, current studies using a scenario that includes technology advances in aviation efficiency suggest the effect of aviation on UTLS ozone could increase to as much as 11% (Olsen et al., 2013; Brasseur et al., 2013). The effect on the total ozone column remains small (<1%).

Supersonic aircraft fly at higher altitudes, where they emit NO_x and H_2O into the stratosphere at altitudes where they can be mixed upwards and globally (instead of being flushed out of the lowermost stratosphere within a season as for subsonic aircraft). Thus high-flying supersonic aircraft can have potentially much greater impacts on ozone and climate forcing. There are no current plans for development of commercial supersonic aircraft, although the technology for supersonic business jets is continuing to be developed, and future growth should be monitored.

ROCKETS AND SUB-ORBITAL VEHICLES

WMO (2011) raised the potential importance of emissions from rockets. Cryogenic rocket engines using liquid oxygen and liquid hydrogen produce water and nitric oxide. Solid rocket motors (SRMs) have emissions of hydrochloric acid (HCl) and alumina (Al_2O_3) and so have more impact on ozone than the cryogenic engines. These SRM emissions can lead to destruction of the ozone in the rocket exhaust plumes (Ross et al., 2009; Voigt et al., 2013). The present-day loss in the globally averaged total ozone column due to these rockets is estimated at ~0.03%, insignificant compared to other processes (Ross et al., 2009). It would take a large increase in the frequency of launches for the impact on ozone to become significant compared to the impacts of other influences. A recent forecast for the commercial sector (currently about 25% of the total) is an increase from about 20 to 30 launches per year (FAA, 2013).

A number of suborbital, reusable vehicles (SRV) are being developed for use for satellite launches and/or for passengers. It is still early in the development of these technologies and so it is hard to predict future usage and growth in the number of launches. One study developed three scenarios (baseline, constrained, and growth) based on different assumptions about cost, level of consumer interest, and governmental/industrial demand (FAA, 2013). In these scenarios, the number of flights ten years after the first year of regular SRV operation ranged from about 250 to 1600. Newer propellants are being considered in the private space market, many of which are liquid oxygen (O_2) with alcohol (FAA, 2011). The effect on stratospheric ozone will depend on the number of launches, the propellant used, and the flight profiles. Few studies have addressed the effects of these vehicles and their potential environmental impacts.

GEOENGINEERING OF CLIMATE

A variety of ideas have been proposed to mitigate the climate effects of rising greenhouse gases concentrations (geoengineering). One of these, the creation of additional particles in the stratosphere, would directly impact stratospheric ozone (Tilmes et al., 2008, 2009). Other methods have indirect effects on stratospheric ozone and are not considered further here.

Stratospheric particles reflect a small amount of the incoming solar radiation back to space, and so lead to a reduction in the incident solar energy reaching the Earth and a resultant surface cooling. An enhancement of the stratospheric particle layer, e.g., following volcanic eruptions, increases this cooling effect. The effect is well established, because the surface of the Earth is observed to cool as a result of the high sulfate aerosol loading in the years following major volcanic eruptions (WMO, 2011; Graf et al., 1998; Free and Lanzante, 2009; IPCC, 2013), although it has recently been suggested that the volcanic response may have been overestimated by as much as a factor of two (Canty et al., 2013).

Increases in stratospheric particles affect the radiative balance in the stratosphere, with consequent changes in the dynamics and in the chemistry (through changes in photolysis rates). In addition, stratospheric chemistry is perturbed by heterogeneous reactions that occur on particle surfaces, with impacts on the HO_x, NO_x, ClO_x, and BrO_x chemical cycles. Three-dimensional models have individually simulated the stratospheric response following the Mt. Pinatubo eruption (the best observed) with some success (e.g., Heckendorn et al., 2009; see also Chapter 2, Section 2.3.4). However, the large inter-model variation in the dynamical response to forcings (SPARC CCMVal, 2010) limits our confidence in the predictive capability of the current models.

The main type of artificial perturbation that has been considered is an augmentation of the background sulfate aerosol layer through the injection of sulfur (Crutzen et al., 2006; Wigley, 2006; WMO, 2011). The observed changes with volcanic eruptions give confidence in our qualitative understanding of the impacts of elevated sulfate aerosol. However, quantitative studies are limited to date. Recent modeling studies of an artificially perturbed stratospheric aerosol layer have concentrated on scenarios defined in the Geoengineering Model Intercomparison Project (GeoMIP) (Kravitz et al., 2011), with nearly all GEOMIP studies to date focusing on impacts on climate rather than stratospheric ozone. Results from four models using the two GEOMIP scenarios that include stratospheric aerosol (Pitari et al., 2014) indicate reductions in total column ozone of a few percent, with the larger losses at high latitudes, consistent with earlier studies based on different scenarios (Heckendorn et al., 2009; Tilmes et al., 2009). The chemical ozone loss is calculated to decrease as the availability of ClO_x and BrO_x decreases. This effect may be offset by any increase in the input of chlorine- and bromine-containing VSLS into the stratosphere (Tilmes et al., 2012; see Section 5.2.4).

Consideration is also being given to particles with different optical properties that could substantially increase the amount of light scattered back to space thereby reducing the mass required for injection (Katz, 2011) or that reduce the absorption of solar radiation by the particles hence leading to a reduced impact on the stratospheric circulation (Ferraro et al., 2011). Such particles could be more effective in producing a surface cooling than sulfate aerosol. The heterogeneous chemistry occurring on the surface of new particles is poorly known (Pope et al., 2012). The surface coating of a particle and how it evolves under stratospheric conditions will be important for the heterogeneous reaction rates. For example, a coating of sulfuric acid (H_2SO_4) on a particle's surface would tend to make the heterogeneous chemistry that occurs more like that of sulfate aerosol. However, the effect on the optical properties would likely be small. If the particles became significantly larger, the sedimentation rate would in general increase and the stratospheric lifetime would shorten.

In our discussion, we have not considered other potential effects of the stratospheric particle geoengineering approach on climate and other aspects of the environment. Overall the gaps in our current understanding of the full impacts of possible geoengineering approaches on stratospheric ozone preclude us from making a full assessment with confidence. Thus, there is still the potential for significant risks to the ozone layer, both known and unknown, from solar radiation management through the use of stratospheric particles.

POLAR OZONE DEPLETION BY COSMIC RAYS

A series of papers (most recently Lu (2013, 2014)) have repeated the hypothesis that cosmic rays can promote the breakdown of organic and inorganic halogenated compounds, including CFCs, on ice and other stratospheric particles in polar regions, with the resulting chlorine compounds playing the dominant role in polar ozone loss. The recent papers have been published despite a number of previous papers showing that this hypothesis is inconsistent with established knowledge of the stratosphere (Harris et al., 2002; Patra and Santhanam, 2002; Grooß and Müller, 2011; Müller and Grooß, 2014 and references therein). Lu (2013) and his earlier papers rely principally on correlations of observed variables (e.g., ozone, temperature, cosmic ray flux) with no quantitative evidence that the proposed mechanism makes a significant difference to the well established understanding of polar ozone loss based on mechanisms demonstrated in laboratory and field measurements as well as model studies (e.g., see Chapter 3). Among other things there is no evidence that the hydrophobic CFC-11 or CFC-12 molecules are absorbed into the

particles in large enough amounts for cosmic-ray-produced electrons to dissociate them (Harris et al., 2002). Nor can the mechanism explain the observed distributions and correlations of long-lived trace gases such as the CFCs, N_2O, and CH_4 which show that CFC depletion occurs in the middle and upper stratosphere at low and midlatitudes and not in the polar lower stratosphere (Grooß and Müller, 2011). The fundamental problem with the hypothesis is that it ignores most of the work that has been done over the last 30–40 years as reported in the series of WMO Assessments prepared in support of the Montreal Protocol. This hypothesis should be rejected.

5.3 METRICS FOR CHANGES IN OZONE AND CLIMATE

For the purpose of this Assessment, metrics are defined as tools used for quantifying and comparing impacts of emissions from human activity. Typically they aggregate and simplify complex information about different gases, placing them on a common scale to simplify comparison of impacts. Metrics such as Equivalent Effective Stratospheric Chlorine (EESC) and Ozone Depletion Potentials (ODPs) have proven to be important tools in policy considerations for stratospheric ozone (see Box 5-2), while other metrics, including radiative forcing (RF) and Global Warming Potentials (GWPs), have proven to be useful tools in climate-policy-related studies (see Box 5-3). These metrics have all been used in past assessment of ozone and climate including the WMO Assessments. In addition, newer metrics, such as Global Temperature change Potentials (GTPs), are introduced in the discussion below.

One advantage of metrics is that they are straightforward to communicate. Some of these metrics express the integrated impact of a given gas relative to that for the release of the same mass of a reference compound (generally CFC-11 for ODPs and CO_2 for GWPs and GTPs). For these metrics using such relative indices, some uncertainties in translating emissions into absolute environmental impacts tend to cancel, and the relative benefits of controlling emissions of different gases are highlighted. However, it should be recognized that the metrics discussed here do not represent the full complexity of the chemistry and physics of the atmosphere (e.g., where and when the ozone depletion occurs). Their simplicity means some caution is required when interpreting the values derived (e.g., how much are these values dependent on the background atmosphere assumed in their derivation). Nonetheless, ODPs and GWPs have found widespread use in national regulatory actions and in international agreements such as the Montreal Protocol and the Kyoto Protocol.

5.3.1 Metrics for Changes in Ozone

Box 5-2 (next page) summarizes the basics of metrics used for describing changes in ozone, namely, Equivalent Effective Stratospheric Chlorine (EESC) and Ozone Depletion Potentials (ODPs).

UPDATING THE EVALUATION OF ODPS

There have been only a few published updates on ODP values since the last Assessment, with most of those concerning VSLS as discussed below. Papanastasiou et al. (2013) provide analyses of updated semi-empirical ODPs for several bromine-containing compounds (halon-1202, -1211, and -2402) using updated lifetimes computed with the NASA GSFC 2-D atmospheric model (Fleming et al., 2011). Their analyses produced somewhat different ODP values compared to WMO (2011): 1.95 for halon-1202 vs. 1.7 in WMO (2011), 8.1 for halon-1211 vs. 7.9 in WMO (2011), and 18.4 for halon-2402 vs. 13.0 in WMO (2011).

New scientific results affect the earlier ODPs, especially from the reanalysis of atmospheric lifetimes in SPARC (2013). The revised SPARC (2013) recommended lifetimes are based on calculations with atmospheric chemical transport models, analysis of observations at the surface and in the stratosphere, laboratory analysis of chemical reactions and photolysis rates, and on inverse modeling. In addition, the SPARC report provides uncertainties in the lifetimes of major halogenated ODSs. The uncertainties in the lifetimes are considerable, ranging from 3% to 33% (one standard deviation, 1σ; also see Velders and Daniel (2014) for further discussion on these uncertainties). The SPARC (2013) atmospheric lifetimes are

Box 5-2. Metrics for Ozone: The Basics

Equivalent Effective Stratospheric Chlorine (EESC)

EESC is a sum of the time-dependent chlorine and bromine derived from ODS tropospheric abundances, weighted to reflect their potential influence on ozone. EESC has become a standard benchmark for estimating ozone depletion relative to a base period, usually taken as 1980 (a time before major ozone depletion). EESC relates surface mixing ratios of chlorine- and bromine-containing ODSs to the stratospheric inorganic chlorine and bromine released from these gases in key regions of the stratosphere and thus to the amount of ozone they will destroy (Daniel et al., 1995; WMO, 1995, 1999, 2003, 2007, 2011; also see Chapter 1). EESC also accounts for the larger efficiency of bromine to destroy stratospheric ozone compared to chlorine (on a per-atom basis) and that different source gases release their chlorine and bromine at different rates and geographic locations. EESC has been reformulated (Newman et al., 2007) to account for the age-of-air spectrum and the age-of-air dependent fractional release values. Not only does this increase its accuracy, but EESC can also then be derived for various latitudes, including effects at midlatitudes or in the Antarctic vortex (Newman et al., 2009; WMO, 2011). The changes in integrated EESC and the date when EESC returns to 1980 levels have both been used in the previous WMO Assessments to quantify the relative impacts of future emissions of ODSs. In Section 5.4, EESC is used in the evaluation of scenarios for various assumptions about future emissions of halocarbons.

The EESC concept has been further revised (Daniel et al., 2010) to account for the effects of nitrous oxide (N_2O), the primary source for nitrogen oxides ($NO_x = NO + NO_2$) in the stratosphere. If this can be done accurately, it is useful because N_2O is increasing and is projected to continue to do so in the future. The NO_x produced from N_2O chemistry not only destroys ozone itself, it also reduces the efficiency of chlorine and bromine in destroying ozone by tying up these halogens in chlorine nitrate ($ClONO_2$) and bromine nitrate ($BrONO_2$) reservoir gases. Projected decreasing levels of reactive chlorine (Cl_y) similarly ties up less reactive nitrogen (NO_y; note that reactive nitrogen does not include N_2O, only the more reactive forms of atmospheric nitrogen) in $ClONO_2$, especially in the lower stratosphere, increasing the efficiency of N_2O to destroy ozone at those altitudes (Ravishankara et al., 2009). However, there is also a decreasing efficiency of N_2O in ozone depletion in the future climate due to the projected CO_2-induced cooling of the stratosphere and enhancement of the stratospheric circulation (Rosenfield and Douglass, 1998; Plummer et al., 2010). The expected decrease, by 2100, in the effectiveness of a unit N_2O emission to destroy ozone ranges from 10–20% (Daniel et al., 2010) to 50% (Plummer et al., 2010). Although these interactions will potentially lead to a complicated relationship between EESC and ozone depletion, we investigate the usefulness of this effect in Section 5.4. Future changes in emissions of methane, as well as potential emissions of other gases and particles, can further complicate the interpretation of EESC but are not considered in the EESC index at this time.

EESC is calculated as in previous Assessments. The only difference between the calculations in WMO (2011) and those here is that we now use an age spectrum for both midlatitude (3-year mean age) and Antarctic conditions (5.5-year mean age), while a full age spectrum was not used before. In both cases, we assume the width of the spectrum is equal to half of the average age (Newman et al., 2007). A complete discussion of the other aspects of the EESC calculation can be found in Chapter 5 of WMO (2011). As in that Assessment, we assume the relative impact of bromine compared to chlorine for ozone destruction, typically referred to as alpha (α), is 60 at midlatitudes and 65 in polar regions.

Ozone Depletion Potentials (ODPs)

The concept of Ozone Depletion Potentials (ODPs) (Wuebbles 1981, 1983; Solomon et al. 1992; the various WMO Assessments) arose as a means of determining the relative ability of a chemical to destroy ozone. Steady-state ODPs are defined as the change in global ozone for a sustained unit mass emission of a specific compound relative to the change in global ozone for the sustained unit mass emission of CFC-11 ($CFCl_3$). This is equivalent to assuming an infinitesimal emission pulse and integrating over the entire decay of the compound. ODPs are an integral part of national and international

Box 5-2, continued.

considerations on ozone-protection policy, including the Montreal Protocol and its Amendments. ODPs provide an important and relatively straightforward way of analyzing the potential for a new chemical to affect ozone relative to the chlorofluorocarbons (CFCs) and other chlorine-, bromine- and iodine-containing halocarbons. It is also now being applied to non-halogenated compounds like nitrous oxide (N_2O) (Ravishankara et al., 2009; Fleming et al., 2011; WMO, 2011) and methane (CH_4) (Fleming et al., 2011). ODPs are currently determined by two different means: calculations from chemical transport models (CTMs) of the global atmosphere, and the semi-empirical approach that depends primarily on observations rather than models (Solomon et al., 1992; WMO, 2003, 2007, 2011). Both approaches have been shown to give very similar ODP values in previous Assessments.

Advantages and disadvantages of using ODPs have been discussed in the prior WMO Assessments. Because ODPs are defined relative to the ozone loss caused by CFC-11, it is generally thought that the ODP values demonstrate less sensitivity to photochemical modeling errors than do absolute ozone loss calculations, but this is only strictly true for other chlorine-containing compounds with similar atmospheric lifetimes. Interpretation of non-halocarbon ODPs could be particularly problematic. For example, ODPs are normally derived relative to the current atmosphere, but there could potentially be some differences in values if they were calculated relative to a future atmosphere with different background composition, temperatures, or circulation.

Originally, the evaluation of ODPs was conducted largely for chemicals with atmospheric lifetimes sufficiently long (> ~1 year) that they are well mixed throughout the troposphere after surface release, and a significant portion of the surface emissions can still reach the stratosphere. However, many of the compounds being considered either for new applications or as replacements for substances controlled under the Montreal Protocol are now designed to be very short lived, on the order of days to a few months, so as to reduce the impacts on ozone and climate. Many of these very short-lived substances (VSLS) still contain chlorine, bromine, or iodine, and can be vertically transported into the lower stratosphere particularly through the tropical troposphere. A major complication with VSLS is that the compounds can decompose into inorganic halogen compounds in the uppermost tropical troposphere, and hence an important uncertainty is the degree to which the inorganic halogens (e.g., HBr, HOBr) are scavenged during the removal of water vapor in ascent. Another issue is that basic assumptions of referencing to CFC-11 to cancel transport and other errors in the model clearly break down since the chemical removal processes are so different; nonetheless there is high value for policymakers in being able to use the modified form of the ODP concept for VSLS.

Due to the difficulties in calculating the dynamical and chemical processes affecting such short-lived compounds, three-dimensional (3-D) models fully representing the troposphere and stratosphere need to be used to predict the halogen loading and resulting effects on global ozone. As a result, the definition of ODPs has been revised for VSLS (Wuebbles et al., 2001; WMO, 2003, 2011; Pisso et al., 2010). The ODPs derived for VSLS now account for variations that can occur in the ODP as a function of where and when (geographic location and time of year) the compound is emitted. The most important factor in evaluating the ODP of VSLS is shown to be geographical distribution, or latitude, of the surface emissions because gases emitted at higher latitudes are less likely to reach the stratosphere before destruction than gases emitted in the tropics (Bridgeman et al., 2000; Olsen et al., 2000; Wuebbles et al., 2001). The discussion of updates to ODPs thus reflects this change in definition for VSLS.

compared to those from WMO (2011) in Table 5-1 (also see discussion of atmospheric lifetimes in Chapter 1). There are a number of differences, but the most important one to the derivation of ODPs is the change in lifetime of CFC-11 from 45 years to 52 years (+15%); CFC-11 is in the denominator in ODP derivation, so this change in lifetime decreases the values of all ODPs in WMO (2011) by 15%. Revisions in the lifetimes for other gases produce the other differences found in ODP values for "This Assessment" found in Table 5-2.

The age-of-air spectrum from Newman et al. (2007) and the age-of-air dependent fractional release factors (FRFs, defined as age of-air-dependent ODS decomposition rates; also see Chapter 1) from

Table 5-1. Atmospheric lifetimes and fractional halogen release factors relative to WMO (2011) for long-lived halocarbons. In this Assessment, lifetimes are based on SPARC (2013). Fractional release factors (midlatitude conditions) used in this Assessment are based on the previous Assessment (WMO, 2011), but we also show in the table those for the 10 compounds updated in Laube et al. (2013) using a mean age of air of 3 years. Lifetime uncertainties are based on SPARC (2013) lifetimes as evaluated by Velders and Daniel (2014). Also see Chapter 1 for further discussion on atmospheric lifetimes.

Halocarbon	Atmospheric Lifetime (years)			Fractional Release Factors	
	WMO (2011)	This Assessment	Lifetime uncertainty (1σ)[c]	This Assessment	Laube et al. (2013)
Annex A-I					
CFC-11	45	52	±22%	0.47	0.35
CFC-12	100	102	±15%	0.23	0.19
CFC-113	85	93	±17%	0.29	0.22
CFC-114	190	189	±12%	0.12	
CFC-115	1020	540	±17%	0.04	
Annex A-II					
halon-1301	65	72	±13%	0.28	0.26
halon-1211	16	16	±29%	0.62	0.52
halon-2402	20	28	±19%	0.65	
Annex B-II					
CCl_4	26[a]	26[a]	±17%	0.56	0.42
Annex B-III					
CH_3CCl_3	5.0	5.0[a]	±3%	0.67	0.61
Annex C-I					
HCFC-22	11.9	12	±16%	0.13	0.07
HCFC-123	1.3				
HCFC-124	5.9				
HCFC-141b	9.2	9.4	±15%	0.34	0.17
HCFC-142b	17.2	18	±14%	0.17	0.05
HCFC-225ca	1.9				
HCFC-225cb	5.9				
Annex E					
CH_3Br	0.75[a,b]	0.8[a]	±17%	0.60	
Others					
halon-1202	2.9	2.5	±33%	0.62	
CH_3Cl	1.0[a]	0.9[a]	±18%	0.44	

[a] Losses due to oceanic and soil processes are taken into account using values from WMO (2011). The partial lifetime for CCl_4 is 44 years for atmospheric loss (from SPARC, 2013) and is assumed to be 95 years for oceanic loss and 195 years for soil loss for a total lifetime of 26 years. The partial lifetime for CH_3CCl_3 is 5.0 years for atmospheric loss (from SPARC, 2013). The total lifetime for CH_3Br is 1.5 years for atmospheric loss (from SPARC, 2013), 3.1 years for oceanic loss, and 3.3–3.4 years for soil loss. The partial lifetime for CH_3Cl is 1.3 years for atmospheric loss (from SPARC, 2013) and 3 years for oceanic and soil loss.

[b] In Table 5-1 a lifetime of 0.7 years is reported. In the scenarios calculations, however, a value of 0.75 years is used to be consistent with natural emission estimates from WMO (2011).

[c] These are 1-σ lifetimes, taken from Velders and Daniel (2014), which are calculated when only the uncertainties in the atmospheric loss rates (inverse of the atmospheric lifetime) from SPARC (2013) are taken into account. A 1-σ uncertainty implies that there is an approximately 68% chance that the actual lifetime will fall within that range. The exclusion of other loss rate uncertainties is relevant for CCl_4, for which the uncertainty could change if the uncertainty in the partial lifetime due to oceanic loss (82–191 years (WMO, 2011)) would be taken into account.

Newman et al. (2006) were used in WMO (2011) for discrete ages-of-air for midlatitude (3 year) and Antarctic (5.5 year) conditions. A new analysis of the FRF for ten ODS by Laube et al. (2013) gives values that are on average about 20% smaller than those derived by Newman et al. (2006) (see comparison in Table 5-1). These have not been adopted for this Assessment although their effect on ODP values is considered in the following discussion and in Chapter 1.

In Table 5-2, the steady-state semi-empirical ODPs for longer-lived halocarbons (those with an atmospheric lifetime greater than 0.5 year) are shown using the atmospheric lifetimes from WMO (2011) and those derived using the lifetimes from SPARC (2013). In general the derived ODP values in Table 5-2 are almost all smaller numerically (ranging from no change (for carbon tetrachloride, CCl_4) to more than a factor of two smaller (for CFC-115), with most smaller by 10–30% than the values reported in WMO (2011), as expected given the longer lifetime for CFC-11. The one major exception is halon-2402, for which the lifetime in SPARC (2013) is appreciably longer than in WMO (2011).

The use of the Laube et al. (2013) FRFs also affects the semi-empirical ODPs, as shown by the values in parentheses in Table 5-2 (based on Velders and Daniel, 2014). Using both the lifetimes from SPARC (2013) and the fractional release values from Laube et al. (2013) results in small changes in ODPs of most species compared with the values reported in WMO (2011). The ODPs of the HCFCs show larger changes: the ODP of HCFC-22 decreases by 37%; that of HCFC-141b, by 40%; and that of HCFC-142b, by 64%. ODPs calculated from the fractional release values of Laube et al. (2013) and using the SPARC (2013) lifetimes are consistent with the assessed values in the Montreal Protocol and WMO (2011) except for HCFC-22, HCFC-141b, and HCFC-142b, all of which have much smaller values using the Laube et al. fractional release values. Uncertainties in the atmospheric lifetimes, the fractional release values, and atmospheric chemistry generally result in overall uncertainties on the order of 30% for the CFCs and CCl_4, but are much higher for HCFCs and halons (roughly 55–58% for the HCFCs and halon-1301 to over 80% for halon-1202 and halon-1211), based on analyses by Velders and Daniel (2014). The 95th percentile confidence intervals are also shown in the table, as taken from Velders and Daniel (2014). They are shown when using the "most likely" and "possible" lifetime uncertainty ranges as presented in SPARC (2013).

Table 5-3 shows analyses of the spatial dependence in ODPs for VSLS primarily based on results using different versions of the National Center for Atmospheric Research (NCAR) global 3-D model (Wuebbles et al., 2009, 2011; Patten and Wuebbles, 2010; Youn et al., 2010; Patten et al., 2011). Note that this model calculates an atmospheric lifetime of 53.7 years for CFC-11, so the published ODPs would not be significantly affected by the revised SPARC (2013) lifetime for CFC-11. In these studies, the VSLS examined all have quite small ODPs based on emissions occurring primarily at midlatitudes. New approaches for estimating VSLS ODPs have been developed since WMO (2011) based on Lagrangian models (Tegtmeier et al., 2012; Pisso et al., 2010; Brioude et al., 2010), with findings similar to previous studies, except for emissions in the tropics, where a different treatment of convection may allow for more VSLS (and their products) to reach the stratosphere.

In addition to these lifetime estimates, Patten and Wuebbles (2010) evaluated the lifetimes and ODPs of (*E*)-1-chloro-3,3,3-trifluoropropylene ((*E*)-CHCl=$CHCF_3$, HCFC-1233zd(*E*)) and (*E*)-1,2-dichloroethylene ((*E*)-CHCl=CHCl), assuming industrial emissions were to occur over all land surfaces in the latitude range 30°N to 60°N. These compounds are proposed foam blowing agents and electronic cleaning substances. Based on 3-D chemical transport model (CTM) calculations, the atmospheric lifetime of HCFC-1233zd(*E*) was 40 days with an ODP of 0.00034. The model-calculated lifetime is shorter than the boundary layer local lifetime given in Table 1-11 (250 days) and longer than the 26-day lifetime reported in Sulbaek Andersen et al. (2008) that was calculated using a specific OH concentration. For (*E*)-CHCl=CHCl the calculated lifetime and ODP were 12.7 days (6.7-day local lifetime in Table 1-11) and 0.00024, respectively. Patten et al. (2011) evaluated the lifetime and ODP of 2-bromo-3,3,3-trifluoropropene (CH_2=$CBrCF_3$), a suggested halon replacement for use in fire extinguishers. They reported a global annually averaged lifetime of 7 days and an ODP of 0.0028, when emissions were distributed between 30°N to 60°N, compared to the 3.9-day local lifetime given in Table 1-11. The differences in the model-calculated and estimated local lifetimes given in Table 1-11 highlight the dependence on the OH climatology used for the lifetime estimate.

Table 5-2. Ozone Depletion Potentials (ODPs) for long-lived halocarbons. Shown are the ODP values assumed in the Montreal Protocol, the ODPs updated in the previous Assessment (WMO, 2011), and the values determined in this Assessment based on the atmospheric lifetimes from SPARC (2013). Values shown as "This Assessment" are based on the fractional release factors from WMO (2011). The ODPs in parentheses are those using the fractional release factors from Laube et al. (2013). In general the derived ODP values in the Assessment are almost all smaller numerically (ranging from no change (for carbon tetrachloride, CCl_4) to more than a factor of two smaller (for CFC-115), with most smaller by 10–30% than the values reported in WMO (2011), as expected given the longer lifetime for CFC-11. The one major exception is halon-2402, for which the lifetime in SPARC (2013) is appreciably longer than in WMO (2011).

Halocarbon	ODP in Montreal Protocol	Semi-Empirical ODP		Uncertainties (95% confidence interval) (from Velders and Daniel, 2014)	
		WMO (2011)	This Assessment	Possible (±)	Most Likely (±)
Annex A-I					
CFC-11	1.0	1.0	1.0		
CFC-12	1.0	0.82	0.73 (0.81)	34%	30%
CFC-113	0.8	0.85	0.81 (0.82)	34%	30%
CFC-114	1.0	0.58	0.50	37%	30%
CFC-115	0.6	0.57	0.26	34%	32%
Annex A-II					
halon-1301	10.0	15.9	15.2 (19.0)	61%	57%
halon-1211	3.0	7.9	6.9 (7.7)	90%	82%
halon-2402	6.0	13.0	15.7	80%	71%
Annex B-II					
CCl_4	1.1	0.82	0.72 (0.72)	34%	30%
Annex B-III					
CH_3CCl_3	0.1	0.16	0.14 (0.17)	52%	36%
Annex C-I					
HCFC-22	0.055	0.04	0.034 (0.024)	69%	58%
HCFC-123	0.02	0.01			
HCFC-124	0.022				
HCFC-141b	0.11	0.12	0.102 (0.069)	68%	57%
HCFC-142b	0.065	0.06	0.057 (0.023)	67%	56%
HCFC-225ca	0.025				
HCFC-225cb	0.033				
Annex E					
CH_3Br	0.6	0.66 [a]	0.57	78%	69%
Others					
halon-1202		*	1.7	96%	88%
CH_3Cl		0.02	0.015		

[a] This value was based on the lifetime of CH_3Br of 0.8 year shown in the ODP table in WMO (2011).

* The value of 2.2 in Velders and Daniel (2014) is attributed to WMO (2011); the value was not in Table 5-1 of WMO (2011) but can be inferred from the fractional release and lifetimes shown in that table.

Table 5-3. Ozone Depletion Potentials (ODPs) for emissions from given latitude bands over land for short-lived halocarbons (very short-lived substances, VSLS) based on analyses from 3-D models. ODPs are from the papers, but modeled lifetimes for CFC-11 were similar to the SPARC (2013) values, so no correction was necessary. See Chapter 1, Table 1-5, for local lifetimes of such VSLS.

VSLS	Reference	Latitudes of Emissions	Reported Annual Lifetimes (days)	ODPs
nPB [1]	Wuebbles et al. (2009, 2011)	30°N – 60°N	24.7	0.0049
		60°S – 70°N	19.6	0.011
TCE [2]	Wuebbles et al. (2011)	30°N – 60°N	13.0	0.00037
PCE [3]	Wuebbles et al. (2011)	30°N – 60°N	111	0.0050
BTP [4]	Patten et al. (2011)	30°N – 60°N	7.0	0.0028
		60°S – 60°N	4.3	0.0052
HFO-1233zd [5]	Patten and Wuebbles (2010)	30°N – 60°N	40.4	0.00034
tDCE [6]	Patten and Wuebbles (2010)	30°N – 60°N	12.7	0.00024
CF_3I [7]	Youn et al. (2010)	30°N – 60°N	5.0	0.008
		20°S – 20°N	1.1	0.016
CH_3I [8]	Youn et al. (2010)	30°N – 60°N	13.6	0.017
CH_2Br_2 [9]	Tegtmeier et al. (2012)	20°S – 13°N	120	3 – 4
$CHBr_3$ [10]	Tegtmeier et al. (2012)	20°S – 20°N	26	1 – 5

[1] n-propyl bromide (C_3H_7Br)
[2] trichloroethylene (C_2HCl_3)
[3] perchloroethylene (C_2Cl_4)
[4] 2-bromo-3,3,3-trifluoropropene ($CH_2 = CBrCF_3$)
[5] (*E*)-1-chloro-3,3,3-trifluoropropylene ((*E*)-CHCl=$CHCF_3$) (also called tCFP)
[6] (*E*)--1,2-dichloroethylene ((*E*)-CHCl=CHCl)
[7] iodotrifluoromethane
[8] methyl iodide
[9] dibromomethane
[10] tribromomethane

Earlier studies (Wuebbles et al., 1999, 2001; Olsen et al., 2000; Bridgeman et al., 2000) have shown that the ODPs for short-lived compounds depend greatly on when or where the emissions occur, with the largest ODPs being found for emissions in the tropics. Although it is generally expected that most emissions from anthropogenic emissions of VSLS will occur at northern midlatitudes, there is no guarantee of this and the locations of future emissions could change. ODPs for tropical emissions of two VSLS compounds from Tegtmeier et al. (2012) are also presented in Table 5-3. The compounds examined, CH_2Br_2 and $CHBr_3$, are important contributors to lower stratospheric reactive bromine (especially through natural oceanic sources, see Chapter1), and have large ODPs for emissions occurring in the tropics.

The recent modeling studies also re-emphasize the point that VSLS ODPs are very dependent on the location of emissions, and not just the latitude; for example, by co-location with efficient vertical transport by deep convection into the stratosphere (semi-empirical ODPs as a function of specific locations of emissions based on Brioude et al. (2010) are shown in Table 5-4). Brioude et al. (2010) showed that these factors are more important than regional variations in VSLS losses by OH or photolysis. Using CO-like emissions to represent anthropogenic VSLS, they estimated ODPs for various compounds and found maximum ODPs over the Indian sub-continent varying from 0.079 in winter to 0.29 in summer for n-propyl bromide (C_3H_7Br or nPB) and from 0.13 in winter to 0.83 in summer for

CH_3I. Pisso et al. (2010) applied their new methodology to an nPB-like tracer with a lifetime of 20 days. They also found higher ODPs over southeast Asia in the summer (and over western Pacific in winter). In July in the tropics (30°N–30°S), ODPs varied from 0.33 in runs with convection to 0.17 in runs with no convection. Locally, values over southeast Asia are as high as 1.00. In general the results from these Lagrangian studies predict higher ODPs regionally compared to the global model results. These differences highlight uncertainties in simulating the transport of VSLS, with boundary layer mixing, convection depth, and advection strength all possibly leading to local differences in VSLS delivery to the stratosphere (e.g., see Hossaini et al., 2012b; Feng et al., 2011; Hoyle et al. 2011). The global model studies (e.g., Wuebbles et al., 2011) used a full chemical treatment for VSLS and CFC-11 degradation in the stratosphere and more realistic degradation and wet deposition schemes for VSLS in the troposphere than the Lagrangian-based studies (e.g., Tegtmeier et al., 2012; Pisso et al., 2010), leading to less VSLS reaching the stratosphere. Overall, these results point to potentially more important impacts from VSLS if emissions occur in regions close to convective regions in the tropics.

Ravishankara et al. (1994) estimated that HFCs and other halocarbons with CF_3 groups, such as HFC-23, -125, and -134a, could lead to ODPs of at most 0.0005 because of degradation product reactions. While the fluorine in HFCs is largely thought to be inert to ozone, it can destroy a small amount of ozone (Ravishankara et al., 1994). This can occur by (barely) catalytic cycles involving FO_x = F + FO and $CF_3O_x = CF_3O + CF_3O_2 + CF_3O_2NO_2$ families (e.g., Lary, 1997). Recent updates to relevant reaction rates suggest that the upper limits of the ODPs for such compounds are likely to be smaller (Sander et al., 2011), indicating that these compounds (not containing chlorine, bromine, or iodine) are unlikely to have a significant effect on stratospheric ozone.

Table 5-4. Estimated annual-mean Ozone Depletion Potentials (ODPs) for short-lived halocarbons (very short-lived substances, VSLS) as a function of specific emissions location. The numbers in brackets show the seasonal variability. These semi-empirical ODP estimates are based on the Lagrangian model study of Brioude et al. (2010) (the numbers shown are from the Supplementary materials of the published paper). The ODP estimates for $CHBr_3$ have been reduced by a factor of 3.1 compared with the Brioude et al. (2010) Supplement values owing to an error discovered after publication.

Species	North America	Europe	East Asia	Indian Subcontinent
C_2H_5Br	0.1300 [0.0780 – 0.2000]	0.1100 [0.0610 – 0.1700]	0.2100 [0.1000 – 0.3100]	0.4600 [0.3400 – 0.6300]
CH_2CBrCF_3	0.0035 [0.0008 – 0.0077	0.0013 [0.0006 – 0.0024]	0.0052 [0.0011 – 0.0130]	0.0440 [0.0130 – 0.0830]
n-C_3H_7Br	0.0235 [0.0150 – 0.0320]	0.0150 [0.0070 – 0.0260]	0.0420 [0.0190 – 0.0600]	0.1700 [0.0790 – 0.1300]
C_2HCl_3	0.0004 [0.0001 – 0.0007]	0.0001 [0.0001 – 0.0002]	0.0006 [0.0002 – 0.0013]	0.0041 [0.0013 – 0.0079]
CCl_3CHO	0.0008 [0.0005 – 0.0010]	0.0004 [0.0002 – 0.0008]	0.0014 [0.0007 – 0.0022]	0.0062 [0.0026 – 0.0110]
CH_3I	0.0360 [0.0130 – 0.0650]	0.0140 [0.0072 – 0.0210]	0.0660 [0.0220 – 0.1500]	0.4200 [0.1300 – 0.8300]
CF_3I	0.0068 [0.0022 – 0.0120]	0.0034 [0.0013 – 0.0061]	0.0120 [0.0020 – 0.0310]	0.0940 [0.0290 – 0.1900]
C_3F_7I	0.0028 [0.0007 – 0.0064]	0.0015 [0.0005 – 0.0031]	0.0033 [0.0006 – 0.0100]	0.0390 [0.0140 – 0.0670]
CH_2ClI	0.0047 [0.0011 – 0.0110]	0.0024 [0.0007 – 0.0050]	0.0051 [0.0009 – 0.0150]	0.0660 [0.0240 – 0.1100]
$CHBr_3$	0.130 [0.094 – 0.201]	0.106 [0.074 – 0.158]	0.216 [0.123 – 0.310]	0.581 [0.387 – 0.806]

5.3.2 Metrics for Changes in Climate

Box 5-3 summarizes the basics of metrics used for describing changes in climate, namely, Global Warming Potentials (GWPs) and Global Temperature change Potentials (GTPs).

Box 5-3. Metrics for Climate: The Basics

Global Warming Potentials (GWPs)

Many metrics are based on the concept of radiative forcing (RF), which is itself a metric. RF has been commonly used to compare different forcing agents (e.g., emissions of gases and particles) affecting climate in assessments of climate change (e.g., IPCC, 1990, 1995, 1996, 1999, 2000, 2001, 2007, 2009, 2013). Traditionally, the use of radiative forcing as a metric has been based on there being a clear relationship between the globally averaged forcing and the globally averaged annual mean surface temperature response at equilibrium. IPCC reports now also use Effective Radiative Forcing (ERF) to compare different climate change mechanisms (Forster et al. in IPCC 2007; Myhre et al., 2013). Forcings can only be accurately compared in a global mean sense, and not all forcings necessarily have the same efficiency or "efficacy" in causing climate to change. The IPCC 5th Assessment Report accounts better for the effects of efficacy by using the concept of ERF. For RF, all surface and tropospheric conditions are assumed to be constant, while for ERF, all physical variables can respond to perturbations except for those concerning the sea surface temperatures and sea ice. The basis for ERF is to account for the rapid adjustments in the troposphere that occur in the climate system such as the effects on clouds. The inclusion of these adjustments makes ERF a better indicator of the eventual temperature response, especially from particles and other forcings on climate that have strong atmospheric responses on short timescales or have large spatial variations. By including many of the rapid adjustments that differ across forcing agents, the ERF concept includes much of their relative efficacy and therefore leads to more uniform climate sensitivity across agents than the traditional RF concept (Myhre et al., 2013). Because the rapid adjustments included in ERF differ in strength across climate models, the uncertainty range for ERF estimates tends to be larger than the range for RF estimates (Myhre et al., 2013). Nonetheless, for well-mixed gases, there is no significant difference between RF and ERF.

The Global Warming Potential (GWP) metric arose out of analyses done for the first IPCC Assessment and is still the most widely used emission metric and the general standard for metric discussion in Climate Assessments (IPCC 1990, 1996, 1999, 2007). It represents the radiative forcing for either pulse or sustained emissions above the current background levels by integrating the radiative forcing over a specific time interval and comparing that integral to the forcing from an equal mass emission of carbon dioxide. GWPs for different gases can be compared for evaluating their relative potential for affecting climate over a given timescale. The Kyoto Protocol and other climate-related policymaking also compares the effects of different emissions using GWPs with a 100-year time horizon, effectively mapping all greenhouse gas emissions into "CO_2-equivalent emissions." It has become common practice to use the 100-year time horizon for analyses of GWPs, but the choice of time horizon has no direct scientific basis (IPCC, 1990; Wuebbles, 1995; Myhre et al., 2013). Its choice is a value judgment since it depends on the relative weight assigned to effects at different times. Other important choices include the background atmosphere underlying the GWP calculations, and the way indirect effects and feedbacks are considered (Myhre et al., 2013).

Essentially, GWPs are a relative measure of the total energy added to the climate system by a component in question relative to that added by CO_2. The GWP is approximately equal to the ratio (normalizing by the similar expression for CO_2) of the *equilibrium temperature response due to a sustained emission* of the species or to the *integrated temperature response for a pulse emission* (assuming efficacies are equal for the gases that are compared) (Myhre et al., 2013; also see O'Neill, 2000; Prather, 2002; Peters et al., 2011; Azar and Johansson, 2012).

Box 5-3, continued.

However, GWPs do not lead to equivalence with the temporal evolution of the temperature response or that of other climate variables. As a result, despite its existing use in policy considerations, there have been many critiques of the GWP concept. Metrics beyond radiative forcing and GWPs have been proposed but have not yet been used for policy decisions. The most prevalently discussed alternative metric is Global Temperature change Potential, also referred to as Global Temperature Potential (GTP).

Global Temperature change Potentials (GTPs)

The GTP metric (Shine et al., 2005; Shine et al., 2007) gives the relative temperature increase on a per unit mass of emissions basis due to emissions of a greenhouse gas relative to that due to CO_2 emissions for the chosen time horizon. GTP takes into account the thermal inertia and response of the climate system, and provides a measure of the temperature responses of the different components for a specific time horizon. GTP is an end-point measure based on temperature change for a selected year. As with GWPs, the choice of time horizon has a strong effect on the metric. Like GWPs, GTPs can be used for weighting the emissions to obtain "CO_2 equivalents."

GWPs and GTPs are fundamentally different by construction (see Figure 5-1) and different numerical values can be expected. By accounting for the climate sensitivity and the exchange of heat between the atmosphere and the ocean, GTPs include physical processes that GWPs do not. GTPs account for the slow response of the (deep) ocean, thereby prolonging the response to emissions beyond what is controlled by the decay time of the atmospheric concentration. GTPs include both the atmospheric adjustment timescale of the component considered and the response timescale of the climate system. However, GTPs also incorporate extra uncertainties relative to GWPs from including the climate response in the analysis, e.g., GTP values can be significantly affected by assumptions about the climate sensitivity and heat-uptake by the ocean (also see discussion in Myhre et al., 2013). As such, GTPs are sensitive to the specific climate model used in their derivation (e.g., see Olivié and Peters, 2013) and to the background scenario used in the analyses. As a result, the relative uncertainty ranges are potentially much wider for GTPs compared to GWPs.

Peters et al. (2011) provide additional useful insights to the GWP and GTP emissions metrics. They found that GWPs are a useful measure of the energy entering the climate system. GWPs and GTPs should be different as GTPs are an instantaneous measure while GWPs are an integrated measure of the system; that is, for the GTP the pathway of the forcing following a pulse emission is important, whereas the GWP depends only on the integral of the forcing. The ultimate choice of emission metric(s) and time horizon(s) depends on policy objectives. To the extent that limiting integrated temperature change over a specific time horizon is consistent with the broader objectives of climate policy, the analysis by Peters et al. suggests that the GWP concept represents a relatively robust, transparent, and policy-relevant emission metric, except for the short-lived gases, but GWPs are quite small for such gases.

ANALYSES OF GWPS AND GTPS

Updated GWPs and GTPs for many compounds based on the analyses in IPCC (Myhre et al., 2013) are shown in the Appendix in Table 5A-1. Also shown are the atmospheric lifetimes and radiative efficiencies used in these analyses. Hodnebrog et al. (2013) provide further descriptions of the analyses of radiative efficiencies for many halocarbons and related compounds (the IPCC values for the GWPs and GTPs are largely based on those in Hodnebrog et al.). Absolute GWP and GTP (AGWP and AGTP) are the absolute integral of RF (W m^{-2} yr; using ERF if possible) and the absolute temperature change (°C) for a kilogram emission of the greenhouse gas. Climate-carbon feedbacks (i.e., feedbacks between climate change and the carbon cycle) are included in the AGWP and AGTP of CO_2, but not for the AGWP of the non-CO_2 gases; see discussion below. In the new IPCC analyses, there is an increase of approximately 1% and 6% relative to IPCC (2007) and WMO (2011) in the AGWP for CO_2 for integrations of 20 and 100

years, respectively. As a result, many of the GWP values decrease slightly, but they also change because of changes in the lifetime and the radiative efficiency of the named greenhouse gas. This is the first time that values are provided for GTPs in the Ozone Assessment. The derivation of GTP in IPCC (2013) assumes a climate sensitivity of 1.06°C (W m^{-2})$^{-1}$, equivalent to a +3.9°C equilibrium response to 2 × CO_2, toward the higher end of the traditional range in climate sensitivity of 1.5 to 4.5°C for doubling of CO_2.

The IPCC (2013) GWP and GTP values do not include the changes in atmospheric lifetimes recommended by SPARC (2013). Table 5-5 adjusts the IPCC GWPs and GTPs for the 24 halocarbons with recommended lifetimes from SPARC (2013). Halon-1211 and CCl_4 were the only ODSs for which the lifetime was unchanged. The changes in GWPs and GTPs are roughly proportional to the changes in atmospheric lifetimes. Although there are some differences for all of the gases (except halon-1211 and CCl_4), the largest differences in GWPs and GTPs relative to Table 5A-1 are found for CFC-11, CFC-115, halon-1301, halon-2402, halon-1202, HFC-125, and HFC-143a.

Uncertainties in GWP values based on the uncertainties given for radiative efficiencies, perturbation lifetimes, and in the AGWP for the reference gas CO_2 are estimated in IPCC AR5 Chapter 8 (Myhre et al., 2013). The uncertainty in GWPs for gases with lifetimes of a few decades is estimated to be approximately ±25% and ±35% for 20 and 100 years, respectively. Velders and Daniel (2014) report uncertainties on a number of ODSs; their results suggest that the uncertainties differ substantially for different ODSs. Table 5-6 shows the estimated uncertainty ranges in 20-year and 100-year GWPs for several HFCs, first due to uncertainties in the SPARC (2013) lifetimes by themselves, and then in combination with other uncertainties in evaluation of the full range of uncertainties.

For shorter-lived gases, the uncertainties in GWPs will be larger but the GWP values are also smaller. For GTPs, few uncertainty estimates are currently available in the literature. In IPCC, the results from Joos et al. (2013), Reisinger et al. (2010, 2011), and Boucher (2012) were used to assess an uncertainty for methane for a 100-year GTP of ±75% (as compared to a range of 14 to +22% for 100-year GWPs, based on Olivié and Peters (2013)). The uncertainty in GTPs for longer-lived gases is much smaller (e.g., −17 to +24% for N_2O). We do not attempt to show the range of uncertainties for GTPs in this Assessment.

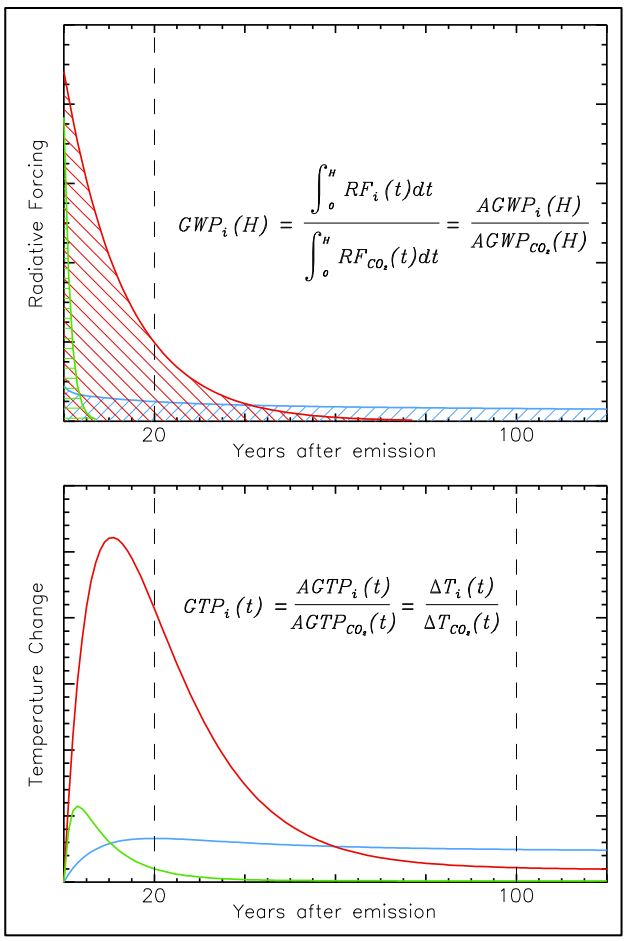

Figure 5-1. (a) The Absolute Global Warming Potential (AGWP) is calculated by integrating the RF due to emission pulses over a chosen time horizon; e.g., 20 and 100 years (vertical lines). The GWP is the ratio of AGWP for component *i* over AGWP for the reference gas CO_2. The blue-hatched field represents the integrated RF from a pulse of CO_2, while the green and red fields represent example gases with 1.5-year and 13-year lifetimes, respectively. (b) The Global Temperature change Potential (GTP) is based on the surface temperature response at a selected year after pulse emission of the same gases; e.g., 20 or 100 years (vertical lines). See IPCC (2013) Supplementary Material Section S8.11 for equations for calculations of GWP and GTP as used here.

Table 5-5. GWPs and GTPs of various halocarbons based on the SPARC (2013) atmospheric lifetimes. Except for the HFCs, the lifetimes are also found in Table 5-1.

Halocarbon	SPARC (2013) Lifetime (years)	GWP 20-yr	GWP 100-yr	GTP 20-yr	GTP 50-yr	GTP 100-yr
Annex A-I						
CFC-11	52	7090	5160	7160	5480	2920
CFC-12	102	10800	10300	11300	11000	8590
CFC-113	93	6560	6080	6830	6510	4860
CFC-114	189	7710	8580	8180	9010	8530
CFC-115	540	5780	7310	6210	7500	8290
Annex A-II						
halon-1301	72	7930	6670	8160	7160	4700
halon-1211	16	4590	1750	3950	1130	297
halon-2402	28	3920	2030	3730	1900	615
Annex B-II						
CCl_4	26	3480	1730	3280	1570	479
Annex B-III						
CH_3CCl_3	4.8	555	153	298	32	21
Annex C-I						
HCFC-22	12	5310	1780	4230	847	265
HCFC-141b	9.4	2590	800	1900	285	114
HCFC-142b	18	5140	2070	4530	1490	387
Annex E						
CH_3Br	0.8	9	2	3	<1	<1
Others						
halon-1202	2.5	719	196	285	35	27
CH_3Cl	0.9	40	11	13	2	2
HFC-23	228	10800	12500	11500	13000	12800
HFC-32	5.4	2530	704	1440	154	98
HFC-125	31	6280	3450	6040	3350	1180
HFC-134a	14	3810	1360	3170	771	214
HFC-143a	51	7050	5080	7110	5390	2830
HFC-152a	1.6	545	148	191	26	21
HFC-227ea	36	5250	3140	5140	3180	1260
HFC-245fa	7.9	2980	882	2040	259	124

Values of the GWP and GTP metrics are dependent on what processes are included. Ideally all indirect effects should be taken into account. The indirect effects of CH_4 on its own lifetime, tropospheric ozone, and stratospheric water have been traditionally included in its GWP (Prather, 1994; IPCC, 1995). The indirect effect of N_2O on its own lifetime has been considered since the IPCC 3rd Assessment Report (Prather, 1998; IPCC, 2001; Prather and Hsu, 2010). The WMO Assessments (e.g., WMO, 2007, 2011) have considered the indirect effects on stratospheric ozone from various halocarbons. In Table 5-7, indirect GWPs based on IPCC (2013) for various halocarbons are updated using the approach for the ozone response first developed by Daniel et al. (1995). The resulting values are similar to those found in the previous Assessments.

Table 5-6. For selected HFCs, lifetime and full uncertainty estimates of the 20- and 100-year GWPs using the SPARC (2013) lifetimes. The number ranges represent the effects of only considering uncertainties in the SPARC lifetimes, while the "full uncertainty" ranges include also uncertainties in the radiative efficiency (10%, from Myhre et al., 2013) and the AGWP for CO_2 (from Joos et al., 2013). The GWP uncertainties are calculated as in Myhre et al. (2013) (see Supplementary Material Section 8.SM.12 in IPCC (2013) for details), except that new information about lifetime uncertainties from SPARC (2013) is included here. The uncertainty estimates are representative of a 5 to 95% (90%) confidence interval. In addition, note that the IPCC (2013) stated uncertainties in the 100-year GWP for HFC-134a is ±35% (90% confidence) as representative for similar gases. The IPCC and updated GWPs that use the SPARC lifetimes are consistent within their uncertainties.

Halocarbon	SPARC (2013) Lifetime (years)	GWP 20-yr Best Estimate	GWP 20-yr Lifetime Uncertainty	GWP 20-yr Full Uncertainty	GWP 100-yr Best Estimate	GWP 100-yr Lifetime Uncertainty	GWP 100-yr Full Uncertainty
HFC-23	228	10800	10700–11100	8640–13100	12500	11800–14000	8880–16300
HFC-32	5.4	2530	2030–3530	1810–3650	704	551–1010	453–1070
HFC-125	31	6280	5840–7110	4930–7800	3450	2720–4830	2230–5140
HFC-134a	14	3810	3300–4690	2890–4980	1360	1040–1930	860–2050
HFC-143a	51	7050	6780–7690	5600–8620	5080	4340–6790	3460–7310
HFC-152a	1.6	545	431–718	386–750	148	117–195	96–211

Table 5-7. Indirect GWPs from ozone depletion (direct forcing from ODS, themselves, is not included) taken from IPCC (2013). Approach is taken from Daniel et al., 1995, assuming a radiative forcing due to ozone depletion in 2011 of −0.15 W m^{-2} (IPCC, 2013). Uncertainty in this radiative forcing leads to an uncertainty in these GWPs of ±100%.

SUBSTANCE	GWP 100-yr
CFC-11	–2640
CFC-12	–2100
CFC-113	–2150
CFC-114	–914
CFC-115	–223
HCFC-22	–98
HCFC-123	–37
HCFC-124	–46
HCFC-141b	–261
HCFC-142b	–152
CH_3CCl_3	–319
CCl_4	–2110
CH_3Br	–1250
halon-1211	–19000
halon-1301	–44500
halon-2402	–32000
HCFC-225ca	–40
HCFC-225cb	–60

It is also important to consider feedbacks between climate and the carbon cycle, effectively the additional amount of CO_2 released from the warming caused by any greenhouse gas. Gillett and Matthews (2010) included climate-carbon feedbacks in calculations of the GWPs for CH_4 and N_2O and found that this increased the values by ~20% for the 100-year GWP. For GTPs they found an increase of ~80%. The AGWP for the CO_2 reference gas has included the climate–carbon feedback in the analyses of GWP in recent Assessments (WMO, 2011; IPCC, 2007, 2013). For the first time, Myhre et al. (2013) include analyses of these indirect climate-carbon feedback effects on GWPs and GTPs for many halocarbons. For many gases, the correction is sizeable, increasing the values of the GWPs and GTPs. However, uncertainties remain large, so more analysis is likely needed before this additional effect is included in policy considerations. Also, the GWPs for the combination of indirect effects on ozone depletion and climate-carbon feedbacks have not been evaluated.

5.4 SCENARIOS AND SENSITIVITY ANALYSES

This section presents an analysis of a set of scenarios and hypothetical test cases that may be of use to decision-makers. The existing Montreal Protocol and its Amendments and adjustments provide the backdrop and a framework for these analyses. Options evaluated include the elimination of future production and future emissions in advance of current controls, and the recapture and destruction of banks (see Box 5-1) in 2015 and 2020. Results are roughly linear, in that a decrease in 50% of future production will have about half the effect on ozone depletion and climate forcing as the scenario evaluated here in which all future production is eliminated. This Ozone Assessment does not evaluate the technical or economical feasibility of these options, but because of the linearity, these results can help guide policymakers in their environmental evaluation of feasible options.

5.4.1 Tools Used in Analyses of Ozone and Climate Effects

As in WMO (2011), both EESC and climate-chemistry modeling studies are used in the scenario analyses relating to ozone impacts. As discussed earlier, EESC is a metric that relates the tropospheric concentration of source gases to their chemically active stratospheric products that are available to destroy ozone. It has been shown (Daniel et al., 2010) that the halogenated ODS mitigation options have about the same percentage impact on integrated EESC as on integrated global stratospheric total column ozone. Because of the computational ease of calculating EESC, an EESC analysis allows for a fast and accurate method for comparing potential ODS mitigation options involving halogenated species without running a full atmospheric model.

Typically, EESC has only been used for halocarbon source gases. However, surface N_2O concentrations due to anthropogenic activity can also be included in EESC (Daniel et al., 2010). The calculation of N_2O's contribution to ozone depletion, and thus to EESC, is complicated by other chemical interactions, such as the concentration of atmospheric chlorine and stratospheric aerosols (Ravishankara et al., 2009), but these obstacles are similar to those encountered by the chlorine- and bromine-containing gases. In this chapter, we do not include N_2O in our standard EESC calculations, but we do include a set of sensitivity runs to show the degree to which the two-dimensional (2-D) modeled ozone response compares with the N_2O EESC response for an N_2O mitigation option.

The NASA/Goddard Space Flight Center (GSFC) 2-D coupled chemistry-radiation-dynamics model (Fleming et al., 2011) is used to evaluate the impact of various ODS and GHG scenarios on past and future ozone, including evaluation of the effects of changes of CO_2 and CH_4 that cannot readily be addressed by EESC as used here. While three-dimensional (3-D) climate-chemistry modeling studies would be ideal for these scenario/test analyses, the computational and time requirements make most of these studies prohibitive for this Assessment. The GSFC 2-D model provides realistic simulations of meridional transport in the stratosphere on timescales >30 days, as seen by good model agreement with a variety of observations in reproducing transport-sensitive features in the meridional plane (Fleming et al.,

2011). Since the computational efficiency of a zonally averaged 2-D model makes it possible to perform multiple long-term simulations in a reasonable amount of time, this 2-D climate-chemistry model is optimal for addressing the ozone-change scenarios discussed here. To be consistent with the model results reported in other Chapters, the model simulations presented here use the recommended chemical rate constants from Sander et al. (2011). Sensitivity simulations revealed that using the updated rate constants from SPARC (2013) resulted in a very minor impact on global total ozone, with changes <±0.2 Dobson units (DU).

Radiative forcing is used to quantify the potential effects of the various scenarios on climate. The radiative forcing is calculated with a radiative transfer model using the spatial distribution of mixing ratios determined from observations or calculated in the given atmospheric chemistry-climate model. For the halocarbons, radiative forcing is determined by multiplying the surface mixing ratio by the appropriate radiative efficiency (see Appendix 5A, Table 5A-1). The radiative forcing of N_2O is based on the analyses in Annex II of IPCC (2013).

In addition to the previously discussed ozone depletion and climate metrics, integrated ODP- and GWP-weighted quantities are also shown in Table 5-8 as another comparative tool.

5.4.2 Background Scenario(s) for Ozone and Climate

To evaluate the impact of potential policy decisions on ozone depletion and climate change, a background or baseline scenario of mixing ratios from 1950 through 2100 has been developed for ODS halocarbons and N_2O (and CH_4 and CO_2 in the 2-D model), against which other scenarios are compared. These alternative scenarios are consistent with various mitigation options and are discussed in more detail in Section 5.4.3. The RCP6.0 scenario is used for the time evolution of CO_2, CH_4, and N_2O abundances in the background scenario.

The baseline scenario for the halocarbon ODSs is consistent with the current upper limits prescribed by the Montreal Protocol on Substances that Deplete the Ozone Layer, and it has been developed to be consistent with mixing ratio observations through the beginning of 2013 (see Chapter 1). In the years before atmospheric observations were made, mixing ratios have been estimated from reported production values and are very similar to values in WMO (2011). Future projections are determined from global lifetime estimates that have been recently updated (SPARC, 2013), future production amounts set to be the maximum allowed under the Montreal Protocol, and bottom-up bank estimates for 2008 are the same as were used in WMO (2011). It is assumed that future releases of halocarbons from equipment and applications will continue at the same fractional rate as estimated over the period 2005 through 2011.

Figure 5-2 compares the current baseline scenario and alternative scenarios (see Section 5.4.3 for a description of these scenarios) with the baseline scenario from WMO (2011). The most significant difference in terms of effects on EESC between the two baseline scenarios results from the longer estimated lifetimes for CFC-11 and CCl_4. These lead to slower atmospheric decay and thus an increased contribution to EESC in the future. Lifetime estimate changes have no effect on historical mixing ratios since those are constrained by observations. Some of the largest relative mixing ratio changes occur for the HCFCs. These are primarily caused by the lower base level against which future HCFC production and consumption in Article 5 Parties are referenced to in the current baseline compared with the one from WMO (2011); they are also partly due to a higher assumed level of production between 2009 and 2012 in the previous Assessment, before the freeze went into effect in 2013. The Article 5 base production level is defined in the Montreal Protocol as the average of the 2009–2010 production. In WMO (2011), it was estimated that the Article 5 base level for the HCFCs would be slightly more than 36 ODP-ktonnes; it is now known to be about 33 ODP-ktonnes. This affects the current HCFC production as well as the production and emissions for decades to come since the future limits on production and consumption are prescribed by the Montreal Protocol to be a decreasing fraction of this base level over time.

Changing concentrations of CO_2, CH_4, and N_2O also affect stratospheric ozone and should be considered in analyses of ozone. CO_2 and CH_4 have never been included in the EESC formalism, and N_2O's contribution to EESC has met with limited use. Therefore, in this chapter, we will consider the impact

Table 5-8. Comparison of scenarios and cases[a]: the year when EESC drops below the 1980 value for both midlatitude and Antarctic vortex cases, and integrated EESC differences (midlatitude case) relative to the baseline (A1) scenario[b]. Also shown are changes in integrated ODP- and GWP-weighted emissions and, for selected cases, integrated global ozone depletion from 2015−2050. Future changes in CH_4 and CO_2 may also significantly alter ozone levels, perhaps by amounts larger than any of the cases considered in this table. However, their effects are not included here because policy choices that would lead to reduced global O_3 depletion would require increased CH_4 and CO_2, which would increase climate forcing.

Scenario and Cases	Percent Difference in Integrated EESC Relative to Baseline Scenario for the Midlatitude Case		Year When EESC is Expected to Drop Below 1980 Value		Change in Cumulative ODP-Weighted[d] Emission: 2015−2050	Change in Cumulative GWP-Weighted[e] Emission: 2015−2050	Percent Difference in Integrated O_3 Depletion[f]: 2015−2050
	Midlatitude [b,c]			Antarctic vortex [c]	(Million tonnes CFC-11-equivalent)	(Billion tonnes CO_2-equivalent)	
	$\int_{1980}^{x} EESC\ dt$	$\int_{2015}^{x} EESC\ dt$					
Scenarios							
A1: Baseline scenario	-	-	2047.6	2073.3	0.0	0.0	
Cases[a] of zero production from 2015 onward of:							
P0: All ODS	−5.9	−20	2042.8	2069.5	−0.91	−9.0	−0.30
CFCs	0.0	0.0	2047.6	2073.3	−0.00	−0.00	-
halons	0.0	0.0	2047.6	2073.3	−0.00	−0.00	-
HCFCs	−1.8	−6.4	2046.3	2072.6	−0.22	−7.8	−0.12
CH_3Br for QPS	−1.6	−5.3	2046.5	2071.9	−0.13	−0.00	−0.07
CCl_4	−2.8	−9.8	2045.3	2071.6	−0.56	−1.2	−0.11
Cases[a] of zero emissions from 2015 onward of:							
E0: All ODS (does not include N_2O)	−12	−40	2036.5	2061.4	−2.72	−18.5	−0.75
CFCs	−2.6	−8.9	2045.0	2069.6	−0.86	−4.7	−0.20
halons	−3.4	−12	2044.8	2070.1	−0.76	−0.24	−0.16
HCFCs	−3.7	−13	2045.3	2072.2	−0.41	−12.4	−0.19
CCl_4 [g]	−2.8	−9.8	2045.3	2071.6	−0.56	−1.2	−0.11
CH_3CCl_3	0	0	2047.6	2073.3	−0.00	−0.00	-
CH_3Br for QPS	−1.6	−5.3	2046.5	2071.9	−0.13	−0.00	−0.07
Total anthropogenic N_2O [h]	-	-	-	-	−6.69	−104	−0.88
N_2O mitigation					−1.25	−19.5	−0.16
Cases[a] of full recovery of the 2015 banks of:							
B0: All ODS	−7.3	−25	2041.3	2065.7	−1.80	−9.6	−0.44
CFCs	−2.6	−8.9	2045.0	2069.6	−0.86	−4.7	−0.20
halons	−3.4	−12	2044.8	2070.1	−0.76	−0.24	−0.16
HCFCs	−1.9	−6.4	2046.8	2072.9	−0.19	−4.6	−0.07
Cases[a] of full recovery of the 2020 banks of:							
B0: All ODS	−4.7	−16	2042.4	2066.8	−1.39	−8.1	−0.38
CFCs	−1.5	−5.3	2045.6	2070.3	−0.64	−3.3	-
halons	−2.0	−6.8	2045.4	2070.6	−0.56	−0.18	-
HCFCs	−1.6	−5.5	2046.5	2072.7	−0.19	−4.6	-
CH_3Br sensitivity: [i]							
Same as A1, but CUEs continue at 2012 levels	+0.2	+0.7	2047.8	2073.5	+0.02	+0.00	-

Table 5-8, continued.

[a] Significance of ozone-depleting substances for future EESC was calculated in the hypothetical "cases" by setting production or emission to zero in 2015 and subsequent years or the bank of the ODS to zero in the year 2015 or 2020.

[b] EESC is integrated until it returns to 1980 levels, denoted as year "x."

[c] For midlatitude conditions, an average age-of-air of 3 years, corresponding fractional release values, and a bromine efficiency factor (alpha) of 60 are assumed. For Antarctic vortex conditions, an average age-of-air of 5.5 years, corresponding fractional release values, and an alpha value of 65 are assumed. In all cases, age spectra are applied as in Newman et al. (2007).

[d] Semi-empirical ODPs from Table 5-2.

[e] GWPs with 100-year time horizon (see Appendix 5A, Table 5A-1).

[f] Integrated globally averaged total column ozone changes are taken from 2-D model runs described in chapter.

[g] Banks are assumed to be zero. Emissions include uncertain sources such as possible fugitive emissions and unintended other emissions.

[h] The integrated ODP- and GWP-weighted emissions correspond to the reduction of anthropogenic N_2O emissions from a business-as-usual case to a strong mitigation case (see text).

[i] Same as A1 but critical-use exemptions continue at 2012 levels.

of these three gases in the 2-D model calculations, but not with the box model EESC analysis, except for a brief discussion of the estimated impact of N_2O on EESC. The baseline scenario chosen for these compounds is taken to be the RCP6.0 scenario. While RCP6.0 is a mitigation scenario, it represents one choice of a central scenario around which we can explore the sensitivity of our results to a stronger mitigation scenario (RCP4.5) and a business-as-usual scenario (RCP8.5). This sensitivity analysis has been performed to explore the impact of this choice on the results, but in general, it has little effect on the impacts of the halocarbon mitigation scenarios in terms of either depletion of globally averaged total ozone or on climate forcing changes. However, the scenario choice could have local effects on the structure of ozone changes with altitude and latitude.

5.4.3 Alternative Future Scenarios

Future scenarios have been developed that reflect the impacts of various mitigation options to further reduce future ozone depletion. Because halocarbons and N_2O are greenhouse gases, these scenarios will reduce climate forcing as well. For the ODS halocarbons, the mitigation options include capture and destruction of the banks (see Box 5-1), elimination of future production beginning in 2015, and elimination of future emissions beginning in 2015. Two sets of bank recapture scenarios have been performed, one for elimination of banks in 2015 and one for 2020. A comparison of these bank scenarios illustrates the reduced impact of the bank capture option on ozone and climate as the halocarbons are released into the atmosphere over this 5-year period and bank sizes are projected to decline for most ODSs. Because all post-2015 emission either originates from production after 2015 or from banks existing in 2015, the production elimination and bank capture and destruction scenarios can be approximately added together to reproduce the "no emission" scenario results. The reason that the results are not always perfectly additive is that some of the metrics quantified here are tied to the return of EESC to 1980 levels and this return time changes differently in each mitigation scenario. The production, bank, and emission scenarios are run for individual ODS groups to evaluate the impact of mitigation options for each group to the future ozone and climate metrics. These individual calculations allow for a straightforward evaluation of the relative importance of future production and bank sizes for each of the ODS groups considered.

Figure 5-2 shows future ODS concentration projections for the various mitigation options. The CFCs should have almost no additional production in the future scenarios and so all future emissions are assumed to originate from current equipment and applications. Thus, bank recapture and destruction is the only approach to reduce future mixing ratios of the CFCs. On the other hand, banks of CH_3Br and CCl_4

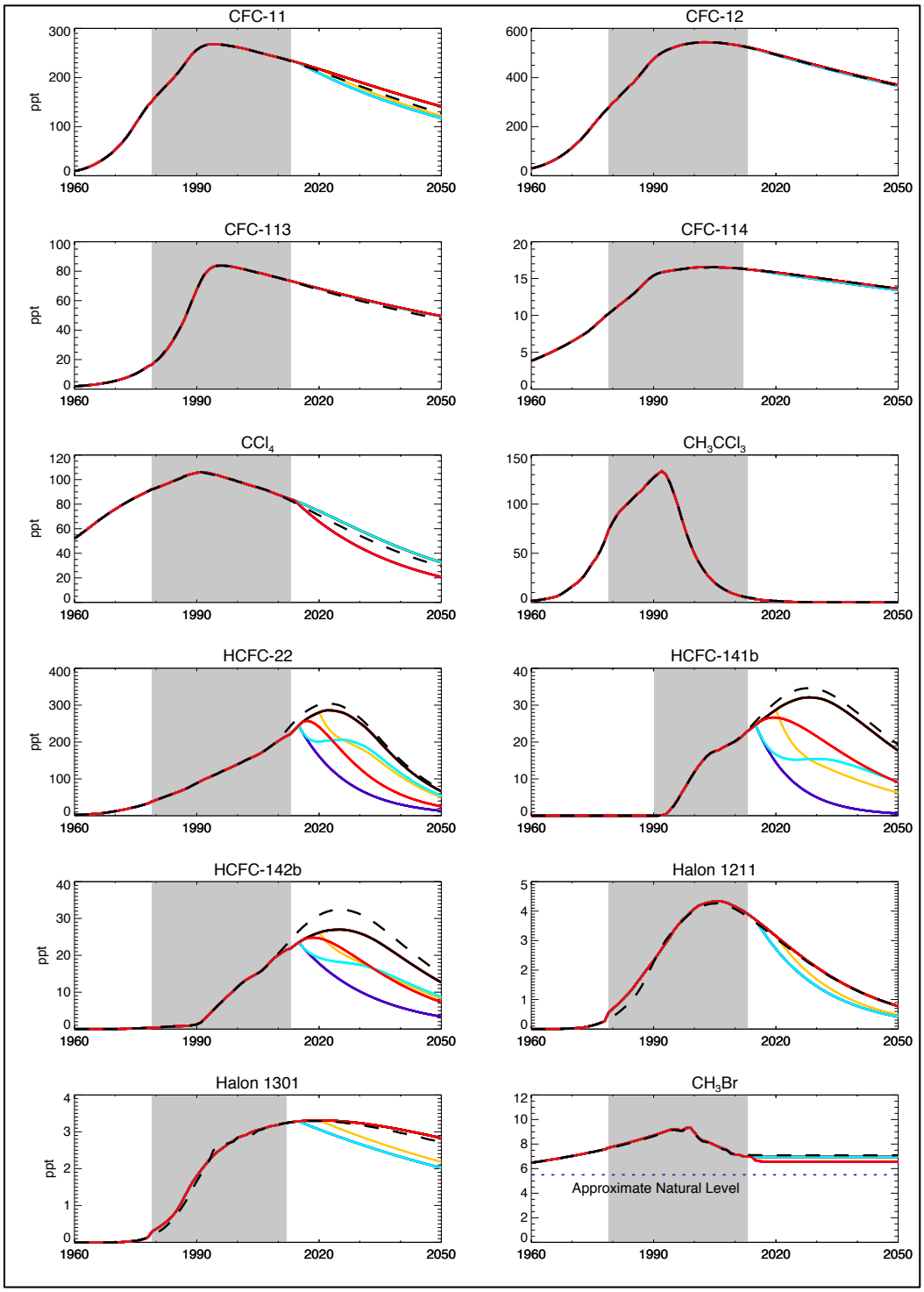

Figure 5-2. Comparison of current baseline halocarbon mixing ratios compared with those from the baseline scenario of WMO (2011); also shown are future mixing ratio projections for "no emission from 2015 onward," "bank capture and destruction in 2015," "bank capture and destruction in 2020," and "no production from 2015 onward" scenarios. Curves are color coded in the same manner as in Figure 5-3 (e.g., solid black is the baseline scenario). Shaded regions represent mixing ratios that are constrained to observational estimates (see Chapter 1; Chapter 5 Appendix 5A, Table 5A-2). The approximate natural concentration of CH_3Br is noted by the dashed dark blue line in the lower right-hand panel (see Chapter 1).

may be small compared with their annual production; for these compounds, eliminating production is the way to reduce their future mixing ratios. Of course, as discussed in Chapter 1, there is a discrepancy between top-down emissions estimates derived from CCl_4 mixing ratio observations and reported production, with reported production too small to be able to account for the observed trend in abundances even if all production were emitted immediately. Thus, to the extent that there is additional unidentified emission that does not come from reported production, elimination of that emission could reduce future EESC and ozone depletion. In this Assessment we adopt current emissions of CCl_4 from the top-down estimates and assume that future emissions will decline at 6% per year in the absence of additional controls. HCFCs can be noticeably reduced in the future by both bank recapture and destruction and by production elimination. It is important to recognize that only emissions resulting from QPS and critical-use exemptions (CUE) applications are considered in our scenario calculations. While controlled uses are thought to lead to small emissions in comparison to QPS emissions (see Chapter 1), we also neglect emissions associated with other activities, such as biomass burning and gasoline and biofuel usage. The baseline scenario for WMO (2011) is shown for comparison in Figure 5-2.

Figure 5-3 shows the impacts of the different mitigation options on total midlatitude EESC. The "No Future Emissions" curve represents the EESC levels to which we are committed even if no ODSs are emitted from 2015 on. This limiting case assumes no further production and no release from existing banks. Both future production and current banks contribute to the elevation of EESC above this level in our baseline scenario approximately equally as shown by the various curves. The difference between the "Zero 2015 Bank" and "Zero 2020 Bank" curves illustrates the impact on EESC of waiting 5 years to capture and destroy the banks; this difference is largest just after 2020 and shrinks over time. Velders and Daniel (2014) have quantified the EESC uncertainty in a scenario that is similar to the baseline scenario shown in Figure 5-3. That calculated uncertainty is determined from uncertainty estimates in all the terms that are used in the EESC calculation. It is found that the 2-σ fractional EESC uncertainty when considering the "most likely" lifetime ranges is comparable to the maximum difference between the baseline scenario and the zero emissions scenario. Overall, the most important single factor to future EESC uncertainty is the uncertainty in the lifetimes of the ODSs.

Table 5-8 shows, as in WMO (2011), how different specific mitigation options affect integrated EESC, ODP- and GWP-weighted emissions, and the return to 1980 EESC levels. In terms of future emissions, HCFCs, halons, CFCs, CCl_4, and CH_3Br all contribute noticeably to increasing future integrated

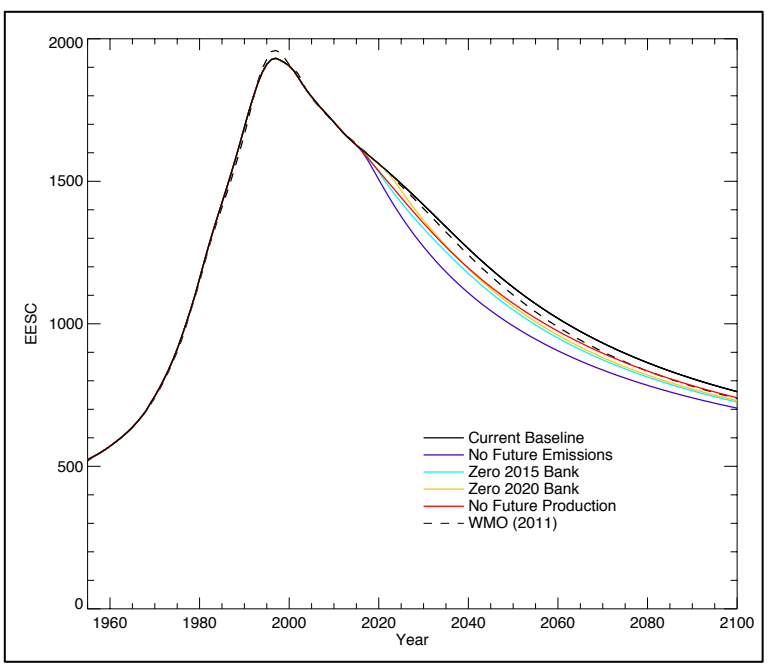

Figure 5-3. EESC for the current baseline scenario (midlatitude conditions) compared with EESC from the WMO (2011) baseline scenario; also shown are four alternative scenarios that reflect current mitigation alternatives considered in this Assessment. Velders and Daniel (2014) have quantified the uncertainty in a similar EESC scenario considering uncertainties in all contributing terms; they found that the 2-σ uncertainty values in the future vary somewhat over time, but are less than 15% when the most likely lifetime ranges are considered and the curves are normalized at 1980 EESC levels.

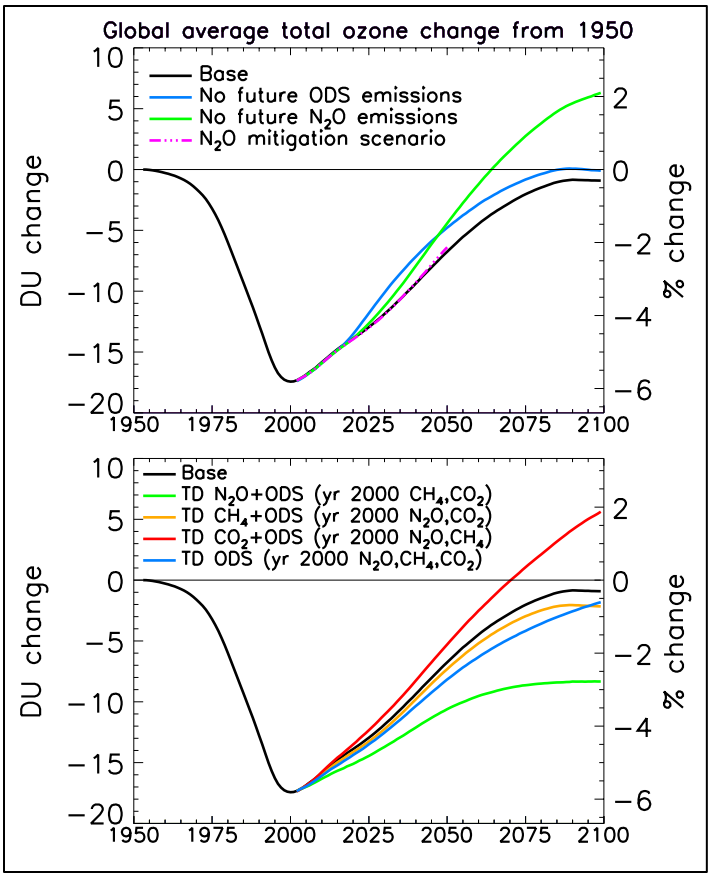

Figure 5-4. Model calculations of the globally averaged total column ozone difference relative to 1950. Upper panel: the baseline scenario, a scenario of no future ODS emissions (blue), no future human-related N_2O emissions (green), and the N_2O mitigation scenario from UNEP (2013) (red dashed-dotted). Bottom panel: the impact due to only the decreasing ODSs, with CO_2, CH_4, and N_2O fixed at 2000 levels (blue), and the separate impacts due to future increasing CO_2 (red), CH_4 (yellow), and N_2O (green) in the presence of decreasing ODSs. The RCP6.0 scenario was used for the greenhouse gases. As stated in the text, these scenarios are different than those presented in Chapter 2.

EESC, where the integration is stopped once total EESC drops below 1980 levels. If all ODS emissions were to be eliminated beginning in 2015, EESC for midlatitudes would return to 1980 levels 11 years sooner than in the baseline scenario. The most significant projected emissions for determining the return time arise from current halon, CFC, and HCFC banks and future production of HCFCs, and CH_3Br. Future emissions of CCl_4 are also projected to be important, but as discussed in Chapter 1 and in this chapter, the sources of these emissions are uncertain. Production of CH_3Br has been eliminated for many historical uses. However, production for quarantine and pre-shipment (QPS) applications is not controlled and is currently the largest remaining emissive anthropogenic component of CH_3Br production. The elimination of future emissions from QPS uses could bring forward the date of EESC return to 1980 levels by 1.1 years, smaller than the 1.6 years estimated in the previous Assessment. Critical-use exemptions for CH_3Br also continue to be granted, but emissions arising from this production are substantially smaller than those from QPS activities. A continuation of critical-use exemptions at the current level would delay the return of EESC to 1980 levels by 0.2 years. For climate considerations, HCFCs play the largest role in future integrated GWP-weighted emissions, contributing almost two-thirds of the total by the ODS halocarbons. These emissions result primarily from future HCFC production, but current banks are also important. Future CFC emissions represent most of the remaining cumulative GWP-weighted emissions through 2050 and are due almost exclusively to current banks.

Table 5-8 also shows the changes in integrated global ozone levels for selected scenarios run with the 2-D model. Figure 5-4 (top panel) shows the two most significant scenarios: 1) no future ODS emissions, and 2) no future human-related N_2O emissions. Also shown is the effect of more modest N_2O mitigation on future ozone. Unlike the ODS halocarbon scenarios, this N_2O alternative mitigation scenario does not assume complete elimination of future production or emission. N_2O has a number of sources but a major one results from the use of fertilizers, i.e., it is to a large degree a by-product of global food production, and because there are no replacements for this use, we have adopted the "concentrated

mitigation" scenario from UNEP (2013) for the alternative mitigation scenario here to compare with the baseline. Even though the reduction in N_2O is only a fraction of the total anthropogenic emissions, the results here are qualitatively consistent with WMO (2011): the impact of all anthropogenic N_2O emissions is very significant compared with the sum of all halocarbon emissions in terms of both ozone depletion and climate. When integrated through 2050, elimination of all anthropogenic N_2O emissions leads to a slightly larger reduction in future CO_2-equivalent emissions than would the elimination of all ODS halocarbon emissions. In terms of integrated ODP-weighted emissions, elimination of anthropogenic N_2O has about half the effect of an elimination of all ODS halocarbon emissions. The alternative N_2O mitigation scenario has an obviously smaller impact on global ozone by 2050. N_2O's impact becomes relatively more important over time because the halocarbon production and consumption is phased out by the Montreal Protocol, while N_2O is projected to continue growing under many future scenarios, including those considered here. It must be recognized, however, that the quantitative impact of N_2O emissions mitigation depends on the baseline scenario chosen (RCP6.0 here). A higher baseline scenario will increase the impact of N_2O mitigation on future climate forcing and ozone depletion.

Figure 5-5 shows the relative importance of historical and future projected N_2O abundances on EESC relative to that of the ODS halocarbons for the baseline scenario used in the chapter. This exemplifies the increasingly important role that N_2O is expected play in the future if its emissions are not reduced. A similar response is seen in the 2-D model calculations of ozone with increasing N_2O but CO_2 and CH_4 fixed at 2000 levels, with increasing ozone flattening and even starting to decrease in the later part of the 21st century (Figure 5-4, bottom, green line). The upper panel of Figure 5-4 shows the relative impact of reducing or eliminating future N_2O emissions compared with that of eliminating future halocarbon ODS emissions on global average total ozone. While total future N_2O emissions cause substantially more depletion in the future than do future halocarbon ODS emissions, many of the N_2O emissions are expected to be very difficult to eliminate (UNEP, 2013). If the UNEP (2013) N_2O mitigation scenario is adopted, which was only analyzed to 2050 (Figure 5-4, top, red dash-dotted line), there is little difference relative to the baseline scenario and much less change than if the no future ODS emissions scenario were adopted (blue line). Again, however, the impact of N_2O mitigation is expect to grow past 2050, while that of ODS halocarbon mitigation will decrease.

It is important to recognize that any future increases in CO_2 and CH_4 not only will have a substantial impact on climate forcing, but also are expected to lead to higher levels of globally averaged total ozone than if these greenhouse gases remained constant. So while CO_2 and CH_4 are likely not considered candidates for altering future ozone depletion themselves, it is important to be aware that policy options for halocarbon ODSs and for N_2O will be made against a backdrop of potentially large ozone changes due to CO_2 and CH_4. The effects on ozone due to increasing CO_2 and CH_4 are discussed in detail in Chapter 2; a summary of the important mechanisms and ozone responses is provided here.

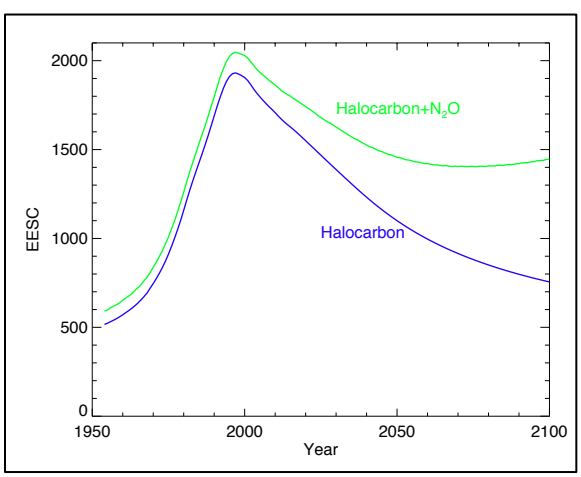

Figure 5-5. Comparison of EESC calculated from halocarbons alone using the midlatitude baseline scenario (Halocarbon), and with the addition of the N_2O contribution (Halocarbon+N_2O) using the formula from Daniel et al. (2010) for including N_2O in EESC.

For most of the scenarios examined, increases in ozone arising from CO_2 and CH_4 increases may be comparable to or larger than the additional depletion caused by N_2O increases. This behavior can be seen from the 2-D model calculations of global total ozone using the RCP6.0 scenario shown in Figure 5-4 (bottom). This illustrates the individual effects of future increases in CO_2 (red line), CH_4 (yellow line), and N_2O (green line) in the presence of decreasing ODSs, and can be compared with the impact due to only the decreasing ODSs (in which the GHGs are all fixed at 2000 levels, blue line). As shown by comparing the red, yellow, and green lines with the blue line in Figure 5-4, increasing CO_2 leads to a substantial global ozone increase by 2100 (+2% relative to 1950) primarily due to stratospheric cooling, which reduces the ozone chemical loss rates (Haigh and Pyle, 1979). Note that these results are for global ozone and that more localized changes may differ (see below and Chapter 2). Another factor is that future CO_2-induced stratospheric changes will indirectly affect ozone by somewhat mitigating the ozone depletion caused by N_2O (see Box 5-2 and Section 2.4.3.1).

Compared to CO_2, methane loading leads to a smaller global total ozone increase (yellow line in Figure 5-4, bottom). CH_4 causes ozone to increase by: 1) mitigation of the chlorine-ozone loss cycles in the stratosphere, and 2) enhanced NO_x-induced ozone production in the troposphere and lowermost stratosphere following CH_4 oxidation (Brasseur and Solomon, 2005, and see Section 2.4.3.1). For total column ozone, these processes dominate the ozone reductions caused by the CH_4-enhanced HO_x-ozone loss cycles that are important primarily in the upper stratosphere (Revell et al., 2012). The slight decline of the CH_4-induced total ozone change during the late 21st century in Figure 5-4 is caused by the decrease in methane in the RCP6.0 scenario. As atmospheric chlorine levels decline through the 21st century, future methane-induced changes in total ozone will be increasingly determined by the NO_x-ozone production cycle in the troposphere and lowermost stratosphere. The large range in CH_4 among the RCP scenarios, mainly due to the very high methane of RCP8.5 (Section 2.4.3.2), is projected to produce a large range of future tropospheric ozone responses. For example, in 2100, CH_4 increases of 1.9–2.0 ppm (approximately the increase from present day to 2100 in RCP8.5) are projected to increase tropospheric column ozone by 3.5–5 DU (10–13%) (Brasseur et al., 2006; Kawase et al., 2011).

The baseline scenario, with all ODS and GHG effects included, gives an ozone level in 2100 that is slightly less (by 1 DU) than in 1960 (Figure 5-4, black line). This is generally similar to the CMIP5 CHEM multi-model mean for the RCP6.0 scenario, in which stratospheric column ozone is 4 DU less in 2100 than 1960 (Eyring et al., 2013, see also Section 2.4.1). Scenarios with higher levels of CO_2 and CH_4 may cause ozone to obtain higher globally averaged levels than historically observed despite the fact that N_2O levels contribute several DU of ozone depletion by 2100. This is seen in the CMIP5 multi-model mean for the RCP8.5 scenario, in which global stratospheric column ozone in 2100 is greater (by 2 DU) than in 1960 (Eyring et al., 2013). Also, the Special Report on Emissions Scenarios (SRES) A1B (medium) scenario used in the CCMVal-2 simulations (also used in WMO (2011) and Section 2.4.1 of this Assessment) had higher levels of CO_2 and CH_4, and lower N_2O compared with RCP6.0; these factors all contribute to higher global ozone (by ~5 DU) in the A1B scenario during the mid to late 21st century (compare baseline simulations in Figure 2-24 (A1B) and Figure 5-4 (RCP6.0) which are from the same model). However, the ozone response to GHG forcing will likely differ in altitude and region. For example, the CO_2-driven enhancement of the stratospheric circulation will increase lower stratospheric ozone at middle to high latitudes (Li et al., 2009). While global and midlatitude ozone may rise above historical levels, the CO_2-driven circulation enhancement may lead to ozone decreases in the tropical lower stratosphere after 2050, as seen in the CCMVal-2 and CMIP5 simulations for different GHG scenarios (SPARC CCMVal, 2010; Eyring et al., 2013; see also Sections 2.3.5 and 2.4.1).

It is sometimes argued that the future projected "super-recovery" of stratospheric ozone, which can occur under certain scenarios of CO_2 and CH_4 future increased abundances, is a reason to not be concerned about increasing N_2O. Scientifically however, it is clear that N_2O increases in the future will lead to lower ozone levels (greater depletion) than if anthropogenic N_2O emissions were mitigated. Depending on the particular $CO_2/CH_4/N_2O$ scenario, this may mean that levels of global total ozone before intervention from human emissions will never be attained again, or that there will be a delay in reaching those levels.

5.4.4 Radiative Forcing on Climate

Figure 5-6 shows the impacts of the various mitigation scenarios on the radiative forcing on climate from the ODS halocarbons. These curves represent the same scenarios as were shown in Figure 5-3 for their impacts on EESC. The relative shapes and positions of the various scenarios are similar to their EESC contributions. It is currently projected that ODS halocarbon climate forcing will decline from its current peak of 0.33 W m^{-2} to close to 0.1 W m^{-2} by 2100, with little dependence on the particular scenario because of controls already adopted under the Montreal Protocol. In the next few decades, the particular scenario can make a somewhat larger impact on radiative forcing reductions compared with the baseline scenario. One of the consequences of the controls on ODSs is that HFCs, climate forcing agents themselves, have become prevalent replacement compounds. These are discussed in the next section. Velders and Daniel (2014) have quantified the RF uncertainties for a scenario very similar to the baseline scenario considered here. They considered uncertainties in a wide variety of factors that go into estimating past and future concentrations, as well as a 5% uncertainty in the radiative efficiency of each compound. That analysis suggests a 2-σ uncertainty of about ±0.02 W m^{-2} from the present through 2100, when considering the "most likely" range of lifetimes. This uncertainty is controlled primarily by the radiative efficiency uncertainty in the past and current time, while lifetime uncertainties dominate further in the future.

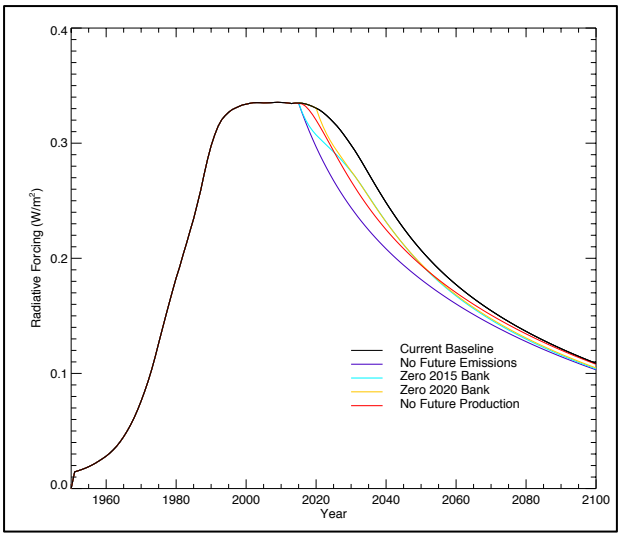

Figure 5-6. Time series of historical and projected radiative forcing from long-lived ODS halocarbons. The radiative forcing projections for the primary mitigation scenarios considered in this Assessment are also shown.

Figure 5-7 shows the derived direct radiative forcing on climate from 2010 to 2050 due to ODSs and other compounds (note that there would be additional indirect forcing due to effects on ozone). The top panel shows the RF due to CFCs and HCFCs to 2050 based on assuming the emissions follow the Montreal Protocol (RF values from Annex II of IPCC, 2013).

The second panel shows the RF for HFCs under various assumptions and demonstrates that increasing RF from HFCs could essentially compensate (or more than compensate) for the decrease in RF from ODSs. The RF curves for HFCs for the RCP scenarios are based on IPCC (2013); these scenarios give lower RFs than those from Velders et al. (2009). Another scenario projecting HFCs growth is taken from Gschrey et al. (2011), which used various sources of information, including the Gross Domestic Product (GDP) and population data underlying the SRES scenarios (IPCC, 2000). Much larger RFs are given in the High and Low scenarios from Velders et al. (2009), which were also based on GDP and population data underlying the SRES scenarios, plus other information, including: the rapid observed growth in demand, substantiated by atmospheric observations; information about products and equipment using HCFCs and HFCs in developing countries; reported increases in consumption of HCFCs in developing countries; replacement patterns of HCFCs by HFCs as reported in developed countries; accelerated phase-out schedules of HCFCs in developed and developing countries; and increases in reported use of HFC-134a in mobile air conditioning in developed and developing countries. The Velders et al. (2009) High scenario describes what happens if the developing world follows the same path in transitioning from CFCs and HCFCs to HFCs (and not-in-kind alternatives) as we have seen in the developed world in the past decade (up to 2009). This in combination with large population and economic

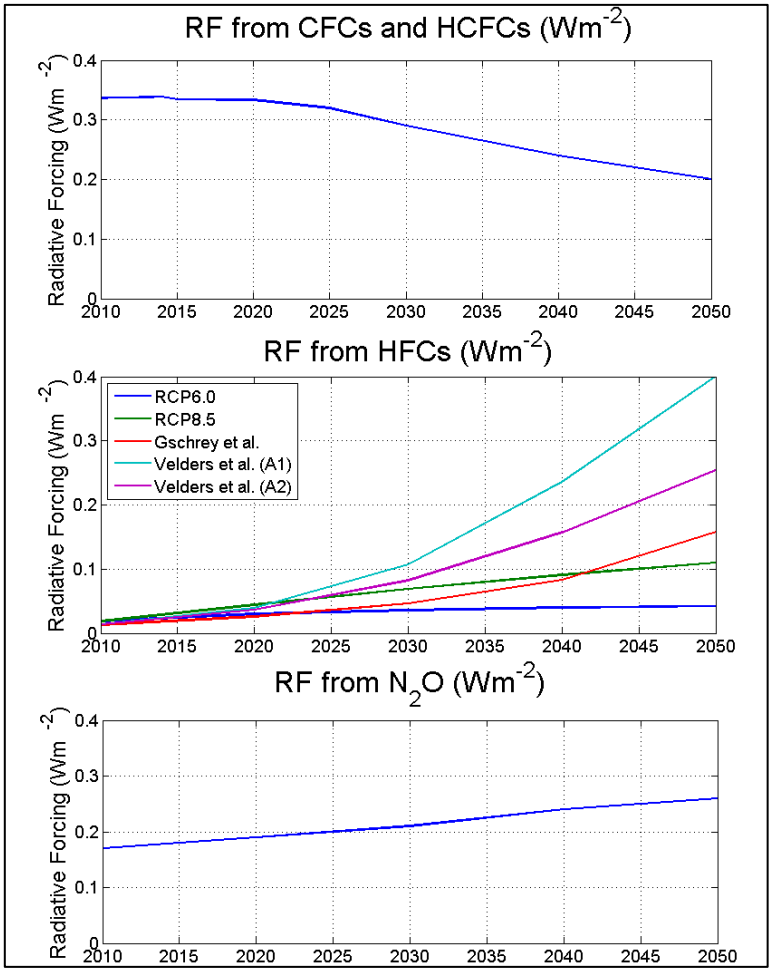

Figure 5-7. Radiative forcing (given as Effective RF) projections for CFCs and HCFCs (following the Montreal Protocol) and the degree to which these decreases might be offset by HFC and N_2O increases. Except for some of the HFC scenarios, the values are based on the scenarios used in Annex II of IPCC (2013). The HFC scenarios represent a range of assumptions and calculations (e.g., see Velders et al. 2009; Gschrey et al., 2011). The Velders et al. A1 and A2 scenarios correspond to the high and low scenarios, respectively, used in Figure 5-8.

growth result in a larger RF for HFCs. If more alternative (low GWP) technologies get a larger market, share the contributions of HFCs to RF will be smaller than in this scenario.

The bottom panel shows the projected growth in RF from N_2O based on the RCP6.0 scenario from IPCC (2013). The increase in N_2O concentration for this scenario results in a direct increase in RF of about 0.09 W m^{-2} by 2050 relative to 2010 (from 0.17 to 0.26 W m^{-2}). This is smaller than, but comparable to, the decrease in RF from ODSs over this time period. By comparison the RF changes for CO_2 and CH_4 for the same scenario over this time period are 1.1 (from 1.8 to 2.9) and 0.05 (from 0.48 to 0.53) W m^{-2}, respectively.

5.4.5 Replacements for High-GWP HFCs

The special report on HFCs by UNEP (2011) found that the climate benefits of the Montreal Protocol could be offset by future increases in the use of the HFCs with longer lifetimes and higher GWPs (those with GWP 100-year values greater than 1000, e.g., including HFC-134a, -143a, and -125). While HFCs are not currently a significant contributor to radiative forcing on climate, they could become important within the next few decades if no action is taken. Switching away from the use of such higher-GWP HFCs to alternatives with much lower GWPs could effectively reduce the effects of halocarbons on climate by 2050. In WMO (2011), a set of different scenarios was considered based on Velders et al. (2009, 2012) that show the phase-out of the higher-GWP HFCs could be an important contributor to reducing future radiative forcing. The analyses can be taken a step further (Wuebbles et al., 2013) by examining a realistic mix of compounds for replacing the uses of the higher-GWP HFCs. As stated in the previous section, the Velders et al. studies assumed growth in HFC use is much larger than in the IPCC (2013) analyses.

Various unsaturated halogenated hydrocarbons with very short atmospheric lifetimes have been recently proposed as substitutes for HCFCs (which are now being phased out under the Montreal Protocol) and longer-lived HFCs. These short-lived substances are expected to have extremely small effects on tropospheric and stratospheric ozone and on climate. Among the possible replacement chemical

compounds are (*E*)-CHCl=CHCF$_3$ (tCFP or HFO-1233zd; included in the ODP analyses in Table 5-3) and at least six possible HFOs: 2,3,3,3-tetrafluoropropene (CF$_3$CF=CH$_2$, HFO-1234yf); (*E*)-1,3,3,3-tetrafluoropropene ((*E*)-CHF=CHCF$_3$, HFO-1234ze(E)); (*Z*)-1,3,3,3-tetrafluoropropene ((*Z*)-CHF=CHCF$_3$, HFO-1234ze(Z)); (*Z*)-1,2,3,3,3-pentafluoropropene ((*Z*)-CF$_3$CF=CHF, HFO-1225ye(Z)); (*E*)-1,2,3,3,3-pentafluoropropene ((*E*)-CF$_3$CF=CHF, HFO-1225ye(E)); and (Z)-1,1,1,4,4,4-hexafluoro-2-butene ((Z)-CF$_3$CH=CHCF$_3$, HFO-1336mzz-Z). In the possible uses, HFO-1234yf can serve as a mobile air conditioning refrigerant; HFO-1234ze(E) can be used as a blowing agent and propellant; HFO-1233zd and HFO-1336mzz-Z can serve as blowing agents; HFO-1234ze(Z) has been suggested as a refrigerant (Brown et al., 2009); HFO-1225ye(Z) and -1225ye(E) have been also proposed as refrigerants (Hurley et al., 2007). The prospect of using HFO-1234yf and HFO-1234ze(E) has been discussed in the literature (UNEP, 2011; Velders et al., 2012). Three-dimensional modeling analyses by Wuebbles et al. (2013) show HFO-1233zd to have an atmospheric lifetime (for realistic locations of emissions) of 30.5 days, while the HFOs have lifetimes ranging from 9.2 days for HFO-1225ye to 17.3 days for HFO-1234ze. The 100-year GWPs range from 0.9 to 4.7 for these six compounds, assuming emissions occur spatially corresponding to current uses of HFCs (Wuebbles et al., 2013).

Scenarios for replacing HFCs with the low-GWP alternatives are developed in Wuebbles et al. (2013) based on the demand for such compounds (e.g., see Velders et al., 2009) with the assumptions that (i) production and consumption of HFCs decrease linearly starting in 2015; (ii) production and consumption of HFC-32, -125, -143a, -245fa, and -365mfc decrease to zero in 2035; (iii) production and consumption of HFC-134a decrease to zero in 2025; (iv) the demand for refrigerants from use of HFC-32, -125, -134a, and -143a is replaced by HFO-1234yf, -1234ze(Z), -1225ye(Z), or -1225ye(E) on a per mass basis; (v) the demand for blowing agents from the use of HFC-152a, -245fa, and -365mfc is replaced by HFO-1234ze(E), or HFO-1233zd on a per mass basis. With these assumptions, the red lines in Figure 5-8 show the radiative forcing of the low-GWP alternatives in 2050 is between 0.00026 and 0.00080 W m^{-2}. As a result, radiative forcing resulting from future requirements for refrigerants and blowing agents is significantly reduced. In contrast, the monotonically increasing radiative forcing of long-lived HFCs (the black lines in Figure 5-8 for low and high HFC growth scenarios from Velders et al., 2009) reaches 0.25 to 0.40 W m^{-2} in 2050. The blue lines in Figure 5-8 show the radiative forcing of the long-lived HFCs for scenarios transitioning to low-GWP alternatives; the HFC radiative forcing for this assumption peaks at 0.046 to 0.053 W m^{-2} near 2030 and decreases to 0.026 to 0.031 W m^{-2} in 2050. The resulting reduction in radiative forcing on climate in 2030 is significant, between 0.04 and 0.07 W m^{-2} (Wuebbles et al., 2013), comparable to the savings of the regulatory black carbon reduction measures, or a sizable fraction of the savings of the technological black carbon reduction measures and CH$_4$ reduction measures recently suggested (Shindell et al., 2012). By 2050, Figure 5-8 shows that the savings could be as large as 0.37 W m^{-2}. Comparably, a recent study by Rigby et al. (2014) suggests that reducing HFC use under the Montreal Protocol could reduce radiative forcing in 2050 by 0.05 to 0.24 W m^{-2}. Some fraction of the replacements could possibly be not-in-kind gases, leading to the possibility for even more reduction in radiative forcing (if those replacements are not greenhouse gases).

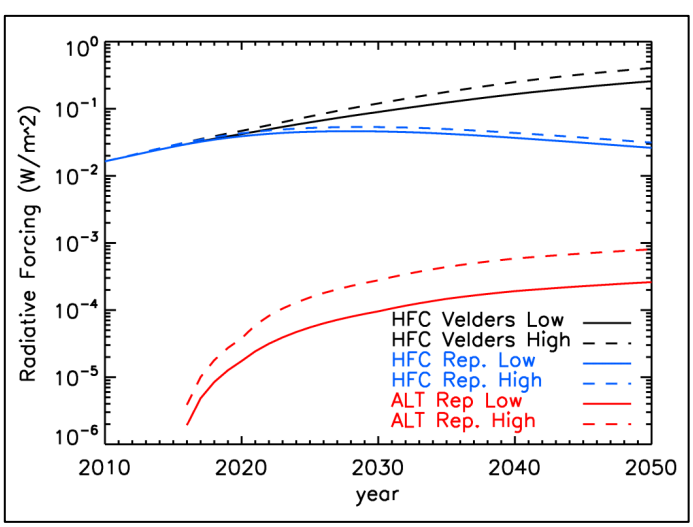

Figure 5-8. Radiative forcing (in W m^{-2}) from 2010–2050 for various scenarios of future HFC usage: high-GWP HFC scenario (Velders et al., 2009; black lines); scenarios for transitioning long-lived high-GWP HFCs to low-GWP alternatives (based on Wuebbles et al., 2013; blue lines) and low-GWP replacement scenarios based on the use of low-GWP alternative compounds (based on Wuebbles et al., 2013; red lines).

Radiative forcing of HFCs would soon be less than that of today if the current mix of HFCs (mean lifetime ~15 yrs) were hypothetically to be entirely replaced within the next few years by a mix of replacements with lifetimes less than 1 month (Velders et al., 2012) but such a rapid transition may be difficult, if not unrealistic. Assuming the slower transition process, the blue lines in Figure 5-8, the radiative forcing due to long-lived HFCs emitted would essentially be the only remaining meaningful direct climate forcing contribution due to the chemicals used in refrigeration and blowing agents. Nonetheless, the quicker the long-lived HFCs are phased out, the less radiative forcing there would be.

Because the applications using HFCs are, in general, less emissive than were those of the CFCs at the same stage, the amount of HFCs stored in existing applications (banks) is projected to be a much larger fraction of annual production (or cumulative production) than was the case for CFCs. As a result, there is an additional future commitment to climate change from HFC banks that would not be apparent if only radiative forcing for a given period is analyzed (Velders et al., 2014). By 2050, HFC banks are estimated to grow to 40 and 65 $GtCO_2$-eq in the high and low scenarios from Velders et al. (2009). In both cases, these bank sizes are approximately 25% of the cumulative production through 2050. Figure 5-9 shows the cumulative production and emissions and their comparisons with the bank sizes for the two scenarios from Velders et al. (2009). While the emissions and forcing from these scenarios are higher than for other published projections, the larger relative importance of the banks compared with the historical CFC situation should hold for all reasonable HFC scenarios. The implication is that earlier phase-outs of HFC production may play a somewhat larger role in mitigating climate forcing than previous estimates have suggested.

Figure 5-9. Projected growth of HFC production, emissions, and banks for two future scenarios (Velders et al., 2014). Figures show the magnitude of the future banks relative to cumulate emissions and production. For example, a phase-out of production in 2020 rather than 2030 would lead to a production decrease of 27–42 $GtCO_2$-eq, of which 8–15 $GtCO_2$ would have remained in banks at the end of that decade and 19–27 $GtCO_2$-eq would have been emitted to the atmosphere during that decade.

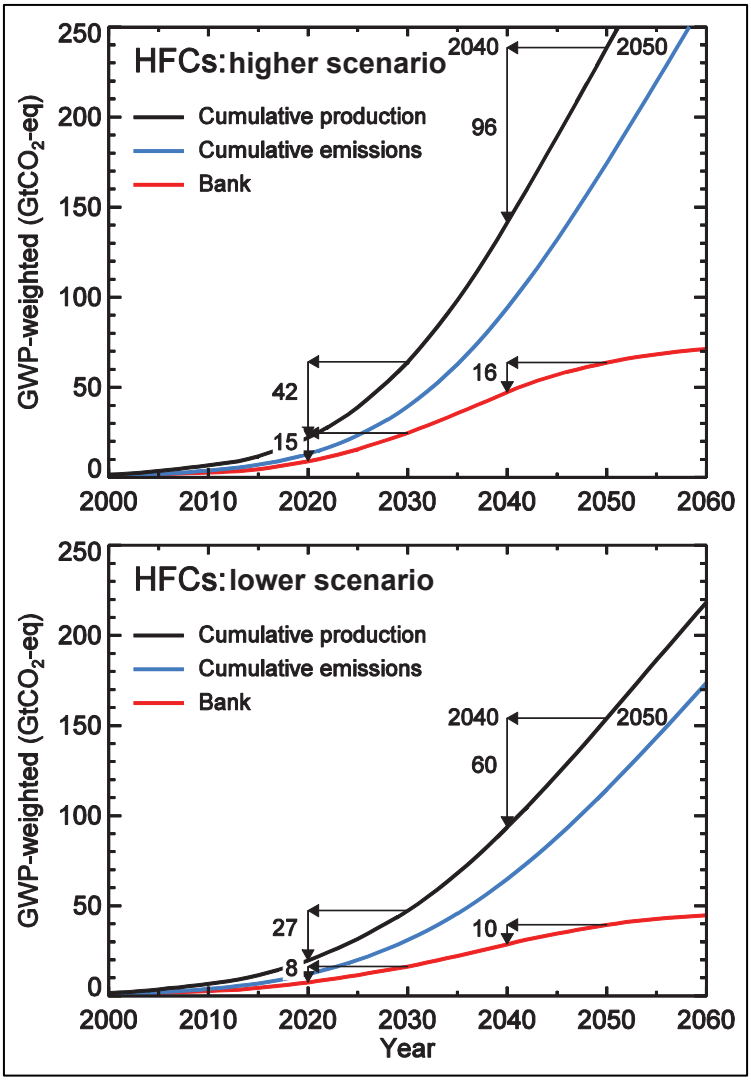

REFERENCES

Anderson, J.G., D.M. Wilmouth, J.B. Smith, and D.S. Sayres, UV dosage levels in summer: Increased risk of ozone loss from convectively injected water vapor, *Science*, *337* (6096), 835-839, doi: 10.1126/science.1222978, 2012.

Azar, C., and D.J.A. Johansson, On the relationship between metrics to compare greenhouse gases – the case of IGTP, GWP and SGTP, *Earth Syst. Dynam.*, *3* (2), 139-147, doi: 10.5194/esd-3-139-2012, 2012.

Benesch, J.A., M.S. Gustin, G.R. Cramer, and T.M. Cahill, Investigation of effects of trifluoroacetate on vernal pool ecosystems, *Environ. Toxicol. Chem.*, *21* (3), 640-647, doi: 10.1002/etc.5620210325, 2002.

Boucher, O., Comparison of physically-and economically-based CO_2-equivalences for methane, *Earth Syst. Dynam.*, *3* (1), 49-61, doi: 10.5194/esd-3-49-2012, 2012.

Boucher, O., P. Friedlingstein, B. Collins, and K.P. Shine, The indirect global warming potential and global temperature change potential due to methane oxidation, *Env. Res. Lett.*, *4* (4), 044007, doi: 10.1088/1748-9326/4/4/044007, 2009.

Boutonnet, J.C., P. Bingham, D. Calamari, C. de Rooij, J. Franklin, T. Kawano, J.-M. Libre, A. McCulloch, G. Malinverno, J.M. Odom, G.M. Rusch, K. Smythe, I. Sobolev, R. Thompson, and J.M. Tiedje, Environmental risk assessment of trifluoroacetic acid, *Hum. Ecol. Risk Assess.*, *5* (1), 59-124, 1999.

Brasseur, G., and S. Solomon, *Aeronomy of the Middle Atmosphere*, 3rd ed., Dordrecht, The Netherlands, 2005.

Brasseur, G.P., M. Schultz, C. Granier, M. Saunois, T. Diehl, M. Botzet, E. Roeckner, and S. Walters, Impact of climate change on the future chemical composition of the global troposphere*, J. Clim.*, *19* (16), 3932-3951, doi: 10.1175/JCLI3832.1, 2006.

Brasseur, G.P., A. Gettelman, M. Jacobson, P. Minnis, J. Penner, R. Prinn, H.B. Selkirk, N. Unger, H.-W. Wong, D.J. Wuebbles, P. Yang, R. Halthore, and S.D. Jacob, *Aviation Climate Change Research Initiative (ACCRI) Phase II Report*, Federal Aviation Administration, Washington, D.C., 2013.

Bridgeman, C.H., J.A. Pyle, and D E. Shallcross, A three-dimensional model calculation of the ozone depletion potential of 1-bromopropane (1-C_3H_7Br), *J. Geophys. Res.*, *105* (D21), 26493-26502, doi: 10.1029/2000 JD900293, 2000.

Brioude, J., R.W. Portmann, J.S. Daniel, O.R. Cooper, G.J. Frost, K.H. Rosenlof, C. Granier, A.R. Ravishankara, S.A. Montzka, and A. Stohl, Variations in ozone depletion potentials of very short-lived substances with season and emission region, *Geophys. Res. Lett.*, *37* (19), L19804, doi: 10.1029/2010GL044856, 2010.

Brown, J.S., C. Zilio, and A. Cavallini, The fluorinated olefin R-1234ze(Z) as a high-temperature heat pumping refrigerant, *International Journal of Refrigeration*, *32* (6), 1412-1422, doi: 10.1016/j.ijrefrig.2009.03.002, 2009.

Brühl, C., J. Lelieveld, P.J. Crutzen, and H. Tost, The role of carbonyl sulphide as a source of stratospheric sulphate aerosol and its impact on climate, *Atmos. Chem. Phys.*, *12* (3), 1239-1253, doi: 10.5194/acp-12-1239-2012, 2012.

Canty, T., N.R. Mascioli, M.D. Smarte, and R.J. Salawitch, An empirical model of global climate – Part 1: A critical evaluation of volcanic cooling, *Atmos. Chem. Phys.*, *13* (8), 3997-4031, doi: 10.5194/acp-13-3997-2013, 2013.

Crutzen, P.J., Albedo enhancement by stratospheric sulfur injections: A contribution to resolve a policy dilemma?, *Clim. Change*, *77* (3-4), 211-220, doi: 10.1007/s10584-006-9101-y, 2006.

Daniel, J.S., S. Solomon, and D.L. Albritton, On the evaluation of halocarbon radiative forcing and global warming potentials, *J. Geophys. Res.*, *100* (D1), 1271-1285, 1995.

Daniel, J.S., E.L. Fleming, R.W. Portmann, G.J.M. Velders, C.H. Jackman, and A.R. Ravishankara, Options to accelerate ozone recovery: Ozone and climate benefits, *Atmos. Chem. Phys.*, *10* (16), 7697-7707, doi: 10.5194/ acp-10-7697-2010, 2010.

Davis, S.M., and K.H. Rosenlof, A multidiagnostic intercomparison of tropical-width time series using reanalyses and satellite observations, *J. Climate*, *25* (4), 1061-1078, doi: 10.1175/JCLI-D-11-00127.1, 2012.

Dessens, O., G. Zeng, N. Warwick, and J. Pyle, Short-lived bromine compounds in the lower stratosphere; impact of climate change on ozone, *Atmos. Sci. Lett.*, *10* (3), 201-206, doi: 10.1002/asl.236, 2009.

Dessler, A.E., M.R. Schoeberl, T. Wang, S.M. Davis, and K.H. Rosenlof,, Stratospheric water vapor feedback, *Proc. Natl. Acad. Sci.*, *110* (45), 18087-18091, doi: 10.1073/pnas.1310344110, 2013.

Eyring, V., J.M. Arblaster, I. Cionni, J. Sedláček, J. Perlwitz, P.J. Young, S. Bekki, D. Bergmann, P. Cameron-Smith, W.J. Collins, G. Faluvegi, K.-D. Gottschaldt, L.W. Horowitz, D.E. Kinnison, J.-F. Lamarque, D.R. Marsh, D. Saint-Martin, D.T. Shindell, K. Sudo, S. Szopa, and S. Watanabe, Long-term ozone changes and associated climate impacts in CMIP5 simulations, *J. Geophys. Res.*, *118* (10), 5029-5060, doi: 10.1002/jgrd. 50316, 2013.

FAA (Federal Aviation Administration), *2011 U.S. Commercial Space Transportation Developments and Concepts:*

Vehicles, Technologies, and Spaceports, 103 pp., Washington D.C., http://www.faa.gov/about/office_org/headquarters_offices/ast/media/111355.pdf, 2011.

FAA (Federal Aviation Administration), *2013 Commercial Space Transportation Forecasts*, FAA Commercial Space Transportation (AST) and the Commercial Space Transportation Advisory Committee (COMSTAC), 96 pp., Washington D.C., http://www.faa.gov/go.ast, 2013.

FAO (Food and Agriculature Organisation), *The State of World Fisheries and Aquaculture 2012*, Food and Agriculture Organisation of the United Nations, Fisheries and Aquaculture Department, 209 pp., Rome, http://www.fao.org/docrep/016/i2727e/i2727e00.htm, 2012.

Feng, W., M.P. Chipperfield, S. Dhomse, B.M. Monge-Sanz, X. Yang, K. Zhang, and M. Ramonet, Evaluation of cloud convection and tracer transport in a three-dimensional chemical transport model, *Atmos. Chem. Phys.*, *11* (12), 5783-5803, doi: 10.5194/acp-11-5783-2011, 2011.

Ferraro, A.J., E.J. Highwood, and A.J. Charlton-Perez, Stratospheric heating by potential geoengineering aerosols, *Geophys. Res. Lett.*, *38* (24), L24706, doi: 10.1029/2011GL049761, 2011.

Fleming, E.L., C.H. Jackman, R.S. Stolarski, and A.R. Douglass, A model study of the impact of source gas changes on the stratosphere for 1850-2100, *Atmos. Chem. Phys.*, *11* (16), 8515-8541, doi: 10.5194/acp-11-8515-2011, 2011.

Free, M., and J. Lanzante, Effect of volcanic eruptions on the vertical temperature profile in radiosonde data and climate models, *J. Clim.*, *22* (11), 2925-2939, doi: 10.1175/2008JCLI2562.1, 2009.

Gillett, N.P., and H.D. Matthews, Accounting for carbon cycle feedbacks in a comparison of the global warming effects of greenhouse gases, *Environ. Res. Lett.*, *5* (3), 034011, doi: 10.1088/1748-9326/5/3/034011, 2010.

Graf, H.-F., B. Langmann, and J. Feichter, The contribution of Earth degassing to the atmospheric sulfur budget, *Chemical Geology*, *147* (1-2), 131-145, doi: 10.1016/S0009-2541(97)00177, 1998.

Grooß, J.-U. and R. Müller, Do cosmic-ray-driven electron-induced reactions impact stratospheric ozone depletion and global climate change?, *Atmos. Environ.*, *45* (20), 3508-3514, doi: 10.1016/j.atmosenv.2011.03.059, 2011.

Gschrey, B., W. Schwarz, C. Elsner, and R. Engelhardt, High increase of global F-gas emissions until 2050, *Greenhouse Gas Measurement and Management, 1* (2), 85-92, doi: 10.1080/20430779.2011.579352, 2011.

Haigh, J.D., and J.A. Pyle, A two-dimensional calculation including atmospheric carbon dioxide and stratospheric ozone, *Nature*, *279*, 222-224, doi: 10.1038/279222a0, 1979.

Harris, N.R, J.C. Farman, and D.W. Fahey, Comment on "Effects of cosmic rays on atmospheric chlorofluorocarbon dissociation and ozone depletion," *Phys. Rev. Lett.*, *89* (21), 219801, doi: 10.1103/PhysRevLett.89.219803, 2002.

Heckendorn, P., D. Weisenstein, S. Fueglistaler, B.P. Luo, E. Rozanov, M. Schraner, L.W. Thomason, and T. Peter, Impact of geoengineering aerosols on stratospheric temperature and ozone, *Env. Res. Lett.*, *4* (4), 045108, doi: 10.1088/1748-9326/4/4/045108, 2009.

Henne, S., D.E. Shallcross, S. Reimann, P. Xiao, D. Brunner, S. O'Doherty, and B. Buchmann, Future emissions and atmospheric fate of HFC-1234yf from mobile air conditioners in Europe, *Environ. Sci. Technol.*, *46* (3), 1650-1658, doi: 10.1021/es2034608, 2012.

Hodnebrog, Ø., M. Etminan, J.S. Fuglestvedt, G. Marston, G. Myhre, C.J. Nielsen, K.P. Shine, and T.J. Wallington, Global warming potentials and radiative efficiencies of halocarbons and related compounds: A comprehensive review, *Rev. Geophys.*, *51* (2), 300-378, doi: 10.1002/rog.20013, 2013.

Holmes, C.D., Q. Tang, and M.J. Prather, Uncertainties in climate assessment for the case of aviation NO, *Proc. Natl. Acad. Sci. USA*, *108* (27), 10997-11002, doi: 10.1073/pnas.1101458108, 2011.

Hossaini, R., M.P. Chipperfield, S. Dhomse, C. Ordóñez, A. Saiz-Lopez, N.L. Abraham, A. Archibald, P. Braesicke, P. Telford, N. Warwick, X. Yang, and J. Pyle, Modelling future changes to the stratospheric source gas injection of biogenic bromocarbons, *Geophys. Res. Lett.*, *39* (20), L20813, doi: 10.1029/2012GL053401, 2012a.

Hossaini, R., M.P. Chipperfield, W. Feng, T.J. Breider, E. Atlas, S.A. Montzka, B.R. Miller, F. Moore, and J. Elkins, The contribution of natural and anthropogenic very short-lived species to stratospheric bromine, *Atmos. Chem. Phys.*, *12* (1), 371-380, doi: 10.5194/acp-12-371-2012, 2012b.

Hoyle, C.R., V. Marécal, M.R. Russo, G. Allen, J. Arteta, C. Chemel, M.P. Chipperfield, F. D'Amato, O. Dessens, W. Feng, J.F. Hamilton, N.R.P. Harris, J.S. Hosking, A.C. Lewis, O. Morgenstern, T. Peter, J.A. Pyle, T. Reddmann, N.A.D. Richards, P.J. Telford, W. Tian, S. Viciani, A. Volz-Thomas, O. Wild, X. Yang, and G. Zeng, Representation of tropical deep convection in atmospheric models - Part 2: Tracer transport, *Atmos. Chem. Phys.*, *11* (15), 8103-8131, doi: 10.5194/acp-11-8103-2011, 2011.

Hurley, M.D., J.C. Ball, and T.J. Wallington, Atmospheric chemistry of the Z and E isomers of $CF_3CF{=}CHF$; Kinetics, mechanisms, and products of gas-phase reactions with Cl atoms, OH radicals, and O_3, *J. Phys. Chem. A*, *111* (39), 9789-9795, doi: 10.1021/jp0753530, 2007.

IPCC (Intergovernmental Panel on Climate Change), *Climate Change: The IPCC Scientific Assessment*, edited by J.T. Houghton, G.J. Jenkins, and J.J. Ephraums, 364 pp., Cambridge University Press, Cambridge, U.K., 1990.

IPCC (Intergovernmental Panel on Climate Change), *Climate Change*, *1994: Radiative Forcing of Climate Change and an Evaluation of the IPCC IS92 Emission Scenarios*, edited by J.T. Houghton, L.G. Meira Filho, J. Bruce, H. Lee, B.A. Callander, E. Haites, N. Harris, and K. Maskell, 339 pp., Cambridge University Press, Cambridge, U.K., 1995.

IPCC (Intergovernmental Panel on Climate Change), *Climate Change 1995: The Science of Climate Change*, edited by J.T. Houghton, L.G. Meira Filho, B.A. Callander, N. Harris, A. Kattenberg, and K. Maskell, 572 pp., Cambridge University Press, Cambridge, U.K., 1996.

IPCC (Intergovernmental Panel on Climate Change), *Aviation and the Global Atmosphere*, A Special Report of the Intergovernmental Panel on Climate Change, edited by J.E. Penner, D. Lister, D.J. Griggs, D.J. Dokken, and M. McFarland, 373 pp., Cambridge University Press, Cambridge, U.K., doi: 10.2277/0521664047, 1999.

IPCC (Intergovernmental Panel on Climate Change), *Emissions Scenarios. A Special Report of Working Group III of the Intergovernmental Panel on Climate Change*, edited by N. Nakicenovic and R. Swart, 570 pp., Cambridge University Press, Cambridge, U.K., and New York, NY, U.S.A., 2000.

IPCC (Intergovernmental Panel on Climate Change), *Climate Change 2001: The Scientific Basis*, *Contribution of Working Group I to the Third Assessment Report of the Intergovernmental Panel on Climate Change*, edited by J.T. Houghton, Y. Ding, D.J. Griggs, M. Noguer, P.J. van der Linden, X. Dai, K. Maskell, and C.A. Johnson, 881 pp., Cambridge University Press, Cambridge, U.K., 2001.

IPCC (Intergovernmental Panel on Climate Change), *Climate Change 2007: The Physical Science Basis: Contribution of Working Group I to the Fourth Assessment Report of the Intergovernmental Panel on Climate Change*, edited by Solomon, S., D. Qin, M. Manning, Z. Chen, M. Marquis, K.B. Averyt, M. Tignor, and H.L. Miller, 996 pp., Cambridge University Press, Cambridge, U.K., and New York, NY, U.S.A., 2007.

IPCC (Intergovernmental Panel on Climate Change), *Summary Report of the IPCC Expert Meeting on the Science of Alternative Metrics*, 18–20 March 2009, Oslo, Norway. IPCC-XXX/Doc.13 (31.III.2009), http://www.ipcc.ch/meetings/session30/doc13.pdf, 2009.

IPCC (Intergovernmental Panel on Climate Change), *Climate Change 2013: The Physical Science Basis: Contribution of Working Group I to the Fifth Assessment Report of the Intergovernmental Panel on Climate Change*, edited by T.F. Stocker, D. Qin, G.-K. Plattner, M. Tignor, S.K. Allen, J. Boschung, A. Nauels, Y. Xia, V. Bex, and P.M. Midgley, 1535 pp., Cambridge University Press, Cambridge, UK and New York, NY, USA, 2013.

IPCC/TEAP (Intergovernmental Panel on Climate Change/Technology and Economic Assessment Panel), *IPCC/TEAP Special Report on Safeguarding the Ozone Layer and the Global Climate System: Issues Related to Hydrofluorocarbons and Perfluorocarbons*, prepared by Working Groups I and III of the Intergovernmental Panel on Climate Change, and the Technical and Economic Assessment Panel, Cambridge University Press, Cambridge, U.K. and New York, NY, U.S.A., 2005.

John, J.G., A.M. Fiore, V. Naik, L.W. Horowitz, and J.P. Dunne, Climate versus emission drivers of methane lifetime against loss by tropospheric OH from 1860–2100, *Atmos. Chem. Phys.*, *12* (24), 12021-12036, doi: 10.5194/acp-12-12021-2012, 2012.

Joos, F., R. Roth J.S. Fuglestvedt G.P. Peters, I.G. Enting, W. von Bloh, V. Brovkin, E.J. Burke, M. Eby, N.R. Edwards, T. Friedrich, T.L. Frölicher, P.R. Halloran, P.B. Holden, C. Jones, T. Kleinen, F.T. Mackenzie, K. Matsumoto, M. Meinshausen, G.-K. Plattner, A. Reisinger, J. Segschneider, G. Shaffer, M. Steinacher, K. Strassmann, K. Tanaka, A. Timmermann, and A.J. Weaver, Carbon dioxide and climate impulse response functions for the computation of greenhouse gas metrics: A multi-model analysis, *Atmos. Chem. Phys.*, *13* (5), 2793-2825, doi: 10.5194/acp-13-2793-2013, 2013.

Katz, J.I., Stratospheric albedo modification, *Energy Environ. Sci.*, *3* (11), 1634-1644, doi: 10.1039/C002441D, 2010.

Kawase, H., T. Nagashima, K. Sudo, and T. Nozawa, Future changes in tropospheric ozone under Representative Concentration Pathways (RCPs), *Geophys. Res. Lett.*, *38* (5), L05801, doi: 10.1029/2010GL046402, 2011.

Kravitz, B., A. Robock, O. Boucher, H. Schmidt, K.E. Taylor, G. Stenchikov, and M. Schulz, The Geoengineering Model Intercomparison Project (GeoMIP), *Atm. Sci. Lett.*, *12* (2), 162-167, doi: 10.1002/asl.316, 2011.

Lary, D.J., Catalytic destruction of stratospheric ozone, *J. Geophys. Res.*, *102* (D17), 21515-21526, doi: 10.1029/97JD00912, 1997.

Laube, J.C., A. Keil, H. Bönisch, A. Engel, T. Röckmann, C.M. Volk, and W.T. Sturges, Observation-based assessment of stratospheric fractional release, lifetimes, and ozone depletion potentials of ten important source gases, *Atmos. Chem. Phys*., *13* (5), 2779-2791, doi: 10.5194/acp-13-2779-2013, 2013.

Lee, D.S., D.W. Fahey, P.M. Forster, P.J. Newton, R.C.N. Wit, L.L. Lim, B. Owen, and R. Sausen, Aviation and global climate change in the 21st century, *Atmos. Environ.*, *43* (22-23), 3520-3537, doi: 10.1016/j.atmosenv.2009.04.024, 2009.

Leedham, E.C., C. Hughes, F.S.L. Keng, S.-M. Phang, G. Malin, and W.T. Sturges, Emission of atmospherically significant halocarbons by naturally occurring and farmed tropical macroalgae, *Biogeosciences*, *10* (6), 3615-3633, doi: 10.5194/bg-10-3615-2013, 2013.

Li, F., R.S. Stolarski, and P.A. Newman, Stratospheric ozone in the post-CFC era, *Atmos. Chem. Phys.*, *9* (6), 2207-2213, doi: 10.5194/acp-9-2207-2009, 2009.

Lu, Q.-B., Cosmic-ray-driven reaction and greenhouse effect of halogenated molecules: Culprits for atmospheric ozone depletion and global climate change, *Int. J. Mod. Phys. B*, *27* (17), 1350073, doi: 10.1142/S0217979213500732, 2013.

Lu, Q.-B., Reply to "Comment on 'Cosmic-ray-driven reaction and greenhouse effect of halogenated molecules: Culprits for atmospheric ozone depletion and global climate change' by Rolf Müller and Jens-Uwe Grooß," *Int. J. Mod. Phys. B*, *28* (13), 1482002, doi: 10.1142/S0217979214820025, 2014.

Luecken, D.J., R.L. Waterland, S. Papasavva, K.N. Taddonio, W.T. Hutzel, J.P. Rugh, and S.O. Andersen, Ozone and TFA impacts in North America from degradation of 2,3,3,3-tetrafluoropropene (HFO-1234yf), a potential greenhouse gas replacement, *Environ. Sci. Technol.*, *44* (1), 343-348, doi: 10.1021/es902481f, 2010.

Miller, B.R., and L.J.M. Kuijpers, Projecting future HFC-23 emissions, *Atmos. Chem. Phys.*, *11* (24), 13259-13267, doi: 10.5194/acp-11-13259-2011, 2011.

Müller, R., and J.-U. Grooß, Comment on "Cosmic-ray-driven reaction and greenhouse effect of halogenated molecules: Culprits for atmospheric ozone depletion and global climate change," *Int. J. Mod. Phys. B*, *28* (13), 1482001, doi: 10.1142/S0217979214820013, 2014.

Myhre, G., D. Shindell, F.-M. Bréon, W. Collins, J. Fuglestvedt, J. Huang, D. Koch, J.-F. Lamarque, D. Lee, B. Mendoza, T. Nakajima, A. Robock, G. Stephens, T. Takemura, and H. Zhang, Anthropogenic and natural radiative forcing, Chapter 8 in *Climate Change 2013: The Physical Science Basis. Contribution of Working Group I to the Fifth Assessment Report of the Intergovernmental Panel on Climate Change*, edited by Stocker, T.F., D. Qin, G.-K. Plattner, M. Tignor, S.K. Allen, J. Boschung, A. Nauels, Y. Xia, V. Bex and P.M. Midgley, Cambridge University Press, Cambridge, U.K. and New York, NY, 2013.

Nagai, T., B. Liley, T. Sakai, T. Shibata, and O. Uchino, Post-Pinatubo evolution and subsequent trend of the stratospheric aerosol layer observed by mid-latitude lidars in both hemispheres, *SOLA*, *6*, 69-72, doi: 10.2151/sola.2010-018, 2010.

Neely III, R.R., O.B. Toon, S. Solomon, J.-P. Vernier, C. Alvarez, J.M. English, K.H. Rosenlof, M.J. Mills, C.G. Bardeen, J.S. Daniel, and J.P. Thayer, Recent anthropogenic increases in SO_2 from Asia have minimal impact on stratospheric aerosol, *Geophys. Res. Lett.*, *40* (5), 999-1004, doi: 10.1002/grl.50263, 2013.

Newman, P.A., E.R. Nash, S.R. Kawa, S.A. Montzka, and S.M. Schauffler, When will the Antarctic ozone hole recover?, *Geophys. Res. Lett.*, *33*, L12814, doi: 10.1029/2005GL025232, 2006.

Newman, P.A., J.S. Daniel, D.W. Waugh, and E.R. Nash, A new formulation of equivalent effective stratospheric chlorine (EESC), *Atmos. Chem. Phys.*, *7* (17), 4537-4522, doi: 10.5194/acp-7-4537-2007, 2007.

Newman, P.A., E.R. Nash, A.R. Douglass, J.E. Nielsen, and R.S. Stolarski, Estimating when the Antarctic ozone hole will recover, in *Twenty Years of Ozone Decline*, *Proceedings of the Symposium for the 20th Anniversary of the Montreal Protocol*, edited by C. Zerefos, G. Contopoulos, and G. Skalkeas, Springer Publishing, Dordrecht, The Netherlands, doi: 10.1007/978-90-481-2469-5, p. 191-200, 2009.

Olivié, D.J.L., and G.P. Peters, Variations in emission metrics due to variation in CO_2 and temperature impulse response functions, *Earth Syst. Dynam.*, *4* (2), 267-286, doi: 10.5194/esd-4-267-2013, 2013.

Olsen, S.C., B.J. Hannegan, X. Zhu, and M.J. Prather, Evaluating ozone depletion from very short-lived halocarbons, *Geophys. Res. Lett.*, *27* (10), 1475-1478, doi: 10.1029/1999GL011040, 2000.

Olsen, S.C., G.P. Brasseur, D.J. Wuebbles, S.R.H. Barrett, H. Dang, S.D. Eastham, M.Z. Jacobson, A. Khodayari, H. Selkirk, A. Sokolov, and N. Unger, Comparison of model estimates of the effects of aviation emissions on atmospheric ozone and methane, *Geophys. Res. Lett.*, *40* (22), 6004-6009, doi: 10.1002/2013GL057660, 2013.

O'Neill, B.C., The jury is still out on global warming potentials, *Clim. Change*, *44* (4), 427-443, doi: 10.1023/A:1005582929198, 2000.

Papadimitriou, V.C., Y.G. Lazarou, R.K. Talukdar, and J.B. Burkholder, Atmospheric chemistry of $CF_3CF{=}CH_2$ and (Z)-$CF_3CF{=}CHF$: Cl and NO_3 rate coefficients, Cl reaction product yields, and thermochemical calculations, *J. Phys. Chem. A*, *115* (2), 167-181, doi: 10.1021/jp110021u, 2011.

Papadimitriou, V.C., M.R. McGillen, S.C. Smith, A.M. Jubb, R.W. Portmann, B.D. Hall, E.L. Fleming, C.H. Jackman, and J.B. Burkholder, 1,2-dichlorohexafluoro-cyclobutane (1,2-c-$C_4F_6Cl_2$, R-316c) a potent ozone

depleting substance and greenhouse gas: Atmospheric loss processes, lifetimes, and ozone depletion and global warming potentials for the (*E*) and (*Z*) stereoisomers, *J. Phys. Chem. A*, *117* (43), 11049-11065, doi: 10.1021/jp407823k, 2013.

Papanastasiou, D.K., N.R. Carlon, J.A. Neuman, E.L. Fleming, C.H. Jackman, and J.B. Burkholder, Revised UV absorption spectra, ozone depletion potentials, and global warming potentials for the ozone-depleting substances CF_2Br_2, CF_2ClBr, and CF_2BrCF_2Br, *Geophys. Res. Lett.*, *40* (2), 464-469, doi: 10.1002/grl.50121, 2013.

Patra, P.K., and M.S. Santhanam, Comment on "Effects of cosmic rays on atmospheric chlorofluorocarbon dissociation and ozone depletion," *Phys. Rev. Lett.*, *89*, 219803, doi: 10.1103/PhysRevLett.89.219803, 2002.

Patten, K.O., and D.J. Wuebbles, Atmospheric lifetimes and Ozone Depletion Potentials of trans-1-chloro-3,3,3-trifluoropropylene and trans-1,2-dichloroethylene in a three-dimensional model, *Atmos. Chem. Phys.*, *10* (22), 10867-10874, doi: 10.5194/acp-10-10867-2010, 2010.

Patten, K.O., V.G. Khamaganov, V.L. Orkin, S.L. Baughcum, and D.J. Wuebbles, OH reaction rate constant, IR absorption spectrum, ozone depletion potentials and global warming potentials of 2-bromo-3,3,3-trifluoropropene, *J. Geophys. Res.*, *116* (D24), D24307, doi: 10.1029/2011JD016518, 2011.

Peters, G.P., B. Aamaas, T. Bernsten, and J.S. Fuglestvedt, The integrated global temperature change potential (iGTP) and relationships between emission metrics, *Environ. Res. Lett.*, *6* (4), 044021, doi: 10.1088/1748-9326/6/4/044021, 2011.

Pisso, I., P.H. Haynes, and K.S. Law, Emission location dependent ozone depletion potentials for very short-lived halogenated species, *Atmos. Chem. Phys.*, *10* (24), 12025-12036, doi: 10.5194/acp-10-12025-2010, 2010.

Pitari, G., V. Aquila, B. Kravitz, A. Robock, S. Watanabe, I. Cionni, N. De Luca, G. Di Genova, E. Mancini, and S. Tilmes, Stratospheric ozone response to sulfate geoengineering: Results from the Geoengineering Model Intercomparison Project (GeoMIP), *J. Geophys. Res.*, *119* (5), 2629-2653, doi: 10.1002/2013JD020566, 2014.

Ploeger, F., G. Günther, P. Konopka, S. Fueglistaler, R. Müller, C. Hoppe, A. Kunz, R. Spang, J.-U. Grooß, and M. Riese, Horizontal water vapor transport in the lower stratosphere from subtropics to high latitudes during boreal summer, *J. Geophys. Res.*, *118* (14), 8111-8127, doi: 10.1002/jgrd.50636, 2013.

Plummer, D.A., J.F. Scinocca, T.G. Shepherd, M.C. Reader, and A.I. Jonsson, Quantifying the contributions of stratospheric ozone changes from ozone depleting substances and greenhouse gases, *Atmos. Chem. Phys.*, *10* (18), 8803-8820, doi: 10.5194/acp-10-8803-2010, 2010.

Pope, F.D., P. Braesicke, R.G. Grainger, M. Kalberer, I.M. Watson, P.J. Davidson, and R.A. Cox, Stratospheric aerosol particles and solar-radiation management, *Nature Clim. Change*, *2* (10), 713-719, doi: 10.1038/nclimate1528, 2012.

Prather, M.J., Lifetimes and eigenstates in atmospheric chemistry, *Geophys. Res. Lett.*, *21* (9), 801-804, doi: 10.1029/94GL00840, 1994.

Prather, M.J., Time scales in atmospheric chemistry: Coupled perturbations to N_2O, NO_y, and O_3, *Science*, *279* (5355), 1339-1341, doi: 10.1126/science.279.5355.1339, 1998.

Prather, M.J., Lifetimes of atmospheric species: Integrating environmental impacts, *Geophys. Res. Lett.*, *29* (22), 2063, doi: 10.1029/2002GL016299, 2002.

Prather, M.J., and J. Hsu, Coupling of nitrous oxide and methane by global atmospheric chemistry, *Science*, *330* (6006), 952-954, doi: 10.1126/science.1196285, 2010.

Pyle, J.A., N.J. Warwick, N.R.P. Harris, M.R. Abas, A.T. Archibald, M.J. Ashfold, K. Ashworth, M.P. Barkley, G.D. Carver, K. Chance, J.R. Dorsey, D. Fowler, S. Gonzi, B. Gostlow, C.N. Hewitt, T.P. Kurosu, J.D. Lee, S.B. Langford, G. Mills, S. Moller, A.R. MacKenzie, A.J. Manning, P. Misztal, M.S.M. Nadzir, E. Nemitz, H.M. Newton, L.M. O'Brien, S. Ong, D. Oram, P.I. Palmer, L.K. Peng, S.M. Phang, R. Pike, T.A.M. Pugh, N.A. Rahman, A.D. Robinson, J. Sentian, A. Abu Samah, U. Skiba, H.E. Ung, S.E. Yong, and P.J. Young, The impact of local surface changes in Borneo on atmospheric composition at wider spatial scales: Coastal processes, land-use change and air quality, *Phil. Trans. R. Soc. B*, *366* (1582), 3210-3224, doi: 10.1098/rstb.2011.0060, 2011.

Randel, W.J., and E.J. Jensen, Physical processes in the tropical tropopause layer and their roles in a changing climate, *Nature Geosci.*, *6* (3), 169-176, doi: 10.1038/ngeo1733, 2013.

Ravishankara, A.R., A.A. Turnipseed, N.R. Jensen, S. Barone, M. Mills, C.J. Howard, and S. Solomon, Do hydrofluorocarbons destroy stratospheric ozone?, *Science*, *263*, 71-75, 1994.

Ravishankara, A.R., J.S. Daniel, and R.W. Portmann, Nitrous oxide (N_2O): The dominant ozone-depleting substance emitted in the 21st century, *Science*, *326* (5949), 123-125, doi: 10.1126/science.1176985, 2009.

Reisinger, A., M. Meinshausen, M. Manning, and G. Bodeker, Uncertainties of global warming metrics: CO_2 and CH_4, *Geophys. Res. Lett.*, *37* (14), L14707, doi: 10.1029/2010GL043803, 2010.

Reisinger, A., M. Meinshausen, and M. Manning, Future changes in global warming potentials under representative concentration pathways, *Environ. Res. Lett.*, *6* (2), 024020, doi: 10.1088/1748-9326/6/2/024020, 2011.

Revell L.E., G.E. Bodeker, P.E. Huck, B.E. Williamson, and E. Rozanov, The sensitivity of stratospheric ozone changes through the 21st century to N_2O and CH_4, *Atmos. Chem. Phys.*, *12* (23), 11309-11317, doi: 10.5194/acp-12-11309-2012, 2012.

Rex, M., I. Wohltmann, T. Ridder, R. Lehmann, K. Rosenlof, P. Wennberg, D. Weisenstein, J. Notholt, K. Krüger, V. Mohr, and S. Tegtmeier, A tropical West Pacific OH minimum and implications for stratospheric composition, *Atmos. Chem. Phys*., *14* (9), 4827-4841, doi: 10.5194/acp-14-4827-2014, 2014.

Rigby, M., R.G. Prinn, S. O'Doherty, B.R. Miller, D. Ivy, J. Mühle, C.M. Harth, P.K. Salameh, T. Arnold, R.F. Weiss, P.B. Krummel, L.P. Steele, P.J. Fraser, D. Young, and P.G. Simmonds, Recent and future trends in synthetic greenhouse gas radiative forcing, *Geophys. Res. Lett*., *41* (7), 2623-2630, doi: 10.1002/2013 GL059099, 2014.

Rosenfield, J.E., and A.R. Douglass, Doubled CO_2 effects on NO_y in a coupled 2D model, *Geophys. Res. Lett.*, *25* (23), 4381-4384, doi: 10.1029/1998GL900147, 2013.

Ross, M., D. Toohey, M. Peinemann, and P. Ross, Limits on the space launch market related to stratospheric ozone depletion, *Astropolitics*, *7* (1), 50-82, doi: 10.1080/14777620902768867, 2009.

Sander, S.P., J. Abbatt, J.R. Barker, J.B. Burkholder, R.R. Friedl, D.M. Golden, R.E. Huie, C.E. Kolb, M.J. Kurylo, G.K. Moortgat, V.L. Orkin and P.H. Wine, *Chemical Kinetics and Photochemical Data for Use in Atmospheric Studies*, *Evaluation Number 17*, JPL Publication 10-6, Jet Propulsion Laboratory, Pasadena, California, http://jpldataeval.jpl.nasa.gov, 2011.

Schofield, R., S. Fueglistaler, I. Wohltmann, and M. Rex, Sensitivity of stratospheric Br_y to uncertainties in very short lived substance emissions and atmospheric transport, *Atmos. Chem. Phys*., *11* (4), 1379-1392, doi: 10.5194/acp-11-1379-2011, 2011.

Schwartz, M.J., W.G. Read, M.L. Santee, N.J. Livesey, L. Froidevaux, A. Lambert, and G.L. Manney, Convectively injected water vapor in the North American summer lowermost stratosphere, *Geophys. Res. Lett.*, *40* (10), 2316-2321, doi: 10.1002/grl.50421, 2013.

Shindell, D., J.C.I. Kuylenstierna, E. Vignati, R. van Dingenen, M. Amann, Z. Klimont, S.C. Anenberg, N. Muller, G. Janssens-Maenhout, F. Raes, J. Schwartz, G. Faluvegi, L. Pozzoli, K. Kupiainen, L. Höglund-Isaksson, L. Emberson, D. Streets, V. Ramanathan, K. Hicks, N.T. Kim Oanh, G. Milly, M. Williams, V. Demkine, and D. Fowler, Simultaneously mitigating near-term climate change and improving human health and food security, *Science*, *335* (6065), 183-189, doi: 10.1126/science.1210026, 2012.

Shine, K.P., J.S. Fuglestvedt, K. Hailemariam, and N. Stuber, Alternatives to the global warming potential for comparing climate impacts of emissions of greenhouse gases, *Clim. Change*, *68,* 281-302, doi: 10.1007/s10584-005-1146-9, 2005.

Shine, K.P., T.K. Berntsen, J.S. Fuglestvedt, R.B. Skeie, and N. Stuber, Comparing the climate effect of emissions of short-and long-lived climate agents, *Phil. Trans. R. Soc. A*, *365* (1856), 1903-1914, doi: 10.1098/rsta.2007. 2050, 2007.

Siddaway, J.M., and S.V. Petelina, Transport and evolution of the 2009 Australian Black Saturday bushfire smoke in the lower stratosphere observed by OSIRIS on Odin, *J. Geophys. Res.*, *116* (D6), D06203, doi: 10.1029/ 2010JD015162, 2011.

Skowron, A., D.S. Lee, and R.R. DeLeòn, The assessment of the impact of aviation NO_x on ozone and other radiative forcing responses - The importance of representing cruise altitudes accurately, *Atmos. Environ*., *74*, 159-168, doi: 10.1016/j.atmosenv.2013.03.034, 2013.

Solomon, S., M. Mills, L.E. Heidt, W.H. Pollock, and A.F. Tuck, On the evaluation of ozone depletion potentials, *J. Geophys. Res.*, *97* (D1), 825-842, doi: 10.1029/91JD02613, 1992.

Solomon, S., R.W. Portmann, R.R. Garcia, L.W. Thomason, L.R. Poole, and M.P. McCormick, The role of aerosol variations in anthropogenic ozone depletion at northern midlatitudes, *J. Geophys. Res.*, *101 (D3)*, 6713-6727, doi: 10.1029/95JD03353, 1996.

Solomon, S., J.S. Daniel, R.R. Neely III, J.-P. Vernier, E.G. Dutton, and L.W. Thomason, The persistently variable "background" stratospheric aerosol layer and global climate change, *Science*, *333* (6044), 866-870, doi: 10.1126/science.1206027, 2011.

SPARC CCMVal (Stratosphere-troposphere Processes And their Role in Climate), *SPARC Report on the Evaluation of Chemistry-Climate Models*, edited by V. Eyring, T.G. Shepherd, and D.W. Waugh, SPARC Report No. 5, WCRP-132, WMO/TD-No. 1526, 478 pp., http://www.atmosp.physics.utoronto.ca/SPARC/ccmval_final/ index.php, 2010.

SPARC (Stratosphere-troposphere Processes And their Role in Climate), *SPARC Report on the Lifetimes of Stratospheric Ozone-Depleting Substances, Their Replacements, and Related Species*, edited by M. Ko, P. Newman, S. Reimann, and S. Strahan, SPARC Report No. 6, WCRP-15/2013, 2013.

Stevenson, D., R. Doherty, M. Sanderson, C. Johnson, B. Collins, and D. Derwent, Impacts of climate change and variability on tropospheric ozone and its precursors, *Faraday Discuss.*, *130*, 41-57, doi: 10.1039/b417412g, 2005.

Sulbaek Andersen, M.P., E.J.K. Nilsson, O.J. Nielsen, M.S. Johnson, M.D. Hurley, and T.J. Wallington, Atmospheric chemistry of *trans*-$CF_3CH{=}CHCl$: Kinetics of the gas-phase reactions with Cl atoms, OH radicals, and O_3, *J. Photochem. Photobio. A: Chemistry*, *199* (1), 92-97, doi: 10.1016/j.jphotochem.2008.05.013, 2008.

Tegtmeier, S., K. Krüger, B. Quack, E.L. Atlas, I. Pisso, A. Stohl, and X. Yang, Emission and transport of bromocarbons: From the West Pacific ocean into the stratosphere, *Atmos. Chem. Phys.*, *12* (22), 10633-10648, doi: 10.5194/acp-12-10633-2012, 2012.

Tilmes, S., R. Müller, and R. Salawitch, The sensitivity of polar ozone depletion to proposed geoengineering schemes, *Science*, *320*, 1201-1204, 2008.

Tilmes, S., R.R. Garcia, D.E. Kinnison, A. Gettelman, and P.J. Rasch, Impact of geoengineered aerosols on the troposphere and stratosphere, *J. Geophys. Res.*, *114*, D12305, doi: 10.1029/2008JD011420, 2009.

Tilmes, S., D.E. Kinnison, R.R. Garcia, R. Salawitch, T. Canty, J. Lee-Taylor, S. Madronich, and K. Chance, Impact of very short-lived halogens on stratospheric ozone abundance and UV radiation in a geo-engineered atmosphere, *Atmos. Chem. Phys.*, *12* (22), 10945-10955, doi: 10.5194/acp-12-10945-2012, 2012.

UNEP (United Nations Environment Programme), *Assessment of Alternatives to HCFCs and HFCs and Update of the TEAP 2005 Supplement Report Data*, Report of the UNEP Technology and Economic Assessment Panel, Task Force Decision XX/8 Report, 129 pp., Nairobi, Kenya, http://ozone.unep.org/teap/Reports/TEAP_Reports/teap-may-2009-decisionXX-8-task-force-report.pdf, 2009.

UNEP (United Nations Environment Programme), *Environmental Effects of Ozone Depletion and Its Interactions with Climate Change: 2010 Assessment*, Report of the UNEP Environmental Effects Assessment Panel, Nairobi, Kenya, http://ozone.unep.org/Assessment_Panels/EEAP/eeap-report2010.pdf, 2010.

UNEP (United Nations Environment Programme), *HFCs: A Critical Link in Protecting Climate and the Ozone Layer*, 36 pp., Nairobi, Kenya, http://www.unep.org/dewa/Portals/67/pdf/HFC_report.pdf, 2011.

UNEP (United Nations Environment Programme), *Volume 2, Additional Information on Alternatives to ODS,* Report of the UNEP Technology and Economic Assessment Panel, ISBN: 978-9966-20-017-4, Nairobi, Kenya, http://ozone.unep.org/Assessment_Panels/TEAP/Reports/TEAP_Reports/TEAP_TaskForce%20XXIV-7-September2013.pdf, 2013.

van Vuuren, D.P., J. Edmonds, M. Kainuma, K. Riahi, A. Thomson, K. Hibbard, G.C. Hurtt, T. Kram, V. Krey, J.-F. Lamarque, T. Masui, M. Meinshausen, N. Nakicenovic, S.J. Smith, and S.K. Rose, The representative concentration pathways: An overview, *Clim. Change*, *109*, 5-31, doi: 10.1007/s10584-011-0148-z, 2011.

Velders, G.J.M., and J.S. Daniel, Uncertainty analysis of projections of ozone-depleting substances: Mixing ratios, EESC, ODPs, and GWPs, *Atmos. Chem. Phys.*, *14* (6), 2757-2776, doi: 10.5194/acp-14-2757-2014, 2014.

Velders, G.J.M., D.W. Fahey, J.S. Daniel, M. McFarland, and S.O. Andersen, The large contribution of projected HFC emissions to future climate forcing, *Proc. Natl. Acad. Sci.*, *106* (27), 10949-10954, doi: 10.1073/pnas.0902817106, 2009.

Velders, G.J.M. A.R. Ravishankara, M.K. Miller, M.J. Molina, J. Alcamo, J.S. Daniel, D.W. Fahey, S.A. Montzka, and S. Reimann, Preserving Montreal Protocol climate benefits by limiting HFCs, *Science*, *335* (6071), 922-923, doi: 10.1126/science.1216414, 2012.

Velders, G.J.M., S. Solomon, and J.S. Daniel, Growth in climate change commitments from HFC banks and emissions, *Atmos. Chem. Phys.*, *14* (9), 4563-4572, doi: 10.5194/acp-14-4563-2014, 2014.

Vernier, J.P., J.P. Pommereau, A. Garnier, J. Pelon, N. Larsen, J. Nielsen, T. Christensen, F. Cairo, L.W. Thomason, T. Leblanc, and I.S. McDermid, Tropical stratospheric aerosol layer from CALIPSO lidar observations, *J. Geophys. Res.*, *114*, D00H10, doi: 10.1029/2009JD011946, 2009.

Vernier, J.-P., L.W. Thomason, J.-P. Pommereau, A. Bourassa, J. Pelon, A. Garnier, A. Hauchecorne, L. Blanot, C. Trepte, D. Degenstein, and F. Vargas, Major influence of tropical volcanic eruptions on the stratospheric aerosol layer during the last decade, *Geophys. Res. Lett.*, *38* (12), L12807, doi: 10.1029/2011GL047563, 2011.

Voigt, Ch., U. Schumann, K. Graf, and K.-D. Gottschaldt, Impact of rocket exhaust plumes on atmospheric composition and climate — an overview, *Progress in Propulsion Physics*, *4*, 657-670, doi: 10.1051/eucass/201304657, 2013.

Voulgarakis, A., V. Naik, J.-F. Lamarque, D.T. Shindell, P.J. Young, M.J. Prather, O. Wild, R.D. Field, D. Bergmann, P. Cameron-Smith, I. Cionni, W.J. Collins, S.B. Dalsøren, R.M. Doherty, V. Eyring, G. Faluvegi,

G.A. Folberth, L.W. Horowitz, B. Josse, I.A. MacKenzie, T. Tagashima, D.A. Plummer, M. Righi, S.T. Rumbold, D.S. Stevenson, S.A. Strode, K. Sudo, S. Szopa, and G. Zeng, Analysis of present day and future OH and methane lifetime in the ACCMIP simulations, *Atmos. Chem. Phys.*, *13* (5), 2563-2587, doi: 10.5194/acp-13-2563-2013, 2013.

Wallington, T.J., W.F. Schneider, D.R. Worsnop, O.J. Nielsen, J. Sehested, W.J. DeBruyn, and J.A. Shorter, The environmental impact of CFC replacements – HFCs and HCFCs, *Environ. Sci. Technol*., *28* (7), 320A-326A, doi: 10.1021/es00056a002, 1994.

Wallington, T.J., M.P. Sulbaek Andersen, and O.J. Nielsen, Estimated photochemical ozone creation potentials (POCPs) of $CF_3CF{=}CH_2$ (HFO-1234yf) and related hydrofluoroolefins (HFOs), *Atmos. Environ*., *44* (11), 1478-1481, doi: 10.1016/j.atmosenv.2010.01.040, 2010.

Wigley, T.M.L., A combined mitigation/geoengineering approach to climate stabilization, *Science*, *314* (5798), 452-454, doi: 10.1126/science.1131728, 2006.

WMO (World Meteorological Organization), *Scientific Assessment of Ozone Depletion: 1994*, Global Ozone Research and Monitoring Project–Report No. 37, Geneva, Switzerland, 1995.

WMO (World Meteorological Organization), *Scientific Assessment of Ozone Depletion: 1998*, Global Ozone Research and Monitoring Project–Report No. 44, Geneva, Switzerland, 1999.

WMO (World Meteorological Organization), *Scientific Assessment of Ozone Depletion: 2002*, Global Ozone Research and Monitoring Project–Report No. 47, Geneva, Switzerland, 2003.

WMO (World Meteorological Organization), *Scientific Assessment of Ozone Depletion: 2006*, Global Ozone Research and Monitoring Project–Report No. 50, 572 pp., Geneva, Switzerland, 2007.

WMO (World Meteorological Organization), *Scientific Assessment of Ozone Depletion: 2010*, *Global Ozone Research and Monitoring Project–Report No. 52*, Geneva, Switzerland, 2011.

Wuebbles, D.J., *The Relative Efficiency of a Number of Halocarbons for Destroying Stratospheric Ozone*, 11 pp., Lawrence Livermore National Laboratory, Livermore, CA, 1981.

Wuebbles, D.J., Chlorocarbon emission scenarios: Potential impact on stratospheric ozone, *Geophys. Res. Lett.*, *88* (C2), 1433-1443, 1983.

Wuebbles, D.J., Weighing functions for ozone depletion and greenhouse gas effects on climate, *Annual Reviews of Energy and the Environment*, *20*, 45-70, doi: 10.1146/annurev.eg.20.110195.000401, 1995.

Wuebbles, D.J., R. Kotamarthi, and K.O. Patten, Updated evaluation of ozone depletion potentials for chlorobromomethane (CH_2ClBr) and 1-bromo-propane ($CH_2BrCH_2CH_3$), *Atmos. Environ.*, *33* (10), 1641-1643, doi: 10.1016/S1352-2310(98)00249-0, 1999.

Wuebbles, D.J., K.O. Patten, M.T. Johnson, and R. Kotamarthi, New methodology for Ozone Depletion Potentials of short-lived compounds: n-Propyl bromide as an example, *J. Geophys. Res.*, *106* (D13), 14551-14571, doi: 10.1029/2001JD900008, 2001.

Wuebbles, D.J., D. Youn, K. Patten, D. Wang, and M. Martinez-Aviles, Metrics for ozone and climate: Three-dimensional modeling studies of ozone depletion potentials and indirect global warming potentials, in *Twenty Years of Ozone Decline*, *Proceedings of the Symposium for the 20th Anniversary of the Montreal Protocol*, edited by C. Zerefos, G. Contopoulos, and G. Skalkeas, 297-326, Springer, Netherlands, doi: 10.1007/978-90-481-2469-5_23, 2009.

Wuebbles, D.J., K.O. Patten, D. Wang, D. Youn, M. Martínez-Avilés, and J.S. Francisco, Three-dimensional model evaluation of the Ozone Depletion Potentials for n-propyl bromide, trichloroethylene and perchloroethylene, *Atmos. Chem. Phys*., *11* (5), 2371-2380, doi: 10.5194/acp-11-2371-2011, 2011.

Wuebbles, D.J., D. Wang, K.O. Patten, and S.C. Olsen, Analyses of short-lived replacements for HFCs with large GWPs, *Geophys. Res. Lett*., *40* (17), 4767-4771, doi: 10.1002/grl.50908, 2013.

Youn, D., K.O. Patten, D.J. Wuebbles, H. Lee, and C.-W. So, Potential impacts of iodinated replacement compounds CF_3I and CH_3I on atmospheric ozone: A three-dimensional modeling study, *Atmos. Chem. Phys*., *10* (20), 10129-10144, doi: 10.5194/acp-10-10129-2010, 2010.

Young, C.J., and S.A. Mabury, Atmospheric perfluorinated acid precursors: Chemistry, occurrence, and impacts, *Rev. of Environ. Contam. Toxicology*, *208*, 1-109, doi: 10.1007/978-1-4419-6880-7_1, 2010.

APPENDIX 5A

5A-1. ANALYSES OF GWPs AND GTPs

Table 5A-1. Atmospheric lifetimes / adjustment times, radiative efficiencies (RE), and GWP values for 20 and 100 years, and GTP values for 20, 50 and 100 years (from IPCC, 2013). Climate-carbon feedbacks are included for CO_2 while no climate feedbacks are included for the other components (see IPCC (2013) for further details). The derivation of GTP assumes a climate sensitivity of 1.06 K (W m^{-2})$^{-1}$, equivalent to a 3.9 K equilibrium response to 2 x CO_2, toward the higher end of the uncertainty in climate sensitivity. For a complete list of chemical names and Chemical Abstracts Service (CAS) numbers, and for accurate replications of metric values, plus further details on the specific values used, see Supplementary Material Section S8.13 and references therein in IPCC (2013). Also see Hodnebrog et al. (2013) for analyses of radiative efficiencies for the halocarbons and related compounds.

Industrial Designation or Chemical Name	Chemical Formula	Lifetime (years)	Radiative Efficiency (W m^{-2} ppb^{-1})	GWP 20-yr	GWP 100-yr	GTP 20-yr	GTP 50-yr	GTP 100-yr
Carbon dioxide	CO_2	See *	1.37e-5	**1**	**1**	**1**	**1**	**1**
Methane	CH_4	12.4^{+}	3.63e-4	**84**	**28**	**67**	**14**	**4**
Fossil methane #	CH_4	12.4^{+}	3.63e-4	**85**	**30**	**68**	**15**	**6**
Nitrous oxide	N_2O	121^{+}	3.00e-3	**264**	**265**	**277**	**282**	**234**
Chlorofluorocarbons								
CFC-11	CCl_3F	45.0	0.26	**6,900**	**4,660**	**6,890**	**4,890**	**2,340**
CFC-12	CCl_2F_2	100.0	0.32	**10,800**	**10,200**	**11,300**	**11,000**	**8,450**
CFC-13	$CClF_3$	640.0	0.25	**10,900**	**13,900**	**11,700**	**14,200**	**15,900**
CFC-113	CCl_2FCClF_2	85.0	0.30	**6,490**	**5,820**	**6,730**	**6,250**	**4,470**
CFC-114	$CClF_2CClF_2$	190.0	0.31	**7,710**	**8,590**	**8,190**	**9,020**	**8,550**
CFC-115	$CClF_2CF_3$	1,020.0	0.20	**5,860**	**7,670**	**6,310**	**7,810**	**8,980**
Hydrochlorofluorocarbons								
HCFC-21	$CHCl_2F$	1.7	0.15	**543**	**148**	**192**	**26**	**20**
HCFC-22	$CHClF_2$	11.9	0.21	**5,280**	**1,760**	**4,200**	**832**	**262**
HCFC-122	$CHCl_2CF_2Cl$	1.0	0.17	**218**	**59**	**70**	**10**	**8**
HCFC-122a	$CHFClCFCl_2$	3.4	0.21	**945**	**258**	**426**	**48**	**36**
HCFC-123	$CHCl_2CF_3$	1.3	0.15	**292**	**79**	**98**	**14**	**11**
HCFC-123a	$CHClFCF_2Cl$	4.0	0.23	**1,350**	**370**	**659**	**72**	**51**
HCFC-124	$CHClFCF_3$	5.9	0.20	**1,870**	**527**	**1,120**	**121**	**74**

Industrial Designation or Chemical Name	Chemical Formula	Lifetime (years)	Radiative Efficiency ($W\ m^{-2}\ ppb^{-1}$)	GWP 20-yr	GWP 100-yr	GTP 20-yr	GTP 50-yr	GTP 100-yr
HCFC-132c	CH_2FCFCl_2	4.3	0.17	**1,230**	**338**	**624**	**67**	**47**
HCFC-141b	CH_3CCl_2F	9.2	0.16	**2,550**	**782**	**1,850**	**271**	**111**
HCFC-142b	CH_3CClF_2	17.2	0.19	**5,020**	**1,980**	**4,390**	**1,370**	**356**
HCFC-225ca	$CHCl_2CF_2CF_3$	1.9	0.22	**469**	**127**	**170**	**22**	**18**
HCFC-225cb	$CHClFCF_2CClF_2$	5.9	0.29	**1,860**	**525**	**1,110**	**120**	**73**
(E)-1-Chloro-3,3,3-trifluoroprop-1-ene	trans-$CF_3CH{=}CHCl$	26.0 days	0.04	**5**	**1**	**2**	**<1**	**<1**
Hydrofluorocarbons								
HFC-23	CHF_3	222.0	0.18	**10,800**	**12,400**	**11,500**	**13,000**	**12,700**
HFC-32	CH_2F_2	5.2	0.11	**2,430**	**677**	**1,360**	**145**	**94**
HFC-41	CH_3F	2.8	0.02	**427**	**116**	**177**	**21**	**16**
HFC-125	CHF_2CF_3	28.2	0.23	**6,090**	**3,170**	**5,800**	**2,980**	**967**
HFC-134	CHF_2CHF_2	9.7	0.19	**3,580**	**1,120**	**2,660**	**412**	**160**
HFC-134a	CH_2FCF_3	13.4	0.16	**3,710**	**1,300**	**3,050**	**703**	**201**
HFC-143	CH_2FCHF_2	3.5	0.13	**1,200**	**328**	**549**	**62**	**46**
HFC-143a	CH_3CF_3	47.1	0.16	**6,940**	**4,800**	**6,960**	**5,060**	**2,500**
HFC-152	CH_2FCH_2F	0.4	0.04	**60**	**16**	**18**	**3**	**2**
HFC-152a	CH_3CHF_2	1.5	0.10	**506**	**138**	**174**	**24**	**19**
HFC-161	CH_3CH_2F	66.0 days	0.02	**13**	**4**	**4**	**<1**	**<1**
HFC-227ca	$CF_3CF_2CHF_2$	28.2	0.27	**5,080**	**2,640**	**4,830**	**2,480**	**806**
HFC-227ea	CF_3CHFCF_3	38.9	0.26	**5,360**	**3,350**	**5,280**	**3,440**	**1,460**
HFC-236cb	$CH_2FCF_2CF_3$	13.1	0.23	**3,480**	**1,210**	**2,840**	**636**	**185**
HFC-236ea	CHF_2CHFCF_3	11.0	0.30	**4,110**	**1,330**	**3,190**	**573**	**195**
HFC-236fa	$CF_3CH_2CF_3$	242.0	0.24	**6,940**	**8,060**	**7,400**	**8,400**	**8,380**
HFC-245ca	$CH_2FCF_2CHF_2$	6.5	0.24	**2,510**	**716**	**1,570**	**176**	**100**
HFC-245cb	$CF_3CF_2CH_3$	47.1	0.24	**6,680**	**4,620**	**6,690**	**4,870**	**2,410**
HFC-245ea	$CHF_2CHFCHF_2$	3.2	0.16	**863**	**235**	**378**	**44**	**33**
HFC-245eb	$CH_2FCHFCF_3$	3.1	0.20	**1,070**	**290**	**460**	**54**	**40**
HFC-245fa	$CHF_2CH_2CF_3$	7.7	0.24	**2,920**	**858**	**1,970**	**245**	**121**
HFC-263fb	$CH_3CH_2CF_3$	1.2	0.10	**278**	**76**	**92**	**13**	**10**
HFC-272ca	$CH_3CF_2CH_3$	2.6	0.07	**530**	**144**	**213**	**26**	**20**
HFC-329p	$CHF_2CF_2CF_2CF_3$	28.4	0.31	**4,510**	**2,360**	**4,290**	**2,220**	**725**
HFC-365mfc	$CH_3CF_2CH_2CF_3$	8.7	0.22	**2,660**	**804**	**1,890**	**262**	**114**
HFC-43-10mee	$CF_3CHFCHFCF_2CF_3$	16.1	0.42	**4,310**	**1,650**	**3,720**	**1,070**	**281**
HFC-1132a	$CH_2{=}CF_2$	4.0 days	0.004	**<1**	**<1**	**<1**	**<1**	**<1**
HFC-1141	$CH_2{=}CHF$	2.1 days	0.002	**<1**	**<1**	**<1**	**<1**	**<1**
(Z)-HFC-1225ye	$CF_3CF{=}CHF(Z)$	8.5 days	0.02	**<1**	**<1**	**<1**	**<1**	**<1**

Industrial Designation or Chemical Name	Chemical Formula	Lifetime (years)	Radiative Efficiency ($W\ m^{-2}\ ppb^{-1}$)	GWP 20-yr	GWP 100-yr	GTP 20-yr	GTP 50-yr	GTP 100-yr
(E)-HFC-1225ye	$CF_3CF{=}CHF(E)$	4.9 days	0.01	**<1**	**<1**	**<1**	**<1**	**<1**
(Z)-HFC-1234ze	$CF_3CH{=}CHF(Z)$	10.0 days	0.02	**1**	**<1**	**<1**	**<1**	**<1**
HFC-1234yf	$CF_3CF{=}CH_2$	10.5 days	0.02	**1**	**<1**	**<1**	**<1**	**<1**
(E)-HFC-1234ze	trans-$CF_3CH{=}CHF$	16.4 days	0.04	**4**	**<1**	**<1**	**<1**	**<1**
(Z)-HFC-1336	$CF_3CH{=}CHCF_3(Z)$	22.0 days	0.07	**6**	**2**	**2**	**<1**	**<1**
HFC-1243zf	$CF_3CH{=}CH_2$	7.0 days	0.01	**<1**	**<1**	**<1**	**<1**	**<1**
HFC-1345zfc	$C_2F_5CH{=}CH_2$	7.6 days	0.01	**<1**	**<1**	**<1**	**<1**	**<1**
3,3,4,4,5,5,6,6,6-Nonafluorohex-1-ene	$C_4F_9CH{=}CH_2$	7.6 days	0.03	**<1**	**<1**	**<1**	**<1**	**<1**
3,3,4,4,5,5,6,6,7,7,8,8,8-Tridecafluorooct-1-ene	$C_6F_{13}CH{=}CH_2$	7.6 days	0.03	**<1**	**<1**	**<1**	**<1**	**<1**
3,3,4,4,5,5,6,6,7,7,8,8,9,9,10,10,10-Heptadecafluorodec-1-ene	$C_8F_{17}CH{=}CH_2$	7.6 days	0.03	**<1**	**<1**	**<1**	**<1**	**<1**
Chlorocarbons and Hydrochlorocarbons								
Methyl chloroform	CH_3CCl_3	5.0	0.07	**578**	**160**	**317**	**34**	**22**
Carbon tetrachloride	CCl_4	26.0	0.17	**3,480**	**1,730**	**3,280**	**1,570**	**479**
Methyl chloride	CH_3Cl	1.0	0.01	**45**	**12**	**15**	**2**	**2**
Methylene chloride	CH_2Cl_2	0.4	0.03	**33**	**9**	**10**	**2**	**1**
Chloroform	$CHCl_3$	0.4	0.08	**60**	**16**	**18**	**3**	**2**
1,2-Dichloroethane	CH_2ClCH_2Cl	65.0 days	0.01	**3**	**<1**	**<1**	**<1**	**<1**
Bromocarbons, Hydrobromocarbons and Halons								
Methyl bromide	CH_3Br	0.8	0.004	**9**	**2**	**3**	**<1**	**<1**
Methylene bromide	CH_2Br_2	0.3	0.01	**4**	**1**	**1**	**<1**	**<1**
Halon-1201	$CHBrF_2$	5.2	0.15	**1,350**	**376**	**756**	**80**	**52**
Halon-1202	CBr_2F_2	2.9	0.27	**848**	**231**	**356**	**42**	**32**
Halon-1211	$CBrClF_2$	16.0	0.29	**4,590**	**1,750**	**3,950**	**1,130**	**297**
Halon-1301	$CBrF_3$	65.0	0.30	**7,800**	**6,290**	**7,990**	**6,750**	**4,170**
Halon-2301	CH_2BrCF_3	3.4	0.14	**635**	**173**	**286**	**33**	**24**
Halon-2311 / Halothane	$CHBrClCF_3$	1.0	0.13	**151**	**41**	**49**	**7**	**6**
Halon-2401	$CHFBrCF_3$	2.9	0.19	**674**	**184**	**283**	**34**	**25**
Halon-2402	$CBrF_2CBrF_2$	20.0	0.31	**3,440**	**1,470**	**3,100**	**1,150**	**304**
Fully Fluorinated Species								
Nitrogen trifluoride	NF_3	500.0	0.20	**12,800**	**16,100**	**13,700**	**16,500**	**18,100**
Sulphur hexafluoride	SF_6	3,200.0	0.57	**17,500**	**23,500**	**18,900**	**23,800**	**28,200**

Industrial Designation or Chemical Name	Chemical Formula	Lifetime (years)	Radiative Efficiency (W m^{-2} ppb^{-1})	GWP 20-yr	GWP 100-yr	GTP 20-yr	GTP 50-yr	GTP 100-yr
(Trifluoromethyl)sulfur pentafluoride	SF_5CF_3	800.0	0.59	**13,500**	**17,400**	**14,500**	**17,800**	**20,200**
Sulfuryl fluoride	SO_2F_2	36.0	0.20	**6,840**	**4,090**	**6,690**	**4,140**	**1,650**
PFC-14	CF_4	50,000.0	0.09	**4,880**	**6,630**	**5,270**	**6,690**	**8,040**
PFC-116	C_2F_6	10,000.0	0.25	**8,210**	**11,100**	**8,880**	**11,200**	**13,500**
PFC-c216	c-C_3F_6	3,000.0	0.23	**6,850**	**9,200**	**7,400**	**9,310**	**11,000**
PFC-218	C_3F_8	2,600.0	0.28	**6,640**	**8,900**	**7,180**	**9,010**	**10,700**
PFC-318	c-C_4F_8	3,200.0	0.32	**7,110**	**9,540**	**7,680**	**9,660**	**11,500**
PFC-31-10	C_4F_{10}	2,600.0	0.36	**6,870**	**9,200**	**7,420**	**9,320**	**11,000**
Perfluorocyclopentene	c-C_5F_8	31.0 days	0.08	**7**	**2**	**2**	**<1**	**<1**
PFC-41-12	n-C_5F_{12}	4,100.0	0.41	**6,350**	**8,550**	**6,860**	**8,650**	**10,300**
PFC-51-14	n-C_6F_{14}	3,100.0	0.44	**5,890**	**7,910**	**6,370**	**8,010**	**9,490**
PFC-61-16	n-C_7F_{16}	3,000.0	0.50	**5,830**	**7,820**	**6,290**	**7,920**	**9,380**
PFC-71-18	C_8F_{18}	3,000.0	0.55	**5,680**	**7,620**	**6,130**	**7,710**	**9,140**
PFC-91-18	$C_{10}F_{18}$	2,000.0	0.55	**5,390**	**7,190**	**5,820**	**7,290**	**8,570**
Perfluorodecalin (Z)	(Z)-$C_{10}F_{18}$	2,000.0	0.56	**5,430**	**7,240**	**5,860**	**7,340**	**8,630**
Perfluorodecalin (E)	(E)-$C_{10}F_{18}$	2,000.0	0.48	**4,720**	**6,290**	**5,090**	**6,380**	**7,500**
PFC-1114	$CF_2{=}CF_2$	1.1 days	0.002	**<1**	**<1**	**<1**	**<1**	**<1**
PFC-1216	$CF_3CF{=}CF_2$	4.9 days	0.01	**<1**	**<1**	**<1**	**<1**	**<1**
Perfluorobuta-1,3-diene	$CF_2{=}CFCF{=}CF_2$	1.1 days	0.003	**<1**	**<1**	**<1**	**<1**	**<1**
Perfluorobut-1-ene	$CF_3CF_2CF{=}CF_2$	6.0 days	0.02	**<1**	**<1**	**<1**	**<1**	**<1**
Perfluorobut-2-ene	$CF_3CF{=}CFCF_3$	31.0 days	0.07	**6**	**2**	**2**	**<1**	**<1**
Halogenated Alcohols and Ethers								
HFE-125	CHF_2OCF_3	119.0	0.41	**12,400**	**12,400**	**13,000**	**13,200**	**10,900**
HFE-134 (HG-00)	CHF_2OCHF_2	24.4	0.44	**11,600**	**5,560**	**10,800**	**4,900**	**1,430**
HFE-143a	CH_3OCF_3	4.8	0.18	**1,890**	**523**	**1,020**	**108**	**73**
HFE-227ea	$CF_3CHFOCF_3$	51.6	0.44	**8,900**	**6,450**	**8,980**	**6,850**	**3,630**
HCFE-235ca2 (enflurane)	CHF_2OCF_2CHFCl	4.3	0.41	**2,120**	**583**	**1,080**	**116**	**81**
HCFE-235da2 (isoflurane)	$CHF_2OCHClCF_3$	3.5	0.42	**1,800**	**491**	**822**	**93**	**68**
HFE-236ca	$CHF_2OCF_2CHF_2$	20.8	0.56	**9,710**	**4,240**	**8,820**	**3,400**	**912**
HFE-236ea2 (desflurane)	$CHF_2OCHFCF_3$	10.8	0.45	**5,550**	**1,790**	**4,280**	**753**	**260**
HFE-236fa	$CF_3CH_2OCF_3$	7.5	0.36	**3,350**	**979**	**2,240**	**273**	**138**
HFE-245cb2	$CF_3CF_2OCH_3$	4.9	0.33	**2,360**	**654**	**1,280**	**136**	**91**
HFE-245fa1	$CHF_2CH_2OCF_3$	6.6	0.31	**2,900**	**828**	**1,820**	**206**	**116**
HFE-245fa2	$CHF_2OCH_2CF_3$	5.5	0.36	**2,910**	**812**	**1,670**	**179**	**114**
2,2,3,3,3-Pentafluoropropan-1-ol	$CF_3CF_2CH_2OH$	0.3	0.14	**69**	**19**	**21**	**3**	**3**
HFE-254cb1	$CH_3OCF_2CHF_2$	2.5	0.26	**1,110**	**301**	**438**	**54**	**42**

Industrial Designation or Chemical Name	Chemical Formula	Lifetime (years)	Radiative Efficiency ($W\ m^{-2}\ ppb^{-1}$)	GWP 20-yr	GWP 100-yr	GTP 20-yr	GTP 50-yr	GTP 100-yr
HFE-263fb2	$CF_3CH_2OCH_3$	23.0 days	0.04	**5**	**1**	**1**	**0**	**0**
HFE-263m1	$CF_3OCH_2CH_3$	0.4	0.13	**108**	**29**	**33**	**5**	**4**
3,3,3-Trifluoropropan-1-ol	$CF_3CH_2CH_2OH$	12.0 days	0.02	**1**	**0**	**0**	**0**	**0**
HFE-329mcc2	$CHF_2CF_2OCF_2CF_3$	22.5	0.53	**6,720**	**3,070**	**6,180**	**2,580**	**718**
HFE-338mmz1	$(CF_3)_2CHOCHF_2$	21.2	0.44	**5,940**	**2,620**	**5,410**	**2,130**	**575**
HFE-338mcf2	$CF_3CH_2OCF_2CF_3$	7.5	0.44	**3,180**	**929**	**2,120**	**259**	**131**
Sevoflurane (HFE-347mmz1)	$(CF_3)_2CHOCH_2F$	2.2	0.32	**795**	**216**	**302**	**38**	**30**
HFE-347mcc3 (HFE-7000)	$CH_3OCF_2CF_2CF_3$	5.0	0.35	**1,910**	**530**	**1,050**	**111**	**74**
HFE-347mcf2	$CHF_2CH_2OCF_2CF_3$	6.6	0.42	**2,990**	**854**	**1,880**	**212**	**120**
HFE-347pcf2	$CHF_2CF_2OCH_2CF_3$	6.0	0.48	**3,150**	**889**	**1,900**	**206**	**124**
HFE-347mmy1	$(CF_3)_2CFOCH_3$	3.7	0.32	**1,330**	**363**	**624**	**69**	**51**
HFE-356mec3	$CH_3OCF_2CHFCF_3$	3.8	0.30	**1,410**	**387**	**673**	**74**	**54**
HFE-356mff2	$CF_3CH_2OCH_2CF_3$	105.0 days	0.17	**62**	**17**	**18**	**3**	**2**
HFE-356pcf2	$CHF_2CH_2OCF_2CHF_2$	5.7	0.37	**2,560**	**719**	**1,500**	**162**	**101**
HFE-356pcf3	$CHF_2OCH_2CF_2CHF_2$	3.5	0.38	**1,640**	**446**	**747**	**84**	**62**
HFE-356pcc3	$CH_3OCF_2CF_2CHF_2$	3.8	0.32	**1,510**	**413**	**718**	**79**	**57**
HFE-356mmz1	$(CF_3)_2CHOCH_3$	97.1 days	0.15	**50**	**14**	**15**	**2**	**2**
HFE-365mcf3	$CF_3CF_2CH_2OCH_3$	19.3 days	0.05	**3**	**<1**	**<1**	**<1**	**<1**
HFE-365mcf2	$CF_3CF_2OCH_2CH_3$	0.6	0.26	**215**	**58**	**66**	**10**	**8**
HFE-374pc2	$CHF_2CF_2OCH_2CH_3$	5.0	0.30	**2,260**	**627**	**1,240**	**132**	**88**
4,4,4-Trifluorobutan-1-ol	$CF_3(CH_2)_2CH_2OH$	4.0 days	0.01	**<1**	**<1**	**<1**	**<1**	**<1**
2,2,3,3,4,4,5,5-Octafluorocyclopentanol	$-(CF_2)_4CH(OH)-$	0.3	0.16	**47**	**13**	**14**	**2**	**2**
HFE-43-10pccc124 (H-Galden 1040x, HG-11)	$CHF_2OCF_2OC_2F_4OCHF_2$	13.5	1.02	**8,010**	**2,820**	**6,600**	**1,530**	**436**
HFE-449s1 (HFE-7100)	$C_4F_9OCH_3$	4.7	0.36	**1,530**	**421**	**809**	**86**	**59**
n-HFE-7100	$n\text{-}C_4F_9OCH_3$	4.7	0.42	**1,760**	**486**	**934**	**99**	**68**
i-HFE-7100	$i\text{-}C_4F_9OCH_3$	4.7	0.35	**1,480**	**407**	**783**	**83**	**57**
HFE-569sf2 (HFE-7200)	$C_4F_9OC_2H_5$	0.8	0.30	**209**	**57**	**66**	**10**	**8**
n-HFE-7200	$n\text{-}C_4F_9OC_2H_5$	0.8	0.35	**237**	**65**	**75**	**11**	**9**
i-HFE-7200	$i\text{-}C_4F_9OC_2H_5$	0.8	0.24	**163**	**44**	**52**	**8**	**6**
HFE-236ca12 (HG-10)	$CHF_2OCF_2OCHF_2$	25.0	0.65	**11,000**	**5,350**	**10,300**	**4,770**	**1,420**
HFE-338pcc13 (HG-01)	$CHF_2OCF_2CF_2OCHF_2$	12.9	0.86	**8,430**	**2,910**	**6,860**	**1,500**	**442**
1,1,1,3,3,3-Hexafluoropropan-2-ol	$(CF_3)_2CHOH$	1.9	0.26	**668**	**182**	**243**	**32**	**25**
HG-02	$HF_2C–(OCF_2CF_2)_2–OCF_2H$	12.9	1.24	**7,900**	**2,730**	**6,430**	**1,410**	**415**

Industrial Designation or Chemical Name	Chemical Formula	Lifetime (years)	Radiative Efficiency (W m^{-2} ppb^{-1})	GWP 20-yr	GWP 100-yr	GTP 20-yr	GTP 50-yr	GTP 100-yr
HG-03	$HF_2C–(OCF_2CF_2)_3–OCF_2H$	12.9	1.76	**8,270**	**2,850**	**6,730**	**1,480**	**434**
HG-20	$HF_2C–(OCF_2)_2–OCF_2H$	25.0	0.92	**10,900**	**5,300**	**10,200**	**4,730**	**1,400**
HG-21	$HF_2C–OCF_2CF_2OCF_2OCF_2O–CF_2H$	13.5	1.71	**11,100**	**3,890**	**9,110**	**2,120**	**602**
HG-30	$HF_2C–(OCF_2)_3–OCF_2H$	25.0	1.65	**15,100**	**7,330**	**14,100**	**6,530**	**1,940**
1-Ethoxy-1,1,2,2,3,3,3-heptafluoropropane	$CF_3CF_2CF_2OCH_2CH_3$	0.8	0.28	**223**	**61**	**70**	**10**	**8**
Fluoroxene	$CF_3CH_2OCH=CH_2$	3.6 days	0.01	**<1**	**<1**	**<1**	**<1**	**<1**
1,1,2,2-Tetrafluoro-1-(fluoromethoxy)ethane	$CH_2FOCF_2CF_2H$	6.2	0.34	**3,080**	**871**	**1,880**	**207**	**122**
2-Ethoxy-3,3,4,4,5-pentafluorotetrahydro-2,5-bis[1,2,2,2-tetrafluoro-1-(trifluoromethyl)ethyl]-furan	$C_{12}H_5F_{19}O_2$	1.0	0.49	**204**	**56**	**66**	**10**	**8**
Fluoro(methoxy)methane	CH_3OCH_2F	73.0 days	0.07	**46**	**13**	**14**	**2**	**2**
Difluoro(methoxy)methane	CH_3OCHF_2	1.1	0.17	**528**	**144**	**173**	**25**	**20**
Fluoro(fluoromethoxy)methane	CH_2FOCH_2F	0.9	0.19	**479**	**130**	**153**	**22**	**18**
Difluoro(fluoromethoxy)methane	CH_2FOCHF_2	3.3	0.30	**2,260**	**617**	**1,010**	**115**	**86**
Trifluoro(fluoromethoxy)methane	CH_2FOCF_3	4.4	0.33	**2,730**	**751**	**1,400**	**150**	**105**
HG'-01	$CH_3OCF_2CF_2OCH_3$	2.0	0.29	**815**	**222**	**301**	**39**	**31**
HG'-02	$CH_3O(CF_2CF_2O)_2CH_3$	2.0	0.56	**868**	**236**	**320**	**42**	**33**
HG'-03	$CH_3O(CF_2CF_2O)_3CH_3$	2.0	0.76	**812**	**221**	**299**	**39**	**31**
HFE-329me3	$CF_3CFHCF_2OCF_3$	40.0	0.48	**7,170**	**4,550**	**7,090**	**4,690**	**2,040**
3,3,4,4,5,5,6,6,7,7,7-Undecafluoroheptan-1-ol	$CF_3(CF_2)_4CH_2CH_2OH$	20.0 days	0.06	**2**	**<1**	**<1**	**<1**	**<1**
3,3,4,4,5,5,6,6,7,7,8,8,9,9,9-Pentadecafluorononan-1-ol	$CF_3(CF_2)_6CH_2CH_2OH$	20.0 days	0.07	**1**	**<1**	**<1**	**<1**	**<1**
3,3,4,4,5,5,6,6,7,7,8,8,9,9,10,10,11,11,11-Nonadecafluoroundecan-1-ol	$CF_3(CF_2)_8CH_2CH_2OH$	20.0 days	0.05	**<1**	**<1**	**<1**	**<1**	**<1**
2-Chloro-1,1,2-trifluoro-1-methoxyethane	CH_3OCF_2CHFCl	1.4	0.21	**449**	**122**	**153**	**21**	**17**
PFPMIE (perfluoropolymethylisopropyl ether)	$CF_3OCF(CF_3)CF_2OCF_2OCF_3$	800.0	0.65	**7,500**	**9,710**	**8,070**	**9,910**	**11,300**
HFE-216	$CF_3OCF=CF_2$	8.4 days	0.02	**<1**	**<1**	**<1**	**<1**	**<1**

Industrial Designation or Chemical Name	Chemical Formula	Lifetime (years)	Radiative Efficiency ($W\ m^{-2}\ ppb^{-1}$)	GWP 20-yr	GWP 100-yr	GTP 20-yr	GTP 50-yr	GTP 100-yr
Trifluoromethyl formate	$HCOOCF_3$	3.5	0.31	**2,150**	**588**	**984**	**111**	**82**
Perfluoroethyl formate	$HCOOCF_2CF_3$	3.5	0.44	**2,130**	**580**	**971**	**110**	**81**
Perfluoropropyl formate	$HCOOCF_2CF_2CF_3$	2.6	0.50	**1,380**	**376**	**555**	**68**	**52**
Perfluorobutyl formate	$HCOOCF_2CF_2CF_2CF_3$	3.0	0.56	**1,440**	**392**	**613**	**72**	**54**
2,2,2-Trifluoroethyl formate	$HCOOCH_2CF_3$	0.4	0.16	**123**	**33**	**37**	**6**	**5**
3,3,3-Trifluoropropyl formate	$HCOOCH_2CH_2CF_3$	0.3	0.13	**64**	**17**	**19**	**3**	**2**
1,2,2,2-Tetrafluoroethyl formate	$HCOOCHFCF_3$	3.2	0.35	**1,720**	**470**	**755**	**87**	**65**
1,1,1,3,3,3-Hexafluoropropan-2-yl formate	$HCOOCH(CF_3)_2$	3.2	0.33	**1,220**	**333**	**535**	**62**	**46**
Perfluorobutyl acetate	$CH_3COOCF_2CF_2CF_2CF_3$	21.9 days	0.12	**6**	**2**	**2**	**<1**	**<1**
Perfluoropropyl acetate	$CH_3COOCF_2CF_2CF_3$	21.9 days	0.11	**6**	**2**	**2**	**<1**	**<1**
Perfluoroethyl acetate	$CH_3COOCF_2CF_3$	21.9 days	0.10	**8**	**2**	**2**	**<1**	**<1**
Trifluoromethyl acetate	CH_3COOCF_3	21.9 days	0.07	**8**	**2**	**2**	**<1**	**<1**
Methyl carbonofluoridate	$FCOOCH_3$	1.8	0.07	**350**	**95**	**126**	**17**	**13**
1,1-Difluoroethyl carbonofluoridate	$FCOOCF_2CH_3$	0.3	0.17	**99**	**27**	**30**	**5**	**4**
1,1-Difluoroethyl 2,2,2-trifluoroacetate	$CF_3COOCF_2CH_3$	0.3	0.27	**113**	**31**	**34**	**5**	**4**
Ethyl 2,2,2-trifluoroacetate	$CF_3COOCH_2CH_3$	21.9 days	0.05	**5**	**1**	**1**	**<1**	**<1**
2,2,2-Trifluoroethyl 2,2,2-trifluoroacetate	$CF_3COOCH_2CF_3$	54.8 days	0.15	**25**	**7**	**7**	**1**	**<1**
Methyl 2,2,2-trifluoroacetate	CF_3COOCH_3	0.6	0.18	**192**	**52**	**60**	**9**	**7**
Methyl 2,2-difluoroacetate	HCF_2COOCH_3	40.1 days	0.05	**12**	**3**	**4**	**<1**	**<1**
Difluoromethyl 2,2,2-trifluoroacetate	$CF_3COOCHF_2$	0.3	0.24	**99**	**27**	**30**	**5**	**4**
2,2,3,3,4,4,4-Heptafluorobutan-1-ol	$C_3F_7CH_2OH$	0.6	0.20	**124**	**34**	**38**	**6**	**5**
1,1,2-Trifluoro-2-(trifluoromethoxy)-ethane	$CHF_2CHFOCF_3$	9.8	0.35	**3,970**	**1,240**	**2,960**	**467**	**178**
1-Ethoxy-1,1,2,3,3,3-hexafluoropropane	$CF_3CHFCF_2OCH_2CH_3$	0.4	0.19	**86**	**23**	**26**	**4**	**3**
1,1,1,2,2,3,3-Heptafluoro-3-(1,2,2,2-tetrafluoroethoxy)-propane	$CF_3CF_2CF_2OCHFCF_3$	67.0	0.58	**7,940**	**6,490**	**8,140**	**6,960**	**4,380**
2,2,3,3-Tetrafluoro-1-propanol	$CHF_2CF_2CH_2OH$	91.2 days	0.11	**48**	**13**	**14**	**2**	**2**
2,2,3,4,4,4-Hexafluoro-1-butanol	$CF_3CHFCF_2CH_2OH$	94.9 days	0.19	**63**	**17**	**19**	**3**	**2**
2,2,3,3,4,4,4-Heptafluoro-1-butanol	$CF_3CF_2CF_2CH_2OH$	0.3	0.16	**60**	**16**	**18**	**3**	**2**
1,1,2,2-Tetrafluoro-3-methoxy-propane	$CHF_2CF_2CH_2OCH_3$	14.2 days	0.03	**2**	**<1**	**<1**	**<1**	**<1**
Perfluoro-2-methyl-3-pentanone	$CF_3CF_2C(O)CF(CF_3)_2$	7.0 days	0.03	**<1**	**<1**	**<1**	**<1**	**<1**

Industrial Designation or Chemical Name	Chemical Formula	Lifetime (years)	Radiative Efficiency ($W\ m^{-2}\ ppb^{-1}$)	GWP 20-yr	GWP 100-yr	GTP 20-yr	GTP 50-yr	GTP 100-yr
3,3,3-Trifluoro-propanal	CF_3CH_2CHO	2.0 days	0.004	**<1**	**<1**	**<1**	**<1**	**<1**
2-Fluoroethanol	CH_2FCH_2OH	20.4 days	0.02	**3**	**<1**	**<1**	**<1**	**<1**
2,2-Difluoroethanol	CHF_2CH_2OH	40.0 days	0.04	**11**	**3**	**3**	**<1**	**<1**
2,2,2-Trifluoroethanol	CF_3CH_2OH	0.3	0.10	**73**	**20**	**22**	**3**	**3**
1,1'-Oxybis[2-(difluoromethoxy)-1,1,2,2-tetrafluoroethane	$HCF_2O(CF_2CF_2O)_2$-CF_2H	26.0	1.15	**9,910**	**4,920**	**9,320**	**4,460**	**1,360**
1,1,3,3,4,4,6,6,7,7,9,9,10,10,12,12-Hexadecafluoro-2,5,8,11-tetraoxadodecane	$HCF_2O(CF_2CF_2O)_3$-CF_2H	26.0	1.43	**9,050**	**4,490**	**8,520**	**4,080**	**1,250**
1,1,3,3,4,4,6,6,7,7,9,9,10,10,12,12,13,13,15,15-Eicosafluoro-2,5,8,11,14-pentaoxapentadecane	$HCF_2O(CF_2CF_2O)_4$-CF_2H	26.0	1.46	**7,320**	**3,630**	**6,880**	**3,300**	**1,010**

For CH_4 we estimate an uncertainty of ±30% and ±40% for 20- and 100-year time horizons, respectively (for 90% uncertainty range). The uncertainty is dominated by AGWP for CO_2 and indirect effects. The uncertainty in GWP for N_2O is estimated to be ±20% and ±30% for 20- and 100-year time horizons, with the largest contributions from CO_2. The uncertainty in GWP for HFC-134a is estimated to be ±25% and ±35% for 20- and 100-year time horizons while for CFC-11, the GWP corresponding uncertainties are approximately ±20% and ±35% (not accounting for the indirect effects). For CFC-12 the corresponding numbers are ±20 and ±30. The uncertainties estimated for HFC-134a and CFC-11 are assessed as representative for most other gases with similar or longer lifetimes. For shorter-lived gases, the uncertainties will be larger. For GTP, few estimates are available in the literature. The uncertainty is assessed to be of the order of ±75% for the methane 100-year GTP.

* No single lifetime can be given. The impulse response function for CO_2 from Joos et al. (2013) has been used. See also Supplementary Material Section S8.11 in IPCC (2013).

\+ Perturbation lifetime is used in calculation of metrics; not the lifetime of the atmospheric burden.

\# Metric values for CH_4 of fossil origin include the oxidation to CO_2 (based on Boucher et al. (2009)). In applications of these values, inclusion of the CO_2 effect of fossil methane must be done with caution to avoid any double counting, since CO_2 emissions numbers are often based on total carbon content. For non-fossil CH_4 we assume balance between CO_2 taken up by the biosphere and CO_2 produced from CH_4 oxidation.

5A-2. BASELINE SCENARIO MIXING RATIOS

Table 5A-2. Mixing ratios (ppt) of the ODSs considered in the baseline (A1) scenario. Values are for the beginning of the corresponding year (see Chapter 1). Potentially important short-lived gases that may currently contribute 5 (2–8) ppt of stratospheric bromine and 95 (50–145) ppt of stratospheric chlorine (see Chapter 1) are not shown in the table. Note: Areas are shaded for compounds in years when mixing ratio values are forced to equal global average estimates inferred from observations (see Chapter 1, Figure 1-1).

Year	CFC-11	CFC-12	CFC-113	CFC-114	CFC-115	CCl_4	CH_3CCl_3	HCFC-22	HCFC-141b	HCFC-142b	halon-1211	halon-1202	halon-1301	halon-2402	CH_3Br	CH_3Cl
1955	3.3	14.3	1.3	2.6	0.0	42.3	0.1	1.0	0.0	0.0	0.00	0.00	0.00	0.00	6.3	491.3
1960	9.5	29.5	1.9	3.8	0.0	52.1	1.5	2.1	0.0	0.0	0.00	0.00	0.00	0.00	6.5	510.3
1965	23.5	58.8	3.1	5.0	0.0	64.4	4.7	4.9	0.0	0.0	0.00	0.00	0.00	0.00	6.7	528.1
1970	52.8	114.3	5.5	6.5	0.2	75.9	16.3	12.1	0.0	0.0	0.02	0.00	0.00	0.02	7.0	539.9
1975	106.1	203.1	10.4	8.3	0.6	85.5	40.0	23.8	0.0	0.2	0.12	0.01	0.04	0.06	7.4	545.8
1980	161.9	297.1	19.0	10.7	1.5	92.9	82.0	42.5	0.0	0.4	0.69	0.01	0.36	0.15	7.8	548.4
1981	170.5	312.1	21.5	11.1	1.7	94.3	89.0	46.6	0.0	0.5	0.81	0.01	0.43	0.17	7.9	548.6
1982	179.2	330.5	24.5	11.6	2.0	95.7	94.1	50.7	0.0	0.6	0.95	0.01	0.51	0.19	8.0	548.9
1983	187.6	346.4	28.0	12.0	2.3	97.0	98.0	54.8	0.0	0.6	1.09	0.02	0.60	0.21	8.0	549.1
1984	196.4	363.7	32.2	12.4	2.7	98.5	102.0	58.8	0.0	0.7	1.23	0.02	0.71	0.23	8.1	549.3
1985	206.2	378.5	36.7	12.9	3.0	99.9	106.5	62.7	0.0	0.7	1.40	0.02	0.85	0.26	8.2	549.4
1986	216.2	397.9	41.8	13.4	3.4	101.3	110.3	66.9	0.0	0.8	1.59	0.02	1.03	0.27	8.3	549.5
1987	227.2	416.4	47.5	14.0	3.9	103.0	113.5	71.5	0.0	0.8	1.77	0.02	1.24	0.29	8.4	549.6
1988	238.7	439.0	54.0	14.5	4.3	104.0	118.7	76.7	0.0	0.9	1.96	0.02	1.45	0.31	8.5	549.7
1989	248.8	459.3	60.9	15.0	4.7	104.8	123.5	82.5	0.0	1.1	2.14	0.02	1.64	0.34	8.6	549.8
1990	256.4	476.4	67.6	15.4	5.2	105.6	127.3	88.2	0.0	1.2	2.32	0.03	1.80	0.37	8.7	549.8
1991	262.0	489.7	73.3	15.7	5.6	105.9	130.8	93.7	0.0	1.8	2.52	0.03	1.95	0.39	8.8	549.9
1992	265.4	500.7	78.2	15.8	6.0	105.8	133.6	99.8	0.1	2.8	2.72	0.03	2.09	0.42	8.9	549.9
1993	267.8	510.0	81.2	16.0	6.4	105.3	130.3	103.9	0.4	3.9	2.92	0.03	2.23	0.44	9.0	549.9
1994	268.1	516.5	83.0	16.1	6.8	104.4	121.9	109.1	1.5	5.1	3.11	0.03	2.35	0.46	9.2	550.0
1995	267.8	523.0	83.8	16.1	7.1	103.7	110.5	113.6	2.8	6.2	3.35	0.04	2.45	0.47	9.2	555.2
1996	267.0	528.7	84.0	16.2	7.4	102.6	98.2	119.4	4.5	7.2	3.53	0.04	2.53	0.48	9.2	539.3
1997	266.0	532.9	83.8	16.3	7.7	101.6	84.1	124.2	6.4	8.3	3.69	0.05	2.61	0.49	9.1	529.6
1998	264.6	536.4	83.4	16.4	7.9	100.7	71.0	128.9	8.2	9.4	3.82	0.05	2.69	0.49	9.3	554.3
1999	263.3	539.3	82.9	16.4	8.0	99.6	59.4	134.3	10.1	10.4	3.96	0.04	2.76	0.49	9.3	555.5
2000	261.6	541.4	82.3	16.5	8.1	98.5	49.7	139.2	11.8	11.4	4.08	0.04	2.84	0.49	9.0	542.8
2001	260.0	542.8	81.7	16.5	8.2	97.5	41.5	144.7	13.5	12.5	4.18	0.03	2.88	0.49	8.5	534.8
2002	258.2	543.6	81.1	16.6	8.3	96.5	34.5	150.5	14.8	13.3	4.24	0.02	2.91	0.49	8.3	533.6

Year	CFC-11	CFC-12	CFC-113	CFC-114	CFC-115	CCl_4	CH_3CCl_3	HCFC-22	HCFC-141b	HCFC-142b	halon-1211	halon-1202	halon-1301	halon-2402	CH_3Br	CH_3Cl
2003	256.0	543.6	80.4	16.6	8.3	95.5	28.8	155.4	16.1	13.9	4.28	0.02	2.97	0.49	8.2	539.6
2004	253.8	543.4	79.7	16.6	8.3	94.5	24.0	160.5	17.0	14.6	4.31	0.02	3.02	0.49	8.1	536.2
2005	251.5	542.5	79.0	16.6	8.4	93.5	20.0	165.7	17.5	15.2	4.34	0.01	3.05	0.49	7.9	539.9
2006	249.4	541.6	78.4	16.5	8.4	92.5	16.7	171.9	17.8	15.9	4.34	0.01	3.08	0.48	7.8	536.9
2007	247.2	539.6	77.7	16.5	8.4	91.4	14.0	179.1	18.5	16.9	4.32	0.01	3.11	0.48	7.6	543.7
2008	245.0	537.5	76.9	16.5	8.4	90.2	11.7	187.3	19.1	18.1	4.28	0.00	3.15	0.47	7.5	545.3
2009	243.0	535.3	76.2	16.5	8.4	88.9	9.8	195.2	19.6	19.3	4.22	0.00	3.17	0.47	7.3	541.0
2010	241.1	532.7	75.5	16.4	8.4	87.6	8.2	202.5	20.1	20.0	4.16	0.00	3.19	0.46	7.1	538.4
2011	239.0	530.1	74.8	16.4	8.4	86.5	6.9	210.0	20.9	20.8	4.08	0.00	3.22	0.45	7.1	533.5
2012	237.0	527.4	74.1	16.4	8.4	85.2	5.7	216.1	21.9	21.5	4.01	0.00	3.24	0.45	7.0	538.1
2013	234.7	525.0	73.4	16.3	8.4	84.1	4.8	221.5	22.9	21.9	3.91	0.00	3.26	0.44	7.0	539.5
2014	232.4	520.9	72.7	16.2	8.4	82.9	4.0	233.8	23.8	22.7	3.81	0.00	3.27	0.43	7.0	539.5
2015	229.9	516.7	71.9	16.1	8.4	81.6	3.3	244.8	24.6	23.5	3.71	0.00	3.28	0.43	7.0	539.5
2016	227.5	512.4	71.2	16.1	8.4	80.3	2.7	254.7	25.5	24.2	3.60	0.00	3.29	0.42	7.0	539.5
2017	224.9	508.0	70.5	16.0	8.4	78.9	2.2	262.9	26.4	24.8	3.49	0.00	3.30	0.41	7.0	539.5
2018	222.4	503.6	69.7	16.0	8.4	77.4	1.8	269.8	27.2	25.3	3.38	0.00	3.31	0.41	7.0	539.5
2019	219.9	499.1	69.0	15.9	8.4	75.9	1.5	275.5	28.0	25.8	3.27	0.00	3.31	0.40	7.0	539.5
2020	217.3	494.6	68.3	15.8	8.4	74.4	1.2	280.3	28.7	26.2	3.15	0.00	3.31	0.39	7.0	539.5
2025	204.2	472.0	64.7	15.5	8.4	66.6	0.4	282.2	31.5	27.0	2.60	0.00	3.29	0.35	7.0	539.5
2030	190.9	449.8	61.4	15.1	8.4	58.8	0.2	251.9	32.0	26.0	2.09	0.00	3.24	0.32	7.0	539.5
2035	177.8	428.5	58.2	14.7	8.3	51.3	0.1	198.8	29.8	23.3	1.66	0.00	3.16	0.28	7.0	539.5
2040	165.1	408.1	55.1	14.3	8.3	44.4	0.0	142.9	26.0	19.6	1.30	0.00	3.06	0.25	7.0	539.5
2045	152.8	388.6	52.3	14.0	8.3	38.1	0.0	98.7	21.7	16.0	1.01	0.00	2.95	0.22	7.0	539.5
2050	141.1	370.0	49.5	13.6	8.2	32.6	0.0	66.4	17.7	12.7	0.77	0.00	2.83	0.19	7.0	539.5
2055	130.0	352.3	46.9	13.3	8.2	27.7	0.0	44.2	14.1	9.9	0.59	0.00	2.71	0.17	7.0	539.5
2060	119.6	335.5	44.5	12.9	8.1	23.4	0.0	29.3	11.1	7.7	0.45	0.00	2.58	0.15	7.0	539.5
2065	109.8	319.4	42.1	12.6	8.0	19.8	0.0	19.3	8.6	5.9	0.34	0.00	2.45	0.13	7.0	539.5
2070	100.7	304.1	39.9	12.2	8.0	16.6	0.0	12.8	6.7	4.5	0.26	0.00	2.32	0.11	7.0	539.5
2075	92.3	289.6	37.9	11.9	7.9	14.0	0.0	8.4	5.1	3.4	0.19	0.00	2.20	0.10	7.0	539.5
2080	84.5	275.7	35.9	11.6	7.9	11.7	0.0	5.6	3.9	2.6	0.14	0.00	2.07	0.08	7.0	539.5
2085	77.2	262.5	34.0	11.3	7.8	9.8	0.0	3.7	3.0	2.0	0.11	0.00	1.96	0.07	7.0	539.5
2090	70.6	250.0	32.2	11.0	7.7	8.2	0.0	2.4	2.3	1.5	0.08	0.00	1.84	0.06	7.0	539.5
2095	64.4	238.0	30.5	10.7	7.7	6.8	0.0	1.6	1.7	1.2	0.06	0.00	1.73	0.05	7.0	539.5
2100	58.8	226.6	28.9	10.5	7.6	5.7	0.0	1.1	1.3	0.9	0.04	0.00	1.63	0.04	7.0	539.5

APPENDICES

APPENDIX A
LIST OF INTERNATIONAL AUTHORS, CONTRIBUTORS, AND REVIEWERS

APPENDIX B
MAJOR ACRONYMS AND ABBREVIATIONS

APPENDIX C
CHEMICAL FORMULAE AND NOMENCLATURE

APPENDIX A

LIST OF INTERNATIONAL AUTHORS, CONTRIBUTORS, AND REVIEWERS

COCHAIRS

Ayité-Lô Nohende Ajavon	North-South Environment	Togo
Paul A. Newman	NASA Goddard Space Flight Center	USA
John A. Pyle	National Centre for Atmospheric Science, UK and University of Cambridge	UK
A.R. Ravishankara	Colorado State University and NOAA ESRL Chemical Sciences Division	USA

SCIENTIFIC STEERING COMMITTEE

Ayité-Lô Nohende Ajavon	North-South Environment	Togo
David J. Karoly	University of Melbourne	Australia
Malcolm K. Ko	NASA Langley Research Center	USA
Paul A. Newman	NASA Goddard Space Flight Center	USA
John A. Pyle	National Centre for Atmospheric Science, UK and University of Cambridge	UK
A.R. Ravishankara	Colorado State University and NOAA ESRL Chemical Sciences Division	USA
Theodore G. Shepherd	University of Reading, Department of Meteorology	UK
Susan Solomon	Massachusetts Institute of Technology, Department of Earth, Atmospheric, and Planetary Sciences	USA

AUTHORS AND CONTRIBUTORS

CHAPTER 1
UPDATE ON OZONE-DEPLETING SUBSTANCES (ODSs) AND OTHER GASES OF INTEREST TO THE MONTREAL PROTOCOL

Lead Authors

Lucy J. Carpenter	University of York	USA
Stefan Reimann	Empa, Swiss Federal Laboratories for Materials Science and Technology	Germany

Chapter Editors

Andreas Engel	Goethe University Frankfurt, Institute for Atmospheric and Environmental Sciences	Germany
Stephen A. Montzka	NOAA ESRL Global Monitoring Division	USA

Coauthors

James B. Burkholder	NOAA ESRL Chemical Sciences Division	USA
Cathy Clerbaux	Sorbonne Universités, UPMC Univ. Paris 06; Université Versailles St-Quentin; CNRS / INSU; LATMOS-IPSL	France
Bradley D. Hall	NOAA ESRL Global Monitoring Division	USA
Ryan Hossaini	University of Leeds	UK
Johannes C. Laube	University of East Anglia	UK
Shari A. Yvon-Lewis	Texas A&M University	USA

Contributors

Donald R. Blake	University of California Irvine	USA
Marcel Dorf	Max-Planck-Institut für Chemie	Germany
Geoffrey S. Dutton	CIRES-University of Colorado / NOAA ESRL Global Monitoring Division	USA
Paul J. Fraser	CSIRO Marine and Atmospheric Research / Centre for Weather and Climate Research	Australia
Lucien Froidevaux	Jet Propulsion Laboratory, California Institute of Technology	USA
François Hendrick	Belgian Institute for Space Aeronomy	Belgium
Jianxin Hu	Peking University, College of Environmental Sciences and Engineering	China
Ashley Jones	University of Toronto	Canada
Paul B. Krummel	Centre for Australian Weather and Climate Research, CSIRO Marine and Atmospheric Research	Australia
Lambert J.M. Kuijpers	Technical University Eindhoven, Eindhoven Center for Sustainability	The Netherlands
Michael J.Kurylo	Universities Space Research Association / Goddard Earth Sciences, Technology, and Research	USA
Qing Liang	Universities Space Research Association / NASA Goddard Space Flight Center	USA
Emmanuel Mahieu	University of Liège	Belgium
Jens Mühle	Scripps Institution of Oceanography, University of California San Diego	USA
Simon O'Doherty	University of Bristol	UK
Keiichi Ohnishi	Asahi Glass Co., Ltd.	Japan
Vladimir L. Orkin	National Institute of Standards and Technology	USA
Klaus Pfeilsticker	University of Heidelberg	Germany
Matt Rigby	University of Bristol	UK
Isobel J. Simpson	University of California Irvine	USA
Yoko Yokouchi	National Institute for Environmental Studies	Japan

Editorial Contributions

Nada Derek	University of York	UK
Jenny Hudson	Commonwealth Scientific and Industrial Research Organisation	Australia

CHAPTER 2
UPDATE ON GLOBAL OZONE: PAST, PRESENT, AND FUTURE

Lead Authors

Steven Pawson	NASA Goddard Space Flight Center	USA
Wolfgang Steinbrecht	Deutscher Wetterdienst, Hohenpeissenberg	Germany

Chapter Editors

Vitali E. Fioletov	Environment Canada, Measurements and Analysis Research Section	Canada
Ulrike Langematz	Freie Universität Berlin, Institut für Meteorologie	Germany

Coauthors

Andrew Charlton-Perez	University of Reading	UK
Masatomo Fujiwara	Hokkaido University	Japan
Alexey Yu. Karpechko	Finnish Meteorological Institute	Finland
Irina Petropavlovskikh	CIRES-University of Colorado / NOAA ESRL Global Monitoring Division	USA
Joachim Urban	Chalmers University of Technology	Sweden
Mark Weber	University of Bremen, Institute of Environmental Physics	Germany

Contributors

Valentina Aquila	GESTAR / The Johns Hopkins University	USA
Wissam Chehade	University of Bremen, Institute of Environmental Physics	Germany
Irene Cionni	Technical Unit for Energy and Environmental Modeling, ENEA	Italy
Melanie Coldewey-Egbers	Deutsches Zentrum für Luft- und Raumfahrt (DLR), Institut für Methodik der Fernerkundung	Germany
Andy Delcloo	Royal Meteorological Institute	Belgium
Sandip Dhomse	University of Leeds, School of Earth and Environment	UK
Veronika Eyring	Deutsches Zentrum für Luft- und Raumfahrt (DLR), Institut für Physik der Atmosphäre	Germany
Eric L. Fleming	Science Systems and Applications, Inc.	USA
Stacey M. Frith	Science Systems and Applications, Inc.	USA
Lucien Froidevaux	Jet Propulsion Laboratory, California Institute of Technology	USA
Nathan P. Gillett	Environment Canada	Canada
Birgit Hassler	CIRES-University of Colorado / NOAA ESRL Chemical Sciences Division	USA
Michaela I. Hegglin	University of Reading, Department of Meteorology	UK
Doug Kinnison	National Center for Atmospheric Research, Atmospheric Chemistry Division	USA
Diego Loyola	Deutsches Zentrum für Luft- und Raumfahrt (DLR), Institut für Methodik der Fernerkundung	Germany
Chris McLinden	Environment Canada, Air Quality Research Division	Canada
Luke D. Oman	NASA Goddard Space Flight Center	USA
David Plummer	Environment Canada	Canada
Laura Revell	Swiss Federal Institute of Technology Zürich	Switzerland
Takatoshi Sakazaki	Kyoto University	Japan
William Seviour	Oxford University	UK

Susann Tegtmeier	GEOMAR Helmholtz Centre for Ocean Research Kiel	Germany
Ronald van der A	Royal Netherlands Meteorological Institute (KNMI)	The Netherlands
Jeannette Wild	Innovim and NOAA / NWS / NCEP Climate Prediction Center	USA

CHAPTER 3
UPDATE ON POLAR OZONE: PAST, PRESENT, AND FUTURE

Lead Authors

Martin Dameris	Deutsches Zentrum für Luft- und Raumfahrt (DLR), Institut für Physik der Atmosphäre	Germany
Sophie Godin-Beekmann	Université de Versailles Saint-Quentin; Sorbonne Universités, UPMC Univ. Paris 06; CNRS / INSU; OVSQ-LATMOS	France

Chapter Editors

Slimane Bekki	Sorbonne Universités, UPMC Univ. Paris 06; Université Versailles St-Quentin; CNRS / INSU; LATMOS-IPSL	France
Judith Perlwitz	CIRES-University of Colorado / NOAA ESRL Physical Sciences Division	USA

Coauthors

Simon Alexander	Australian Antarctic Division	Australia
Peter Braesicke	Karlsruhe Institute of Technology, Institute for Meteorology and Climate Research	Germany
Martyn P. Chipperfield	University of Leeds, School of Earth and Environment	UK
A.T. Jos de Laat	Royal Netherlands Meteorological Institute (KNMI)	The Netherlands
Yvan J. Orsolini	Norwegian Institute for Air Research (NILU)	Norway
Markus Rex	Alfred Wegener Institute – Helmholtz Centre for Polar and Marine Research	Germany
Michelle L. Santee	Jet Propulsion Laboratory, California Institute of Technology	USA

Contributors

Ronald van der A	Royal Netherlands Meteorological Institute (KNMI)	The Netherlands
Irene Cionni	Technical Unit for Energy and Environmental Modeling, ENEA	Italy
Sandip Dhomse	University of Leeds, School of Earth and Environment	UK
Susana B. Diaz	Instituto de Investigaciones en Ingenieria Genetica y Biologia molecular (INGEBI), Consejo Nacional de Investigaciones Cientificas y Tecnologicas (CONICET)	Argentina
Ines Engel	Forschungszentrum Jülich, Institute of Energy and Climate Research – Stratosphere	Germany
Peter von der Gathen	Alfred Wegener Institute – Helmholtz Centre for Polar and Marine Research	Germany
Jens-Uwe Grooß	Forschungszentrum Jülich	Germany
Birgit Hassler	CIRES-University of Colorado / NOAA ESRL Chemical Sciences Division	USA
Larry Horowitz	NOAA Geophysical Fluid Dynamics Laboratory	USA
Karin Kreher	Bodeker Scientific and NIWA	New Zealand
Markus Kunze	Freie Universität Berlin, Institut für Meteorologie	Germany

Ulrike Langematz	Freie Universität Berlin, Institut für Meteorologie	Germany
Gloria L. Manney	NorthWest Research Associates	USA
Rolf Müller	Forschungszentrum Jülich GmbH	Germany
Giovanni Pitari	Università degli Studi de L'Aquila, Dipartimento di Scienze Fisiche e Chimiche	Italy
Michael C. Pitts	NASA Langley Research Center, Atmospheric Composition Branch	USA
Lamont R. Poole	Science Systems and Applications, Inc.	USA
Robyn Schofield	University of Melbourne, ARC Centre of Excellence for Climate System Science	Australia
Simone Tilmes	National Center for Atmospheric Research	USA
Mark Weber	University of Bremen, Institute of Environmental Physics	Germany

CHAPTER 4
STRATOSPHERIC OZONE CHANGES AND CLIMATE

Lead Authors

Julie M. Arblaster	Australian Bureau of Meteorology and National Center for Atmospheric Research	Australia / USA
Nathan P. Gillett	Environment Canada	Canada

Chapter Editors

Lesley J. Gray	National Centre for Atmospheric Science, UK and University of Oxford	UK
David W.J. Thompson	Colorado State University	USA

Coauthors

Natalia Calvo	Complutense University of Madrid	Spain
Piers M. Forster	University of Leeds	UK
Lorenzo M. Polvani	Columbia University	USA
Seok-Woo Son	Seoul National University	Korea
Darryn W. Waugh	The Johns Hopkins University	USA
Paul J. Young	Lancaster University	UK

Contributors

Elizabeth A. Barnes	Colorado State University	USA
Irene Cionni	Technical Unit for Energy and Environmental Modeling, ENEA	Italy
Chaim I. Garfinkel	Hebrew University	Israel
Edwin P. Gerber	New York University	USA
Steven C. Hardiman	Met Office Hadley Centre	UK
Dale F. Hurst	CIRES-University of Colorado / NOAA ESRL Global Monitoring Division	USA
Jean-François Lamarque	National Center for Atmospheric Research	USA
Eun-Pa Lim	Australian Bureau of Meteorology	Australia
Michael P. Meredith	British Antarctic Survey	UK
Judith Perlwitz	CIRES-University of Colorado / NOAA ESRL Physical Sciences Division	USA

Robert W. Portmann	NOAA ESRL Chemical Sciences Division	USA
Michael Previdi	Columbia University, Lamont-Doherty Earth Observatory	USA
Michael Sigmond	Environment Canada	Canada
Neil C. Swart	Environment Canada	Canada
Jean-Paul Vernier	NASA Langley Research Center	USA
Yutian Wu	Purdue University	USA

CHAPTER 5
SCENARIOS AND INFORMATION FOR POLICYMAKERS

Lead Authors

Neil R.P. Harris	University of Cambridge	UK
Donald J. Wuebbles	University of Illinois	USA

Chapter Editors

Mack McFarland	DuPont Chemicals & Fluoroproducts	USA
Guus J.M. Velders	National Institute for Public Health and the Environment (RIVM)	The Netherlands

Coauthors

John S. Daniel	NOAA ESRL Chemical Sciences Division	USA
Jianxin Hu	Peking University, College of Environmental Sciences and Engineering	China
Lambert J.M. Kuijpers	Technical University Eindhoven, Eindhoven Center for Sustainability	The Netherlands
Katharine S. Law	Sorbonne Universités, UPMC Univ. Paris 06; Université Versailles St-Quentin; CNRS / INSU; LATMOS-IPSL	France
Michael J. Prather	University of California Irvine / Earth System Science Department	USA
Robyn Schofield	University of Melbourne, ARC Centre of Excellence for Climate System Science	Australia

Contributors

James B. Burkholder	NOAA ESRL Chemical Sciences Division	USA
Eric L. Fleming	Science Systems and Applications, Inc.	USA
Øivind Hodnebrog	Center for International Climate and Environmental Research – Oslo (CICERO)	Norway
Ryan Hossaini	University of Leeds	UK
Charles H. Jackman	NASA Goddard Space Flight Center	USA
Daniel Phoenix	University of Illinois	USA

TWENTY QUESTIONS AND ANSWERS ABOUT THE OZONE LAYER: 2014 UPDATE

Lead Author

Michaela I. Hegglin	University of Reading, Department of Meteorology	UK

REVIEWERS

Jon Abbatt	University of Toronto	Canada
Ayité-Lô Nohende Ajavon	North-South Environment	Togo
Hideharu Akiyoshi	National Institute for Environmental Studies	Japan
Joan M. Alexander	NorthWest Research Associates	USA
Simon Alexander	Australian Antarctic Division	Australia
Stephen O. Andersen	Institute for Governance & Sustainable Development	USA
Julie M. Arblaster	Australian Bureau of Meteorology and National Center for Atmospheric Research	Australia / USA
Matthew Ashfold	University of Nottingham Malaysia Campus	Malaysia
Ghassem Asrar	Joint Global Change Research Institute (PNNL / UMD)	USA
Pieter J. Aucamp	Ptersa Environmental Management Consultants, South Africa	South Africa
Alkiviadis F. Bais	Aristotle University of Thessaloniki	Greece
Mark P. Baldwin	University of Exeter	UK
Steven L. Baughcum	Boeing Company	USA
Gufran Beig	Indian Institute of Tropical Meteorology	India
Slimane Bekki	Sorbonne Universités, UPMC Univ. Paris 06; Université Versailles St-Quentin; CNRS / INSU; LATMOS-IPSL	France
Peter Bernath	Old Dominion University	USA
Thomas Birner	Colorado State University, Department of Atmospheric Science	USA
Greg Bodeker	Bodeker Scientific	New Zealand
Rumen D. Bojkov	Consultant on ozone and climate change	Germany
Geir O. Braathen	World Meteorological Organization	Switzerland
Stefan Brönnimann	University of Bern, Institute of Geography	Switzerland
Dominik Brunner	Empa, Swiss Federal Laboratories for Materials Science and Technology	Switzerland
John P. Burrows	University of Bremen, Institute of Environmental Physics / Institute of Remote Sensing	Germany
Neal Butchart	Met Office Hadley Centre	UK
Amy H. Butler	CIRES-University of Colorado / NOAA ESRL Chemical Sciences Division	USA
Wenju Cai	Commonwealth Scientific and Industrial Research Organization, Division of Marine and Atmospheric Research	Australia
Francesco Cairo	National Research Council – Institute of Atmospheric Sciences and Climate	Italy
Pablo O. Canziani	Pontificia Universidad Católica Argentina / Consejo Nacional de Investigaciones Científicas y Técnicas) / PEPACG	Argentina
Lucy J. Carpenter	University of York	UK
Kenneth S. Carslaw	University of Leeds, School of Earth and Environment	UK
Andrew Charlton-Perez	University of Reading	UK
Martyn P. Chipperfield	University of Leeds, School of Earth and Environment	UK
Bo Christiansen	Danish Meteorological Institute	Denmark
Cathy Clerbaux	Sorbonne Universités, UPMC Univ. Paris 06; Université Versailles St-Quentin; CNRS / INSU; LATMOS-IPSL	France
Martin Dameris	Deutsches Zentrum für Luft- und Raumfahrt (DLR), Institut für Physik der Atmosphäre	Germany
John S. Daniel	NOAA ESRL Chemical Sciences Division	USA
Sandip Dhomse	University of Leeds, School of Earth and Environment	UK

Susana B. Diaz	Instituto de Investigaciones en Ingenieria Genetica y Biologia molecular (INGEBI), Consejo Nacional de Investigaciones Cientificas y Tecnologicas (CONICET)	Argentina
Anne R. Douglass	NASA Goddard Space Flight Center	USA
Richard S. Eckman	NASA Headquarters	USA
Nawo Eguchi	Kyushu University, Research Institute for Applied Mechanics	Japan
James William Elkins	NOAA ESRL Global Monitoring Division	USA
Andreas Engel	Goethe University Frankfurt, Institute for Atmospheric and Environmental Sciences	Germany
Christine A. Ennis	CIRES-University of Colorado / NOAA ESRL Chemical Sciences Division	USA
Veronika Eyring	Deutsches Zentrum für Luft- und Raumfahrt (DLR), Institut für Physik der Atmosphäre	Germany
David W. Fahey	NOAA ESRL Chemical Sciences Division	USA
Vitali E. Fioletov	Environment Canada, Measurements and Analysis Research Section	Canada
Piers M. Forster	University of Leeds	UK
Paul J. Fraser	CSIRO Marine and Atmospheric Research / Centre for Weather and Climate Research	Australia
Lucien Froidevaux	Jet Propulsion Laboratory, California Institute of Technology	USA
Jan Fuglestvedt	Center for International Climate and Environmental Research – Oslo (CICERO)	Norway
John C. Fyfe	Environment Canada, Canadian Centre for Climate Modeling and Analysis	Canada
Annie Gabriel	Department of the Environment	Australia
Lenah Gaoetswe	Department of Meteorological Services	Botswana
Hella Garny	Deutsches Zentrum für Luft- und Raumfahrt (DLR), Institut für Physik der Atmosphäre	Germany
Marvin A. Geller	Stony Brook University	USA
Edwin P. Gerber	New York University	USA
Andrew Gettelman	National Center for Atmospheric Research	USA
Tomasz Gierczak	Warsaw University	Poland
Manuel Gil-Ojeda	Área de Investigación e Instrumentación Atmosférica, Instituto Nacional de Técnica Aeroespacial-INTA	Spain
Nathan P. Gillett	Environment Canada	Canada
Sophie Godin-Beekmann	Université de Versailles Saint-Quentin; Sorbonne Universités, UPMC Univ. Paris 06; CNRS / INSU; OVSQ-LATMOS	France
Marco González	Sistemas de Energia	Costa Rica
Lesley J. Gray	National Centre for Atmospheric Science, UK and University of Oxford	UK
Kevin M. Grise	Columbia University, Lamont-Doherty Earth Observatory	USA
Jens-Uwe Grooß	Forschungszentrum Jülich	Germany
Serge Guillas	University College London	UK
Joanna D. Haigh	Imperial College London	UK
Bradley D. Hall	NOAA ESRL Global Monitoring Division	USA
Neil R.P. Harris	University of Cambridge	UK
Birgit Hassler	CIRES-University of Colorado / NOAA ESRL Chemical Sciences Division	USA
Alain Hauchecorne	Université Versailles St-Quentin; Sorbonne Universités, UPMC Univ. Paris 06; CNRS / INSU; LATMOS-IPSL	France
Peter Haynes	University of Cambridge, Centre for Mathematical Sciences	UK

Michaela I. Hegglin	University of Reading, Department of Meteorology	UK
Peter Hitchcock	University of Cambridge, Department of Applied Mathematics and Theoretical Physics	UK
Øivind Hodnebrog	Center for International Climate and Environmental Research – Oslo (CICERO)	Norway
Jianxin Hu	Peking University, College of Environmental Sciences and Engineering	China
Nathalie Huret	Université d'Orléans / OSUC, CNRS / Laboratoire de Physique et Chimie de l'Environnement et de l'Espace	France
Iolanda Ialongo	Finnish Meteorological Institute, Earth Observation unit	Finland
Mohammad Ilyas	University of Malaysia Perlis	Malaysia
Franz Immler	European Commission	Belgium
Ivar S.A. Isaksen	University of Oslo	Norway
Michal Janouch	Czech Hydrometeorological Institute, Solar and Ozone Observatory	Czech Republic
Julie M. Jones	University of Sheffield, Department of Geography	UK
Kenneth W. Jucks	NASA Headquarters	USA
David J. Karoly	University of Melbourne	Australia
Alexey Yu. Karpechko	Finnish Meteorological Institute	Finland
Yasuko Kasai	National Institute of Information and Communications Technology	Japan
Philippe Keckhut	Université Versailles St-Quentin; Sorbonne Universités, UPMC Univ. Paris 06; CNRS / INSU, LATMOS-IPSL	France
Sergey Khaykin	Central Aerological Observatory of Roshydromet	Russia
Andrew R. Klekociuk	Australian Antarctic Division	Australia
Jeff R. Knight	Met Office Hadley Centre	UK
Malcolm K. Ko	NASA Langley Research Center	USA
Yutaka Kondo	Department of Earth and Planetary Science, Graduate School of Science, The University of Tokyo	Japan
Karin Kreher	Bodeker Scientific and NIWA	New Zealand
Kirstin Krüger	University of Oslo, Department of Geosciences	Norway
Paul B. Krummel	Centre for Australian Weather and Climate Research, CSIRO Marine and Atmospheric Research	Australia
Lambert J.M. Kuijpers	Technical University Eindhoven, Eindhoven Center for Sustainability	The Netherlands
Michael J.Kurylo	Universities Space Research Association / Goddard Earth Sciences, Technology, and Research	USA
Paul J. Kushner	University of Toronto, Department of Physics	Canada
Erkki Kyrölä	Finnish Meteorological Institute, Earth Observation	Finland
Gabriela Lakkis	Pontificia Universidad Católica Argentina, PEPACG	Argentina
Shyam Lal	Physical Research Laboratory	India
Jean-François Lamarque	National Center for Atmospheric Research, Earth System Laboratory	USA
Tom Land	U.S. Environmental Protection Agency, Office of Atmospheric Programs, Stratospheric Protection Division	USA
Ulrike Langematz	Freie Universität Berlin, Institut für Meteorologie	Germany
Franck Lefèvre	Sorbonne Universités, UPMC Univ. Paris 06; Université Versailles St-Quentin; CNRS / INSU; LATMOS-IPSL	France
Bernard Legras	Laboratoire de Météorologie Dynamique, CNRS / Ecole Normale Supérieure / UPMC / Ecole Polytechnique / IPSL	France
Jos Lelieveld	Max Planck Institute for Chemistry – Mainz	Germany

Jintai Lin	Peking University, Department of Atmospheric and Oceanic Sciences	China
Nathaniel Livesey	Jet Propulsion Laboratory, California Institute of Technology	USA
Desmond Manatsa	Bindura University of Science	Zimbabwe
Gloria L. Manney	NorthWest Research Associates	USA
Martin R. Manning	New Zealand Climate Change Research Institute	New Zealand
Elisa Manzini	Max-Planck-Institut für Meteorologie – Hamburg	Germany
Bella Maranion	U.S. Environmental Protection Agency	USA
Daniel R. Marsh	National Center for Atmospheric Research	USA
Amanda C. Maycock	University of Cambridge, Centre for Atmospheric Science	UK
Mack McFarland	DuPont Chemicals & Fluoroproducts	USA
Charles McLandress	University of Toronto, Department of Physics	Canada
Johan Mellqvist	Chalmers University of Technology	Sweden
Pauline M. Midgley	University of Bern	Switzerland
Daniel M. Mitchell	University of Oxford, Department of Physics	UK
Mario J. Molina	University of California San Diego, Department of Chemistry and Biochemistry	USA
Stephen A. Montzka	NOAA ESRL Global Monitoring Division	USA
Olaf Morgenstern	National Institute of Water and Atmospheric Research (NIWA) Lauder	New Zealand
Rolf Müller	Forschungszentrum Jülich GmbH	Germany
Hiroaki Naoe	Japan Meteorological Agency	Japan
Thando Ndarana	South African Weather Service	South Africa
Paul A. Newman	NASA Goddard Space Flight Center	USA
Ole John Nielsen	Copenhagen Center for Atmospheric Research (CCAR), Department of Chemistry, University of Copenhagen	Denmark
Luke D. Oman	NASA Goddard Space Flight Center	USA
Vladimir L. Orkin	National Institute of Standards and Technology	USA
Andrew Orr	British Antarctic Survey	UK
Steven Pawson	NASA Goddard Space Flight Center	USA
Juan Carlos Peláez	Centro de Física de la Atmósfera, Instituto de Meteorología de Cuba	Cuba
Stuart A. Penkett	University of East Anglia	UK
Judith Perlwitz	CIRES-University of Colorado / NOAA ESRL Physical Sciences Division	USA
Thomas Peter	Swiss Federal Institute of Technology Zürich, Institute for Atmospheric and Climate Science	Switzerland
Damaris K. Pinheiro	Federal University of Santa Maria	Brazil
Giovanni Pitari	Università degli Studi de L'Aquila, Dipartimento di Scienze Fisiche e Chimiche	Italy
David Plummer	Environment Canada	Canada
Lorenzo M. Polvani	Columbia University	USA
Jean-Pierre Pommereau	Université Versailles St-Quentin; Sorbonne Universités, UPMC Univ. Paris 06; CNRS / INSU; LATMOS-IPSL	France
Ronald G. Prinn	Massachusetts Institute of Technology, Center for Global Change Science	USA
John A. Pyle	National Centre for Atmospheric Science, UK and University of Cambridge	UK
Birgit Quack	GEOMAR Helmholtz Centre for Ocean Research Kiel	Germany
B. Rajakumar	Indian Institute of Technology Madras, Department of Chemistry	India

S. Ramachandran	Physical Research Laboratory	India
V. Ramaswamy	NOAA Geophysical Fluid Dynamics Laboratory	USA
Cora Randall	University of Colorado / Laboratory for Atmospheric and Space Physics	USA
William Randel	National Center for Atmospheric Research	USA
Marilyn Raphael	University of California Los Angeles, Department of Geography	USA
A.R. Ravishankara	NOAA ESRL Chemical Sciences Division and Colorado State University, Department of Chemistry and Department of Atmospheric Science	USA
Stefan Reimann	Empa, Swiss Federal Laboratories for Materials Science and Technology	Switzerland
James Renwick	Victoria University of Wellington	New Zealand
Markus Rex	Alfred Wegener Institute – Helmholtz Centre for Polar and Marine Research	Germany
Robert C. Rhew	University of California Berkeley	USA
Harald E. Rieder	University of Graz, Austria	Austria
Martin Riese	Forschungszentrum Jülich, Institute of Energy and Climate Research – Stratosphere	Germany
Vincenzo Rizi	CETEMPS, Dipartimento di Scienze Fisiche e Chimiche, Università Degli Studi dell'Aquila	Italy
Alan Robock	Rutgers University, Department of Environmental Sciences	USA
Jose M. Rodriguez	NASA Goddard Space Flight Center	USA
Eugene Rozanov	World Radiation Center / Swiss Federal Institute of Technology Zürich	Switzerland
Vladimir Ryabinin	World Climate Research Programme	Switzerland
Alfonso Saiz-Lopez	Consejo Superior de Investigaciones Cientificas, Institute of Physical Chemistry Rocasolano	Spain
Ross J. Salawitch	University of Maryland, College Park	USA
Michelle L. Santee	Jet Propulsion Laboratory, California Institute of Technology	USA
Robert Sausen	Deutsches Zentrum für Luft- und Raumfahrt (DLR), Institut für Physik der Atmosphäre	Germany
Sue Schauffler	National Center for Atmospheric Research	USA
Robyn Schofield	University of Melbourne, ARC Centre of Excellence for Climate System Science	Australia
Dian J. Seidel	NOAA Air Resources Laboratory	USA
Megumi Seki	United Nations Environment Programme, Ozone Secretariat	Kenya
Jonathan Shanklin	British Antarctic Survey	UK
Tiffany A. Shaw	Columbia University, Lamont-Doherty Earth Observatory	USA
Rajendra Shende	TERRE Policy Centre	India
Theodore G. Shepherd	University of Reading, Department of Meteorology	UK
Kiyotaka Shibata	Meteorological Research Institute	Japan
Keith Shine	University of Reading, Department of Meteorology	UK
Masato Shiotani	Kyoto University, Research Institute for Sustainable Humanosphere	Japan
Peter Simmonds	University of Bristol (retired)	UK
Isla R. Simpson	Columbia University, Lamont-Doherty Earth Observatory	USA
Rajiv R. Singh	Honeywell International	USA
Björn-Martin Sinnhuber	Karlsruhe Institute of Technology	Germany
Karen L. Smith	Columbia University, Lamont-Doherty Earth Observatory	USA

Susan Solomon	Massachusetts Institute of Technology, Department of Earth, Atmospheric, and Planetary Sciences	USA
Johannes Staehelin	Swiss Federal Institute of Technology Zürich, Institute for Atmospheric and Climate Science	Switzerland
Wolfgang Steinbrecht	Deutscher Wetterdienst, Hohenpeissenberg	Germany
Gabriele P. Stiller	Karlsruhe Institute of Technology, Institute for Meteorology and Climate Research	Germany
Richard S. Stolarski	The Johns Hopkins University	USA
William T. Sturges	University of East Anglia	UK
Tove M. Svendby	Norwegian Institute for Air Research (NILU)	Norway
Neil C. Swart	Environment Canada	Canada
David W. Tarasick	Environment Canada	Canada
Susann Tegtmeier	GEOMAR Helmholtz Centre for Ocean Research Kiel	Germany
Said Ali Thaoubane	Université des Comores	Comoros
Larry W. Thomason	NASA Langley Research Center	USA
David W.J. Thompson	Colorado State University	USA
Simone Tilmes	National Center for Atmospheric Research	USA
Owen Brian Toon	University of Colorado, Laboratory for Atmospheric and Space Physics, Department of Atmospheric and Oceanic Sciences	USA
Matthew B. Tully	Australian Bureau of Meteorology	Australia
John Turner	British Antarctic Survey	UK
Guus J.M. Velders	National Institute for Public Health and the Environment (RIVM)	The Netherlands
Daniel P. Verdonik	Hughes Associates, Inc.	USA
Martin K. Vollmer	Empa, Swiss Federal Laboratories for Materials Science and Technology	Switzerland
Christian von Savigny	Ernst-Moritz-Arndt-University of Greifswald, Institute of Physics	Germany
Timothy J. Wallington	Ford Motor Company	USA
Darryn W. Waugh	The Johns Hopkins University	USA
Ann R. Webb	University of Manchester	UK
Debra K. Weisenstein	Harvard University, School of Engineering and Applied Science	USA
Ray F. Weiss	University of California San Diego, Scripps Institution of Oceanography	USA
Laura J. Wilcox	University of Reading, Department of Meteorology	UK
Elian Augusto Wolfram	Laser Research Center and Applications, CEILAP (CITEDEF-CONICET)	Argentina
Donald J. Wuebbles	University of Illinois	USA
Shi-Keng Yang	NOAA / NWS / NCEP Climate Prediction Center	USA
Shigeo Yoden	Kyoto University	Japan
Durwood Zaelke	Institute for Governance and Sustainable Development	USA
Christos S. Zerefos	Academy of Athens	Greece
Lingxi Zhou	Chinese Meteorological Administration, Chinese Academy of Meteorological Sciences	China
Jerry Ziemke	NASA Goddard Space Flight Center	USA

OZONE PEER-REVIEW MEETING

Les Diablerets, Switzerland
23-27 June 2014

by Maria Montzka, Fall 2006

Ayité-Lô Nohende Ajavon	North-South Environment	Togo
Stephen O. Andersen	Institute for Governance & Sustainable Development	USA
Julie M. Arblaster *(remote)*	Australian Bureau of Meteorology and National Center for Atmospheric Research	Australia/USA
Pieter J. Aucamp	Ptersa Environmental Management Consultants, South Africa	South Africa
Gufran Beig	Indian Institute of Tropical Meteorology	India
Geir O. Braathen	World Meteorological Organization	Switzerland
John P. Burrows	University of Bremen, Institute of Environmental Physics / Institute of Remote Sensing	Germany
Pablo O. Canziani	Pontificia Universidad Católica Argentina / Consejo Nacional de Investigaciones Científicas y Técnicas) / PEPACG	Argentina
Lucy J. Carpenter	University of York	UK
Martyn P. Chipperfield	University of Leeds, School of Earth and Environment	UK
Martin Dameris	Deutsches Zentrum für Luft- und Raumfahrt (DLR), Institut für Physik der Atmosphäre	Germany
John S. Daniel	NOAA ESRL Chemical Sciences Division	USA
Christine A. Ennis	CIRES-University of Colorado / NOAA ESRL Chemical Sciences Division	USA
David W. Fahey	NOAA ESRL Chemical Sciences Division	USA
Vitali E. Fioletov	Environment Canada, Measurements and Analysis Research Section	Canada
Lucien Froidevaux	Jet Propulsion Laboratory, California Institute of Technology	USA
Nathan P. Gillett	Environment Canada	Canada
Sophie Godin-Beekmann	Université de Versailles Saint-Quentin; Sorbonne Universités, UPMC Univ. Paris 06; CNRS / INSU; OVSQ-LATMOS	France
Marco González	Sistemas de Energia	Costa Rica
Neil R.P. Harris	University of Cambridge	UK
Michaela I. Hegglin	University of Reading, Department of Meteorology	UK
Kenneth W. Jucks	NASA Headquarters	USA

David J. Karoly	University of Melbourne	Australia
Malcolm K. Ko	NASA Langley Research Center	USA
Lambert J.M. Kuijpers	Technical University Eindhoven, Eindhoven Center for Sustainability	The Netherlands
Michael J.Kurylo	Universities Space Research Association / Goddard Earth Sciences, Technology, and Research	USA
Ulrike Langematz	Freie Universität Berlin, Institut für Meteorologie	Germany
Martin R. Manning	New Zealand Climate Change Research Institute	New Zealand
Amanda C. Maycock	University of Cambridge, Centre for Atmospheric Science	UK
Mack McFarland	DuPont Chemicals & Fluoroproducts	USA
Pauline M. Midgley	University of Bern	Switzerland
Stephen A. Montzka	NOAA ESRL Global Monitoring Division	USA
Olaf Morgenstern	National Institute of Water and Atmospheric Research (NIWA) Lauder	New Zealand
Rolf Müller	Forschungszentrum Jülich GmbH	Germany
Hiroaki Naoe	Japan Meteorological Agency	Japan
Paul A. Newman	NASA Goddard Space Flight Center	USA
Steven Pawson	NASA Goddard Space Flight Center	USA
Thomas Peter	Swiss Federal Institute of Technology Zürich, Institute for Atmospheric and Climate Science	Switzerland
David Plummer	Environment Canada	Canada
Lorenzo M. Polvani	Columbia University	USA
Ronald G. Prinn	Massachusetts Institute of Technology, Center for Global Change Science	USA
John A. Pyle	National Centre for Atmospheric Science, UK and University of Cambridge	UK
A.R. Ravishankara	NOAA ESRL Chemical Sciences Division and Colorado State University, Department of Chemistry and Department of Atmospheric Science	USA
Stefan Reimann	Empa, Swiss Federal Laboratories for Materials Science and Technology	Switzerland
Jose M. Rodriguez	NASA Goddard Space Flight Center	USA
Ross J. Salawitch	University of Maryland, College Park	USA
Megumi Seki	United Nations Environment Programme, Ozone Secretariat	Kenya
Rajendra Shende	TERRE Policy Centre	India
Theodore G. Shepherd	University of Reading, Department of Meteorology	UK
Susan Solomon	Massachusetts Institute of Technology, Department of Earth, Atmospheric, and Planetary Sciences	USA
Wolfgang Steinbrecht	Deutscher Wetterdienst, Hohenpeissenberg	Germany
William T. Sturges	University of East Anglia	UK
David W.J. Thompson	Colorado State University	USA
Guus J.M. Velders	National Institute for Public Health and the Environment (RIVM)	The Netherlands
Timothy J. Wallington	Ford Motor Company	USA
Darryn W. Waugh	The Johns Hopkins University	USA
Ray F. Weiss	University of California San Diego, Scripps Institution of Oceanography	USA
Donald J. Wuebbles	University of Illinois	USA
Shigeo Yoden	Kyoto University	Japan
Lingxi Zhou	Chinese Meteorological Administration, Chinese Academy of Meteorological Sciences	China

Liaisons of Sponsoring Organizations

Geir O. Braathen World Meteorological Organization Switzerland
Tina Birmpili United Nations Environment Programme Kenya
A.R. Ravishankara National Oceanic and Atmospheric Administration USA
Kenneth Jucks National Aeronautics and Space Administration USA
Claus Brüning European Commission Belgium

Assessment Coordinator and Technical Editor

Christine A. Ennis CIRES/NOAA ESRL Chemical Sciences Division USA

Publication/Graphics Design and Layout

Full Report: Christine A. Ennis CIRES/NOAA ESRL Chemical Sciences Division USA
ADM: Debra A. Dailey-Fisher NOAA ESRL Chemical Sciences Division USA

Conference Coordination and Documentation

Christine A. Ennis CIRES/NOAA ESRL Chemical Sciences Division USA
Geir O. Braathen World Meteorological Organization Switzerland
Debra A. Dailey-Fisher NOAA ESRL Chemical Sciences Division USA
John A. Pyle University of Cambridge UK

Conference Support

Debra Dailey-Fisher NOAA ESRL Chemical Sciences Division USA
Jennifer Fox NOAA ESRL Chemical Sciences Division USA
Jeanne S. Waters NOAA ESRL Chemical Sciences Division USA
Kathy A. Thompson CSC USA
Chantal Renaudot World Meteorological Organization Switzerland
Alice Wood University of Cambridge UK
Megumi Seki UNEP Ozone Secretariat Kenya
James S. Curlin UNEP Division of Technology, Industry, and Economics France
Benedictine Desbois UNEP Division of Technology, Industry, and Economics France

Computing and Networking Support

Richard J. Tisinai CIRES/NOAA ESRL Chemical Sciences Division USA
Jennifer Fox NOAA ESRL Chemical Sciences Division USA

Document Distribution

Jeanne S. Waters NOAA ESRL Chemical Sciences Division USA
Debra A. Dailey-Fisher NOAA ESRL Chemical Sciences Division USA
Suzette M. Milano-Schoser NOAA ESRL Chemical Sciences Division USA
Geir O. Braathen / Chantal Renaudot World Meteorological Organization Switzerland
Megumi Seki UNEP Ozone Secretariat Kenya
Kathleen Creavalle UNEP Ozone Secretariat Kenya

Reference Research and Editing

Scout D. Ennis CIRES/NOAA ESRL Chemical Sciences Division USA
Zita N. Toth STC and NOAA ESRL Chemical Sciences Division USA

APPENDIX B

MAJOR ACRONYMS AND ABBREVIATIONS

A1	baseline (or most likely) halocarbon scenario of the Ozone Assessment
A1-2006	baseline (or most likely) halocarbon scenario of the 2006 Ozone Assessment
A1-2010	baseline (or most likely) halocarbon scenario of the 2010 Ozone Assessment
A1B	scenario of the IPCC Special Report on Emissions Scenarios (SRES)
A5	Article 5 countries of the Montreal Protocol
AAO	Antarctic Oscillation
ACC	Antarctic Circumpolar Current
ACCMIP	Atmospheric Chemistry and Climate Model Intercomparison Project
ACE-FTS	Atmospheric Chemistry Experiment Fourier Transform Spectrometer
ADEOS	Advanced Earth Observing Satellite
ADM	Assessment for Decision-Makers (of the 2014 WMO/UNEP Ozone Assessment)
AGAGE	Advanced Global Atmospheric Gases Experiment
AGTP	Absolute Global Temperature Potential
AGWP	Absolute Global Warming Potential
AIRS	Atmospheric Infrared Sounder
AMSU	Advanced Microwave Sounding Unit
AO	Arctic Oscillation
AOGCM	atmosphere-ocean general circulation model
AR4	IPCC Fourth Assessment Report
AR5	IPCC Fifth Assessment Report
ARC	Australian Research Council (Australia)
ARCTAS	Arctic Research of the Composition of the Troposphere from Aircraft and Satellites
ARCPAC	Aerosol, Radiation, and Cloud Processes affecting Arctic Climate
ATLAS	Atmospheric Laboratory for Applications and Science
ATTREX	Airborne Tropical TRopopause Experiment
AVE	Aura Validation Experiment
B1	a lower-emissions scenario of the IPCC Special Report on Emissions Scenarios (SRES)
B2	scenario of the IPCC Special Report on Emissions Scenarios (SRES)
BDBP	Binary Database of Profiles
BDC	Brewer-Dobson circulation
BL	boundary layer
BUV	Backscatter (or Backscattered) Ultraviolet (spectrometer)
C	Celsius (unit of temperature)
CALIOP	Cloud-Aerosol Lidar with Orthogonal Polarization
CALIPSO	Cloud-Aerosol Lidar and Infrared Pathfinder Satellite Observation
CAM	Community Atmosphere Model
CanESM	Canadian Earth System Model

CARIBIC	Civil Aircraft for the Regular Investigation of the atmosphere Based on an Instrument Container
CAS	Chemical Abstracts Service
CBL	Convective boundary layer
CCM	chemistry-climate model
CCMI	Chemistry-Climate Model Initiative
CCMVal	Chemistry-Climate Model (CCM) Validation Activity (SPARC)
CCMVal-2	Chemistry-Climate Model (CCM) Validation Activity-2 (SPARC)
CCSM	Community Climate System Model
CCSRNIES	Center for Climate-Systems Research–National Institute for Environmental Studies CCM
CDIAC	Carbon Dioxide Information Analysis Center
CDM	Clean Development Mechanism
CDW	circumpolar deep water
CESM	Community Earth System Model
CFC	chlorofluorocarbon
CFSR	Climate Forecast System Reanalysis
CICERO	Center for International Climate and Environmental Research-Oslo (Norway)
CIRES	Cooperative Institute for Research in Environmental Sciences (United States)
CLAES	Cryogenic Limb Array Etalon Spectrometer
CLaMS	Chemical Lagrangian Model of the Stratosphere
cm	centimeters (unit of length)
CMAM	Canadian Middle Atmosphere Model
CMIP3	Couples Model Intercomparison Project Phase 3
CMIP5	Coupled Model Intercomparison Project Phase 5
CMIP5-CHEM	CMIP5 models with chemistry
CNRM	Centre National de Recherches Météorologiques (France)
CNRM-CMM	CNRM Centre de Meteorologie Marine
CNRS	Centre National de la Recherche Scientifique (France)
COBALD	Compact Optical Backscatter Aerosol Detector
CONICET	Consejo de Investigaciones Cientificas y Técnicas (Argentina)
CO_2-eq	carbon dioxide equivalents
COSI	COde for Solar Irradiance
CPT	cold point tropopause
CR-AVE	Costa Rica-Aura Validation Experiment
CRISTA	Cryogenic Infrared Spectrometers and Telescopes for the Atmosphere
CSIRO	Commonwealth Scientific and Industrial Research Organisation (Australia)
CTM	chemical transport model
CUE	critical-use exemption
DJF	December-January-February
DLAPSE	Denitrification by Lagrangian Particle Sedimentation
DLR	Deutschen Zentrum für Luft- und Raumfahrt (Germany)
DMS	dimethyl sulfide
DOAS	Differential Optical Absorption Spectroscopy
DU	Dobson unit
E39CA	a coupled chemistry-climate model of DLR
ECl	Equivalent Chlorine
ECMWF	European Centre for Medium-Range Weather Forecasts (United Kingdom)

EEAP	Environmental Effects Assessment Panel
EESC	Equivalent Effective Stratospheric Chlorine
ENEA	Italian National Agency for New Technologies, Energy (Italy)
ENSO	El Niño-Southern Oscillation
Envisat	Environmental Satellite
EOS	Earth Observing System
EP	Eliassen-Palm
eq	equivalent
ERA	ECMWF Re-Analysis
ERA-40	ECMWF 40-year Re-Analysis
ERA-Interim	ECMWF Interim Re-Analysis
ERF	Effective Radiative Forcing
ESA	European Space Agency
ESA O3-CCI	European Space Agency Ozone Climate Change Initiative
ESRL	Earth System Research Laboratory (NOAA)
FAA	Federal Aviation Administration
FPH	Frost Point Hygrometers
FRF	fractional release factors
FTIR	Fourier transform infrared
FU-Berlin	Freie Universität Berlin (Germany)
GAW	Global Atmosphere Watch
GCM	general circulation model
GDP	Gross Domestic Product
GES DISC	Goddard Earth Sciences Data and Information Services Center
GeoMIP	Geoengineering Model Intercomparison Project
GEOS CHEM	Goddard Earth Observing System global 3-D chemical transport model
GEOSCCM	Goddard Earth Observing System Chemistry-Climate Model (Table 3-1)
GFDL	Geophysical Fluid Dynamics Laboratory (NOAA)
Gg	gigagrams (10^9 grams) (unit of mass)
GHG	greenhouse gas
GISS	Goddard Institute for Space Studies (NASA)
GMD	Global Monitoring Division (NOAA/ESRL)
GODFIT	GOME Direct-FITing
GOME	Global Ozone Monitoring Experiment
GOME-2	Global Ozone Monitoring Experiment-2
GOMOS	Global Ozone Monitoring by Occultation of Stars
GOSAT	Greenhouse gases Observing SATellite
GOZCARDS	Global Ozone Chemistry and Related Trace Gas Data Records for the Stratosphere
GPCP	Global Precipitation Climatology Project
GROMOS	Ground-Based Millimeter-Wave Ozone Spectrometer
GSFC	Goddard Space Flight Center (NASA)
GSG	GOME, SCIAMACY, and GOME-2
Gt	gigatonnes
$GtCO_2$-eq	gigatonnes of carbon dioxide equivalents
GTO	Global Total Ozone
GTP	Global Temperature Potential; Global Temperature change Potential
GWP	Global Warming Potential

HadAT	Hadley Centre radiosonde temperature product
HALOE	Halogen Occultation Experiment
HARMOZ	HARMonized dataset of OZone profiles
HCFC	hydrochlorofluorocarbon
HF	hydrogen fluoride
HFC	hydrofluorocarbon
HFE	hydrofluorinated ether or hydrofluoroether
HFO	hydrofluoro-olefin
HIAPER	High-performance Instrumented Airborne Platform for Environmental Research
HIPPO	HIAPER Pole-to-Pole Observations
HIRDLS	High Resolution Dynamics Limb Sounder
hPa	hectoPascal (10^2 Pascal) (unit of pressure)
HTOC	Halons Technical Options Committee (TEAP)
IAM	Integrated Assessment Models
IASI	Infrared Atmospheric Sounding Interferometer
IGAC	International Global Atmospheric Chemistry
IGACO-O3	Integrated Global Atmospheric Chemistry Observations-Ozone
IHALACE	International Halocarbons in Air Comparison Experiment
INGEBI	Instituto de Investigaciones en Ingeniería Genética y Biología Molecular (Argentina)
INSU	Institut National des Sciences de l'Univers (France)
IO3C	International Ozone Commission
IPCC	Intergovernmental Panel on Climate Change
IPSL	Institut Pierre-Simon Laplace (France)
IR	infrared
IUP	Institute of Environmental Physics, University of Bremen (Germany)
JJA	June-July-August
JMA	Japan Meteorological Agency (Japan)
JPL	Jet Propulsion Laboratory (NASA)
K	Kelvin (unit of temperature)
kg	kilogram (10^3 grams) (unit of mass)
km	kilometer (10^3 meters) (unit of length)
KNMI	Royal Netherlands Meteorological Institute (The Netherlands)
Kt	kilotons (10^3 tons) (unit of mass)
LATMOS	Laboratoire Atmosphères, Milieux, Observations Spatiales (France)
LIMS	Limb Infrared Monitor of the Stratosphere
LMDZrepro	general circulation model of the Laboratory of Dynamic Meteorology (IPSL)
LS	lower stratosphere
LT	local time
LZRH	level of zero radiative heating

m	meter (unit of length)
MAESTRO	Measurements of Aerosol Extinction in the Stratosphere and Troposphere Retrieved by Occultation
MAM	March-April-May
MATCH	Model for Atmospheric Transport and Chemistry
MBL	marine boundary layer
MEaSUREs	Making Earth System Data Records for Use in Research Environments
MERRA	Modern-Era Retrospective Analysis for Research and Applications
MetOp	Meteorological Operational satellite
MFA	monofluoroacetic acid
MIPAS	Michelson Interferometer for Passive Atmospheric Sounding
MLR	multiple linear regression
MLS	Microwave Limb Sounder
mm	millimeters (10^{-3} meters) (unit of length)
µm	micrometer; micron (10^{-6} meters) (unit of length)
MMBtu	million British thermal units (1MMBtu = 1.055 gigajoules)
MMM	multi-model mean
MOD	merged ozone data set
mol	mole (unit, amount of substance)
MRI	Meteorological Research Institute (Japan)
MSR	Multi Sensor Reanalysis
MSU	Microwave Sounding Unit
mW	milliWatt (10^{-3} Watts)
NAM	Northern Annular Mode
NAO	North Atlantic Oscillation
NASA	National Aeronautics and Space Administration (United States)
NAT	nitric acid trihydrate
NCAR	National Center for Atmospheric Research (United States)
NCEP	National Centers for Environmental Prediction (NOAA) (United States)
NDACC	Network for the Detection of Atmospheric Composition Change
NH	Northern Hemisphere
NIES	National Institute for Environmental Studies (Japan)
NIWA	National Institute of Water and Atmospheric Research (New Zealand)
nm	nanometers (10^{-9} meters) (unit of length)
NOAA	National Oceanic and Atmospheric Administration (United States)
nPB	n-propyl bromide
NPLS	nonparametric least-squares fit
NPP	net primary production
NRL	Naval Research Laboratory
NRLSSI	Naval Research Laboratory Solar Spectral Irradiance model
NWS	National Weather Service (NOAA) (United States)
OCS	carbonyl sulfide (also COS)
ODP	Ozone Depletion Potential
ODS	ozone-depleting substance
OMI	Ozone Monitoring Instrument
OMPS	Ozone Mapping and Profiler Suite

OMPS-LP	Ozone Mapping and Profiler Suite-Limb Profiler
OMPS-NM	Ozone Mapping and Profiler Suite-Nadir Mapper
OMPS-NP	Ozone Mapping and Profiler Suite-Nadir Profiler
OSIRIS	Optical Spectrograph and InfraRed Imager System
OSUC	Observatoire des Sciences de l'Univers en région Centre (France)
PCE	perchloroethylene, also known as tetrachloroethylene
PDO	Pacific Decadal Oscillation
PEARL	Polar Environment Atmospheric Research Laboratory
PEM	Pacific Exploratory Mission
PEPACG	Programa para el Estudio de Procesos Atmosféricos en el Cambio Global (Argentina)
PFC	perfluorocarbon
PFOS	perfluorooctanyl sulfonate
PG	product gas
PGI	product gas injection
PI	pre-industrial
PNNL	Pacific Northwest National Laboratory (United States)
POAM	Polar Ozone and Aerosol Measurement
ppb	parts per billion
ppbv	parts per billion by volume
ppm	parts per million
ppmv	parts per million by volume
ppt	parts per trillion
pptv	part per trillion by volume
PSC	polar stratospheric cloud
PTFE	polytetrafluoroethylene
PWLT	piecewise linear trend
QBO	quasi-biennial oscillation
QPS	quarantine and pre-shipment
RCP	Representative Concentration Pathway
RE	radiative efficiencies
REF-B1	reference “future” simulation of SPARC CCMVal-2
REF-B2	reference “future” simulation of SPARC CCMVal-2
RF	radiative forcing
RICH	Radiosonde Innovation Composite Homogenization
RSS	Remote Sensing Systems Inc.
s	second (unit of time)
SABER	Sounding of the Atmosphere using Broadband Emission Radiometry
SAGE	Stratospheric Aerosol and Gas Experiment
SAM	Southern Annular Mode
SAM II	Stratospheric Aerosol Measurement II
SAMW	Subantarctic Mode Water
SAOZ	Système d’Analyse par Observation Zénithale
SAP	Scientific Assessment Panel (Montreal Protocol)

SATIRE	Spectral and Total Irradiance REconstruction
SBUV/SBUV2	Solar Backscatter (or Backscattered) Ultraviolet (spectrometer)
SCIAMACHY	Scanning Imaging Absorption Spectrometer for Atmospheric Chartography
SCISAT	a Canadian satellite also known as Atmospheric Chemistry Experiment (ACE)
SD-WACCM	Specified Dynamics version of the Whole Atmosphere Community Climate Model
SG	source gas
SGI	source gas injection
SH	Southern Hemisphere
SHADOZ	Southern Hemisphere Additional Ozonesondes
SHIVA	Stratospheric Ozone: Halogen Impacts in a Varying Atmosphere
SI2N	SPARC/IO_3C/IGACO-O3/NDACC initiative
SLIMCAT	Single-Layer Isentropic Model of Chemistry and Transport
SLS	Submillimeterwave Heterodyne Limb Sounder
SMILES	Superconducting Submillimeter-Wave Limb-Emission Sounder
SMR	Sub-Millimetre Radiometer (Odin satellite)
SOCOL	modeling tool for studies of Solar-Climate-Ozone Links
SON	September-October-November
SORCE	Solar Radiation and Climate Experiment
SPARC	Stratosphere-troposphere Processes and Their Role in Climate (WCRP)
SRES	Special Report on Emissions Scenarios (IPCC)
SRM	solid rocket motor
SRV	suborbital, reusable vehicles
SSA	stratospheric sulfate aerosol
SSA	single scattering albedo
SSI	spectral solar irradiance
SST	sea surface temperature
SSU	Stratospheric Sounding Unit
SSW	sudden stratospheric warming
STAR	System for Transfer of Atmospheric Radiation
STE	stratosphere-troposphere exchange
STRAT	Stratospheric Tracers of Atmospheric Transport
STS	supercooled ternary solution
Suomi-NPP	Suomi National Polar-orbiting Partnership
SUSIM	Solar Ultraviolet Spectral Irradiance Monitor
SWOOSH	Stratospheric Water and Ozone Satellite Homogenized
SZA	solar zenith angle

2-D	two-dimensional
3-D	three-dimensional
TANSO-FTS	Thermal And Near infrared Sensor for carbon Observation-Fourier Transform Spectrometer
TC4	Tropical Composition, Cloud and Climate Coupling mission
TCE	trichloroethene, trichloroethylene
TEAP	Technology and Economic Assessment Panel (Montreal Protocol)
TES	Tropospheric Emission Spectrometer
TFA	trifluoroacetic acid
Tg	teragrams (10^{12} grams) (unit of mass; equivalent to megatonne)
TOMCAT	Toulouse Off-line Model of Chemistry and Transport
TOMS	Total Ozone Mapping Spectrometer
TOSOMI	SCIAMACHY total ozone retrieval algorithm

TOGOMI	GOME total ozone retrieval algorithm
TOU	Total Ozone Unit
TSAM	time series additive model
TTL	tropical tropopause layer
UAH	University of Alabama–Huntsville
UARS	Upper Atmosphere Research Satellite
UCI	University of California, Irvine
UEA	University of East Anglia (United Kingdom)
UK	United Kingdom
UKCA	United Kingdom Chemistry and Aerosols chemistry-climate model
ULAQ	University of L'Aquila chemistry-climate model (Italy)
UMD	University of Maryland (United States)
UMETRAC	Unified Model with Eulerian Transport and Chemistry
UMSLIMCAT	Unified Model Single-Layer Isentropic Model of Chemistry and Transport CCM
UMUKCA	Unified Model of the UK – Chemistry and Aerosol
UNEP	United Nations Environment Programme
UNFCCC	United Nations Framework Convention on Climate Change
UPMC	Université Pierre et Marie Curie (France)
US, USA	United States of America
UT	upper troposphere
UTLS	upper troposphere/lower stratosphere
UV	ultraviolet
VIRGO	Variability of solar IRadiance and Gravity Oscillations
VSL	very short-lived
VSLS	very short-lived substance(s)
W	watt (unit of energy)
WACCM	Whole-Atmosphere Community Climate Model
WCRP	World Climate Research Programme
WFDOAS	Weighting Function Differential Optical Absorption Spectroscopy
WOUDC	World Ozone and Ultraviolet Data Centre
W/m^2, $W\ m^{-2}$	watts per square meter
WMO	World Meteorological Organization

APPENDIX C
CHEMICAL FORMULAE AND NOMENCLATURE

HALOGEN-CONTAINING SPECIES

Cl	atomic chlorine	Br	atomic bromine
Cl_y	total inorganic chlorine	Br_y	total inorganic bromine
CCl_y	organic chlorine	CBr_y	organic bromine
Cl_2	molecular chlorine	Br_2	molecular bromine
ClO	chlorine monoxide	BrO	bromine monoxide
Cl_2O	dichlorine monoxide	Br_2O	dibromine monoxide
ClO_x	chlorine radicals ([ClO] + 2×[ClOOCl])	BrO_x	bromine radicals
OClO	chlorine dioxide		
ClOO	chloroperoxy radical		
Cl_2O_2, ClOOCl	dichlorine peroxide (ClO dimer)		
$ClONO_2$, $ClNO_3$	chlorine nitrate	$BrONO_2$, $BrNO_3$	bromine nitrate
HCl	hydrogen chloride (hydrochloric acid)	HBr	hydrogen bromide
HOCl	hypochlorous acid	HOBr	hypobromous acid

F	atomic fluorine	I	atomic iodine
F_2	molecular fluorine	I_2	molecular iodine
F_y	total inorganic fluorine	I_y	total inorganic iodine
HF	hydrogen fluoride (hydrofluoric acid)	IO	iodine monoxide
FO_x	fluorine radicals, F + FO	IO_x	iodine radicals
		OIO	iodine dioxide
		HOI	hypoiodous acid

SF_6	sulfur hexafluoride	NF_3	nitrogen trifluoride
SO_2F_2	sulfuryl fluoride	PBr_3	phosphorus tribromide

HALOCARBONS

CHLOROFLUOROCARBONS (CFCS)

CFC-11	CCl_3F
CFC-12	CCl_2F_2
CFC-13	$CClF_3$
CFC-112	CCl_2FCCl_2F
CFC-112a	$CClF_2CCl_3$
CFC-113	CCl_2FCClF_2
CFC-113a	CCl_3CF_3
CFC-114	$CClF_2CClF_2$
CFC-114a	CCl_2FCF_3
CFC-115	$CClF_2CF_3$
CFC-316c	cyclic $C_4Cl_2F_6$

HALONS

halon-1202	CBr_2F_2
halon-1211	$CBrClF_2$
halon-1301	$CBrF_3$
halon-2402	$CBrF_2CBrF_2$
halon-2311(Halothane)	$CHBrClCF_3$

HYDROCHLOROFLUOROCARBONS (HCFCS)

HCFC-21	$CHCl_2F$
HCFC-22	$CHClF_2$
HCFC-31	CH_2ClF
HCFC-123	$CHCl_2CF_3$
HCFC-123a	$CHClFCF_2Cl$
HCFC-123b	CHF_2CCl_2F
HCFC-124	$CHClFCF_3$
HCFC-124a	CHF_2CClF_2
HCFC-133a	CH_2ClCF_3
HCFC-141b	CH_3CCl_2F
HCFC-142b	CH_3CClF_2
HCFC-225ca	$CHCl_2CF_2CF_3$
HCFC-225cb	$CHClFCF_2CClF_2$
HCFC-234fb	$CF_3CH_2CCl_2F$
HCFC-243cc	$CH_3CF_2CCl_2F$
HCFC-1233zd(*E*)	(*E*)-$CHClCHCF_3$

HYDROFLUOROCARBONS (HFCS)

HFC-23	CHF_3
HFC-32	CH_2F_2
HFC-41	CH_3F
HFC-125	CHF_2CF_3
HFC-134	CHF_2CHF_2
HFC-134a	CH_2FCF_3
HFC-143	CH_2FCHF_2
HFC-143a	CH_3CF_3
HFC-152	CH_2FCH_2F
HFC-152a	CH_3CHF_2
HFC-161	CH_3CH_2F
HFC-227ea	CF_3CHFCF_3
HFC-236cb	$CH_2FCF_2CF_3$
HFC-236ea	CHF_2CHFCF_3
HFC-236fa	$CF_3CH_2CF_3$
HFC-245cb	$CH_3CF_2CF_3$
HFC-245ca	$CH_2FCF_2CHF_2$
HFC-245ea	$CHF_2CHFCHF_2$
HFC-245eb	$CH_2FCHFCF_3$
HFC-245fa	$CHF_2CH_2CF_3$
HFC-263fb	$CH_3CH_2CF_3$
HFC-272ca	$CH_3CF_2CH_3$
HFC-281ea	CH_3CHFCH_3
HFC-365mfc	$CH_3CF_2CH_2CF_3$
HFC-356mcf	$CH_2FCH_2CF_2CF_3$
HFC-356mff	$CF_3CH_2CH_2CF_3$
HFC-338pcc	$CHF_2CF_2CF_2CHF_2$
HFC-43-10mee	$CF_3CHFCHFCF_2CF_3$
HFC-458mfcf	$CF_3CH_2CF_2CH_2CF_3$
HFC-55-10mcff	$CF_3CF_2CH_2CH_2CF_2CF_3$

CHLOROCARBONS

CH_3Cl	methyl chloride, chloromethane
CH_2Cl_2	dichloromethane, methylene chloride
$CHCl_3$	chloroform, trichloromethane
CCl_4	carbon tetrachloride, CTC
$CHClCCl_2$	trichloroethylene, trichloroethene, TCE
CCl_2CCl_2	tetrachloroethene, perchloroethene, PCE
CH_3CH_2Cl, C_2H_5Cl	ethyl chloride, chloroethane
CH_2ClCH_2Cl	1,2 dichloroethane
CH_3CCl_3	methyl chloroform
$CH_3CHClCH_3$	isopropylchloride, 2-chloropropane
$CH_3CH_2CH_2Cl$	n-propyl chloride, 1-chloropropane
$COCl_2$, $Cl_2C(O)$	phosgene, carbonyl chloride

BROMOCARBONS

CH_3Br	methyl bromide, bromomethane
CH_2Br_2	dibromomethane, methylene bromide
$CHBr_3$	bromoform, tribromomethane
CH_3CH_2Br, C_2H_5Br	ethyl bromide, bromoethane
CH_2BrCH_2Br	1,2 dibromoethane
$CH_3CH_2CH_2Br$,	n-propyl bromide, n-PB, n-C_3H_7Br, 1-bromopropane
$COBr_2$	carbonyl bromide

IODOCARBONS

CH_3I	methyl iodide, iodomethane
CH_2I_2	diiodomethane
CH_3CH_2I, C_2H_5I	ethyl iodide, iodoethane
CH_3CHICH_3	isopropyl iodide, 2-iodopropane
$CH_3CH_2CH_2I$ (n-C_3H_7I)	n-propyl iodide, 1-iodopropane

OTHERS

$CHBr_2Cl$	dibromochloromethane
CH_2BrCl	bromochloromethane
$CHBrCl_2$	bromodichloromethane
CH_2BrI	bromoiodomethane
$CHBrF_2$	bromodifluoromethane
CH_2ClI	chloroiodomethane
CF_3I	trifluoroiodomethane
CH_2CBrCF_3	bromotrifluoropropene
$CF_3CF_2CF_2I$, C_3F_7I	1-iodo-heptafluoropropane
COClF	chlorofluorocarbonyl
CCl_3CHO	trichloroacetaldehyde, chloral
SF_5CF_3	trifluoromethylsulfurpentafluoride

FLUOROCARBONS

CF_4 (PFC-14)	perfluoromethane, carbon tetrafluoride
C_2F_6, CF_3CF_3 (PFC-116)	perfluoroethane
C_3F_8, $CF_3CF_2CF_3$ (PFC-218)	perfluoropropane
c-C_3F_6 (PFC-C216)	perfluorocyclopropane
C_4F_{10} (PFC-31-10)	perfluorobutane
c-C_4F_8 (PFC-C318)	perfluorocyclobutane
C_5F_{12} (PFC-41-12)	perfluoropentane
C_6F_{14} (PFC-51-14)	perfluorohexane
C_7H_{16} (PFC-61-16)	perflouoroheptane
$C_{10}F_{18}$	perfluorodecalin
COF_2	carbonyl fluoride
$CH_2FC(O)OH$	monofluoroacetic acid (MFA)
$CHF_2C(O)OH$	difluoroacetic acid (DFA)
$CF_3C(O)OH$	trifluoroacetic acid (TFA)
CF_3O_x	$CF_3O + CF_3O_2 + CF_3O_2NO_2$

HYDROFLUORO-OLEFINS

CH_2CFCF_3	HFO-1234yf

OTHER CHEMICAL SPECIES

O	atomic oxygen
$O(^3P)$	atomic oxygen (ground state)
$O(^1D)$	atomic oxygen (first excited state)
O_2	molecular oxygen
O_3	ozone
O_x	odd oxygen (O, $O(^1D)$, O_3) or oxidant ($O_3 + NO_2$)
H	atomic hydrogen
H_2	molecular hydrogen
OH	hydroxyl radical
HO_2	hydroperoxyl radical
H_2O	water
HO_x	odd hydrogen (H, OH, HO_2, H_2O_2)

N	atomic nitrogen
N_2	molecular nitrogen
N_2O	nitrous oxide
NO	nitric oxide
NO_2	nitrogen dioxide
NO_3	nitrogen trioxide, nitrate radical
N_2O_5	dinitrogen pentoxide
NO_x	nitrogen oxides ($NO + NO_2$)
NO_y	total reactive nitrogen (usually includes NO, NO_2, NO_3, N_2O_5, $ClONO_2$, HNO_4, HNO_3)
HNO_2, HONO	nitrous acid
HOONO	pernitrous acid
HNO_3	nitric acid
NH_3	ammonia
NH_4NO_3	ammonium nitrate

S	atomic sulfur
SO_2	sulfur dioxide
H_2SO_4	sulfuric acid
CH_3SCH_3	DMS, dimethyl sulfide
H_2S	hydrogen sulfide
CS_2	carbon disulfide
COS, OCS	carbonyl sulfide

C	carbon atom
CO	carbon monoxide
CO_2	carbon dioxide

CH_4	methane
CH_3CH_3	ethane
$CH_3CH_2CH_3$	propane
CH_3OH	methyl alcohol, methanol